Stable Isotope Hydrology of the Table Mountain Group

Roger Diamond

Submitted for the degree of
Doctor of Philosophy
in Geology.

Department of Geological Sciences
University of Cape Town

2014

Towerkop, 2189m, Skurweberg Formation of the Table Mountain Group, viewed from the north, showing the fractured nature of this quartzite aquifer. The Towerkop water point is just out of view, around the corner to the east, at about the level of the horizon.

"It ain't the water that's not right around here."

from Black Eyed Man, 1992

Cowboy Junkies.

ABSTRACT

Rain was collected from 2010 to 2012 at 15 locations around the Cape Fold Belt, at the same time as samples from rivers, springs, seeps and boreholes, totalling 435 samples. Precipitation ranged from -75 ‰ to +40 ‰ for δD and -12 ‰ to +8 ‰ for $\delta^{18}O$, showing seasonal patterns, with lower δ values in winter and higher in summer. Certain anomalous δ values can be attributed to individual weather events, such as thunderstorms. Using weighted data, the meteoric water line is δD = 6.15 $\delta^{18}O$ + 8.21, which is similar to previous equations. The best fit line for groundwater δ values is δD = 7.09 $\delta^{18}O$ + 10.08, the steeper gradient and higher intercept reflecting the predominance of heavy rainfall events with lower δ values in recharge, known as selection. The range of -47 ‰ to 0 ‰ for δD and -8 ‰ to -1 ‰ for $\delta^{18}O$ values for all groundwater data is about half that of the rain values, due to the averaging effect from mixing during groundwater flow. Rainfall isotope composition is negatively correlated with continentality, as defined by the product of distance to the Atlantic and the closest coast. Isotope composition of rainfall is also strongly negatively correlated with altitude, with gradients from -0.48 to -2.2 $\frac{\Delta\delta D}{100m}$ and -0.075 to -0.34 $\frac{\Delta\delta^{18}O}{100m}$. Sites that are elevated within the landscape have a reduced altitude effect, such as tall peaks, whereas mountain valleys display enhanced altitude effects. Temporal and spatial variations in the strength of the amount effect reveal meteorological variability and emphasise the need for long term monitoring.

Groundwater-fed surface waters show little systematic variation in isotope composition within catchments, indicating groundwater mixing. Differences between catchments are significant and reveal continental and altitude effects across the Cape Fold Belt. There is no significant change in hot spring isotope compositions over 40 years, confirming deep, well mixed groundwater flow. In the greater Cederberg region, groundwater abstracted from the Peninsula Formation in the Olifants River Mountains appears to be locally recharged and not in the Cederberg mountains. Abstraction in the Rietvlei Formation north and south of the Hex River anticline is being recharged at higher altitude, around 1200-1600masl, probably in the Goudini or Skurweberg Formation and moves up the stratigraphy prior to discharge. Discharge of increasingly negative δ values, a sign of deeper groundwater from higher recharge areas, could warn against overabstraction. Similar relations occur at Gamkaberg (Little Karoo) and Rooihoogte (Great Karoo), where groundwater, having been recharged at higher altitude, moves up the stratigraphy in the Skurweberg aquifer. At Gamkaberg, selective recharge of isotopically more negative large rainfall amount events, or interannual shifts in isotope composition of rainfall may account for the more negative δ values of groundwater than rain and warns against overinterpretation of short term precipitation monitoring. The δD and $\delta^{18}O$ values of springs around Table Mountain correlate positively with distance from the mountain, an amount effect. The altitude effect gradient revealed that the typical spring is recharged an average of 1km upslope of the spring at an average elevation of 330masl, into the scree aquifer. Shifts in annual mean δ values of precipitation are mimicked in the springs, proving that a component of groundwater flow is fast and shallow, whilst a deeper component must also exist to account for the steady discharge of perennial springs. An average hydraulic conductivity of 15–20m/day was calculated for the scree aquifer.

Contents

Abstract **1**

Contents **2**

List of Figures **5**

List of Tables **8**

1 Introduction **9**

1.1 Water in South Africa 9

1.1.1 Water in the Western Cape 9

1.2 Introduction to Stable Isotope Hydrology 13

1.2.1 Isotope Geochemistry 13

1.2.2 Isotope Fractionation 14

1.2.3 Kinetic Fractionation 14

1.2.4 Equilibrium Fractionation 14

1.2.5 Fractionation Factors 15

1.2.6 Measurement and Standards 16

1.2.7 Stable Isotope Hydrology 17

1.3 Stable Isotope Hydrology in South Africa 22

1.3.1 Motivation Behind this Study 25

2 Background **27**

2.1 Introduction 27

2.2 Geology — Lithostratigraphy 27

2.2.1 Saldania Belt 27

2.2.2 Cape Granite Suite 30

2.2.3 Cape Supergroup 30

2.2.4 Karoo Supergroup 38

2.2.5 Younger Rocks 38

2.3 Geology — Structure 41

2.4 Climate and Weather 43

2.4.1 Rain . . . 43
2.4.2 Temperature . . . 52
2.5 Hydrogeology . . . 52
2.5.1 Porosity and Permeability . . . 52
2.5.2 Hydraulic Parameters . . . 55
2.5.3 Hydrostratigraphy . . . 57
2.5.4 Significance of the Table Mountain Group . . . 60

3 Methods **63**
3.1 Introduction . . . 63
3.2 Sample Collection . . . 63
3.2.1 Rain . . . 63
3.2.2 Surface Water . . . 66
3.2.3 Groundwater . . . 66
3.3 Sample Preparation . . . 66
3.3.1 Mass Spectrometry . . . 66
3.3.2 Laser Cavity Ringdown Spectroscopy . . . 69
3.4 Sample Analysis and Data Correction . . . 69
3.4.1 Mass Spectrometry . . . 69
3.4.2 Laser Cavity Ringdown Spectroscopy . . . 70
3.4.3 Standards . . . 72
3.5 Data Analysis . . . 75
3.6 Maps . . . 76

4 Results **94**
4.1 Introduction . . . 94
4.2 Rain . . . 94
4.2.1 Rainfall Amount . . . 97
4.2.2 Rainfall Seasonality . . . 98
4.3 Rain Isotopes . . . 98
4.3.1 Temporal Variations . . . 100
4.3.2 Means and Weighting . . . 104
4.3.3 Deuterium Excess . . . 108
4.3.4 Local Meteoric Water Lines . . . 108
4.4 Groundwater . . . 113
4.5 Surface Water . . . 114
4.6 Other Samples . . . 116
4.6.1 Snow . . . 116
4.7 Summary . . . 117

5 Discussion **129**
5.1 Introduction . . . 129
5.2 Precipitation . . . 129
5.2.1 Source Area and Pathway Effects . . . 129
5.2.2 Isotope Effects . . . 132
5.3 Surface Water . . . 146
5.3.1 Altitude . . . 146
5.3.2 Springs, Seeps and Tributaries . . . 146
5.3.3 Baseflow . . . 148
5.4 Groundwater . . . 151
5.4.1 Altitude . . . 151
5.4.2 Hot Springs . . . 153
5.5 Regional Analyses . . . 154
5.5.1 Cederberg . . . 155
5.5.2 Hex River Mountains . . . 159
5.5.3 Langeberg – Gamkaberg – Swartberg . . . 166
5.5.4 Swartberg to Goukamma . . . 168
5.5.5 Cape Town . . . 173

6 Conclusions and Recommendations **181**

7 Abbreviations, Acronyms and Units **188**

8 Acknowledgements **191**

References **193**

List of Figures

1.1 Mean annual precipitation for the Western Cape . . . 11
1.2 Geological map of the study area . . . 12
1.3 The global water cycle . . . 17
1.4 The global meteoric water line . . . 18
1.5 Local meteoric water lines . . . 20
1.6 Source region humidity measured through d-excess . . . 23

2.1 Revised stratigraphy of the western Saldania Belt . . . 29
2.2 Stratigraphy of the Table Mountain Group . . . 32
2.3 Photograph of Peninsula Formation pebbly quartzite . . . 34
2.4 Photograph of the Hex River anticline . . . 41
2.5 Mean annual precipitation map for South Africa . . . 42
2.6 Rainfall and temperatures for stations in the Western Cape . . . 45
2.7 Rainfall and temperatures for stations in the Western Cape . . . 46
2.8 Synoptic chart: westerly wave . . . 47
2.9 Synoptic chart: southerly meridional flow . . . 48
2.10 Synoptic chart: ridging anticyclone . . . 49
2.11 Synoptic chart: cut-off low . . . 50
2.12 Synoptic chart: west coast trough . . . 51
2.13 Photograph of seeps in the Skurweberg Formation . . . 53
2.14 Piekenierskloof Formation fracture measurements . . . 54
2.15 Theoretical models of fracture porosity . . . 54
2.16 Fracture trace map for the Cederberg region . . . 55
2.17 Detailed fracture trace map for the Peninsula Formation . . . 57
2.18 Hydrostratigraphy of the Cape Supergroup . . . 62

3.1 Map of the study area . . . 65
3.2 Cumulative rainfall collector . . . 67
3.3 Hydrogen isotope sample preparation apparatus . . . 67
3.4 Oxygen isotope sample preparation apparatus . . . 68
3.5 Isotope correction procedure . . . 71

3.6 Map legend . . . 77
3.7 Cape Town map . . . 78
3.8 Twaktuin map . . . 79
3.9 Cederberg map . . . 80
3.10 Wolfkop map . . . 81
3.11 Matroosberg map . . . 82
3.12 Waaihoek and Witels map . . . 83
3.13 Drakenstein map . . . 84
3.14 Meulkloof map . . . 85
3.15 Riverndale map . . . 86
3.16 Klein Swartberg map . . . 87
3.17 Gamkaberg map . . . 88
3.18 Robinson Pass map . . . 89
3.19 Kammanassie map . . . 90
3.20 Blesberg map . . . 91
3.21 Lentelus map . . . 92
3.22 Goukamma map . . . 93

4.1 South African monthly rainfall maps . . . 99
4.2 Sample altitude histogram . . . 101
4.3 Rainfall: δD vs. time . . . 102
4.4 Rainfall: $\delta^{18}O$ vs. time . . . 103
4.5 Photograph of convective rainfall over the Cederberg . . . 105
4.6 Rainfall δD vs. $\delta^{18}O$: arithmetic means and weighted means . . . 106
4.7 Rainfall: difference between arithmetic and weighted mean δ values vs. MAP . . . 107
4.8 Rainfall: d-excess vs. MAP and continentality . . . 109
4.9 All rain water and groundwater δ values . . . 110
4.10 Local meteoric water lines . . . 111
4.11 Local meteoric water line map . . . 112
4.12 Photograph of Seweweekspoort Peak Cave seep . . . 114
4.13 Surface water: δD vs. $\delta^{18}O$ . . . 115
4.14 Monthly rainfall graphs . . . 118

5.1 Isotope data from various studies in South Africa . . . 131
5.2 Rainfall: the continental effect . . . 135
5.3 Map of the study area, showing sample locations and cross section lines . . . 139
5.4 Rainfall and groundwater: altitude effects . . . 141
5.5 Topography around sample sites . . . 144
5.6 Rainfall: annual amount effects . . . 145

5.7 Rainfall: monthly amount effects . . . 147
5.8 Surface water: δ vs. altitude . . . 149
5.9 Groundwater: δ vs. altitude . . . 151
5.10 Hot springs: δD vs. $\delta^{18}O$ . . . 154
5.11 Cederberg cross section . . . 156
5.12 Cederberg δD vs. $\delta^{18}O$ . . . 157
5.13 Schematic hydrogeology of the Olifants River Mountains . . . 158
5.14 Photograph of duplexes in the Peninsula Formation . . . 159
5.15 Hex River Mountains δD vs. $\delta^{18}O$ . . . 161
5.16 Possible south-easter snow air trajectories. . . . 162
5.17 Hex River Mountains cross section . . . 165
5.18 Langeberg–Gamkaberg δD vs. $\delta^{18}O$ . . . 167
5.19 Swartberg to Goukamma δD vs. $\delta^{18}O$ . . . 169
5.20 Little Karoo cross section . . . 171
5.21 Cape Town δD vs. $\delta^{18}O$ . . . 172
5.22 Cape Town springs δD vs. $\delta^{18}O$ . . . 174
5.23 Cape Town springs interannual shifts in δ values . . . 176
5.24 Rainfall interannual shifts in δ values . . . 177
5.25 Conceptual model for Cape Town springs . . . 179
5.26 Calculation of recharge altitude for Cape Town springs . . . 180

List of Tables

1.1 Isotopologues of water 13
1.2 Publications on stable isotopes in the Table Mountain Group 26

2.1 Hydraulic parameters for the Table Mountain Group 56
2.2 Spring and wellfield yields from the Table Mountain Group 61

3.1 Rainfall collection stations 64
3.2 UCT internal isotope standards 69
3.3 Raw data for internal standards: δD 73
3.4 Raw data for internal standards: $\delta^{18}O$ 74

4.1 Rainfall collection periods at each station 95
4.2 Rainfall collection stations 96
4.3 Rainfall: arithmetic and weighted means 107
4.4 Snow: isotope composition 117
4.5 Isotope data for rain for 2010 123
4.6 Isotope data for rain for 2011 124
4.7 Isotope data for rain for 2012 125
4.8 Isotope data for the Table Mountain springs 126
4.9 Isotope data for surface water 127
4.10 Isotope data for groundwater 128

5.1 Cape meteoric water line equations 132
5.2 Global examples of the continental effect 133
5.3 Distances from rainfall stations to the sea 134
5.4 Global examples of the altitude effect 136
5.5 Rainfall and groundwater: altitude effect gradients 137
5.6 Topographic position of sample sites 142
5.7 Description of the five rivers sampled 149

7.1 Acronyms, Units and Abbreviations 190

Chapter 1

Introduction

1.1 Water in South Africa

South Africa is a dry country. With an average annual rainfall of 450 mm/a (Dent et al., 1987; Schulze and Lynch, 2001), South Africa is clearly drier than most of the world, which averages around 1000 mm/a (Wikipedia, 2013a; Encyclopaedia Brittanica, 2013). The warm, dry climate compounds the problem of low rainfall and it is estimated that less than 10 % of rainfall becomes runoff, the rest being lost to evaporation or used by plants for transpiration (Nkondo et al., 2012). This runoff is estimated to be 50 000 GL/a, which equates to the total possible surface water yield of South Africa, although *at least* 25% of this should be set aside for ecological flows. In comparison, the estimated sustainable groundwater yield is 7500 GL/a. Actual consumption of water is around 15 000 GL/a for the country, with groundwater making up 13 %, at around 2000 GL/a (DTI, 2009; Nkondo et al., 2012; Stats SA, 2006). This shows the generally minor status of groundwater in South Africa, in contrast to aquifers such as the Ogallala in the United States midwest region where 26 000 Gl/a are abstracted (Wikipedia, 2013b) in an area of moderate rainfall, or the Nubian Sandstone Aquifer, in the eastern Sahara Desert, where Libya alone is planning to abstract over 2000 GL/a (IAEA, 2013). These are however, unsustainable abstraction rates, being higher than the recharge rates in these moderate to very low rainfall areas, and therefore qualify as groundwater mining, a practice with dire environmental, social and economic consequences.

1.1.1 Water in the Western Cape

The Western Cape has the greatest extremes of rainfall of any province in South Africa, with a maximum measured average annual rainfall of 3345 mm/a at Jonkershoek, 50 km east of Cape Town, and a minimum of 60 mm/a in the Tankwa Karoo (Schulze and Lynch, 2001). The actual maximum and minimum are likely to be higher and lower, respectively, as the rain gauges have probably not been sited in the ultimate locations that experience the extremes. Despite such a high maximum, the province receives an average of only 348 mm/a. The mean annual precipitation (MAP) map of the country, as developed by Dent et al. (1987), was refined for the Western

Cape by Beuster et al. (2009) and is shown in **Figure 1.1**. To produce this rainfall map, they used the MAP of 321 rainfall stations to select four out of six factors, based on regression analysis, as determinants of rainfall at any point: altitude, continentality, terrain roughness and distance from selected "barrier" mountain chains. From this map it can be seen that much of the Western Cape receives little rain, in the region of 200–300 mm/a, but the mountainous areas receive over 1000 mm/a. These mountains are largely made up of the rocks of the Table Mountain Group (TMG), the outcrop area of which can be seen in **Figure 1.2** and it can be concluded that most of the rainfall in the Western Cape occurs on the TMG outcrop area. Of the rain that falls, some evaporates from plants (interception) and soil, some is transpired by plants, some becomes runoff and the remainder is recharged to the TMG, a fractured rock aquifer. Due to the rugged terrain and stormy weather in the Cape Mountains, minimal research has been done on hydrological processes and our understanding of recharge, discharge and groundwater flow is poorly constrained. For example, at the biennial groundwater conference held by the Groundwater Division of the Geological Society of South Africa in 2013 in Durban, only 5 of the 70 papers presented dealt with the Table Mountain Group, and only 1 of those was from work done in a mountain area. The best studies are in the extensive compilation on the Table Mountain Group edited by Pietersen and Parsons (2002). **Table 1.2**, at the end of this chapter, contains a list of all publications that make use of stable isotopes of hydrogen and oxygen and relate to the Table Mountain Group.

The most direct way to understand groundwater flow in an aquifer is by using hydraulics, which requires water level or pressure measurements taken from boreholes penetrating the aquifer. This is not easily done, not only because of the practical difficulty and cost of siting boreholes in the Cape Mountains, but also because the fractured rock nature of the TMG porosity complicates water level interpretations. Water chemistry in the TMG aquifer is remarkably consistent across the Cape Fold Belt and in addition to the consistency, the water is very low in dissolved constituents, being generally well under 100 mg/L total dissolved solids (Rosewarne, 2002b). Although it may be possible to use dissolved chemical species as tracers of groundwater flow in the TMG aquifers (Saayman et al., 2003; Richey et al., 1998), the very low concentrations make this challenging. Stable isotopes of oxygen and hydrogen offer a solution to these problems in that they are cheaper than constructing boreholes and making hydraulic measurements. Stable isotopes are known to vary on a regional scale (hundreds of kilometres) (Rozanski et al., 1993) and with altitude (Gonfiantini et al., 2001) and the Cape Fold Belt has sufficient area and altitude change to expect isotopic variation.

Variations in hydrogen and oxygen stable isotopes are used frequently in hydrological applications, such as identifying sources of groundwater recharge (Ladouche et al., 2009), changes in vapour source or oceanic surface water and in resultant precipitation (Breitenbach et al., 2010), leaking water pipes or canals (Harvey and Sibray, 2001) and sources of bottled water (Rangarajan and Ghosh, 2011).

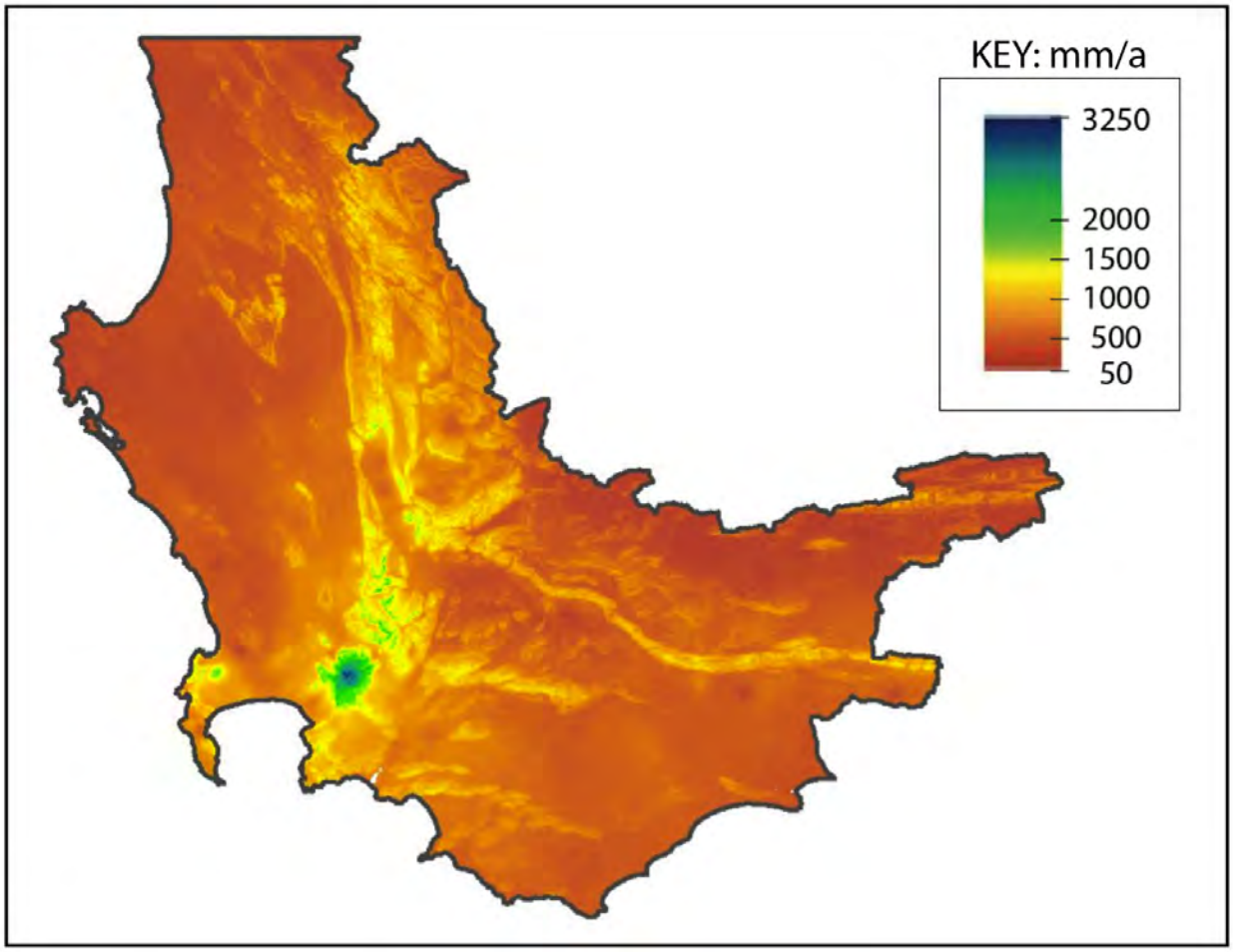

Figure 1.1: Mean annual precipitation for the western portion of the Western Cape, as calculated by Beuster et al. (2009). Precipitation amount was calculated using four factors – altitude, continentality, terrain roughness and distance from "barrier" mountains – and quantified from long term (>20 a) rainfall records from 321 stations.

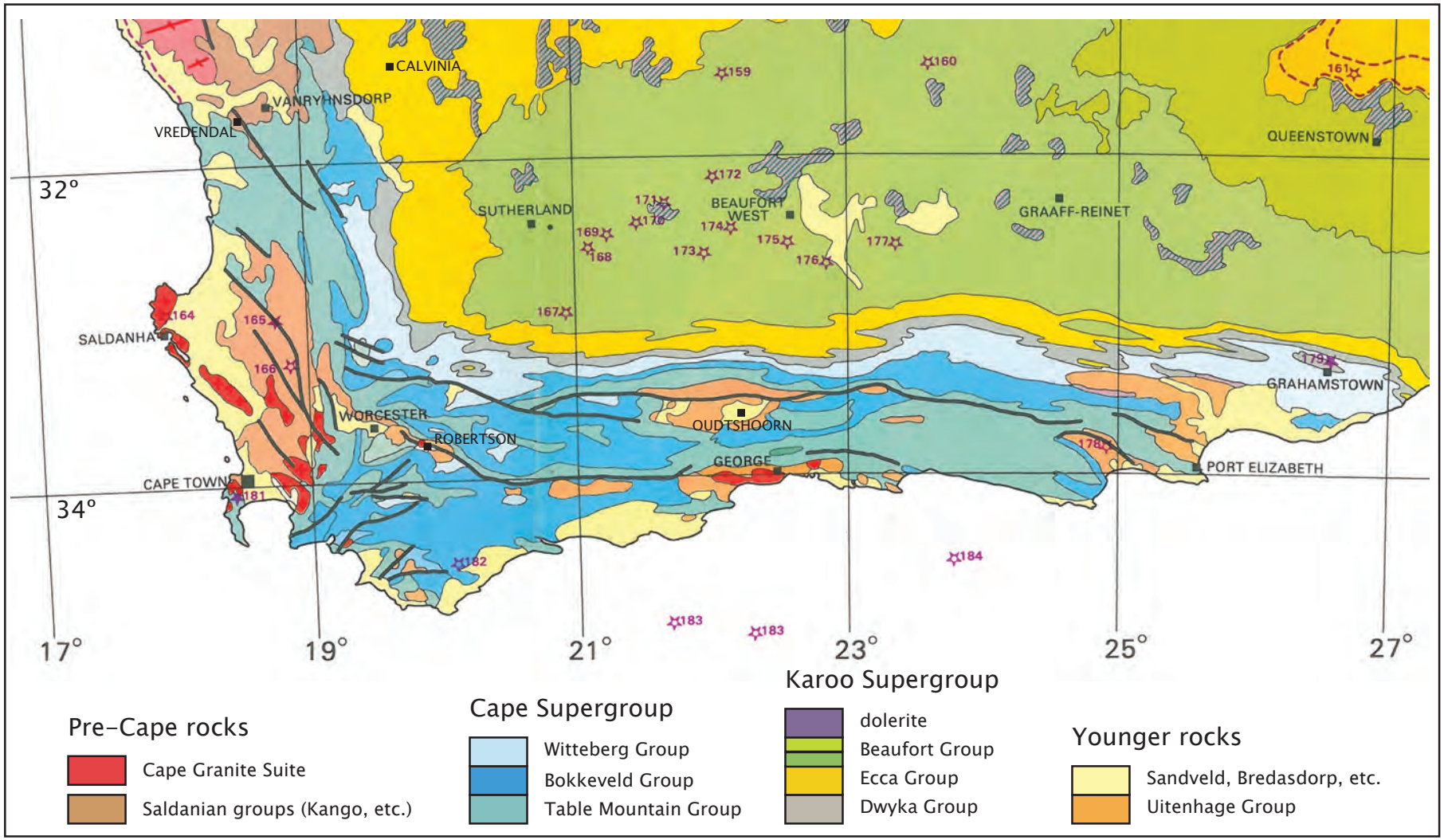

Figure 1.2: Geological map of the study area, showing the outcrop of the Table Mountain Group, where the focus of sample collection occurred. Map from Hammerbeck and Allcock (1985).

1.2 Introduction to Stable Isotope Hydrology

1.2.1 Isotope Geochemistry

The stable isotopes of oxygen were discovered in the 1920s by Blackett, and Giauque and Johnston. In 1931, deuterium was discovered by Harold Urey, who would turn out to be a major force in the understanding of the variations in stable isotope compositions (Gat, 1981b). By the 1940s, pioneering scientists were making the first attempts to apply stable isotope measurements to earth science questions, but it was only after improvements by Alfred Nier to the mass spectrometer in the late 1940s that the precision enabled the true birth of stable isotope geochemistry with early papers by Sam Epstein, Irving Friedman and Stan McCrea (Sharp, 2007). Applications to hydrology were immediately apparent and so widespread measurement of stable isotope ratios of hydrogen and oxygen commenced around the world in the 1950s, driven substantially by the World Meteorological Association and the International Atomic Energy Agency.

Isotope geochemistry can be broken into several sub-disciplines, the major break being that between radioactive or radiogenic isotopes and stable isotopes. The stable isotopes are futher broken down into light and heavy, with hydrogen, carbon, nitrogen and oxygen being the most commonly used stable light isotopes. However, the stable light isotopes and certain radioactive isotopes, such as tritium and ^{14}C, are also grouped into a branch known as the environmental isotopes, referring to their application to earth surface processes, typically in and around the biosphere, hydrosphere and atmosphere.

Hydrogen occurs as protium, ^{1}H (sometimes simply referred to as hydrogen), deuterium, ^{2}H, also written as D, and the radioactive tritium, ^{3}H, or T, with a half life of 12.33 a (Emiliani, 1987). Oxygen occurs as ^{16}O, ^{17}O and ^{18}O, all of which are stable. As a result of this spread of isotopes, water can occur as nine different isotopologues, chemically identical but isotopically different molecules, as shown in **Table 1.1**.

isotopologue	mass	abundance (%)
$^{1}H^{1}H^{16}O$	18	99.732
$^{1}H^{1}H^{18}O$	20	0.200
$^{1}H^{1}H^{17}O$	19	0.038
$^{1}H^{2}H^{16}O$	19	0.015
$^{1}H^{2}H^{18}O$	21	0.00003
$^{1}H^{2}H^{17}O$	20	0.0000057
$^{2}H^{2}H^{16}O$	20	0.0000022
$^{2}H^{2}H^{18}O$	22	0.0000000045
$^{2}H^{2}H^{17}O$	21	0.00000000086

Table 1.1: Isotopologues (isotopically different, chemically identical molecules) of water with the average abundances on earth (Emiliani, 1987).

1.2.2 Isotope Fractionation

The ratios of one isotope to another, such as $\frac{^{18}O}{^{16}O}$, vary slightly between different materials or even different reservoirs of the same substance. These differences in isotope ratios come about through preferential diffusion of the lighter or heavier isotope (or isotopologues, if in a compound) or through preferential location of the lighter or heavier isotope due to different bond energies related to mass, and are known as fractionation.

Processes that can cause isotope fractionation are chemical reactions, physical reactions or changes of state, diffusion and exchange. A chemical reaction is when two or more elements or compounds react to form different compounds; a physical reaction is where an element or compound undergoes a change of state; diffusion is when atoms or molecules disperse from high to low concentration through other material; exchange is when atoms of the same element swap places from one compound to another without causing any chemical changes. In all of these processes, molecules or atoms bearing different isotopes will proceed through these reactions at different speeds and this is known as kinetic fractionation.

1.2.3 Kinetic Fractionation

For physical, chemical and exchange reactions, the dissociation energy of molecular bonds control the reaction rate. A bond involving lighter isotopes has a lesser dissociation energy and can break more easily than the same bond involving a heavier isotope. For example, when a body of liquid water evaporates into air, the resultant water vapour (H_2O gas mixed in air) will be relatively enriched in the lighter isotopes and therefore have lower values for the ratios $\frac{D}{H}$ and $\frac{^{18}O}{^{16}O}$ than the source body. This kinetic effect will be exaggerated if the vapour is being removed rapidly, as happens in windy situations or low humidities with evaporation from natural water bodies. On the other hand, a lack of mixing in the source water body will result in a lesser fractionation effect, because the surface water layer will become depleted in ^{16}O with time.

For diffusion, the diffusive velocity is inversely proportional to the mass of the molecule and therefore molecules with lighter isotopes will diffuse faster. For kinetic fractionation there is no fixed difference in isotope ratios between the source and receptor reservoirs, as this is dependent upon factors such as time, degree of removal of one reservoir and degree of mixing of the reservoirs, as well as the actual reaction or change of state taking place.

1.2.4 Equilibrium Fractionation

If chemical, physical or exchange reactions are allowed to run to completion, then there will be a fixed isotope difference between the source and receptor reservoirs, given a certain temperature. Reactions will continue, but backwards and forwards at an equal rate, and without any net effect on isotopic composition of either reservoir. For example, at 25 °C, there is a fixed difference between the $\frac{^{18}O}{^{16}O}$ ratio in $H_2O_{(l)}$ and $CO_{2(g)}$ in equilibrium with each other. In this situation, the

kinetic effects of reaction rate are no longer important, and it is the relative preference for a heavier or lighter isotope within a chemical bond that determines which isotopes locate where. Heavier isotopes are favoured in bond positions with higher strength. To continue the above example, the covalent bonds between oxygen and carbon in CO_2 are stronger than the covalent bonds between oxygen and hydrogen in H_2O, and as the heavier isotopes remain preferentially in the stronger bond positions, the result is that $CO_{2(g)}$ will have higher values for $\frac{^{18}O}{^{16}O}$ than the $H_2O_{(l)}$.

Temperature plays a very important role in fractionation. The higher the temperature, the less the degree of fractionation, because fractionation processes are thermodynamically controlled.

1.2.5 Fractionation Factors

In order to quantify the fractionation of isotopes between two phases or compounds, the fractionation factor, α, is used, where:

$$\alpha = \frac{R_{reactant}}{R_{product}} \ ,$$

and R is the isotope ratio, such as $\frac{D}{H}$. For example:

$$\alpha D_{water-vapour} = \frac{\left(\frac{D}{H}\right)_{water}}{\left(\frac{D}{H}\right)_{vapour}} \ .$$

This factor describes the partitioning of an isotope between two phases or compounds, which is determined by the chemical bonds and other atomic scale properties of the element. Importantly, the fractionation factor is temperature dependant; in other words, at equilibrium, the isotope ratios in the reactant and product vary with temperature, as was first outlined by Urey (1947). Furthermore, this variation is systematic, in that lower temperatures result in higher fractionation factors and vica versa.

Fractionation factors are mostly numbers just above 1, and if one takes 1000 ln α, the result is approximately the difference in δ values of the reactant and product, because 1000 ln (1.00x) is approximately equal to x, and so:

$$\Delta_{X-Y} = \delta_X - \delta_Y \approx 1000 \ln \alpha_{X-Y} \ .$$

For example:

$\alpha_{(H_2O_{(l)}-H_2O_{(g)},25^\circ C)} = 1.0094$ (Kakiuchi and Matsuo (1979) in Beaudoin and Therrien (2014)),

and $1000 \ln 1.0094 = 9.4$,

so $\Delta_{(H_2O_{(l)}-H_2O_{(g)},25°C)} = 9.4$ ‰ .

This relationship holds best for smaller fractionation factors, where $\alpha < 1.01$.

1.2.6 Measurement and Standards

Isotope ratios are, by convention, the ratio of the heavier (and less abundant) isotope to the lighter (and more abundant) one. The differences in isotope ratios between materials are very slight and are not easily measured in an absolute sense. However, if measured as a relative difference between the sample and a standard of known isotope ratio, then the precision increases substantially. This is how measurements in light stable isotope mass spectrometers are made, using either a dual inlet or continuous flow system, where a reference gas is analysed alternately with the sample gas.

Stable isotope ratios are reported as deviation from an international standard. For both hydrogen and oxygen in water, the standard is SMOW, Standard Mean Ocean Water. SMOW was devised by Harmon Craig in 1961 (Craig, 1961b) as an average of previous ocean water samples from Epstein and Mayeda (1953) and Horibe and Kobayakawa (1960), but no actual sample existed. Because of this, SMOW was defined relative to NBS1 (National Bureau of Standards), a United States administered sample from the Potomac River. Because of the difficulties of not having an actual standard to analyse, the International Atomic Energy Agency in Vienna commissioned the creation of VSMOW in 1966, which was to mimic SMOW. Although VSMOW is not isotopically identical to SMOW (Clark and Fritz, 1997), it is similar enough and most workers use the acronym SMOW to define their isotope reference scale, even though VSMOW may have been used in their laboratory to calibrate their local laboratory standards (Gonfiantini, 1981; Sharp, 2007).

The Greek letter δ is used to denote the deviation of a sample from a standard, as follows:

$$\delta = \frac{R_{sample} - R_{standard}}{R_{standard}},$$

where R is an isotope ratio, such as $\frac{D}{H}$. Where relatively more of the heavy isotope (e.g. ^{18}O) is present in the sample than the standard, then the δ value will be greater than zero, whereas samples relatively depleted in the heavy isotope will have negative δ values. The $\delta^{18}O$ and δD values of SMOW are equal to 0. As the variations in isotope ratios are generally quite small, these δ values are reported in per mille (parts per thousand), using the ‰ notation. The equation combining these definitions is then:

$$\delta^{18}O_{sample-SMOW} = \left(\frac{\left(\frac{^{18}O}{^{16}O}\right)_{sample}}{\left(\frac{^{18}O}{^{16}O}\right)_{standard(SMOW)}} - 1 \right) \times 1000.$$

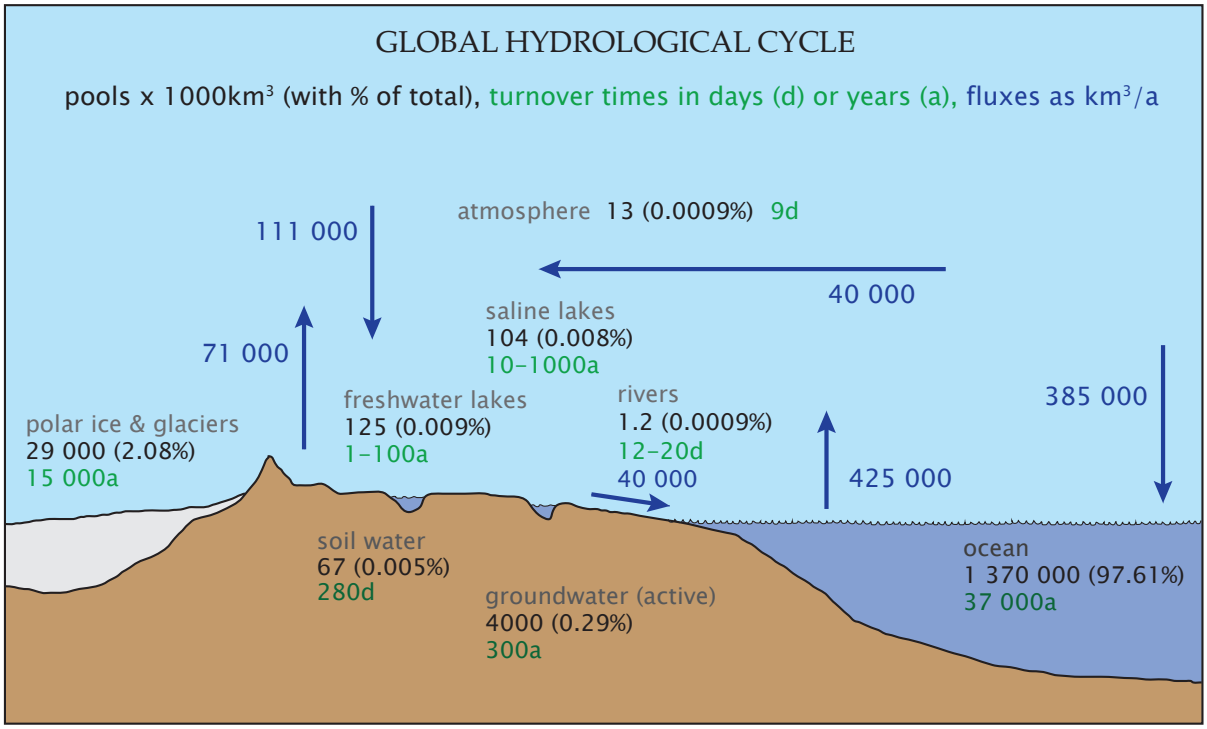

Figure 1.3: A simplified and schematic diagram of the global water cycle, showing also the reservoir sizes and turnover times within those reservoirs. It excludes water within the crust or mantle, which is unavailable, except on a timescale of many millions of years. After Reeburgh (1994).

1.2.7 Stable Isotope Hydrology

The global water cycle is extremely complex if all the interactions with geological and biological materials are taken into account, including things as diverse as weathering and volcanic eruptions in the geosphere and organic decay and drinking in the biosphere. Fortunately, the flows of water are involved in those interactions are orders of magnitude less than the major flows of water, such as evaporation from the oceans or precipitation over land, except perhaps for transpiration by plants. An attempted quantification of these flows is shown in **Figure 1.3**. This global flow of water is known as the hydrological cycle and most of the steps in this cycle are key points where the isotopic composition of parcels of water gets changed. With such complexity in this cycle, it is perhaps surprising that the variation in δD and $\delta^{18}O$ is very defined, as can be seen in the diagram in **Figure 1.4** from the landmark publication by Craig in 1961 (Craig, 1961a).

The most important observation to note in **Figure 1.4** is that most precipitation has δD and $\delta^{18}O$ values less than zero. This is primarily because evaporation from the oceans produces vapour that is depleted in the heavier isotopes relative to sea water which is similar to SMOW and has δD and $\delta^{18}O$ values close to zero. During evaporation from the ocean surface the vapour is continuously removed by diffusion and wind and mixed upwards in the atmosphere, so the air in contact with the ocean surface never becomes saturated and isotopic equilibrium cannot be reached, which means that this is a kinetic fractionation process. This results in the water vapour

in the atmosphere being more depleted in the heavier isotopes than would occur if equilibrium fractionation was taking place (Clark and Fritz, 1997). The measured values of $\delta^{18}O$ over the oceans vary from about -10 ‰ to -15 ‰, as latitude increases (temperature decreases), which are about 4 ‰ less than the equilibrium values would be. The values for δD are similarly lower than theoretical equilibrium values and range from -70 ‰ to -100 ‰ (Sharp, 2007).

Generation of atmospheric water vapour occurs mainly over the warmer oceans and it has been estimated that around 65 % is generated between 30°S and 30°N (Rozanski et al., 1993). Once an air mass is cooled, either by advection to colder climates and over a cool surface or by convection, the air can become saturated and condensation may commence. Actual condensation is dependant not only on temperature and humidity, but on the availability of condensation nucleii of the correct type (Sumner, 1988). Condensation generally proceeds slowly in response to reduced pressure or further cooling and this takes place in the presence of the vapour. As a result, condensation is an equilibrium fractionation process.

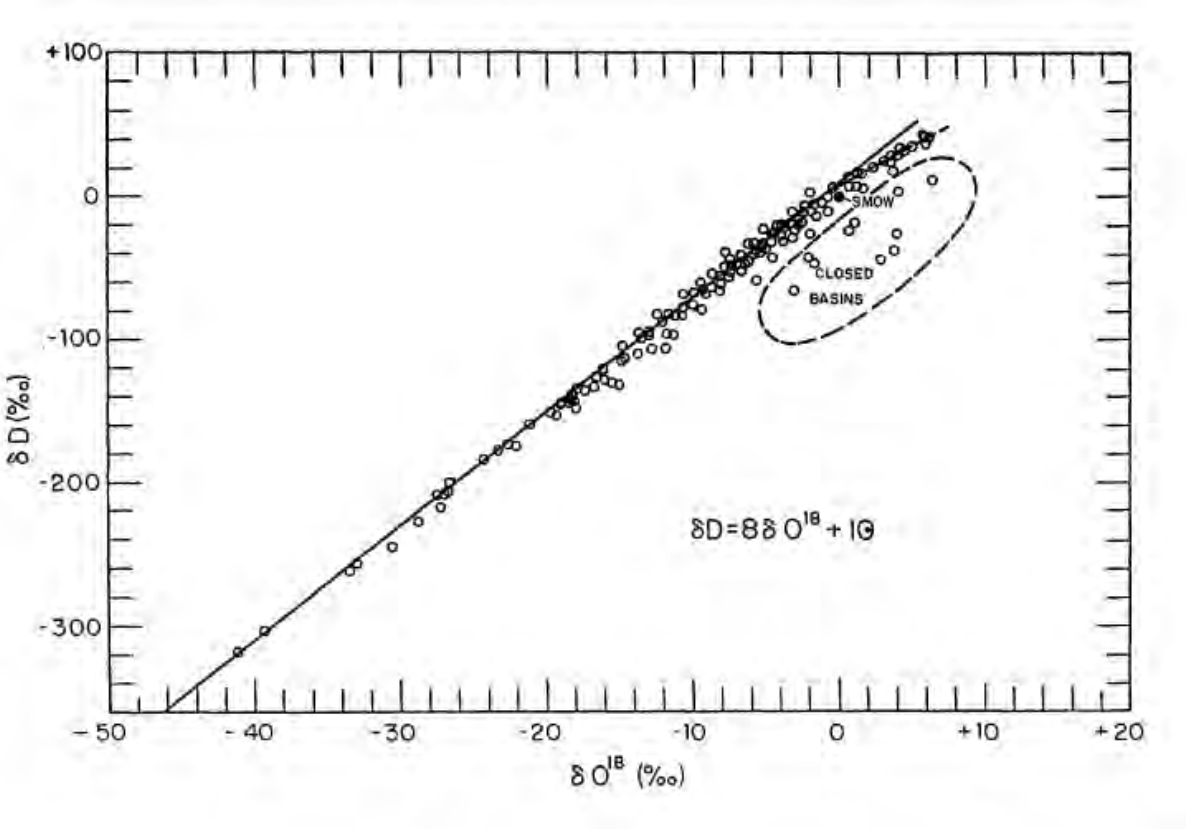

Figure 1.4: The diagram that established the relationship between δD and $\delta^{18}O$ in precipitation. The equation that describes this relationship is called the Global Meteoric Water Line (GMWL) (from Craig, 1961a).

The spread of data along the GMWL is influenced by several meteorological processes or factors, such as humidity and temperature, but it is probably rainout of atmospheric moisture, as air masses move from the tropics to the poles, that accounts for the bulk of the variation in δ values (Yurtsever and Gat, 1981). As a moisture laden air mass moves from the tropics to the poles, the moisture is removed by precipitation and the temperature or climate tends towards being colder, which not only allows further precipitation by causing more condensation, but enhances the removal of heavy isotopes by increasing equilibrium isotope fractionation factors. As the process of rainout is governed by condensation, which is is an equilibrium process, δD and $\delta^{18}O$ co-vary but with a factor of 8 difference, which is the factor by which the atomic weights vary:

$$\frac{\frac{D-H}{H}}{\frac{^{18}O-^{16}O}{^{16}O}} = \frac{\frac{1}{1}}{\frac{2}{16}} = \frac{1}{\frac{1}{8}} = 8 \quad = \frac{\Delta\delta D}{\Delta\delta^{18}O} \text{ (from GMWL of Craig (1961a)) .}$$

For a given area, with limited rainout and temperature variation, samples of precipitation will plot along a local meteoric water line (LMWL). Most LMWLs have slopes ($\frac{\Delta\delta D}{\Delta\delta^{18}O}$) of < 8, usually around 5 to 7 and a very much more limited range of δD and $\delta^{18}O$ values compared to the GMWL. When several LMWLs for areas with different climates are drawn, these lines lie semi-parallel, but displaced 'up' or 'down' on the δD–$\delta^{18}O$ plot and stack on top of each other to form the GMWL. An example is given in **Figure 1.5** that shows the data for a wide range of areas, and although each area forms more of a cluster, as the study was not to determine MWLs for each area, it nonetheless illustrates how the various areas stack up upon each other in the $\delta - -\delta$ space. The GMWL is the cumulative result of lots of LMWLs for regions of different climate, with degree of rainout being the main discriminant for the position of each LMWL. LMWLs for higher latitude regions will tend to plot lower on the diagram and vica-versa, which is clearly illustrated in **Figure 1.5**.

The reason only general, rough statements can be made about the causes of the distribution of isotope ratios in meteoric water is the extreme complexity of the hydrological cycle. Attempts have been made to build equations or conceptual models to predict isotopic values, but these have not been adequate (Sharp, 2007; Yurtsever and Gat, 1981). However, several key factors have been identified, some of which have already been alluded to above, by the first workers to interpret stable isotopes in water samples, for instance Friedman (1953), Epstein and Mayeda (1953), Craig (1961a) and Dansgaard (1964). Subsequent workers continued to develop the understanding of these key factors, until they became widely accepted as a fundamental part of isotope hydrology (e.g. Rozanski et al., 1993; Gat, 1996; Sharp, 2007). These factors are known as the latitude effect, continental effect, altitude effect and amount effect. With increasing latitude, increasing distance from the coast, increasing altitude or increasing amount of rain in a rainfall event, the isotopic composition of the precipitation becomes lighter (depleted in D and ^{18}O).

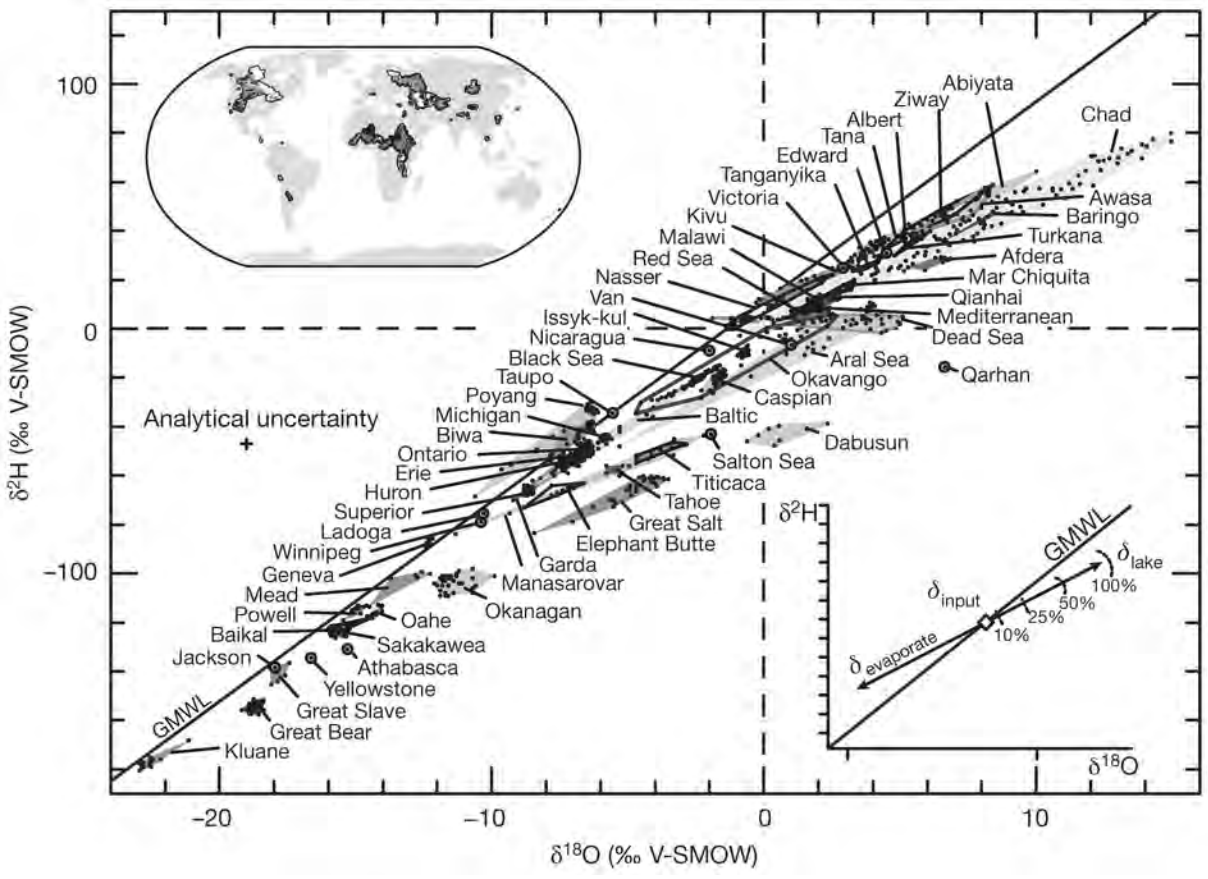

Figure 1.5: A graph illustrating the limited ranges of isotopic compositions in particular areas and how these ranges, or LMWLs, stack upon each other to form the GMWL. Diagram from Jasechko et al. (2013).

1.2.7.1 The Latitude Effect

As most moisture is sourced from the tropical oceans, because the higher temperature of the sea allows greater evaporation than in mid- or high latitude ocean areas, atmospheric moisture evolves isotopically as it moves away from the tropics. Condensation and rainout favours the removal of the heavier isotopes and so the precipitation at higher latitudes has more negative δ values. However, evaporation does still occur off the mid-latitude oceans and because the temperatures are colder, the fractionation factors will be greater, resulting in vapour relatively more depleted in the heavier isotopes than vapour that forms above the tropical oceans.

1.2.7.2 The Continental Effect

Progressive rainout is the main cause of increasingly negative δ values for precipitation that is further and further inland. In some cases, where winter rainfall occurs, cooler air inland may also reduce the amount of evaporation and isotopic change that occurs as rain drops fall through unsaturated air below the cloud. These colder inland temperatures will also increase the equilibrium fractionation factor that applies during condensation, so removing heavier isotopes more effectively from the vapour and resulting in precipitation further inland being even lighter isotopically.

1.2.7.3 The Altitude Effect

Again, the altitude effect is caused mainly by rainout that is triggered by orographic uplift, as well as a decrease in temperature, resulting in greater fractionation factors, which will drive rainout of heavier isotopes and cause a faster shift to lighter isotopes at higher altitude. Also, rain falling at higher elevations will have less distance to travel to the ground and less chance for evaporative enrichment, in which the lighter isotopes evaporate preferentially.

1.2.7.4 The Amount Effect

The amount effect also has a close relationship with rainout. Firstly, heavy individual rainstorms will tend to remove more of the vapour and cloud droplets in the air, and so with increasing rainfall in one location, the isotopic signature should become lighter. Secondly, the air below the cloud base will gradually become more saturated and colder, both of which will reduce evaporative enrichment of the later rain drops.

As can be seen from the above decriptions of the four effects, temperature and rainout are the main underlying processes that drive the various 'effects'. It is important to note that all of these effects and their underlying causes occur in a highly complex natural system where many variables contribute to the final isotopic composition of a rainwater sample. Other than temperature and rainout, factors such as humidity and source region also modify the isotopic composition. Isotope content of rainwater varies by the minute in a rainstorm (Lawrence and White, 1991; Harris et al., 2010) and between rain events, as is typical of most meteorological phenomena. Averaging the isotope composition of rainfall over longer periods, such as a month, has been found to be the most useful way of understanding the variation in isotopic signatures in an area (Yurtsever and Gat, 1981).

1.2.7.5 The Deuterium Excess

Kinetic fractionation during evaporation from the ocean surface takes place because of diffusion of water vapour molecules from a saturated boundary layer at the sea surface and into the open atmosphere . The $HH^{16}O$ isotopologue diffuses faster than all the others and so the vapour is

depleted in the heavier isotopes. If the atmosphere was saturated, then isotope exchange would occur fully between the sea and water vapour in the air, resulting in isotopic equilibrium, where the vapour would also be depleted in the heavier isotopes. However, the differences between the equilibrium and diffusion fractionation factors for D-H and ^{16}O-^{18}O are not the same and so the relative depletion of D and of ^{18}O changes with the degree of saturation, or relative humidity, **h**. As **h** increases, so more isotope exchange will occur and the closer to equilibrium fractionation the system will come (Clark and Fritz, 1997).

This means the slope along which vapour and residual water plot on a $\delta D - \delta^{18}O$ diagram will vary as a result of the degree of exchange, or isotopic equilibrium. Evaporation under lower relative humidities will generate lines with lower slopes. **Figure 1.6** shows how evaporation from sea water under 85% relative humidity conditions and then condensation at equilibrium generates water with isotopic compositions that plot along the GMWL. At different relative humidities, vapour and the resulting water samples will be displaced from the GMWL. The deuterium excess of a water samples measures this displacement with the formula:

$$d - excess = \delta D - 8\delta^{18}O$$

where δD and $\delta^{18}O$ are the values for the water sample. The d value is a proxy of the humidity of the source region.

1.3 Stable Isotope Hydrology in South Africa

Water is the single most important compound for all life. Humans need water daily, both for direct consumption and for all the other activities taking place in our society. Pre-colonial settlements in South Africa were influenced by the availability of water and the very first permanent European settlement, Cape Town, was chosen over Saldanha Bay with its better harbour, on the presence of superb quality perennial water coming from the springs at the foot of Table Mountain.

Scientific interest in groundwater has often been secondary to the practical concerns of locating and using it, a notable exception being hot springs, which seem to have attracted much attention over the years, in particular by Kent (e.g. Kent, 1949). One of the first investigations to make use of stable isotopes of hydrogen and oxygen also focused on hot springs, specifically those in Swaziland (Mazor et al., 1974) and was closely followed in 1976 by similar work by the two main authors on the hot springs of Zimbabwe (then Rhodesia) (Mazor and Verhagen, 1976). The same two authors eventually did similar work on the South African hot springs (Mazor and Verhagen, 1983), where they found a wide scatter of δD and $\delta^{18}O$ values with no systematic variation by location or average annual rainfall.

Surveys of the isotopic composition of the Gariep (Orange) River were undertaken around 1968-74 by the Council for Scientific and Industrial Research and the International Atomic Energy

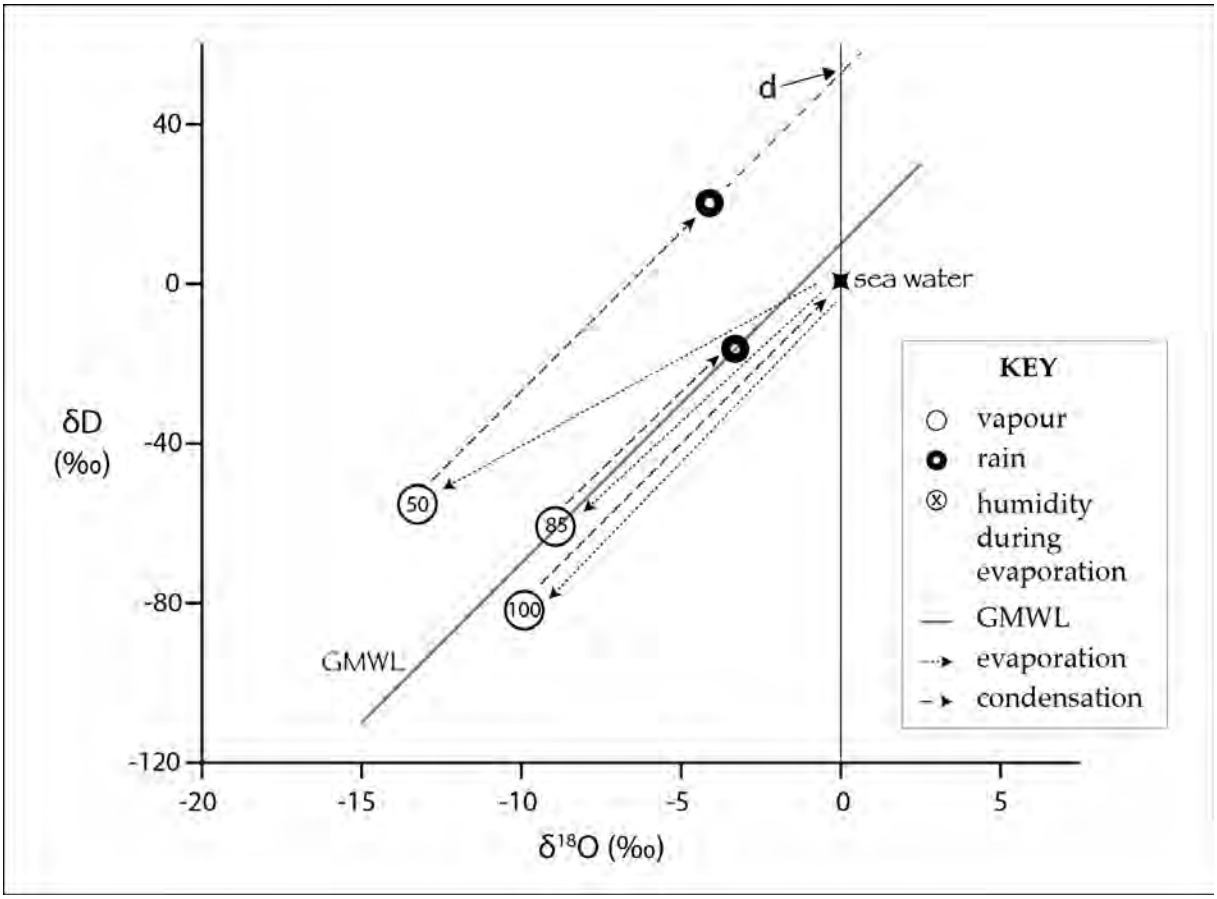

Figure 1.6: Different relative humidities in the source regions during evaporation create moisture masses with different isotope compositions due to kinetic effects as explained in this chapter. Examples in the figure show how the GMWL suggests an average global humidity at the sea surface of around 85 %, where the deuterium excess parameter is 10. For a hypothetical region with evaporation occurring under 50 % relative humidity conditions, d ≈ 50 (after Clark and Fritz (1997)).

Agency with reports being written by S Talma and others, but not published. This work found, despite disturbances to flow in the river caused by the large Gariep (then Hendrik Verwoerd) and Vanderkloof (then P K Le Roux) dams, a negative correlation between $\delta^{18}O$ and flow volume, presumably as a result of the amount effect and perhaps also for samples further downstream, an evaporation effect during low flows.

In 1975, Vogel and Van Urk surveyed ^{18}O content of precipitation and groundwater in the semi-arid regions of southern Africa, finding the groundwater $\delta^{18}O$ values to be remarkably consistent and generally more negative than the highly varied precipitation values. They concluded that groundwater is recharged during heavy rainfall events only. A similar conclusion was reached by Sami (1992) but using hydrogen and oxygen isotopes in conjunction with soil and groundwater chemistry to understand soil and groundwater salinisation in the interior of the Eastern Cape. It was concluded that periods of salt accumulation in the soil, from weathering and evaporative

enrichment of meteoric water, are followed by intense rainfall which flushes these salts to the water table. A study by Adams et al. (2001) in the Sutherland area of the Karoo reached much the same conclusions, also by using isotopic and hydrochemical observations.

Midgley and Scott (1994) compared surface water discharge to rainfall during rain events in the mountainous Jonkershoek area, east of Stellenbosch, concluding that the bulk of streamflow is from groundwater displaced by rain recharging the soil or aquifer. They also calculated a local meteoric water line (LMWL) for Jonkershoek: $\delta D = 6.99\delta^{18}O + 9.63$. A LMWL for the Western Cape was calculated by Diamond and Harris (1997) to be: $\delta D = 6.2\delta^{18}O + 10.6$, which is rather different, but closer to the best LMWL calculation, based on 12 years of data giving an equation of $\delta D = 6.41\delta^{18}O + 8.66$ (Harris et al., 2010).

A thorough examination of the hot springs of the Western Cape was done by Diamond and Harris (2000) in which monthly samples of spring discharge were taken. The spring discharge isotope ratios were seen to have a slight scatter, but no systematic variations. This study also concluded, on the basis of isotopic and geological evidence, that the springs are being recharged at high altitude in mountains made up of the Table Mountain Group and circulating to depths of over 2 km below sea level before discharging at surface. Cavé et al. (2002) used oxygen and hydrogen isotopes in the Agter-Witzenberg Valley to develop a conceptual groundwater flow model. This study also found that recharge was occurring at high altitude and circulating down before rising up in the valley area, where boreholes were intercepting flow. Deep boreholes, up to 350 m below surface, in the Citrusdal Valley contained water with more negative δ values than for shallow boreholes and surface water in the region, and was interpreted to indicate the deeper groundwater was being recharged at higher elevations than the shallow groundwater (Hartnady and Hay, 2002a). On the basis of these studies, it seems that groundwater flow occurs simultaneously at multiple levels, with more shallow local circulation occurring above deeper, more regional flow paths, which is an accepted model for groundwater flow (e.g. Domenico and Schwartz, 1998, p.79).

Determination of the source of water used by plants makes it possible to predict impacts on plant life from changes in the water table caused by groundwater abstraction. It has been found for fynbos plants growing on soils above the Table Mountain Group that different species have different water requirements and make use of water from different levels within the soil, with the conclusion that certain species will be more affected than others if groundwater levels do drop (February et al., 2004). Declining groundwater levels have been experienced in the Kammanassie Mountains, as part of the Klein Karoo Rural Water Supply Scheme. Substantial work has been done around this scheme (e.g. Kotze, 2002; Jolly, 2002; Woodford, 2002; Jolly and Kotze, 2002), including analysis of groundwater for stable isotopes of hydrogen and oxygen (Kotze et al., 2000). This study revealed that boreholes sited in low lying valleys may be tapping groundwater that was recharged at high elevation and has travelled through highly fractured 'aquizones' to reach the lower lying areas.

More applied uses of stable isotopes include fingerprinting water in urban areas in order to determine sources of leakage or pollution. In South Africa, various workers have identified isotopic differences in local groundwater versus public water supply (mains) water in Cape Town (Harris et al., 1999), local groundwater and a wastewater treatment works in Bellville, Cape Town (Saayman et al., 2000) and local rain or groundwater and mains water supply in Pretoria (Butler et al., 2000). The latter study found many boreholes with 30–50 % mains water contributions, highlighting the severe extent of leakage and water wastage.

Oxygen and hydrogen isotopes from groundwater in deep gold mines in the Witwatersrand Supergroup often have δ values that do not match current precipitation and suggest recharge during a previous, colder climate. This helps determine that primitive organisms found in these deep groundwaters are well removed from the earth's surface and do not regularly interact with the bulk of the biosphere, having profound implications for our understanding of evolution and the functioning of the biosphere (Takai et al., 2001).

1.3.1 Motivation Behind this Study

Groundwater from the Table Mountain Group is used extensively by people and the environment of the Western (and Eastern) Cape. This occurs both directly, where boreholes and springs tap the aquifer, and indirectly, where discharge from the aquifer supplies springs and wetlands, and maintains surface water flows through summer, forming the basis of much agriculture and most of the ecosystems of the region. Boreholes are used by many farmers and also for public water supply in towns such as Citrusdal and Hermanus. There is intense interest in the water resource of the Table Mountain Group aquifer system, not only from the existing users, but many other potential users, including the country's second largest metropolitan area, Cape Town.

Stable isotopes of water offer one method of improving our understanding of the Table Mountain Group aquifer system. The source of all groundwater and surface water is precipitation, and therefore, in order to interpret stable isotope measurements of groundwater or surface water, a handle on the spatial and temporal variation in stable isotope composition of precipitation is needed. This was the primary motivation behind the deployment of 15 rainfall collection stations across the Western Cape, from coast to mountaintop, over a period of two years. The focus of this study was to quantify, as much as is possible given the duration of monitoring, the patterns in stable isotope composition of precipitation. Sampling of groundwater and surface water at selected sites was included to demonstrate the possible findings that stable isotope hydrology can reveal about the inner workings of the Table Mountain Group aquifer system.

authors	date	title
E Mazor & B T Verhagen	1983	Dissolved ions, stable and radioactive isotopes and noble gases in thermal waters of South Africa.
J Midgley & D F Scott	1994	The use of stable isotopes of water (D and ^{18}O) in hydrological studies in the Jonkershoek Valley.
R E Diamond & C Harris	1997	Oxygen and hydrogen isotope composition of Western Cape meteoric water.
J M Weaver, A S Talma & L C Cavé	1999	Geochemistry and isotopes for resource evaluation in the fractured rock aquifers of the Table Mountain Group.
C Harris, B Oom & R E Diamond	1999	A preliminary investigation of the oxygen and hydrogen isotope hydrology of the greater Cape Town area and an assessment of the potential for using stable isotopes as tracers.
R E Diamond & C Harris	2000	Oxygen and hydrogen isotope geochemistry of thermal springs of the Western Cape, South Africa: Recharge at high altitude?
J C Kotze, B T Verhagen & M J Butler	2000	An aquifer model based on chemistry, isotopes and lineament mapping: Little Karoo, South Africa.
C J Hartnady & E R Hay	2002	Boschkloof groundwater discovery.
E C February, W Bond, R Taylor & R Newton	2004	Will water abstraction from the Table Mountain aquifer threaten endemic species?
C Harris, C Burgers, J Miller & F Rawoot	2010	O- and H-isotope record of Cape Town rainfall from 1996 to 2008, and its application to recharge studies of Table Mountain groundwater, South Africa.
D Barrow & R E Diamond	2011	Stable Isotopes of rain, surface water and groundwater in the Kogelberg.

Table 1.2: Oxygen and hydrogen stable isotope publications relating to the Table Mountain Group.

Chapter 2

Background

2.1 Introduction

The Table Mountain Group dominates the geology of the Western Cape, but due to extensive folding and faulting during the Permo-Triassic Cape Orogeny and subsequent sedimentation during the Mesozoic and Cenozoic, it comes into contact with numerous other geological units. A good overall knowledge of these various units is necessary to understand how groundwater within the Table Mountain Group may be constrained, recharged by, or discharged into these other units. The geological map in Chapter 1 and the cross sections in Chapter 5 may be useful to consult when reading through this chapter.

This chapter describes the geology of the Western Cape in brief, the climate of the region, with an emphasis on the rainfall and rain producing weather systems, and then concludes with a summary of the understanding of the hydrogeology of the Table Mountain Group.

2.2 Geology — Lithostratigraphy

The geology of the Cape Fold Belt region can be split into three main packages: the basement, the Cape and Karoo Supergroups, and the younger rocks. This chapter summarizes these three packages and their components, with an emphasis on the Cape Supergroup and the Table Mountain Group in particular. The basement of the Cape Fold Belt region can also be divided into three packages: the various parts of the Pan-African Saldania Belt, the Cape Granite Suite, and some transitional formations that undoubtedly precede the Cape Supergroup, but have uncertain relationships with the Saldania Belt rocks.

2.2.1 Saldania Belt

The Saldania Belt refers to a set of units in the Cape Fold Belt region that display similar stratigraphic position and deformation style, although they contain a wide array of rock types and are geographically separated. These units are exposed where the Cape Supergroup has been

stripped away by erosion, typically either on the coastward side of the Cape Fold Mountains or where large anticlines or normal faults have aided exposure of inliers. The Saldania Belt abuts the Kalahari Craton to the north (Gresse et al., 2006) and is made up of the Malmesbury Group to the north-east of Cape Town, the Cango Caves and Kansa Groups to the north of Oudtshoorn, the Kaaimans Group around George and the Gamtoos Group west of Port Elizabeth.

The Malmesbury Group has the largest area of exposure of all these groups, although the quality and area of actual outcrop is very poor due to low relief and the easily weathered nature of the formations. As such, this Group is poorly understood. The first substantial synthesis was put forward by Hartnady et al. (1974), in which the Group was subdivided into three "domains" (now called terranes), separated by fault zones. These are, from the south-west to the north-east, the Tygerberg, Swartland and Boland Terranes, with zones of tectonized rocks between them, known as the Saldanha-Franschhoek Fault, now called the Colenso Fault, between the Tygerberg and Swartland Terranes and the Piketberg-Wellington Fault between the Swartland and Boland Terranes (SACS, 1980).

The stratigraphy of the Malmesbury Group remained largely unchanged from Hartnady et al. (1974) in Tankard et al. (1982). Rozendaal et al. (1999) reported an improved understanding of the depositional setting, tectonic history and radiometric dates, as well as correlations across the various groups within the Saldania, Gariep and Dom Feliciano (in South America) Belts, but the basic lithostratigraphy remained unchanged. Then, in 2003, Belcher & Kisters substantially revised the Malmesbury Group lithostratigraphy based upon detailed structural observations within formations. These dramatic revisions appear to have not, however, been accepted by the time of publication of the 2006 volume of The Geology of South Africa, in which Gresse et al. (2006) summarize the present understanding of the Neoproterozoic to Cambrian successions of South Africa. The Belcher & Kisters revision, see **Figure 2.1**, resulted in three groups. These are, from the oldest: strongly deformed low grade metamorphic rocks, predominantly schists with minor carbonates, chert and metavolcanics, of the Swartland Group; low grade metamorphic rocks, mainly shale, greywacke and sandstone with minor conglomerate, limestone and andesite; conglomerate, grit, sandstone and shale of the Klipheuwel Group.

The Kaaimans Group, exposed along the south coast at the core of a regional anticline, comprises low grade metamorphic rocks of a great variety, include shale, phyllite, greywacke, sandstone, schist and calc-silicate. The Kansa and Cango Caves Groups occur to the north of the regional Cango Fault, a normal fault that causes repetition of the south-to-north basement to Cape Supergroup to Karoo Supergroup sequence. In contrast to the diverse rock types of the Kaaimans Group, the Cango Caves Group is dominated by greywackes and carbonates with lesser shale, sandstone and conglomerate, and the Kansa Group is made up of conglomerate, sandstone and minor shale. The Gamtoos Group, exposed in a sliver shaped inlier within a fault bounded anticlinal hinge, features mainly carbonates, phllitic greywackes and various arkosic sandstones and conglomerates (Gresse et al., 2006).

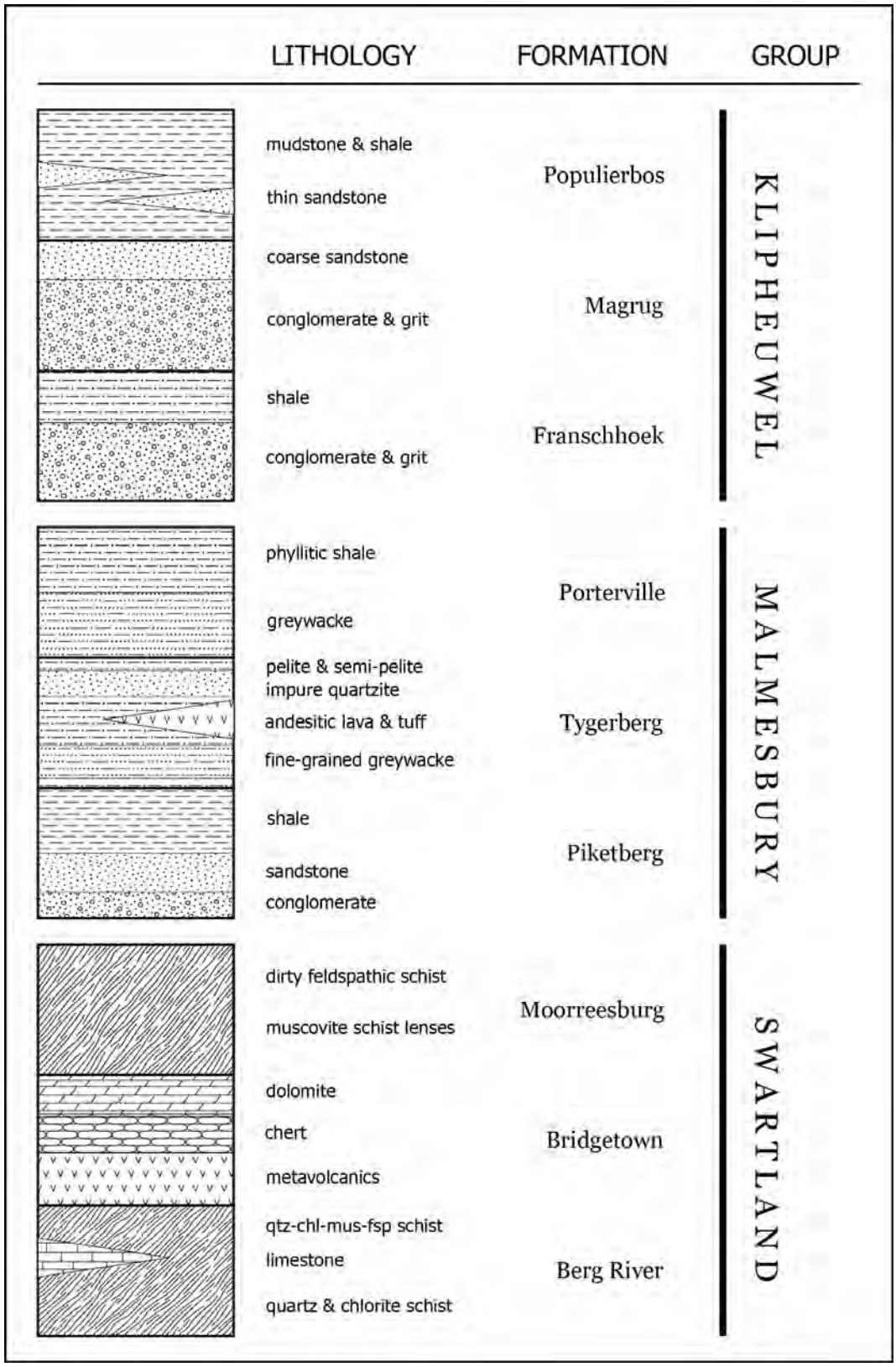

Figure 2.1: Revised stratigraphy of the western Saldania Belt formations within the Western Cape, based on Belcher and Kisters (2003).

2.2.2 Cape Granite Suite

The Cape Granite Suite consists of numerous bodies that have mostly been intruded as plutons into the metasediments of the Saldania Belt, or have been thrust into their current positions during the Cape Orogeny. The plutons occur in three clusters: a minor Richtersveld cluster, a minor George cluster and the large south-western cluster in the Saldanha Bay - Cape Peninsula - Overberg area (e.g. Schoch et al., 1977). In reality, the south-western and eastern clusters may be two parts of the same large cluster, as the lack of evidence of any granites in the intervening area coincides with a lack of outcrop of any basement at all.

The Cape Granite Suite occurs as multiple intrusions, mostly plutons, that in places have been grouped into batholiths, for example the Cape Peninsula and Darling Batholiths. Although composed mostly of granitic plutons, there is quite a range of rock types and intrusive forms in the Cape Granite Suite. Aside from a range of granitic compositions, rock types include gabbro, diorite, quartz porphyry and quartz syenite (Scheepers and Schoch, 2006). Similarly, although intrusions occur mostly as plutons, other structures such as dykes, ignimbrite flows and tectonically bounded sheets also occur (Gresse and Theron, 1992).

The plutons of the Cape Granite Suite have been dated by various workers and yield ages that range from very late Neoproterozoic to late Cambrian. Scheepers and Armstrong (2002) found the Hoedjiespunt granite gave a U-Pb zircon age of 552±4 Ma; in the same year, Scheepers & Poujol found an ignimbrite, also in the Saldanha Bay area to give a U-Pb zircon age of 515±3 Ma. These ages bracket those of da Silva et al. (2000) who reported U-Pb zircon ages of 547±6 Ma and 536±5 Ma, Schoch and Burger (1976) who found a Pb-Pb zircon age of 522±12 Ma, Jordaan et al. (1995) who found a U-Pb zircon age of 519±7 Ma on the monzonite Yzerfontein pluton and other ages, around 540 Ma, reported by Scheepers and Armstrong (2002) for plutons in the Saldanha Bay area.

Based on the above ages, field relations and petrography, 4 stages of igneous activity have been identified (Scheepers and Schoch, 2006; Rozendaal et al., 1999). These can be summarized as S-type granites in phase 1, I-type granites in phase 2, A-type granites and intermediate and mafic plutons in phase 3, and intrusive and extrusive felsic rocks in phase 4, all within a 40-50 Ma period during the Pan-African.

2.2.3 Cape Supergroup

The Cape Supergroup is one of only 9 supergroups in South Africa. It dominates the geology of the Western Cape and extends substantially into the Eastern Cape and is composed of three groups: the thickest, basal, arenaceous Table Mountain Group, the argillaceous Bokkeveld Group and the lithologically intermediate Witteberg Group. The succession was deposited during the Palaeozoic, on top of the Saldanian basement, and then overlain by the Karoo Supergroup, the youngest of all South Africa's supergroups. The Cape Supergroup, underlying basement and the older formations of the Karoo Supergroup were deformed in the Permo-Triassic Cape Orogeny.

2.2.3.1 Table Mountain Group

The Table Mountain Group is the dominant group of the Cape Supergroup due to the stratigraphic thickness and highly arenaceous character, causing resistance to weathering and leading to formation of mountains that define the geography of the Western Cape. **Figure 2.2** shows the lithostratigraphy of the Table Mountain Group in the western half of the Cape Fold Belt. The basal formations in the Cape Supergroup vary from east to west and north to south: in the west the Piekenierskloof and then Graafwater Formation occur; in the far south-east the Sardinia Bay Formation occurs; in the central to eastern areas these are absent and the Peninsula Formation lies directly on the basement; in the far north-western areas where the Cape Supergroup ends, the lower formations pinch out and the Nardouw Subgroup formations lie at the base. Controversy does exist over the assignment of the Sardinia Bay Formation, in part or whole, to the Cape Supergroup, the Saldanian Gamtoos Group or to neither.

Sardinia Bay Formation

Toerien and Hill (1989) and Bell (1980) included all the rocks between the Gamtoos Group and the Peninsula Formation as the Sardinia Bay Formation and treat this unit as the basal formation of the Table Mountain Group, possibly correlating with the Graafwater Formation to the far west. In contrast, Shone (1979, 1983) as cited in Gaucher and Germs (2006) included only the untectonized rocks into the Sardinia Bay Formation. Such differences aside, the Sardinia Bay Formation is a sequence of alternating dominant feldspathic, quartzitic sandstones, thin to medium bedded with some cross-bedding, subordinate greenish-grey to black phyllitic shales, and minor vein-quartz-pebble conglomerates (Toerien and Hill, 1989).

Piekenierskloof Formation

The Piekenierskloof Formation forms the base of the Cape Supergroup only in the north-western part of the Western Cape. The contact with the underlying Klipheuwel Formation, or Populierbos Formation of the Klipheuwel Group, if using Belcher and Kisters (2003) revision, is either an angular unconformity or disconformity (Rust, 1967), although Vos and Tankard (1981) considered that the Piekenierskloof and Klipheuwel Formations may be contemporaneous, in spite of observations by Rust (1973) that show variable clast lithologies in the Piekenierskloof Formation in contrast to locally derived (Cape Granite Suite) clasts in the Klipheuwel Formation. The southernmost outcrops are a mere 10 m thick, occuring in the Kasteelberg outlier in the middle of the Swartland (Theron et al., 1992), whilst outcrops reaching a maximum thickness of 900 m occur further north-west near Lamberts Bay (Thamm and Johnson, 2006). The Piekenierskloof Formation consists of very mature arenite and conglomerate, the latter containing identifiable clasts of resistant sedimentary and metamorphic rocks (Rust, 1967).

Graafwater Formation

The Graafwater Formation overlies the Piekenierskloof Formation conformably where the latter occurs, but extends beyond the boundaries of the Piekenierskloof basin and there overlies Saldanian basement. The Graafwater basin extended from beyond the present day Atlantic Ocean

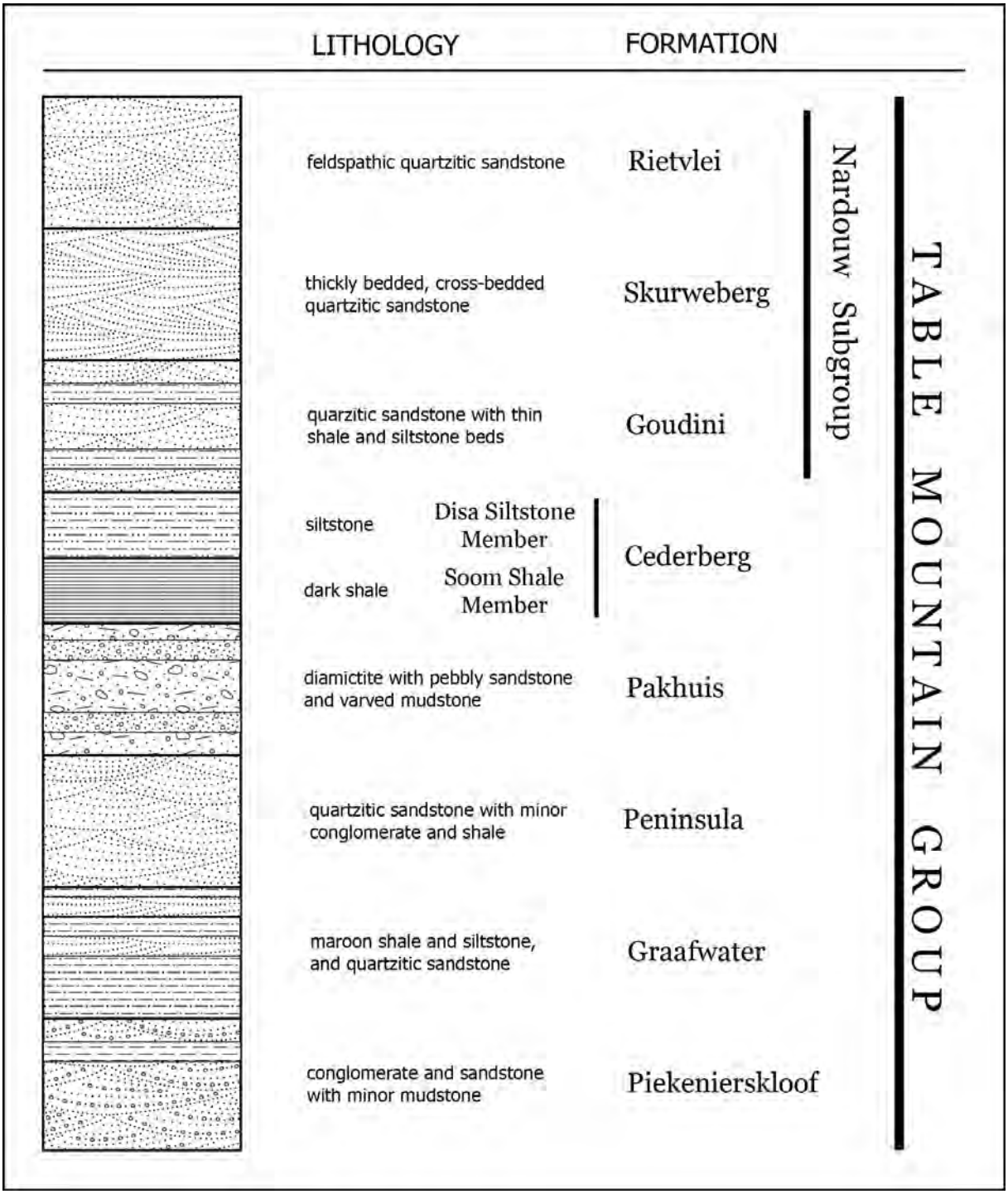

Figure 2.2: Stratigraphy of the Table Mountain Group for the western side of the Cape Fold Belt.

coast at the Olifants River Mouth, southwards to the Cape Peninsula and eastwards to the Ceres-Worcester area (Rust, 1967). The southern part of the Graafwater Formation, south of Piketberg, averages 50–100 m thickness, whilst there is a defined north-west trending trough in the Citrusdal to Lamberts Bay region where the Formation averages 250 m and reaches 430 m thickness (Rust, 1967; Thamm and Johnson, 2006). Although nearly 700 km apart and therefore probably never linked originally, several factors indicate that the Sardinia Bay Formation could be equivalent to the Graafwater Formation. These factors include: stratigraphic position, rock types and an underlying conglomerate with similarities to the Piekenierskloof Formation (Shone and Booth, 2005). The Graafwater Formation features upwards fining cycles of three distinct lithologies: a fine to medium grained quartzose sandstone; an interbedded finer grained sandstone, siltstone and maroon mudstone with dessication cracks; and a maroon mudstone (Tankard and Hobday, 1977; Rust, 1977).

Peninsula Formation

The Peninsula Formation is the dominant formation of the Table Mountain Group and indeed of the Cape Supergroup, due to its widespread occurrence, thickness and remarkably consistent, highly quartzose nature. The formation occurs throughout the Cape Basin except for the very north-western margin in the Niewoudtville vicinity where it is absent (Rust, 1973). Thickness estimation in the Peninsula Formation is hampered as one moves east by extensive thrusting, much of which is bedding-parallel and difficult to detect, leading to estimates of as much as 3000-4000 m by Rust (1973), whereas the less deformed sequences of the west, in the Cape Peninsula, reveal the thickness to be 530 m, according to Fuller and Broquet (1990).

The Peninsula Formation is remarkable for the great thickness of consistently mature quartzose sandstone. The sandstone is light grey, medium to coarse grained, mainly planar bedded, but commonly with trough cross bedding, usually thickly bedded, but in places massive or thinly bedded (Shone and Booth, 2005; Gresse and Theron, 1992). Occasional thin quartz pebble lags are found and channels also occur, reportedly a few metres in width (Theron et al., 1992) or up to 40 m deep and kilometres in extent (Hobday and Tankard, 1978; Tankard et al., 1982). In the upper 100 m of the Peninsula Formation, a zone of folding is sometimes present (Gresse and Theron, 1992), varying from simple, metre scale deformation to complex overturned and refolded zones of 75 m thickness. It occurs in the west only and the fold axes trend northwards (Rust, 1973).

Pakhuis Formation

The Pakhuis Formation occurs only in the western half of the Cape Basin, west of Swartberg Pass (SACS, 1980; Thamm and Johnson, 2006). Its thickness is given as 40 m by SACS (1980), but 150 m by Young et al. (2004), 160 m by Tankard et al. (1982) and 190 m by Rust (1981) as cited in Shone and Booth (2005). The lowermost Sneeukop Member is a structureless sandstone, with abundant striated and faceted erratics, that occurs only within the synclines of the Peninsula Formation fold-zone (Rust, 1967; Gresse and Theron, 1992). A thin sandstone, the Oskop Member, overlies the Sneeukop Member or the Peninsula Formation directly, and although continuous, is

Figure 2.3: A coarse grained example of quartzite in the Table Mountain Group. Rounded pebbles of vein quartz and gritty layers can be seen in this photograph from the upper Peninsula Formation.

lensoid in thickness with indistinct or thick bedding. The north-west Cape Basin contains the Kobe Member whilst the south-west Cape Basin contains the Steenbras Member, both quartzose diamictites with plentiful clasts, although the latter is a darker, more mature facies (Tankard et al., 1982; Gresse and Theron, 1992).

Cederberg Formation

The Cederberg Formation occurs widely in the Cape Basin, from the far west, eastwards to about 100 km west of Port Elizabeth, although in the eastern areas it is discontinuous because of smearing out along fold limbs (Shone and Booth, 2005). The contact with the underlying Pakhuis Formation is known to be both gradational (Rust, 1967) and sharp (Gresse and Theron, 1992). The formation thickness is given as between 50 m and 120 m (SACS, 1980; Thamm and Johnson, 2006). The Cederberg Formation is divided into two members. The basal Soom Shale Member is the thinner unit, seldom exceeding 15 m and is a dark grey, usually thinly laminated, micaceous shale (Theron et al., 1990). It contains a variety of fossils of some significance globally, such as conodonts, trilobites and ostracods (Theron et al., 1990; Gabbott et al., 2003). It coarsens upwards into the Disa Silstone Member, which itself continues the upwards coarsening trend and in turn has a gradational contact with the overlying Goudini Formation. The Disa Siltstone Member is a thinly bedded, argillaceous and carbonaceous siltstone and fine grained sandstone that reaches 75 m thickness and contains fossil brachiopods (Rust, 1967; Gresse and Theron, 1992).

Nardouw Subgroup

The Nardouw Subgroup used to have formation status, with three members, Goudini, Skurweberg and Rietvlei, recognized (SACS, 1980), but these have been upgraded to formations (Thamm and Johnson, 2006). In the east, corresponding names Tchando, Kouga and Baviaanskloof were in use for the three formations (Toerien, 1979), but now that the Goudini and Skurweberg are formations, they have been extended across the Cape Basin and only Baviaanskloof Formation is still in use for the area east of 21° 30' E as the continuation of the Rietvlei Formation (Thamm and Johnson, 2006).

The Nardouw Subgroup is characterized by a return to arenaceous rocks with similar depositional environments to the Peninsula Formation, after the unusual interlude of the Pakhuis and Cederberg Formations. The Nardouw Subgroup occurs across the whole Cape Basin and is the last single unit of the Cape Supergroup that pinches out in the northern extremities of the Basin (Rust, 1967). Thicknesses for the Subgroup are given as 900 m in the east and 700 m in the west (Thamm and Johnson, 2006), or 500 m (SACS, 1980).

Goudini Formation

The Goudini Formation is the lowermost formation of the Nardouw Subgroup and has a gradational contact with both the underlying and overlying formations. It occurs throughout the Cape Basin and its thickness is given as 200-300 m (Thamm and Johnson, 2006; Toerien and Hill, 1989) to as little as 30 m on Franschhoek Pass (Gresse and Theron, 1992). It is composed of thinly bedded, grey, medium grained quartzose sandstone that distinctively weathers to a reddish brown colour. Thin, pinkish, micaceous shale and siltstone layers are interspersed through the formation and some bluish grey siltstone occur nearer the top (Theron et al., 1991; Gresse and Theron, 1992).

Skurweberg Formation

This formation occurs throughout the Cape Basin and is around 200-400 m thick. The top and bottom contacts are gradational. It is composed of light grey, massive, medium to coarse grained quartzose sandstone with profuse cross-bedding, occasional thin quartz pebble lags and very minor shale (Toerien and Hill, 1989; Theron et al., 1991; Gresse and Theron, 1992). The highly quartzose nature of the Skurweberg Formation results in it forming steep cliffs and mountains, similarly but to a lesser extent than the Peninsula Formation does. The abundance of trough cross bedding can help distinguish the Skurweberg Formation from the planar bedding dominated Peninsula Formation.

Rietvlei Formation

The Rietvlei Formation occurs in the western half of the Cape Basin, up until a notional boundary at 21° 30' E, from where its stratigraphic equivalent, the Baviaanskloof Formation, then occurs eastwards. The typical thicknesses of the Formation are 90-200 m (Theron et al., 1991; Thamm and Johnson, 2006). It is generally similar to the Goudini Formation in that the bedding is thinner,

the sandstones dirtier and there are more thin shale bands than in the intervening Skurweberg Formation. Specifically, the Rietvlei Formation consists of alternating light grey quartzose sandstone, feldspathic sandstone, siltstone, micaceous shale and quartz pebble conglomerate, with some of the more quartzose sandstone units traceable for long distances (Theron and Basson, 1989; Theron et al., 1991; Gresse and Theron, 1992).

Baviaanskloof Formation

The Baviaanskloof Formation is the eastern, east of 21° 30' E, equivalent of the Rietvlei Formation. It contains the Kareedouw Sandstone Member which is lithologically similar to the Rietvlei Formation and most likely represents the easterly extension of this formation (Theron et al., 1991). The Baviaanskloof Formation thickness is given as 200 m by Toerien (1979) and Thamm and Johnson (2006). Above and below the 50 m thick Kareedouw Member, which is composed of light grey, medium grained, feldspathic sandstone, occurs greenish grey, fine grained, impure micaceous sandstone interbedded with subordinate greyish black, carbonaceous and micaceous shale (Toerien and Hill, 1989; Theron et al., 1991). Contacts with the overlying Bokkeveld Group are conformable and can be either gradational or sharp.

2.2.3.2 Bokkeveld Group

Whereas the Table Mountain Group is primarily arenaceous and has irregular stratigraphy, the Bokkeveld Group is argillaceous and distinctly cyclic. This group is distributed throughout the Cape Basin, except for the very northernmost margin near Nieuwoudtville. The deposit thickens to the south, being 1000 m near Citrusdal, 2500 m in the south-west near Bredasdorp and reaching 4000 m in the south-east near Uitenhage (Rust, 1967; Broquet, 1992).

Several upwards coarsening cycles occur, the lower three of which form the basinwide Ceres Subgroup, which itself ranges from 600 m to 1700 m thick, west to east (Thamm and Johnson, 2006). The persistence of these cycles basinwide has allowed the finer and coarser units to be given formation status: cycle 1 is formed by the basal mudrock and siltstone of the Gydo Formation coarsening into the greywacke of the Gamka Formation, overlain by cycle 2 siltstone and mudrock of the Voorstehoek Formation grading again into greywacke of the Hex River Formation, and similarly overlain by the fine grained Tra-Tra Formation and coarser Boplaas Formation of cycle 3. The argillaceous units do include minor sandstone, just as the arenaceous units of feldspathic greywacke and arenite include minor mudrocks and siltstones.

The upper portion of the Bokkeveld Group shows substantial facies variation spatially and is therefore divided into the Bidouw Subgroup in the west and the Traka Subgroup east of 21° E (Tankard et al., 1982). The Bidouw Subgroup is similar to the underlying Ceres Subgroup in lithologies and cyclicity, although the absence of marine invertebrate fossils is in contrast to their abundance in the latter (Broquet, 1992). The argillaceous Waboomsberg Formation forms the base of the Subgroup, followed by the arenaceous Wupperthal Formation, overlain by the argillaceous Klipbokkop Formation, overlain by the arenaceous Osberg Formation and capped by the

argillaceous Karoopoort Formation. In the east, the Traka Subgroup is quite different: it develops great thickness, is thoroughly dominated by clay-rich and silt-rich rocks and does not display widespread, regular cyclicity. As a result, only three formations are recognized: the thick, lithologically variable but mudrock dominated Karies Formation; the siltstone dominated Adolphspoort Formation; and the topmost mudrock-rich Sandpoort Formation (Thamm and Johnson, 2006).

2.2.3.3 Witteberg Group

The Witteberg Group caps the Cape Supergroup and, although similarly cyclic to the Bokkeveld Group, is lithologically intermediate to the Bokkeveld and Table Mountain Groups, having approximately balanced proportions of arenaceous and argillaceous rocks. The Witteberg Group is widespread in the Cape Basin, although it thins rapidly northwards in the western areas (Thamm and Johnson, 2006). The thickness of the Group is is given as over 2000 m by both Tankard et al. (1982) and Broquet (1992), but has been revised downwards by Thamm and Johnson (2006) to 1700 m, and as with the Bokkeveld Group, the thickest portions lie in the east. Not only does the abundance of sandstone increase relative to the underlying group, but the arenaceous units are more mature, and therefore lighter in colour, than the greywackes of the Bokkeveld Group, and in contrast to both the other groups of the Cape Supergroup, Witteberg Group sandstones are more micaceous (Gresse and Theron, 1992).

As with the Bokkeveld Group, the lower section of the Witteberg Group is broken into an eastern and western portion, this time along the 22° E meridian. The thinner western portion is called the Weltevrede Subgroup and is divided into the basal argillaceous Wagendrift Formation, the middle arenaceous Blinkberg Formation and the upper argillaceous Swartruggens Formation, whereas ironically, in the eastern areas where this package is thicker these units are all lumped into the Weltevrede Formation containing the Blinkberg Member, the arenaceous extension of the Blinkberg Formation (Thamm and Johnson, 2006). Running through the Witteberg Group distinctively, east and west, is the thick quartzose sandstone unit of the Witpoort Formation, which has not been assigned to any subgroup. The Witteberg Group draws its name from the low mountain range east of Touwsrivier, which in turn derives its name from the abundant exposures of the resistant, thick, white-weathering outcrops of the Witpoort Formation.

Overlying the Witpoort Formation is the Lake Mentz Subgroup, in which the Kweekvlei, Floriskraal and Waaipoort Formations form another clay-rich, sand-rich, clay-rich triplet across the whole basin. Above this, in the eastern area only, the Kommadagga Subgroup contains four formations, which tend to be less micaceous than the older formations. The basal Miller Formation, a diamictite with grit to pebble sized clasts, is followed and interfingers with the thin, pebbly quartz sandstone of the Swartwaterspoort Formation. These are overlain by the rythmically bedded shales of the Soutkloof Formation and finally the fine to medium grained sandstone of the Dirkskraal Formation (Toerien and Hill, 1989; Broquet, 1992; Thamm and Johnson, 2006).

2.2.4 Karoo Supergroup

The Karoo Supergroup covers over a third of the surface area of South Africa and reaches a total thickness of at least 4–5 km. Along the southern boundary of the Karoo Basin, it overlies the Cape Supergroup paraconformably to disconformably and extended over the current lines of mountains where it has been eroded away, evidence for this being outcrops of the lowermost units between Worcester and Robertson and even further south at Greyton (Gresse and Theron, 1992). These outliers aside, the Karoo Supergroup lies to the north of the southern arm and to the east of the western arm of the Cape Fold Belt. Only the two lowermost groups will be mentioned here, as they are the only ones that occur in any reasonable proximity to the Table Mountain Group.

2.2.4.1 Dwyka Group

The Dwyka Group is a succession of several different facies of diamictite, often repeated, to reach thicknesses of 800 m in the southern Karoo Basin. Except for two rare facies, an irregular or lensoid esker-like deposit and the variable sandstone facies, the matrix of all the diamictites and mudrocks is very fine grained, but with clasts that vary from the matrix up to large boulders (>1 m) in size (Johnson et al., 2006). The extremely varied lithological composition, size and angularity of the clasts have, amongst other properties, led to interpreting the Dwyka Group as glacial and ice-sheet deposits.

2.2.4.2 Ecca Group

This group of diverse formations formed in marine environments and is dominated by fine grained rocks, mostly shales and mudstones with some chert and tuff present; although moderately arenaceous rocks such as greywacke do occur. The Ecca Group overlies the Dwyka Group conformably and is around 2-3 km thick along the southern margin of the Karoo Basin where it occurs within the northern limit of the Cape Fold Belt (Johnson et al., 2006).

2.2.5 Younger Rocks

Rocks from the Cretaceous and Tertiary form minor yet significant components in the geology of the study area. All of these rocks are younger than the Cape Orogeny and therefore have experienced very little deformation. Most are lithified, although this becomes weaker and eventually non-existent with the very youngest formations.

2.2.5.1 The Uitenhage Group

The Uitenhage Group is a set of Mesozoic deposits that fill basins along the coast and in valleys within the Cape Fold Belt. Stretching from Worcester eastwards to Algoa Bay, the current distribution is not continuous, mainly due to the originally sporadic occurrence of the depocentre basins, but also because of some subsequent erosion. The various sub-basins are cumulatively

called the Outeniqua Basin, which has both onshore and offshore components, the latter of which will not be mentioned further here. The basins are typically half-grabens with the deeper, faulted edge being to the north, except for the largest, the Algoa Basin, which is more complex and has full graben structures (Shone, 2006; Dingle et al., 1983). Sediment reaches to around 3 km thickness in the deeper basins and thins distally, to the south. The Uitenhage Group comprises 3 formations; all 3 only occur in the Algoa and Oudtshoorn Basins and all other basins contain only the basal Enon Formation.

Enon Formation

The Enon Formation reaches 3 km thickness and is a very distinctive coarse conglomerate of well rounded Cape Supergroup quartzite pebbles and cobbles that generally weathers to dark red in outcrop, although yellow and grey colours also occur. The matrix of grit, sand and silt is cemented by red limonite and the formation can develop high, steep cliffs. Minor siltstone and sandstone lenses do occur (Shone, 2006).

Kirkwood Formation

This is a poorly cemented succession of coarse to medium grained lithic sandstone, siltstone and mudstones, reaching 2 km thickness (Shone, 2006).

Sundays River Formation

Attaining a similar thickness to the Kirkwood Formation, this formation consists of fine to medium grained, sometimes shelly, moderately cemented sandstone, siltstone and mudstone (Shone, 2006).

Cenozoic Deposits

Cenozoic deposits in the study area come in several different forms, including lithified and unlithified coastal deposits, various terraces and ancient duricrusted landsurfaces inland and on the coastal plain, more recent pedogenic duricrusts, minor alluvial, lacustrine, spring and other deposits, and ubiquitous scree and soil. Only the coastal and ancient terrace deposits will be considered here, as the others tend to be thin or scattered (Partridge et al., 2006).

Due to the primarily erosional nature of the southern African subcontinent since 65 Ma and because of the high gradient of the land surface, accumulations of most Cenozoic materials on land tend to be thin. The coastal deposits fall into 4 groups based on position along the coast.

2.2.5.2 The Algoa Group

This group largely falls outside the study area, being found from Plettenberg Bay to Port Edward. It consists of 6 formations, made up mainly of limestone, conglomerate, shelly deposits, calcareous sand and loose sand (Roberts et al., 2006).

2.2.5.3 The Bredasdorp Group

The Bredasdorp Group occurs from Plettenberg Bay to Cape Hangklip and typically overlies the Table Mountain or Bokkeveld Groups, or in places the Enon Formation, or in the George area the

Kaaimans Group and Cape Granite Suite. A highly simplified stratigraphic summary is given here.

The lowermost, thin De Hoop Formation (≤17 m) is a shelly version of the thick overlying Wankoe Formation calcarenite (≤290 m). Above this lies the thin, shelly, pebbly, quartz sand of the Klein Brak Formation (≤10 m), followed by aeolianite and calcrete of the Waenhuiskrans Formation (≤60 m) and topped by unconsolidated sand of the Strandveld Formation (≤100 m) (Roberts et al., 2006).

2.2.5.4 The Sandveld Group

The Sandveld Group is found from False Bay in the south to Elands Bay on the west coast. It generally overlies either Malmesbury Group or Cape Granite, but in the Elands Bay vicinity overlies the Table Mountain Group. The areas of greatest thickness are developed in bedrock depressions controlled by rock type and structure. A highly simplified stratigraphic summary is given here.

The basal Elandsfontyn (≤70 m) and generally overlying Varswater (≤60 m) Formations consist primarily of sand with minor carbonaceous clay and lignite layers and pebbles in places. North of Saldanha Bay, the Prospect Hill Formation (≤70 m) lies below the Varswater Formation and is made up of bioclastic aeolianite, often reddish. Overlying the Varswater Formation is the thin gravelly and shelly Velddrif Formation (about 7 m), followed by the calcarenite and calcrete layers of the thicker Langebaan Formation and capped by unconsolidated quartz sand and then calcareous sand of the Springfontyn and Witzand Formations, respectively (Roberts et al., 2006).

2.2.5.5 The West Coast Group

From Elands Bay to the Orange River mouth another series of coastal formations occurs. These formations overlie the Table Mountain Group in the southern area, from Elands Bay to north of Papendorp, where the very north-westernmost outcrops/subcrops of the Table Mountain Group are found. Although only the Alexander Bay and Curlew Strand Formations have been named, other units overlie and underlie these. Overall the group is dominated by sand, with minor mud, calcified sand, gravel and other rock or sediment types (Roberts et al., 2006).

2.2.5.6 The African Surface

Erosion and planation across southern Africa in the Tertiary led to the development of what is referred to as the African Surface. Remnants of this surface are still found today and are characterized by a duricrust, up to 8 m thick (SACS, 1980), overlying a thick weathered profile, usually kaolinitic and up to 50 m thick (Partridge and Maud, 1987), although this is not always the case and depends on the bedrock. Interestingly, the duricrust may be composed of silcrete, calcrete or ferricrete (Dingle et al., 1983). Subsequent erosional surfaces, the most notable being the *post-African I* and *post-African II* have not developed significant profiles of either weathered or consolidated material (Partridge and Maud, 1987; Partridge et al., 2006).

Figure 2.4: View south-west from the Matroosberg rainfall collector site looking along the hinge of the Hex River anticline in the syntaxis of the Cape Fold Belt. The fractured nature of the Table Mountain Group formations is apparent in this photograph. Two faults, both with limited displacement on them (tens of metres at most), are indicated.

2.3 Geology — Structure

The Table Mountain Group was deformed during the Cape Orogeny, a multiphase compressional tectonic event spanning the Permo-Triassic boundary, with four episodes of deformation having been dated: 278, 258, 247 and 230 Ma (Hälbich, 1992). Deformation occurred in such a way that three major structural domains are evident. The western branch of the Cape Fold Belt with open, upright folding and normal faulting is arcuate and convex inland, striking in a north–south direction in the southern parts near Paarl, and north-northwest–south-southeast in the northern parts near Vanrhynsdorp. The southern branch of the Cape Fold Belt is similarly arcuate and convex inland, but with folding and faulting striking east–west at the western end near Robertson and east-southeast–west-northwest in the eastern parts near Port Elizabeth. Deformation in the southern branch is more intense, with strong northward vergence, overturning and thrusting. The

southern and western branches merge in the syntaxis, stretching from the coast at Hermanus to the Karoo near Touwsrivier. In this domain, folding and faulting is more chaotic, although mainly striking north-east–south-west, and deformation is intense (Söhnge, 1983; de Beer, 2002).

Throughout the Cape Fold Belt, the compressional tectonic regime that reigned during the Cape Orogeny was inverted (became extensional) upon breakup of Gondwana during the Triassic and Cretaceous (de Wit and Ransome, 1992). Hälbich (1992) shows that both new faults with normal movement probably developed and some of the previous reverse faults were reactivated and experienced normal motion as the continents moved apart. This is most clearly demonstrated by the Cretaceous graben or half-graben basins in which the Uitenhage Group was deposited. Of note are the Kango and Worcester Faults, which have normal vertical displacements up to several kilometres and have moulded the mega-scale geography of the Western Cape, in which the TMG is duplicated, forming parallel rows of 2000 m high mountains.

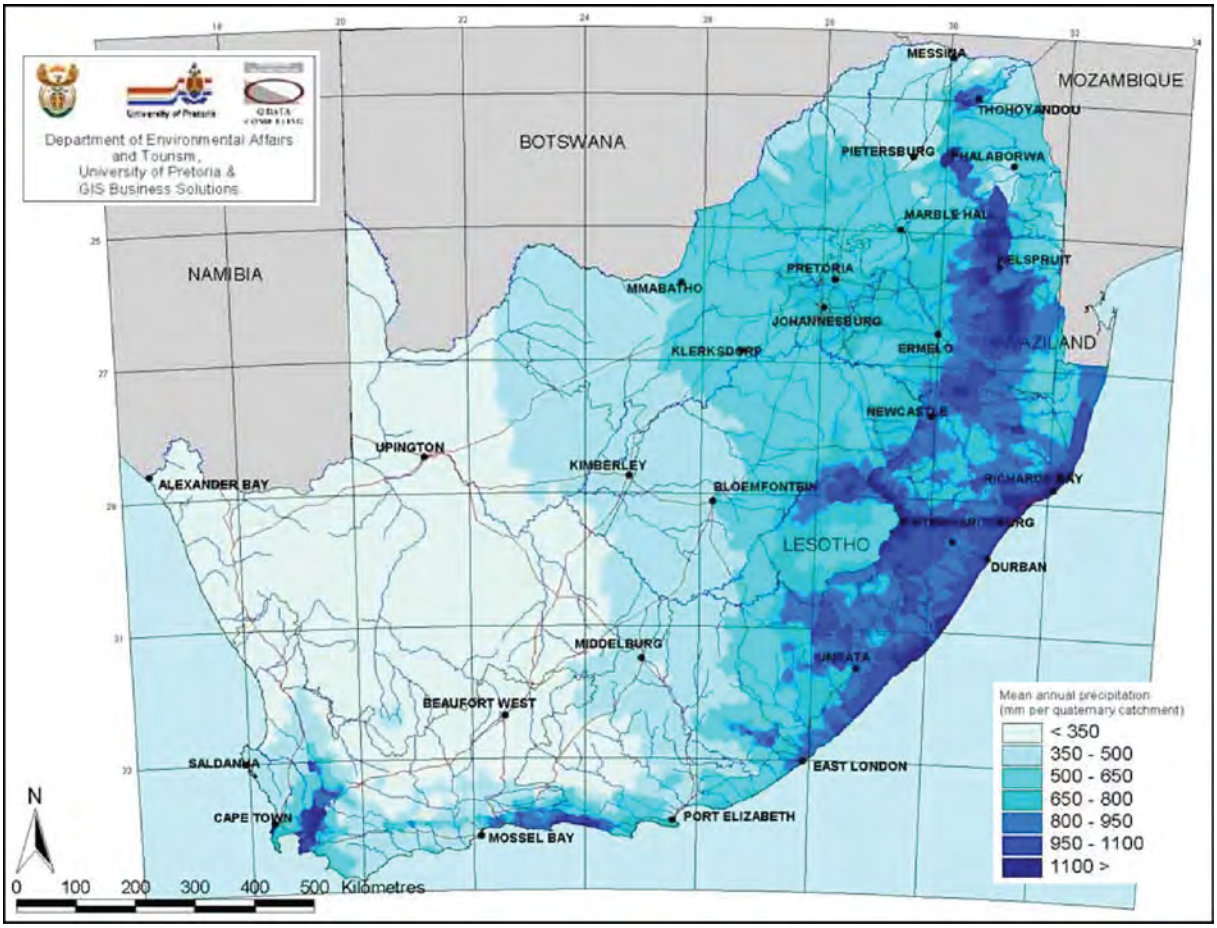

Figure 2.5: Mean annual precipitation map for South Africa.

2.4 Climate and Weather

The climate and weather of an area has an equal importance to the geology in determining the hydrogeology of an area. Various aspects of the climate, such average annual rainfall and seasonality of rainfall and temperature are important. The weather too plays a role in determining the hydrogeology as it dictates the intensity and duration of rainfall events, the reliability of rain bearing storms and the forms of precipitation that occur. Very importantly, all of this influences the isotopic composition of the precipitation and a thorough understanding of the climate and weather is essential for interpretation of the measured isotopes.

In 1911, Alexander Knox, a member of the convocation of the University of the Cape of Good Hope (a previous name for The University of Cape Town), had this to say in the opening of the chapter on South Africa in his book *The Climate of the Continent of Africa*: "Speaking generally of Southern Africa south of, say, 19° or 20° S., it may be said that the rainfall increases from west to east along any parallel, except in the extreme south of Cape Colony where irregularities exist, ... " (Knox, 1911). It is within these "irregularities" that the study area wholly falls and therefore, a brief mention of the climate and weather patterns is warranted. The study area experiences a wide range of climates due to three main factors, these being size, position and geography.

The size of the study area is somewhat over 100 000 km^2, encompassing most of the Western Cape and going into the Eastern Cape. This is large enough to experience gradients in climate simply due to distance. The position of the study area at the southernmost tip of Africa places the region just far south enough to be within the westerly wind belt and experience mid-latitude cyclones regularly in winter and occasionally in summer. However, the region is still close enough to the equator that it experiences tropical influences in summer and is on the fringes of the global southern desert belt, centred along the 30th parallel. The position is also unique in that the region is subjected to effects from both the cold upwelling of the Benguela Current on the west coast and the warm, tropically derived water of the Agulhas Current on the east and south coast. Finally, the geography of the region is complex, with variations in climate caused by the coast to inland gradient and the presence of mountain ranges, which block or funnel weather systems around, generate orographic rainfall and cause rain shadows.

Climate in the study area ranges from *warm temperate* along the south coast, where rain falls all year round, especially against the south-facing slopes of the Langeberg, from Swellendam to Port Elizabeth, to *hot desert* in the Tankwa Karoo, where some years there is no rain.

2.4.1 Rain

Cape Town experiences a typical *Mediterranean* climate with cold wet winters and warm dry summers. Moving north from Cape Town, the winter rainfall decreases until desert conditions are reached at the Gariep River; moving north-east, the winter rainfall decreases and summer rainfall increases until the central Karoo which experiences only summer rainfall; moving east,

winter rainfall is maintained and summer rainfall increases, until the coast veers north-east at Port Elizabeth, cutting out winter rain by East London. The general pattern of rainfall is greatly modified by mountains, as seen in **Figure 2.5**. Rainfall is increased in the immediate vicinity of mountains, both the windward and leeward side, and only a significant distance beyond the leeward mountain flank does the rainfall decrease.

The above patterns are illustrated in the diagrams in **Figures 2.6 & 2.7**. The decrease in rain northwards is seen by the drop in rainfall from Cape Town to Vredendal. At the same latitude as Vredental, rainfall increase due to both some summer rain and the effect of elevation can be seen at Calvinia. The change from Cape Town to Robertson shows three effects: decreasing winter rain because of distance eastwards; decreased rainfall because of a rain shadow behind the first line of mountains of the Cape Fold Belt; and a small increase in summer rain. The difference between Cape Town and Port Elizabeth shows a clear decrease in winter and increase in summer rain. The same two effects are visible at George, as well as an overall increase caused by proximity to the Outenikwa (Langeberg) Mountains. George to Oudtshoorn illustrates the combined effect of rainfall decreases from the coastal-inland gradient and a rain shadow.

The study area has a remarkable array of weather scenarios that can produce rain. A brief discussion of these follows, based largely on Preston-Whyte and Tyson (1988) and SAWB (1996). There are 5 main weather scenarios that can cause rain and all of these are related to some form of pressure trough of cyclonic feature (both low pressure) at the surface and into the middle and sometimes upper atmosphere. Of these 5, 4 occur in conjunction with or after the passage of a frontal depression, also known as a mid-latitude cyclone.

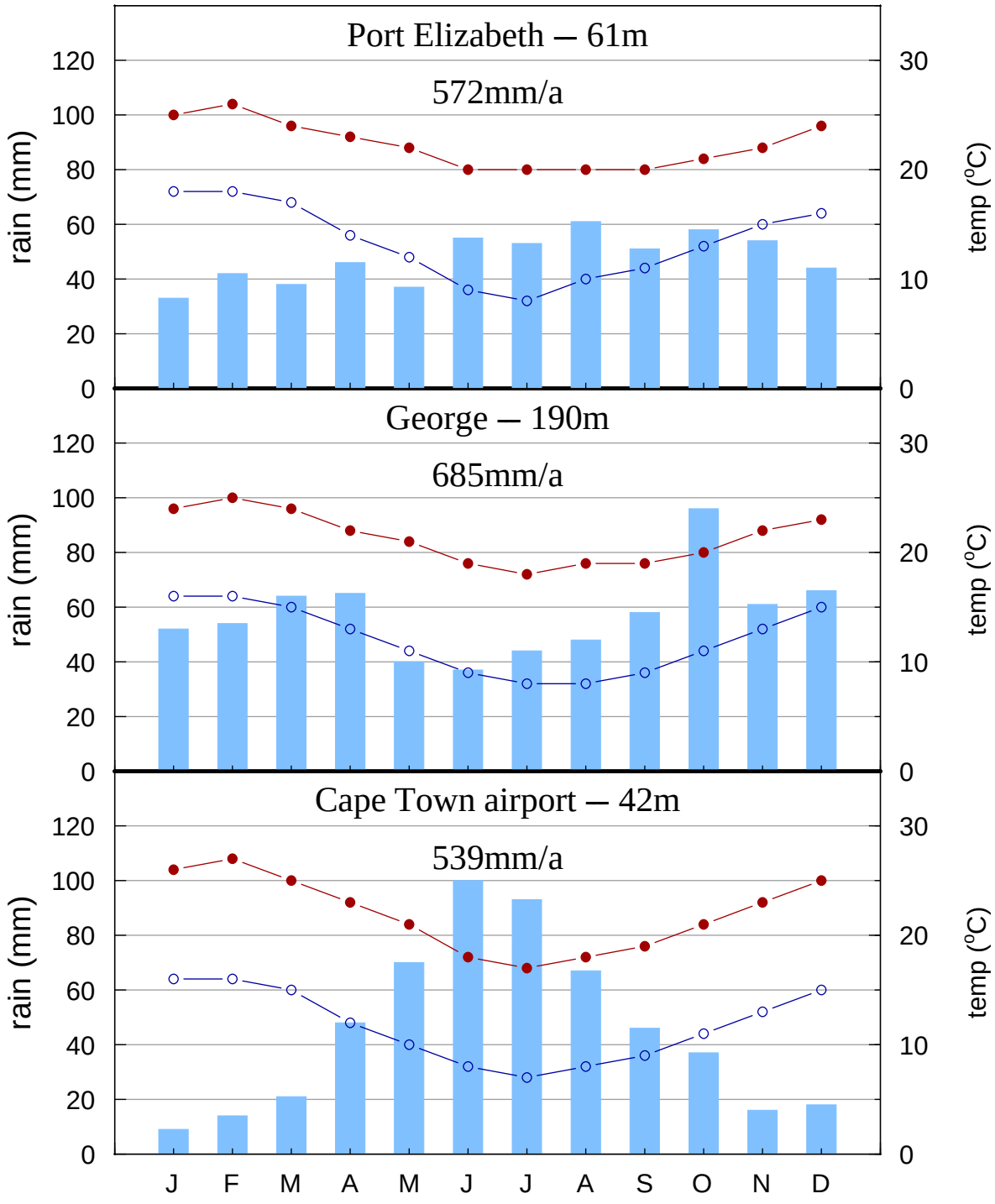

Figure 2.6: Rainfall and minimum and maximum temperature graphs for selected locations in the Cape Fold Belt region. The station altitude is given in metres above sea level. Locations are shown in the map in Chapter 1. Data for 1979–2000 (CSAG, 2013).

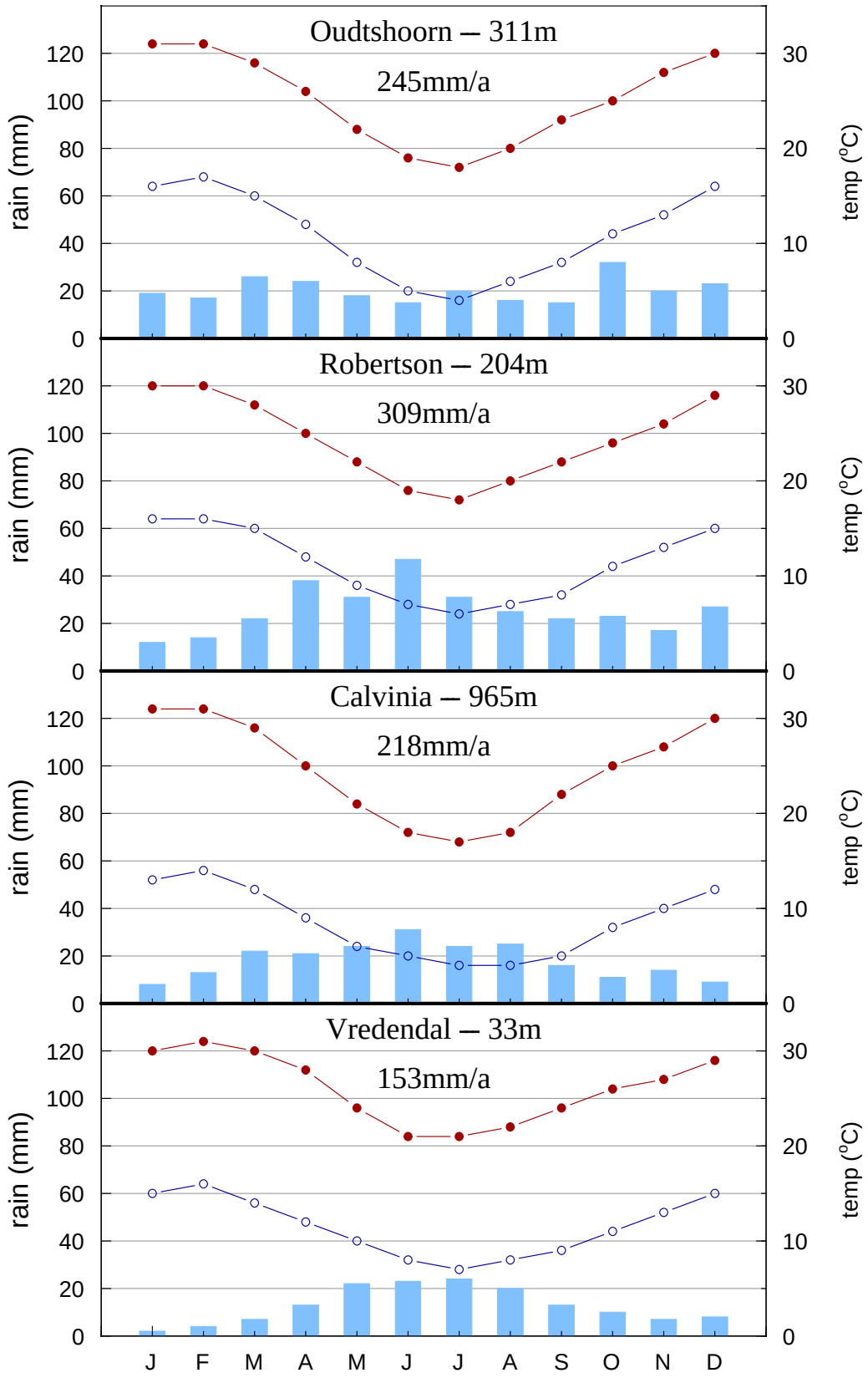

Figure 2.7: Rainfall and minimum and maximum temperature graphs for selected locations in the Cape Fold Belt region. The station altitude is given in metres above sea level. Locations are shown in the map in Chapter 1. Data for 1979–2000 (CSAG, 2013).

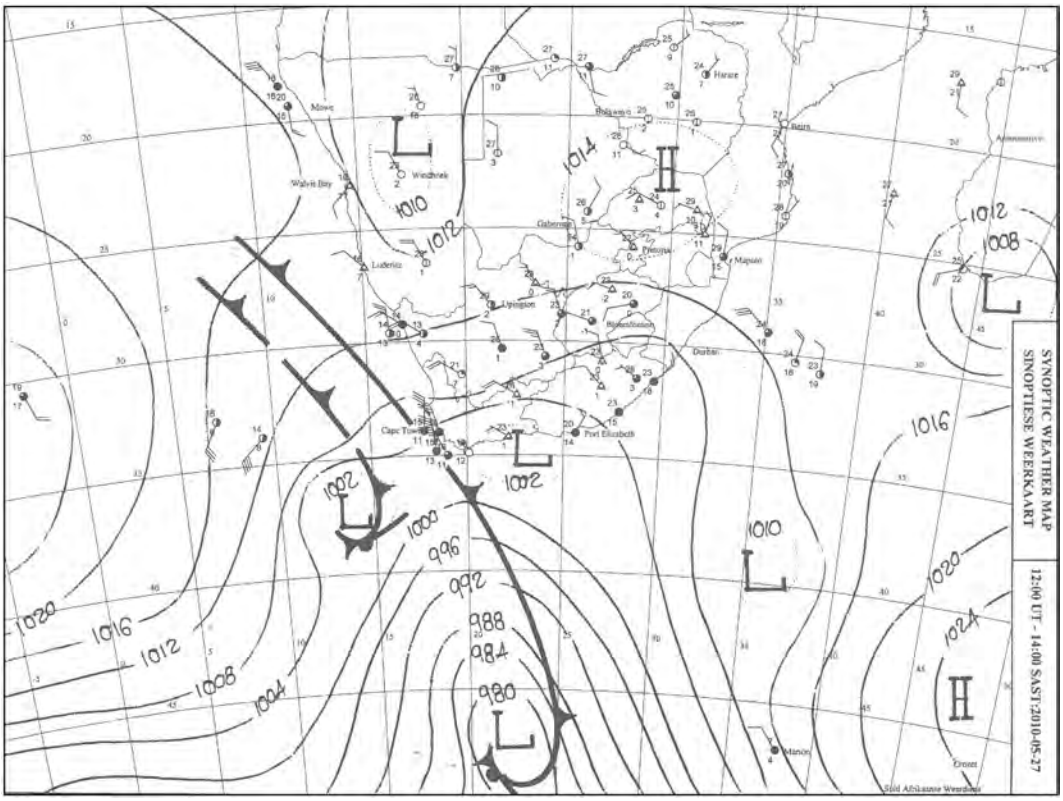

Figure 2.8: Synoptic chart from SAWS for 14h00 SAST on 27th May 2010 in which a westerly wave can be seen approaching South Africa. Rainfall from this system on this day was up to 73 mm, at Kirstenbosch and reached far north, with 10 mm at Springbok and 3 mm even at Alexander Bay.

2.4.1.1 Westerly Wave

Frontal depressions form at the polar front, at around 60°S in the south Atlantic Ocean, and move north-eastwards until they begin to decay and move south-eastwards. They feature a warm front and cold front, where air masses of different temperature meet, and the whole system rotates clockwise in the southern hemisphere. If they move far enough north, they can push a cold front over southern Africa. Uplift of warmer, moist air ahead of the cold front can cause a line of continuous rain at the front typically lasting a few hours, and instability behind the front can lead to typical intermittent 'clearing showers' that may persist for a day or two. Rainfall is mainly in the south-western Cape, but can, in extreme cases, once or twice a year, occur over the whole subcontinent, even precipitating rain or snow as far north and inland as Windhoek and Johannesburg. The example in **Figure 2.8** shows the wave shape of the isobars as the system moves west to east.

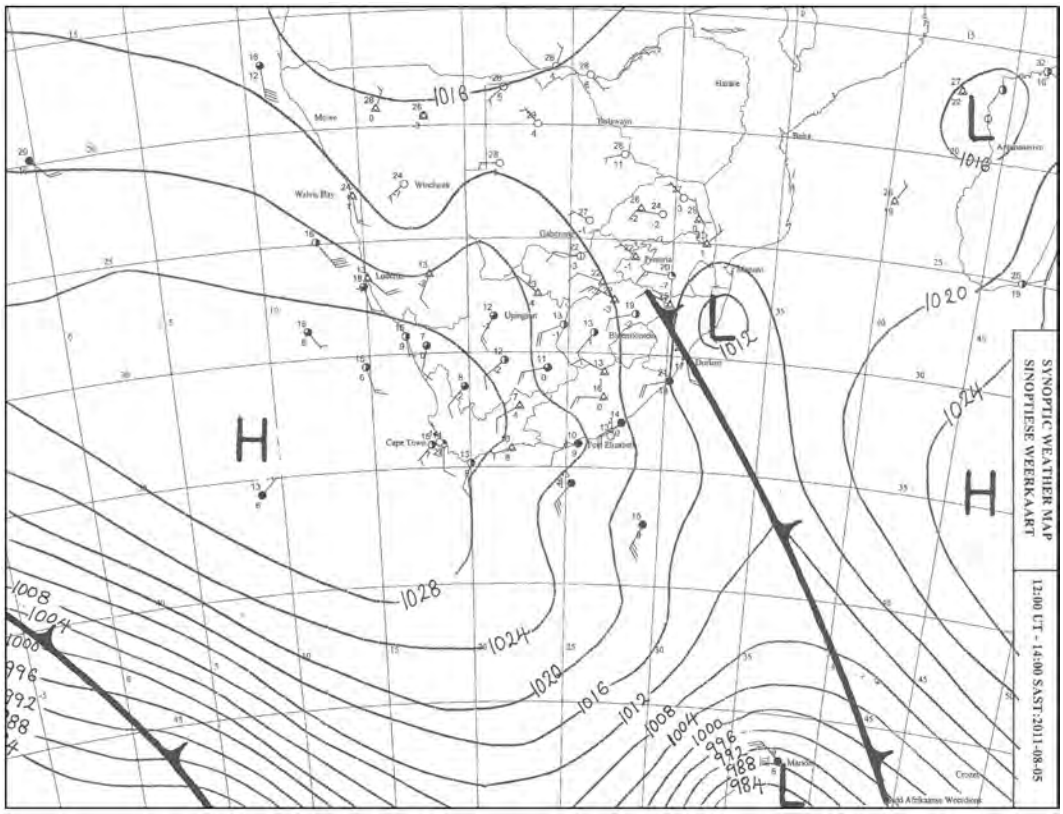

Figure 2.9: Synoptic chart from SAWS for 14h00 SAST on 5th August 2011 in which post-frontal conditions are causing southerly meridional flow. Rainfall was up to only 11 mm, at Mossel Bay, but was widespread, occurring at almost every SAWS station in the Western Cape as well as into the southern parts of the Northern Cape.

2.4.1.2 Southerly Meridional Flow

After the passage of a cold front, strong southerly airflow can persist for a day or two, starting off as south-westerly airflow immediately after the passage of the cold front, and then swinging to southerly flow (**Figure 2.9**). This usually advects very cold air and showers to the southern Cape and Eastern Cape coastal regions. Snow on mountains of the Western and Eastern Cape can result. Much of the rain in the central parts of the Western Cape results from this weather pattern, as the frontal rain that approaches from the north-west and west has fallen out on the western peaks of the Cape Mountains and so these central regions are in a rain shadow for westerly winds.

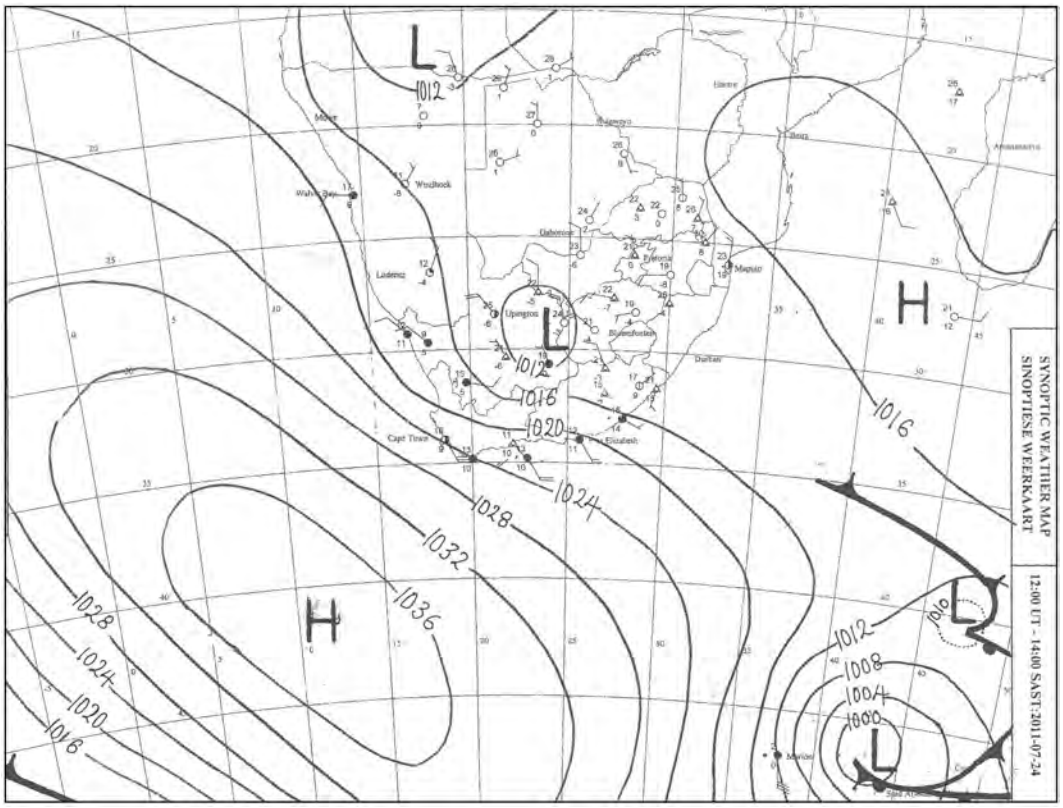

Figure 2.10: Synoptic chart from SAWS for 14h00 SAST on 24th July 2011 in which the South Atlantic High Pressure is moving south-eastwards after the passage of a cold front, seen dissipating to the south-east. Rainfall from this system was concentrated in the southern and eastern portions of the Western Cape, with up to 68 mm for the day, at George.

2.4.1.3 Ridging Anticyclone

A day or two after the passage of a cold front, the South Atlantic High Pressure cell can ridge south of the subcontinent. Moisture is picked up off the Indian Ocean and advected into an area of unstable conditions. The rainfall that results is usually confined to the eastern and central parts of the country with only orographically induced cloud evident in the far west, but when this system intensifies, the rain becomes more widespread in the eastern or central parts and the orographically induced cloud in the west increases to the point where it precipitates. This condition is known as a *black south easter*, named for the low, dark clouds that accompany this type of rain event. The normal white, fluffy or smooth *table cloth* on Table Mountain thickens and emits rain, often at a 45° angle or less, due to the intense wind, from the base of the darkened cloud. Ridging anticyclones typically cause rainfall in the eastern and southern portions of the Western Cape, as occurred in the example given in **Figure 2.10**.

The westerly wave, southern meridional flow and ridging anticyclone above are common weather scenarios, although a black south easter develops only infrequently, a few times per year. The cut-off low and west coast trough described below are not common.

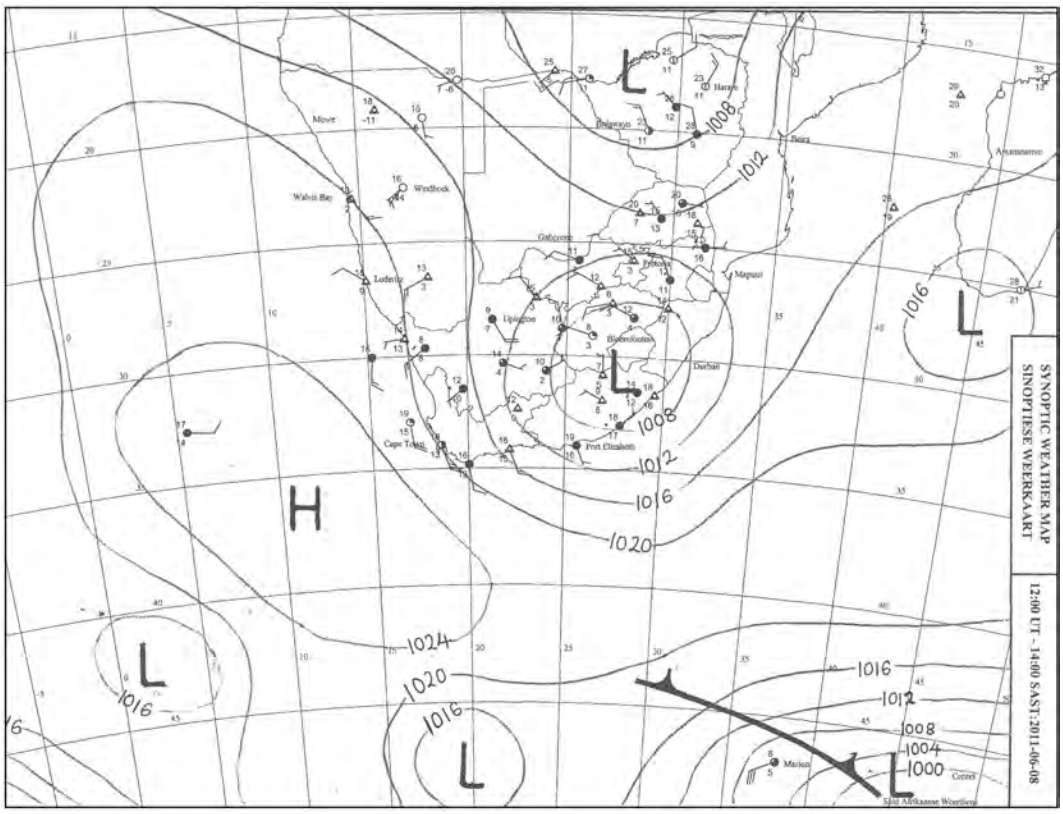

Figure 2.11: Synoptic chart from SAWS for 14h00 SAST on 8th June 2011 in which a cut-off low can be seen over the Eastern Cape. This system started south-west of the country on the 6th and intensified, exiting the country to the south-east on the 9th and dissipating thereafter. Rainfall from this system on this day (8th) reached 103 mm, in Ladismith.

2.4.1.4 Cut-Off Low

A cut-off low occurs when a cold front spawns a closed cyclonic cell that drifts northwards, out of the westerly wind belt. The cut-off low is a deep system with substantial uplift and generates heavy rain. As the low is out of the flow of the westerlies, it is often stationary or slow moving and the rain therefore falls on a relatively small area and can be for a period of days, usually causing floods. The example in **Figure 2.11** shows the most intense, third day of a four day cut-off low system, where rain occurred over the whole of the Western Cape, starting in the west and moving east. The floods of January 1981 that nearly obliterated the small town of Laingsburg were caused by a cut-off low. These systems can affect most of the country, but particularly the southern portions.

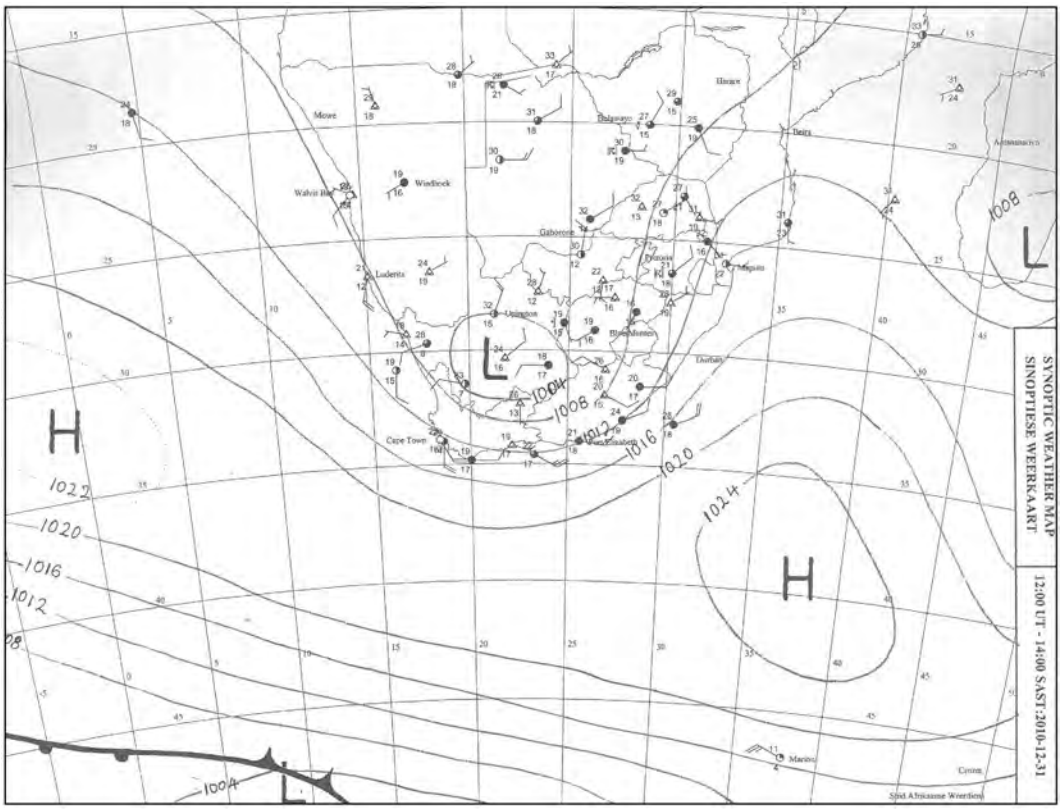

Figure 2.12: Synoptic chart from SAWS for 14h00 SAST on 31st December 2010 in which a trough near the west coast is causing significant rainfall in the Western Cape. Rainfall on this day reached 26 mm, at Beaufort West, and continued the next day, with up to 19 mm, at Excelsior Ceres.

2.4.1.5 West Coast Trough

This is the only weather pattern discussed here that may have no association with a frontal depression. Although the weather pattern may develop several times per year, rainfall from this system is less frequent. The rain that results usually falls in the central, southern and eastern parts of the country, but it is one of the few systems that can bring significant rain to the far west desert areas. The trough is a region of low pressure that develops west of the country, as the name suggests, and deepens and strengthens as it moves south-eastwards, as these systems generally do. The system shown in **Figure 2.12** was stationary for about two days, generating widespread rain over the Western Cape, with some heavy falls of rain and hail from thunderstorms. Rain typically occurs in the west if the system had its genesis far out in the Atlantic and had time to develop rain-bearing clouds by the time it makes landfall on the west coast.

2.4.2 Temperature

The study area experiences mostly moderate temperatures, although there are extremes of heat in the dry areas and cold on the mountain tops. Temperatures near the coast are more consistent (see Cape Town and Port Elizabeth), being moderated by the presence of the ocean and the more humid air. Inland temperatures are more extreme, with greater daily and seasonal ranges (see Oudtshoorn and Robertson). The effect of altitude reduces temperatures (see Calvinia). Interestingly, the annual average temperatures do not vary much, being from 16.5–19 °C for the selected stations.

2.5 Hydrogeology

2.5.1 Porosity and Permeability

The Table Mountain Group is largely composed of quartzose sandstones, a rock type that would generally exhibit a primary porosity of 5 to 30 % , depending on coarseness and sorting (Domenico and Schwartz, 1998, p.14). However, burial and diagenesis during the Cape Orogeny reached lowermost greenschist facies (not exceeding 300 °C), sufficient to result in conversion of most of the sandstones to quartzite (Frimmel et al., 2001). The changes in porosity that occur during diagenesis are complex and include mechanical rearrangement of the matrix, partial dissolution of sediment grains and precipitation of new minerals (the cement). In the case of the Table Mountain Group, silica was dissolved from the quartz sand grains and reprecipitated to the extent that the rock has been thoroughly recrystallized and virtually no primary porosity remains (Rosewarne, 2002b).

However, the Table Mountain Group contains abundant secondary porosity due to fractures (see **Figure 2.13**. The great thickness of quartzose sandstones has predisposed the rocks to brittle behaviour under stress and the thorough recrystallization of the Table Mountain Group formations has only made the units more competent and therefore subject to an even greater degree of brittle failure (Kotze, 2002). Fractures in the Table Mountain Group have developed in relation to folding, faulting and cleavage formation, but also include bedding planes, as can be seen in **Figure 2.14**. Up to a point, the more deformation, the greater the degree of fracturing and therefore secondary porosity. However, there is a limit to this and zones of extreme deformation, or cataclasis, often have experienced intense silicification that closes or partially blocks openings and thereby reduces permeability (de Beer, 2002).

In the absence of any porosity measurements for the TMG, general models of porosity can be instructive. For rocks with fracture porosity, three possible broad classes exist, as shown in **Figure 2.15**: one, single porosity from major fractures only; two, dual porosity of major fractures and intergranular, primary porosity; three, dual porosity of major and minor fractures. Kotze (2002) maintained the Table Mountain Group has a dual porosity of major and minor fractures, at least as was observed in the Peninsula aquifer in the Kammanassie Mountains. This dual fracture

Figure 2.13: Groundwater discharging as seeps from fractures in quartzite of the Skurweberg Formation on the Spout at Cederberg Tafelberg. The fractures are horizontal bedding planes and vertical joints.

porosity model may operate at numerous scales and in fact be a multiple level phenomenon with fractures or fracture systems being found at many scales, from regional or mega-fault structures, through local and outcrop scale, to hand specimen size. Mapping as done by Hartnady and Hay (2002c) using remote sensing techniques gives some indication of this at the regional to local scale in **Figure 2.16** and at the local to outcrop scale in **Figure 2.17**.

Groundwater discoveries support this multilevel fracture model because water strikes during drilling can give an order of magnitude difference in water yield. For example, borehole BK4 drilled in the Citrusdal Valley in 1997-8 yielded a 5 L/s blowyield until, at 220 m depth, a major water strike allowed blow yields of around 100 L/s to be realised (Hartnady and Hay, 2002a). The low yield was presumably from minor, more common fractures encountered through much of the borehole, and the very high yield corresponds to intersection of a major, regional scale fracture or fracture system.

Although the commonly held belief is that fracture density decreases with depth, it seems that this might only occur at a very low rate, or at great depths (more than 1 km) in the Table Mountain Group. Lin et al. (2007) recorded a very weak negative correlation between fracture density and depth over a vertical distance of 750 m in the Piekenierskloof Formation; in other words, there was only a marginal decrease in fracture density with depth.

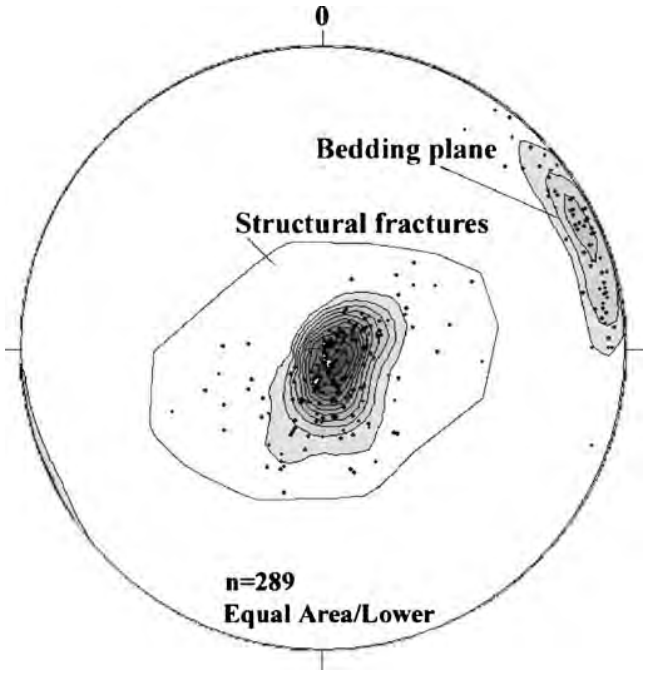

Figure 2.14: Fracture measurements (strike and dip) taken at surface in the Piekenierskloof Formation between Lamberts Bay and Graafwater, showing the separation between near horizontal bedding planes and near vertical structurally formed fractures. From Lin et al. (2007).

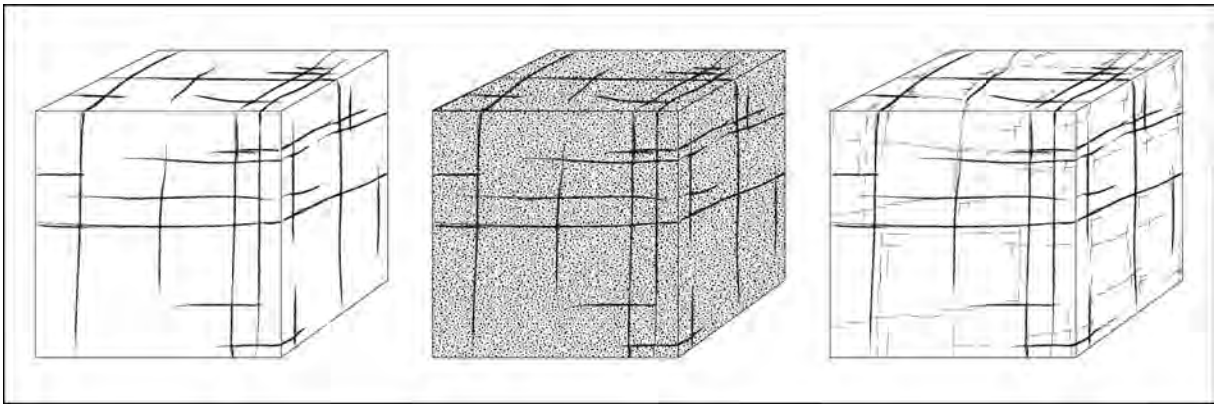

Figure 2.15: Theoretical models of possible fracture porosity: one, major fractures; two, major fractures and primary porosity; three, major and minor fractures. After Kruseman and De Ridder (1994) as cited in Woodford (2002).

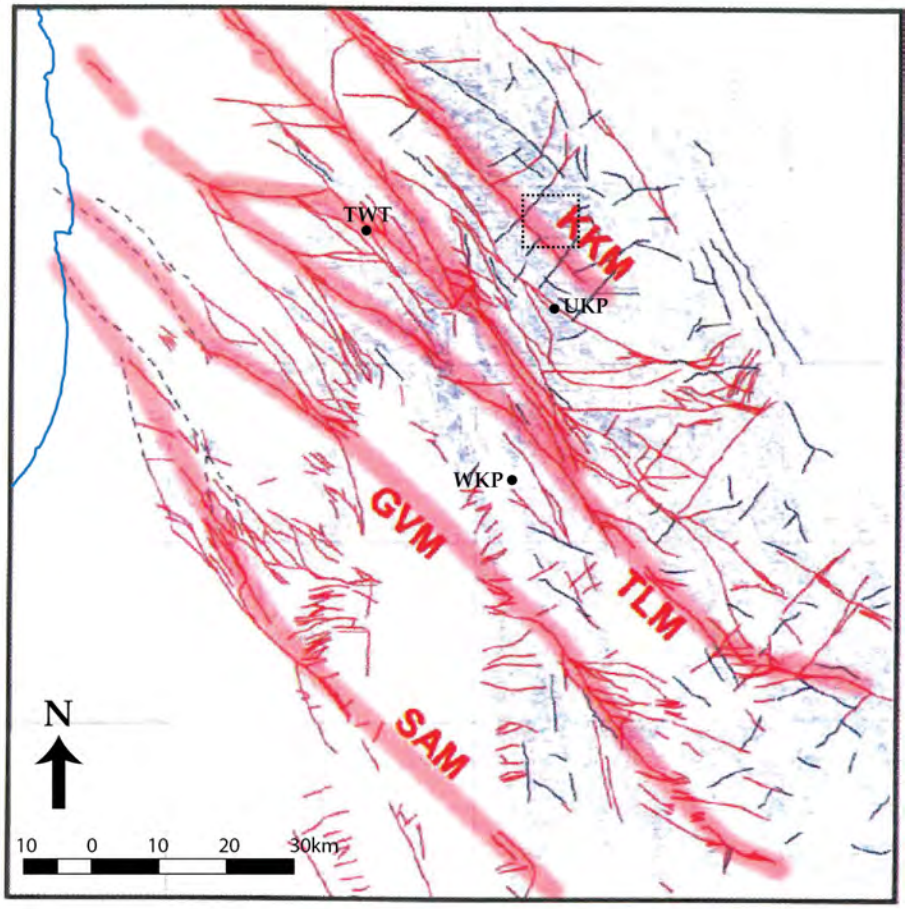

Figure 2.16: A fault and fracture trace map for the Cederberg–West Coast region showing mapped faults from the 1:250 000 geology maps as thin red lines, and additional mapped or remoted derived fracture traces, from Landsat, SPOT or aerial photographs, as thin black lines. The area includes outcrop of all formations within the Table Mountain Group. Large regions with few structures (in the south-west) are areas where the Malmesbury Group is exposed. SAM - Saron-Aurora megafault; GVM - Gydo-Verlorenvlei megafault; TLM - Twee Riviere-Leipoldtville megafault; KKM - Krakadouw-Klawer megafault. The dotted black square shows the location of **Figure 2.17**. From Hartnady and Hay (2002c).

2.5.2 Hydraulic Parameters

Aquifers can be defined in several ways, including geology, structure and spatial occurrence. The ability of an aquifer to conduct water is typically described by three hydraulic parameters: the hydraulic conductivity (K), the transmissivity (T) and the storativity (S). Hydraulic conductivity is a measure of permeability; transmissivity is a measure of the total flow possible along a vertical line through the aquifer and is calculated by multiplying the hydraulic conductivity by the aquifer thickness, and it gives some indication of the possible borehole yields or flow rates; storativity measures the amount of water released from a confined aquifer per unit drop in hydraulic head and gives an indication of how much water can be abstracted. All of these parameters are derived

location	aquifer	K m/d	T m^2/d	S	source
Lamberts Bay	Piekenierskloof	0.00069			Lin et al. (2007)
The Baths, Citrusdal	Peninsula	0.002 - 2	10 - 200	0.0001 - 0.001	Umvoto and SRK (2000)
Roode Elsberg, Hex	Peninsula	0.26			Brink (1981)
Villiersdorp	Peninsula	017			Brink (1981)
Kammanassie	Peninsula			0.01 - 0.05	Kotze (2002)
Lakenvalley, Hex	Skurweberg	0.26			Brink (1981)
Kouga Dam	Skurweberg	0.07			Brink (1981)
Villiersdorp	Skurweberg	0.3			Rosewarne (2002b)
Agter Witzenberg	Skurweberg	0.05			Weaver et al. (1999)
Kleinmond	Skurweberg		70 - 320	0.0001 - 0.0005	Parsons (2002)
St Francis on Sea	Skurweberg		100	0.0018 - 0.0033	Rosewarne (2002b)
Struisbaai	Pen/Skbg		15 - 200	0.0086	Weaver et al. (1999)
Uitenhage	Pen/Skbg		10 - 400	0.0002 - 0.05	Maclear (2002)
Cape Fold Belt	TMG			0.001	Vegter (1995)
Cape Fold Belt	TMG			0.0032 - 0.015	Weaver et al. (2002)

Table 2.1: Hydraulic parameters (K - hydraulic conductivity, T - transmissivity, S - storativity) for aquifers of the TMG, based on calculations from pumping tests, conceptual or numerical models and other estimates. Table is based on a compilation by Rosewarne (2002b).

from borehole pumping tests and are best suited to homogenous, isotropic, primary porosity aquifers. The Table Mountain Group may fit the characteristic of being homogenous, but it is anisotropic because of the preferential directions in which fractures have developed (see **Figure 2.14**) and it is of course a secondary porosity aquifer. In addition, the very size of the Table Mountain Group, even simply the depth at one locality, never mind the vast horizontal dimensions, makes the aquifer difficult to quantify, not only theoretically, but in a very practical sense; i.e. the cost and effort of drilling a fully penetrating borehole, even through just one formation (e.g. Peninsula), is in most cases immense. For these reasons there are few reliable estimates of the three hydraulic parameters for the Table Mountain Group.

Rosewarne (2002b) collated some hydraulic parameters for the TMG; these have been reproduced here in **Table 2.1** with some rearranging and additions.

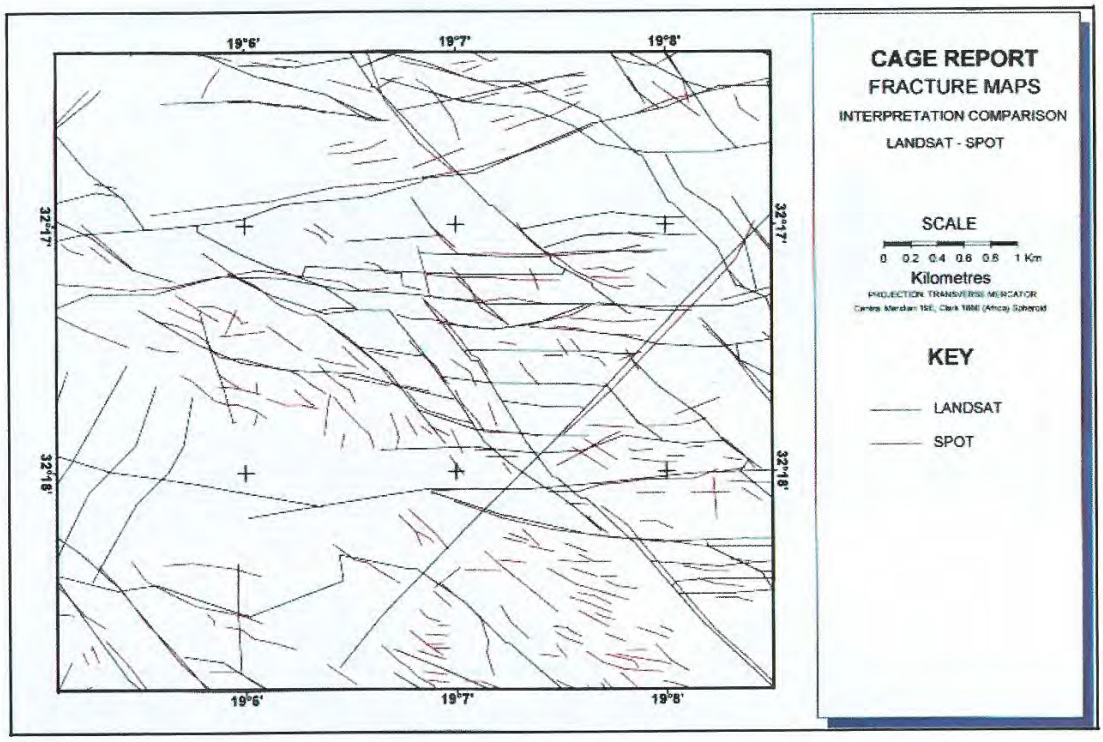

Figure 2.17: A detailed fracture trace map for a small area of Peninsula Formation outcrop, shown as the region in the dotted black square in **Figure 2.16**. Fracture traces derived from Landsat images (black lines) and SPOT satellite images (red lines). The diagrams shows how fractures occurs in parallel sets that often intersect and that many fractures are short and some, typically associated with local to regional faults, are much longer. From Hartnady and Hay (2002c).

2.5.3 Hydrostratigraphy

The Table Mountain Group is not a simple, single aquifer with a neat geometrical shape, but rather an interconnected aquifer system, semi-continuous in space, with an extremely complex three dimensional form and multiple aquifers. The highest parts of the aquifer are over 2000 m above sea level and form the crests and peaks of mountain ranges, mainly comprising the Peninsula Formation, but also the Nardouw Subgroup, especially the Skurweberg Formation. The lowest parts of the aquifer reach depths of 5–6 km below sea level along the Worcester and Kango Faults (see the cross-sections in Chapter 5), and in places the Table Mountain Group outcrops or subcrops beneath the sea bed, to a distance of at least tens of kilometres offshore. There is no location where all the Table Mountain Group formations occur, from Piekenierskloof or Sardinia Bay Formation to Rietvlei or Baviaanskloof Formation, however the succession from Peninsula to Rietvlei Formation is preserved in many areas and probably reaches 4000 m true thickness (perpendicular to the formation contacts), especially in the southern branch of the Cape Fold Belt where structural thickening has been substantial.

Hydrogeologists have traditionally only recognized the terms aquifer and aquitard for geolog-

ical units that do and do not conduct significant quantities of groundwater. These are relative terms and factors such as depth, thickness, economics and demand for water are almost as important as the actual hydraulic parameters of the unit in determining which term to apply. In addition, the term aquiclude is sometimes used as a synonym for aquitard, although Poehls and Smith (2009) maintain the term aquiclude should be reserved for extremely impermeable formations. It is important to realise that hydrostratigraphic units may or may not overlap with geological units; an aquifer may be only a part of a geological formation, or several geological formations may constitute one aquifer, and similarly for aquitards. Furthermore, there was no accepted heirarchy of hydrogeological units, such as the familiar geological *member*, *formation*, *group* and other categories.

Al-Aswad and Al-Bassam (1997) have created a hydrostratigraphical nomenclature, but even this is inadequate under many common geological situations where layers are lenticular, where folding has occurred and even more so in a faulted environment, where substantial flow along faults through aquitards connects different aquifers, or different aquifers are faulted into direct contact with each other. All of the above occurs in the Cape Fold Belt. For example, Rosewarne (2002a) found the Bokkeveld Group sandstone layers to deliver high yields, because leakage from the underlying Table Mountain Group into these sandstone layers occurred once they had been pumped. The high hydraulic head of the underlying Table Mountain Group was due to recharge in the adjacent Skurweberg mountain range and allowed this groundwater to leak upwards and recharge the Bokkeveld Group sandstones.

Using the Al-Aswad and Al-Bassam (1997) system yields a classification for the Cape Supergroup as shown in **Figure 2.18**. Each geological formation can be roughly evaluated as either an aquifer or aquitard. Aquitards may contain water bearing layers, such as the sandstone beds within the Graafwater Formation; equally, aquifers may only offer some portion of their thickness as an aquifer, the rest being an aquitard, such as the sandstone beds within the dominantly silty Floriskraal Formation, but the reason for calling the Floriskraal Formation an aquifer is that it bears water within a predominantly non-water bearing setting.

The proposed hydrostratigraphy attempts to simplify and highlight major aquifers and aquitards. Where aquifer-aquitard boundaries coincide with geological boundaries, no reclassification has been done. In the Witteberg and Bokkeveld Groups where the geology alternates regularly between arenaceous and argillaceous, the hydrostratigraphy mimics the geostratrigraphy, but in the TMG this is not the case. The Piekenierskloof and Graafwater Formations have limited areal extents.

The Piekenierskloof Formation is a significant aquifer in the Sandveld region (Lin et al., 2007). The Graafwater Formation may have fractured, water bearing sandstone layers, but their limited vertical and areal extent (Rust, 1977) will render them low yielding, unless they are connected via faults to the Piekenierskloof or Peninsula Formation.

The Peninsula Superaquifer may include some portion of the Pakhuis Formation, where this

is permeable, although Hartnady and Hay (2002b) consider the Pakhuis Formation to be an aquitard, based on the similarity in gamma and neutron-neutron downhole geophysical logging of the Pakhuis and Cederberg Formations. Superaquifer status is assigned on account of the extreme thickness (up to 2000 m) and areal extent over the Cape Fold Belt, as well as the high yielding nature of this unit (Hartnady and Hay, 2002a). The Cederberg Aquitard may include portions of the Pakhuis Formation where it is less permeable and portions of the Goudini Formation where the siltstone and shale layers are substantial enough to restrict groundwater flow. Although rather thin (100–200 m) the fact that this aquitard either separates the Peninsula Superaquifer from the Skurweberg aquifer or simply acts as a cap to the Peninsula Superaquifer, makes this unit of extreme importance in understanding groundwater flow in the Table Mountain Group. The Skurweberg Aquifer is centred on the highly fractured mature quartzites of the Skurweberg Formation, but includes portions of the underlying Goudini and overlying Rietvlei Formations where they are more permeable and have good connectivity with the Skurweberg Formation.

The Bokkeveld Group, although it contains sandstone aquifers that can yield substantial water at the local scale (Rosewarne, 2002a), acts as an aquitard on a regional scale, particularly as a confining layer to the Table Mountain Group. Good examples of this are seen in the Olifants River Valley (Geological Survey, 1973) and under the Little Karoo (Geological Survey, 1979) where the Bokkeveld Group confines the Table Mountain Group under the valley floors and allows deep groundwater to flow many kilometres from one side of the valley to the other and emerge in hot springs, under pressure gradients derived from mountain recharge areas (Diamond and Harris, 2000).

The Witteberg Group contains both substantial aquifers and aquitards. It probably acts as an aquitard on a regional scale, although the extensive structural deformation, particularly intense folding and thrusting, probably allow good connections between the various sandstone (aquifer) layers to the extent that in some areas these may act as a single aquifer. The great thickness and highly competent nature and therefore extensive fracturing of the Witpoort Formation mean this unit is potentially a significant aquifer, although low recharge because of low rainfall is probably a limiting factor for achieving high and sustainable borehole yields from this unit. The Witteberg Group tends to receive low rainfall because of its usual position inland and therefore in the rain shadow of mountains formed by the Table Mountain Group.

Overall, the Bokkeveld and Witteberg Groups possess similar hydrogeological characteristics, in that they both contain numerous minor aquifers that may be connected to each other, or to the larger aquifers in the Table Mountain Group, if structural features allow. These similarities suggest that the multiple aquifers and aquitards of these two groups can be collectively known as the Bokkeveld-Witteberg aquagroup (Al-Aswad and Al-Bassam, 1997). The Table Mountain aquagroup is essentially the Peninsula-Cederberg-Skurweberg configuration that persists over much of the Cape Fold Belt, with some localised variations at the base of the group, where other formations are present.

Below and above the Cape Supergroup lie thick aquitards that generally conduct little groundwater: the Saldanian basement of metasediments and granite beneath and the Dwyka Group above. The Cape Supergroup can therefore be termed the Cape aquasystem, bounded by these basement and cover mega-aquitards, and with a fixed configuration of the aquifer dominated Table Mountain aquagroup at the base, and the regular aquifer-aquitard alternations of the Bokkeveld-Witteberg aquagroup above.

In some instances, aquifers within the Cape aquasystem will be connected to more recent cover rocks of the West Coast, Sandveld, Bredasdorp or Algoa Groups, which contain calcarenites, unconsolidated sand and other lithologies that can form aquifers. These linkages occur mainly near the coast and are generally limited in area. The Sandveld region around Elands Bay is the largest area where the Table Mountain Group interacts with surficial rocks and sediments.

2.5.4 Significance of the Table Mountain Group

The Table Mountain Group is critical in sustaining surface water in the Western Cape (Roets et al., 2008; Colvin et al., 2009). Baseflow during the summer dry season is sustained through discharge of groundwater (le Maitre et al., 2002; Colvin et al., 2009) and it has been shown that peak or flood discharge surface water during rain events is mainly composed of groundwater that has discharge from the aquifer in response to increased hyrdaulic head caused by fast recharge of rainwater (Midgley and Scott, 1994). A substantial portion of the ecosystems of the Western Cape are directly dependant upon water, being wetlands, riparian zones and estuaries. Furthermore, these vegetation and plant communities are more important as habitat and for ecosystem services than the dryland areas. As such, the Table Mountain Group is the ultimate water source for most surface water and therefore controls both the natural and human environment through most of the Western Cape.

Various attempts have been made at calculating the groundwater yield potential of the Table Mountain Group. From the information presented above, it should be clear that this exercise is subject to two huge challenges, being the great size of the aquifer system and the sparse and often unreliable information. As a first step, Rosewarne (2002b) has collated pumping data from active wellfields, giving an indication of available water in particular locations, and Meyer (2002) gives the flow rates of the thermal springs in the Cape Fold Belt. These data are summarized in **Table 2.2**.

THERMAL SPRINGS		WELLFIELDS	
name	GL/a	name	GL/a
Baden	1.16	Albertinia	0.26
Brandvlei	4.00	Caledon	0.10
Caledon	0.28	Ceres	1.51
Calitzdorp	0.25	Hermanus	0.35
Citrusdal (The Baths)	0.91	Humansdorp	0.68
Goudini	0.35	Jeffreys Bay	0.80
Montagu	1.20	Lamberts Bay	0.13
Studtis	0.98	Plettenberg Bay	0.28
Toverwater	0.35	Steytlerville	0.07
Uitenhage	1.42	St Francis-on-Sea	0.73
Warmwaterberg	0.28	Uitenhage	1.58
TOTAL	11.2	TOTAL	6.5

Table 2.2: Point source (springs) or small area (wellfield) abstraction figures give an indication of possible yields for deep boreholes or small wellfields in the Table Mountain Group. Data from Meyer (2002) and Rosewarne (2002b).

Hartnady and Hay in Weaver et al. (2002) calculated groundwater yield for an area of less than 2000 km^2 in the Citrusdal region as 5–25 GL per 1 m decrease in hydraulic head, concluding that for a technically and probably environmentally acceptable decrease in head of 20 m, 100–500 GL could be withdrawn annually. Scaling up to the whole of the Table Mountain Group, they calculate an aquifer rock volume of 100 000 km^3, which, for a fracture porosity of 0.1-1 % gives a volume of 100 000 – 1 000 000 GL of groundwater, although much of this water is not available because of practical challenges, as well as potential environmental impacts. Similarly, Rosewarne (2002b) calculates an aquifer rock volume of 47 000 km^3 and using storatitivity values shown in **Table 2.1**, he concludes that 10 000 – 100 000 GL of groundwater is in storage, again, most of which is not available. However, even if only a small percentage of this groundwater is available, when compared to the total volume of all surface water reservoirs fed by Table Mountain Group catchments, 1500 GL, it should be clear that the aquifer system stores a very large amount of water.

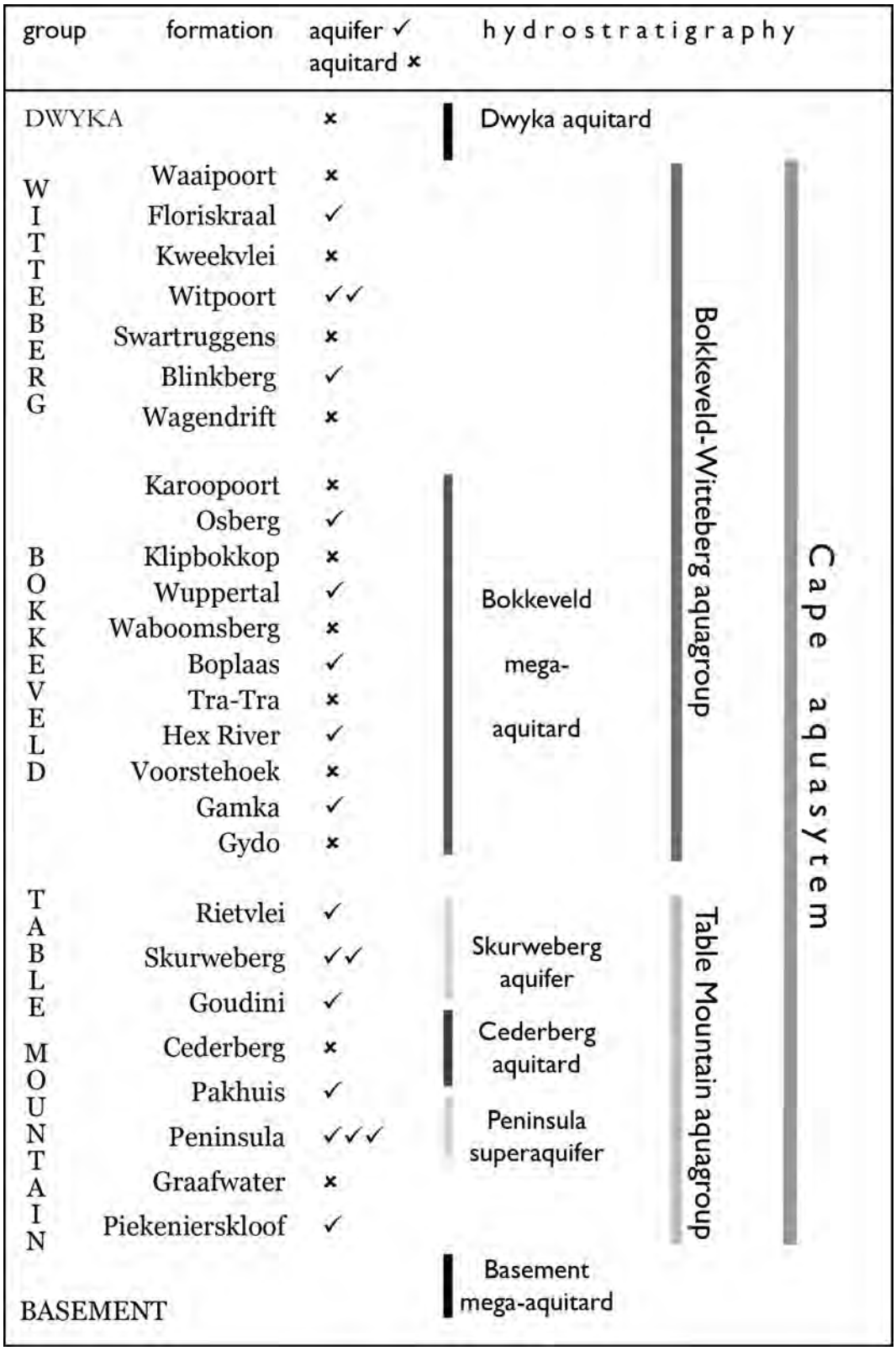

Figure 2.18: Proposed hydrostratigraphic classification for the Cape Supergroup in the western half of the Cape Fold Belt.

Chapter 3

Methods

3.1 Introduction

This chapter describes the methods used for collection of samples, laboratory preparation and instrumental analysis, including correction factors and equations. The locations of all the sample sites are shown on various maps and the major rainfall collection stations are all listed in a table with coordinates and elevations. Information on the calculation of regression lines is also included.

3.2 Sample Collection

3.2.1 Rain

Rainfall was collected at 15 sites across the Western Cape. Most of the collection stations operated for 2 years, from 2010 to 2012, with some having a continuous record and others an interrupted or shorter operational period. Factors that caused a station to cease operating were instrument problems from animal or weather damage, lack of access due to weather conditions and also human error. Maps of the sample locations are included below, approximately in a west to east direction, starting with Cape Town (**Figures 5.21 to 3.22**).

Rain collection depended on access to the rain gauge. Where gauges were easily accessible, rainfall was collected daily and emptied into a glass jar, from which a sample was taken at the end of each month. At remote sites, a cumulative collector (**Figure 3.2**) was erected and emptied at approximately the end of each month. In each case, the daily or monthly rainfall amounts were recorded. Bosman (1981) noted that plastic raingauges collect around 7 % less rainfall than standard metal raingauges, attributable to splash out from the receiving funnel and higher retention of raindrops on the plastic surface, which then evaporate. Given the extreme variation in rainfall in the field area due to orographic effects and that rainfall amount is used indirectly to weight isotope values, this discrepancy is considered acceptable. Furthermore, all rainfall for this study was collected using similar plastic raingauges and so the data is internally consistent.

station			location		
code	name	description	latitude	longitude	altitude
UCT	University of Cape Town	Department of Geological Sciences building	33° 57’ 31.9" S	18° 27’ 37.6" E	135 m
TMC	Table Mountain Cableway	upper cableway station	33° 57’ 26.6" S	18° 24’ 10.3" E	1074 m
TWT	Twaktuin	Twaktuin farm in Olifants River Mountains	32° 19’ 17.6" S	18° 49’ 31.9" E	412 m
UKP	Uitkyk Pass	crest of pass in Cederberg	32° 24’ 14.8" S	19° 06’ 05.4" E	1013 m
WKP	Wolfkop	house in Wolfkop Private Nature Reserve, south of Citrusdal	32° 38’ 19.2" S	19° 03’ 20.4" E	355 m
MTB	Matroosberg	nek between Matroosberg and Conical Peaks, Hex River Mountains	33° 22’ 27.2" S	19° 39’ 53.1" E	1910 m
DDN	De Doorns	Tweespruit farm near De Doorns in Hex River Valley	33° 26’ 34.3" S	19° 40’ 30.9" E	482 m
RVD	Riverndale	Riverndale farm, foot of the Langeberg, north-east of Heidelberg	33° 58’ 22.9" S	20° 59’ 56.2" E	251 m
RBP	Robinson Pass	crest of pass over Langeberg, north of Mossel Bay	33° 52’ 26.3" S	22° 01’ 54.7" E	885 m
BKK	Bakenskop	highest point of the Gamkaberg, Gamka Mountain Nature Reserve	33° 43’ 07.8" S	21° 55’ 28.4" E	1101 m
GST	Gamkaberg store	store shed at Gamka Mountain Nature Reserve	33° 40’ 20.0" S	21° 53’ 15.5" E	350 m
BBG	Blesberg	highest peak in the eastern Groot Swartberg	33° 25’ 03.8" S	22° 41’ 15.0" E	2080 m
KMN	Kammanassie	Vermaaks River Gorge in western Kammanassie Mountain	33° 36’ 11.4" S	22° 31’ 56.2" E	666 m
LTL	Lentelus	Lentelus farm in Bo-Kouga region	33° 40’ 42.2" S	23° 29’ 58.0" E	642 m
GKM	Goukamma	house near Goukamma railway station and Goukamma River	33° 02’ 21.1" S	22° 56’ 25.3" E	62 m

Table 3.1: Location information for the 15 rainfall collection stations of this study.

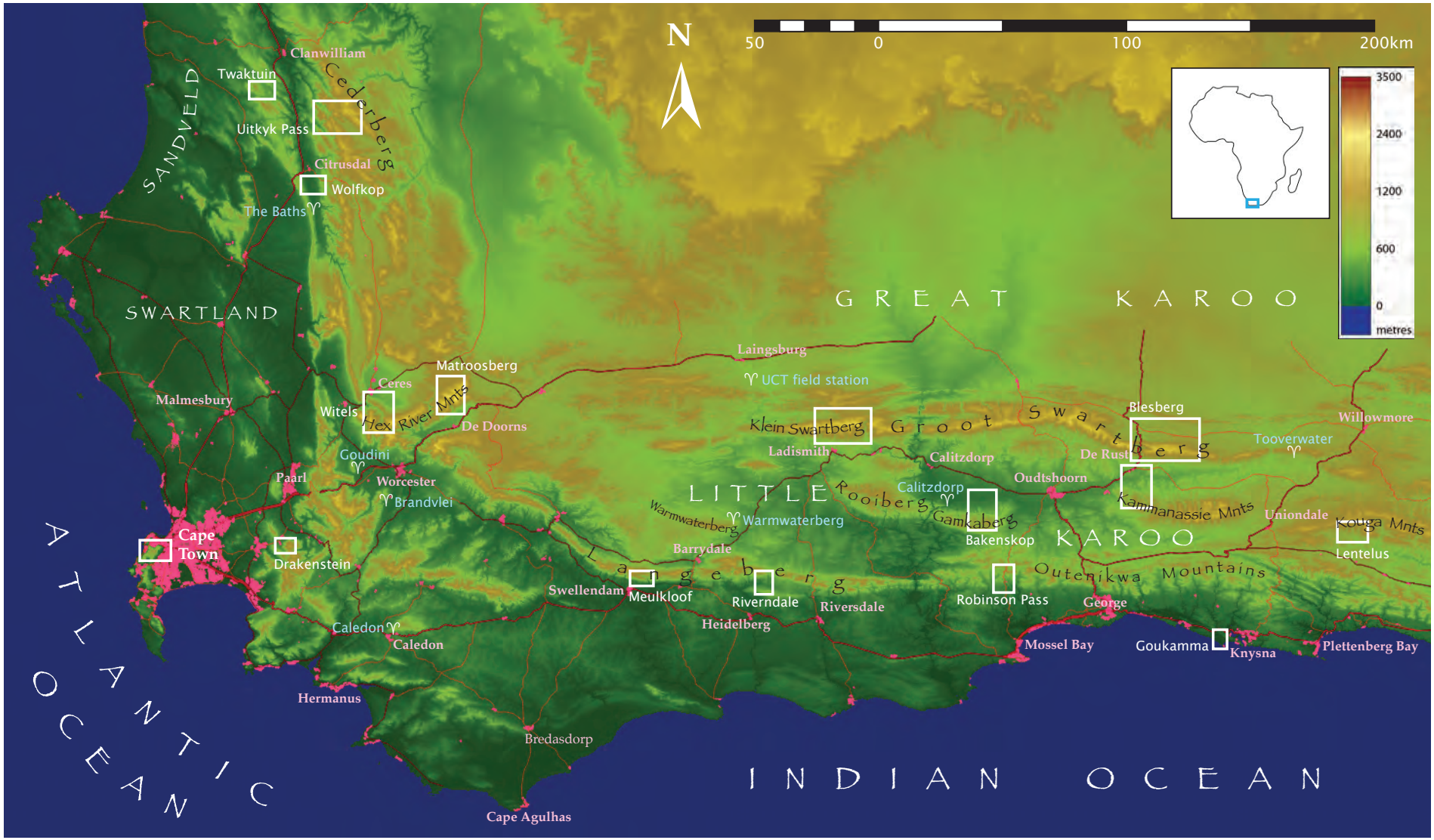

Figure 3.1: Map of the whole study area with white rectangles showing the areas for each of the detailed maps that follow. DEM from NASA (2013) and roads shapefile from NGI (2012).

For the monthly collectors, prevention of evaporation was achieved by use of a long thin plastic tube, as seen in the diagram, although oil was also added to some collectors, but it was found that this was unnecessary, as collectors without oil seemed to yield samples with acceptable isotope compositions. The oil contaminated some samples, but care was taken to avoid getting the oil into the laboratory preparation equipment and as a result, no effect on isotope values was observed. Spikes were placed on top to discourage birds from sitting on the rim and adding non-meteoric contributions to the funnel.

3.2.2 Surface Water

Surface water was collected from five rivers in the Western Cape. The water was collected directly from the surface of the flowing stream, except for one sample collected from the cold bottom water in a deep river pool. The sample locations are also shown in the maps in this chapter.

3.2.3 Groundwater

Groundwater was sampled from both natural sources, springs and seeps, and boreholes. If boreholes were not in frequent use, a short period of purging was done to flush water out from the borehole volume and associated piping and allow true aquifer water to be sampled. Springs and seeps were sampled at or as near as possible to the source, in cases where the spring was capped. The borehole locations are also shown in the maps in this chapter.

3.3 Sample Preparation

3.3.1 Mass Spectrometry

3.3.1.1 Hydrogen Isotopes

Sample preparation for hydrogen isotope analysis was done using established single sample preparation procedures (e.g. Tanweer et al., 1988; Schimmelman and DeNiro, 1993). The procedure starts by loading 100 mg ($\pm$3 mg) of Indiana zinc shavings into a glass tube of 3 mm internal diameter which was heated with a hot air gun under vacuum to degas the zinc, removed from vacuum and allowed to cool down before a 2 μL microcapillary pipette containing the sample water was dropped into the glass tube. The tube was then placed back on the vacuum line and evacuated after the sample had been frozen with liquid nitrogen, then sealed with an oxygen-propane flame; see **Figure 3.3**. The glass tube was then loaded into a furnace and baked at 450 °C for 30 minutes, allowing the following reaction to take place:

$$Zn + 2H_2O \rightarrow ZnO_2 + 2H_2 \quad .$$

This glass tube could then be loaded into the mass spectrometer to allow for analysis of the hydrogen gas.

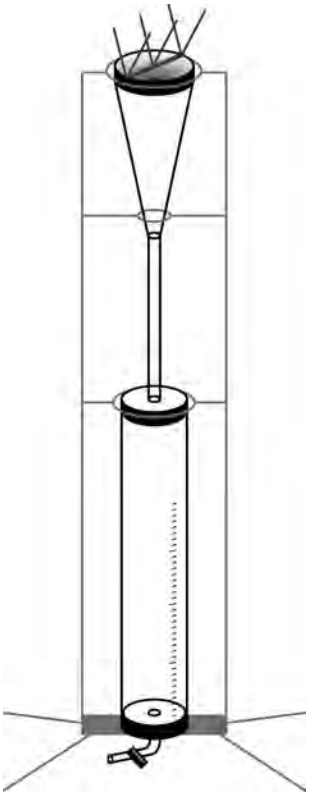

Figure 3.2: Cumulative rainfall collector, designed to collect rain for one month and prevent significant evaporation until collection.

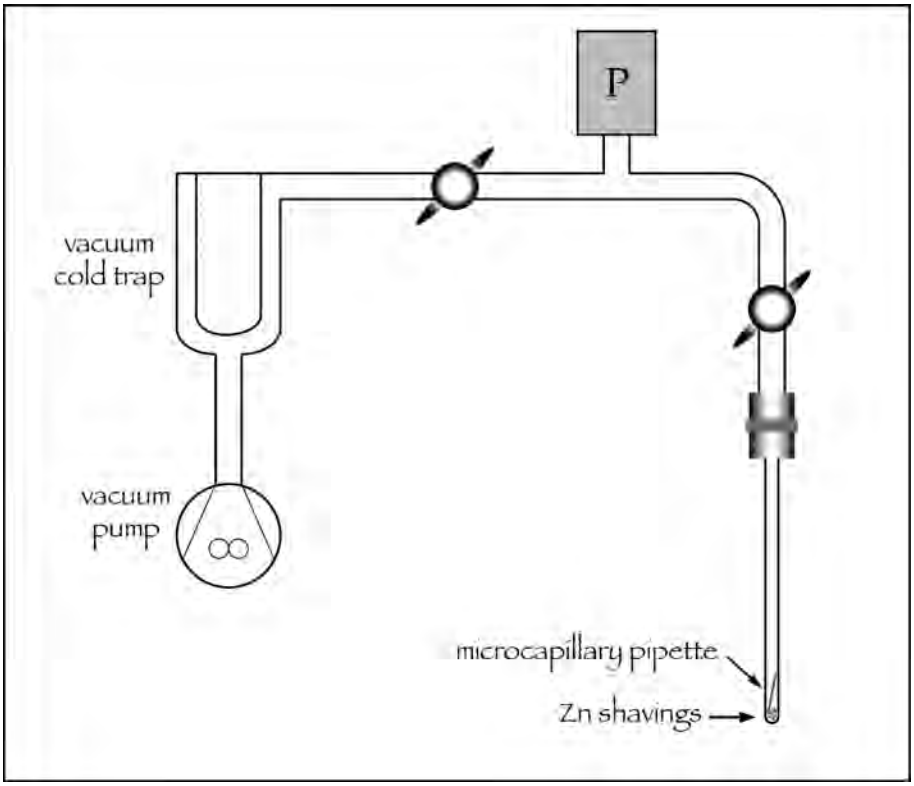

Figure 3.3: Vacuum line for preparing water samples for hydrogen isotope analysis.

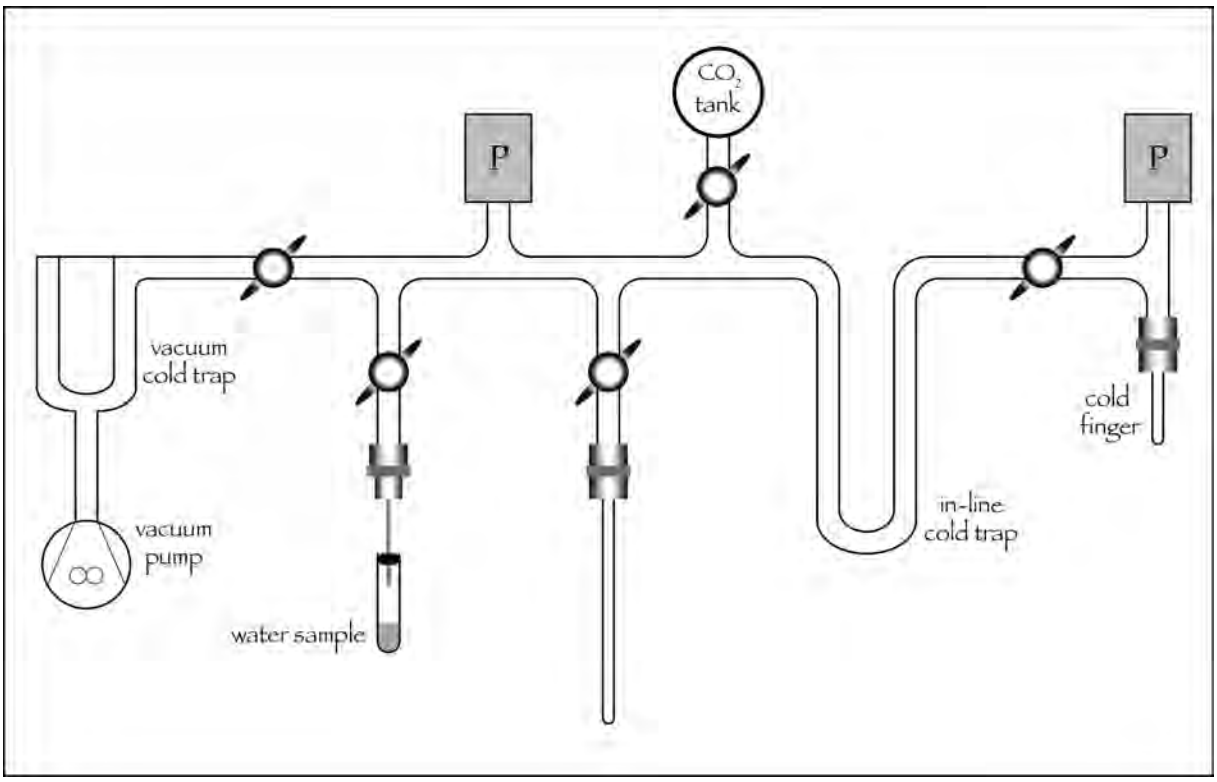

Figure 3.4: Vacuum line for preparing water samples for oxygen isotope analysis.

3.3.1.2 Oxygen Isotopes

Sample preparation for oxygen isotope analysis was done by the method of equilibrating sample water with CO_2 and analysing this, as described in Socki et al. (1992), based on that of previous workers, such as Epstein and Mayeda (1953). The method entailed injecting 2 mL of sample water into a 7 mL sealed plastic vial (vacutainer) that had been evacuated and then loaded with $\frac{1}{3}$ atm of CO_2. The vial was then submerged in a 25 °C water bath and agitated for 2 hours to allow oxygen exchange between the H_2O and CO_2 to reach equilibrium. Then the vial was placed onto the vacuum line and submerged in liquid nitrogen to freeze the H_2O and CO_2. Once frozen, the vial was opened to the vacuum to evacuate any gases. The liquid nitrogen was then moved to the in-line vacuum trap and nearly frozen 2-propanol (isopropyl alcohol) was placed around the vial to retain the ice but liberate the CO_2 as gas. Once all the CO_2 had frozen at the in-line cold trap, the vial was closed off from the vacuum line and the vacuum was opened again to remove any unwanted gases. After closing the valve to the vacuum pump, the liquid nitrogen was moved to the cold finger and the 2-propanol to the cold trap, to transfer the CO_2 where it could be measured with a pressure gauge. Unwanted gases can again be pumped away to vacuum in this step. Finally the CO_2 was frozen into a glass tube using liquid nitrogen, and flamed closed with an oxygen-propane torch.

For both hydrogen and oxygen isotope preparation, each batch of samples was accompanied by 2 laboratory standards, both duplicated. The two standards were initially CTMP2010, which

standard		$\delta D_{(SMOW)}$ (‰)	$\delta^{18}O_{(SMOW)}$ (‰)
CTMP2010	Cape Town Millipore Water 2010	-7.4	-2.69
ACTMP	Adam's CTMP2010	+1.6	-0.60
Evian	Evian bottled water	-70	-10.0
EvianA	Adam's Evian	-71.7	-10.20
RMW	Rocky Mountain Water	-129.5	-17.27

Table 3.2: Delta values for the various internal standards used in this study.

stands for Cape Town Millipore Water and is filtered 2010 University of Cape Town tap water and Evian bottled spring water, from the Alps. Later during the study, Evian was replaced with a more isotopically depleted water, RMW, which stands for Rocky Mountain Water, bottled spring water with a source in the American Rocky Mountains.

3.3.2 Laser Cavity Ringdown Spectroscopy

No sample preparation is generally needed for this method. One millilitre of sample water is injected into a vial which is capped with a septum and then put into an automated sample loading tray. Hydrogen and oxygen isotopes are analysed simultaneously. Only samples with traces of oil or other dirt were injected through a micropore filter to remove the contaminants.

Sample runs using this method made use of 3 standards: ACTMP (Adam's CTMP), EvianA (Evian Adam's) and RMW, reflecting the use of Adam West's laboratory in the Botany Department at the University of Cape Town.

3.4 Sample Analysis and Data Correction

3.4.1 Mass Spectrometry

A 2004 Thermo Corporation Delta Plus XP stable light isotope ratio mass spectrometer was used for conventional dual inlet analysis of hydrogen and oxygen isotope ratios at separate times. The machine was set to make 4 and 6 measurements of the δ value of the sample relative to the reference gas for H_2 and CO_2, respectively. Over years of experience it was found that the machine precision for hydrogen was better than the preparation procedure and so making more than 4 measurements would not improve overall accuracy. For CO_2 however, a slight memory effect seemed to occur as the first measurement was often slightly different from the other five, and the preparation procedure precision was slightly better, so 6 measurements resulted in the optimal balance between accuracy and time for analysis.

Each time the machine was switched over from hydrogen to carbon dioxide, a peak optimisation or focus procedure was performed, in which the ion source and other beam parameters were adjusted to reduce H_3 production and focus the beam squarely into the collector cups. This was

followed by an H_3-factor correction for the molecules of H_3 produced in the ion source, which interfere with the measurement of HD.

Data from the mass spectrometer were corrected using the following method. The first correction applied was for fractionation of oxygen between H_2O_l and CO_2, which at 25 °C has a fractionation factor of 1.0412. This equates to the CO_2 being 40.37 ‰ heavier than the water, once equilibrated. Then a correction was applied for the difference between the reference gas and SMOW. Finally, the sample values were adjusted by correcting the two laboratory standards (CTMP2010 and RMW) to their known values and applying the same correction to the samples. This was done by assuming the error between the measured and actual values varies linearly and therefore a straight line equation can be found that will transform the two standards from their measured values to their actual values, as shown in **Figure 3.5**.

The equation for a straight line is:

$$y = mx + c$$

where **y** is the unknown actual sample value, **m** is the gradient and **c** the intercept of the straight line, and **x** is the measured value of the sample. Both m and c can be calculated individually and the above equation used to calculate the actual sample value, or the equation below can be used to perform the calculation in one step:

$$SAMPLE_{actual} = \left(SAMPLE_{meas} \times \left(\frac{CTMP_{actual} - RMW_{actual}}{CTMP_{meas} - RMW_{meas}} \right) \right) + \left(RMW_{actual} - \left(RMW_{meas} \times \left(\frac{CTMP_{actual} - RMW_{actual}}{CTMP_{meas} - RMW_{meas}} \right) \right) \right)$$

As seen in **Figure 3.5**, a straight line is used to convert measured values (x-axis) to actual values, based on analysis of two standards (RMW and CTMP) of known value. For each analytical run of samples, the straight line will vary in both gradient and intercept. This method replaces the 'shift' and 'stretch' technique commonly used to correct measured values (e.g. Sharp, 2007, p.332).

3.4.2 Laser Cavity Ringdown Spectroscopy

A L2120-i Picarro wavelength scanning cavity ringdown spectrometer was used to analyse for oxygen and hydrogen isotope values simultaneously. Certain wavelengths of infrared light are scanned and the ringdown time is used to calculate the abundance of the various isotopes of oxygen and hydrogen (Lis et al., 2008). Six injections of microlitre amounts of sample were

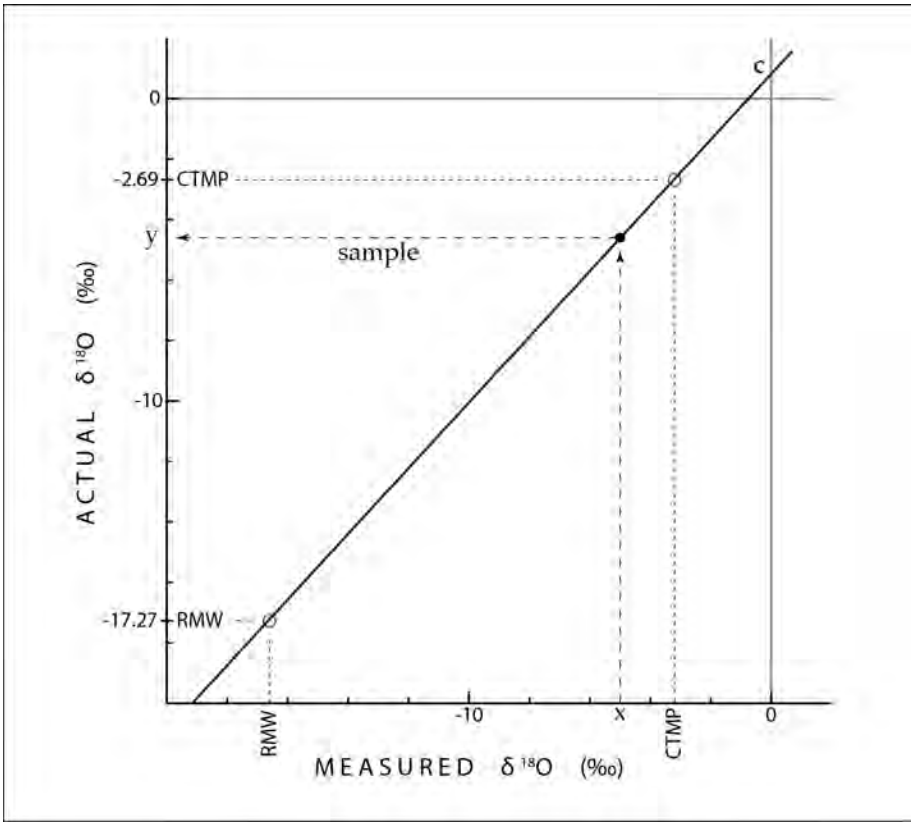

Figure 3.5: The final correction applied to isotope data to correct for instrument drift and laboratory preparation procedure variations. Two standards allow calculation of a straight line equation which is then applied to all the sample data for that run. The example is given for $\delta^{18}O$ but is equally applicable to δD.

made through a septum, vapourised and then transported by N_2 gas into the cavity for analysis. Standards were run at the beginning and end as well as after every ten to twelve samples during a given run. The first two injections show a clear memory effect and these values were discarded, the remaining four being averaged to give an instrument measurement. These instrument measurements were then corrected using the same final correction procedure as shown in **Figure 3.5**. Issues with contaminants, particularly organic compounds such as alcohols, have been noted (West et al., 2010), however, pure water samples tend to give good results. Quality assurance software was used to scan the raw data from the machine and highlight poor analytical indicators (West et al., 2011).

3.4.3 Standards

As shown in **Table 3.2**, several standards were used to correct for laboratory and instrument errors. An analysis of long term laboratory and mass-spectrometer precision can be made by looking at the raw data values for these working standards over time. These values are shown in **Tables 3.3 and 3.4** for δD and $\delta^{18}O$. The latter table shows rather stable values for the three standards, although a small possible drift in CTMP2010 from more to less negative values appears to occur over time. This is likely to be due to drift in the reference gas for the mass-spectrometer, although it could also be due to a change in the laboratory CO_2 tank or in the CTMP2010 standard. The mean difference in replicates (the two values against each date) is around 0.2 ‰ $\delta^{18}O$ for the three standards, which represents the overall precision of the laboratory preparation procedure and mass-spectrometer analysis.

Table 3.3 reveals substantial drift in the values for the three standards, although the period over which Evian was analysed is a bit short. Changes in hydrogen analysis results could be due to several factors. As with oxygen (carbon dioxide) analysis, there could be drift in the reference gas and in the working standards. The zinc used was changed around mid-2012, from batch S83B4 to S38r, and this in fact coincides with substantial changes in values. The 31-05-2012 sample run was the first with the new batch of zinc, the 08-08-2012 and 15-08-2012 again used the old batch, and from 20-08-2012 thereafter the new zinc was used. It can be seen that these changes coincide with the big changes in values. With this in mind, the drift in working standards appears reasonable. More importantly for precision, the mean difference in replicates can be seen to be a little over 1 ‰, which is assurance of the reliability of the preparation and analytical procedures.

The Picarro LASER instrument was only used twice, so no meaningful statements can be made about long term precision. Aside from the working standards, certain samples were run through the LASER and mass-spectrometer methods and the results were found to be similar, with approximately the same level of precision between instruments as within, as reported above.

The final correction procedure, making use of these measured values and adjusting them and the samples for each run to the known values, was able to produce data of acceptable accuracy.

δD ‰						
date	**CTMP2010**		**Evian**		**RMW**	
28-03-2011	-15.1	-12.8	-75.8	-76.0		
12-04-2011			-68.9	-70.2		
27-05-2011	-15.4	-13.3	-69.6	-67.2		
01-06-2011	-12.1	-9.8	-67.2	-59.7		
17-06-2011	-11.4	-11.3	-67.2	-70.3		
30-06-2011	-4.5	-0.6	-58.9	-59.2		
18-10-2011	-9.1	-12.2			-125.6	-125.7
13-12-2011	-4.1	-1.8			-119.6	-119.5
19-12-2011	-1.0	-1.1			-119.2	-119.1
03-02-2012	-2.0	-2.6			-115.8	-116.4
24-05-2012	-1.7	+0.4			-114.6	-115.2
31-05-2012	+9.0	+9.7			-104.6	-105.6
08-08-2012	-2.2	-3.0			-120.1	-121.6
15-08-2012	-0.7	-3.0			-122.9	-120.8
20-08-2012	+6.9	+6.3			-115.3	-116.0
04-10-2012	+12.9	+12.2			-98.0	-98.7
05-11-2012	+9.4	+7.9			-108.2	-108.0
21-02-2013	+8.7	+8.0			-105.0	104.2
03-04-2013	+11.5	+12.8			-100.0	-98.7
05-04-2013	+10.0	+9.9			-101.7	-102.2
02-05-2014	+7.8	-7.1			-107.6	-105.2
mean		-0.0075		-67.6		-111.8
maximum — minimum	+12.9 — -15.4		-58.9 — -76.0		-98.0 — -125.7	
standard deviation		8.9		5.7		8.7
mean difference		1.4		2.3		0.85
difference std. dev.		1.1		2.8		0.71

Table 3.3: Raw data for δD analyses of standards during this project. The values above are the mass-spectrometer values with the zinc correction applied.

$\delta^{18}O$ ‰						
date	**CTMP2010**		**Evian**		**RMW**	
15-03-2011	-4.46	-4.56	-10.5	-10.2		
12-04-2011			-10.44	-10.40		
26-05-2011	-5.75	-4.11	-9.76	-10.18		
02-06-2011	-4.10	-3.40	-9.65	-9.62		
07-06-2011	-3.27	-3.12				
20-06-2011	-3.48	-3.30	-9.61	-9.53		
07-07-2011	-3.63	-3.55	-9.61	-9.67		
01-08-2011		-2.54		-9.31		
03-08.2011		-4.25		-10.21		
04-08-2011		-3.86		-10.10		
12-08-2011		-3.63			-17.44	-17.59
24-10-2011		-3.61			-17.58	-17.77
21-12-2011	-3.53	-3.63			-17.50	-17.54
11-01-2012	-3.40	-3.09			-17.46	-17.61
01-02-2012	-4.58	-3.71			-17.56	-17.68
21-05-2012	-4.27	-4.16			-17.47	-18.09
28-05-2012		-3.63				-17.49
18-06-2012	-3.60	-3.80			-17.94	-18.45
18-07-2012	-3.62	-3.40			-17.82	-17.76
19-07-2012	-3.73	-3.68			-17.98	-17.86
23-07-2012	-4.04	-3.96			-17.57	-17.51
01-08-2012	-3.55	-3.67			-17.62	-17.51
10-10-2012	-4.57	-3.93				-17.27
11-10-2012	-3.42	-3.38			-17.61	-17.74
15-10-2012	-3.97	-3.82			-17.77	-17.83
06-11-2012	-3.67	-3.45			-17.44	-17.50
08-11-2012	-3.43	-3.49			-17.60	-18.47
19-02-2013	-3.18	-3.34			-17.56	-17.36
26-03-2013	-3.71	-3.35			-17.34	-17.42
27-03-2013	-3.41	-3.03			-17.13	-17.16
28-03-2013	-3.11	-3.05			-17.27	-17.36
04-04-2013	-2.92	-3.11				-17.01
02-05-2014	-3.42	-3.43			-17.19	-17.22
mean		-3.65		-9.92		-17.58
maximum — minimum	-2.54 — -5.75		-9.31 — -10.50		-17.01 — -18.47	
standard deviation		0.51		0.38		0.30
mean difference		0.28		0.15		0.18
difference std. dev.		0.35		0.16		0.22

Table 3.4: Raw data for $\delta^{18}O$ analyses of standards. The values above are the mass-spectrometer values with the reference gas and $CO_2 - H_2O$ equilibration corrections applied.

3.5 Data Analysis

A substantial portion of the analysis of stable isotope data consists of finding correlations and calculating regressions. The most common regression analysis is known as the *least squares method*. This assumes the x-variable is independent and accurately known, whereas the y-variable depends upon the x-value and has errors and random variations. An example of an independent x-variable would be time or distance, and a dependent y-variable could be temperature, rainfall or an isotope ratio. For analysis of one stable isotope ratio, say δD against one of these independent variables, the *least squares regression* is suitable. However, where both variables are dependent, such as δD and $\delta^{18}O$, no one should be treated as more certain than the other and so the *reduced major axis* form of a structural regression is suitable.

Least Squares Regression

To calculate a straight line of the form:

$$y = mx + c\,,$$

using the least squares regression:

$$\begin{aligned} m &= \frac{SP_{xy}}{SS_x} \\ \text{and} \quad c &= \bar{y} - m\bar{x}\,, \\ \text{where} \quad SS_x &= \sum_{i=1}^{n}(x_i - \bar{x})^2 \\ \text{and} \quad SP_{xy} &= \sum_{i=1}^{n}(x_i - \bar{x})(y_i - \bar{y})\,. \end{aligned}$$

Reduced Major Axis Regression

The RMA regression line is calculated in a similar way to above, with the single difference that the gradient, m, is calculated as follows:

$$\begin{aligned} m &= \sqrt{\frac{SS_y}{SS_x}} \\ \text{where} \quad SS_y &= \sum_{i=1}^{n}(y_i - \bar{y})^2\,. \end{aligned}$$

Weighted Regression Line Calculations

As noted by Hughes and Crawford (2012), weighting of isotopic values for monthly cumulative

rainfall by the rainfall amount produces regression lines (meteoric water lines) with higher gradients, as a result of minimising the influence of evaporated samples from low rainfall events. The difference in gradient between weighted and unweighted regression lines depends on the dataset. These meteoric water lines better characterise the average rainfall and especially heavier events that are more likely to play an important role in hydrological processes such as groundwater recharge. Calculation of such regressions uses methods similar to above, but by adding the rainfall term into the statistical quantities as follows:

$$SS_x = \sum_{i=1}^{n} (rain_i)(x_i - \bar{x})^2 \ ,$$
$$SS_y = \sum_{i=1}^{n} (rain_i)(y_i - \bar{y})^2 \ ,$$
$$SP_{xy} = \sum_{i=1}^{n} (rain_i)(x_i - \bar{x})(y_i - \bar{y}) \ .$$

3.6 Maps

The maps that follow were prepared using the QGIS programme with shapefiles of 1:50 000 tile data from the Chief Directorate for National Geo-Spatial Information of the South African Department of Rural Development & Land Reform. Dotted grey circles around some sampling sites are 5 km radius circles and will be mentioned in the Discussion chapter.

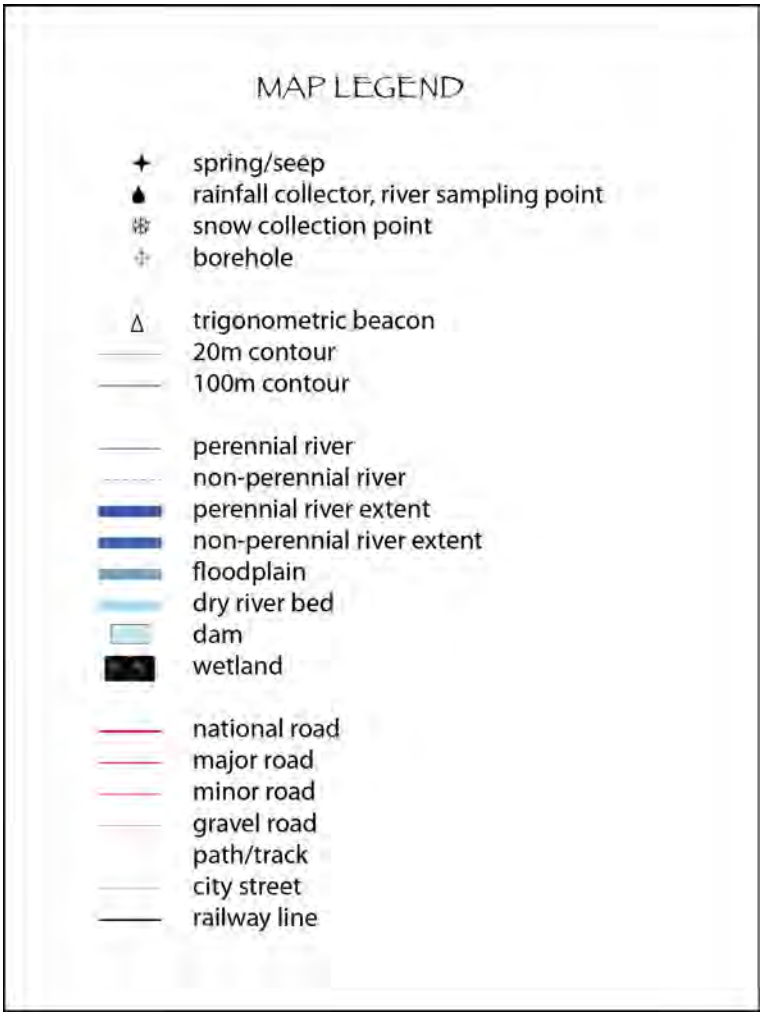

Figure 3.6: Legend for the location maps.

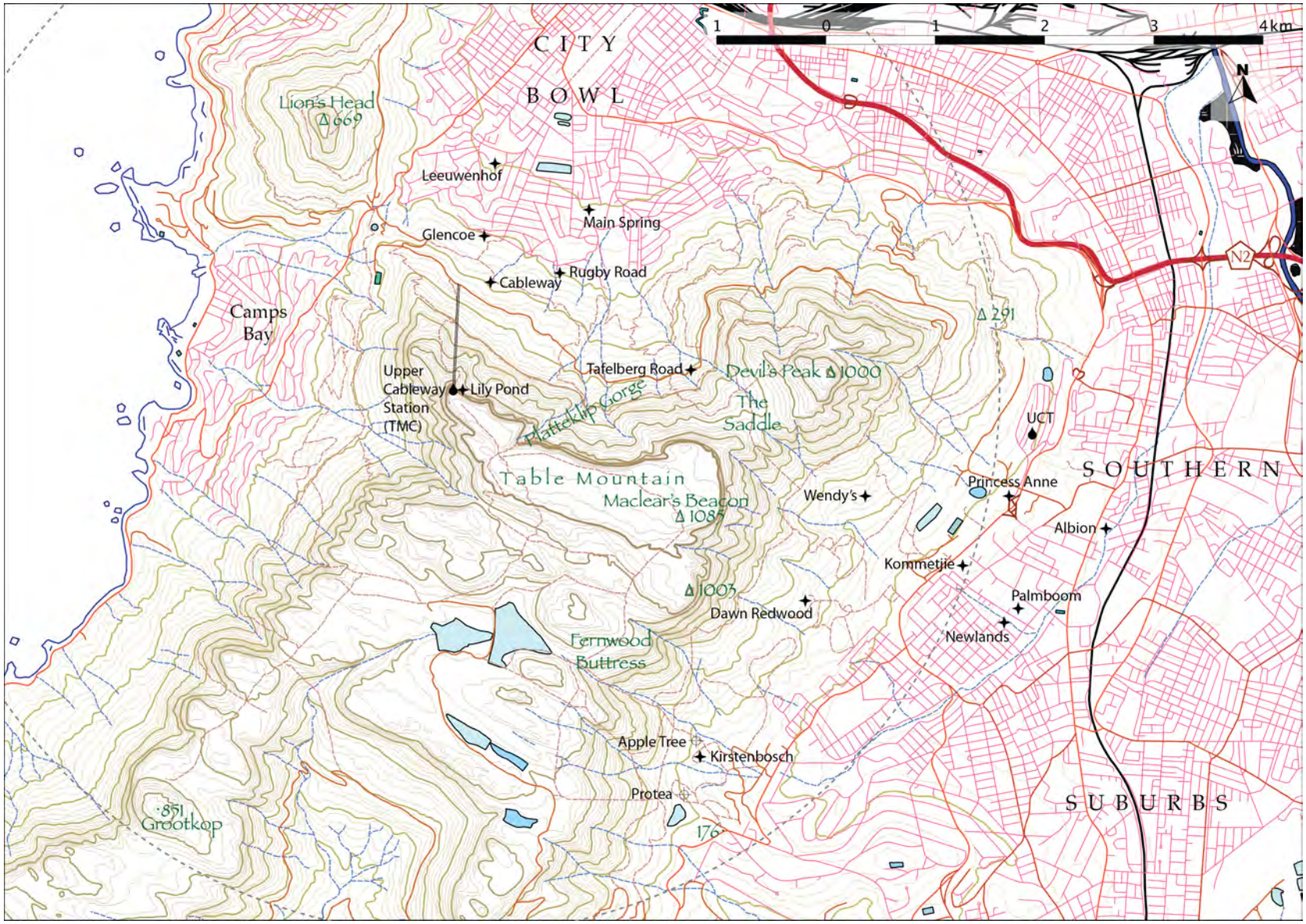

Figure 3.7: Locations of sampling points in the Cape Town area.

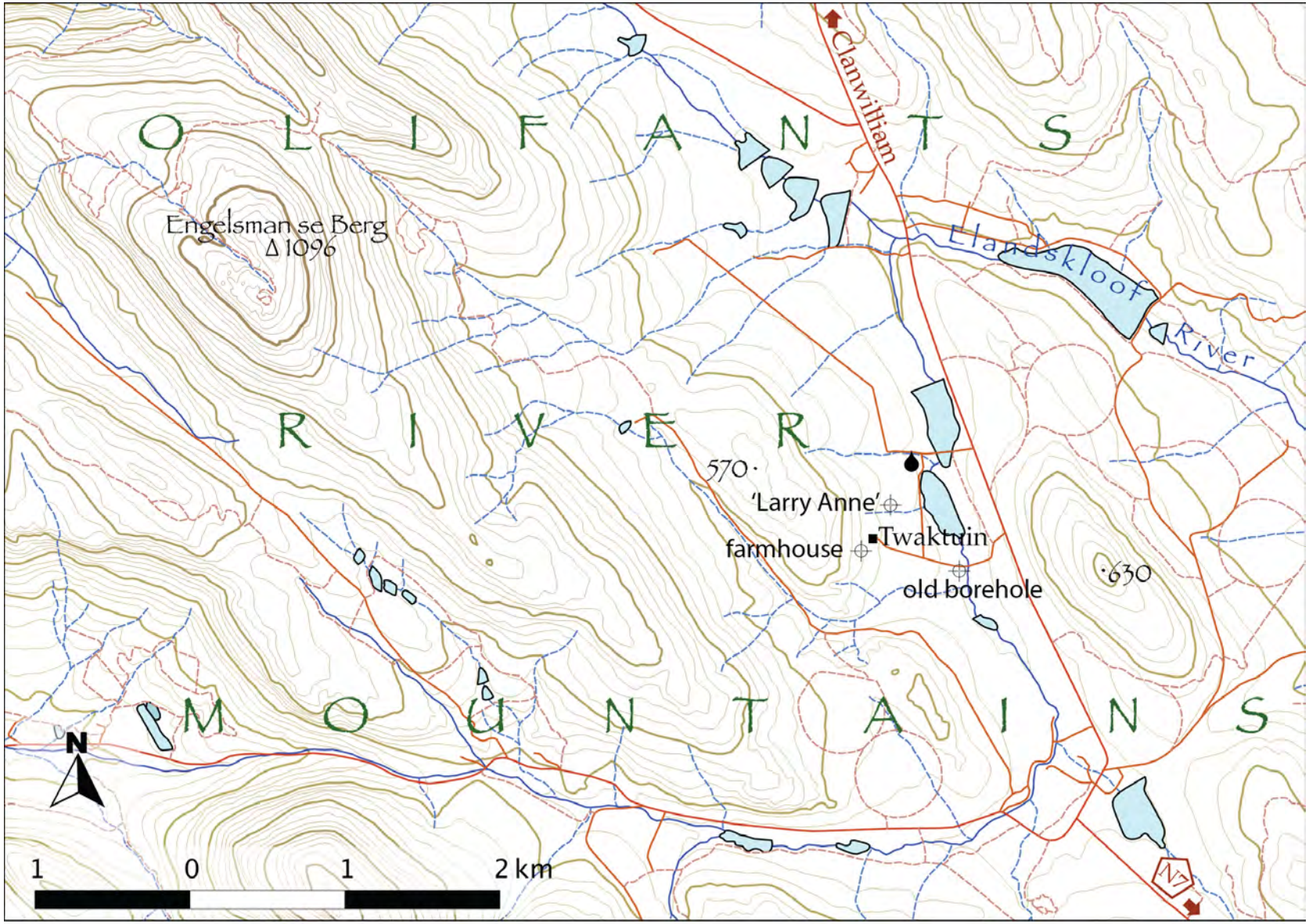

Figure 3.8: Locations of the rainfall collector and three boreholes sampled on Twaktuin Farm, south-west of Clanwilliam.

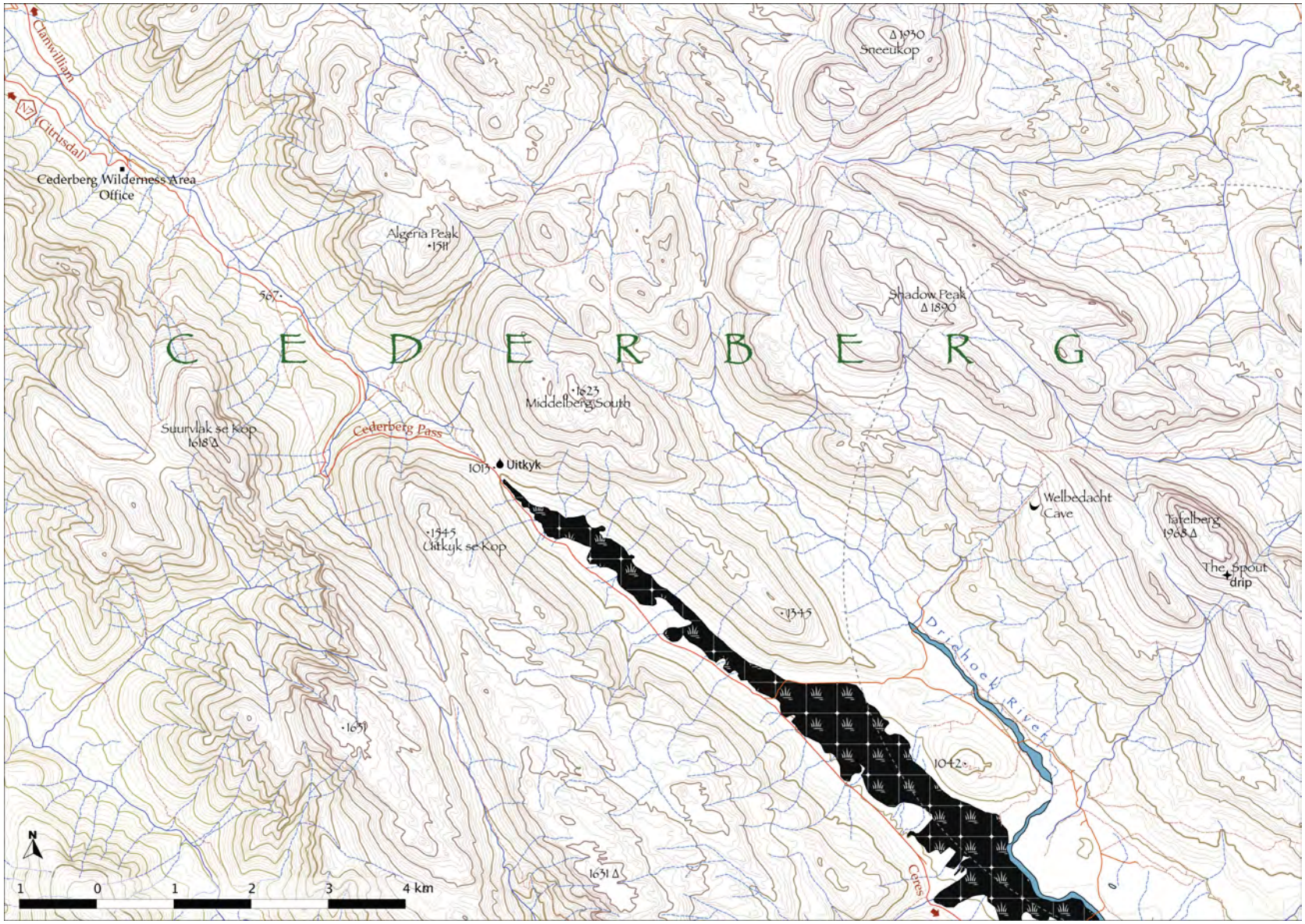

Figure 3.9: Locations of the rainfall collector and high altitude seep sampled in the Cederberg, south-east of Clanwilliam.

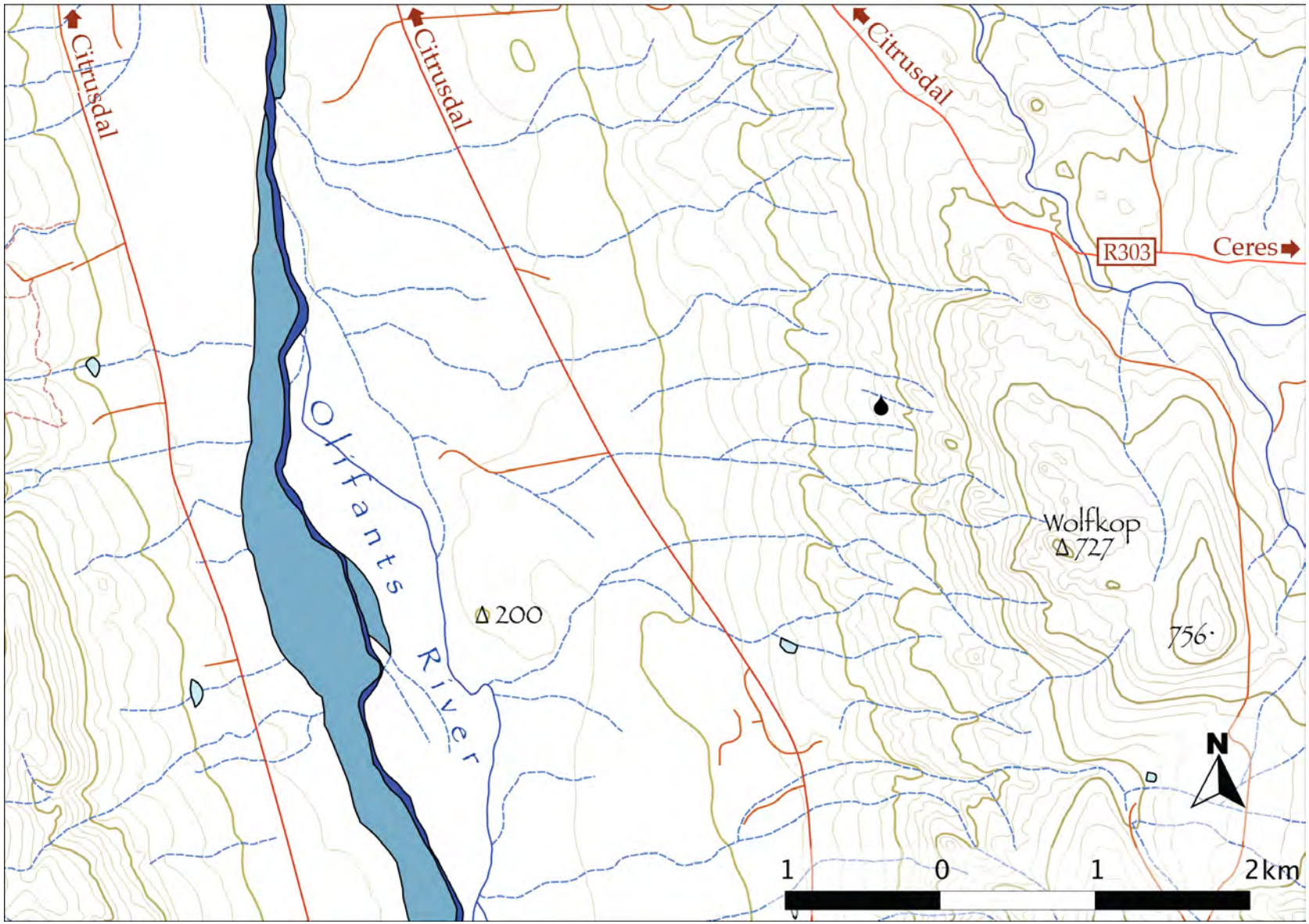

Figure 3.10: Location of the rainfall collector at Wolfkop Nature Reserve, south of Citrusdal.

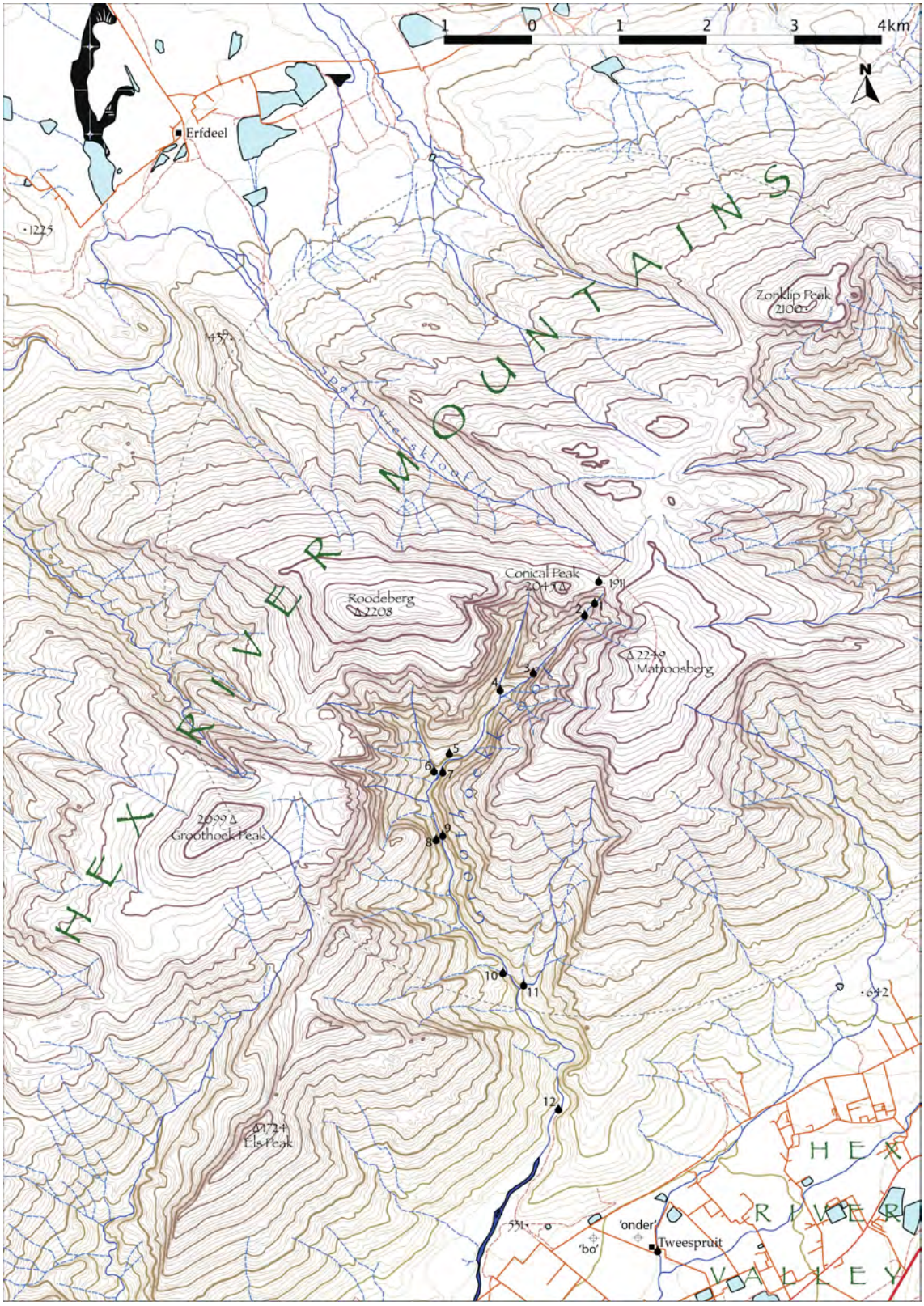

Figure 3.11: Locations of the Erfdeel and Tweespruit rainfall collectors and boreholes and the Groothoekkloof river samples in the vicinity of Matroosberg, the highest peak in the south-western Cape.

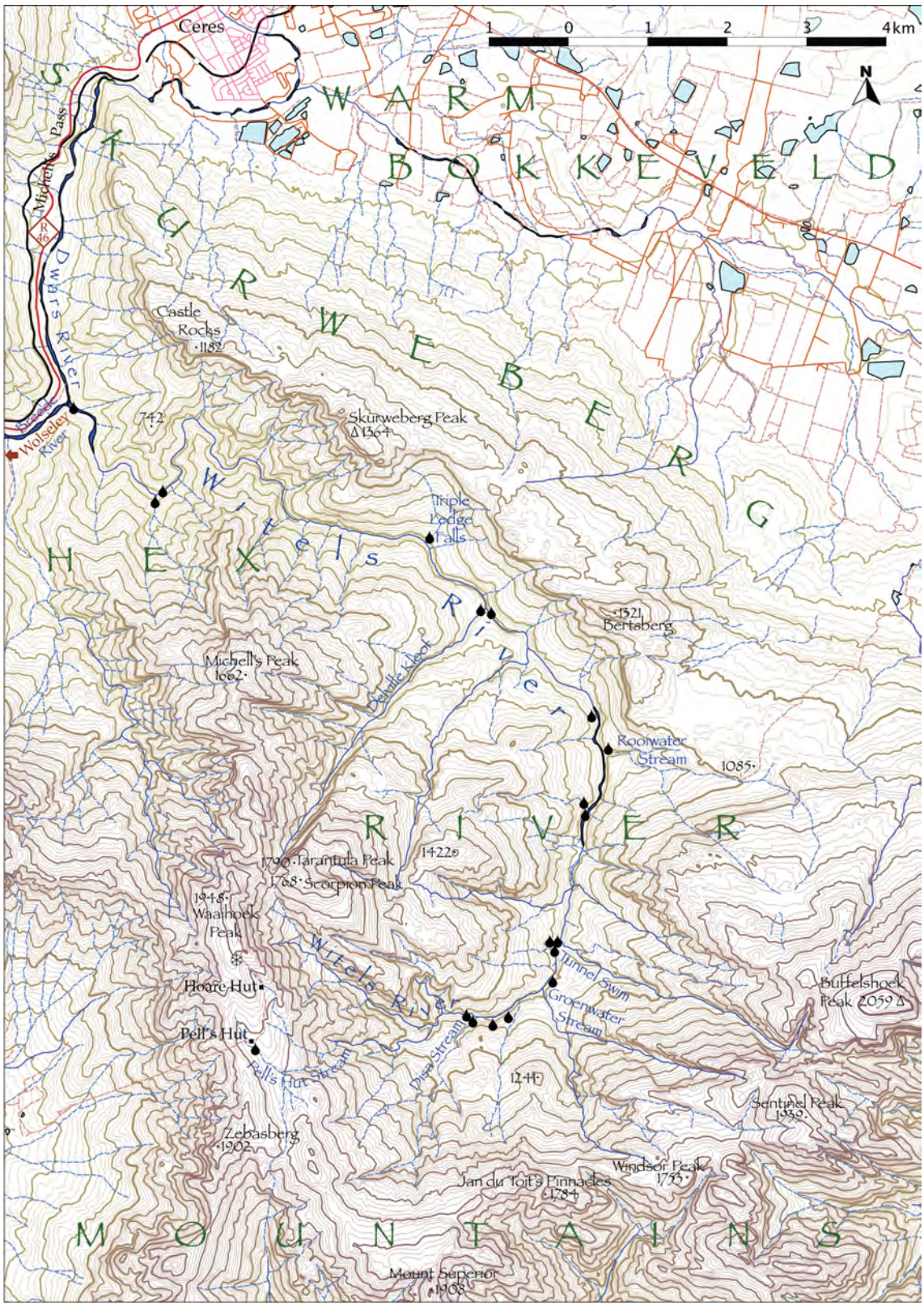

Figure 3.12: Locations of the Waaihoek Peak snow and Witels River samples taken in the Hex River Mountains, south of Ceres.

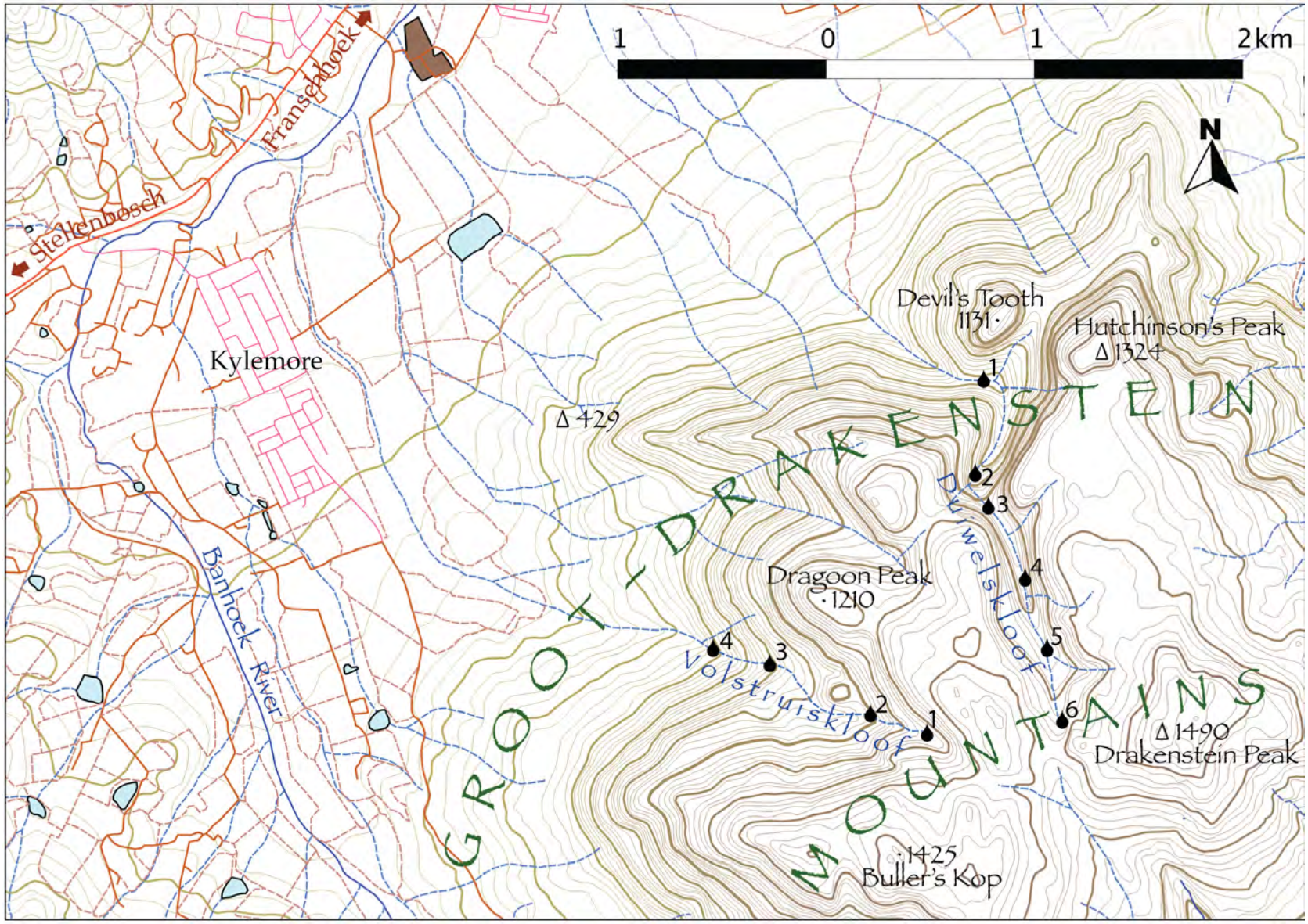

Figure 3.13: Locations of the Duiwelskloof and Volstruiskloof river samples taken in the Groot Drakenstein Mountains, east of Stellenbosch.

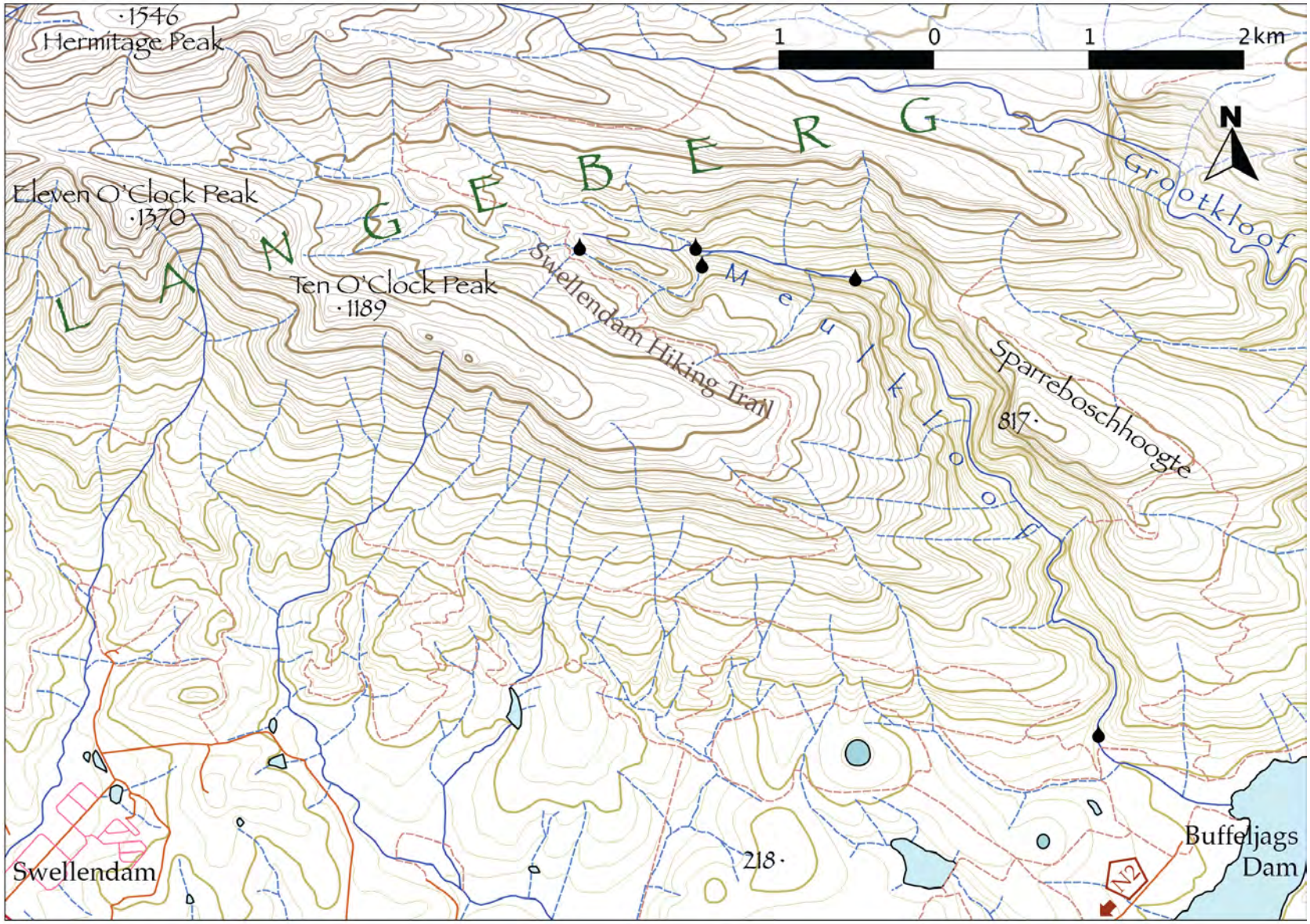

Figure 3.14: Locations of the Meulkloof river samples taken in the Langeberg, east of Swellendam.

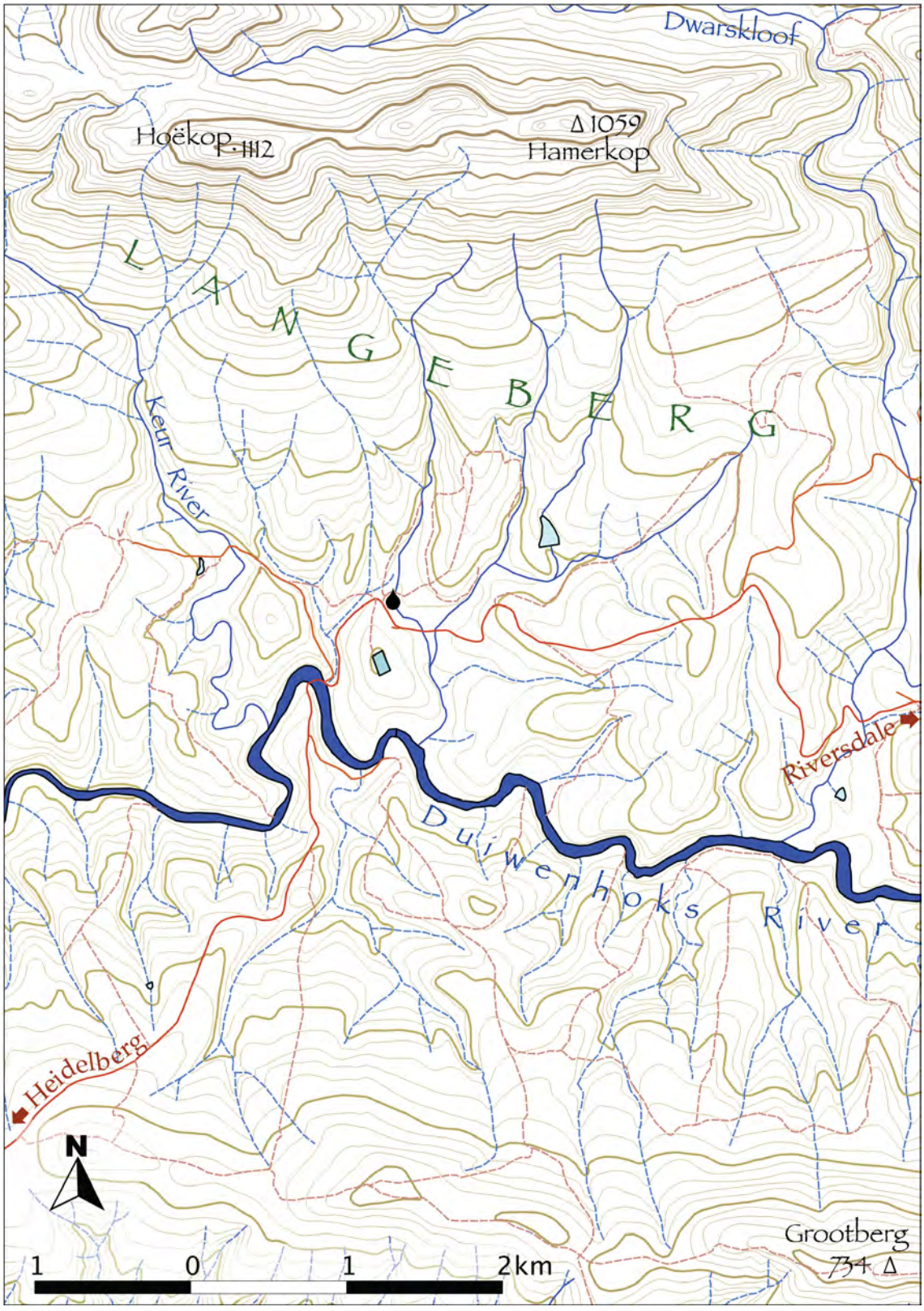

Figure 3.15: Location of the Riverndale rainfall collector, north of Heidelberg.

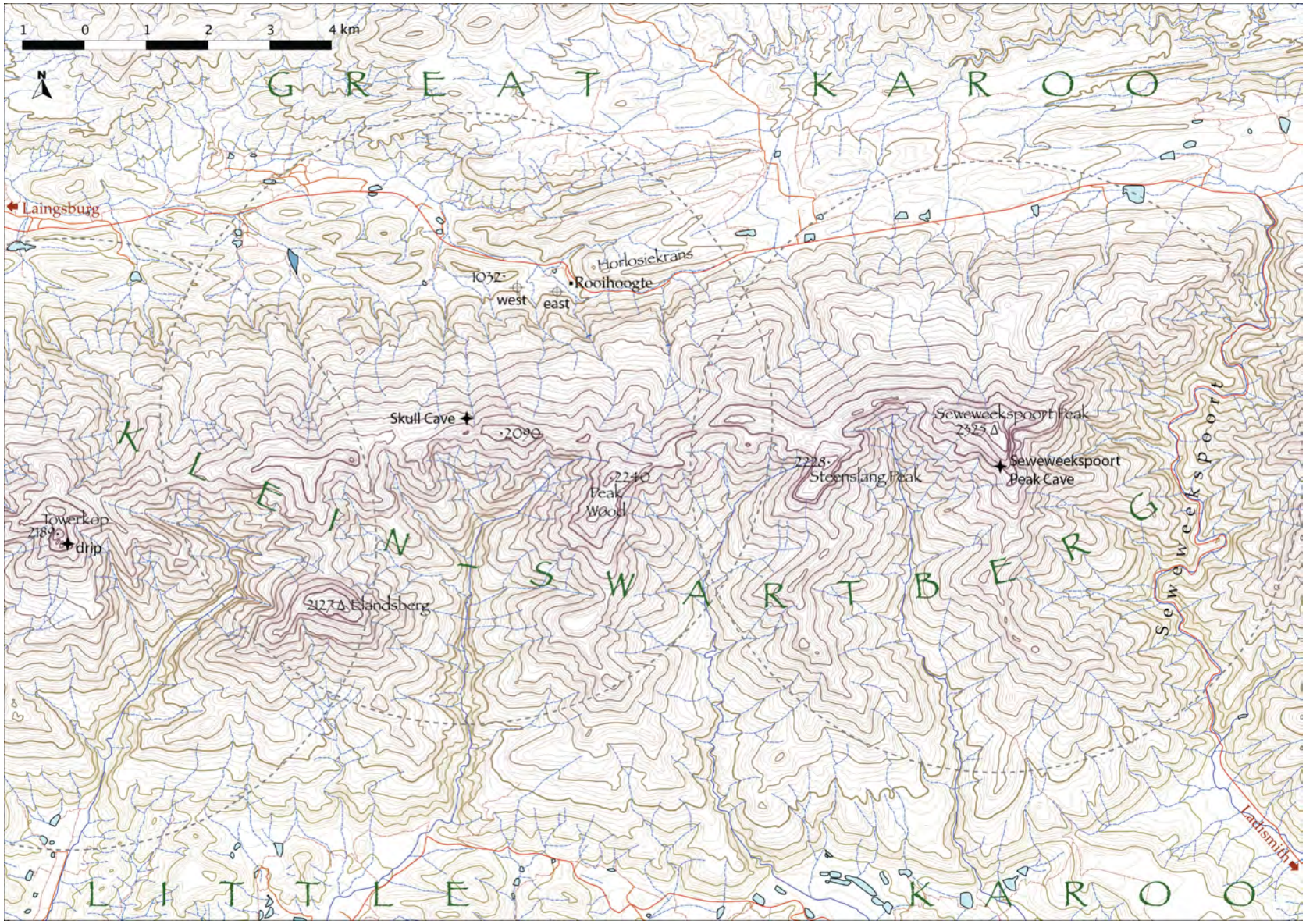

Figure 3.16: Locations of high altitude seeps in the Klein Swartberg and boreholes on Rooihoogte Farm.

Figure 3.17: Locations of the Bakenskop mountain and the store rainfall collectors as well as the boreholes at Gamkaberg, south-east of Calitzdorp.

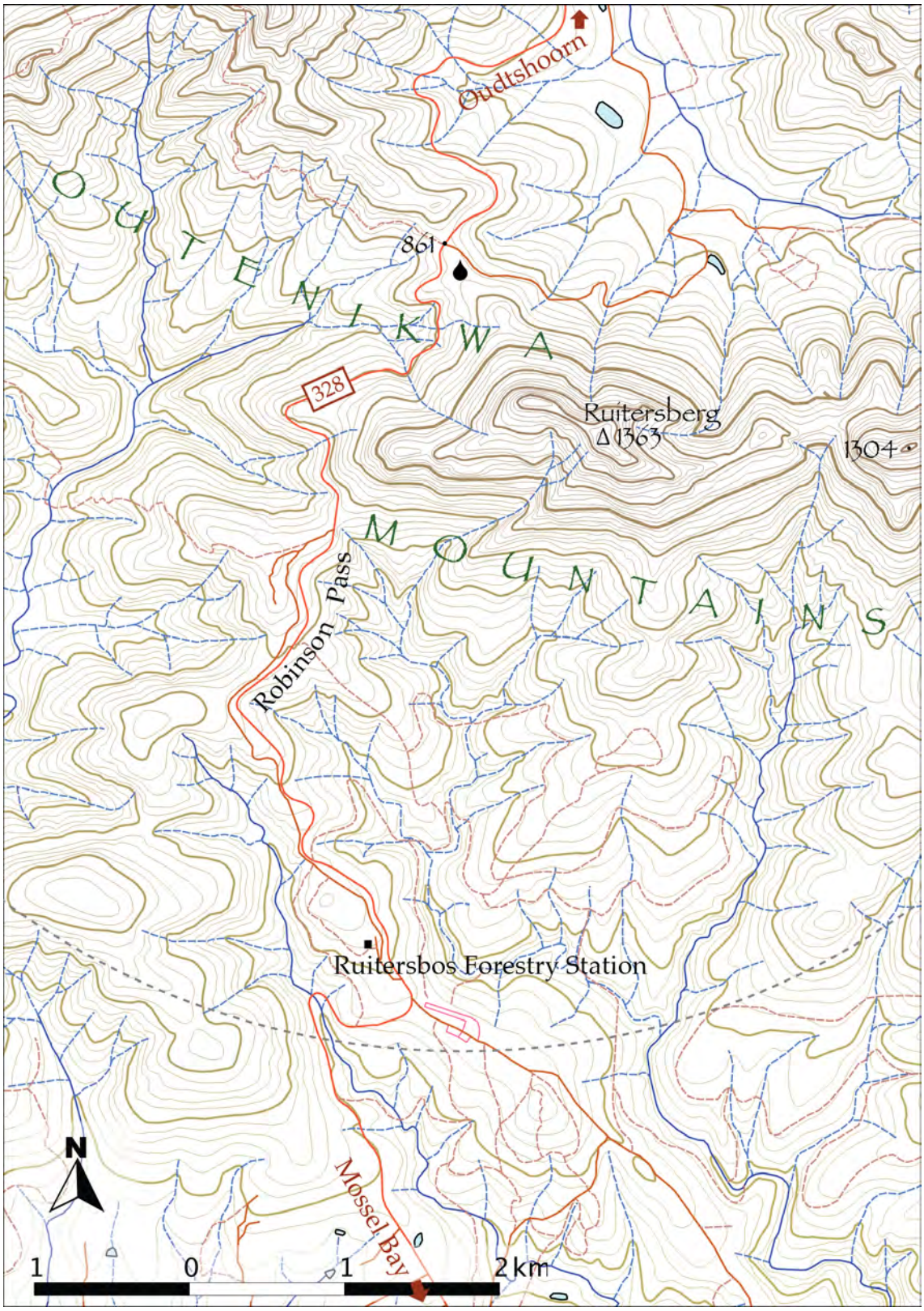

Figure 3.18: Location of the rainfall collector on Robinson Pass, north of Mossel Bay.

Figure 3.19: Location of the rainfall collector in the Kammanassie Mountains, south of De Rust.

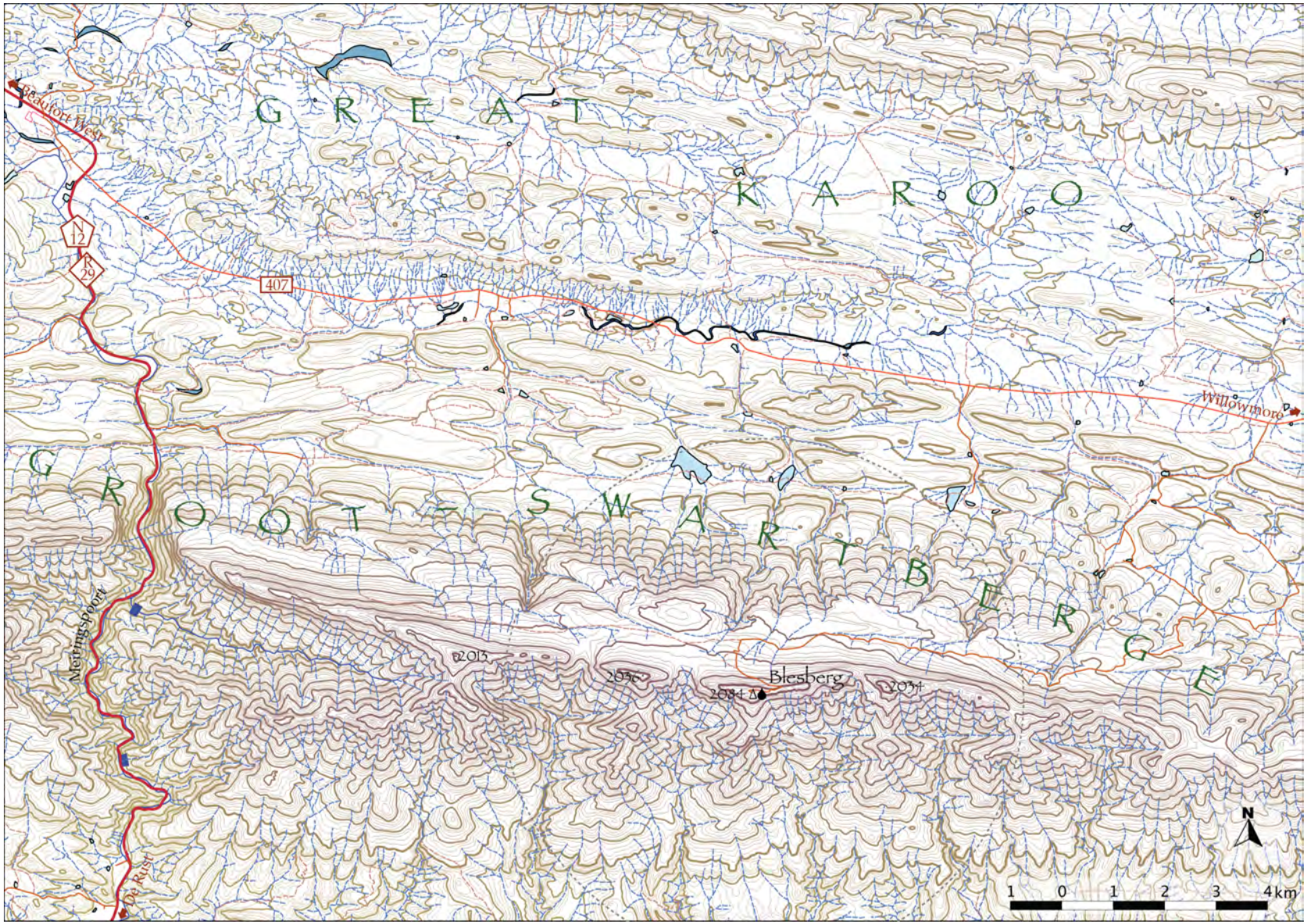

Figure 3.20: Location of the rainfall collector on top of Blesberg in the Groot Swartberg, north-east of De Rust.

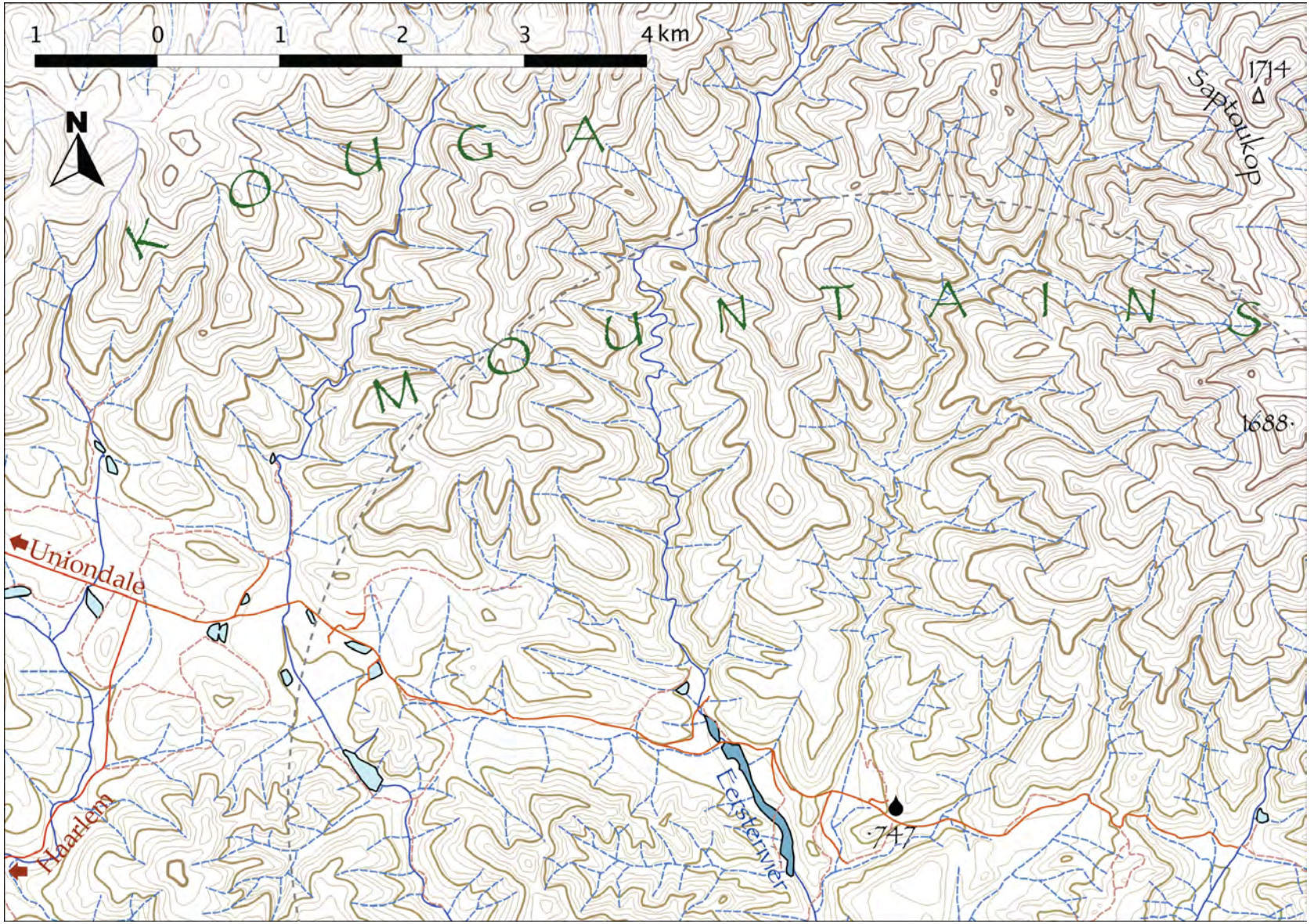

Figure 3.21: Location of the rainfall collector on Lentelus Farm in the Kouga Mountains, south-east of Uniondale.

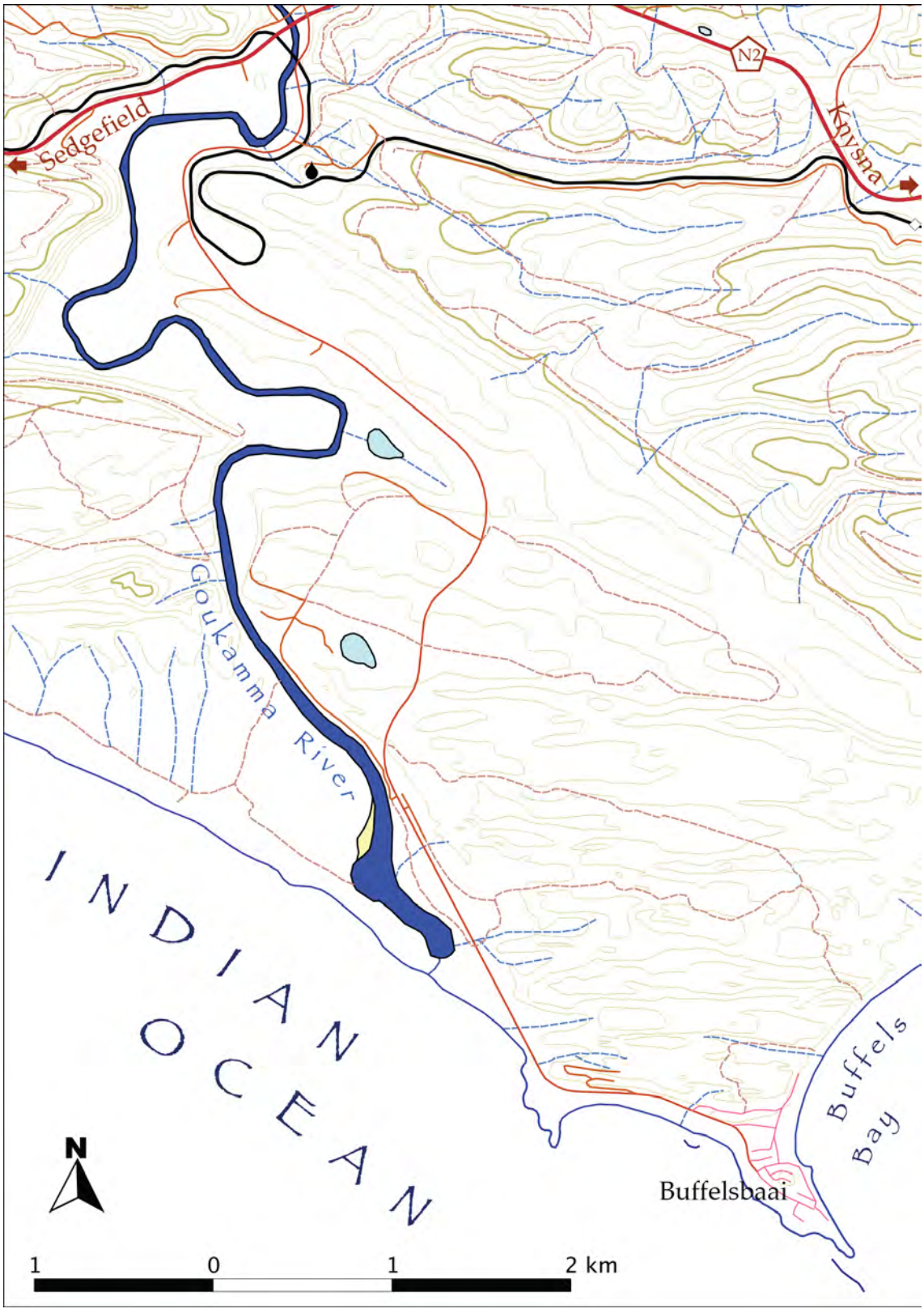

Figure 3.22: Location of the rainfall collector above the Goukamma River, west of Knysna.

Chapter 4

Results

4.1 Introduction

This chapter reports the data collected in this study, namely rainfall amounts and hydrogen and oxygen isotope values of various water samples, including rain, snow, river water and groundwater, the latter from both natural sources such as springs and seeps as well as from boreholes. The rainfall is presented as monthly amounts and some of the notable variations in space and time are described. Isotope data of rainfall is presented over time and compared with weather events to make sense of some of the outlier isotopic compositions. The rain isotope data is also analysed by generating means and weighted means for each rainfall station, d-excess values for these means, and meteoric water lines. Groundwater isotope data and the best-fit line through this data is compared to the rainfall isotope data and meteoric water lines. Mention is also made of other samples, such as surface water and snow. The isotope data for this study is reproduced in **Tables 4.5 to 4.10** at the end of this chapter.

4.2 Rain

In order to understand the hydrological impact of hydrogen and oxygen isotope ratios in monthly cumulative rainfall samples, the amount of rain for each month must be known. Isotope values from months with high rainfall have a greater effect on the isotope signatures in the hydrological cycle than months with low rainfall and therefore the isotope values need to be weighted accordingly when calculating means and meteoric water line equations. All the regular rainfall samples taken for this study are shown in **Table 4.1**.

	2010												2011												2012											
stn.	J	F	M	A	M	J	J	A	S	O	N	D	J	F	M	A	M	J	J	A	S	O	N	D	J	F	M	A	M	J	J	A	S	O	N	D
UCT	–	–	–	–	–	–	–	–	–	–	–	–	–	–	–	–	–	–	–	–	–	–	–	–	–	–	–	–	–	–	–	–	–	–	–	–
TMC					–	–	–	–	–	–	–	–	–			–	–	–	–	–	–	–	–	–	–	–	–									
TWT					–	–	–	–	–	–	–	–	–	–	–	–	–	–	–	–	–	–	–	–	–	–	–	–	–	–	–	–				
UKP								–	–	–	–	–	–	–	–	–	–	–	–	–		–	–	–	–	–	–	–	–		–	–				
WKP					–	–	–	–	–	–	–	–	–	–	–	–	–	–	–	–	–	–	–	–	–	–	–	–	–	–	–	–				
MTB					–								–	–	–	–	–	–	–	–	–	–	–	–	–										
DDN																		–	–	–	–	–	–	–	–					–					
RVD						–	–	–	–	–	–	–	–	–	–	–	–	–	–	–	–	–	–	–	–	–	–	–								
RBP						–	–	–	–	–	–								–																
BKK						–	–	–	–	–	–					–	–	–	–	–	–	–	–	–											
GST													–	–	–	–	–	–	–	–			–	–	–	–	–	–	–	–	–	–				
BBG						–	–	–	–	–	–	–	–	–	–	–				–	–	–	–			–	–	–	–	–	–					
KMN						–	–	–	–	–	–					–	–	–	–		–														
LTL						–	–	–		–	–		–	–	–	–	–	–	–	–	–	–	–	–	–	–	–								
GKM						–	–	–	–	–	–	–	–	–	–	–	–	–	–	–	–	–	–	–	–	–	–	–	–							

Table 4.1: Bars indicate the months for which total monthly rainfall was analysed for hydrogen and oxygen isotopic composition.

station code and name		elevation	continentality		MAP	SI	n	weighted mean & standard deviation				d-excess
			Atlantic	'sea'				δD	$\sigma_{\delta D}$	$\delta^{18}O$	$\sigma_{\delta^{18}O}$	
		(masl)	(km)	(km)	(mm/a)			‰	‰	‰	‰	‰
UCT	University of Cape Town	135	8	8	1210	0.63	36	-9.2	6.0	-2.89	1.19	14.0
TMC	Table Mountain	1074	3	2	1328	0.43	23	-13.9	5.7	-3.77	1.04	16.3
TWT	Twaktuin	412	48	45	510	0.76	17	-11.4	19.6	-2.96	3.41	12.3
UKP	Uitkyk Pass	1013	70	70	1177	0.81	20	-21.7	9.8	-4.67	2.23	15.6
WKP	Wolfkop	355	72	70	565	0.81	25	-15.9	11.4	-3.82	1.42	14.7
MTB	Matroosberg	1910	143	110	702	0.83	14	-43.1	9.6	-7.95	1.44	20.5
DDN	Tweespruit	482	133	105	213	0.91	6	-19.4	15.8	-3.14	2.09	5.8
RVD	Riverndale	251	242	42	671	0.40	23	-10.3	13.7	-3.44	2.38	17.2
RBP	Robinson Pass	885	330	30	1093	0.47	7	-23.3	11.3	-4.91	2.39	16.0
BKK	Bakenskop	1101	314	50	529	0.46	15	-29.2	12.2	-5.84	2.63	17.5
GST	Gamka Store	350	315	55	297	0.50	15	-15.6	13.5	-3.37	2.76	11.4
BBG	Blesberg	2080	410	65	735	0.50	18	-28.3	8.0	-6.16	1.04	21.0
KMN	Kammanassie	666	482	50	400	0.56	11	-36.3	23.1	-7.37	2.95	22.7
LTL	Lentelus	642	573	35	567	0.51	20	-26.9	20.4	-5.62	3.16	18.1
GKM	Goukamma	62	526	5	701	0.54	25	-14.3	15.3	-3.82	1.98	16.3
	all				713		275	-17.7	14.2	-4.22	2.33	16.0

Table 4.2: Continentality distance from Atlantic Ocean measured along a line of latitude; 'sea' distance is distance in any direction to the closest coast. Mean annual precipitation (MAP) and seasonality index (SI) based on 3 years of rainfall records; stable isotope weighted means and standard deviations using 'n' number of cumulative monthly rainfall samples. Deuterium excess for each station and the region, calculated from the weighted means.

These rainfall amounts should have been recorded when the rain was collected, however, due largely to human error, not all the figures were recorded or retained for each sample. In some cases people collecting rain forgot to record the amount, in other cases, the data was mislaid. However, it was possible to estimate these missing rainfall amounts by interpolation between South African Weather Service stations (SAWS, 2010-12), rainfall stations within this study and by using the SAWS monthly rainfall maps, examples of which are given in **Figure 4.1**. When estimating missing rainfall amounts, consideration was also given to factors known to affect rainfall, in particular the altitude, proximity and leeward or windward relationship to mountains, and distance from the sea.

The resultant rainfall figures, both measured and estimated, for each rainfall collection station are displayed in time series graphs in **Figure 4.14**. The most obvious pattern seen in these graphs is the seasonal signature caused by the higher rainfall occurring in winter from cold fronts (westerly waves) and the subsequent southerly meridional flow, as explained in Chapter 2. The second most noticeable pattern is the change from highly seasonal rain in the west to less seasonal in the east, as discussed below in **Section 4.2.2**.

4.2.1 Rainfall Amount

The average annual rainfall at the rain collection stations is shown in **Table 4.2**. Although this figure is only for three years and for most of the stations is based on many estimations, the averages do illustrate the range of rainfall amounts recorded and some general trends. Stations at higher latitude, altitude and nearer to the sea tend to receive more rain. Other factors, such as proximity to mountains, steepness of slopes and aspect (relative to rain-bearing winds) also influence the rainfall at a site. These were the factors used by Dent et al. (1987) and Beuster et al. (2009) to produce the MAP (mean annual precipitation) map for the south-western Cape, as discussed in Chapter 1.

Examination of the graphs in **Figure 4.14** shows how variable rainfall is across the Western Cape. Rainfall collection stations less than 50 km apart can receive vastly different quantities of rain in a month. For example, in August 2010, Twaktuin recorded 69 mm, Uitkyk Pass 215 mm and Wolfkop 84 mm. These sorts of variations are epitomized by the famous microclimates of Cape Town, as is revealed from the UCT and Table Mountain Cableway stations, less than 5 km apart, where in December 2010 those two stations recorded 17 mm and 60 mm respectively, and similarly for October 2012 with 44 mm and 123 mm. This variation is not always systematic; the generally wetter station may sometimes receive less rain. For example, in February 2011, Lentelus, which averages 80 % of the rainfall of Goukamma, recorded 65 mm in comparison to Goukamma's 39 mm; this is 160 %, or double the expected amount; or one could say that Goukamma was half as wet as would be expected from the Lentelus rainfall. Similarly, in November 2012 UCT recorded 6 0mm in comparison to the normally wetter Table Mountain Cableway's 44 mm.

4.2.2 Rainfall Seasonality

The seasonality index (SI), as described by Walsch and Lawler (1981), has been calculated for the rainfall collection stations in this study, according to the formula:

$$SI = \frac{1}{\bar{R}} \sum_{n=1}^{n=12} \left| \bar{x}_n - \frac{\bar{R}}{12} \right|$$

where $\bar{R}$ is the MAP and $\bar{x}_n$ is the mean monthly precipitation for month n.

The SI values may not be very meaningful after only 3 years of collection, however, they still provide a reasonable idea of seasonality. The SI values, as shown in **Table 4.2**, all fall within moderately seasonal categories: SI from 0.40 to 0.59 is "rather seasonal with a short drier season"; SI from 0.60 to 0.79 is "seasonal" and SI from 0.80 to 0.99 is "markedly seasonal with a long drier season" (Walsch and Lawler, 1981). There is a general decrease in SI eastwards, as would be expected given that summer rainfall gradually increases from Cape Town eastwards. To the east of the study area, seasonality will again increase eastwards as the winter rainfall decreases.

The two maps in **Figure 4.1** also show the strong seasonality of rainfall in South Africa. The June 2010 map shows a typical winter rainfall pattern with most rain occurring in the Western Cape, high amounts being on the Boland, Hex River and Tsitsikamma Mountains and some other substantial rainfalls along the coast of the Eastern Cape and KwaZulu-Natal as well as on the high ground around the Lesotho - Free State - Eastern Cape borders. The December 2012 map shows a typical summer rainfall pattern, although with above average rainfall amounts, especially those over the Karoo and Namaqualand, while the Western Cape experiences negligible rainfall, except for the futhest eastern portions.

4.3 Rain Isotopes

Four hundred and thirty-five water samples have been analysed for their hydrogen and oxygen isotope composition, excluding duplicates, repeats, laboratory standards or blanks. The graph in **Figure 4.2** shows the distribution of the water samples according to major water type and collection altitude of sample. Rain waters make up the bulk of the samples at 279, groundwaters are intermediate at 110 and surface waters the minority at 46 samples. The altitude distribution reflects the dominance of samples taken in settled areas, which are generally at lower elevations, either near the coast or in valleys, with two spikes at higher elevations due to the rain and groundwater samples taken on peaks or passes at 1000–1200 m, or on the high peaks of the Cape Fold Belt at 1800–2200 m.

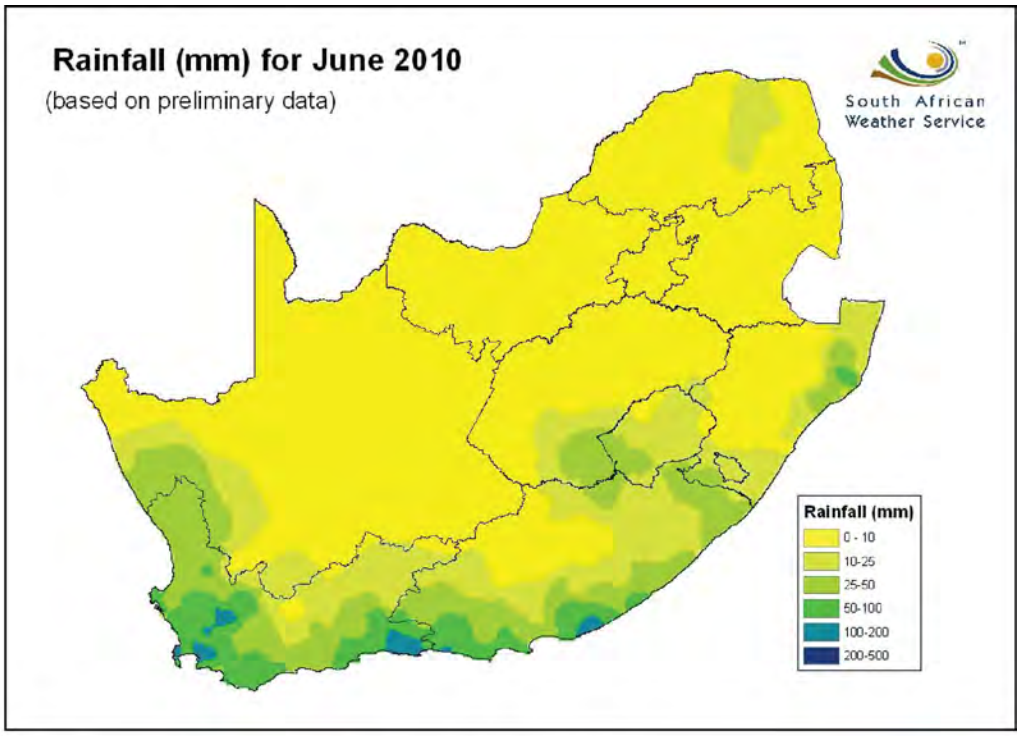

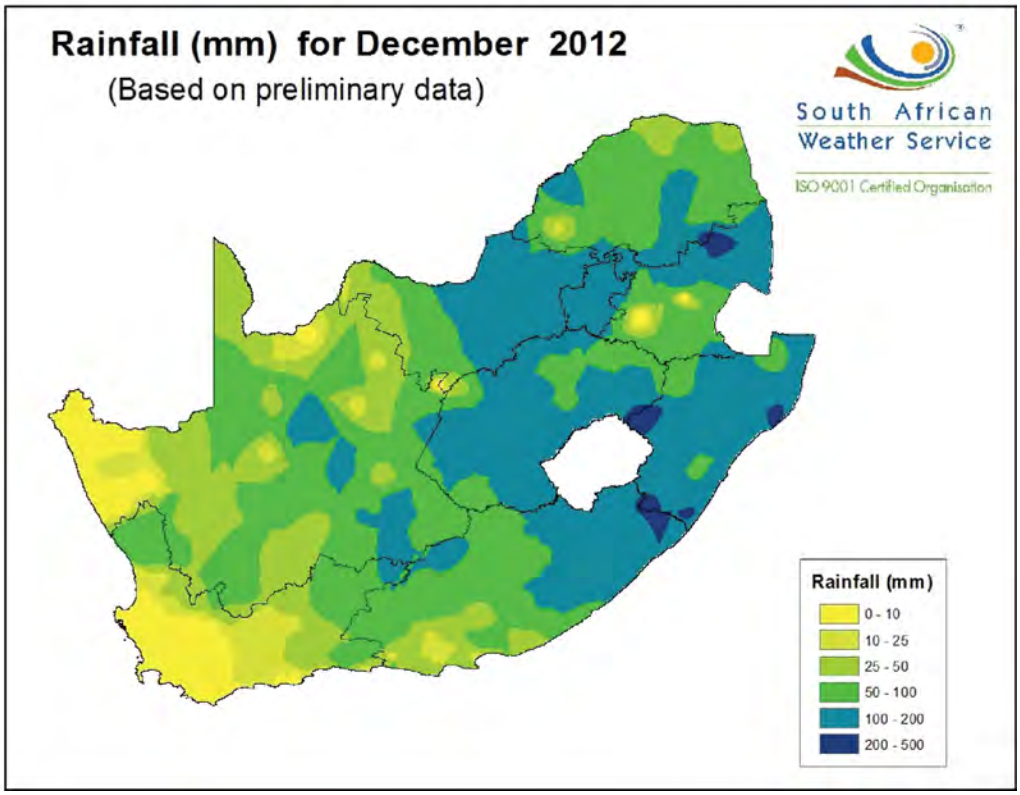

Figure 4.1: Two examples of the monthly rainfall maps produced by the South African Weather Service and available for download from their website (www.weathersa.co.za). The June 2011 map shows a typical winter rainfall pattern and the December 2012 map shows a typical summer rainfall pattern, although about 20 % wetter than normal.

4.3.1 Temporal Variations

Time series graphs have been plotted of all the isotope data from all the rainfall collection stations (**Figures 4.3 and 4.4**), separated into an eastern cluster (Riverndale, Robinson Pass, Bakenskop, Gamka Store, Blesberg, Kammanassie, Lentelus and Goukamma) and western cluster (UCT, Table Mountain, Twaktuin, Uitkyk, Wolfkop, Matroosberg and De Doorns) for ease of viewing. Several features stand out from these graphs. Firstly, although the isotope δ values correlate amongst stations some of the time, at other times they do not. In a few cases there may be field sampling errors, such as evaporation, causing a poor correlation. Most of the time, however, the samples are probably unaltered, based on discussions with the samplers, and the poor correlation indicates the spatial variation of isotope content of precipitation. This interpretation is reinforced by the observations made in **Section 4.2.1** showing how spatially variable rainfall amounts are. If the rainfall amounts are variable, the weather systems are heterogenous and it follows that the isotopic content of the rain may be varied.

Secondly, there is a general pattern of more negative δ values over winter and less negative δ values over summer, as would be expected for areas with a Mediterranean climate (e.g. Jaunat et al., 2013). This pattern is most noticeable in the eastern cluster, both for δD and $\delta^{18}O$. This pattern results from several of the meteoric water isotope effects, as mentioned in Chapter 1, such as the temperature effect and amount effect; in winter, temperatures are colder and rainfall amounts are greater, so rainout removes heavier isotopes faster and the lighter isotopes become more abundant in rain, resulting in more negative δ values. In summer the reverse is true; rainfall amounts are lesser and temperatures are warmer, resulting in less negative δ values. In particular, the effect of evaporation of raindrops during small amount rainfall events shifts the isotopic content to less negative or even positive δ values.

In the western cluster in particular, the data shows greater variation over summer and more similar values over winter. In winter, regional weather systems sweep over all the rainfall stations and produce rain of similar isotope content. In summer, weather systems may be more localised with the result that some stations receive almost no rain, others receive small, highly evaporated amounts with less negative or even positive δ values, and summer thunderstorms may deposit large amounts of rain with very negative δ values. As a result, summer isotopic ratios are less consistent between stations.

In addition to these general patterns, there are occasional spikes in δ values. July 2010 was a month with very negative δ values in the eastern cluster of rain collection stations. The weather systems that caused this month's rain have been compared to those in months without a negative spike in δ values, such as June 2010 or July 2011. For example, in July 2010 there were only two major rain producing systems, the first being a cold front followed by southerly meridional flow over 10–11th and the second being another cold front followed by south-westerly air flow on the 14–15th (SAWS, 2010-12). These rain producing weather systems are very similar to those for June 2010, in which a double cold front was followed by southerly meridional flow from 7–9th

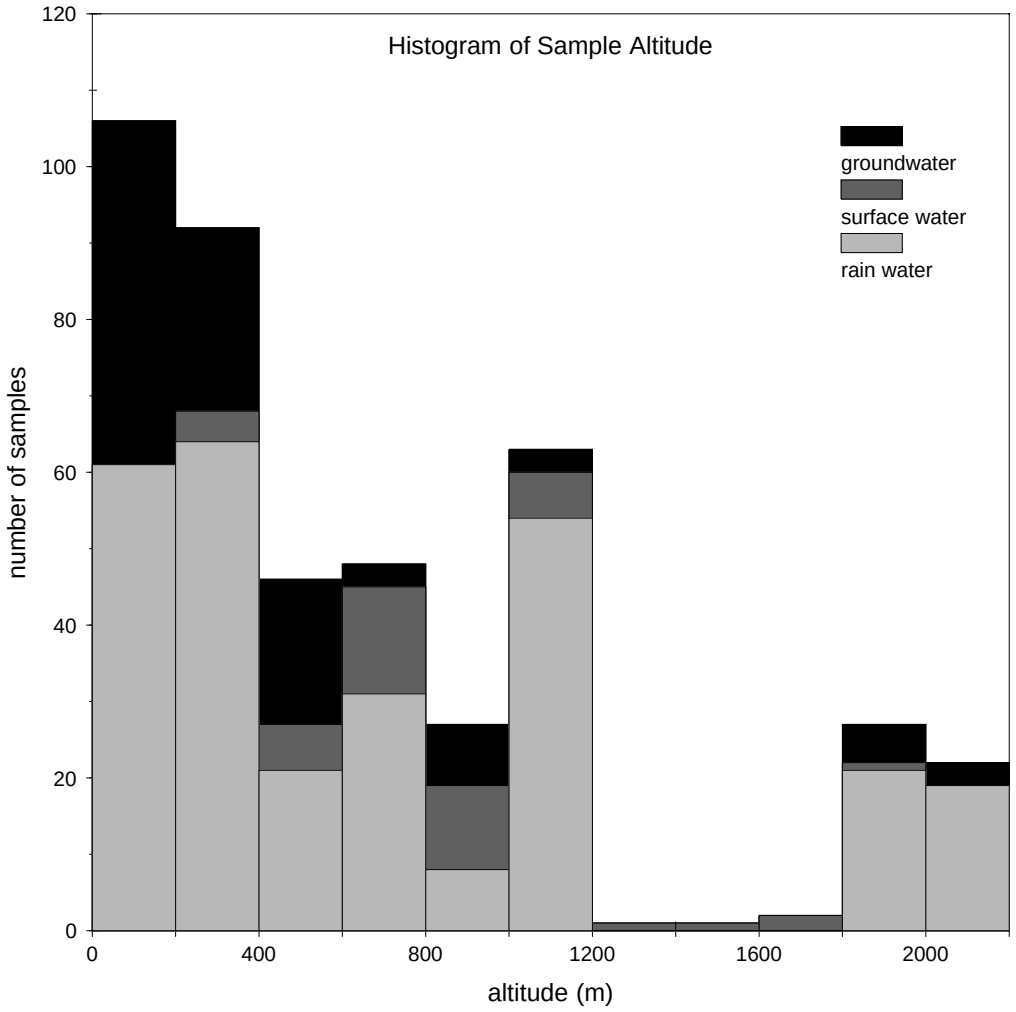

Figure 4.2: A plot of the distribution of the sampling altitude of all samples taken in this study.

and another double cold front was followed by southerly and then south-westerly flow over the 12–16th. For all these events, maximum daily rainfalls across the study area were typically in the 30–60 mm range, with averages being in the 10–20 mm range (SAWS, 2010-12). There is no unusual weather system or anomalously high rainfall for July 2010.

Temperatures at a weather station may undergo various changes as a weather system passes over. Maximum temperatures typically decrease as the cloudy, wet weather arrives and recover once clearing takes place, although may stay depressed if the southerly or south-westerly airflow is strong. Minimum temperatures however, may either decrease or increase, depending on the weather preceding the arrival of the cold front and the timing of the system (SAWB, 1996). Temperatures behaved variably in the June 2010 and July 2010 rainfall producing weather events, with no remarkable cold or change in July 2010. In the case of this distinctive spike in isotope values, it is therefore not easy to find something exceptional about the weather that could account for these results.

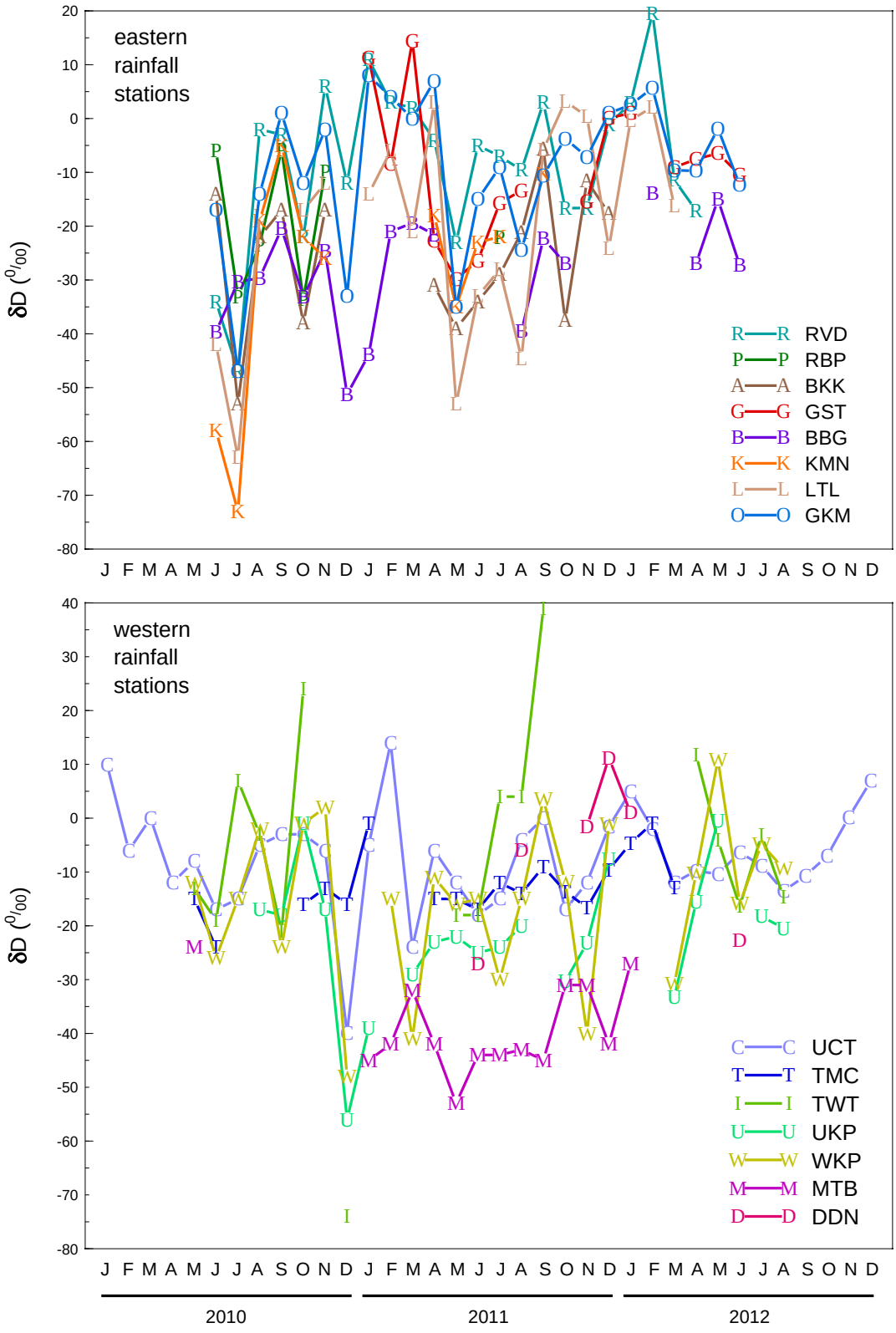

Figure 4.3: Time series graphs for δD for all rainfall stations, the eastern cluster on top and western cluster at the bottom. Stations with missing months have broken lines.

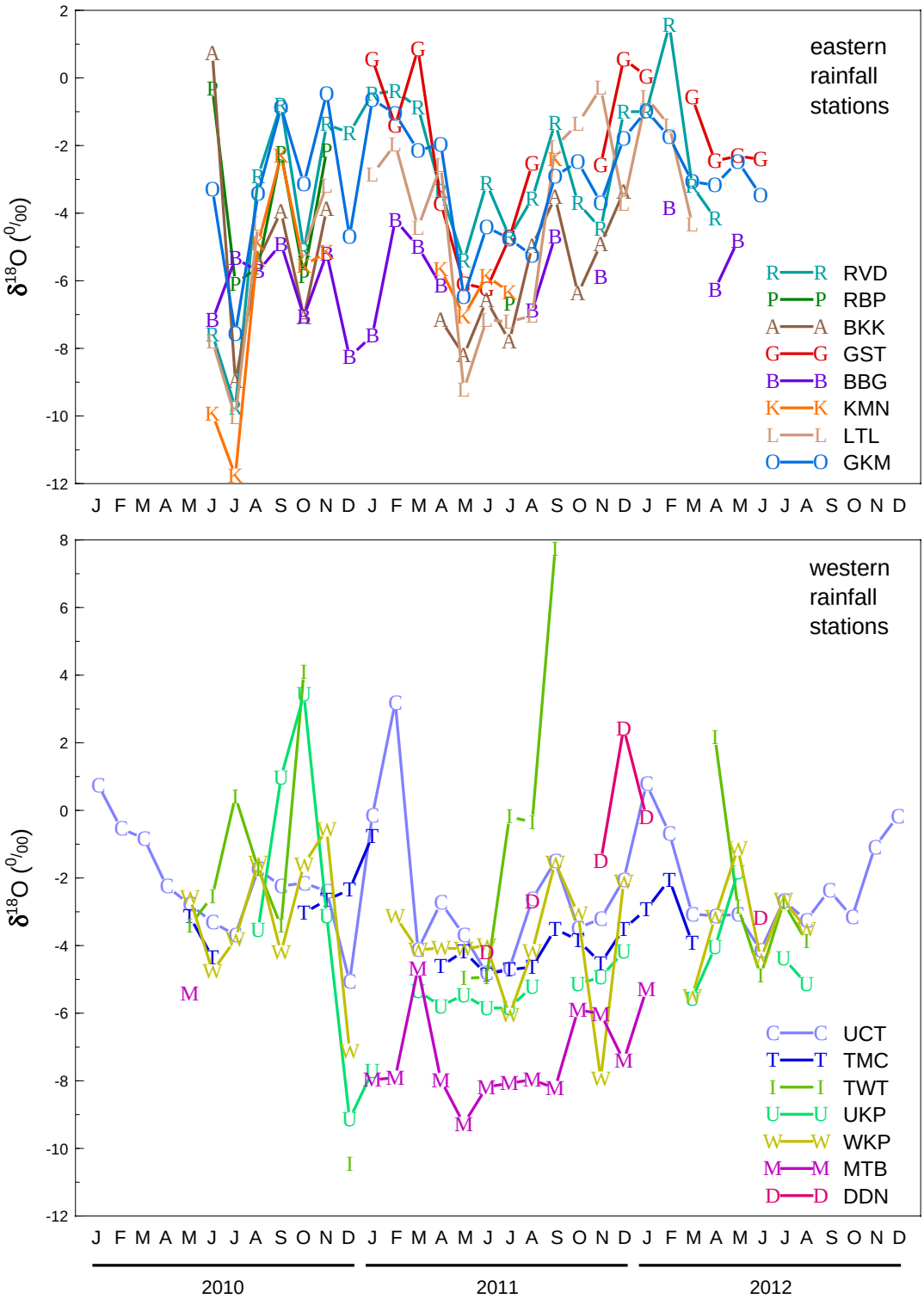

Figure 4.4: Time series graphs for $\delta^{18}O$ for all rainfall stations, the eastern cluster on top and western cluster at the bottom. Stations with missing months have broken lines.

December 2010 also features a negative spike in delta values, most noticeable for the Cederberg cluster of stations. In this case, it is easy to find the weather systems responsible for these results. During this month, several west coast troughs established and ridges of low pressure, connected to the summer rainfall producing *Kalahari Low*, penetrated far south into the Western Cape, but only twice did these result in appreciable rainfall in the Western Cape. The first occurred on 15–16th and delivered daily rainfall up to 60 mm at Vredendal, with lesser amounts of 30 mm at Lamberts Bay, 23 mm at Excelsior Ceres and other more minor amounts. The second event straddled the New Year, with up to 14 mm at Porterville on the 31st. Similar rainfalls occurred on 1st January 2011, such as 19 mm at Excelsior Ceres and 12 mm at Wellington, and it is quite possible that these were included in the December 2010 rainfall sample by the rainfall collectors. These low pressure systems produce convective style rain (thunderstorms) and hail was experienced by the author on top of Tafelberg at 1960 m in the Cederberg on 1st January 2011 (see **Figure 4.5**). The convective nature of these clouds can result in precipitation forming at high altitudes and hence low temperatures, which can result in relatively negative delta values, compared with the more stratified winter rainfall systems. Also, rainfall occurs in short, heavy showers in which minimal evaporation from raindrops occurs, reducing the extent to which the isotopic ratios will be driven to less negative delta values.

In November 2011 there was a very strong negative spike in the delta values for Wolfkop only. This can be traced to a low pressure trough extending southwards from the Kalahari on the 19th and causing convective rainfall. The rainfall amounts recorded were low, with daily totals of only 6 mm at Vredendal, 4 mm at Lamberts Bay and even lower elsewhere, but clearly the rain/hail that fell during this event must have been generated in systems with very low temperatures to account for the very negative delta values measured.

Some highly positive delta values, from +10 – +40 ‰ δD and +2 – +8 ‰ $\delta^{18}O$, were also measured, particularly at the Twaktuin station, but also at Uitkyk Pass, UCT and DeDoorns. These values have most probably been caused through extensive evaporation, both during the actual rainfall event of 19th November 2011 and possibly also from the rain gauge after the event. The latter is probably the reason for the extremely high spike at Twaktuin in September 2011, as there is no indication of similar behaviour at the other stations. However, the October 2010 spike is recorded at both Twaktuin and Uitkyk Pass and in that case probably reflects evaporation during rain drop descent. Similarly, the February 2011 measurements show more positive delta values at both UCT and Wolfkop, as well as for Wolfkop and DeDoorns in December 2011, and so these are likely to be real atmospheric isotopic enrichment during rain drop descent.

4.3.2 Means and Weighting

Mean delta values for each rain collection station have been calculated, both a simple arithmetic mean, and also a weighted mean, weighted according to the rainfall amount for each month (see **Table 4.2**). These results are shown in **Figure 4.6**, which demonstrates two significant patterns.

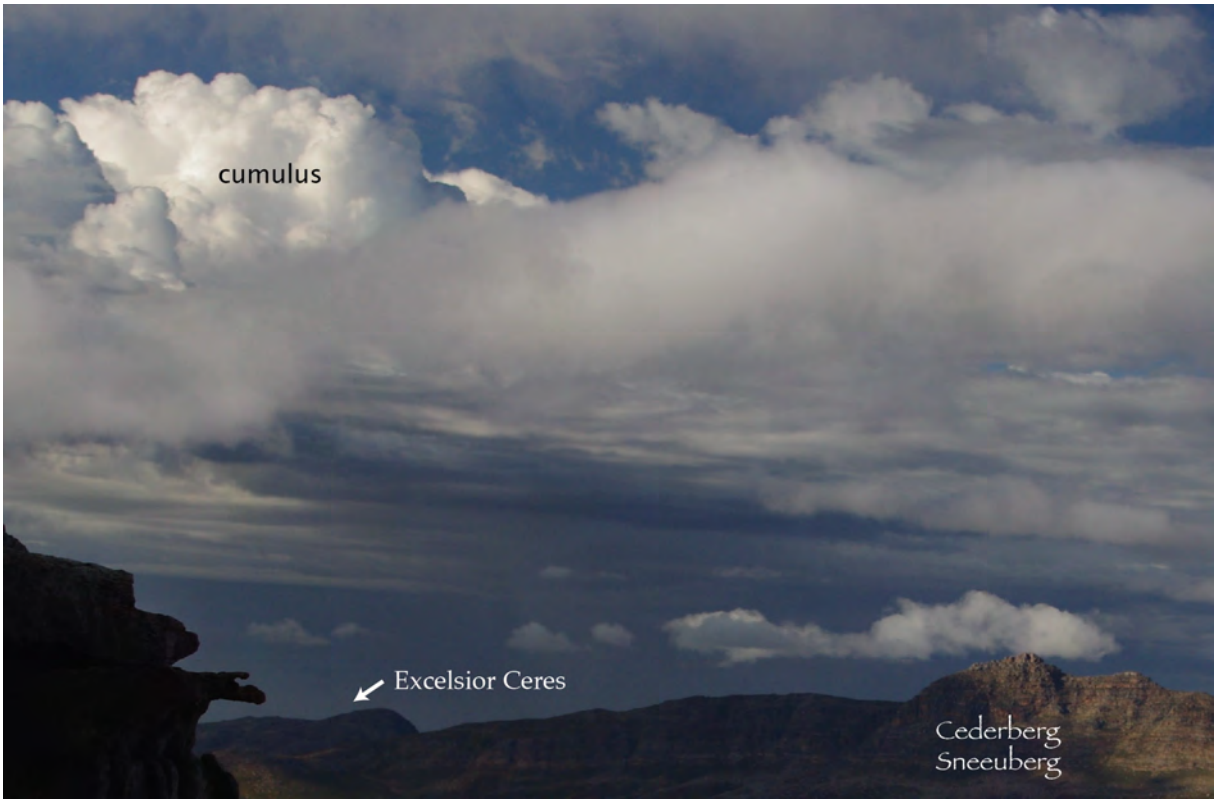

Figure 4.5: A view of the convective cumulus clouds and heavy rainfall (dark grey area in photo) that occurred in the West Coast and Cederberg region of the Western Cape over 31 December 2010 to 1st January 2011. Photograph taken from Cederberg Tafelberg, looking south over Sneeuberg and towards rain at Excelsior Ceres SAWS weather station.

Firstly, in all cases except one (δD at Uitkyk Pass), the weighted mean has a lower delta value for both δD and $\delta^{18}O$ than the unweighted mean, as is commonly observed in such studies (e.g. Iacumin et al., 2009). This is because the less negative delta values are associated with low rainfall events, mostly during summer where temperatures are higher and delta values of rain are less negative and where evaporation further increases the delta values. Put otherwise, the high rainfall, cold and isotopically more depleted winter rains bring the weighted means down towards more negative delta values.

Secondly, the degree of difference between the arithmetic mean and weighted mean is negatively correlated with the mean annual precipitation (see **Figure 4.7**). Sites with low total rainfall have more of the isotopically enriched very low rainfall months. These values drive the unweighted, or arithmetic, mean to unrealistically high delta values. When the weighted mean is calculated, the relatively few, but high rainfall months cause the weighted mean to have more negative delta values, so increasing the difference with the unweighted mean. It can be concluded that recording the rainfall amount when sampling rain is more important at drier locations, although still of value at all locations. According to Yurtsever and Gat (1981), when analysing the IAEA/WMO data: "The difference between the two means is not generally significant for stations

with a rather uniform monthly distribution of rainfall...". Our study, however, found that the correlation of difference between delta values with the seasonality index was very poor: δD and $\delta^{18}O$ vs SI gave Pearson's r correlations of 0.18 and 0.014 respectively, whereas the δD and $\delta^{18}O$ vs MAP correlations (as seen in **Figure 4.7**) are -0.71 and -0.65, respectively.

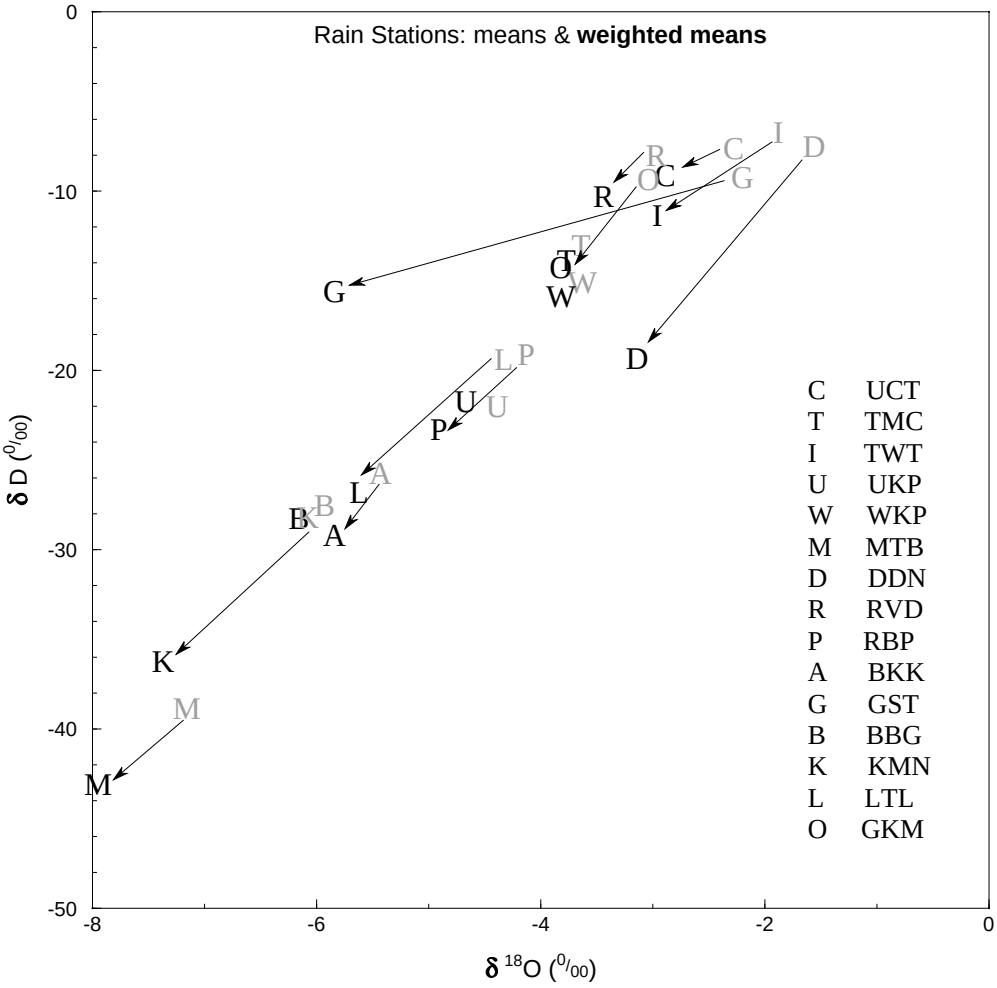

Figure 4.6: Arithmetic means and weighted means, by rainfall amount, for each rain collection station. Arrows show change from unweighted (arithmetic) means to weighted means.

The arithmetic and weighted mean δD and $\delta^{18}O$ values for UCT from this study compare favourably with previous studies in the Cape Town area, as shown in **Table 4.3**, although the results from this study are slightly less negative. There is a fair correlation between the amount of rainfall and the delta values, especially for δD, for the UCT data. The CTIA site is quite different, in terms of MAP and location, and most data is from 1960-80's and hence is not readily comparable, so it is displayed here more for interest.

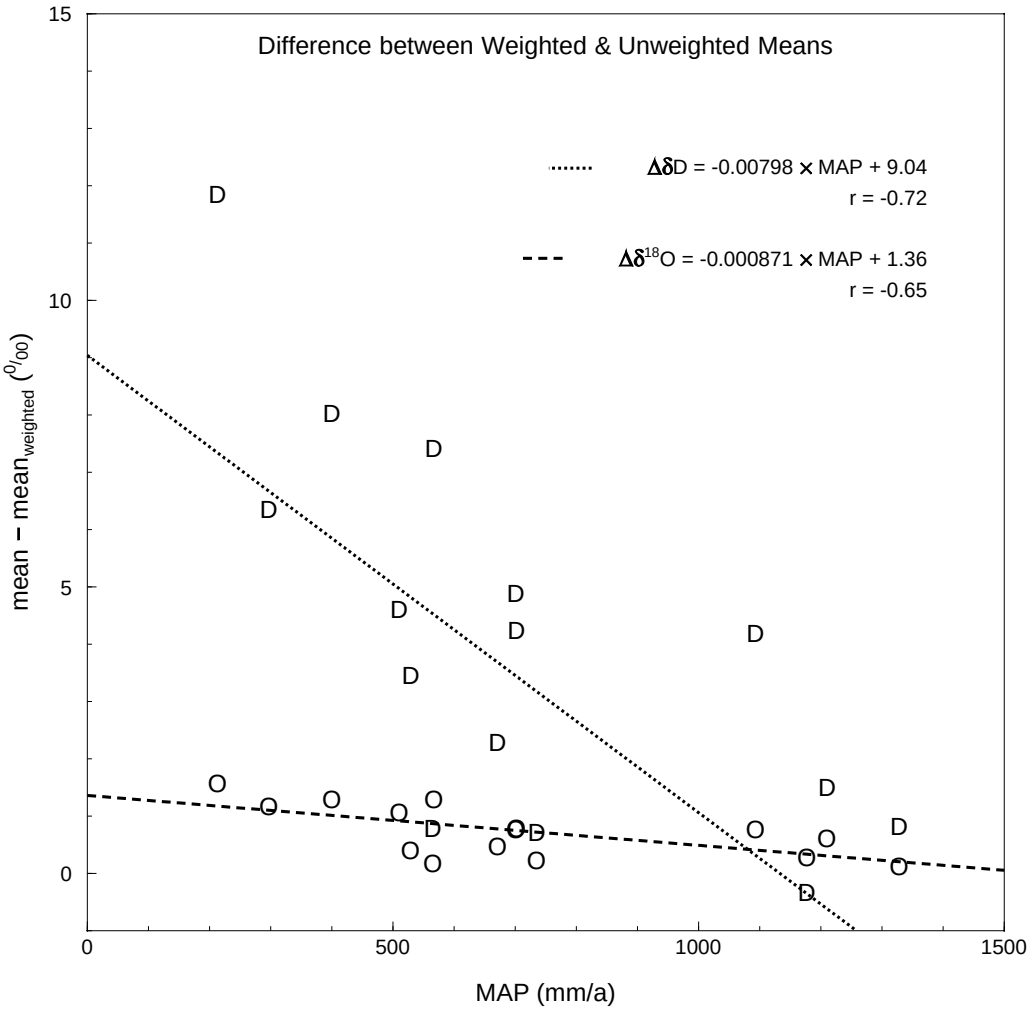

Figure 4.7: The difference between the mean and weighted mean for δD (D) and $\delta^{18}O$ (O) versus the MAP (mean annual precipitation), for each rain collection station.

			arithmetic		weighted		
study	altitude	MAP	δD	$\delta^{18}O$	δD	$\delta^{18}O$	source
	masl	mm	‰	‰	‰	‰	
UCT 2010–2012	130	1210	-7.6	-2.28	-9.2	-2.89	this study
UCT 1995–1997	130	1260	-13.0	-3.46	-11.7	-3.74	Diamond and Harris (1997)
UCT 1996–2008	130	1365	-8.5	-2.68	-12.5	-3.29	Harris et al. (2010)
'Malan'/CTIA	40	513	-8.2	-2.72	-12.8	-3.36	Rozanski et al. (1993)

Table 4.3: Arithmetic (unweighted) and weighted mean δD and $\delta^{18}O$ values of rainfall from various studies in Cape Town. CTIA refers to the Cape Town International Airport (DF Malan) where the IAEA/WMO GNIP station was located.

4.3.3 Deuterium Excess

The d-excess, often referred to simply as 'd' in the literature, is calculated for a sample of known δD and $\delta^{18}O$ values by the equation:

$$d - excess = \delta D - 8\delta^{18}O.$$

The d-excess values for the 15 rainfall collection stations range from 5.8 to 22.7 ‰ and average 16.0 ‰, which is similar to d-excess values from other studies in Mediterranean climates (Vreča et al., 2006; Argiriou and Lykoudis, 2006) (see **Table 4.2**). No correlations are apparent with MAP, seasonality or any other obvious geographic parameters, for example latitude and altitude, as can be seen in **Figure 4.8**. The best correlation is found against a continentality factor, which is the product of the distance between the rainfall station and the Atlantic Ocean (along a line of latitude due west) and the distance to the closest coast ('sea'). This factor is discussed further in Chapter 5, but even this correlation is rather poor, with a Pearson's r of only 0.42.

4.3.4 Local Meteoric Water Lines

All rain water isotope results have been plotted in the upper graph in **Figure 4.9**. The most noticeable feature of this graph is the well defined correlation between δD and $\delta^{18}O$, as is expected, according to isotopic fractionation, as described in the Introduction. This correlation defines the trend of the local meteoric water line. Using the data set to calculate lines of best fit (local meteoric water lines), the equations are as follows:

♢ unweighted rain water data: δD = 6.11$\delta^{18}O$ + 7.09

♢ rain water data, weighted by rainfall amount: δD = 6.15$\delta^{18}O$ + 8.21 .

Several points can be made about these equations. Firstly, there is only a small difference between the weighted and unweighted equations. This suggests that the statistical outliers, the rain water samples with unusual isotopic composition, are nearly symmetrical about the data. Additionally, the unweighted and weighted rain water means (n = 275) are, for δD and $\delta^{18}O$: -15.9 ‰ and -3.76 ‰ , -17.7 ‰ and -4.22 ‰. These also show only a small difference and if plotted together on a $\delta D - \delta^{18}O$ diagram, the two means lie along the same orientation as the two nearly parallel local meteroric water lines. The small shift between the two equations does however reveal that the unweighted line tends towards a lower gradient and lower intercept, both of which are a sign of evaporated waters. The bulk of the outliers are therefore the low rainfall, highly evaporated, summertime rainfall samples, as seen in the time series plots in **Figures 4.3 and 4.4**.

Local meteoric water lines have also been calculated for each of the rainfall stations and

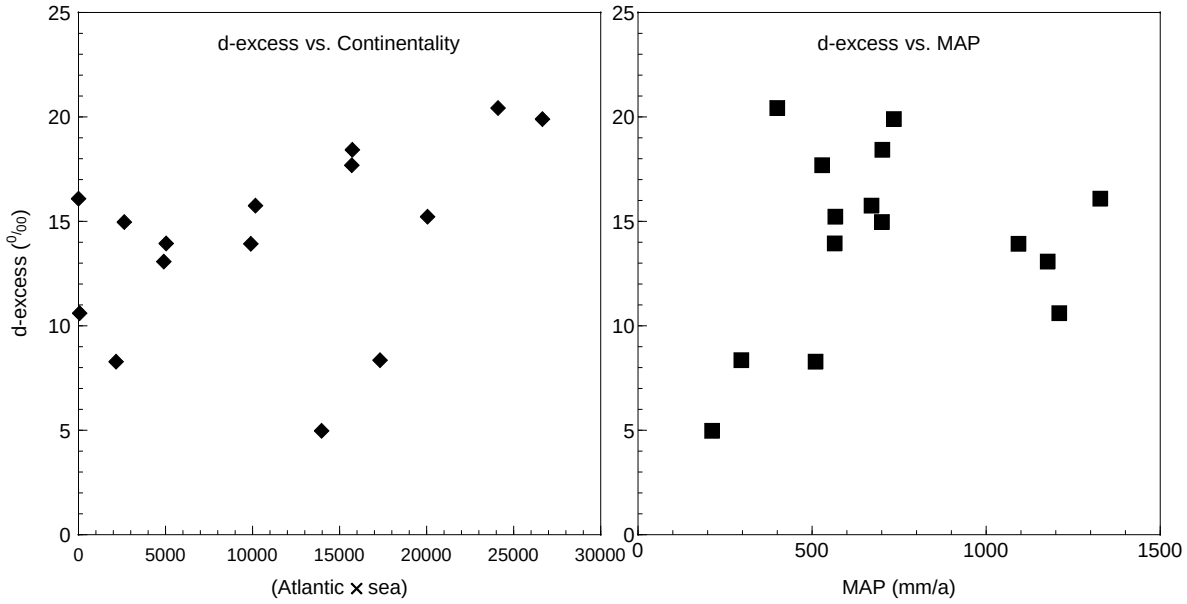

Figure 4.8: d-excess values for the weighted means for the 15 rainfall collection stations, plotted against a continentality factor and against MAP.

these are displayed in **Figure 4.10**. Ellipses have been drawn on the graph, using the standard deviations from **Table 4.2**, to show where most of the data actually lies; 67 % of points should lie within the 1σ ellipse and 98 % within the 2σ ellipse. The graph region was extended to show some separation in the meteoric water lines and allow labelling of each line.

The LMWL gradients range from 4.42 for Uitkyk Pass to 8.17 for Kammanassie, and intercepts from -3.0 for Bakenskop to 23.9 for Kammanassie. Although no single, clear correlation between these local meteoric water line equations and geographic factors such as mean annual precipitation, altitude or longitude is apparent, the equations do display geographic clustering (see **Figure 4.11**). The following groups can be distinguished by the similarity of their gradient and intercept values: a western cluster of UCT (University of Cape Town), TMC (Table Mountain Cableway) and TWT (Twaktuin) have gradients in the 5 to 6 range with intercepts from 6 to 7.5; the Hex River Mountain stations MTB (Matroosberg) and DDN (DeDoorns) have similar gradients, although different intercepts; the Langeberg-Gamkaberg group of RBP (Robinson Pass), BKK (Bakenskop) and GST (Gamka Store) all have gradients around 4.5 and intercepts close to zero; the eastern stations BBG (Blesberg), KMN (Kammanassie), LTL (Lentelus) and GKM (Goukamma) have high gradients, from 6.5 to 8.2, and high intercepts, from 10 to 24. Some stations do not fit into these groups, despite being geographical neighbours, these being Uitkyk Pass and Wolfkop, 30 km apart in the north-west, and Riverndale, less than 100 km from the Langeberg-Gamkaberg group in the south. The large range in gradients and intercepts for the 15 LMWLs is likely due to the short duration of sampling, whereby unusual weather (humidity, series of storms, drought) can affect the small dataset. Longer term monitoring should see some convergence in LWMLs.

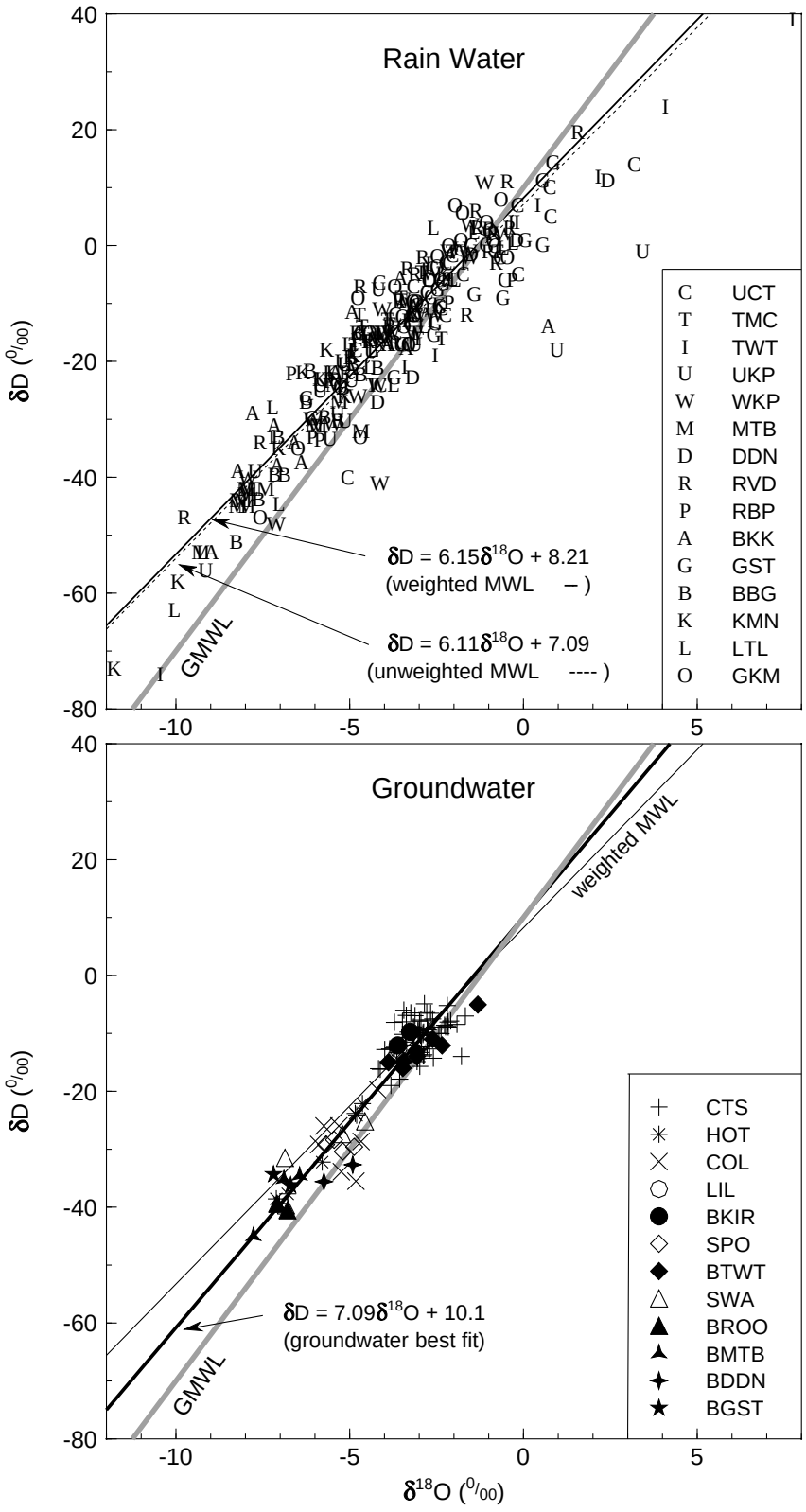

Figure 4.9: δD–$\delta^{18}O$ plots of all rain water and groundwater samples for this study. Key for the groundwater graph: CTS Cape Town springs; HOT hot springs; COL cold springs; LIL Table Mountain lily pond; BKIR Kirstenbosch boreholes; SPO Cederberg Tafelberg spout drip; BTWT Twaktuin boreholes; SWA Klein Swartberg seeps; BROO Rooihoogte boreholes; BMTB Matroosberg boreholes; BDDN DeDoorns boreholes; BGST Gamka Store boreholes.

The significance of the clustering of these local meteoric water lines is that they reveal affinities not seen when looking at the means and d-excess values. For instance, the two stations Matroosberg and DeDoorns, only 10 km apart, have very different means and d-excess values, and although the intercepts of their local meteoric water lines do show a large difference, the gradients are nearly identical, showing some parallels in meteoric processes between the two stations. A similar thing can be said for the 'sister' stations, Bakenskop and Gamka Store.

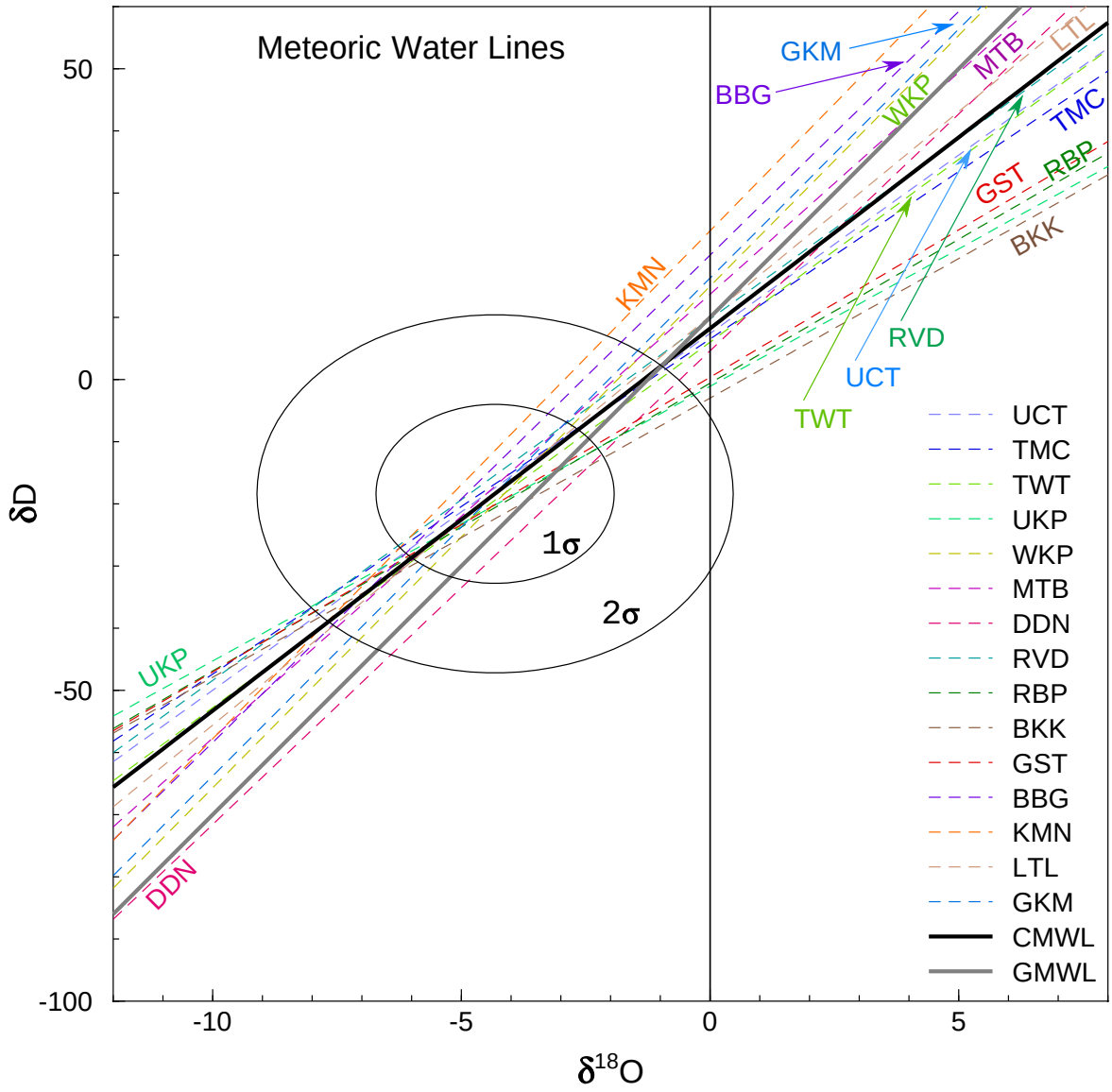

Figure 4.10: Local meteoric water lines for each of the 15 rainfall stations, calculated from monthly cumulative rainfall samples weighted by rainfall amount and using the RMA regression method. The LMWL for the all the stations (also weighted), called the Cape MWL (CMWL), and the GMWL of Craig (1961a) are also shown. The 1σ and 2σ distribution ellipses are for all rainfall data, showing how the graph has been extended well beyond the δ values found in this study, in order to show separation and allow labelling of the LMWLs.

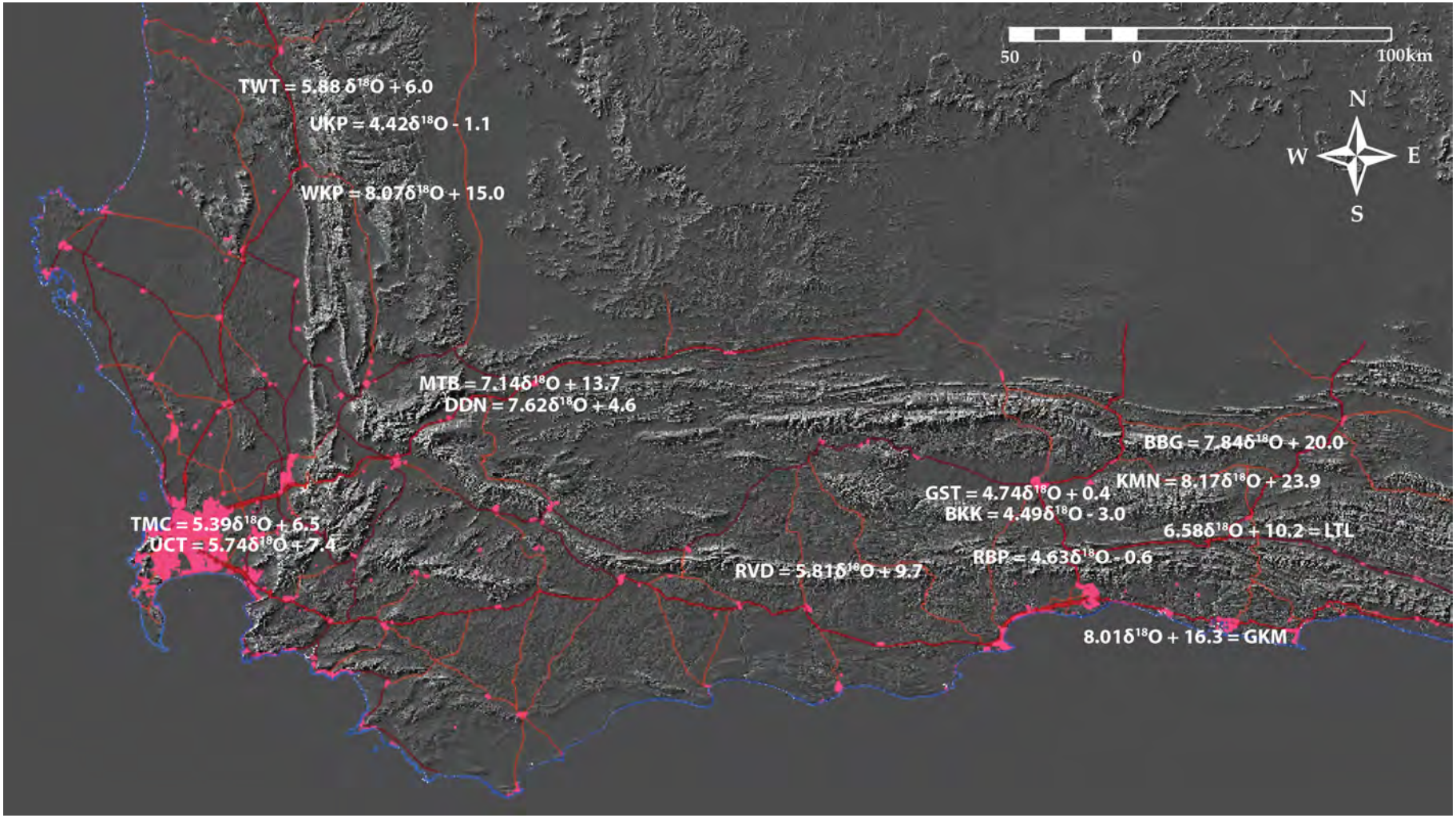

Figure 4.11: Local meteoric water line equations for each rainfall collection station, calculated with data weighted by monthly rainfall amount. The station code (e.g. BBG) lies approximately over the station location. Background image is a hillshade DEM (NASA, 2013) with roads and streets overlain (NGI, 2012).

4.4 Groundwater

Groundwater was sampled from a variety of sources: springs, seeps and boreholes. Except for the springs around Table Mountain, almost all of the groundwater was taken from sources discharging from the Table Mountain Group.

The Table Mountain springs lie below the unconformity between the overlying Table Mountain Group and the Cape Granite or Malmesbury Group, but they do not discharge from unaltered granitic or metamorphic rock. These springs discharge from areas with no bedrock outcrop and are likely to be discharging from an aquifer made of colluvial material such as scree and some weathered rock.

The springs and seeps around the Western Cape vary from widely known, high discharge rate hot springs such as Calitzdorp and Citrusdal, to virtually unknown drips that are used as high altitude water points by mountaineers, such as Cederberg Tafelberg Spout drip and the Klein-Swartberg Toverkop drip. The former, major springs, have often been capped and the ground is covered with recent material, both natural and anthropogenic, and so the exact geological formation at the discharge point is uncertain. Additionally, these larger springs mostly lie on faults and stratigraphic units can be juxtaposed, such as the Peninsula Formation of the Table Mountain Group and the Gamka Formation of the Bokkeveld Group at the Caledon hot spring (e.g. Council for Geoscience, 1997). In contrast, for the seeps, not only can the geological formation be identified, but the exact fracture from which the groundwater emerges is often visible.

The boreholes sampled are of moderate depths, around 30–100 m, and most (except for the Kirstenbosch boreholes) penetrate the Table Mountain Group, although the surface outcrop in some cases (e.g. DeDoorns) is Bokkeveld Group.

All groundwater data have been plotted in the lower graph in **Figure 4.9**. The contrast with the upper graph of all the rain water data is very noticeable, the lack of scatter being the result of the smoothing that occurs for the following reasons: small rain volume events with unusual isotopic signatures do not contribute to recharge; mixing of meteoric water takes place during recharge and subsequent underground flow, averaging out the composition of discharge. The former of these effects has been dubbed selection by Gat & Tzur (1967) (in Gat, 1981a). Using this data set to calculate a best fit line gives the following equation:

$\diamondsuit$ groundwater data, which cannot be weighted: $\delta D = 7.09\delta^{18}O + 10.08$.

This equation is substantially different from the rain water MWL equations and is much closer to the GMWL of Craig (1961a). The means for all the groundwater data are, for δD and $\delta^{18}O$: -16.9 ‰ and -3.8 ‰, respectively. These means are biased towards the Table Mountain springs, as about 60 % of the groundwater data is from these springs, which accounts for the relatively isotopically enriched values of these means.

Figure 4.12: The Seweweekspoort Peak Cave water point at 2020m in the Klein Swartberg. The fractured nature of the folded, duplexed and competent quartzite of the Peninsula Formation is apparent.

4.5 Surface Water

Water samples were collected from five rivers in the Cape Mountains. The extent of each river that was sampled falls wholly within the outcrop of the Table Mountain Group, although shortly downstream of the lowest sample the rivers exit onto other stratigraphic units, except for the Witels as described below.

Duiwelskloof and Volstruiskloof are both in the Drakenstein Mountains between Stellenbosch and Franschhoek where the Table Mountain Group is fairly flat lying on top of granite of the Stellenbosch Pluton of the Cape Granite Suite. The rivers are both very steep: Duiwelskloof has an average gradient of 30° over a distance of 2.4 km and Volstruiskloof drops 700 m in a distance of 1.5 km, giving an average gradient of around 45° (see **Table 5.7**). The rivers flow through Peninsula Formation and exit onto scree over granite at the foot of the mountains.

The Witels and Groothoekkloof Rivers both lie in the Hex River Mountains, but at opposite ends. The Witels lies in the western side of the Hex River Mountains, south of Ceres, and is the longest mountain river in the Western Cape, protected from the impact of agriculture and urbanisation by virtue of the mountainous terrain. This makes it potentially useful for understanding interaction between surface water and Table Mountain Group groundwater. The Witels has an

average gradient of 7.5° over the full 20 km length, starting at around 1900 masl and ending at 300 m in Michells Pass, but bar one high altitude sample, the main 16 km stretch of the river that was sampled drops only 600 m and so has an average gradient of only 3.5°. The Witels mainly flows through Peninsula Formation, but due to folded beds that dip north-east, it flows through Pakhuis, Cederberg and Goudini Formations for a portion of its course. The sampling of the Witels stops at its junction with the Dwars River in Michells Pass, an impacted river that drains the agricultural and urban land of the Ceres Valley. The Dwars (with the Witels) continue for a few kilometres in Table Mountain Group before exiting onto a substrate of Malmesbury Group in the Tulbagh–Wolseley Valley.

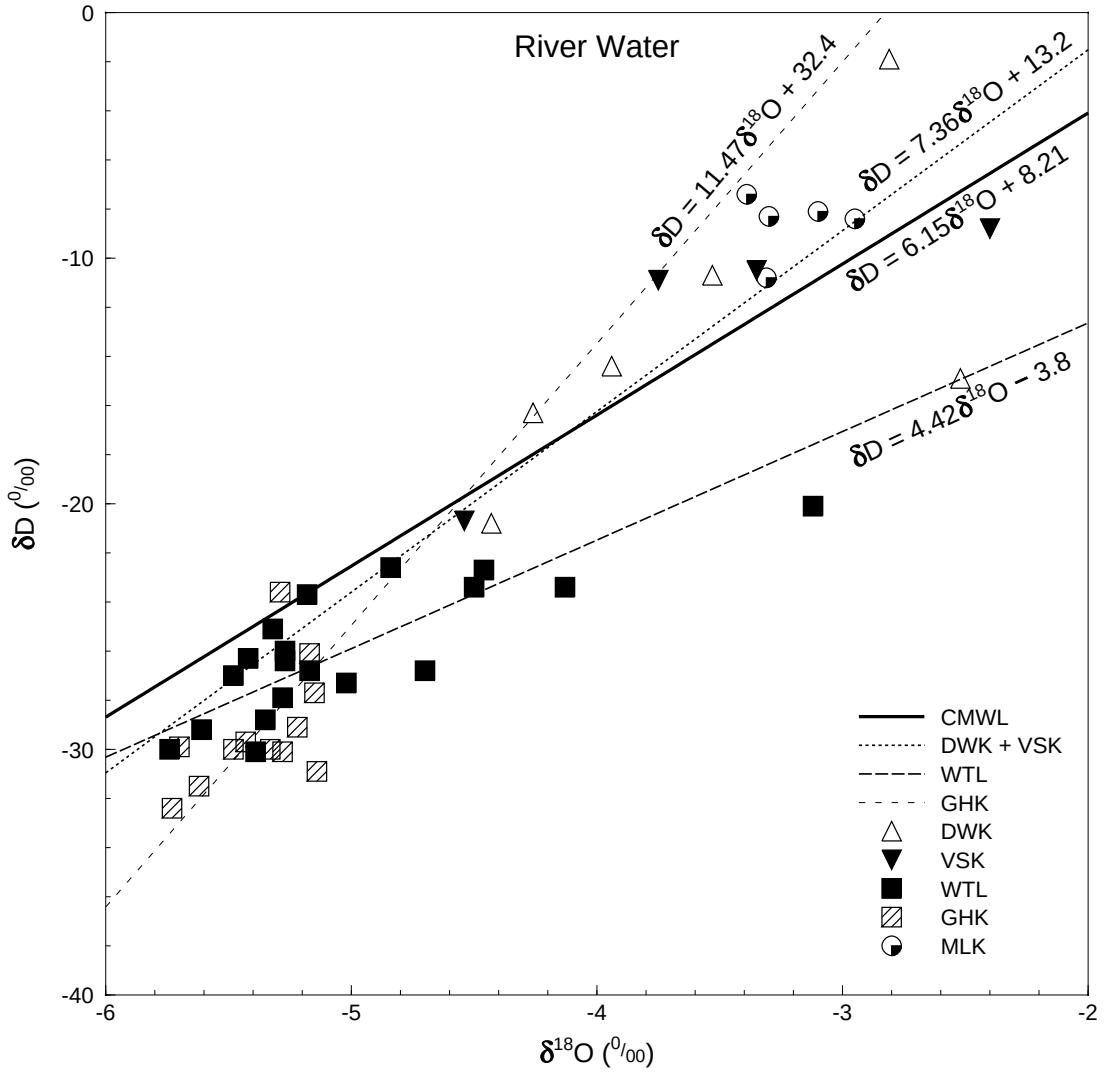

Figure 4.13: $\delta D - \delta^{18}O$ plot for all surface water samples. Best fit lines have been calculated for some data sets and the Cape Meteoric Water Line, as calculated from this study, has been added for reference.

The Groothoekkloof River arises in the highest mountains of the south-western Cape, namely

Matroosberg and Roodeberg in the far north-eastern Hex River Mountains, both over 2200 masl. It exits into Bokkeveld Group and covering gravels in the Hex River Valley Syncline at 500 masl, having flowed only through Peninsula Formation, although the high peaks above perennial water are capped with cliffs of the Skurweberg Formation and the catchment therefore includes outcrop of the Pakuis, Cederberg and Goudini Formations. This river's average gradient from perennial water at about 1800 m is around 13° (see **Table 5.7**).

Meulkloof River lies in the Swellendam region of the Langeberg Mountains. It's source is around Hermitage Peak, over 1500 masl, and it flows through Peninsula Formation only until it exits the mountains across a faulted contact with the Bokkeveld Group at 130 masl.

The $\delta D - \delta^{18}O$ plot of all surface water samples is shown in **Figure 4.13**. A clear separation exists between the two rivers from the higher mountains of the Hex River Mountains and the three other rivers located in lower mountain ranges. Best fit lines have been calculated for Groothoekkloof, Witels and a combined line for Volstruiskloof and Duiwelskloof. Meulkloof does not have enough of a linear spread of data to calculate a meaningful correlation. The correlation coefficient, Pearson's r, is only 0.53 for Groothoekkloof, but for Witels it is 0.81 and Volstruiskloof-Duiwelskloof it is 0.72, both of which are fair correlations. There is a large separation in the Witels and Groothoekkloof lines, and they straddle the MWL equations for De Doorns and Matroosberg, the two rainfall stations in the area.

The river water samples have a weak correlation with altitude, mainly between rivers. More detailed analysis of these results is necessary, as samples include those from not only the trunk stream, but also tributaries, and certain samples are highly evaporated after descent over exposed cliffs (trickling waterfalls). This will be done in the next chapter.

4.6 Other Samples

4.6.1 Snow

Six samples of snow and ice were taken from about 1900 masl on Waaihoek Peak on 29 July 2011. An unusual weather event occurred on 24–25th July 2011 when snow fell on some of the high peaks of the Cape Fold Belt from a *black south-easter*. This event can be summarised as follows. On the 2nd July a cold front and ensuing southerly meridional flow caused widespread light rain over the Western Cape with very cold ($0 - 10°C$) minimum daily temperatures. On the 4th July southerly meridional flow caused large amounts of rain (40–50 mm daily totals) on the south coast and light rain in the south-central mountain areas. Thereafter, a blocking high sat south of the country for nearly three weeks and prevented any cold fronts from causing rain until the 21st–22nd when a cold front brushed past, resulting in a few millimetres of rain along the south coast. This was followed by the South Atlantic High Pressure re-establishing itself south of the country, but this time with abundant moisture and resulting in rain falling from 23–25th mostly along the southern parts of the Province, with a maximum daily rainfall of 68 mm in George on the 24th.

On the 27th–28th a typical winter cold front caused widespread rain, and snow on the high peaks, across the Province.

Snow from both the black south-easter event and the following north-wester event was sampled near the top of Waaihoek Peak in the Hex River Mountains. It was possible to differentiate the two snowfalls from the granular snow (firn) which develops at the top of a snowpack due to freeze-thaw. The isotope results of these samples are shown in **Table 4.4**. Two different profiles were cored into the snow, WHK1-3 and WHK5-6 and a sample was also taken of rime ice (formed by sublimation directly from the atmosphere) that forms on these windy summits. The rime ice was formed during the recent north-wester, as it was on the western side of the rocks and would also not have survived the intervening sunny days between the south-east and north-west weather events.

sample ID	sample description	depth	δD	$\delta^{18}O$
		mm	‰	‰
WH1	recent powder snow from NW cold front	0-50	-60.6	-11.56
WH2	granular (melted and refrozen) top of SE snow	100-150	-38.3	-9.11
WH3	powder snow from SE at base of snowpack	300-400	-30.6	-9.16
WH4	rime ice stalactite on west facing rock	n/a	-20.5	-7.16
Wh5	granular snow at top of SE snowfall	100-200	-38.0	-8.69
WH6	podwer SE snow at base of snowpack	300-350	-33.6	-8.46

Table 4.4: Waaihoek Peak snow samples taken on 29 July 2011.

4.7 Summary

The stable isotope data from this study has a wide range of values because of seasonal variations, specific weather events, differing continentality and altitude of sample sites, and modification by evaporation. Some results can easily be attributed to such factors, whereas others have a less clear cause. Mean δD and $\delta^{18}O$ values for each rainfall station were calculated by weighting the monthly values by rainfall amount. Meteoric water lines for each station were also calculated using weighted data. The weighted results differ more from the unweighted results for less rainy areas, as weighting removes the effect of highly evaporated, low rainfall isotopically outlying data points.

Groundwater data is more tightly clustered than precipitation, as a result of selective recharge of more isotopically negative, higher rainfall events, and mixing of groundwater. Water from rivers tends to vary unsystematically isotopically down the length of the streams and each river's isotope data tends to form a cluster. Snow from a south-easter weather event has a markedly different isotope content to a subsequent north-wester weather system.

More detailed analysis of these and other results follows in the Discussion.

Figure 4.14: Monthly rainfall graphs for the 15 rain collection stations over January 2010 to December 2012. Estimates were made based on nearby rainfall stations from this study and SAWS, as well as monthly rainfall maps from the SAWS.

(a) Monthly rainfall as measured (solid bars) and estimated (striped bars) for the two Cape Town area stations.

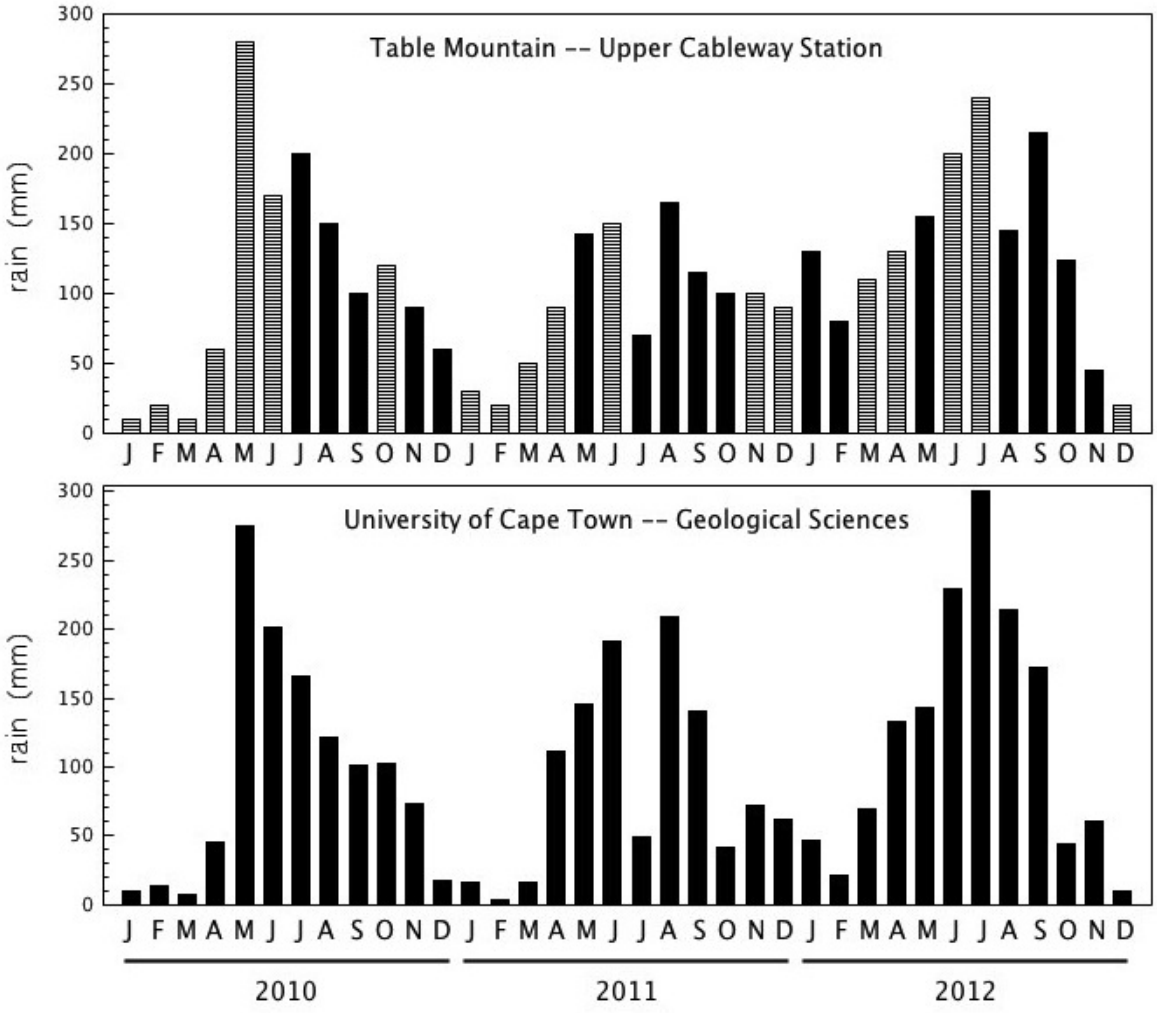

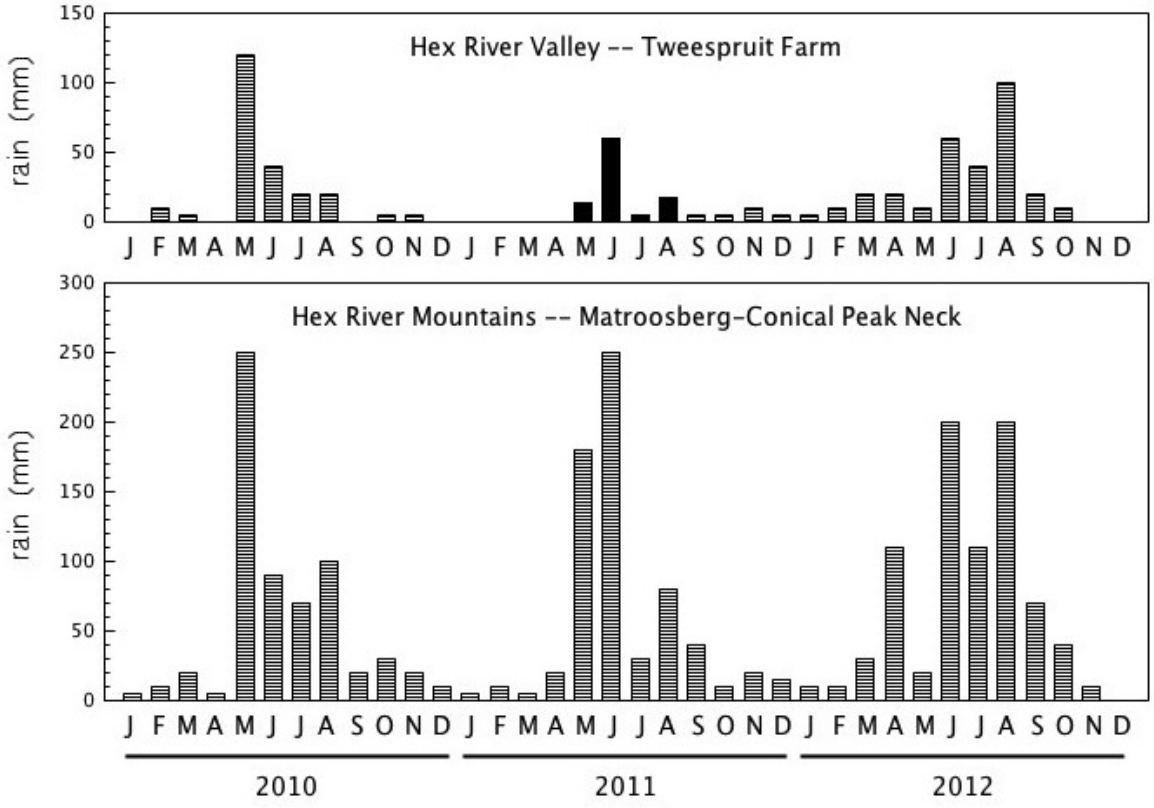

(b) Monthly rainfall as measured (solid bars) and estimated (striped bars) for the two Hex River region stations.

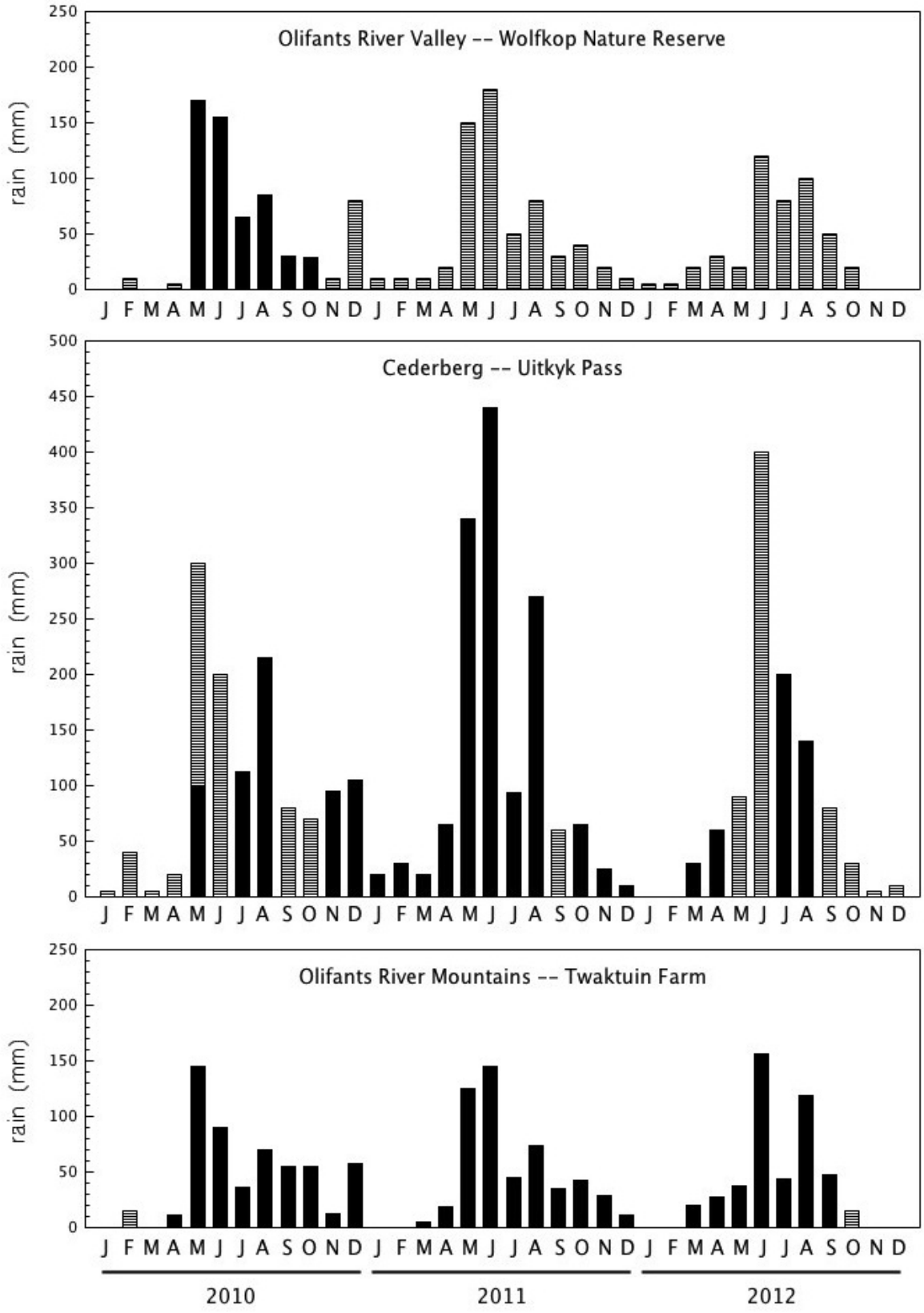

(c) Monthly rainfall as measured (solid bars) and estimated (striped bars) for the three Cederberg area stations.

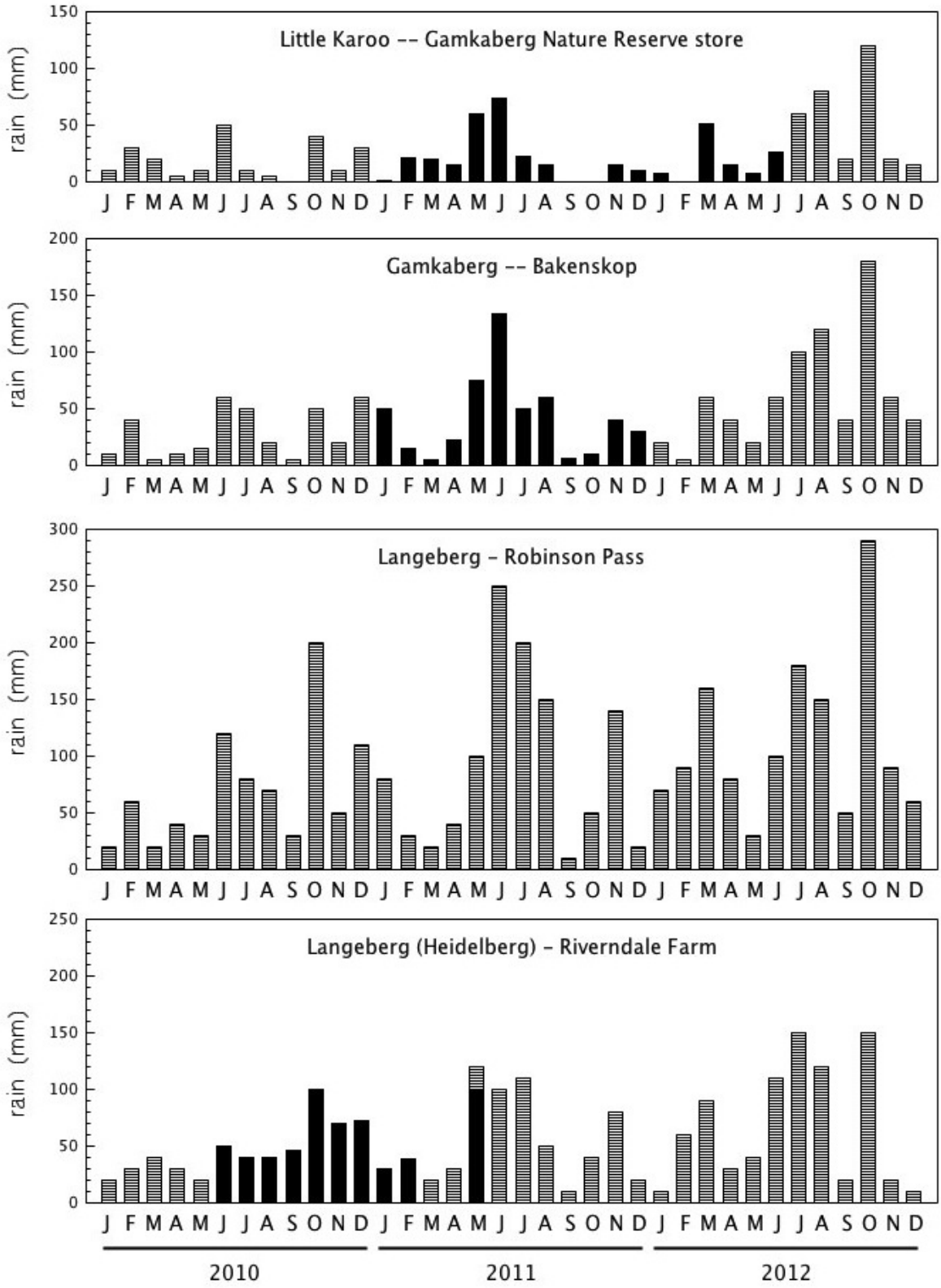

(d) Monthly rainfall as measured (solid bars) and estimated (striped bars) for the Langeberg and Gamkaberg region stations.

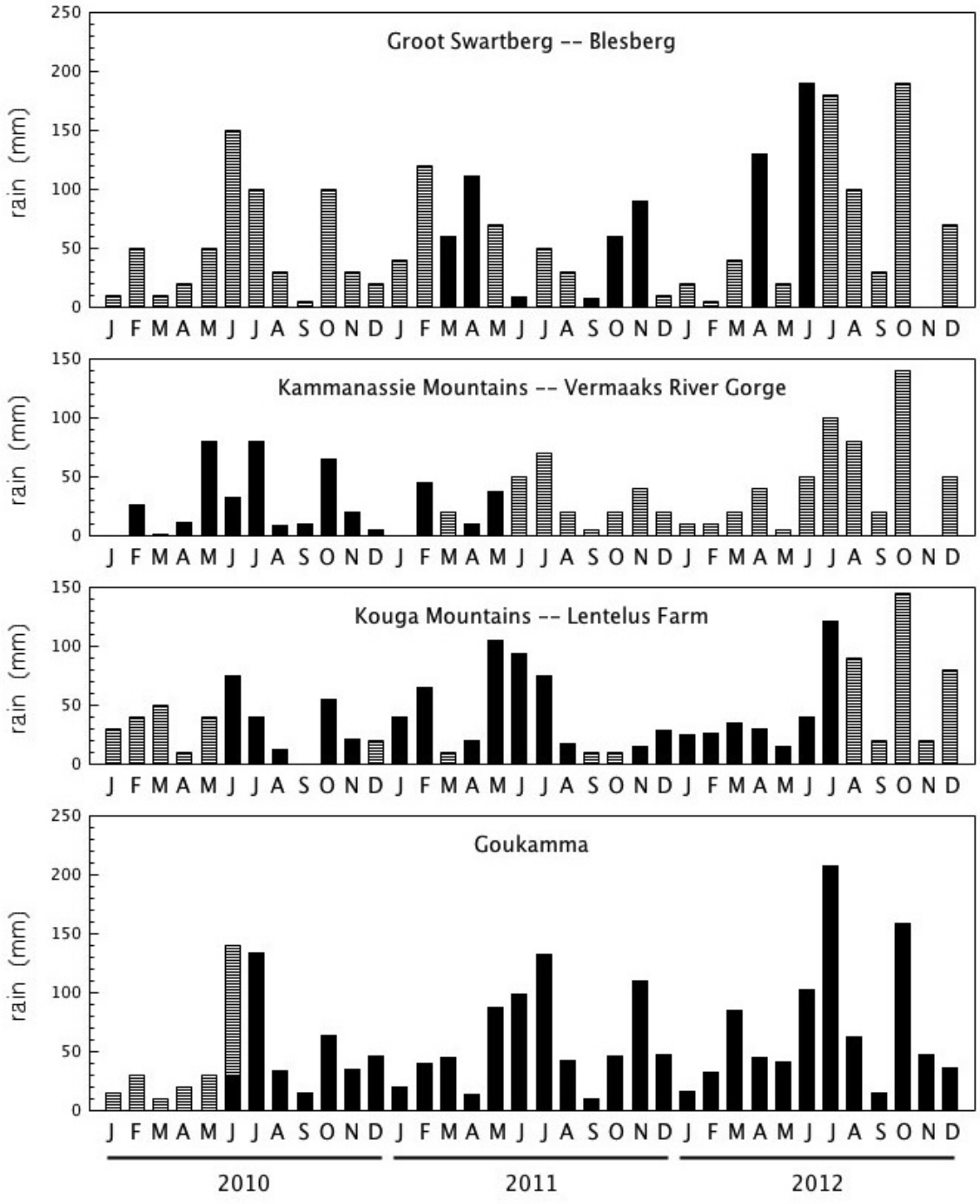

(e) Monthly rainfall as measured (solid bars) and estimated (striped bars) for the eastern region stations.

rain — 2010

	J		F		M		A		M		J		J		A		S		O		N		D	
	δD	$\delta^{18}O$	δD	$\delta^{18}O$	δD	$\delta^{18}O$	δD	$\delta^{18}O$	δD	$\delta^{18}O$	δD	$\delta^{18}O$	δD	$\delta^{18}O$	δD	$\delta^{18}O$	δD	$\delta^{18}O$	δD	$\delta^{18}O$	δD	$\delta^{18}O$	δD	$\delta^{18}O$
	‰	‰	‰	‰	‰	‰	‰	‰	‰	‰	‰	‰	‰	‰	‰	‰	‰	‰	‰	‰	‰	‰	‰	‰
UCT	9.7	0.75	-5.8	-0.54	0.4	-0.83	-12.1	-2.25	-8.4	-2.78	-17.0	-3.31	-15.0	-3.69	-4.9	-1.74	-3.3	-2.24	-3.3	-2.15	-6.2	-2.39	-39.9	-5.06
TMC									-15.0	-3.14	-24.4	-4.35							-16.3	-3.04	-13.1	-2.65	-16.0	-2.35
TWT									-13.5	-3.41	-18.8	-2.54	6.6	0.41	-2.7	-1.73	-21.4	-3.42	23.7	4.09			-74.4	-10.45
WKP									-11.7	-2.57	-25.8	-4.77	-14.7	-3.82	-1.5	-1.55	-24.1	-4.21	-0.9	-1.60	2.2	-0.56	-47.8	-7.12
UKP															-16.6	-3.53	-18.2	0.97	-1.0	3.43	-17.4	-3.12	-56.2	-9.14
MTB									-23.7	-5.43														
DDN																								
RVD											-33.8	-7.58	-47.5	-9.76	-2.4	-2.90	-3.0	-0.79	-21.5	-5.11	5.5	-1.37	-12.0	-1.63
RBP											-5.9	-0.32	-33.1	-6.08	-23.5	-5.6	-5.8	-2.22	-33.5	-5.86	-9.9	-2.14		
BKK											-13.6	0.72	-52.7	-8.97	-22.2	-5.39	-16.8	-3.95	-38.2	-7.08	-16.5	-3.88		
GST																								
BBG											-39.6	-7.17	-30.3	-5.34	-29.6	-5.72	-20.5	-4.91	-33.1	-7.06	-24.6	-5.19	-51.3	-8.26
KMN											-58.3	-9.94	-73.0	-11.77	-18.9	-4.90	-5.0	-2.30	-21.9	-5.55	-26.4	-5.15		
LTL											-42.3	-7.80	-62.9	-10.04	-17.8	-4.32			-16.5	-5.04	-12.1	-3.18		
GKM											-16.9	-3.30	-47.1	-7.60	-14.4	-3.43	0.9	-0.87	-12.1	-3.13	-1.9	-0.46	-32.5	-4.69

Table 4.5: Isotope data for rain for 2010. For locations of the rainfall stations, see the maps in Chapter 3.

rain — 2011

	J		F		M		A		M		J		J		A		S		O		N		D	
	δD	$\delta^{18}O$	δD	$\delta^{18}O$	δD	$\delta^{18}O$	δD	$\delta^{18}O$	δD	$\delta^{18}O$	δD	$\delta^{18}O$	δD	$\delta^{18}O$	δD	$\delta^{18}O$	δD	$\delta^{18}O$	δD	$\delta^{18}O$	δD	$\delta^{18}O$	δD	$\delta^{18}O$
	‰	‰	‰	‰	‰	‰	‰	‰	‰	‰	‰	‰	‰	‰	‰	‰	‰	‰	‰	‰	‰	‰	‰	‰
UCT	-5.2	-0.15	13.9	3.19	-23.6	-4.12	-5.8	-2.73	-12.3	-3.69	-18.3	-4.82	-14.6	-4.68	-3.8	-2.63	-0.1	-1.51	-17.0	-3.48	-12.0	-3.21	-1.6	-2.05
TMC	-1.2	-0.75					-14.8	-4.61	-14.7	-4.17	-16.9	-4.85	-11.6	-4.71	-14.4	-4.64	-9.2	-3.51	-13.6	-3.84	-17.4	-4.64	-9.6	-3.51
TWT									-17.7	-4.97	-17.7	-4.94	3.8	-0.19	4.2	-0.35	39.2	7.74						
UKP					-29.2	-5.35	-22.7	-5.79	-22.4	-5.46	-24.9	-5.85	-23.9	-5.85	-20.2	-5.21			-30.3	-5.13	-23.2	-4.94	-7.6	-4.17
WKP			-15.1	-3.13	-41.4	-4.13	-11.2	-4.07	-16.0	-4.10	-15.0	-4.00	-30.4	-6.06	-14.6	-4.17	3.5	-1.54	-11.8	-3.06	-40.0	-7.94	-1.1	-2.11
MTB	-44.7	-7.97	-41.9	-7.91	-31.9	-4.67	-42.4	-7.98	-52.9	-9.28	-44.4	-8.19	-44.0	-8.07	-42.9	-7.97	-44.6	-8.22	-30.9	-5.90	-31.3	-6.02	-41.8	-7.41
DDN											-27.0	-4.20			-6.0	-2.71					-1.5	-1.5	11.2	2.43
RVD	11.0	-0.47	3.2	-0.39	2.2	-0.87	-3.6	-3.35	-22.7	-5.41	-5.0	-3.12	-7.5	-4.70	-9.6	-3.57	3.0	-1.33	-16.7	-3.70	-16.6	-4.46	-1.1	-1.01
RBP													-22.1	-6.68										
BKK							-30.9	-7.16	-39.2	-8.21	-33.7	-6.58	-28.9	-7.79	-21.1	-4.97	-5.7	-3.53	-37.5	-6.38	-11.6	-4.92	-17.7	-3.37
GST	11.2	0.56	-8.4	-1.82	14.4	1.61	-22.7	-3.72	-29.8	-6.08	-26.4	-6.24	-15.7	-4.73	-13.4	-2.54					-15.4	-2.57	0.1	0.56
BBG	-43.9	-7.62	-21.1	-4.20	-19.4	-4.99	-21.6	-6.14							-39.5	-6.88	-22.3	-4.69	-26.9		-14.8	-6.55		
KMN							-17.5	-5.66	-34.5	-7.05	-23.0	-5.86	-21.7	-6.34			-10.2	-2.41						
LTL	-13.8	-2.86	-6.3	-1.96	-21.3	-4.43	2.9	-2.59	-52.7	-9.23	-32.5	-7.15	-27.7	-7.22	-44.7	-7.03	-5.8	-2.05	3.2	-1.35	0.4	-0.30	-24.1	-3.73
GKM	8.1	-0.64	4.4	-1.06	-0.1	-2.15	7.2	-1.96	-35.4	-6.48	-15.1	-4.41	-8.8	-4.76	-24.4	-5.26	-10.6	-2.90	-3.7	1.0	-1.79			

Table 4.6: Isotope data for rain for 2011. For locations of the rainfall stations, see the maps in Chapter 3.

rain — 2012

	J		F		M		A		M		J		J		A		S		O		N		D	
	δD	$\delta^{18}O$	δD	$\delta^{18}O$	δD	$\delta^{18}O$	δD	$\delta^{18}O$	δD	$\delta^{18}O$	δD	$\delta^{18}O$	δD	$\delta^{18}O$	δD	$\delta^{18}O$	δD	$\delta^{18}O$	δD	$\delta^{18}O$	δD	$\delta^{18}O$	δD	$\delta^{18}O$
	‰	‰	‰	‰	‰	‰	‰	‰	‰	‰	‰	‰	‰	‰	‰	‰	‰	‰	‰	‰	‰	‰	‰	‰
UCT	5.4	0.78	-2.5	-0.68	-11.9	-3.07	-9.8	-3.12	-10.4	-3.08	-6.4	-4.15	-8.8	-2.67	-13.5	-3.25	-10.8	-2.36	-7.1	-3.16	0.1	-1.08	6.9	-0.17
TMC	-4.7	-2.93	-1.0	-2.05	-12.9	-3.91	-13.7	-4.34			-8.7	-2.32	-7.6	-2.93	-20.8	-4.82	-22.4	-5.75						
TWT							11.8	2.15	-4.1	-2.86	-16.4	-4.88	-3.1	-2.73	-14.6	-3.88								
UKP					-33.3	-5.57	-15.6	-4.05	-0.5	-1.82			-18.3	-4.37	-20.5	-5.14								
WKP					-30.8	-5.49	-10.2	-3.16	10.9	-1.12	-15.9	-4.40	-4.8	-2.65	-9.4	-3.51								
MTB	-26.5	-5.30																						
DDN	1.0	-0.20									-22.72	-3.19												
RVD	2.9	-0.99	19.6	1.56	-11.4	-3.19	-17.1	-4.15																
RBP																								
BKK																								
GST	1.0	0.05			-9.1	-0.58	-7.6	-2.46	-6.5	-2.31	-10.5	-2.41												
BBG			-13.9	-3.86	-26.9	-6.26	-15.0	-4.81	-28.2	-7.02														
KMN																								
LTL	-0.3	-0.57	2.2	-1.42	-16.2	-4.33																		
GKM	2.5	-0.97	5.7	-1.75	-9.6	-3.07	-9.7	-3.17	-1.9	-2.47	-12.4	-3.47												

Table 4.7: Isotope data for rain for 2012. For locations of the rainfall stations, see the maps in Chapter 3.

Table Mountain springs

	2010-03		2010-11		2011-05		2011-10		2012-05		2012-09	
	δD	$\delta^{18}O$	δD	$\delta^{18}O$	δD	$\delta^{18}O$	δD	$\delta^{18}O$	δD	$\delta^{18}O$	δD	$\delta^{18}O$
	‰	‰	‰	‰	‰	‰	‰	‰	‰	‰	‰	‰
Redwood			-10.3	-2.96			-10.8	-3.36	-8.0	-3.48	-9.6	-3.03
Wendy's			-9.4	-2.74			-10.7	-3.38	-9.8	-3.32	-9.1	-2.77
Kirstenbosch	-13.7	-3.01	-9.4	-3.03	-12.4	-3.71	-12.9	-3.04	-10.2	-3.48	-10.1	-2.37
Kommetjie	-13.9	-2.88	-8.9	-2.16	-8.9	-3.16	-10.2	-2.89	-6.5	-3.24	-8.5	-1.91
Newlands	-13.3	-2.94	-7.5	-2.61	-6.9	-3.37	-10.2	-3.01	-6.5	-2.67	-7.9	-2.09
Palmboom	-13.7	-2.86	-10.0	-2.43	-4.9	-2.85	-9.9	-2.99	-7.7	-2.95	-8.9	-2.24
Princess Anne							-12.0	-3.21			-8.9	-2.57
Albion	-8.7	-2.18	-7.0	-1.67	-7.9	-2.99	-9.8	-2.87	-7.7	-2.71	-8.0	-2.17
CT Main	-15.7	-2.98	-12.7	-2.70	-12.8	-3.99	-13.3	-3.64	-10.7	-3.40	-12.3	-2.77
Cableway	-19.0	-3.81	-10.4	-3.17							-14.9	-3.06
Glencoe	-17.9	-3.56	-10.0	-3.19	-16.1	-4.17	-16.2	-4.12	-12.5	-3.74	-14.4	-3.04
Leeuwenhof	-14.0	-1.78	-5.2	-2.19	-8.1	-3.71	-11.5	-3.17	-6.4	-2.78	-14.3	-2.59
Tafelberg Rd			-8.6	-2.27	-6.0	-3.44	-12.7	-3.85	-7.0	-3.12	-12.3	-2.93

Table 4.8: Isotope data for the Table Mountain springs. For locations of the springs, see the Cape Town map in Chapter 3.

Western Cape rivers

	Duiwelskloof March 2011		Volstruiskloof March 2011		Witels February 2010		Groothoekkloof January 2012		Meulkloof March 2012	
	δD ‰	$\delta^{18}O$ ‰	δD ‰	$\delta^{18}O$ ‰	δD ‰	$\delta^{18}O$ ‰	δD ‰	$\delta^{18}O$ ‰	δD ‰	$\delta^{18}O$ ‰
1	-14.4	-3.94	-20.7	-4.54	-26.8	-4.70	-27.7	-5.15	-7.4	-3.39
2	-16.3	-4.25	-10.9	-3.75	-30.1	-5.39	-32.4	-5.73	-8.4	-2.95
3	-10.7	-3.53	-8.8	-2.40	-28.8	-5.35	-30.1	-5.28	-10.8	-3.31
4	-14.9	-2.52	-10.5	-3.35	-23.4	-4.13	-23.6	-5.29	-8.1	-3.10
5	-20.8	-4.43			-23.4	4.50	-29.9	5.70	-8.3	-3.30
6	-1.9	-2.81			-27.9	-5.28	-26.1	-5.17		
7					-30.0	-5.74	29.1	-5.22		
8					-20.1	-3.12	-31.5	5.62		
9					-27.3	-5.02	-30.0	-5.48		
10					-27.0	-5.48	-30.9	-5.14		
11					-29.2	-5.61	-30.0	-5.33		
12					-22.7	-4.46	-29.7	-5.43		
13					-26.0	-5.27				
14					-25.1	-5.32				
15					-26.8	-5.17				
16					-22.6	-4.84				
17					-26.4	-5.27				
18					-23.7	-5.18				
19					-26.3	-5.42				

Table 4.9: Isotope data for the five rivers sampled. For locations of the rivers and sample points 1→n, see the maps in Chapter 3.

groundwaters

sample type	location		date	δD ‰	$\delta^{18}O$ ‰
hot spring	The Baths	Citrusdal	May 2010	-22.1	-4.63
hot spring	Goudini Spa	Worcester	February 2011	-24.1	-4.80
hot spring	Brandvlei	Worcester	February 2011	-32.2	-5.79
hot spring	Caledon	Caledon	May 2011	-23.8	-4.84
hot spring	Warmwaterberg	Barrydale	September 2010	-37.7	-6.78
hot spring	Calitzdorp Spa	Calitzdorp	May 2011	-39.4	-7.02
hot spring	Tooverwater	Willowmore	May 2011	-38.6	-7.11
spring	Goudini cool	Worcester	February 2011	-19.7	-4.20
spring	UCT field station	Laingsburg	September 2010	-28.7	-4.67
spring	UCT field station	Laingsburg	September 2011	-33.9	-5.24
spring	UCT field station	Laingsburg	September 2012	-35.5	-4.82
seep	Lily Pond	Table Mountain	February 2011	-12.8	-3.60
seep	Lily Pond	Table Mountain	March 2012	-11.4	-2.95
seep	Tafelberg Spout	Cederberg	December 2010	-29.2	-5.68
seep	Tafelberg Spout	Cederberg	January 2011	-29.6	-4.87
seep	Tafelberg Spout	Cederberg	March 2011	-30.4	-5.20
seep	Tafelberg Spout	Cederberg	December 2011	-28.4	-5.45
seep	Toverkop water cave	Klein Swartberg	September 2010	-25.2	-4.56
seep	Toverkop water cave	Klein Swartberg	October 2011	-27.4	-5.21
seep	Skull Cave	Klein Swartberg	March 2011	-39.7	-6.83
seep	Seweweekspoort Peak Cave	Klein Swartberg	March 2011	-31.5	-6.86
borehole	'Protea'	Kirstenbosch	May 2012	-12.1	-3.62
borehole	'Apple'	Kirstenbosch	May 2012	-9.73	-3.26
borehole	house borehole	Twaktuin	February 2011	-15.5	-3.47
borehole	vlei borehole	Twaktuin	February 2011	-14.4	-3.07
borehole	C&D borehole	Twaktuin	February 2011	-11.3	-2.61
borehole	house borehole	Twaktuin	September 2011	-15.2	-3.88
spring	house spring	Twaktuin	September 2012	-14.9	-3.45
borehole	house borehole	Twaktuin	September 2012	-13.1	-3.09
borehole	vlei borehole	Twaktuin	September 2012	-12.1	-2.34
borehole	C&D borehole	Twaktuin	September 2012	-5.1	-1.31
borehole	Erfdeel 1	Erfdeel	February 2012	-34.6	-6.44
borehole	Grootvlak 1	Erfdeel	February 2012	-45.0	-7.77
borehole	Grootvlak 2	Erfdeel	February 2012	-35.2	-6.89
borehole	upper borehole	Tweespruit	July 2012	-32.7	-4.91
borehole	lower borehole	Tweespruit	July 2012	-35.6	-5.74
borehole	house borehole	Gamkaberg	June 2012	-36.3	-6.70
borehole	Tierkloof	Gamkaberg	June 2012	-34.4	-7.19
borehole	east	Rooihoogte	July 2012	-40.6	-6.79
borehole	west	Rooihoogte	July 2012	-39.4	-7.09

Table 4.10: Stable isotope data for various sample types. Hot springs have T > 37 °C. Locations are shown in the maps of Chapter 3.

Chapter 5

Discussion

5.1 Introduction

This chapter has two major parts. The first part contains findings on the isotope data for rainfall, surface water and groundwater separately, concentrating on the isotope effects, especially the altitude effect. The second part is made up of regional analyses of all data types within an area, such as the Cederberg or Hex River Mountains. The interpretations are proposed on the grounds of stable isotope evidence, but are checked against the geological and hydrogeological setting for feasibility. Attempts are made to draw conclusions that have relevance for groundwater flow in the Table Mountain Group.

5.2 Precipitation

Widespread collection of rainfall across the Western Cape has allowed a thorough consideration of hydrogen and oxygen stable isotope variations for the first time in this region. In particular, the rainfall stations vary greatly in their altitude, from 60–2080 m above sea level, their mean annual precipitation, from 200–1300 mm per year, and distance from the sea, from 2–110 km. Establishing the stable isotope variation with factors such as altitude, continentality and temperature allows for application to hydrological problems such as finding groundwater recharge areas (e.g. D'Alessandro et al., 2004).

5.2.1 Source Area and Pathway Effects

Precipitation in a given area may be derived from differing weather systems or the moisture causing the precipitation may have had different trajectories, hence the rainfall may display distinctive isotopic compositions (e.g. Peng et al., 2010; Breitenbach et al., 2010). South Africa receives precipitation from several types of weather systems, but these can broadly be divided into convective type summer rainfall over the eastern, central and northern parts of the country and frontal winter rain over the western and southern regions. The summer rain is brought over

land anticyclonically by the South Indian High Pressure cell, whereas the winter rain arrives with cyclonic frontal depressions from the southern Atlantic Ocean. Although the frontal depressions originate at approximately 60°S in the Atlantic Ocean and gather some of their moisture over the mid-latitude ocean before making landfall on the southern west coast of Africa, much of the water vapour in these weather systems has been derived from evaporation off the tropical sea surface (Rozanski et al., 1993). The summer rainfall systems develop over the land, but the air mass containing the moisture is derived from the mid-latitudes, 30-60°S, in the southern Indian Ocean. Moisture in the summer and winter rainfall in South Africa has therefore followed different trajectories since evaporation over the tropical ocean and has acquired additional moisture at different latitudes over different oceans at different temperatures of evaporation. It is therefore possible that the summer and winter rainfall may have different isotopic compositions.

Plotted in **Figure 5.1** is data from this study, for the winter rainfall region, and data from three other studies for other parts of South Africa, representing summer rainfall regions. No striking differences are apparent. This could be for two possible reasons: either there is no actual isotopic difference, or the amount of data is insufficient to show any differences.

For the latter, it is possible that the treatment of the data is deficient and a more detailed separation of the Western Cape rainfall is needed, based on weather patterns. This is because rainfall in the Western Cape, although dominated by winter frontal rain, does have elements of other rain-producing weather systems, especially further east, as with rainfall stations like Lentelus and Goukamma. A substantial quantity of the rainfall at these far eastern stations does in fact come from weather related to advection of moisture by the South Indian High Pressure cell. However, this explanation does not seem likely, as the rainfall stations in this study show no significant difference in average δD and δ^{18}O values, d-excess values (see **Table 4.2**) or meteoric water lines between the rainfall stations in the west, which are winter rain dominated, and those further east, with all-year round rain.

It is also possible the duration of sample collection is too short, being only 2 years and having some months not recorded. However, this also does not seem likely for the following reasons. The various Cape meteoric water lines calculated using different data sets do not vary much, in spite of these data sets being vastly different in size, as shown in **Table 5.1**. Also, a lot of groundwater data has been collected and groundwater isotopic values are known to reflect the longer term average precipitation isotope values (e.g Clark and Fritz, 1997). As the groundwater data overlap the precipitation data and the array of compositions is centred within the spread of precipitation data (see **Figure 5.1**), this can be seen as a validation that the precipitation samples are representative of longer term precipitation averages.

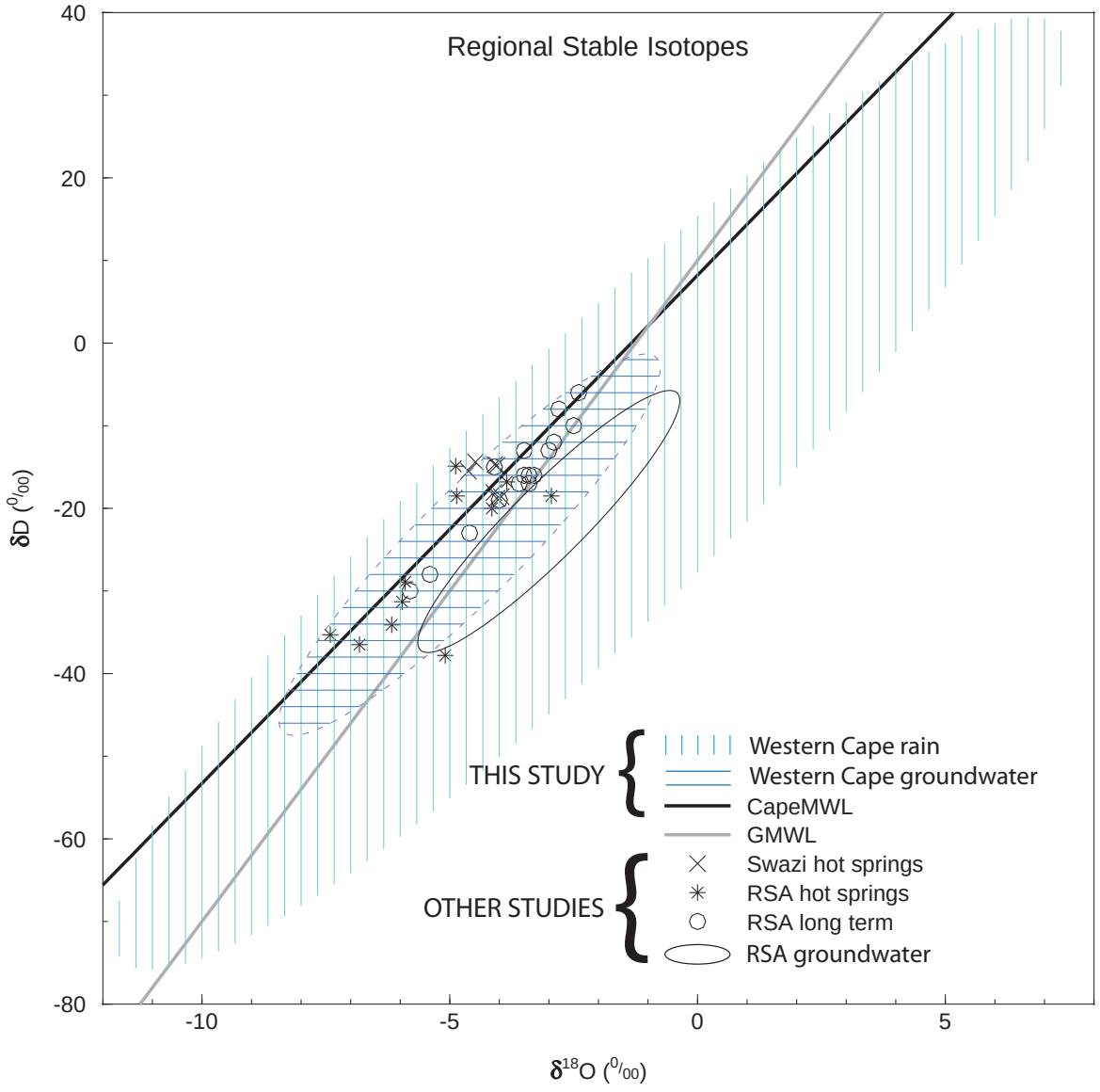

Figure 5.1: Comparison of isotope compositions of water from various South African studies with the results fields (shaded areas) for this study. Data for Swaziland hot springs from Mazor et al. (1974), RSA hot springs from Mazor and Verhagen (1983), RSA long term precipitation from Talma and van Wyk (2013) and RSA groundwater from West et al. (2014). The CMWL has the equation: $\delta D = 6.15\delta^{18}O + 8.21$.

meteoric water line equation	years		stations	reference
$\delta D = 6.1\delta^{18}O + 8.6$	1	1995-6	4	(Diamond and Harris, 1997)
$\delta D = 6.41\delta^{18}O + 8.66$	12	1996-2008	1	(Harris et al., 2010)
$\delta D = 6.15\delta^{18}O + 8.21$	2	2010-12	15	this study

Table 5.1: Meteoric water line equations calculated for rainfall in the Western Cape, illustrating the subtle differences in equations in spite of substantial differences in the date, duration and scale, as determined by the number of stations, for each study.

It does, however, remain possible that a more detailed analysis of South African isotope data will reveal a slight yet significant difference in isotopic composition for the summer and winter rainfall regions, but this is beyond the scope of this study. The alternative hypothesis may therefore be correct, which is that, in spite of different weather systems and moisture mass trajectories, there are no observable differences in isotope signatures between the summer and winter rainfall systems.

5.2.2 Isotope Effects

5.2.2.1 Temperature

Temperatures vary substantially across the Western Cape. This includes the daily maxima and minima, which are often over 40 °C in summer at low altitude, inland locations, and less than 0 °C in winter on mountains and at inland locations. Also, during precipitation events anticyclonic summer rain can occur with air temperatures over 20 °C whereas cyclonic winter precipitation frequently occurs as snow (SAWB, 1996). The isotopic content of precipitation is known to vary greatly temporally, and although correlations and patterns can at times be found with temperature, there is much noise in the data, associated with the complex dynamics of each and every weather system or rain event. Dansgaard (1964) states that, even if assuming no kinetic, exchange or evaporation effects, the isotopic composition of a sample of rain cannot be used to calculate the condensation temperature. This is because many other parameters, such as humidity, cloud height and rain event duration, also play a role in determining the eventual isotope composition of the rain.

The strong correlations of stable isotopes with average annual temperature reported in the literature (e.g Craig, 1961a; Dansgaard, 1964; Yurtsever and Gat, 1981) are summarized by Yurtsever and Gat (1981) as follows: "...it is evident that the spatial variations in the mean isotopic composition of precipitation of [GNIP] network stations are essentially correlated to the temperature variations." It is important to note that these correlations are based on long term averages of both the δD and $\delta^{18}O$ values of rainfall and of temperature (T) at each station and strong correlations are only formed with global or continental scale data sets and in particular at middle and high latitudes. This T-δ correlation is largely a product of the rainout process, where T reflects

species	gradient $\frac{\Delta‰}{1000km}$	location	reference
δD	13	Europe: Belgium to Poland - summer	Rozanski et al. (1982)
δD	33	Europe: Belgium to Poland - winter	Rozanski et al. (1982)
$\delta^{18}O$	1.6	Europe: Poland to Russia	Rozanski et al. (1993)
$\delta^{18}O$	3.8	Europe: Poland to Russia	Rozanski et al. (1993)
$\delta^{18}O$	3–4	North America: Atlantic to Rockies	Clark and Fritz (1997)
$\delta^{18}O$	10	Canada: Pacific to Prairies	Yonge et al. (1989)
$\delta^{18}O$	0.75	Amazon: Atlantic to Andes	Salati et al. (1979)

Table 5.2: Some examples of the continental effect from around the world.

distance from the tropical oceans and is therefore a proxy of the length of the air mass trajectory (Araguás-Araguás et al., 2000). At a single location where two (or more) weather system types produce precipitation, it has been shown that the rainout process has a greater effect in reducing the δ values of precipitation than seasonal changes in temperature of as much as 10 °C (Araguás-Araguás et al., 1998).

The situation in the Western Cape is that, in spite of the variety of climates in the study area, the mean annual temperatures at the 15 rainfall stations are between 16.5 and 19 °C. This small range in temperature makes it difficult to attempt a meaningful analysis of isotopic variations against average annual temperature. It may be possible to explore variations in stable isotopes against seasonal temperatures, but the precipitation during summer is erratic at many of the stations and more years of data would be needed. Isotopic trends will instead be explored against continentality and altitude, both also proxies for the rainout process.

5.2.2.2 Continentality

There is often a correlation between isotope composition of rainfall and distance from the coast (e.g. Liu et al., 2010). This has either been applied over large distances, 1000s of kilometres, and for this purpose the GNIP (IAEA/WMO) data has usually been used, such as Araguás-Araguás et al. (1998), or over a smaller scale, typically using non-GNIP data, such as Hunjak et al. (2013) who sampled around Croatia. The former studies often reveal a clear gradient in isotope values and result in a $\frac{\Delta\delta}{\Delta distance}$ ratio, whereas the latter studies may only find a difference between coastal and inland sites and not be able to calculate a meaningful gradient (e.g. Vreča et al., 2006). Some examples of calculated continental isotope gradients are given in **Table 5.2**.

Developing a continentality model for the Western Cape is challenging in several ways. Firstly, the area of study is only sub-continental and so isotopic depletion is limited, although this is offset by orographically induced rainout on the 2000 m high mountain ranges of the Cape. Secondly, the area is almost surrounded by ocean and so most locations are never further than 100 km

station	Atlantic distance	coast distance	Atlantic × coast
UCT	8	8	64
TMC	2	2	4
TWT	48	45	2160
UKP	70	70	4900
WKP	72	70	5040
MTB	143	110	15730
DDN	133	105	13965
RVD	242	42	10164
RBP	330	30	9900
BKK	314	50	15700
GST	315	55	17325
BBG	410	65	26650
KMN	482	50	24100
LTL	573	35	20055
GKM	526	5	2630
r for δD	-0.39	-0.44	-0.71
r for δ^{18}O	-0.44	-0.37	-0.68

Table 5.3: Calculation of a continentality factor, by multiplication of the distance to the Atlantic in a line due west and the distance to the closest coastline irrespective of direction. Correlation coefficients between weighted mean delta values at each station and the various distances are shown.

from the nearest stretch of coastline (see **Table 5.3**). Thirdly, several types of weather system are responsible for producing rain in the province and these may approach from any direction between north-west, through west, south-west and south, to south-east, a range of 180°. Ocean is located in all of these directions from the rainfall collection stations, but by very different amounts. For example, the Goukamma sampling station is very close to the Indian Ocean and rainfall approaching from the south will have travelled a mere 5km over land before reaching there, whereas a trough approaching from the Atlantic Ocean at the west coast will have travelled over 500km before arriving at this station. No simple single factor can therefore be expected to describe a continentality correlation and indeed, correlations between δD or $\delta^{18}O$ and 'distance-to-Atlantic' or 'distance-to-closest-coast' are poor, with Pearson's r values of -0.39 for δD – Atlantic, -0.44 for $\delta^{18}O$ – Atlantic, -0.53 for δD – coast and -0.37 for $\delta^{18}O$ – coast.

A factor that somehow combines the effects of multiple weather systems approaching from the Atlantic and Indian Oceans to represent the average length of rainout pathways to each rainfall station is needed. The two measurements of 'distance-to-Atlantic', which is a line from the rainfall station due west to the Atlantic Ocean, and 'distance-to-closest-coast', which is a line in any di-

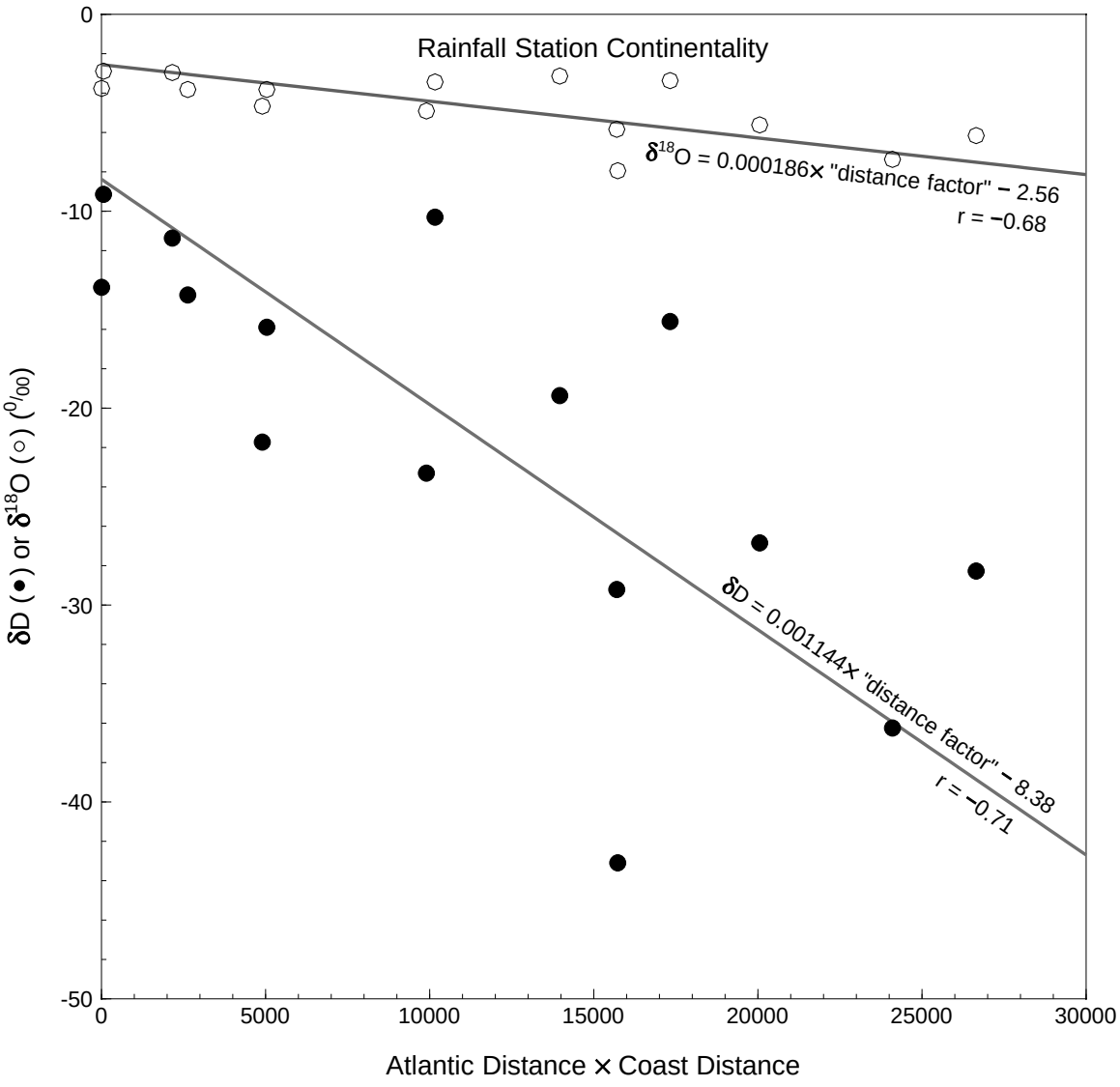

Figure 5.2: The continental effects calculated from this study.

location	**country**	$\delta^{18}O$ **gradient** $\frac{‰}{100m}$	**altitude** m asl	**reference**
Mt Cameroon	Cameroon	-0.16	0–4000	Gonfiantini et al. (2001)
Eastern Andes	Bolivia	-0.24	200–5200	Gonfiantini et al. (2001)
Hérault	France	-0.27	500–1800	Ladouche et al. (2009)
whole island	Taiwan	-0.20	0–2500	Peng et al. (2010)
Fuego volcano	Guatemala	-0.67	800–1200	Mulligan et al. (2011)

Table 5.4: Some examples of the altitude effect from around the world.

rection to measure the shortest distance to the coast from a rainfall station, have been multiplied to create a composite factor. Using this factor produces much better correlations; -0.71 for δD and -0.68 for $\delta^{18}O$ (**Figure 5.2**). The best fit lines to this data also have more realistic δD and $\delta^{18}O$ intercept values, close to those measured at UCT. These values are those expected for precipitation falling at the coast. Unfortunately this correlation does not allow easy comparison with isotope gradients that have been reported as $\frac{\Delta\delta}{\Delta distance}$, such as in Salati et al. (1979) or Rozanski et al. (1982).

5.2.2.3 Altitude

The altitude effect is the most easily measured and quantified meteoric isotope effect and many studies report values of $\frac{\Delta\delta}{\Delta altitude}$ for $\delta^{18}O$ and sometimes δD of precipitation at myriad locations around the world. **Table 5.4** shows a selection of these results from various recent studies; Clark and Fritz (1997, p.71) give results from similar studies in a slightly older selection of the literature.

The altitude effect is, as with the temperature and continental effects, also largely a consequence of progressive rainout as weather systems move up a mountain or escarpment and the heavier isotopes are depleted initially, leaving the subsequent precipitation to have lower and lower δ values. There is, however, an additional factor causing these lower δ values found at greater elevations and this is a reduction in the evaporative enrichment of raindrops as they descend below the cloud base, through unsaturated air. At higher elevations, the land surface is closer, or indeed above the cloud bottom, so reducing or eliminating the path length in which evaporative enrichment can occur.

Table 5.5 shows the altitude effect results calculated for this study. The range of $\frac{\Delta\delta^{18}O}{\Delta altitude}$ values can be seen to be similar to that reported in the literature, except that the Table Mountain and Cederberg region gradients seem on the low side. Unfortunately not many examples of $\frac{\Delta\delta D}{\Delta altitude}$ values have been reported in the literature. As would be expected from the physics governing isotopic fractionation of H and O in water, the δD gradients are around 6–8X that of $\delta^{18}O$.

locations	**distance***	**altitude change**		**gradient**	
				δ**D**	δ^{18}**O**
	km	m	masl	$\frac{‰}{100m}$	$\frac{‰}{100m}$
UCT - Lily Pond - TMC	6	940	135–1075	-0.48	-0.075
WKP - TWT - UKP - Cederberg Tafelberg	40	1550	350–1900	-1.1	-0.11
DDN - MTB	10	1430	480–1910	-1.6	-0.34
RVD - RBP	100	635	250–885	-2.0	-0.24
GST - BKK	6	750	350–1100	-1.8	-0.33
GKM - LTL	70	580	60–640	-2.2	-0.31
all stations: least squares regression	480	2020	60–2080	-1.2	-0.19
all stations: reduced major axis regression	480	2020	60–2080	-1.7	-0.27

Table 5.5: Altitude effect gradients calculated for this study. *Distance refers to the distance between the furthest of the listed locations.

The first point to note about the altitude effect calculations for this study is that many of the individually calculated gradients are similar, such as DeDoorns – Matroosberg and Gamka Store – Bakenskop, even though the altitudes are not the same and the pairs of stations are hundreds of kilometres apart. This is best seen graphically in **Figure 5.4**. Second to note, again most easily visible in the graphs, is the general agreement between the local gradients and the regional line calculated by using all the rainfall station data gathered in this study. Slight exceptions to this are the Table Mountain area (C – Lily Pond – T) and the Cederberg area (I – W – U – Spout).

Looking more closely at the data, there is a trend, especially noticeable in the δD gradients, of increasing gradient eastwards; the locations are arranged approximately in a west to east order in **Table 5.5**. This trend is not well displayed by the $\delta^{18}O$ gradients, however, the high gradients for DDN – MTB and to a lesser extent GST – BKK, the two locations which are disturbing the trend, are probably due to the evaporative enrichment of rain at DDN and GST, both of which are low altitude, low rainfall sites. The ratio of $\frac{\Delta\delta D}{\Delta\delta^{18}O}$ should be around 6–8X, and if less than this, is a sign of evaporative enrichment. Substantial evaporation of falling raindrops will increase $\delta^{18}O$ values more than δD values because of kinetic fractionation, and so increase the difference in $\delta^{18}O$ values between the high and low altitude sites, resulting in a steepening of the $\delta^{18}O$ gradient and therefore a reduction in the multiplication factor between the δD and $\delta^{18}O$ gradients.

The very low gradient in $\frac{\Delta\delta}{\Delta distance}$ reported for Table Mountain can be explained by the following argument. Normally weather systems move from low to high ground and so, as explained above, the altitude effect is a reflection of rainout of heavier isotopes at lower elevations. The dramatic topography of Table Mountain means that the high altitude station, TMC (1074 m), is only 2 km from the Atlantic Ocean coast, whereas the lower station, UCT (135 m), is 6 km further inland. This is a reversal of the usual situation in studies of the altitude effect, where the higher altitude station is also further inland (or in the direction of rain-bearing weather in the case of the

Andes and the Amazon in Gonfiantini et al. (2001)) than the lower altitude station. The altitude effects measured in these studies are the cumulative effect of altitude and distance on rainout. The Table Mountain sub-study is therefore an unusual and valuable example that demonstrates how the pure altitude component of rainout is less than is generally found in these other studies, where a composite distance and altitude induced rainout is being measured.

Two regression lines are plotted on each of the graphs in **Figure 5.4**; the altitude data is shown in **Table 5.6**. These lines have been regressed on all the rainfall station data (letters); they exclude the points for the high altitude seeps (symbols), such as the Lily Pond and Spout. The least squares method (thinner line) assumes no error on the x-variable as this is accurately known and does not change; this regression can be thought of as y on x. This method is appropriate for this type of analysis, where y (δ) is variable and imperfectly known and is dependent upon x (altitude), which is perfectly known and unchanging. However, these lines, for both δD – altitude and $\delta^{18}O$ – altitude are not good matches for the local gradient lines, as seen in the graphs and in the gradient values in **Table 5.5**, where the least squares gradients are at the low end of the spectrum.

The reduced major axis method of regression (thick lines) has been used throughout this study for the δD – $\delta^{18}O$ regressions and is ideally suited to data where both x and y have variance and neither are independent of the other. Interestingly, although this method is theoretically statistically sub-optimal for the δ – altitude regressions, the resulting regression lines and $\frac{\Delta\delta}{\Delta altitude}$ gradients seem to describe and fit the data better.

Figure 5.3: Map of the study area with sample locations and cross section lines indicated. Background DEM from NASA (2013) and roads shapefile from NGI (2012).

Island Mountains and Mountain Valleys

Island Mountains is a term coined here to describe sample collection points that are located at or near the top of a mountain peak and are therefore at a position much higher than the surrounding area.

The two rainfall collection stations, Blesberg and Kammanassie, which are only 25 km apart and have a 1400 m altitude difference, would seem to make a useful pair for a local estimate of the altitude effect. However, Blesberg, the highest station of the whole study, at 2080 m, has δD and $\delta^{18}O$ that would be expected for a station of half that height, based on the average altitude effect relationship for this study. In contrast, Kammanassie, with a moderate altitude of 666 m, has isotope ratios that would be expected for a station at triple the height. Only Matroosberg, at 1910 m, has more negative δ values than Kammanassie. The result of these departures from the average pattern is that the local altitude effect gradient is reversed between these stations, with δ values that increase with altitude.

The Blesberg mean δ values seem to fall on a line with Cederberg Tafelberg (Spout) and Cape Town's Table Mountain (and Lily Pond); see **Figure 5.4**. All four of these points lie to the right of the $\frac{\Delta\delta}{\Delta altitude}$ best fit regression line, meaning the δ values are less negative than expected, based on the average for this study. Robinson Pass, Bakenskop and Matroosberg are close to the average for all of the data. Kammanassie and Lentelus lie to the left of the average, meaning their δ values are more negative than would be expected for their altitude. These three sets of locations have morphological similarities that may account for their location on the δ–altitude plot. The first group can be thought of as "island peaks", sharply rising peaks that are much higher than the general surrounds. The last group can be thought of as "mountain valleys", where the elevation of the sample site is lower than that of the general surrounds. The intermediate group are at a position in the landscape where there are substantial amounts of higher and lower ground around, or, in the case of Bakenskop, on a plateau-like summit where the station is surrounded by lots of land at a very similar elevation (less than 100 m difference).

Rainout on the "island peaks" is not substantial, because of the sudden change in elevation, and so the isotopic signature is more typical of that for a site at lower elevation. The "mountain valleys" are the reverse, where the station elevation does not reflect the amount of rainout that occurs on the surrounding higher ground, and so the isotope composition tends towards those expected at these surrounding, higher elevations.

Table 5.6 summarizes the landscapes around some of the rainfall collection stations, as well as some high altitude seeps. The average altitudes were generated from the ASTER DEM (Advanced Spaceborne Thermal Emission and Reflection Radiometer Digital Elevation Model) by averaging the elevations of all pixels within a 5 km radius of the point of interest (ASTER, 2014). The seeps discharge high up in the mountains with minimal ground above the seep and so the discharge altitude cannot be much different to the recharge altitude, as there is very little more mountain available above the seep point for recharge to occur. These seeps can be thought of as proxies for

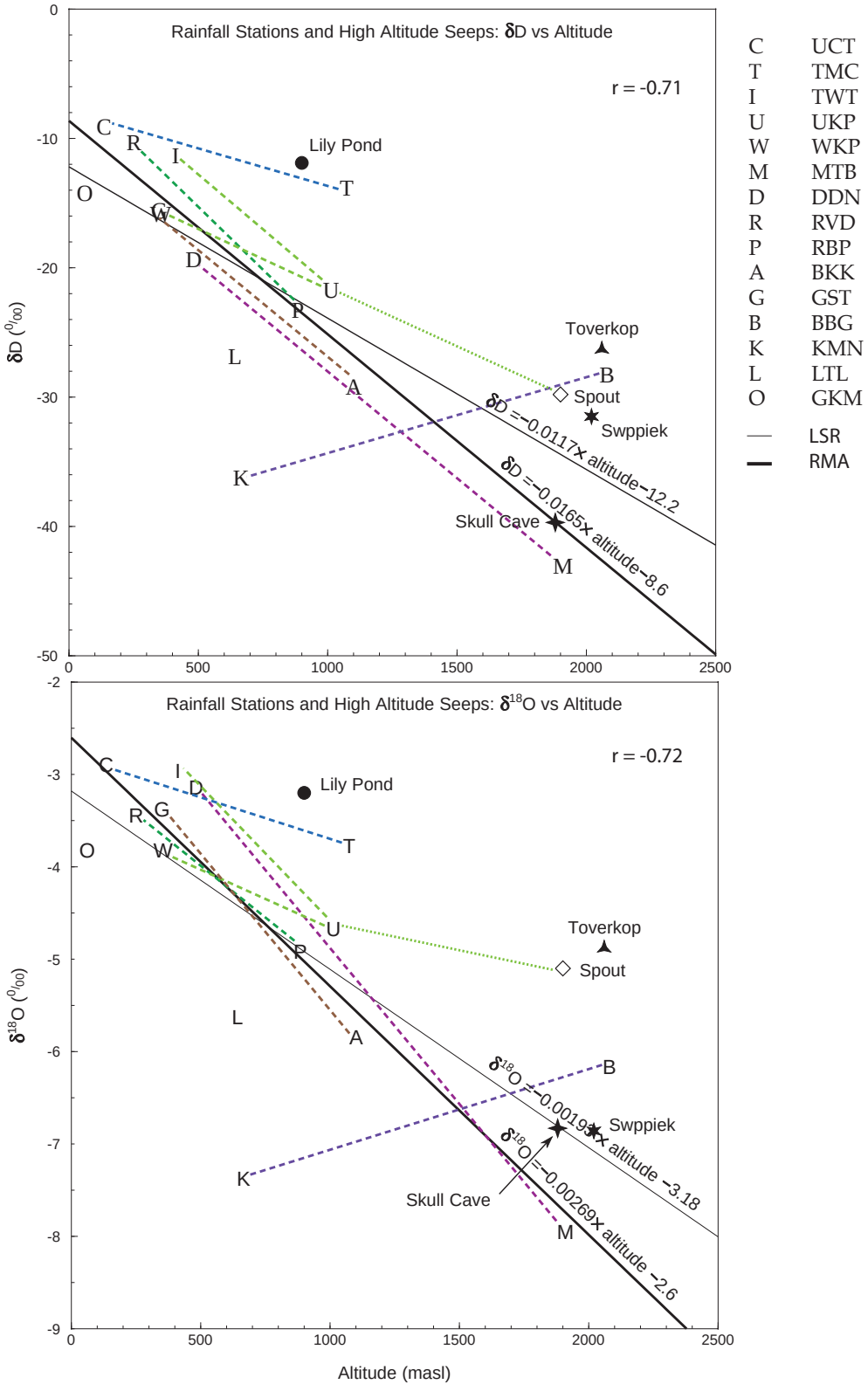

Figure 5.4: Relations between altitude and δ values. Letters indicate weighted averages of monthly precipitation at rainfall collection stations; symbols are high altitude seeps. Dashed lines connect rainfall nearby stations; dots to a nearby seep. Colours are from the theme colours for one of the stations in the pair. Both the RMA regression (thick line) and LSR (thin line) are shown, calculated from the rainfall station data, excluding the seeps.

station		elevations				stn - avg
		m asl in 5km radius from station				m
		station	**highest**	**average**	**lowest**	
Cederberg Spout		1900	1969	1266	940	+634
Table Mountain Cableway	TMC	1074	1086	289	0	+785
Table Mountain Lily Pond		900	1086	289	0	+611
Matroosberg	MTB	1910	2249	1561	550	+349
Robinson Pass	RBP	885	1363	723	350	+162
Bakenskop	BKK	1100	1106	772	350	+328
Toverkop	TVK	2060	2189	1281	550	+779
Skull Cave	SKC	1880	2240	1393	750	+487
Seweweekspoortpiek Cave	SWP	2020	2324	1368	650	+652
Blesberg	BBG	2080	2084	1329	600	+751
Kammanassie	KMN	666	1205	794	500	-128
Lentelus	LTL	710	1688	854	550	-144

Table 5.6: Relative position in the landscape of selected rainfall stations and high altitude seeps, which are proxies for rainfall. The last column summarizes the situation by showing the difference in height between the station or seep elevation and average elevation for an area of 5 km radius around the station.

rainfall at much the same elevation. It can be seen from **Table 5.6**, especially the final column, that some stations lie well elevated from the average surrounding landscape, Blesberg, Toverkop and Table Mountain being good examples – these are the "island peaks". Other stations are at similar altitudes to the average and only two, Lentelus and Kammanassie, are examples of the "mountain valleys". A good correlation exists between this difference from the average elevation, and the position on the δ–altitude graphs, as described above. A visual representation of the relative altitude of sampling points is shown in **Figure 5.5**.

The correlation is not exact, at least one reason of which is the seep data consists of between one and three samples only per seep. Much noise exists in isotope data, due to the specifics of the weather, and so single samples are not ideal, although being groundwater, these seep samples will be more stable and representative values than for rain. Another reason for the extreme position of Kammanassie is the large amount and isotopically negative rainfall in June and July 2010. The July value in particular, with 80 mm rainfall for the month, caused the average to be displaced towards low δ values.

In conclusion, due to the steep slopes and small area of the high peaks in the Cape Mountains, the altitude effect is supressed and the isotopic composition of rainfall on these summits is less negative than one might expect. The reverse is also true for valleys in mountainous areas, where the isotopic composition reflects a slightly higher altitude, closer to that of the average ground

elevation around the site, and not the specific, low, elevation of the valley floor. To get an accurate measure of the altitude effect, sites for rainfall collection should be chosen on broader peaks where substantial areas of high ground occur, such that the rainout process is significant enough to drive the isotope ratios to more negative δ values.

This altitude effect distortion is probably the reason the RMA regressions fit the data better than the least squares method, as the RMA regression assumes an error in 'x' as well as 'y'. As discussed above, the ground altitude at the rainfall stations is not always representative of the area around the location, which is what influences the isotope content of the rain, and so 'x', or altitude, can also be thought of as being subject to some error.

5.2.2.4 Amount

Correlations between δD or $\delta^{18}O$ and rainfall amount have been described by many authors since Dansgaard (1964) first reported it. As the amount of rainfall increases, the δ values decrease, both for single rainfall events (e.g. Dody and Ziv, 2013) and for monthly average rainfall amounts (e.g. Uemura et al., 2012). Reasons for the amount effect include, firstly, a drop in air temperature to cause condensation of progressively isotopically lighter vapour, as the heavier isotopes have already condensed and rained out of the air mass. Secondly, the more rain that has fallen, the more the air below the cloud becomes moist and so less evaporative enrichment of the raindrops occurs as they fall to the ground. And thirdly, similarly, in clouds with great vertical development where rain may form at high elevations, raindrops falling through the cloud may undergo isotope exchange with cloud droplets and vapour lower down, which will make slight rains tend towards heavier isotopic content, but will affect substantial rains less and so substantial rains will tend to retain their more negative isotopic signatures.

The data from this study is not ideally suited to quantification of an amount effect, primarily because the short period of sampling (two years) leads to averages for rainfall and isotope data possibly being far from the long term means. No correlations exists between the average annual rainfall and the weighted mean isotope values, as can be seen in **Figure 5.6**, both graphically and from the 'r' values that are near zero. For monthly data, a similar restriction on data quality results from the short duration of this study, as each month (e.g. July) may only be based on zero to three samples. At some stations there are months with no samples, although this is often due to a consistent lack of rain for that month(s) over two or three years, for example January at De Doorns. Nevertheless, for the stations with more complete records, comparison of mean monthly δD and $\delta^{18}O$ values with mean monthly rainfall has been done: see **Figure 5.7**.

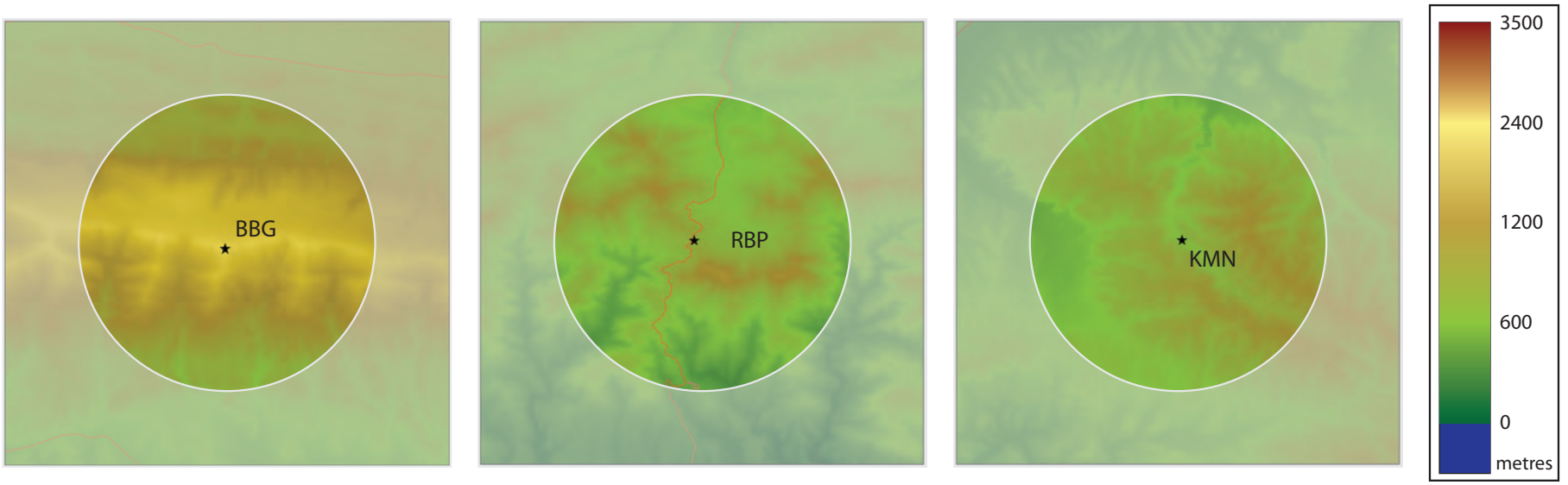

Figure 5.5: Digital elevation models for three of the rainfall collection stations with a highlighted circle of 5km radius around each station, illustrating the relative position in the landscape, in terms of altitude, of each station. Blesberg (BBG) is an example of an "island peak", Robinson Pass (RBP) of a station in a more or less representative position and Kammanassie (KMN) a "mountain valley". See **Table 5.6** for similar information in a numerical format for these and other sampling points.

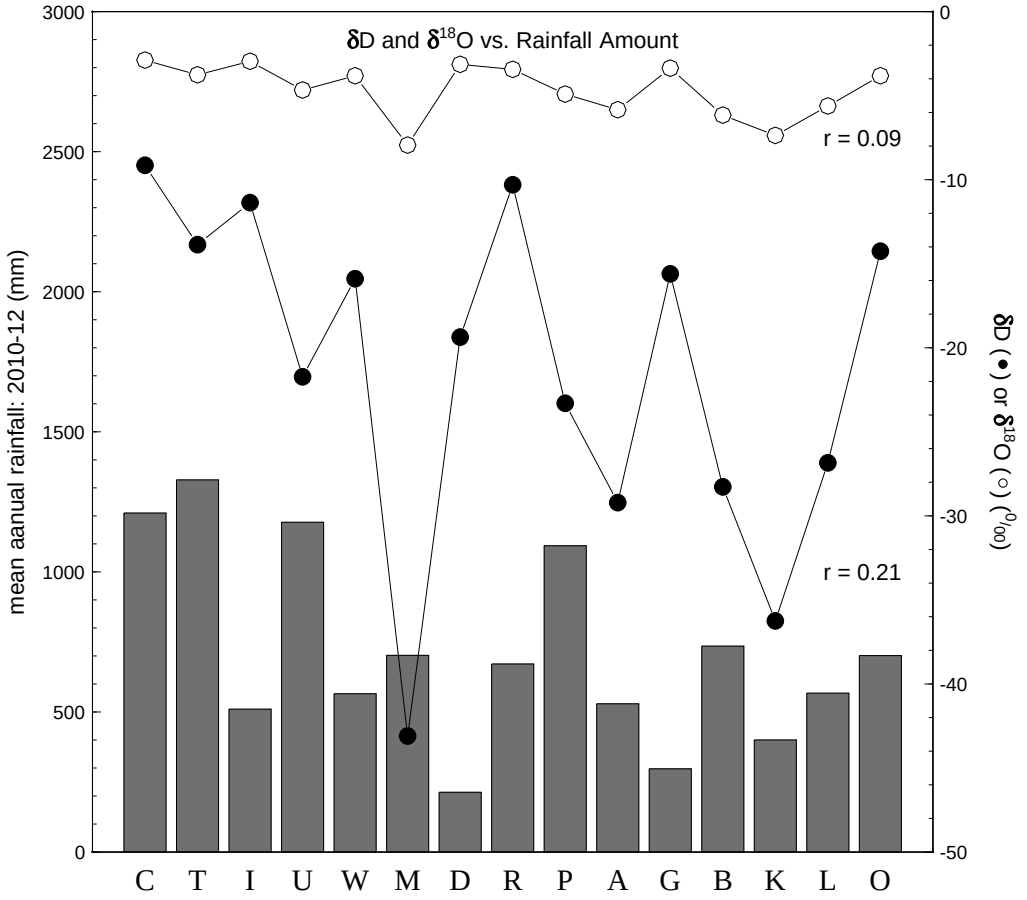

Figure 5.6: Comparison of weighted mean isotope composition and mean annual rainfall at each station: C = UCT, T = Table Mountain, I = Twaktuin, U = Uitkyk Pass, W = Wolfkop, M = Matroosberg, D = De Doorns, R = Riverndale, P = Robinson Pass, A = Bakenskop, G = Gamka Store, B = Blesberg, K = Kammanassie, L = Lentelus and O = Goukamma.

These stations were not selected on the grounds of displaying a "better" amount effect, but purely on the completeness of the record. The amount effect at these stations is generally noticeable in that there is a fair to good correlation between the δD or $\delta^{18}O$ values and rainfall amount. The Pearson's 'r' correlation coefficients shown on the graphs in **Figure 5.7** confirm the validity of the visual impressions given by the graphs. The Wolfkop station, however, shows no correlation between rainfall amount and δ values, due to some months with low rainfall having the isotopically lightest water, particularly March and December. The 30th March 2011 featured an unusual low pressure trough preceding a frontal depression over the Atlantic Coast area, causing widespread rain over the Western Cape and into the western parts of the Northern Cape, with falls of 8 mm at Clanwilliam and 10 mm at Excelsior Ceres. Rain from these systems is typically convective in nature (similar to thunderstorms) and generates rain of light isotopic composition. The rainfall of 31st December 2010 to 1st January 2011 has already been discussed in the previous chapter (Chapter 4), and was a significant event environmentally, causing floods and mass

wasting erosion in the Cederberg region, and resulted in rain and hail with highly negative delta values. A longer term record for a station like Wolfkop would be expected to see the influence of these unusual events decline and a better amount effect correlation develop.

The amount effects from the stations at UCT, Riverndale and Goukamma are all significantly better than that found by Harris et al. (2010) for UCT rainfall over 1996–2008, which gave 'r' values of -0.388 for δD–amount and -0.425 for $\delta^{18}O$–amount. Of the three stations shown in **Figure 5.7**, the UCT 2010–2012 record gave the poorest correlations with 'r' values of -0.51 and -0.68, similarly, but these are still substantially better correlations than the previous work. This suggests that some years have a particularly clear amount effect, exceeding the long term average. This finding emphasizes the value of long term monitoring in revealing average meteorological patterns and warns against overinterpretation of data based on short term precipitation records.

5.3 Surface Water

5.3.1 Altitude

The five rivers sampled reveal a wide range of isotopic compositions over an altitude range of approximately 130–1900 m (see **Figure 5.8**). The data for each river generally forms a cluster, with no significant correlations against altitude. The best correlation is at Volstruiskloof, which is the only river to have 'r' values more positive or more negative than +0.5 or -0.5, respectively (the threshhold for a reasonable correlation). However, removal of only one of the four Volstruiskloof data points reduces the remaining three points to a cluster. For the neighbouring river, Duiwelskloof, a better correlation can be created if the data point with the highest δ values is removed; this can be motivated as this sample is from the base of a very low flowing drip waterfall that flowed over exposed, sunny rock for many metres and has been substantially evaporated in the process. However, this still does not create a good correlation between isotope values and altitude. The outlier Volstruiskloof and Duiwelskloof points have been included in analyses and graphs.

5.3.2 Springs, Seeps and Tributaries

Samples of seeps and springs were taken along Groothoekkloof and in the Witels, often paired with a sample from the main stream just above mixing with the new source, but these showed surprisingly little variation. Similarly, tributaries were also sampled and paired with a sample in the main stream just upstream of mixing with the tributaries' waters, and again these often showed little difference. No systematic variation could be found between the isotope composition of a sample and the characteristics of its source, such as being a main stream or spring sample, or the size or average elevation of its sub-catchment, in the case of a tributary.

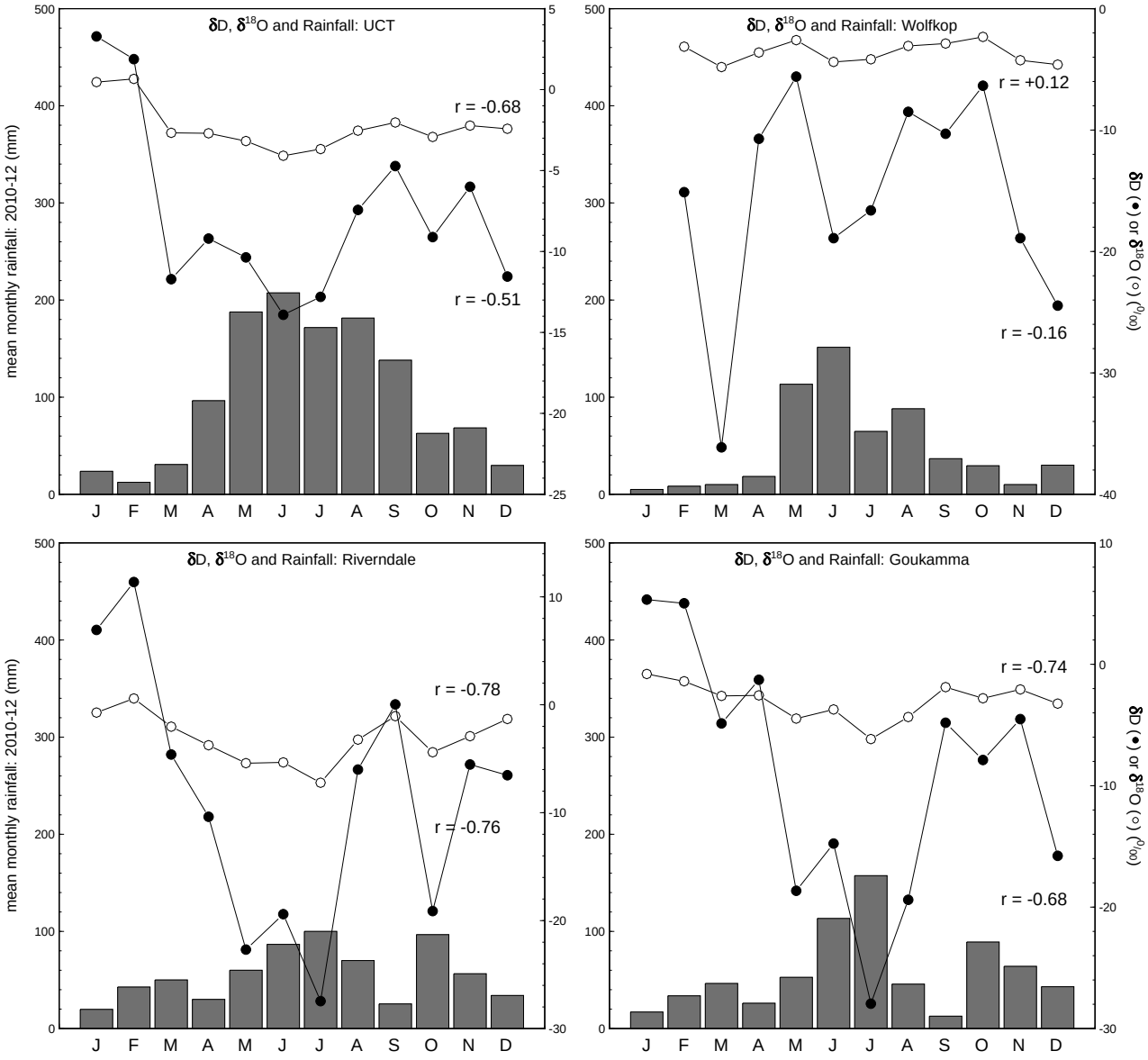

Figure 5.7: Mean monthly rainfall, δD and $\delta^{18}O$ values for the four rain stations with most complete record.

5.3.3 Baseflow

The rivers were all sampled in summer or early autumn when rainfall had been low for many months, with the exception of Meulkloof, near Swellendam in the southern Cape, which experiences all year round rainfall. The other rivers would all have been fed exclusively by groundwater (see **Section 2.5.4**), whether deeper groundwater discharging from fractured Table Mountain Group aquifers or shallow groundwater from soil and scree slopes. The surface water flows that remain steady over the dry season and are groundwater fed are known as baseflow.

Several factors could cause the baseflow to show little isotopic variation down the length of the river, as seen in **Figure 5.8**. The most obvious factor is that river samples are a mixture of the various groundwater sources that feed them, and so mixing of all the water sources would dilute any unusual isotope composition feeding into the river at any point. The rivers all have a steady increase in flow downstream, caused by addition of groundwater. However, the sampling of springs, seeps and tributaries directly showed that it is not mixing and dilution of surface water that is responsible for the lack of isotopic trends or changes, but rather the sources themselves that do not vary much.

Groundwater flow through the Table Mountain Group aquifers is directed by fracture networks that are aligned with structural features and bedding (Hartnady and Hay, 2002b). Groundwater does not simply flow from peaks to valley bottoms in the shortest distance as it would in a primary porosity aquifer. This complex flow dynamic means that water emerging as springs and seeps to feed surface water may come from a range of directions and be recharged at a variety of positions at different altitudes. This complexity is possibly the reason the rather limited surface water data set is unable to yield any patterns. Interestingly, the variations in δD and $\delta^{18}O$ values tend to decrease eastwards, as seen in the last two columns of **Table 5.7**. This could be caused by an increase in fracturing of the Table Mountain Group as one moves from the relatively undeformed strata of the Drakenstein Mountains in the west, through the syntaxial region of the Hex River Mountains to the southern Cape, known to have experienced the greatest tectonic deformation during the Cape Orogeny (Söhnge, 1983; de Beer, 2002). The greater the degree of fracturing, the more likely the groundwater becomes well mixed and variation in isotope composition is homogenised. The sample size of 5 rivers is perhaps a bit small to take this as a real trend, but it is interesting that greater river length, greater change in altitude or greater catchment size does not cause a greater range in isotope values.

Work by Negrel et al. (2011) on groundwater from shallow fractured rock aquifers showed substantial variation in isotope composition. This is in contrast to the more homogenous isotope compositions measured in this study and supports the model of complex and deep groundwater flow in the Peninsula aquifer.

code	river	mountain range	catchment						sampling		range	
			highest peak	height	highest sample	lowest sample	area	flow	length	gradient	δD	$\delta^{18}O$
				m asl	m asl	m asl	km^2	L/s	km	m/km	‰	‰
DWK	Duiwelskloof	Drakenstein Mountains	Drakenstein Peak	1490	1240	680	2	2	2.4	300	10.1	1.91
VSK	Volstruiskloof	Drakenstein Mountains	Buller's Kop	1425	1160	580	1.5	2	1.5	450	11.9	2.14
WTL	Witels	Hex River Mountains	Buffelshoek Peak	2060	1650	310	50	100	20	70	7.5	1.61
GHK	Groothoekkloof	Hex River Mountains	Matroosberg	2249	1800	580	15	10	8	150	8.8	0.59
MLK	Meulkloof	Langeberg	Hermitage Peak	1546	820	130	11	20	6	120	3.4	0.44

Table 5.7: Description of the five rivers sampled, with rough flow estimates and gradient for the sampled length.

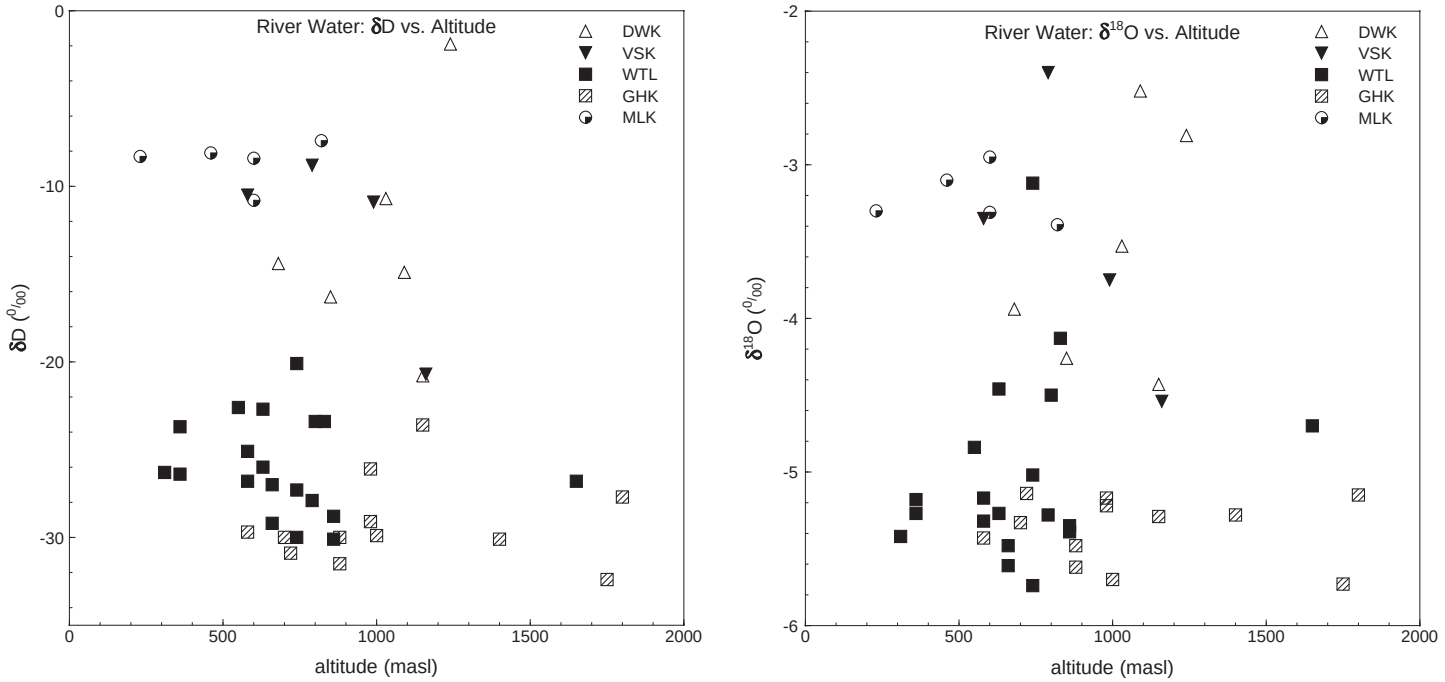

Figure 5.8: Plots of δD and $\delta^{18}O$ against altitude for surface water samples from five rivers in the Western Cape.

5.3.3.1 Sharp Relief

The lack of a distinct change in isotopic composition with altitude in the rivers and their sources (springs and seeps) suggests that the groundwater in each catchment does not vary significantly isotopically. The would occur if the rainfall is isotopically similar across the catchment, as might be expected because of the small size of these mountain catchments. This finding concurs with the rainfall analysis where it was found that the variation in isotopes is less than is expected given the range in altitude between sites. The average elevation around a site, in an area of 50–100 km^2, is as important as the actual altitude of the site in determining the isotopic composition of rainfall. This works for both sharp, high peaks that are much higher than the surrounding terrain, and for deep, steep valleys that are much lower than the surrounding terrain. So although the rivers traverse wide ranges of elevations, from peak to valley bottom, the range in isotopic composition for rainfall is more restricted than the elevation range would suggest.

The best fit lines shown for the five rivers in Chapter 4 also reveal something about the catchments. The line with the lowest gradient and intercept is for the Witels ($\delta D = 4.42\delta^{18}O - 3.8$), and is similar to typical evaporation lines (e.g. Gat, 1996). This river is the longest, the gradient is the lowest and the catchment is the largest, all of which are likely to contribute to evaporation in the area. If evaporation was occurring only in the main stream as it flows through the catchment, then the lowest samples would have the least negative isotope compositions. The samples with the least negative isotope composition are not concentrated towards the bottom of the river catchment and as seen in **Figure 5.8**, there is no systematic variation of isotope values against parameters such as altitude. This suggests that the evaporation is widespread and affects all waters in the catchment and is not simply the result of evaporation in the main stream.

5.3.3.2 Summary

Isotope compositions are clustered for each river sampled. Variation in each river is minimal and is generally poorly correlated with any obvious parameter, although it is known that rivers often display limited variation in isotope values (Fritz, 1981). The isotopic variation in rainfall has been shown to be smaller than would be expected, given the range of altitude. Furthermore, complex groundwater flow causing mixing, and also mixing and dilution along the length of the streams, will reduce the range in isotope compositions in the surface water. From the rivers sampled it seems that isotopes are unable to help pinpoint groundwater flow directions or recharge areas for the water that discharges into the streams via springs and seeps. Isotopes may still be of value for longer rivers or larger catchments, but appear to have little value in small, rugged mountain catchments. Decreasing range in isotope compositions within each river, as one moves eastwards, may reflect more complex groundwater flow and greater mixing, due to more intense fracturing related to position within the Cape Fold Belt, which has varying degrees of structural deformation from the Cape Orogeny.

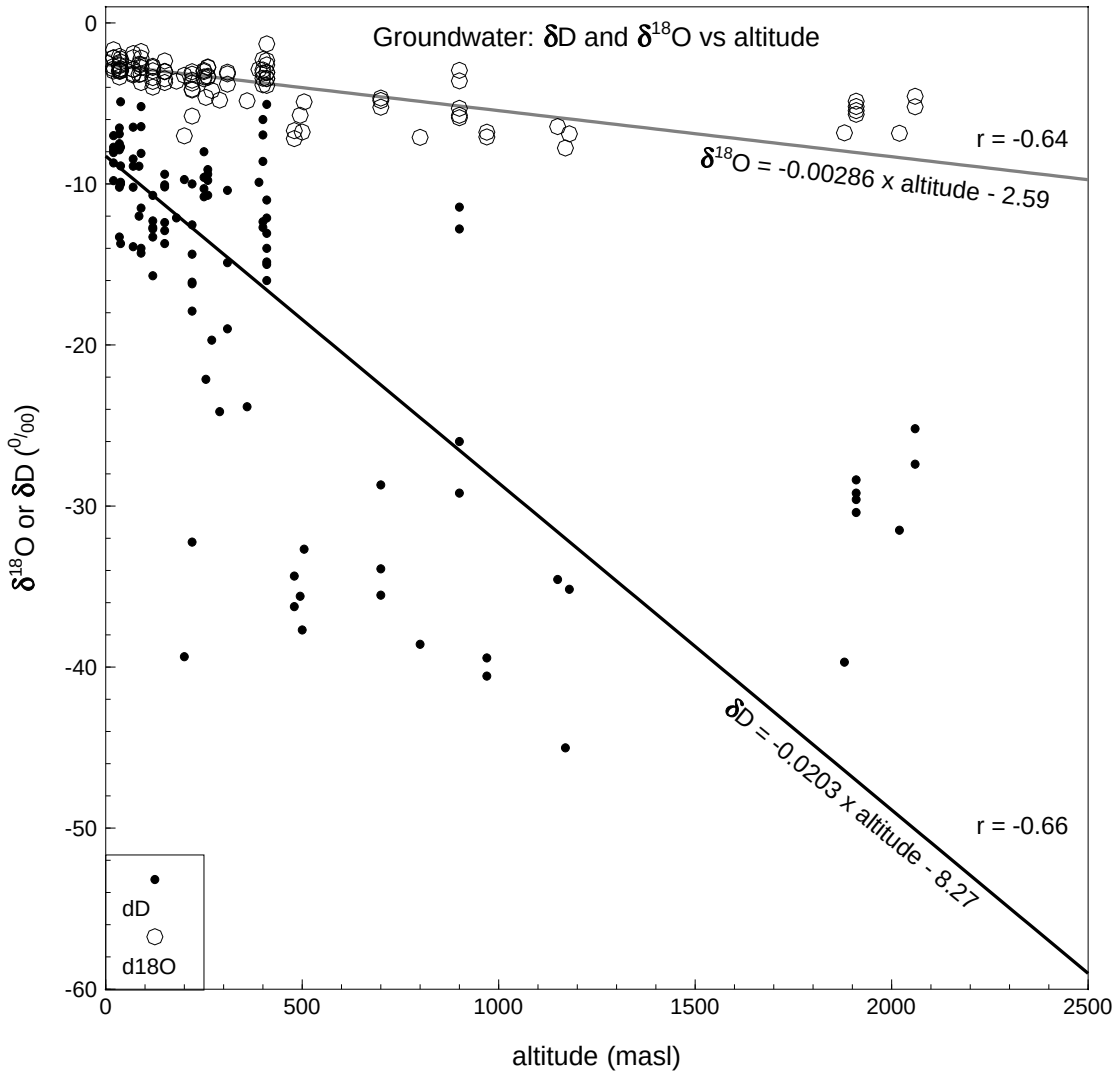

Figure 5.9: Groundwater isotope composition as a function of sampling (discharge) altitude.

5.4 Groundwater

5.4.1 Altitude

The isotope composition of recharge should be similar to that of the rainfall in the recharge area, although some changes will take place, primarily due to evaporation and selective recharge. Selective recharge takes place because not all rainfall events are the same in magnitude and intensity, and depending upon the recharge process, some of the rain may not recharge. This can occur when an event is too small and all the rainfall gets used up through interception, transpiration or evaporation. A larger event may generate recharge, but a portion of it will still be taken up in interception, transpiration and evaporation. More intense events may result in high runoff, none of which recharges locally, but may recharge in another area downslope. The isotope

composition of groundwaters can therefore vary from very similar to that of rain in the recharge area, to something quite different, and this variation may itself vary year to year, depending on changes in the weather and possibly also vegetation and soil.

Brandvlei hot spring, at 64 °C, is the hottest spring in the region (and in the country). No actively circulating groundwater in the Western Cape is therefore likely to reach temperatures over 70 °C and by far most of the groundwater circulates at temperatures between 0 °C and 20 °C. No isotope exchange between the water and host rock takes place at these temperatures (Clark and Fritz, 1997). Assuming a simple flow model from recharge area to discharge area with no mixing, the isotope composition of water at discharge must be the same as at the recharge area.

Groundwater flow through landscapes varies from highly local, over hundreds of metres or less, to regional, over distances of tens to hundreds, such as in the Perth Basin (Davidson, 1995) and sometimes even thousands of kilometres, such as in the Great Artesian Basin in Australia (White, 2000). In South Africa, the absence of large, unmetamorphosed sedimentary basins to form regional aquifers is the main reason groundwater flow is restricted in extent and quantity. The Karoo Basin contains mostly argillaceous rocks and the more arenaceous units are too well cemented to be highly transmissive primary porosity aquifers. Changes in rock type also tend to block flow as aquifers come up against impermeable units, for example the Table Mountain Group abutting the Malmesbury Group as on the Kango Fault (see **Figure 5.20**). Lastly, the highly dissected topography tends to make flow paths short, because of steep hydraulic gradients and short distances between wet, high altitude mountains, and dry, low altitude valleys where discharge feeds into rivers (Domenico and Schwartz, 1998, p.77).

A correlation exists between the isotopic composition of groundwater and altitude (**Figure 5.9**). The altitude plotted is that of the discharge point of springs and seeps, or that of the collar (ground level), if sampled from a borehole. The equations of the best fit lines describing the δD and $\delta^{18}O$ relationships with altitude have been plotted on the graph. These lines were calculated using the reduced major axis regression method, as the least squares regression method again generated lines of best fit with rather gentle gradients and unrealistically negative intercepts, as was noted for the regression of the rainfall station data against altitude, in **Figure 5.4**. These least squares regression equations are:

$$\delta D = 0.0134 \times altitude - 11.15 \quad (r = -0.66)$$

$$\delta^{18}O = 0.00184 \times altitude - 3.02 \quad (r = -0.64).$$

Where recharge areas are far from discharge points, the isotope composition of the groundwater might be different from the rainfall at the discharge area. In particular, because changes in altitude generate noticeable changes in rainfall (and hence recharge) isotope composition over relatively short distances, if groundwater flow paths were several kilometres and more, there

would be a poor correlation between groundwater delta values and altitude. The graph in **Figure 5.9** shows the opposite. The slopes and intercepts of the best fit lines similar to those for the rainfall station – altitude correlation (see **Figure 5.4**). This suggests that the flow paths, at least for the groundwater sampled in this project, are mostly short, and in particular, there are not large differences between the elevation of the recharge and discharge sites.

5.4.2 Hot Springs

Hot springs have always been a target for hydrological (e.g. Bond, 1953), hydrochemical (e.g. Kent, 1949) and isotopic (e.g. Mazor and Verhagen, 1976) studies. The hot springs of the Western Cape have been analysed for their stable isotope content previously, so an analysis of the changes over time is possible. From **Figure 5.10**, it is clear that there are no systematic changes between the three studies in 1971-2 (Mazor and Verhagen, 1983), 1995-6 (Diamond and Harris, 2000) and 2010-12 (this study). The 'random' variation in isotopic values of discharge at the springs, measured from month to month in the Diamond and Harris (2000) work is equal to the magnitude of variation seen over 40 years, between 1971 and 2011. It is possible that some of the larger shifts in isotope composition could reflect yearly or multi-year shifts in the average isotope composition of recharge. However, these large shifts (10 ‰ for δD and 2 ‰ for δ^{18}O) were recorded over months by Diamond and Harris (2000) over only 2 years at Laingsburg. It is possible that inter-annual shifts in isotope composition become compressed in the groundwater flow path and issue over monthly timescales, but this would require a piston-like flowpath with very little groundwater mixing, which is not likely given the depth and length of the flowpath.

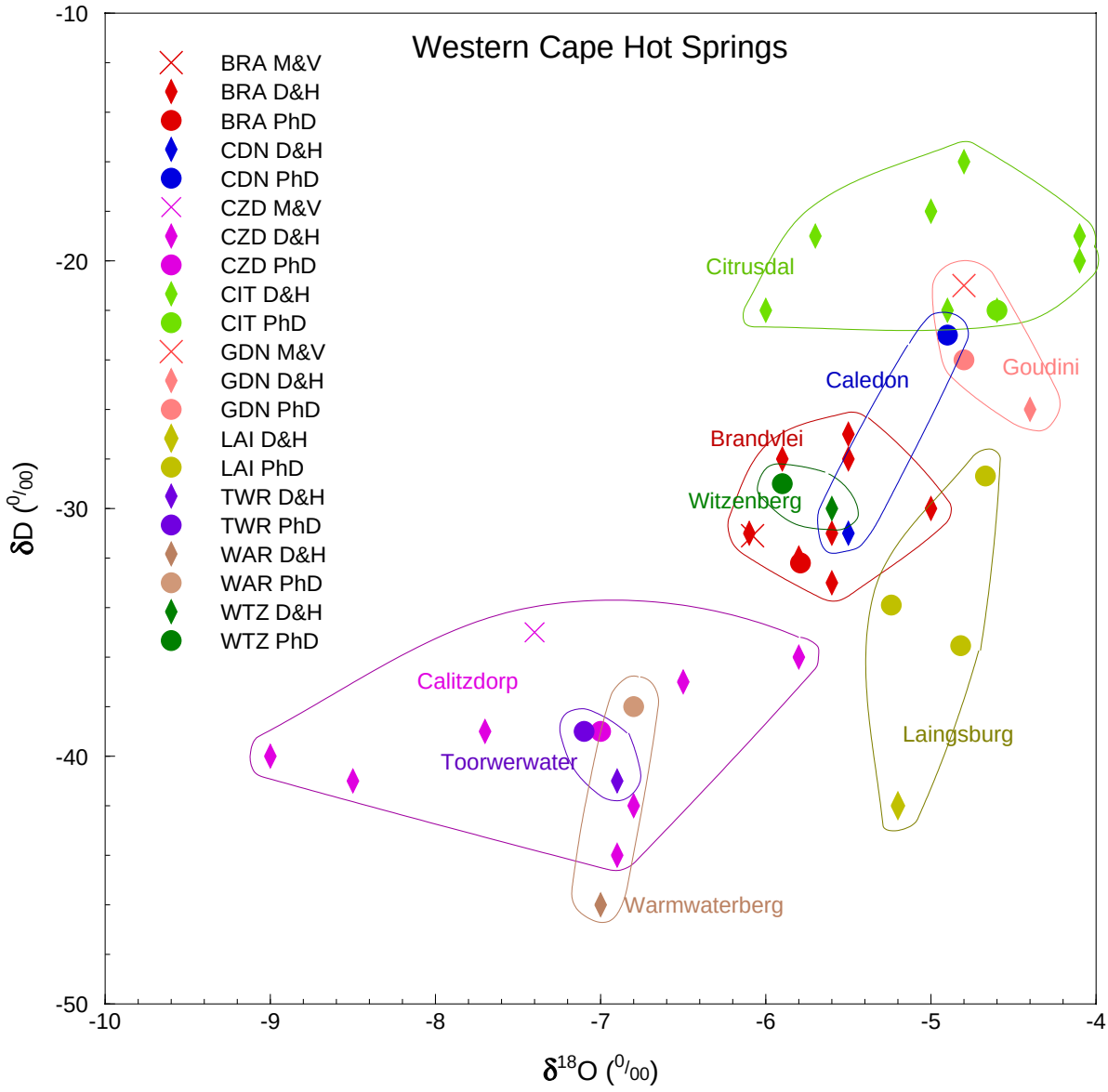

Figure 5.10: Stable isotope compositions for the Western Cape hot springs from three different studies, showing no obvious long term change. Data from Mazor and Verhagen (1983) (M&V), Diamond and Harris (2000) (D&H) and this study (PhD).

5.5 Regional Analyses

This study attempted an overview of stable isotopes of water in and around the Table Mountain Group, including rain, surface water and groundwater. In such a broad study, large areas naturally are neglected, but some areas have had sufficient analysis that a more detailed interpretation can be attempted in those areas. These interpretations should provide, firstly, an indication of the usefulness of stable isotope hydrology in unravelling the hydrogeology of the Table Mountain Group, and secondly, some actual insights into the flow of groundwater through the Table

Mountain Group. On the δD–δ^{18}O plots in this section, the symbol size is approximately that of the analytical error.

5.5.1 Cederberg

Substantial quantities (gigalitres per year) of groundwater are utilized by farmers in the Olifants River Mountains area (pers. comm. Robert Paterson of Twaktuin Farm). The possibility exists that this groundwater, or some of it, is recharged in the Cederberg and, by means of faults and fracture networks in the Peninsula Formation, passes beneath the Olifants River Valley before discharging to the west of the Olifants River Syncline in the Olifants River Mountains area. The cross section in **Figure 5.11** illustrates how the geology can allow this to occur, although the geometry of the Olifants River Syncline changes to the north and south of this line. In general, the syncline deepens and is dominated by a simple synclinal fold structure southwards, whereas northwards the syncline shallows and faults displace the Cederberg aquitard such that hydraulic connections are established between the Peninsula and Skurweberg aquifers. The fault shown in the Olifants River Syncline in the cross section does not quite achieve this linkage, but another fault, a few kilometres north of the cross section line, does.

The result of these changes in structure in the Olifants River Syncline is that futher south the Peninsula aquifer is more of a confined system under the Olifants River Valley, and does indeed transfer groundwater from the higher, eastern mountains, the Koue Bokkeveld range, to the lower, western range, the Warmbadberg, as shown in Diamond and Harris (2000). Evidence for this comes from the Citrusdal hot spring, The Baths, and is twofold: firstly, the temperature of discharge, at 43 °C, requires circulation to around 2 km depth, assuming a geothermal gradient of 20 °C/km and an input temperature for rain of 5–10 °C (Jones, 1992); secondly, as can be seen in **Figure 5.12**, the isotopic composition of the spring water is more negative than local rainfall at Citrusdal (Diamond and Harris, 1997) or Wolfkop, but matches rainfall at Uitkyk, 1000 m high in the Cederberg, which will be similar to rainfall in the Koue Bokkeveld ranges due east of the spring. Further north in the Olifants River Syncline movement of groundwater under a hydraulic gradient from the higher Cederberg range in the east to the lower Olifants River Mountains in the west may not be as easy due to the shallower syncline and the presence of the faults. These faults can lead to an upward leakage out of the Peninsula aquifer and directly into surface water, such as is postulated to occur at The Baths, or via the Skurweberg aquifer and then into surface water. The juxtaposition of the Peninsula and Skurweberg aquifers, because of the faulting, can also allow loss of groundwater from the Peninsula aquifer into the Skurweberg aquifer. The shallowness of the syncline also leaves a relatively thin layer of the Peninsula Formation remaining to conduct groundwater westwards, as seen in the areas just east and west of the Olifants River Valley in **Figure 5.11**.

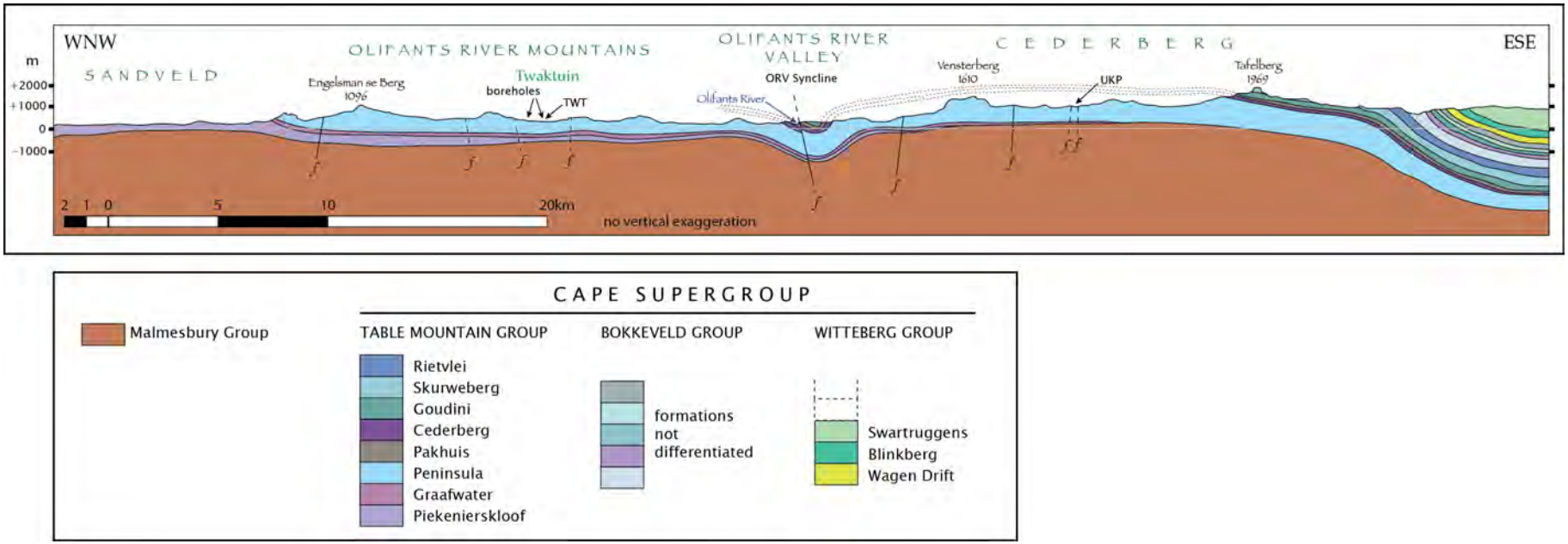

Figure 5.11: A geological cross section through the northern part of the western limb of the Cape Fold Belt, drawn from the Clanwilliam 1:250 000 geological map (Geological Survey, 1973). The section line is indicated on the map in **Figure 5.3**.

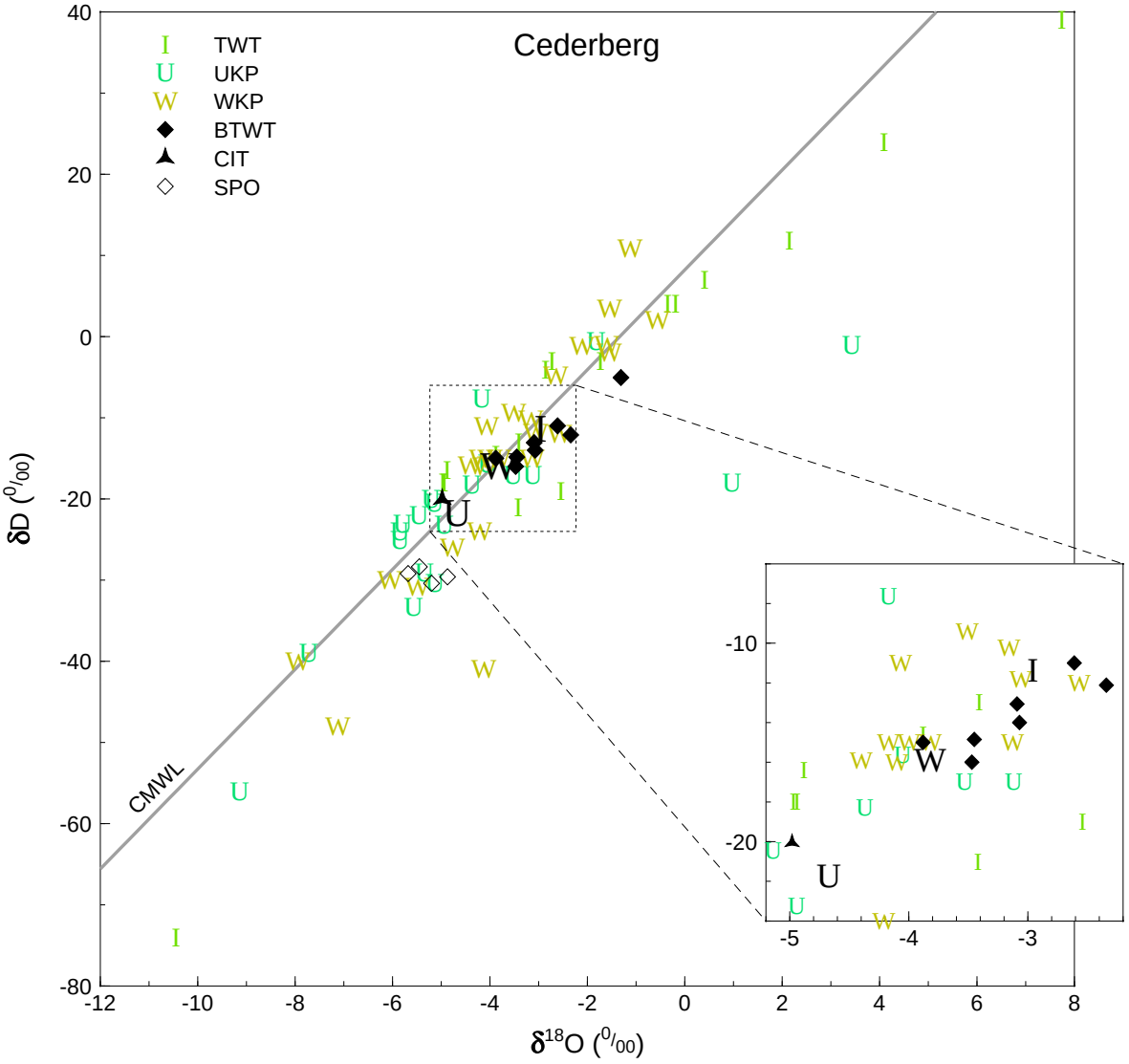

Figure 5.12: A δD – $\delta^{18}O$ plot for all data for the Cederberg region. Weighted means for Twaktuin (I), Uitkyk Pass (U) and Wolfkop (W) rainfall stations are shown as large black letters. Abbreviations: TWT = Twaktuin monthly rainfall, UKP = Uitkyk Pass monthly rainfall, WKP = Wolfkop monthly rainfall, BTWT = Twaktuin boreholes, CIT = The Baths hot spring, SPO = Tafelberg Spout seep.

Samples of groundwater from Twaktuin Farm in the Olifants River Mountains are compared **Figure 5.12** to possible sources of recharge: local rainfall at Twaktuin Farm; rainfall across the Olifants River Valley in the Cederberg at Uitkyk Pass; rainfall higher in the Cederberg, such as at the high altitude seep on Tafelberg at 1900 m. The groundwater discharging at this seep is from rainfall at around 1950 m on top of The Spout, a rock tower peak. The δ values of Twaktuin groundwater are more negative than the weighted mean for Twaktuin rainfall. The amount effect for Twaktuin has a similarly poor correlation to Wolfkop, primarily because of the 31 December 2010 thunderstorm event; Pearson's r values for Twaktuin are -0.12 for δD – rain-amount and

-0.30 for $\delta^{18}O$ – rain-amount. However, in general one can expect the heavier winter rains (more intense rainfall) are more likely to result in groundwater recharge and to have more negative δ values. The mean Twaktuin recharge δ values are probably more negative than the mean Twaktuin rainfall δ values. Also, the Farm is in a valley and the surrounding hills and peaks will contribute more negative isotopic value rainfall to recharge the groundwater of the area.

The δD and $\delta^{18}O$ values of Twaktuin groundwater are not as negative as Uitkyk Pass rainfall (**Figure 5.12**. They are however, similar to Wolfkop rainfall. The Wolfkop values represent all the lower elevation hills on the east of the Olifants River Valley, but these areas do not have the elevation necessary to produce a hydraulic head sufficient to drive groundwater to the Twaktuin region. If recharge is occurring east of the Olifants River Valley, it must be from the high peaks of the Cederberg proper, such as Vensterberg in the cross section. The isotopic evidence suggests that groundwater in the Olifants River Mountains area is locally recharged, as shown in the sketch in **Figure 5.13**. This fits with the geological structure of the region which shows numerous obstacles, as outlined above, to groundwater flow occurring in any significant quantities on such a regional scale.

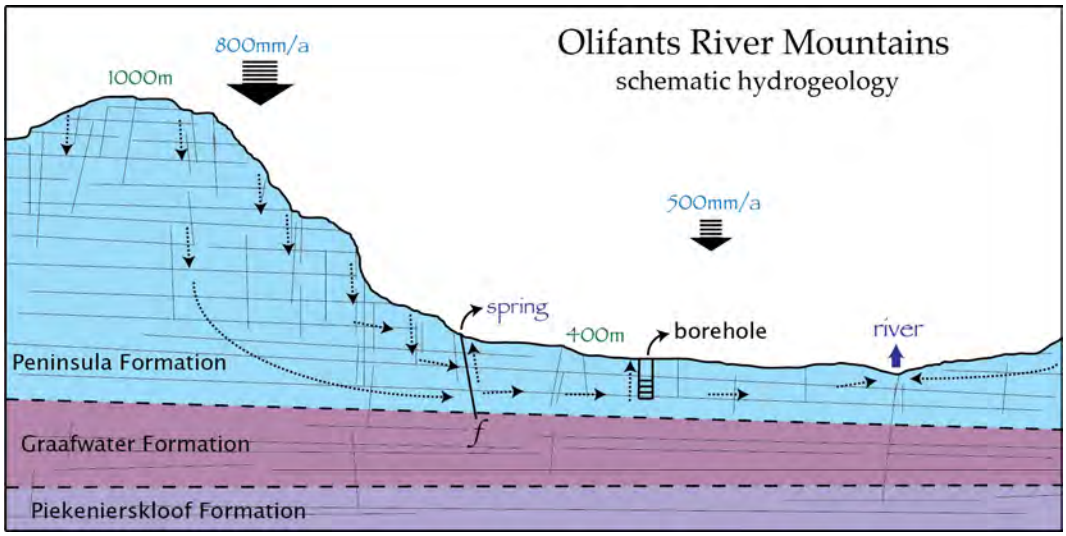

Figure 5.13: Sketch cross section showing the conceptual hydrogeological model suggested by isotopic compositions measured in this study.

The possibility does remain that there is a component of groundwater flow that is travelling east to west through the Olifants River Syncline, perhaps discharging closer to the Olifants River Valley, not as far west as Twaktuin, or contributing just a portion to groundwater in the Twaktuin area through limited flow in deep fractures near the base of the Peninsula Formation. More widespread monitoring of boreholes and springs in west of the Olifants River Valley could help shed light on the former possibility, whilst more detailed monitoring over time at Twaktuin and neighbouring farms' boreholes may reveal changes in isotopic composition as deeper groundwater is tapped later in the irrigation season, or after several low rainfall years.

Figure 5.14: Duplexes (piggyback thrusts) in the Hex River Mountains. Multiple thrust ramps can be seen, some of which have been labelled. The extensively fractured nature of the rock, both thrusts and near vertical jointing, are evident.

5.5.2 Hex River Mountains

The Hex River Mountains are formed by erosion into a large north-east trending anticline in the inland portion of the syntaxis (meeting zone of the western and southern limbs) of the Cape Fold Belt. East of the syntaxial region most folds trend east-west, while to the west and north of the syntaxis, folds trend north-south. The Hex River Mountains include several of the highest peaks in the Western Cape, including the second highest, Matroosberg, at 2249 m, just north-east of the cross-section in **Figure 5.17**. The Table Mountain Group, especially the Peninsula Formation, is structurally thickened in this region and duplexing is evident in the cliff forming outcrops of the Peninsula Formation, as seen in the annotated photograph in **Figure 5.14**.

The two surface water bodies sampled, the Witels and Groothoekkloof rivers, have been discussed in the Surface Water section above, but in summary they show a difference in the mean δD and $\delta^{18}O$ values. This probably reflects continental and altitude effects operating in concert to gause the Groothoekkloof isotope values to be more negative than the Witels.

Six snow and ice samples were taken at 1900 m elevation on Waaihoek Peak in the western Hex. They were taken by coring vertically into the thin snowpack, 0.2–0.4 m thick at two sites, and by removing a stalactite of rime ice hanging from a rock. The stalactite (*1) has the least negative δ values of the six samples. Four samples of snow (*2–*5) record the unusual weather

event described in Chapter 4, where a south-east wind caused widespread snow on mountains of the Western Cape. These samples show that the first snow to fall (the base of the snowpack, *2 and *3) had higher δ values than the later snow (*4 and *5). Snow from a more typical north-west wind from a frontal depression has the most isotopically negative signature (*6).

Previous snow samples (+) (Diamond and Harris, 1997; Harris et al., 2010) taken from Gydo Pass, Hex River Pass, Theronsberg Pass and Waaihoek Peak, all in the vicinity of the Hex River Mountains, overlap with the results from this study, as seen in **Figure 5.15**. The most negative cluster of points is from three different seasons, 1996, 2000 and 2011, and from three different locations, Theronsberg and Hex River Passes and Waaihoek Peak, suggest that this is a typical value for snow from a mid-winter north-west frontal storm in the south-western Cape: –55 > δD > –60, –10.5 > $\delta^{18}O$ > –11.5. The two less isotopically negative samples from the previous studies may have undergone melting, causing the lighter isotopes to be preferentially melted and removed (Arnason, 1981), or may have been rained upon and undergone exchange with heavier isotopes in rain, or may simply have been derived from a weather system that deposited snow of an isotopically heavier nature, such as was observed for the south-easter snowfall in this study.

The difference between the early and late south-easter snow is consistent in the two profiles sampled. It was possible to distinguish the top of the south-easter snowpack from the overlying north-west event snowfall, as the former was granular from freeze-thaw over a few sunny days prior to the north-west event, and the latter was still in powder form. The freeze-thaw process that turns powder snow to firn should have increased δ values at the top of the snowpack as the lighter isotopes are preferentially incorporated into snowmelt, so these points may have had lower δ values originally. A movement from less to more negative δ values during this precipitation event could occur if the temperature decreases or as a result of rainout. A decrease in temperature often accompanies the passage of a cold front, as the wind shifts from westerly to southerly, however, this snow was from a south-easter event. In this case the decrease in δ values during the event suggests that colder air from further south was being fed into the system as it developed and that perhaps increased rainout occurred for the later snow, as shown in **Figure 5.16**. The isotope composition of snow may be useful in understanding air mass trajectories during weather events. Clearly there are several processes at play, and complex relations occur between the three phases of water in this semi-alpine zone of the Cape Mountains. Unfortunately, there are probably insufficient data to draw major conclusions, except to note the large range in values that could be useful in meteorological and hydrological applications if such differences are consistent. A more comprehensive study with more widespread sampling of snow over a greater time frame would assist in identifying any trends.

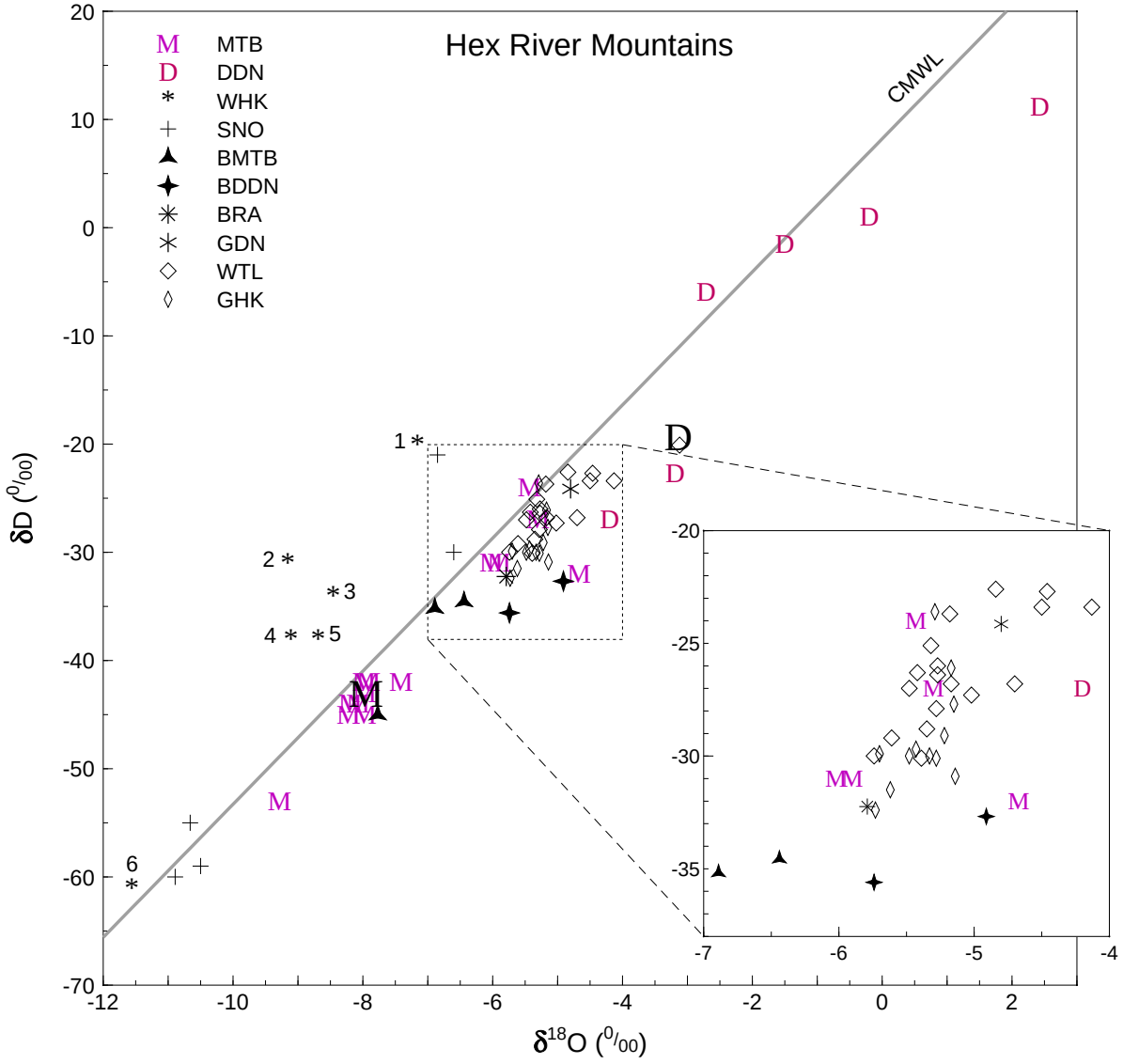

Figure 5.15: A δD – $\delta^{18}O$ plot for all data for the Hex River Mountains region. Weighted means for the Matroosberg (M) and DeDoorns (D) rainfall stations are shown as large black letters. Abbreviations: MTB = Matroosberg monthly rainfall, DDN = Tweespruit monthly rainfall, WHK = Waaihoek Peak snow, SNO = snow from previous studies, BMTB = Erfdeel boreholes, BDDN = Tweespruit boreholes, BRA = Brandvlei hot spring, GDN = Goudini hot spring, WTL = Witels River, GHK = Groothoekkloof River.

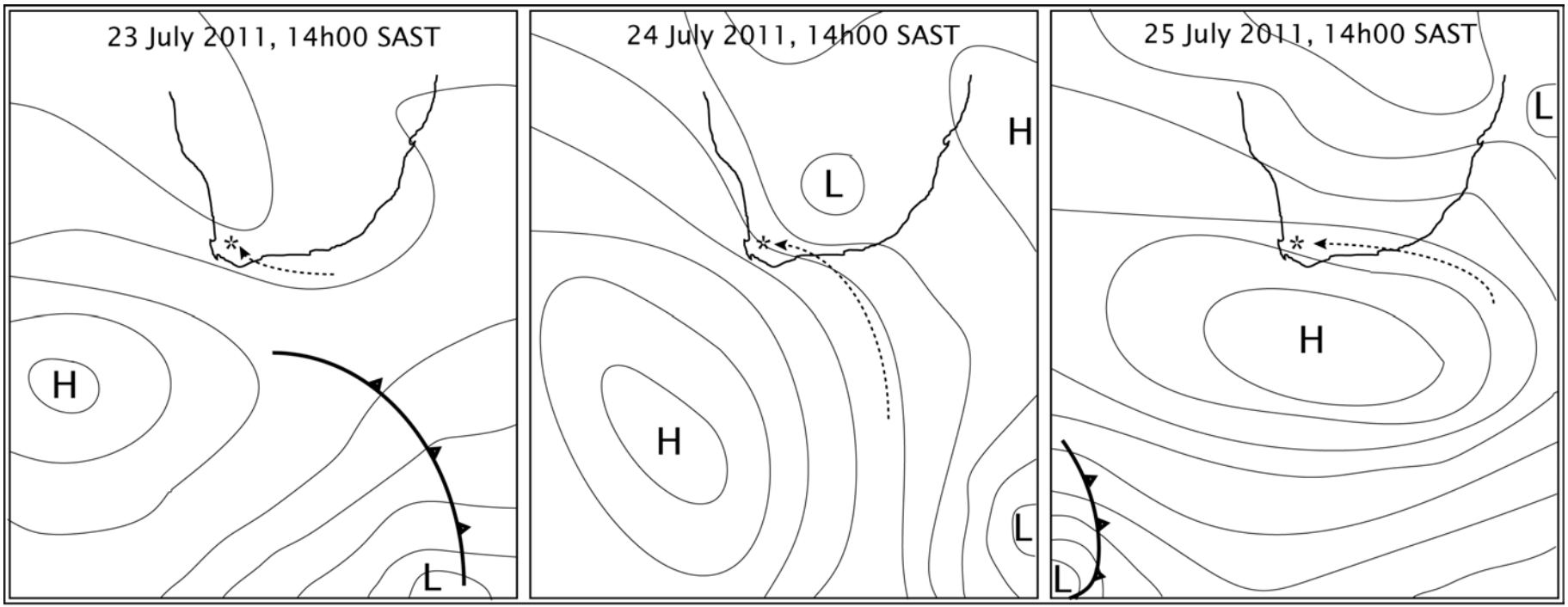

Figure 5.16: Simplified synoptic weather charts from SAWS (2010-12) with possible air trajectories for snowfall in the Hex River Mountains shown. The 23rd July shows a short air trajectory from warmer areas that caused rain. The 24th July shows a much longer air trajectory bringing very cold sub-antarctic air and resulting in snow. Later snow on the 25th July may have travelled even further and probably experienced more rainout over land, resulting in lighter isotope composition.

The most significant hydrogeological interpretations that can be made from the data for the Hex River Mountains region are from comparing the values for borehole water at Erfdeel, on the northern side of the Hex River Anticline (BMTB), and at Tweespruit, on the southern side (BDDN), with the rainfall data for the two stations in this area (see **Figure 5.17**). The mean δ values for rainfall at Tweespruit, the large 'D' in **Figure 5.15**, are less negative than the water from the two boreholes sampled on this farm. These boreholes are drilled into the Rietvlei Formation and although they may not penetrate deep enough to encounter the Skurweberg Formation (see **Figure 5.17**), the Rietvlei Formation is part of the Skurweberg aquifer. This large difference in δ values, 15 ‰ for δD and 2 ‰ for $\delta^{18}O$, can be accounted for by recharge at high altitude on the slopes of the Hex River Mountains. Based on a linear altitude effect between the DDN and MTB rainfall stations, using the gradients shown in **Table 5.5**, the δ values of the Tweespruit boreholes suggest an average recharge elevation for this groundwater of around 1200 masl. Weaver et al. (1999) showed a similar hydrogeological setting for groundwater flow in the Agter-Witzenberg Valley, north-west of Ceres, although with smaller differences in elevation.

Although the cross section shows the Skurweberg Formation only reaching around 1000 masl, the areas west and north of the section line contain outcrops up to 1500 m and 2000 masl, respectively. Additionally, the Goudini Formation, which is hydraulically part of the Skurweberg aquifer occurs at even higher elevations closer to the core of the Hex River Anticline. It is easy then for groundwater in the Skurweberg aquifer to have isotopic compositions similar to those found in the Tweespruit boreholes. However, it does suggest this groundwater originally was recharged in the Skurweberg or Goudini Formation outcrop areas and is flowing upwards through the stratigraphy in the Hex River Valley. This would probably have occurred naturally due to the hydraulic head in these lower formations being higher than that in the Rietvlei Formation, but it may also be enhanced by pumping, causing an upconing flow towards the boreholes. Should the isotope composition of the groundwater from the boreholes become lighter over time, this might suggest that deeper and deeper water from the Skurweberg aquifer is being abstracted. This is because the deeper parts of the aquifer (the Skurweberg and Goudini Formations) are recharged at higher elevation than the Rietvlei Formation and will therefore transmit groundwater with lower δ values. Long term monitoring of the isotope content of the boreholes may be useful to warn of depletion of the groundwater resource.

Groundwater from boreholes at Erfdeel displays a wider range of δ values than at Tweespruit, although in both cases the sample numbers are too low for this to be a firm observation. Two of the boreholes have similar and less negative δ values than the third, which has similar δ values to the weighted mean for the MTB rainfall station. The Erfdeel boreholes also tap the Rietvlei Formation, part of the Skurweberg aquifer, which reaches over 2000 m elevation south-east of the farm, two kilometres south of the section line. The range in isotope composition of the Erfdeep borehole water and the geological structure of the area suggest that groundwater recharge occurs from relatively low down on the mountain slopes, on the northern flank of the Hex River Anticline, to

high up, amongst the peaks on the hinge of the Anticline. The altitude range for groundwater recharge at Erfdeel can be estimated as 1300–2000 masl.

Groothoekkloof river samples display less negative δ values than the MTB rainfall station and the boreholes at Tweespruit and Erfdeel. This suggests that either the GHK samples, being from late summer, display an evaporated signature, or the Erfdeel groundwater was selectively recharged by the most isotopically negative rainfall, a phenomenon known as 'selection' (Gat, 1981a). If the latter is the case, it suggests that the groundwater responsible for creating summer baseflow in the Groothoekkloof river is mostly shallow circulating and recharged by rainfall of varied isotopic composition, whereas the groundwater being pumped out at Erfdeel taps deeper circulating water that has been selectively recharged in heavy winter rainfall events subject to colder temperatures and the amount effect to drive the isotope composition to more negative values.

The Erfdeel borehole δ values lie closer to the Cape Meteoric Water Line (**Figure 5.15**) than the Tweespruit borehole points that seem to lie on an evaporation line trend. As the recharge for the Tweespruit boreholes is on the eastern side of the Hex River Mountains, it is in the lee of the highest peaks. Rainfall here may take place through drier air that has lost some of its moisture when precipitating over the crest of the range. Evaporative enrichment during raindrop descent could account for these points being displaced from the CMWL.

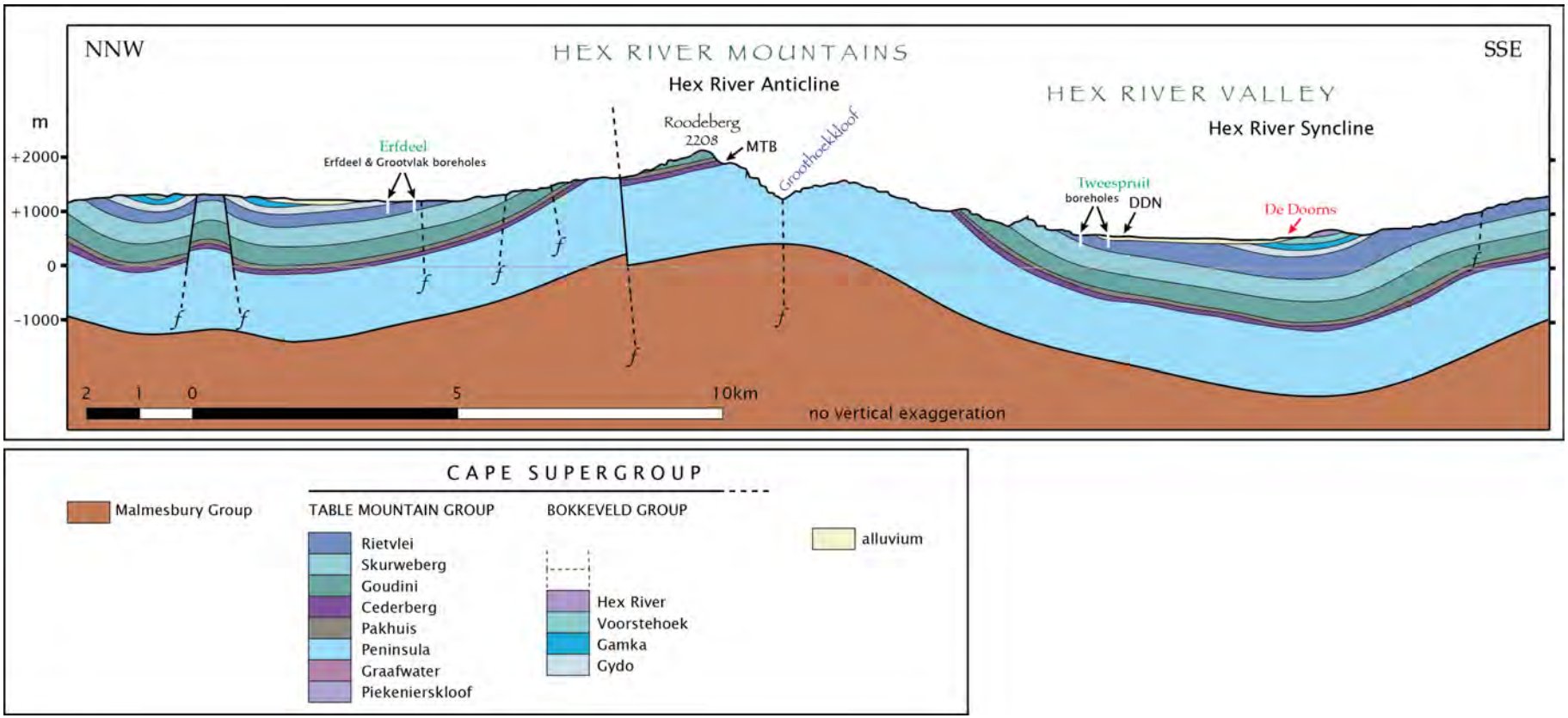

Figure 5.17: A geological cross section through the Hex River Mountains and Hex River Valley, drawn from the 1:250 000 geological map for Worcester (Council for Geoscience, 1997). Borehole positions and depths are illustrative only.

5.5.3 Langeberg – Gamkaberg – Swartberg

Gamkaberg Nature Reserve lies in the Little Karoo and the adjacent Gamka Mountain. The Little Karoo is a semi-arid area and the nature reserve gets its water from boreholes at the foot of the Gamkaberg. The Gamkaberg boreholes are drilled into Rietvlei Formation and perhaps some through unconformably overlying Enon Formation (**Figure 5.20**). They therefore abstract groundwater from the Skurweberg aquifer. The δ values for the groundwater from these boreholes are extremely low relative to rainfall collected at the same place, the Gamka Store location (GST). The groundwater has 20 ‰ lower δD and almost 4 ‰ lower $\delta^{18}O$ than the weighted mean for Gamka Store rain and almost 10 ‰ δD and almost 1.5 ‰ $\delta^{18}O$ less than the weighted mean for Bakenskop on the summit plateau of Gamkaberg. It is almost as negative as water from the hot springs at Warmwaterberg and Calitzdorp Spa. Three possible explanations could account for this result.

Firstly, as proposed by Diamond and Harris (2000) for the Calitzdorp Spa, the recharge area for this groundwater could be the Swartberg. That study did not collect high altitude rainfall and it was simply assumed that rainfall on the Swartberg around 2000 m would be isotopically negative enough to account for the very negative δ values at the Calitzdorp Spa (see **Figure 5.18 and 5.10**). Data from this study shows that this assumption was partly true: the high altitude seeps of the Klein Swartberg, to be discussed in the next regional analysis, do have δ values similar to Calitzdorp Spa discharge. On the other hand, the high altitude rainfall collected at 2080 m on Blesberg does not have such negative δ values and the weighted mean at Blesberg is similar to that of Bakenskop, at half the altitude.

The cross section in **Figure 5.20** shows that the Table Mountain Group has been eroded away over the inlier of Cango Group basement south of the Groot Swartberg and so no groundwater flow can occur from the Swartberg southwards along this line. However, to the north-west of Gamkaberg, the basement is much lower and the Table Mountain Group is continuous from the Swartberg, via the Huisrivier Mountains and the Rooiberg, to Gamkaberg and the Langeberg, as shown in Diamond and Harris (2000). Although this hydraulic connection exists, it is about 40 km, very folded and passes one major fault at the southern edge of the Swartberg. Groundwater would have to be recharged in the Peninsula aquifer in the Swartberg, move into the Skurweberg aquifer at the fault and then through the anticline of the Huisrivier Mountains and a syncline before discharging at the Gamkaberg boreholes. The water would have circulated to great depths and should be heated. For Calitzdorp Spa, the temperature of discharge is 52 °C, which is evidence for deep circulation and concurs with the isotopic evidence, but the Gamkaberg groundwater is not noticeably warm and therefore it is unlikely to have travelled this route. The Outeniqua Mountains (Langeberg) are very unlikely as sources of groundwater at the Gamkaberg boreholes because the discontinuity of the Skurweberg aquifer does not allow flow of groundwater to the northern side of the Gamkaberg. The Cederberg aquitard prevents groundwater flowing from the Peninsula aquifer into the Skurweberg aquifer without the presence of a major fault, of which

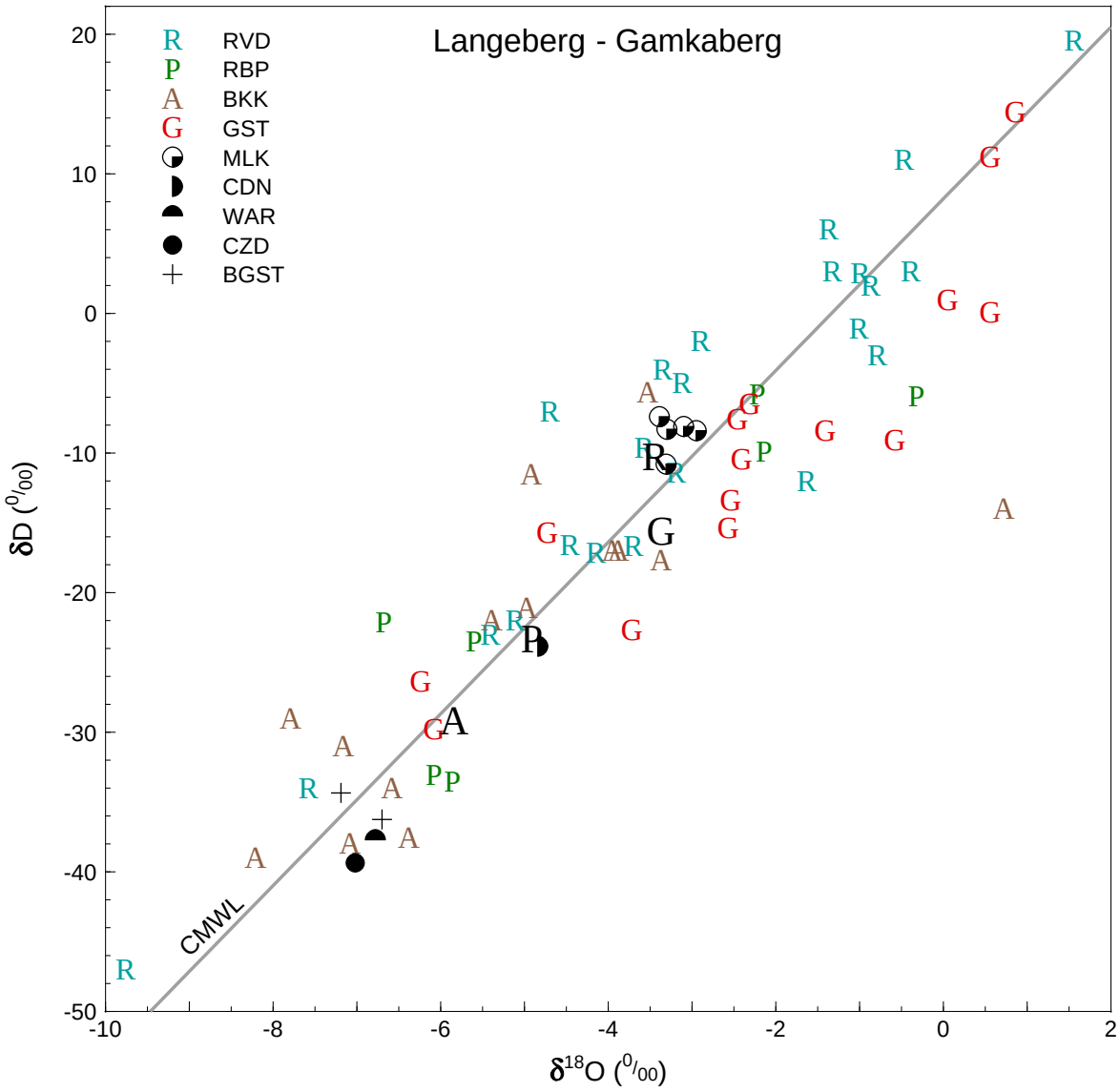

Figure 5.18: A δD – $\delta^{18}O$ plot for all samples taken in the Langeberg–Gamkaberg region, including rain, surface water and groundwater. Larger black letters indicate weighted means for rainfall at Riverndale (R), Robinson Pass (P), Bakenskop (A) and Gamka Store (G). RVD = Riverndale, RBP = Robinson Pass, BKK = Bakenskop, GST = Gamka Store, MLK = Meulkloof river, CDN = Caledon hot spring, WAR = Warmwaterberg hot spring, CZD = Calitzdorp hot spring, BGST = Gamkaberg boreholes.

none are mapped. The isotopic evidence also shows the Robinson Pass rainfall to have higher δD and $\delta^{18}O$ values than the Gamkaberg boreholes.

In the second and third possibilities, the recharge area is the crest of the Gamkaberg, around the Bakenskop rainfall collection station, but two possible factors may be causing the discrepancy between the weighted mean delta values at Bakenskop and the values found at the Gamkaberg boreholes. The first is *selection*, whereby heavy rainfall events, subject to the amount effect and hence with lighter isotope composition, are preferentially recharged over lighter rains with heavier isotope composition (e.g. Dogramaci et al., 2012). The second is that the 2010–12 rainfall at Bakenskop may have been less negative than normal. Although not generally reported in the literature, weighted mean annual isotope composition of rainfall has been shown to vary from year to year locally (Harris et al., 2010) and is discussed in **Section 5.21**. Specifically, observations at UCT show the 2010–12 weighted annual rainfall means lying at the less negative end of the spread of weighted annual means for 1996–2012, as seen in **Figure 5.24**, which supports the hypothesis that the sampled Bakenskop rainfall may not be typical. Lastly, a combination of *selection* and unusual rainfall isotope composition could be responsible for the discrepancy observed at Gamkaberg.

5.5.4 Swartberg to Goukamma

Figure 5.19 is a δD–$\delta^{18}O$ plot of all the samples analysed from the Klein Swartberg, north of Ladismith, to Goukamma, near Knysna. This graph provides some excellent examples of the amount effect at the moderate rainfall sites of Kammanassie and Lentelus, with MAP of 660 mm/a and 640 mm/a, respectively. The lowest δ values for these two sites are both from July 2010 where 80 mm and 40 mm, respectively, fell at these two locations. June 2010 also shows low values for Kammanassie and Lentelus where 30 mm and 75 mm, respectively, fell in that month.

Figure 5.19 shows the unexpected isotopic distribution of the Klein Swartberg high altitude seeps at Toverkop (2060 m), Skull Cave (1880 m) and Seweweekspoort Peak Cave (2020 m); these were discussed in **Section 5.2.2.3**. Two boreholes on the farm Rooihoogte on the northern side of the Klein Swartberg (due north of Skull Cave) were sampled are labelled BROO on **Figure 5.19**. The boreholes are drilled into the Rietvlei Formation and therefore abstract water from the Skurweberg aquifer. The Table Mountain Group here is tilted steeply to the north, dipping beneath the Bokkeveld and Witteberg Groups. The isotope composition of the Rooihoogte boreholes matches that of Skull Cave very closely, which suggests that recharge takes place at the crest of the range, which here is Goudini Formation and therefore also part of the Skurweberg aquifer, before travelling down-dip towards the Great Karoo. Another possibility is that recharge takes place at slightly lower altitudes, which would have less isotopically negative rainfall on average, but is subject to *selection*, whereby only the high volume rain events with the most negative isotope ratios recharge the aquifer.

As with the Tweespruit and Gamkaberg boreholes, it seems likely that the groundwater is

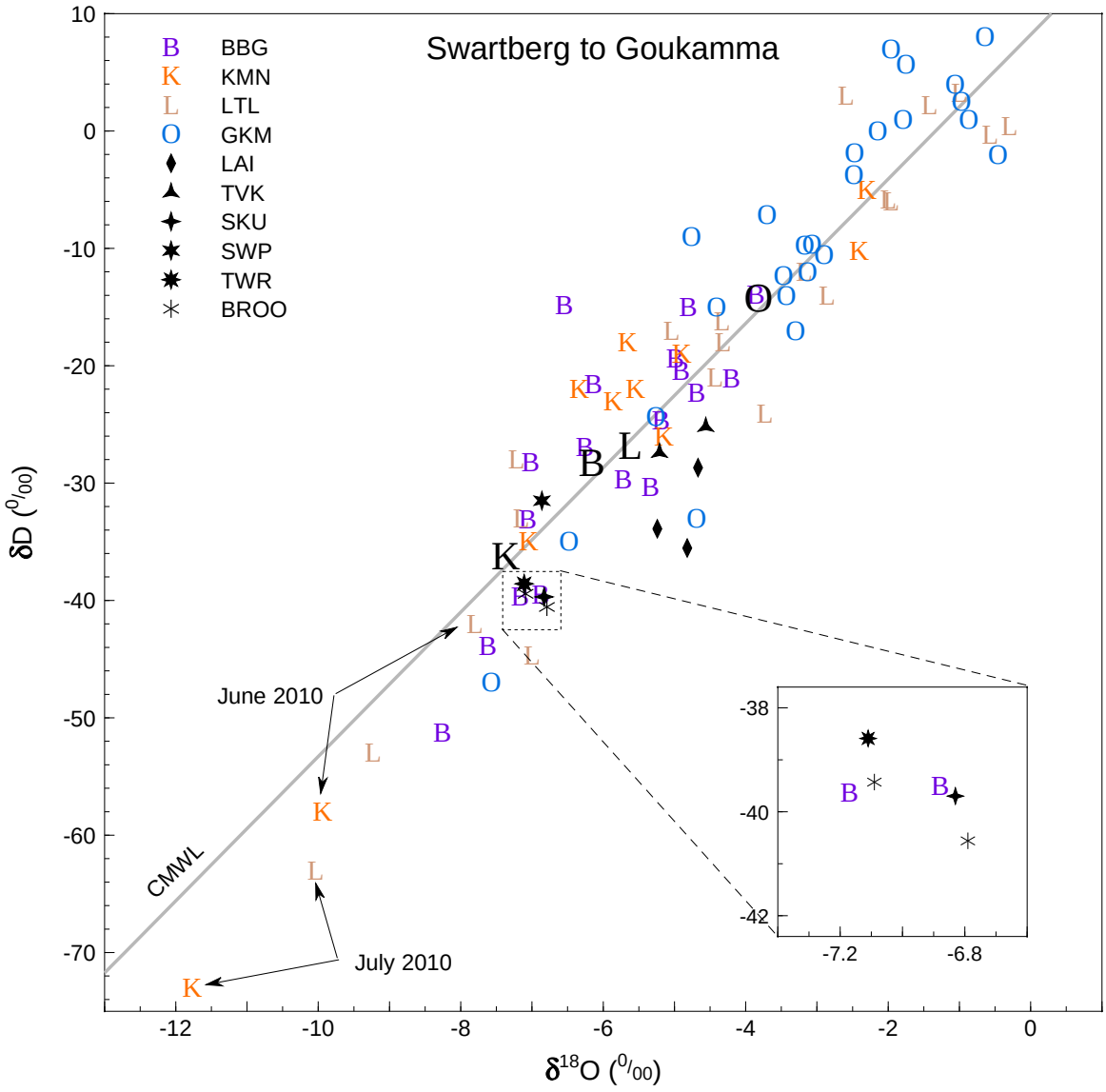

Figure 5.19: A δD – $\delta^{18}O$ plot for all samples taken in the Swartberg to Goukamma region. Larger black letters indicate weighted means for rainfall at Blesberg (B), Kammanassie (K), Lentelus (L) and Goukamma (O). BBG = Blesberg, KMN = Kammanassie, LTL = Lentelus, GKM = Goukamma, LAI = UCT field station spring, TVK = Toverkop seep, SKU = Skull Cave seep, SWP = Seweweek-spoort Peak Cave seep, TWR = Toowerwater hot spring, BROO = Rooihoogte boreholes.

recharged in the Goudini or Skurweberg Formations and discharged via the Rietvlei Formation, all part of the Skurweberg aquifer. To what extent this upgradient flow is natural or in induced by pumping remains open to speculation. From both the Gamkaberg and Swartberg (Rooihoogte) settings, the very negative nature of the borehole isotope values suggests the groundwater flow is already from the highest parts of the crest to the valley, whereas for Tweespruit there is space for the groundwater to be recharged at higher elevations, based on the calculated recharge elevation of 1200 m on the flanks of a 2000 m high mountain range.

Samples from a spring 10 km south of Laingsburg at the UCT Geological Sciences field station in the Great Karoo were taken in 2010, 2011 and 2012. This spring emerges from the Dwyka Group at about 700 m altitude and could be recharged in the south in low mountains of Witteberg Group rocks. The Witteberg Group contains quartzite formations that are extensively fractured, providing secondary porosity. The relatively negative δ values for the 'Laingsburg' spring suggest either a higher altitude of recharge than at the spring, or are the result of the local rainfall displaying a significant continental effect and amount effect. The continental effect is likely to be significant as this location is inland of 2000 m high mountain ranges in almost all directions, so rainout will have been substantial because of orographically driven rainfall. The amount effect is known from arid regions (Dody and Ziv, 2013) and has been seen in South African arid zone rainfall by Vogel and van Urk (1975).

The 'Laingsburg' spring samples plot quite far to the right of the Cape Meteoric Water Line, in the area on the δD – $\delta^{18}O$ plot associated with evaporated waters. This would be expected for precipitation, and hence all other meteoric waters, in an arid zone. It confirms that the recharge area is in the Karoo and not in the Table Mountain Group in the Cape Mountains, where less evaporated isotopic signatures are expected, as can be seen for most of the data in this study.

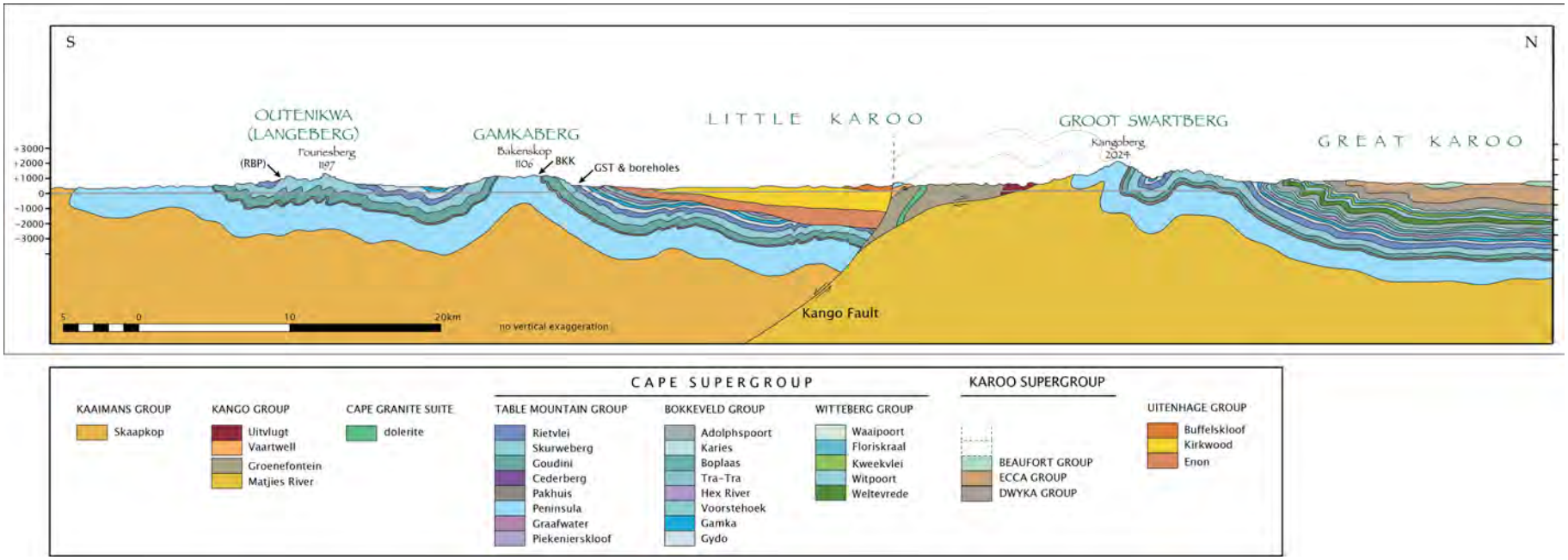

Figure 5.20: A geological cross section from the coastal plain to the Great Karoo, drawn from the 1:250 000 geological map for Ladismith (Geological Survey, 1991).

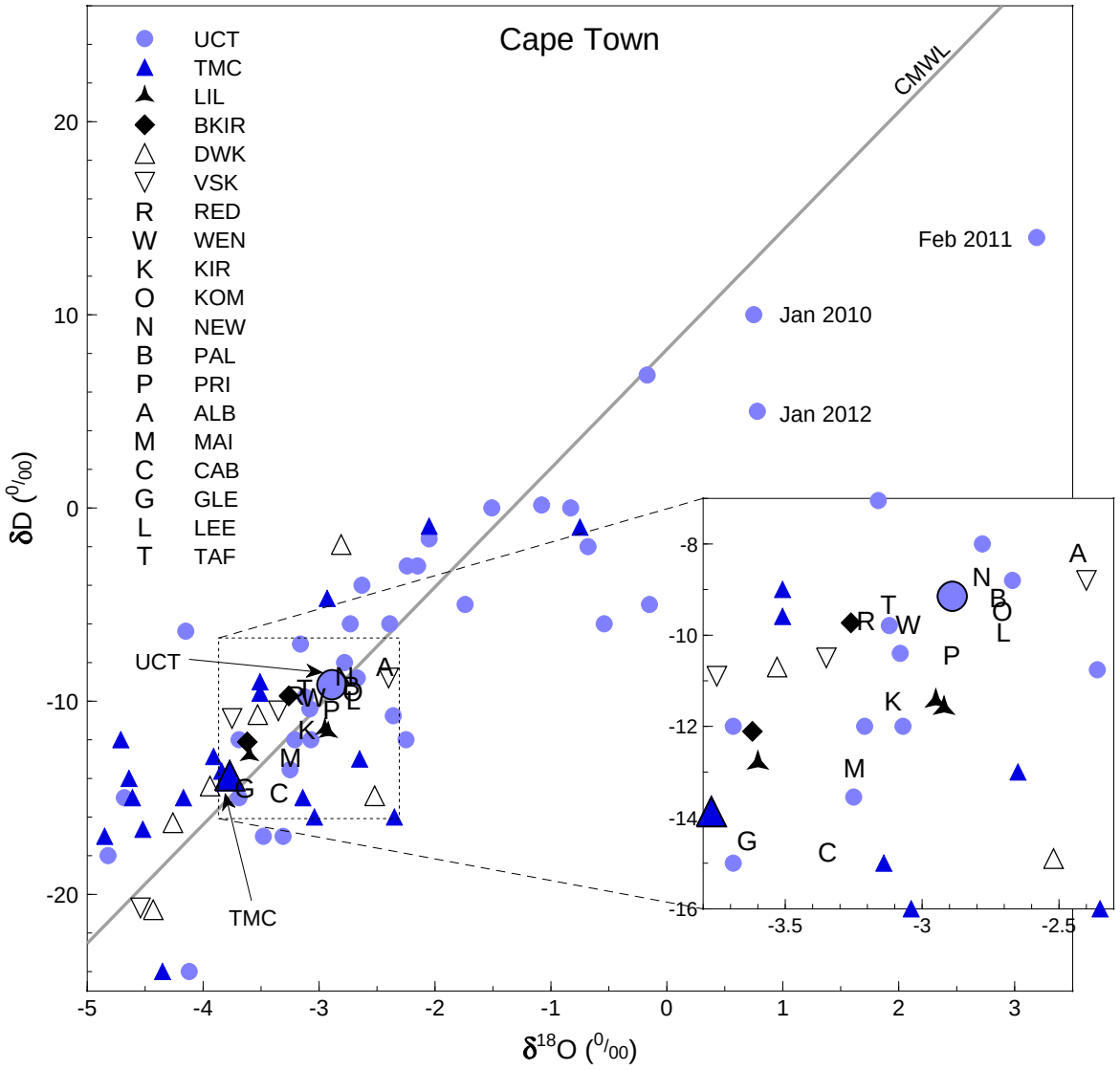

Figure 5.21: A δD versus $\delta^{18}O$ plot for all samples taken in the Cape Town region. The large circle and triangle indicate the weighted mean values for UCT and TMC rainfall. UCT = University of Cape Town, TMC = Table Mountain Cableway, LIL = Lily Pond seep, BKIR = Kirstenbosch boreholes, DWK = Duiwelskloof river, VSK = Volstruiskloof river, R = mean Redwood spring, W = mean Wendy's spring, K = mean Kirstenbosch spring, O = mean Kommetjie spring, N = mean Newlands spring, B = mean Palmboom spring, P = mean Princess Anne spring, A = mean Albion spring, M = mean Main CT spring, C = mean Cableway spring, G = mean Glencoe spring, L = mean Leeuwenhof spring, T = mean Tafelberg Rd spring.

5.5.5 Cape Town

Samples in the Cape Town area include regular samples over three years of the major springs that issue from the slopes of the mountain, both on the northern, city side and on the eastern, Kirstenbosch side. A detailed analysis of this data will be made, but first, a brief analysis of data from the two rainfall stations in the area, UCT and Table Mountain Cableway, will be made. As was mentioned in **Section 5.2.2.3**, the difference in isotope ratios between UCT and TMC is less than would be expected based on global averages for the altitude effect, because of both an "island peak" effect and because the higher location (TMC) is not in the direction of increasing rainout.

The UCT data shows some excellent examples of highly evaporated rainfall typical of summer months in a Mediterranean climate (e.g. Argiriou and Lykoudis, 2006). Table Mountain Cableway does not show the same degree of evaporative enrichment due to the shorter path of raindrops through the atmosphere in which evaporation can occur. The meteoric water lines of these two stations are similar in both gradient and δD-intercept values **Figure 4.10**.

The mean values for each of the sampled Cape Town springs have been plotted in **Figure 5.21**. The Kirstenbosch cluster of springs sit on the lower slopes below the east face of Table Mountain, Kirstenbosch being the most southerly and Albion one of the most northerly of those sampled. The Albion Spring (A) discharges water with the highest δ values of these springs and also happens to discharge at the lowest altitude. Its position places it furthest from the steep cliffs and the summit near the east face of Table Mountain, where the most isotopically light rainfall would be expected. The isotope values at Albion indicate the recharge area receives the least isotopically negative rainfall of all the Kirstenbosch springs, which corresponds with its geographic position and elevation. The opposite holds for Kirstenbosch (K), and to a lesser extent Redwood (R) and Wendy's (W), which have more isotopically negative discharge and are closer to the high cliffs of Table Mountain. The position of the spring waters on the δD – $\delta^{18}O$ graph roughly corresponds to the geographic position, resulting in a sequence from more to less negative δ values as the springs are located further from the site of highest rainfall on the southern end of the east face of Table Mountain, known as Fernwood Buttress. The sequence of springs, from most negative to most positive δ values is: Kirstenbosch (K) $\rightarrow$ Redwood (R) and Wendy's (W) $\rightarrow$ Princess Anne (P) $\rightarrow$ Kommetjie (O) and Palmboom (B) and Newlands (N) $\rightarrow$ Albion (A).

As this trend is based on the isotopic values of spring discharge, which is reliant upon isotopic changes inherited from precipitation in the recharge area, it suggests the position of a spring is closely related to the position of the recharge area. This in turn means long distance groundwater flow is probably not occurring. It also means if there is a distance between the spring and the recharge area, a similar distance exists for all the springs. The weighted average for UCT rainfall lies very close to many of these springs, especially Wendy's, Princess Anne and the Newlands, Palmboom and Kommetjie group, which are geographically also very close to UCT. All this evidence points to extremely local recharge on the lower slopes of the mountain. The most likely

aquifer for these springs is the scree and weathered material overlying the basement, comprising granite in the southern areas around Kirstenbosch and Redwood, and Malmesbury Group in the northern areas around UCT. The Table Mountain Group is not directly involved, except as a supply of boulders and sand that make up the scree material on the slopes of the mountain.

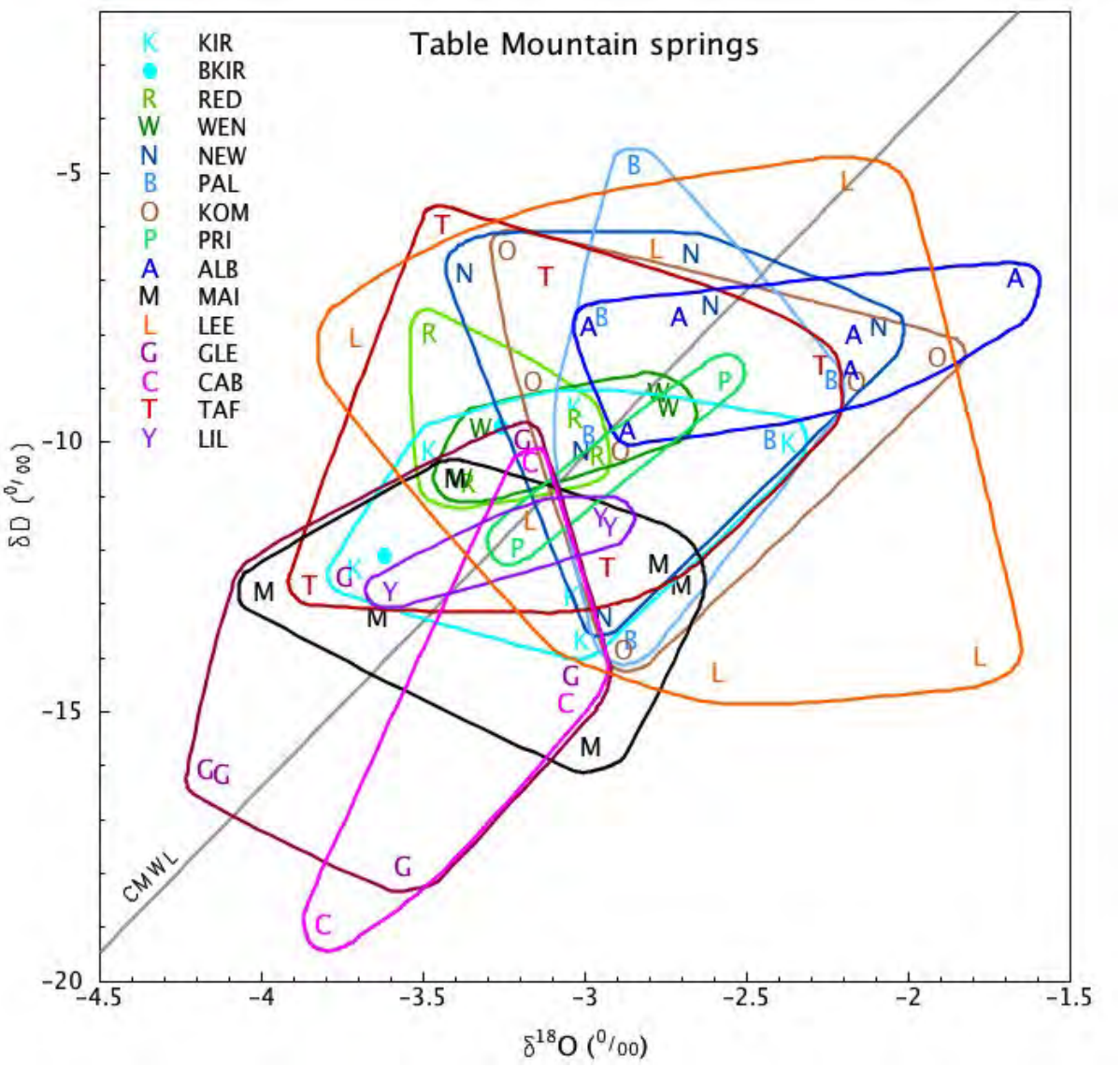

Figure 5.22: All the data for all the Table Mountain springs, with each springs' cluster of points circled. K = Kirstenbosch, BKIR = Kirstenbosch boreholes, R = Redwood, W = Wendy's, N = Newlands, B = Palmboom, O = Kommetjie, P = Princess Anne, A = Albion, M = main spring, L = Leeuwenhof, G = Glencoe, C = Cableway, T = Tafelberg Road, Y = Lily Pond.

Two boreholes at Kirstenbosch were sampled, "Protea" and "Apple Tree". Their isotope values are amongst the most negative of the Kirstenbosch springs and fall neatly within the distribution for the samples from the Kirstenbosch spring itself, as seen in **Figure 5.22**. They fit into the overall pattern noted above, where position on the δD – $\delta^{18}O$ diagram in **Figure 5.21** broadly

relates to geographic position relative to Table Mountain.

Several observations can be made from the isotope data for the springs analysed on the city side of Table Mountain. Cableway (C) and Glencoe (G) have the lowest δ values. These springs emerge from large scree fans that cover the north-west slopes of Table Mountain. Recharge into these screes is not only from rainfall directly onto their surfaces at 200–500 m elevation, but also from streams that drain the steep cliffs on the northern face of the western Table. These streams' catchments include areas up to the Upper Cableway Station at 1070 m. The similarity between the weighted mean for TMC and for Glencoe and Cableway springs confirm this as being part of the recharge area for these springs. An amount effect and selective recharge of heavier rainfall events will drive the Glencoe and Cableway recharge to lower δ values, compensated for by a shift to higher δ values from recharge occurring at lower elevation as well.

The Tafelberg Road spring (T) has less negative δ values, probably because its position below The Saddle, the area separating Devils Peak from Table Mountain, where recharge can only occur up to a maximum altitude of 700 m. The Leeuwenhof Spring (L) has the largest range of values of any of the springs by a factor of 2, as seen in **Figure 5.22**. This spring was sampled about 100 m from the source, an area of about half a hectare of seepage, because it is within the official residence of the Western Cape premier and access is restricted. The spring is undoubtedly the reason for the location of this historical homestead. The diffuse discharge area and the possibility for contamination from rain, Cape Town scheme water, stormwater or sewage leaks, as well as evaporation in the seepage area, explain the abnormally wide range in isotopic values at this spring. The position of the Leeuwenhof mean on the δD – $\delta^{18}O$ diagram, however, is consistent with its geographic position furthest from Table Mountain and at the lowest altitude of the city springs, and therefore subject to recharge at lower elevations with higher δ values. This suggests that dilution or alteration of isotope composition was minor.

The "main spring" (M) was sampled at the collection chamber in the "field of springs" east of Upper Orange Street in Oranjezicht. This collection chamber receives water from a few springs at the top of Oranjezicht, such as above Rugby Road cul-de-sac, and from the adjacent Stadsfontein at the field of springs, one of the original springs deciding the settlement of Cape Town by the Dutch East India Company in 1652. Assuming a similar relationship applies to the City Bowl springs as has been shown to apply to the Kirstenbosch springs, namely a positive correlation between distance from mountain and δ values, then the water from the "main spring" should be more isotopically negative than the position of the collection chamber on the map would suggest. The average position of these feeder springs would be in line with Glencoe's altitude and at the base of the large screen cones below Platteklip Gorge. Balancing these springs closer to the mountain is the position of Stadsfontein at the "field of springs." The expected isotope composition for the main spring should be intermediate to the Glencoe and Cableway values (closer to the mountain), and to Leeuwenhof (further from the mountain). This is indeed where the "main spring" plots in **Figure 5.21**.

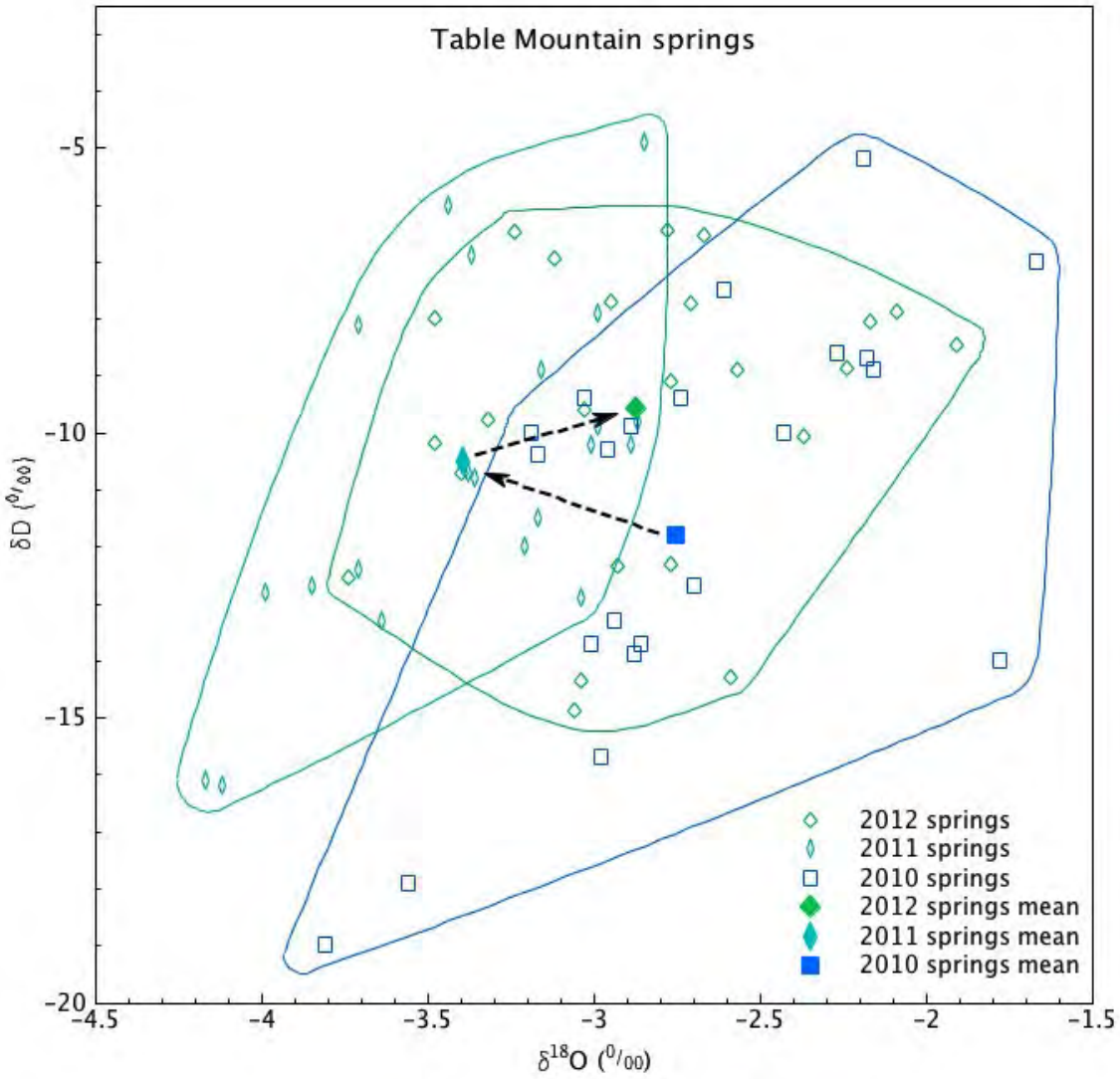

Figure 5.23: Data for all the Table Mountain springs plotted according to year, with the annual means also shown and arrows to indicate the yearly shift between annual means.

Groundwater Flow

Figure 5.23 shows the data for all the Cape Town springs plotted by year; most of the springs were sampled twice a year. A significant shift occurs in the isotope values, to the extent that less than 25 % of the 2010 samples fall within the range of the 2011 samples. This is clearly a significant shift and is quite unlike the random variability as noted for the hot springs in **Section 5.4.2**. The means for all the springs for the three years, 2010–2012, have also been plotted in **Figure 5.23** with arrows indicating the progression from year to year.

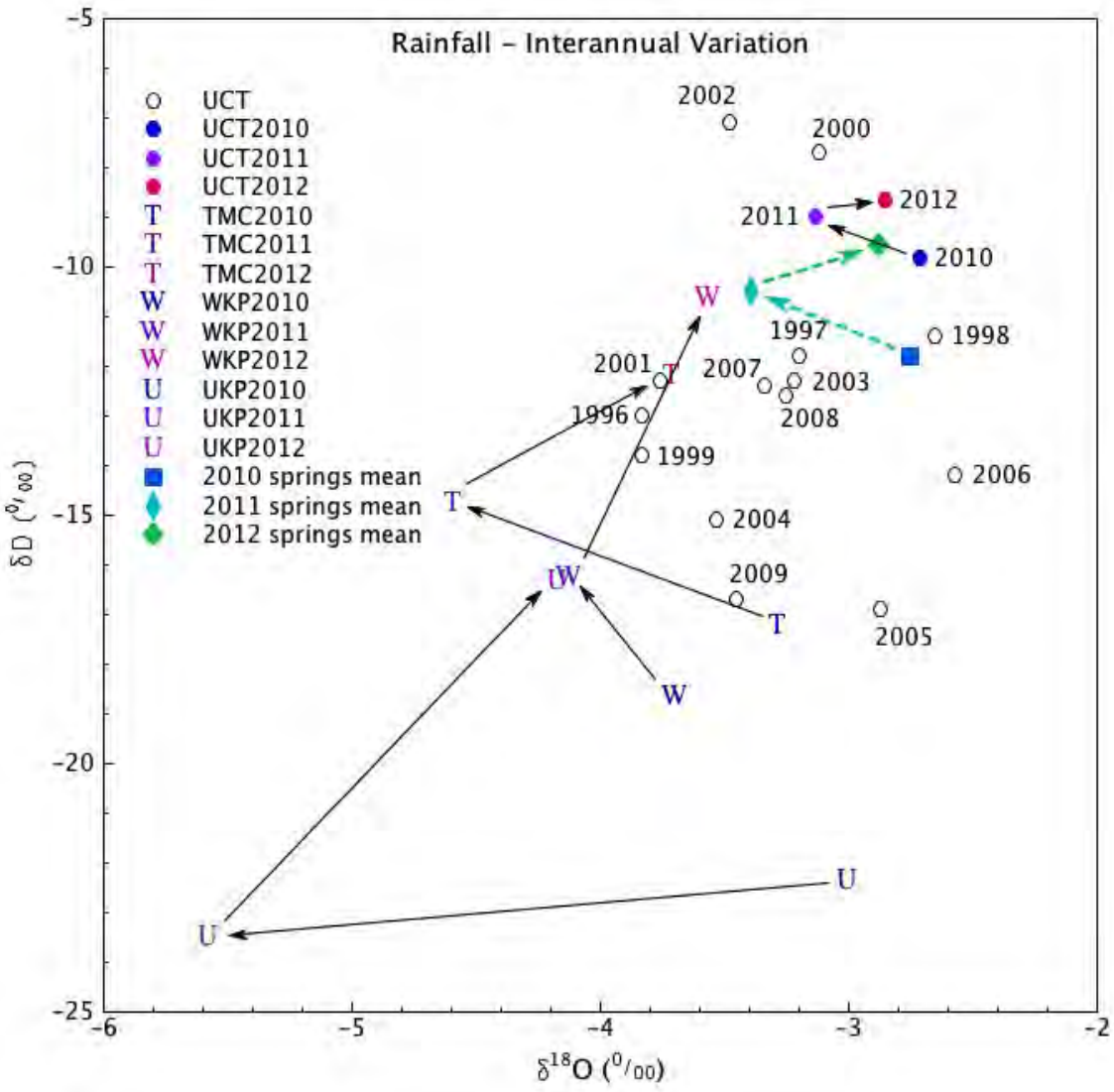

Figure 5.24: Weighted annual means for rainfall from several stations, including the long term records from UCT, as well as the average annual values for the Table Mountain springs, plotted in the δD – $\delta^{18}O$ space. UCT = University of Cape Town, T = Table Mountain Cableway, W = Wolfkop, U = Uitkyk Pass. Note the similarity in shift of annual means of UCT rain and Cape Town springs.

The weighted annual means for several of the rainfall stations have been plotted on **Figure 5.24**, including the long term records for UCT, from 1996 until this study. The shifts in the UCT annual means are interesting, if not somewhat puzzling, and some very large shifts can be seen, for example 1999 to 2000 and 2009 to 2010. The overall range in variation of these means is also noteworthy and suggests quite different weather conditions can dominate particular years.

Interestingly, the 2010–11–12 pattern in shifts of means at UCT mimics that of the Table Mountain springs, which have been added to the graph. Three of the other rainfall stations, Table Mountain Cableway (T), Uitkyk Pass (U) and to a lesser extent Wolfkop (W), also show similar

shifts in the weighted annual means. Seeing a similar pattern of shifts in annual mean values from more than one collection station is verification that these shifts are caused by widespread changes in weather conditions from year to year and not just site specific random variation. A small difference between the UCT averages and the spring averages probably reflects selection, altitude and amount effects, as the springs are recharged at higher elevations and during heavy rainfall events. Notwithstanding this small difference in actual isotope composition, the remarkable coincidence of the interannual shifts suggests that the Table Mountain springs discharge groundwater that has been recharged in that same year.

If recharge and discharge happens in the same year and the aquifer conforms to a piston flow model, then springs would only flow weeks to months after the first winter rain around April/May, in other words, around June/July, and cease flowing around November/December once the spring rains have passed. This is not seen, except in a few of the springs: Princess Anne and Rhodes Memorial (not sampled in this study) on the Kirstenbosch side, and Cableway and Tafelberg Road on the City Bowl side. The bulk of the springs flow perennially with little seasonal variation. Even after a drought, in which rainfall is well below average for a few years, all of the perennial springs continue to flow, although perhaps at lower rates (pers. comm. Caron von Zeil, Marius Bonthuis). Many of the springs are so reliable that they are used daily by the South African National Botanical Institute (Kirstenbosch), South African Breweries (Kommetjie), Provincial Government of the Western Cape (Leeuwenhof), City of Cape Town (Stadsfontein) and the public (Newlands) for industrial, irrigation and personal use. The aquifers are clearly able to sustain flow over a time period much greater than the half-year long rainy season.

The springs' aquifer must be able to accomodate longer term groundwater flow to sustain the steady, perennial flow, as well as shorter term groundwater flow to conduct the recently recharged groundwater with an isotope composition that is similar to the precipitation of that year. An attempt was made to isolate groups of springs to see if the higher flow rate springs showed less of a shift, or if those further from the mountain showed a greater delay in the isotope composition shift, but no trends could be found. A better data set, with monthly spring samples for all the springs would perhaps yield better resolution and show such trends. Nonetheless, it seems the aquifers are able to conduct recent recharge within months or less from the recharge area to the spring, as well as sustain groundwater flow over the summer months and through dry years.

A conceptual hydrogeological model is proposed whereby recently recharged groundwater is able to flow near the water table and at speed to discharge within weeks of heavy rain, usually at the start of winter. At the same time, slower movement of groundwater deeper in the aquifer is able to sustain discharge in the long term. This model is shown in a sketch cross section in **Figure 5.25**.

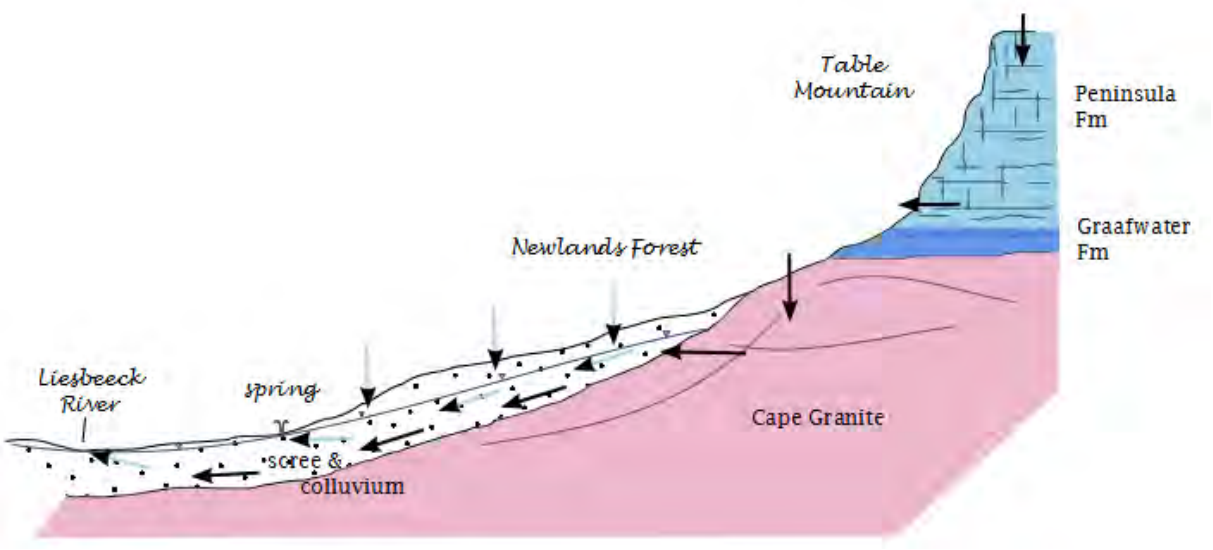

Figure 5.25: A sketch cross section looking south over Newlands Forest, showing a proposed conceptual hydrogeological model for the Kirstenbosch set of springs. Recently recharged groundwater is able to flow at shallow depths and discharge within weeks or months, whilst deeper groundwater is able to flow more slowly and sustain steady discharge over years. This model is equally applicable to the City Bowl springs.

Recharge Altitude

Figure 5.26 shows the weighted means for rainfall over 2010–12 at UCT and Table Mountain Cableway, and the mean for all the Cape Town spring samples, both those in the City Bowl and on the Kirstenbosch side of the mountain. As can be seen from the Figure, the springs plot in an intermediate position to UCT and TMC. Because the elevations of the rainfall stations are known, if a linear gradient for $\frac{\Delta\delta}{\Delta altitude}$ is assumed, the average recharge elevation for the springs can be interpolated. This works out to 304 masl.

The mean spring elevation is 156 masl, and so:

$$304masl - 156masl = 148m \ ,$$

which is the average altitude difference between spring recharge areas and discharge points. Given the typical topographic gradient of the lower slopes of Table Mountain is around 9°,

$$\Delta s = \frac{148m}{cosine9^\circ} = 946m \ ,$$

which is the average slope distance between recharge area and discharge point. Given that recharge occurs over a wide area, it would be reasonable to assume that recharge for each spring occurs in an area about 0.5–1.5 km upslope from the spring. Using the average distance of about 1 km, and an estimated duration of 2 months between rainfall and discharge for the shallow

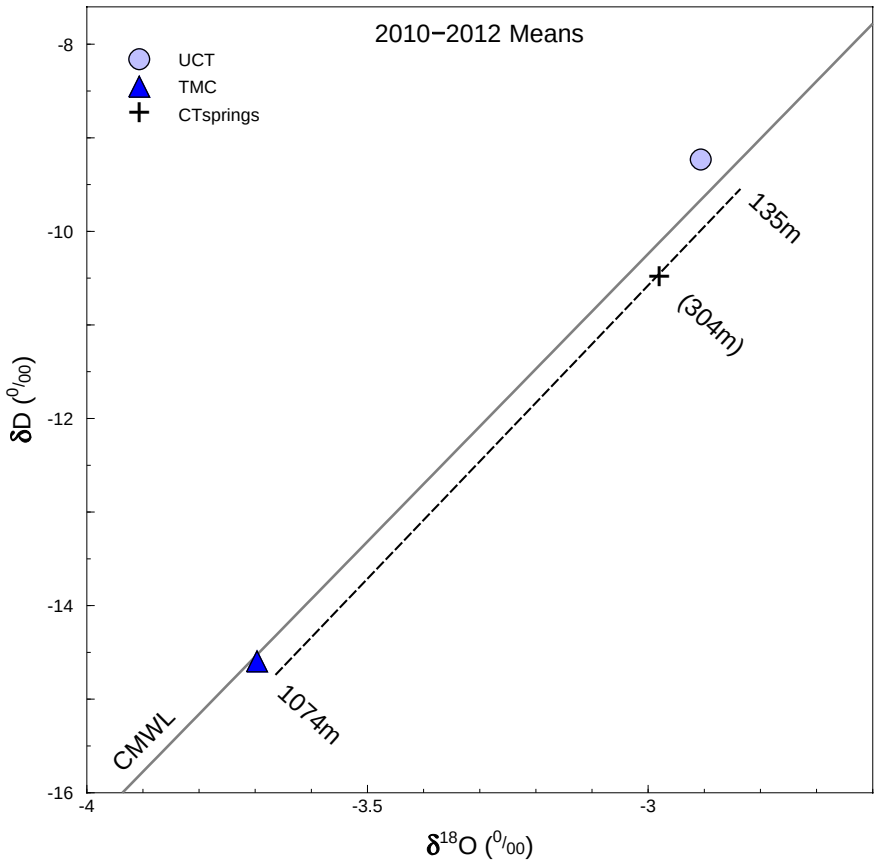

Figure 5.26: Calculation of average recharge altitude for Cape Town springs by interpolation between the altitudes of the UCT and Table Mountain Cableway (TMC) rainfall stations along a line of the same gradient as the Cape MWL.

groundwater component of the aquifer, a hydraulic conductivity of around 15–20 m/d is arrived at. This falls within the ranges of hydraulic conductivity of fine to coarse sand and gravel given in Domenico and Schwartz (1998, p.39).

These figures are rough values and will vary substantially between each spring, because of geological and topographic differences, and over different years, depending primarily upon rainfall amounts and intensities. Nonetheless, the calculation of recharge altitude and average flow path length based on isotope composition confirms the scree apron on Table Mountain as being the aquifer supporting the Cape Town springs, as presented in the conceptual model in **Figure 5.25**.

Chapter 6

Conclusions and Recommendations

This chapter summarizes the major findings of this study. The details of the data and reasoning behind these findings are to be found in both the Results and Discussion chapters above. Some key numerical results are repeated here.

1. **Weather affects isotopes** (p.100)
   The isotope composition of cumulative monthly samples of rain sometimes shows unusual values. With the help of records of past weather, individual weather systems can be found to be responsible for generation of unusual isotope composition (e.g. Dody and Ziv, 2013). In particular, convective rainfall events (thunderstorms) in summer can generate relatively negative δ values in precipitation in the Western Cape. Knowing the rarity of such weather systems can help determine whether the measured isotope composition is representative of that site.

   Recommendation: Weather records should be used when interpreting the isotope composition of rainfall.

2. **Weighted δ values of precipitation are more important in dry climates** (p.104)
   The difference between weighted and unweighted mean δ values for precipitation at a site is negatively correlated with mean annual precipitation. Weighting δ values of monthly precipitation samples by precipitation amount removes the effect of low volume rain events with extreme isotope composition, most particularly summer rains that are highly evaporated, with less negative or positive δ values. This has a greater effect on the mean in drier climates where highly evaporated and low volume rain events are more common than in wetter climates. This is in contrast to Yurtsever and Gat (1981), who found the difference in means is positively correlated with seasonality.

   Result: The weighted means for all rainfall for this study are: δD = -17.7 ‰ and $\delta^{18}O$ = -4.22 ‰, similar to those in drier parts of Jordan (Salameh, 2004).

Recommendation: Means should always be calculated by weighting δ values of monthly cumulative rain samples by the rainfall amount.

3. **The weighted LMWL is more relevant in hydrological studies** (p.108)
   The local meteoric water line equation is calculated using reduced-major-axis (RMA) regression between δD and $\delta^{18}O$. Weighting the monthly δ values by rainfall amount changes the best fit line and generally results in a steeper gradient and higher δD intercept. As low volume rains have less impact on hydrology, especially groundwater recharge, and weighting removes the effect of low volume rains, the weighted LMWL is more applicable to hydrological studies (Hughes and Crawford, 2012). Use of weighted data and the more applicable RMA regression method is either not done or not clearly stated in the global literature.

   Result: The weighted LMWL for this study, or Cape MWL is: δD = 6.15 $\delta^{18}O$ + 8.21, which is similar to those previously calculated for this area (Diamond and Harris, 1997; Harris et al., 2010).

   Recommendation: Local meteoric water lines should be calculated by weighted reduced-major-axis regression.

4. **Groundwater has a lesser spread of δ values than precipitation** (p.113)
   The range of δ values for groundwater at one site or across a region is less than for precipitation (e.g. Majumder et al., 2011). Groundwater averages out the short term variations in precipitation to reveal the long term mean δ values of precipitation. Where the recharge area is well defined, such as for high altitude mountain seeps in the Table Mountain Group, where there is very little aquifer above the discharge point, the isotope composition of the water from the seep is a good proxy for the local precipitation.

   Result: The ranges in values of δD and $\delta^{18}O$ are, for precipitation: -75 ‰ to +40 ‰ and -12 ‰ to +8 ‰; and for groundwater: -47 ‰ to 0 ‰ and -8 ‰ to -1 ‰ .

   Recommendation: High altitude mountain seeps in the Table Mountain Group can be collected instead of difficult and costly long term precipitation monitoring at high altitude.

5. **Western Cape stable isotope compositions are similar to South Africa** (p.129)
   In spite of having different climates, the isotope compositions for the Western Cape and for the rest of South Africa overlap. The current data sets have insufficient separation according to season, climatic region, weather events and other factors to be able to draw out trends, although there are most likely differences in means from different regions. Differences in mean isotope composition of precipitation at specific sites across Australia are also minor, in spite of vast distances and different climates (Liu et al., 2010).

Recommendation: More samples of meteoric water throughout South Africa are needed. In particular, thoughtful analysis of these samples, according to geographic and meteorological parameters, is needed to draw out regional patterns in stable isotope composition.

6. **The Western Cape displays a complex continentality effect** (p.133)
   Poor correlations are displayed between δ values and simple distance from sea parameters, such as have been used by Salati et al. (1979) and Yonge et al. (1989). A compound "distance to the Atlantic" and "distance to the closest coast" parameter shows much better correlations with δ values. This is likely because rain bearing weather systems can approach from any direction from NW, through W and S to SE, due to the Western Cape's position at the southern end of Africa. Continentality effects in regions where rain bearing weather systems can approach from more than one direction are likely to be complex.

   Recommendation: To calculate the best index of continentality for the Western Cape, generate average weather system tracks for different locations, or more simply measure the area of land between the rainfall station and the ocean within the semi-circle facing SW.

7. **Small and steep mountains display a reduced altitude effect due to reduced rainout** (p.136)
   Small, steep mountains do not generate sufficient rainout to drive isotope compositions towards the negative δ values that would be expected based on the site altitude. The isotope composition is a function of the average altitude over several square kilometres around a site. The reverse is also true: sites surrounded by higher elevation, such as valleys within mountains, record δ values that are more negative than would be expected based on the actual site altitude. The altitude effect gradients calculated for this study are on the low side compared to reported gradients from around the world (Clark and Fritz, 1997, p.71). This is because of the steep terrain gradients of the Cape Mountains and suggests that many of the altitude effects calculated worldwide are in fact combination effects of pure altitude change as well as rainout with distance.

   Result: Calculated altitude effect gradients varied from -0.48 to -2.2 $\frac{\Delta\delta D}{100m}$ and -0.075 to -0.34 $\frac{\Delta\delta^{18}O}{100m}$.

   Recommendation: Precipitation collection stations should be placed at an elevation that is representative of the general surrounds, rather than atop a high peak or in a deep valley. Where stations are in topographically unrepresentative positions, the average elevation around the site should be used when calculating altitude effect gradients.

8. **The amount effect varies between stations and over time at single stations** (p.143)
   The amount effect was not noticeable for average annual precipitation, but for mean monthly precipitation (e.g. Dansgaard, 1964; Rozanski et al., 1993). To calculate useful monthly means of precipitation and δ values, several years of monitoring are needed. The scale of the effect varied significantly between stations and even at a single station over different groups of years, emphasising the need for longer term monitoring to calculate reliable relationships.

   Recommendation: Long term monitoring is needed to calculate such isotope effects accurately. In the absence of longer term data, overinterpretation of trends should be avoided.

9. **Surface waters show little variation within catchments, suggesting complex groundwater flow paths with significant mixing in the Peninsula aquifer** (p.148)
   Samples from rivers showed great variation between rivers, but not within each catchment, despite substantial ranges in altitude and sometimes distance. The surface waters were sampled in late summer, so representing baseflow, made up of groundwater discharge. Direct samples of springs and seeps adjacent to rivers were also taken. The well averaged nature of surface water in each catchment suggests the groundwaters are well mixed between recharge and discharge points, which suggests complex flow paths through deep fracture networks in the Table Mountain Group, mostly the Peninsula Formation, in contrast to isotopically varied groundwater from shallow fracture networks (e.g. Negrel et al., 2011).

   Recommendation: Surface water samples should not be used to understand details of groundwater flow, but do offer averaged δ values for the catchment. The homogeneity of surface water baseflow can be used as a measure of groundwater mixing.

10. **Groundwater flow paths are often shallow and short** (p.151)
    A negative correlation exists between δ values of groundwater samples and the discharge elevation. If groundwater flow paths were long or variable in length, the recharge altitude, which is what determines the δ values, would not be correlated with the discharge altitude. The correlation suggests that much of the groundwater sampled circulates shallowly and has a short flow path of hundreds of metres to perhaps a kilometre or two. This means the aquifer is more easily impacted by surface activities and overabstraction.

    Recommendation: Determine the size and depth of the aquifer by comparing groundwater and precipitation isotope composition, to determine its vulnerability to surface impacts and overabstraction. Long term precipitation monitoring will be needed.

11. **Hot springs reveal long term, long distance, deep circulation in the Table Mountain Group** (p.153)

    Stable isotope composition of several hot springs did not change appreciably over 40 years, although significant variations occur in isotope composition of discharge, even on a monthly timescale. Interannual or interdecadal variations in recharge (precipitation) are not obvious and indicate that circulation is well mixed, deep and regional (e.g. Delalande et al., 2011). The Table Mountain Group is able to conduct deep (more than one or two kilometres), long distance (tens of kilometres) groundwater flow.

12. **Agricultural abstraction in the Olifants River Mountains taps locally recharged groundwater of the Peninsula aquifer** (p.155)

    Isotope composition of rainfall and groundwater in the Olifants River and Cederberg region revealed that groundwater being abstracted from the Peninsula Formation in the Olifants River Mountains was not coming from the Cederberg region and was being locally recharged. The aquifer is relatively limited in extent and more likely to become depleted.

    Recommendation: Local monitoring of hydrological parameters (water levels, rainfall) may be useful in warning of potential groundwater depletion, especially if climate change predictions of decreased rainfall come to pass. Stable isotopes can be employed to elucidate more details about the local groundwater circulation.

13. **Mountain recharge into the Skurweberg aquifer supplies agricultural boreholes on both sides of the Hex River anticline** (p.159)

    Comparison of the isotope composition of boreholes with precipitation has allowed the calculation of approximate recharge altitude. Groundwater abstracted from the Rietvlei Formation at 500 masl on the south side of the Hex River anticline is recharged in the Skurweberg or Goudini Formation at 1200 masl, and groundwater abstracted from the Rietvlei Formation at 1100 masl on the north side of the Hex River anticline is recharged in the Skurweberg or Goudini Formation at 1600 masl. The Skurweberg aquifer is an important, high yielding aquifer for agriculture in the Hex River Mountains region, as has been noted in the nearby Agter-Witzenberg Valley (Weaver et al., 1999). Increasing groundwater abstraction will draw water from deeper in the Skurweberg aquifer, which will have been recharged at higher elevation and therefore have more negative δ values.

    Recommendation: Where an aquifer is recharged over a range of altitudes, monitor stable isotope composition of borehole water to detect signs of overabstraction.

14. **Snow isotope composition varies greatly and preserves that of precipitation events**

    A profile through a snowpack revealed that the isotope composition changed both during a

precipitation event and between different events. Some of this change may have been due to post-depositional changes (Arnason, 1981).

Recommendation: Snow may be sampled to examine recent past precipitation events, but care must be taken to evaluate the degree of post-depositional change.

15. **Groundwater is recharged selectively during large amount rainfall events** (p.166)
    The isotope composition of groundwater discharge at Gamkaberg boreholes has more negative δ values than rainfall at the top of the Gamkaberg, so either selective recharge during isotopically more negative large amount rainfall events occurs (e.g. Dogramaci et al., 2012), or interannual variation in isotope composition of rainfall accounts for the relatively high δ values on top of Gamkaberg.

    Recommendation: Long term precipitation monitoring is needed to quantify the range of interannual variations in δ values.

16. **The Skurweberg aquifer conducts groundwater from the crest of the Klein Swartberg into the Great Karoo** (p.166)
    Boreholes on the northern side of the Klein Swartberg at 1000 masl discharge groundwater with δ values that match recharge at the crest of the range at 2000 m. The recharge occurs in the Goudini or Skurweberg Formation and is discharged through the Rietvlei Formation.

17. **Table Mountain springs are fed by groundwater from the scree aquifer** (p.173)
    Using the altitude effect calculated for Table Mountain it was shown that the typical groundwater flow path for each spring is 1 km long. The aquifer is the scree apron that lies on the middle to lower slopes of Table Mountain, contrary to popularly held belief that the Peninsula Formation is the aquifer (Bryant and Blake, 2014). The springs may be more susceptible to climate change and human activities on the lower slopes than would be the case if the Peninsula aquifer higher on the mountain was directly involved, being in a higher rainfall zone and further removed from human activities.

18. **Table Mountain scree aquifers allow layered groundwater flow to take place** (p.173)
    By tracking changes in annual mean δ values for precipitation and for the springs, the scree aquifer must allow shallow, fast groundwater flow to take place on top of slower, deeper groundwater flow. The former is needed to explain the identical pattern in shifts of annual mean δ values between rain and springs, and the latter is needed to explain the perennial flow of many of the springs. Changes in mean annual isotope composition are generally regarded as noise in data, caused by variations in the weather from year to year, and long

term averages are usually sought (Yurtsever and Gat, 1981). This study has shown the value of using shorter term data and in particular, the interannual changes in mean isotope composition to unravel hydrogeological relations.

Summary

In an international review on stable isotope hydrology, Gat (1996, p.253) stated: "In order to take full advantage of the possibilities of understanding groundwater formation, the detailed isotope effects of the recharge and runoff processes need to be established for different climate conditions and for each watershed. Such studies are still few and incomplete." And in the closing chapter of the Water Research Commission report on the Table Mountain Group, Pietersen and Parsons (2002, p.257) stated: "The WRC recognises the need to... Develop an understanding of the occurrence, attributes and dynamics of the TMG aquifer systems... ". This study has made a start on these recommendations and being regional in nature, has paved the way for more detailed work in and around the Cape Fold Belt.

Findings have been made regarding the continental and altitude effects. Both have been shown to contain more complexity than some other studies have shown, suggesting that either weather in the Cape is more complex, or that other studies have overlooked such details. Changes in mean annual isotope composition of precipitation have been shown to be useful tracers of groundwater flow, something which has not been done before.

Regarding the Table Mountain Group, this study has shown strong evidence for mountain recharge and flow of groundwater to adjacent valleys. Much of the groundwater in the Table Mountain Group has a short flow path of one or two kilometres or less, in keeping with the steep terrain of the Cape Mountains. Despite these short flow distances, groundwater appears to be well mixed, which indicates substantial fracture networks in multiple orientations. Recharge displays selection behaviour, where large amount rainfall events with lighter isotope compositions are favoured.

The range in isotope compositions, due largely to continental and altitude effects, allowed their use as hydrological tracers and helped develop conceptual models of groundwater flow in the Cape Fold Belt. With increasing pressure on water resources in the region, stable isotopes should be employed to help understand the hydrogeology and then better manage water resources to reduce environmental impacts and allow sustainable use of groundwater, at the same time as adding to the global picture on the behaviour of stable isotopes in the hydrological cycle.

Chapter 7

Abbreviations, Acronyms and Units

acronym	explanation
ASTER	Advanced Spaceborne Thermal Emission and Reflection Radiometer
CMWL	Cape meteoric water line
CTIA	Cape Town International Airport
CTMP	Cape Town millipore water
DEM	digital elevation model
GIS	geographic information system
GMWL	Global Meteoric Water Line
GNIP	global network for isotopes in precipitation
IAEA	International Atomic Energy Agency
LASER	light amplification by stimulated emission of radiation
LMWL	local meteoric water line
LSR	least squares regression
MAP	mean annual precipitation
masl	metres above sea level
MWL	meteoric water line
RMA	reduced major axis regression
RMW	Rocky Mountain Water
SAST	South African Standard Time
SAWS	South African Weather Service
SS	sum of the squares (statistical parameter)
SP	sum of the products (statistical parameter)
T	temperature
WMO	World Meteorological Organisation

symbol	explanation
mm	millimetre
m	metre
km	kilometre
μL	microlitre
mL	millilitre
L	litre
kL	kilolitre
ML	megalitre
GL	gigalitre
mg	milligram
s	second
h	hour
d	day
a	annum (year)
Ma	megannum (million years)

letter	abbreviation	explanation
		rainfall stations
C	UCT	University of Cape Town
T	TMC	Table Mountain Upper Cableway Station
I	TWT	Twaktuin
U	UKP	Uitkyk Pass
W	WKP	Wolfkop
M	MTB	Matroosberg
D	DDN	DeDoorns
R	RVD	Riverndale
P	RBP	Robinson Pass
A	BKK	Bakenskop
G	GST	Gamka Store
B	BBG	Blesberg
K	KMN	Kammanassie
L	LTL	Lentelus
O	GKM	Goukamma
		rivers
	DWK	Duiwelskloof
	VSK	Volstruiskloof
	WTL	Witels

	GHK	Groothoekkloof
		hot springs
	CIT	Citrusdal (The Baths)
	WTZ	Witzenberg (Tulbagh)
	GDN	Goudini
	BRA	Brandvlei
	CDN	Caledon
	WAR	Warmwaterberg
	LAI	Laingsburg (UCT field station)
	CZD	Calitzdorp
	TWR	Toowerwater
		Table Mountain (Cape Town) springs
K	KIR	Kirstenbosch
O	KOM	Kommetjie
P	PRI	Princess Anne Drive
N	NEW	Newlands
B	PAL	Palmboom
A	ALB	Albion
R	RED	Redwood
W	WEN	Wendy’s
M	MAI	Cape Town main spring (collection chamber)
C	CAB	Cableway
G	GLE	Glencoe Road
L	LEE	Leeuwenhof
T	TAF	Tafelberg Road
Y	LIL	Lily Pond

Table 7.1: Tables of Acronyms, Units and Abbreviations

Chapter 8

Acknowledgements

I would like to thank the following organisations and people:

Professor Chris Harris for supervision, funding, advice and climbing;

National Research Foundation and Water Research Commission for funding;

Dr John Lanham for analytical assistance on the mass spectrometer;

Dr Adam West for analytical assistance on the LASER spectrometer and advice;

for sampling rain:
Fayrooza Rawoot at University of Cape Town,
Sabine Lehmann, Marie Abraham and Kim van Reenen at the Table Mountain Aerial Cableway Company,
Robert and Anne Paterson at Twaktuin,
Patrick Lane at the Cederberg (Cape Nature),
Richard Humphris at Wolfkop,
Waldo and Didi Smith at Erfdeel,
Retief Jordaan at Tweespruit,
Jeremy Wakeford at Riverndale,
Jan Makampies at Ruitersbos (Cape Nature), Robinson Pass,
Tom Barry and team at Gamkaberg (Cape Nature),
Jan Coetzee, Theo Taute and team at the Groot Swartberg (Cape Nature),
Philip Esau and team at the Kammanassie (Cape Nature),
Dirk Versfeld and Rachel Moos at Lentelus,
Marina Botha at Goukamma;

for sampling boreholes:
Robert Paterson at Twaktuin,
Waldo Smith at Erfdeel,
Retief Jordaan at Tweespruit,
Tom Barry at Gamkaberg,
Geoff Grundlingh at Rooihoogte;

for sampling springs:
Caron von Zeil and Pixie Littlewort for assistance and passion for the Cape Town springs,
Marius Bonthuis at Cape Town Main (City of Cape Town),
Philip le Roux and Aida van Reenen at Kirstenbosch (South African National Biodiversity Institute),
Paul Teuchert at Kommetjie (South African Breweries),
the managers at the various hot springs;

and to all the friends and family who accompanied me on various missions to collect samples, service rainfall collectors and sample springs and seeps in the wild yet wonderful Cape Mountains:
Alexis Aronson,
Anyik Duku,
Phil Ginsberg,
John Glover,
Richard Halsey,
Martin Kleynhans,
Lucille Krige,
Mikhaela Levitas,
Elinor Milewski,
Sonia van Essen,
Luke Viljoen,
Xolani Zekani.

References

Adams, S., Titus, R., Pietersen, K., Tredoux, G., Harris, C., 2001. Hydrochemical characteristics of aquifers near Sutherland in the Western Karoo, South Africa. Journal of Hydrology 241, 91–103.

Al-Aswad, A.A., Al-Bassam, A.M., 1997. Proposed hydrostratigraphical classification and nomenclature: application to the Palaeozoic in Saudi Arabia. Journal of African Earth Sciences 24, 497–510.

Araguás-Araguás, L., Froehlich, K., Rozanski, K., 1998. Stable isotope composition of precipitation over southeast Asia. Journal of Geophysical Research 103, 28721–28742.

Araguás-Araguás, L., Froehlich, K., Rozanski, K., 2000. Deuterium and oxygen-18 isotope composition of precipitation and atmospheric moisture. Hydrological Processes 14, 1341–1355.

Argiriou, A.A., Lykoudis, S., 2006. Isotopic composition of precipitation in Greece. Journal of Hydrology 327, 486–495.

Arnason, B., 1981. Ice and Snow Hydrology, in: Gat, J.R., Gonfiantini, R. (Eds.), Stable Isotope Hydrology. International Atomic Energy Agency, Vienna. number 210 in Technical Reports Series. chapter 7, pp. 143–175.

ASTER, 2014. Advanced Spaceborne Thermal Emission and Reflection Radiometer. URL: http://www.jspacesystems.or.jp/ersdac/GDEM/E/index.html.

Barrow, D., Diamond, R.E., 2011. Stable isotopes of rain, surface water and groundwater in the Kogelberg, in: Groundwater: Our Source of Security in an Uncertain Future, Groundwater Division: Geological Society of South Africa, Pretoria.

Beaudoin, G., Therrien, P., 2014. AlphaDelta: Stable Isotope Fractionation Calculator. URL: http://www2.ggl.ulaval.ca/cgi-bin/alphadelta/alphadelta.cgi.

Belcher, R.W., Kisters, A.F., 2003. Lithostratigraphic correlations in the western branch of the Pan-African Saldania Belt, South Africa: the Malmesbury Group revisited. South African Journal of Geology 106, 327–342.

Bell, C.M., 1980. Deformation of the Table Mountain Group in the Cape Fold Belt south of Port Elizabeth. Transactions of the Geological Society of South Africa 83, 115–124.

Beuster, H., Thompson, I., Gögens, A.H., Jonker, V., Clarke, F.A., 2009. Application of geostatistical analyses to develop a new mean annual rainfall surface for the south-western Cape, in: South African National Committee for the International Association of Hydrological Sciences: Symposium 2009, p. 18p.

Bond, G., 1953. The origin of thermal and mineral waters in the middle Zambezi Valley and adjoining territory. Geological Society of South Africa 56, 131–148.

Bosman, H.H., 1981. Raingauges: Quality pays. Water SA 7, 190–191.

Breitenbach, S.F., Adkins, J.F., Meyer, H., Marwan, N., Kumar, K.K., Haug, G.H., 2010. Strong influence of water vapor source dynamics on stable isotopes in precipitation observed in southern Meghalaya, NE India. Earth & Planetary Science Letters 292, 212–220.

Brink, A.B., 1981. Engineering Geology of Southern Africa. volume 2: Case Study: Dams founded on rocks and The Table Mountain Group. Building Publications, Pretoria.

Broquet, C.A., 1992. The sedimentary record of the Cape Supergroup: A review, in: de Wit, M.J., Ransome, I.G. (Eds.), Inversion Tectonics of the Cape Fold Belt, Karoo and Cretaceous Basins of Southern Africa. A.A.Balkema, pp. 159–184.

Bryant, J., Blake, D., 2014. Investigating the springs and boreholes of Groote Schuur. Veld & Flora , 63.

Butler, M.J., Verhagen, B.T., Levin, M., 2000. Application of environmental isotope techniques to hydrological and pollution problems in the urban environment, in: Sililo, O. (Ed.), Groundwater: Past Achievements and Future Challenges. A.A.Balkema, Rotterdam, pp. 459–464.

Cavé, L.C., Weaver, J.M., Talma, A.S., 2002. The use of geochemistry and isotopes in resource evaluation: a case study from the Agter-Witzenberg Valley, in: Pietersen, K., Parsons, R. (Eds.), A Synthesis of the Hydrogeology of the Table Mountain Group - Formation of a Research Strategy. Water Research Commission, Pretoria. TT 158/01, pp. 143–149.

Clark, I.D., Fritz, P., 1997. Environmental Isotopes in Hydrogeology. CRC Press, Boca Raton.

Colvin, C., Riemann, K., Brown, C., Maitre, D.L., Mlisa, A., Blake, D., Aston, T., Maherry, A., Engelbrecht, J., Pemberton, C., Magoba, R., Soltau, L., Prinsloo, E., 2009. Ecological and environmental impacts of large-scale groundwater development in the Table Mountain Group) TMG aquifer system. Technical Report 1327/1/08. Water Research Commission. Pretoria.

Council for Geoscience, 1997. 3319 Worcester. 1:250 000 geological series. Council for Geoscience. Pretoria.

Craig, H., 1961a. Isotopic variations in meteoric waters. Science 133, 1702–1703.

Craig, H., 1961b. Standard for reporting concentrations of deuterium and oxygen-18 in natural waters. Science 133, 1833–1834.

CSAG, 2013. Climate Information Portal, Climate Systems Analysis Group, University of Cape Town. http://cip.csag.uct.ac.za/webclient2/app/.

da Silva, L.C., Gresse, P.G., Scheepers, R., McNaughton, N.J., Hartmann, L.A., Fletcher, I., 2000. U-Pb SHRIMP and Sm-Nd age constraints on the timing and sources of the Pan-African Cape Granite Suite, South Africa. Journal of African Earth Sciences 30, 795–815.

D'Alessandro, W., Federico, C., Longo, M., Parello, F., 2004. Oxygen isotope composition of natural waters in the Mt Etna area. Journal of Hydrology 296, 282–299.

Dansgaard, W., 1964. Stable Isotopes in Precipitation. Tellus 16, 436–468.

Davidson, W.A., 1995. Hydrogeology and groundwater resources of the Perth Basin. Technical Report Bulletin 142. Western Australia Geological Survey. Perth.

de Beer, C.H., 2002. The Stratigraphy, Lithology and Structure of the Table Mountain Group, in: Pietersen, K., Parsons, R. (Eds.), A Synthesis of the Hydrogeology of the Table Mountain Group - Formation of a Research Strategy. Water Research Commission, Pretoria. TT 158/01, pp. 9–18.

de Wit, M.J., Ransome, I.G., 1992. Regional inversion tectonics along the southern margin of Gondwana, in: de Wit, M.J., Ransome, I.G. (Eds.), Inversion Tectonics of the Cape Fold Belt, Karoo and Cretaceous Basins of Southern Africa. A.A.Balkema, Rotterdam, pp. 15–22.

Delalande, M., Bergonzini, L., Gherardi, F., Guidi, M., Andre, L., Abdallah, I., Williamson, D., 2011. Fluid geochemistry of natural manifestations from the Southern Poroto-Rungwe hydrothermal system (Tanzania): Preliminary conceptual model. Journal of Volcanology and Geothermal Research 199, 127–141.

Dent, M.C., Lynch, S.D., Schulze, R.E., 1987. Mapping mean annual and other rainfall statistics over Southern Africa. Technical Report 109/1/89. Water Research Commission. Pretoria.

Diamond, R.E., Harris, C., 1997. Oxygen and hydrogen isotope composition of Western Cape meteoric water. South African Journal of Science 93, 371–374.

Diamond, R.E., Harris, C., 2000. Oxygen and hydrogen isotope geochemistry of thermal springs of the Western Cape, South Africa: recharge at high altitude? Journal of African Earth Sciences 31, 467–481.

Dingle, R.V., Siesser, W.G., Newton, A.R., 1983. Mesozoic and Tertiary Geology of Southern Africa. A.A.Balkema.

Dody, A., Ziv, B., 2013. Factors affecting isotopic composition of the rainwater in the Negev Desert, Israel. Journal of Geophysical Research: Atmospheres 118, 8274–8284.

Dogramaci, S., Skrzypek, G., Dodson, W., Grierson, P.F., 2012. Stable isotope and hydrochemical evolution of groundwater in the semi-arid Hamersley Basin of subtropical northwest Australia. Journal of Hydrology 475, 281–293.

Domenico, P.A., Schwartz, F.W., 1998. Physical and Chemical Hydrogeology. John Wiley & Sons, Inc.

DTI, 2009. SA Risk and Vulnerability Atlas. URL: http://rava.qsens.net/themes/groundwater.

Emiliani, C., 1987. Dictionary of the Physical Sciences. Oxford University Press, Oxford.

Encyclopaedia Brittanica, 2013. Climate. URL: http://www.britannica.com/EBchecked/topic/121560/c

Epstein, S., Mayeda, T., 1953. Variation of 18O content of waters from natural sources. Geochimica et Cosmochimica Acta 4, 213–224.

February, E.C., Bond, W., Taylor, R., Newton, R., 2004. Will water abstraction from the Table Mountain aquifer threaten endemic species? A case study at Cape Point, Cape Town. South African Journal of Science 100, 253–255.

Friedman, I., 1953. Deuterium content of natural waters and other substances. Geochimica et Cosmochimica Acta 4, 89–103.

Frimmel, H.E., Fölling, P.G., Diamond, R.E., 2001. Metamorphism of the Permo-Triassic Cape Fold Belt and its basement, South Africa. Mineralogy and Petrology 73, 325–346.

Fritz, P., 1981. River Waters, in: Gat, J.R., Gonfiantini, R. (Eds.), Stable Isotope Hydrology. International Atomic Energy Agency, Vienna. number 210 in Technical Reports Series. chapter 8, pp. 177–202.

Fuller, A.O., Broquet, C.A., 1990. Aspects of the Peninsula Formation - Table Mountain Group, in: Geocongress ’90 - abstracts, Geological Society of South Africa. Geological Society of South Africa, Johannesburg. pp. 169–172.

Gabbott, S.E., Siveter, D.J., Aldridge, R.J., Theron, J.N., 2003. The earliest myodocopes: ostracodes from the late Ordovician Soom Shale Lagerstätte. Lethaia 36, 151–160.

Gat, J.R., 1981a. Groundwater, in: Gat, J.R., Gonfiantini, R. (Eds.), Stable Isotope Hydrology. International Atomic Energy Agency, Vienna. number 210 in Technical Reports Series. chapter 10, pp. 223–240.

Gat, J.R., 1981b. Historical Introduction, in: Gat, J.R., Gonfiantini, R. (Eds.), Stable Isotope Hydrology. International Atomic Energy Agency, Vienna. number 210 in Technical Reports Series. chapter 1, pp. 1–6.

Gat, J.R., 1996. Oxygen and hydrogen isotopes in the hydrological cycle. Annual Reviews in Earth and Planetary Sciences 24, 225–262.

Gaucher, C., Germs, G.J., 2006. Recent advances in South African Neoproterozoic-Early Palaeozoic biostratigraphy: correlation of the Cango Caves and Gamtoos Groups and acritarchs of the Sardinia Bay Formation, Saldania Belt. South African Journal of Geology 109, 193–214.

Geological Survey, 1973. 3218 Clanwilliam. 1:250 000 geological series. Department of Mines. Pretoria.

Geological Survey, 1979. 3322 Oudtshoorn. 1:250 000 geological series. Geological Survey. Pretoria.

Geological Survey, 1991. 3320 Ladismith. 1:250 000 geological series. Geological Survey. Pretoria.

Gonfiantini, R., 1981. The δ notation and the mass-spectrometric measurement techniques, in: Gat, J.R., Gonfiantini, R. (Eds.), Stable Isotope Hydrology. International Atomic Energy Agency, Vienna. number 210 in Technical Reports Series. chapter 4, pp. 35–84.

Gonfiantini, R., Roche, M.A., Olivry, J.C., Fontes, J.C., Zuppi, G.M., 2001. The altitude effect on the isotopic composition of tropical rains. Chemical Geology 181, 147–167.

Gresse, P.G., Theron, J.N., 1992. The Geology of the Worcester Area, explanation of sheet 3319. Technical Report. Geological Survey, Department of Mineral and Energy Affairs. Pretoria.

Gresse, P.G., von Veh, M.W., Frimmel, H.E., 2006. Namibian (Neoproterozoic) to Early Cambrian Successions, in: Johnson, M.R., Annhaeusser, C.R., Thomas, R.J. (Eds.), The Geology of South Africa. Geological Society of South Africa, Council for Geoscience, Pretoria. chapter 18, pp. 395–420.

Hälbich, I.W., 1992. The Cape Fold Belt Orogeny: State of the art 1970’s - 1980’s, in: de Wit, M.J., Ransome, I.G. (Eds.), Inversion Tectonics of the Cape Fold Belt, Karoo and Cretaceous Basins of Southern Africa. A.A.Balkema, Rotterdam, pp. 141–158.

Hammerbeck, E.C., Allcock, R.J., 1985. Geological Map of Southern Africa. Technical Report. Geological Society of South Africa. Pretoria.

Harris, C., Burgers, C., Miller, J., Rawoot, F., 2010. O- and H-isotope record of Cape Town rainfall from 1996 to 2008, and its application to recharge studies of Table Mountain groundwater, South Africa. South African Journal of Geology 113, 33–56.

Harris, C., Oom, B.M., Diamond, R.E., 1999. A preliminary investigation of the oxygen and hydrogen isotope hydrology of the greater Cape Town area and an assessment of the potential for using stable isotopes as tracers. Water SA 25, 15–24.

Hartnady, C.J., Hay, E.R., 2002a. Boschkloof groundwater discovery, in: Pietersen, K., Parsons, R. (Eds.), A Synthesis of the Hydrogeology of the Table Mountain Group - Formation of a Research Strategy. Water Research Commission, Pretoria. TT 158/01, pp. 168–177.

Hartnady, C.J., Hay, E.R., 2002b. Experimental deep drilling at Blikhuis, Olifants River Valley, Western Cape: Motivation, setting and current progress, in: Pietersen, K., Parsons, R. (Eds.), A Synthesis of the Hydrogeology of the Table Mountain Group - Formation of a Research Strategy. Water Research Commission, Pretoria. TT 158/01, pp. 192–197.

Hartnady, C.J., Hay, E.R., 2002c. Use of structural geology and remote sensing in hydrogeological exploration of the Olifants and Doring River catchments, in: Pietersen, K., Parsons, R. (Eds.), A Synthesis of the Hydrogeology of the Table Mountain Group - Formation of a Research Strategy. Water Research Commission, Pretoria. TT 158/01, pp. 19–30.

Hartnady, C.J., Newton, A.R., Theron, J.N., 1974. The stratigraphy and structure of the Malmesbury Group in the southwestern Cape. Bulletin of the Precambrian Research Unit, UCT 15, 195–213.

Harvey, F.E., Sibray, S.S., 2001. Delineating Groundwater recharge from leaking irrigation canals using water chemistry and isotopes. Groundwater 39, 408–421.

Hobday, D.K., Tankard, A.J., 1978. Transgressive-barrier and shallow-shelf interpretation of the lower Paleozoic Peninsula Formation, South Africa. Geological Society of America Bulletin 89, 1733–1744.

Horibe, Y., Kobayakawa, M., 1960. Deuterium abundance of natural waters. Geochimica et Cosmochimica Acta 20, 273.

Hughes, C.E., Crawford, J., 2012. A new precipitation weighted method for determining the meteoric water line for hydrological applications demonstrated using Australian and global GNIP data. Journal of Hydrology 464, 344–351.

Hunjak, T., Lutz, H.O., Roller-Lutz, Z., 2013. Stable isotope composition of the meteoric precipitation in Croatia. Isotopes in Environmental and Health Studies 49, 336–345.

Iacumin, P., Venturelli, G., Selmo, E., 2009. Isotopic features of rivers and groundwater of the Parma Province (Northern Italy) and their relationships with precipitation. Journal of Geochemical Exploration 102, 56–62.

IAEA, 2013. The Nubian Aquifer Project. URL: http://www-naweb.iaea.org/napc/ih/IHS projects nubian development.html.

Jasechko, S., Sharp, Z., Gibson, J., Birks, S., Yi, Y., Fawcett, P., 2013. Terrestrial water fluxes dominated by transpiration. Nature 496, 347–350.

Jaunat, J., Celle-Jeanton, H., Huneau, F., Dupuy, A., Le Coustumer, P., 2013. Characterisation of the input signal to aquifers in the French Basque Country: Emphasis on parameters influencing the chemical and isotopic composition of recharge waters. Journal of Hydrology 496, 57–70.

Johnson, M.R., van Vuuren, C.J., Visser, J.N., Cole, D.I., Wickens, H., Christie, A.D., Roberts, D.L., Brandl, G., 2006. Sedimentary rocks of the Karoo Supergroup, in: Johnson, M.R., Annhaeusser, C.R., Thomas, R.J. (Eds.), The Geology of South Africa. Geological Society of South Africa, Council for Geoscience, Pretoria. chapter 22, pp. 461–500.

Jolly, J.L., 2002. Sustainable use of Table Mountain Group aquifers and problems related to scheme failure, in: Pietersen, K., Parsons, R. (Eds.), A Synthesis of the Hydrogeology of the Table Mountain Group - Formation of a Research Strategy. Water Research Commission, Pretoria. TT 158/01, pp. 108–111.

Jolly, J.L., Kotze, J.C., 2002. The Klein Karoo Rural Water Supply Scheme, in: Pietersen, K., Parsons, R. (Eds.), A Synthesis of the Hydrogeology of the Table Mountain Group - Formation of a Research Strategy. Water Research Commission, Pretoria. TT 158/01, pp. 198–201.

Jones, M., 1992. Heat flow in South Africa. Handbook of the Geological Survey 14. Geological Survey. Pretoria.

Jordaan, L.J., Scheepers, R., Barton, E.S., 1995. The geochemistry and isotopic composition of the mafic and intermediate igneous components of the Cape Granite Suite, South Africa. Journal of African Earth Sciences 21, 59–70.

Kakiuchi, M., Matsuo, S., 1979. Direct measurements of D/D and 18O/16O fractionation factors between vapor and liquid water in the temperature range from 10 to 40C. Geochemical Journal 13, 307–311.

Kent, L.E., 1949. The thermal waters of the Union of South Africa and South West Africa. Transactions of the Geological Society of South Africa 52, 231–264.

Knox, A., 1911. The Climate of the Continent of Africa. Cambridge University Press, Cambridge.

Kotze, J.C., 2002. Towards a management tool for groundwater exploitation in the Table Mountain sandstone fractured aquifer. Technical Report 729/1/02. Water Research Commission. Pretoria.

Kotze, J.C., Verhagen, B.T., Butler, M.J., 2000. An aquifer model based on chemistry, isotopes and lineament mapping: Little Karoo, South Africa, in: Sililo, O. (Ed.), Groundwater: Past Achievements and Future Challenges. Balkema, Rotterdam, pp. 539–544.

Ladouche, B., Luc, A., Nathalie, D., 2009. Chemical and isotopic investigation of rainwater in southern France (1996-2002): Potential use as input signal for karst functioning investigation. Journal of Hydrology 367, 150–164.

Lawrence, J.R., White, J.W., 1991. The elusive climate signal if the isotopic composition of precipitation, in: Taylor, H.P., O'Neil, J.R., Kaplan, I.R. (Eds.), Stable Isotope Geochemistry: A Tribute to Samuel Epstein. The Geochemical Society, San Antonio. number 3 in Special Publication, pp. 169–185.

le Maitre, D.C., Colvin, C., Scott, D.F., 2002. Groundwater dependent ecosystems in the Fynbos Biome, and their vulnerability to groundwater abstraction, in: Pietersen, K., Parsons, R. (Eds.), A Synthesis of the Hydrogeology of the Table Mountain Group - Formation of a Research Strategy. Water Research Commission, Pretoria. TT 158/01, pp. 112–117.

Lin, L., Jia, H., Xu, Y., 2007. Fracture network characteristics of a deep borehole in the Table Mountain Group, South Africa. Hydrogeology Journal 15, 1419–1432.

Lis, G., Wassenaar, L.I., Hendry, M.J., 2008. High-Precision LASER spectroscopy D/H and 18O/16O measurements of microliter natural water samples. Analytical Chemistry 80, 287–293.

Liu, J., Fu, G., Song, X., Charles, S.P., Zhang, Y., Han, D., Wang, S., 2010. Stable isotopic compositions in Australian precipitation. Journal of Geophysical Research 115, 16.

Maclear, L.G., 2002. The hydrogeology of the Uitenhage Artesian Basin with reference to the Table Mountain Group aquifer, in: Pietersen, K., Parsons, R. (Eds.), A Synthesis of the Hydrogeology of the Table Mountain Group - Formation of a Research Strategy. Water Research Commission, Pretoria. TT 158/01, pp. 216 – 223.

Majumder, R.K., Halim, M.A., Saha, B.B., Ikawa, R., Nakamura, T., Kagabu, M., Shimada, J., 2011. Groundwater flow systems in Bengal Delta, Bangladesh revealed by environmental isotopes. Environmental Earth Science 64, 1343–1352.

Mazor, E., Verhagen, B.T., 1976. Hot springs of Rhodesia – their noble gases, isotopic and chemical composition. Journal of Hydrology 28, 29–43.

Mazor, E., Verhagen, B.T., 1983. Dissolved ions, stable and radioactive isotopes and noble gases in thermal waters of South Africa. Journal of Hydrology 63, 315–329.

Mazor, E., Verhagen, B.T., Negreanu, E., 1974. Hot springs of the igneous terrain of Swaziland – their noble gases, hydrogen, oxygen and carbon isotopes and dissolved ions, in: Isotope Techniques in Groundwater Hydrology. International Atomic Energy Agency, Vienna. volume 2, pp. 29–47.

Meyer, P.S., 2002. Springs in the Table Mountain Group, with special reference to fault controlled springs, in: Pietersen, K., Parsons, R. (Eds.), A Synthesis of the Hydrogeology of the Table Mountain Group - Formation of a Research Strategy. Water Research Commission, Pretoria. TT 158/01, pp. 224–229.

Midgley, J., Scott, D.F., 1994. The use of stable isotopes of water (D and ^{18}O) in hydrological studies in the Jonkershoek Valley. Water SA 20, 151–154.

Mulligan, B.M., Ryan, M.C., Cámbara, T.P., 2011. Delineating volcanic aquifer recharge areas using geochemical and isotopic tools. Hydrogeology Journal 19, 1335–1347.

NASA, 2013. Shuttle Radar Topography Mission. URL: http://www2.jpl.nasa.gov/srtm/.

Negrel, P., Pauwels, H., Dewandel, B., Gandolfi, J.M., Mascré, C., Ahmed, S., 2011. Understanding groundwater systems and their functioning through the study of stable isotopes in a hard-rock aquifer (Maheshwaram watershed, India). Journal of Hydrology 397, 55–70.

NGI, 2012. RSA National Geo-Spatial Information 1:50 000 shape files. URL: http://www.ngi.gov.za/.

Nkondo, M.N., van Zyl, F.C., Keuris, H., Schreiner, B., 2012. National Water Resource Strategy 2. Technical Report. Department of Water Affairs. Pretoria.

Parsons, R., 2002. Development of Groundwater Resources of the Arabella Country Estate, in: Pietersen, K., Parsons, R. (Eds.), A Synthesis of the Hydrogeology of the Table Mountain Group - Formation of a Research Strategy. Water Research Commission, Pretoria. TT 158/01, pp. 150–154.

Partridge, T.C., Botha, G.A., Haddon, I.G., 2006. Cenozoic Deposits of the Interior, in: Johnson, M.R., Annhaeusser, C.R., Thomas, R.J. (Eds.), The Geology of South Africa. Geological Society of South Africa, Council for Geoscience, Pretoria. chapter 29, pp. 585–604.

Partridge, T.C., Maud, R.R., 1987. Geomorphic evolution of southern Africa since the Mesozoic. South African Journal of Geology 90, 179–208.

Peng, T.R., Wang, C.H., Huang, C.C., Fei, L.Y., Chen, C.T., Hwong, J.L., 2010. Stable isotope characteristics of Taiwan's precipitation: A case study of western Pacific monsoon region. Earth & Planetary Science Letters 289, 357–366.

Pietersen, K., Parsons, R. (Eds.), 2002. A Synthesis of the Hydrogeology of the Table Mountain Group - Formation of a Research Strategy. TT 158/01, Water Research Commission, Pretoria.

Poehls, D.J., Smith, G.J., 2009. Encyclopedic Dictionary of Hydrogeology. Elsevier, Amsterdam.

Preston-Whyte, R.A., Tyson, P.D., 1988. The Atmosphere and Weather of Southern Africa. Oxford University Press, Cape Town.

Rangarajan, R., Ghosh, P., 2011. Tracing the source of bottled water using stable isotope techniques. Rapid Communications in Mass Spectrometry 25, 3323–3330.

Reeburgh, W.S., 1994. Global water reservoirs, fluxes and turnover times. URL: http://www.ess.uci.edu/ reeburgh/fig8.html.

Richey, D.G., McDonnell, J.J., Erbe, M.W., Hurd, T.M., 1998. Hydrograph separations based on chemical and isotopic concentrations: a critical appraisal of published studies from New Zealand, North America and Europe. Journal of Hydrology (NZ) 37, 95–111.

Roberts, D.L., Botha, G.A., Maud, R.R., Pether, J., 2006. Coastal Cenozoic Deposits, in: Johnson, M.R., Annhaeusser, C.R., Thomas, R.J. (Eds.), The Geology of South Africa. Geological Society of South Africa, Council for Geoscience, Pretoria. chapter 30, pp. 605–628.

Roets, W., Xu, Y., Raitt, L., El-Kahloun, M., Meire, P., Calitz, F., Batelaan, O., Anibas, C., Paridaens, K., Vandenbroucke, T., Verhoest, N., Brendonck, L., 2008. Determining discharges from the Table Mountain Group (TMG) aquifer to wetlands in the Southern Cape, South Africa. Hydrobiologia 607, 175–186.

Rosewarne, P., 2002a. Case Study: Ceres Municipality, in: Pietersen, K., Parsons, R. (Eds.), A Synthesis of the Hydrogeology of the Table Mountain Group - Formation of a Research Strategy. Water Research Commission, Pretoria. TT 158/01, pp. 160–163.

Rosewarne, P., 2002b. Hydrogeological Characteristics of the Table Mountain Group Aquifers, in: Pietersen, K., Parsons, R. (Eds.), A Synthesis of the Hydrogeology of the Table Mountain Group - Formation of a Research Strategy. Water Research Commission, Pretoria. TT 158/01, pp. 33–44.

Rozanski, K., Araguás-Araguás, L., Gonfiantini, R., 1993. Isotopic patterns in modern global precipitation, in: Swart, P.K., Lohmann, K.C., McKenzie, J., Savin, S. (Eds.), Climate Change in Continental Isotopic Records. American Geophysical Union. number 78 in Geophysical Monograph. chapter 1, pp. 1–36.

Rozanski, K., Sonntag, C., Munnich, K.O., 1982. Factors controlling stable isotope composition of European precipitation. Tellus 34, 142–150.

Rozendaal, A., Gresse, P.G., Scheepers, R., le Roux, J.P., 1999. Neoproterozoic to early Cambrian crustal evolution of the Pan-African Saldania Belt, South Africa. Precambrian Research 97, 303–323.

Rust, I.C., 1967. On the sedimentation of the Table Mountain Group in the Western Cape Province, D.Sc. thesis. Ph.D. thesis. Stellenbosch University.

Rust, I.C., 1973. The evolution of the Palaeozoic Cape basin, southern margin of Africa. Plenum, New York, New York. volume 1 of *The Ocean Basins and Margins*. chapter 6. pp. 247–276.

Rust, I.C., 1977. Evidence of shallow marine and tidal sedimentation in the Ordovician Graafwater Formation, Cape Province, South Africa. Sedimentary Geology 18, 123–133.

Saayman, I.C., Adams, S., Harris, C., 2000. Example of O- and H-isotope use to identify surface water pollution in groundwater, in: Sililo, O. (Ed.), Groundwater: Past Achievements and Future Challenges. A.A.Balkema, Rotterdam, pp. 599–603.

Saayman, I.C., Scott, D.F., Prinsloo, F.W., Moses, G., Weaver, J.M., Talma, S., 2003. Evaluation of the application of natural isotopes in the identification of the dominant streamflow generation mechanisms in TMG catchments. Technical Report 1234/1/03. Water Research Commission. Pretoria.

SACS, 1980. Stratigraphy of South Africa. volume Part 1: Lithostratigraphy of the Republic of South Africa, South West Africa/Namibia, and the Republics of Boputhatswana, Transkei and Venda. South African Committee for Stratigraphy, Geological Survey, Pretoria.

Salameh, E., 2004. Using environmental isotopes in the study of the recharge-discharge mechanisms of the Yarmouk catchment area in Jordan. Hydrogeology Journal 12, 451–463.

Salati, E., Dall'Olio, A., Matsui, E., Gat, J.R., 1979. Recycling of water in the Amazon Basin: an isotopic study. Water Resources Research 15, 1250–1258.

Sami, K., 1992. Recharge mechanisms and geochemical processes in a semi-arid sedimentary basin, Eastern Cape, South Africa. Journal of Hydrology 139, 27–48.

SAWB, 1996. The weather and climate of the extreme south-western Cape. South African Weather Bureau, Department of Environmental Affairs and Tourism. Pretoria.

SAWS, 2010-12. Daily Weather Bulletin, ISSN 0011-5517. Monthly. Pretoria.

Scheepers, R., Armstrong, R., 2002. New U-Pb SHRIMP zircon ages of the Cape Granite Suite: implications for the magmatic evolution of the Saldania Belt. South African Journal of Geology 105, 241–256.

Scheepers, R., Poujol, M., 2002. U-Pb zircon age of Cape Granite Suite ignimbrites: characteristics of the last phases of the Saldanian magmatism. South African Journal of Geology 105, 163–178.

Scheepers, R., Schoch, A.E., 2006. The Cape Granite Suite, in: Johnson, M.R., Annhaeusser, C.R., Thomas, R.J. (Eds.), The Geology of South Africa. Geological Society of South Africa, Council for Geoscience, Pretoria. chapter 19, pp. 421–432.

Schimmelman, A., DeNiro, M.J., 1993. Preparation of organic and water hydrogen for stable isotope analysis: Effects due to reaction vessels and zinc reagent. Analytical Chemistry 65, 789–792.

Schoch, A.E., Burger, A.J., 1976. U-Pb zircon age of the Saldanha Quartz Porphyry, Western Cape Province. Transactions of the Geological Society of South Africa 79, 239–241.

Schoch, A.E., Leterrier, J., de la Roche, H., 1977. Major element geochemical trends in the Cape Granites. Transactions of the Geological Society of South Africa 80, 197–209.

Schulze, R.E., Lynch, S.D., 2001. South African Atlas of Agrohydrology and Climatology. URL: http://planet.uwc.ac.za/NISL/Invasives/Assignments/GARP/atlas/atlas toc.htm.

Sharp, Z., 2007. Principles of Stable Isotope Geochemistry. Pearson Prentice Hall.

Shone, R.W., 2006. Onshore post-Karoo Mesozoic deposits, in: Johnson, M.R., Annhaeusser, C.R., Thomas, R.J. (Eds.), The Geology of South Africa. Geological Society of South Africa, Council for Geoscience, Pretoria. chapter 26, pp. 541–552.

Shone, R.W., Booth, P.W., 2005. The Cape basin, South Africa: A review. Journal of African Earth Sciences 43, 196–210.

Socki, R.A., Karlsson, H.R., Gibson, Jr., E.K., 1992. Extraction technique for the determination of oxygen-18 in water using preevacuated glass vials. Analytical Chemistry 64, 829–831.

Söhnge, A.P., 1983. The Cape Fold Belt - Perspective, in: Söhnge, A.P., Hälbich, I.W. (Eds.), Geodynamics of the Cape Fold Belt. Geological Society of South Africa, Johannesburg. number 12 in Special Publication. chapter 1, pp. 1–6.

Stats SA, 2006. Updated water accounts for South Africa: 2000. Technical Report. Statistics South Africa. Pretoria.

Sumner, G., 1988. Precipitation: Process and Analysis. John Wiley & Sons, Inc., Singapore.

Takai, K., Moser, D.P., DeFlaun, M., Onstott, T.C., Frederickson, J.K., 2001. Archaeal diversity in waters from deep South African gold mines. Applied and Environmental Microbiology 67, 5750–5760.

Talma, A.S., van Wyk, E., 2013. Rainfall and Groundwater Isotope Atlas, in: Abiye, T. (Ed.), The Use of Isotope Hydrology to Characterise and Assess Water Resources in Southern Africa. Water Research Commission, Pretoria. TT570/13. chapter 6, pp. 83–101.

Tankard, A.J., Hobday, D.K., 1977. Tide dominated back-barrier sedimentation, early Ordovician Cape Basin, Cape Peninsula, South Africa. Sedimentary Geology 18, 135–159.

Tankard, A.J., Jackson, M.P., Eriksson, K.A., Hobday, D.K., Hunter, D.R., Minter, W.E.L., 1982. Crustal Evolution of Southern Africa, 3.8 Billion Years of Earth History. Springer, New York.

Tanweer, A., Hut, G., Burgman, J.O., 1988. Optimal conditions for the reduction of water to hydrogen by zinc for mass spectrometric analysis of the deuterium content. Chemical Geology (Isotope Geoscience Section) 73, 199–203.

Thamm, A.G., Johnson, M.R., 2006. The Cape Supergroup, in: Johnson, M.R., Annhaeusser, C.R., Thomas, R.J. (Eds.), The Geology of South Africa. Geological Society of South Africa, Council for Geoscience, Pretoria. chapter 21, pp. 443–460.

Theron, J.N., Basson, W.A., 1989. Lithostratigraphy of the Rietvlei Formation (Table Mountain Group). Lithostratigraphic Series 7. Geological Survey. Pretoria.

Theron, J.N., Gresse, P.G., Siegfried, H.P., Rogers, J., 1992. The Geology of the Cape Town area, explanation of sheet 3318. Technical Report. Geological Survey, Department of Mineral and Energy Affairs. Pretoria.

Theron, J.N., Rickards, R.B., Aldridge, R.J., 1990. Bedding plane assemblages of *Promissum pulchrum*, a new giant ashgill conodont from the Table Mountain Group, South Africa. Palaeontology 33, 577–594.

Theron, J.N., Wickens, H., Gresse, P.G., 1991. The Geology of the Ladismith area, explanation of sheet 3320. Technical Report. Geological Survey, Department of Mineral and Energy Affairs.

Toerien, D.K., 1979. The Geology of the Oudtshoorn area, explanation of sheet 3222. Technical Report. Geological Survey, Department of Mines.

Toerien, D.K., Hill, R.S., 1989. The Geology of the Port Elizabeth Area, explanation of sheet 3324. Technical Report. Geological Survey, Department of Mineral and Energy Affairs. Pretoria.

Uemura, R., Yonezawa, N., Yoshimura, K., Asami, R., Kadena, H., Yamada, K., Yoshida, N., 2012. Factors controlling isotopic composition of precipitation on Okinawa Island, Japan: Implications for palaeoclimate reconstruction in the East Asian Monsoon region. Journal of Hydrology 475, 314–322.

Umvoto, SRK, 2000. Reconnaissance Investigation into the Development and Utilization of Table Mountain Group Artesian Groundwater using the E10 Catchment as a Pilot Study Area: CAGE project - interim report. Technical Report. Geohydrology and Project Planning Directorate, Department of Water Affairs & Forestry.

Urey, H.C., 1947. The thermodynamic properties of isotopic substances. Journal of the Chemical Society of London , 562–581.

Vegter, J.R., 1995. An explanation of a set of National Groundwater Maps. Technical Report TT 74/95. Water Research Commission, Department of Water Affairs & Forestry. Pretoria.

Vogel, J.C., van Urk, H., 1975. Isotopic composition of groundwater in semi-arid regions of southern Africa. Journal of Hydrology 25, 23–36.

Vos, R.G., Tankard, A.J., 1981. Braided fluvial sedimentation in the lower Palaeozoic Cape Basin, South Africa. Sedimentary Geology 29, 171–193.

Vreča, P., Bronić, I.K., Horvatiničić, N., Barešić, J., 2006. Isotopic characteristics of precipitation in Slovenia and Croatia: Comparison of continental and maritime stations. Journal of Hydrology 330, 457–469.

Walsch, R.P., Lawler, D.M., 1981. Rainfall seasonality: Description, spatial patterns and change through time. Weather 36, 201–208.

Weaver, J.M., Rosewarne, P., Hartnady, C.J., Hay, E.R., 2002. Potential of Table Mountain Group aquifers and integration into catchment water management, in: Pietersen, K., Parsons, R. (Eds.), A Synthesis of the Hydrogeology of the Table Mountain Group - Formation of a Research Strategy. Water Research Commission, Pretoria. TT 158/01, pp. 239–255.

Weaver, J.M., Talma, A.S., Cavé, C., 1999. Geochemistry and Isotopes for resource evaluation in the fractured rock aquifers of the Table Mountain Group. Technical Report 481/1/99. Water Research Commission. Pretoria.

West, A.G., February, E.C., Bowen, G.J., 2014. Spatial analysis of hydrogen and oxygen stable isotopes ("isoscapes") in ground water and tap water across South Africa. Journal of Geochemical Exploration 145, 213–222.

West, A.G., Goldsmith, G.R., Brooks, P.D., Dawson, T.E., 2010. Discrepancies between isotope ratio infrared spectroscopy and isotope ratio mass spectrometry for the stable isotope analysis of plant and soil waters. Rapid Communications in Mass Spectrometry 24, 1948–1954.

West, A.G., Goldsmith, G.R., Matimati, I., Dawson, T.E., 2011. Spectral analysis software improves confidence in plant and soil water stable isotope analyses performed by isotope ratio infrared spectroscopy (IRIS). Rapid Communications in Mass Spectrometry 25, 2268–2274.

White, M.E., 2000. Running Down. Kangaroo Press, Sydney.

Wikipedia, 2013a. Rain. URL: http://www.wikipedia.org/wiki/rain.

Wikipedia, 2013b. Ogallala aquifer. URL: http://www.wikipedia.org/wiki/Ogallala aquifer.

Woodford, A.C., 2002. Interpretation and applicability of pumping-tests in Table Mountain Group aquifers, in: Pietersen, K., Parsons, R. (Eds.), A Synthesis of the Hydrogeology of the Table Mountain Group - Formation of a Research Strategy. Water Research Commission, Pretoria. TT 158/01, pp. 71–84.

Yonge, C.J., Goldenberg, L., Krouse, H.R., 1989. An isotopic study of water bodies along a traverse of southwestern Canada. Journal of Hydrology 106, 245–255.

Young, G.M., Minter, W.E.L., Theron, J.N., 2004. Geochemistry and palaeogeography of upper Ordovician glaciogenic sedimentary rocks in the Table Mountain Group, South Africa. Palaeogeography, Palaeoclimatology, Palaeoecology 214, 323–345.

Yurtsever, Y., Gat, J.R., 1981. Atmospheric waters, in: Gat, J.R., Gonfiantini, R. (Eds.), Stable Isotope Hydrology. International Atomic Energy Agency, Vienna. number 20 in Technical Reports Series. chapter 6, pp. 103–142.

Stable Isotope Hydrology of the Table Mountain Group

Roger Diamond

Submitted for the degree of
Doctor of Philosophy
in Geology.

Department of Geological Sciences
University of Cape Town

2014

ABSTRACT

Rain was collected from 2010 to 2012 at 15 locations around the Cape Fold Belt, at the same time as samples from rivers, springs, seeps and boreholes, totalling 435 samples. Precipitation ranged from -75 ‰ to +40 ‰ for δD and -12 ‰ to +8 ‰ for $\delta^{18}O$, showing seasonal patterns, with lower δ values in winter and higher in summer. Certain anomalous δ values can be attributed to individual weather events, such as thunderstorms. Using weighted data, the meteoric water line is δD = 6.15 $\delta^{18}O$ + 8.21, which is similar to previous equations. The best fit line for groundwater δ values is δD = 7.09 $\delta^{18}O$ + 10.08, the steeper gradient and higher intercept reflecting the predominance of heavy rainfall events with lower δ values in recharge, known as selection. The range of -47 ‰ to 0 ‰ for δD and -8 ‰ to -1 ‰ for $\delta^{18}O$ values for all groundwater data is about half that of the rain values, due to the averaging effect from mixing during groundwater flow. Rainfall isotope composition is negatively correlated with continentality, as defined by the product of distance to the Atlantic and the closest coast. Isotope composition of rainfall is also strongly negatively correlated with altitude, with gradients from -0.48 to -2.2 $\frac{\Delta\delta D}{100m}$ and -0.075 to -0.34 $\frac{\Delta\delta^{18}O}{100m}$. Sites that are elevated within the landscape have a reduced altitude effect, such as tall peaks, whereas mountain valleys display enhanced altitude effects. Temporal and spatial variations in the strength of the amount effect reveal meteorological variability and emphasise the need for long term monitoring.

Groundwater-fed surface waters show little systematic variation in isotope composition within catchments, indicating groundwater mixing. Differences between catchments are significant and reveal continental and altitude effects across the Cape Fold Belt. There is no significant change in hot spring isotope compositions over 40 years, confirming deep, well mixed groundwater flow. In the greater Cederberg region, groundwater abstracted from the Peninsula Formation in the Olifants River Mountains appears to be locally recharged and not in the Cederberg mountains. Abstraction in the Rietvlei Formation north and south of the Hex River anticline is being recharged at higher altitude, around 1200-1600masl, probably in the Goudini or Skurweberg Formation and moves up the stratigraphy prior to discharge. Discharge of increasingly negative δ values, a sign of deeper groundwater from higher recharge areas, could warn against overabstraction. Similar relations occur at Gamkaberg (Little Karoo) and Rooihoogte (Great Karoo), where groundwater, having been recharged at higher altitude, moves up the stratigraphy in the Skurweberg aquifer. At Gamkaberg, selective recharge of isotopically more negative large rainfall amount events, or interannual shifts in isotope composition of rainfall may account for the more negative δ values of groundwater than rain and warns against overinterpretation of short term precipitation monitoring. The δD and $\delta^{18}O$ values of springs around Table Mountain correlate positively with distance from the mountain, an amount effect. The altitude effect gradient revealed that the typical spring is recharged an average of 1km upslope of the spring at an average elevation of 330masl, into the scree aquifer. Shifts in annual mean δ values of precipitation are mimicked in the springs, proving that a component of groundwater flow is fast and shallow, whilst a deeper component must also exist to account for the steady discharge of perennial springs. An average hydraulic conductivity of 15–20m/day was calculated for the scree aquifer.

Stable Isotope Hydrology of the Table Mountain Group

Roger Diamond

Submitted for the degree of
Doctor of Philosophy
in Geology.

Department of Geological Sciences
University of Cape Town

2014

Towerkop, 2189m, Skurweberg Formation of the Table Mountain Group, viewed from the north, showing the fractured nature of this quartzite aquifer. The Towerkop water point is just out of view, around the corner to the east, at about the level of the horizon.

"It ain't the water that's not right around here."

from Black Eyed Man, 1992

Cowboy Junkies.

ABSTRACT

Rain was collected from 2010 to 2012 at 15 locations around the Cape Fold Belt, at the same time as samples from rivers, springs, seeps and boreholes, totalling 435 samples. Precipitation ranged from -75 ‰ to +40 ‰ for δD and -12 ‰ to +8 ‰ for $\delta^{18}O$, showing seasonal patterns, with lower δ values in winter and higher in summer. Certain anomalous δ values can be attributed to individual weather events, such as thunderstorms. Using weighted data, the meteoric water line is δD = 6.15 $\delta^{18}O$ + 8.21, which is similar to previous equations. The best fit line for groundwater δ values is δD = 7.09 $\delta^{18}O$ + 10.08, the steeper gradient and higher intercept reflecting the predominance of heavy rainfall events with lower δ values in recharge, known as selection. The range of -47 ‰ to 0 ‰ for δD and -8 ‰ to -1 ‰ for $\delta^{18}O$ values for all groundwater data is about half that of the rain values, due to the averaging effect from mixing during groundwater flow. Rainfall isotope composition is negatively correlated with continentality, as defined by the product of distance to the Atlantic and the closest coast. Isotope composition of rainfall is also strongly negatively correlated with altitude, with gradients from -0.48 to -2.2 $\frac{\Delta\delta D}{100m}$ and -0.075 to -0.34 $\frac{\Delta\delta^{18}O}{100m}$. Sites that are elevated within the landscape have a reduced altitude effect, such as tall peaks, whereas mountain valleys display enhanced altitude effects. Temporal and spatial variations in the strength of the amount effect reveal meteorological variability and emphasise the need for long term monitoring.

Groundwater-fed surface waters show little systematic variation in isotope composition within catchments, indicating groundwater mixing. Differences between catchments are significant and reveal continental and altitude effects across the Cape Fold Belt. There is no significant change in hot spring isotope compositions over 40 years, confirming deep, well mixed groundwater flow. In the greater Cederberg region, groundwater abstracted from the Peninsula Formation in the Olifants River Mountains appears to be locally recharged and not in the Cederberg mountains. Abstraction in the Rietvlei Formation north and south of the Hex River anticline is being recharged at higher altitude, around 1200-1600masl, probably in the Goudini or Skurweberg Formation and moves up the stratigraphy prior to discharge. Discharge of increasingly negative δ values, a sign of deeper groundwater from higher recharge areas, could warn against overabstraction. Similar relations occur at Gamkaberg (Little Karoo) and Rooihoogte (Great Karoo), where groundwater, having been recharged at higher altitude, moves up the stratigraphy in the Skurweberg aquifer. At Gamkaberg, selective recharge of isotopically more negative large rainfall amount events, or interannual shifts in isotope composition of rainfall may account for the more negative δ values of groundwater than rain and warns against overinterpretation of short term precipitation monitoring. The δD and $\delta^{18}O$ values of springs around Table Mountain correlate positively with distance from the mountain, an amount effect. The altitude effect gradient revealed that the typical spring is recharged an average of 1km upslope of the spring at an average elevation of 330masl, into the scree aquifer. Shifts in annual mean δ values of precipitation are mimicked in the springs, proving that a component of groundwater flow is fast and shallow, whilst a deeper component must also exist to account for the steady discharge of perennial springs. An average hydraulic conductivity of 15–20m/day was calculated for the scree aquifer.

Contents

Abstract **1**

Contents **2**

List of Figures **5**

List of Tables **8**

1 Introduction **9**

1.1 Water in South Africa 9

1.1.1 Water in the Western Cape 9

1.2 Introduction to Stable Isotope Hydrology 13

1.2.1 Isotope Geochemistry 13

1.2.2 Isotope Fractionation 14

1.2.3 Kinetic Fractionation 14

1.2.4 Equilibrium Fractionation 14

1.2.5 Fractionation Factors 15

1.2.6 Measurement and Standards 16

1.2.7 Stable Isotope Hydrology 17

1.3 Stable Isotope Hydrology in South Africa 22

1.3.1 Motivation Behind this Study 25

2 Background **27**

2.1 Introduction 27

2.2 Geology — Lithostratigraphy 27

2.2.1 Saldania Belt 27

2.2.2 Cape Granite Suite 30

2.2.3 Cape Supergroup 30

2.2.4 Karoo Supergroup 38

2.2.5 Younger Rocks 38

2.3 Geology — Structure 41

2.4 Climate and Weather 43

2.4.1 Rain . . . 43
2.4.2 Temperature . . . 52
2.5 Hydrogeology . . . 52
2.5.1 Porosity and Permeability . . . 52
2.5.2 Hydraulic Parameters . . . 55
2.5.3 Hydrostratigraphy . . . 57
2.5.4 Significance of the Table Mountain Group . . . 60

3 Methods **63**
3.1 Introduction . . . 63
3.2 Sample Collection . . . 63
3.2.1 Rain . . . 63
3.2.2 Surface Water . . . 66
3.2.3 Groundwater . . . 66
3.3 Sample Preparation . . . 66
3.3.1 Mass Spectrometry . . . 66
3.3.2 Laser Cavity Ringdown Spectroscopy . . . 69
3.4 Sample Analysis and Data Correction . . . 69
3.4.1 Mass Spectrometry . . . 69
3.4.2 Laser Cavity Ringdown Spectroscopy . . . 70
3.4.3 Standards . . . 72
3.5 Data Analysis . . . 75
3.6 Maps . . . 76

4 Results **94**
4.1 Introduction . . . 94
4.2 Rain . . . 94
4.2.1 Rainfall Amount . . . 97
4.2.2 Rainfall Seasonality . . . 98
4.3 Rain Isotopes . . . 98
4.3.1 Temporal Variations . . . 100
4.3.2 Means and Weighting . . . 104
4.3.3 Deuterium Excess . . . 108
4.3.4 Local Meteoric Water Lines . . . 108
4.4 Groundwater . . . 113
4.5 Surface Water . . . 114
4.6 Other Samples . . . 116
4.6.1 Snow . . . 116
4.7 Summary . . . 117

5 Discussion **129**
5.1 Introduction . . . 129
5.2 Precipitation . . . 129
5.2.1 Source Area and Pathway Effects . . . 129
5.2.2 Isotope Effects . . . 132
5.3 Surface Water . . . 146
5.3.1 Altitude . . . 146
5.3.2 Springs, Seeps and Tributaries . . . 146
5.3.3 Baseflow . . . 148
5.4 Groundwater . . . 151
5.4.1 Altitude . . . 151
5.4.2 Hot Springs . . . 153
5.5 Regional Analyses . . . 154
5.5.1 Cederberg . . . 155
5.5.2 Hex River Mountains . . . 159
5.5.3 Langeberg – Gamkaberg – Swartberg . . . 166
5.5.4 Swartberg to Goukamma . . . 168
5.5.5 Cape Town . . . 173

6 Conclusions and Recommendations **181**

7 Abbreviations, Acronyms and Units **188**

8 Acknowledgements **191**

References **193**

List of Figures

1.1 Mean annual precipitation for the Western Cape . . . 11
1.2 Geological map of the study area . . . 12
1.3 The global water cycle . . . 17
1.4 The global meteoric water line . . . 18
1.5 Local meteoric water lines . . . 20
1.6 Source region humidity measured through d-excess . . . 23

2.1 Revised stratigraphy of the western Saldania Belt . . . 29
2.2 Stratigraphy of the Table Mountain Group . . . 32
2.3 Photograph of Peninsula Formation pebbly quartzite . . . 34
2.4 Photograph of the Hex River anticline . . . 41
2.5 Mean annual precipitation map for South Africa . . . 42
2.6 Rainfall and temperatures for stations in the Western Cape . . . 45
2.7 Rainfall and temperatures for stations in the Western Cape . . . 46
2.8 Synoptic chart: westerly wave . . . 47
2.9 Synoptic chart: southerly meridional flow . . . 48
2.10 Synoptic chart: ridging anticyclone . . . 49
2.11 Synoptic chart: cut-off low . . . 50
2.12 Synoptic chart: west coast trough . . . 51
2.13 Photograph of seeps in the Skurweberg Formation . . . 53
2.14 Piekenierskloof Formation fracture measurements . . . 54
2.15 Theoretical models of fracture porosity . . . 54
2.16 Fracture trace map for the Cederberg region . . . 55
2.17 Detailed fracture trace map for the Peninsula Formation . . . 57
2.18 Hydrostratigraphy of the Cape Supergroup . . . 62

3.1 Map of the study area . . . 65
3.2 Cumulative rainfall collector . . . 67
3.3 Hydrogen isotope sample preparation apparatus . . . 67
3.4 Oxygen isotope sample preparation apparatus . . . 68
3.5 Isotope correction procedure . . . 71

3.6 Map legend . . . 77
3.7 Cape Town map . . . 78
3.8 Twaktuin map . . . 79
3.9 Cederberg map . . . 80
3.10 Wolfkop map . . . 81
3.11 Matroosberg map . . . 82
3.12 Waaihoek and Witels map . . . 83
3.13 Drakenstein map . . . 84
3.14 Meulkloof map . . . 85
3.15 Riverndale map . . . 86
3.16 Klein Swartberg map . . . 87
3.17 Gamkaberg map . . . 88
3.18 Robinson Pass map . . . 89
3.19 Kammanassie map . . . 90
3.20 Blesberg map . . . 91
3.21 Lentelus map . . . 92
3.22 Goukamma map . . . 93

4.1 South African monthly rainfall maps . . . 99
4.2 Sample altitude histogram . . . 101
4.3 Rainfall: δD vs. time . . . 102
4.4 Rainfall: $\delta^{18}O$ vs. time . . . 103
4.5 Photograph of convective rainfall over the Cederberg . . . 105
4.6 Rainfall δD vs. $\delta^{18}O$: arithmetic means and weighted means . . . 106
4.7 Rainfall: difference between arithmetic and weighted mean δ values vs. MAP . . . 107
4.8 Rainfall: d-excess vs. MAP and continentality . . . 109
4.9 All rain water and groundwater δ values . . . 110
4.10 Local meteoric water lines . . . 111
4.11 Local meteoric water line map . . . 112
4.12 Photograph of Seweweekspoort Peak Cave seep . . . 114
4.13 Surface water: δD vs. $\delta^{18}O$ . . . 115
4.14 Monthly rainfall graphs . . . 118

5.1 Isotope data from various studies in South Africa . . . 131
5.2 Rainfall: the continental effect . . . 135
5.3 Map of the study area, showing sample locations and cross section lines . . . 139
5.4 Rainfall and groundwater: altitude effects . . . 141
5.5 Topography around sample sites . . . 144
5.6 Rainfall: annual amount effects . . . 145

5.7 Rainfall: monthly amount effects . . . 147
5.8 Surface water: δ vs. altitude . . . 149
5.9 Groundwater: δ vs. altitude . . . 151
5.10 Hot springs: δD vs. $\delta^{18}O$ . . . 154
5.11 Cederberg cross section . . . 156
5.12 Cederberg δD vs. $\delta^{18}O$ . . . 157
5.13 Schematic hydrogeology of the Olifants River Mountains . . . 158
5.14 Photograph of duplexes in the Peninsula Formation . . . 159
5.15 Hex River Mountains δD vs. $\delta^{18}O$ . . . 161
5.16 Possible south-easter snow air trajectories. . . . 162
5.17 Hex River Mountains cross section . . . 165
5.18 Langeberg–Gamkaberg δD vs. $\delta^{18}O$ . . . 167
5.19 Swartberg to Goukamma δD vs. $\delta^{18}O$ . . . 169
5.20 Little Karoo cross section . . . 171
5.21 Cape Town δD vs. $\delta^{18}O$ . . . 172
5.22 Cape Town springs δD vs. $\delta^{18}O$ . . . 174
5.23 Cape Town springs interannual shifts in δ values . . . 176
5.24 Rainfall interannual shifts in δ values . . . 177
5.25 Conceptual model for Cape Town springs . . . 179
5.26 Calculation of recharge altitude for Cape Town springs . . . 180

List of Tables

1.1 Isotopologues of water 13
1.2 Publications on stable isotopes in the Table Mountain Group 26

2.1 Hydraulic parameters for the Table Mountain Group 56
2.2 Spring and wellfield yields from the Table Mountain Group 61

3.1 Rainfall collection stations 64
3.2 UCT internal isotope standards 69
3.3 Raw data for internal standards: δD 73
3.4 Raw data for internal standards: $\delta^{18}O$ 74

4.1 Rainfall collection periods at each station 95
4.2 Rainfall collection stations 96
4.3 Rainfall: arithmetic and weighted means 107
4.4 Snow: isotope composition 117
4.5 Isotope data for rain for 2010 123
4.6 Isotope data for rain for 2011 124
4.7 Isotope data for rain for 2012 125
4.8 Isotope data for the Table Mountain springs 126
4.9 Isotope data for surface water 127
4.10 Isotope data for groundwater 128

5.1 Cape meteoric water line equations 132
5.2 Global examples of the continental effect 133
5.3 Distances from rainfall stations to the sea 134
5.4 Global examples of the altitude effect 136
5.5 Rainfall and groundwater: altitude effect gradients 137
5.6 Topographic position of sample sites 142
5.7 Description of the five rivers sampled 149

7.1 Acronyms, Units and Abbreviations 190

Chapter 1

Introduction

1.1 Water in South Africa

South Africa is a dry country. With an average annual rainfall of 450 mm/a (Dent et al., 1987; Schulze and Lynch, 2001), South Africa is clearly drier than most of the world, which averages around 1000 mm/a (Wikipedia, 2013a; Encyclopaedia Brittanica, 2013). The warm, dry climate compounds the problem of low rainfall and it is estimated that less than 10 % of rainfall becomes runoff, the rest being lost to evaporation or used by plants for transpiration (Nkondo et al., 2012). This runoff is estimated to be 50 000 GL/a, which equates to the total possible surface water yield of South Africa, although *at least* 25% of this should be set aside for ecological flows. In comparison, the estimated sustainable groundwater yield is 7500 GL/a. Actual consumption of water is around 15 000 GL/a for the country, with groundwater making up 13 %, at around 2000 GL/a (DTI, 2009; Nkondo et al., 2012; Stats SA, 2006). This shows the generally minor status of groundwater in South Africa, in contrast to aquifers such as the Ogallala in the United States midwest region where 26 000 Gl/a are abstracted (Wikipedia, 2013b) in an area of moderate rainfall, or the Nubian Sandstone Aquifer, in the eastern Sahara Desert, where Libya alone is planning to abstract over 2000 GL/a (IAEA, 2013). These are however, unsustainable abstraction rates, being higher than the recharge rates in these moderate to very low rainfall areas, and therefore qualify as groundwater mining, a practice with dire environmental, social and economic consequences.

1.1.1 Water in the Western Cape

The Western Cape has the greatest extremes of rainfall of any province in South Africa, with a maximum measured average annual rainfall of 3345 mm/a at Jonkershoek, 50 km east of Cape Town, and a minimum of 60 mm/a in the Tankwa Karoo (Schulze and Lynch, 2001). The actual maximum and minimum are likely to be higher and lower, respectively, as the rain gauges have probably not been sited in the ultimate locations that experience the extremes. Despite such a high maximum, the province receives an average of only 348 mm/a. The mean annual precipitation (MAP) map of the country, as developed by Dent et al. (1987), was refined for the Western

Cape by Beuster et al. (2009) and is shown in **Figure 1.1**. To produce this rainfall map, they used the MAP of 321 rainfall stations to select four out of six factors, based on regression analysis, as determinants of rainfall at any point: altitude, continentality, terrain roughness and distance from selected "barrier" mountain chains. From this map it can be seen that much of the Western Cape receives little rain, in the region of 200–300 mm/a, but the mountainous areas receive over 1000 mm/a. These mountains are largely made up of the rocks of the Table Mountain Group (TMG), the outcrop area of which can be seen in **Figure 1.2** and it can be concluded that most of the rainfall in the Western Cape occurs on the TMG outcrop area. Of the rain that falls, some evaporates from plants (interception) and soil, some is transpired by plants, some becomes runoff and the remainder is recharged to the TMG, a fractured rock aquifer. Due to the rugged terrain and stormy weather in the Cape Mountains, minimal research has been done on hydrological processes and our understanding of recharge, discharge and groundwater flow is poorly constrained. For example, at the biennial groundwater conference held by the Groundwater Division of the Geological Society of South Africa in 2013 in Durban, only 5 of the 70 papers presented dealt with the Table Mountain Group, and only 1 of those was from work done in a mountain area. The best studies are in the extensive compilation on the Table Mountain Group edited by Pietersen and Parsons (2002). **Table 1.2**, at the end of this chapter, contains a list of all publications that make use of stable isotopes of hydrogen and oxygen and relate to the Table Mountain Group.

The most direct way to understand groundwater flow in an aquifer is by using hydraulics, which requires water level or pressure measurements taken from boreholes penetrating the aquifer. This is not easily done, not only because of the practical difficulty and cost of siting boreholes in the Cape Mountains, but also because the fractured rock nature of the TMG porosity complicates water level interpretations. Water chemistry in the TMG aquifer is remarkably consistent across the Cape Fold Belt and in addition to the consistency, the water is very low in dissolved constituents, being generally well under 100 mg/L total dissolved solids (Rosewarne, 2002b). Although it may be possible to use dissolved chemical species as tracers of groundwater flow in the TMG aquifers (Saayman et al., 2003; Richey et al., 1998), the very low concentrations make this challenging. Stable isotopes of oxygen and hydrogen offer a solution to these problems in that they are cheaper than constructing boreholes and making hydraulic measurements. Stable isotopes are known to vary on a regional scale (hundreds of kilometres) (Rozanski et al., 1993) and with altitude (Gonfiantini et al., 2001) and the Cape Fold Belt has sufficient area and altitude change to expect isotopic variation.

Variations in hydrogen and oxygen stable isotopes are used frequently in hydrological applications, such as identifying sources of groundwater recharge (Ladouche et al., 2009), changes in vapour source or oceanic surface water and in resultant precipitation (Breitenbach et al., 2010), leaking water pipes or canals (Harvey and Sibray, 2001) and sources of bottled water (Rangarajan and Ghosh, 2011).

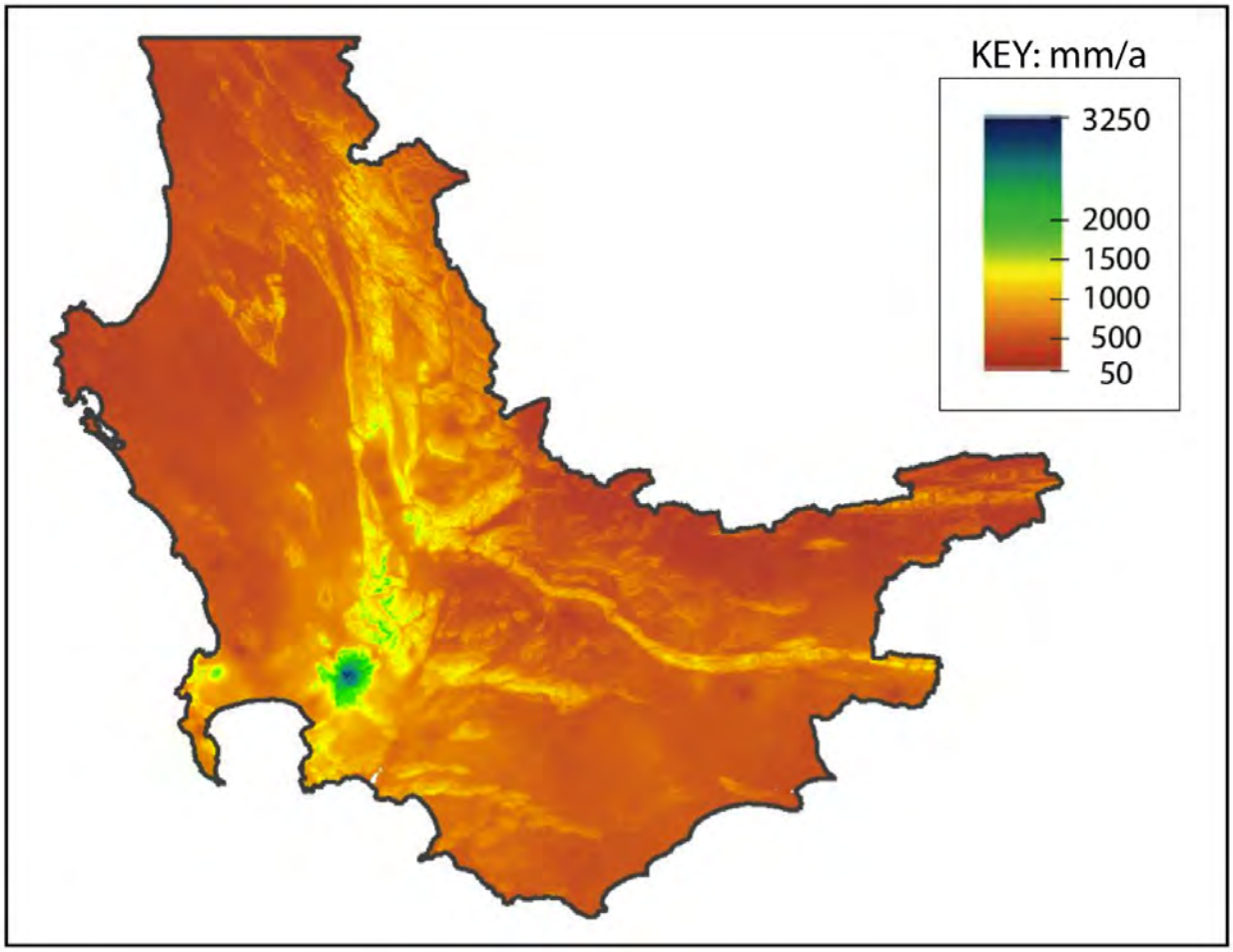

Figure 1.1: Mean annual precipitation for the western portion of the Western Cape, as calculated by Beuster et al. (2009). Precipitation amount was calculated using four factors – altitude, continentality, terrain roughness and distance from "barrier" mountains – and quantified from long term (>20 a) rainfall records from 321 stations.

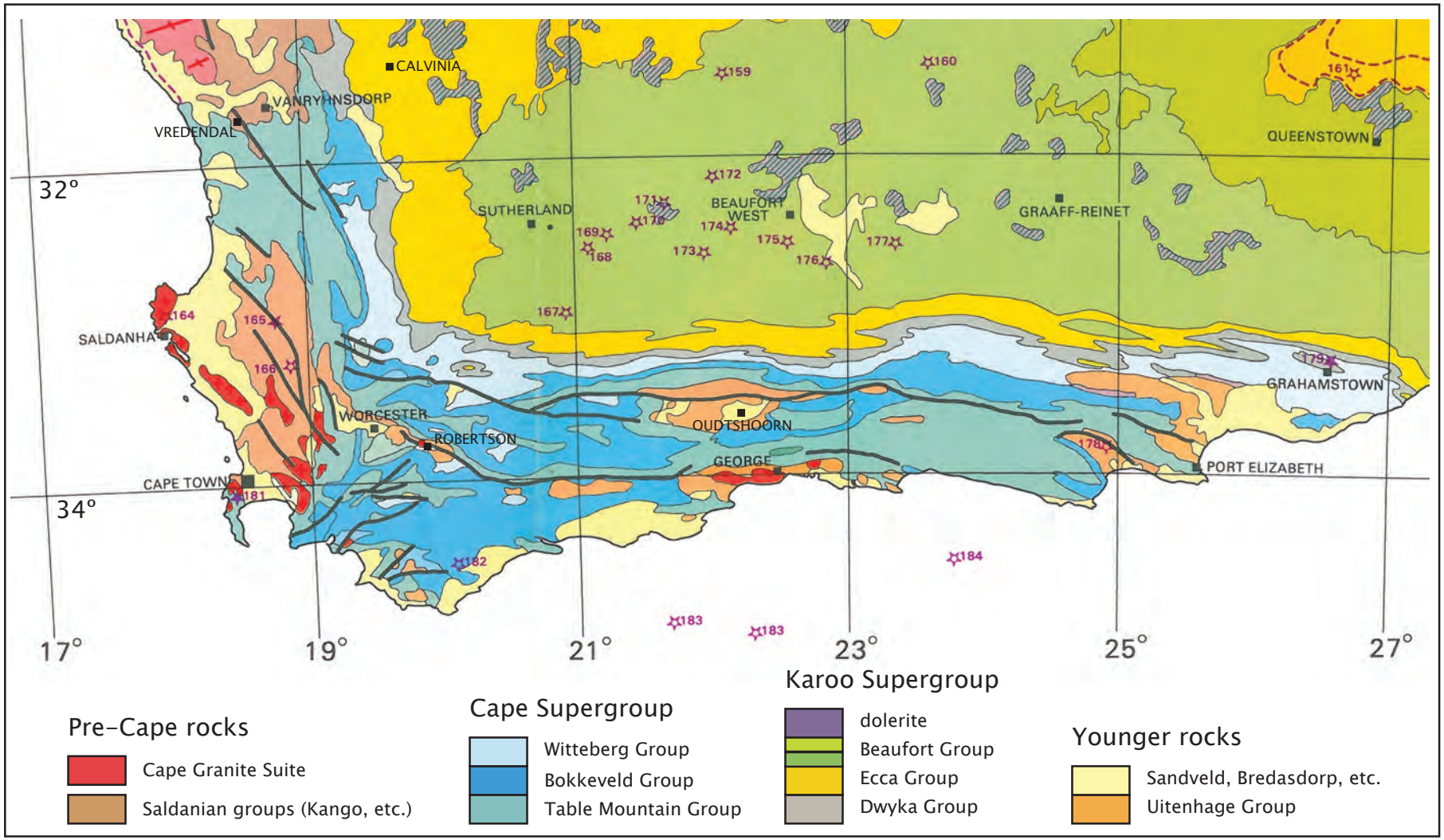

Figure 1.2: Geological map of the study area, showing the outcrop of the Table Mountain Group, where the focus of sample collection occurred. Map from Hammerbeck and Allcock (1985).

1.2 Introduction to Stable Isotope Hydrology

1.2.1 Isotope Geochemistry

The stable isotopes of oxygen were discovered in the 1920s by Blackett, and Giauque and Johnston. In 1931, deuterium was discovered by Harold Urey, who would turn out to be a major force in the understanding of the variations in stable isotope compositions (Gat, 1981b). By the 1940s, pioneering scientists were making the first attempts to apply stable isotope measurements to earth science questions, but it was only after improvements by Alfred Nier to the mass spectrometer in the late 1940s that the precision enabled the true birth of stable isotope geochemistry with early papers by Sam Epstein, Irving Friedman and Stan McCrea (Sharp, 2007). Applications to hydrology were immediately apparent and so widespread measurement of stable isotope ratios of hydrogen and oxygen commenced around the world in the 1950s, driven substantially by the World Meteorological Association and the International Atomic Energy Agency.

Isotope geochemistry can be broken into several sub-disciplines, the major break being that between radioactive or radiogenic isotopes and stable isotopes. The stable isotopes are futher broken down into light and heavy, with hydrogen, carbon, nitrogen and oxygen being the most commonly used stable light isotopes. However, the stable light isotopes and certain radioactive isotopes, such as tritium and ^{14}C, are also grouped into a branch known as the environmental isotopes, referring to their application to earth surface processes, typically in and around the biosphere, hydrosphere and atmosphere.

Hydrogen occurs as protium, ^{1}H (sometimes simply referred to as hydrogen), deuterium, ^{2}H, also written as D, and the radioactive tritium, ^{3}H, or T, with a half life of 12.33 a (Emiliani, 1987). Oxygen occurs as ^{16}O, ^{17}O and ^{18}O, all of which are stable. As a result of this spread of isotopes, water can occur as nine different isotopologues, chemically identical but isotopically different molecules, as shown in **Table 1.1**.

isotopologue	mass	abundance (%)
$^{1}H^{1}H^{16}O$	18	99.732
$^{1}H^{1}H^{18}O$	20	0.200
$^{1}H^{1}H^{17}O$	19	0.038
$^{1}H^{2}H^{16}O$	19	0.015
$^{1}H^{2}H^{18}O$	21	0.00003
$^{1}H^{2}H^{17}O$	20	0.0000057
$^{2}H^{2}H^{16}O$	20	0.0000022
$^{2}H^{2}H^{18}O$	22	0.0000000045
$^{2}H^{2}H^{17}O$	21	0.00000000086

Table 1.1: Isotopologues (isotopically different, chemically identical molecules) of water with the average abundances on earth (Emiliani, 1987).

1.2.2 Isotope Fractionation

The ratios of one isotope to another, such as $\frac{^{18}O}{^{16}O}$, vary slightly between different materials or even different reservoirs of the same substance. These differences in isotope ratios come about through preferential diffusion of the lighter or heavier isotope (or isotopologues, if in a compound) or through preferential location of the lighter or heavier isotope due to different bond energies related to mass, and are known as fractionation.

Processes that can cause isotope fractionation are chemical reactions, physical reactions or changes of state, diffusion and exchange. A chemical reaction is when two or more elements or compounds react to form different compounds; a physical reaction is where an element or compound undergoes a change of state; diffusion is when atoms or molecules disperse from high to low concentration through other material; exchange is when atoms of the same element swap places from one compound to another without causing any chemical changes. In all of these processes, molecules or atoms bearing different isotopes will proceed through these reactions at different speeds and this is known as kinetic fractionation.

1.2.3 Kinetic Fractionation

For physical, chemical and exchange reactions, the dissociation energy of molecular bonds control the reaction rate. A bond involving lighter isotopes has a lesser dissociation energy and can break more easily than the same bond involving a heavier isotope. For example, when a body of liquid water evaporates into air, the resultant water vapour (H_2O gas mixed in air) will be relatively enriched in the lighter isotopes and therefore have lower values for the ratios $\frac{D}{H}$ and $\frac{^{18}O}{^{16}O}$ than the source body. This kinetic effect will be exaggerated if the vapour is being removed rapidly, as happens in windy situations or low humidities with evaporation from natural water bodies. On the other hand, a lack of mixing in the source water body will result in a lesser fractionation effect, because the surface water layer will become depleted in ^{16}O with time.

For diffusion, the diffusive velocity is inversely proportional to the mass of the molecule and therefore molecules with lighter isotopes will diffuse faster. For kinetic fractionation there is no fixed difference in isotope ratios between the source and receptor reservoirs, as this is dependent upon factors such as time, degree of removal of one reservoir and degree of mixing of the reservoirs, as well as the actual reaction or change of state taking place.

1.2.4 Equilibrium Fractionation

If chemical, physical or exchange reactions are allowed to run to completion, then there will be a fixed isotope difference between the source and receptor reservoirs, given a certain temperature. Reactions will continue, but backwards and forwards at an equal rate, and without any net effect on isotopic composition of either reservoir. For example, at 25 °C, there is a fixed difference between the $\frac{^{18}O}{^{16}O}$ ratio in $H_2O_{(l)}$ and $CO_{2(g)}$ in equilibrium with each other. In this situation, the

kinetic effects of reaction rate are no longer important, and it is the relative preference for a heavier or lighter isotope within a chemical bond that determines which isotopes locate where. Heavier isotopes are favoured in bond positions with higher strength. To continue the above example, the covalent bonds between oxygen and carbon in CO_2 are stronger than the covalent bonds between oxygen and hydrogen in H_2O, and as the heavier isotopes remain preferentially in the stronger bond positions, the result is that $CO_{2(g)}$ will have higher values for $\frac{^{18}O}{^{16}O}$ than the $H_2O_{(l)}$.

Temperature plays a very important role in fractionation. The higher the temperature, the less the degree of fractionation, because fractionation processes are thermodynamically controlled.

1.2.5 Fractionation Factors

In order to quantify the fractionation of isotopes between two phases or compounds, the fractionation factor, α, is used, where:

$$\alpha = \frac{R_{reactant}}{R_{product}} \ ,$$

and R is the isotope ratio, such as $\frac{D}{H}$. For example:

$$\alpha D_{water-vapour} = \frac{\left(\frac{D}{H}\right)_{water}}{\left(\frac{D}{H}\right)_{vapour}} \ .$$

This factor describes the partitioning of an isotope between two phases or compounds, which is determined by the chemical bonds and other atomic scale properties of the element. Importantly, the fractionation factor is temperature dependant; in other words, at equilibrium, the isotope ratios in the reactant and product vary with temperature, as was first outlined by Urey (1947). Furthermore, this variation is systematic, in that lower temperatures result in higher fractionation factors and vica versa.

Fractionation factors are mostly numbers just above 1, and if one takes 1000 ln α, the result is approximately the difference in δ values of the reactant and product, because 1000 ln (1.00x) is approximately equal to x, and so:

$$\Delta_{X-Y} = \delta_X - \delta_Y \approx 1000 \ln \alpha_{X-Y} \ .$$

For example:

$\alpha_{(H_2O_{(l)}-H_2O_{(g)},25^\circ C)} = 1.0094$ (Kakiuchi and Matsuo (1979) in Beaudoin and Therrien (2014)),

and $1000 \ln 1.0094 = 9.4$,

so $\Delta_{(H_2O_{(l)}-H_2O_{(g)},25°C)} = 9.4$ ‰ .

This relationship holds best for smaller fractionation factors, where $\alpha < 1.01$.

1.2.6 Measurement and Standards

Isotope ratios are, by convention, the ratio of the heavier (and less abundant) isotope to the lighter (and more abundant) one. The differences in isotope ratios between materials are very slight and are not easily measured in an absolute sense. However, if measured as a relative difference between the sample and a standard of known isotope ratio, then the precision increases substantially. This is how measurements in light stable isotope mass spectrometers are made, using either a dual inlet or continuous flow system, where a reference gas is analysed alternately with the sample gas.

Stable isotope ratios are reported as deviation from an international standard. For both hydrogen and oxygen in water, the standard is SMOW, Standard Mean Ocean Water. SMOW was devised by Harmon Craig in 1961 (Craig, 1961b) as an average of previous ocean water samples from Epstein and Mayeda (1953) and Horibe and Kobayakawa (1960), but no actual sample existed. Because of this, SMOW was defined relative to NBS1 (National Bureau of Standards), a United States administered sample from the Potomac River. Because of the difficulties of not having an actual standard to analyse, the International Atomic Energy Agency in Vienna commissioned the creation of VSMOW in 1966, which was to mimic SMOW. Although VSMOW is not isotopically identical to SMOW (Clark and Fritz, 1997), it is similar enough and most workers use the acronym SMOW to define their isotope reference scale, even though VSMOW may have been used in their laboratory to calibrate their local laboratory standards (Gonfiantini, 1981; Sharp, 2007).

The Greek letter δ is used to denote the deviation of a sample from a standard, as follows:

$$\delta = \frac{R_{sample} - R_{standard}}{R_{standard}},$$

where R is an isotope ratio, such as $\frac{D}{H}$. Where relatively more of the heavy isotope (e.g. ^{18}O) is present in the sample than the standard, then the δ value will be greater than zero, whereas samples relatively depleted in the heavy isotope will have negative δ values. The $\delta^{18}O$ and δD values of SMOW are equal to 0. As the variations in isotope ratios are generally quite small, these δ values are reported in per mille (parts per thousand), using the ‰ notation. The equation combining these definitions is then:

$$\delta^{18}O_{sample-SMOW} = \left(\frac{\left(\frac{^{18}O}{^{16}O}\right)_{sample}}{\left(\frac{^{18}O}{^{16}O}\right)_{standard(SMOW)}} - 1 \right) \times 1000.$$

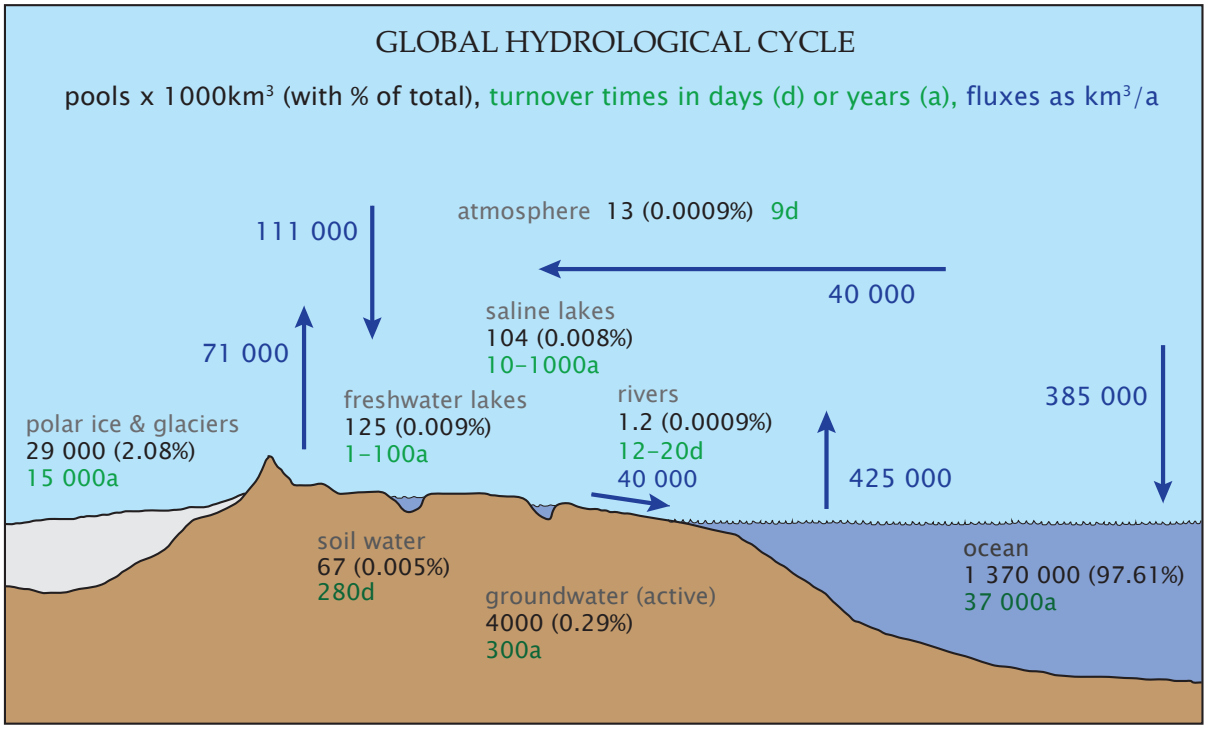

Figure 1.3: A simplified and schematic diagram of the global water cycle, showing also the reservoir sizes and turnover times within those reservoirs. It excludes water within the crust or mantle, which is unavailable, except on a timescale of many millions of years. After Reeburgh (1994).

1.2.7 Stable Isotope Hydrology

The global water cycle is extremely complex if all the interactions with geological and biological materials are taken into account, including things as diverse as weathering and volcanic eruptions in the geosphere and organic decay and drinking in the biosphere. Fortunately, the flows of water are involved in those interactions are orders of magnitude less than the major flows of water, such as evaporation from the oceans or precipitation over land, except perhaps for transpiration by plants. An attempted quantification of these flows is shown in **Figure 1.3**. This global flow of water is known as the hydrological cycle and most of the steps in this cycle are key points where the isotopic composition of parcels of water gets changed. With such complexity in this cycle, it is perhaps surprising that the variation in δD and $\delta^{18}O$ is very defined, as can be seen in the diagram in **Figure 1.4** from the landmark publication by Craig in 1961 (Craig, 1961a).

The most important observation to note in **Figure 1.4** is that most precipitation has δD and $\delta^{18}O$ values less than zero. This is primarily because evaporation from the oceans produces vapour that is depleted in the heavier isotopes relative to sea water which is similar to SMOW and has δD and $\delta^{18}O$ values close to zero. During evaporation from the ocean surface the vapour is continuously removed by diffusion and wind and mixed upwards in the atmosphere, so the air in contact with the ocean surface never becomes saturated and isotopic equilibrium cannot be reached, which means that this is a kinetic fractionation process. This results in the water vapour

in the atmosphere being more depleted in the heavier isotopes than would occur if equilibrium fractionation was taking place (Clark and Fritz, 1997). The measured values of $\delta^{18}O$ over the oceans vary from about -10 ‰ to -15 ‰, as latitude increases (temperature decreases), which are about 4 ‰ less than the equilibrium values would be. The values for δD are similarly lower than theoretical equilibrium values and range from -70 ‰ to -100 ‰ (Sharp, 2007).

Generation of atmospheric water vapour occurs mainly over the warmer oceans and it has been estimated that around 65 % is generated between 30°S and 30°N (Rozanski et al., 1993). Once an air mass is cooled, either by advection to colder climates and over a cool surface or by convection, the air can become saturated and condensation may commence. Actual condensation is dependant not only on temperature and humidity, but on the availability of condensation nucleii of the correct type (Sumner, 1988). Condensation generally proceeds slowly in response to reduced pressure or further cooling and this takes place in the presence of the vapour. As a result, condensation is an equilibrium fractionation process.

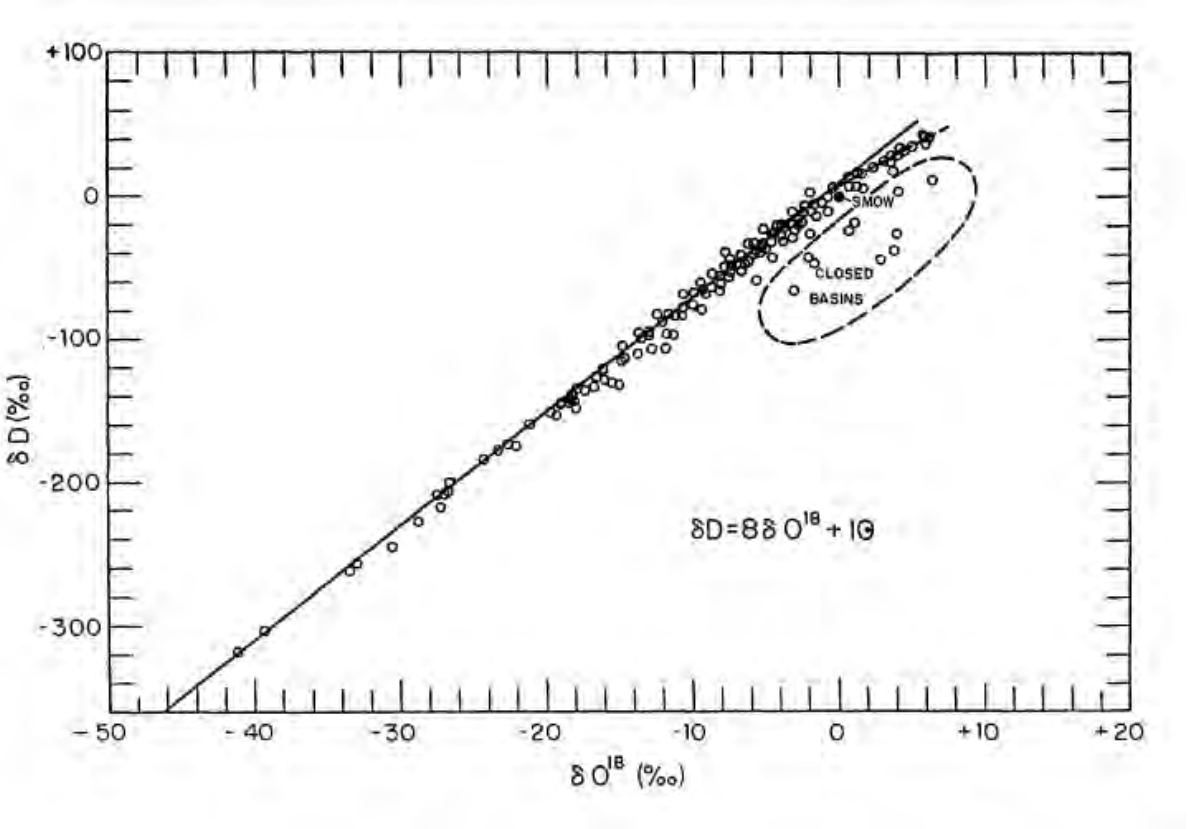

Figure 1.4: The diagram that established the relationship between δD and $\delta^{18}O$ in precipitation. The equation that describes this relationship is called the Global Meteoric Water Line (GMWL) (from Craig, 1961a).

The spread of data along the GMWL is influenced by several meteorological processes or factors, such as humidity and temperature, but it is probably rainout of atmospheric moisture, as air masses move from the tropics to the poles, that accounts for the bulk of the variation in δ values (Yurtsever and Gat, 1981). As a moisture laden air mass moves from the tropics to the poles, the moisture is removed by precipitation and the temperature or climate tends towards being colder, which not only allows further precipitation by causing more condensation, but enhances the removal of heavy isotopes by increasing equilibrium isotope fractionation factors. As the process of rainout is governed by condensation, which is is an equilibrium process, δD and $\delta^{18}O$ co-vary but with a factor of 8 difference, which is the factor by which the atomic weights vary:

$$\frac{\frac{D-H}{H}}{\frac{^{18}O-^{16}O}{^{16}O}} = \frac{\frac{1}{1}}{\frac{2}{16}} = \frac{1}{\frac{1}{8}} = 8 \quad = \frac{\Delta\delta D}{\Delta\delta^{18}O} \text{ (from GMWL of Craig (1961a)) .}$$

For a given area, with limited rainout and temperature variation, samples of precipitation will plot along a local meteoric water line (LMWL). Most LMWLs have slopes ($\frac{\Delta\delta D}{\Delta\delta^{18}O}$) of < 8, usually around 5 to 7 and a very much more limited range of δD and $\delta^{18}O$ values compared to the GMWL. When several LMWLs for areas with different climates are drawn, these lines lie semi-parallel, but displaced 'up' or 'down' on the δD–$\delta^{18}O$ plot and stack on top of each other to form the GMWL. An example is given in **Figure 1.5** that shows the data for a wide range of areas, and although each area forms more of a cluster, as the study was not to determine MWLs for each area, it nonetheless illustrates how the various areas stack up upon each other in the $\delta - -\delta$ space. The GMWL is the cumulative result of lots of LMWLs for regions of different climate, with degree of rainout being the main discriminant for the position of each LMWL. LMWLs for higher latitude regions will tend to plot lower on the diagram and vica-versa, which is clearly illustrated in **Figure 1.5**.

The reason only general, rough statements can be made about the causes of the distribution of isotope ratios in meteoric water is the extreme complexity of the hydrological cycle. Attempts have been made to build equations or conceptual models to predict isotopic values, but these have not been adequate (Sharp, 2007; Yurtsever and Gat, 1981). However, several key factors have been identified, some of which have already been alluded to above, by the first workers to interpret stable isotopes in water samples, for instance Friedman (1953), Epstein and Mayeda (1953), Craig (1961a) and Dansgaard (1964). Subsequent workers continued to develop the understanding of these key factors, until they became widely accepted as a fundamental part of isotope hydrology (e.g. Rozanski et al., 1993; Gat, 1996; Sharp, 2007). These factors are known as the latitude effect, continental effect, altitude effect and amount effect. With increasing latitude, increasing distance from the coast, increasing altitude or increasing amount of rain in a rainfall event, the isotopic composition of the precipitation becomes lighter (depleted in D and ^{18}O).

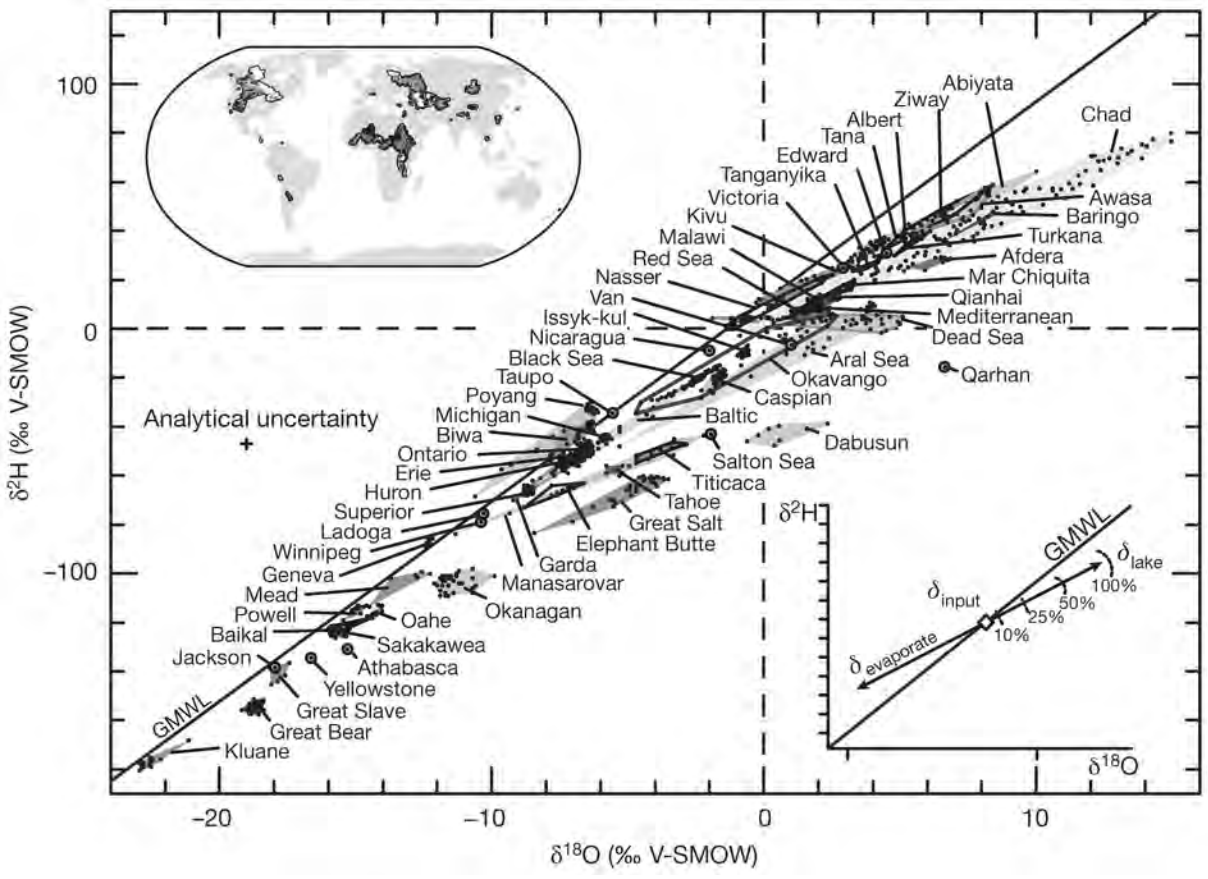

Figure 1.5: A graph illustrating the limited ranges of isotopic compositions in particular areas and how these ranges, or LMWLs, stack upon each other to form the GMWL. Diagram from Jasechko et al. (2013).

1.2.7.1 The Latitude Effect

As most moisture is sourced from the tropical oceans, because the higher temperature of the sea allows greater evaporation than in mid- or high latitude ocean areas, atmospheric moisture evolves isotopically as it moves away from the tropics. Condensation and rainout favours the removal of the heavier isotopes and so the precipitation at higher latitudes has more negative δ values. However, evaporation does still occur off the mid-latitude oceans and because the temperatures are colder, the fractionation factors will be greater, resulting in vapour relatively more depleted in the heavier isotopes than vapour that forms above the tropical oceans.

1.2.7.2 The Continental Effect

Progressive rainout is the main cause of increasingly negative δ values for precipitation that is further and further inland. In some cases, where winter rainfall occurs, cooler air inland may also reduce the amount of evaporation and isotopic change that occurs as rain drops fall through unsaturated air below the cloud. These colder inland temperatures will also increase the equilibrium fractionation factor that applies during condensation, so removing heavier isotopes more effectively from the vapour and resulting in precipitation further inland being even lighter isotopically.

1.2.7.3 The Altitude Effect

Again, the altitude effect is caused mainly by rainout that is triggered by orographic uplift, as well as a decrease in temperature, resulting in greater fractionation factors, which will drive rainout of heavier isotopes and cause a faster shift to lighter isotopes at higher altitude. Also, rain falling at higher elevations will have less distance to travel to the ground and less chance for evaporative enrichment, in which the lighter isotopes evaporate preferentially.

1.2.7.4 The Amount Effect

The amount effect also has a close relationship with rainout. Firstly, heavy individual rainstorms will tend to remove more of the vapour and cloud droplets in the air, and so with increasing rainfall in one location, the isotopic signature should become lighter. Secondly, the air below the cloud base will gradually become more saturated and colder, both of which will reduce evaporative enrichment of the later rain drops.

As can be seen from the above decriptions of the four effects, temperature and rainout are the main underlying processes that drive the various 'effects'. It is important to note that all of these effects and their underlying causes occur in a highly complex natural system where many variables contribute to the final isotopic composition of a rainwater sample. Other than temperature and rainout, factors such as humidity and source region also modify the isotopic composition. Isotope content of rainwater varies by the minute in a rainstorm (Lawrence and White, 1991; Harris et al., 2010) and between rain events, as is typical of most meteorological phenomena. Averaging the isotope composition of rainfall over longer periods, such as a month, has been found to be the most useful way of understanding the variation in isotopic signatures in an area (Yurtsever and Gat, 1981).

1.2.7.5 The Deuterium Excess

Kinetic fractionation during evaporation from the ocean surface takes place because of diffusion of water vapour molecules from a saturated boundary layer at the sea surface and into the open atmosphere . The $HH^{16}O$ isotopologue diffuses faster than all the others and so the vapour is

depleted in the heavier isotopes. If the atmosphere was saturated, then isotope exchange would occur fully between the sea and water vapour in the air, resulting in isotopic equilibrium, where the vapour would also be depleted in the heavier isotopes. However, the differences between the equilibrium and diffusion fractionation factors for D-H and ^{16}O-^{18}O are not the same and so the relative depletion of D and of ^{18}O changes with the degree of saturation, or relative humidity, **h**. As **h** increases, so more isotope exchange will occur and the closer to equilibrium fractionation the system will come (Clark and Fritz, 1997).

This means the slope along which vapour and residual water plot on a $\delta D - \delta^{18}O$ diagram will vary as a result of the degree of exchange, or isotopic equilibrium. Evaporation under lower relative humidities will generate lines with lower slopes. **Figure 1.6** shows how evaporation from sea water under 85% relative humidity conditions and then condensation at equilibrium generates water with isotopic compositions that plot along the GMWL. At different relative humidities, vapour and the resulting water samples will be displaced from the GMWL. The deuterium excess of a water samples measures this displacement with the formula:

$$d - excess = \delta D - 8\delta^{18}O$$

where δD and $\delta^{18}O$ are the values for the water sample. The d value is a proxy of the humidity of the source region.

1.3 Stable Isotope Hydrology in South Africa

Water is the single most important compound for all life. Humans need water daily, both for direct consumption and for all the other activities taking place in our society. Pre-colonial settlements in South Africa were influenced by the availability of water and the very first permanent European settlement, Cape Town, was chosen over Saldanha Bay with its better harbour, on the presence of superb quality perennial water coming from the springs at the foot of Table Mountain.

Scientific interest in groundwater has often been secondary to the practical concerns of locating and using it, a notable exception being hot springs, which seem to have attracted much attention over the years, in particular by Kent (e.g. Kent, 1949). One of the first investigations to make use of stable isotopes of hydrogen and oxygen also focused on hot springs, specifically those in Swaziland (Mazor et al., 1974) and was closely followed in 1976 by similar work by the two main authors on the hot springs of Zimbabwe (then Rhodesia) (Mazor and Verhagen, 1976). The same two authors eventually did similar work on the South African hot springs (Mazor and Verhagen, 1983), where they found a wide scatter of δD and $\delta^{18}O$ values with no systematic variation by location or average annual rainfall.

Surveys of the isotopic composition of the Gariep (Orange) River were undertaken around 1968-74 by the Council for Scientific and Industrial Research and the International Atomic Energy

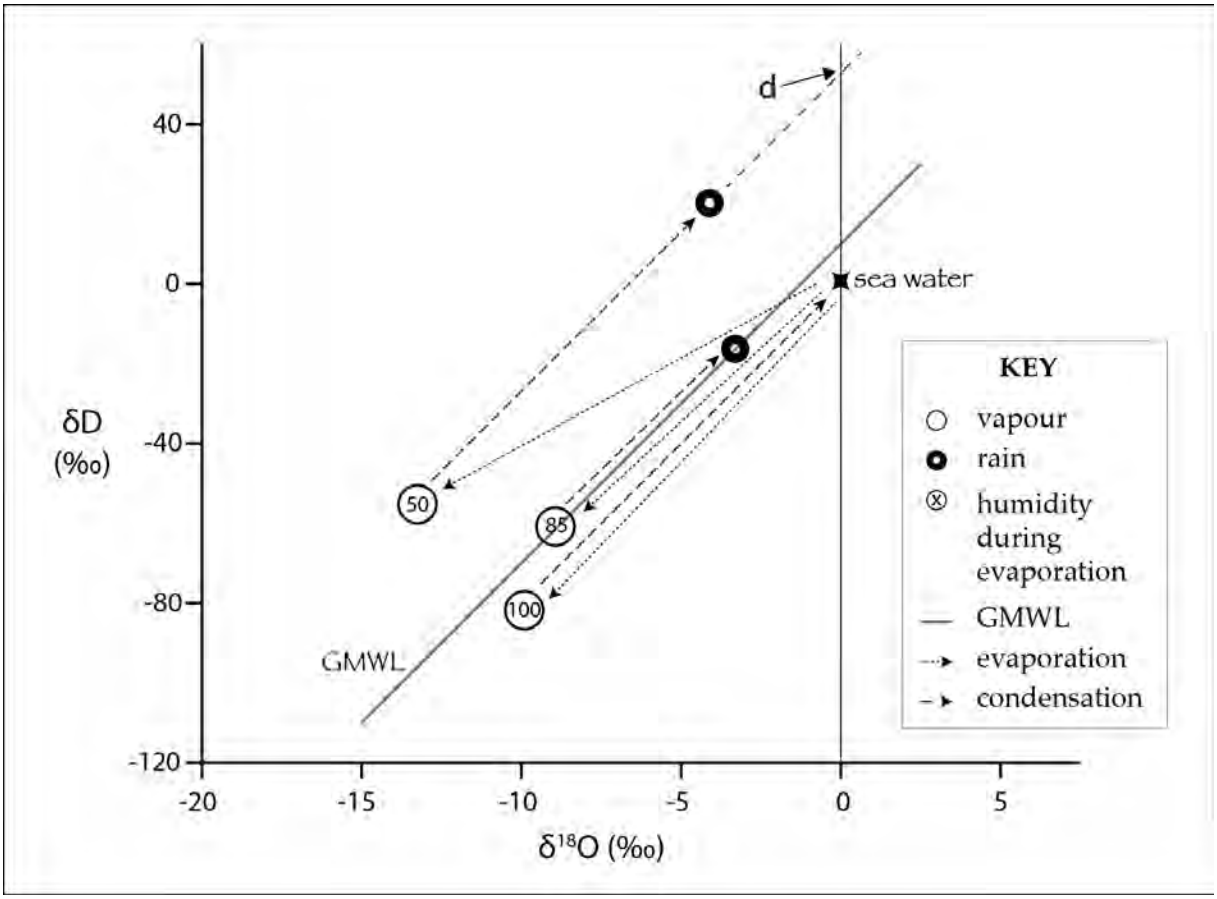

Figure 1.6: Different relative humidities in the source regions during evaporation create moisture masses with different isotope compositions due to kinetic effects as explained in this chapter. Examples in the figure show how the GMWL suggests an average global humidity at the sea surface of around 85 %, where the deuterium excess parameter is 10. For a hypothetical region with evaporation occurring under 50 % relative humidity conditions, d ≈ 50 (after Clark and Fritz (1997)).

Agency with reports being written by S Talma and others, but not published. This work found, despite disturbances to flow in the river caused by the large Gariep (then Hendrik Verwoerd) and Vanderkloof (then P K Le Roux) dams, a negative correlation between $\delta^{18}O$ and flow volume, presumably as a result of the amount effect and perhaps also for samples further downstream, an evaporation effect during low flows.

In 1975, Vogel and Van Urk surveyed ^{18}O content of precipitation and groundwater in the semi-arid regions of southern Africa, finding the groundwater $\delta^{18}O$ values to be remarkably consistent and generally more negative than the highly varied precipitation values. They concluded that groundwater is recharged during heavy rainfall events only. A similar conclusion was reached by Sami (1992) but using hydrogen and oxygen isotopes in conjunction with soil and groundwater chemistry to understand soil and groundwater salinisation in the interior of the Eastern Cape. It was concluded that periods of salt accumulation in the soil, from weathering and evaporative

enrichment of meteoric water, are followed by intense rainfall which flushes these salts to the water table. A study by Adams et al. (2001) in the Sutherland area of the Karoo reached much the same conclusions, also by using isotopic and hydrochemical observations.

Midgley and Scott (1994) compared surface water discharge to rainfall during rain events in the mountainous Jonkershoek area, east of Stellenbosch, concluding that the bulk of streamflow is from groundwater displaced by rain recharging the soil or aquifer. They also calculated a local meteoric water line (LMWL) for Jonkershoek: $\delta D = 6.99\delta^{18}O + 9.63$. A LMWL for the Western Cape was calculated by Diamond and Harris (1997) to be: $\delta D = 6.2\delta^{18}O + 10.6$, which is rather different, but closer to the best LMWL calculation, based on 12 years of data giving an equation of $\delta D = 6.41\delta^{18}O + 8.66$ (Harris et al., 2010).

A thorough examination of the hot springs of the Western Cape was done by Diamond and Harris (2000) in which monthly samples of spring discharge were taken. The spring discharge isotope ratios were seen to have a slight scatter, but no systematic variations. This study also concluded, on the basis of isotopic and geological evidence, that the springs are being recharged at high altitude in mountains made up of the Table Mountain Group and circulating to depths of over 2 km below sea level before discharging at surface. Cavé et al. (2002) used oxygen and hydrogen isotopes in the Agter-Witzenberg Valley to develop a conceptual groundwater flow model. This study also found that recharge was occurring at high altitude and circulating down before rising up in the valley area, where boreholes were intercepting flow. Deep boreholes, up to 350 m below surface, in the Citrusdal Valley contained water with more negative δ values than for shallow boreholes and surface water in the region, and was interpreted to indicate the deeper groundwater was being recharged at higher elevations than the shallow groundwater (Hartnady and Hay, 2002a). On the basis of these studies, it seems that groundwater flow occurs simultaneously at multiple levels, with more shallow local circulation occurring above deeper, more regional flow paths, which is an accepted model for groundwater flow (e.g. Domenico and Schwartz, 1998, p.79).

Determination of the source of water used by plants makes it possible to predict impacts on plant life from changes in the water table caused by groundwater abstraction. It has been found for fynbos plants growing on soils above the Table Mountain Group that different species have different water requirements and make use of water from different levels within the soil, with the conclusion that certain species will be more affected than others if groundwater levels do drop (February et al., 2004). Declining groundwater levels have been experienced in the Kammanassie Mountains, as part of the Klein Karoo Rural Water Supply Scheme. Substantial work has been done around this scheme (e.g. Kotze, 2002; Jolly, 2002; Woodford, 2002; Jolly and Kotze, 2002), including analysis of groundwater for stable isotopes of hydrogen and oxygen (Kotze et al., 2000). This study revealed that boreholes sited in low lying valleys may be tapping groundwater that was recharged at high elevation and has travelled through highly fractured 'aquizones' to reach the lower lying areas.

More applied uses of stable isotopes include fingerprinting water in urban areas in order to determine sources of leakage or pollution. In South Africa, various workers have identified isotopic differences in local groundwater versus public water supply (mains) water in Cape Town (Harris et al., 1999), local groundwater and a wastewater treatment works in Bellville, Cape Town (Saayman et al., 2000) and local rain or groundwater and mains water supply in Pretoria (Butler et al., 2000). The latter study found many boreholes with 30–50 % mains water contributions, highlighting the severe extent of leakage and water wastage.

Oxygen and hydrogen isotopes from groundwater in deep gold mines in the Witwatersrand Supergroup often have δ values that do not match current precipitation and suggest recharge during a previous, colder climate. This helps determine that primitive organisms found in these deep groundwaters are well removed from the earth's surface and do not regularly interact with the bulk of the biosphere, having profound implications for our understanding of evolution and the functioning of the biosphere (Takai et al., 2001).

1.3.1 Motivation Behind this Study

Groundwater from the Table Mountain Group is used extensively by people and the environment of the Western (and Eastern) Cape. This occurs both directly, where boreholes and springs tap the aquifer, and indirectly, where discharge from the aquifer supplies springs and wetlands, and maintains surface water flows through summer, forming the basis of much agriculture and most of the ecosystems of the region. Boreholes are used by many farmers and also for public water supply in towns such as Citrusdal and Hermanus. There is intense interest in the water resource of the Table Mountain Group aquifer system, not only from the existing users, but many other potential users, including the country's second largest metropolitan area, Cape Town.

Stable isotopes of water offer one method of improving our understanding of the Table Mountain Group aquifer system. The source of all groundwater and surface water is precipitation, and therefore, in order to interpret stable isotope measurements of groundwater or surface water, a handle on the spatial and temporal variation in stable isotope composition of precipitation is needed. This was the primary motivation behind the deployment of 15 rainfall collection stations across the Western Cape, from coast to mountaintop, over a period of two years. The focus of this study was to quantify, as much as is possible given the duration of monitoring, the patterns in stable isotope composition of precipitation. Sampling of groundwater and surface water at selected sites was included to demonstrate the possible findings that stable isotope hydrology can reveal about the inner workings of the Table Mountain Group aquifer system.

authors	date	title
E Mazor & B T Verhagen	1983	Dissolved ions, stable and radioactive isotopes and noble gases in thermal waters of South Africa.
J Midgley & D F Scott	1994	The use of stable isotopes of water (D and ^{18}O) in hydrological studies in the Jonkershoek Valley.
R E Diamond & C Harris	1997	Oxygen and hydrogen isotope composition of Western Cape meteoric water.
J M Weaver, A S Talma & L C Cavé	1999	Geochemistry and isotopes for resource evaluation in the fractured rock aquifers of the Table Mountain Group.
C Harris, B Oom & R E Diamond	1999	A preliminary investigation of the oxygen and hydrogen isotope hydrology of the greater Cape Town area and an assessment of the potential for using stable isotopes as tracers.
R E Diamond & C Harris	2000	Oxygen and hydrogen isotope geochemistry of thermal springs of the Western Cape, South Africa: Recharge at high altitude?
J C Kotze, B T Verhagen & M J Butler	2000	An aquifer model based on chemistry, isotopes and lineament mapping: Little Karoo, South Africa.
C J Hartnady & E R Hay	2002	Boschkloof groundwater discovery.
E C February, W Bond, R Taylor & R Newton	2004	Will water abstraction from the Table Mountain aquifer threaten endemic species?
C Harris, C Burgers, J Miller & F Rawoot	2010	O- and H-isotope record of Cape Town rainfall from 1996 to 2008, and its application to recharge studies of Table Mountain groundwater, South Africa.
D Barrow & R E Diamond	2011	Stable Isotopes of rain, surface water and groundwater in the Kogelberg.

Table 1.2: Oxygen and hydrogen stable isotope publications relating to the Table Mountain Group.

Chapter 2

Background

2.1 Introduction

The Table Mountain Group dominates the geology of the Western Cape, but due to extensive folding and faulting during the Permo-Triassic Cape Orogeny and subsequent sedimentation during the Mesozoic and Cenozoic, it comes into contact with numerous other geological units. A good overall knowledge of these various units is necessary to understand how groundwater within the Table Mountain Group may be constrained, recharged by, or discharged into these other units. The geological map in Chapter 1 and the cross sections in Chapter 5 may be useful to consult when reading through this chapter.

This chapter describes the geology of the Western Cape in brief, the climate of the region, with an emphasis on the rainfall and rain producing weather systems, and then concludes with a summary of the understanding of the hydrogeology of the Table Mountain Group.

2.2 Geology — Lithostratigraphy

The geology of the Cape Fold Belt region can be split into three main packages: the basement, the Cape and Karoo Supergroups, and the younger rocks. This chapter summarizes these three packages and their components, with an emphasis on the Cape Supergroup and the Table Mountain Group in particular. The basement of the Cape Fold Belt region can also be divided into three packages: the various parts of the Pan-African Saldania Belt, the Cape Granite Suite, and some transitional formations that undoubtedly precede the Cape Supergroup, but have uncertain relationships with the Saldania Belt rocks.

2.2.1 Saldania Belt

The Saldania Belt refers to a set of units in the Cape Fold Belt region that display similar stratigraphic position and deformation style, although they contain a wide array of rock types and are geographically separated. These units are exposed where the Cape Supergroup has been

stripped away by erosion, typically either on the coastward side of the Cape Fold Mountains or where large anticlines or normal faults have aided exposure of inliers. The Saldania Belt abuts the Kalahari Craton to the north (Gresse et al., 2006) and is made up of the Malmesbury Group to the north-east of Cape Town, the Cango Caves and Kansa Groups to the north of Oudtshoorn, the Kaaimans Group around George and the Gamtoos Group west of Port Elizabeth.

The Malmesbury Group has the largest area of exposure of all these groups, although the quality and area of actual outcrop is very poor due to low relief and the easily weathered nature of the formations. As such, this Group is poorly understood. The first substantial synthesis was put forward by Hartnady et al. (1974), in which the Group was subdivided into three "domains" (now called terranes), separated by fault zones. These are, from the south-west to the north-east, the Tygerberg, Swartland and Boland Terranes, with zones of tectonized rocks between them, known as the Saldanha-Franschhoek Fault, now called the Colenso Fault, between the Tygerberg and Swartland Terranes and the Piketberg-Wellington Fault between the Swartland and Boland Terranes (SACS, 1980).

The stratigraphy of the Malmesbury Group remained largely unchanged from Hartnady et al. (1974) in Tankard et al. (1982). Rozendaal et al. (1999) reported an improved understanding of the depositional setting, tectonic history and radiometric dates, as well as correlations across the various groups within the Saldania, Gariep and Dom Feliciano (in South America) Belts, but the basic lithostratigraphy remained unchanged. Then, in 2003, Belcher & Kisters substantially revised the Malmesbury Group lithostratigraphy based upon detailed structural observations within formations. These dramatic revisions appear to have not, however, been accepted by the time of publication of the 2006 volume of The Geology of South Africa, in which Gresse et al. (2006) summarize the present understanding of the Neoproterozoic to Cambrian successions of South Africa. The Belcher & Kisters revision, see **Figure 2.1**, resulted in three groups. These are, from the oldest: strongly deformed low grade metamorphic rocks, predominantly schists with minor carbonates, chert and metavolcanics, of the Swartland Group; low grade metamorphic rocks, mainly shale, greywacke and sandstone with minor conglomerate, limestone and andesite; conglomerate, grit, sandstone and shale of the Klipheuwel Group.

The Kaaimans Group, exposed along the south coast at the core of a regional anticline, comprises low grade metamorphic rocks of a great variety, include shale, phyllite, greywacke, sandstone, schist and calc-silicate. The Kansa and Cango Caves Groups occur to the north of the regional Cango Fault, a normal fault that causes repetition of the south-to-north basement to Cape Supergroup to Karoo Supergroup sequence. In contrast to the diverse rock types of the Kaaimans Group, the Cango Caves Group is dominated by greywackes and carbonates with lesser shale, sandstone and conglomerate, and the Kansa Group is made up of conglomerate, sandstone and minor shale. The Gamtoos Group, exposed in a sliver shaped inlier within a fault bounded anticlinal hinge, features mainly carbonates, phllitic greywackes and various arkosic sandstones and conglomerates (Gresse et al., 2006).

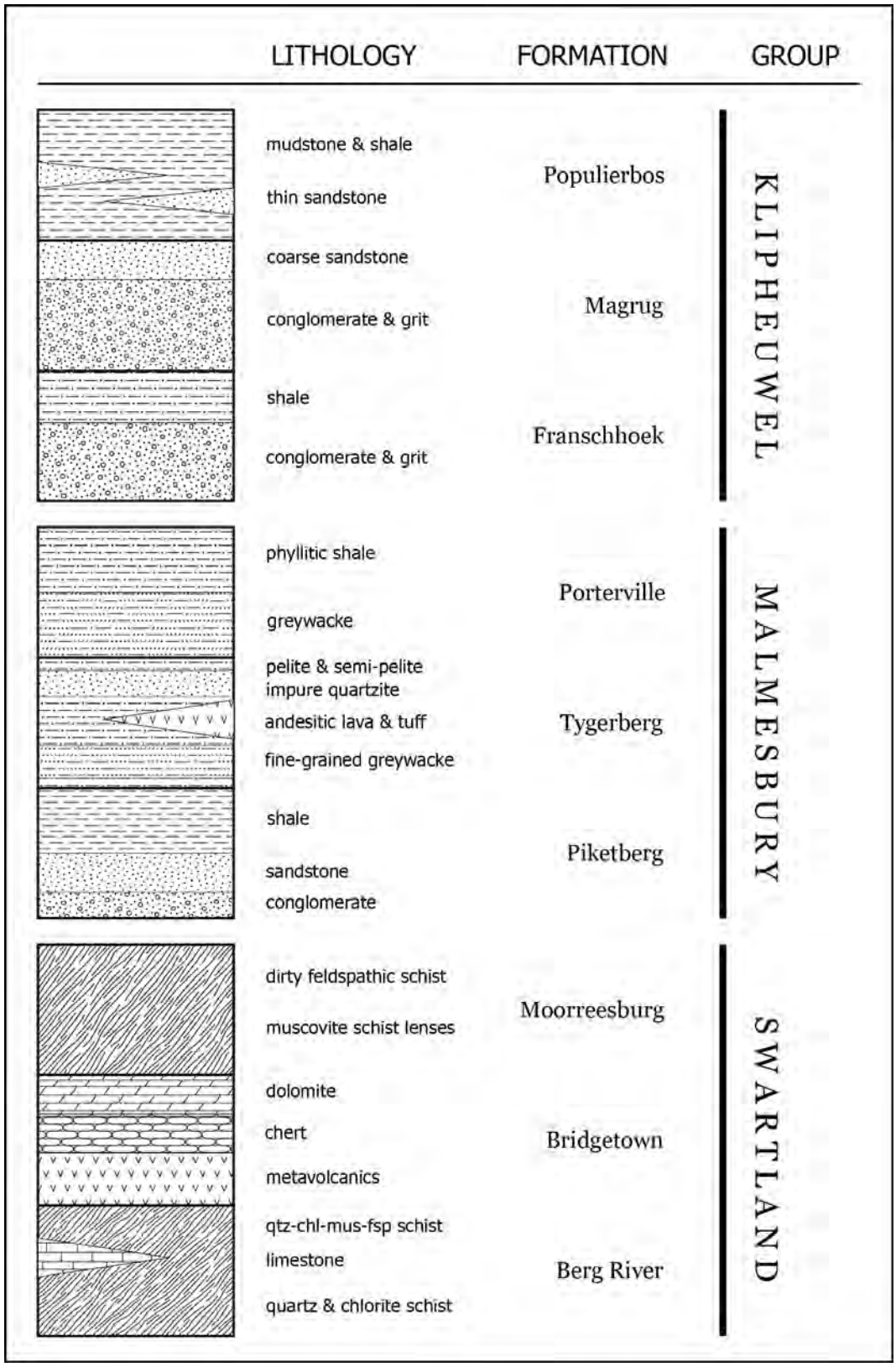

Figure 2.1: Revised stratigraphy of the western Saldania Belt formations within the Western Cape, based on Belcher and Kisters (2003).

2.2.2 Cape Granite Suite

The Cape Granite Suite consists of numerous bodies that have mostly been intruded as plutons into the metasediments of the Saldania Belt, or have been thrust into their current positions during the Cape Orogeny. The plutons occur in three clusters: a minor Richtersveld cluster, a minor George cluster and the large south-western cluster in the Saldanha Bay - Cape Peninsula - Overberg area (e.g. Schoch et al., 1977). In reality, the south-western and eastern clusters may be two parts of the same large cluster, as the lack of evidence of any granites in the intervening area coincides with a lack of outcrop of any basement at all.

The Cape Granite Suite occurs as multiple intrusions, mostly plutons, that in places have been grouped into batholiths, for example the Cape Peninsula and Darling Batholiths. Although composed mostly of granitic plutons, there is quite a range of rock types and intrusive forms in the Cape Granite Suite. Aside from a range of granitic compositions, rock types include gabbro, diorite, quartz porphyry and quartz syenite (Scheepers and Schoch, 2006). Similarly, although intrusions occur mostly as plutons, other structures such as dykes, ignimbrite flows and tectonically bounded sheets also occur (Gresse and Theron, 1992).

The plutons of the Cape Granite Suite have been dated by various workers and yield ages that range from very late Neoproterozoic to late Cambrian. Scheepers and Armstrong (2002) found the Hoedjiespunt granite gave a U-Pb zircon age of 552±4 Ma; in the same year, Scheepers & Poujol found an ignimbrite, also in the Saldanha Bay area to give a U-Pb zircon age of 515±3 Ma. These ages bracket those of da Silva et al. (2000) who reported U-Pb zircon ages of 547±6 Ma and 536±5 Ma, Schoch and Burger (1976) who found a Pb-Pb zircon age of 522±12 Ma, Jordaan et al. (1995) who found a U-Pb zircon age of 519±7 Ma on the monzonite Yzerfontein pluton and other ages, around 540 Ma, reported by Scheepers and Armstrong (2002) for plutons in the Saldanha Bay area.

Based on the above ages, field relations and petrography, 4 stages of igneous activity have been identified (Scheepers and Schoch, 2006; Rozendaal et al., 1999). These can be summarized as S-type granites in phase 1, I-type granites in phase 2, A-type granites and intermediate and mafic plutons in phase 3, and intrusive and extrusive felsic rocks in phase 4, all within a 40-50 Ma period during the Pan-African.

2.2.3 Cape Supergroup

The Cape Supergroup is one of only 9 supergroups in South Africa. It dominates the geology of the Western Cape and extends substantially into the Eastern Cape and is composed of three groups: the thickest, basal, arenaceous Table Mountain Group, the argillaceous Bokkeveld Group and the lithologically intermediate Witteberg Group. The succession was deposited during the Palaeozoic, on top of the Saldanian basement, and then overlain by the Karoo Supergroup, the youngest of all South Africa's supergroups. The Cape Supergroup, underlying basement and the older formations of the Karoo Supergroup were deformed in the Permo-Triassic Cape Orogeny.

2.2.3.1 Table Mountain Group

The Table Mountain Group is the dominant group of the Cape Supergroup due to the stratigraphic thickness and highly arenaceous character, causing resistance to weathering and leading to formation of mountains that define the geography of the Western Cape. **Figure 2.2** shows the lithostratigraphy of the Table Mountain Group in the western half of the Cape Fold Belt. The basal formations in the Cape Supergroup vary from east to west and north to south: in the west the Piekenierskloof and then Graafwater Formation occur; in the far south-east the Sardinia Bay Formation occurs; in the central to eastern areas these are absent and the Peninsula Formation lies directly on the basement; in the far north-western areas where the Cape Supergroup ends, the lower formations pinch out and the Nardouw Subgroup formations lie at the base. Controversy does exist over the assignment of the Sardinia Bay Formation, in part or whole, to the Cape Supergroup, the Saldanian Gamtoos Group or to neither.

Sardinia Bay Formation

Toerien and Hill (1989) and Bell (1980) included all the rocks between the Gamtoos Group and the Peninsula Formation as the Sardinia Bay Formation and treat this unit as the basal formation of the Table Mountain Group, possibly correlating with the Graafwater Formation to the far west. In contrast, Shone (1979, 1983) as cited in Gaucher and Germs (2006) included only the untectonized rocks into the Sardinia Bay Formation. Such differences aside, the Sardinia Bay Formation is a sequence of alternating dominant feldspathic, quartzitic sandstones, thin to medium bedded with some cross-bedding, subordinate greenish-grey to black phyllitic shales, and minor vein-quartz-pebble conglomerates (Toerien and Hill, 1989).

Piekenierskloof Formation

The Piekenierskloof Formation forms the base of the Cape Supergroup only in the north-western part of the Western Cape. The contact with the underlying Klipheuwel Formation, or Populierbos Formation of the Klipheuwel Group, if using Belcher and Kisters (2003) revision, is either an angular unconformity or disconformity (Rust, 1967), although Vos and Tankard (1981) considered that the Piekenierskloof and Klipheuwel Formations may be contemporaneous, in spite of observations by Rust (1973) that show variable clast lithologies in the Piekenierskloof Formation in contrast to locally derived (Cape Granite Suite) clasts in the Klipheuwel Formation. The southernmost outcrops are a mere 10 m thick, occuring in the Kasteelberg outlier in the middle of the Swartland (Theron et al., 1992), whilst outcrops reaching a maximum thickness of 900 m occur further north-west near Lamberts Bay (Thamm and Johnson, 2006). The Piekenierskloof Formation consists of very mature arenite and conglomerate, the latter containing identifiable clasts of resistant sedimentary and metamorphic rocks (Rust, 1967).

Graafwater Formation

The Graafwater Formation overlies the Piekenierskloof Formation conformably where the latter occurs, but extends beyond the boundaries of the Piekenierskloof basin and there overlies Saldanian basement. The Graafwater basin extended from beyond the present day Atlantic Ocean

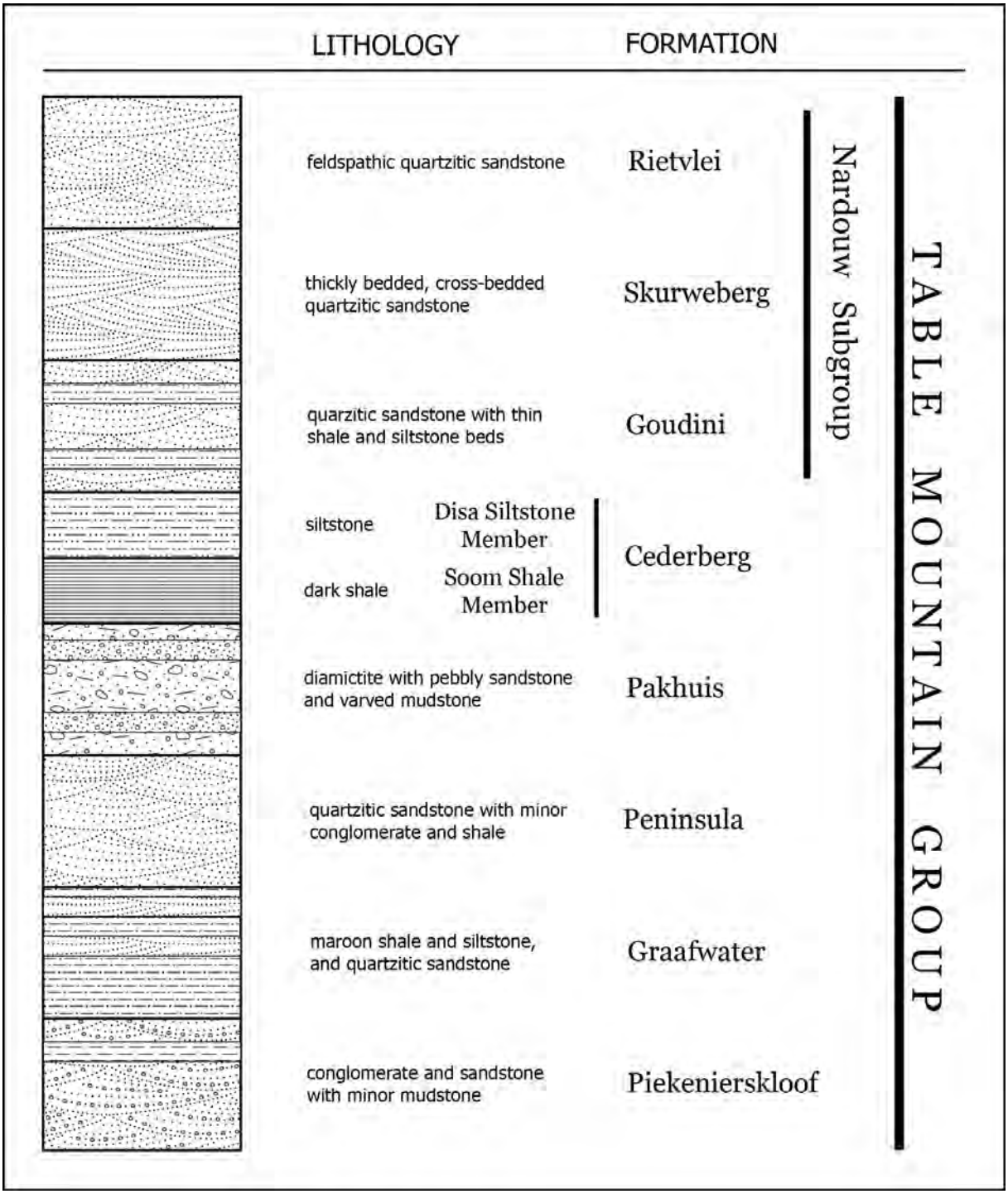

Figure 2.2: Stratigraphy of the Table Mountain Group for the western side of the Cape Fold Belt.

coast at the Olifants River Mouth, southwards to the Cape Peninsula and eastwards to the Ceres-Worcester area (Rust, 1967). The southern part of the Graafwater Formation, south of Piketberg, averages 50–100 m thickness, whilst there is a defined north-west trending trough in the Citrusdal to Lamberts Bay region where the Formation averages 250 m and reaches 430 m thickness (Rust, 1967; Thamm and Johnson, 2006). Although nearly 700 km apart and therefore probably never linked originally, several factors indicate that the Sardinia Bay Formation could be equivalent to the Graafwater Formation. These factors include: stratigraphic position, rock types and an underlying conglomerate with similarities to the Piekenierskloof Formation (Shone and Booth, 2005). The Graafwater Formation features upwards fining cycles of three distinct lithologies: a fine to medium grained quartzose sandstone; an interbedded finer grained sandstone, siltstone and maroon mudstone with dessication cracks; and a maroon mudstone (Tankard and Hobday, 1977; Rust, 1977).

Peninsula Formation

The Peninsula Formation is the dominant formation of the Table Mountain Group and indeed of the Cape Supergroup, due to its widespread occurrence, thickness and remarkably consistent, highly quartzose nature. The formation occurs throughout the Cape Basin except for the very north-western margin in the Niewoudtville vicinity where it is absent (Rust, 1973). Thickness estimation in the Peninsula Formation is hampered as one moves east by extensive thrusting, much of which is bedding-parallel and difficult to detect, leading to estimates of as much as 3000-4000 m by Rust (1973), whereas the less deformed sequences of the west, in the Cape Peninsula, reveal the thickness to be 530 m, according to Fuller and Broquet (1990).

The Peninsula Formation is remarkable for the great thickness of consistently mature quartzose sandstone. The sandstone is light grey, medium to coarse grained, mainly planar bedded, but commonly with trough cross bedding, usually thickly bedded, but in places massive or thinly bedded (Shone and Booth, 2005; Gresse and Theron, 1992). Occasional thin quartz pebble lags are found and channels also occur, reportedly a few metres in width (Theron et al., 1992) or up to 40 m deep and kilometres in extent (Hobday and Tankard, 1978; Tankard et al., 1982). In the upper 100 m of the Peninsula Formation, a zone of folding is sometimes present (Gresse and Theron, 1992), varying from simple, metre scale deformation to complex overturned and refolded zones of 75 m thickness. It occurs in the west only and the fold axes trend northwards (Rust, 1973).

Pakhuis Formation

The Pakhuis Formation occurs only in the western half of the Cape Basin, west of Swartberg Pass (SACS, 1980; Thamm and Johnson, 2006). Its thickness is given as 40 m by SACS (1980), but 150 m by Young et al. (2004), 160 m by Tankard et al. (1982) and 190 m by Rust (1981) as cited in Shone and Booth (2005). The lowermost Sneeukop Member is a structureless sandstone, with abundant striated and faceted erratics, that occurs only within the synclines of the Peninsula Formation fold-zone (Rust, 1967; Gresse and Theron, 1992). A thin sandstone, the Oskop Member, overlies the Sneeukop Member or the Peninsula Formation directly, and although continuous, is

Figure 2.3: A coarse grained example of quartzite in the Table Mountain Group. Rounded pebbles of vein quartz and gritty layers can be seen in this photograph from the upper Peninsula Formation.

lensoid in thickness with indistinct or thick bedding. The north-west Cape Basin contains the Kobe Member whilst the south-west Cape Basin contains the Steenbras Member, both quartzose diamictites with plentiful clasts, although the latter is a darker, more mature facies (Tankard et al., 1982; Gresse and Theron, 1992).

Cederberg Formation

The Cederberg Formation occurs widely in the Cape Basin, from the far west, eastwards to about 100 km west of Port Elizabeth, although in the eastern areas it is discontinuous because of smearing out along fold limbs (Shone and Booth, 2005). The contact with the underlying Pakhuis Formation is known to be both gradational (Rust, 1967) and sharp (Gresse and Theron, 1992). The formation thickness is given as between 50 m and 120 m (SACS, 1980; Thamm and Johnson, 2006). The Cederberg Formation is divided into two members. The basal Soom Shale Member is the thinner unit, seldom exceeding 15 m and is a dark grey, usually thinly laminated, micaceous shale (Theron et al., 1990). It contains a variety of fossils of some significance globally, such as conodonts, trilobites and ostracods (Theron et al., 1990; Gabbott et al., 2003). It coarsens upwards into the Disa Silstone Member, which itself continues the upwards coarsening trend and in turn has a gradational contact with the overlying Goudini Formation. The Disa Siltstone Member is a thinly bedded, argillaceous and carbonaceous siltstone and fine grained sandstone that reaches 75 m thickness and contains fossil brachiopods (Rust, 1967; Gresse and Theron, 1992).

Nardouw Subgroup

The Nardouw Subgroup used to have formation status, with three members, Goudini, Skurweberg and Rietvlei, recognized (SACS, 1980), but these have been upgraded to formations (Thamm and Johnson, 2006). In the east, corresponding names Tchando, Kouga and Baviaanskloof were in use for the three formations (Toerien, 1979), but now that the Goudini and Skurweberg are formations, they have been extended across the Cape Basin and only Baviaanskloof Formation is still in use for the area east of 21° 30' E as the continuation of the Rietvlei Formation (Thamm and Johnson, 2006).

The Nardouw Subgroup is characterized by a return to arenaceous rocks with similar depositional environments to the Peninsula Formation, after the unusual interlude of the Pakhuis and Cederberg Formations. The Nardouw Subgroup occurs across the whole Cape Basin and is the last single unit of the Cape Supergroup that pinches out in the northern extremities of the Basin (Rust, 1967). Thicknesses for the Subgroup are given as 900 m in the east and 700 m in the west (Thamm and Johnson, 2006), or 500 m (SACS, 1980).

Goudini Formation

The Goudini Formation is the lowermost formation of the Nardouw Subgroup and has a gradational contact with both the underlying and overlying formations. It occurs throughout the Cape Basin and its thickness is given as 200-300 m (Thamm and Johnson, 2006; Toerien and Hill, 1989) to as little as 30 m on Franschhoek Pass (Gresse and Theron, 1992). It is composed of thinly bedded, grey, medium grained quartzose sandstone that distinctively weathers to a reddish brown colour. Thin, pinkish, micaceous shale and siltstone layers are interspersed through the formation and some bluish grey siltstone occur nearer the top (Theron et al., 1991; Gresse and Theron, 1992).

Skurweberg Formation

This formation occurs throughout the Cape Basin and is around 200-400 m thick. The top and bottom contacts are gradational. It is composed of light grey, massive, medium to coarse grained quartzose sandstone with profuse cross-bedding, occasional thin quartz pebble lags and very minor shale (Toerien and Hill, 1989; Theron et al., 1991; Gresse and Theron, 1992). The highly quartzose nature of the Skurweberg Formation results in it forming steep cliffs and mountains, similarly but to a lesser extent than the Peninsula Formation does. The abundance of trough cross bedding can help distinguish the Skurweberg Formation from the planar bedding dominated Peninsula Formation.

Rietvlei Formation

The Rietvlei Formation occurs in the western half of the Cape Basin, up until a notional boundary at 21° 30' E, from where its stratigraphic equivalent, the Baviaanskloof Formation, then occurs eastwards. The typical thicknesses of the Formation are 90-200 m (Theron et al., 1991; Thamm and Johnson, 2006). It is generally similar to the Goudini Formation in that the bedding is thinner,

the sandstones dirtier and there are more thin shale bands than in the intervening Skurweberg Formation. Specifically, the Rietvlei Formation consists of alternating light grey quartzose sandstone, feldspathic sandstone, siltstone, micaceous shale and quartz pebble conglomerate, with some of the more quartzose sandstone units traceable for long distances (Theron and Basson, 1989; Theron et al., 1991; Gresse and Theron, 1992).

Baviaanskloof Formation

The Baviaanskloof Formation is the eastern, east of 21° 30' E, equivalent of the Rietvlei Formation. It contains the Kareedouw Sandstone Member which is lithologically similar to the Rietvlei Formation and most likely represents the easterly extension of this formation (Theron et al., 1991). The Baviaanskloof Formation thickness is given as 200 m by Toerien (1979) and Thamm and Johnson (2006). Above and below the 50 m thick Kareedouw Member, which is composed of light grey, medium grained, feldspathic sandstone, occurs greenish grey, fine grained, impure micaceous sandstone interbedded with subordinate greyish black, carbonaceous and micaceous shale (Toerien and Hill, 1989; Theron et al., 1991). Contacts with the overlying Bokkeveld Group are conformable and can be either gradational or sharp.

2.2.3.2 Bokkeveld Group

Whereas the Table Mountain Group is primarily arenaceous and has irregular stratigraphy, the Bokkeveld Group is argillaceous and distinctly cyclic. This group is distributed throughout the Cape Basin, except for the very northernmost margin near Nieuwoudtville. The deposit thickens to the south, being 1000 m near Citrusdal, 2500 m in the south-west near Bredasdorp and reaching 4000 m in the south-east near Uitenhage (Rust, 1967; Broquet, 1992).

Several upwards coarsening cycles occur, the lower three of which form the basinwide Ceres Subgroup, which itself ranges from 600 m to 1700 m thick, west to east (Thamm and Johnson, 2006). The persistence of these cycles basinwide has allowed the finer and coarser units to be given formation status: cycle 1 is formed by the basal mudrock and siltstone of the Gydo Formation coarsening into the greywacke of the Gamka Formation, overlain by cycle 2 siltstone and mudrock of the Voorstehoek Formation grading again into greywacke of the Hex River Formation, and similarly overlain by the fine grained Tra-Tra Formation and coarser Boplaas Formation of cycle 3. The argillaceous units do include minor sandstone, just as the arenaceous units of feldspathic greywacke and arenite include minor mudrocks and siltstones.

The upper portion of the Bokkeveld Group shows substantial facies variation spatially and is therefore divided into the Bidouw Subgroup in the west and the Traka Subgroup east of 21° E (Tankard et al., 1982). The Bidouw Subgroup is similar to the underlying Ceres Subgroup in lithologies and cyclicity, although the absence of marine invertebrate fossils is in contrast to their abundance in the latter (Broquet, 1992). The argillaceous Waboomsberg Formation forms the base of the Subgroup, followed by the arenaceous Wupperthal Formation, overlain by the argillaceous Klipbokkop Formation, overlain by the arenaceous Osberg Formation and capped by the

argillaceous Karoopoort Formation. In the east, the Traka Subgroup is quite different: it develops great thickness, is thoroughly dominated by clay-rich and silt-rich rocks and does not display widespread, regular cyclicity. As a result, only three formations are recognized: the thick, lithologically variable but mudrock dominated Karies Formation; the siltstone dominated Adolphspoort Formation; and the topmost mudrock-rich Sandpoort Formation (Thamm and Johnson, 2006).

2.2.3.3 Witteberg Group

The Witteberg Group caps the Cape Supergroup and, although similarly cyclic to the Bokkeveld Group, is lithologically intermediate to the Bokkeveld and Table Mountain Groups, having approximately balanced proportions of arenaceous and argillaceous rocks. The Witteberg Group is widespread in the Cape Basin, although it thins rapidly northwards in the western areas (Thamm and Johnson, 2006). The thickness of the Group is is given as over 2000 m by both Tankard et al. (1982) and Broquet (1992), but has been revised downwards by Thamm and Johnson (2006) to 1700 m, and as with the Bokkeveld Group, the thickest portions lie in the east. Not only does the abundance of sandstone increase relative to the underlying group, but the arenaceous units are more mature, and therefore lighter in colour, than the greywackes of the Bokkeveld Group, and in contrast to both the other groups of the Cape Supergroup, Witteberg Group sandstones are more micaceous (Gresse and Theron, 1992).

As with the Bokkeveld Group, the lower section of the Witteberg Group is broken into an eastern and western portion, this time along the 22° E meridian. The thinner western portion is called the Weltevrede Subgroup and is divided into the basal argillaceous Wagendrift Formation, the middle arenaceous Blinkberg Formation and the upper argillaceous Swartruggens Formation, whereas ironically, in the eastern areas where this package is thicker these units are all lumped into the Weltevrede Formation containing the Blinkberg Member, the arenaceous extension of the Blinkberg Formation (Thamm and Johnson, 2006). Running through the Witteberg Group distinctively, east and west, is the thick quartzose sandstone unit of the Witpoort Formation, which has not been assigned to any subgroup. The Witteberg Group draws its name from the low mountain range east of Touwsrivier, which in turn derives its name from the abundant exposures of the resistant, thick, white-weathering outcrops of the Witpoort Formation.

Overlying the Witpoort Formation is the Lake Mentz Subgroup, in which the Kweekvlei, Floriskraal and Waaipoort Formations form another clay-rich, sand-rich, clay-rich triplet across the whole basin. Above this, in the eastern area only, the Kommadagga Subgroup contains four formations, which tend to be less micaceous than the older formations. The basal Miller Formation, a diamictite with grit to pebble sized clasts, is followed and interfingers with the thin, pebbly quartz sandstone of the Swartwaterspoort Formation. These are overlain by the rythmically bedded shales of the Soutkloof Formation and finally the fine to medium grained sandstone of the Dirkskraal Formation (Toerien and Hill, 1989; Broquet, 1992; Thamm and Johnson, 2006).

2.2.4 Karoo Supergroup

The Karoo Supergroup covers over a third of the surface area of South Africa and reaches a total thickness of at least 4–5 km. Along the southern boundary of the Karoo Basin, it overlies the Cape Supergroup paraconformably to disconformably and extended over the current lines of mountains where it has been eroded away, evidence for this being outcrops of the lowermost units between Worcester and Robertson and even further south at Greyton (Gresse and Theron, 1992). These outliers aside, the Karoo Supergroup lies to the north of the southern arm and to the east of the western arm of the Cape Fold Belt. Only the two lowermost groups will be mentioned here, as they are the only ones that occur in any reasonable proximity to the Table Mountain Group.

2.2.4.1 Dwyka Group

The Dwyka Group is a succession of several different facies of diamictite, often repeated, to reach thicknesses of 800 m in the southern Karoo Basin. Except for two rare facies, an irregular or lensoid esker-like deposit and the variable sandstone facies, the matrix of all the diamictites and mudrocks is very fine grained, but with clasts that vary from the matrix up to large boulders (>1 m) in size (Johnson et al., 2006). The extremely varied lithological composition, size and angularity of the clasts have, amongst other properties, led to interpreting the Dwyka Group as glacial and ice-sheet deposits.

2.2.4.2 Ecca Group

This group of diverse formations formed in marine environments and is dominated by fine grained rocks, mostly shales and mudstones with some chert and tuff present; although moderately arenaceous rocks such as greywacke do occur. The Ecca Group overlies the Dwyka Group conformably and is around 2-3 km thick along the southern margin of the Karoo Basin where it occurs within the northern limit of the Cape Fold Belt (Johnson et al., 2006).

2.2.5 Younger Rocks

Rocks from the Cretaceous and Tertiary form minor yet significant components in the geology of the study area. All of these rocks are younger than the Cape Orogeny and therefore have experienced very little deformation. Most are lithified, although this becomes weaker and eventually non-existent with the very youngest formations.

2.2.5.1 The Uitenhage Group

The Uitenhage Group is a set of Mesozoic deposits that fill basins along the coast and in valleys within the Cape Fold Belt. Stretching from Worcester eastwards to Algoa Bay, the current distribution is not continuous, mainly due to the originally sporadic occurrence of the depocentre basins, but also because of some subsequent erosion. The various sub-basins are cumulatively

called the Outeniqua Basin, which has both onshore and offshore components, the latter of which will not be mentioned further here. The basins are typically half-grabens with the deeper, faulted edge being to the north, except for the largest, the Algoa Basin, which is more complex and has full graben structures (Shone, 2006; Dingle et al., 1983). Sediment reaches to around 3 km thickness in the deeper basins and thins distally, to the south. The Uitenhage Group comprises 3 formations; all 3 only occur in the Algoa and Oudtshoorn Basins and all other basins contain only the basal Enon Formation.

Enon Formation

The Enon Formation reaches 3 km thickness and is a very distinctive coarse conglomerate of well rounded Cape Supergroup quartzite pebbles and cobbles that generally weathers to dark red in outcrop, although yellow and grey colours also occur. The matrix of grit, sand and silt is cemented by red limonite and the formation can develop high, steep cliffs. Minor siltstone and sandstone lenses do occur (Shone, 2006).

Kirkwood Formation

This is a poorly cemented succession of coarse to medium grained lithic sandstone, siltstone and mudstones, reaching 2 km thickness (Shone, 2006).

Sundays River Formation

Attaining a similar thickness to the Kirkwood Formation, this formation consists of fine to medium grained, sometimes shelly, moderately cemented sandstone, siltstone and mudstone (Shone, 2006).

Cenozoic Deposits

Cenozoic deposits in the study area come in several different forms, including lithified and unlithified coastal deposits, various terraces and ancient duricrusted landsurfaces inland and on the coastal plain, more recent pedogenic duricrusts, minor alluvial, lacustrine, spring and other deposits, and ubiquitous scree and soil. Only the coastal and ancient terrace deposits will be considered here, as the others tend to be thin or scattered (Partridge et al., 2006).

Due to the primarily erosional nature of the southern African subcontinent since 65 Ma and because of the high gradient of the land surface, accumulations of most Cenozoic materials on land tend to be thin. The coastal deposits fall into 4 groups based on position along the coast.

2.2.5.2 The Algoa Group

This group largely falls outside the study area, being found from Plettenberg Bay to Port Edward. It consists of 6 formations, made up mainly of limestone, conglomerate, shelly deposits, calcareous sand and loose sand (Roberts et al., 2006).

2.2.5.3 The Bredasdorp Group

The Bredasdorp Group occurs from Plettenberg Bay to Cape Hangklip and typically overlies the Table Mountain or Bokkeveld Groups, or in places the Enon Formation, or in the George area the

Kaaimans Group and Cape Granite Suite. A highly simplified stratigraphic summary is given here.

The lowermost, thin De Hoop Formation (≤17 m) is a shelly version of the thick overlying Wankoe Formation calcarenite (≤290 m). Above this lies the thin, shelly, pebbly, quartz sand of the Klein Brak Formation (≤10 m), followed by aeolianite and calcrete of the Waenhuiskrans Formation (≤60 m) and topped by unconsolidated sand of the Strandveld Formation (≤100 m) (Roberts et al., 2006).

2.2.5.4 The Sandveld Group

The Sandveld Group is found from False Bay in the south to Elands Bay on the west coast. It generally overlies either Malmesbury Group or Cape Granite, but in the Elands Bay vicinity overlies the Table Mountain Group. The areas of greatest thickness are developed in bedrock depressions controlled by rock type and structure. A highly simplified stratigraphic summary is given here.

The basal Elandsfontyn (≤70 m) and generally overlying Varswater (≤60 m) Formations consist primarily of sand with minor carbonaceous clay and lignite layers and pebbles in places. North of Saldanha Bay, the Prospect Hill Formation (≤70 m) lies below the Varswater Formation and is made up of bioclastic aeolianite, often reddish. Overlying the Varswater Formation is the thin gravelly and shelly Velddrif Formation (about 7 m), followed by the calcarenite and calcrete layers of the thicker Langebaan Formation and capped by unconsolidated quartz sand and then calcareous sand of the Springfontyn and Witzand Formations, respectively (Roberts et al., 2006).

2.2.5.5 The West Coast Group

From Elands Bay to the Orange River mouth another series of coastal formations occurs. These formations overlie the Table Mountain Group in the southern area, from Elands Bay to north of Papendorp, where the very north-westernmost outcrops/subcrops of the Table Mountain Group are found. Although only the Alexander Bay and Curlew Strand Formations have been named, other units overlie and underlie these. Overall the group is dominated by sand, with minor mud, calcified sand, gravel and other rock or sediment types (Roberts et al., 2006).

2.2.5.6 The African Surface

Erosion and planation across southern Africa in the Tertiary led to the development of what is referred to as the African Surface. Remnants of this surface are still found today and are characterized by a duricrust, up to 8 m thick (SACS, 1980), overlying a thick weathered profile, usually kaolinitic and up to 50 m thick (Partridge and Maud, 1987), although this is not always the case and depends on the bedrock. Interestingly, the duricrust may be composed of silcrete, calcrete or ferricrete (Dingle et al., 1983). Subsequent erosional surfaces, the most notable being the *post-African I* and *post-African II* have not developed significant profiles of either weathered or consolidated material (Partridge and Maud, 1987; Partridge et al., 2006).

Figure 2.4: View south-west from the Matroosberg rainfall collector site looking along the hinge of the Hex River anticline in the syntaxis of the Cape Fold Belt. The fractured nature of the Table Mountain Group formations is apparent in this photograph. Two faults, both with limited displacement on them (tens of metres at most), are indicated.

2.3 Geology — Structure

The Table Mountain Group was deformed during the Cape Orogeny, a multiphase compressional tectonic event spanning the Permo-Triassic boundary, with four episodes of deformation having been dated: 278, 258, 247 and 230 Ma (Hälbich, 1992). Deformation occurred in such a way that three major structural domains are evident. The western branch of the Cape Fold Belt with open, upright folding and normal faulting is arcuate and convex inland, striking in a north–south direction in the southern parts near Paarl, and north-northwest–south-southeast in the northern parts near Vanrhynsdorp. The southern branch of the Cape Fold Belt is similarly arcuate and convex inland, but with folding and faulting striking east–west at the western end near Robertson and east-southeast–west-northwest in the eastern parts near Port Elizabeth. Deformation in the southern branch is more intense, with strong northward vergence, overturning and thrusting. The

southern and western branches merge in the syntaxis, stretching from the coast at Hermanus to the Karoo near Touwsrivier. In this domain, folding and faulting is more chaotic, although mainly striking north-east–south-west, and deformation is intense (Söhnge, 1983; de Beer, 2002).

Throughout the Cape Fold Belt, the compressional tectonic regime that reigned during the Cape Orogeny was inverted (became extensional) upon breakup of Gondwana during the Triassic and Cretaceous (de Wit and Ransome, 1992). Hälbich (1992) shows that both new faults with normal movement probably developed and some of the previous reverse faults were reactivated and experienced normal motion as the continents moved apart. This is most clearly demonstrated by the Cretaceous graben or half-graben basins in which the Uitenhage Group was deposited. Of note are the Kango and Worcester Faults, which have normal vertical displacements up to several kilometres and have moulded the mega-scale geography of the Western Cape, in which the TMG is duplicated, forming parallel rows of 2000 m high mountains.

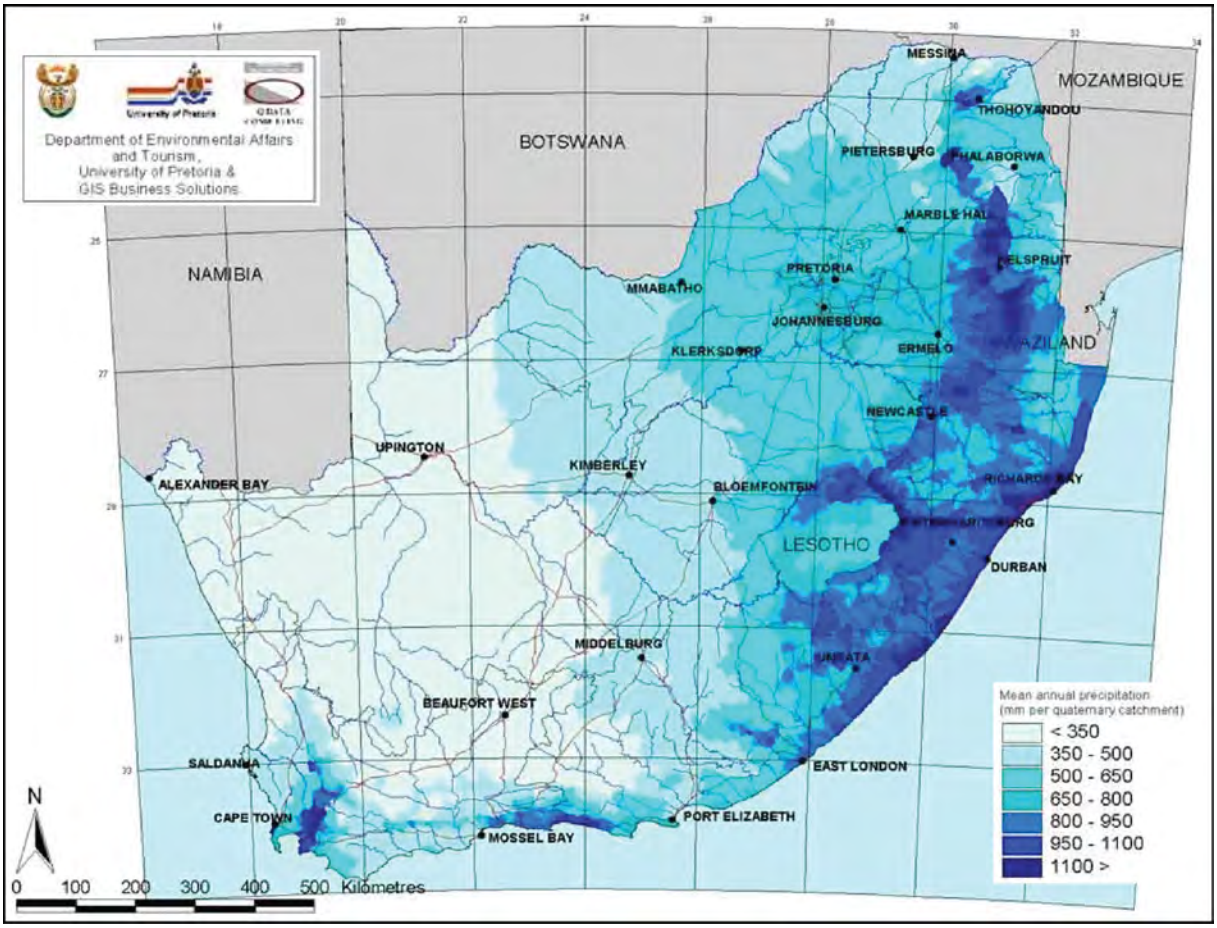

Figure 2.5: Mean annual precipitation map for South Africa.

2.4 Climate and Weather

The climate and weather of an area has an equal importance to the geology in determining the hydrogeology of an area. Various aspects of the climate, such average annual rainfall and seasonality of rainfall and temperature are important. The weather too plays a role in determining the hydrogeology as it dictates the intensity and duration of rainfall events, the reliability of rain bearing storms and the forms of precipitation that occur. Very importantly, all of this influences the isotopic composition of the precipitation and a thorough understanding of the climate and weather is essential for interpretation of the measured isotopes.

In 1911, Alexander Knox, a member of the convocation of the University of the Cape of Good Hope (a previous name for The University of Cape Town), had this to say in the opening of the chapter on South Africa in his book *The Climate of the Continent of Africa*: "Speaking generally of Southern Africa south of, say, 19° or 20° S., it may be said that the rainfall increases from west to east along any parallel, except in the extreme south of Cape Colony where irregularities exist, ... " (Knox, 1911). It is within these "irregularities" that the study area wholly falls and therefore, a brief mention of the climate and weather patterns is warranted. The study area experiences a wide range of climates due to three main factors, these being size, position and geography.

The size of the study area is somewhat over 100 000 km^2, encompassing most of the Western Cape and going into the Eastern Cape. This is large enough to experience gradients in climate simply due to distance. The position of the study area at the southernmost tip of Africa places the region just far south enough to be within the westerly wind belt and experience mid-latitude cyclones regularly in winter and occasionally in summer. However, the region is still close enough to the equator that it experiences tropical influences in summer and is on the fringes of the global southern desert belt, centred along the 30th parallel. The position is also unique in that the region is subjected to effects from both the cold upwelling of the Benguela Current on the west coast and the warm, tropically derived water of the Agulhas Current on the east and south coast. Finally, the geography of the region is complex, with variations in climate caused by the coast to inland gradient and the presence of mountain ranges, which block or funnel weather systems around, generate orographic rainfall and cause rain shadows.

Climate in the study area ranges from *warm temperate* along the south coast, where rain falls all year round, especially against the south-facing slopes of the Langeberg, from Swellendam to Port Elizabeth, to *hot desert* in the Tankwa Karoo, where some years there is no rain.

2.4.1 Rain

Cape Town experiences a typical *Mediterranean* climate with cold wet winters and warm dry summers. Moving north from Cape Town, the winter rainfall decreases until desert conditions are reached at the Gariep River; moving north-east, the winter rainfall decreases and summer rainfall increases until the central Karoo which experiences only summer rainfall; moving east,

winter rainfall is maintained and summer rainfall increases, until the coast veers north-east at Port Elizabeth, cutting out winter rain by East London. The general pattern of rainfall is greatly modified by mountains, as seen in **Figure 2.5**. Rainfall is increased in the immediate vicinity of mountains, both the windward and leeward side, and only a significant distance beyond the leeward mountain flank does the rainfall decrease.

The above patterns are illustrated in the diagrams in **Figures 2.6 & 2.7**. The decrease in rain northwards is seen by the drop in rainfall from Cape Town to Vredendal. At the same latitude as Vredental, rainfall increase due to both some summer rain and the effect of elevation can be seen at Calvinia. The change from Cape Town to Robertson shows three effects: decreasing winter rain because of distance eastwards; decreased rainfall because of a rain shadow behind the first line of mountains of the Cape Fold Belt; and a small increase in summer rain. The difference between Cape Town and Port Elizabeth shows a clear decrease in winter and increase in summer rain. The same two effects are visible at George, as well as an overall increase caused by proximity to the Outenikwa (Langeberg) Mountains. George to Oudtshoorn illustrates the combined effect of rainfall decreases from the coastal-inland gradient and a rain shadow.

The study area has a remarkable array of weather scenarios that can produce rain. A brief discussion of these follows, based largely on Preston-Whyte and Tyson (1988) and SAWB (1996). There are 5 main weather scenarios that can cause rain and all of these are related to some form of pressure trough of cyclonic feature (both low pressure) at the surface and into the middle and sometimes upper atmosphere. Of these 5, 4 occur in conjunction with or after the passage of a frontal depression, also known as a mid-latitude cyclone.

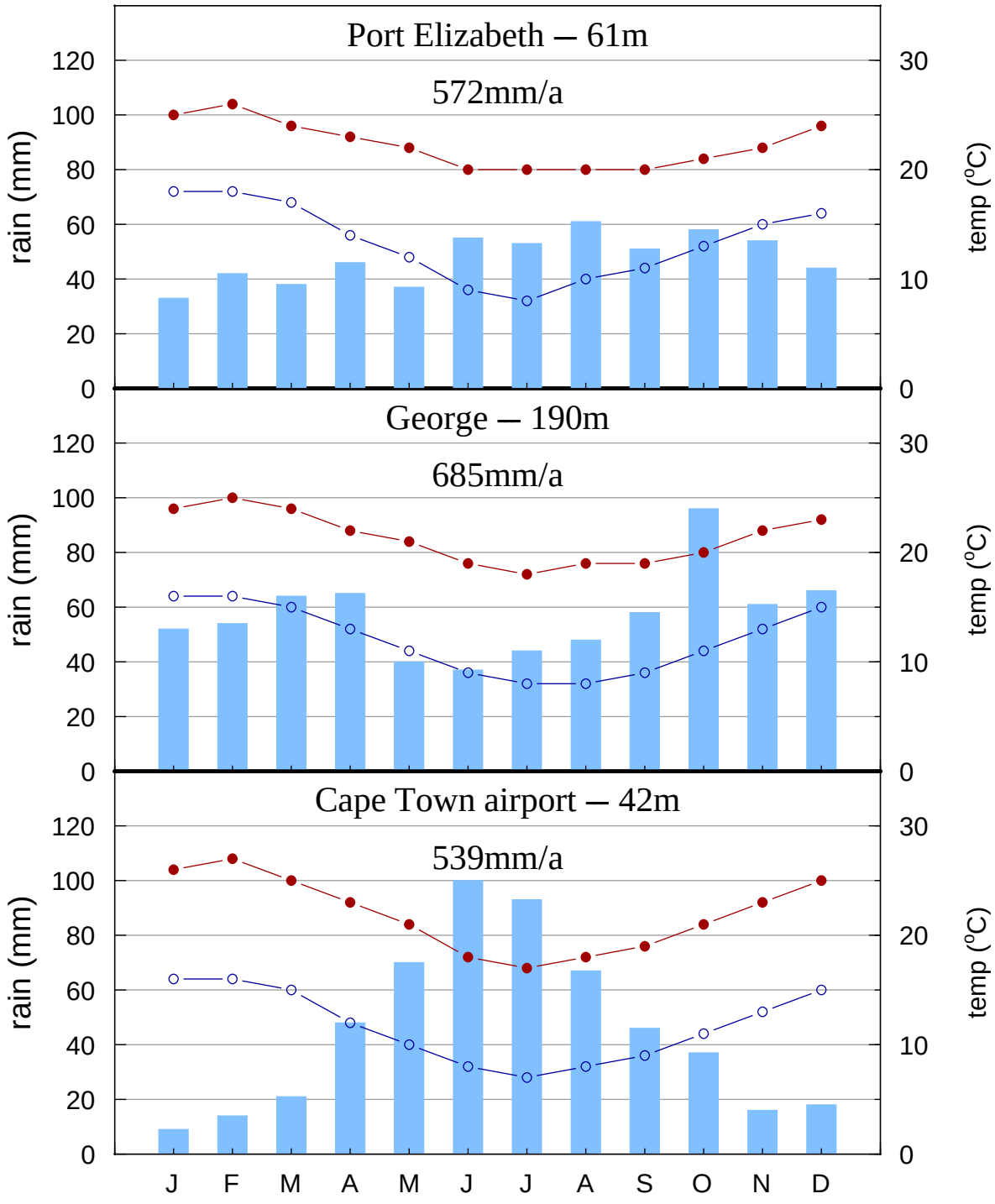

Figure 2.6: Rainfall and minimum and maximum temperature graphs for selected locations in the Cape Fold Belt region. The station altitude is given in metres above sea level. Locations are shown in the map in Chapter 1. Data for 1979–2000 (CSAG, 2013).

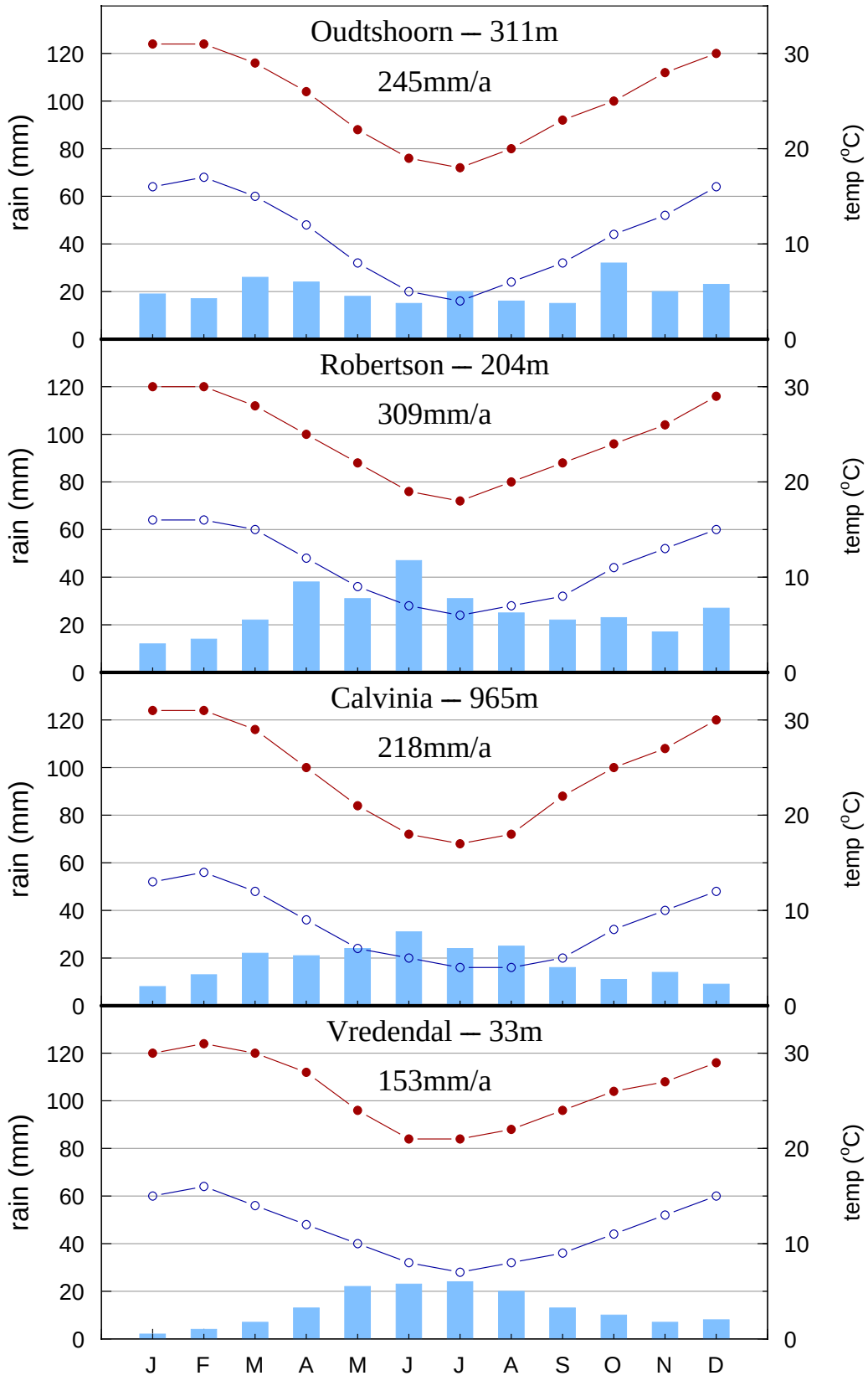

Figure 2.7: Rainfall and minimum and maximum temperature graphs for selected locations in the Cape Fold Belt region. The station altitude is given in metres above sea level. Locations are shown in the map in Chapter 1. Data for 1979–2000 (CSAG, 2013).

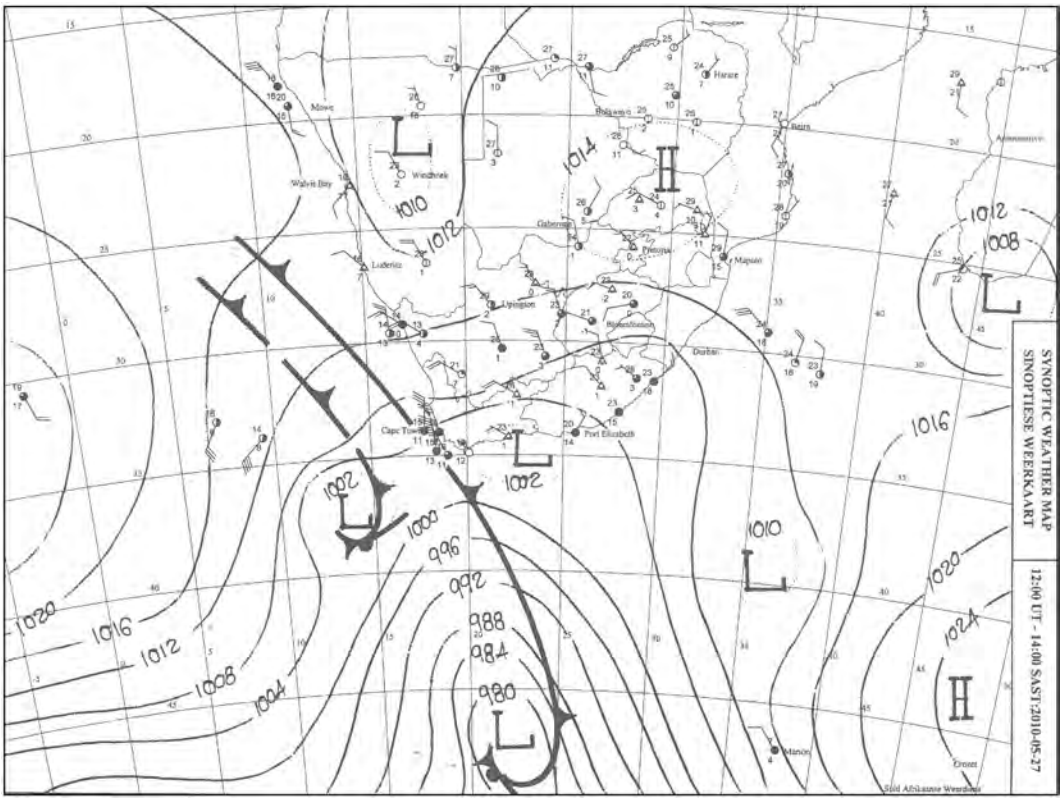

Figure 2.8: Synoptic chart from SAWS for 14h00 SAST on 27th May 2010 in which a westerly wave can be seen approaching South Africa. Rainfall from this system on this day was up to 73 mm, at Kirstenbosch and reached far north, with 10 mm at Springbok and 3 mm even at Alexander Bay.

2.4.1.1 Westerly Wave

Frontal depressions form at the polar front, at around 60°S in the south Atlantic Ocean, and move north-eastwards until they begin to decay and move south-eastwards. They feature a warm front and cold front, where air masses of different temperature meet, and the whole system rotates clockwise in the southern hemisphere. If they move far enough north, they can push a cold front over southern Africa. Uplift of warmer, moist air ahead of the cold front can cause a line of continuous rain at the front typically lasting a few hours, and instability behind the front can lead to typical intermittent 'clearing showers' that may persist for a day or two. Rainfall is mainly in the south-western Cape, but can, in extreme cases, once or twice a year, occur over the whole subcontinent, even precipitating rain or snow as far north and inland as Windhoek and Johannesburg. The example in **Figure 2.8** shows the wave shape of the isobars as the system moves west to east.

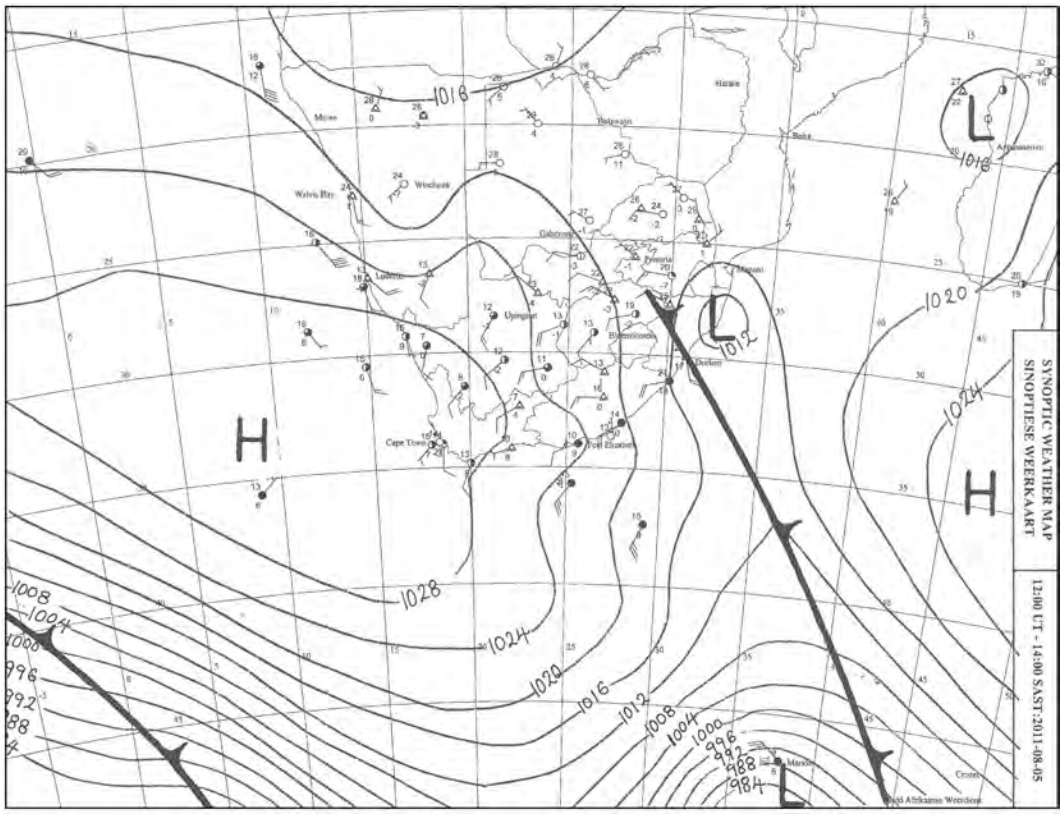

Figure 2.9: Synoptic chart from SAWS for 14h00 SAST on 5th August 2011 in which post-frontal conditions are causing southerly meridional flow. Rainfall was up to only 11 mm, at Mossel Bay, but was widespread, occurring at almost every SAWS station in the Western Cape as well as into the southern parts of the Northern Cape.

2.4.1.2 Southerly Meridional Flow

After the passage of a cold front, strong southerly airflow can persist for a day or two, starting off as south-westerly airflow immediately after the passage of the cold front, and then swinging to southerly flow (**Figure 2.9**). This usually advects very cold air and showers to the southern Cape and Eastern Cape coastal regions. Snow on mountains of the Western and Eastern Cape can result. Much of the rain in the central parts of the Western Cape results from this weather pattern, as the frontal rain that approaches from the north-west and west has fallen out on the western peaks of the Cape Mountains and so these central regions are in a rain shadow for westerly winds.

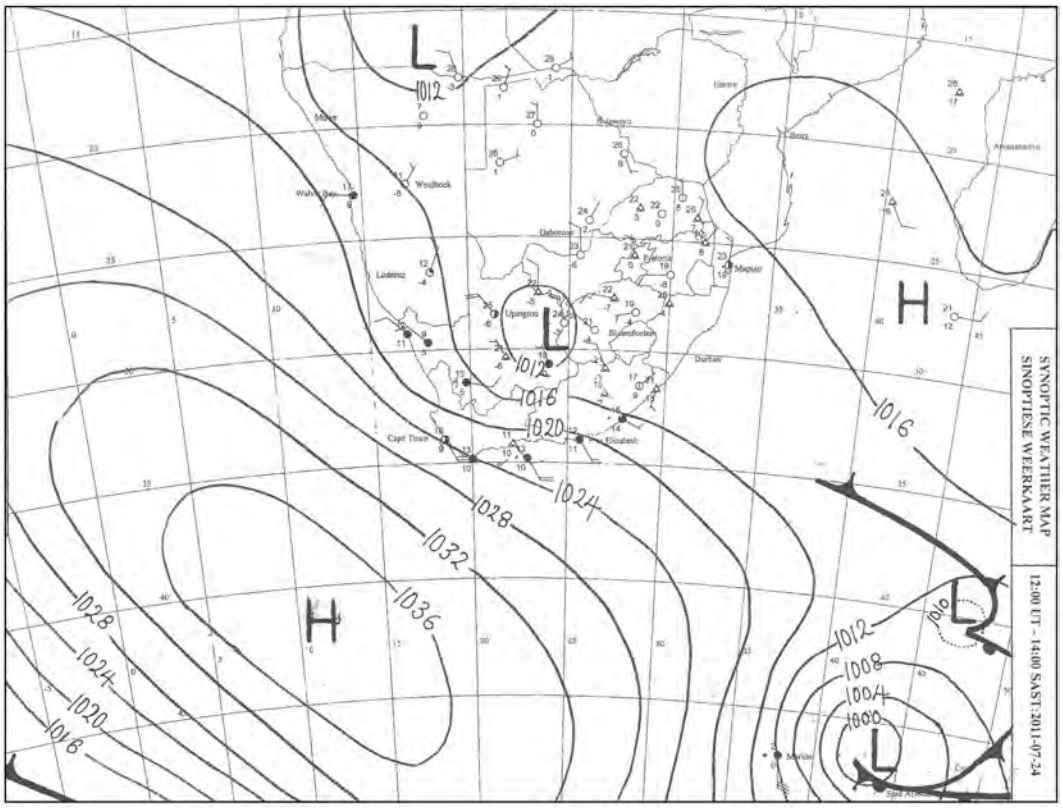

Figure 2.10: Synoptic chart from SAWS for 14h00 SAST on 24th July 2011 in which the South Atlantic High Pressure is moving south-eastwards after the passage of a cold front, seen dissipating to the south-east. Rainfall from this system was concentrated in the southern and eastern portions of the Western Cape, with up to 68 mm for the day, at George.

2.4.1.3 Ridging Anticyclone

A day or two after the passage of a cold front, the South Atlantic High Pressure cell can ridge south of the subcontinent. Moisture is picked up off the Indian Ocean and advected into an area of unstable conditions. The rainfall that results is usually confined to the eastern and central parts of the country with only orographically induced cloud evident in the far west, but when this system intensifies, the rain becomes more widespread in the eastern or central parts and the orographically induced cloud in the west increases to the point where it precipitates. This condition is known as a *black south easter*, named for the low, dark clouds that accompany this type of rain event. The normal white, fluffy or smooth *table cloth* on Table Mountain thickens and emits rain, often at a 45° angle or less, due to the intense wind, from the base of the darkened cloud. Ridging anticyclones typically cause rainfall in the eastern and southern portions of the Western Cape, as occurred in the example given in **Figure 2.10**.

The westerly wave, southern meridional flow and ridging anticyclone above are common weather scenarios, although a black south easter develops only infrequently, a few times per year. The cut-off low and west coast trough described below are not common.

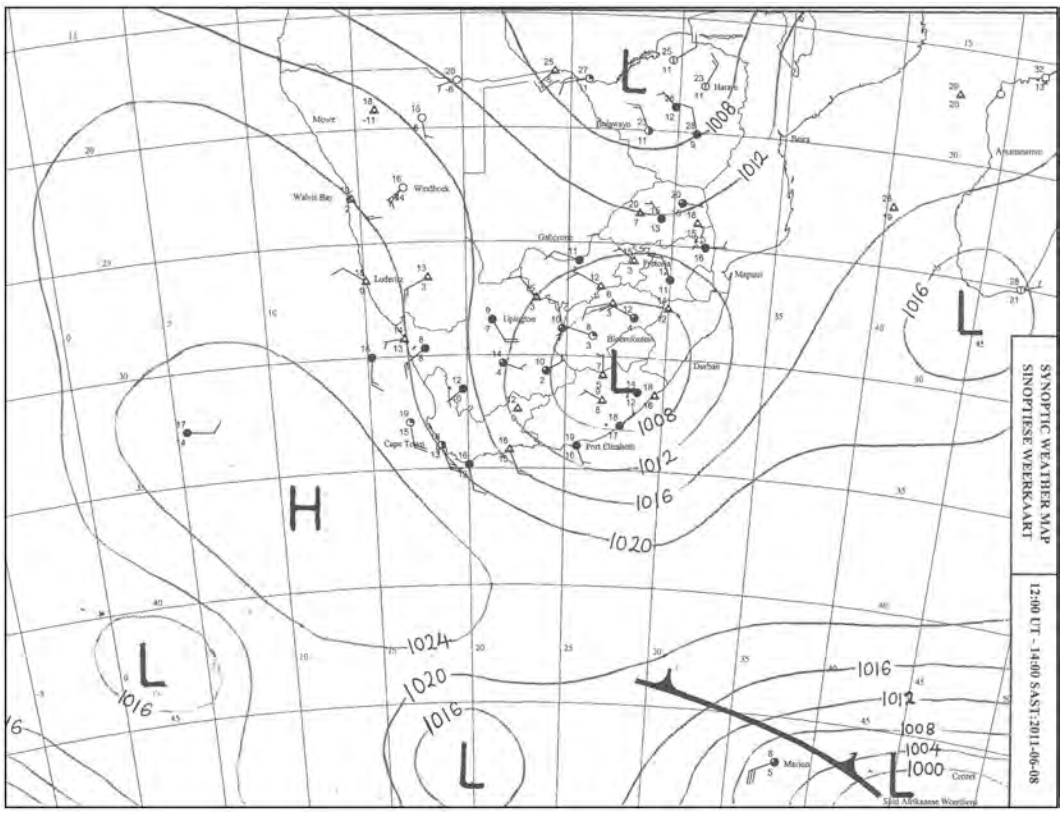

Figure 2.11: Synoptic chart from SAWS for 14h00 SAST on 8th June 2011 in which a cut-off low can be seen over the Eastern Cape. This system started south-west of the country on the 6th and intensified, exiting the country to the south-east on the 9th and dissipating thereafter. Rainfall from this system on this day (8th) reached 103 mm, in Ladismith.

2.4.1.4 Cut-Off Low

A cut-off low occurs when a cold front spawns a closed cyclonic cell that drifts northwards, out of the westerly wind belt. The cut-off low is a deep system with substantial uplift and generates heavy rain. As the low is out of the flow of the westerlies, it is often stationary or slow moving and the rain therefore falls on a relatively small area and can be for a period of days, usually causing floods. The example in **Figure 2.11** shows the most intense, third day of a four day cut-off low system, where rain occurred over the whole of the Western Cape, starting in the west and moving east. The floods of January 1981 that nearly obliterated the small town of Laingsburg were caused by a cut-off low. These systems can affect most of the country, but particularly the southern portions.

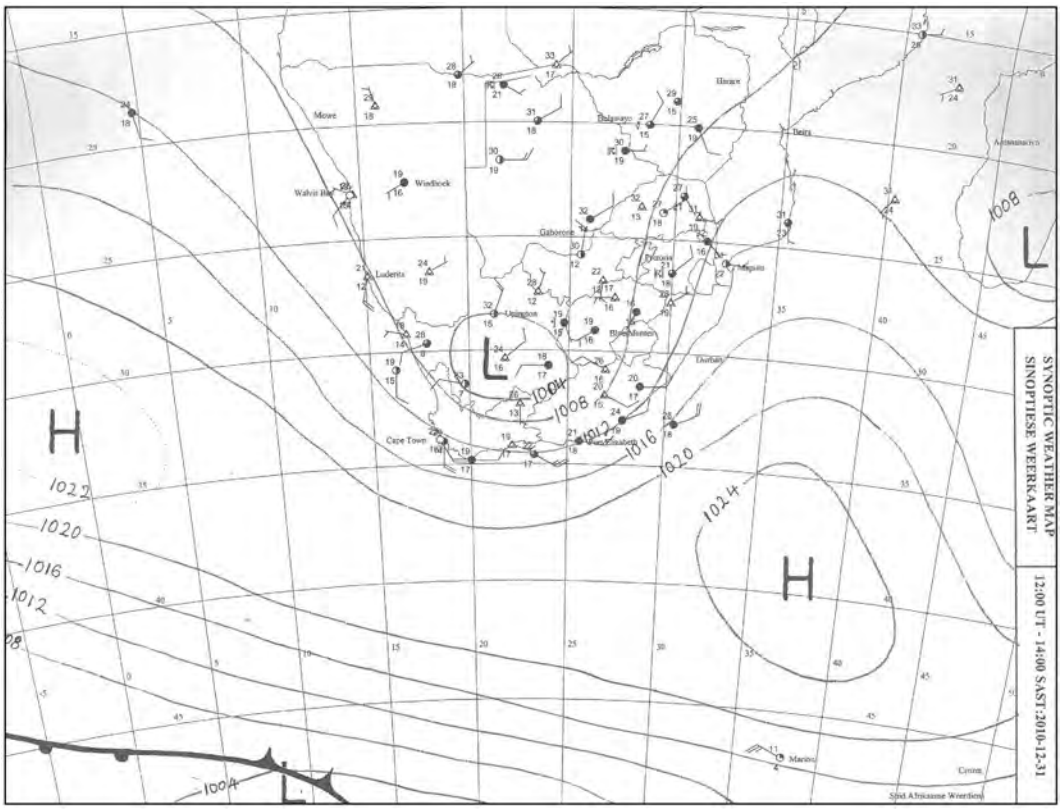

Figure 2.12: Synoptic chart from SAWS for 14h00 SAST on 31st December 2010 in which a trough near the west coast is causing significant rainfall in the Western Cape. Rainfall on this day reached 26 mm, at Beaufort West, and continued the next day, with up to 19 mm, at Excelsior Ceres.

2.4.1.5 West Coast Trough

This is the only weather pattern discussed here that may have no association with a frontal depression. Although the weather pattern may develop several times per year, rainfall from this system is less frequent. The rain that results usually falls in the central, southern and eastern parts of the country, but it is one of the few systems that can bring significant rain to the far west desert areas. The trough is a region of low pressure that develops west of the country, as the name suggests, and deepens and strengthens as it moves south-eastwards, as these systems generally do. The system shown in **Figure 2.12** was stationary for about two days, generating widespread rain over the Western Cape, with some heavy falls of rain and hail from thunderstorms. Rain typically occurs in the west if the system had its genesis far out in the Atlantic and had time to develop rain-bearing clouds by the time it makes landfall on the west coast.

2.4.2 Temperature

The study area experiences mostly moderate temperatures, although there are extremes of heat in the dry areas and cold on the mountain tops. Temperatures near the coast are more consistent (see Cape Town and Port Elizabeth), being moderated by the presence of the ocean and the more humid air. Inland temperatures are more extreme, with greater daily and seasonal ranges (see Oudtshoorn and Robertson). The effect of altitude reduces temperatures (see Calvinia). Interestingly, the annual average temperatures do not vary much, being from 16.5–19 °C for the selected stations.

2.5 Hydrogeology

2.5.1 Porosity and Permeability

The Table Mountain Group is largely composed of quartzose sandstones, a rock type that would generally exhibit a primary porosity of 5 to 30 % , depending on coarseness and sorting (Domenico and Schwartz, 1998, p.14). However, burial and diagenesis during the Cape Orogeny reached lowermost greenschist facies (not exceeding 300 °C), sufficient to result in conversion of most of the sandstones to quartzite (Frimmel et al., 2001). The changes in porosity that occur during diagenesis are complex and include mechanical rearrangement of the matrix, partial dissolution of sediment grains and precipitation of new minerals (the cement). In the case of the Table Mountain Group, silica was dissolved from the quartz sand grains and reprecipitated to the extent that the rock has been thoroughly recrystallized and virtually no primary porosity remains (Rosewarne, 2002b).

However, the Table Mountain Group contains abundant secondary porosity due to fractures (see **Figure 2.13**. The great thickness of quartzose sandstones has predisposed the rocks to brittle behaviour under stress and the thorough recrystallization of the Table Mountain Group formations has only made the units more competent and therefore subject to an even greater degree of brittle failure (Kotze, 2002). Fractures in the Table Mountain Group have developed in relation to folding, faulting and cleavage formation, but also include bedding planes, as can be seen in **Figure 2.14**. Up to a point, the more deformation, the greater the degree of fracturing and therefore secondary porosity. However, there is a limit to this and zones of extreme deformation, or cataclasis, often have experienced intense silicification that closes or partially blocks openings and thereby reduces permeability (de Beer, 2002).

In the absence of any porosity measurements for the TMG, general models of porosity can be instructive. For rocks with fracture porosity, three possible broad classes exist, as shown in **Figure 2.15**: one, single porosity from major fractures only; two, dual porosity of major fractures and intergranular, primary porosity; three, dual porosity of major and minor fractures. Kotze (2002) maintained the Table Mountain Group has a dual porosity of major and minor fractures, at least as was observed in the Peninsula aquifer in the Kammanassie Mountains. This dual fracture

Figure 2.13: Groundwater discharging as seeps from fractures in quartzite of the Skurweberg Formation on the Spout at Cederberg Tafelberg. The fractures are horizontal bedding planes and vertical joints.

porosity model may operate at numerous scales and in fact be a multiple level phenomenon with fractures or fracture systems being found at many scales, from regional or mega-fault structures, through local and outcrop scale, to hand specimen size. Mapping as done by Hartnady and Hay (2002c) using remote sensing techniques gives some indication of this at the regional to local scale in **Figure 2.16** and at the local to outcrop scale in **Figure 2.17**.

Groundwater discoveries support this multilevel fracture model because water strikes during drilling can give an order of magnitude difference in water yield. For example, borehole BK4 drilled in the Citrusdal Valley in 1997-8 yielded a 5 L/s blowyield until, at 220 m depth, a major water strike allowed blow yields of around 100 L/s to be realised (Hartnady and Hay, 2002a). The low yield was presumably from minor, more common fractures encountered through much of the borehole, and the very high yield corresponds to intersection of a major, regional scale fracture or fracture system.

Although the commonly held belief is that fracture density decreases with depth, it seems that this might only occur at a very low rate, or at great depths (more than 1 km) in the Table Mountain Group. Lin et al. (2007) recorded a very weak negative correlation between fracture density and depth over a vertical distance of 750 m in the Piekenierskloof Formation; in other words, there was only a marginal decrease in fracture density with depth.

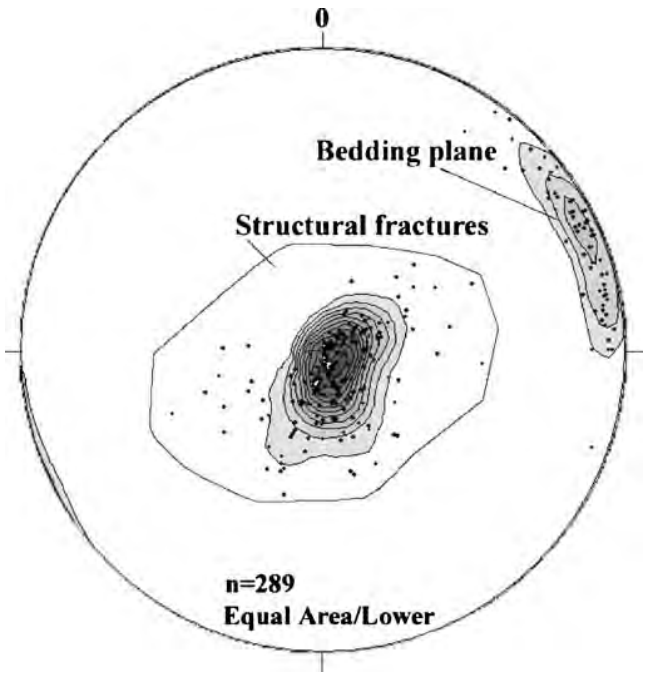

Figure 2.14: Fracture measurements (strike and dip) taken at surface in the Piekenierskloof Formation between Lamberts Bay and Graafwater, showing the separation between near horizontal bedding planes and near vertical structurally formed fractures. From Lin et al. (2007).

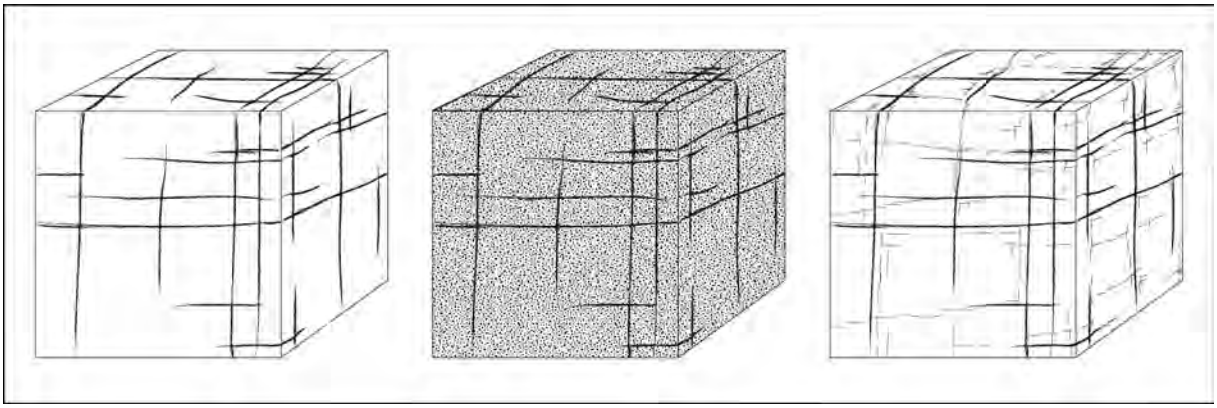

Figure 2.15: Theoretical models of possible fracture porosity: one, major fractures; two, major fractures and primary porosity; three, major and minor fractures. After Kruseman and De Ridder (1994) as cited in Woodford (2002).

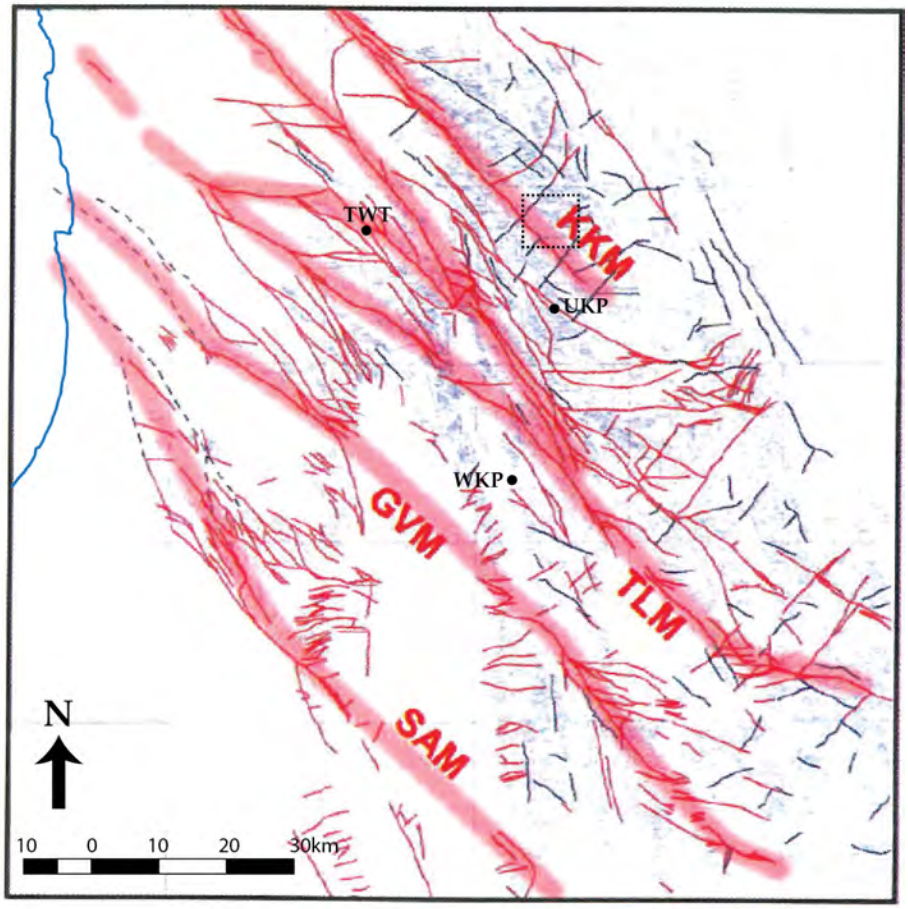

Figure 2.16: A fault and fracture trace map for the Cederberg–West Coast region showing mapped faults from the 1:250 000 geology maps as thin red lines, and additional mapped or remoted derived fracture traces, from Landsat, SPOT or aerial photographs, as thin black lines. The area includes outcrop of all formations within the Table Mountain Group. Large regions with few structures (in the south-west) are areas where the Malmesbury Group is exposed. SAM - Saron-Aurora megafault; GVM - Gydo-Verlorenvlei megafault; TLM - Twee Riviere-Leipoldtville megafault; KKM - Krakadouw-Klawer megafault. The dotted black square shows the location of **Figure 2.17**. From Hartnady and Hay (2002c).

2.5.2 Hydraulic Parameters

Aquifers can be defined in several ways, including geology, structure and spatial occurrence. The ability of an aquifer to conduct water is typically described by three hydraulic parameters: the hydraulic conductivity (K), the transmissivity (T) and the storativity (S). Hydraulic conductivity is a measure of permeability; transmissivity is a measure of the total flow possible along a vertical line through the aquifer and is calculated by multiplying the hydraulic conductivity by the aquifer thickness, and it gives some indication of the possible borehole yields or flow rates; storativity measures the amount of water released from a confined aquifer per unit drop in hydraulic head and gives an indication of how much water can be abstracted. All of these parameters are derived

location	aquifer	K m/d	T m^2/d	S	source
Lamberts Bay	Piekenierskloof	0.00069			Lin et al. (2007)
The Baths, Citrusdal	Peninsula	0.002 - 2	10 - 200	0.0001 - 0.001	Umvoto and SRK (2000)
Roode Elsberg, Hex	Peninsula	0.26			Brink (1981)
Villiersdorp	Peninsula	017			Brink (1981)
Kammanassie	Peninsula			0.01 - 0.05	Kotze (2002)
Lakenvalley, Hex	Skurweberg	0.26			Brink (1981)
Kouga Dam	Skurweberg	0.07			Brink (1981)
Villiersdorp	Skurweberg	0.3			Rosewarne (2002b)
Agter Witzenberg	Skurweberg	0.05			Weaver et al. (1999)
Kleinmond	Skurweberg		70 - 320	0.0001 - 0.0005	Parsons (2002)
St Francis on Sea	Skurweberg		100	0.0018 - 0.0033	Rosewarne (2002b)
Struisbaai	Pen/Skbg		15 - 200	0.0086	Weaver et al. (1999)
Uitenhage	Pen/Skbg		10 - 400	0.0002 - 0.05	Maclear (2002)
Cape Fold Belt	TMG			0.001	Vegter (1995)
Cape Fold Belt	TMG			0.0032 - 0.015	Weaver et al. (2002)

Table 2.1: Hydraulic parameters (K - hydraulic conductivity, T - transmissivity, S - storativity) for aquifers of the TMG, based on calculations from pumping tests, conceptual or numerical models and other estimates. Table is based on a compilation by Rosewarne (2002b).

from borehole pumping tests and are best suited to homogenous, isotropic, primary porosity aquifers. The Table Mountain Group may fit the characteristic of being homogenous, but it is anisotropic because of the preferential directions in which fractures have developed (see **Figure 2.14**) and it is of course a secondary porosity aquifer. In addition, the very size of the Table Mountain Group, even simply the depth at one locality, never mind the vast horizontal dimensions, makes the aquifer difficult to quantify, not only theoretically, but in a very practical sense; i.e. the cost and effort of drilling a fully penetrating borehole, even through just one formation (e.g. Peninsula), is in most cases immense. For these reasons there are few reliable estimates of the three hydraulic parameters for the Table Mountain Group.

Rosewarne (2002b) collated some hydraulic parameters for the TMG; these have been reproduced here in **Table 2.1** with some rearranging and additions.

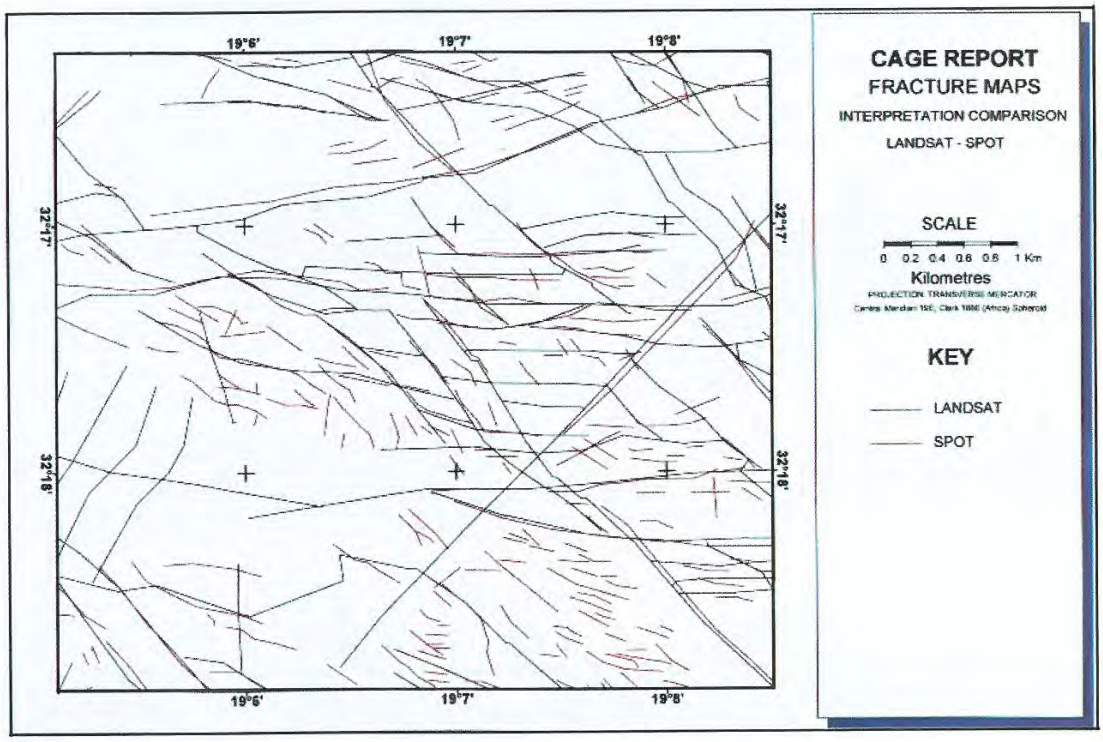

Figure 2.17: A detailed fracture trace map for a small area of Peninsula Formation outcrop, shown as the region in the dotted black square in **Figure 2.16**. Fracture traces derived from Landsat images (black lines) and SPOT satellite images (red lines). The diagrams shows how fractures occurs in parallel sets that often intersect and that many fractures are short and some, typically associated with local to regional faults, are much longer. From Hartnady and Hay (2002c).

2.5.3 Hydrostratigraphy

The Table Mountain Group is not a simple, single aquifer with a neat geometrical shape, but rather an interconnected aquifer system, semi-continuous in space, with an extremely complex three dimensional form and multiple aquifers. The highest parts of the aquifer are over 2000 m above sea level and form the crests and peaks of mountain ranges, mainly comprising the Peninsula Formation, but also the Nardouw Subgroup, especially the Skurweberg Formation. The lowest parts of the aquifer reach depths of 5–6 km below sea level along the Worcester and Kango Faults (see the cross-sections in Chapter 5), and in places the Table Mountain Group outcrops or subcrops beneath the sea bed, to a distance of at least tens of kilometres offshore. There is no location where all the Table Mountain Group formations occur, from Piekenierskloof or Sardinia Bay Formation to Rietvlei or Baviaanskloof Formation, however the succession from Peninsula to Rietvlei Formation is preserved in many areas and probably reaches 4000 m true thickness (perpendicular to the formation contacts), especially in the southern branch of the Cape Fold Belt where structural thickening has been substantial.

Hydrogeologists have traditionally only recognized the terms aquifer and aquitard for geolog-

ical units that do and do not conduct significant quantities of groundwater. These are relative terms and factors such as depth, thickness, economics and demand for water are almost as important as the actual hydraulic parameters of the unit in determining which term to apply. In addition, the term aquiclude is sometimes used as a synonym for aquitard, although Poehls and Smith (2009) maintain the term aquiclude should be reserved for extremely impermeable formations. It is important to realise that hydrostratigraphic units may or may not overlap with geological units; an aquifer may be only a part of a geological formation, or several geological formations may constitute one aquifer, and similarly for aquitards. Furthermore, there was no accepted heirarchy of hydrogeological units, such as the familiar geological *member*, *formation*, *group* and other categories.

Al-Aswad and Al-Bassam (1997) have created a hydrostratigraphical nomenclature, but even this is inadequate under many common geological situations where layers are lenticular, where folding has occurred and even more so in a faulted environment, where substantial flow along faults through aquitards connects different aquifers, or different aquifers are faulted into direct contact with each other. All of the above occurs in the Cape Fold Belt. For example, Rosewarne (2002a) found the Bokkeveld Group sandstone layers to deliver high yields, because leakage from the underlying Table Mountain Group into these sandstone layers occurred once they had been pumped. The high hydraulic head of the underlying Table Mountain Group was due to recharge in the adjacent Skurweberg mountain range and allowed this groundwater to leak upwards and recharge the Bokkeveld Group sandstones.

Using the Al-Aswad and Al-Bassam (1997) system yields a classification for the Cape Supergroup as shown in **Figure 2.18**. Each geological formation can be roughly evaluated as either an aquifer or aquitard. Aquitards may contain water bearing layers, such as the sandstone beds within the Graafwater Formation; equally, aquifers may only offer some portion of their thickness as an aquifer, the rest being an aquitard, such as the sandstone beds within the dominantly silty Floriskraal Formation, but the reason for calling the Floriskraal Formation an aquifer is that it bears water within a predominantly non-water bearing setting.

The proposed hydrostratigraphy attempts to simplify and highlight major aquifers and aquitards. Where aquifer-aquitard boundaries coincide with geological boundaries, no reclassification has been done. In the Witteberg and Bokkeveld Groups where the geology alternates regularly between arenaceous and argillaceous, the hydrostratigraphy mimics the geostratrigraphy, but in the TMG this is not the case. The Piekenierskloof and Graafwater Formations have limited areal extents.

The Piekenierskloof Formation is a significant aquifer in the Sandveld region (Lin et al., 2007). The Graafwater Formation may have fractured, water bearing sandstone layers, but their limited vertical and areal extent (Rust, 1977) will render them low yielding, unless they are connected via faults to the Piekenierskloof or Peninsula Formation.

The Peninsula Superaquifer may include some portion of the Pakhuis Formation, where this

is permeable, although Hartnady and Hay (2002b) consider the Pakhuis Formation to be an aquitard, based on the similarity in gamma and neutron-neutron downhole geophysical logging of the Pakhuis and Cederberg Formations. Superaquifer status is assigned on account of the extreme thickness (up to 2000 m) and areal extent over the Cape Fold Belt, as well as the high yielding nature of this unit (Hartnady and Hay, 2002a). The Cederberg Aquitard may include portions of the Pakhuis Formation where it is less permeable and portions of the Goudini Formation where the siltstone and shale layers are substantial enough to restrict groundwater flow. Although rather thin (100–200 m) the fact that this aquitard either separates the Peninsula Superaquifer from the Skurweberg aquifer or simply acts as a cap to the Peninsula Superaquifer, makes this unit of extreme importance in understanding groundwater flow in the Table Mountain Group. The Skurweberg Aquifer is centred on the highly fractured mature quartzites of the Skurweberg Formation, but includes portions of the underlying Goudini and overlying Rietvlei Formations where they are more permeable and have good connectivity with the Skurweberg Formation.

The Bokkeveld Group, although it contains sandstone aquifers that can yield substantial water at the local scale (Rosewarne, 2002a), acts as an aquitard on a regional scale, particularly as a confining layer to the Table Mountain Group. Good examples of this are seen in the Olifants River Valley (Geological Survey, 1973) and under the Little Karoo (Geological Survey, 1979) where the Bokkeveld Group confines the Table Mountain Group under the valley floors and allows deep groundwater to flow many kilometres from one side of the valley to the other and emerge in hot springs, under pressure gradients derived from mountain recharge areas (Diamond and Harris, 2000).

The Witteberg Group contains both substantial aquifers and aquitards. It probably acts as an aquitard on a regional scale, although the extensive structural deformation, particularly intense folding and thrusting, probably allow good connections between the various sandstone (aquifer) layers to the extent that in some areas these may act as a single aquifer. The great thickness and highly competent nature and therefore extensive fracturing of the Witpoort Formation mean this unit is potentially a significant aquifer, although low recharge because of low rainfall is probably a limiting factor for achieving high and sustainable borehole yields from this unit. The Witteberg Group tends to receive low rainfall because of its usual position inland and therefore in the rain shadow of mountains formed by the Table Mountain Group.

Overall, the Bokkeveld and Witteberg Groups possess similar hydrogeological characteristics, in that they both contain numerous minor aquifers that may be connected to each other, or to the larger aquifers in the Table Mountain Group, if structural features allow. These similarities suggest that the multiple aquifers and aquitards of these two groups can be collectively known as the Bokkeveld-Witteberg aquagroup (Al-Aswad and Al-Bassam, 1997). The Table Mountain aquagroup is essentially the Peninsula-Cederberg-Skurweberg configuration that persists over much of the Cape Fold Belt, with some localised variations at the base of the group, where other formations are present.

Below and above the Cape Supergroup lie thick aquitards that generally conduct little groundwater: the Saldanian basement of metasediments and granite beneath and the Dwyka Group above. The Cape Supergroup can therefore be termed the Cape aquasystem, bounded by these basement and cover mega-aquitards, and with a fixed configuration of the aquifer dominated Table Mountain aquagroup at the base, and the regular aquifer-aquitard alternations of the Bokkeveld-Witteberg aquagroup above.

In some instances, aquifers within the Cape aquasystem will be connected to more recent cover rocks of the West Coast, Sandveld, Bredasdorp or Algoa Groups, which contain calcarenites, unconsolidated sand and other lithologies that can form aquifers. These linkages occur mainly near the coast and are generally limited in area. The Sandveld region around Elands Bay is the largest area where the Table Mountain Group interacts with surficial rocks and sediments.

2.5.4 Significance of the Table Mountain Group

The Table Mountain Group is critical in sustaining surface water in the Western Cape (Roets et al., 2008; Colvin et al., 2009). Baseflow during the summer dry season is sustained through discharge of groundwater (le Maitre et al., 2002; Colvin et al., 2009) and it has been shown that peak or flood discharge surface water during rain events is mainly composed of groundwater that has discharge from the aquifer in response to increased hyrdaulic head caused by fast recharge of rainwater (Midgley and Scott, 1994). A substantial portion of the ecosystems of the Western Cape are directly dependant upon water, being wetlands, riparian zones and estuaries. Furthermore, these vegetation and plant communities are more important as habitat and for ecosystem services than the dryland areas. As such, the Table Mountain Group is the ultimate water source for most surface water and therefore controls both the natural and human environment through most of the Western Cape.

Various attempts have been made at calculating the groundwater yield potential of the Table Mountain Group. From the information presented above, it should be clear that this exercise is subject to two huge challenges, being the great size of the aquifer system and the sparse and often unreliable information. As a first step, Rosewarne (2002b) has collated pumping data from active wellfields, giving an indication of available water in particular locations, and Meyer (2002) gives the flow rates of the thermal springs in the Cape Fold Belt. These data are summarized in **Table 2.2**.

THERMAL SPRINGS		WELLFIELDS	
name	GL/a	name	GL/a
Baden	1.16	Albertinia	0.26
Brandvlei	4.00	Caledon	0.10
Caledon	0.28	Ceres	1.51
Calitzdorp	0.25	Hermanus	0.35
Citrusdal (The Baths)	0.91	Humansdorp	0.68
Goudini	0.35	Jeffreys Bay	0.80
Montagu	1.20	Lamberts Bay	0.13
Studtis	0.98	Plettenberg Bay	0.28
Toverwater	0.35	Steytlerville	0.07
Uitenhage	1.42	St Francis-on-Sea	0.73
Warmwaterberg	0.28	Uitenhage	1.58
TOTAL	11.2	TOTAL	6.5

Table 2.2: Point source (springs) or small area (wellfield) abstraction figures give an indication of possible yields for deep boreholes or small wellfields in the Table Mountain Group. Data from Meyer (2002) and Rosewarne (2002b).

Hartnady and Hay in Weaver et al. (2002) calculated groundwater yield for an area of less than 2000 km^2 in the Citrusdal region as 5–25 GL per 1 m decrease in hydraulic head, concluding that for a technically and probably environmentally acceptable decrease in head of 20 m, 100–500 GL could be withdrawn annually. Scaling up to the whole of the Table Mountain Group, they calculate an aquifer rock volume of 100 000 km^3, which, for a fracture porosity of 0.1-1 % gives a volume of 100 000 – 1 000 000 GL of groundwater, although much of this water is not available because of practical challenges, as well as potential environmental impacts. Similarly, Rosewarne (2002b) calculates an aquifer rock volume of 47 000 km^3 and using storatitivity values shown in **Table 2.1**, he concludes that 10 000 – 100 000 GL of groundwater is in storage, again, most of which is not available. However, even if only a small percentage of this groundwater is available, when compared to the total volume of all surface water reservoirs fed by Table Mountain Group catchments, 1500 GL, it should be clear that the aquifer system stores a very large amount of water.

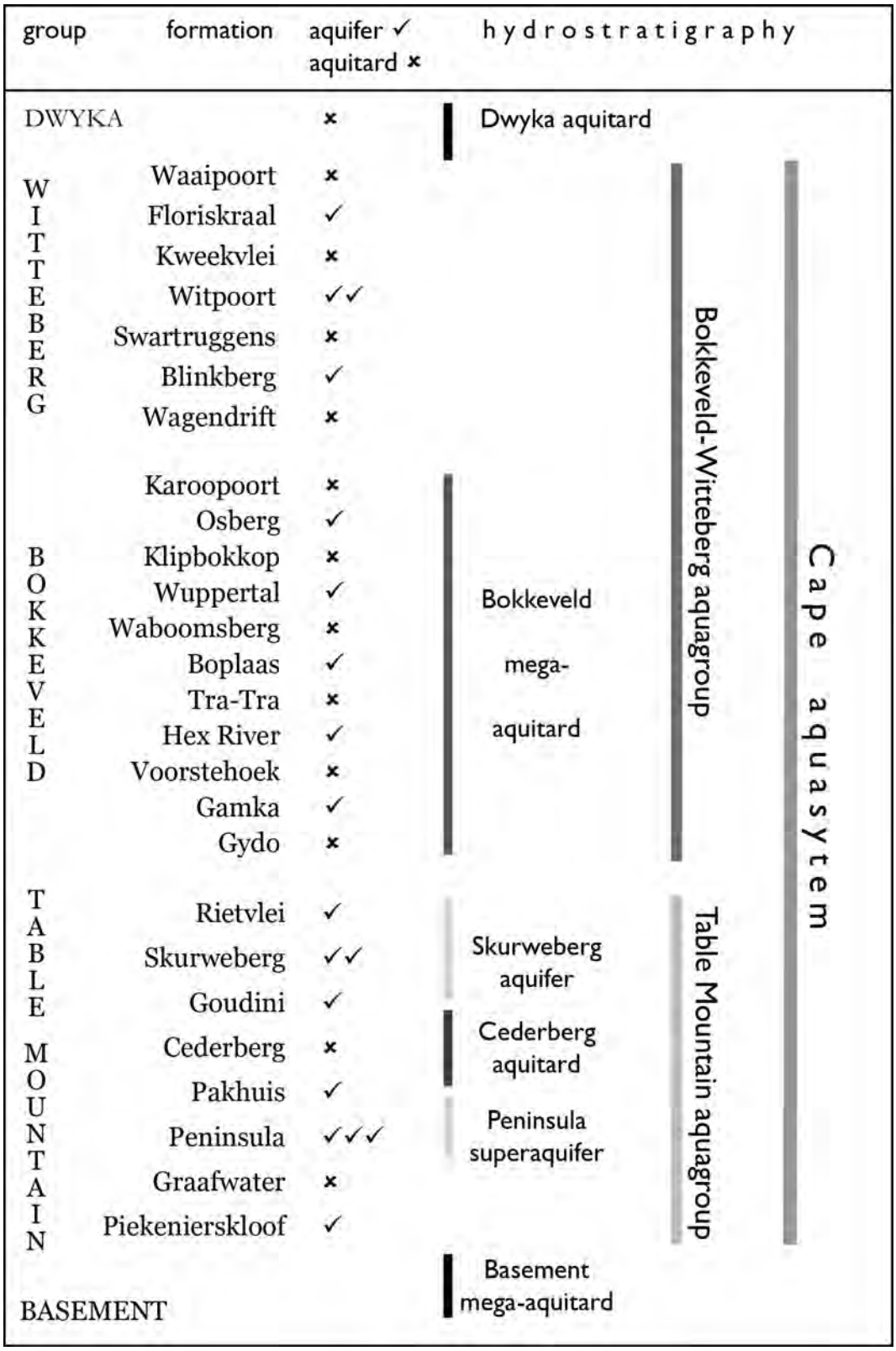

Figure 2.18: Proposed hydrostratigraphic classification for the Cape Supergroup in the western half of the Cape Fold Belt.

Chapter 3

Methods

3.1 Introduction

This chapter describes the methods used for collection of samples, laboratory preparation and instrumental analysis, including correction factors and equations. The locations of all the sample sites are shown on various maps and the major rainfall collection stations are all listed in a table with coordinates and elevations. Information on the calculation of regression lines is also included.

3.2 Sample Collection

3.2.1 Rain

Rainfall was collected at 15 sites across the Western Cape. Most of the collection stations operated for 2 years, from 2010 to 2012, with some having a continuous record and others an interrupted or shorter operational period. Factors that caused a station to cease operating were instrument problems from animal or weather damage, lack of access due to weather conditions and also human error. Maps of the sample locations are included below, approximately in a west to east direction, starting with Cape Town (**Figures 5.21 to 3.22**).

Rain collection depended on access to the rain gauge. Where gauges were easily accessible, rainfall was collected daily and emptied into a glass jar, from which a sample was taken at the end of each month. At remote sites, a cumulative collector (**Figure 3.2**) was erected and emptied at approximately the end of each month. In each case, the daily or monthly rainfall amounts were recorded. Bosman (1981) noted that plastic raingauges collect around 7 % less rainfall than standard metal raingauges, attributable to splash out from the receiving funnel and higher retention of raindrops on the plastic surface, which then evaporate. Given the extreme variation in rainfall in the field area due to orographic effects and that rainfall amount is used indirectly to weight isotope values, this discrepancy is considered acceptable. Furthermore, all rainfall for this study was collected using similar plastic raingauges and so the data is internally consistent.

station			location		
code	name	description	latitude	longitude	altitude
UCT	University of Cape Town	Department of Geological Sciences building	33° 57’ 31.9" S	18° 27’ 37.6" E	135 m
TMC	Table Mountain Cableway	upper cableway station	33° 57’ 26.6" S	18° 24’ 10.3" E	1074 m
TWT	Twaktuin	Twaktuin farm in Olifants River Mountains	32° 19’ 17.6" S	18° 49’ 31.9" E	412 m
UKP	Uitkyk Pass	crest of pass in Cederberg	32° 24’ 14.8" S	19° 06’ 05.4" E	1013 m
WKP	Wolfkop	house in Wolfkop Private Nature Reserve, south of Citrusdal	32° 38’ 19.2" S	19° 03’ 20.4" E	355 m
MTB	Matroosberg	nek between Matroosberg and Conical Peaks, Hex River Mountains	33° 22’ 27.2" S	19° 39’ 53.1" E	1910 m
DDN	De Doorns	Tweespruit farm near De Doorns in Hex River Valley	33° 26’ 34.3" S	19° 40’ 30.9" E	482 m
RVD	Riverndale	Riverndale farm, foot of the Langeberg, north-east of Heidelberg	33° 58’ 22.9" S	20° 59’ 56.2" E	251 m
RBP	Robinson Pass	crest of pass over Langeberg, north of Mossel Bay	33° 52’ 26.3" S	22° 01’ 54.7" E	885 m
BKK	Bakenskop	highest point of the Gamkaberg, Gamka Mountain Nature Reserve	33° 43’ 07.8" S	21° 55’ 28.4" E	1101 m
GST	Gamkaberg store	store shed at Gamka Mountain Nature Reserve	33° 40’ 20.0" S	21° 53’ 15.5" E	350 m
BBG	Blesberg	highest peak in the eastern Groot Swartberg	33° 25’ 03.8" S	22° 41’ 15.0" E	2080 m
KMN	Kammanassie	Vermaaks River Gorge in western Kammanassie Mountain	33° 36’ 11.4" S	22° 31’ 56.2" E	666 m
LTL	Lentelus	Lentelus farm in Bo-Kouga region	33° 40’ 42.2" S	23° 29’ 58.0" E	642 m
GKM	Goukamma	house near Goukamma railway station and Goukamma River	33° 02’ 21.1" S	22° 56’ 25.3" E	62 m

Table 3.1: Location information for the 15 rainfall collection stations of this study.

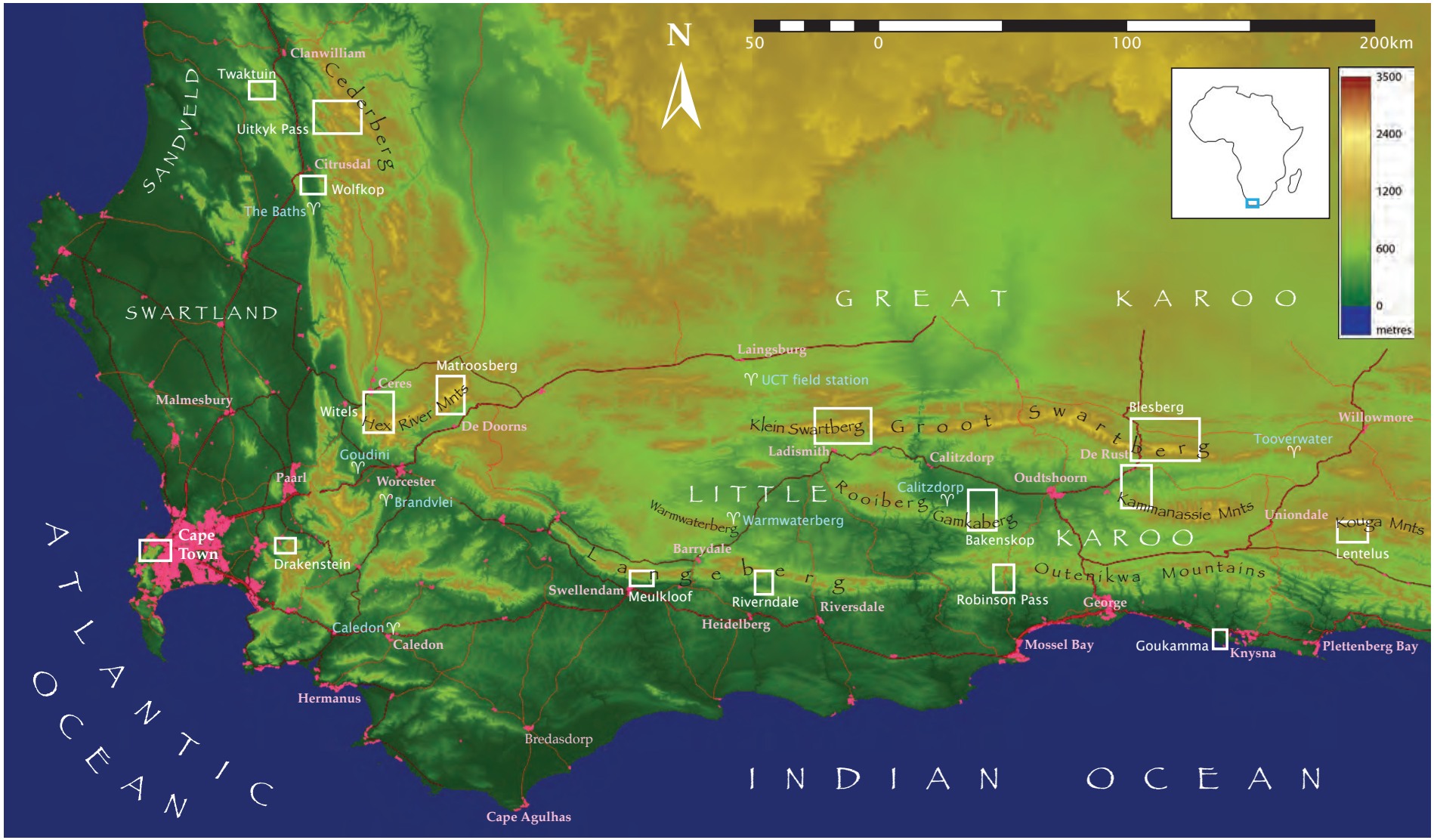

Figure 3.1: Map of the whole study area with white rectangles showing the areas for each of the detailed maps that follow. DEM from NASA (2013) and roads shapefile from NGI (2012).

For the monthly collectors, prevention of evaporation was achieved by use of a long thin plastic tube, as seen in the diagram, although oil was also added to some collectors, but it was found that this was unnecessary, as collectors without oil seemed to yield samples with acceptable isotope compositions. The oil contaminated some samples, but care was taken to avoid getting the oil into the laboratory preparation equipment and as a result, no effect on isotope values was observed. Spikes were placed on top to discourage birds from sitting on the rim and adding non-meteoric contributions to the funnel.

3.2.2 Surface Water

Surface water was collected from five rivers in the Western Cape. The water was collected directly from the surface of the flowing stream, except for one sample collected from the cold bottom water in a deep river pool. The sample locations are also shown in the maps in this chapter.

3.2.3 Groundwater

Groundwater was sampled from both natural sources, springs and seeps, and boreholes. If boreholes were not in frequent use, a short period of purging was done to flush water out from the borehole volume and associated piping and allow true aquifer water to be sampled. Springs and seeps were sampled at or as near as possible to the source, in cases where the spring was capped. The borehole locations are also shown in the maps in this chapter.

3.3 Sample Preparation

3.3.1 Mass Spectrometry

3.3.1.1 Hydrogen Isotopes

Sample preparation for hydrogen isotope analysis was done using established single sample preparation procedures (e.g. Tanweer et al., 1988; Schimmelman and DeNiro, 1993). The procedure starts by loading 100 mg ($\pm$3 mg) of Indiana zinc shavings into a glass tube of 3 mm internal diameter which was heated with a hot air gun under vacuum to degas the zinc, removed from vacuum and allowed to cool down before a 2 μL microcapillary pipette containing the sample water was dropped into the glass tube. The tube was then placed back on the vacuum line and evacuated after the sample had been frozen with liquid nitrogen, then sealed with an oxygen-propane flame; see **Figure 3.3**. The glass tube was then loaded into a furnace and baked at 450 °C for 30 minutes, allowing the following reaction to take place:

$$Zn + 2H_2O \rightarrow ZnO_2 + 2H_2 \quad .$$

This glass tube could then be loaded into the mass spectrometer to allow for analysis of the hydrogen gas.

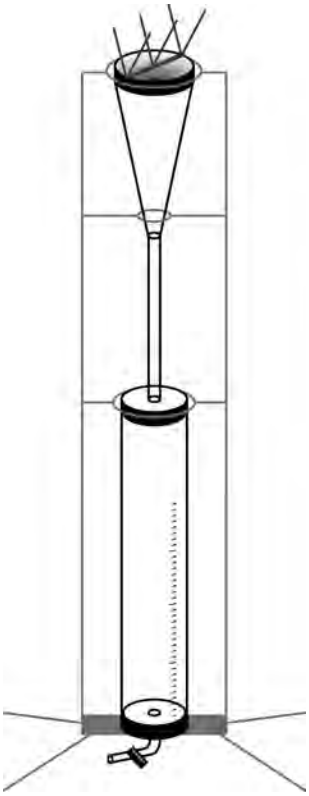

Figure 3.2: Cumulative rainfall collector, designed to collect rain for one month and prevent significant evaporation until collection.

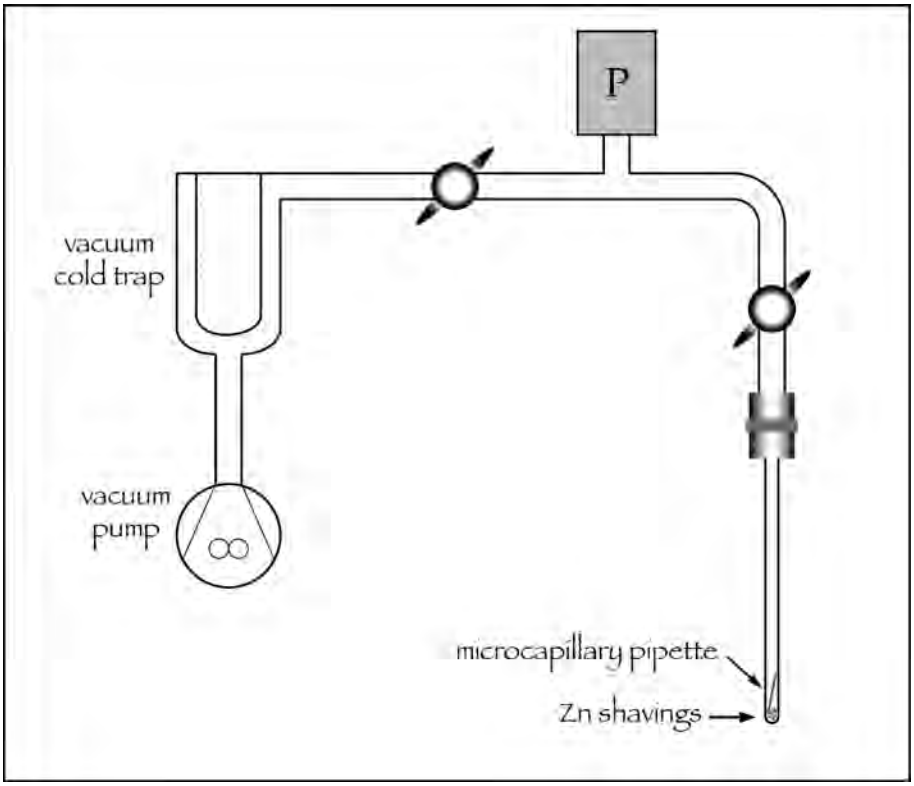

Figure 3.3: Vacuum line for preparing water samples for hydrogen isotope analysis.

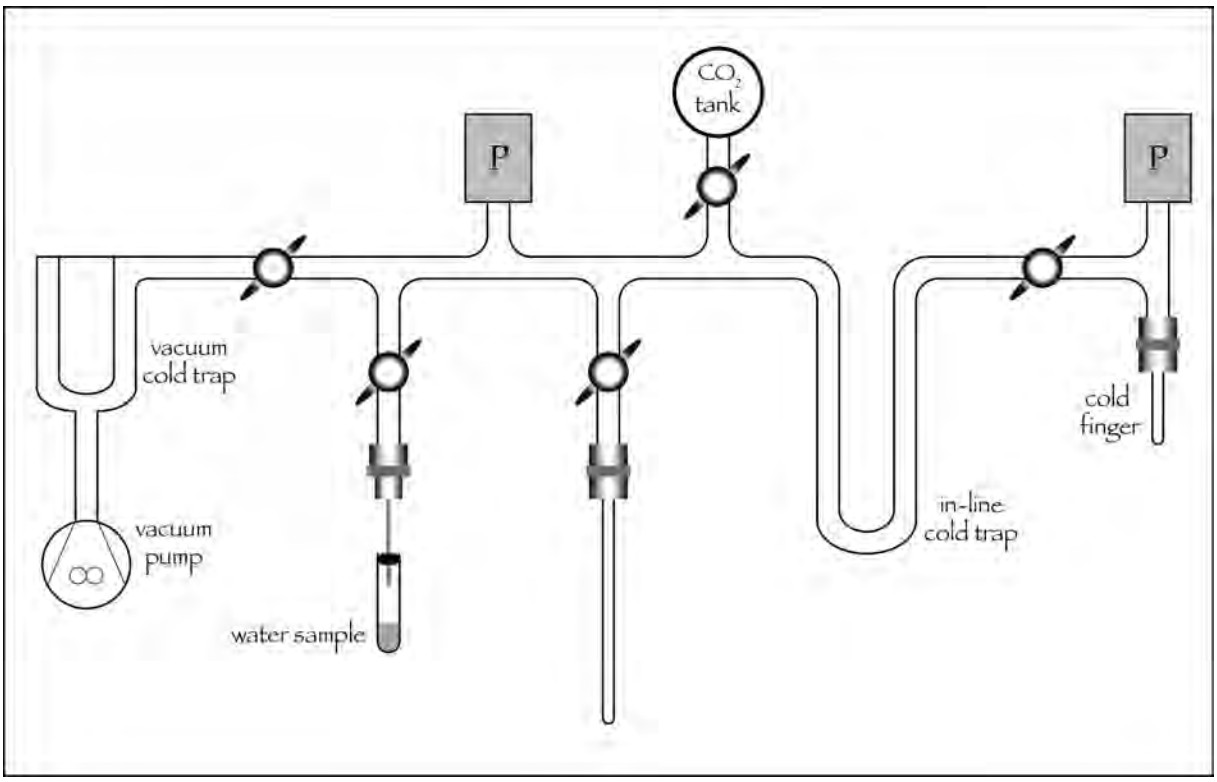

Figure 3.4: Vacuum line for preparing water samples for oxygen isotope analysis.

3.3.1.2 Oxygen Isotopes

Sample preparation for oxygen isotope analysis was done by the method of equilibrating sample water with CO_2 and analysing this, as described in Socki et al. (1992), based on that of previous workers, such as Epstein and Mayeda (1953). The method entailed injecting 2 mL of sample water into a 7 mL sealed plastic vial (vacutainer) that had been evacuated and then loaded with $\frac{1}{3}$ atm of CO_2. The vial was then submerged in a 25 °C water bath and agitated for 2 hours to allow oxygen exchange between the H_2O and CO_2 to reach equilibrium. Then the vial was placed onto the vacuum line and submerged in liquid nitrogen to freeze the H_2O and CO_2. Once frozen, the vial was opened to the vacuum to evacuate any gases. The liquid nitrogen was then moved to the in-line vacuum trap and nearly frozen 2-propanol (isopropyl alcohol) was placed around the vial to retain the ice but liberate the CO_2 as gas. Once all the CO_2 had frozen at the in-line cold trap, the vial was closed off from the vacuum line and the vacuum was opened again to remove any unwanted gases. After closing the valve to the vacuum pump, the liquid nitrogen was moved to the cold finger and the 2-propanol to the cold trap, to transfer the CO_2 where it could be measured with a pressure gauge. Unwanted gases can again be pumped away to vacuum in this step. Finally the CO_2 was frozen into a glass tube using liquid nitrogen, and flamed closed with an oxygen-propane torch.

For both hydrogen and oxygen isotope preparation, each batch of samples was accompanied by 2 laboratory standards, both duplicated. The two standards were initially CTMP2010, which

standard		$\delta D_{(SMOW)}$ (‰)	$\delta^{18}O_{(SMOW)}$ (‰)
CTMP2010	Cape Town Millipore Water 2010	-7.4	-2.69
ACTMP	Adam's CTMP2010	+1.6	-0.60
Evian	Evian bottled water	-70	-10.0
EvianA	Adam's Evian	-71.7	-10.20
RMW	Rocky Mountain Water	-129.5	-17.27

Table 3.2: Delta values for the various internal standards used in this study.

stands for Cape Town Millipore Water and is filtered 2010 University of Cape Town tap water and Evian bottled spring water, from the Alps. Later during the study, Evian was replaced with a more isotopically depleted water, RMW, which stands for Rocky Mountain Water, bottled spring water with a source in the American Rocky Mountains.

3.3.2 Laser Cavity Ringdown Spectroscopy

No sample preparation is generally needed for this method. One millilitre of sample water is injected into a vial which is capped with a septum and then put into an automated sample loading tray. Hydrogen and oxygen isotopes are analysed simultaneously. Only samples with traces of oil or other dirt were injected through a micropore filter to remove the contaminants.

Sample runs using this method made use of 3 standards: ACTMP (Adam's CTMP), EvianA (Evian Adam's) and RMW, reflecting the use of Adam West's laboratory in the Botany Department at the University of Cape Town.

3.4 Sample Analysis and Data Correction

3.4.1 Mass Spectrometry

A 2004 Thermo Corporation Delta Plus XP stable light isotope ratio mass spectrometer was used for conventional dual inlet analysis of hydrogen and oxygen isotope ratios at separate times. The machine was set to make 4 and 6 measurements of the δ value of the sample relative to the reference gas for H_2 and CO_2, respectively. Over years of experience it was found that the machine precision for hydrogen was better than the preparation procedure and so making more than 4 measurements would not improve overall accuracy. For CO_2 however, a slight memory effect seemed to occur as the first measurement was often slightly different from the other five, and the preparation procedure precision was slightly better, so 6 measurements resulted in the optimal balance between accuracy and time for analysis.

Each time the machine was switched over from hydrogen to carbon dioxide, a peak optimisation or focus procedure was performed, in which the ion source and other beam parameters were adjusted to reduce H_3 production and focus the beam squarely into the collector cups. This was

followed by an H_3-factor correction for the molecules of H_3 produced in the ion source, which interfere with the measurement of HD.

Data from the mass spectrometer were corrected using the following method. The first correction applied was for fractionation of oxygen between H_2O_l and CO_2, which at 25 °C has a fractionation factor of 1.0412. This equates to the CO_2 being 40.37 ‰ heavier than the water, once equilibrated. Then a correction was applied for the difference between the reference gas and SMOW. Finally, the sample values were adjusted by correcting the two laboratory standards (CTMP2010 and RMW) to their known values and applying the same correction to the samples. This was done by assuming the error between the measured and actual values varies linearly and therefore a straight line equation can be found that will transform the two standards from their measured values to their actual values, as shown in **Figure 3.5**.

The equation for a straight line is:

$$y = mx + c$$

where **y** is the unknown actual sample value, **m** is the gradient and **c** the intercept of the straight line, and **x** is the measured value of the sample. Both m and c can be calculated individually and the above equation used to calculate the actual sample value, or the equation below can be used to perform the calculation in one step:

$$SAMPLE_{actual} = \left(SAMPLE_{meas} \times \left(\frac{CTMP_{actual} - RMW_{actual}}{CTMP_{meas} - RMW_{meas}} \right) \right) + \left(RMW_{actual} - \left(RMW_{meas} \times \left(\frac{CTMP_{actual} - RMW_{actual}}{CTMP_{meas} - RMW_{meas}} \right) \right) \right)$$

As seen in **Figure 3.5**, a straight line is used to convert measured values (x-axis) to actual values, based on analysis of two standards (RMW and CTMP) of known value. For each analytical run of samples, the straight line will vary in both gradient and intercept. This method replaces the 'shift' and 'stretch' technique commonly used to correct measured values (e.g. Sharp, 2007, p.332).

3.4.2 Laser Cavity Ringdown Spectroscopy

A L2120-i Picarro wavelength scanning cavity ringdown spectrometer was used to analyse for oxygen and hydrogen isotope values simultaneously. Certain wavelengths of infrared light are scanned and the ringdown time is used to calculate the abundance of the various isotopes of oxygen and hydrogen (Lis et al., 2008). Six injections of microlitre amounts of sample were

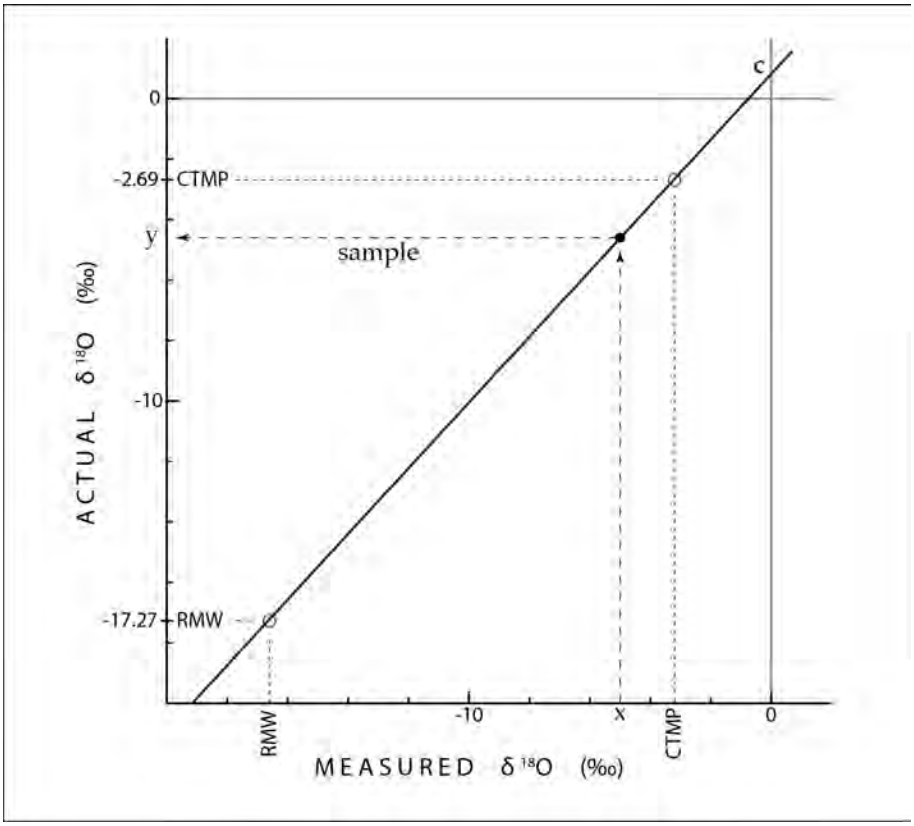

Figure 3.5: The final correction applied to isotope data to correct for instrument drift and laboratory preparation procedure variations. Two standards allow calculation of a straight line equation which is then applied to all the sample data for that run. The example is given for $\delta^{18}O$ but is equally applicable to δD.

made through a septum, vapourised and then transported by N_2 gas into the cavity for analysis. Standards were run at the beginning and end as well as after every ten to twelve samples during a given run. The first two injections show a clear memory effect and these values were discarded, the remaining four being averaged to give an instrument measurement. These instrument measurements were then corrected using the same final correction procedure as shown in **Figure 3.5**. Issues with contaminants, particularly organic compounds such as alcohols, have been noted (West et al., 2010), however, pure water samples tend to give good results. Quality assurance software was used to scan the raw data from the machine and highlight poor analytical indicators (West et al., 2011).

3.4.3 Standards

As shown in **Table 3.2**, several standards were used to correct for laboratory and instrument errors. An analysis of long term laboratory and mass-spectrometer precision can be made by looking at the raw data values for these working standards over time. These values are shown in **Tables 3.3 and 3.4** for δD and $\delta^{18}O$. The latter table shows rather stable values for the three standards, although a small possible drift in CTMP2010 from more to less negative values appears to occur over time. This is likely to be due to drift in the reference gas for the mass-spectrometer, although it could also be due to a change in the laboratory CO_2 tank or in the CTMP2010 standard. The mean difference in replicates (the two values against each date) is around 0.2 ‰ $\delta^{18}O$ for the three standards, which represents the overall precision of the laboratory preparation procedure and mass-spectrometer analysis.

Table 3.3 reveals substantial drift in the values for the three standards, although the period over which Evian was analysed is a bit short. Changes in hydrogen analysis results could be due to several factors. As with oxygen (carbon dioxide) analysis, there could be drift in the reference gas and in the working standards. The zinc used was changed around mid-2012, from batch S83B4 to S38r, and this in fact coincides with substantial changes in values. The 31-05-2012 sample run was the first with the new batch of zinc, the 08-08-2012 and 15-08-2012 again used the old batch, and from 20-08-2012 thereafter the new zinc was used. It can be seen that these changes coincide with the big changes in values. With this in mind, the drift in working standards appears reasonable. More importantly for precision, the mean difference in replicates can be seen to be a little over 1 ‰, which is assurance of the reliability of the preparation and analytical procedures.

The Picarro LASER instrument was only used twice, so no meaningful statements can be made about long term precision. Aside from the working standards, certain samples were run through the LASER and mass-spectrometer methods and the results were found to be similar, with approximately the same level of precision between instruments as within, as reported above.

The final correction procedure, making use of these measured values and adjusting them and the samples for each run to the known values, was able to produce data of acceptable accuracy.

δD ‰						
date	**CTMP2010**		**Evian**		**RMW**	
28-03-2011	-15.1	-12.8	-75.8	-76.0		
12-04-2011			-68.9	-70.2		
27-05-2011	-15.4	-13.3	-69.6	-67.2		
01-06-2011	-12.1	-9.8	-67.2	-59.7		
17-06-2011	-11.4	-11.3	-67.2	-70.3		
30-06-2011	-4.5	-0.6	-58.9	-59.2		
18-10-2011	-9.1	-12.2			-125.6	-125.7
13-12-2011	-4.1	-1.8			-119.6	-119.5
19-12-2011	-1.0	-1.1			-119.2	-119.1
03-02-2012	-2.0	-2.6			-115.8	-116.4
24-05-2012	-1.7	+0.4			-114.6	-115.2
31-05-2012	+9.0	+9.7			-104.6	-105.6
08-08-2012	-2.2	-3.0			-120.1	-121.6
15-08-2012	-0.7	-3.0			-122.9	-120.8
20-08-2012	+6.9	+6.3			-115.3	-116.0
04-10-2012	+12.9	+12.2			-98.0	-98.7
05-11-2012	+9.4	+7.9			-108.2	-108.0
21-02-2013	+8.7	+8.0			-105.0	104.2
03-04-2013	+11.5	+12.8			-100.0	-98.7
05-04-2013	+10.0	+9.9			-101.7	-102.2
02-05-2014	+7.8	-7.1			-107.6	-105.2
mean		-0.0075		-67.6		-111.8
maximum — minimum	+12.9 — -15.4		-58.9 — -76.0		-98.0 — -125.7	
standard deviation		8.9		5.7		8.7
mean difference		1.4		2.3		0.85
difference std. dev.		1.1		2.8		0.71

Table 3.3: Raw data for δD analyses of standards during this project. The values above are the mass-spectrometer values with the zinc correction applied.

$\delta^{18}O$ ‰						
date	**CTMP2010**		**Evian**		**RMW**	
15-03-2011	-4.46	-4.56	-10.5	-10.2		
12-04-2011			-10.44	-10.40		
26-05-2011	-5.75	-4.11	-9.76	-10.18		
02-06-2011	-4.10	-3.40	-9.65	-9.62		
07-06-2011	-3.27	-3.12				
20-06-2011	-3.48	-3.30	-9.61	-9.53		
07-07-2011	-3.63	-3.55	-9.61	-9.67		
01-08-2011		-2.54		-9.31		
03-08.2011		-4.25		-10.21		
04-08-2011		-3.86		-10.10		
12-08-2011		-3.63			-17.44	-17.59
24-10-2011		-3.61			-17.58	-17.77
21-12-2011	-3.53	-3.63			-17.50	-17.54
11-01-2012	-3.40	-3.09			-17.46	-17.61
01-02-2012	-4.58	-3.71			-17.56	-17.68
21-05-2012	-4.27	-4.16			-17.47	-18.09
28-05-2012		-3.63				-17.49
18-06-2012	-3.60	-3.80			-17.94	-18.45
18-07-2012	-3.62	-3.40			-17.82	-17.76
19-07-2012	-3.73	-3.68			-17.98	-17.86
23-07-2012	-4.04	-3.96			-17.57	-17.51
01-08-2012	-3.55	-3.67			-17.62	-17.51
10-10-2012	-4.57	-3.93				-17.27
11-10-2012	-3.42	-3.38			-17.61	-17.74
15-10-2012	-3.97	-3.82			-17.77	-17.83
06-11-2012	-3.67	-3.45			-17.44	-17.50
08-11-2012	-3.43	-3.49			-17.60	-18.47
19-02-2013	-3.18	-3.34			-17.56	-17.36
26-03-2013	-3.71	-3.35			-17.34	-17.42
27-03-2013	-3.41	-3.03			-17.13	-17.16
28-03-2013	-3.11	-3.05			-17.27	-17.36
04-04-2013	-2.92	-3.11				-17.01
02-05-2014	-3.42	-3.43			-17.19	-17.22
mean		-3.65		-9.92		-17.58
maximum — minimum	-2.54 — -5.75		-9.31 — -10.50		-17.01 — -18.47	
standard deviation		0.51		0.38		0.30
mean difference		0.28		0.15		0.18
difference std. dev.		0.35		0.16		0.22

Table 3.4: Raw data for $\delta^{18}O$ analyses of standards. The values above are the mass-spectrometer values with the reference gas and $CO_2 - H_2O$ equilibration corrections applied.

3.5 Data Analysis

A substantial portion of the analysis of stable isotope data consists of finding correlations and calculating regressions. The most common regression analysis is known as the *least squares method*. This assumes the x-variable is independent and accurately known, whereas the y-variable depends upon the x-value and has errors and random variations. An example of an independent x-variable would be time or distance, and a dependent y-variable could be temperature, rainfall or an isotope ratio. For analysis of one stable isotope ratio, say δD against one of these independent variables, the *least squares regression* is suitable. However, where both variables are dependent, such as δD and $\delta^{18}O$, no one should be treated as more certain than the other and so the *reduced major axis* form of a structural regression is suitable.

Least Squares Regression

To calculate a straight line of the form:

$$y = mx + c\,,$$

using the least squares regression:

$$\begin{aligned} m &= \frac{SP_{xy}}{SS_x} \\ \text{and} \quad c &= \bar{y} - m\bar{x}\,, \\ \text{where} \quad SS_x &= \sum_{i=1}^{n}(x_i - \bar{x})^2 \\ \text{and} \quad SP_{xy} &= \sum_{i=1}^{n}(x_i - \bar{x})(y_i - \bar{y})\,. \end{aligned}$$

Reduced Major Axis Regression

The RMA regression line is calculated in a similar way to above, with the single difference that the gradient, m, is calculated as follows:

$$\begin{aligned} m &= \sqrt{\frac{SS_y}{SS_x}} \\ \text{where} \quad SS_y &= \sum_{i=1}^{n}(y_i - \bar{y})^2\,. \end{aligned}$$

Weighted Regression Line Calculations

As noted by Hughes and Crawford (2012), weighting of isotopic values for monthly cumulative

rainfall by the rainfall amount produces regression lines (meteoric water lines) with higher gradients, as a result of minimising the influence of evaporated samples from low rainfall events. The difference in gradient between weighted and unweighted regression lines depends on the dataset. These meteoric water lines better characterise the average rainfall and especially heavier events that are more likely to play an important role in hydrological processes such as groundwater recharge. Calculation of such regressions uses methods similar to above, but by adding the rainfall term into the statistical quantities as follows:

$$SS_x = \sum_{i=1}^{n} (rain_i)(x_i - \bar{x})^2 \ ,$$
$$SS_y = \sum_{i=1}^{n} (rain_i)(y_i - \bar{y})^2 \ ,$$
$$SP_{xy} = \sum_{i=1}^{n} (rain_i)(x_i - \bar{x})(y_i - \bar{y}) \ .$$

3.6 Maps

The maps that follow were prepared using the QGIS programme with shapefiles of 1:50 000 tile data from the Chief Directorate for National Geo-Spatial Information of the South African Department of Rural Development & Land Reform. Dotted grey circles around some sampling sites are 5 km radius circles and will be mentioned in the Discussion chapter.

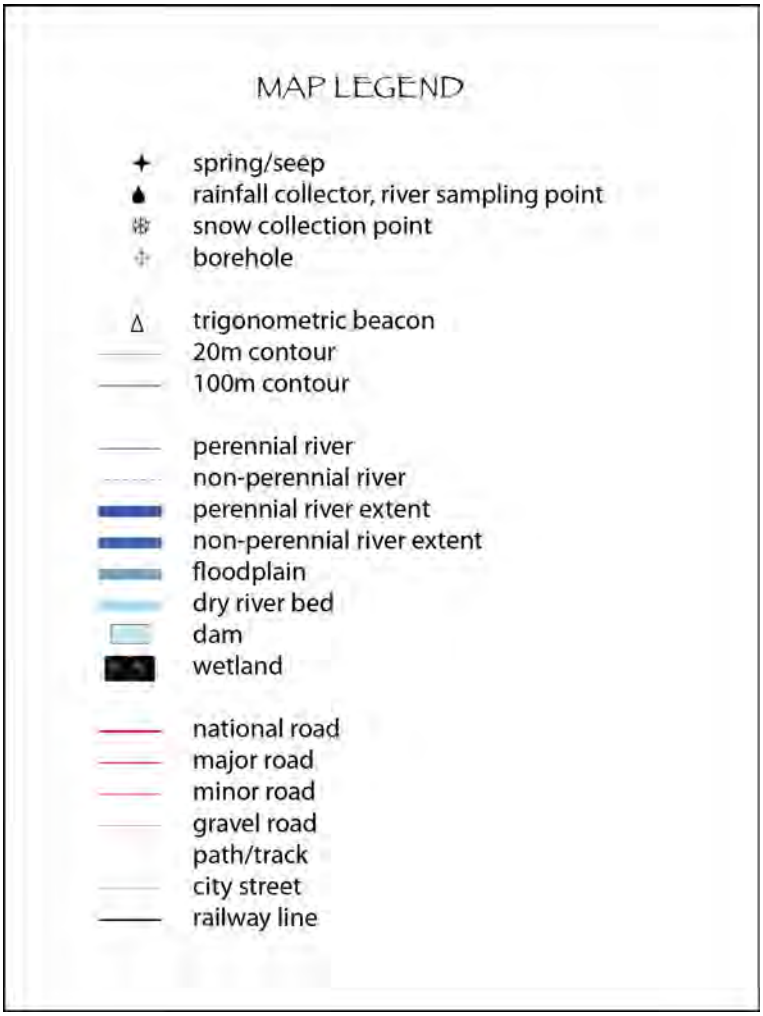

Figure 3.6: Legend for the location maps.

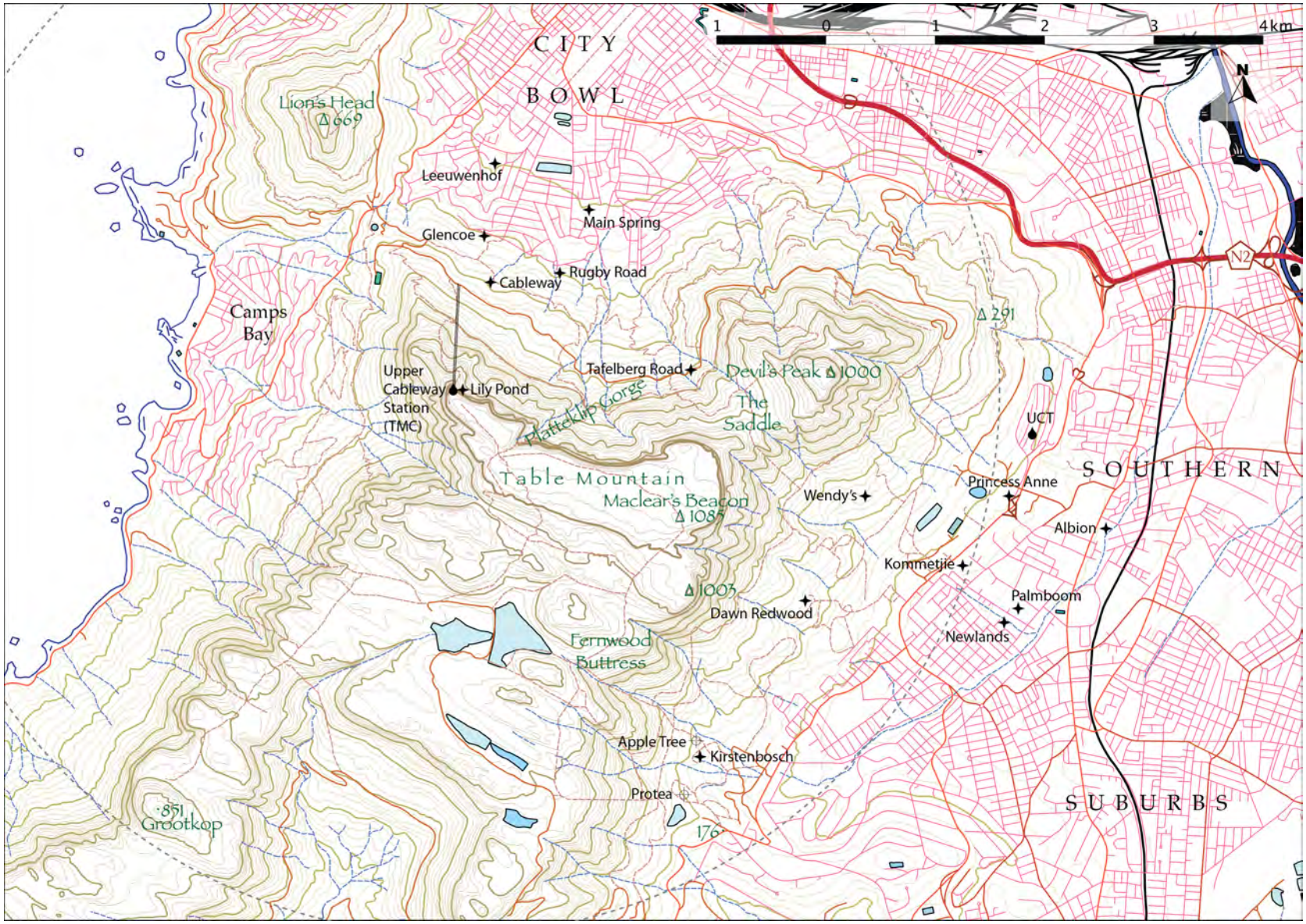

Figure 3.7: Locations of sampling points in the Cape Town area.

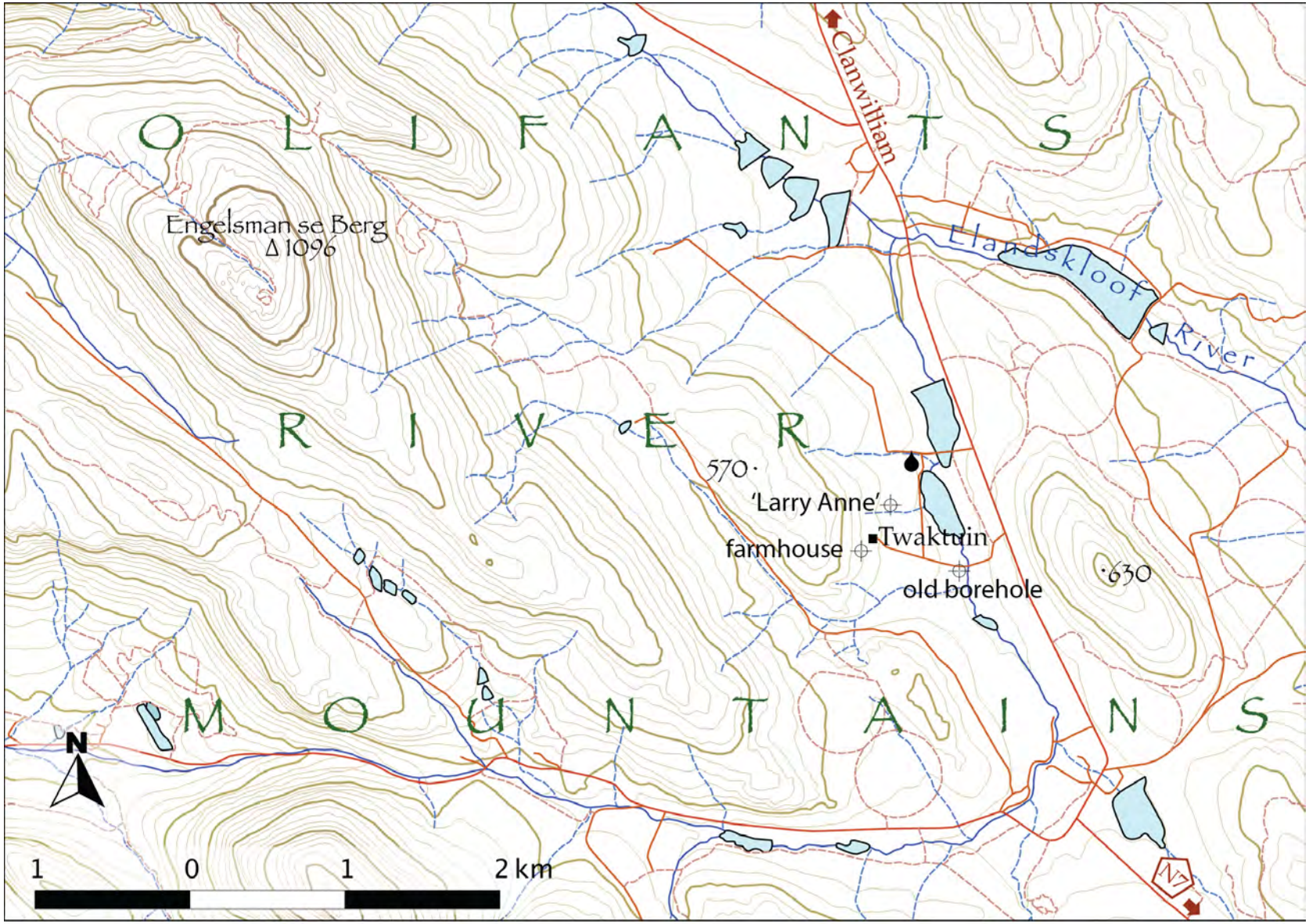

Figure 3.8: Locations of the rainfall collector and three boreholes sampled on Twaktuin Farm, south-west of Clanwilliam.

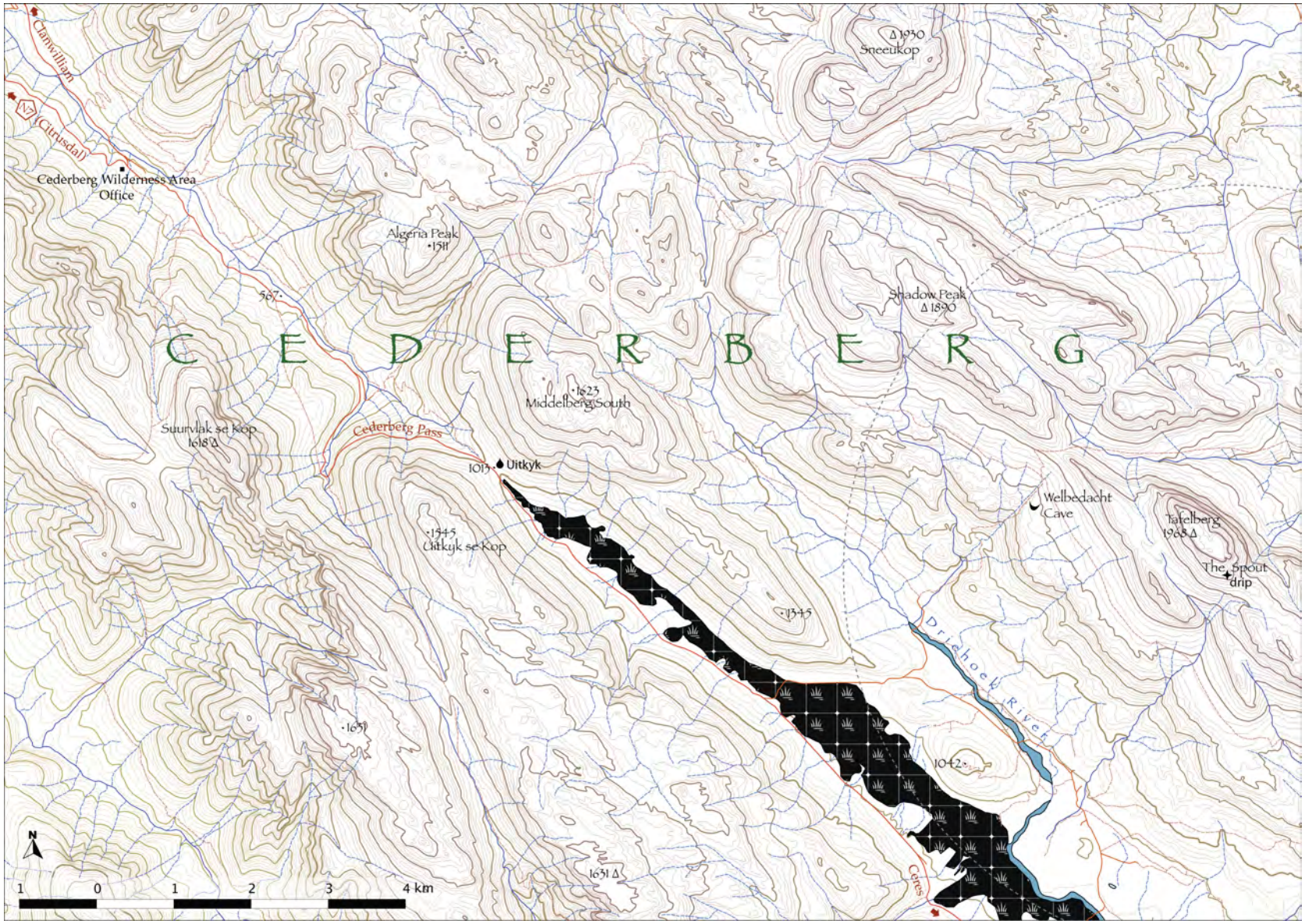

Figure 3.9: Locations of the rainfall collector and high altitude seep sampled in the Cederberg, south-east of Clanwilliam.

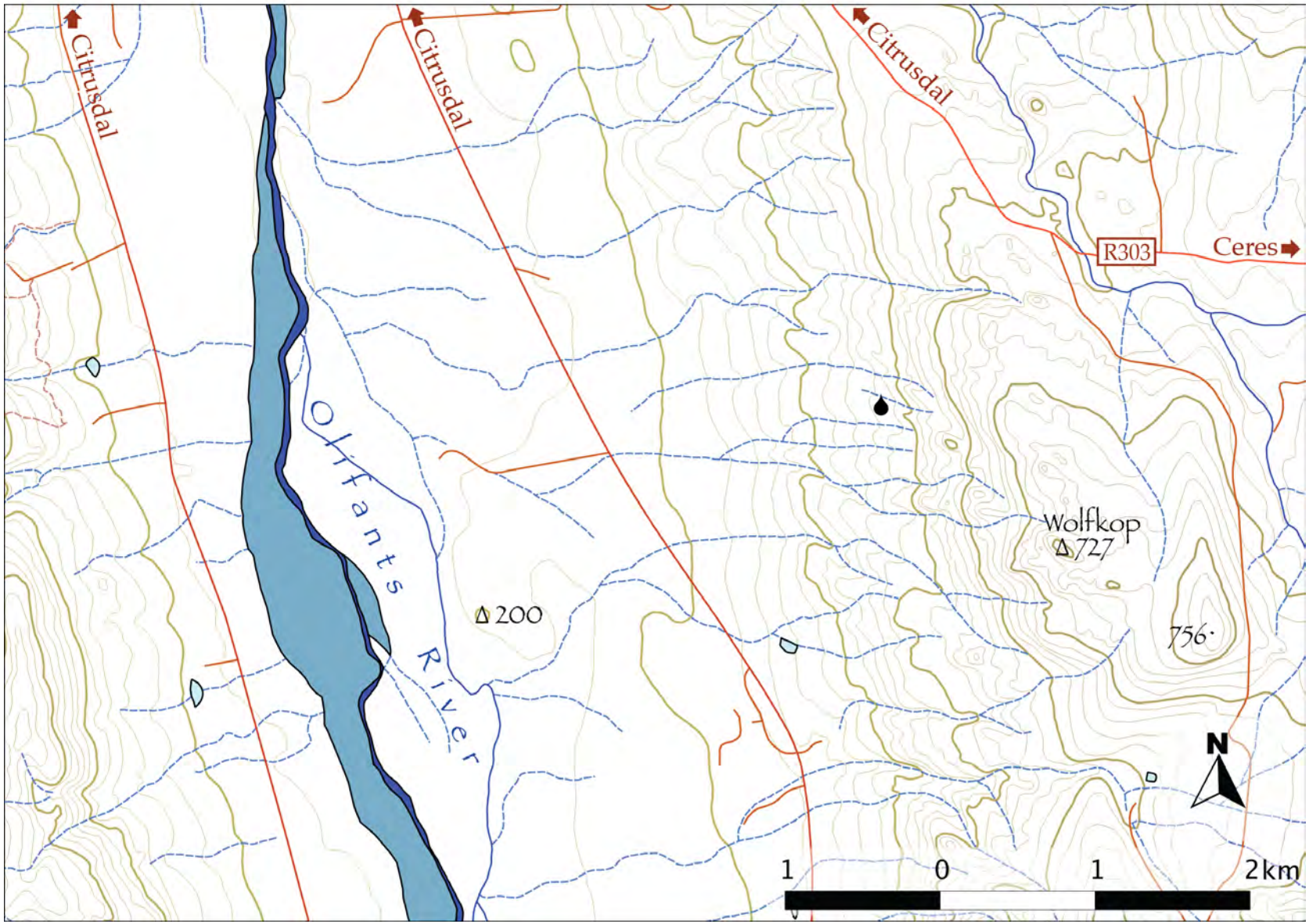

Figure 3.10: Location of the rainfall collector at Wolfkop Nature Reserve, south of Citrusdal.

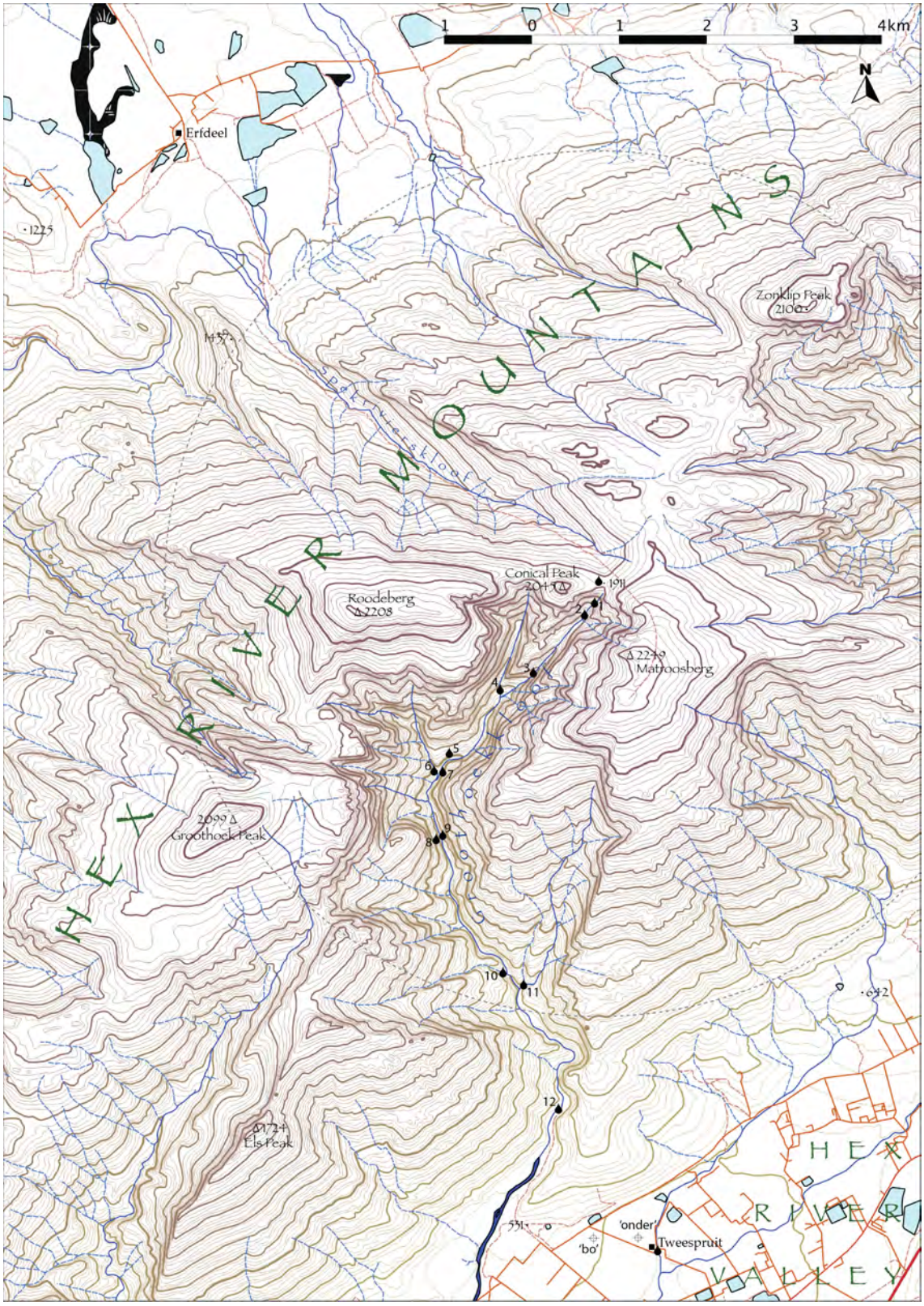

Figure 3.11: Locations of the Erfdeel and Tweespruit rainfall collectors and boreholes and the Groothoekkloof river samples in the vicinity of Matroosberg, the highest peak in the south-western Cape.

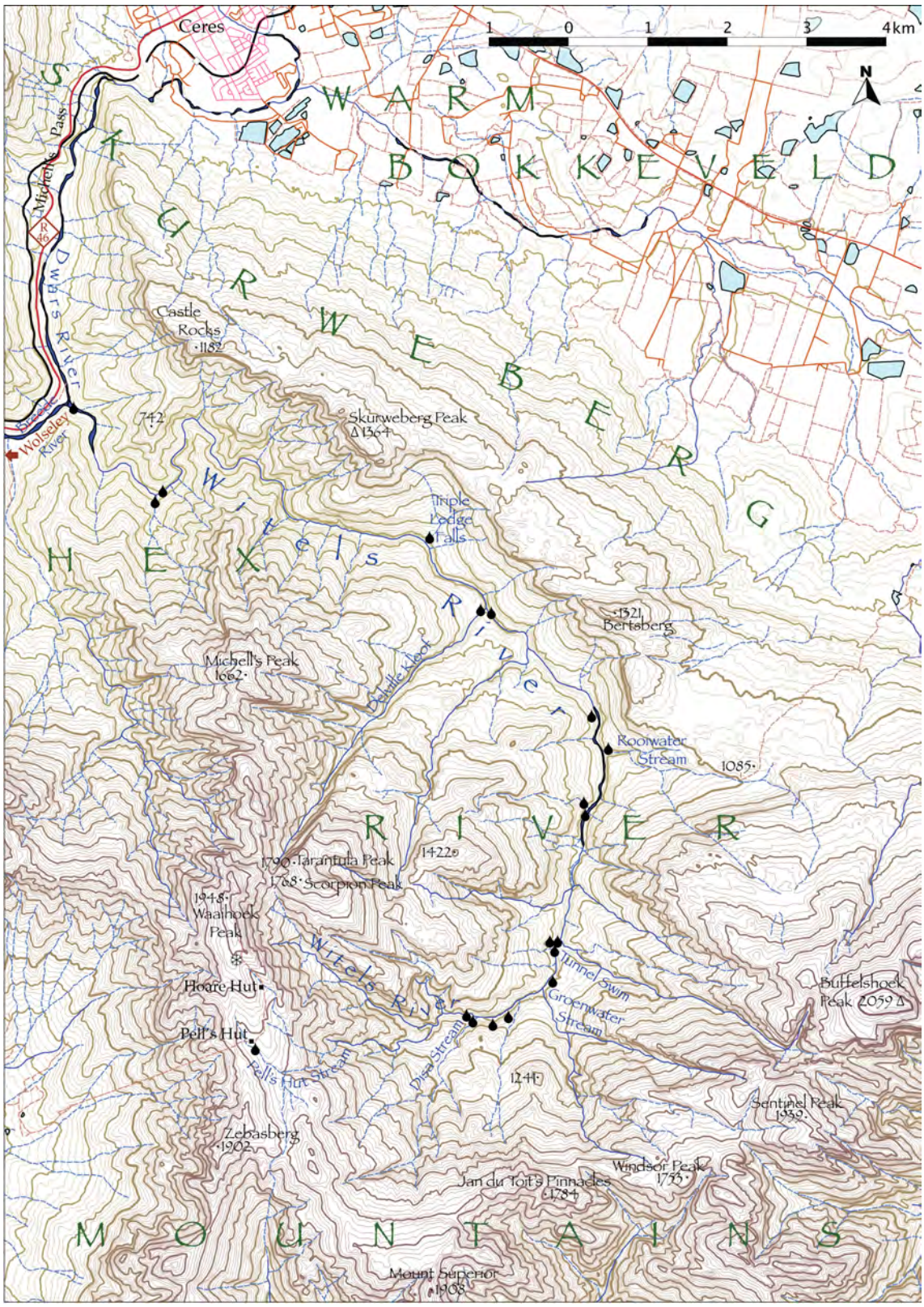

Figure 3.12: Locations of the Waaihoek Peak snow and Witels River samples taken in the Hex River Mountains, south of Ceres.

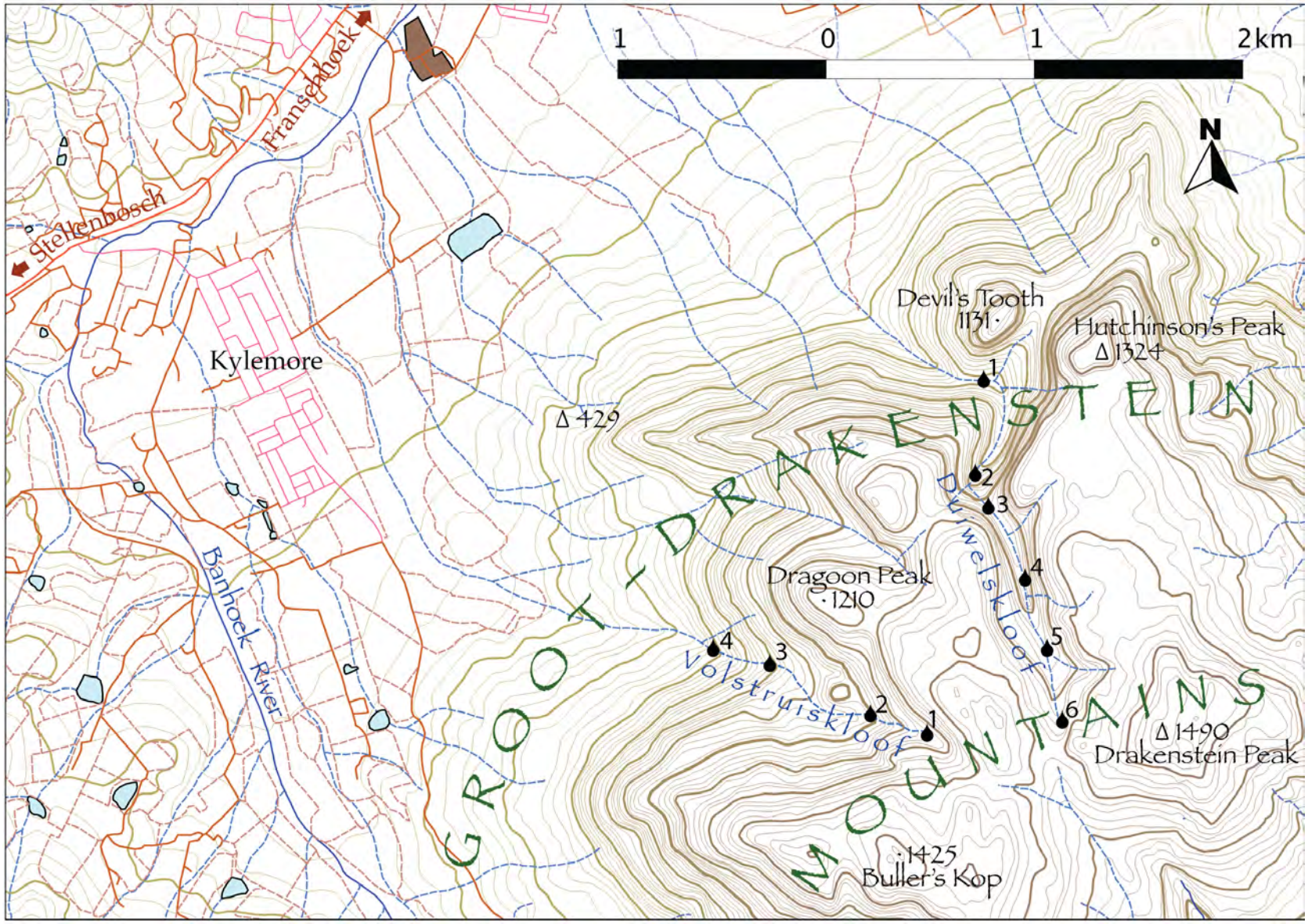

Figure 3.13: Locations of the Duiwelskloof and Volstruiskloof river samples taken in the Groot Drakenstein Mountains, east of Stellenbosch.

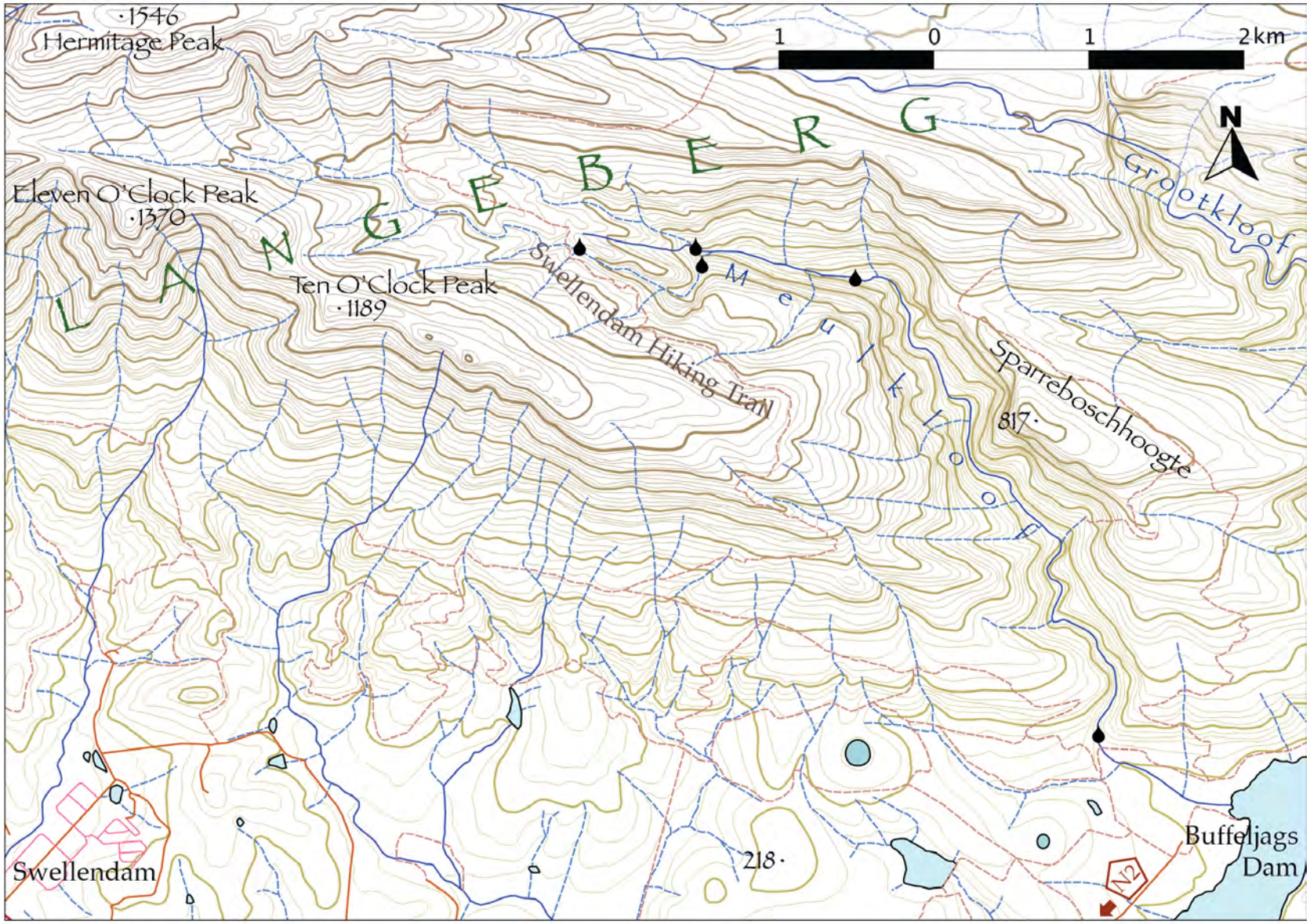

Figure 3.14: Locations of the Meulkloof river samples taken in the Langeberg, east of Swellendam.

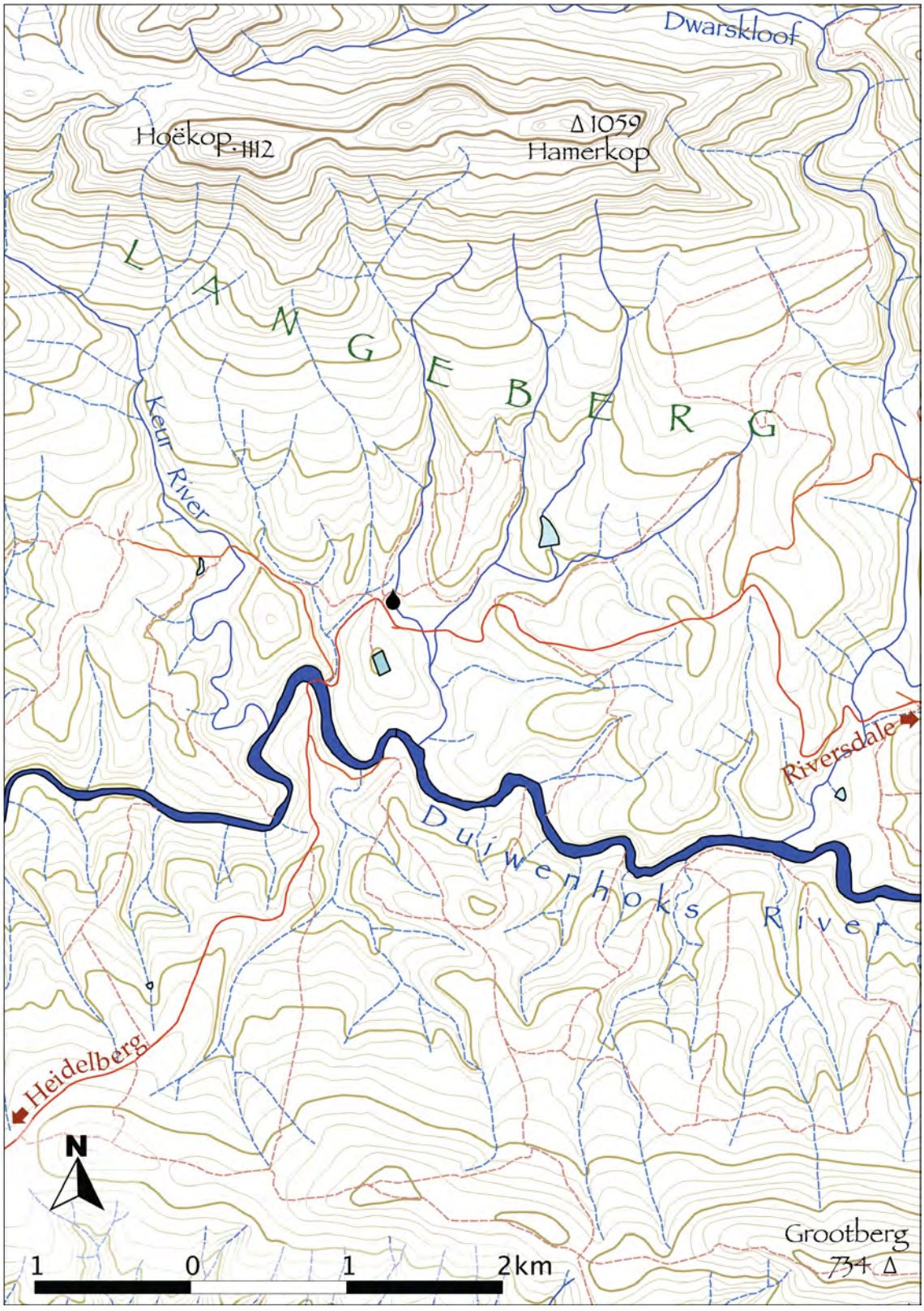

Figure 3.15: Location of the Riverndale rainfall collector, north of Heidelberg.

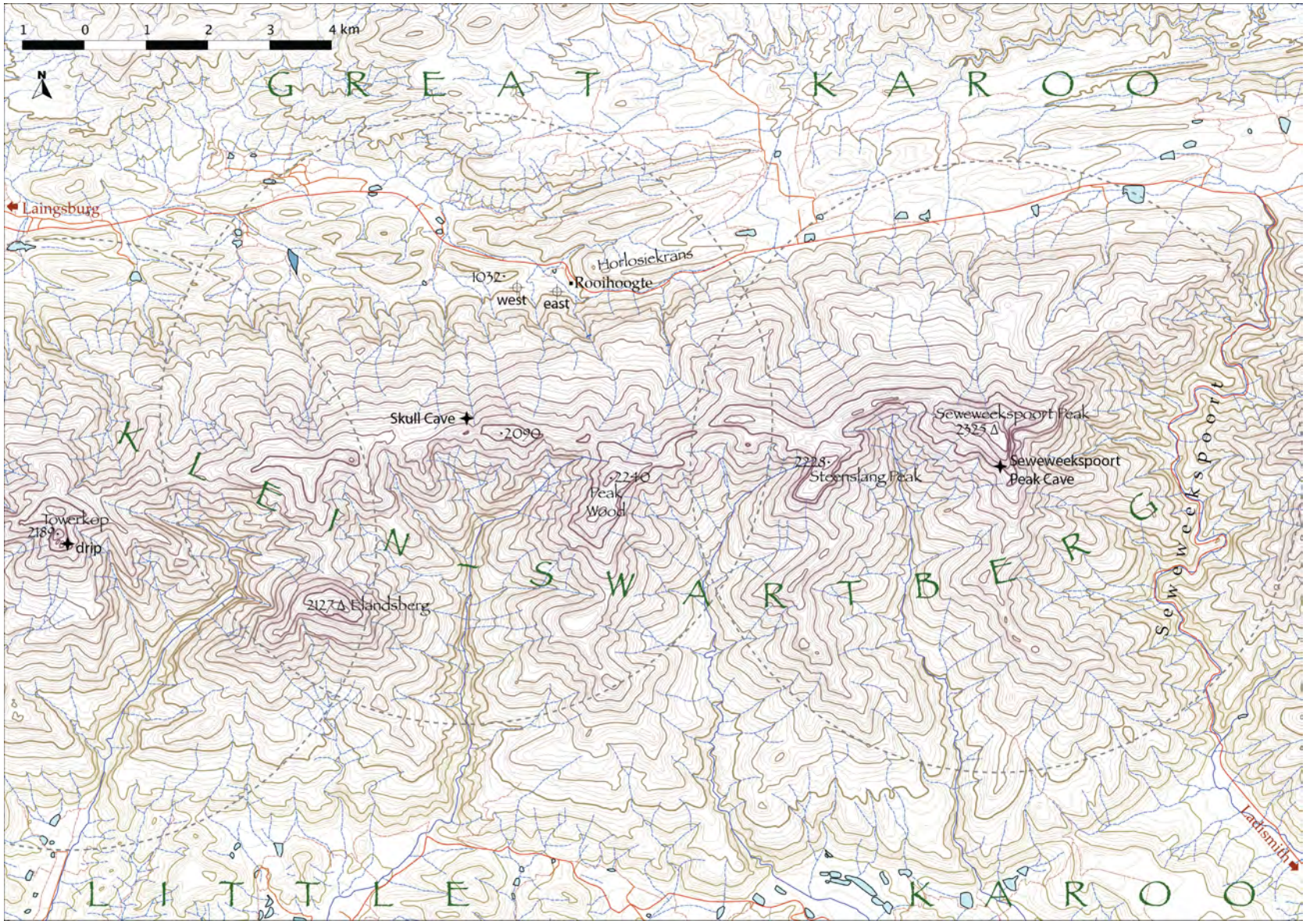

Figure 3.16: Locations of high altitude seeps in the Klein Swartberg and boreholes on Rooihoogte Farm.

Figure 3.17: Locations of the Bakenskop mountain and the store rainfall collectors as well as the boreholes at Gamkaberg, south-east of Calitzdorp.

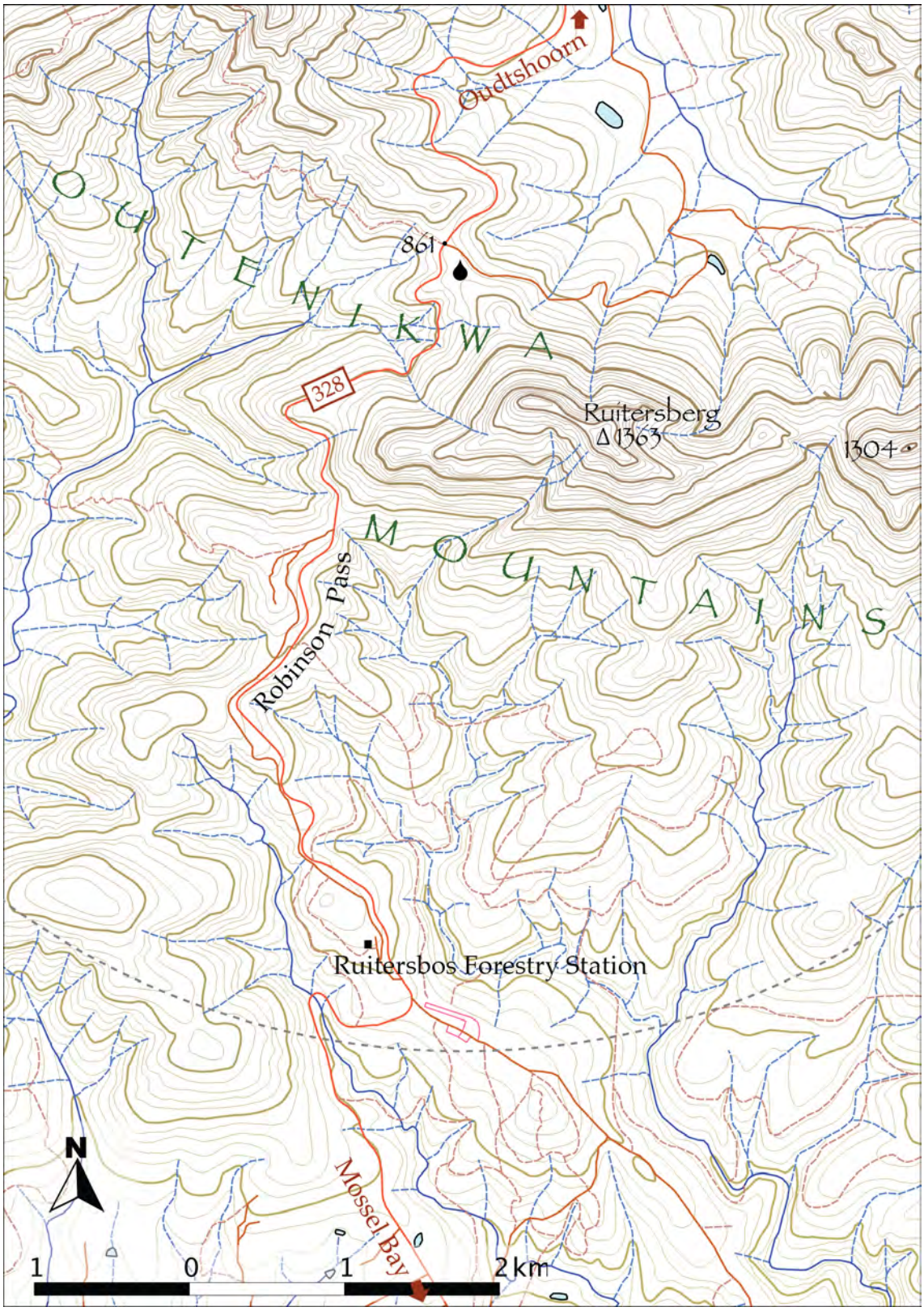

Figure 3.18: Location of the rainfall collector on Robinson Pass, north of Mossel Bay.

Figure 3.19: Location of the rainfall collector in the Kammanassie Mountains, south of De Rust.

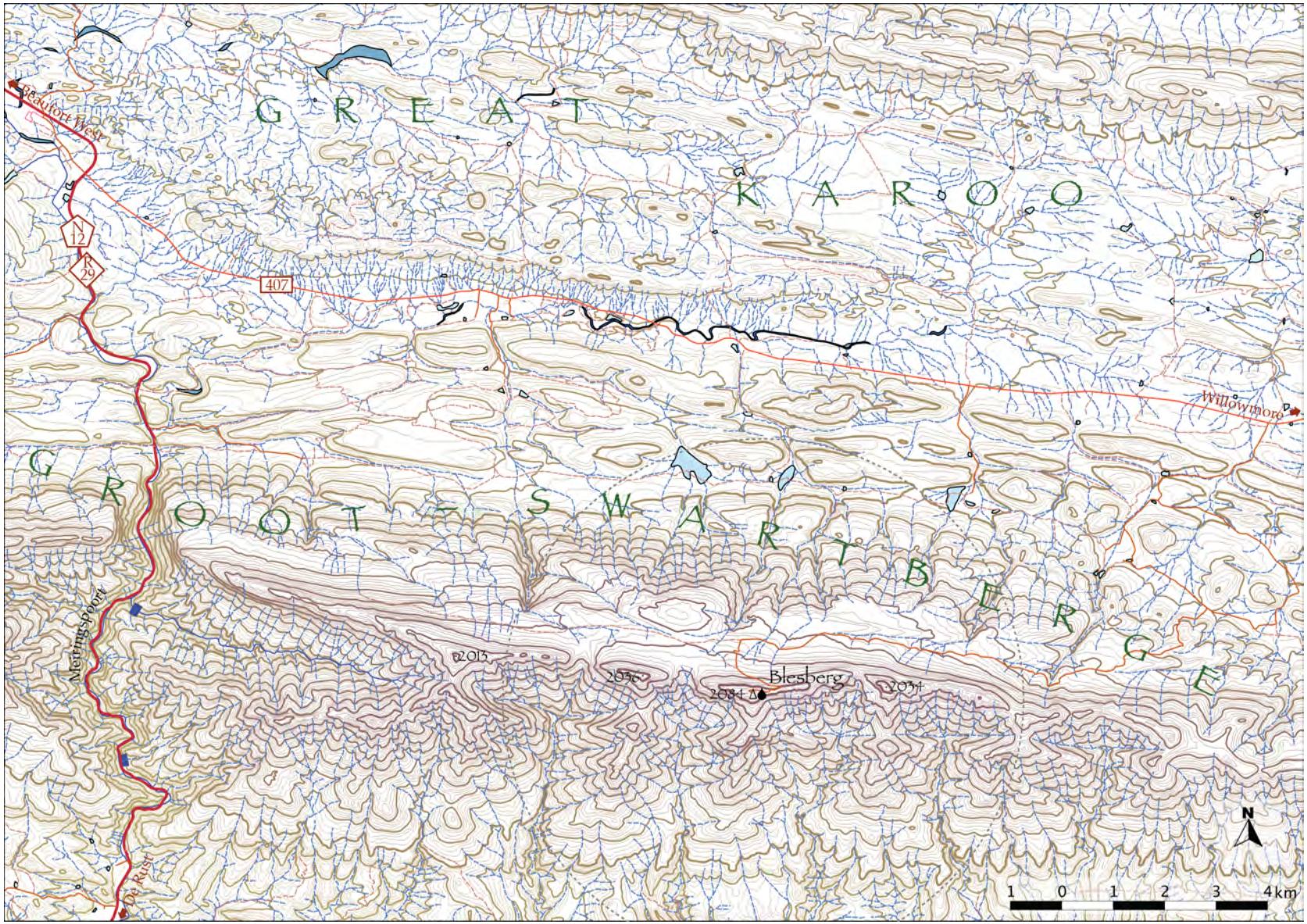

Figure 3.20: Location of the rainfall collector on top of Blesberg in the Groot Swartberg, north-east of De Rust.

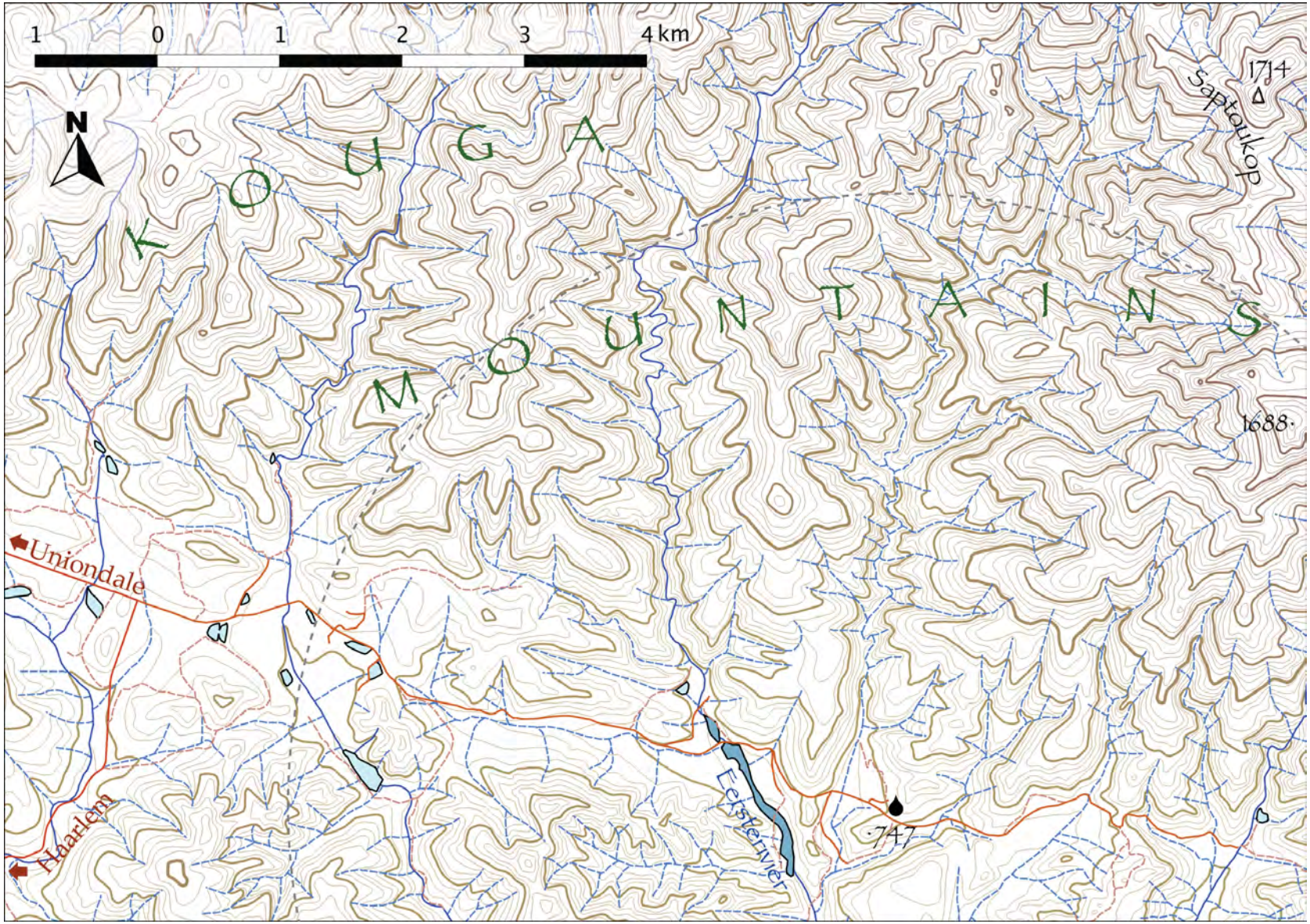

Figure 3.21: Location of the rainfall collector on Lentelus Farm in the Kouga Mountains, south-east of Uniondale.

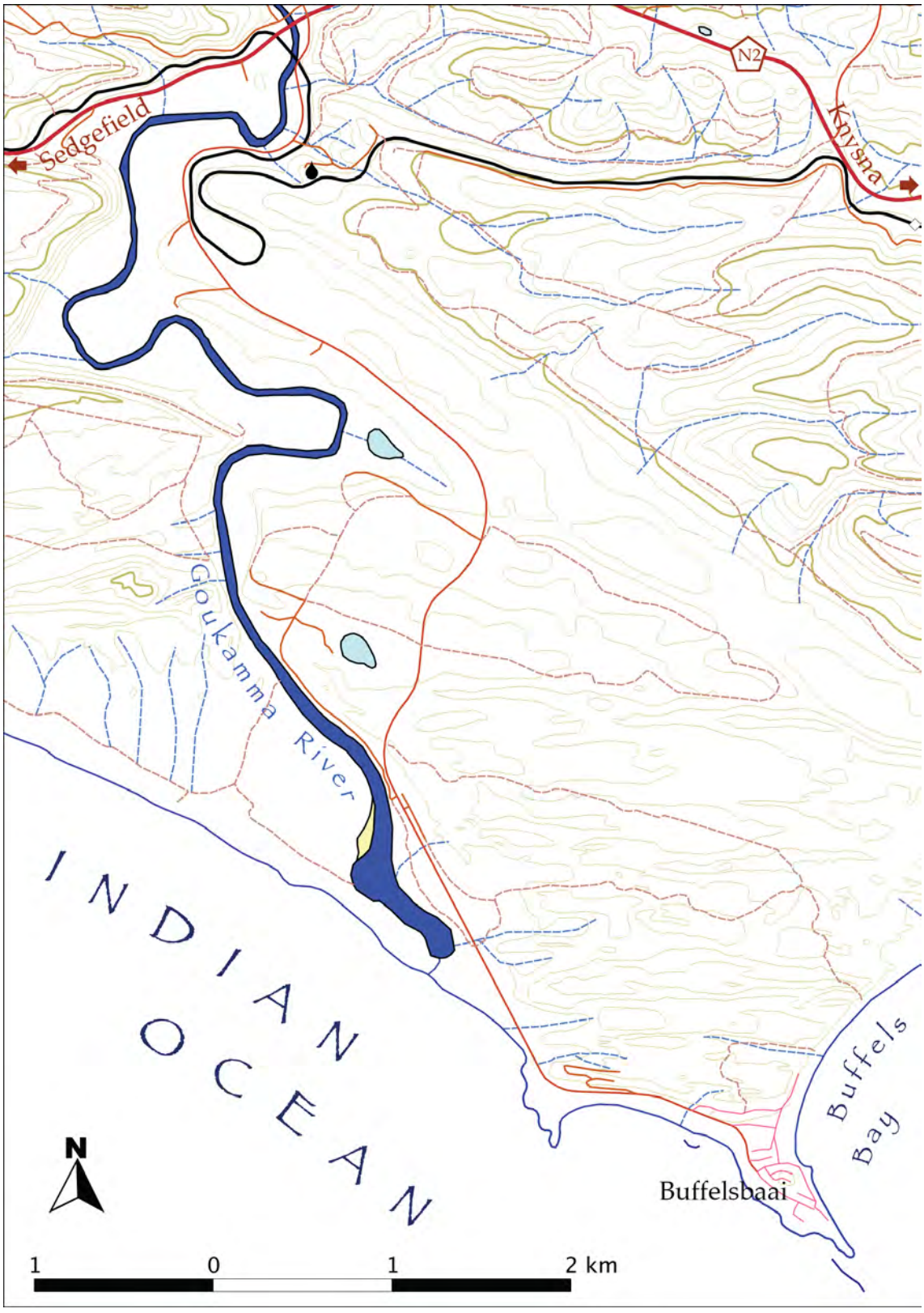

Figure 3.22: Location of the rainfall collector above the Goukamma River, west of Knysna.

Chapter 4

Results

4.1 Introduction

This chapter reports the data collected in this study, namely rainfall amounts and hydrogen and oxygen isotope values of various water samples, including rain, snow, river water and groundwater, the latter from both natural sources such as springs and seeps as well as from boreholes. The rainfall is presented as monthly amounts and some of the notable variations in space and time are described. Isotope data of rainfall is presented over time and compared with weather events to make sense of some of the outlier isotopic compositions. The rain isotope data is also analysed by generating means and weighted means for each rainfall station, d-excess values for these means, and meteoric water lines. Groundwater isotope data and the best-fit line through this data is compared to the rainfall isotope data and meteoric water lines. Mention is also made of other samples, such as surface water and snow. The isotope data for this study is reproduced in **Tables 4.5 to 4.10** at the end of this chapter.

4.2 Rain

In order to understand the hydrological impact of hydrogen and oxygen isotope ratios in monthly cumulative rainfall samples, the amount of rain for each month must be known. Isotope values from months with high rainfall have a greater effect on the isotope signatures in the hydrological cycle than months with low rainfall and therefore the isotope values need to be weighted accordingly when calculating means and meteoric water line equations. All the regular rainfall samples taken for this study are shown in **Table 4.1**.

	2010												2011												2012											
stn.	J	F	M	A	M	J	J	A	S	O	N	D	J	F	M	A	M	J	J	A	S	O	N	D	J	F	M	A	M	J	J	A	S	O	N	D
UCT	–	–	–	–	–	–	–	–	–	–	–	–	–	–	–	–	–	–	–	–	–	–	–	–	–	–	–	–	–	–	–	–	–	–	–	–
TMC					–	–	–	–	–	–	–	–	–			–	–	–	–	–	–	–	–	–	–	–	–									
TWT					–	–	–	–	–	–	–	–	–	–	–	–	–	–	–	–	–	–	–	–	–	–	–	–	–	–	–	–				
UKP								–	–	–	–	–	–	–	–	–	–	–	–	–		–	–	–	–	–	–	–	–		–	–				
WKP					–	–	–	–	–	–	–	–	–	–	–	–	–	–	–	–	–	–	–	–	–	–	–	–	–	–	–	–				
MTB					–								–	–	–	–	–	–	–	–	–	–	–	–	–										
DDN																		–	–	–	–	–	–	–	–					–					
RVD						–	–	–	–	–	–	–	–	–	–	–	–	–	–	–	–	–	–	–	–	–	–	–								
RBP						–	–	–	–	–	–								–																
BKK						–	–	–	–	–	–					–	–	–	–	–	–	–	–	–											
GST													–	–	–	–	–	–	–	–			–	–	–	–	–	–	–	–	–	–				
BBG						–	–	–	–	–	–	–	–	–	–	–				–	–	–	–			–	–	–	–	–	–					
KMN						–	–	–	–	–	–					–	–	–	–		–														
LTL						–	–	–		–	–		–	–	–	–	–	–	–	–	–	–	–	–	–	–	–								
GKM						–	–	–	–	–	–	–	–	–	–	–	–	–	–	–	–	–	–	–	–	–	–	–	–							

Table 4.1: Bars indicate the months for which total monthly rainfall was analysed for hydrogen and oxygen isotopic composition.

station code and name		elevation	continentality		MAP	SI	n	weighted mean & standard deviation				d-excess
			Atlantic	'sea'				δD	$\sigma_{\delta D}$	$\delta^{18}O$	$\sigma_{\delta^{18}O}$	
		(masl)	(km)	(km)	(mm/a)			‰	‰	‰	‰	‰
UCT	University of Cape Town	135	8	8	1210	0.63	36	-9.2	6.0	-2.89	1.19	14.0
TMC	Table Mountain	1074	3	2	1328	0.43	23	-13.9	5.7	-3.77	1.04	16.3
TWT	Twaktuin	412	48	45	510	0.76	17	-11.4	19.6	-2.96	3.41	12.3
UKP	Uitkyk Pass	1013	70	70	1177	0.81	20	-21.7	9.8	-4.67	2.23	15.6
WKP	Wolfkop	355	72	70	565	0.81	25	-15.9	11.4	-3.82	1.42	14.7
MTB	Matroosberg	1910	143	110	702	0.83	14	-43.1	9.6	-7.95	1.44	20.5
DDN	Tweespruit	482	133	105	213	0.91	6	-19.4	15.8	-3.14	2.09	5.8
RVD	Riverndale	251	242	42	671	0.40	23	-10.3	13.7	-3.44	2.38	17.2
RBP	Robinson Pass	885	330	30	1093	0.47	7	-23.3	11.3	-4.91	2.39	16.0
BKK	Bakenskop	1101	314	50	529	0.46	15	-29.2	12.2	-5.84	2.63	17.5
GST	Gamka Store	350	315	55	297	0.50	15	-15.6	13.5	-3.37	2.76	11.4
BBG	Blesberg	2080	410	65	735	0.50	18	-28.3	8.0	-6.16	1.04	21.0
KMN	Kammanassie	666	482	50	400	0.56	11	-36.3	23.1	-7.37	2.95	22.7
LTL	Lentelus	642	573	35	567	0.51	20	-26.9	20.4	-5.62	3.16	18.1
GKM	Goukamma	62	526	5	701	0.54	25	-14.3	15.3	-3.82	1.98	16.3
	all				713		275	-17.7	14.2	-4.22	2.33	16.0

Table 4.2: Continentality distance from Atlantic Ocean measured along a line of latitude; 'sea' distance is distance in any direction to the closest coast. Mean annual precipitation (MAP) and seasonality index (SI) based on 3 years of rainfall records; stable isotope weighted means and standard deviations using 'n' number of cumulative monthly rainfall samples. Deuterium excess for each station and the region, calculated from the weighted means.

These rainfall amounts should have been recorded when the rain was collected, however, due largely to human error, not all the figures were recorded or retained for each sample. In some cases people collecting rain forgot to record the amount, in other cases, the data was mislaid. However, it was possible to estimate these missing rainfall amounts by interpolation between South African Weather Service stations (SAWS, 2010-12), rainfall stations within this study and by using the SAWS monthly rainfall maps, examples of which are given in **Figure 4.1**. When estimating missing rainfall amounts, consideration was also given to factors known to affect rainfall, in particular the altitude, proximity and leeward or windward relationship to mountains, and distance from the sea.

The resultant rainfall figures, both measured and estimated, for each rainfall collection station are displayed in time series graphs in **Figure 4.14**. The most obvious pattern seen in these graphs is the seasonal signature caused by the higher rainfall occurring in winter from cold fronts (westerly waves) and the subsequent southerly meridional flow, as explained in Chapter 2. The second most noticeable pattern is the change from highly seasonal rain in the west to less seasonal in the east, as discussed below in **Section 4.2.2**.

4.2.1 Rainfall Amount

The average annual rainfall at the rain collection stations is shown in **Table 4.2**. Although this figure is only for three years and for most of the stations is based on many estimations, the averages do illustrate the range of rainfall amounts recorded and some general trends. Stations at higher latitude, altitude and nearer to the sea tend to receive more rain. Other factors, such as proximity to mountains, steepness of slopes and aspect (relative to rain-bearing winds) also influence the rainfall at a site. These were the factors used by Dent et al. (1987) and Beuster et al. (2009) to produce the MAP (mean annual precipitation) map for the south-western Cape, as discussed in Chapter 1.

Examination of the graphs in **Figure 4.14** shows how variable rainfall is across the Western Cape. Rainfall collection stations less than 50 km apart can receive vastly different quantities of rain in a month. For example, in August 2010, Twaktuin recorded 69 mm, Uitkyk Pass 215 mm and Wolfkop 84 mm. These sorts of variations are epitomized by the famous microclimates of Cape Town, as is revealed from the UCT and Table Mountain Cableway stations, less than 5 km apart, where in December 2010 those two stations recorded 17 mm and 60 mm respectively, and similarly for October 2012 with 44 mm and 123 mm. This variation is not always systematic; the generally wetter station may sometimes receive less rain. For example, in February 2011, Lentelus, which averages 80 % of the rainfall of Goukamma, recorded 65 mm in comparison to Goukamma's 39 mm; this is 160 %, or double the expected amount; or one could say that Goukamma was half as wet as would be expected from the Lentelus rainfall. Similarly, in November 2012 UCT recorded 6 0mm in comparison to the normally wetter Table Mountain Cableway's 44 mm.

4.2.2 Rainfall Seasonality

The seasonality index (SI), as described by Walsch and Lawler (1981), has been calculated for the rainfall collection stations in this study, according to the formula:

$$SI = \frac{1}{\bar{R}} \sum_{n=1}^{n=12} \left| \bar{x}_n - \frac{\bar{R}}{12} \right|$$

where $\bar{R}$ is the MAP and $\bar{x}_n$ is the mean monthly precipitation for month n.

The SI values may not be very meaningful after only 3 years of collection, however, they still provide a reasonable idea of seasonality. The SI values, as shown in **Table 4.2**, all fall within moderately seasonal categories: SI from 0.40 to 0.59 is "rather seasonal with a short drier season"; SI from 0.60 to 0.79 is "seasonal" and SI from 0.80 to 0.99 is "markedly seasonal with a long drier season" (Walsch and Lawler, 1981). There is a general decrease in SI eastwards, as would be expected given that summer rainfall gradually increases from Cape Town eastwards. To the east of the study area, seasonality will again increase eastwards as the winter rainfall decreases.

The two maps in **Figure 4.1** also show the strong seasonality of rainfall in South Africa. The June 2010 map shows a typical winter rainfall pattern with most rain occurring in the Western Cape, high amounts being on the Boland, Hex River and Tsitsikamma Mountains and some other substantial rainfalls along the coast of the Eastern Cape and KwaZulu-Natal as well as on the high ground around the Lesotho - Free State - Eastern Cape borders. The December 2012 map shows a typical summer rainfall pattern, although with above average rainfall amounts, especially those over the Karoo and Namaqualand, while the Western Cape experiences negligible rainfall, except for the futhest eastern portions.

4.3 Rain Isotopes

Four hundred and thirty-five water samples have been analysed for their hydrogen and oxygen isotope composition, excluding duplicates, repeats, laboratory standards or blanks. The graph in **Figure 4.2** shows the distribution of the water samples according to major water type and collection altitude of sample. Rain waters make up the bulk of the samples at 279, groundwaters are intermediate at 110 and surface waters the minority at 46 samples. The altitude distribution reflects the dominance of samples taken in settled areas, which are generally at lower elevations, either near the coast or in valleys, with two spikes at higher elevations due to the rain and groundwater samples taken on peaks or passes at 1000–1200 m, or on the high peaks of the Cape Fold Belt at 1800–2200 m.

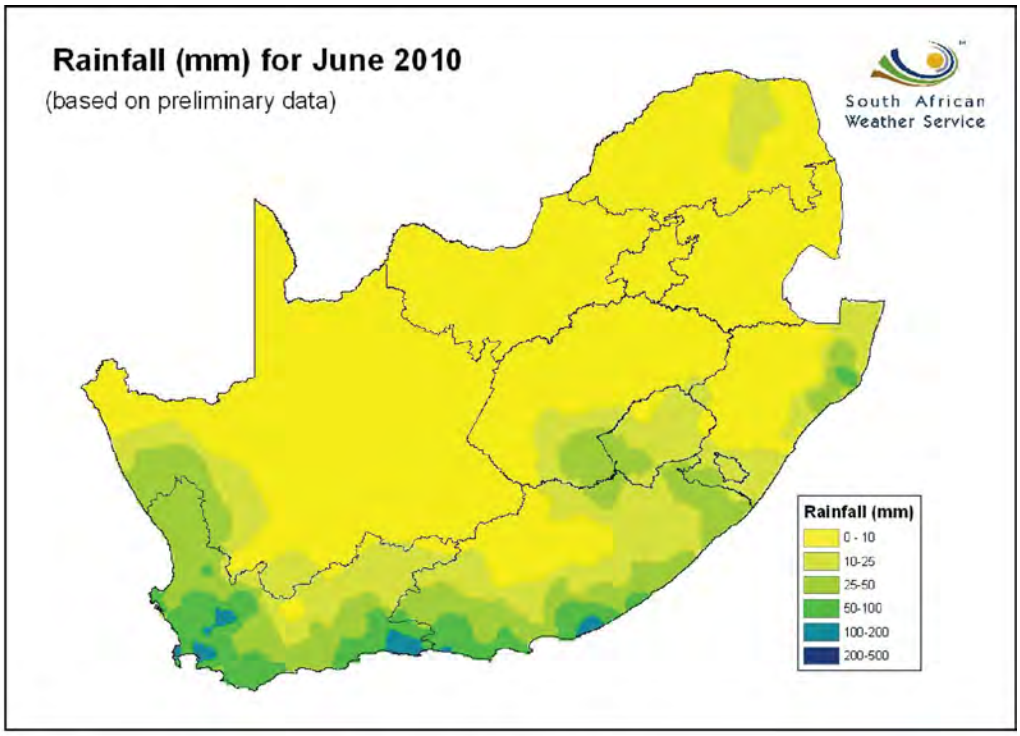

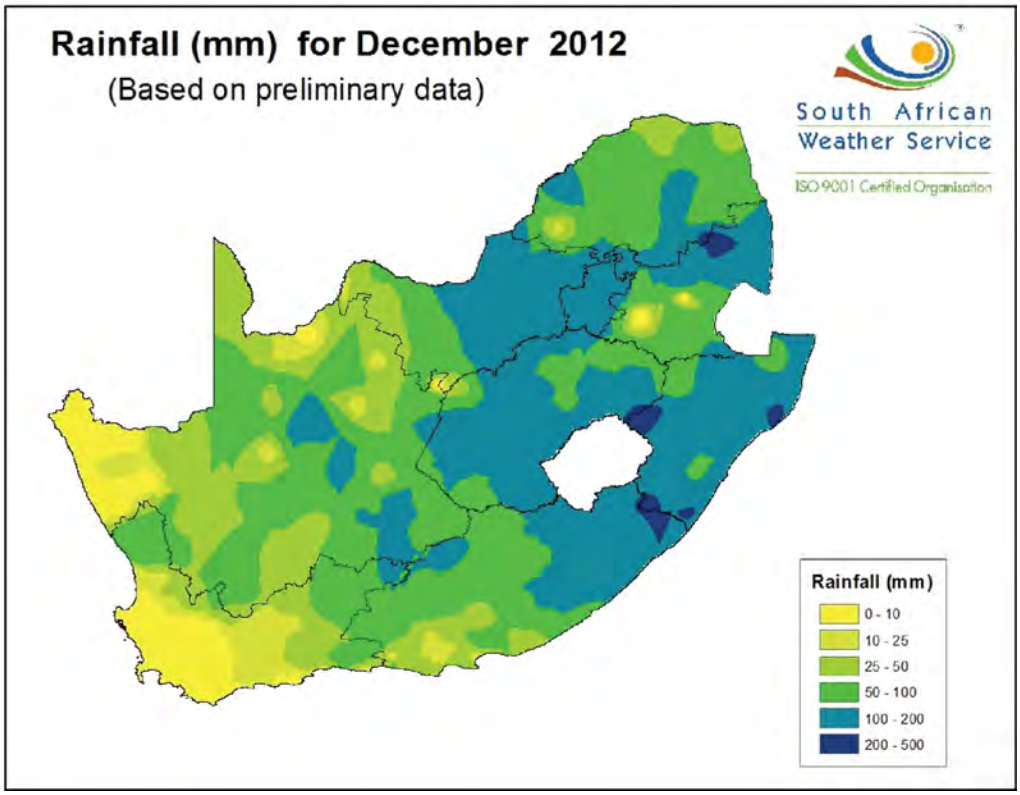

Figure 4.1: Two examples of the monthly rainfall maps produced by the South African Weather Service and available for download from their website (www.weathersa.co.za). The June 2011 map shows a typical winter rainfall pattern and the December 2012 map shows a typical summer rainfall pattern, although about 20 % wetter than normal.

4.3.1 Temporal Variations

Time series graphs have been plotted of all the isotope data from all the rainfall collection stations (**Figures 4.3 and 4.4**), separated into an eastern cluster (Riverndale, Robinson Pass, Bakenskop, Gamka Store, Blesberg, Kammanassie, Lentelus and Goukamma) and western cluster (UCT, Table Mountain, Twaktuin, Uitkyk, Wolfkop, Matroosberg and De Doorns) for ease of viewing. Several features stand out from these graphs. Firstly, although the isotope δ values correlate amongst stations some of the time, at other times they do not. In a few cases there may be field sampling errors, such as evaporation, causing a poor correlation. Most of the time, however, the samples are probably unaltered, based on discussions with the samplers, and the poor correlation indicates the spatial variation of isotope content of precipitation. This interpretation is reinforced by the observations made in **Section 4.2.1** showing how spatially variable rainfall amounts are. If the rainfall amounts are variable, the weather systems are heterogenous and it follows that the isotopic content of the rain may be varied.

Secondly, there is a general pattern of more negative δ values over winter and less negative δ values over summer, as would be expected for areas with a Mediterranean climate (e.g. Jaunat et al., 2013). This pattern is most noticeable in the eastern cluster, both for δD and $\delta^{18}O$. This pattern results from several of the meteoric water isotope effects, as mentioned in Chapter 1, such as the temperature effect and amount effect; in winter, temperatures are colder and rainfall amounts are greater, so rainout removes heavier isotopes faster and the lighter isotopes become more abundant in rain, resulting in more negative δ values. In summer the reverse is true; rainfall amounts are lesser and temperatures are warmer, resulting in less negative δ values. In particular, the effect of evaporation of raindrops during small amount rainfall events shifts the isotopic content to less negative or even positive δ values.

In the western cluster in particular, the data shows greater variation over summer and more similar values over winter. In winter, regional weather systems sweep over all the rainfall stations and produce rain of similar isotope content. In summer, weather systems may be more localised with the result that some stations receive almost no rain, others receive small, highly evaporated amounts with less negative or even positive δ values, and summer thunderstorms may deposit large amounts of rain with very negative δ values. As a result, summer isotopic ratios are less consistent between stations.

In addition to these general patterns, there are occasional spikes in δ values. July 2010 was a month with very negative δ values in the eastern cluster of rain collection stations. The weather systems that caused this month's rain have been compared to those in months without a negative spike in δ values, such as June 2010 or July 2011. For example, in July 2010 there were only two major rain producing systems, the first being a cold front followed by southerly meridional flow over 10–11th and the second being another cold front followed by south-westerly air flow on the 14–15th (SAWS, 2010-12). These rain producing weather systems are very similar to those for June 2010, in which a double cold front was followed by southerly meridional flow from 7–9th

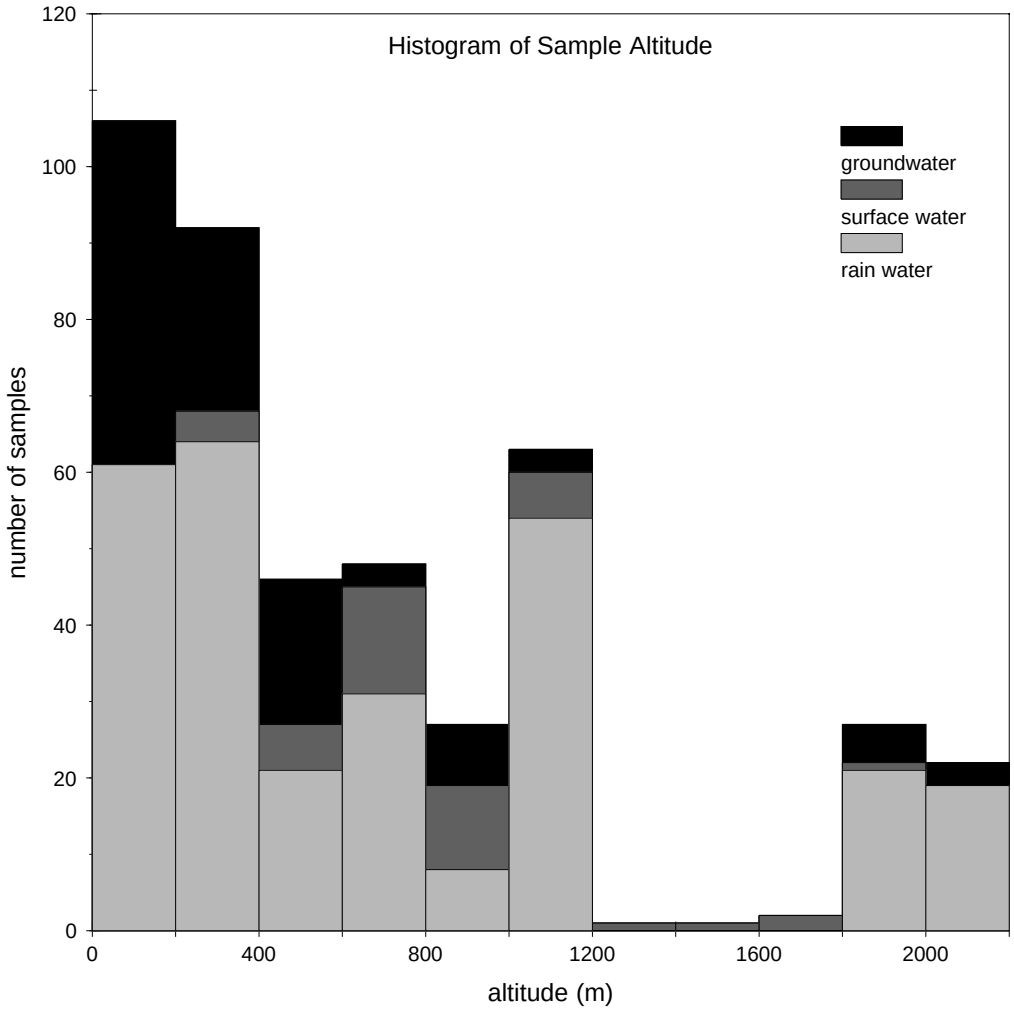

Figure 4.2: A plot of the distribution of the sampling altitude of all samples taken in this study.

and another double cold front was followed by southerly and then south-westerly flow over the 12–16th. For all these events, maximum daily rainfalls across the study area were typically in the 30–60 mm range, with averages being in the 10–20 mm range (SAWS, 2010-12). There is no unusual weather system or anomalously high rainfall for July 2010.

Temperatures at a weather station may undergo various changes as a weather system passes over. Maximum temperatures typically decrease as the cloudy, wet weather arrives and recover once clearing takes place, although may stay depressed if the southerly or south-westerly airflow is strong. Minimum temperatures however, may either decrease or increase, depending on the weather preceding the arrival of the cold front and the timing of the system (SAWB, 1996). Temperatures behaved variably in the June 2010 and July 2010 rainfall producing weather events, with no remarkable cold or change in July 2010. In the case of this distinctive spike in isotope values, it is therefore not easy to find something exceptional about the weather that could account for these results.

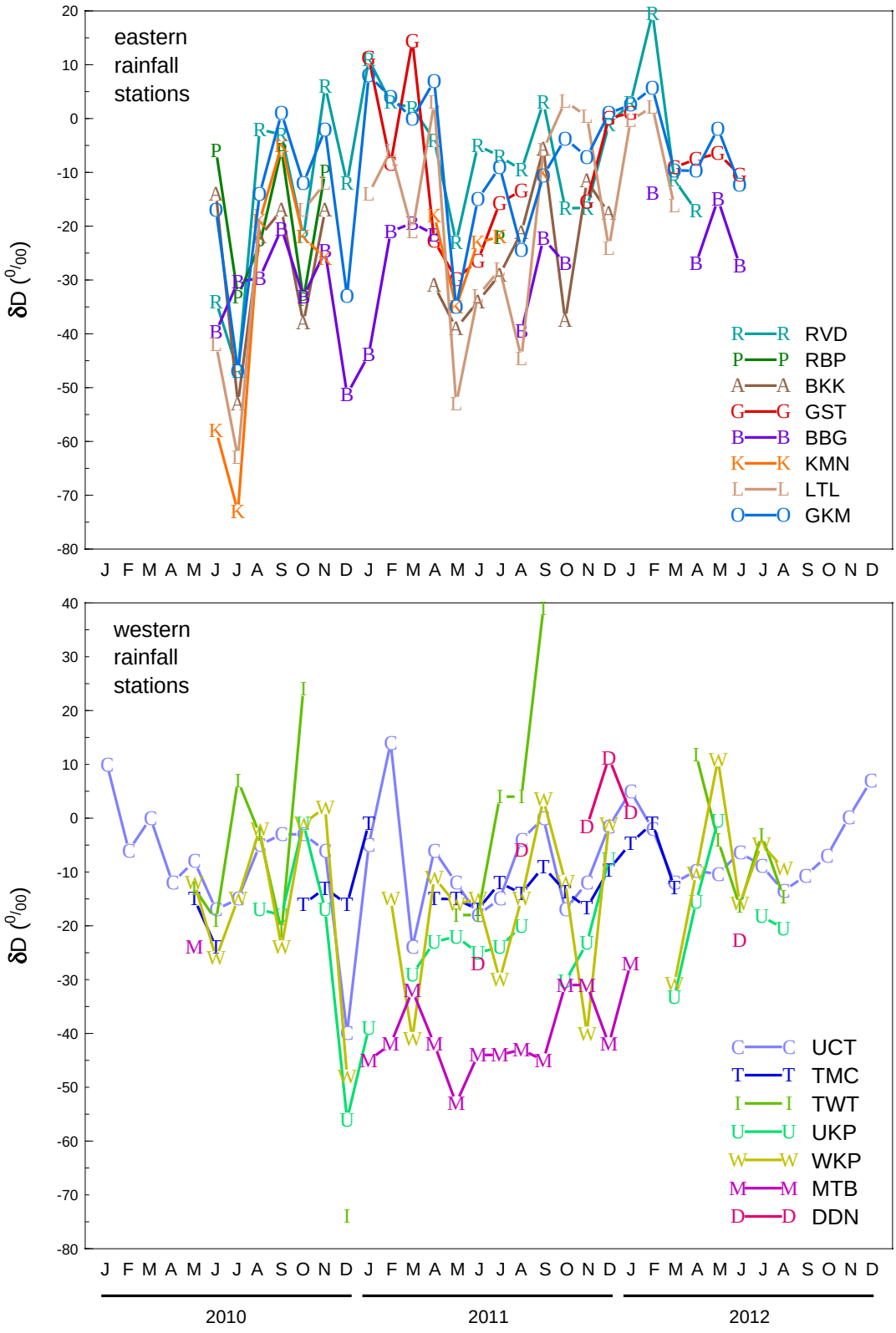

Figure 4.3: Time series graphs for δD for all rainfall stations, the eastern cluster on top and western cluster at the bottom. Stations with missing months have broken lines.

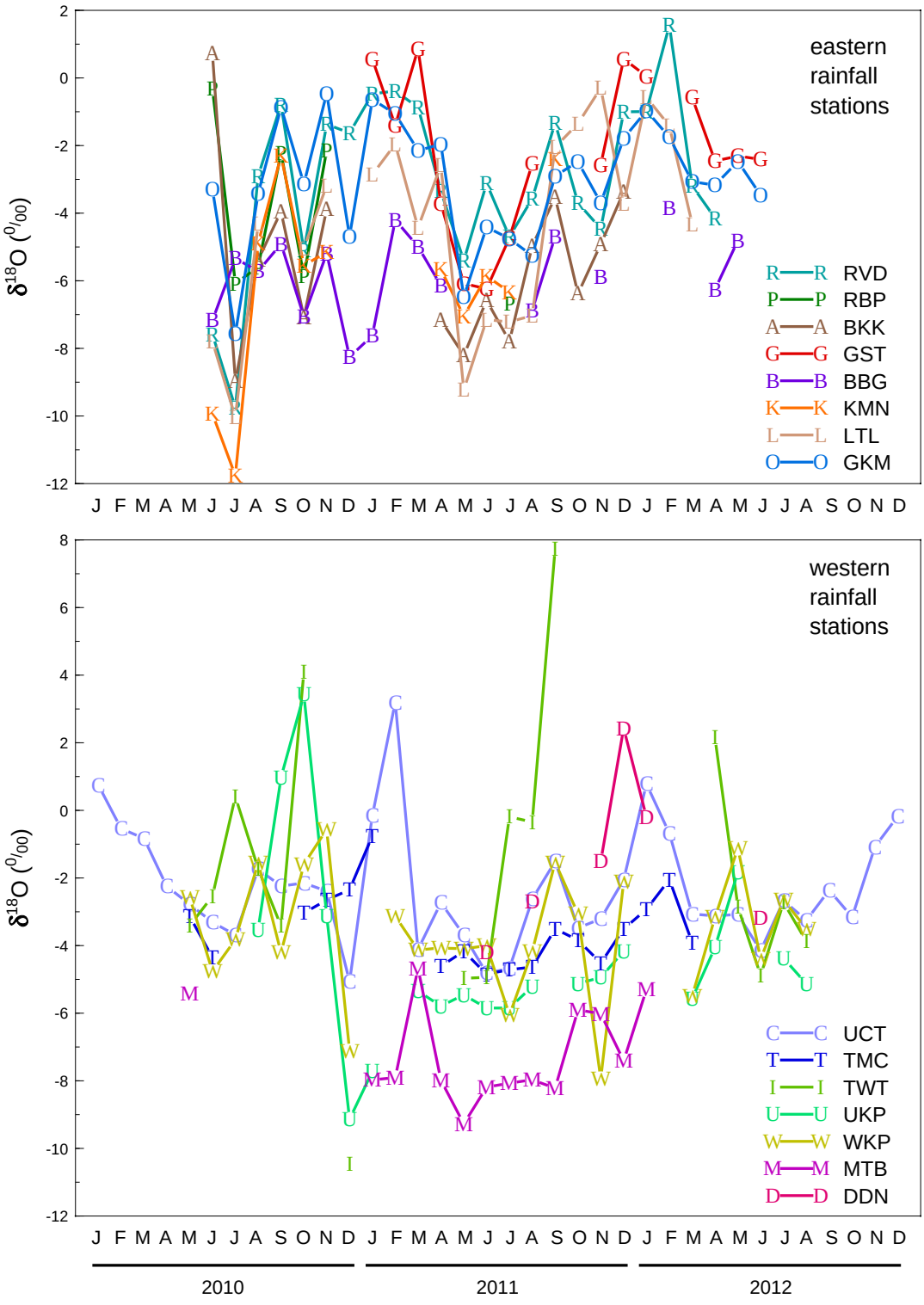

Figure 4.4: Time series graphs for $\delta^{18}O$ for all rainfall stations, the eastern cluster on top and western cluster at the bottom. Stations with missing months have broken lines.

December 2010 also features a negative spike in delta values, most noticeable for the Cederberg cluster of stations. In this case, it is easy to find the weather systems responsible for these results. During this month, several west coast troughs established and ridges of low pressure, connected to the summer rainfall producing *Kalahari Low*, penetrated far south into the Western Cape, but only twice did these result in appreciable rainfall in the Western Cape. The first occurred on 15–16th and delivered daily rainfall up to 60 mm at Vredendal, with lesser amounts of 30 mm at Lamberts Bay, 23 mm at Excelsior Ceres and other more minor amounts. The second event straddled the New Year, with up to 14 mm at Porterville on the 31st. Similar rainfalls occurred on 1st January 2011, such as 19 mm at Excelsior Ceres and 12 mm at Wellington, and it is quite possible that these were included in the December 2010 rainfall sample by the rainfall collectors. These low pressure systems produce convective style rain (thunderstorms) and hail was experienced by the author on top of Tafelberg at 1960 m in the Cederberg on 1st January 2011 (see **Figure 4.5**). The convective nature of these clouds can result in precipitation forming at high altitudes and hence low temperatures, which can result in relatively negative delta values, compared with the more stratified winter rainfall systems. Also, rainfall occurs in short, heavy showers in which minimal evaporation from raindrops occurs, reducing the extent to which the isotopic ratios will be driven to less negative delta values.

In November 2011 there was a very strong negative spike in the delta values for Wolfkop only. This can be traced to a low pressure trough extending southwards from the Kalahari on the 19th and causing convective rainfall. The rainfall amounts recorded were low, with daily totals of only 6 mm at Vredendal, 4 mm at Lamberts Bay and even lower elsewhere, but clearly the rain/hail that fell during this event must have been generated in systems with very low temperatures to account for the very negative delta values measured.

Some highly positive delta values, from +10 – +40 ‰ δD and +2 – +8 ‰ $\delta^{18}O$, were also measured, particularly at the Twaktuin station, but also at Uitkyk Pass, UCT and DeDoorns. These values have most probably been caused through extensive evaporation, both during the actual rainfall event of 19th November 2011 and possibly also from the rain gauge after the event. The latter is probably the reason for the extremely high spike at Twaktuin in September 2011, as there is no indication of similar behaviour at the other stations. However, the October 2010 spike is recorded at both Twaktuin and Uitkyk Pass and in that case probably reflects evaporation during rain drop descent. Similarly, the February 2011 measurements show more positive delta values at both UCT and Wolfkop, as well as for Wolfkop and DeDoorns in December 2011, and so these are likely to be real atmospheric isotopic enrichment during rain drop descent.

4.3.2 Means and Weighting

Mean delta values for each rain collection station have been calculated, both a simple arithmetic mean, and also a weighted mean, weighted according to the rainfall amount for each month (see **Table 4.2**). These results are shown in **Figure 4.6**, which demonstrates two significant patterns.

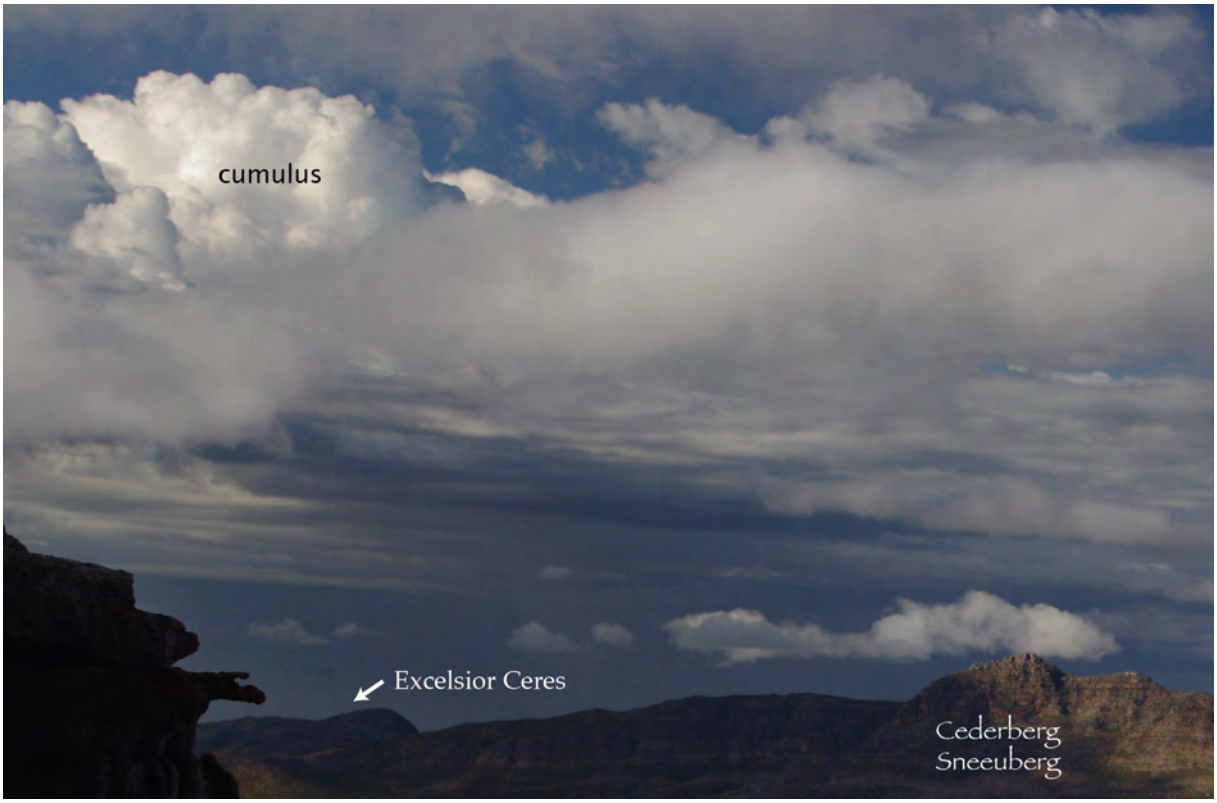

Figure 4.5: A view of the convective cumulus clouds and heavy rainfall (dark grey area in photo) that occurred in the West Coast and Cederberg region of the Western Cape over 31 December 2010 to 1st January 2011. Photograph taken from Cederberg Tafelberg, looking south over Sneeuberg and towards rain at Excelsior Ceres SAWS weather station.

Firstly, in all cases except one (δD at Uitkyk Pass), the weighted mean has a lower delta value for both δD and $\delta^{18}O$ than the unweighted mean, as is commonly observed in such studies (e.g. Iacumin et al., 2009). This is because the less negative delta values are associated with low rainfall events, mostly during summer where temperatures are higher and delta values of rain are less negative and where evaporation further increases the delta values. Put otherwise, the high rainfall, cold and isotopically more depleted winter rains bring the weighted means down towards more negative delta values.

Secondly, the degree of difference between the arithmetic mean and weighted mean is negatively correlated with the mean annual precipitation (see **Figure 4.7**). Sites with low total rainfall have more of the isotopically enriched very low rainfall months. These values drive the unweighted, or arithmetic, mean to unrealistically high delta values. When the weighted mean is calculated, the relatively few, but high rainfall months cause the weighted mean to have more negative delta values, so increasing the difference with the unweighted mean. It can be concluded that recording the rainfall amount when sampling rain is more important at drier locations, although still of value at all locations. According to Yurtsever and Gat (1981), when analysing the IAEA/WMO data: "The difference between the two means is not generally significant for stations

with a rather uniform monthly distribution of rainfall...". Our study, however, found that the correlation of difference between delta values with the seasonality index was very poor: δD and $\delta^{18}O$ vs SI gave Pearson's r correlations of 0.18 and 0.014 respectively, whereas the δD and $\delta^{18}O$ vs MAP correlations (as seen in **Figure 4.7**) are -0.71 and -0.65, respectively.

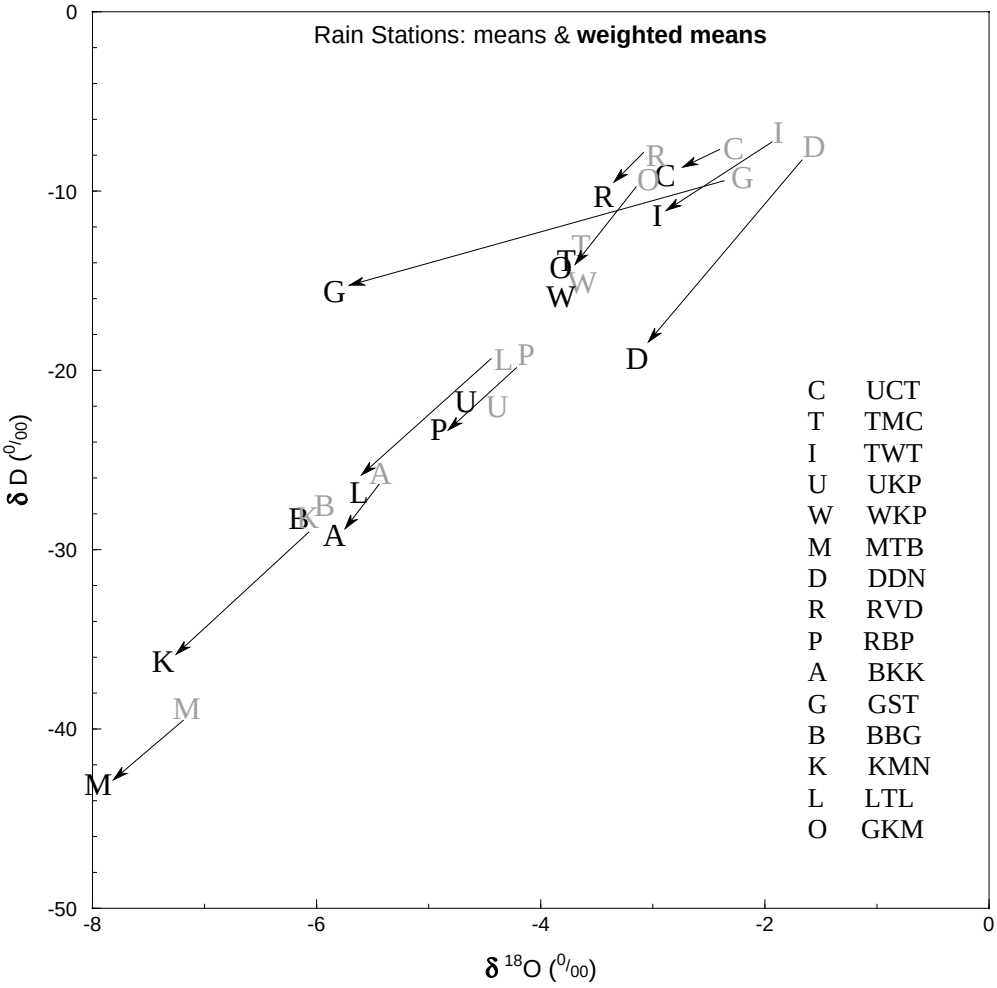

Figure 4.6: Arithmetic means and weighted means, by rainfall amount, for each rain collection station. Arrows show change from unweighted (arithmetic) means to weighted means.

The arithmetic and weighted mean δD and $\delta^{18}O$ values for UCT from this study compare favourably with previous studies in the Cape Town area, as shown in **Table 4.3**, although the results from this study are slightly less negative. There is a fair correlation between the amount of rainfall and the delta values, especially for δD, for the UCT data. The CTIA site is quite different, in terms of MAP and location, and most data is from 1960-80's and hence is not readily comparable, so it is displayed here more for interest.

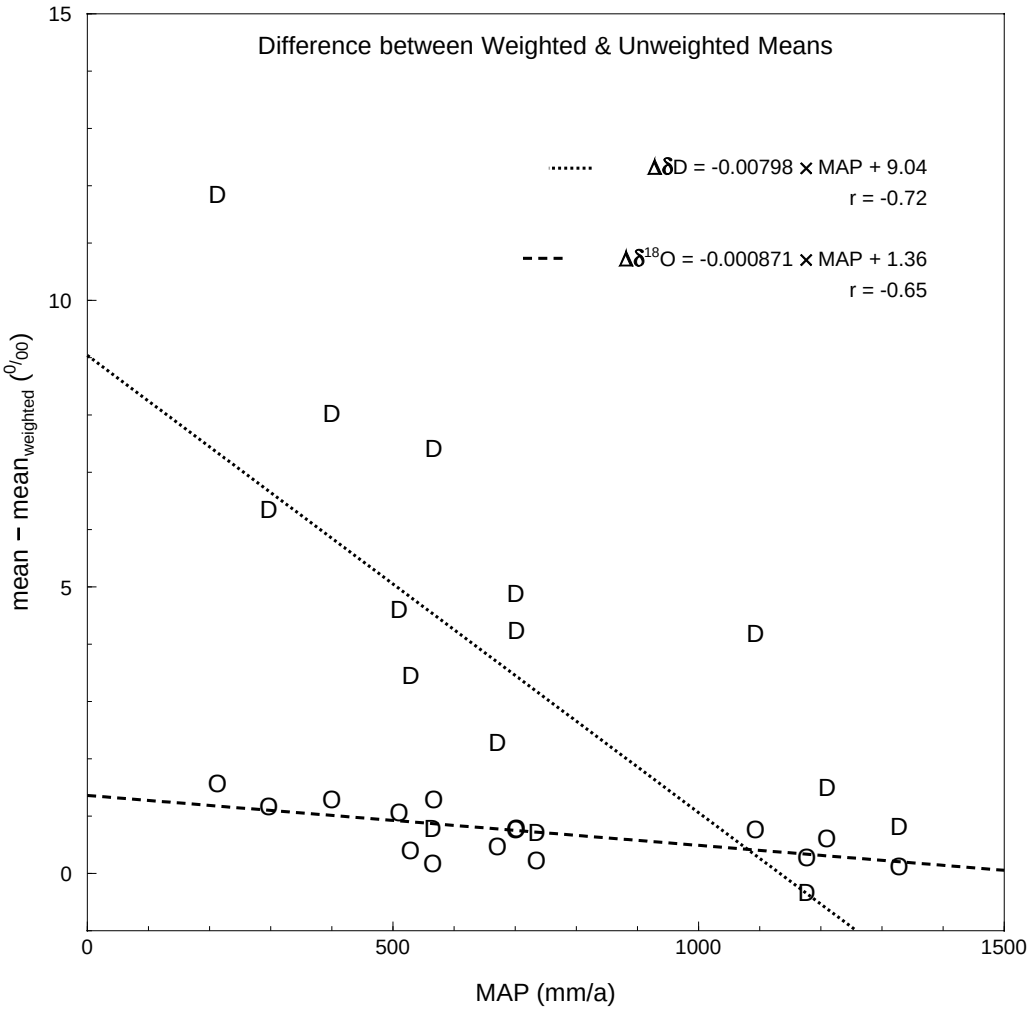

Figure 4.7: The difference between the mean and weighted mean for δD (D) and $\delta^{18}O$ (O) versus the MAP (mean annual precipitation), for each rain collection station.

			arithmetic		weighted		
study	altitude	MAP	δD	$\delta^{18}O$	δD	$\delta^{18}O$	source
	masl	mm	‰	‰	‰	‰	
UCT 2010–2012	130	1210	-7.6	-2.28	-9.2	-2.89	this study
UCT 1995–1997	130	1260	-13.0	-3.46	-11.7	-3.74	Diamond and Harris (1997)
UCT 1996–2008	130	1365	-8.5	-2.68	-12.5	-3.29	Harris et al. (2010)
'Malan'/CTIA	40	513	-8.2	-2.72	-12.8	-3.36	Rozanski et al. (1993)

Table 4.3: Arithmetic (unweighted) and weighted mean δD and $\delta^{18}O$ values of rainfall from various studies in Cape Town. CTIA refers to the Cape Town International Airport (DF Malan) where the IAEA/WMO GNIP station was located.

4.3.3 Deuterium Excess

The d-excess, often referred to simply as 'd' in the literature, is calculated for a sample of known δD and $\delta^{18}O$ values by the equation:

$$d - excess = \delta D - 8\delta^{18}O.$$

The d-excess values for the 15 rainfall collection stations range from 5.8 to 22.7 ‰ and average 16.0 ‰, which is similar to d-excess values from other studies in Mediterranean climates (Vreča et al., 2006; Argiriou and Lykoudis, 2006) (see **Table 4.2**). No correlations are apparent with MAP, seasonality or any other obvious geographic parameters, for example latitude and altitude, as can be seen in **Figure 4.8**. The best correlation is found against a continentality factor, which is the product of the distance between the rainfall station and the Atlantic Ocean (along a line of latitude due west) and the distance to the closest coast ('sea'). This factor is discussed further in Chapter 5, but even this correlation is rather poor, with a Pearson's r of only 0.42.

4.3.4 Local Meteoric Water Lines

All rain water isotope results have been plotted in the upper graph in **Figure 4.9**. The most noticeable feature of this graph is the well defined correlation between δD and $\delta^{18}O$, as is expected, according to isotopic fractionation, as described in the Introduction. This correlation defines the trend of the local meteoric water line. Using the data set to calculate lines of best fit (local meteoric water lines), the equations are as follows:

♢ unweighted rain water data: δD = 6.11$\delta^{18}O$ + 7.09

♢ rain water data, weighted by rainfall amount: δD = 6.15$\delta^{18}O$ + 8.21 .

Several points can be made about these equations. Firstly, there is only a small difference between the weighted and unweighted equations. This suggests that the statistical outliers, the rain water samples with unusual isotopic composition, are nearly symmetrical about the data. Additionally, the unweighted and weighted rain water means (n = 275) are, for δD and $\delta^{18}O$: -15.9 ‰ and -3.76 ‰ , -17.7 ‰ and -4.22 ‰. These also show only a small difference and if plotted together on a $\delta D - \delta^{18}O$ diagram, the two means lie along the same orientation as the two nearly parallel local meteroric water lines. The small shift between the two equations does however reveal that the unweighted line tends towards a lower gradient and lower intercept, both of which are a sign of evaporated waters. The bulk of the outliers are therefore the low rainfall, highly evaporated, summertime rainfall samples, as seen in the time series plots in **Figures 4.3 and 4.4**.

Local meteoric water lines have also been calculated for each of the rainfall stations and

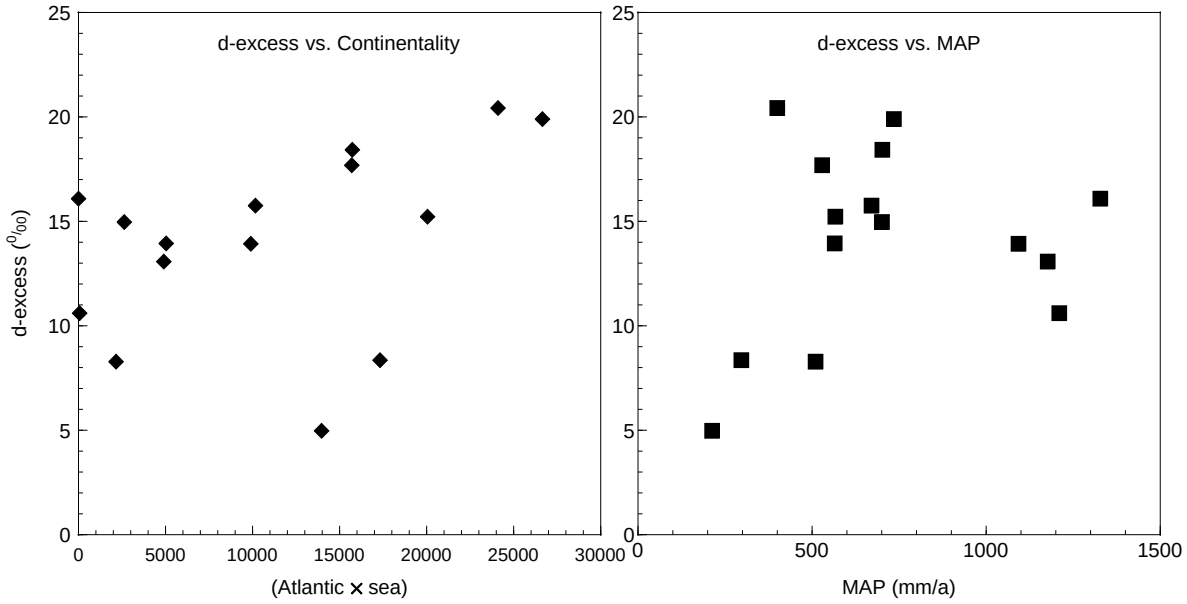

Figure 4.8: d-excess values for the weighted means for the 15 rainfall collection stations, plotted against a continentality factor and against MAP.

these are displayed in **Figure 4.10**. Ellipses have been drawn on the graph, using the standard deviations from **Table 4.2**, to show where most of the data actually lies; 67 % of points should lie within the 1σ ellipse and 98 % within the 2σ ellipse. The graph region was extended to show some separation in the meteoric water lines and allow labelling of each line.

The LMWL gradients range from 4.42 for Uitkyk Pass to 8.17 for Kammanassie, and intercepts from -3.0 for Bakenskop to 23.9 for Kammanassie. Although no single, clear correlation between these local meteoric water line equations and geographic factors such as mean annual precipitation, altitude or longitude is apparent, the equations do display geographic clustering (see **Figure 4.11**). The following groups can be distinguished by the similarity of their gradient and intercept values: a western cluster of UCT (University of Cape Town), TMC (Table Mountain Cableway) and TWT (Twaktuin) have gradients in the 5 to 6 range with intercepts from 6 to 7.5; the Hex River Mountain stations MTB (Matroosberg) and DDN (DeDoorns) have similar gradients, although different intercepts; the Langeberg-Gamkaberg group of RBP (Robinson Pass), BKK (Bakenskop) and GST (Gamka Store) all have gradients around 4.5 and intercepts close to zero; the eastern stations BBG (Blesberg), KMN (Kammanassie), LTL (Lentelus) and GKM (Goukamma) have high gradients, from 6.5 to 8.2, and high intercepts, from 10 to 24. Some stations do not fit into these groups, despite being geographical neighbours, these being Uitkyk Pass and Wolfkop, 30 km apart in the north-west, and Riverndale, less than 100 km from the Langeberg-Gamkaberg group in the south. The large range in gradients and intercepts for the 15 LMWLs is likely due to the short duration of sampling, whereby unusual weather (humidity, series of storms, drought) can affect the small dataset. Longer term monitoring should see some convergence in LWMLs.

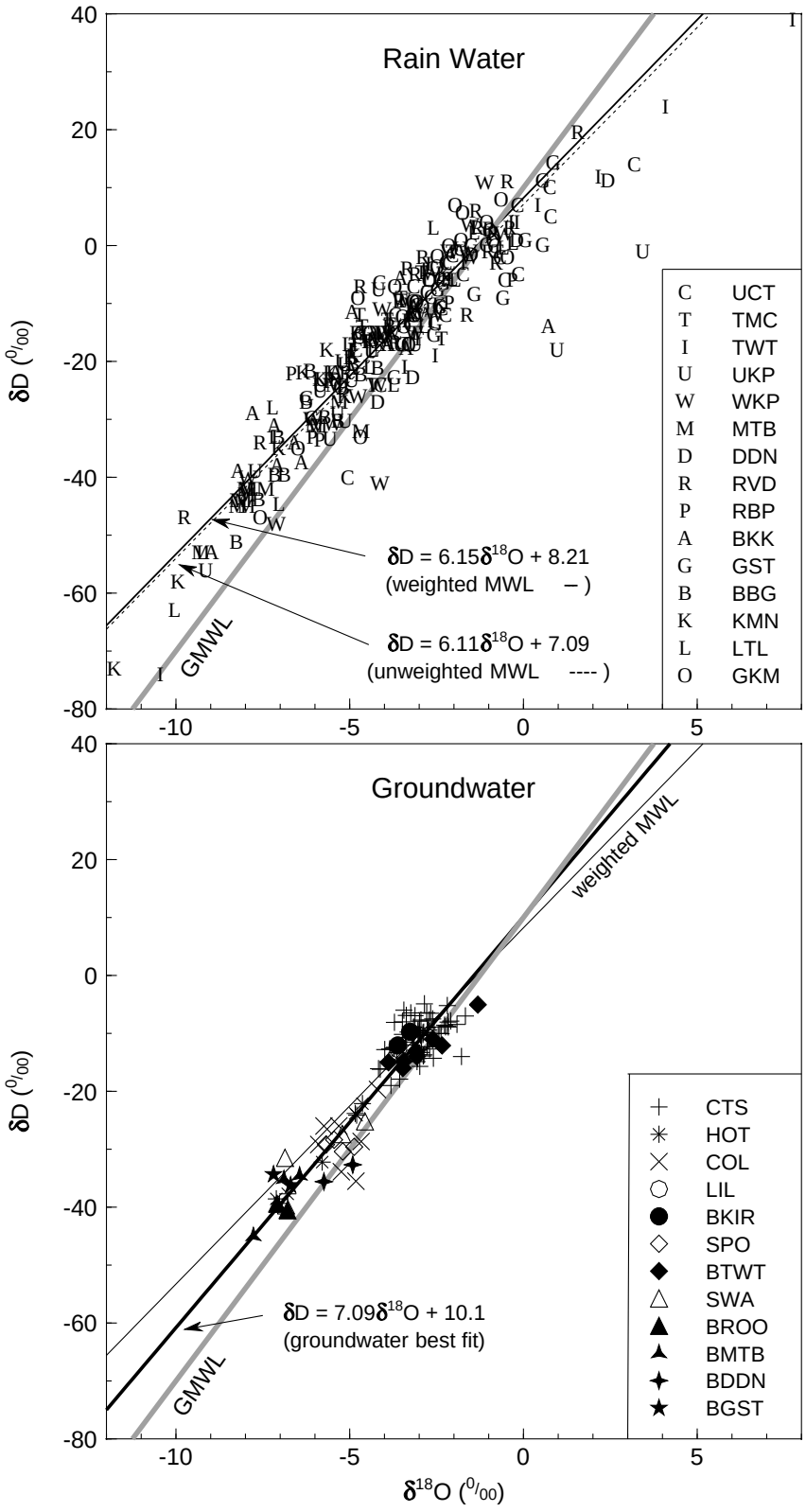

Figure 4.9: δD–$\delta^{18}O$ plots of all rain water and groundwater samples for this study. Key for the groundwater graph: CTS Cape Town springs; HOT hot springs; COL cold springs; LIL Table Mountain lily pond; BKIR Kirstenbosch boreholes; SPO Cederberg Tafelberg spout drip; BTWT Twaktuin boreholes; SWA Klein Swartberg seeps; BROO Rooihoogte boreholes; BMTB Matroosberg boreholes; BDDN DeDoorns boreholes; BGST Gamka Store boreholes.

The significance of the clustering of these local meteoric water lines is that they reveal affinities not seen when looking at the means and d-excess values. For instance, the two stations Matroosberg and DeDoorns, only 10 km apart, have very different means and d-excess values, and although the intercepts of their local meteoric water lines do show a large difference, the gradients are nearly identical, showing some parallels in meteoric processes between the two stations. A similar thing can be said for the 'sister' stations, Bakenskop and Gamka Store.

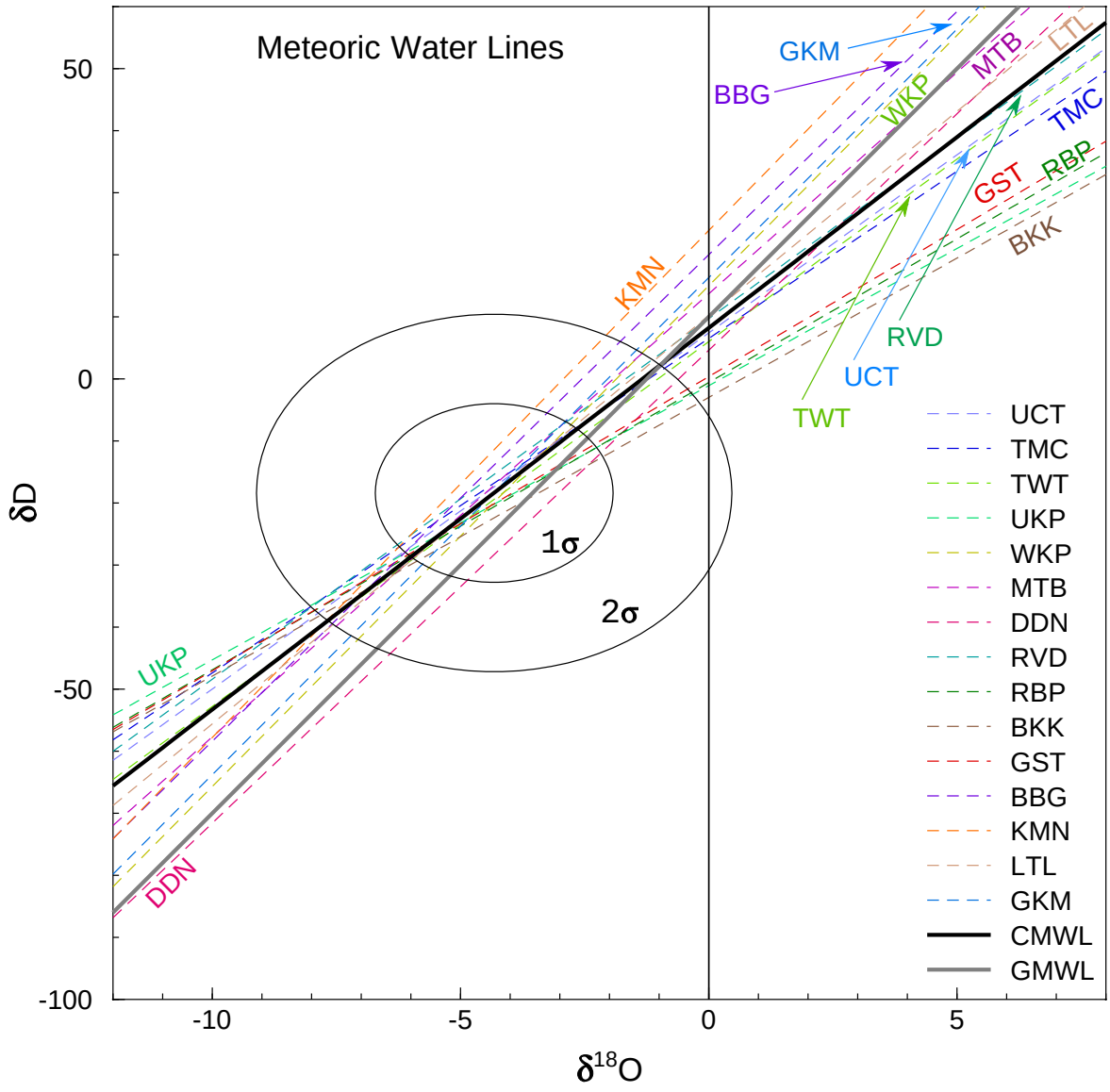

Figure 4.10: Local meteoric water lines for each of the 15 rainfall stations, calculated from monthly cumulative rainfall samples weighted by rainfall amount and using the RMA regression method. The LMWL for the all the stations (also weighted), called the Cape MWL (CMWL), and the GMWL of Craig (1961a) are also shown. The 1σ and 2σ distribution ellipses are for all rainfall data, showing how the graph has been extended well beyond the δ values found in this study, in order to show separation and allow labelling of the LMWLs.

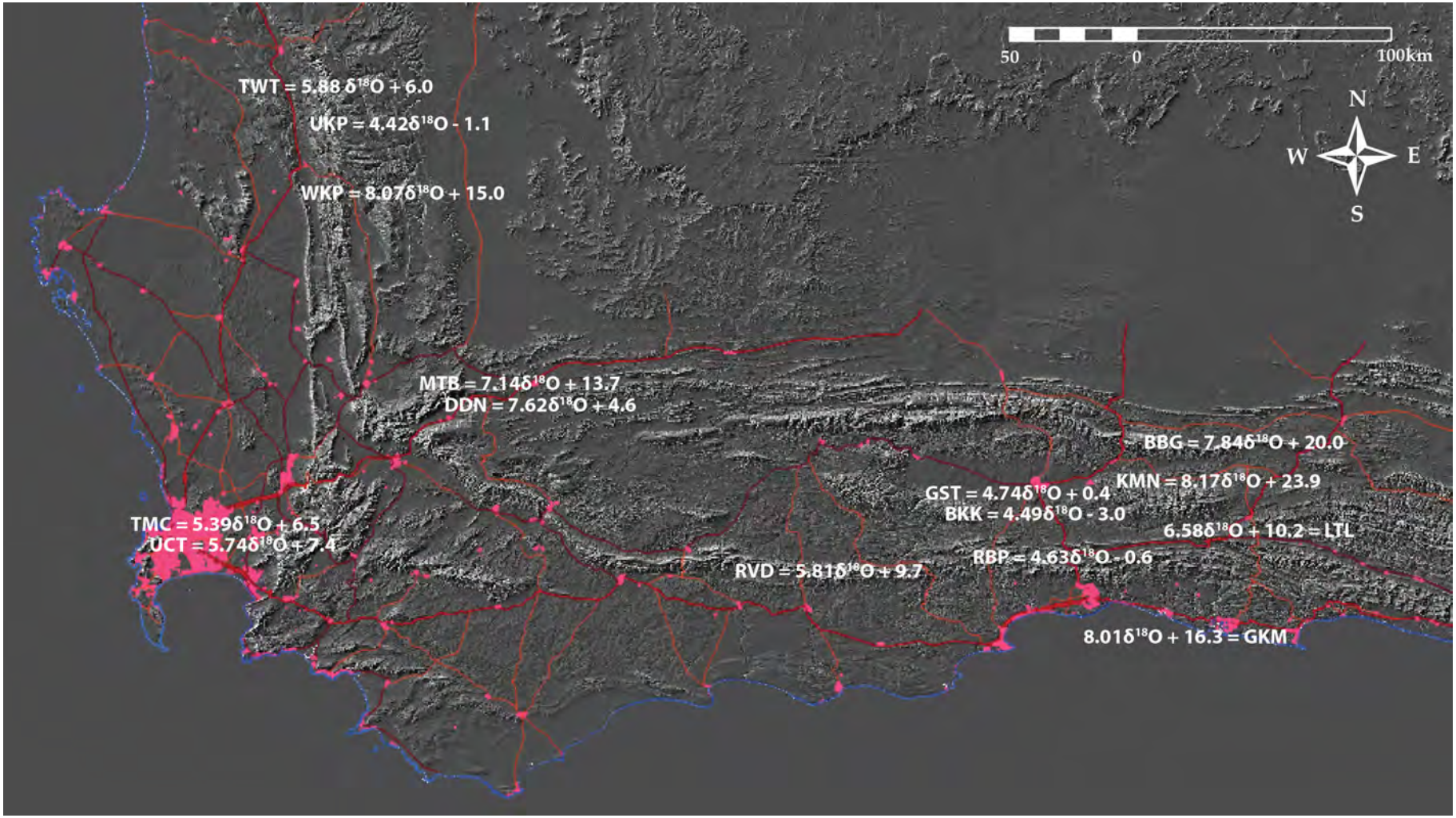

Figure 4.11: Local meteoric water line equations for each rainfall collection station, calculated with data weighted by monthly rainfall amount. The station code (e.g. BBG) lies approximately over the station location. Background image is a hillshade DEM (NASA, 2013) with roads and streets overlain (NGI, 2012).

4.4 Groundwater

Groundwater was sampled from a variety of sources: springs, seeps and boreholes. Except for the springs around Table Mountain, almost all of the groundwater was taken from sources discharging from the Table Mountain Group.

The Table Mountain springs lie below the unconformity between the overlying Table Mountain Group and the Cape Granite or Malmesbury Group, but they do not discharge from unaltered granitic or metamorphic rock. These springs discharge from areas with no bedrock outcrop and are likely to be discharging from an aquifer made of colluvial material such as scree and some weathered rock.

The springs and seeps around the Western Cape vary from widely known, high discharge rate hot springs such as Calitzdorp and Citrusdal, to virtually unknown drips that are used as high altitude water points by mountaineers, such as Cederberg Tafelberg Spout drip and the Klein-Swartberg Toverkop drip. The former, major springs, have often been capped and the ground is covered with recent material, both natural and anthropogenic, and so the exact geological formation at the discharge point is uncertain. Additionally, these larger springs mostly lie on faults and stratigraphic units can be juxtaposed, such as the Peninsula Formation of the Table Mountain Group and the Gamka Formation of the Bokkeveld Group at the Caledon hot spring (e.g. Council for Geoscience, 1997). In contrast, for the seeps, not only can the geological formation be identified, but the exact fracture from which the groundwater emerges is often visible.

The boreholes sampled are of moderate depths, around 30–100 m, and most (except for the Kirstenbosch boreholes) penetrate the Table Mountain Group, although the surface outcrop in some cases (e.g. DeDoorns) is Bokkeveld Group.

All groundwater data have been plotted in the lower graph in **Figure 4.9**. The contrast with the upper graph of all the rain water data is very noticeable, the lack of scatter being the result of the smoothing that occurs for the following reasons: small rain volume events with unusual isotopic signatures do not contribute to recharge; mixing of meteoric water takes place during recharge and subsequent underground flow, averaging out the composition of discharge. The former of these effects has been dubbed selection by Gat & Tzur (1967) (in Gat, 1981a). Using this data set to calculate a best fit line gives the following equation:

$\diamondsuit$ groundwater data, which cannot be weighted: $\delta D = 7.09\delta^{18}O + 10.08$.

This equation is substantially different from the rain water MWL equations and is much closer to the GMWL of Craig (1961a). The means for all the groundwater data are, for δD and $\delta^{18}O$: -16.9 ‰ and -3.8 ‰, respectively. These means are biased towards the Table Mountain springs, as about 60 % of the groundwater data is from these springs, which accounts for the relatively isotopically enriched values of these means.

Figure 4.12: The Seweweekspoort Peak Cave water point at 2020m in the Klein Swartberg. The fractured nature of the folded, duplexed and competent quartzite of the Peninsula Formation is apparent.

4.5 Surface Water

Water samples were collected from five rivers in the Cape Mountains. The extent of each river that was sampled falls wholly within the outcrop of the Table Mountain Group, although shortly downstream of the lowest sample the rivers exit onto other stratigraphic units, except for the Witels as described below.

Duiwelskloof and Volstruiskloof are both in the Drakenstein Mountains between Stellenbosch and Franschhoek where the Table Mountain Group is fairly flat lying on top of granite of the Stellenbosch Pluton of the Cape Granite Suite. The rivers are both very steep: Duiwelskloof has an average gradient of 30° over a distance of 2.4 km and Volstruiskloof drops 700 m in a distance of 1.5 km, giving an average gradient of around 45° (see **Table 5.7**). The rivers flow through Peninsula Formation and exit onto scree over granite at the foot of the mountains.

The Witels and Groothoekkloof Rivers both lie in the Hex River Mountains, but at opposite ends. The Witels lies in the western side of the Hex River Mountains, south of Ceres, and is the longest mountain river in the Western Cape, protected from the impact of agriculture and urbanisation by virtue of the mountainous terrain. This makes it potentially useful for understanding interaction between surface water and Table Mountain Group groundwater. The Witels has an

average gradient of 7.5° over the full 20 km length, starting at around 1900 masl and ending at 300 m in Michells Pass, but bar one high altitude sample, the main 16 km stretch of the river that was sampled drops only 600 m and so has an average gradient of only 3.5°. The Witels mainly flows through Peninsula Formation, but due to folded beds that dip north-east, it flows through Pakhuis, Cederberg and Goudini Formations for a portion of its course. The sampling of the Witels stops at its junction with the Dwars River in Michells Pass, an impacted river that drains the agricultural and urban land of the Ceres Valley. The Dwars (with the Witels) continue for a few kilometres in Table Mountain Group before exiting onto a substrate of Malmesbury Group in the Tulbagh–Wolseley Valley.

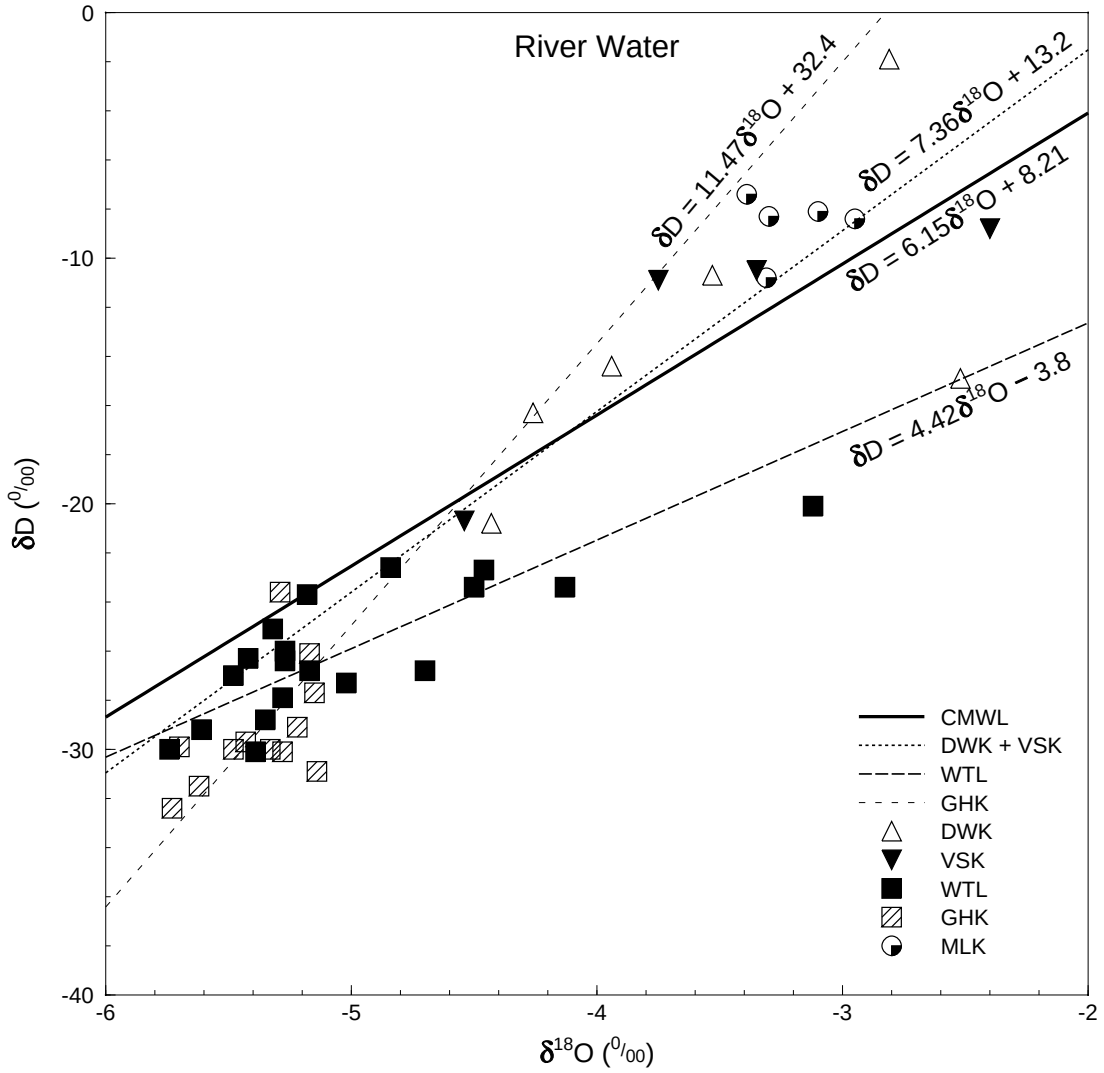

Figure 4.13: $\delta D - \delta^{18}O$ plot for all surface water samples. Best fit lines have been calculated for some data sets and the Cape Meteoric Water Line, as calculated from this study, has been added for reference.

The Groothoekkloof River arises in the highest mountains of the south-western Cape, namely

Matroosberg and Roodeberg in the far north-eastern Hex River Mountains, both over 2200 masl. It exits into Bokkeveld Group and covering gravels in the Hex River Valley Syncline at 500 masl, having flowed only through Peninsula Formation, although the high peaks above perennial water are capped with cliffs of the Skurweberg Formation and the catchment therefore includes outcrop of the Pakuis, Cederberg and Goudini Formations. This river's average gradient from perennial water at about 1800 m is around 13° (see **Table 5.7**).

Meulkloof River lies in the Swellendam region of the Langeberg Mountains. It's source is around Hermitage Peak, over 1500 masl, and it flows through Peninsula Formation only until it exits the mountains across a faulted contact with the Bokkeveld Group at 130 masl.

The $\delta D - \delta^{18}O$ plot of all surface water samples is shown in **Figure 4.13**. A clear separation exists between the two rivers from the higher mountains of the Hex River Mountains and the three other rivers located in lower mountain ranges. Best fit lines have been calculated for Groothoekkloof, Witels and a combined line for Volstruiskloof and Duiwelskloof. Meulkloof does not have enough of a linear spread of data to calculate a meaningful correlation. The correlation coefficient, Pearson's r, is only 0.53 for Groothoekkloof, but for Witels it is 0.81 and Volstruiskloof-Duiwelskloof it is 0.72, both of which are fair correlations. There is a large separation in the Witels and Groothoekkloof lines, and they straddle the MWL equations for De Doorns and Matroosberg, the two rainfall stations in the area.

The river water samples have a weak correlation with altitude, mainly between rivers. More detailed analysis of these results is necessary, as samples include those from not only the trunk stream, but also tributaries, and certain samples are highly evaporated after descent over exposed cliffs (trickling waterfalls). This will be done in the next chapter.

4.6 Other Samples

4.6.1 Snow

Six samples of snow and ice were taken from about 1900 masl on Waaihoek Peak on 29 July 2011. An unusual weather event occurred on 24–25th July 2011 when snow fell on some of the high peaks of the Cape Fold Belt from a *black south-easter*. This event can be summarised as follows. On the 2nd July a cold front and ensuing southerly meridional flow caused widespread light rain over the Western Cape with very cold ($0 - 10°C$) minimum daily temperatures. On the 4th July southerly meridional flow caused large amounts of rain (40–50 mm daily totals) on the south coast and light rain in the south-central mountain areas. Thereafter, a blocking high sat south of the country for nearly three weeks and prevented any cold fronts from causing rain until the 21st–22nd when a cold front brushed past, resulting in a few millimetres of rain along the south coast. This was followed by the South Atlantic High Pressure re-establishing itself south of the country, but this time with abundant moisture and resulting in rain falling from 23–25th mostly along the southern parts of the Province, with a maximum daily rainfall of 68 mm in George on the 24th.

On the 27th–28th a typical winter cold front caused widespread rain, and snow on the high peaks, across the Province.

Snow from both the black south-easter event and the following north-wester event was sampled near the top of Waaihoek Peak in the Hex River Mountains. It was possible to differentiate the two snowfalls from the granular snow (firn) which develops at the top of a snowpack due to freeze-thaw. The isotope results of these samples are shown in **Table 4.4**. Two different profiles were cored into the snow, WHK1-3 and WHK5-6 and a sample was also taken of rime ice (formed by sublimation directly from the atmosphere) that forms on these windy summits. The rime ice was formed during the recent north-wester, as it was on the western side of the rocks and would also not have survived the intervening sunny days between the south-east and north-west weather events.

sample ID	sample description	depth	δD	$\delta^{18}O$
		mm	‰	‰
WH1	recent powder snow from NW cold front	0-50	-60.6	-11.56
WH2	granular (melted and refrozen) top of SE snow	100-150	-38.3	-9.11
WH3	powder snow from SE at base of snowpack	300-400	-30.6	-9.16
WH4	rime ice stalactite on west facing rock	n/a	-20.5	-7.16
Wh5	granular snow at top of SE snowfall	100-200	-38.0	-8.69
WH6	podwer SE snow at base of snowpack	300-350	-33.6	-8.46

Table 4.4: Waaihoek Peak snow samples taken on 29 July 2011.

4.7 Summary

The stable isotope data from this study has a wide range of values because of seasonal variations, specific weather events, differing continentality and altitude of sample sites, and modification by evaporation. Some results can easily be attributed to such factors, whereas others have a less clear cause. Mean δD and $\delta^{18}O$ values for each rainfall station were calculated by weighting the monthly values by rainfall amount. Meteoric water lines for each station were also calculated using weighted data. The weighted results differ more from the unweighted results for less rainy areas, as weighting removes the effect of highly evaporated, low rainfall isotopically outlying data points.

Groundwater data is more tightly clustered than precipitation, as a result of selective recharge of more isotopically negative, higher rainfall events, and mixing of groundwater. Water from rivers tends to vary unsystematically isotopically down the length of the streams and each river's isotope data tends to form a cluster. Snow from a south-easter weather event has a markedly different isotope content to a subsequent north-wester weather system.

More detailed analysis of these and other results follows in the Discussion.

Figure 4.14: Monthly rainfall graphs for the 15 rain collection stations over January 2010 to December 2012. Estimates were made based on nearby rainfall stations from this study and SAWS, as well as monthly rainfall maps from the SAWS.

(a) Monthly rainfall as measured (solid bars) and estimated (striped bars) for the two Cape Town area stations.

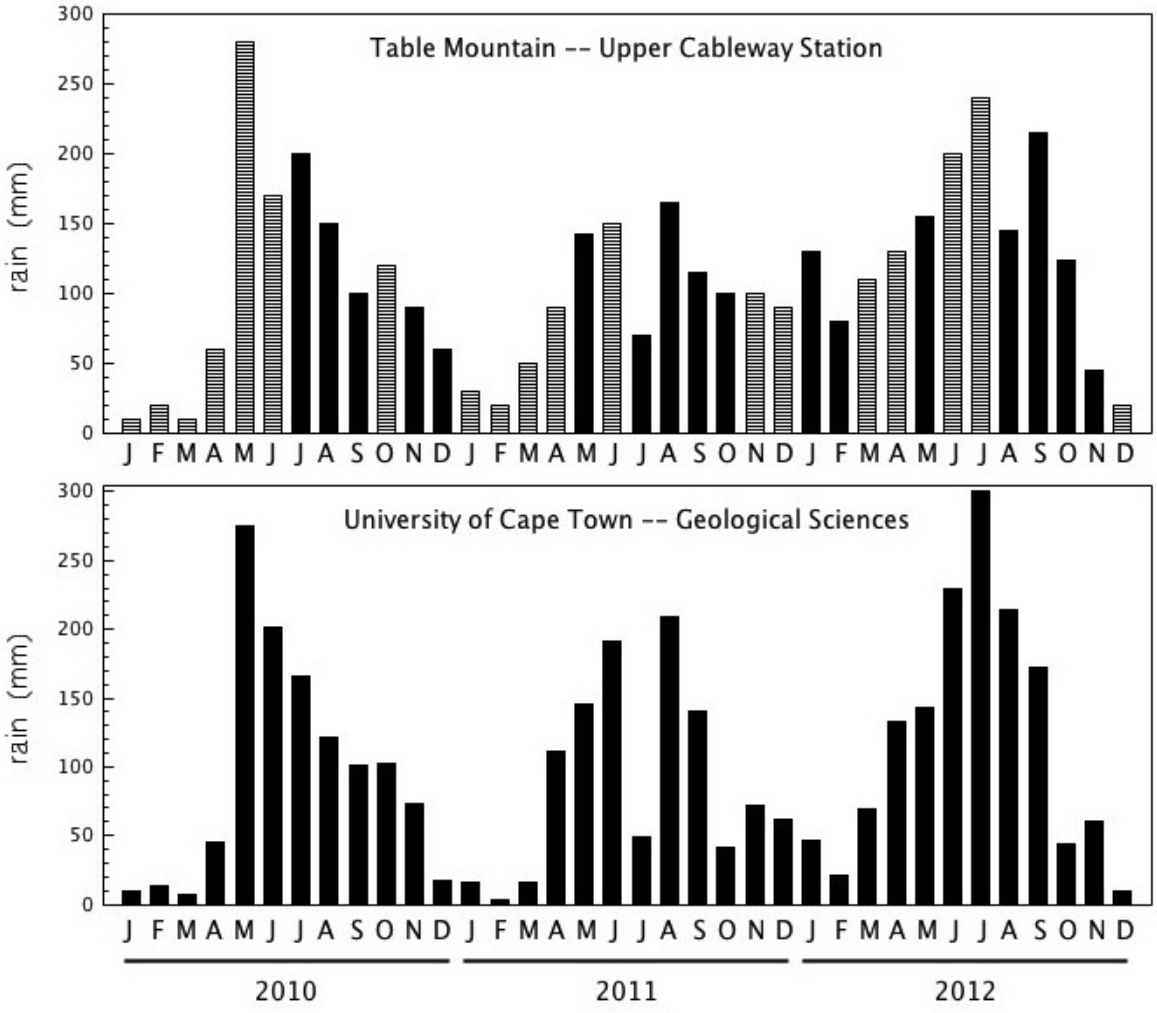

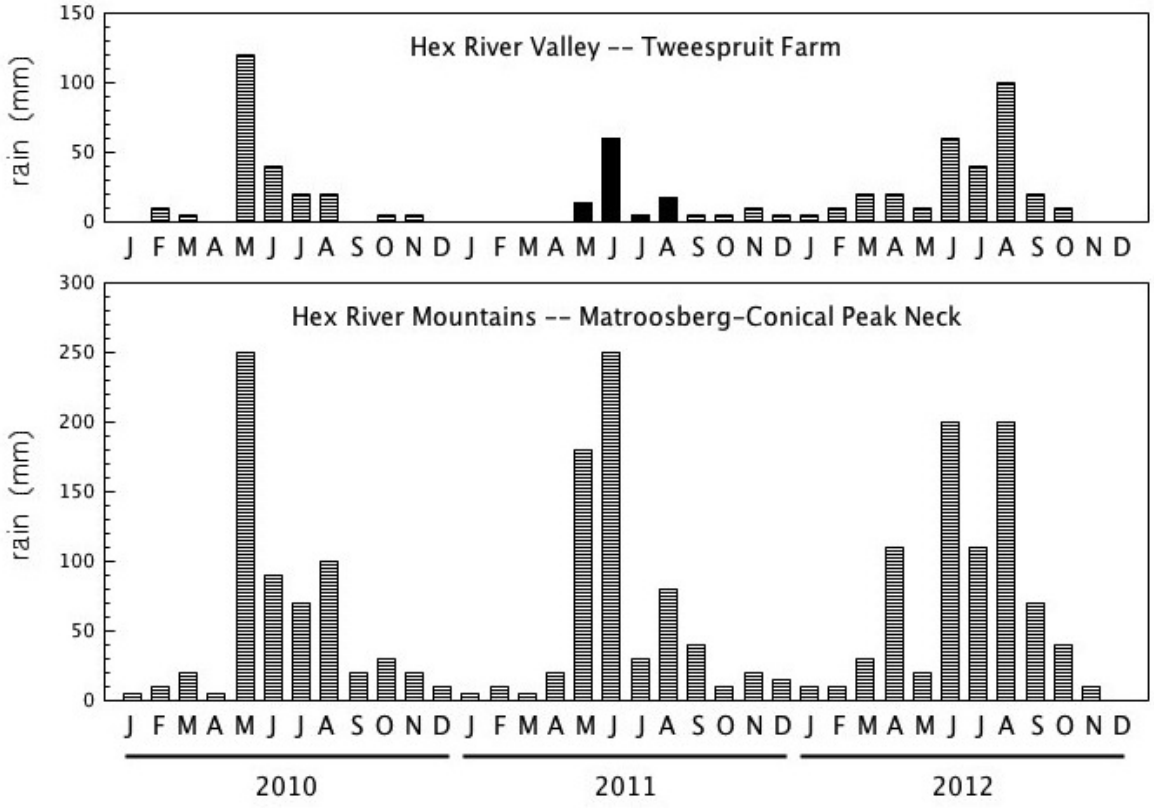

(b) Monthly rainfall as measured (solid bars) and estimated (striped bars) for the two Hex River region stations.

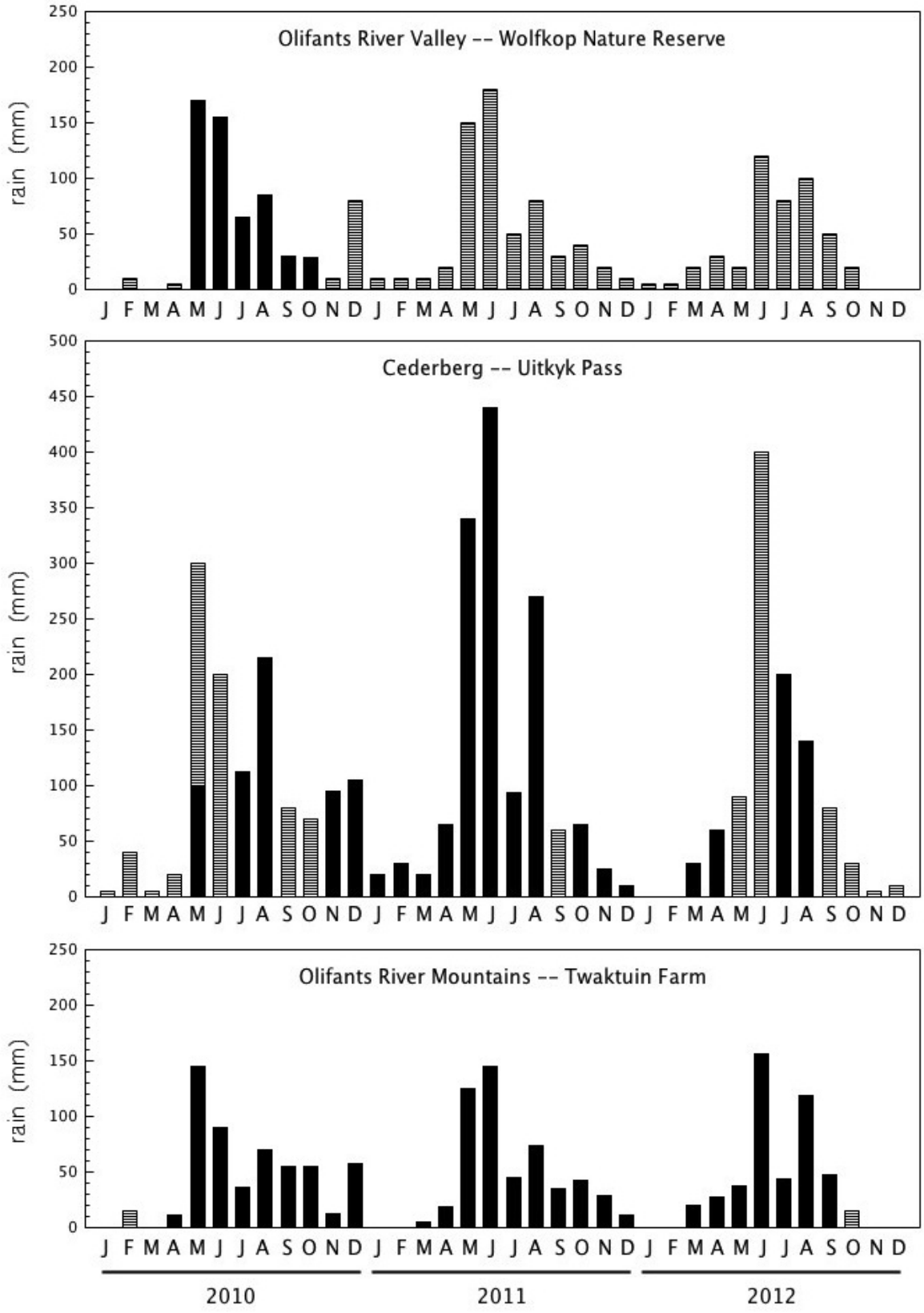

(c) Monthly rainfall as measured (solid bars) and estimated (striped bars) for the three Cederberg area stations.

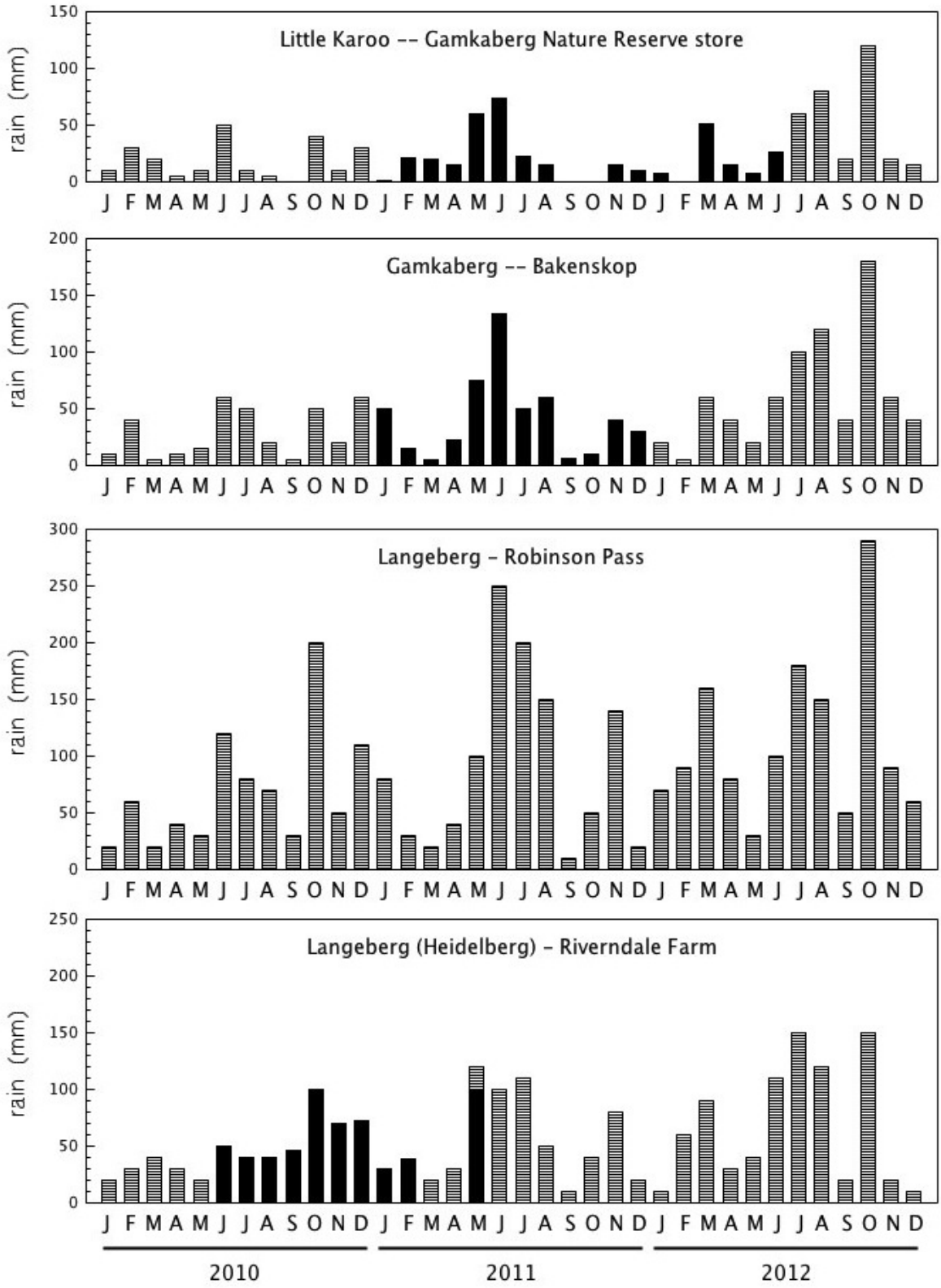

(d) Monthly rainfall as measured (solid bars) and estimated (striped bars) for the Langeberg and Gamkaberg region stations.

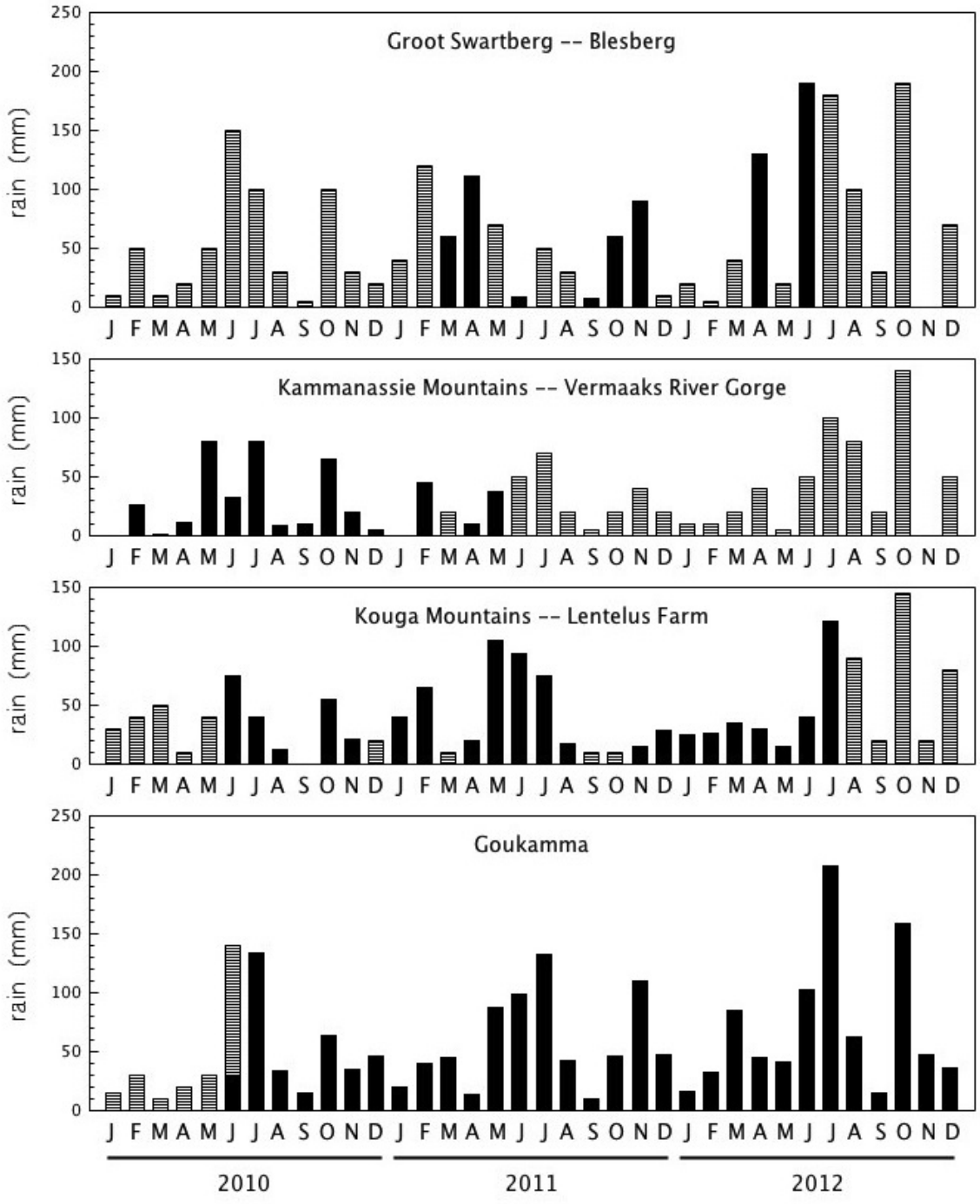

(e) Monthly rainfall as measured (solid bars) and estimated (striped bars) for the eastern region stations.

rain — 2010

	J		F		M		A		M		J		J		A		S		O		N		D	
	δD	$\delta^{18}O$	δD	$\delta^{18}O$	δD	$\delta^{18}O$	δD	$\delta^{18}O$	δD	$\delta^{18}O$	δD	$\delta^{18}O$	δD	$\delta^{18}O$	δD	$\delta^{18}O$	δD	$\delta^{18}O$	δD	$\delta^{18}O$	δD	$\delta^{18}O$	δD	$\delta^{18}O$
	‰	‰	‰	‰	‰	‰	‰	‰	‰	‰	‰	‰	‰	‰	‰	‰	‰	‰	‰	‰	‰	‰	‰	‰
UCT	9.7	0.75	-5.8	-0.54	0.4	-0.83	-12.1	-2.25	-8.4	-2.78	-17.0	-3.31	-15.0	-3.69	-4.9	-1.74	-3.3	-2.24	-3.3	-2.15	-6.2	-2.39	-39.9	-5.06
TMC									-15.0	-3.14	-24.4	-4.35							-16.3	-3.04	-13.1	-2.65	-16.0	-2.35
TWT									-13.5	-3.41	-18.8	-2.54	6.6	0.41	-2.7	-1.73	-21.4	-3.42	23.7	4.09			-74.4	-10.45
WKP									-11.7	-2.57	-25.8	-4.77	-14.7	-3.82	-1.5	-1.55	-24.1	-4.21	-0.9	-1.60	2.2	-0.56	-47.8	-7.12
UKP															-16.6	-3.53	-18.2	0.97	-1.0	3.43	-17.4	-3.12	-56.2	-9.14
MTB									-23.7	-5.43														
DDN																								
RVD											-33.8	-7.58	-47.5	-9.76	-2.4	-2.90	-3.0	-0.79	-21.5	-5.11	5.5	-1.37	-12.0	-1.63
RBP											-5.9	-0.32	-33.1	-6.08	-23.5	-5.6	-5.8	-2.22	-33.5	-5.86	-9.9	-2.14		
BKK											-13.6	0.72	-52.7	-8.97	-22.2	-5.39	-16.8	-3.95	-38.2	-7.08	-16.5	-3.88		
GST																								
BBG											-39.6	-7.17	-30.3	-5.34	-29.6	-5.72	-20.5	-4.91	-33.1	-7.06	-24.6	-5.19	-51.3	-8.26
KMN											-58.3	-9.94	-73.0	-11.77	-18.9	-4.90	-5.0	-2.30	-21.9	-5.55	-26.4	-5.15		
LTL											-42.3	-7.80	-62.9	-10.04	-17.8	-4.32			-16.5	-5.04	-12.1	-3.18		
GKM											-16.9	-3.30	-47.1	-7.60	-14.4	-3.43	0.9	-0.87	-12.1	-3.13	-1.9	-0.46	-32.5	-4.69

Table 4.5: Isotope data for rain for 2010. For locations of the rainfall stations, see the maps in Chapter 3.

rain — 2011

	J		F		M		A		M		J		J		A		S		O		N		D	
	δD	$\delta^{18}O$	δD	$\delta^{18}O$	δD	$\delta^{18}O$	δD	$\delta^{18}O$	δD	$\delta^{18}O$	δD	$\delta^{18}O$	δD	$\delta^{18}O$	δD	$\delta^{18}O$	δD	$\delta^{18}O$	δD	$\delta^{18}O$	δD	$\delta^{18}O$	δD	$\delta^{18}O$
	‰	‰	‰	‰	‰	‰	‰	‰	‰	‰	‰	‰	‰	‰	‰	‰	‰	‰	‰	‰	‰	‰	‰	‰
UCT	-5.2	-0.15	13.9	3.19	-23.6	-4.12	-5.8	-2.73	-12.3	-3.69	-18.3	-4.82	-14.6	-4.68	-3.8	-2.63	-0.1	-1.51	-17.0	-3.48	-12.0	-3.21	-1.6	-2.05
TMC	-1.2	-0.75					-14.8	-4.61	-14.7	-4.17	-16.9	-4.85	-11.6	-4.71	-14.4	-4.64	-9.2	-3.51	-13.6	-3.84	-17.4	-4.64	-9.6	-3.51
TWT									-17.7	-4.97	-17.7	-4.94	3.8	-0.19	4.2	-0.35	39.2	7.74						
UKP					-29.2	-5.35	-22.7	-5.79	-22.4	-5.46	-24.9	-5.85	-23.9	-5.85	-20.2	-5.21			-30.3	-5.13	-23.2	-4.94	-7.6	-4.17
WKP			-15.1	-3.13	-41.4	-4.13	-11.2	-4.07	-16.0	-4.10	-15.0	-4.00	-30.4	-6.06	-14.6	-4.17	3.5	-1.54	-11.8	-3.06	-40.0	-7.94	-1.1	-2.11
MTB	-44.7	-7.97	-41.9	-7.91	-31.9	-4.67	-42.4	-7.98	-52.9	-9.28	-44.4	-8.19	-44.0	-8.07	-42.9	-7.97	-44.6	-8.22	-30.9	-5.90	-31.3	-6.02	-41.8	-7.41
DDN											-27.0	-4.20			-6.0	-2.71					-1.5	-1.5	11.2	2.43
RVD	11.0	-0.47	3.2	-0.39	2.2	-0.87	-3.6	-3.35	-22.7	-5.41	-5.0	-3.12	-7.5	-4.70	-9.6	-3.57	3.0	-1.33	-16.7	-3.70	-16.6	-4.46	-1.1	-1.01
RBP													-22.1	-6.68										
BKK							-30.9	-7.16	-39.2	-8.21	-33.7	-6.58	-28.9	-7.79	-21.1	-4.97	-5.7	-3.53	-37.5	-6.38	-11.6	-4.92	-17.7	-3.37
GST	11.2	0.56	-8.4	-1.82	14.4	1.61	-22.7	-3.72	-29.8	-6.08	-26.4	-6.24	-15.7	-4.73	-13.4	-2.54					-15.4	-2.57	0.1	0.56
BBG	-43.9	-7.62	-21.1	-4.20	-19.4	-4.99	-21.6	-6.14							-39.5	-6.88	-22.3	-4.69	-26.9		-14.8	-6.55		
KMN							-17.5	-5.66	-34.5	-7.05	-23.0	-5.86	-21.7	-6.34			-10.2	-2.41						
LTL	-13.8	-2.86	-6.3	-1.96	-21.3	-4.43	2.9	-2.59	-52.7	-9.23	-32.5	-7.15	-27.7	-7.22	-44.7	-7.03	-5.8	-2.05	3.2	-1.35	0.4	-0.30	-24.1	-3.73
GKM	8.1	-0.64	4.4	-1.06	-0.1	-2.15	7.2	-1.96	-35.4	-6.48	-15.1	-4.41	-8.8	-4.76	-24.4	-5.26	-10.6	-2.90	-3.7	1.0	-1.79			

Table 4.6: Isotope data for rain for 2011. For locations of the rainfall stations, see the maps in Chapter 3.

rain — 2012

	J		F		M		A		M		J		J		A		S		O		N		D	
	δD	$\delta^{18}O$	δD	$\delta^{18}O$	δD	$\delta^{18}O$	δD	$\delta^{18}O$	δD	$\delta^{18}O$	δD	$\delta^{18}O$	δD	$\delta^{18}O$	δD	$\delta^{18}O$	δD	$\delta^{18}O$	δD	$\delta^{18}O$	δD	$\delta^{18}O$	δD	$\delta^{18}O$
	‰	‰	‰	‰	‰	‰	‰	‰	‰	‰	‰	‰	‰	‰	‰	‰	‰	‰	‰	‰	‰	‰	‰	‰
UCT	5.4	0.78	-2.5	-0.68	-11.9	-3.07	-9.8	-3.12	-10.4	-3.08	-6.4	-4.15	-8.8	-2.67	-13.5	-3.25	-10.8	-2.36	-7.1	-3.16	0.1	-1.08	6.9	-0.17
TMC	-4.7	-2.93	-1.0	-2.05	-12.9	-3.91	-13.7	-4.34			-8.7	-2.32	-7.6	-2.93	-20.8	-4.82	-22.4	-5.75						
TWT							11.8	2.15	-4.1	-2.86	-16.4	-4.88	-3.1	-2.73	-14.6	-3.88								
UKP					-33.3	-5.57	-15.6	-4.05	-0.5	-1.82			-18.3	-4.37	-20.5	-5.14								
WKP					-30.8	-5.49	-10.2	-3.16	10.9	-1.12	-15.9	-4.40	-4.8	-2.65	-9.4	-3.51								
MTB	-26.5	-5.30																						
DDN	1.0	-0.20									-22.72	-3.19												
RVD	2.9	-0.99	19.6	1.56	-11.4	-3.19	-17.1	-4.15																
RBP																								
BKK																								
GST	1.0	0.05			-9.1	-0.58	-7.6	-2.46	-6.5	-2.31	-10.5	-2.41												
BBG			-13.9	-3.86	-26.9	-6.26	-15.0	-4.81	-28.2	-7.02														
KMN																								
LTL	-0.3	-0.57	2.2	-1.42	-16.2	-4.33																		
GKM	2.5	-0.97	5.7	-1.75	-9.6	-3.07	-9.7	-3.17	-1.9	-2.47	-12.4	-3.47												

Table 4.7: Isotope data for rain for 2012. For locations of the rainfall stations, see the maps in Chapter 3.

Table Mountain springs

	2010-03		2010-11		2011-05		2011-10		2012-05		2012-09	
	δD	$\delta^{18}O$	δD	$\delta^{18}O$	δD	$\delta^{18}O$	δD	$\delta^{18}O$	δD	$\delta^{18}O$	δD	$\delta^{18}O$
	‰	‰	‰	‰	‰	‰	‰	‰	‰	‰	‰	‰
Redwood			-10.3	-2.96			-10.8	-3.36	-8.0	-3.48	-9.6	-3.03
Wendy's			-9.4	-2.74			-10.7	-3.38	-9.8	-3.32	-9.1	-2.77
Kirstenbosch	-13.7	-3.01	-9.4	-3.03	-12.4	-3.71	-12.9	-3.04	-10.2	-3.48	-10.1	-2.37
Kommetjie	-13.9	-2.88	-8.9	-2.16	-8.9	-3.16	-10.2	-2.89	-6.5	-3.24	-8.5	-1.91
Newlands	-13.3	-2.94	-7.5	-2.61	-6.9	-3.37	-10.2	-3.01	-6.5	-2.67	-7.9	-2.09
Palmboom	-13.7	-2.86	-10.0	-2.43	-4.9	-2.85	-9.9	-2.99	-7.7	-2.95	-8.9	-2.24
Princess Anne							-12.0	-3.21			-8.9	-2.57
Albion	-8.7	-2.18	-7.0	-1.67	-7.9	-2.99	-9.8	-2.87	-7.7	-2.71	-8.0	-2.17
CT Main	-15.7	-2.98	-12.7	-2.70	-12.8	-3.99	-13.3	-3.64	-10.7	-3.40	-12.3	-2.77
Cableway	-19.0	-3.81	-10.4	-3.17							-14.9	-3.06
Glencoe	-17.9	-3.56	-10.0	-3.19	-16.1	-4.17	-16.2	-4.12	-12.5	-3.74	-14.4	-3.04
Leeuwenhof	-14.0	-1.78	-5.2	-2.19	-8.1	-3.71	-11.5	-3.17	-6.4	-2.78	-14.3	-2.59
Tafelberg Rd			-8.6	-2.27	-6.0	-3.44	-12.7	-3.85	-7.0	-3.12	-12.3	-2.93

Table 4.8: Isotope data for the Table Mountain springs. For locations of the springs, see the Cape Town map in Chapter 3.

Western Cape rivers

	Duiwelskloof March 2011		Volstruiskloof March 2011		Witels February 2010		Groothoekkloof January 2012		Meulkloof March 2012	
	δD ‰	$\delta^{18}O$ ‰	δD ‰	$\delta^{18}O$ ‰	δD ‰	$\delta^{18}O$ ‰	δD ‰	$\delta^{18}O$ ‰	δD ‰	$\delta^{18}O$ ‰
1	-14.4	-3.94	-20.7	-4.54	-26.8	-4.70	-27.7	-5.15	-7.4	-3.39
2	-16.3	-4.25	-10.9	-3.75	-30.1	-5.39	-32.4	-5.73	-8.4	-2.95
3	-10.7	-3.53	-8.8	-2.40	-28.8	-5.35	-30.1	-5.28	-10.8	-3.31
4	-14.9	-2.52	-10.5	-3.35	-23.4	-4.13	-23.6	-5.29	-8.1	-3.10
5	-20.8	-4.43			-23.4	4.50	-29.9	5.70	-8.3	-3.30
6	-1.9	-2.81			-27.9	-5.28	-26.1	-5.17		
7					-30.0	-5.74	29.1	-5.22		
8					-20.1	-3.12	-31.5	5.62		
9					-27.3	-5.02	-30.0	-5.48		
10					-27.0	-5.48	-30.9	-5.14		
11					-29.2	-5.61	-30.0	-5.33		
12					-22.7	-4.46	-29.7	-5.43		
13					-26.0	-5.27				
14					-25.1	-5.32				
15					-26.8	-5.17				
16					-22.6	-4.84				
17					-26.4	-5.27				
18					-23.7	-5.18				
19					-26.3	-5.42				

Table 4.9: Isotope data for the five rivers sampled. For locations of the rivers and sample points 1→n, see the maps in Chapter 3.

groundwaters

sample type	location		date	δD ‰	$\delta^{18}O$ ‰
hot spring	The Baths	Citrusdal	May 2010	-22.1	-4.63
hot spring	Goudini Spa	Worcester	February 2011	-24.1	-4.80
hot spring	Brandvlei	Worcester	February 2011	-32.2	-5.79
hot spring	Caledon	Caledon	May 2011	-23.8	-4.84
hot spring	Warmwaterberg	Barrydale	September 2010	-37.7	-6.78
hot spring	Calitzdorp Spa	Calitzdorp	May 2011	-39.4	-7.02
hot spring	Tooverwater	Willowmore	May 2011	-38.6	-7.11
spring	Goudini cool	Worcester	February 2011	-19.7	-4.20
spring	UCT field station	Laingsburg	September 2010	-28.7	-4.67
spring	UCT field station	Laingsburg	September 2011	-33.9	-5.24
spring	UCT field station	Laingsburg	September 2012	-35.5	-4.82
seep	Lily Pond	Table Mountain	February 2011	-12.8	-3.60
seep	Lily Pond	Table Mountain	March 2012	-11.4	-2.95
seep	Tafelberg Spout	Cederberg	December 2010	-29.2	-5.68
seep	Tafelberg Spout	Cederberg	January 2011	-29.6	-4.87
seep	Tafelberg Spout	Cederberg	March 2011	-30.4	-5.20
seep	Tafelberg Spout	Cederberg	December 2011	-28.4	-5.45
seep	Toverkop water cave	Klein Swartberg	September 2010	-25.2	-4.56
seep	Toverkop water cave	Klein Swartberg	October 2011	-27.4	-5.21
seep	Skull Cave	Klein Swartberg	March 2011	-39.7	-6.83
seep	Seweweekspoort Peak Cave	Klein Swartberg	March 2011	-31.5	-6.86
borehole	'Protea'	Kirstenbosch	May 2012	-12.1	-3.62
borehole	'Apple'	Kirstenbosch	May 2012	-9.73	-3.26
borehole	house borehole	Twaktuin	February 2011	-15.5	-3.47
borehole	vlei borehole	Twaktuin	February 2011	-14.4	-3.07
borehole	C&D borehole	Twaktuin	February 2011	-11.3	-2.61
borehole	house borehole	Twaktuin	September 2011	-15.2	-3.88
spring	house spring	Twaktuin	September 2012	-14.9	-3.45
borehole	house borehole	Twaktuin	September 2012	-13.1	-3.09
borehole	vlei borehole	Twaktuin	September 2012	-12.1	-2.34
borehole	C&D borehole	Twaktuin	September 2012	-5.1	-1.31
borehole	Erfdeel 1	Erfdeel	February 2012	-34.6	-6.44
borehole	Grootvlak 1	Erfdeel	February 2012	-45.0	-7.77
borehole	Grootvlak 2	Erfdeel	February 2012	-35.2	-6.89
borehole	upper borehole	Tweespruit	July 2012	-32.7	-4.91
borehole	lower borehole	Tweespruit	July 2012	-35.6	-5.74
borehole	house borehole	Gamkaberg	June 2012	-36.3	-6.70
borehole	Tierkloof	Gamkaberg	June 2012	-34.4	-7.19
borehole	east	Rooihoogte	July 2012	-40.6	-6.79
borehole	west	Rooihoogte	July 2012	-39.4	-7.09

Table 4.10: Stable isotope data for various sample types. Hot springs have T > 37 °C. Locations are shown in the maps of Chapter 3.

Chapter 5

Discussion

5.1 Introduction

This chapter has two major parts. The first part contains findings on the isotope data for rainfall, surface water and groundwater separately, concentrating on the isotope effects, especially the altitude effect. The second part is made up of regional analyses of all data types within an area, such as the Cederberg or Hex River Mountains. The interpretations are proposed on the grounds of stable isotope evidence, but are checked against the geological and hydrogeological setting for feasibility. Attempts are made to draw conclusions that have relevance for groundwater flow in the Table Mountain Group.

5.2 Precipitation

Widespread collection of rainfall across the Western Cape has allowed a thorough consideration of hydrogen and oxygen stable isotope variations for the first time in this region. In particular, the rainfall stations vary greatly in their altitude, from 60–2080 m above sea level, their mean annual precipitation, from 200–1300 mm per year, and distance from the sea, from 2–110 km. Establishing the stable isotope variation with factors such as altitude, continentality and temperature allows for application to hydrological problems such as finding groundwater recharge areas (e.g. D'Alessandro et al., 2004).

5.2.1 Source Area and Pathway Effects

Precipitation in a given area may be derived from differing weather systems or the moisture causing the precipitation may have had different trajectories, hence the rainfall may display distinctive isotopic compositions (e.g. Peng et al., 2010; Breitenbach et al., 2010). South Africa receives precipitation from several types of weather systems, but these can broadly be divided into convective type summer rainfall over the eastern, central and northern parts of the country and frontal winter rain over the western and southern regions. The summer rain is brought over

land anticyclonically by the South Indian High Pressure cell, whereas the winter rain arrives with cyclonic frontal depressions from the southern Atlantic Ocean. Although the frontal depressions originate at approximately 60°S in the Atlantic Ocean and gather some of their moisture over the mid-latitude ocean before making landfall on the southern west coast of Africa, much of the water vapour in these weather systems has been derived from evaporation off the tropical sea surface (Rozanski et al., 1993). The summer rainfall systems develop over the land, but the air mass containing the moisture is derived from the mid-latitudes, 30-60°S, in the southern Indian Ocean. Moisture in the summer and winter rainfall in South Africa has therefore followed different trajectories since evaporation over the tropical ocean and has acquired additional moisture at different latitudes over different oceans at different temperatures of evaporation. It is therefore possible that the summer and winter rainfall may have different isotopic compositions.

Plotted in **Figure 5.1** is data from this study, for the winter rainfall region, and data from three other studies for other parts of South Africa, representing summer rainfall regions. No striking differences are apparent. This could be for two possible reasons: either there is no actual isotopic difference, or the amount of data is insufficient to show any differences.

For the latter, it is possible that the treatment of the data is deficient and a more detailed separation of the Western Cape rainfall is needed, based on weather patterns. This is because rainfall in the Western Cape, although dominated by winter frontal rain, does have elements of other rain-producing weather systems, especially further east, as with rainfall stations like Lentelus and Goukamma. A substantial quantity of the rainfall at these far eastern stations does in fact come from weather related to advection of moisture by the South Indian High Pressure cell. However, this explanation does not seem likely, as the rainfall stations in this study show no significant difference in average δD and δ^{18}O values, d-excess values (see **Table 4.2**) or meteoric water lines between the rainfall stations in the west, which are winter rain dominated, and those further east, with all-year round rain.

It is also possible the duration of sample collection is too short, being only 2 years and having some months not recorded. However, this also does not seem likely for the following reasons. The various Cape meteoric water lines calculated using different data sets do not vary much, in spite of these data sets being vastly different in size, as shown in **Table 5.1**. Also, a lot of groundwater data has been collected and groundwater isotopic values are known to reflect the longer term average precipitation isotope values (e.g Clark and Fritz, 1997). As the groundwater data overlap the precipitation data and the array of compositions is centred within the spread of precipitation data (see **Figure 5.1**), this can be seen as a validation that the precipitation samples are representative of longer term precipitation averages.

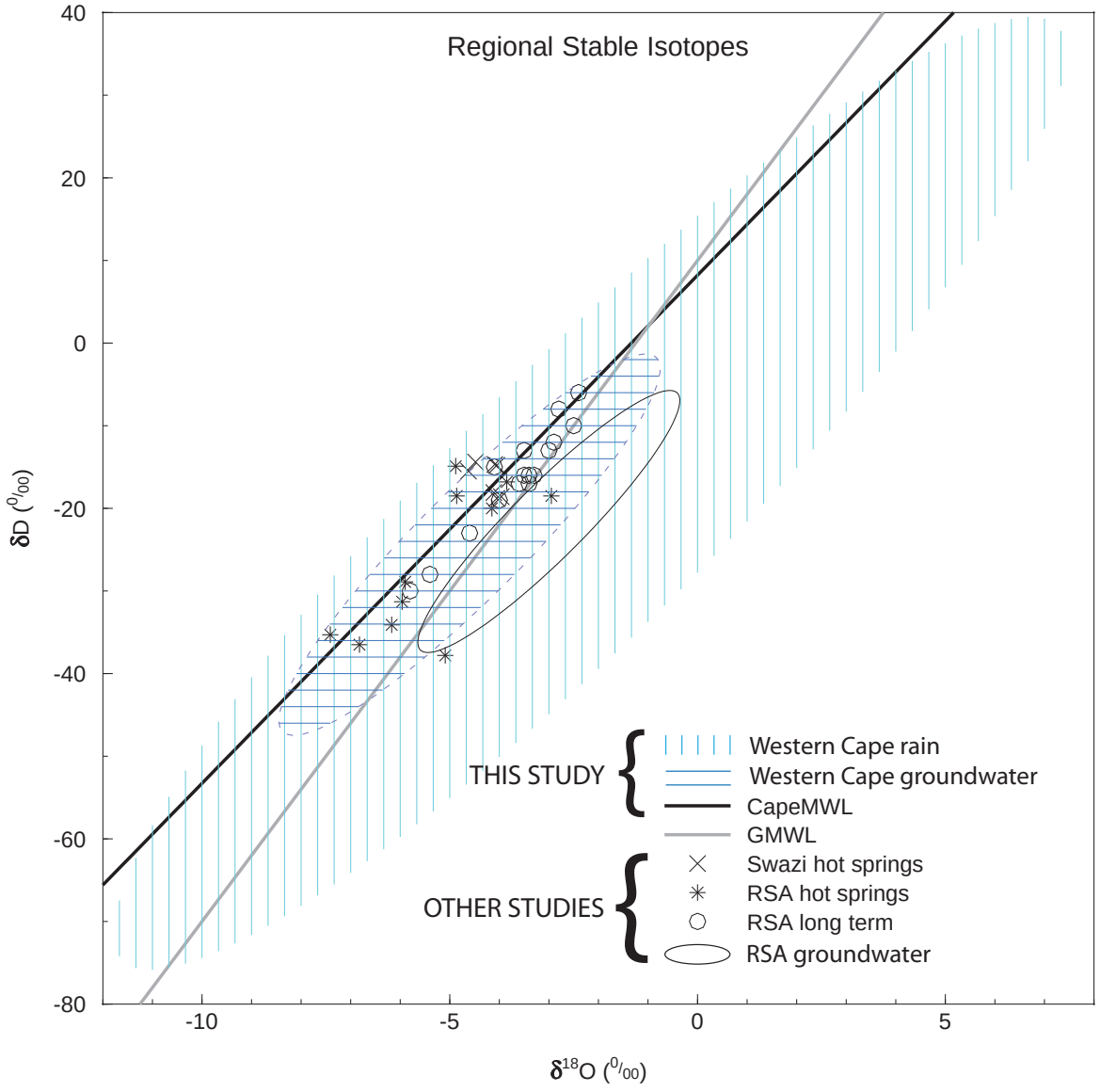

Figure 5.1: Comparison of isotope compositions of water from various South African studies with the results fields (shaded areas) for this study. Data for Swaziland hot springs from Mazor et al. (1974), RSA hot springs from Mazor and Verhagen (1983), RSA long term precipitation from Talma and van Wyk (2013) and RSA groundwater from West et al. (2014). The CMWL has the equation: $\delta D = 6.15\delta^{18}O + 8.21$.

meteoric water line equation	years		stations	reference
$\delta D = 6.1\delta^{18}O + 8.6$	1	1995-6	4	(Diamond and Harris, 1997)
$\delta D = 6.41\delta^{18}O + 8.66$	12	1996-2008	1	(Harris et al., 2010)
$\delta D = 6.15\delta^{18}O + 8.21$	2	2010-12	15	this study

Table 5.1: Meteoric water line equations calculated for rainfall in the Western Cape, illustrating the subtle differences in equations in spite of substantial differences in the date, duration and scale, as determined by the number of stations, for each study.

It does, however, remain possible that a more detailed analysis of South African isotope data will reveal a slight yet significant difference in isotopic composition for the summer and winter rainfall regions, but this is beyond the scope of this study. The alternative hypothesis may therefore be correct, which is that, in spite of different weather systems and moisture mass trajectories, there are no observable differences in isotope signatures between the summer and winter rainfall systems.

5.2.2 Isotope Effects

5.2.2.1 Temperature

Temperatures vary substantially across the Western Cape. This includes the daily maxima and minima, which are often over 40 °C in summer at low altitude, inland locations, and less than 0 °C in winter on mountains and at inland locations. Also, during precipitation events anticyclonic summer rain can occur with air temperatures over 20 °C whereas cyclonic winter precipitation frequently occurs as snow (SAWB, 1996). The isotopic content of precipitation is known to vary greatly temporally, and although correlations and patterns can at times be found with temperature, there is much noise in the data, associated with the complex dynamics of each and every weather system or rain event. Dansgaard (1964) states that, even if assuming no kinetic, exchange or evaporation effects, the isotopic composition of a sample of rain cannot be used to calculate the condensation temperature. This is because many other parameters, such as humidity, cloud height and rain event duration, also play a role in determining the eventual isotope composition of the rain.

The strong correlations of stable isotopes with average annual temperature reported in the literature (e.g Craig, 1961a; Dansgaard, 1964; Yurtsever and Gat, 1981) are summarized by Yurtsever and Gat (1981) as follows: "...it is evident that the spatial variations in the mean isotopic composition of precipitation of [GNIP] network stations are essentially correlated to the temperature variations." It is important to note that these correlations are based on long term averages of both the δD and $\delta^{18}O$ values of rainfall and of temperature (T) at each station and strong correlations are only formed with global or continental scale data sets and in particular at middle and high latitudes. This T-δ correlation is largely a product of the rainout process, where T reflects

species	gradient $\frac{\Delta‰}{1000km}$	location	reference
δD	13	Europe: Belgium to Poland - summer	Rozanski et al. (1982)
δD	33	Europe: Belgium to Poland - winter	Rozanski et al. (1982)
$\delta^{18}O$	1.6	Europe: Poland to Russia	Rozanski et al. (1993)
$\delta^{18}O$	3.8	Europe: Poland to Russia	Rozanski et al. (1993)
$\delta^{18}O$	3–4	North America: Atlantic to Rockies	Clark and Fritz (1997)
$\delta^{18}O$	10	Canada: Pacific to Prairies	Yonge et al. (1989)
$\delta^{18}O$	0.75	Amazon: Atlantic to Andes	Salati et al. (1979)

Table 5.2: Some examples of the continental effect from around the world.

distance from the tropical oceans and is therefore a proxy of the length of the air mass trajectory (Araguás-Araguás et al., 2000). At a single location where two (or more) weather system types produce precipitation, it has been shown that the rainout process has a greater effect in reducing the δ values of precipitation than seasonal changes in temperature of as much as 10 °C (Araguás-Araguás et al., 1998).

The situation in the Western Cape is that, in spite of the variety of climates in the study area, the mean annual temperatures at the 15 rainfall stations are between 16.5 and 19 °C. This small range in temperature makes it difficult to attempt a meaningful analysis of isotopic variations against average annual temperature. It may be possible to explore variations in stable isotopes against seasonal temperatures, but the precipitation during summer is erratic at many of the stations and more years of data would be needed. Isotopic trends will instead be explored against continentality and altitude, both also proxies for the rainout process.

5.2.2.2 Continentality

There is often a correlation between isotope composition of rainfall and distance from the coast (e.g. Liu et al., 2010). This has either been applied over large distances, 1000s of kilometres, and for this purpose the GNIP (IAEA/WMO) data has usually been used, such as Araguás-Araguás et al. (1998), or over a smaller scale, typically using non-GNIP data, such as Hunjak et al. (2013) who sampled around Croatia. The former studies often reveal a clear gradient in isotope values and result in a $\frac{\Delta\delta}{\Delta distance}$ ratio, whereas the latter studies may only find a difference between coastal and inland sites and not be able to calculate a meaningful gradient (e.g. Vreča et al., 2006). Some examples of calculated continental isotope gradients are given in **Table 5.2**.

Developing a continentality model for the Western Cape is challenging in several ways. Firstly, the area of study is only sub-continental and so isotopic depletion is limited, although this is offset by orographically induced rainout on the 2000 m high mountain ranges of the Cape. Secondly, the area is almost surrounded by ocean and so most locations are never further than 100 km

station	Atlantic distance	coast distance	Atlantic × coast
UCT	8	8	64
TMC	2	2	4
TWT	48	45	2160
UKP	70	70	4900
WKP	72	70	5040
MTB	143	110	15730
DDN	133	105	13965
RVD	242	42	10164
RBP	330	30	9900
BKK	314	50	15700
GST	315	55	17325
BBG	410	65	26650
KMN	482	50	24100
LTL	573	35	20055
GKM	526	5	2630
r for δD	-0.39	-0.44	-0.71
r for δ^{18}O	-0.44	-0.37	-0.68

Table 5.3: Calculation of a continentality factor, by multiplication of the distance to the Atlantic in a line due west and the distance to the closest coastline irrespective of direction. Correlation coefficients between weighted mean delta values at each station and the various distances are shown.

from the nearest stretch of coastline (see **Table 5.3**). Thirdly, several types of weather system are responsible for producing rain in the province and these may approach from any direction between north-west, through west, south-west and south, to south-east, a range of 180°. Ocean is located in all of these directions from the rainfall collection stations, but by very different amounts. For example, the Goukamma sampling station is very close to the Indian Ocean and rainfall approaching from the south will have travelled a mere 5km over land before reaching there, whereas a trough approaching from the Atlantic Ocean at the west coast will have travelled over 500km before arriving at this station. No simple single factor can therefore be expected to describe a continentality correlation and indeed, correlations between δD or $\delta^{18}O$ and 'distance-to-Atlantic' or 'distance-to-closest-coast' are poor, with Pearson's r values of -0.39 for δD – Atlantic, -0.44 for $\delta^{18}O$ – Atlantic, -0.53 for δD – coast and -0.37 for $\delta^{18}O$ – coast.

A factor that somehow combines the effects of multiple weather systems approaching from the Atlantic and Indian Oceans to represent the average length of rainout pathways to each rainfall station is needed. The two measurements of 'distance-to-Atlantic', which is a line from the rainfall station due west to the Atlantic Ocean, and 'distance-to-closest-coast', which is a line in any di-

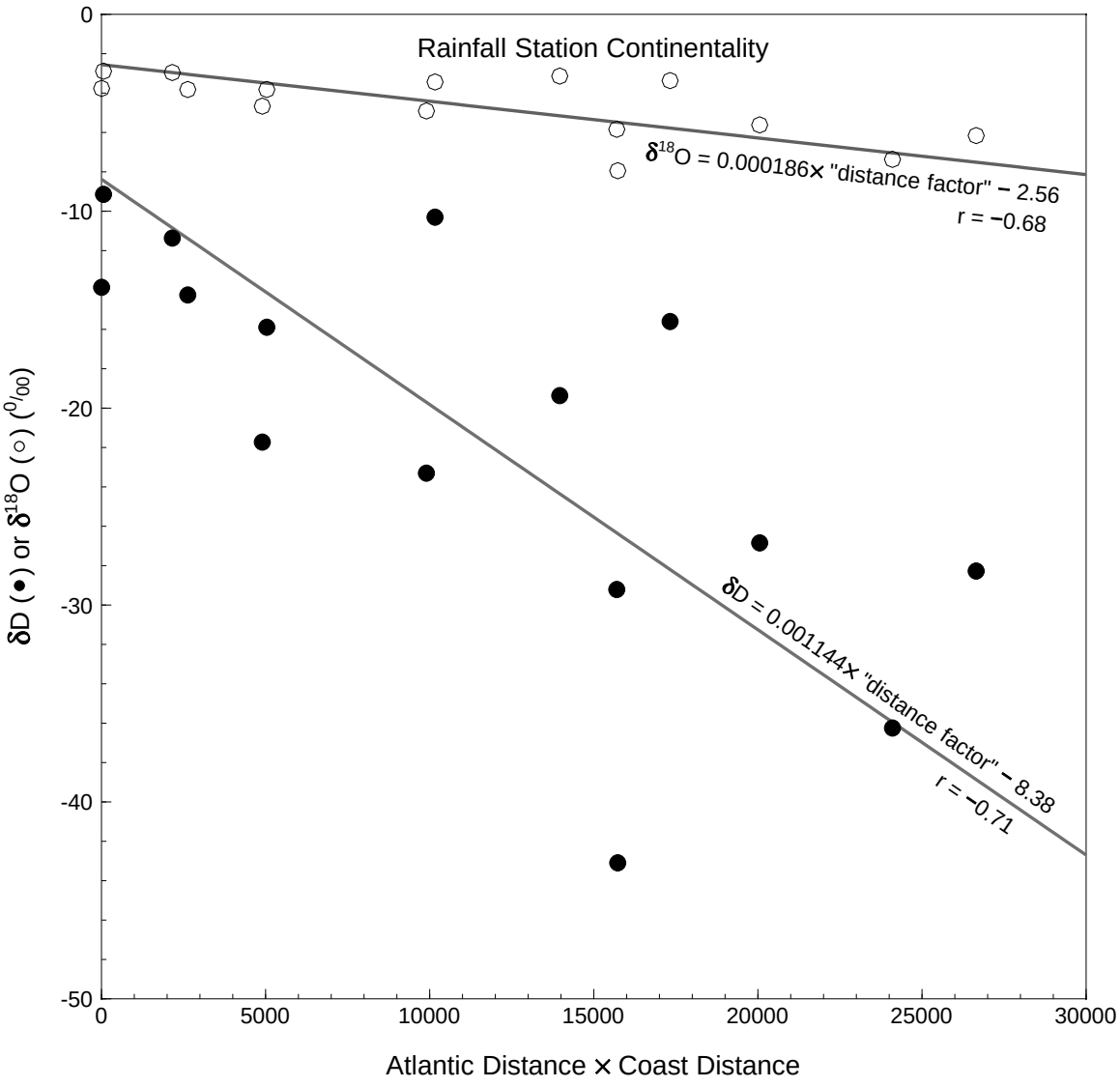

Figure 5.2: The continental effects calculated from this study.

location	**country**	$\delta^{18}O$ **gradient** $\frac{‰}{100m}$	**altitude** m asl	**reference**
Mt Cameroon	Cameroon	-0.16	0–4000	Gonfiantini et al. (2001)
Eastern Andes	Bolivia	-0.24	200–5200	Gonfiantini et al. (2001)
Hérault	France	-0.27	500–1800	Ladouche et al. (2009)
whole island	Taiwan	-0.20	0–2500	Peng et al. (2010)
Fuego volcano	Guatemala	-0.67	800–1200	Mulligan et al. (2011)

Table 5.4: Some examples of the altitude effect from around the world.

rection to measure the shortest distance to the coast from a rainfall station, have been multiplied to create a composite factor. Using this factor produces much better correlations; -0.71 for δD and -0.68 for $\delta^{18}O$ (**Figure 5.2**). The best fit lines to this data also have more realistic δD and $\delta^{18}O$ intercept values, close to those measured at UCT. These values are those expected for precipitation falling at the coast. Unfortunately this correlation does not allow easy comparison with isotope gradients that have been reported as $\frac{\Delta\delta}{\Delta distance}$, such as in Salati et al. (1979) or Rozanski et al. (1982).

5.2.2.3 Altitude

The altitude effect is the most easily measured and quantified meteoric isotope effect and many studies report values of $\frac{\Delta\delta}{\Delta altitude}$ for $\delta^{18}O$ and sometimes δD of precipitation at myriad locations around the world. **Table 5.4** shows a selection of these results from various recent studies; Clark and Fritz (1997, p.71) give results from similar studies in a slightly older selection of the literature.

The altitude effect is, as with the temperature and continental effects, also largely a consequence of progressive rainout as weather systems move up a mountain or escarpment and the heavier isotopes are depleted initially, leaving the subsequent precipitation to have lower and lower δ values. There is, however, an additional factor causing these lower δ values found at greater elevations and this is a reduction in the evaporative enrichment of raindrops as they descend below the cloud base, through unsaturated air. At higher elevations, the land surface is closer, or indeed above the cloud bottom, so reducing or eliminating the path length in which evaporative enrichment can occur.

Table 5.5 shows the altitude effect results calculated for this study. The range of $\frac{\Delta\delta^{18}O}{\Delta altitude}$ values can be seen to be similar to that reported in the literature, except that the Table Mountain and Cederberg region gradients seem on the low side. Unfortunately not many examples of $\frac{\Delta\delta D}{\Delta altitude}$ values have been reported in the literature. As would be expected from the physics governing isotopic fractionation of H and O in water, the δD gradients are around 6–8X that of $\delta^{18}O$.

locations	**distance***	**altitude change**		**gradient**	
				δ**D**	δ^{18}**O**
	km	m	masl	$\frac{‰}{100m}$	$\frac{‰}{100m}$
UCT - Lily Pond - TMC	6	940	135–1075	-0.48	-0.075
WKP - TWT - UKP - Cederberg Tafelberg	40	1550	350–1900	-1.1	-0.11
DDN - MTB	10	1430	480–1910	-1.6	-0.34
RVD - RBP	100	635	250–885	-2.0	-0.24
GST - BKK	6	750	350–1100	-1.8	-0.33
GKM - LTL	70	580	60–640	-2.2	-0.31
all stations: least squares regression	480	2020	60–2080	-1.2	-0.19
all stations: reduced major axis regression	480	2020	60–2080	-1.7	-0.27

Table 5.5: Altitude effect gradients calculated for this study. *Distance refers to the distance between the furthest of the listed locations.

The first point to note about the altitude effect calculations for this study is that many of the individually calculated gradients are similar, such as DeDoorns – Matroosberg and Gamka Store – Bakenskop, even though the altitudes are not the same and the pairs of stations are hundreds of kilometres apart. This is best seen graphically in **Figure 5.4**. Second to note, again most easily visible in the graphs, is the general agreement between the local gradients and the regional line calculated by using all the rainfall station data gathered in this study. Slight exceptions to this are the Table Mountain area (C – Lily Pond – T) and the Cederberg area (I – W – U – Spout).

Looking more closely at the data, there is a trend, especially noticeable in the δD gradients, of increasing gradient eastwards; the locations are arranged approximately in a west to east order in **Table 5.5**. This trend is not well displayed by the $\delta^{18}O$ gradients, however, the high gradients for DDN – MTB and to a lesser extent GST – BKK, the two locations which are disturbing the trend, are probably due to the evaporative enrichment of rain at DDN and GST, both of which are low altitude, low rainfall sites. The ratio of $\frac{\Delta\delta D}{\Delta\delta^{18}O}$ should be around 6–8X, and if less than this, is a sign of evaporative enrichment. Substantial evaporation of falling raindrops will increase $\delta^{18}O$ values more than δD values because of kinetic fractionation, and so increase the difference in $\delta^{18}O$ values between the high and low altitude sites, resulting in a steepening of the $\delta^{18}O$ gradient and therefore a reduction in the multiplication factor between the δD and $\delta^{18}O$ gradients.

The very low gradient in $\frac{\Delta\delta}{\Delta distance}$ reported for Table Mountain can be explained by the following argument. Normally weather systems move from low to high ground and so, as explained above, the altitude effect is a reflection of rainout of heavier isotopes at lower elevations. The dramatic topography of Table Mountain means that the high altitude station, TMC (1074 m), is only 2 km from the Atlantic Ocean coast, whereas the lower station, UCT (135 m), is 6 km further inland. This is a reversal of the usual situation in studies of the altitude effect, where the higher altitude station is also further inland (or in the direction of rain-bearing weather in the case of the

Andes and the Amazon in Gonfiantini et al. (2001)) than the lower altitude station. The altitude effects measured in these studies are the cumulative effect of altitude and distance on rainout. The Table Mountain sub-study is therefore an unusual and valuable example that demonstrates how the pure altitude component of rainout is less than is generally found in these other studies, where a composite distance and altitude induced rainout is being measured.

Two regression lines are plotted on each of the graphs in **Figure 5.4**; the altitude data is shown in **Table 5.6**. These lines have been regressed on all the rainfall station data (letters); they exclude the points for the high altitude seeps (symbols), such as the Lily Pond and Spout. The least squares method (thinner line) assumes no error on the x-variable as this is accurately known and does not change; this regression can be thought of as y on x. This method is appropriate for this type of analysis, where y (δ) is variable and imperfectly known and is dependent upon x (altitude), which is perfectly known and unchanging. However, these lines, for both δD – altitude and $\delta^{18}O$ – altitude are not good matches for the local gradient lines, as seen in the graphs and in the gradient values in **Table 5.5**, where the least squares gradients are at the low end of the spectrum.

The reduced major axis method of regression (thick lines) has been used throughout this study for the δD – $\delta^{18}O$ regressions and is ideally suited to data where both x and y have variance and neither are independent of the other. Interestingly, although this method is theoretically statistically sub-optimal for the δ – altitude regressions, the resulting regression lines and $\frac{\Delta\delta}{\Delta altitude}$ gradients seem to describe and fit the data better.

Figure 5.3: Map of the study area with sample locations and cross section lines indicated. Background DEM from NASA (2013) and roads shapefile from NGI (2012).

Island Mountains and Mountain Valleys

Island Mountains is a term coined here to describe sample collection points that are located at or near the top of a mountain peak and are therefore at a position much higher than the surrounding area.

The two rainfall collection stations, Blesberg and Kammanassie, which are only 25 km apart and have a 1400 m altitude difference, would seem to make a useful pair for a local estimate of the altitude effect. However, Blesberg, the highest station of the whole study, at 2080 m, has δD and $\delta^{18}O$ that would be expected for a station of half that height, based on the average altitude effect relationship for this study. In contrast, Kammanassie, with a moderate altitude of 666 m, has isotope ratios that would be expected for a station at triple the height. Only Matroosberg, at 1910 m, has more negative δ values than Kammanassie. The result of these departures from the average pattern is that the local altitude effect gradient is reversed between these stations, with δ values that increase with altitude.

The Blesberg mean δ values seem to fall on a line with Cederberg Tafelberg (Spout) and Cape Town's Table Mountain (and Lily Pond); see **Figure 5.4**. All four of these points lie to the right of the $\frac{\Delta\delta}{\Delta altitude}$ best fit regression line, meaning the δ values are less negative than expected, based on the average for this study. Robinson Pass, Bakenskop and Matroosberg are close to the average for all of the data. Kammanassie and Lentelus lie to the left of the average, meaning their δ values are more negative than would be expected for their altitude. These three sets of locations have morphological similarities that may account for their location on the δ–altitude plot. The first group can be thought of as "island peaks", sharply rising peaks that are much higher than the general surrounds. The last group can be thought of as "mountain valleys", where the elevation of the sample site is lower than that of the general surrounds. The intermediate group are at a position in the landscape where there are substantial amounts of higher and lower ground around, or, in the case of Bakenskop, on a plateau-like summit where the station is surrounded by lots of land at a very similar elevation (less than 100 m difference).

Rainout on the "island peaks" is not substantial, because of the sudden change in elevation, and so the isotopic signature is more typical of that for a site at lower elevation. The "mountain valleys" are the reverse, where the station elevation does not reflect the amount of rainout that occurs on the surrounding higher ground, and so the isotope composition tends towards those expected at these surrounding, higher elevations.

Table 5.6 summarizes the landscapes around some of the rainfall collection stations, as well as some high altitude seeps. The average altitudes were generated from the ASTER DEM (Advanced Spaceborne Thermal Emission and Reflection Radiometer Digital Elevation Model) by averaging the elevations of all pixels within a 5 km radius of the point of interest (ASTER, 2014). The seeps discharge high up in the mountains with minimal ground above the seep and so the discharge altitude cannot be much different to the recharge altitude, as there is very little more mountain available above the seep point for recharge to occur. These seeps can be thought of as proxies for

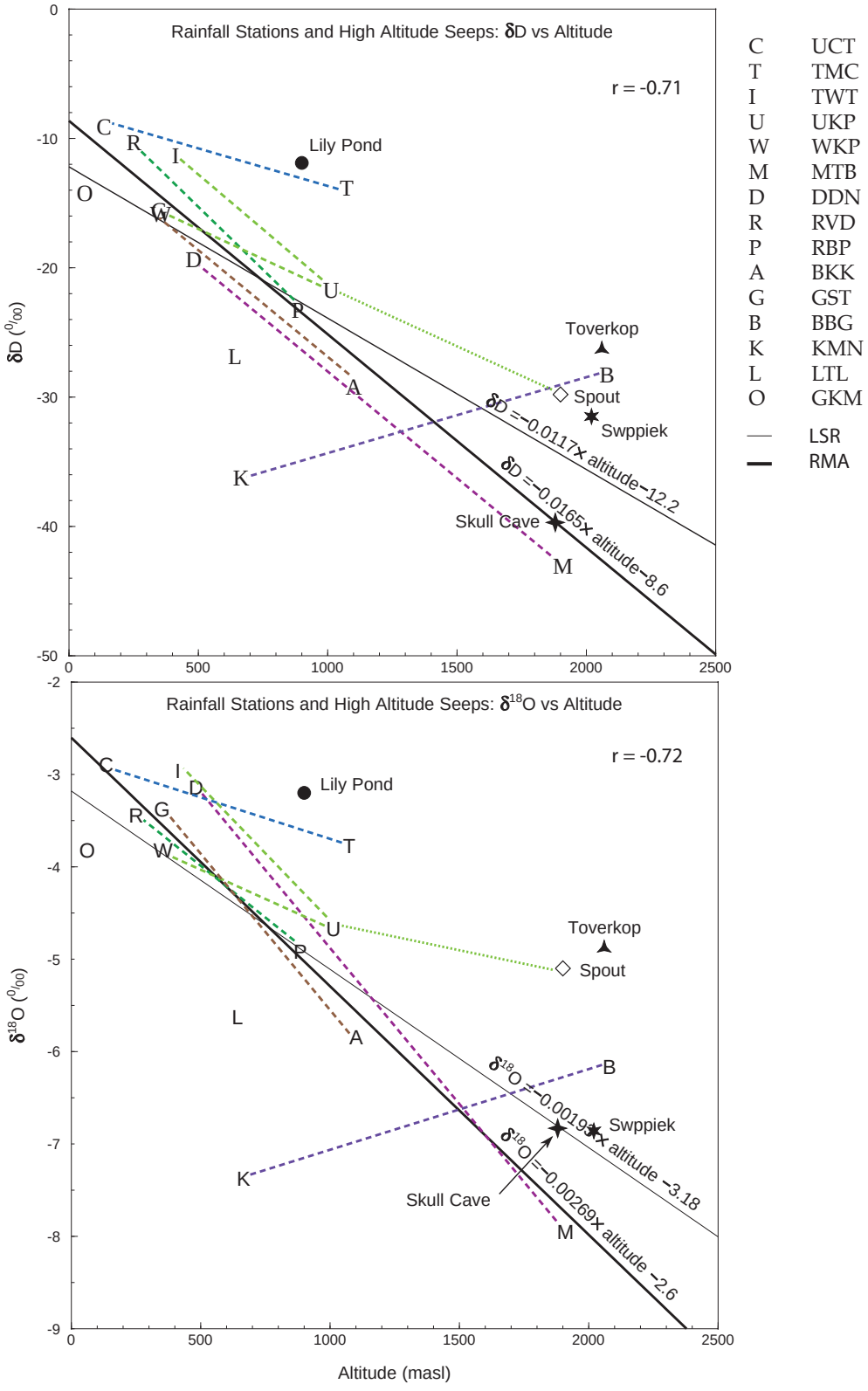

Figure 5.4: Relations between altitude and δ values. Letters indicate weighted averages of monthly precipitation at rainfall collection stations; symbols are high altitude seeps. Dashed lines connect rainfall nearby stations; dots to a nearby seep. Colours are from the theme colours for one of the stations in the pair. Both the RMA regression (thick line) and LSR (thin line) are shown, calculated from the rainfall station data, excluding the seeps.

station		elevations				stn - avg
		m asl in 5km radius from station				m
		station	**highest**	**average**	**lowest**	
Cederberg Spout		1900	1969	1266	940	+634
Table Mountain Cableway	TMC	1074	1086	289	0	+785
Table Mountain Lily Pond		900	1086	289	0	+611
Matroosberg	MTB	1910	2249	1561	550	+349
Robinson Pass	RBP	885	1363	723	350	+162
Bakenskop	BKK	1100	1106	772	350	+328
Toverkop	TVK	2060	2189	1281	550	+779
Skull Cave	SKC	1880	2240	1393	750	+487
Seweweekspoortpiek Cave	SWP	2020	2324	1368	650	+652
Blesberg	BBG	2080	2084	1329	600	+751
Kammanassie	KMN	666	1205	794	500	-128
Lentelus	LTL	710	1688	854	550	-144

Table 5.6: Relative position in the landscape of selected rainfall stations and high altitude seeps, which are proxies for rainfall. The last column summarizes the situation by showing the difference in height between the station or seep elevation and average elevation for an area of 5 km radius around the station.

rainfall at much the same elevation. It can be seen from **Table 5.6**, especially the final column, that some stations lie well elevated from the average surrounding landscape, Blesberg, Toverkop and Table Mountain being good examples – these are the "island peaks". Other stations are at similar altitudes to the average and only two, Lentelus and Kammanassie, are examples of the "mountain valleys". A good correlation exists between this difference from the average elevation, and the position on the δ–altitude graphs, as described above. A visual representation of the relative altitude of sampling points is shown in **Figure 5.5**.

The correlation is not exact, at least one reason of which is the seep data consists of between one and three samples only per seep. Much noise exists in isotope data, due to the specifics of the weather, and so single samples are not ideal, although being groundwater, these seep samples will be more stable and representative values than for rain. Another reason for the extreme position of Kammanassie is the large amount and isotopically negative rainfall in June and July 2010. The July value in particular, with 80 mm rainfall for the month, caused the average to be displaced towards low δ values.

In conclusion, due to the steep slopes and small area of the high peaks in the Cape Mountains, the altitude effect is supressed and the isotopic composition of rainfall on these summits is less negative than one might expect. The reverse is also true for valleys in mountainous areas, where the isotopic composition reflects a slightly higher altitude, closer to that of the average ground

elevation around the site, and not the specific, low, elevation of the valley floor. To get an accurate measure of the altitude effect, sites for rainfall collection should be chosen on broader peaks where substantial areas of high ground occur, such that the rainout process is significant enough to drive the isotope ratios to more negative δ values.

This altitude effect distortion is probably the reason the RMA regressions fit the data better than the least squares method, as the RMA regression assumes an error in 'x' as well as 'y'. As discussed above, the ground altitude at the rainfall stations is not always representative of the area around the location, which is what influences the isotope content of the rain, and so 'x', or altitude, can also be thought of as being subject to some error.

5.2.2.4 Amount

Correlations between δD or $\delta^{18}O$ and rainfall amount have been described by many authors since Dansgaard (1964) first reported it. As the amount of rainfall increases, the δ values decrease, both for single rainfall events (e.g. Dody and Ziv, 2013) and for monthly average rainfall amounts (e.g. Uemura et al., 2012). Reasons for the amount effect include, firstly, a drop in air temperature to cause condensation of progressively isotopically lighter vapour, as the heavier isotopes have already condensed and rained out of the air mass. Secondly, the more rain that has fallen, the more the air below the cloud becomes moist and so less evaporative enrichment of the raindrops occurs as they fall to the ground. And thirdly, similarly, in clouds with great vertical development where rain may form at high elevations, raindrops falling through the cloud may undergo isotope exchange with cloud droplets and vapour lower down, which will make slight rains tend towards heavier isotopic content, but will affect substantial rains less and so substantial rains will tend to retain their more negative isotopic signatures.

The data from this study is not ideally suited to quantification of an amount effect, primarily because the short period of sampling (two years) leads to averages for rainfall and isotope data possibly being far from the long term means. No correlations exists between the average annual rainfall and the weighted mean isotope values, as can be seen in **Figure 5.6**, both graphically and from the 'r' values that are near zero. For monthly data, a similar restriction on data quality results from the short duration of this study, as each month (e.g. July) may only be based on zero to three samples. At some stations there are months with no samples, although this is often due to a consistent lack of rain for that month(s) over two or three years, for example January at De Doorns. Nevertheless, for the stations with more complete records, comparison of mean monthly δD and $\delta^{18}O$ values with mean monthly rainfall has been done: see **Figure 5.7**.

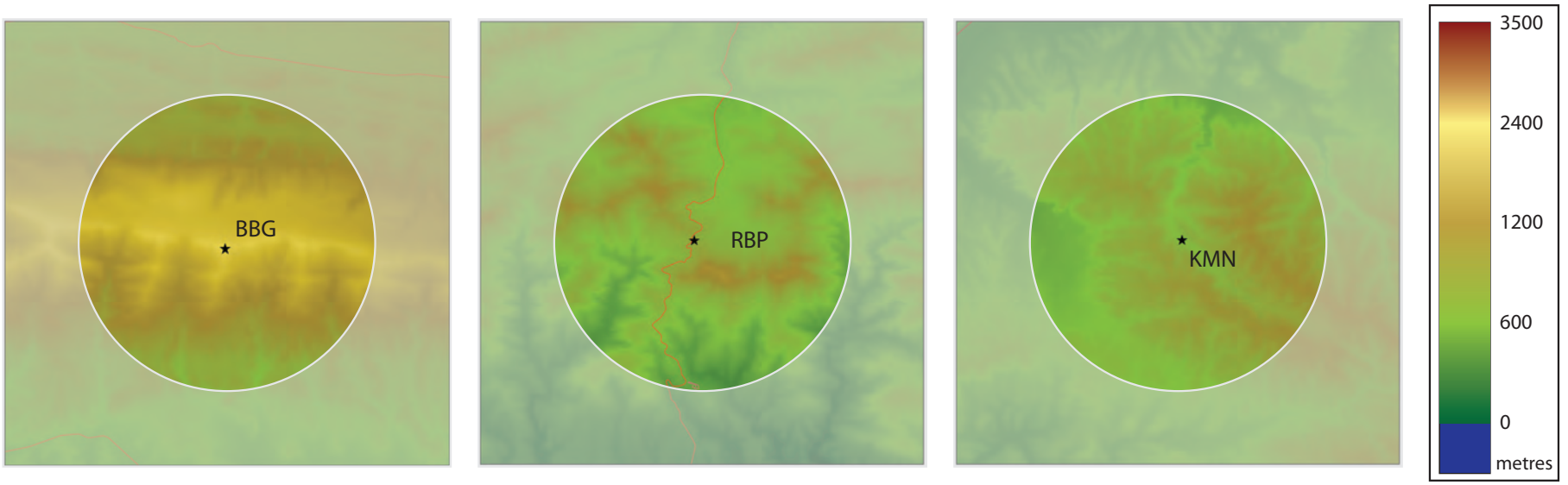

Figure 5.5: Digital elevation models for three of the rainfall collection stations with a highlighted circle of 5km radius around each station, illustrating the relative position in the landscape, in terms of altitude, of each station. Blesberg (BBG) is an example of an "island peak", Robinson Pass (RBP) of a station in a more or less representative position and Kammanassie (KMN) a "mountain valley". See **Table 5.6** for similar information in a numerical format for these and other sampling points.

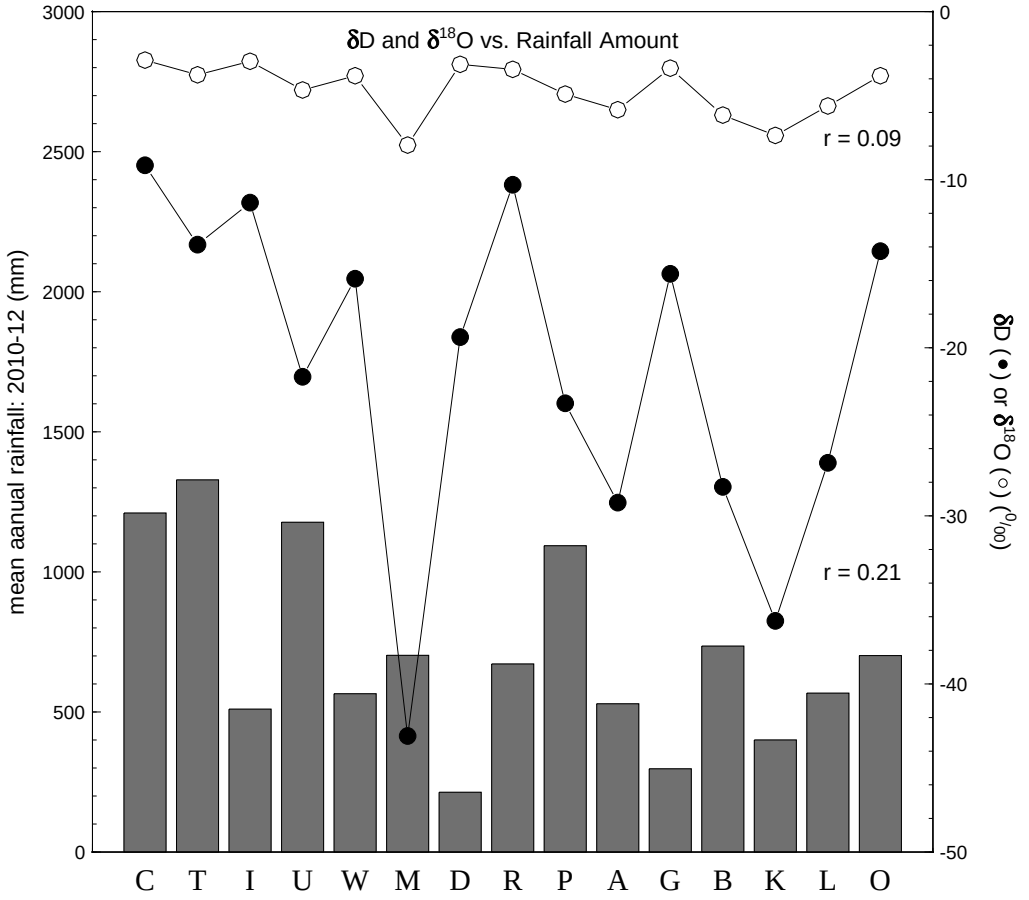

Figure 5.6: Comparison of weighted mean isotope composition and mean annual rainfall at each station: C = UCT, T = Table Mountain, I = Twaktuin, U = Uitkyk Pass, W = Wolfkop, M = Matroosberg, D = De Doorns, R = Riverndale, P = Robinson Pass, A = Bakenskop, G = Gamka Store, B = Blesberg, K = Kammanassie, L = Lentelus and O = Goukamma.

These stations were not selected on the grounds of displaying a "better" amount effect, but purely on the completeness of the record. The amount effect at these stations is generally noticeable in that there is a fair to good correlation between the δD or $\delta^{18}O$ values and rainfall amount. The Pearson's 'r' correlation coefficients shown on the graphs in **Figure 5.7** confirm the validity of the visual impressions given by the graphs. The Wolfkop station, however, shows no correlation between rainfall amount and δ values, due to some months with low rainfall having the isotopically lightest water, particularly March and December. The 30th March 2011 featured an unusual low pressure trough preceding a frontal depression over the Atlantic Coast area, causing widespread rain over the Western Cape and into the western parts of the Northern Cape, with falls of 8 mm at Clanwilliam and 10 mm at Excelsior Ceres. Rain from these systems is typically convective in nature (similar to thunderstorms) and generates rain of light isotopic composition. The rainfall of 31st December 2010 to 1st January 2011 has already been discussed in the previous chapter (Chapter 4), and was a significant event environmentally, causing floods and mass

wasting erosion in the Cederberg region, and resulted in rain and hail with highly negative delta values. A longer term record for a station like Wolfkop would be expected to see the influence of these unusual events decline and a better amount effect correlation develop.

The amount effects from the stations at UCT, Riverndale and Goukamma are all significantly better than that found by Harris et al. (2010) for UCT rainfall over 1996–2008, which gave 'r' values of -0.388 for δD–amount and -0.425 for $\delta^{18}O$–amount. Of the three stations shown in **Figure 5.7**, the UCT 2010–2012 record gave the poorest correlations with 'r' values of -0.51 and -0.68, similarly, but these are still substantially better correlations than the previous work. This suggests that some years have a particularly clear amount effect, exceeding the long term average. This finding emphasizes the value of long term monitoring in revealing average meteorological patterns and warns against overinterpretation of data based on short term precipitation records.

5.3 Surface Water

5.3.1 Altitude

The five rivers sampled reveal a wide range of isotopic compositions over an altitude range of approximately 130–1900 m (see **Figure 5.8**). The data for each river generally forms a cluster, with no significant correlations against altitude. The best correlation is at Volstruiskloof, which is the only river to have 'r' values more positive or more negative than +0.5 or -0.5, respectively (the threshhold for a reasonable correlation). However, removal of only one of the four Volstruiskloof data points reduces the remaining three points to a cluster. For the neighbouring river, Duiwelskloof, a better correlation can be created if the data point with the highest δ values is removed; this can be motivated as this sample is from the base of a very low flowing drip waterfall that flowed over exposed, sunny rock for many metres and has been substantially evaporated in the process. However, this still does not create a good correlation between isotope values and altitude. The outlier Volstruiskloof and Duiwelskloof points have been included in analyses and graphs.

5.3.2 Springs, Seeps and Tributaries

Samples of seeps and springs were taken along Groothoekkloof and in the Witels, often paired with a sample from the main stream just above mixing with the new source, but these showed surprisingly little variation. Similarly, tributaries were also sampled and paired with a sample in the main stream just upstream of mixing with the tributaries' waters, and again these often showed little difference. No systematic variation could be found between the isotope composition of a sample and the characteristics of its source, such as being a main stream or spring sample, or the size or average elevation of its sub-catchment, in the case of a tributary.

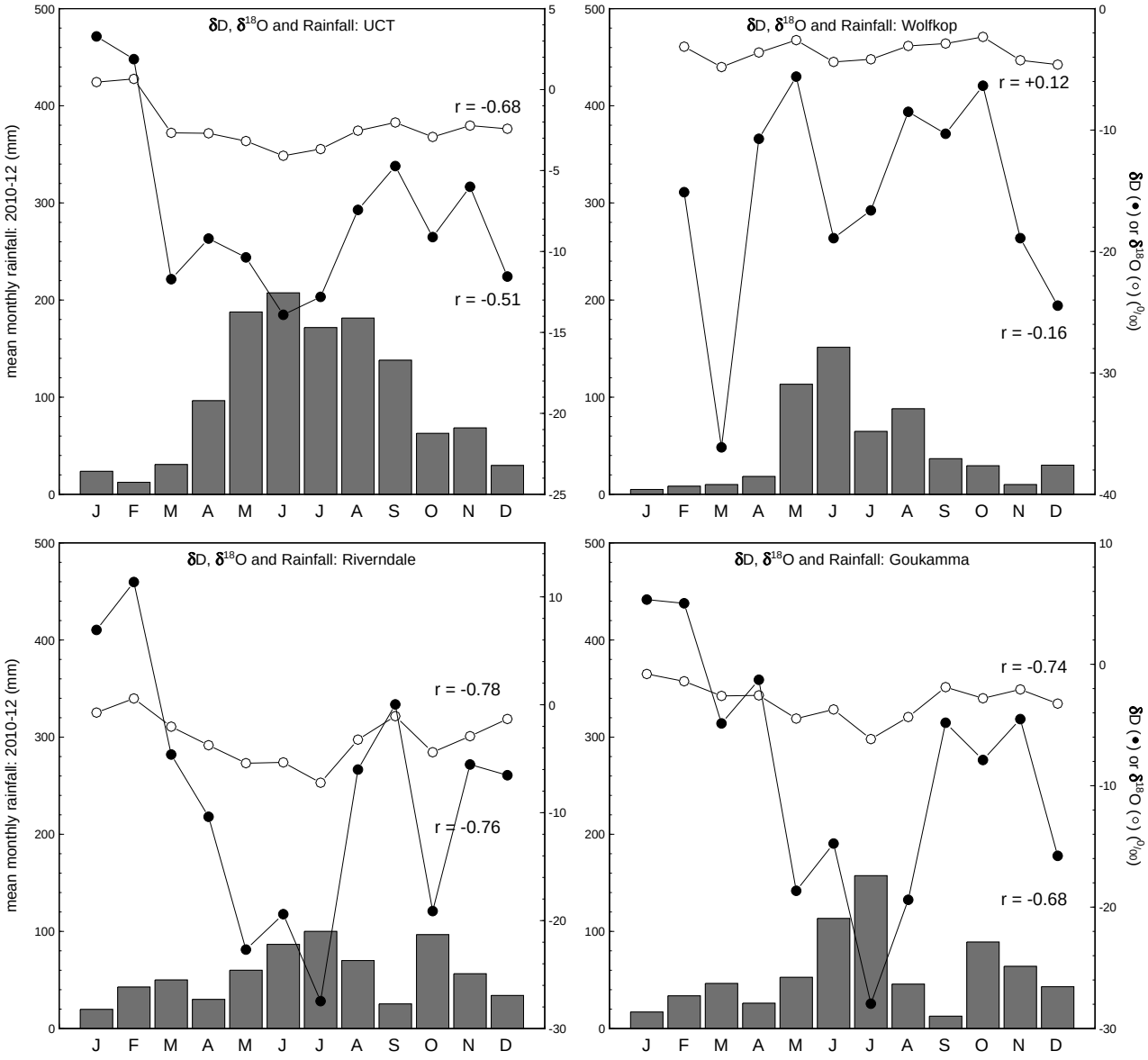

Figure 5.7: Mean monthly rainfall, δD and $\delta^{18}O$ values for the four rain stations with most complete record.

5.3.3 Baseflow

The rivers were all sampled in summer or early autumn when rainfall had been low for many months, with the exception of Meulkloof, near Swellendam in the southern Cape, which experiences all year round rainfall. The other rivers would all have been fed exclusively by groundwater (see **Section 2.5.4**), whether deeper groundwater discharging from fractured Table Mountain Group aquifers or shallow groundwater from soil and scree slopes. The surface water flows that remain steady over the dry season and are groundwater fed are known as baseflow.

Several factors could cause the baseflow to show little isotopic variation down the length of the river, as seen in **Figure 5.8**. The most obvious factor is that river samples are a mixture of the various groundwater sources that feed them, and so mixing of all the water sources would dilute any unusual isotope composition feeding into the river at any point. The rivers all have a steady increase in flow downstream, caused by addition of groundwater. However, the sampling of springs, seeps and tributaries directly showed that it is not mixing and dilution of surface water that is responsible for the lack of isotopic trends or changes, but rather the sources themselves that do not vary much.

Groundwater flow through the Table Mountain Group aquifers is directed by fracture networks that are aligned with structural features and bedding (Hartnady and Hay, 2002b). Groundwater does not simply flow from peaks to valley bottoms in the shortest distance as it would in a primary porosity aquifer. This complex flow dynamic means that water emerging as springs and seeps to feed surface water may come from a range of directions and be recharged at a variety of positions at different altitudes. This complexity is possibly the reason the rather limited surface water data set is unable to yield any patterns. Interestingly, the variations in δD and $\delta^{18}O$ values tend to decrease eastwards, as seen in the last two columns of **Table 5.7**. This could be caused by an increase in fracturing of the Table Mountain Group as one moves from the relatively undeformed strata of the Drakenstein Mountains in the west, through the syntaxial region of the Hex River Mountains to the southern Cape, known to have experienced the greatest tectonic deformation during the Cape Orogeny (Söhnge, 1983; de Beer, 2002). The greater the degree of fracturing, the more likely the groundwater becomes well mixed and variation in isotope composition is homogenised. The sample size of 5 rivers is perhaps a bit small to take this as a real trend, but it is interesting that greater river length, greater change in altitude or greater catchment size does not cause a greater range in isotope values.

Work by Negrel et al. (2011) on groundwater from shallow fractured rock aquifers showed substantial variation in isotope composition. This is in contrast to the more homogenous isotope compositions measured in this study and supports the model of complex and deep groundwater flow in the Peninsula aquifer.

code	river	mountain range	catchment						sampling		range	
			highest peak	height	highest sample	lowest sample	area	flow	length	gradient	δD	$\delta^{18}O$
				m asl	m asl	m asl	km^2	L/s	km	m/km	‰	‰
DWK	Duiwelskloof	Drakenstein Mountains	Drakenstein Peak	1490	1240	680	2	2	2.4	300	10.1	1.91
VSK	Volstruiskloof	Drakenstein Mountains	Buller's Kop	1425	1160	580	1.5	2	1.5	450	11.9	2.14
WTL	Witels	Hex River Mountains	Buffelshoek Peak	2060	1650	310	50	100	20	70	7.5	1.61
GHK	Groothoekkloof	Hex River Mountains	Matroosberg	2249	1800	580	15	10	8	150	8.8	0.59
MLK	Meulkloof	Langeberg	Hermitage Peak	1546	820	130	11	20	6	120	3.4	0.44

Table 5.7: Description of the five rivers sampled, with rough flow estimates and gradient for the sampled length.

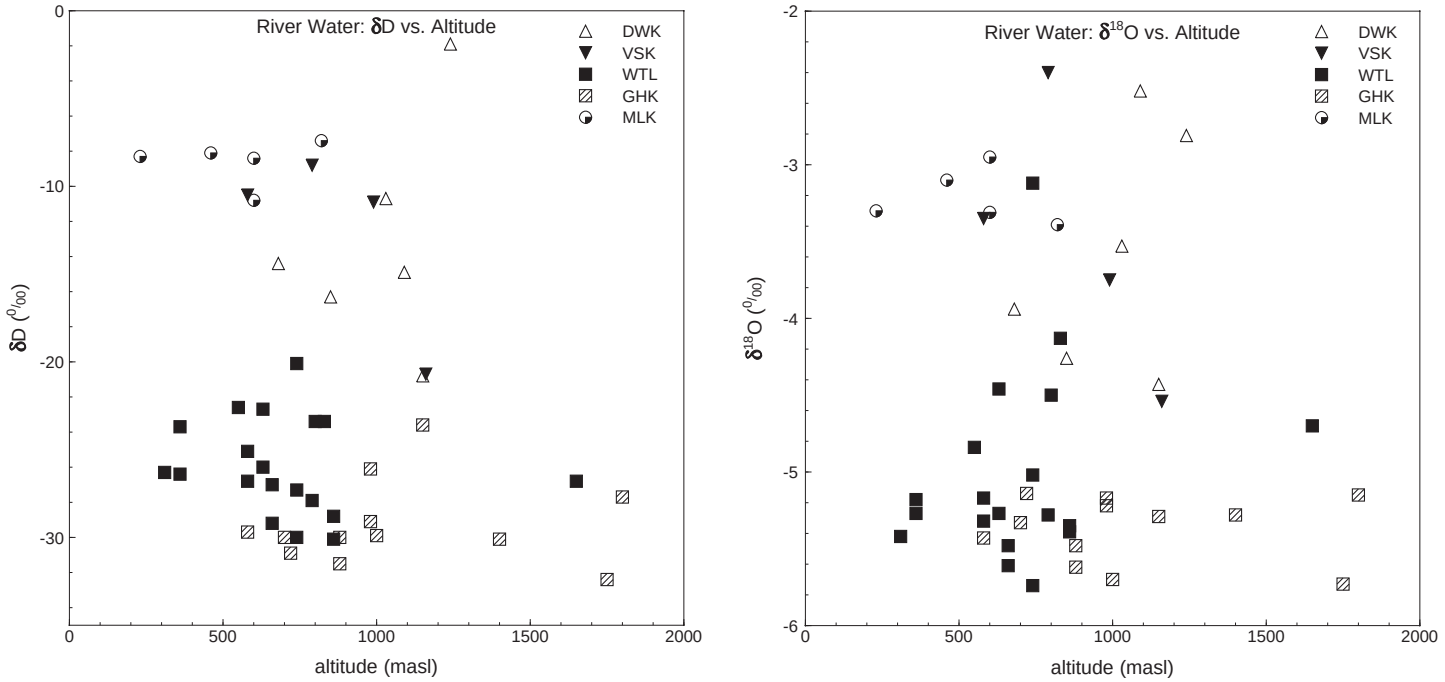

Figure 5.8: Plots of δD and $\delta^{18}O$ against altitude for surface water samples from five rivers in the Western Cape.

5.3.3.1 Sharp Relief

The lack of a distinct change in isotopic composition with altitude in the rivers and their sources (springs and seeps) suggests that the groundwater in each catchment does not vary significantly isotopically. The would occur if the rainfall is isotopically similar across the catchment, as might be expected because of the small size of these mountain catchments. This finding concurs with the rainfall analysis where it was found that the variation in isotopes is less than is expected given the range in altitude between sites. The average elevation around a site, in an area of 50–100 km^2, is as important as the actual altitude of the site in determining the isotopic composition of rainfall. This works for both sharp, high peaks that are much higher than the surrounding terrain, and for deep, steep valleys that are much lower than the surrounding terrain. So although the rivers traverse wide ranges of elevations, from peak to valley bottom, the range in isotopic composition for rainfall is more restricted than the elevation range would suggest.

The best fit lines shown for the five rivers in Chapter 4 also reveal something about the catchments. The line with the lowest gradient and intercept is for the Witels ($\delta D = 4.42\delta^{18}O - 3.8$), and is similar to typical evaporation lines (e.g. Gat, 1996). This river is the longest, the gradient is the lowest and the catchment is the largest, all of which are likely to contribute to evaporation in the area. If evaporation was occurring only in the main stream as it flows through the catchment, then the lowest samples would have the least negative isotope compositions. The samples with the least negative isotope composition are not concentrated towards the bottom of the river catchment and as seen in **Figure 5.8**, there is no systematic variation of isotope values against parameters such as altitude. This suggests that the evaporation is widespread and affects all waters in the catchment and is not simply the result of evaporation in the main stream.

5.3.3.2 Summary

Isotope compositions are clustered for each river sampled. Variation in each river is minimal and is generally poorly correlated with any obvious parameter, although it is known that rivers often display limited variation in isotope values (Fritz, 1981). The isotopic variation in rainfall has been shown to be smaller than would be expected, given the range of altitude. Furthermore, complex groundwater flow causing mixing, and also mixing and dilution along the length of the streams, will reduce the range in isotope compositions in the surface water. From the rivers sampled it seems that isotopes are unable to help pinpoint groundwater flow directions or recharge areas for the water that discharges into the streams via springs and seeps. Isotopes may still be of value for longer rivers or larger catchments, but appear to have little value in small, rugged mountain catchments. Decreasing range in isotope compositions within each river, as one moves eastwards, may reflect more complex groundwater flow and greater mixing, due to more intense fracturing related to position within the Cape Fold Belt, which has varying degrees of structural deformation from the Cape Orogeny.

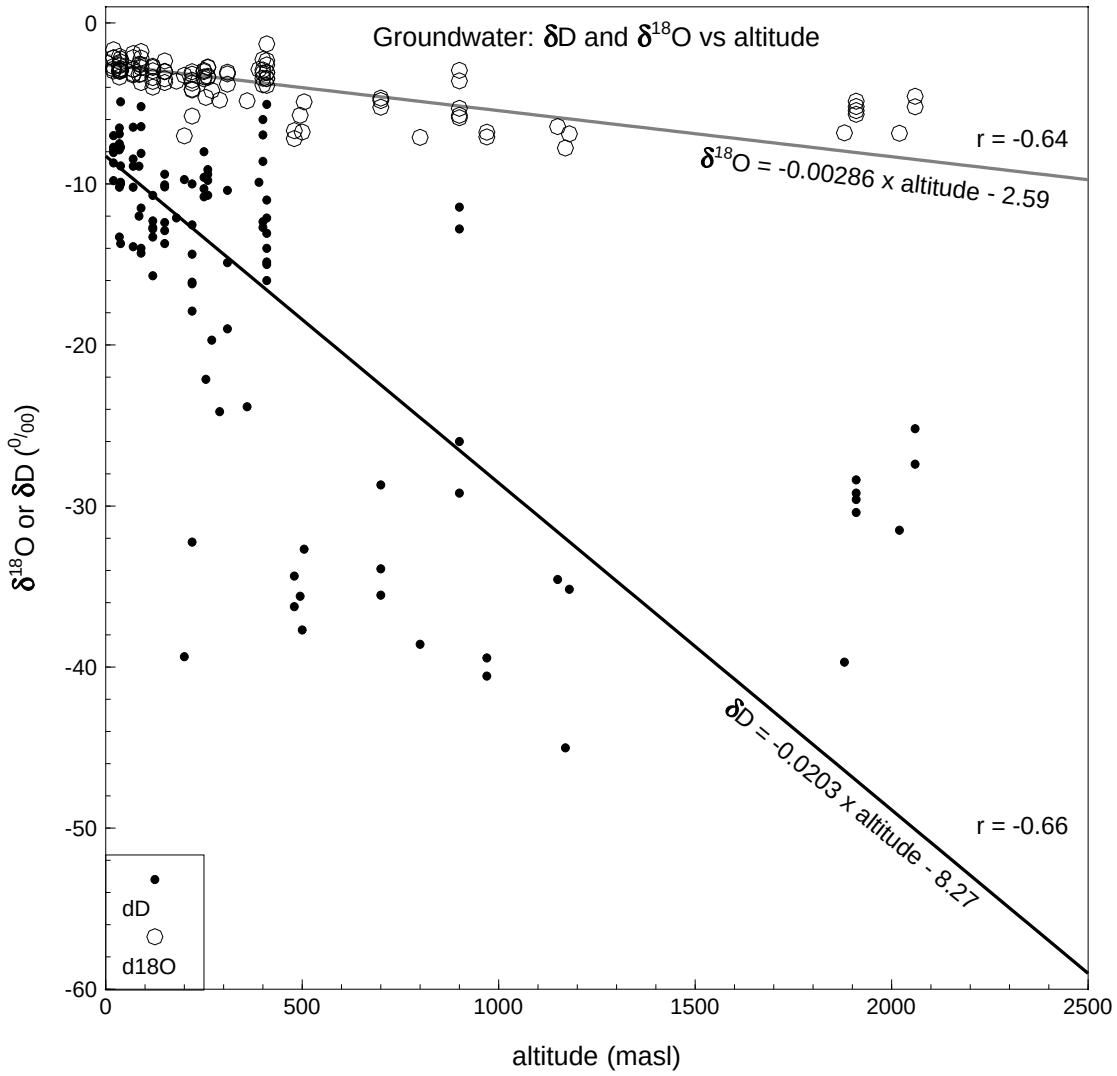

Figure 5.9: Groundwater isotope composition as a function of sampling (discharge) altitude.

5.4 Groundwater

5.4.1 Altitude

The isotope composition of recharge should be similar to that of the rainfall in the recharge area, although some changes will take place, primarily due to evaporation and selective recharge. Selective recharge takes place because not all rainfall events are the same in magnitude and intensity, and depending upon the recharge process, some of the rain may not recharge. This can occur when an event is too small and all the rainfall gets used up through interception, transpiration or evaporation. A larger event may generate recharge, but a portion of it will still be taken up in interception, transpiration and evaporation. More intense events may result in high runoff, none of which recharges locally, but may recharge in another area downslope. The isotope

composition of groundwaters can therefore vary from very similar to that of rain in the recharge area, to something quite different, and this variation may itself vary year to year, depending on changes in the weather and possibly also vegetation and soil.

Brandvlei hot spring, at 64 °C, is the hottest spring in the region (and in the country). No actively circulating groundwater in the Western Cape is therefore likely to reach temperatures over 70 °C and by far most of the groundwater circulates at temperatures between 0 °C and 20 °C. No isotope exchange between the water and host rock takes place at these temperatures (Clark and Fritz, 1997). Assuming a simple flow model from recharge area to discharge area with no mixing, the isotope composition of water at discharge must be the same as at the recharge area.

Groundwater flow through landscapes varies from highly local, over hundreds of metres or less, to regional, over distances of tens to hundreds, such as in the Perth Basin (Davidson, 1995) and sometimes even thousands of kilometres, such as in the Great Artesian Basin in Australia (White, 2000). In South Africa, the absence of large, unmetamorphosed sedimentary basins to form regional aquifers is the main reason groundwater flow is restricted in extent and quantity. The Karoo Basin contains mostly argillaceous rocks and the more arenaceous units are too well cemented to be highly transmissive primary porosity aquifers. Changes in rock type also tend to block flow as aquifers come up against impermeable units, for example the Table Mountain Group abutting the Malmesbury Group as on the Kango Fault (see **Figure 5.20**). Lastly, the highly dissected topography tends to make flow paths short, because of steep hydraulic gradients and short distances between wet, high altitude mountains, and dry, low altitude valleys where discharge feeds into rivers (Domenico and Schwartz, 1998, p.77).

A correlation exists between the isotopic composition of groundwater and altitude (**Figure 5.9**). The altitude plotted is that of the discharge point of springs and seeps, or that of the collar (ground level), if sampled from a borehole. The equations of the best fit lines describing the δD and $\delta^{18}O$ relationships with altitude have been plotted on the graph. These lines were calculated using the reduced major axis regression method, as the least squares regression method again generated lines of best fit with rather gentle gradients and unrealistically negative intercepts, as was noted for the regression of the rainfall station data against altitude, in **Figure 5.4**. These least squares regression equations are:

$$\delta D = 0.0134 \times altitude - 11.15 \quad (r = -0.66)$$

$$\delta^{18}O = 0.00184 \times altitude - 3.02 \quad (r = -0.64).$$

Where recharge areas are far from discharge points, the isotope composition of the groundwater might be different from the rainfall at the discharge area. In particular, because changes in altitude generate noticeable changes in rainfall (and hence recharge) isotope composition over relatively short distances, if groundwater flow paths were several kilometres and more, there

would be a poor correlation between groundwater delta values and altitude. The graph in **Figure 5.9** shows the opposite. The slopes and intercepts of the best fit lines similar to those for the rainfall station – altitude correlation (see **Figure 5.4**). This suggests that the flow paths, at least for the groundwater sampled in this project, are mostly short, and in particular, there are not large differences between the elevation of the recharge and discharge sites.

5.4.2 Hot Springs

Hot springs have always been a target for hydrological (e.g. Bond, 1953), hydrochemical (e.g. Kent, 1949) and isotopic (e.g. Mazor and Verhagen, 1976) studies. The hot springs of the Western Cape have been analysed for their stable isotope content previously, so an analysis of the changes over time is possible. From **Figure 5.10**, it is clear that there are no systematic changes between the three studies in 1971-2 (Mazor and Verhagen, 1983), 1995-6 (Diamond and Harris, 2000) and 2010-12 (this study). The 'random' variation in isotopic values of discharge at the springs, measured from month to month in the Diamond and Harris (2000) work is equal to the magnitude of variation seen over 40 years, between 1971 and 2011. It is possible that some of the larger shifts in isotope composition could reflect yearly or multi-year shifts in the average isotope composition of recharge. However, these large shifts (10 ‰ for δD and 2 ‰ for δ^{18}O) were recorded over months by Diamond and Harris (2000) over only 2 years at Laingsburg. It is possible that inter-annual shifts in isotope composition become compressed in the groundwater flow path and issue over monthly timescales, but this would require a piston-like flowpath with very little groundwater mixing, which is not likely given the depth and length of the flowpath.

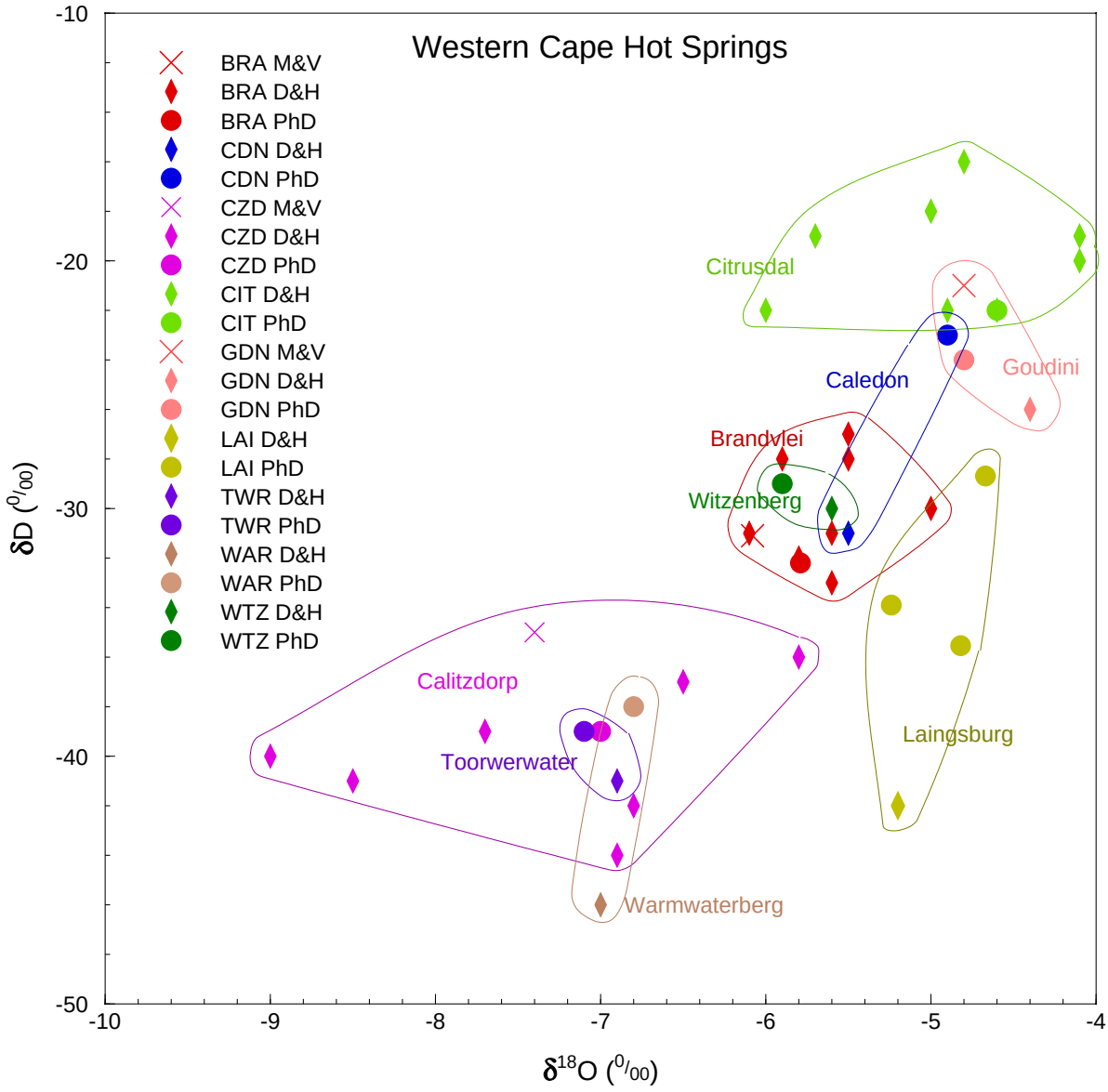

Figure 5.10: Stable isotope compositions for the Western Cape hot springs from three different studies, showing no obvious long term change. Data from Mazor and Verhagen (1983) (M&V), Diamond and Harris (2000) (D&H) and this study (PhD).

5.5 Regional Analyses

This study attempted an overview of stable isotopes of water in and around the Table Mountain Group, including rain, surface water and groundwater. In such a broad study, large areas naturally are neglected, but some areas have had sufficient analysis that a more detailed interpretation can be attempted in those areas. These interpretations should provide, firstly, an indication of the usefulness of stable isotope hydrology in unravelling the hydrogeology of the Table Mountain Group, and secondly, some actual insights into the flow of groundwater through the Table

Mountain Group. On the δD–δ^{18}O plots in this section, the symbol size is approximately that of the analytical error.

5.5.1 Cederberg

Substantial quantities (gigalitres per year) of groundwater are utilized by farmers in the Olifants River Mountains area (pers. comm. Robert Paterson of Twaktuin Farm). The possibility exists that this groundwater, or some of it, is recharged in the Cederberg and, by means of faults and fracture networks in the Peninsula Formation, passes beneath the Olifants River Valley before discharging to the west of the Olifants River Syncline in the Olifants River Mountains area. The cross section in **Figure 5.11** illustrates how the geology can allow this to occur, although the geometry of the Olifants River Syncline changes to the north and south of this line. In general, the syncline deepens and is dominated by a simple synclinal fold structure southwards, whereas northwards the syncline shallows and faults displace the Cederberg aquitard such that hydraulic connections are established between the Peninsula and Skurweberg aquifers. The fault shown in the Olifants River Syncline in the cross section does not quite achieve this linkage, but another fault, a few kilometres north of the cross section line, does.

The result of these changes in structure in the Olifants River Syncline is that futher south the Peninsula aquifer is more of a confined system under the Olifants River Valley, and does indeed transfer groundwater from the higher, eastern mountains, the Koue Bokkeveld range, to the lower, western range, the Warmbadberg, as shown in Diamond and Harris (2000). Evidence for this comes from the Citrusdal hot spring, The Baths, and is twofold: firstly, the temperature of discharge, at 43 °C, requires circulation to around 2 km depth, assuming a geothermal gradient of 20 °C/km and an input temperature for rain of 5–10 °C (Jones, 1992); secondly, as can be seen in **Figure 5.12**, the isotopic composition of the spring water is more negative than local rainfall at Citrusdal (Diamond and Harris, 1997) or Wolfkop, but matches rainfall at Uitkyk, 1000 m high in the Cederberg, which will be similar to rainfall in the Koue Bokkeveld ranges due east of the spring. Further north in the Olifants River Syncline movement of groundwater under a hydraulic gradient from the higher Cederberg range in the east to the lower Olifants River Mountains in the west may not be as easy due to the shallower syncline and the presence of the faults. These faults can lead to an upward leakage out of the Peninsula aquifer and directly into surface water, such as is postulated to occur at The Baths, or via the Skurweberg aquifer and then into surface water. The juxtaposition of the Peninsula and Skurweberg aquifers, because of the faulting, can also allow loss of groundwater from the Peninsula aquifer into the Skurweberg aquifer. The shallowness of the syncline also leaves a relatively thin layer of the Peninsula Formation remaining to conduct groundwater westwards, as seen in the areas just east and west of the Olifants River Valley in **Figure 5.11**.

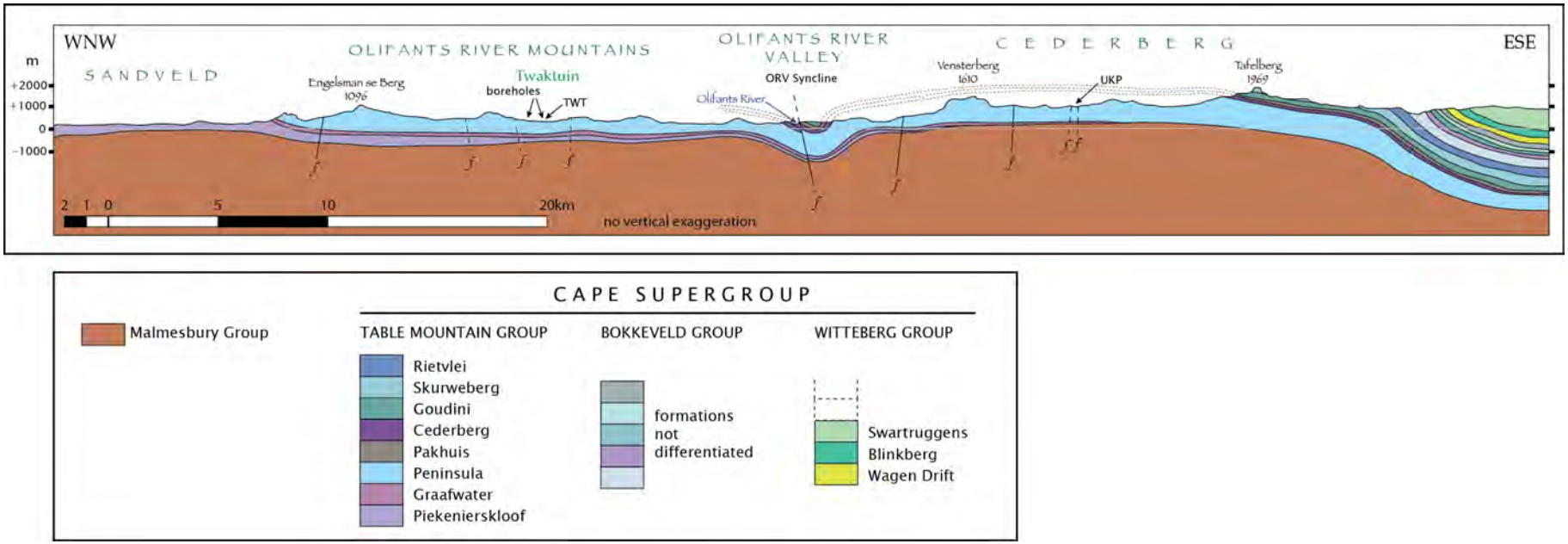

Figure 5.11: A geological cross section through the northern part of the western limb of the Cape Fold Belt, drawn from the Clanwilliam 1:250 000 geological map (Geological Survey, 1973). The section line is indicated on the map in **Figure 5.3**.

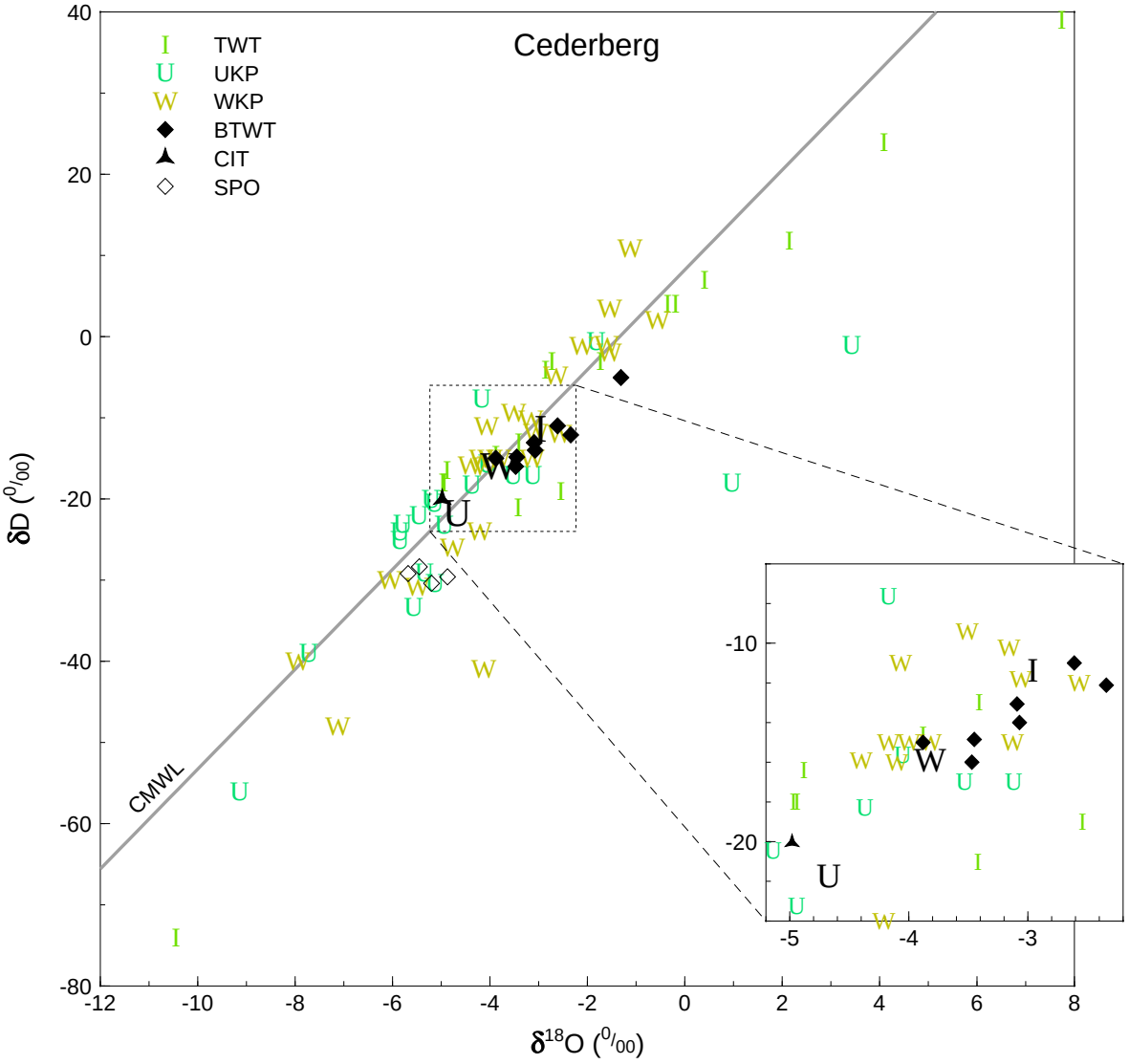

Figure 5.12: A δD – $\delta^{18}O$ plot for all data for the Cederberg region. Weighted means for Twaktuin (I), Uitkyk Pass (U) and Wolfkop (W) rainfall stations are shown as large black letters. Abbreviations: TWT = Twaktuin monthly rainfall, UKP = Uitkyk Pass monthly rainfall, WKP = Wolfkop monthly rainfall, BTWT = Twaktuin boreholes, CIT = The Baths hot spring, SPO = Tafelberg Spout seep.

Samples of groundwater from Twaktuin Farm in the Olifants River Mountains are compared **Figure 5.12** to possible sources of recharge: local rainfall at Twaktuin Farm; rainfall across the Olifants River Valley in the Cederberg at Uitkyk Pass; rainfall higher in the Cederberg, such as at the high altitude seep on Tafelberg at 1900 m. The groundwater discharging at this seep is from rainfall at around 1950 m on top of The Spout, a rock tower peak. The δ values of Twaktuin groundwater are more negative than the weighted mean for Twaktuin rainfall. The amount effect for Twaktuin has a similarly poor correlation to Wolfkop, primarily because of the 31 December 2010 thunderstorm event; Pearson's r values for Twaktuin are -0.12 for δD – rain-amount and

-0.30 for $\delta^{18}O$ – rain-amount. However, in general one can expect the heavier winter rains (more intense rainfall) are more likely to result in groundwater recharge and to have more negative δ values. The mean Twaktuin recharge δ values are probably more negative than the mean Twaktuin rainfall δ values. Also, the Farm is in a valley and the surrounding hills and peaks will contribute more negative isotopic value rainfall to recharge the groundwater of the area.

The δD and $\delta^{18}O$ values of Twaktuin groundwater are not as negative as Uitkyk Pass rainfall (**Figure 5.12**. They are however, similar to Wolfkop rainfall. The Wolfkop values represent all the lower elevation hills on the east of the Olifants River Valley, but these areas do not have the elevation necessary to produce a hydraulic head sufficient to drive groundwater to the Twaktuin region. If recharge is occurring east of the Olifants River Valley, it must be from the high peaks of the Cederberg proper, such as Vensterberg in the cross section. The isotopic evidence suggests that groundwater in the Olifants River Mountains area is locally recharged, as shown in the sketch in **Figure 5.13**. This fits with the geological structure of the region which shows numerous obstacles, as outlined above, to groundwater flow occurring in any significant quantities on such a regional scale.

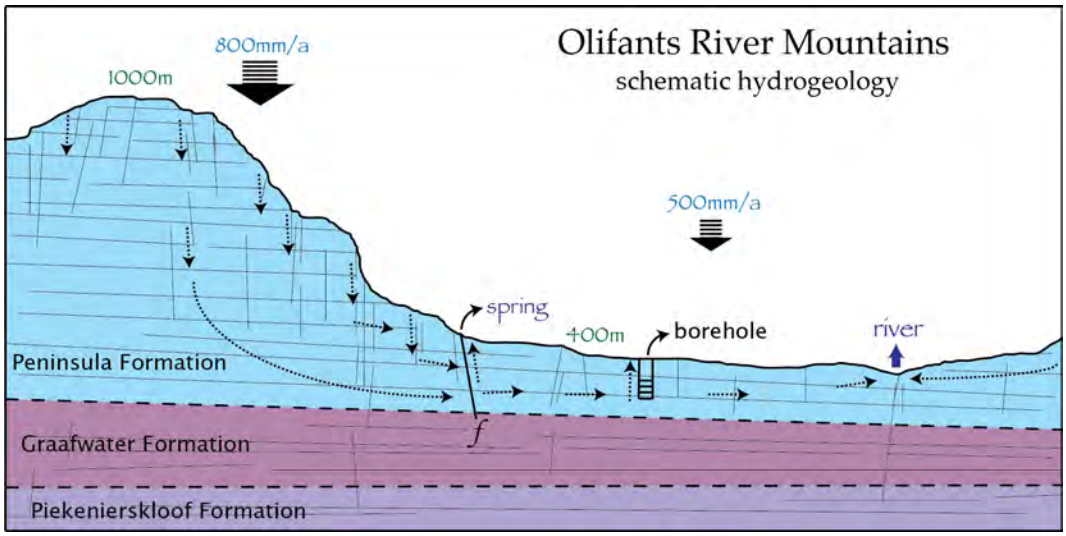

Figure 5.13: Sketch cross section showing the conceptual hydrogeological model suggested by isotopic compositions measured in this study.

The possibility does remain that there is a component of groundwater flow that is travelling east to west through the Olifants River Syncline, perhaps discharging closer to the Olifants River Valley, not as far west as Twaktuin, or contributing just a portion to groundwater in the Twaktuin area through limited flow in deep fractures near the base of the Peninsula Formation. More widespread monitoring of boreholes and springs in west of the Olifants River Valley could help shed light on the former possibility, whilst more detailed monitoring over time at Twaktuin and neighbouring farms' boreholes may reveal changes in isotopic composition as deeper groundwater is tapped later in the irrigation season, or after several low rainfall years.

Figure 5.14: Duplexes (piggyback thrusts) in the Hex River Mountains. Multiple thrust ramps can be seen, some of which have been labelled. The extensively fractured nature of the rock, both thrusts and near vertical jointing, are evident.

5.5.2 Hex River Mountains

The Hex River Mountains are formed by erosion into a large north-east trending anticline in the inland portion of the syntaxis (meeting zone of the western and southern limbs) of the Cape Fold Belt. East of the syntaxial region most folds trend east-west, while to the west and north of the syntaxis, folds trend north-south. The Hex River Mountains include several of the highest peaks in the Western Cape, including the second highest, Matroosberg, at 2249 m, just north-east of the cross-section in **Figure 5.17**. The Table Mountain Group, especially the Peninsula Formation, is structurally thickened in this region and duplexing is evident in the cliff forming outcrops of the Peninsula Formation, as seen in the annotated photograph in **Figure 5.14**.

The two surface water bodies sampled, the Witels and Groothoekkloof rivers, have been discussed in the Surface Water section above, but in summary they show a difference in the mean δD and $\delta^{18}O$ values. This probably reflects continental and altitude effects operating in concert to gause the Groothoekkloof isotope values to be more negative than the Witels.

Six snow and ice samples were taken at 1900 m elevation on Waaihoek Peak in the western Hex. They were taken by coring vertically into the thin snowpack, 0.2–0.4 m thick at two sites, and by removing a stalactite of rime ice hanging from a rock. The stalactite (*1) has the least negative δ values of the six samples. Four samples of snow (*2–*5) record the unusual weather

event described in Chapter 4, where a south-east wind caused widespread snow on mountains of the Western Cape. These samples show that the first snow to fall (the base of the snowpack, *2 and *3) had higher δ values than the later snow (*4 and *5). Snow from a more typical north-west wind from a frontal depression has the most isotopically negative signature (*6).

Previous snow samples (+) (Diamond and Harris, 1997; Harris et al., 2010) taken from Gydo Pass, Hex River Pass, Theronsberg Pass and Waaihoek Peak, all in the vicinity of the Hex River Mountains, overlap with the results from this study, as seen in **Figure 5.15**. The most negative cluster of points is from three different seasons, 1996, 2000 and 2011, and from three different locations, Theronsberg and Hex River Passes and Waaihoek Peak, suggest that this is a typical value for snow from a mid-winter north-west frontal storm in the south-western Cape: –55 > δD > –60, –10.5 > $\delta^{18}O$ > –11.5. The two less isotopically negative samples from the previous studies may have undergone melting, causing the lighter isotopes to be preferentially melted and removed (Arnason, 1981), or may have been rained upon and undergone exchange with heavier isotopes in rain, or may simply have been derived from a weather system that deposited snow of an isotopically heavier nature, such as was observed for the south-easter snowfall in this study.

The difference between the early and late south-easter snow is consistent in the two profiles sampled. It was possible to distinguish the top of the south-easter snowpack from the overlying north-west event snowfall, as the former was granular from freeze-thaw over a few sunny days prior to the north-west event, and the latter was still in powder form. The freeze-thaw process that turns powder snow to firn should have increased δ values at the top of the snowpack as the lighter isotopes are preferentially incorporated into snowmelt, so these points may have had lower δ values originally. A movement from less to more negative δ values during this precipitation event could occur if the temperature decreases or as a result of rainout. A decrease in temperature often accompanies the passage of a cold front, as the wind shifts from westerly to southerly, however, this snow was from a south-easter event. In this case the decrease in δ values during the event suggests that colder air from further south was being fed into the system as it developed and that perhaps increased rainout occurred for the later snow, as shown in **Figure 5.16**. The isotope composition of snow may be useful in understanding air mass trajectories during weather events. Clearly there are several processes at play, and complex relations occur between the three phases of water in this semi-alpine zone of the Cape Mountains. Unfortunately, there are probably insufficient data to draw major conclusions, except to note the large range in values that could be useful in meteorological and hydrological applications if such differences are consistent. A more comprehensive study with more widespread sampling of snow over a greater time frame would assist in identifying any trends.

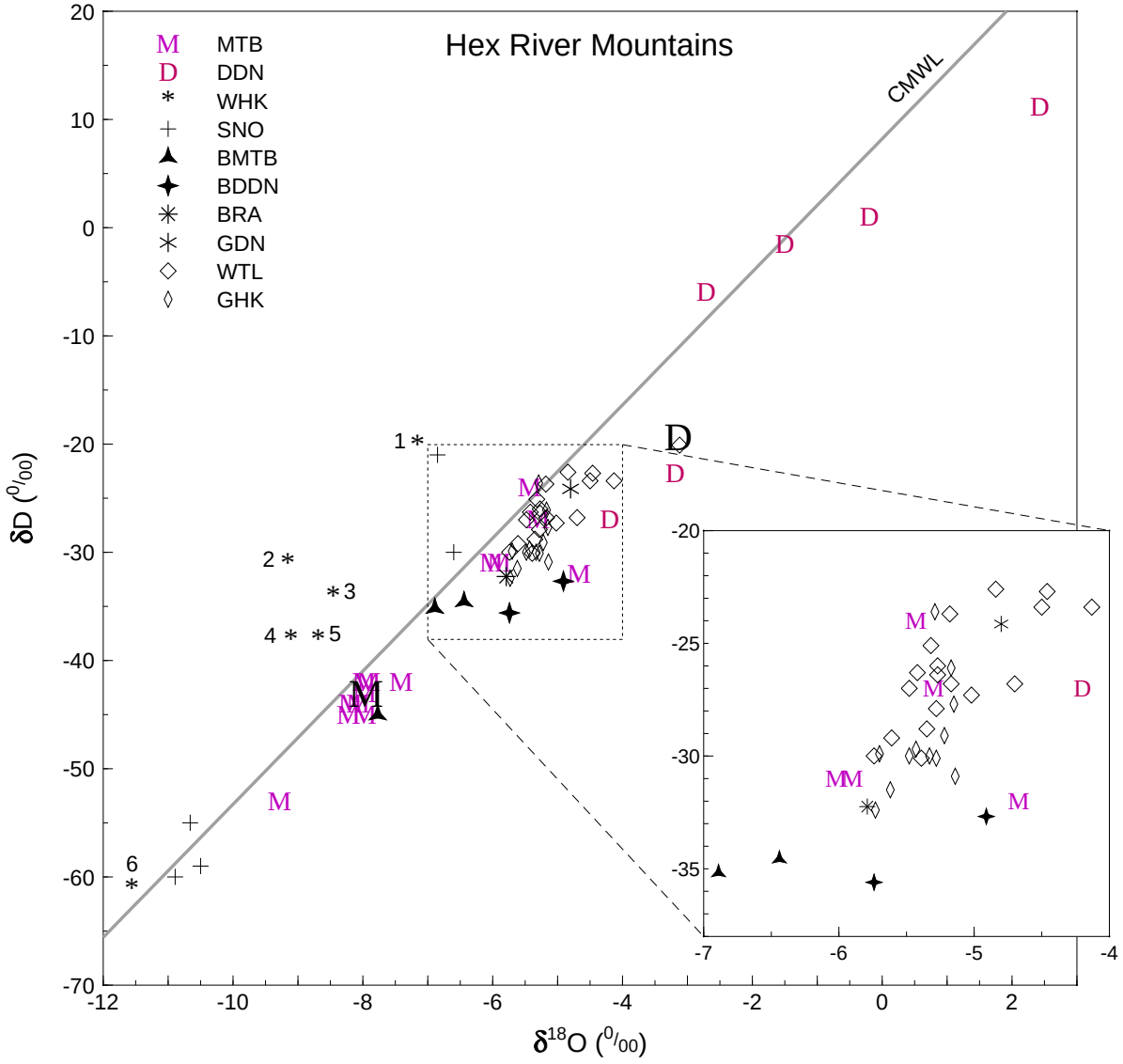

Figure 5.15: A δD – $\delta^{18}O$ plot for all data for the Hex River Mountains region. Weighted means for the Matroosberg (M) and DeDoorns (D) rainfall stations are shown as large black letters. Abbreviations: MTB = Matroosberg monthly rainfall, DDN = Tweespruit monthly rainfall, WHK = Waaihoek Peak snow, SNO = snow from previous studies, BMTB = Erfdeel boreholes, BDDN = Tweespruit boreholes, BRA = Brandvlei hot spring, GDN = Goudini hot spring, WTL = Witels River, GHK = Groothoekkloof River.

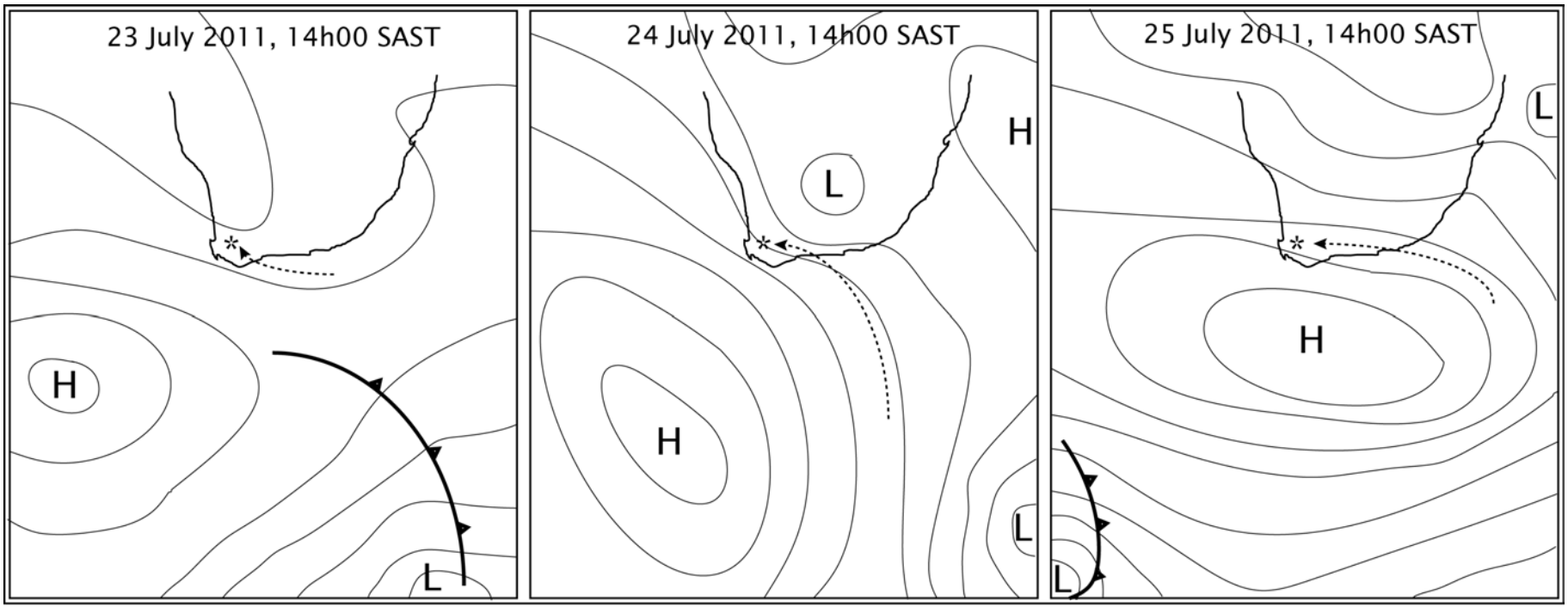

Figure 5.16: Simplified synoptic weather charts from SAWS (2010-12) with possible air trajectories for snowfall in the Hex River Mountains shown. The 23rd July shows a short air trajectory from warmer areas that caused rain. The 24th July shows a much longer air trajectory bringing very cold sub-antarctic air and resulting in snow. Later snow on the 25th July may have travelled even further and probably experienced more rainout over land, resulting in lighter isotope composition.

The most significant hydrogeological interpretations that can be made from the data for the Hex River Mountains region are from comparing the values for borehole water at Erfdeel, on the northern side of the Hex River Anticline (BMTB), and at Tweespruit, on the southern side (BDDN), with the rainfall data for the two stations in this area (see **Figure 5.17**). The mean δ values for rainfall at Tweespruit, the large 'D' in **Figure 5.15**, are less negative than the water from the two boreholes sampled on this farm. These boreholes are drilled into the Rietvlei Formation and although they may not penetrate deep enough to encounter the Skurweberg Formation (see **Figure 5.17**), the Rietvlei Formation is part of the Skurweberg aquifer. This large difference in δ values, 15 ‰ for δD and 2 ‰ for $\delta^{18}O$, can be accounted for by recharge at high altitude on the slopes of the Hex River Mountains. Based on a linear altitude effect between the DDN and MTB rainfall stations, using the gradients shown in **Table 5.5**, the δ values of the Tweespruit boreholes suggest an average recharge elevation for this groundwater of around 1200 masl. Weaver et al. (1999) showed a similar hydrogeological setting for groundwater flow in the Agter-Witzenberg Valley, north-west of Ceres, although with smaller differences in elevation.

Although the cross section shows the Skurweberg Formation only reaching around 1000 masl, the areas west and north of the section line contain outcrops up to 1500 m and 2000 masl, respectively. Additionally, the Goudini Formation, which is hydraulically part of the Skurweberg aquifer occurs at even higher elevations closer to the core of the Hex River Anticline. It is easy then for groundwater in the Skurweberg aquifer to have isotopic compositions similar to those found in the Tweespruit boreholes. However, it does suggest this groundwater originally was recharged in the Skurweberg or Goudini Formation outcrop areas and is flowing upwards through the stratigraphy in the Hex River Valley. This would probably have occurred naturally due to the hydraulic head in these lower formations being higher than that in the Rietvlei Formation, but it may also be enhanced by pumping, causing an upconing flow towards the boreholes. Should the isotope composition of the groundwater from the boreholes become lighter over time, this might suggest that deeper and deeper water from the Skurweberg aquifer is being abstracted. This is because the deeper parts of the aquifer (the Skurweberg and Goudini Formations) are recharged at higher elevation than the Rietvlei Formation and will therefore transmit groundwater with lower δ values. Long term monitoring of the isotope content of the boreholes may be useful to warn of depletion of the groundwater resource.

Groundwater from boreholes at Erfdeel displays a wider range of δ values than at Tweespruit, although in both cases the sample numbers are too low for this to be a firm observation. Two of the boreholes have similar and less negative δ values than the third, which has similar δ values to the weighted mean for the MTB rainfall station. The Erfdeel boreholes also tap the Rietvlei Formation, part of the Skurweberg aquifer, which reaches over 2000 m elevation south-east of the farm, two kilometres south of the section line. The range in isotope composition of the Erfdeep borehole water and the geological structure of the area suggest that groundwater recharge occurs from relatively low down on the mountain slopes, on the northern flank of the Hex River Anticline, to

high up, amongst the peaks on the hinge of the Anticline. The altitude range for groundwater recharge at Erfdeel can be estimated as 1300–2000 masl.

Groothoekkloof river samples display less negative δ values than the MTB rainfall station and the boreholes at Tweespruit and Erfdeel. This suggests that either the GHK samples, being from late summer, display an evaporated signature, or the Erfdeel groundwater was selectively recharged by the most isotopically negative rainfall, a phenomenon known as 'selection' (Gat, 1981a). If the latter is the case, it suggests that the groundwater responsible for creating summer baseflow in the Groothoekkloof river is mostly shallow circulating and recharged by rainfall of varied isotopic composition, whereas the groundwater being pumped out at Erfdeel taps deeper circulating water that has been selectively recharged in heavy winter rainfall events subject to colder temperatures and the amount effect to drive the isotope composition to more negative values.

The Erfdeel borehole δ values lie closer to the Cape Meteoric Water Line (**Figure 5.15**) than the Tweespruit borehole points that seem to lie on an evaporation line trend. As the recharge for the Tweespruit boreholes is on the eastern side of the Hex River Mountains, it is in the lee of the highest peaks. Rainfall here may take place through drier air that has lost some of its moisture when precipitating over the crest of the range. Evaporative enrichment during raindrop descent could account for these points being displaced from the CMWL.

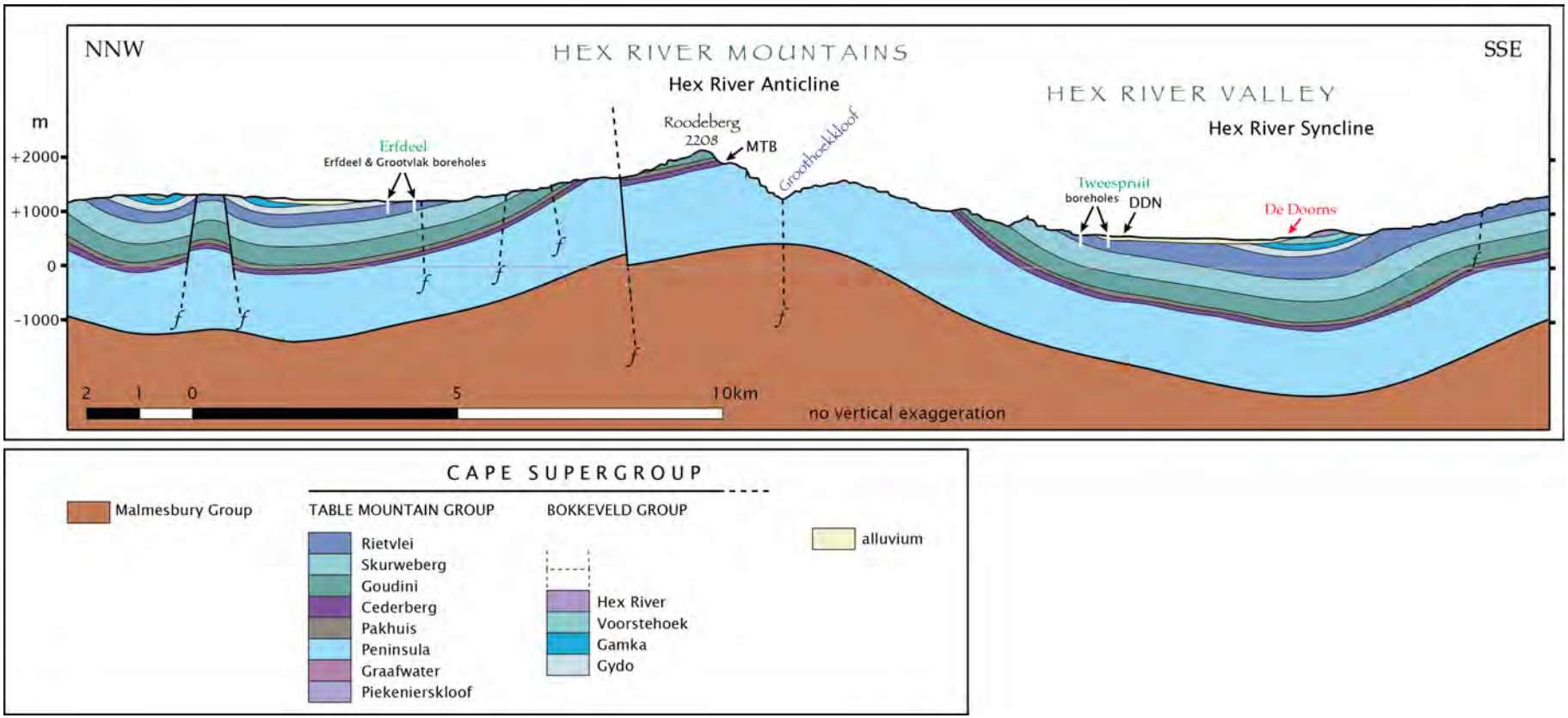

Figure 5.17: A geological cross section through the Hex River Mountains and Hex River Valley, drawn from the 1:250 000 geological map for Worcester (Council for Geoscience, 1997). Borehole positions and depths are illustrative only.

5.5.3 Langeberg – Gamkaberg – Swartberg

Gamkaberg Nature Reserve lies in the Little Karoo and the adjacent Gamka Mountain. The Little Karoo is a semi-arid area and the nature reserve gets its water from boreholes at the foot of the Gamkaberg. The Gamkaberg boreholes are drilled into Rietvlei Formation and perhaps some through unconformably overlying Enon Formation (**Figure 5.20**). They therefore abstract groundwater from the Skurweberg aquifer. The δ values for the groundwater from these boreholes are extremely low relative to rainfall collected at the same place, the Gamka Store location (GST). The groundwater has 20 ‰ lower δD and almost 4 ‰ lower $\delta^{18}O$ than the weighted mean for Gamka Store rain and almost 10 ‰ δD and almost 1.5 ‰ $\delta^{18}O$ less than the weighted mean for Bakenskop on the summit plateau of Gamkaberg. It is almost as negative as water from the hot springs at Warmwaterberg and Calitzdorp Spa. Three possible explanations could account for this result.

Firstly, as proposed by Diamond and Harris (2000) for the Calitzdorp Spa, the recharge area for this groundwater could be the Swartberg. That study did not collect high altitude rainfall and it was simply assumed that rainfall on the Swartberg around 2000 m would be isotopically negative enough to account for the very negative δ values at the Calitzdorp Spa (see **Figure 5.18 and 5.10**). Data from this study shows that this assumption was partly true: the high altitude seeps of the Klein Swartberg, to be discussed in the next regional analysis, do have δ values similar to Calitzdorp Spa discharge. On the other hand, the high altitude rainfall collected at 2080 m on Blesberg does not have such negative δ values and the weighted mean at Blesberg is similar to that of Bakenskop, at half the altitude.

The cross section in **Figure 5.20** shows that the Table Mountain Group has been eroded away over the inlier of Cango Group basement south of the Groot Swartberg and so no groundwater flow can occur from the Swartberg southwards along this line. However, to the north-west of Gamkaberg, the basement is much lower and the Table Mountain Group is continuous from the Swartberg, via the Huisrivier Mountains and the Rooiberg, to Gamkaberg and the Langeberg, as shown in Diamond and Harris (2000). Although this hydraulic connection exists, it is about 40 km, very folded and passes one major fault at the southern edge of the Swartberg. Groundwater would have to be recharged in the Peninsula aquifer in the Swartberg, move into the Skurweberg aquifer at the fault and then through the anticline of the Huisrivier Mountains and a syncline before discharging at the Gamkaberg boreholes. The water would have circulated to great depths and should be heated. For Calitzdorp Spa, the temperature of discharge is 52 °C, which is evidence for deep circulation and concurs with the isotopic evidence, but the Gamkaberg groundwater is not noticeably warm and therefore it is unlikely to have travelled this route. The Outeniqua Mountains (Langeberg) are very unlikely as sources of groundwater at the Gamkaberg boreholes because the discontinuity of the Skurweberg aquifer does not allow flow of groundwater to the northern side of the Gamkaberg. The Cederberg aquitard prevents groundwater flowing from the Peninsula aquifer into the Skurweberg aquifer without the presence of a major fault, of which

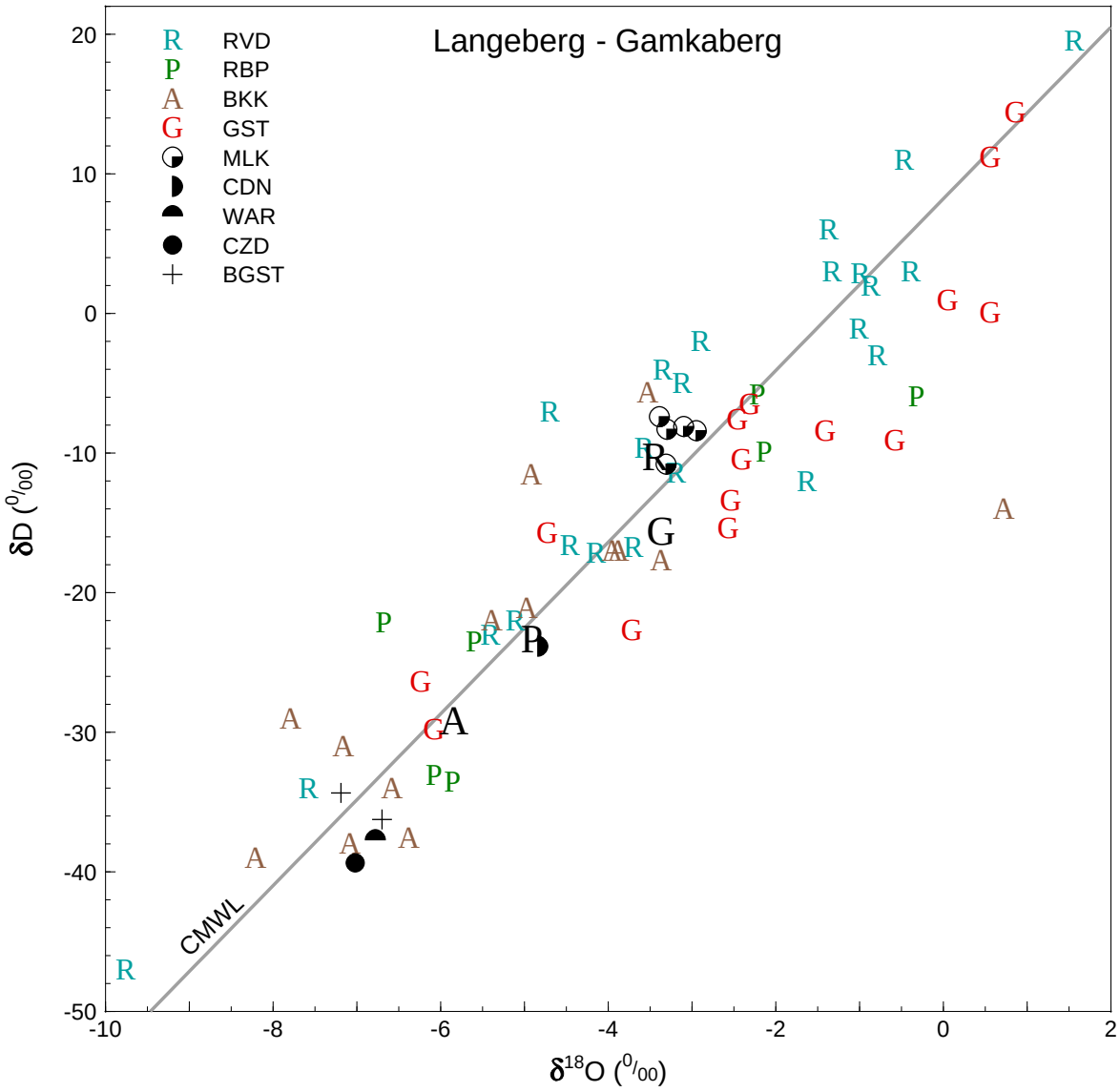

Figure 5.18: A δD – $\delta^{18}O$ plot for all samples taken in the Langeberg–Gamkaberg region, including rain, surface water and groundwater. Larger black letters indicate weighted means for rainfall at Riverndale (R), Robinson Pass (P), Bakenskop (A) and Gamka Store (G). RVD = Riverndale, RBP = Robinson Pass, BKK = Bakenskop, GST = Gamka Store, MLK = Meulkloof river, CDN = Caledon hot spring, WAR = Warmwaterberg hot spring, CZD = Calitzdorp hot spring, BGST = Gamkaberg boreholes.

none are mapped. The isotopic evidence also shows the Robinson Pass rainfall to have higher δD and $\delta^{18}O$ values than the Gamkaberg boreholes.

In the second and third possibilities, the recharge area is the crest of the Gamkaberg, around the Bakenskop rainfall collection station, but two possible factors may be causing the discrepancy between the weighted mean delta values at Bakenskop and the values found at the Gamkaberg boreholes. The first is *selection*, whereby heavy rainfall events, subject to the amount effect and hence with lighter isotope composition, are preferentially recharged over lighter rains with heavier isotope composition (e.g. Dogramaci et al., 2012). The second is that the 2010–12 rainfall at Bakenskop may have been less negative than normal. Although not generally reported in the literature, weighted mean annual isotope composition of rainfall has been shown to vary from year to year locally (Harris et al., 2010) and is discussed in **Section 5.21**. Specifically, observations at UCT show the 2010–12 weighted annual rainfall means lying at the less negative end of the spread of weighted annual means for 1996–2012, as seen in **Figure 5.24**, which supports the hypothesis that the sampled Bakenskop rainfall may not be typical. Lastly, a combination of *selection* and unusual rainfall isotope composition could be responsible for the discrepancy observed at Gamkaberg.

5.5.4 Swartberg to Goukamma

Figure 5.19 is a δD–$\delta^{18}O$ plot of all the samples analysed from the Klein Swartberg, north of Ladismith, to Goukamma, near Knysna. This graph provides some excellent examples of the amount effect at the moderate rainfall sites of Kammanassie and Lentelus, with MAP of 660 mm/a and 640 mm/a, respectively. The lowest δ values for these two sites are both from July 2010 where 80 mm and 40 mm, respectively, fell at these two locations. June 2010 also shows low values for Kammanassie and Lentelus where 30 mm and 75 mm, respectively, fell in that month.

Figure 5.19 shows the unexpected isotopic distribution of the Klein Swartberg high altitude seeps at Toverkop (2060 m), Skull Cave (1880 m) and Seweweekspoort Peak Cave (2020 m); these were discussed in **Section 5.2.2.3**. Two boreholes on the farm Rooihoogte on the northern side of the Klein Swartberg (due north of Skull Cave) were sampled are labelled BROO on **Figure 5.19**. The boreholes are drilled into the Rietvlei Formation and therefore abstract water from the Skurweberg aquifer. The Table Mountain Group here is tilted steeply to the north, dipping beneath the Bokkeveld and Witteberg Groups. The isotope composition of the Rooihoogte boreholes matches that of Skull Cave very closely, which suggests that recharge takes place at the crest of the range, which here is Goudini Formation and therefore also part of the Skurweberg aquifer, before travelling down-dip towards the Great Karoo. Another possibility is that recharge takes place at slightly lower altitudes, which would have less isotopically negative rainfall on average, but is subject to *selection*, whereby only the high volume rain events with the most negative isotope ratios recharge the aquifer.

As with the Tweespruit and Gamkaberg boreholes, it seems likely that the groundwater is

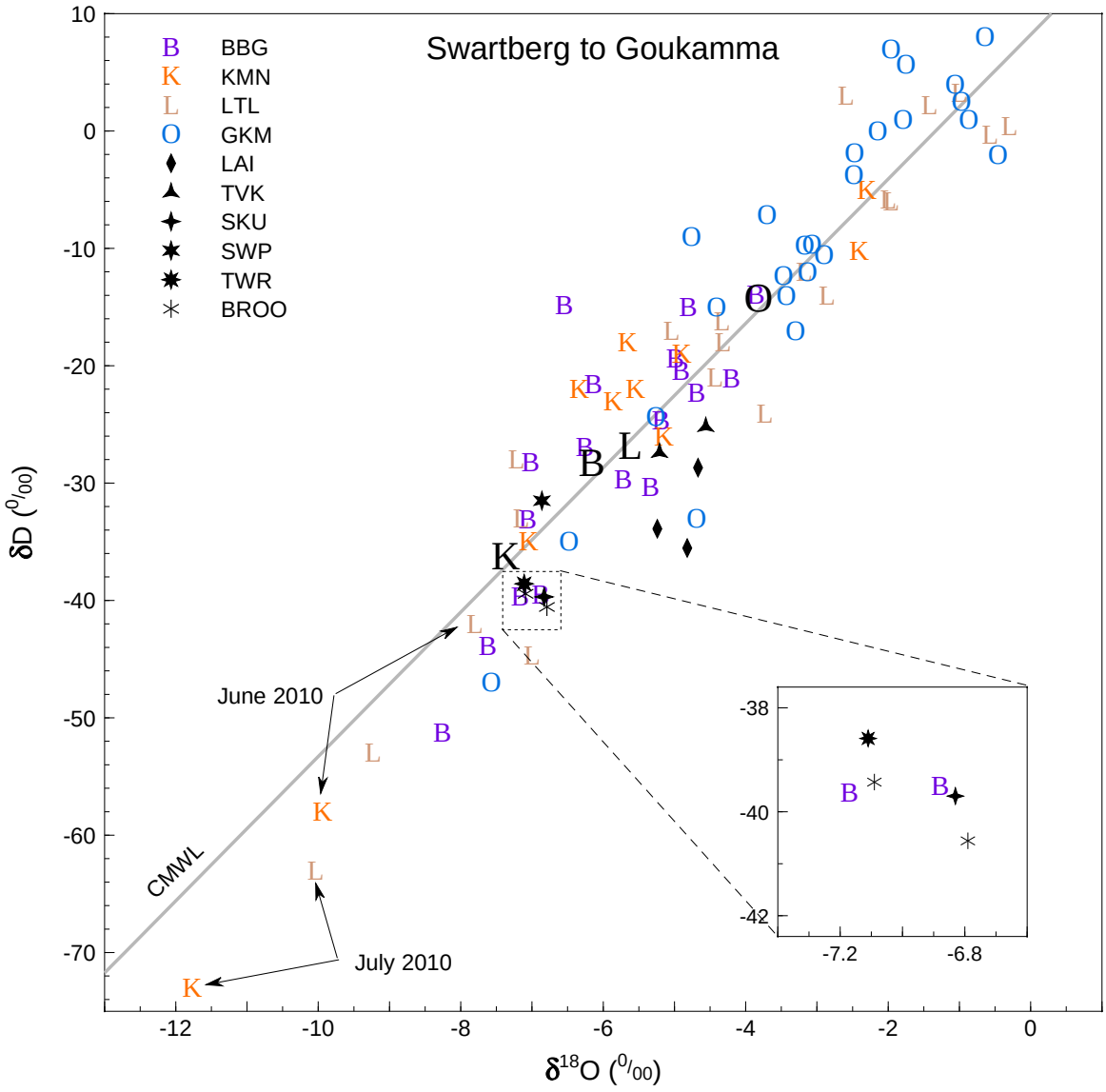

Figure 5.19: A δD – $\delta^{18}O$ plot for all samples taken in the Swartberg to Goukamma region. Larger black letters indicate weighted means for rainfall at Blesberg (B), Kammanassie (K), Lentelus (L) and Goukamma (O). BBG = Blesberg, KMN = Kammanassie, LTL = Lentelus, GKM = Goukamma, LAI = UCT field station spring, TVK = Toverkop seep, SKU = Skull Cave seep, SWP = Seweweek-spoort Peak Cave seep, TWR = Toowerwater hot spring, BROO = Rooihoogte boreholes.

recharged in the Goudini or Skurweberg Formations and discharged via the Rietvlei Formation, all part of the Skurweberg aquifer. To what extent this upgradient flow is natural or in induced by pumping remains open to speculation. From both the Gamkaberg and Swartberg (Rooihoogte) settings, the very negative nature of the borehole isotope values suggests the groundwater flow is already from the highest parts of the crest to the valley, whereas for Tweespruit there is space for the groundwater to be recharged at higher elevations, based on the calculated recharge elevation of 1200 m on the flanks of a 2000 m high mountain range.

Samples from a spring 10 km south of Laingsburg at the UCT Geological Sciences field station in the Great Karoo were taken in 2010, 2011 and 2012. This spring emerges from the Dwyka Group at about 700 m altitude and could be recharged in the south in low mountains of Witteberg Group rocks. The Witteberg Group contains quartzite formations that are extensively fractured, providing secondary porosity. The relatively negative δ values for the 'Laingsburg' spring suggest either a higher altitude of recharge than at the spring, or are the result of the local rainfall displaying a significant continental effect and amount effect. The continental effect is likely to be significant as this location is inland of 2000 m high mountain ranges in almost all directions, so rainout will have been substantial because of orographically driven rainfall. The amount effect is known from arid regions (Dody and Ziv, 2013) and has been seen in South African arid zone rainfall by Vogel and van Urk (1975).

The 'Laingsburg' spring samples plot quite far to the right of the Cape Meteoric Water Line, in the area on the δD – $\delta^{18}O$ plot associated with evaporated waters. This would be expected for precipitation, and hence all other meteoric waters, in an arid zone. It confirms that the recharge area is in the Karoo and not in the Table Mountain Group in the Cape Mountains, where less evaporated isotopic signatures are expected, as can be seen for most of the data in this study.

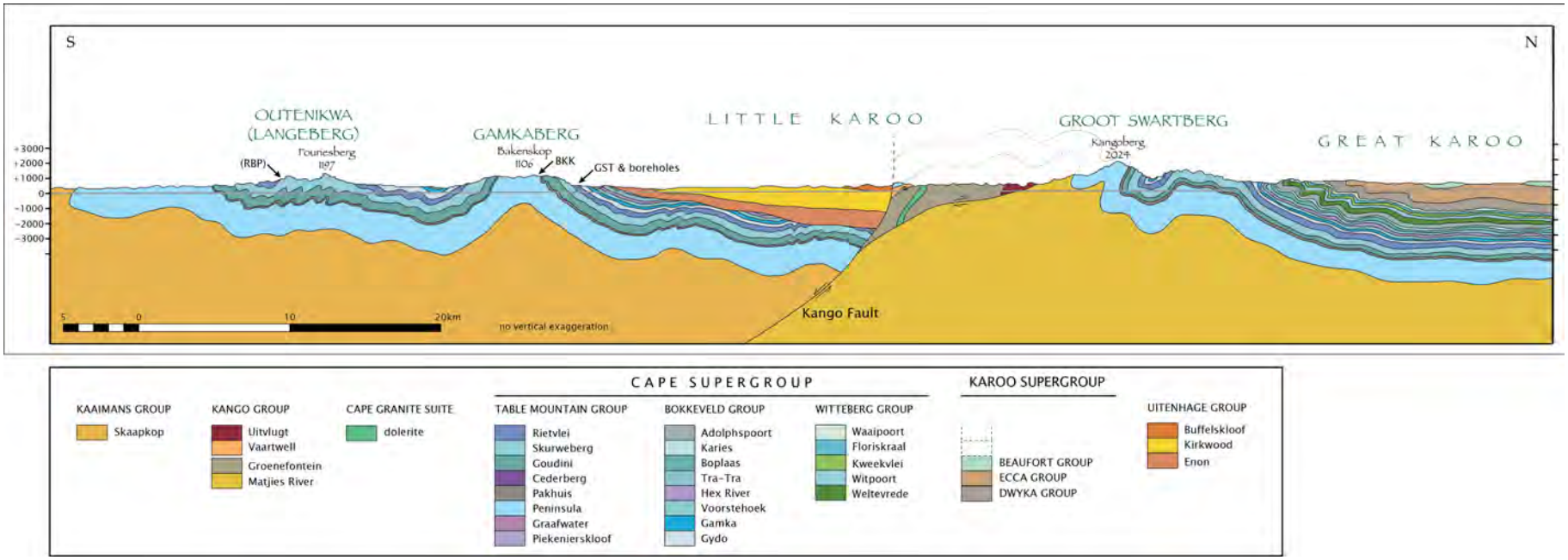

Figure 5.20: A geological cross section from the coastal plain to the Great Karoo, drawn from the 1:250 000 geological map for Ladismith (Geological Survey, 1991).

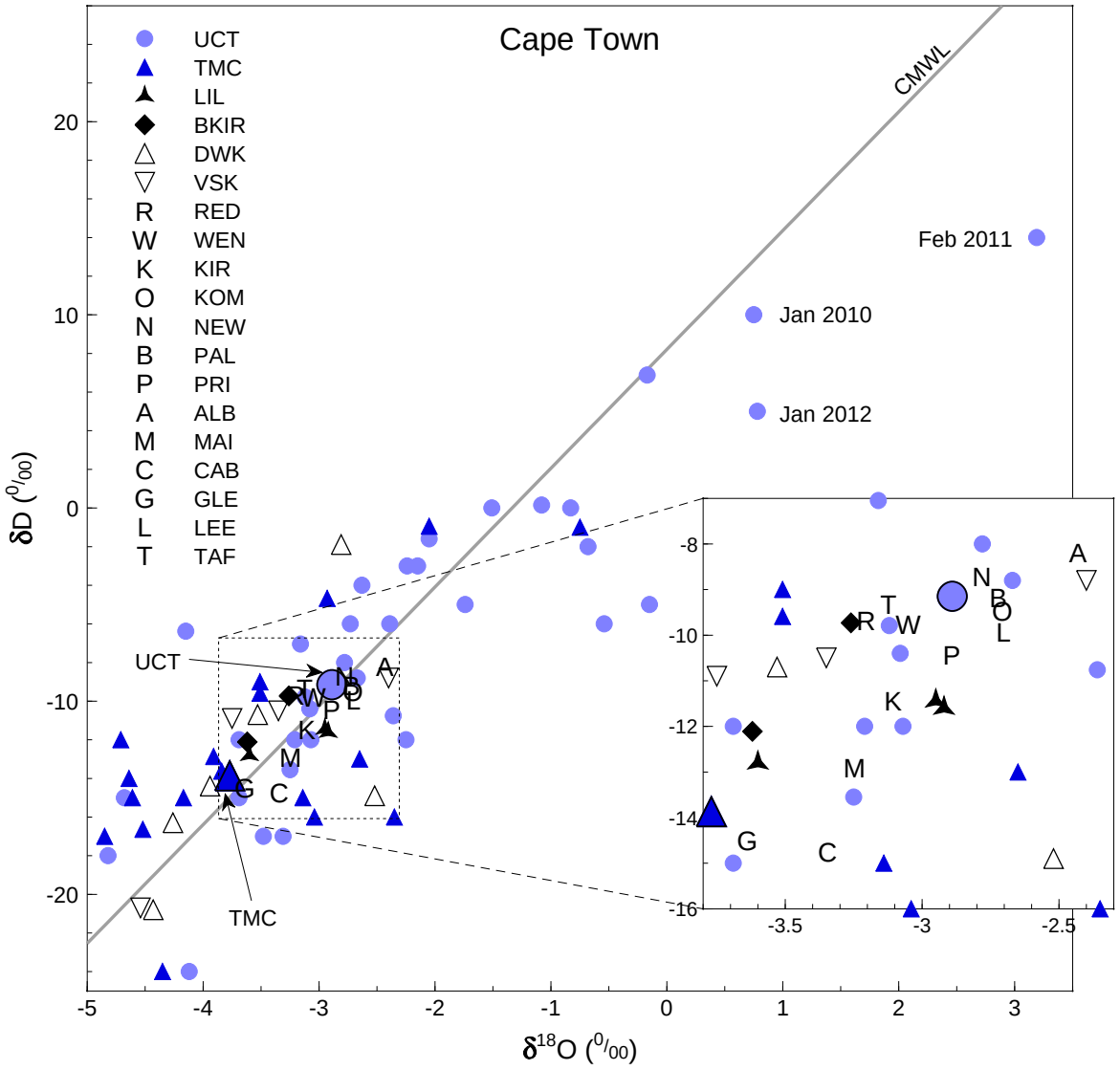

Figure 5.21: A δD versus $\delta^{18}O$ plot for all samples taken in the Cape Town region. The large circle and triangle indicate the weighted mean values for UCT and TMC rainfall. UCT = University of Cape Town, TMC = Table Mountain Cableway, LIL = Lily Pond seep, BKIR = Kirstenbosch boreholes, DWK = Duiwelskloof river, VSK = Volstruiskloof river, R = mean Redwood spring, W = mean Wendy's spring, K = mean Kirstenbosch spring, O = mean Kommetjie spring, N = mean Newlands spring, B = mean Palmboom spring, P = mean Princess Anne spring, A = mean Albion spring, M = mean Main CT spring, C = mean Cableway spring, G = mean Glencoe spring, L = mean Leeuwenhof spring, T = mean Tafelberg Rd spring.

5.5.5 Cape Town

Samples in the Cape Town area include regular samples over three years of the major springs that issue from the slopes of the mountain, both on the northern, city side and on the eastern, Kirstenbosch side. A detailed analysis of this data will be made, but first, a brief analysis of data from the two rainfall stations in the area, UCT and Table Mountain Cableway, will be made. As was mentioned in **Section 5.2.2.3**, the difference in isotope ratios between UCT and TMC is less than would be expected based on global averages for the altitude effect, because of both an "island peak" effect and because the higher location (TMC) is not in the direction of increasing rainout.

The UCT data shows some excellent examples of highly evaporated rainfall typical of summer months in a Mediterranean climate (e.g. Argiriou and Lykoudis, 2006). Table Mountain Cableway does not show the same degree of evaporative enrichment due to the shorter path of raindrops through the atmosphere in which evaporation can occur. The meteoric water lines of these two stations are similar in both gradient and δD-intercept values **Figure 4.10**.

The mean values for each of the sampled Cape Town springs have been plotted in **Figure 5.21**. The Kirstenbosch cluster of springs sit on the lower slopes below the east face of Table Mountain, Kirstenbosch being the most southerly and Albion one of the most northerly of those sampled. The Albion Spring (A) discharges water with the highest δ values of these springs and also happens to discharge at the lowest altitude. Its position places it furthest from the steep cliffs and the summit near the east face of Table Mountain, where the most isotopically light rainfall would be expected. The isotope values at Albion indicate the recharge area receives the least isotopically negative rainfall of all the Kirstenbosch springs, which corresponds with its geographic position and elevation. The opposite holds for Kirstenbosch (K), and to a lesser extent Redwood (R) and Wendy's (W), which have more isotopically negative discharge and are closer to the high cliffs of Table Mountain. The position of the spring waters on the δD – $\delta^{18}O$ graph roughly corresponds to the geographic position, resulting in a sequence from more to less negative δ values as the springs are located further from the site of highest rainfall on the southern end of the east face of Table Mountain, known as Fernwood Buttress. The sequence of springs, from most negative to most positive δ values is: Kirstenbosch (K) $\rightarrow$ Redwood (R) and Wendy's (W) $\rightarrow$ Princess Anne (P) $\rightarrow$ Kommetjie (O) and Palmboom (B) and Newlands (N) $\rightarrow$ Albion (A).

As this trend is based on the isotopic values of spring discharge, which is reliant upon isotopic changes inherited from precipitation in the recharge area, it suggests the position of a spring is closely related to the position of the recharge area. This in turn means long distance groundwater flow is probably not occurring. It also means if there is a distance between the spring and the recharge area, a similar distance exists for all the springs. The weighted average for UCT rainfall lies very close to many of these springs, especially Wendy's, Princess Anne and the Newlands, Palmboom and Kommetjie group, which are geographically also very close to UCT. All this evidence points to extremely local recharge on the lower slopes of the mountain. The most likely

aquifer for these springs is the scree and weathered material overlying the basement, comprising granite in the southern areas around Kirstenbosch and Redwood, and Malmesbury Group in the northern areas around UCT. The Table Mountain Group is not directly involved, except as a supply of boulders and sand that make up the scree material on the slopes of the mountain.

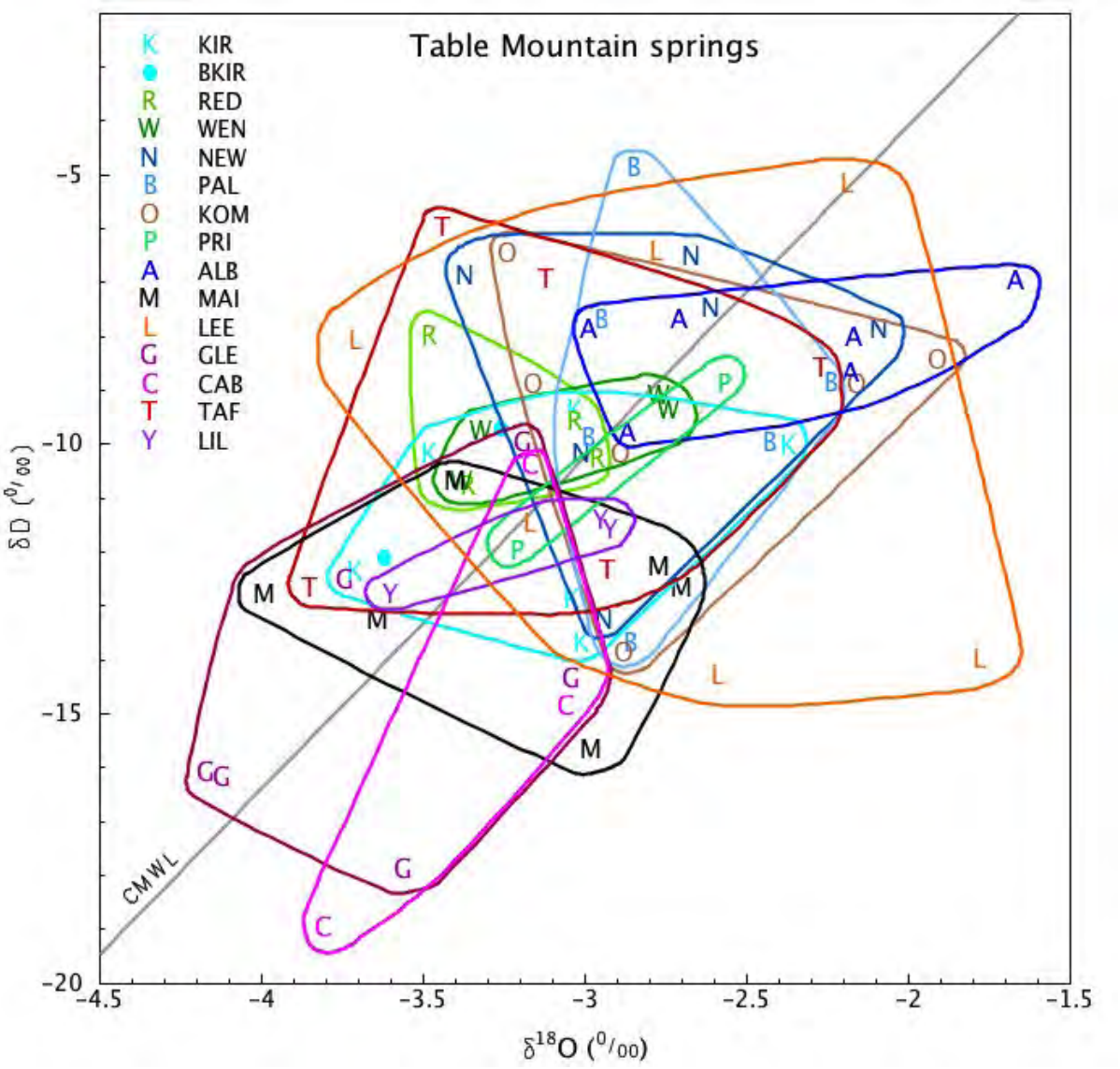

Figure 5.22: All the data for all the Table Mountain springs, with each springs' cluster of points circled. K = Kirstenbosch, BKIR = Kirstenbosch boreholes, R = Redwood, W = Wendy's, N = Newlands, B = Palmboom, O = Kommetjie, P = Princess Anne, A = Albion, M = main spring, L = Leeuwenhof, G = Glencoe, C = Cableway, T = Tafelberg Road, Y = Lily Pond.

Two boreholes at Kirstenbosch were sampled, "Protea" and "Apple Tree". Their isotope values are amongst the most negative of the Kirstenbosch springs and fall neatly within the distribution for the samples from the Kirstenbosch spring itself, as seen in **Figure 5.22**. They fit into the overall pattern noted above, where position on the δD – $\delta^{18}O$ diagram in **Figure 5.21** broadly

relates to geographic position relative to Table Mountain.

Several observations can be made from the isotope data for the springs analysed on the city side of Table Mountain. Cableway (C) and Glencoe (G) have the lowest δ values. These springs emerge from large scree fans that cover the north-west slopes of Table Mountain. Recharge into these screes is not only from rainfall directly onto their surfaces at 200–500 m elevation, but also from streams that drain the steep cliffs on the northern face of the western Table. These streams' catchments include areas up to the Upper Cableway Station at 1070 m. The similarity between the weighted mean for TMC and for Glencoe and Cableway springs confirm this as being part of the recharge area for these springs. An amount effect and selective recharge of heavier rainfall events will drive the Glencoe and Cableway recharge to lower δ values, compensated for by a shift to higher δ values from recharge occurring at lower elevation as well.

The Tafelberg Road spring (T) has less negative δ values, probably because its position below The Saddle, the area separating Devils Peak from Table Mountain, where recharge can only occur up to a maximum altitude of 700 m. The Leeuwenhof Spring (L) has the largest range of values of any of the springs by a factor of 2, as seen in **Figure 5.22**. This spring was sampled about 100 m from the source, an area of about half a hectare of seepage, because it is within the official residence of the Western Cape premier and access is restricted. The spring is undoubtedly the reason for the location of this historical homestead. The diffuse discharge area and the possibility for contamination from rain, Cape Town scheme water, stormwater or sewage leaks, as well as evaporation in the seepage area, explain the abnormally wide range in isotopic values at this spring. The position of the Leeuwenhof mean on the δD – $\delta^{18}O$ diagram, however, is consistent with its geographic position furthest from Table Mountain and at the lowest altitude of the city springs, and therefore subject to recharge at lower elevations with higher δ values. This suggests that dilution or alteration of isotope composition was minor.

The "main spring" (M) was sampled at the collection chamber in the "field of springs" east of Upper Orange Street in Oranjezicht. This collection chamber receives water from a few springs at the top of Oranjezicht, such as above Rugby Road cul-de-sac, and from the adjacent Stadsfontein at the field of springs, one of the original springs deciding the settlement of Cape Town by the Dutch East India Company in 1652. Assuming a similar relationship applies to the City Bowl springs as has been shown to apply to the Kirstenbosch springs, namely a positive correlation between distance from mountain and δ values, then the water from the "main spring" should be more isotopically negative than the position of the collection chamber on the map would suggest. The average position of these feeder springs would be in line with Glencoe's altitude and at the base of the large screen cones below Platteklip Gorge. Balancing these springs closer to the mountain is the position of Stadsfontein at the "field of springs." The expected isotope composition for the main spring should be intermediate to the Glencoe and Cableway values (closer to the mountain), and to Leeuwenhof (further from the mountain). This is indeed where the "main spring" plots in **Figure 5.21**.

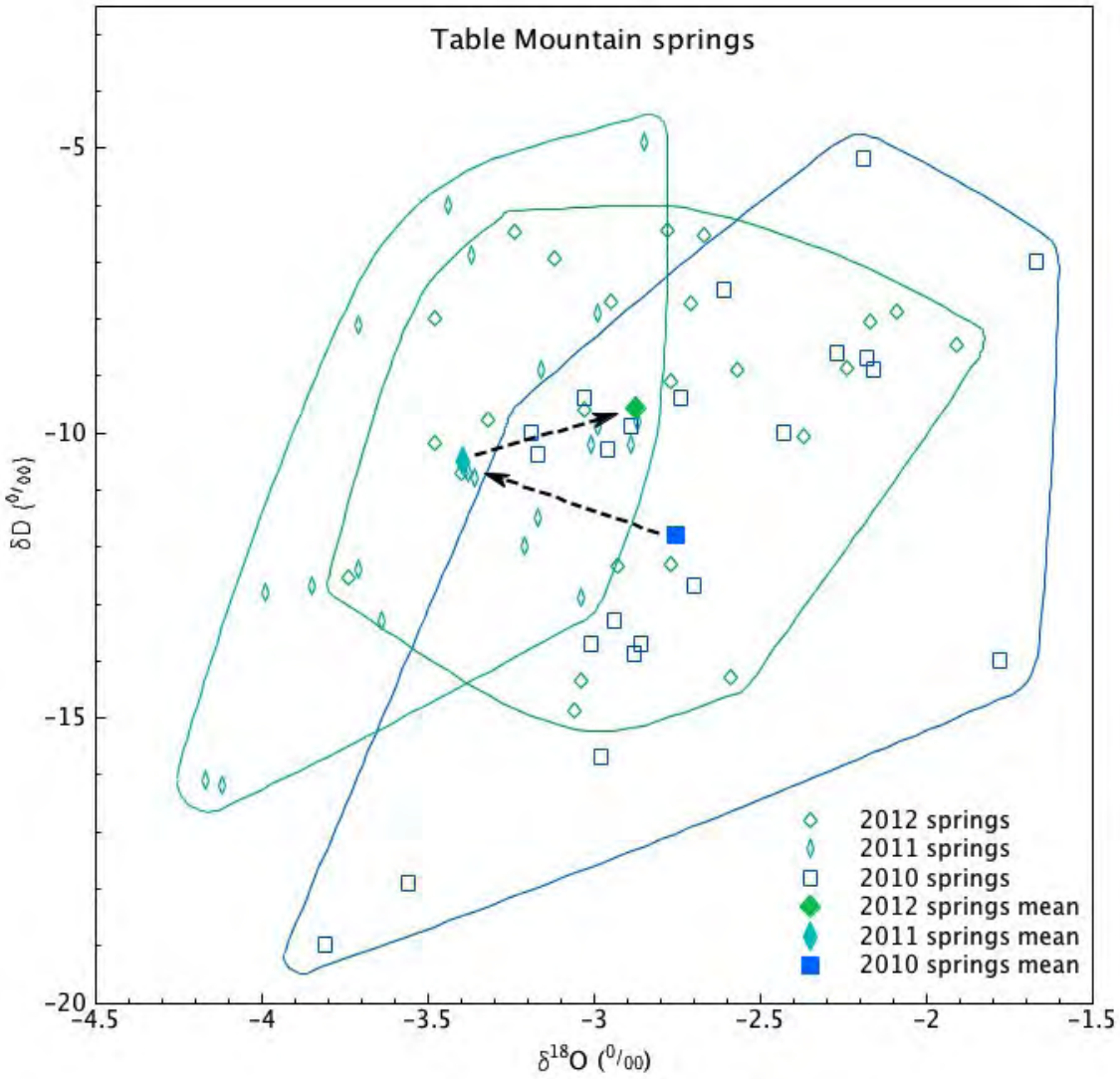

Figure 5.23: Data for all the Table Mountain springs plotted according to year, with the annual means also shown and arrows to indicate the yearly shift between annual means.

Groundwater Flow

Figure 5.23 shows the data for all the Cape Town springs plotted by year; most of the springs were sampled twice a year. A significant shift occurs in the isotope values, to the extent that less than 25 % of the 2010 samples fall within the range of the 2011 samples. This is clearly a significant shift and is quite unlike the random variability as noted for the hot springs in **Section 5.4.2**. The means for all the springs for the three years, 2010–2012, have also been plotted in **Figure 5.23** with arrows indicating the progression from year to year.

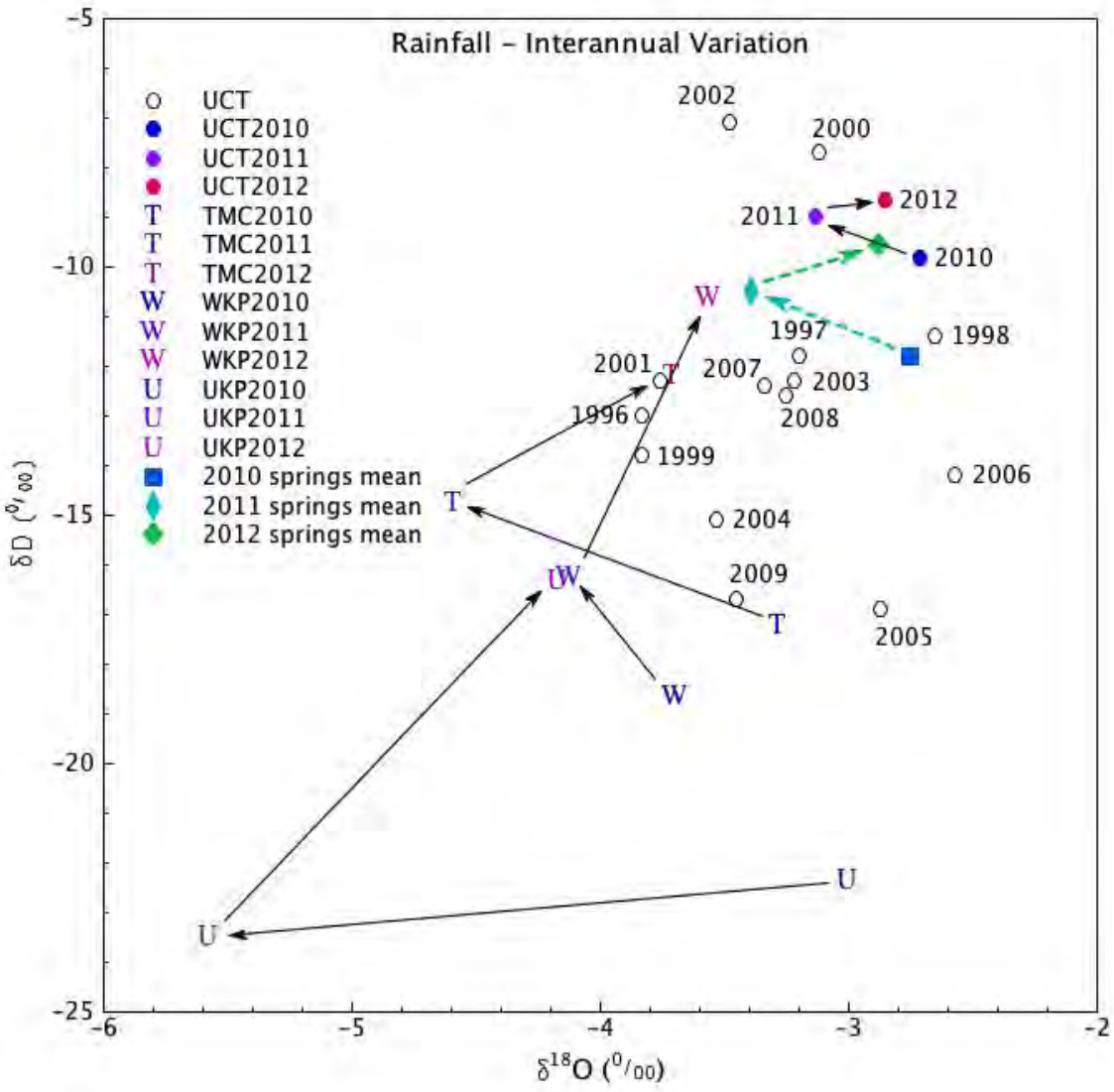

Figure 5.24: Weighted annual means for rainfall from several stations, including the long term records from UCT, as well as the average annual values for the Table Mountain springs, plotted in the δD – $\delta^{18}O$ space. UCT = University of Cape Town, T = Table Mountain Cableway, W = Wolfkop, U = Uitkyk Pass. Note the similarity in shift of annual means of UCT rain and Cape Town springs.

The weighted annual means for several of the rainfall stations have been plotted on **Figure 5.24**, including the long term records for UCT, from 1996 until this study. The shifts in the UCT annual means are interesting, if not somewhat puzzling, and some very large shifts can be seen, for example 1999 to 2000 and 2009 to 2010. The overall range in variation of these means is also noteworthy and suggests quite different weather conditions can dominate particular years.

Interestingly, the 2010–11–12 pattern in shifts of means at UCT mimics that of the Table Mountain springs, which have been added to the graph. Three of the other rainfall stations, Table Mountain Cableway (T), Uitkyk Pass (U) and to a lesser extent Wolfkop (W), also show similar

shifts in the weighted annual means. Seeing a similar pattern of shifts in annual mean values from more than one collection station is verification that these shifts are caused by widespread changes in weather conditions from year to year and not just site specific random variation. A small difference between the UCT averages and the spring averages probably reflects selection, altitude and amount effects, as the springs are recharged at higher elevations and during heavy rainfall events. Notwithstanding this small difference in actual isotope composition, the remarkable coincidence of the interannual shifts suggests that the Table Mountain springs discharge groundwater that has been recharged in that same year.

If recharge and discharge happens in the same year and the aquifer conforms to a piston flow model, then springs would only flow weeks to months after the first winter rain around April/May, in other words, around June/July, and cease flowing around November/December once the spring rains have passed. This is not seen, except in a few of the springs: Princess Anne and Rhodes Memorial (not sampled in this study) on the Kirstenbosch side, and Cableway and Tafelberg Road on the City Bowl side. The bulk of the springs flow perennially with little seasonal variation. Even after a drought, in which rainfall is well below average for a few years, all of the perennial springs continue to flow, although perhaps at lower rates (pers. comm. Caron von Zeil, Marius Bonthuis). Many of the springs are so reliable that they are used daily by the South African National Botanical Institute (Kirstenbosch), South African Breweries (Kommetjie), Provincial Government of the Western Cape (Leeuwenhof), City of Cape Town (Stadsfontein) and the public (Newlands) for industrial, irrigation and personal use. The aquifers are clearly able to sustain flow over a time period much greater than the half-year long rainy season.

The springs' aquifer must be able to accomodate longer term groundwater flow to sustain the steady, perennial flow, as well as shorter term groundwater flow to conduct the recently recharged groundwater with an isotope composition that is similar to the precipitation of that year. An attempt was made to isolate groups of springs to see if the higher flow rate springs showed less of a shift, or if those further from the mountain showed a greater delay in the isotope composition shift, but no trends could be found. A better data set, with monthly spring samples for all the springs would perhaps yield better resolution and show such trends. Nonetheless, it seems the aquifers are able to conduct recent recharge within months or less from the recharge area to the spring, as well as sustain groundwater flow over the summer months and through dry years.

A conceptual hydrogeological model is proposed whereby recently recharged groundwater is able to flow near the water table and at speed to discharge within weeks of heavy rain, usually at the start of winter. At the same time, slower movement of groundwater deeper in the aquifer is able to sustain discharge in the long term. This model is shown in a sketch cross section in **Figure 5.25**.

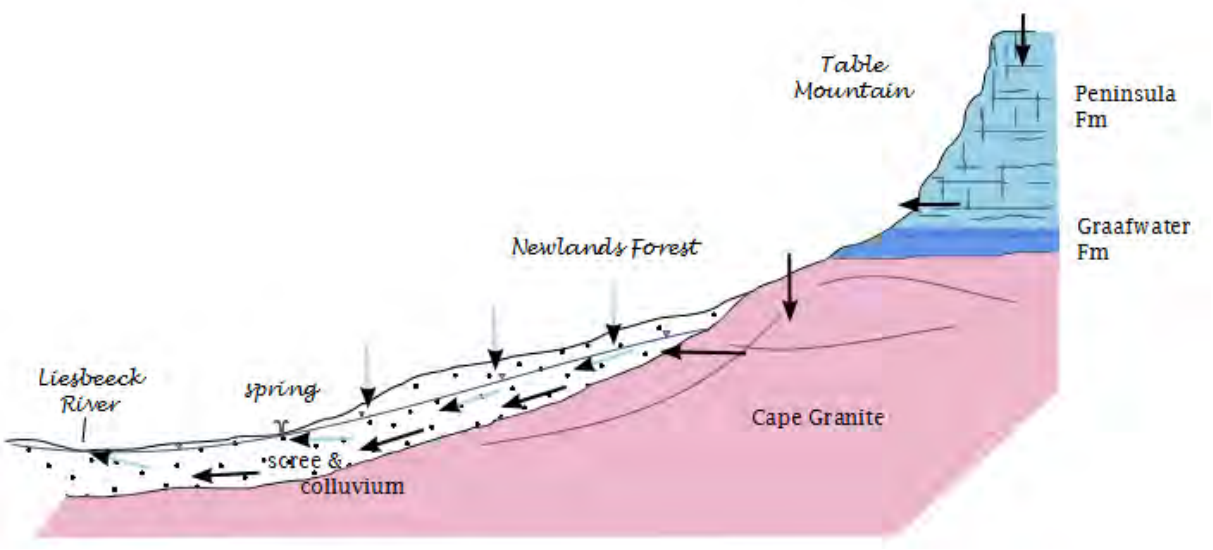

Figure 5.25: A sketch cross section looking south over Newlands Forest, showing a proposed conceptual hydrogeological model for the Kirstenbosch set of springs. Recently recharged groundwater is able to flow at shallow depths and discharge within weeks or months, whilst deeper groundwater is able to flow more slowly and sustain steady discharge over years. This model is equally applicable to the City Bowl springs.

Recharge Altitude

Figure 5.26 shows the weighted means for rainfall over 2010–12 at UCT and Table Mountain Cableway, and the mean for all the Cape Town spring samples, both those in the City Bowl and on the Kirstenbosch side of the mountain. As can be seen from the Figure, the springs plot in an intermediate position to UCT and TMC. Because the elevations of the rainfall stations are known, if a linear gradient for $\frac{\Delta\delta}{\Delta altitude}$ is assumed, the average recharge elevation for the springs can be interpolated. This works out to 304 masl.

The mean spring elevation is 156 masl, and so:

$$304masl - 156masl = 148m \ ,$$

which is the average altitude difference between spring recharge areas and discharge points. Given the typical topographic gradient of the lower slopes of Table Mountain is around 9°,

$$\Delta s = \frac{148m}{cosine9^\circ} = 946m \ ,$$

which is the average slope distance between recharge area and discharge point. Given that recharge occurs over a wide area, it would be reasonable to assume that recharge for each spring occurs in an area about 0.5–1.5 km upslope from the spring. Using the average distance of about 1 km, and an estimated duration of 2 months between rainfall and discharge for the shallow

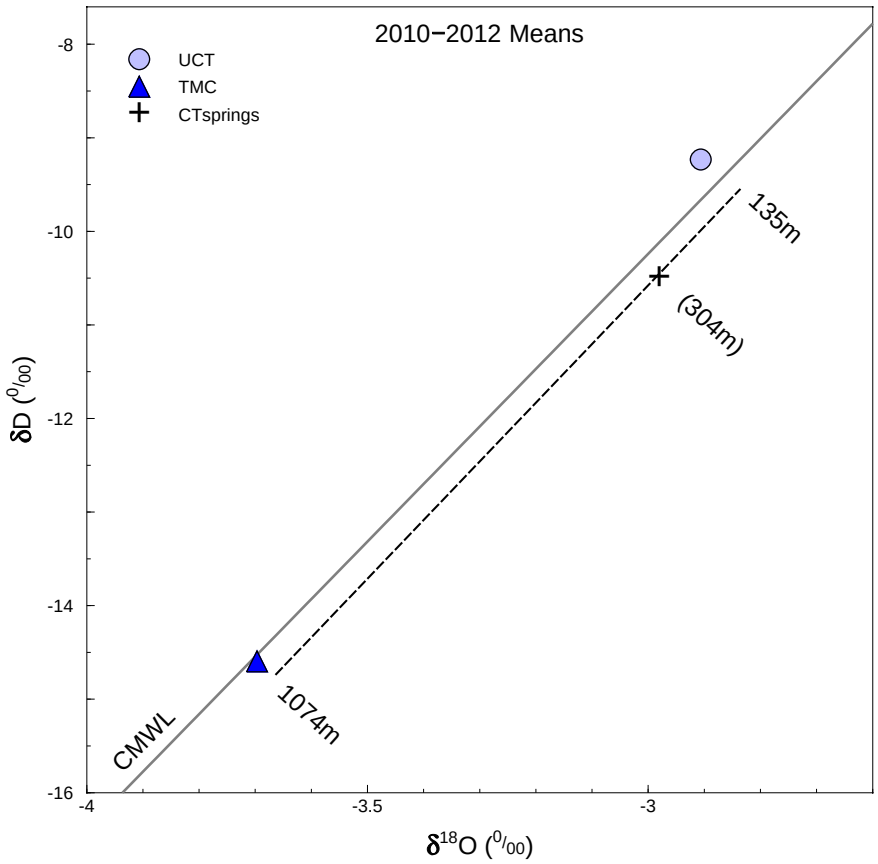

Figure 5.26: Calculation of average recharge altitude for Cape Town springs by interpolation between the altitudes of the UCT and Table Mountain Cableway (TMC) rainfall stations along a line of the same gradient as the Cape MWL.

groundwater component of the aquifer, a hydraulic conductivity of around 15–20 m/d is arrived at. This falls within the ranges of hydraulic conductivity of fine to coarse sand and gravel given in Domenico and Schwartz (1998, p.39).

These figures are rough values and will vary substantially between each spring, because of geological and topographic differences, and over different years, depending primarily upon rainfall amounts and intensities. Nonetheless, the calculation of recharge altitude and average flow path length based on isotope composition confirms the scree apron on Table Mountain as being the aquifer supporting the Cape Town springs, as presented in the conceptual model in **Figure 5.25**.

Chapter 6

Conclusions and Recommendations

This chapter summarizes the major findings of this study. The details of the data and reasoning behind these findings are to be found in both the Results and Discussion chapters above. Some key numerical results are repeated here.

1. **Weather affects isotopes** (p.100)
   The isotope composition of cumulative monthly samples of rain sometimes shows unusual values. With the help of records of past weather, individual weather systems can be found to be responsible for generation of unusual isotope composition (e.g. Dody and Ziv, 2013). In particular, convective rainfall events (thunderstorms) in summer can generate relatively negative δ values in precipitation in the Western Cape. Knowing the rarity of such weather systems can help determine whether the measured isotope composition is representative of that site.

   Recommendation: Weather records should be used when interpreting the isotope composition of rainfall.

2. **Weighted δ values of precipitation are more important in dry climates** (p.104)
   The difference between weighted and unweighted mean δ values for precipitation at a site is negatively correlated with mean annual precipitation. Weighting δ values of monthly precipitation samples by precipitation amount removes the effect of low volume rain events with extreme isotope composition, most particularly summer rains that are highly evaporated, with less negative or positive δ values. This has a greater effect on the mean in drier climates where highly evaporated and low volume rain events are more common than in wetter climates. This is in contrast to Yurtsever and Gat (1981), who found the difference in means is positively correlated with seasonality.

   Result: The weighted means for all rainfall for this study are: δD = -17.7 ‰ and $\delta^{18}O$ = -4.22 ‰, similar to those in drier parts of Jordan (Salameh, 2004).

Recommendation: Means should always be calculated by weighting δ values of monthly cumulative rain samples by the rainfall amount.

3. **The weighted LMWL is more relevant in hydrological studies** (p.108)
   The local meteoric water line equation is calculated using reduced-major-axis (RMA) regression between δD and $\delta^{18}O$. Weighting the monthly δ values by rainfall amount changes the best fit line and generally results in a steeper gradient and higher δD intercept. As low volume rains have less impact on hydrology, especially groundwater recharge, and weighting removes the effect of low volume rains, the weighted LMWL is more applicable to hydrological studies (Hughes and Crawford, 2012). Use of weighted data and the more applicable RMA regression method is either not done or not clearly stated in the global literature.

   Result: The weighted LMWL for this study, or Cape MWL is: δD = 6.15 $\delta^{18}O$ + 8.21, which is similar to those previously calculated for this area (Diamond and Harris, 1997; Harris et al., 2010).

   Recommendation: Local meteoric water lines should be calculated by weighted reduced-major-axis regression.

4. **Groundwater has a lesser spread of δ values than precipitation** (p.113)
   The range of δ values for groundwater at one site or across a region is less than for precipitation (e.g. Majumder et al., 2011). Groundwater averages out the short term variations in precipitation to reveal the long term mean δ values of precipitation. Where the recharge area is well defined, such as for high altitude mountain seeps in the Table Mountain Group, where there is very little aquifer above the discharge point, the isotope composition of the water from the seep is a good proxy for the local precipitation.

   Result: The ranges in values of δD and $\delta^{18}O$ are, for precipitation: -75 ‰ to +40 ‰ and -12 ‰ to +8 ‰; and for groundwater: -47 ‰ to 0 ‰ and -8 ‰ to -1 ‰ .

   Recommendation: High altitude mountain seeps in the Table Mountain Group can be collected instead of difficult and costly long term precipitation monitoring at high altitude.

5. **Western Cape stable isotope compositions are similar to South Africa** (p.129)
   In spite of having different climates, the isotope compositions for the Western Cape and for the rest of South Africa overlap. The current data sets have insufficient separation according to season, climatic region, weather events and other factors to be able to draw out trends, although there are most likely differences in means from different regions. Differences in mean isotope composition of precipitation at specific sites across Australia are also minor, in spite of vast distances and different climates (Liu et al., 2010).

Recommendation: More samples of meteoric water throughout South Africa are needed. In particular, thoughtful analysis of these samples, according to geographic and meteorological parameters, is needed to draw out regional patterns in stable isotope composition.

6. **The Western Cape displays a complex continentality effect** (p.133)
   Poor correlations are displayed between δ values and simple distance from sea parameters, such as have been used by Salati et al. (1979) and Yonge et al. (1989). A compound "distance to the Atlantic" and "distance to the closest coast" parameter shows much better correlations with δ values. This is likely because rain bearing weather systems can approach from any direction from NW, through W and S to SE, due to the Western Cape's position at the southern end of Africa. Continentality effects in regions where rain bearing weather systems can approach from more than one direction are likely to be complex.

   Recommendation: To calculate the best index of continentality for the Western Cape, generate average weather system tracks for different locations, or more simply measure the area of land between the rainfall station and the ocean within the semi-circle facing SW.

7. **Small and steep mountains display a reduced altitude effect due to reduced rainout** (p.136)
   Small, steep mountains do not generate sufficient rainout to drive isotope compositions towards the negative δ values that would be expected based on the site altitude. The isotope composition is a function of the average altitude over several square kilometres around a site. The reverse is also true: sites surrounded by higher elevation, such as valleys within mountains, record δ values that are more negative than would be expected based on the actual site altitude. The altitude effect gradients calculated for this study are on the low side compared to reported gradients from around the world (Clark and Fritz, 1997, p.71). This is because of the steep terrain gradients of the Cape Mountains and suggests that many of the altitude effects calculated worldwide are in fact combination effects of pure altitude change as well as rainout with distance.

   Result: Calculated altitude effect gradients varied from -0.48 to -2.2 $\frac{\Delta\delta D}{100m}$ and -0.075 to -0.34 $\frac{\Delta\delta^{18}O}{100m}$.

   Recommendation: Precipitation collection stations should be placed at an elevation that is representative of the general surrounds, rather than atop a high peak or in a deep valley. Where stations are in topographically unrepresentative positions, the average elevation around the site should be used when calculating altitude effect gradients.

8. **The amount effect varies between stations and over time at single stations** (p.143)
   The amount effect was not noticeable for average annual precipitation, but for mean monthly precipitation (e.g. Dansgaard, 1964; Rozanski et al., 1993). To calculate useful monthly means of precipitation and δ values, several years of monitoring are needed. The scale of the effect varied significantly between stations and even at a single station over different groups of years, emphasising the need for longer term monitoring to calculate reliable relationships.

   Recommendation: Long term monitoring is needed to calculate such isotope effects accurately. In the absence of longer term data, overinterpretation of trends should be avoided.

9. **Surface waters show little variation within catchments, suggesting complex groundwater flow paths with significant mixing in the Peninsula aquifer** (p.148)
   Samples from rivers showed great variation between rivers, but not within each catchment, despite substantial ranges in altitude and sometimes distance. The surface waters were sampled in late summer, so representing baseflow, made up of groundwater discharge. Direct samples of springs and seeps adjacent to rivers were also taken. The well averaged nature of surface water in each catchment suggests the groundwaters are well mixed between recharge and discharge points, which suggests complex flow paths through deep fracture networks in the Table Mountain Group, mostly the Peninsula Formation, in contrast to isotopically varied groundwater from shallow fracture networks (e.g. Negrel et al., 2011).

   Recommendation: Surface water samples should not be used to understand details of groundwater flow, but do offer averaged δ values for the catchment. The homogeneity of surface water baseflow can be used as a measure of groundwater mixing.

10. **Groundwater flow paths are often shallow and short** (p.151)
    A negative correlation exists between δ values of groundwater samples and the discharge elevation. If groundwater flow paths were long or variable in length, the recharge altitude, which is what determines the δ values, would not be correlated with the discharge altitude. The correlation suggests that much of the groundwater sampled circulates shallowly and has a short flow path of hundreds of metres to perhaps a kilometre or two. This means the aquifer is more easily impacted by surface activities and overabstraction.

    Recommendation: Determine the size and depth of the aquifer by comparing groundwater and precipitation isotope composition, to determine its vulnerability to surface impacts and overabstraction. Long term precipitation monitoring will be needed.

11. **Hot springs reveal long term, long distance, deep circulation in the Table Mountain Group** (p.153)

    Stable isotope composition of several hot springs did not change appreciably over 40 years, although significant variations occur in isotope composition of discharge, even on a monthly timescale. Interannual or interdecadal variations in recharge (precipitation) are not obvious and indicate that circulation is well mixed, deep and regional (e.g. Delalande et al., 2011). The Table Mountain Group is able to conduct deep (more than one or two kilometres), long distance (tens of kilometres) groundwater flow.

12. **Agricultural abstraction in the Olifants River Mountains taps locally recharged groundwater of the Peninsula aquifer** (p.155)

    Isotope composition of rainfall and groundwater in the Olifants River and Cederberg region revealed that groundwater being abstracted from the Peninsula Formation in the Olifants River Mountains was not coming from the Cederberg region and was being locally recharged. The aquifer is relatively limited in extent and more likely to become depleted.

    Recommendation: Local monitoring of hydrological parameters (water levels, rainfall) may be useful in warning of potential groundwater depletion, especially if climate change predictions of decreased rainfall come to pass. Stable isotopes can be employed to elucidate more details about the local groundwater circulation.

13. **Mountain recharge into the Skurweberg aquifer supplies agricultural boreholes on both sides of the Hex River anticline** (p.159)

    Comparison of the isotope composition of boreholes with precipitation has allowed the calculation of approximate recharge altitude. Groundwater abstracted from the Rietvlei Formation at 500 masl on the south side of the Hex River anticline is recharged in the Skurweberg or Goudini Formation at 1200 masl, and groundwater abstracted from the Rietvlei Formation at 1100 masl on the north side of the Hex River anticline is recharged in the Skurweberg or Goudini Formation at 1600 masl. The Skurweberg aquifer is an important, high yielding aquifer for agriculture in the Hex River Mountains region, as has been noted in the nearby Agter-Witzenberg Valley (Weaver et al., 1999). Increasing groundwater abstraction will draw water from deeper in the Skurweberg aquifer, which will have been recharged at higher elevation and therefore have more negative δ values.

    Recommendation: Where an aquifer is recharged over a range of altitudes, monitor stable isotope composition of borehole water to detect signs of overabstraction.

14. **Snow isotope composition varies greatly and preserves that of precipitation events**

    A profile through a snowpack revealed that the isotope composition changed both during a

precipitation event and between different events. Some of this change may have been due to post-depositional changes (Arnason, 1981).

Recommendation: Snow may be sampled to examine recent past precipitation events, but care must be taken to evaluate the degree of post-depositional change.

15. **Groundwater is recharged selectively during large amount rainfall events** (p.166)
    The isotope composition of groundwater discharge at Gamkaberg boreholes has more negative δ values than rainfall at the top of the Gamkaberg, so either selective recharge during isotopically more negative large amount rainfall events occurs (e.g. Dogramaci et al., 2012), or interannual variation in isotope composition of rainfall accounts for the relatively high δ values on top of Gamkaberg.

    Recommendation: Long term precipitation monitoring is needed to quantify the range of interannual variations in δ values.

16. **The Skurweberg aquifer conducts groundwater from the crest of the Klein Swartberg into the Great Karoo** (p.166)
    Boreholes on the northern side of the Klein Swartberg at 1000 masl discharge groundwater with δ values that match recharge at the crest of the range at 2000 m. The recharge occurs in the Goudini or Skurweberg Formation and is discharged through the Rietvlei Formation.

17. **Table Mountain springs are fed by groundwater from the scree aquifer** (p.173)
    Using the altitude effect calculated for Table Mountain it was shown that the typical groundwater flow path for each spring is 1 km long. The aquifer is the scree apron that lies on the middle to lower slopes of Table Mountain, contrary to popularly held belief that the Peninsula Formation is the aquifer (Bryant and Blake, 2014). The springs may be more susceptible to climate change and human activities on the lower slopes than would be the case if the Peninsula aquifer higher on the mountain was directly involved, being in a higher rainfall zone and further removed from human activities.

18. **Table Mountain scree aquifers allow layered groundwater flow to take place** (p.173)
    By tracking changes in annual mean δ values for precipitation and for the springs, the scree aquifer must allow shallow, fast groundwater flow to take place on top of slower, deeper groundwater flow. The former is needed to explain the identical pattern in shifts of annual mean δ values between rain and springs, and the latter is needed to explain the perennial flow of many of the springs. Changes in mean annual isotope composition are generally regarded as noise in data, caused by variations in the weather from year to year, and long

term averages are usually sought (Yurtsever and Gat, 1981). This study has shown the value of using shorter term data and in particular, the interannual changes in mean isotope composition to unravel hydrogeological relations.

Summary

In an international review on stable isotope hydrology, Gat (1996, p.253) stated: "In order to take full advantage of the possibilities of understanding groundwater formation, the detailed isotope effects of the recharge and runoff processes need to be established for different climate conditions and for each watershed. Such studies are still few and incomplete." And in the closing chapter of the Water Research Commission report on the Table Mountain Group, Pietersen and Parsons (2002, p.257) stated: "The WRC recognises the need to... Develop an understanding of the occurrence, attributes and dynamics of the TMG aquifer systems... ". This study has made a start on these recommendations and being regional in nature, has paved the way for more detailed work in and around the Cape Fold Belt.

Findings have been made regarding the continental and altitude effects. Both have been shown to contain more complexity than some other studies have shown, suggesting that either weather in the Cape is more complex, or that other studies have overlooked such details. Changes in mean annual isotope composition of precipitation have been shown to be useful tracers of groundwater flow, something which has not been done before.

Regarding the Table Mountain Group, this study has shown strong evidence for mountain recharge and flow of groundwater to adjacent valleys. Much of the groundwater in the Table Mountain Group has a short flow path of one or two kilometres or less, in keeping with the steep terrain of the Cape Mountains. Despite these short flow distances, groundwater appears to be well mixed, which indicates substantial fracture networks in multiple orientations. Recharge displays selection behaviour, where large amount rainfall events with lighter isotope compositions are favoured.

The range in isotope compositions, due largely to continental and altitude effects, allowed their use as hydrological tracers and helped develop conceptual models of groundwater flow in the Cape Fold Belt. With increasing pressure on water resources in the region, stable isotopes should be employed to help understand the hydrogeology and then better manage water resources to reduce environmental impacts and allow sustainable use of groundwater, at the same time as adding to the global picture on the behaviour of stable isotopes in the hydrological cycle.

Chapter 7

Abbreviations, Acronyms and Units

acronym	explanation
ASTER	Advanced Spaceborne Thermal Emission and Reflection Radiometer
CMWL	Cape meteoric water line
CTIA	Cape Town International Airport
CTMP	Cape Town millipore water
DEM	digital elevation model
GIS	geographic information system
GMWL	Global Meteoric Water Line
GNIP	global network for isotopes in precipitation
IAEA	International Atomic Energy Agency
LASER	light amplification by stimulated emission of radiation
LMWL	local meteoric water line
LSR	least squares regression
MAP	mean annual precipitation
masl	metres above sea level
MWL	meteoric water line
RMA	reduced major axis regression
RMW	Rocky Mountain Water
SAST	South African Standard Time
SAWS	South African Weather Service
SS	sum of the squares (statistical parameter)
SP	sum of the products (statistical parameter)
T	temperature
WMO	World Meteorological Organisation

symbol	explanation
mm	millimetre
m	metre
km	kilometre
μL	microlitre
mL	millilitre
L	litre
kL	kilolitre
ML	megalitre
GL	gigalitre
mg	milligram
s	second
h	hour
d	day
a	annum (year)
Ma	megannum (million years)

letter	abbreviation	explanation
		rainfall stations
C	UCT	University of Cape Town
T	TMC	Table Mountain Upper Cableway Station
I	TWT	Twaktuin
U	UKP	Uitkyk Pass
W	WKP	Wolfkop
M	MTB	Matroosberg
D	DDN	DeDoorns
R	RVD	Riverndale
P	RBP	Robinson Pass
A	BKK	Bakenskop
G	GST	Gamka Store
B	BBG	Blesberg
K	KMN	Kammanassie
L	LTL	Lentelus
O	GKM	Goukamma
		rivers
	DWK	Duiwelskloof
	VSK	Volstruiskloof
	WTL	Witels

	GHK	Groothoekkloof
		hot springs
	CIT	Citrusdal (The Baths)
	WTZ	Witzenberg (Tulbagh)
	GDN	Goudini
	BRA	Brandvlei
	CDN	Caledon
	WAR	Warmwaterberg
	LAI	Laingsburg (UCT field station)
	CZD	Calitzdorp
	TWR	Toowerwater
		Table Mountain (Cape Town) springs
K	KIR	Kirstenbosch
O	KOM	Kommetjie
P	PRI	Princess Anne Drive
N	NEW	Newlands
B	PAL	Palmboom
A	ALB	Albion
R	RED	Redwood
W	WEN	Wendy’s
M	MAI	Cape Town main spring (collection chamber)
C	CAB	Cableway
G	GLE	Glencoe Road
L	LEE	Leeuwenhof
T	TAF	Tafelberg Road
Y	LIL	Lily Pond

Table 7.1: Tables of Acronyms, Units and Abbreviations

Chapter 8

Acknowledgements

I would like to thank the following organisations and people:

Professor Chris Harris for supervision, funding, advice and climbing;

National Research Foundation and Water Research Commission for funding;

Dr John Lanham for analytical assistance on the mass spectrometer;

Dr Adam West for analytical assistance on the LASER spectrometer and advice;

for sampling rain:
Fayrooza Rawoot at University of Cape Town,
Sabine Lehmann, Marie Abraham and Kim van Reenen at the Table Mountain Aerial Cableway Company,
Robert and Anne Paterson at Twaktuin,
Patrick Lane at the Cederberg (Cape Nature),
Richard Humphris at Wolfkop,
Waldo and Didi Smith at Erfdeel,
Retief Jordaan at Tweespruit,
Jeremy Wakeford at Riverndale,
Jan Makampies at Ruitersbos (Cape Nature), Robinson Pass,
Tom Barry and team at Gamkaberg (Cape Nature),
Jan Coetzee, Theo Taute and team at the Groot Swartberg (Cape Nature),
Philip Esau and team at the Kammanassie (Cape Nature),
Dirk Versfeld and Rachel Moos at Lentelus,
Marina Botha at Goukamma;

for sampling boreholes:
Robert Paterson at Twaktuin,
Waldo Smith at Erfdeel,
Retief Jordaan at Tweespruit,
Tom Barry at Gamkaberg,
Geoff Grundlingh at Rooihoogte;

for sampling springs:
Caron von Zeil and Pixie Littlewort for assistance and passion for the Cape Town springs,
Marius Bonthuis at Cape Town Main (City of Cape Town),
Philip le Roux and Aida van Reenen at Kirstenbosch (South African National Biodiversity Institute),
Paul Teuchert at Kommetjie (South African Breweries),
the managers at the various hot springs;

and to all the friends and family who accompanied me on various missions to collect samples, service rainfall collectors and sample springs and seeps in the wild yet wonderful Cape Mountains:
Alexis Aronson,
Anyik Duku,
Phil Ginsberg,
John Glover,
Richard Halsey,
Martin Kleynhans,
Lucille Krige,
Mikhaela Levitas,
Elinor Milewski,
Sonia van Essen,
Luke Viljoen,
Xolani Zekani.

References

Adams, S., Titus, R., Pietersen, K., Tredoux, G., Harris, C., 2001. Hydrochemical characteristics of aquifers near Sutherland in the Western Karoo, South Africa. Journal of Hydrology 241, 91–103.

Al-Aswad, A.A., Al-Bassam, A.M., 1997. Proposed hydrostratigraphical classification and nomenclature: application to the Palaeozoic in Saudi Arabia. Journal of African Earth Sciences 24, 497–510.

Araguás-Araguás, L., Froehlich, K., Rozanski, K., 1998. Stable isotope composition of precipitation over southeast Asia. Journal of Geophysical Research 103, 28721–28742.

Araguás-Araguás, L., Froehlich, K., Rozanski, K., 2000. Deuterium and oxygen-18 isotope composition of precipitation and atmospheric moisture. Hydrological Processes 14, 1341–1355.

Argiriou, A.A., Lykoudis, S., 2006. Isotopic composition of precipitation in Greece. Journal of Hydrology 327, 486–495.

Arnason, B., 1981. Ice and Snow Hydrology, in: Gat, J.R., Gonfiantini, R. (Eds.), Stable Isotope Hydrology. International Atomic Energy Agency, Vienna. number 210 in Technical Reports Series. chapter 7, pp. 143–175.

ASTER, 2014. Advanced Spaceborne Thermal Emission and Reflection Radiometer. URL: http://www.jspacesystems.or.jp/ersdac/GDEM/E/index.html.

Barrow, D., Diamond, R.E., 2011. Stable isotopes of rain, surface water and groundwater in the Kogelberg, in: Groundwater: Our Source of Security in an Uncertain Future, Groundwater Division: Geological Society of South Africa, Pretoria.

Beaudoin, G., Therrien, P., 2014. AlphaDelta: Stable Isotope Fractionation Calculator. URL: http://www2.ggl.ulaval.ca/cgi-bin/alphadelta/alphadelta.cgi.

Belcher, R.W., Kisters, A.F., 2003. Lithostratigraphic correlations in the western branch of the Pan-African Saldania Belt, South Africa: the Malmesbury Group revisited. South African Journal of Geology 106, 327–342.

Bell, C.M., 1980. Deformation of the Table Mountain Group in the Cape Fold Belt south of Port Elizabeth. Transactions of the Geological Society of South Africa 83, 115–124.

Beuster, H., Thompson, I., Gögens, A.H., Jonker, V., Clarke, F.A., 2009. Application of geostatistical analyses to develop a new mean annual rainfall surface for the south-western Cape, in: South African National Committee for the International Association of Hydrological Sciences: Symposium 2009, p. 18p.

Bond, G., 1953. The origin of thermal and mineral waters in the middle Zambezi Valley and adjoining territory. Geological Society of South Africa 56, 131–148.

Bosman, H.H., 1981. Raingauges: Quality pays. Water SA 7, 190–191.

Breitenbach, S.F., Adkins, J.F., Meyer, H., Marwan, N., Kumar, K.K., Haug, G.H., 2010. Strong influence of water vapor source dynamics on stable isotopes in precipitation observed in southern Meghalaya, NE India. Earth & Planetary Science Letters 292, 212–220.

Brink, A.B., 1981. Engineering Geology of Southern Africa. volume 2: Case Study: Dams founded on rocks and The Table Mountain Group. Building Publications, Pretoria.

Broquet, C.A., 1992. The sedimentary record of the Cape Supergroup: A review, in: de Wit, M.J., Ransome, I.G. (Eds.), Inversion Tectonics of the Cape Fold Belt, Karoo and Cretaceous Basins of Southern Africa. A.A.Balkema, pp. 159–184.

Bryant, J., Blake, D., 2014. Investigating the springs and boreholes of Groote Schuur. Veld & Flora , 63.

Butler, M.J., Verhagen, B.T., Levin, M., 2000. Application of environmental isotope techniques to hydrological and pollution problems in the urban environment, in: Sililo, O. (Ed.), Groundwater: Past Achievements and Future Challenges. A.A.Balkema, Rotterdam, pp. 459–464.

Cavé, L.C., Weaver, J.M., Talma, A.S., 2002. The use of geochemistry and isotopes in resource evaluation: a case study from the Agter-Witzenberg Valley, in: Pietersen, K., Parsons, R. (Eds.), A Synthesis of the Hydrogeology of the Table Mountain Group - Formation of a Research Strategy. Water Research Commission, Pretoria. TT 158/01, pp. 143–149.

Clark, I.D., Fritz, P., 1997. Environmental Isotopes in Hydrogeology. CRC Press, Boca Raton.

Colvin, C., Riemann, K., Brown, C., Maitre, D.L., Mlisa, A., Blake, D., Aston, T., Maherry, A., Engelbrecht, J., Pemberton, C., Magoba, R., Soltau, L., Prinsloo, E., 2009. Ecological and environmental impacts of large-scale groundwater development in the Table Mountain Group) TMG aquifer system. Technical Report 1327/1/08. Water Research Commission. Pretoria.

Council for Geoscience, 1997. 3319 Worcester. 1:250 000 geological series. Council for Geoscience. Pretoria.

Craig, H., 1961a. Isotopic variations in meteoric waters. Science 133, 1702–1703.

Craig, H., 1961b. Standard for reporting concentrations of deuterium and oxygen-18 in natural waters. Science 133, 1833–1834.

CSAG, 2013. Climate Information Portal, Climate Systems Analysis Group, University of Cape Town. http://cip.csag.uct.ac.za/webclient2/app/.

da Silva, L.C., Gresse, P.G., Scheepers, R., McNaughton, N.J., Hartmann, L.A., Fletcher, I., 2000. U-Pb SHRIMP and Sm-Nd age constraints on the timing and sources of the Pan-African Cape Granite Suite, South Africa. Journal of African Earth Sciences 30, 795–815.

D'Alessandro, W., Federico, C., Longo, M., Parello, F., 2004. Oxygen isotope composition of natural waters in the Mt Etna area. Journal of Hydrology 296, 282–299.

Dansgaard, W., 1964. Stable Isotopes in Precipitation. Tellus 16, 436–468.

Davidson, W.A., 1995. Hydrogeology and groundwater resources of the Perth Basin. Technical Report Bulletin 142. Western Australia Geological Survey. Perth.

de Beer, C.H., 2002. The Stratigraphy, Lithology and Structure of the Table Mountain Group, in: Pietersen, K., Parsons, R. (Eds.), A Synthesis of the Hydrogeology of the Table Mountain Group - Formation of a Research Strategy. Water Research Commission, Pretoria. TT 158/01, pp. 9–18.

de Wit, M.J., Ransome, I.G., 1992. Regional inversion tectonics along the southern margin of Gondwana, in: de Wit, M.J., Ransome, I.G. (Eds.), Inversion Tectonics of the Cape Fold Belt, Karoo and Cretaceous Basins of Southern Africa. A.A.Balkema, Rotterdam, pp. 15–22.

Delalande, M., Bergonzini, L., Gherardi, F., Guidi, M., Andre, L., Abdallah, I., Williamson, D., 2011. Fluid geochemistry of natural manifestations from the Southern Poroto-Rungwe hydrothermal system (Tanzania): Preliminary conceptual model. Journal of Volcanology and Geothermal Research 199, 127–141.

Dent, M.C., Lynch, S.D., Schulze, R.E., 1987. Mapping mean annual and other rainfall statistics over Southern Africa. Technical Report 109/1/89. Water Research Commission. Pretoria.

Diamond, R.E., Harris, C., 1997. Oxygen and hydrogen isotope composition of Western Cape meteoric water. South African Journal of Science 93, 371–374.

Diamond, R.E., Harris, C., 2000. Oxygen and hydrogen isotope geochemistry of thermal springs of the Western Cape, South Africa: recharge at high altitude? Journal of African Earth Sciences 31, 467–481.

Dingle, R.V., Siesser, W.G., Newton, A.R., 1983. Mesozoic and Tertiary Geology of Southern Africa. A.A.Balkema.

Dody, A., Ziv, B., 2013. Factors affecting isotopic composition of the rainwater in the Negev Desert, Israel. Journal of Geophysical Research: Atmospheres 118, 8274–8284.

Dogramaci, S., Skrzypek, G., Dodson, W., Grierson, P.F., 2012. Stable isotope and hydrochemical evolution of groundwater in the semi-arid Hamersley Basin of subtropical northwest Australia. Journal of Hydrology 475, 281–293.

Domenico, P.A., Schwartz, F.W., 1998. Physical and Chemical Hydrogeology. John Wiley & Sons, Inc.

DTI, 2009. SA Risk and Vulnerability Atlas. URL: http://rava.qsens.net/themes/groundwater.

Emiliani, C., 1987. Dictionary of the Physical Sciences. Oxford University Press, Oxford.

Encyclopaedia Brittanica, 2013. Climate. URL: http://www.britannica.com/EBchecked/topic/121560/c

Epstein, S., Mayeda, T., 1953. Variation of 18O content of waters from natural sources. Geochimica et Cosmochimica Acta 4, 213–224.

February, E.C., Bond, W., Taylor, R., Newton, R., 2004. Will water abstraction from the Table Mountain aquifer threaten endemic species? A case study at Cape Point, Cape Town. South African Journal of Science 100, 253–255.

Friedman, I., 1953. Deuterium content of natural waters and other substances. Geochimica et Cosmochimica Acta 4, 89–103.

Frimmel, H.E., Fölling, P.G., Diamond, R.E., 2001. Metamorphism of the Permo-Triassic Cape Fold Belt and its basement, South Africa. Mineralogy and Petrology 73, 325–346.

Fritz, P., 1981. River Waters, in: Gat, J.R., Gonfiantini, R. (Eds.), Stable Isotope Hydrology. International Atomic Energy Agency, Vienna. number 210 in Technical Reports Series. chapter 8, pp. 177–202.

Fuller, A.O., Broquet, C.A., 1990. Aspects of the Peninsula Formation - Table Mountain Group, in: Geocongress ’90 - abstracts, Geological Society of South Africa. Geological Society of South Africa, Johannesburg. pp. 169–172.

Gabbott, S.E., Siveter, D.J., Aldridge, R.J., Theron, J.N., 2003. The earliest myodocopes: ostracodes from the late Ordovician Soom Shale Lagerstätte. Lethaia 36, 151–160.

Gat, J.R., 1981a. Groundwater, in: Gat, J.R., Gonfiantini, R. (Eds.), Stable Isotope Hydrology. International Atomic Energy Agency, Vienna. number 210 in Technical Reports Series. chapter 10, pp. 223–240.

Gat, J.R., 1981b. Historical Introduction, in: Gat, J.R., Gonfiantini, R. (Eds.), Stable Isotope Hydrology. International Atomic Energy Agency, Vienna. number 210 in Technical Reports Series. chapter 1, pp. 1–6.

Gat, J.R., 1996. Oxygen and hydrogen isotopes in the hydrological cycle. Annual Reviews in Earth and Planetary Sciences 24, 225–262.

Gaucher, C., Germs, G.J., 2006. Recent advances in South African Neoproterozoic-Early Palaeozoic biostratigraphy: correlation of the Cango Caves and Gamtoos Groups and acritarchs of the Sardinia Bay Formation, Saldania Belt. South African Journal of Geology 109, 193–214.

Geological Survey, 1973. 3218 Clanwilliam. 1:250 000 geological series. Department of Mines. Pretoria.

Geological Survey, 1979. 3322 Oudtshoorn. 1:250 000 geological series. Geological Survey. Pretoria.

Geological Survey, 1991. 3320 Ladismith. 1:250 000 geological series. Geological Survey. Pretoria.

Gonfiantini, R., 1981. The δ notation and the mass-spectrometric measurement techniques, in: Gat, J.R., Gonfiantini, R. (Eds.), Stable Isotope Hydrology. International Atomic Energy Agency, Vienna. number 210 in Technical Reports Series. chapter 4, pp. 35–84.

Gonfiantini, R., Roche, M.A., Olivry, J.C., Fontes, J.C., Zuppi, G.M., 2001. The altitude effect on the isotopic composition of tropical rains. Chemical Geology 181, 147–167.

Gresse, P.G., Theron, J.N., 1992. The Geology of the Worcester Area, explanation of sheet 3319. Technical Report. Geological Survey, Department of Mineral and Energy Affairs. Pretoria.

Gresse, P.G., von Veh, M.W., Frimmel, H.E., 2006. Namibian (Neoproterozoic) to Early Cambrian Successions, in: Johnson, M.R., Annhaeusser, C.R., Thomas, R.J. (Eds.), The Geology of South Africa. Geological Society of South Africa, Council for Geoscience, Pretoria. chapter 18, pp. 395–420.

Hälbich, I.W., 1992. The Cape Fold Belt Orogeny: State of the art 1970’s - 1980’s, in: de Wit, M.J., Ransome, I.G. (Eds.), Inversion Tectonics of the Cape Fold Belt, Karoo and Cretaceous Basins of Southern Africa. A.A.Balkema, Rotterdam, pp. 141–158.

Hammerbeck, E.C., Allcock, R.J., 1985. Geological Map of Southern Africa. Technical Report. Geological Society of South Africa. Pretoria.

Harris, C., Burgers, C., Miller, J., Rawoot, F., 2010. O- and H-isotope record of Cape Town rainfall from 1996 to 2008, and its application to recharge studies of Table Mountain groundwater, South Africa. South African Journal of Geology 113, 33–56.

Harris, C., Oom, B.M., Diamond, R.E., 1999. A preliminary investigation of the oxygen and hydrogen isotope hydrology of the greater Cape Town area and an assessment of the potential for using stable isotopes as tracers. Water SA 25, 15–24.

Hartnady, C.J., Hay, E.R., 2002a. Boschkloof groundwater discovery, in: Pietersen, K., Parsons, R. (Eds.), A Synthesis of the Hydrogeology of the Table Mountain Group - Formation of a Research Strategy. Water Research Commission, Pretoria. TT 158/01, pp. 168–177.

Hartnady, C.J., Hay, E.R., 2002b. Experimental deep drilling at Blikhuis, Olifants River Valley, Western Cape: Motivation, setting and current progress, in: Pietersen, K., Parsons, R. (Eds.), A Synthesis of the Hydrogeology of the Table Mountain Group - Formation of a Research Strategy. Water Research Commission, Pretoria. TT 158/01, pp. 192–197.

Hartnady, C.J., Hay, E.R., 2002c. Use of structural geology and remote sensing in hydrogeological exploration of the Olifants and Doring River catchments, in: Pietersen, K., Parsons, R. (Eds.), A Synthesis of the Hydrogeology of the Table Mountain Group - Formation of a Research Strategy. Water Research Commission, Pretoria. TT 158/01, pp. 19–30.

Hartnady, C.J., Newton, A.R., Theron, J.N., 1974. The stratigraphy and structure of the Malmesbury Group in the southwestern Cape. Bulletin of the Precambrian Research Unit, UCT 15, 195–213.

Harvey, F.E., Sibray, S.S., 2001. Delineating Groundwater recharge from leaking irrigation canals using water chemistry and isotopes. Groundwater 39, 408–421.

Hobday, D.K., Tankard, A.J., 1978. Transgressive-barrier and shallow-shelf interpretation of the lower Paleozoic Peninsula Formation, South Africa. Geological Society of America Bulletin 89, 1733–1744.

Horibe, Y., Kobayakawa, M., 1960. Deuterium abundance of natural waters. Geochimica et Cosmochimica Acta 20, 273.

Hughes, C.E., Crawford, J., 2012. A new precipitation weighted method for determining the meteoric water line for hydrological applications demonstrated using Australian and global GNIP data. Journal of Hydrology 464, 344–351.

Hunjak, T., Lutz, H.O., Roller-Lutz, Z., 2013. Stable isotope composition of the meteoric precipitation in Croatia. Isotopes in Environmental and Health Studies 49, 336–345.

Iacumin, P., Venturelli, G., Selmo, E., 2009. Isotopic features of rivers and groundwater of the Parma Province (Northern Italy) and their relationships with precipitation. Journal of Geochemical Exploration 102, 56–62.

IAEA, 2013. The Nubian Aquifer Project. URL: http://www-naweb.iaea.org/napc/ih/IHS projects nubian development.html.

Jasechko, S., Sharp, Z., Gibson, J., Birks, S., Yi, Y., Fawcett, P., 2013. Terrestrial water fluxes dominated by transpiration. Nature 496, 347–350.

Jaunat, J., Celle-Jeanton, H., Huneau, F., Dupuy, A., Le Coustumer, P., 2013. Characterisation of the input signal to aquifers in the French Basque Country: Emphasis on parameters influencing the chemical and isotopic composition of recharge waters. Journal of Hydrology 496, 57–70.

Johnson, M.R., van Vuuren, C.J., Visser, J.N., Cole, D.I., Wickens, H., Christie, A.D., Roberts, D.L., Brandl, G., 2006. Sedimentary rocks of the Karoo Supergroup, in: Johnson, M.R., Annhaeusser, C.R., Thomas, R.J. (Eds.), The Geology of South Africa. Geological Society of South Africa, Council for Geoscience, Pretoria. chapter 22, pp. 461–500.

Jolly, J.L., 2002. Sustainable use of Table Mountain Group aquifers and problems related to scheme failure, in: Pietersen, K., Parsons, R. (Eds.), A Synthesis of the Hydrogeology of the Table Mountain Group - Formation of a Research Strategy. Water Research Commission, Pretoria. TT 158/01, pp. 108–111.

Jolly, J.L., Kotze, J.C., 2002. The Klein Karoo Rural Water Supply Scheme, in: Pietersen, K., Parsons, R. (Eds.), A Synthesis of the Hydrogeology of the Table Mountain Group - Formation of a Research Strategy. Water Research Commission, Pretoria. TT 158/01, pp. 198–201.

Jones, M., 1992. Heat flow in South Africa. Handbook of the Geological Survey 14. Geological Survey. Pretoria.

Jordaan, L.J., Scheepers, R., Barton, E.S., 1995. The geochemistry and isotopic composition of the mafic and intermediate igneous components of the Cape Granite Suite, South Africa. Journal of African Earth Sciences 21, 59–70.

Kakiuchi, M., Matsuo, S., 1979. Direct measurements of D/D and 18O/16O fractionation factors between vapor and liquid water in the temperature range from 10 to 40C. Geochemical Journal 13, 307–311.

Kent, L.E., 1949. The thermal waters of the Union of South Africa and South West Africa. Transactions of the Geological Society of South Africa 52, 231–264.

Knox, A., 1911. The Climate of the Continent of Africa. Cambridge University Press, Cambridge.

Kotze, J.C., 2002. Towards a management tool for groundwater exploitation in the Table Mountain sandstone fractured aquifer. Technical Report 729/1/02. Water Research Commission. Pretoria.

Kotze, J.C., Verhagen, B.T., Butler, M.J., 2000. An aquifer model based on chemistry, isotopes and lineament mapping: Little Karoo, South Africa, in: Sililo, O. (Ed.), Groundwater: Past Achievements and Future Challenges. Balkema, Rotterdam, pp. 539–544.

Ladouche, B., Luc, A., Nathalie, D., 2009. Chemical and isotopic investigation of rainwater in southern France (1996-2002): Potential use as input signal for karst functioning investigation. Journal of Hydrology 367, 150–164.

Lawrence, J.R., White, J.W., 1991. The elusive climate signal if the isotopic composition of precipitation, in: Taylor, H.P., O'Neil, J.R., Kaplan, I.R. (Eds.), Stable Isotope Geochemistry: A Tribute to Samuel Epstein. The Geochemical Society, San Antonio. number 3 in Special Publication, pp. 169–185.

le Maitre, D.C., Colvin, C., Scott, D.F., 2002. Groundwater dependent ecosystems in the Fynbos Biome, and their vulnerability to groundwater abstraction, in: Pietersen, K., Parsons, R. (Eds.), A Synthesis of the Hydrogeology of the Table Mountain Group - Formation of a Research Strategy. Water Research Commission, Pretoria. TT 158/01, pp. 112–117.

Lin, L., Jia, H., Xu, Y., 2007. Fracture network characteristics of a deep borehole in the Table Mountain Group, South Africa. Hydrogeology Journal 15, 1419–1432.

Lis, G., Wassenaar, L.I., Hendry, M.J., 2008. High-Precision LASER spectroscopy D/H and 18O/16O measurements of microliter natural water samples. Analytical Chemistry 80, 287–293.

Liu, J., Fu, G., Song, X., Charles, S.P., Zhang, Y., Han, D., Wang, S., 2010. Stable isotopic compositions in Australian precipitation. Journal of Geophysical Research 115, 16.

Maclear, L.G., 2002. The hydrogeology of the Uitenhage Artesian Basin with reference to the Table Mountain Group aquifer, in: Pietersen, K., Parsons, R. (Eds.), A Synthesis of the Hydrogeology of the Table Mountain Group - Formation of a Research Strategy. Water Research Commission, Pretoria. TT 158/01, pp. 216 – 223.

Majumder, R.K., Halim, M.A., Saha, B.B., Ikawa, R., Nakamura, T., Kagabu, M., Shimada, J., 2011. Groundwater flow systems in Bengal Delta, Bangladesh revealed by environmental isotopes. Environmental Earth Science 64, 1343–1352.

Mazor, E., Verhagen, B.T., 1976. Hot springs of Rhodesia – their noble gases, isotopic and chemical composition. Journal of Hydrology 28, 29–43.

Mazor, E., Verhagen, B.T., 1983. Dissolved ions, stable and radioactive isotopes and noble gases in thermal waters of South Africa. Journal of Hydrology 63, 315–329.

Mazor, E., Verhagen, B.T., Negreanu, E., 1974. Hot springs of the igneous terrain of Swaziland – their noble gases, hydrogen, oxygen and carbon isotopes and dissolved ions, in: Isotope Techniques in Groundwater Hydrology. International Atomic Energy Agency, Vienna. volume 2, pp. 29–47.

Meyer, P.S., 2002. Springs in the Table Mountain Group, with special reference to fault controlled springs, in: Pietersen, K., Parsons, R. (Eds.), A Synthesis of the Hydrogeology of the Table Mountain Group - Formation of a Research Strategy. Water Research Commission, Pretoria. TT 158/01, pp. 224–229.

Midgley, J., Scott, D.F., 1994. The use of stable isotopes of water (D and ^{18}O) in hydrological studies in the Jonkershoek Valley. Water SA 20, 151–154.

Mulligan, B.M., Ryan, M.C., Cámbara, T.P., 2011. Delineating volcanic aquifer recharge areas using geochemical and isotopic tools. Hydrogeology Journal 19, 1335–1347.

NASA, 2013. Shuttle Radar Topography Mission. URL: http://www2.jpl.nasa.gov/srtm/.

Negrel, P., Pauwels, H., Dewandel, B., Gandolfi, J.M., Mascré, C., Ahmed, S., 2011. Understanding groundwater systems and their functioning through the study of stable isotopes in a hard-rock aquifer (Maheshwaram watershed, India). Journal of Hydrology 397, 55–70.

NGI, 2012. RSA National Geo-Spatial Information 1:50 000 shape files. URL: http://www.ngi.gov.za/.

Nkondo, M.N., van Zyl, F.C., Keuris, H., Schreiner, B., 2012. National Water Resource Strategy 2. Technical Report. Department of Water Affairs. Pretoria.

Parsons, R., 2002. Development of Groundwater Resources of the Arabella Country Estate, in: Pietersen, K., Parsons, R. (Eds.), A Synthesis of the Hydrogeology of the Table Mountain Group - Formation of a Research Strategy. Water Research Commission, Pretoria. TT 158/01, pp. 150–154.

Partridge, T.C., Botha, G.A., Haddon, I.G., 2006. Cenozoic Deposits of the Interior, in: Johnson, M.R., Annhaeusser, C.R., Thomas, R.J. (Eds.), The Geology of South Africa. Geological Society of South Africa, Council for Geoscience, Pretoria. chapter 29, pp. 585–604.

Partridge, T.C., Maud, R.R., 1987. Geomorphic evolution of southern Africa since the Mesozoic. South African Journal of Geology 90, 179–208.

Peng, T.R., Wang, C.H., Huang, C.C., Fei, L.Y., Chen, C.T., Hwong, J.L., 2010. Stable isotope characteristics of Taiwan's precipitation: A case study of western Pacific monsoon region. Earth & Planetary Science Letters 289, 357–366.

Pietersen, K., Parsons, R. (Eds.), 2002. A Synthesis of the Hydrogeology of the Table Mountain Group - Formation of a Research Strategy. TT 158/01, Water Research Commission, Pretoria.

Poehls, D.J., Smith, G.J., 2009. Encyclopedic Dictionary of Hydrogeology. Elsevier, Amsterdam.

Preston-Whyte, R.A., Tyson, P.D., 1988. The Atmosphere and Weather of Southern Africa. Oxford University Press, Cape Town.

Rangarajan, R., Ghosh, P., 2011. Tracing the source of bottled water using stable isotope techniques. Rapid Communications in Mass Spectrometry 25, 3323–3330.

Reeburgh, W.S., 1994. Global water reservoirs, fluxes and turnover times. URL: http://www.ess.uci.edu/ reeburgh/fig8.html.

Richey, D.G., McDonnell, J.J., Erbe, M.W., Hurd, T.M., 1998. Hydrograph separations based on chemical and isotopic concentrations: a critical appraisal of published studies from New Zealand, North America and Europe. Journal of Hydrology (NZ) 37, 95–111.

Roberts, D.L., Botha, G.A., Maud, R.R., Pether, J., 2006. Coastal Cenozoic Deposits, in: Johnson, M.R., Annhaeusser, C.R., Thomas, R.J. (Eds.), The Geology of South Africa. Geological Society of South Africa, Council for Geoscience, Pretoria. chapter 30, pp. 605–628.

Roets, W., Xu, Y., Raitt, L., El-Kahloun, M., Meire, P., Calitz, F., Batelaan, O., Anibas, C., Paridaens, K., Vandenbroucke, T., Verhoest, N., Brendonck, L., 2008. Determining discharges from the Table Mountain Group (TMG) aquifer to wetlands in the Southern Cape, South Africa. Hydrobiologia 607, 175–186.

Rosewarne, P., 2002a. Case Study: Ceres Municipality, in: Pietersen, K., Parsons, R. (Eds.), A Synthesis of the Hydrogeology of the Table Mountain Group - Formation of a Research Strategy. Water Research Commission, Pretoria. TT 158/01, pp. 160–163.

Rosewarne, P., 2002b. Hydrogeological Characteristics of the Table Mountain Group Aquifers, in: Pietersen, K., Parsons, R. (Eds.), A Synthesis of the Hydrogeology of the Table Mountain Group - Formation of a Research Strategy. Water Research Commission, Pretoria. TT 158/01, pp. 33–44.

Rozanski, K., Araguás-Araguás, L., Gonfiantini, R., 1993. Isotopic patterns in modern global precipitation, in: Swart, P.K., Lohmann, K.C., McKenzie, J., Savin, S. (Eds.), Climate Change in Continental Isotopic Records. American Geophysical Union. number 78 in Geophysical Monograph. chapter 1, pp. 1–36.

Rozanski, K., Sonntag, C., Munnich, K.O., 1982. Factors controlling stable isotope composition of European precipitation. Tellus 34, 142–150.

Rozendaal, A., Gresse, P.G., Scheepers, R., le Roux, J.P., 1999. Neoproterozoic to early Cambrian crustal evolution of the Pan-African Saldania Belt, South Africa. Precambrian Research 97, 303–323.

Rust, I.C., 1967. On the sedimentation of the Table Mountain Group in the Western Cape Province, D.Sc. thesis. Ph.D. thesis. Stellenbosch University.

Rust, I.C., 1973. The evolution of the Palaeozoic Cape basin, southern margin of Africa. Plenum, New York, New York. volume 1 of *The Ocean Basins and Margins*. chapter 6. pp. 247–276.

Rust, I.C., 1977. Evidence of shallow marine and tidal sedimentation in the Ordovician Graafwater Formation, Cape Province, South Africa. Sedimentary Geology 18, 123–133.

Saayman, I.C., Adams, S., Harris, C., 2000. Example of O- and H-isotope use to identify surface water pollution in groundwater, in: Sililo, O. (Ed.), Groundwater: Past Achievements and Future Challenges. A.A.Balkema, Rotterdam, pp. 599–603.

Saayman, I.C., Scott, D.F., Prinsloo, F.W., Moses, G., Weaver, J.M., Talma, S., 2003. Evaluation of the application of natural isotopes in the identification of the dominant streamflow generation mechanisms in TMG catchments. Technical Report 1234/1/03. Water Research Commission. Pretoria.

SACS, 1980. Stratigraphy of South Africa. volume Part 1: Lithostratigraphy of the Republic of South Africa, South West Africa/Namibia, and the Republics of Boputhatswana, Transkei and Venda. South African Committee for Stratigraphy, Geological Survey, Pretoria.

Salameh, E., 2004. Using environmental isotopes in the study of the recharge-discharge mechanisms of the Yarmouk catchment area in Jordan. Hydrogeology Journal 12, 451–463.

Salati, E., Dall'Olio, A., Matsui, E., Gat, J.R., 1979. Recycling of water in the Amazon Basin: an isotopic study. Water Resources Research 15, 1250–1258.

Sami, K., 1992. Recharge mechanisms and geochemical processes in a semi-arid sedimentary basin, Eastern Cape, South Africa. Journal of Hydrology 139, 27–48.

SAWB, 1996. The weather and climate of the extreme south-western Cape. South African Weather Bureau, Department of Environmental Affairs and Tourism. Pretoria.

SAWS, 2010-12. Daily Weather Bulletin, ISSN 0011-5517. Monthly. Pretoria.

Scheepers, R., Armstrong, R., 2002. New U-Pb SHRIMP zircon ages of the Cape Granite Suite: implications for the magmatic evolution of the Saldania Belt. South African Journal of Geology 105, 241–256.

Scheepers, R., Poujol, M., 2002. U-Pb zircon age of Cape Granite Suite ignimbrites: characteristics of the last phases of the Saldanian magmatism. South African Journal of Geology 105, 163–178.

Scheepers, R., Schoch, A.E., 2006. The Cape Granite Suite, in: Johnson, M.R., Annhaeusser, C.R., Thomas, R.J. (Eds.), The Geology of South Africa. Geological Society of South Africa, Council for Geoscience, Pretoria. chapter 19, pp. 421–432.

Schimmelman, A., DeNiro, M.J., 1993. Preparation of organic and water hydrogen for stable isotope analysis: Effects due to reaction vessels and zinc reagent. Analytical Chemistry 65, 789–792.

Schoch, A.E., Burger, A.J., 1976. U-Pb zircon age of the Saldanha Quartz Porphyry, Western Cape Province. Transactions of the Geological Society of South Africa 79, 239–241.

Schoch, A.E., Leterrier, J., de la Roche, H., 1977. Major element geochemical trends in the Cape Granites. Transactions of the Geological Society of South Africa 80, 197–209.

Schulze, R.E., Lynch, S.D., 2001. South African Atlas of Agrohydrology and Climatology. URL: http://planet.uwc.ac.za/NISL/Invasives/Assignments/GARP/atlas/atlas toc.htm.

Sharp, Z., 2007. Principles of Stable Isotope Geochemistry. Pearson Prentice Hall.

Shone, R.W., 2006. Onshore post-Karoo Mesozoic deposits, in: Johnson, M.R., Annhaeusser, C.R., Thomas, R.J. (Eds.), The Geology of South Africa. Geological Society of South Africa, Council for Geoscience, Pretoria. chapter 26, pp. 541–552.

Shone, R.W., Booth, P.W., 2005. The Cape basin, South Africa: A review. Journal of African Earth Sciences 43, 196–210.

Socki, R.A., Karlsson, H.R., Gibson, Jr., E.K., 1992. Extraction technique for the determination of oxygen-18 in water using preevacuated glass vials. Analytical Chemistry 64, 829–831.

Söhnge, A.P., 1983. The Cape Fold Belt - Perspective, in: Söhnge, A.P., Hälbich, I.W. (Eds.), Geodynamics of the Cape Fold Belt. Geological Society of South Africa, Johannesburg. number 12 in Special Publication. chapter 1, pp. 1–6.

Stats SA, 2006. Updated water accounts for South Africa: 2000. Technical Report. Statistics South Africa. Pretoria.

Sumner, G., 1988. Precipitation: Process and Analysis. John Wiley & Sons, Inc., Singapore.

Takai, K., Moser, D.P., DeFlaun, M., Onstott, T.C., Frederickson, J.K., 2001. Archaeal diversity in waters from deep South African gold mines. Applied and Environmental Microbiology 67, 5750–5760.

Talma, A.S., van Wyk, E., 2013. Rainfall and Groundwater Isotope Atlas, in: Abiye, T. (Ed.), The Use of Isotope Hydrology to Characterise and Assess Water Resources in Southern Africa. Water Research Commission, Pretoria. TT570/13. chapter 6, pp. 83–101.

Tankard, A.J., Hobday, D.K., 1977. Tide dominated back-barrier sedimentation, early Ordovician Cape Basin, Cape Peninsula, South Africa. Sedimentary Geology 18, 135–159.

Tankard, A.J., Jackson, M.P., Eriksson, K.A., Hobday, D.K., Hunter, D.R., Minter, W.E.L., 1982. Crustal Evolution of Southern Africa, 3.8 Billion Years of Earth History. Springer, New York.

Tanweer, A., Hut, G., Burgman, J.O., 1988. Optimal conditions for the reduction of water to hydrogen by zinc for mass spectrometric analysis of the deuterium content. Chemical Geology (Isotope Geoscience Section) 73, 199–203.

Thamm, A.G., Johnson, M.R., 2006. The Cape Supergroup, in: Johnson, M.R., Annhaeusser, C.R., Thomas, R.J. (Eds.), The Geology of South Africa. Geological Society of South Africa, Council for Geoscience, Pretoria. chapter 21, pp. 443–460.

Theron, J.N., Basson, W.A., 1989. Lithostratigraphy of the Rietvlei Formation (Table Mountain Group). Lithostratigraphic Series 7. Geological Survey. Pretoria.

Theron, J.N., Gresse, P.G., Siegfried, H.P., Rogers, J., 1992. The Geology of the Cape Town area, explanation of sheet 3318. Technical Report. Geological Survey, Department of Mineral and Energy Affairs. Pretoria.

Theron, J.N., Rickards, R.B., Aldridge, R.J., 1990. Bedding plane assemblages of *Promissum pulchrum*, a new giant ashgill conodont from the Table Mountain Group, South Africa. Palaeontology 33, 577–594.

Theron, J.N., Wickens, H., Gresse, P.G., 1991. The Geology of the Ladismith area, explanation of sheet 3320. Technical Report. Geological Survey, Department of Mineral and Energy Affairs.

Toerien, D.K., 1979. The Geology of the Oudtshoorn area, explanation of sheet 3222. Technical Report. Geological Survey, Department of Mines.

Toerien, D.K., Hill, R.S., 1989. The Geology of the Port Elizabeth Area, explanation of sheet 3324. Technical Report. Geological Survey, Department of Mineral and Energy Affairs. Pretoria.

Uemura, R., Yonezawa, N., Yoshimura, K., Asami, R., Kadena, H., Yamada, K., Yoshida, N., 2012. Factors controlling isotopic composition of precipitation on Okinawa Island, Japan: Implications for palaeoclimate reconstruction in the East Asian Monsoon region. Journal of Hydrology 475, 314–322.

Umvoto, SRK, 2000. Reconnaissance Investigation into the Development and Utilization of Table Mountain Group Artesian Groundwater using the E10 Catchment as a Pilot Study Area: CAGE project - interim report. Technical Report. Geohydrology and Project Planning Directorate, Department of Water Affairs & Forestry.

Urey, H.C., 1947. The thermodynamic properties of isotopic substances. Journal of the Chemical Society of London , 562–581.

Vegter, J.R., 1995. An explanation of a set of National Groundwater Maps. Technical Report TT 74/95. Water Research Commission, Department of Water Affairs & Forestry. Pretoria.

Vogel, J.C., van Urk, H., 1975. Isotopic composition of groundwater in semi-arid regions of southern Africa. Journal of Hydrology 25, 23–36.

Vos, R.G., Tankard, A.J., 1981. Braided fluvial sedimentation in the lower Palaeozoic Cape Basin, South Africa. Sedimentary Geology 29, 171–193.

Vreča, P., Bronić, I.K., Horvatiničić, N., Barešić, J., 2006. Isotopic characteristics of precipitation in Slovenia and Croatia: Comparison of continental and maritime stations. Journal of Hydrology 330, 457–469.

Walsch, R.P., Lawler, D.M., 1981. Rainfall seasonality: Description, spatial patterns and change through time. Weather 36, 201–208.

Weaver, J.M., Rosewarne, P., Hartnady, C.J., Hay, E.R., 2002. Potential of Table Mountain Group aquifers and integration into catchment water management, in: Pietersen, K., Parsons, R. (Eds.), A Synthesis of the Hydrogeology of the Table Mountain Group - Formation of a Research Strategy. Water Research Commission, Pretoria. TT 158/01, pp. 239–255.

Weaver, J.M., Talma, A.S., Cavé, C., 1999. Geochemistry and Isotopes for resource evaluation in the fractured rock aquifers of the Table Mountain Group. Technical Report 481/1/99. Water Research Commission. Pretoria.

West, A.G., February, E.C., Bowen, G.J., 2014. Spatial analysis of hydrogen and oxygen stable isotopes ("isoscapes") in ground water and tap water across South Africa. Journal of Geochemical Exploration 145, 213–222.

West, A.G., Goldsmith, G.R., Brooks, P.D., Dawson, T.E., 2010. Discrepancies between isotope ratio infrared spectroscopy and isotope ratio mass spectrometry for the stable isotope analysis of plant and soil waters. Rapid Communications in Mass Spectrometry 24, 1948–1954.

West, A.G., Goldsmith, G.R., Matimati, I., Dawson, T.E., 2011. Spectral analysis software improves confidence in plant and soil water stable isotope analyses performed by isotope ratio infrared spectroscopy (IRIS). Rapid Communications in Mass Spectrometry 25, 2268–2274.

White, M.E., 2000. Running Down. Kangaroo Press, Sydney.

Wikipedia, 2013a. Rain. URL: http://www.wikipedia.org/wiki/rain.

Wikipedia, 2013b. Ogallala aquifer. URL: http://www.wikipedia.org/wiki/Ogallala aquifer.

Woodford, A.C., 2002. Interpretation and applicability of pumping-tests in Table Mountain Group aquifers, in: Pietersen, K., Parsons, R. (Eds.), A Synthesis of the Hydrogeology of the Table Mountain Group - Formation of a Research Strategy. Water Research Commission, Pretoria. TT 158/01, pp. 71–84.

Yonge, C.J., Goldenberg, L., Krouse, H.R., 1989. An isotopic study of water bodies along a traverse of southwestern Canada. Journal of Hydrology 106, 245–255.

Young, G.M., Minter, W.E.L., Theron, J.N., 2004. Geochemistry and palaeogeography of upper Ordovician glaciogenic sedimentary rocks in the Table Mountain Group, South Africa. Palaeogeography, Palaeoclimatology, Palaeoecology 214, 323–345.

Yurtsever, Y., Gat, J.R., 1981. Atmospheric waters, in: Gat, J.R., Gonfiantini, R. (Eds.), Stable Isotope Hydrology. International Atomic Energy Agency, Vienna. number 20 in Technical Reports Series. chapter 6, pp. 103–142.

Stable Isotope Hydrology of the Table Mountain Group

Roger Diamond

Submitted for the degree of
Doctor of Philosophy
in Geology.

Department of Geological Sciences
University of Cape Town

2014

Towerkop, 2189m, Skurweberg Formation of the Table Mountain Group, viewed from the north, showing the fractured nature of this quartzite aquifer. The Towerkop water point is just out of view, around the corner to the east, at about the level of the horizon.

"It ain't the water that's not right around here."

from Black Eyed Man, 1992

Cowboy Junkies.

ABSTRACT

Rain was collected from 2010 to 2012 at 15 locations around the Cape Fold Belt, at the same time as samples from rivers, springs, seeps and boreholes, totalling 435 samples. Precipitation ranged from -75 ‰ to +40 ‰ for δD and -12 ‰ to +8 ‰ for $\delta^{18}O$, showing seasonal patterns, with lower δ values in winter and higher in summer. Certain anomalous δ values can be attributed to individual weather events, such as thunderstorms. Using weighted data, the meteoric water line is δD = 6.15 $\delta^{18}O$ + 8.21, which is similar to previous equations. The best fit line for groundwater δ values is δD = 7.09 $\delta^{18}O$ + 10.08, the steeper gradient and higher intercept reflecting the predominance of heavy rainfall events with lower δ values in recharge, known as selection. The range of -47 ‰ to 0 ‰ for δD and -8 ‰ to -1 ‰ for $\delta^{18}O$ values for all groundwater data is about half that of the rain values, due to the averaging effect from mixing during groundwater flow. Rainfall isotope composition is negatively correlated with continentality, as defined by the product of distance to the Atlantic and the closest coast. Isotope composition of rainfall is also strongly negatively correlated with altitude, with gradients from -0.48 to -2.2 $\frac{\Delta\delta D}{100m}$ and -0.075 to -0.34 $\frac{\Delta\delta^{18}O}{100m}$. Sites that are elevated within the landscape have a reduced altitude effect, such as tall peaks, whereas mountain valleys display enhanced altitude effects. Temporal and spatial variations in the strength of the amount effect reveal meteorological variability and emphasise the need for long term monitoring.

Groundwater-fed surface waters show little systematic variation in isotope composition within catchments, indicating groundwater mixing. Differences between catchments are significant and reveal continental and altitude effects across the Cape Fold Belt. There is no significant change in hot spring isotope compositions over 40 years, confirming deep, well mixed groundwater flow. In the greater Cederberg region, groundwater abstracted from the Peninsula Formation in the Olifants River Mountains appears to be locally recharged and not in the Cederberg mountains. Abstraction in the Rietvlei Formation north and south of the Hex River anticline is being recharged at higher altitude, around 1200-1600masl, probably in the Goudini or Skurweberg Formation and moves up the stratigraphy prior to discharge. Discharge of increasingly negative δ values, a sign of deeper groundwater from higher recharge areas, could warn against overabstraction. Similar relations occur at Gamkaberg (Little Karoo) and Rooihoogte (Great Karoo), where groundwater, having been recharged at higher altitude, moves up the stratigraphy in the Skurweberg aquifer. At Gamkaberg, selective recharge of isotopically more negative large rainfall amount events, or interannual shifts in isotope composition of rainfall may account for the more negative δ values of groundwater than rain and warns against overinterpretation of short term precipitation monitoring. The δD and $\delta^{18}O$ values of springs around Table Mountain correlate positively with distance from the mountain, an amount effect. The altitude effect gradient revealed that the typical spring is recharged an average of 1km upslope of the spring at an average elevation of 330masl, into the scree aquifer. Shifts in annual mean δ values of precipitation are mimicked in the springs, proving that a component of groundwater flow is fast and shallow, whilst a deeper component must also exist to account for the steady discharge of perennial springs. An average hydraulic conductivity of 15–20m/day was calculated for the scree aquifer.

Contents

Abstract **1**

Contents **2**

List of Figures **5**

List of Tables **8**

1 Introduction **9**

1.1 Water in South Africa 9

1.1.1 Water in the Western Cape 9

1.2 Introduction to Stable Isotope Hydrology 13

1.2.1 Isotope Geochemistry 13

1.2.2 Isotope Fractionation 14

1.2.3 Kinetic Fractionation 14

1.2.4 Equilibrium Fractionation 14

1.2.5 Fractionation Factors 15

1.2.6 Measurement and Standards 16

1.2.7 Stable Isotope Hydrology 17

1.3 Stable Isotope Hydrology in South Africa 22

1.3.1 Motivation Behind this Study 25

2 Background **27**

2.1 Introduction 27

2.2 Geology — Lithostratigraphy 27

2.2.1 Saldania Belt 27

2.2.2 Cape Granite Suite 30

2.2.3 Cape Supergroup 30

2.2.4 Karoo Supergroup 38

2.2.5 Younger Rocks 38

2.3 Geology — Structure 41

2.4 Climate and Weather 43

2.4.1 Rain . . . 43
2.4.2 Temperature . . . 52
2.5 Hydrogeology . . . 52
2.5.1 Porosity and Permeability . . . 52
2.5.2 Hydraulic Parameters . . . 55
2.5.3 Hydrostratigraphy . . . 57
2.5.4 Significance of the Table Mountain Group . . . 60

3 Methods **63**
3.1 Introduction . . . 63
3.2 Sample Collection . . . 63
3.2.1 Rain . . . 63
3.2.2 Surface Water . . . 66
3.2.3 Groundwater . . . 66
3.3 Sample Preparation . . . 66
3.3.1 Mass Spectrometry . . . 66
3.3.2 Laser Cavity Ringdown Spectroscopy . . . 69
3.4 Sample Analysis and Data Correction . . . 69
3.4.1 Mass Spectrometry . . . 69
3.4.2 Laser Cavity Ringdown Spectroscopy . . . 70
3.4.3 Standards . . . 72
3.5 Data Analysis . . . 75
3.6 Maps . . . 76

4 Results **94**
4.1 Introduction . . . 94
4.2 Rain . . . 94
4.2.1 Rainfall Amount . . . 97
4.2.2 Rainfall Seasonality . . . 98
4.3 Rain Isotopes . . . 98
4.3.1 Temporal Variations . . . 100
4.3.2 Means and Weighting . . . 104
4.3.3 Deuterium Excess . . . 108
4.3.4 Local Meteoric Water Lines . . . 108
4.4 Groundwater . . . 113
4.5 Surface Water . . . 114
4.6 Other Samples . . . 116
4.6.1 Snow . . . 116
4.7 Summary . . . 117

5 Discussion **129**
5.1 Introduction . . . 129
5.2 Precipitation . . . 129
5.2.1 Source Area and Pathway Effects . . . 129
5.2.2 Isotope Effects . . . 132
5.3 Surface Water . . . 146
5.3.1 Altitude . . . 146
5.3.2 Springs, Seeps and Tributaries . . . 146
5.3.3 Baseflow . . . 148
5.4 Groundwater . . . 151
5.4.1 Altitude . . . 151
5.4.2 Hot Springs . . . 153
5.5 Regional Analyses . . . 154
5.5.1 Cederberg . . . 155
5.5.2 Hex River Mountains . . . 159
5.5.3 Langeberg – Gamkaberg – Swartberg . . . 166
5.5.4 Swartberg to Goukamma . . . 168
5.5.5 Cape Town . . . 173

6 Conclusions and Recommendations **181**

7 Abbreviations, Acronyms and Units **188**

8 Acknowledgements **191**

References **193**

List of Figures

1.1 Mean annual precipitation for the Western Cape . . . 11
1.2 Geological map of the study area . . . 12
1.3 The global water cycle . . . 17
1.4 The global meteoric water line . . . 18
1.5 Local meteoric water lines . . . 20
1.6 Source region humidity measured through d-excess . . . 23

2.1 Revised stratigraphy of the western Saldania Belt . . . 29
2.2 Stratigraphy of the Table Mountain Group . . . 32
2.3 Photograph of Peninsula Formation pebbly quartzite . . . 34
2.4 Photograph of the Hex River anticline . . . 41
2.5 Mean annual precipitation map for South Africa . . . 42
2.6 Rainfall and temperatures for stations in the Western Cape . . . 45
2.7 Rainfall and temperatures for stations in the Western Cape . . . 46
2.8 Synoptic chart: westerly wave . . . 47
2.9 Synoptic chart: southerly meridional flow . . . 48
2.10 Synoptic chart: ridging anticyclone . . . 49
2.11 Synoptic chart: cut-off low . . . 50
2.12 Synoptic chart: west coast trough . . . 51
2.13 Photograph of seeps in the Skurweberg Formation . . . 53
2.14 Piekenierskloof Formation fracture measurements . . . 54
2.15 Theoretical models of fracture porosity . . . 54
2.16 Fracture trace map for the Cederberg region . . . 55
2.17 Detailed fracture trace map for the Peninsula Formation . . . 57
2.18 Hydrostratigraphy of the Cape Supergroup . . . 62

3.1 Map of the study area . . . 65
3.2 Cumulative rainfall collector . . . 67
3.3 Hydrogen isotope sample preparation apparatus . . . 67
3.4 Oxygen isotope sample preparation apparatus . . . 68
3.5 Isotope correction procedure . . . 71

3.6 Map legend . . . 77
3.7 Cape Town map . . . 78
3.8 Twaktuin map . . . 79
3.9 Cederberg map . . . 80
3.10 Wolfkop map . . . 81
3.11 Matroosberg map . . . 82
3.12 Waaihoek and Witels map . . . 83
3.13 Drakenstein map . . . 84
3.14 Meulkloof map . . . 85
3.15 Riverndale map . . . 86
3.16 Klein Swartberg map . . . 87
3.17 Gamkaberg map . . . 88
3.18 Robinson Pass map . . . 89
3.19 Kammanassie map . . . 90
3.20 Blesberg map . . . 91
3.21 Lentelus map . . . 92
3.22 Goukamma map . . . 93

4.1 South African monthly rainfall maps . . . 99
4.2 Sample altitude histogram . . . 101
4.3 Rainfall: δD vs. time . . . 102
4.4 Rainfall: $\delta^{18}O$ vs. time . . . 103
4.5 Photograph of convective rainfall over the Cederberg . . . 105
4.6 Rainfall δD vs. $\delta^{18}O$: arithmetic means and weighted means . . . 106
4.7 Rainfall: difference between arithmetic and weighted mean δ values vs. MAP . . . 107
4.8 Rainfall: d-excess vs. MAP and continentality . . . 109
4.9 All rain water and groundwater δ values . . . 110
4.10 Local meteoric water lines . . . 111
4.11 Local meteoric water line map . . . 112
4.12 Photograph of Seweweekspoort Peak Cave seep . . . 114
4.13 Surface water: δD vs. $\delta^{18}O$ . . . 115
4.14 Monthly rainfall graphs . . . 118

5.1 Isotope data from various studies in South Africa . . . 131
5.2 Rainfall: the continental effect . . . 135
5.3 Map of the study area, showing sample locations and cross section lines . . . 139
5.4 Rainfall and groundwater: altitude effects . . . 141
5.5 Topography around sample sites . . . 144
5.6 Rainfall: annual amount effects . . . 145

5.7 Rainfall: monthly amount effects . . . 147
5.8 Surface water: δ vs. altitude . . . 149
5.9 Groundwater: δ vs. altitude . . . 151
5.10 Hot springs: δD vs. $\delta^{18}O$ . . . 154
5.11 Cederberg cross section . . . 156
5.12 Cederberg δD vs. $\delta^{18}O$ . . . 157
5.13 Schematic hydrogeology of the Olifants River Mountains . . . 158
5.14 Photograph of duplexes in the Peninsula Formation . . . 159
5.15 Hex River Mountains δD vs. $\delta^{18}O$ . . . 161
5.16 Possible south-easter snow air trajectories. . . . 162
5.17 Hex River Mountains cross section . . . 165
5.18 Langeberg–Gamkaberg δD vs. $\delta^{18}O$ . . . 167
5.19 Swartberg to Goukamma δD vs. $\delta^{18}O$ . . . 169
5.20 Little Karoo cross section . . . 171
5.21 Cape Town δD vs. $\delta^{18}O$ . . . 172
5.22 Cape Town springs δD vs. $\delta^{18}O$ . . . 174
5.23 Cape Town springs interannual shifts in δ values . . . 176
5.24 Rainfall interannual shifts in δ values . . . 177
5.25 Conceptual model for Cape Town springs . . . 179
5.26 Calculation of recharge altitude for Cape Town springs . . . 180

List of Tables

1.1 Isotopologues of water 13
1.2 Publications on stable isotopes in the Table Mountain Group 26

2.1 Hydraulic parameters for the Table Mountain Group 56
2.2 Spring and wellfield yields from the Table Mountain Group 61

3.1 Rainfall collection stations 64
3.2 UCT internal isotope standards 69
3.3 Raw data for internal standards: δD 73
3.4 Raw data for internal standards: $\delta^{18}O$ 74

4.1 Rainfall collection periods at each station 95
4.2 Rainfall collection stations 96
4.3 Rainfall: arithmetic and weighted means 107
4.4 Snow: isotope composition 117
4.5 Isotope data for rain for 2010 123
4.6 Isotope data for rain for 2011 124
4.7 Isotope data for rain for 2012 125
4.8 Isotope data for the Table Mountain springs 126
4.9 Isotope data for surface water 127
4.10 Isotope data for groundwater 128

5.1 Cape meteoric water line equations 132
5.2 Global examples of the continental effect 133
5.3 Distances from rainfall stations to the sea 134
5.4 Global examples of the altitude effect 136
5.5 Rainfall and groundwater: altitude effect gradients 137
5.6 Topographic position of sample sites 142
5.7 Description of the five rivers sampled 149

7.1 Acronyms, Units and Abbreviations 190

Chapter 1

Introduction

1.1 Water in South Africa

South Africa is a dry country. With an average annual rainfall of 450 mm/a (Dent et al., 1987; Schulze and Lynch, 2001), South Africa is clearly drier than most of the world, which averages around 1000 mm/a (Wikipedia, 2013a; Encyclopaedia Brittanica, 2013). The warm, dry climate compounds the problem of low rainfall and it is estimated that less than 10 % of rainfall becomes runoff, the rest being lost to evaporation or used by plants for transpiration (Nkondo et al., 2012). This runoff is estimated to be 50 000 GL/a, which equates to the total possible surface water yield of South Africa, although *at least* 25% of this should be set aside for ecological flows. In comparison, the estimated sustainable groundwater yield is 7500 GL/a. Actual consumption of water is around 15 000 GL/a for the country, with groundwater making up 13 %, at around 2000 GL/a (DTI, 2009; Nkondo et al., 2012; Stats SA, 2006). This shows the generally minor status of groundwater in South Africa, in contrast to aquifers such as the Ogallala in the United States midwest region where 26 000 Gl/a are abstracted (Wikipedia, 2013b) in an area of moderate rainfall, or the Nubian Sandstone Aquifer, in the eastern Sahara Desert, where Libya alone is planning to abstract over 2000 GL/a (IAEA, 2013). These are however, unsustainable abstraction rates, being higher than the recharge rates in these moderate to very low rainfall areas, and therefore qualify as groundwater mining, a practice with dire environmental, social and economic consequences.

1.1.1 Water in the Western Cape

The Western Cape has the greatest extremes of rainfall of any province in South Africa, with a maximum measured average annual rainfall of 3345 mm/a at Jonkershoek, 50 km east of Cape Town, and a minimum of 60 mm/a in the Tankwa Karoo (Schulze and Lynch, 2001). The actual maximum and minimum are likely to be higher and lower, respectively, as the rain gauges have probably not been sited in the ultimate locations that experience the extremes. Despite such a high maximum, the province receives an average of only 348 mm/a. The mean annual precipitation (MAP) map of the country, as developed by Dent et al. (1987), was refined for the Western

Cape by Beuster et al. (2009) and is shown in **Figure 1.1**. To produce this rainfall map, they used the MAP of 321 rainfall stations to select four out of six factors, based on regression analysis, as determinants of rainfall at any point: altitude, continentality, terrain roughness and distance from selected "barrier" mountain chains. From this map it can be seen that much of the Western Cape receives little rain, in the region of 200–300 mm/a, but the mountainous areas receive over 1000 mm/a. These mountains are largely made up of the rocks of the Table Mountain Group (TMG), the outcrop area of which can be seen in **Figure 1.2** and it can be concluded that most of the rainfall in the Western Cape occurs on the TMG outcrop area. Of the rain that falls, some evaporates from plants (interception) and soil, some is transpired by plants, some becomes runoff and the remainder is recharged to the TMG, a fractured rock aquifer. Due to the rugged terrain and stormy weather in the Cape Mountains, minimal research has been done on hydrological processes and our understanding of recharge, discharge and groundwater flow is poorly constrained. For example, at the biennial groundwater conference held by the Groundwater Division of the Geological Society of South Africa in 2013 in Durban, only 5 of the 70 papers presented dealt with the Table Mountain Group, and only 1 of those was from work done in a mountain area. The best studies are in the extensive compilation on the Table Mountain Group edited by Pietersen and Parsons (2002). **Table 1.2**, at the end of this chapter, contains a list of all publications that make use of stable isotopes of hydrogen and oxygen and relate to the Table Mountain Group.

The most direct way to understand groundwater flow in an aquifer is by using hydraulics, which requires water level or pressure measurements taken from boreholes penetrating the aquifer. This is not easily done, not only because of the practical difficulty and cost of siting boreholes in the Cape Mountains, but also because the fractured rock nature of the TMG porosity complicates water level interpretations. Water chemistry in the TMG aquifer is remarkably consistent across the Cape Fold Belt and in addition to the consistency, the water is very low in dissolved constituents, being generally well under 100 mg/L total dissolved solids (Rosewarne, 2002b). Although it may be possible to use dissolved chemical species as tracers of groundwater flow in the TMG aquifers (Saayman et al., 2003; Richey et al., 1998), the very low concentrations make this challenging. Stable isotopes of oxygen and hydrogen offer a solution to these problems in that they are cheaper than constructing boreholes and making hydraulic measurements. Stable isotopes are known to vary on a regional scale (hundreds of kilometres) (Rozanski et al., 1993) and with altitude (Gonfiantini et al., 2001) and the Cape Fold Belt has sufficient area and altitude change to expect isotopic variation.

Variations in hydrogen and oxygen stable isotopes are used frequently in hydrological applications, such as identifying sources of groundwater recharge (Ladouche et al., 2009), changes in vapour source or oceanic surface water and in resultant precipitation (Breitenbach et al., 2010), leaking water pipes or canals (Harvey and Sibray, 2001) and sources of bottled water (Rangarajan and Ghosh, 2011).

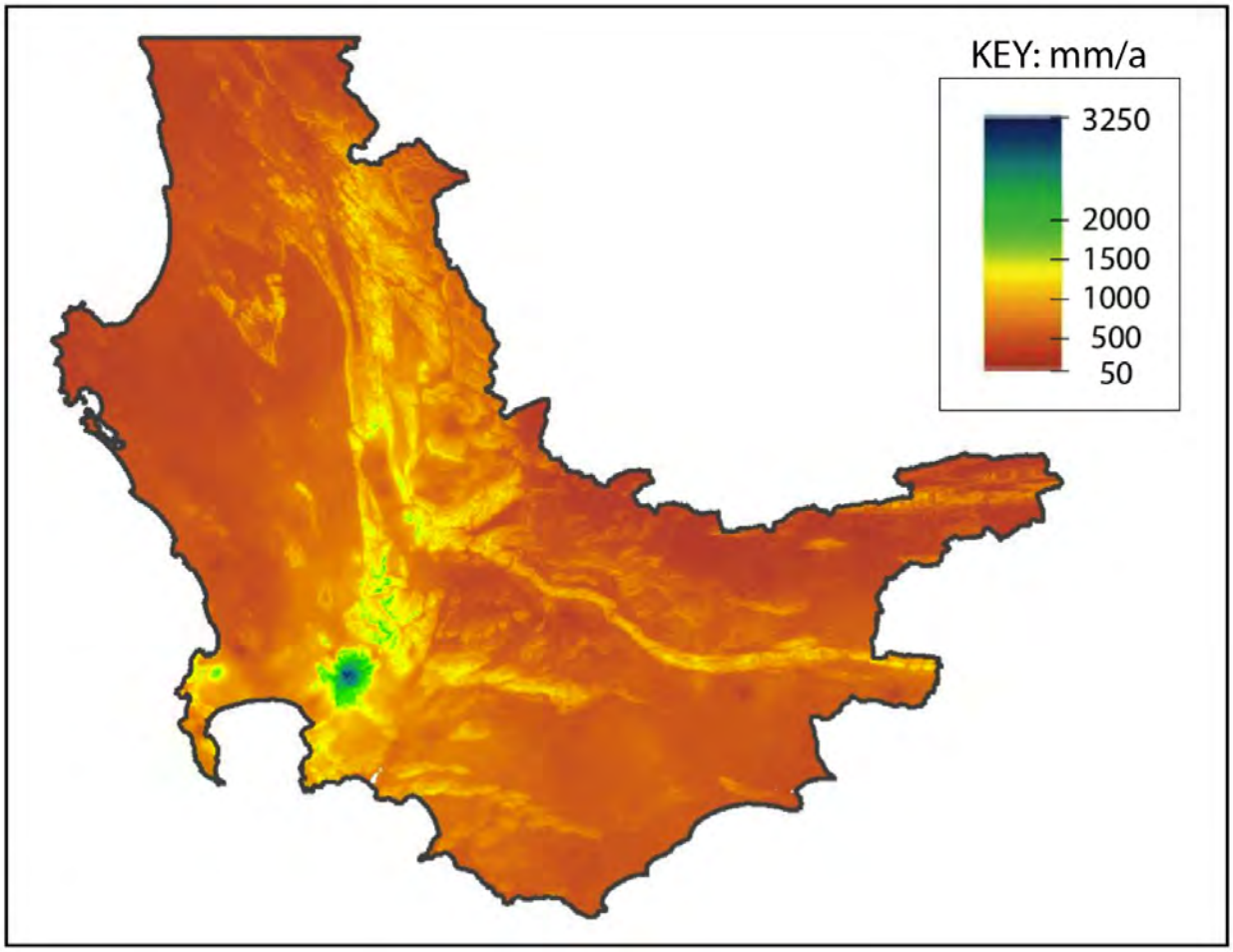

Figure 1.1: Mean annual precipitation for the western portion of the Western Cape, as calculated by Beuster et al. (2009). Precipitation amount was calculated using four factors – altitude, continentality, terrain roughness and distance from "barrier" mountains – and quantified from long term (>20 a) rainfall records from 321 stations.

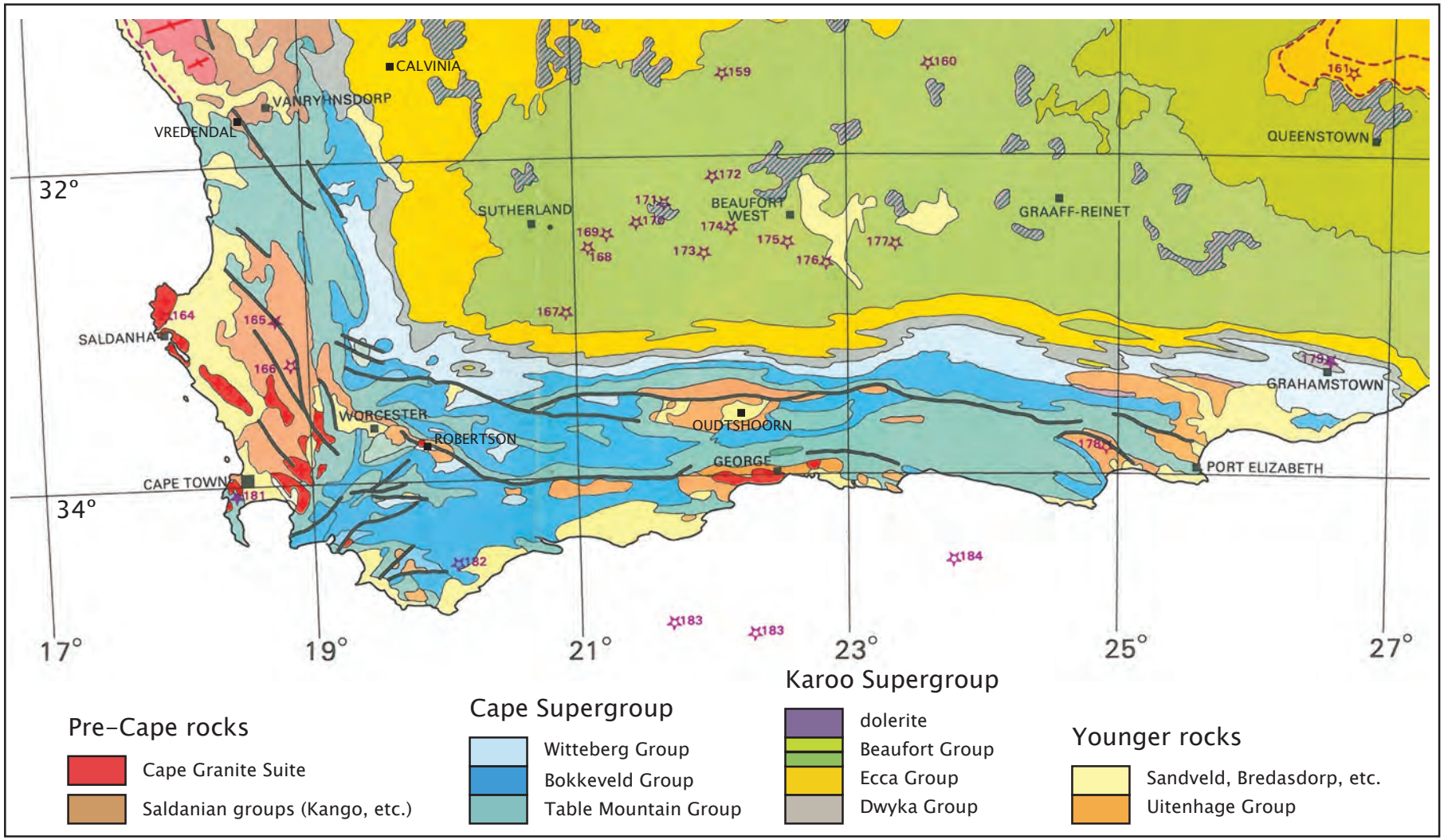

Figure 1.2: Geological map of the study area, showing the outcrop of the Table Mountain Group, where the focus of sample collection occurred. Map from Hammerbeck and Allcock (1985).

1.2 Introduction to Stable Isotope Hydrology

1.2.1 Isotope Geochemistry

The stable isotopes of oxygen were discovered in the 1920s by Blackett, and Giauque and Johnston. In 1931, deuterium was discovered by Harold Urey, who would turn out to be a major force in the understanding of the variations in stable isotope compositions (Gat, 1981b). By the 1940s, pioneering scientists were making the first attempts to apply stable isotope measurements to earth science questions, but it was only after improvements by Alfred Nier to the mass spectrometer in the late 1940s that the precision enabled the true birth of stable isotope geochemistry with early papers by Sam Epstein, Irving Friedman and Stan McCrea (Sharp, 2007). Applications to hydrology were immediately apparent and so widespread measurement of stable isotope ratios of hydrogen and oxygen commenced around the world in the 1950s, driven substantially by the World Meteorological Association and the International Atomic Energy Agency.

Isotope geochemistry can be broken into several sub-disciplines, the major break being that between radioactive or radiogenic isotopes and stable isotopes. The stable isotopes are futher broken down into light and heavy, with hydrogen, carbon, nitrogen and oxygen being the most commonly used stable light isotopes. However, the stable light isotopes and certain radioactive isotopes, such as tritium and ^{14}C, are also grouped into a branch known as the environmental isotopes, referring to their application to earth surface processes, typically in and around the biosphere, hydrosphere and atmosphere.

Hydrogen occurs as protium, ^{1}H (sometimes simply referred to as hydrogen), deuterium, ^{2}H, also written as D, and the radioactive tritium, ^{3}H, or T, with a half life of 12.33 a (Emiliani, 1987). Oxygen occurs as ^{16}O, ^{17}O and ^{18}O, all of which are stable. As a result of this spread of isotopes, water can occur as nine different isotopologues, chemically identical but isotopically different molecules, as shown in **Table 1.1**.

isotopologue	mass	abundance (%)
$^{1}H^{1}H^{16}O$	18	99.732
$^{1}H^{1}H^{18}O$	20	0.200
$^{1}H^{1}H^{17}O$	19	0.038
$^{1}H^{2}H^{16}O$	19	0.015
$^{1}H^{2}H^{18}O$	21	0.00003
$^{1}H^{2}H^{17}O$	20	0.0000057
$^{2}H^{2}H^{16}O$	20	0.0000022
$^{2}H^{2}H^{18}O$	22	0.0000000045
$^{2}H^{2}H^{17}O$	21	0.00000000086

Table 1.1: Isotopologues (isotopically different, chemically identical molecules) of water with the average abundances on earth (Emiliani, 1987).

1.2.2 Isotope Fractionation

The ratios of one isotope to another, such as $\frac{^{18}O}{^{16}O}$, vary slightly between different materials or even different reservoirs of the same substance. These differences in isotope ratios come about through preferential diffusion of the lighter or heavier isotope (or isotopologues, if in a compound) or through preferential location of the lighter or heavier isotope due to different bond energies related to mass, and are known as fractionation.

Processes that can cause isotope fractionation are chemical reactions, physical reactions or changes of state, diffusion and exchange. A chemical reaction is when two or more elements or compounds react to form different compounds; a physical reaction is where an element or compound undergoes a change of state; diffusion is when atoms or molecules disperse from high to low concentration through other material; exchange is when atoms of the same element swap places from one compound to another without causing any chemical changes. In all of these processes, molecules or atoms bearing different isotopes will proceed through these reactions at different speeds and this is known as kinetic fractionation.

1.2.3 Kinetic Fractionation

For physical, chemical and exchange reactions, the dissociation energy of molecular bonds control the reaction rate. A bond involving lighter isotopes has a lesser dissociation energy and can break more easily than the same bond involving a heavier isotope. For example, when a body of liquid water evaporates into air, the resultant water vapour (H_2O gas mixed in air) will be relatively enriched in the lighter isotopes and therefore have lower values for the ratios $\frac{D}{H}$ and $\frac{^{18}O}{^{16}O}$ than the source body. This kinetic effect will be exaggerated if the vapour is being removed rapidly, as happens in windy situations or low humidities with evaporation from natural water bodies. On the other hand, a lack of mixing in the source water body will result in a lesser fractionation effect, because the surface water layer will become depleted in ^{16}O with time.

For diffusion, the diffusive velocity is inversely proportional to the mass of the molecule and therefore molecules with lighter isotopes will diffuse faster. For kinetic fractionation there is no fixed difference in isotope ratios between the source and receptor reservoirs, as this is dependent upon factors such as time, degree of removal of one reservoir and degree of mixing of the reservoirs, as well as the actual reaction or change of state taking place.

1.2.4 Equilibrium Fractionation

If chemical, physical or exchange reactions are allowed to run to completion, then there will be a fixed isotope difference between the source and receptor reservoirs, given a certain temperature. Reactions will continue, but backwards and forwards at an equal rate, and without any net effect on isotopic composition of either reservoir. For example, at 25 °C, there is a fixed difference between the $\frac{^{18}O}{^{16}O}$ ratio in $H_2O_{(l)}$ and $CO_{2(g)}$ in equilibrium with each other. In this situation, the

kinetic effects of reaction rate are no longer important, and it is the relative preference for a heavier or lighter isotope within a chemical bond that determines which isotopes locate where. Heavier isotopes are favoured in bond positions with higher strength. To continue the above example, the covalent bonds between oxygen and carbon in CO_2 are stronger than the covalent bonds between oxygen and hydrogen in H_2O, and as the heavier isotopes remain preferentially in the stronger bond positions, the result is that $CO_{2(g)}$ will have higher values for $\frac{^{18}O}{^{16}O}$ than the $H_2O_{(l)}$.

Temperature plays a very important role in fractionation. The higher the temperature, the less the degree of fractionation, because fractionation processes are thermodynamically controlled.

1.2.5 Fractionation Factors

In order to quantify the fractionation of isotopes between two phases or compounds, the fractionation factor, α, is used, where:

$$\alpha = \frac{R_{reactant}}{R_{product}} \ ,$$

and R is the isotope ratio, such as $\frac{D}{H}$. For example:

$$\alpha D_{water-vapour} = \frac{\left(\frac{D}{H}\right)_{water}}{\left(\frac{D}{H}\right)_{vapour}} \ .$$

This factor describes the partitioning of an isotope between two phases or compounds, which is determined by the chemical bonds and other atomic scale properties of the element. Importantly, the fractionation factor is temperature dependant; in other words, at equilibrium, the isotope ratios in the reactant and product vary with temperature, as was first outlined by Urey (1947). Furthermore, this variation is systematic, in that lower temperatures result in higher fractionation factors and vica versa.

Fractionation factors are mostly numbers just above 1, and if one takes 1000 ln α, the result is approximately the difference in δ values of the reactant and product, because 1000 ln (1.00x) is approximately equal to x, and so:

$$\Delta_{X-Y} = \delta_X - \delta_Y \approx 1000 \ln \alpha_{X-Y} \ .$$

For example:

$\alpha_{(H_2O_{(l)}-H_2O_{(g)},25^\circ C)} = 1.0094$ (Kakiuchi and Matsuo (1979) in Beaudoin and Therrien (2014)),

and $1000 \ln 1.0094 = 9.4$,

so $\Delta_{(H_2O_{(l)}-H_2O_{(g)},25°C)} = 9.4$ ‰ .

This relationship holds best for smaller fractionation factors, where $\alpha < 1.01$.

1.2.6 Measurement and Standards

Isotope ratios are, by convention, the ratio of the heavier (and less abundant) isotope to the lighter (and more abundant) one. The differences in isotope ratios between materials are very slight and are not easily measured in an absolute sense. However, if measured as a relative difference between the sample and a standard of known isotope ratio, then the precision increases substantially. This is how measurements in light stable isotope mass spectrometers are made, using either a dual inlet or continuous flow system, where a reference gas is analysed alternately with the sample gas.

Stable isotope ratios are reported as deviation from an international standard. For both hydrogen and oxygen in water, the standard is SMOW, Standard Mean Ocean Water. SMOW was devised by Harmon Craig in 1961 (Craig, 1961b) as an average of previous ocean water samples from Epstein and Mayeda (1953) and Horibe and Kobayakawa (1960), but no actual sample existed. Because of this, SMOW was defined relative to NBS1 (National Bureau of Standards), a United States administered sample from the Potomac River. Because of the difficulties of not having an actual standard to analyse, the International Atomic Energy Agency in Vienna commissioned the creation of VSMOW in 1966, which was to mimic SMOW. Although VSMOW is not isotopically identical to SMOW (Clark and Fritz, 1997), it is similar enough and most workers use the acronym SMOW to define their isotope reference scale, even though VSMOW may have been used in their laboratory to calibrate their local laboratory standards (Gonfiantini, 1981; Sharp, 2007).

The Greek letter δ is used to denote the deviation of a sample from a standard, as follows:

$$\delta = \frac{R_{sample} - R_{standard}}{R_{standard}},$$

where R is an isotope ratio, such as $\frac{D}{H}$. Where relatively more of the heavy isotope (e.g. ^{18}O) is present in the sample than the standard, then the δ value will be greater than zero, whereas samples relatively depleted in the heavy isotope will have negative δ values. The $\delta^{18}O$ and δD values of SMOW are equal to 0. As the variations in isotope ratios are generally quite small, these δ values are reported in per mille (parts per thousand), using the ‰ notation. The equation combining these definitions is then:

$$\delta^{18}O_{sample-SMOW} = \left(\frac{\left(\frac{^{18}O}{^{16}O}\right)_{sample}}{\left(\frac{^{18}O}{^{16}O}\right)_{standard(SMOW)}} - 1 \right) \times 1000.$$

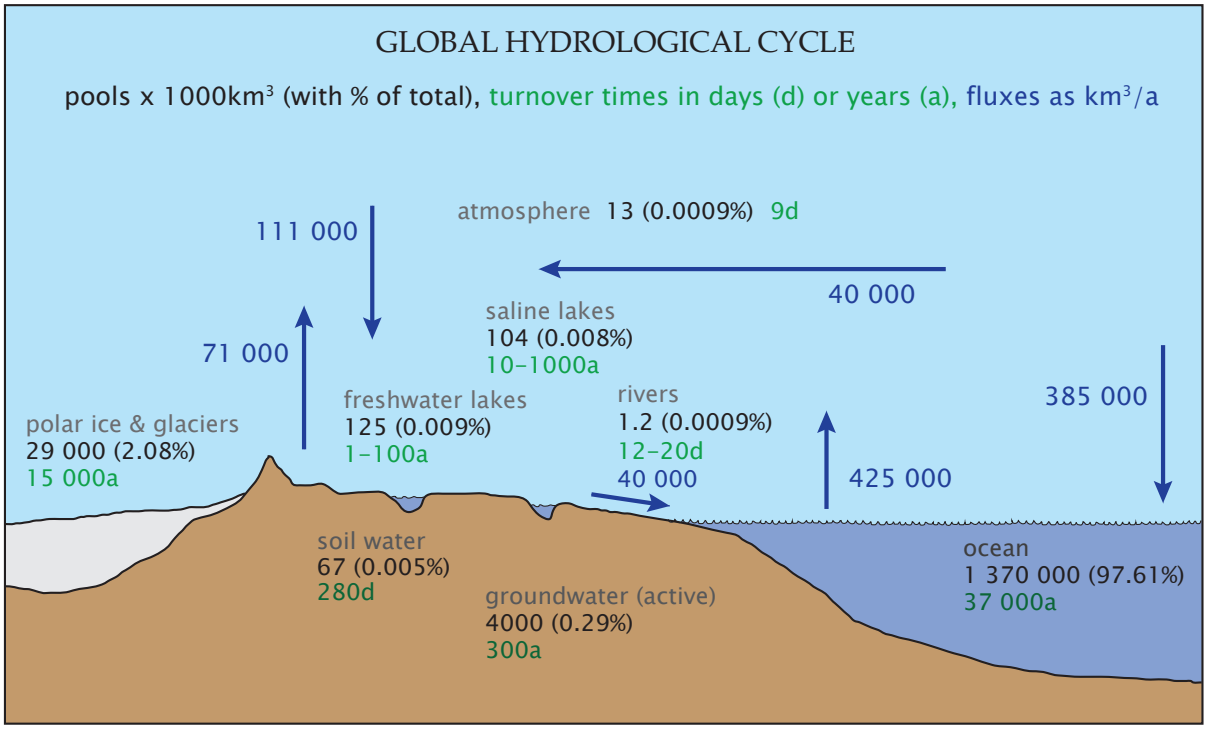

Figure 1.3: A simplified and schematic diagram of the global water cycle, showing also the reservoir sizes and turnover times within those reservoirs. It excludes water within the crust or mantle, which is unavailable, except on a timescale of many millions of years. After Reeburgh (1994).

1.2.7 Stable Isotope Hydrology

The global water cycle is extremely complex if all the interactions with geological and biological materials are taken into account, including things as diverse as weathering and volcanic eruptions in the geosphere and organic decay and drinking in the biosphere. Fortunately, the flows of water are involved in those interactions are orders of magnitude less than the major flows of water, such as evaporation from the oceans or precipitation over land, except perhaps for transpiration by plants. An attempted quantification of these flows is shown in **Figure 1.3**. This global flow of water is known as the hydrological cycle and most of the steps in this cycle are key points where the isotopic composition of parcels of water gets changed. With such complexity in this cycle, it is perhaps surprising that the variation in δD and $\delta^{18}O$ is very defined, as can be seen in the diagram in **Figure 1.4** from the landmark publication by Craig in 1961 (Craig, 1961a).

The most important observation to note in **Figure 1.4** is that most precipitation has δD and $\delta^{18}O$ values less than zero. This is primarily because evaporation from the oceans produces vapour that is depleted in the heavier isotopes relative to sea water which is similar to SMOW and has δD and $\delta^{18}O$ values close to zero. During evaporation from the ocean surface the vapour is continuously removed by diffusion and wind and mixed upwards in the atmosphere, so the air in contact with the ocean surface never becomes saturated and isotopic equilibrium cannot be reached, which means that this is a kinetic fractionation process. This results in the water vapour

in the atmosphere being more depleted in the heavier isotopes than would occur if equilibrium fractionation was taking place (Clark and Fritz, 1997). The measured values of $\delta^{18}O$ over the oceans vary from about -10 ‰ to -15 ‰, as latitude increases (temperature decreases), which are about 4 ‰ less than the equilibrium values would be. The values for δD are similarly lower than theoretical equilibrium values and range from -70 ‰ to -100 ‰ (Sharp, 2007).

Generation of atmospheric water vapour occurs mainly over the warmer oceans and it has been estimated that around 65 % is generated between 30°S and 30°N (Rozanski et al., 1993). Once an air mass is cooled, either by advection to colder climates and over a cool surface or by convection, the air can become saturated and condensation may commence. Actual condensation is dependant not only on temperature and humidity, but on the availability of condensation nucleii of the correct type (Sumner, 1988). Condensation generally proceeds slowly in response to reduced pressure or further cooling and this takes place in the presence of the vapour. As a result, condensation is an equilibrium fractionation process.

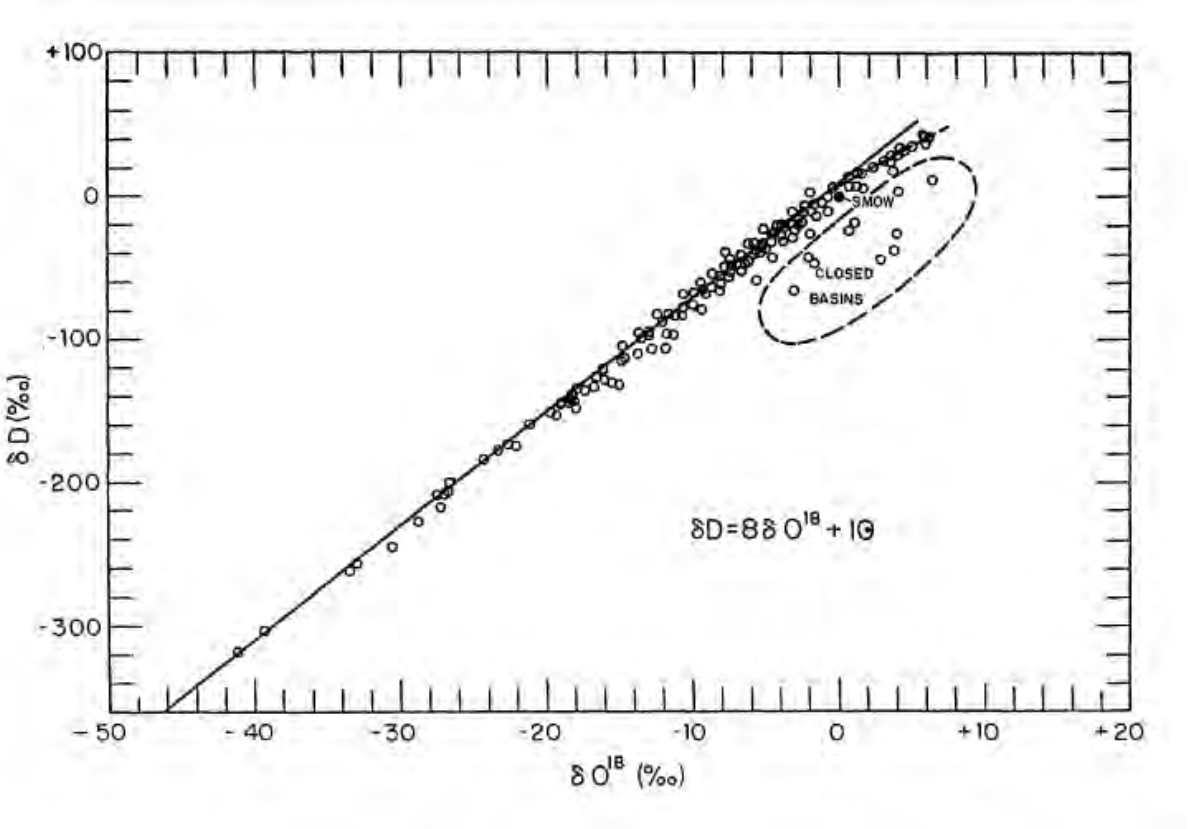

Figure 1.4: The diagram that established the relationship between δD and $\delta^{18}O$ in precipitation. The equation that describes this relationship is called the Global Meteoric Water Line (GMWL) (from Craig, 1961a).

The spread of data along the GMWL is influenced by several meteorological processes or factors, such as humidity and temperature, but it is probably rainout of atmospheric moisture, as air masses move from the tropics to the poles, that accounts for the bulk of the variation in δ values (Yurtsever and Gat, 1981). As a moisture laden air mass moves from the tropics to the poles, the moisture is removed by precipitation and the temperature or climate tends towards being colder, which not only allows further precipitation by causing more condensation, but enhances the removal of heavy isotopes by increasing equilibrium isotope fractionation factors. As the process of rainout is governed by condensation, which is is an equilibrium process, δD and $\delta^{18}O$ co-vary but with a factor of 8 difference, which is the factor by which the atomic weights vary:

$$\frac{\frac{D-H}{H}}{\frac{^{18}O-^{16}O}{^{16}O}} = \frac{\frac{1}{1}}{\frac{2}{16}} = \frac{1}{\frac{1}{8}} = 8 \quad = \frac{\Delta\delta D}{\Delta\delta^{18}O} \text{ (from GMWL of Craig (1961a)) .}$$

For a given area, with limited rainout and temperature variation, samples of precipitation will plot along a local meteoric water line (LMWL). Most LMWLs have slopes ($\frac{\Delta\delta D}{\Delta\delta^{18}O}$) of < 8, usually around 5 to 7 and a very much more limited range of δD and $\delta^{18}O$ values compared to the GMWL. When several LMWLs for areas with different climates are drawn, these lines lie semi-parallel, but displaced 'up' or 'down' on the δD–$\delta^{18}O$ plot and stack on top of each other to form the GMWL. An example is given in **Figure 1.5** that shows the data for a wide range of areas, and although each area forms more of a cluster, as the study was not to determine MWLs for each area, it nonetheless illustrates how the various areas stack up upon each other in the $\delta - -\delta$ space. The GMWL is the cumulative result of lots of LMWLs for regions of different climate, with degree of rainout being the main discriminant for the position of each LMWL. LMWLs for higher latitude regions will tend to plot lower on the diagram and vica-versa, which is clearly illustrated in **Figure 1.5**.

The reason only general, rough statements can be made about the causes of the distribution of isotope ratios in meteoric water is the extreme complexity of the hydrological cycle. Attempts have been made to build equations or conceptual models to predict isotopic values, but these have not been adequate (Sharp, 2007; Yurtsever and Gat, 1981). However, several key factors have been identified, some of which have already been alluded to above, by the first workers to interpret stable isotopes in water samples, for instance Friedman (1953), Epstein and Mayeda (1953), Craig (1961a) and Dansgaard (1964). Subsequent workers continued to develop the understanding of these key factors, until they became widely accepted as a fundamental part of isotope hydrology (e.g. Rozanski et al., 1993; Gat, 1996; Sharp, 2007). These factors are known as the latitude effect, continental effect, altitude effect and amount effect. With increasing latitude, increasing distance from the coast, increasing altitude or increasing amount of rain in a rainfall event, the isotopic composition of the precipitation becomes lighter (depleted in D and ^{18}O).

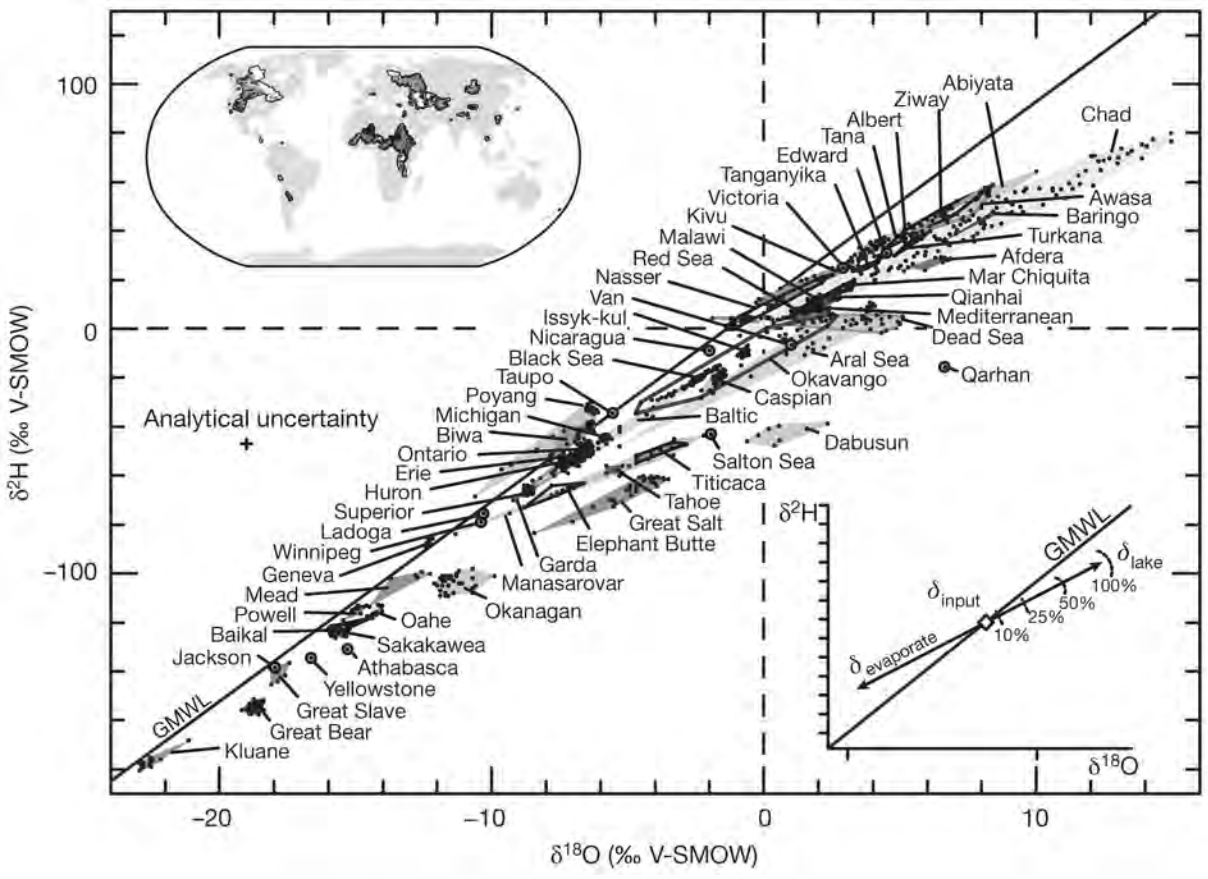

Figure 1.5: A graph illustrating the limited ranges of isotopic compositions in particular areas and how these ranges, or LMWLs, stack upon each other to form the GMWL. Diagram from Jasechko et al. (2013).

1.2.7.1 The Latitude Effect

As most moisture is sourced from the tropical oceans, because the higher temperature of the sea allows greater evaporation than in mid- or high latitude ocean areas, atmospheric moisture evolves isotopically as it moves away from the tropics. Condensation and rainout favours the removal of the heavier isotopes and so the precipitation at higher latitudes has more negative δ values. However, evaporation does still occur off the mid-latitude oceans and because the temperatures are colder, the fractionation factors will be greater, resulting in vapour relatively more depleted in the heavier isotopes than vapour that forms above the tropical oceans.

1.2.7.2 The Continental Effect

Progressive rainout is the main cause of increasingly negative δ values for precipitation that is further and further inland. In some cases, where winter rainfall occurs, cooler air inland may also reduce the amount of evaporation and isotopic change that occurs as rain drops fall through unsaturated air below the cloud. These colder inland temperatures will also increase the equilibrium fractionation factor that applies during condensation, so removing heavier isotopes more effectively from the vapour and resulting in precipitation further inland being even lighter isotopically.

1.2.7.3 The Altitude Effect

Again, the altitude effect is caused mainly by rainout that is triggered by orographic uplift, as well as a decrease in temperature, resulting in greater fractionation factors, which will drive rainout of heavier isotopes and cause a faster shift to lighter isotopes at higher altitude. Also, rain falling at higher elevations will have less distance to travel to the ground and less chance for evaporative enrichment, in which the lighter isotopes evaporate preferentially.

1.2.7.4 The Amount Effect

The amount effect also has a close relationship with rainout. Firstly, heavy individual rainstorms will tend to remove more of the vapour and cloud droplets in the air, and so with increasing rainfall in one location, the isotopic signature should become lighter. Secondly, the air below the cloud base will gradually become more saturated and colder, both of which will reduce evaporative enrichment of the later rain drops.

As can be seen from the above decriptions of the four effects, temperature and rainout are the main underlying processes that drive the various 'effects'. It is important to note that all of these effects and their underlying causes occur in a highly complex natural system where many variables contribute to the final isotopic composition of a rainwater sample. Other than temperature and rainout, factors such as humidity and source region also modify the isotopic composition. Isotope content of rainwater varies by the minute in a rainstorm (Lawrence and White, 1991; Harris et al., 2010) and between rain events, as is typical of most meteorological phenomena. Averaging the isotope composition of rainfall over longer periods, such as a month, has been found to be the most useful way of understanding the variation in isotopic signatures in an area (Yurtsever and Gat, 1981).

1.2.7.5 The Deuterium Excess

Kinetic fractionation during evaporation from the ocean surface takes place because of diffusion of water vapour molecules from a saturated boundary layer at the sea surface and into the open atmosphere . The $HH^{16}O$ isotopologue diffuses faster than all the others and so the vapour is

depleted in the heavier isotopes. If the atmosphere was saturated, then isotope exchange would occur fully between the sea and water vapour in the air, resulting in isotopic equilibrium, where the vapour would also be depleted in the heavier isotopes. However, the differences between the equilibrium and diffusion fractionation factors for D-H and ^{16}O-^{18}O are not the same and so the relative depletion of D and of ^{18}O changes with the degree of saturation, or relative humidity, **h**. As **h** increases, so more isotope exchange will occur and the closer to equilibrium fractionation the system will come (Clark and Fritz, 1997).

This means the slope along which vapour and residual water plot on a $\delta D - \delta^{18}O$ diagram will vary as a result of the degree of exchange, or isotopic equilibrium. Evaporation under lower relative humidities will generate lines with lower slopes. **Figure 1.6** shows how evaporation from sea water under 85% relative humidity conditions and then condensation at equilibrium generates water with isotopic compositions that plot along the GMWL. At different relative humidities, vapour and the resulting water samples will be displaced from the GMWL. The deuterium excess of a water samples measures this displacement with the formula:

$$d - excess = \delta D - 8\delta^{18}O$$

where δD and $\delta^{18}O$ are the values for the water sample. The d value is a proxy of the humidity of the source region.

1.3 Stable Isotope Hydrology in South Africa

Water is the single most important compound for all life. Humans need water daily, both for direct consumption and for all the other activities taking place in our society. Pre-colonial settlements in South Africa were influenced by the availability of water and the very first permanent European settlement, Cape Town, was chosen over Saldanha Bay with its better harbour, on the presence of superb quality perennial water coming from the springs at the foot of Table Mountain.

Scientific interest in groundwater has often been secondary to the practical concerns of locating and using it, a notable exception being hot springs, which seem to have attracted much attention over the years, in particular by Kent (e.g. Kent, 1949). One of the first investigations to make use of stable isotopes of hydrogen and oxygen also focused on hot springs, specifically those in Swaziland (Mazor et al., 1974) and was closely followed in 1976 by similar work by the two main authors on the hot springs of Zimbabwe (then Rhodesia) (Mazor and Verhagen, 1976). The same two authors eventually did similar work on the South African hot springs (Mazor and Verhagen, 1983), where they found a wide scatter of δD and $\delta^{18}O$ values with no systematic variation by location or average annual rainfall.

Surveys of the isotopic composition of the Gariep (Orange) River were undertaken around 1968-74 by the Council for Scientific and Industrial Research and the International Atomic Energy

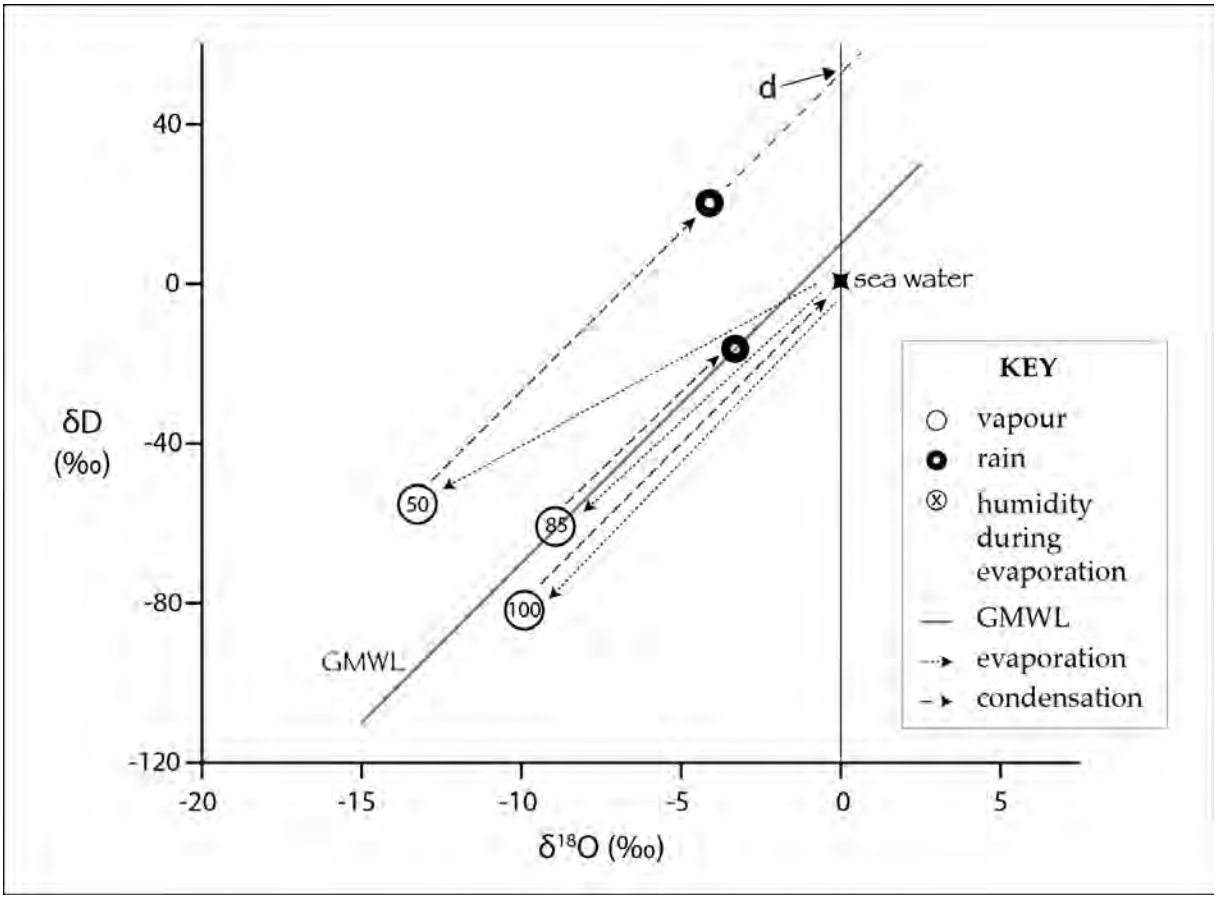

Figure 1.6: Different relative humidities in the source regions during evaporation create moisture masses with different isotope compositions due to kinetic effects as explained in this chapter. Examples in the figure show how the GMWL suggests an average global humidity at the sea surface of around 85 %, where the deuterium excess parameter is 10. For a hypothetical region with evaporation occurring under 50 % relative humidity conditions, d ≈ 50 (after Clark and Fritz (1997)).

Agency with reports being written by S Talma and others, but not published. This work found, despite disturbances to flow in the river caused by the large Gariep (then Hendrik Verwoerd) and Vanderkloof (then P K Le Roux) dams, a negative correlation between $\delta^{18}O$ and flow volume, presumably as a result of the amount effect and perhaps also for samples further downstream, an evaporation effect during low flows.

In 1975, Vogel and Van Urk surveyed ^{18}O content of precipitation and groundwater in the semi-arid regions of southern Africa, finding the groundwater $\delta^{18}O$ values to be remarkably consistent and generally more negative than the highly varied precipitation values. They concluded that groundwater is recharged during heavy rainfall events only. A similar conclusion was reached by Sami (1992) but using hydrogen and oxygen isotopes in conjunction with soil and groundwater chemistry to understand soil and groundwater salinisation in the interior of the Eastern Cape. It was concluded that periods of salt accumulation in the soil, from weathering and evaporative

enrichment of meteoric water, are followed by intense rainfall which flushes these salts to the water table. A study by Adams et al. (2001) in the Sutherland area of the Karoo reached much the same conclusions, also by using isotopic and hydrochemical observations.

Midgley and Scott (1994) compared surface water discharge to rainfall during rain events in the mountainous Jonkershoek area, east of Stellenbosch, concluding that the bulk of streamflow is from groundwater displaced by rain recharging the soil or aquifer. They also calculated a local meteoric water line (LMWL) for Jonkershoek: $\delta D = 6.99\delta^{18}O + 9.63$. A LMWL for the Western Cape was calculated by Diamond and Harris (1997) to be: $\delta D = 6.2\delta^{18}O + 10.6$, which is rather different, but closer to the best LMWL calculation, based on 12 years of data giving an equation of $\delta D = 6.41\delta^{18}O + 8.66$ (Harris et al., 2010).

A thorough examination of the hot springs of the Western Cape was done by Diamond and Harris (2000) in which monthly samples of spring discharge were taken. The spring discharge isotope ratios were seen to have a slight scatter, but no systematic variations. This study also concluded, on the basis of isotopic and geological evidence, that the springs are being recharged at high altitude in mountains made up of the Table Mountain Group and circulating to depths of over 2 km below sea level before discharging at surface. Cavé et al. (2002) used oxygen and hydrogen isotopes in the Agter-Witzenberg Valley to develop a conceptual groundwater flow model. This study also found that recharge was occurring at high altitude and circulating down before rising up in the valley area, where boreholes were intercepting flow. Deep boreholes, up to 350 m below surface, in the Citrusdal Valley contained water with more negative δ values than for shallow boreholes and surface water in the region, and was interpreted to indicate the deeper groundwater was being recharged at higher elevations than the shallow groundwater (Hartnady and Hay, 2002a). On the basis of these studies, it seems that groundwater flow occurs simultaneously at multiple levels, with more shallow local circulation occurring above deeper, more regional flow paths, which is an accepted model for groundwater flow (e.g. Domenico and Schwartz, 1998, p.79).

Determination of the source of water used by plants makes it possible to predict impacts on plant life from changes in the water table caused by groundwater abstraction. It has been found for fynbos plants growing on soils above the Table Mountain Group that different species have different water requirements and make use of water from different levels within the soil, with the conclusion that certain species will be more affected than others if groundwater levels do drop (February et al., 2004). Declining groundwater levels have been experienced in the Kammanassie Mountains, as part of the Klein Karoo Rural Water Supply Scheme. Substantial work has been done around this scheme (e.g. Kotze, 2002; Jolly, 2002; Woodford, 2002; Jolly and Kotze, 2002), including analysis of groundwater for stable isotopes of hydrogen and oxygen (Kotze et al., 2000). This study revealed that boreholes sited in low lying valleys may be tapping groundwater that was recharged at high elevation and has travelled through highly fractured 'aquizones' to reach the lower lying areas.

More applied uses of stable isotopes include fingerprinting water in urban areas in order to determine sources of leakage or pollution. In South Africa, various workers have identified isotopic differences in local groundwater versus public water supply (mains) water in Cape Town (Harris et al., 1999), local groundwater and a wastewater treatment works in Bellville, Cape Town (Saayman et al., 2000) and local rain or groundwater and mains water supply in Pretoria (Butler et al., 2000). The latter study found many boreholes with 30–50 % mains water contributions, highlighting the severe extent of leakage and water wastage.

Oxygen and hydrogen isotopes from groundwater in deep gold mines in the Witwatersrand Supergroup often have δ values that do not match current precipitation and suggest recharge during a previous, colder climate. This helps determine that primitive organisms found in these deep groundwaters are well removed from the earth's surface and do not regularly interact with the bulk of the biosphere, having profound implications for our understanding of evolution and the functioning of the biosphere (Takai et al., 2001).

1.3.1 Motivation Behind this Study

Groundwater from the Table Mountain Group is used extensively by people and the environment of the Western (and Eastern) Cape. This occurs both directly, where boreholes and springs tap the aquifer, and indirectly, where discharge from the aquifer supplies springs and wetlands, and maintains surface water flows through summer, forming the basis of much agriculture and most of the ecosystems of the region. Boreholes are used by many farmers and also for public water supply in towns such as Citrusdal and Hermanus. There is intense interest in the water resource of the Table Mountain Group aquifer system, not only from the existing users, but many other potential users, including the country's second largest metropolitan area, Cape Town.

Stable isotopes of water offer one method of improving our understanding of the Table Mountain Group aquifer system. The source of all groundwater and surface water is precipitation, and therefore, in order to interpret stable isotope measurements of groundwater or surface water, a handle on the spatial and temporal variation in stable isotope composition of precipitation is needed. This was the primary motivation behind the deployment of 15 rainfall collection stations across the Western Cape, from coast to mountaintop, over a period of two years. The focus of this study was to quantify, as much as is possible given the duration of monitoring, the patterns in stable isotope composition of precipitation. Sampling of groundwater and surface water at selected sites was included to demonstrate the possible findings that stable isotope hydrology can reveal about the inner workings of the Table Mountain Group aquifer system.

authors	date	title
E Mazor & B T Verhagen	1983	Dissolved ions, stable and radioactive isotopes and noble gases in thermal waters of South Africa.
J Midgley & D F Scott	1994	The use of stable isotopes of water (D and ^{18}O) in hydrological studies in the Jonkershoek Valley.
R E Diamond & C Harris	1997	Oxygen and hydrogen isotope composition of Western Cape meteoric water.
J M Weaver, A S Talma & L C Cavé	1999	Geochemistry and isotopes for resource evaluation in the fractured rock aquifers of the Table Mountain Group.
C Harris, B Oom & R E Diamond	1999	A preliminary investigation of the oxygen and hydrogen isotope hydrology of the greater Cape Town area and an assessment of the potential for using stable isotopes as tracers.
R E Diamond & C Harris	2000	Oxygen and hydrogen isotope geochemistry of thermal springs of the Western Cape, South Africa: Recharge at high altitude?
J C Kotze, B T Verhagen & M J Butler	2000	An aquifer model based on chemistry, isotopes and lineament mapping: Little Karoo, South Africa.
C J Hartnady & E R Hay	2002	Boschkloof groundwater discovery.
E C February, W Bond, R Taylor & R Newton	2004	Will water abstraction from the Table Mountain aquifer threaten endemic species?
C Harris, C Burgers, J Miller & F Rawoot	2010	O- and H-isotope record of Cape Town rainfall from 1996 to 2008, and its application to recharge studies of Table Mountain groundwater, South Africa.
D Barrow & R E Diamond	2011	Stable Isotopes of rain, surface water and groundwater in the Kogelberg.

Table 1.2: Oxygen and hydrogen stable isotope publications relating to the Table Mountain Group.

Chapter 2

Background

2.1 Introduction

The Table Mountain Group dominates the geology of the Western Cape, but due to extensive folding and faulting during the Permo-Triassic Cape Orogeny and subsequent sedimentation during the Mesozoic and Cenozoic, it comes into contact with numerous other geological units. A good overall knowledge of these various units is necessary to understand how groundwater within the Table Mountain Group may be constrained, recharged by, or discharged into these other units. The geological map in Chapter 1 and the cross sections in Chapter 5 may be useful to consult when reading through this chapter.

This chapter describes the geology of the Western Cape in brief, the climate of the region, with an emphasis on the rainfall and rain producing weather systems, and then concludes with a summary of the understanding of the hydrogeology of the Table Mountain Group.

2.2 Geology — Lithostratigraphy

The geology of the Cape Fold Belt region can be split into three main packages: the basement, the Cape and Karoo Supergroups, and the younger rocks. This chapter summarizes these three packages and their components, with an emphasis on the Cape Supergroup and the Table Mountain Group in particular. The basement of the Cape Fold Belt region can also be divided into three packages: the various parts of the Pan-African Saldania Belt, the Cape Granite Suite, and some transitional formations that undoubtedly precede the Cape Supergroup, but have uncertain relationships with the Saldania Belt rocks.

2.2.1 Saldania Belt

The Saldania Belt refers to a set of units in the Cape Fold Belt region that display similar stratigraphic position and deformation style, although they contain a wide array of rock types and are geographically separated. These units are exposed where the Cape Supergroup has been

stripped away by erosion, typically either on the coastward side of the Cape Fold Mountains or where large anticlines or normal faults have aided exposure of inliers. The Saldania Belt abuts the Kalahari Craton to the north (Gresse et al., 2006) and is made up of the Malmesbury Group to the north-east of Cape Town, the Cango Caves and Kansa Groups to the north of Oudtshoorn, the Kaaimans Group around George and the Gamtoos Group west of Port Elizabeth.

The Malmesbury Group has the largest area of exposure of all these groups, although the quality and area of actual outcrop is very poor due to low relief and the easily weathered nature of the formations. As such, this Group is poorly understood. The first substantial synthesis was put forward by Hartnady et al. (1974), in which the Group was subdivided into three "domains" (now called terranes), separated by fault zones. These are, from the south-west to the north-east, the Tygerberg, Swartland and Boland Terranes, with zones of tectonized rocks between them, known as the Saldanha-Franschhoek Fault, now called the Colenso Fault, between the Tygerberg and Swartland Terranes and the Piketberg-Wellington Fault between the Swartland and Boland Terranes (SACS, 1980).

The stratigraphy of the Malmesbury Group remained largely unchanged from Hartnady et al. (1974) in Tankard et al. (1982). Rozendaal et al. (1999) reported an improved understanding of the depositional setting, tectonic history and radiometric dates, as well as correlations across the various groups within the Saldania, Gariep and Dom Feliciano (in South America) Belts, but the basic lithostratigraphy remained unchanged. Then, in 2003, Belcher & Kisters substantially revised the Malmesbury Group lithostratigraphy based upon detailed structural observations within formations. These dramatic revisions appear to have not, however, been accepted by the time of publication of the 2006 volume of The Geology of South Africa, in which Gresse et al. (2006) summarize the present understanding of the Neoproterozoic to Cambrian successions of South Africa. The Belcher & Kisters revision, see **Figure 2.1**, resulted in three groups. These are, from the oldest: strongly deformed low grade metamorphic rocks, predominantly schists with minor carbonates, chert and metavolcanics, of the Swartland Group; low grade metamorphic rocks, mainly shale, greywacke and sandstone with minor conglomerate, limestone and andesite; conglomerate, grit, sandstone and shale of the Klipheuwel Group.

The Kaaimans Group, exposed along the south coast at the core of a regional anticline, comprises low grade metamorphic rocks of a great variety, include shale, phyllite, greywacke, sandstone, schist and calc-silicate. The Kansa and Cango Caves Groups occur to the north of the regional Cango Fault, a normal fault that causes repetition of the south-to-north basement to Cape Supergroup to Karoo Supergroup sequence. In contrast to the diverse rock types of the Kaaimans Group, the Cango Caves Group is dominated by greywackes and carbonates with lesser shale, sandstone and conglomerate, and the Kansa Group is made up of conglomerate, sandstone and minor shale. The Gamtoos Group, exposed in a sliver shaped inlier within a fault bounded anticlinal hinge, features mainly carbonates, phllitic greywackes and various arkosic sandstones and conglomerates (Gresse et al., 2006).

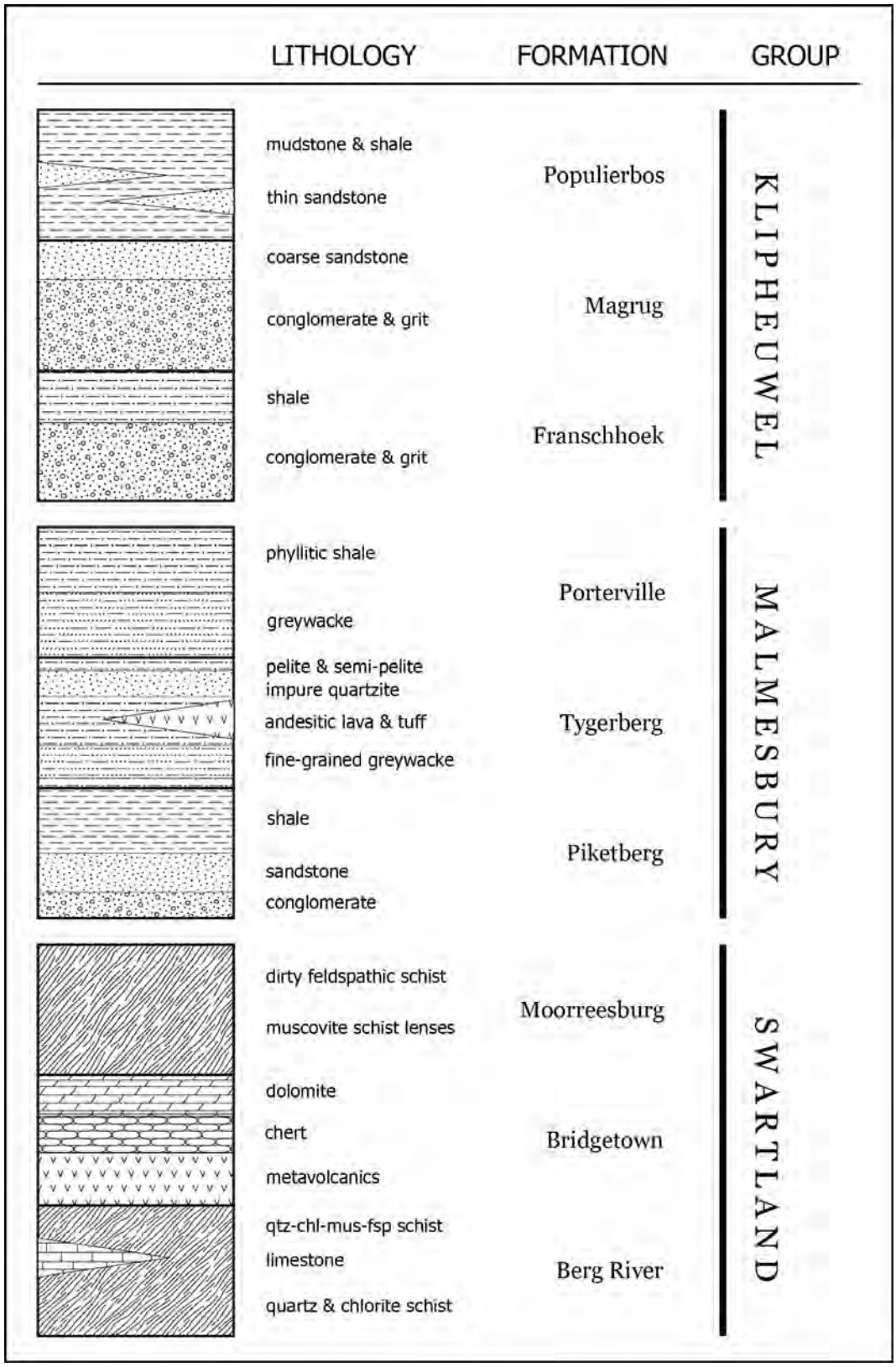

Figure 2.1: Revised stratigraphy of the western Saldania Belt formations within the Western Cape, based on Belcher and Kisters (2003).

2.2.2 Cape Granite Suite

The Cape Granite Suite consists of numerous bodies that have mostly been intruded as plutons into the metasediments of the Saldania Belt, or have been thrust into their current positions during the Cape Orogeny. The plutons occur in three clusters: a minor Richtersveld cluster, a minor George cluster and the large south-western cluster in the Saldanha Bay - Cape Peninsula - Overberg area (e.g. Schoch et al., 1977). In reality, the south-western and eastern clusters may be two parts of the same large cluster, as the lack of evidence of any granites in the intervening area coincides with a lack of outcrop of any basement at all.

The Cape Granite Suite occurs as multiple intrusions, mostly plutons, that in places have been grouped into batholiths, for example the Cape Peninsula and Darling Batholiths. Although composed mostly of granitic plutons, there is quite a range of rock types and intrusive forms in the Cape Granite Suite. Aside from a range of granitic compositions, rock types include gabbro, diorite, quartz porphyry and quartz syenite (Scheepers and Schoch, 2006). Similarly, although intrusions occur mostly as plutons, other structures such as dykes, ignimbrite flows and tectonically bounded sheets also occur (Gresse and Theron, 1992).

The plutons of the Cape Granite Suite have been dated by various workers and yield ages that range from very late Neoproterozoic to late Cambrian. Scheepers and Armstrong (2002) found the Hoedjiespunt granite gave a U-Pb zircon age of 552±4 Ma; in the same year, Scheepers & Poujol found an ignimbrite, also in the Saldanha Bay area to give a U-Pb zircon age of 515±3 Ma. These ages bracket those of da Silva et al. (2000) who reported U-Pb zircon ages of 547±6 Ma and 536±5 Ma, Schoch and Burger (1976) who found a Pb-Pb zircon age of 522±12 Ma, Jordaan et al. (1995) who found a U-Pb zircon age of 519±7 Ma on the monzonite Yzerfontein pluton and other ages, around 540 Ma, reported by Scheepers and Armstrong (2002) for plutons in the Saldanha Bay area.

Based on the above ages, field relations and petrography, 4 stages of igneous activity have been identified (Scheepers and Schoch, 2006; Rozendaal et al., 1999). These can be summarized as S-type granites in phase 1, I-type granites in phase 2, A-type granites and intermediate and mafic plutons in phase 3, and intrusive and extrusive felsic rocks in phase 4, all within a 40-50 Ma period during the Pan-African.

2.2.3 Cape Supergroup

The Cape Supergroup is one of only 9 supergroups in South Africa. It dominates the geology of the Western Cape and extends substantially into the Eastern Cape and is composed of three groups: the thickest, basal, arenaceous Table Mountain Group, the argillaceous Bokkeveld Group and the lithologically intermediate Witteberg Group. The succession was deposited during the Palaeozoic, on top of the Saldanian basement, and then overlain by the Karoo Supergroup, the youngest of all South Africa's supergroups. The Cape Supergroup, underlying basement and the older formations of the Karoo Supergroup were deformed in the Permo-Triassic Cape Orogeny.

2.2.3.1 Table Mountain Group

The Table Mountain Group is the dominant group of the Cape Supergroup due to the stratigraphic thickness and highly arenaceous character, causing resistance to weathering and leading to formation of mountains that define the geography of the Western Cape. **Figure 2.2** shows the lithostratigraphy of the Table Mountain Group in the western half of the Cape Fold Belt. The basal formations in the Cape Supergroup vary from east to west and north to south: in the west the Piekenierskloof and then Graafwater Formation occur; in the far south-east the Sardinia Bay Formation occurs; in the central to eastern areas these are absent and the Peninsula Formation lies directly on the basement; in the far north-western areas where the Cape Supergroup ends, the lower formations pinch out and the Nardouw Subgroup formations lie at the base. Controversy does exist over the assignment of the Sardinia Bay Formation, in part or whole, to the Cape Supergroup, the Saldanian Gamtoos Group or to neither.

Sardinia Bay Formation

Toerien and Hill (1989) and Bell (1980) included all the rocks between the Gamtoos Group and the Peninsula Formation as the Sardinia Bay Formation and treat this unit as the basal formation of the Table Mountain Group, possibly correlating with the Graafwater Formation to the far west. In contrast, Shone (1979, 1983) as cited in Gaucher and Germs (2006) included only the untectonized rocks into the Sardinia Bay Formation. Such differences aside, the Sardinia Bay Formation is a sequence of alternating dominant feldspathic, quartzitic sandstones, thin to medium bedded with some cross-bedding, subordinate greenish-grey to black phyllitic shales, and minor vein-quartz-pebble conglomerates (Toerien and Hill, 1989).

Piekenierskloof Formation

The Piekenierskloof Formation forms the base of the Cape Supergroup only in the north-western part of the Western Cape. The contact with the underlying Klipheuwel Formation, or Populierbos Formation of the Klipheuwel Group, if using Belcher and Kisters (2003) revision, is either an angular unconformity or disconformity (Rust, 1967), although Vos and Tankard (1981) considered that the Piekenierskloof and Klipheuwel Formations may be contemporaneous, in spite of observations by Rust (1973) that show variable clast lithologies in the Piekenierskloof Formation in contrast to locally derived (Cape Granite Suite) clasts in the Klipheuwel Formation. The southernmost outcrops are a mere 10 m thick, occuring in the Kasteelberg outlier in the middle of the Swartland (Theron et al., 1992), whilst outcrops reaching a maximum thickness of 900 m occur further north-west near Lamberts Bay (Thamm and Johnson, 2006). The Piekenierskloof Formation consists of very mature arenite and conglomerate, the latter containing identifiable clasts of resistant sedimentary and metamorphic rocks (Rust, 1967).

Graafwater Formation

The Graafwater Formation overlies the Piekenierskloof Formation conformably where the latter occurs, but extends beyond the boundaries of the Piekenierskloof basin and there overlies Saldanian basement. The Graafwater basin extended from beyond the present day Atlantic Ocean

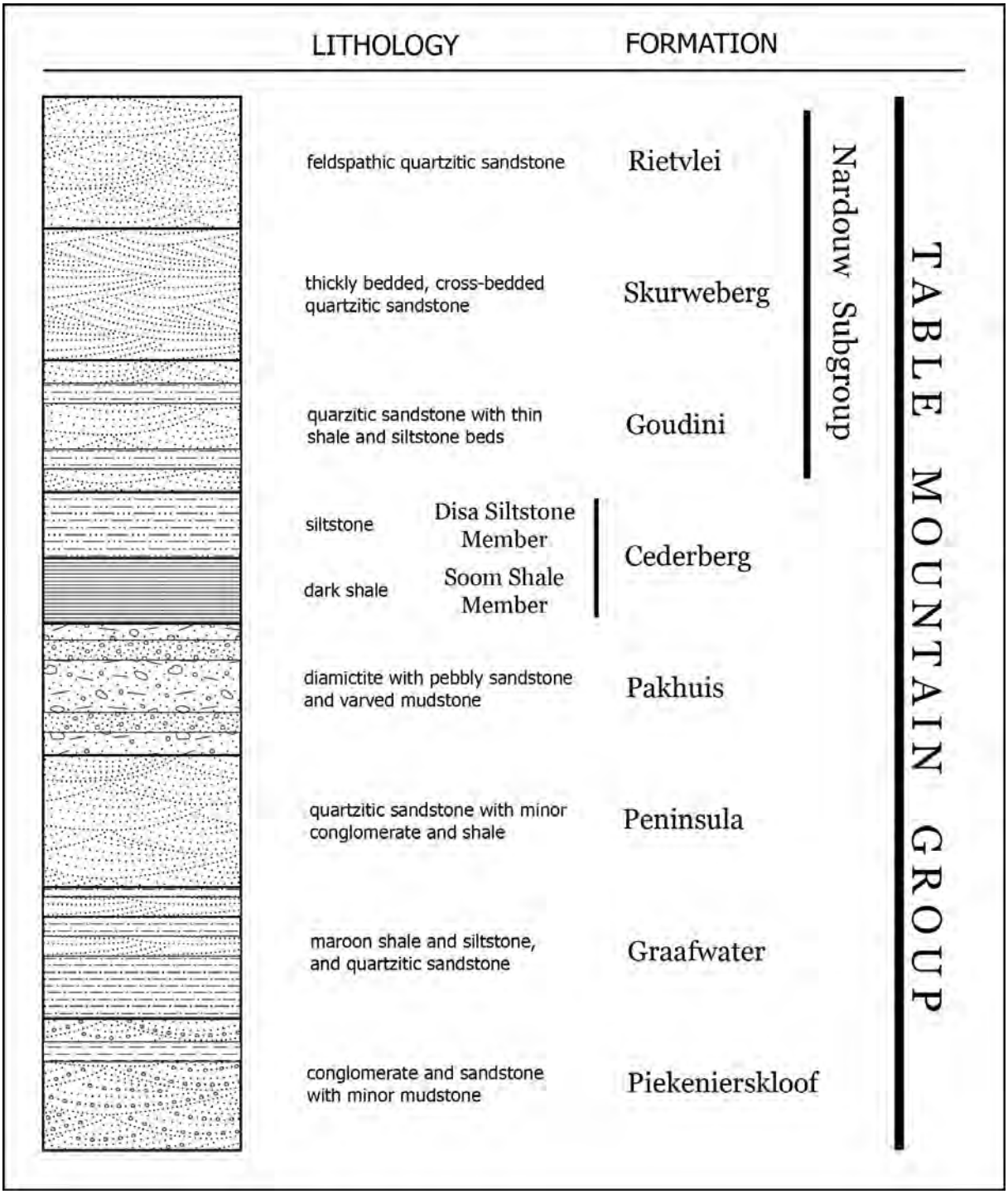

Figure 2.2: Stratigraphy of the Table Mountain Group for the western side of the Cape Fold Belt.

coast at the Olifants River Mouth, southwards to the Cape Peninsula and eastwards to the Ceres-Worcester area (Rust, 1967). The southern part of the Graafwater Formation, south of Piketberg, averages 50–100 m thickness, whilst there is a defined north-west trending trough in the Citrusdal to Lamberts Bay region where the Formation averages 250 m and reaches 430 m thickness (Rust, 1967; Thamm and Johnson, 2006). Although nearly 700 km apart and therefore probably never linked originally, several factors indicate that the Sardinia Bay Formation could be equivalent to the Graafwater Formation. These factors include: stratigraphic position, rock types and an underlying conglomerate with similarities to the Piekenierskloof Formation (Shone and Booth, 2005). The Graafwater Formation features upwards fining cycles of three distinct lithologies: a fine to medium grained quartzose sandstone; an interbedded finer grained sandstone, siltstone and maroon mudstone with dessication cracks; and a maroon mudstone (Tankard and Hobday, 1977; Rust, 1977).

Peninsula Formation

The Peninsula Formation is the dominant formation of the Table Mountain Group and indeed of the Cape Supergroup, due to its widespread occurrence, thickness and remarkably consistent, highly quartzose nature. The formation occurs throughout the Cape Basin except for the very north-western margin in the Niewoudtville vicinity where it is absent (Rust, 1973). Thickness estimation in the Peninsula Formation is hampered as one moves east by extensive thrusting, much of which is bedding-parallel and difficult to detect, leading to estimates of as much as 3000-4000 m by Rust (1973), whereas the less deformed sequences of the west, in the Cape Peninsula, reveal the thickness to be 530 m, according to Fuller and Broquet (1990).

The Peninsula Formation is remarkable for the great thickness of consistently mature quartzose sandstone. The sandstone is light grey, medium to coarse grained, mainly planar bedded, but commonly with trough cross bedding, usually thickly bedded, but in places massive or thinly bedded (Shone and Booth, 2005; Gresse and Theron, 1992). Occasional thin quartz pebble lags are found and channels also occur, reportedly a few metres in width (Theron et al., 1992) or up to 40 m deep and kilometres in extent (Hobday and Tankard, 1978; Tankard et al., 1982). In the upper 100 m of the Peninsula Formation, a zone of folding is sometimes present (Gresse and Theron, 1992), varying from simple, metre scale deformation to complex overturned and refolded zones of 75 m thickness. It occurs in the west only and the fold axes trend northwards (Rust, 1973).

Pakhuis Formation

The Pakhuis Formation occurs only in the western half of the Cape Basin, west of Swartberg Pass (SACS, 1980; Thamm and Johnson, 2006). Its thickness is given as 40 m by SACS (1980), but 150 m by Young et al. (2004), 160 m by Tankard et al. (1982) and 190 m by Rust (1981) as cited in Shone and Booth (2005). The lowermost Sneeukop Member is a structureless sandstone, with abundant striated and faceted erratics, that occurs only within the synclines of the Peninsula Formation fold-zone (Rust, 1967; Gresse and Theron, 1992). A thin sandstone, the Oskop Member, overlies the Sneeukop Member or the Peninsula Formation directly, and although continuous, is

Figure 2.3: A coarse grained example of quartzite in the Table Mountain Group. Rounded pebbles of vein quartz and gritty layers can be seen in this photograph from the upper Peninsula Formation.

lensoid in thickness with indistinct or thick bedding. The north-west Cape Basin contains the Kobe Member whilst the south-west Cape Basin contains the Steenbras Member, both quartzose diamictites with plentiful clasts, although the latter is a darker, more mature facies (Tankard et al., 1982; Gresse and Theron, 1992).

Cederberg Formation

The Cederberg Formation occurs widely in the Cape Basin, from the far west, eastwards to about 100 km west of Port Elizabeth, although in the eastern areas it is discontinuous because of smearing out along fold limbs (Shone and Booth, 2005). The contact with the underlying Pakhuis Formation is known to be both gradational (Rust, 1967) and sharp (Gresse and Theron, 1992). The formation thickness is given as between 50 m and 120 m (SACS, 1980; Thamm and Johnson, 2006). The Cederberg Formation is divided into two members. The basal Soom Shale Member is the thinner unit, seldom exceeding 15 m and is a dark grey, usually thinly laminated, micaceous shale (Theron et al., 1990). It contains a variety of fossils of some significance globally, such as conodonts, trilobites and ostracods (Theron et al., 1990; Gabbott et al., 2003). It coarsens upwards into the Disa Silstone Member, which itself continues the upwards coarsening trend and in turn has a gradational contact with the overlying Goudini Formation. The Disa Siltstone Member is a thinly bedded, argillaceous and carbonaceous siltstone and fine grained sandstone that reaches 75 m thickness and contains fossil brachiopods (Rust, 1967; Gresse and Theron, 1992).

Nardouw Subgroup

The Nardouw Subgroup used to have formation status, with three members, Goudini, Skurweberg and Rietvlei, recognized (SACS, 1980), but these have been upgraded to formations (Thamm and Johnson, 2006). In the east, corresponding names Tchando, Kouga and Baviaanskloof were in use for the three formations (Toerien, 1979), but now that the Goudini and Skurweberg are formations, they have been extended across the Cape Basin and only Baviaanskloof Formation is still in use for the area east of 21° 30' E as the continuation of the Rietvlei Formation (Thamm and Johnson, 2006).

The Nardouw Subgroup is characterized by a return to arenaceous rocks with similar depositional environments to the Peninsula Formation, after the unusual interlude of the Pakhuis and Cederberg Formations. The Nardouw Subgroup occurs across the whole Cape Basin and is the last single unit of the Cape Supergroup that pinches out in the northern extremities of the Basin (Rust, 1967). Thicknesses for the Subgroup are given as 900 m in the east and 700 m in the west (Thamm and Johnson, 2006), or 500 m (SACS, 1980).

Goudini Formation

The Goudini Formation is the lowermost formation of the Nardouw Subgroup and has a gradational contact with both the underlying and overlying formations. It occurs throughout the Cape Basin and its thickness is given as 200-300 m (Thamm and Johnson, 2006; Toerien and Hill, 1989) to as little as 30 m on Franschhoek Pass (Gresse and Theron, 1992). It is composed of thinly bedded, grey, medium grained quartzose sandstone that distinctively weathers to a reddish brown colour. Thin, pinkish, micaceous shale and siltstone layers are interspersed through the formation and some bluish grey siltstone occur nearer the top (Theron et al., 1991; Gresse and Theron, 1992).

Skurweberg Formation

This formation occurs throughout the Cape Basin and is around 200-400 m thick. The top and bottom contacts are gradational. It is composed of light grey, massive, medium to coarse grained quartzose sandstone with profuse cross-bedding, occasional thin quartz pebble lags and very minor shale (Toerien and Hill, 1989; Theron et al., 1991; Gresse and Theron, 1992). The highly quartzose nature of the Skurweberg Formation results in it forming steep cliffs and mountains, similarly but to a lesser extent than the Peninsula Formation does. The abundance of trough cross bedding can help distinguish the Skurweberg Formation from the planar bedding dominated Peninsula Formation.

Rietvlei Formation

The Rietvlei Formation occurs in the western half of the Cape Basin, up until a notional boundary at 21° 30' E, from where its stratigraphic equivalent, the Baviaanskloof Formation, then occurs eastwards. The typical thicknesses of the Formation are 90-200 m (Theron et al., 1991; Thamm and Johnson, 2006). It is generally similar to the Goudini Formation in that the bedding is thinner,

the sandstones dirtier and there are more thin shale bands than in the intervening Skurweberg Formation. Specifically, the Rietvlei Formation consists of alternating light grey quartzose sandstone, feldspathic sandstone, siltstone, micaceous shale and quartz pebble conglomerate, with some of the more quartzose sandstone units traceable for long distances (Theron and Basson, 1989; Theron et al., 1991; Gresse and Theron, 1992).

Baviaanskloof Formation

The Baviaanskloof Formation is the eastern, east of 21° 30' E, equivalent of the Rietvlei Formation. It contains the Kareedouw Sandstone Member which is lithologically similar to the Rietvlei Formation and most likely represents the easterly extension of this formation (Theron et al., 1991). The Baviaanskloof Formation thickness is given as 200 m by Toerien (1979) and Thamm and Johnson (2006). Above and below the 50 m thick Kareedouw Member, which is composed of light grey, medium grained, feldspathic sandstone, occurs greenish grey, fine grained, impure micaceous sandstone interbedded with subordinate greyish black, carbonaceous and micaceous shale (Toerien and Hill, 1989; Theron et al., 1991). Contacts with the overlying Bokkeveld Group are conformable and can be either gradational or sharp.

2.2.3.2 Bokkeveld Group

Whereas the Table Mountain Group is primarily arenaceous and has irregular stratigraphy, the Bokkeveld Group is argillaceous and distinctly cyclic. This group is distributed throughout the Cape Basin, except for the very northernmost margin near Nieuwoudtville. The deposit thickens to the south, being 1000 m near Citrusdal, 2500 m in the south-west near Bredasdorp and reaching 4000 m in the south-east near Uitenhage (Rust, 1967; Broquet, 1992).

Several upwards coarsening cycles occur, the lower three of which form the basinwide Ceres Subgroup, which itself ranges from 600 m to 1700 m thick, west to east (Thamm and Johnson, 2006). The persistence of these cycles basinwide has allowed the finer and coarser units to be given formation status: cycle 1 is formed by the basal mudrock and siltstone of the Gydo Formation coarsening into the greywacke of the Gamka Formation, overlain by cycle 2 siltstone and mudrock of the Voorstehoek Formation grading again into greywacke of the Hex River Formation, and similarly overlain by the fine grained Tra-Tra Formation and coarser Boplaas Formation of cycle 3. The argillaceous units do include minor sandstone, just as the arenaceous units of feldspathic greywacke and arenite include minor mudrocks and siltstones.

The upper portion of the Bokkeveld Group shows substantial facies variation spatially and is therefore divided into the Bidouw Subgroup in the west and the Traka Subgroup east of 21° E (Tankard et al., 1982). The Bidouw Subgroup is similar to the underlying Ceres Subgroup in lithologies and cyclicity, although the absence of marine invertebrate fossils is in contrast to their abundance in the latter (Broquet, 1992). The argillaceous Waboomsberg Formation forms the base of the Subgroup, followed by the arenaceous Wupperthal Formation, overlain by the argillaceous Klipbokkop Formation, overlain by the arenaceous Osberg Formation and capped by the

argillaceous Karoopoort Formation. In the east, the Traka Subgroup is quite different: it develops great thickness, is thoroughly dominated by clay-rich and silt-rich rocks and does not display widespread, regular cyclicity. As a result, only three formations are recognized: the thick, lithologically variable but mudrock dominated Karies Formation; the siltstone dominated Adolphspoort Formation; and the topmost mudrock-rich Sandpoort Formation (Thamm and Johnson, 2006).

2.2.3.3 Witteberg Group

The Witteberg Group caps the Cape Supergroup and, although similarly cyclic to the Bokkeveld Group, is lithologically intermediate to the Bokkeveld and Table Mountain Groups, having approximately balanced proportions of arenaceous and argillaceous rocks. The Witteberg Group is widespread in the Cape Basin, although it thins rapidly northwards in the western areas (Thamm and Johnson, 2006). The thickness of the Group is is given as over 2000 m by both Tankard et al. (1982) and Broquet (1992), but has been revised downwards by Thamm and Johnson (2006) to 1700 m, and as with the Bokkeveld Group, the thickest portions lie in the east. Not only does the abundance of sandstone increase relative to the underlying group, but the arenaceous units are more mature, and therefore lighter in colour, than the greywackes of the Bokkeveld Group, and in contrast to both the other groups of the Cape Supergroup, Witteberg Group sandstones are more micaceous (Gresse and Theron, 1992).

As with the Bokkeveld Group, the lower section of the Witteberg Group is broken into an eastern and western portion, this time along the 22° E meridian. The thinner western portion is called the Weltevrede Subgroup and is divided into the basal argillaceous Wagendrift Formation, the middle arenaceous Blinkberg Formation and the upper argillaceous Swartruggens Formation, whereas ironically, in the eastern areas where this package is thicker these units are all lumped into the Weltevrede Formation containing the Blinkberg Member, the arenaceous extension of the Blinkberg Formation (Thamm and Johnson, 2006). Running through the Witteberg Group distinctively, east and west, is the thick quartzose sandstone unit of the Witpoort Formation, which has not been assigned to any subgroup. The Witteberg Group draws its name from the low mountain range east of Touwsrivier, which in turn derives its name from the abundant exposures of the resistant, thick, white-weathering outcrops of the Witpoort Formation.

Overlying the Witpoort Formation is the Lake Mentz Subgroup, in which the Kweekvlei, Floriskraal and Waaipoort Formations form another clay-rich, sand-rich, clay-rich triplet across the whole basin. Above this, in the eastern area only, the Kommadagga Subgroup contains four formations, which tend to be less micaceous than the older formations. The basal Miller Formation, a diamictite with grit to pebble sized clasts, is followed and interfingers with the thin, pebbly quartz sandstone of the Swartwaterspoort Formation. These are overlain by the rythmically bedded shales of the Soutkloof Formation and finally the fine to medium grained sandstone of the Dirkskraal Formation (Toerien and Hill, 1989; Broquet, 1992; Thamm and Johnson, 2006).

2.2.4 Karoo Supergroup

The Karoo Supergroup covers over a third of the surface area of South Africa and reaches a total thickness of at least 4–5 km. Along the southern boundary of the Karoo Basin, it overlies the Cape Supergroup paraconformably to disconformably and extended over the current lines of mountains where it has been eroded away, evidence for this being outcrops of the lowermost units between Worcester and Robertson and even further south at Greyton (Gresse and Theron, 1992). These outliers aside, the Karoo Supergroup lies to the north of the southern arm and to the east of the western arm of the Cape Fold Belt. Only the two lowermost groups will be mentioned here, as they are the only ones that occur in any reasonable proximity to the Table Mountain Group.

2.2.4.1 Dwyka Group

The Dwyka Group is a succession of several different facies of diamictite, often repeated, to reach thicknesses of 800 m in the southern Karoo Basin. Except for two rare facies, an irregular or lensoid esker-like deposit and the variable sandstone facies, the matrix of all the diamictites and mudrocks is very fine grained, but with clasts that vary from the matrix up to large boulders (>1 m) in size (Johnson et al., 2006). The extremely varied lithological composition, size and angularity of the clasts have, amongst other properties, led to interpreting the Dwyka Group as glacial and ice-sheet deposits.

2.2.4.2 Ecca Group

This group of diverse formations formed in marine environments and is dominated by fine grained rocks, mostly shales and mudstones with some chert and tuff present; although moderately arenaceous rocks such as greywacke do occur. The Ecca Group overlies the Dwyka Group conformably and is around 2-3 km thick along the southern margin of the Karoo Basin where it occurs within the northern limit of the Cape Fold Belt (Johnson et al., 2006).

2.2.5 Younger Rocks

Rocks from the Cretaceous and Tertiary form minor yet significant components in the geology of the study area. All of these rocks are younger than the Cape Orogeny and therefore have experienced very little deformation. Most are lithified, although this becomes weaker and eventually non-existent with the very youngest formations.

2.2.5.1 The Uitenhage Group

The Uitenhage Group is a set of Mesozoic deposits that fill basins along the coast and in valleys within the Cape Fold Belt. Stretching from Worcester eastwards to Algoa Bay, the current distribution is not continuous, mainly due to the originally sporadic occurrence of the depocentre basins, but also because of some subsequent erosion. The various sub-basins are cumulatively

called the Outeniqua Basin, which has both onshore and offshore components, the latter of which will not be mentioned further here. The basins are typically half-grabens with the deeper, faulted edge being to the north, except for the largest, the Algoa Basin, which is more complex and has full graben structures (Shone, 2006; Dingle et al., 1983). Sediment reaches to around 3 km thickness in the deeper basins and thins distally, to the south. The Uitenhage Group comprises 3 formations; all 3 only occur in the Algoa and Oudtshoorn Basins and all other basins contain only the basal Enon Formation.

Enon Formation

The Enon Formation reaches 3 km thickness and is a very distinctive coarse conglomerate of well rounded Cape Supergroup quartzite pebbles and cobbles that generally weathers to dark red in outcrop, although yellow and grey colours also occur. The matrix of grit, sand and silt is cemented by red limonite and the formation can develop high, steep cliffs. Minor siltstone and sandstone lenses do occur (Shone, 2006).

Kirkwood Formation

This is a poorly cemented succession of coarse to medium grained lithic sandstone, siltstone and mudstones, reaching 2 km thickness (Shone, 2006).

Sundays River Formation

Attaining a similar thickness to the Kirkwood Formation, this formation consists of fine to medium grained, sometimes shelly, moderately cemented sandstone, siltstone and mudstone (Shone, 2006).

Cenozoic Deposits

Cenozoic deposits in the study area come in several different forms, including lithified and unlithified coastal deposits, various terraces and ancient duricrusted landsurfaces inland and on the coastal plain, more recent pedogenic duricrusts, minor alluvial, lacustrine, spring and other deposits, and ubiquitous scree and soil. Only the coastal and ancient terrace deposits will be considered here, as the others tend to be thin or scattered (Partridge et al., 2006).

Due to the primarily erosional nature of the southern African subcontinent since 65 Ma and because of the high gradient of the land surface, accumulations of most Cenozoic materials on land tend to be thin. The coastal deposits fall into 4 groups based on position along the coast.

2.2.5.2 The Algoa Group

This group largely falls outside the study area, being found from Plettenberg Bay to Port Edward. It consists of 6 formations, made up mainly of limestone, conglomerate, shelly deposits, calcareous sand and loose sand (Roberts et al., 2006).

2.2.5.3 The Bredasdorp Group

The Bredasdorp Group occurs from Plettenberg Bay to Cape Hangklip and typically overlies the Table Mountain or Bokkeveld Groups, or in places the Enon Formation, or in the George area the

Kaaimans Group and Cape Granite Suite. A highly simplified stratigraphic summary is given here.

The lowermost, thin De Hoop Formation (≤17 m) is a shelly version of the thick overlying Wankoe Formation calcarenite (≤290 m). Above this lies the thin, shelly, pebbly, quartz sand of the Klein Brak Formation (≤10 m), followed by aeolianite and calcrete of the Waenhuiskrans Formation (≤60 m) and topped by unconsolidated sand of the Strandveld Formation (≤100 m) (Roberts et al., 2006).

2.2.5.4 The Sandveld Group

The Sandveld Group is found from False Bay in the south to Elands Bay on the west coast. It generally overlies either Malmesbury Group or Cape Granite, but in the Elands Bay vicinity overlies the Table Mountain Group. The areas of greatest thickness are developed in bedrock depressions controlled by rock type and structure. A highly simplified stratigraphic summary is given here.

The basal Elandsfontyn (≤70 m) and generally overlying Varswater (≤60 m) Formations consist primarily of sand with minor carbonaceous clay and lignite layers and pebbles in places. North of Saldanha Bay, the Prospect Hill Formation (≤70 m) lies below the Varswater Formation and is made up of bioclastic aeolianite, often reddish. Overlying the Varswater Formation is the thin gravelly and shelly Velddrif Formation (about 7 m), followed by the calcarenite and calcrete layers of the thicker Langebaan Formation and capped by unconsolidated quartz sand and then calcareous sand of the Springfontyn and Witzand Formations, respectively (Roberts et al., 2006).

2.2.5.5 The West Coast Group

From Elands Bay to the Orange River mouth another series of coastal formations occurs. These formations overlie the Table Mountain Group in the southern area, from Elands Bay to north of Papendorp, where the very north-westernmost outcrops/subcrops of the Table Mountain Group are found. Although only the Alexander Bay and Curlew Strand Formations have been named, other units overlie and underlie these. Overall the group is dominated by sand, with minor mud, calcified sand, gravel and other rock or sediment types (Roberts et al., 2006).

2.2.5.6 The African Surface

Erosion and planation across southern Africa in the Tertiary led to the development of what is referred to as the African Surface. Remnants of this surface are still found today and are characterized by a duricrust, up to 8 m thick (SACS, 1980), overlying a thick weathered profile, usually kaolinitic and up to 50 m thick (Partridge and Maud, 1987), although this is not always the case and depends on the bedrock. Interestingly, the duricrust may be composed of silcrete, calcrete or ferricrete (Dingle et al., 1983). Subsequent erosional surfaces, the most notable being the *post-African I* and *post-African II* have not developed significant profiles of either weathered or consolidated material (Partridge and Maud, 1987; Partridge et al., 2006).

Figure 2.4: View south-west from the Matroosberg rainfall collector site looking along the hinge of the Hex River anticline in the syntaxis of the Cape Fold Belt. The fractured nature of the Table Mountain Group formations is apparent in this photograph. Two faults, both with limited displacement on them (tens of metres at most), are indicated.

2.3 Geology — Structure

The Table Mountain Group was deformed during the Cape Orogeny, a multiphase compressional tectonic event spanning the Permo-Triassic boundary, with four episodes of deformation having been dated: 278, 258, 247 and 230 Ma (Hälbich, 1992). Deformation occurred in such a way that three major structural domains are evident. The western branch of the Cape Fold Belt with open, upright folding and normal faulting is arcuate and convex inland, striking in a north–south direction in the southern parts near Paarl, and north-northwest–south-southeast in the northern parts near Vanrhynsdorp. The southern branch of the Cape Fold Belt is similarly arcuate and convex inland, but with folding and faulting striking east–west at the western end near Robertson and east-southeast–west-northwest in the eastern parts near Port Elizabeth. Deformation in the southern branch is more intense, with strong northward vergence, overturning and thrusting. The

southern and western branches merge in the syntaxis, stretching from the coast at Hermanus to the Karoo near Touwsrivier. In this domain, folding and faulting is more chaotic, although mainly striking north-east–south-west, and deformation is intense (Söhnge, 1983; de Beer, 2002).

Throughout the Cape Fold Belt, the compressional tectonic regime that reigned during the Cape Orogeny was inverted (became extensional) upon breakup of Gondwana during the Triassic and Cretaceous (de Wit and Ransome, 1992). Hälbich (1992) shows that both new faults with normal movement probably developed and some of the previous reverse faults were reactivated and experienced normal motion as the continents moved apart. This is most clearly demonstrated by the Cretaceous graben or half-graben basins in which the Uitenhage Group was deposited. Of note are the Kango and Worcester Faults, which have normal vertical displacements up to several kilometres and have moulded the mega-scale geography of the Western Cape, in which the TMG is duplicated, forming parallel rows of 2000 m high mountains.

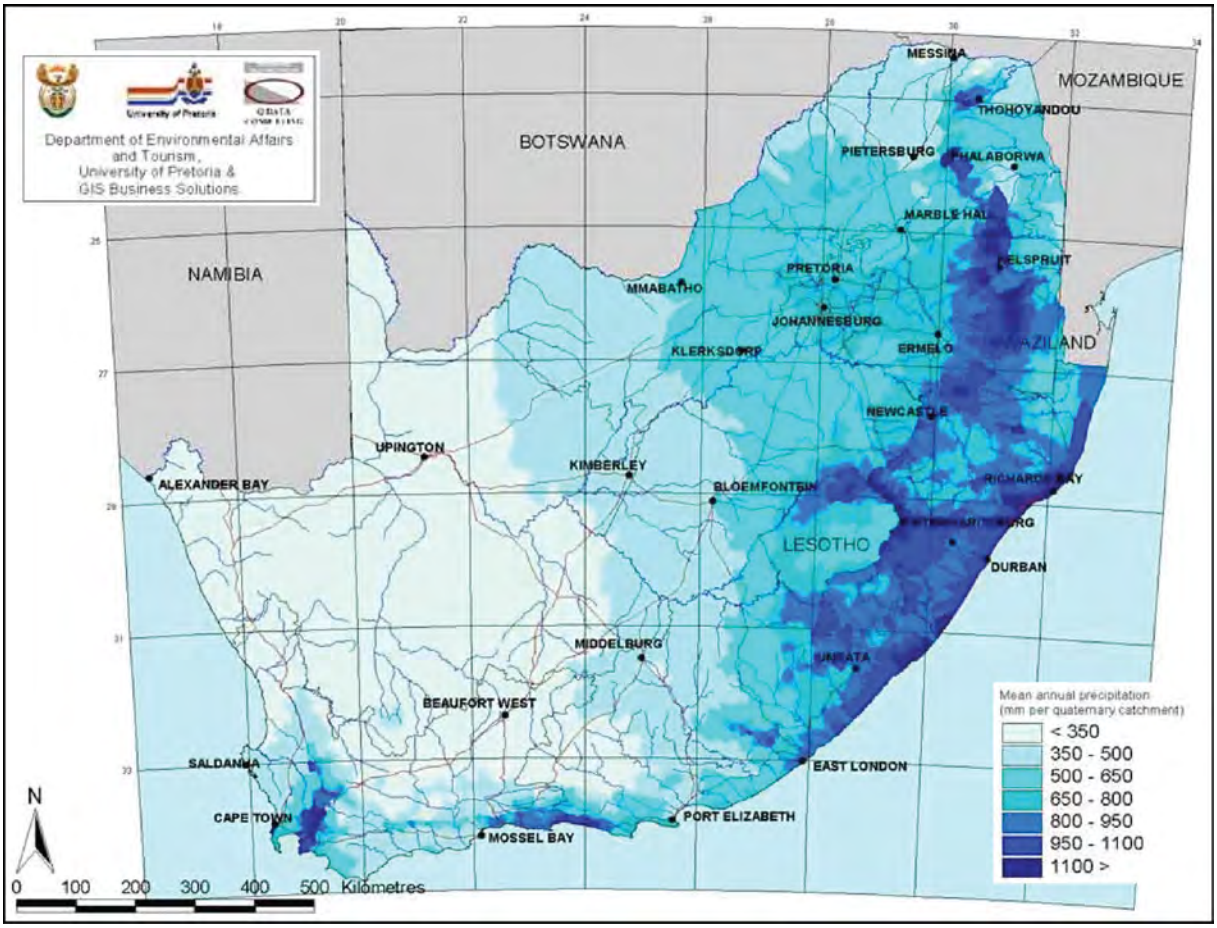

Figure 2.5: Mean annual precipitation map for South Africa.

2.4 Climate and Weather

The climate and weather of an area has an equal importance to the geology in determining the hydrogeology of an area. Various aspects of the climate, such average annual rainfall and seasonality of rainfall and temperature are important. The weather too plays a role in determining the hydrogeology as it dictates the intensity and duration of rainfall events, the reliability of rain bearing storms and the forms of precipitation that occur. Very importantly, all of this influences the isotopic composition of the precipitation and a thorough understanding of the climate and weather is essential for interpretation of the measured isotopes.

In 1911, Alexander Knox, a member of the convocation of the University of the Cape of Good Hope (a previous name for The University of Cape Town), had this to say in the opening of the chapter on South Africa in his book *The Climate of the Continent of Africa*: "Speaking generally of Southern Africa south of, say, 19° or 20° S., it may be said that the rainfall increases from west to east along any parallel, except in the extreme south of Cape Colony where irregularities exist, ... " (Knox, 1911). It is within these "irregularities" that the study area wholly falls and therefore, a brief mention of the climate and weather patterns is warranted. The study area experiences a wide range of climates due to three main factors, these being size, position and geography.

The size of the study area is somewhat over 100 000 km^2, encompassing most of the Western Cape and going into the Eastern Cape. This is large enough to experience gradients in climate simply due to distance. The position of the study area at the southernmost tip of Africa places the region just far south enough to be within the westerly wind belt and experience mid-latitude cyclones regularly in winter and occasionally in summer. However, the region is still close enough to the equator that it experiences tropical influences in summer and is on the fringes of the global southern desert belt, centred along the 30th parallel. The position is also unique in that the region is subjected to effects from both the cold upwelling of the Benguela Current on the west coast and the warm, tropically derived water of the Agulhas Current on the east and south coast. Finally, the geography of the region is complex, with variations in climate caused by the coast to inland gradient and the presence of mountain ranges, which block or funnel weather systems around, generate orographic rainfall and cause rain shadows.

Climate in the study area ranges from *warm temperate* along the south coast, where rain falls all year round, especially against the south-facing slopes of the Langeberg, from Swellendam to Port Elizabeth, to *hot desert* in the Tankwa Karoo, where some years there is no rain.

2.4.1 Rain

Cape Town experiences a typical *Mediterranean* climate with cold wet winters and warm dry summers. Moving north from Cape Town, the winter rainfall decreases until desert conditions are reached at the Gariep River; moving north-east, the winter rainfall decreases and summer rainfall increases until the central Karoo which experiences only summer rainfall; moving east,

winter rainfall is maintained and summer rainfall increases, until the coast veers north-east at Port Elizabeth, cutting out winter rain by East London. The general pattern of rainfall is greatly modified by mountains, as seen in **Figure 2.5**. Rainfall is increased in the immediate vicinity of mountains, both the windward and leeward side, and only a significant distance beyond the leeward mountain flank does the rainfall decrease.

The above patterns are illustrated in the diagrams in **Figures 2.6 & 2.7**. The decrease in rain northwards is seen by the drop in rainfall from Cape Town to Vredendal. At the same latitude as Vredental, rainfall increase due to both some summer rain and the effect of elevation can be seen at Calvinia. The change from Cape Town to Robertson shows three effects: decreasing winter rain because of distance eastwards; decreased rainfall because of a rain shadow behind the first line of mountains of the Cape Fold Belt; and a small increase in summer rain. The difference between Cape Town and Port Elizabeth shows a clear decrease in winter and increase in summer rain. The same two effects are visible at George, as well as an overall increase caused by proximity to the Outenikwa (Langeberg) Mountains. George to Oudtshoorn illustrates the combined effect of rainfall decreases from the coastal-inland gradient and a rain shadow.

The study area has a remarkable array of weather scenarios that can produce rain. A brief discussion of these follows, based largely on Preston-Whyte and Tyson (1988) and SAWB (1996). There are 5 main weather scenarios that can cause rain and all of these are related to some form of pressure trough of cyclonic feature (both low pressure) at the surface and into the middle and sometimes upper atmosphere. Of these 5, 4 occur in conjunction with or after the passage of a frontal depression, also known as a mid-latitude cyclone.

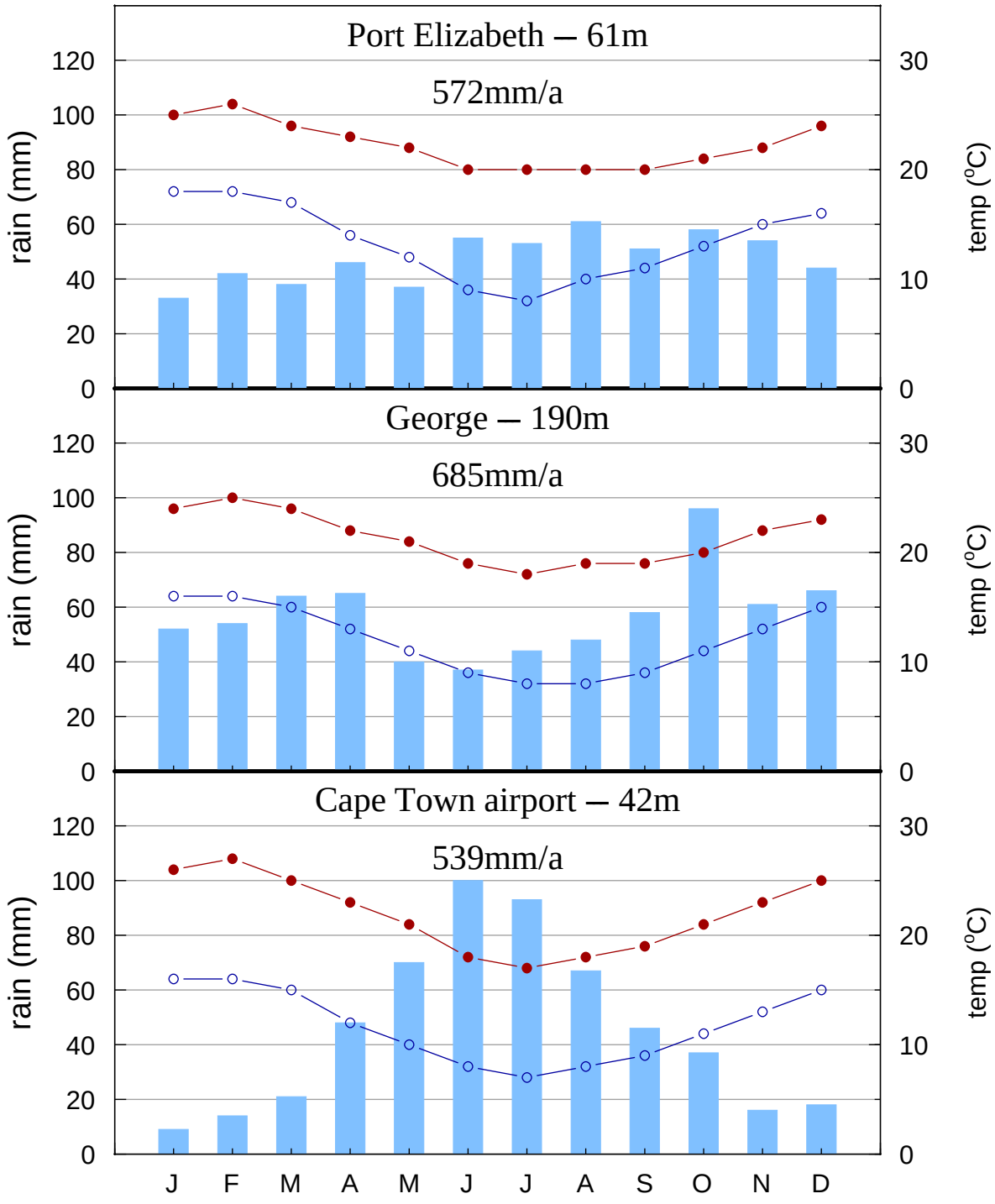

Figure 2.6: Rainfall and minimum and maximum temperature graphs for selected locations in the Cape Fold Belt region. The station altitude is given in metres above sea level. Locations are shown in the map in Chapter 1. Data for 1979–2000 (CSAG, 2013).

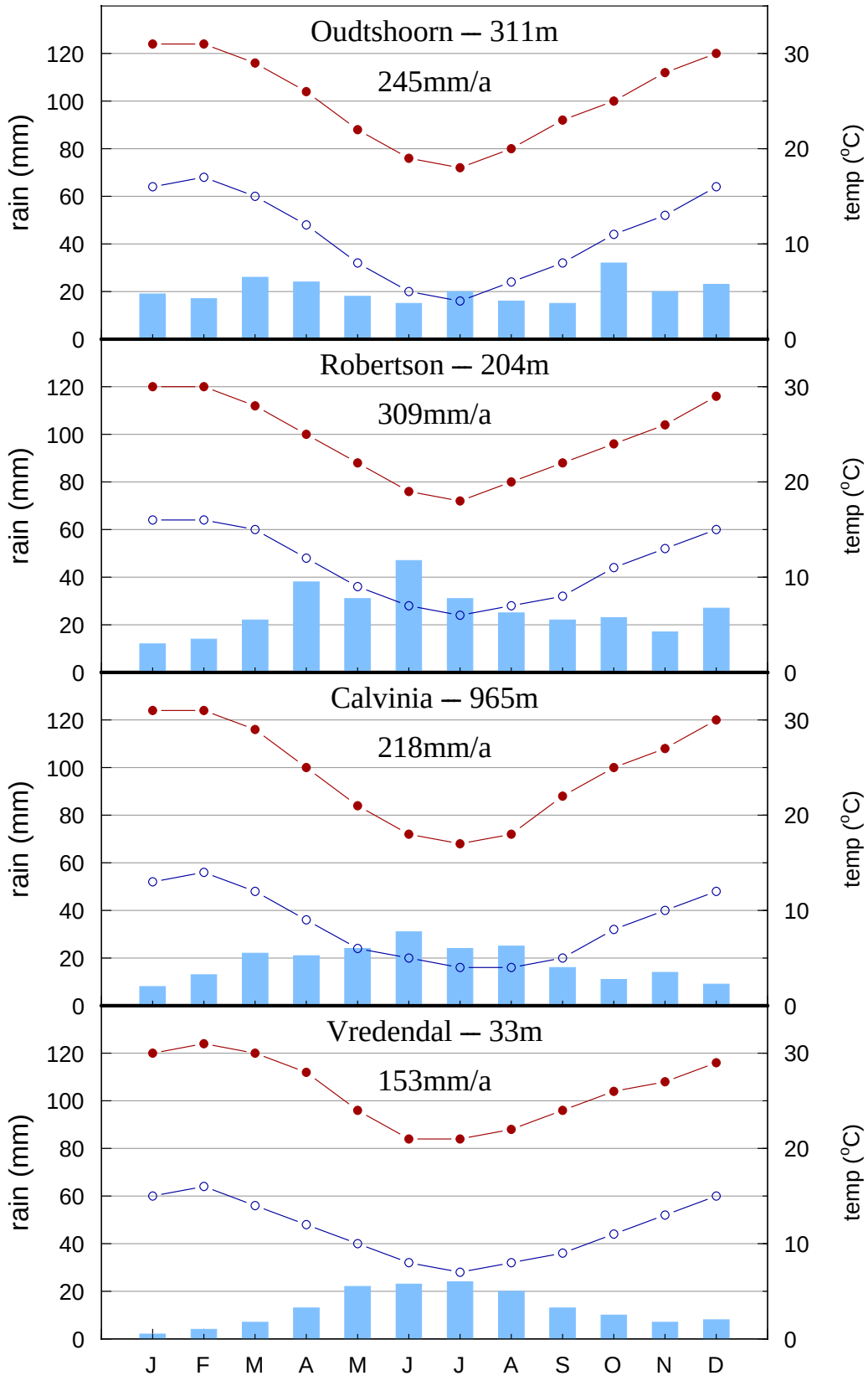

Figure 2.7: Rainfall and minimum and maximum temperature graphs for selected locations in the Cape Fold Belt region. The station altitude is given in metres above sea level. Locations are shown in the map in Chapter 1. Data for 1979–2000 (CSAG, 2013).

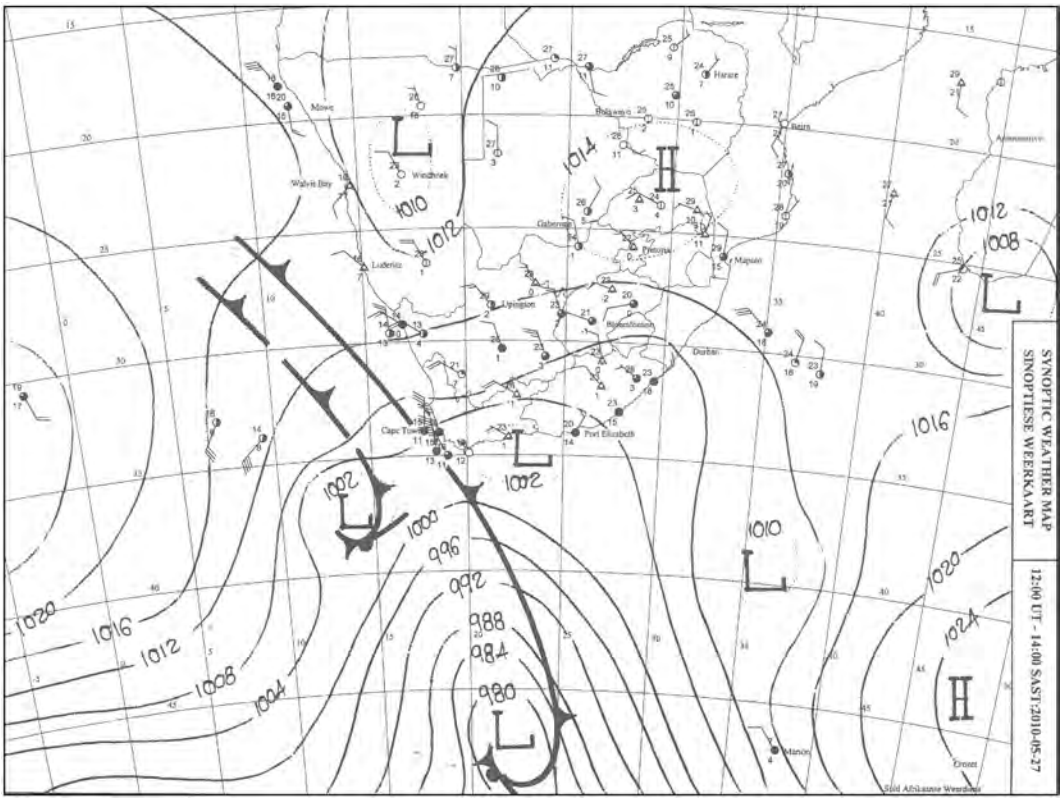

Figure 2.8: Synoptic chart from SAWS for 14h00 SAST on 27th May 2010 in which a westerly wave can be seen approaching South Africa. Rainfall from this system on this day was up to 73 mm, at Kirstenbosch and reached far north, with 10 mm at Springbok and 3 mm even at Alexander Bay.

2.4.1.1 Westerly Wave

Frontal depressions form at the polar front, at around 60°S in the south Atlantic Ocean, and move north-eastwards until they begin to decay and move south-eastwards. They feature a warm front and cold front, where air masses of different temperature meet, and the whole system rotates clockwise in the southern hemisphere. If they move far enough north, they can push a cold front over southern Africa. Uplift of warmer, moist air ahead of the cold front can cause a line of continuous rain at the front typically lasting a few hours, and instability behind the front can lead to typical intermittent 'clearing showers' that may persist for a day or two. Rainfall is mainly in the south-western Cape, but can, in extreme cases, once or twice a year, occur over the whole subcontinent, even precipitating rain or snow as far north and inland as Windhoek and Johannesburg. The example in **Figure 2.8** shows the wave shape of the isobars as the system moves west to east.

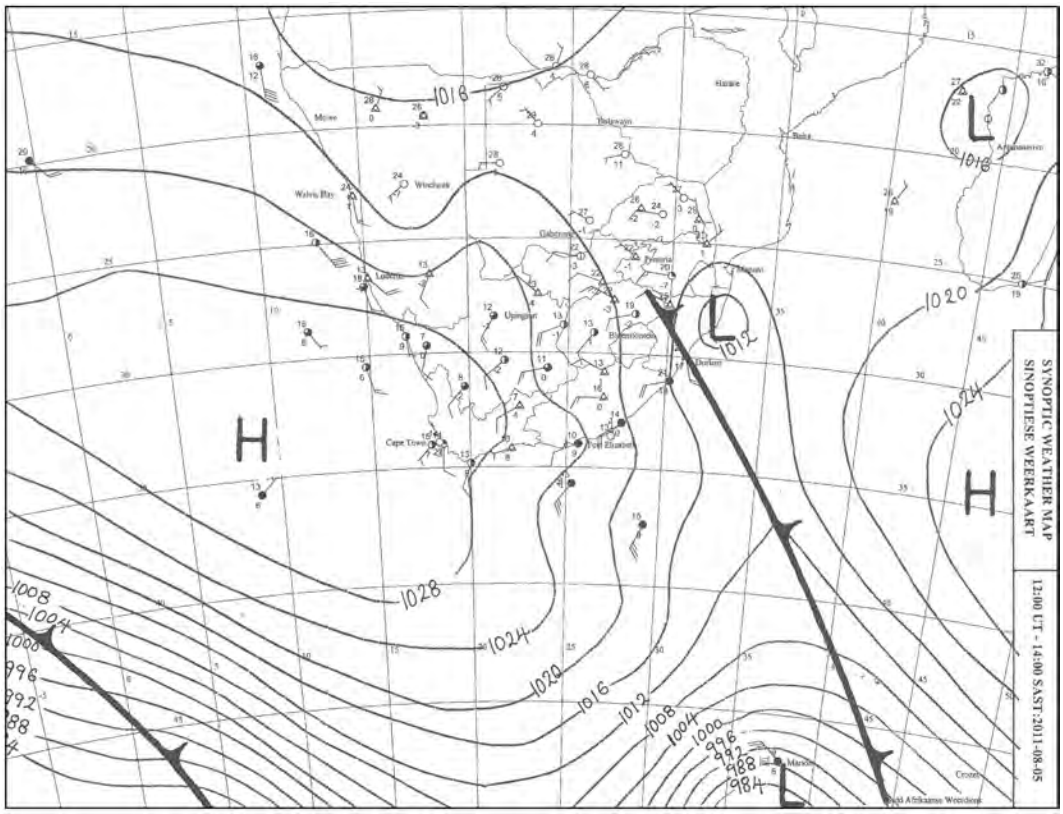

Figure 2.9: Synoptic chart from SAWS for 14h00 SAST on 5th August 2011 in which post-frontal conditions are causing southerly meridional flow. Rainfall was up to only 11 mm, at Mossel Bay, but was widespread, occurring at almost every SAWS station in the Western Cape as well as into the southern parts of the Northern Cape.

2.4.1.2 Southerly Meridional Flow

After the passage of a cold front, strong southerly airflow can persist for a day or two, starting off as south-westerly airflow immediately after the passage of the cold front, and then swinging to southerly flow (**Figure 2.9**). This usually advects very cold air and showers to the southern Cape and Eastern Cape coastal regions. Snow on mountains of the Western and Eastern Cape can result. Much of the rain in the central parts of the Western Cape results from this weather pattern, as the frontal rain that approaches from the north-west and west has fallen out on the western peaks of the Cape Mountains and so these central regions are in a rain shadow for westerly winds.

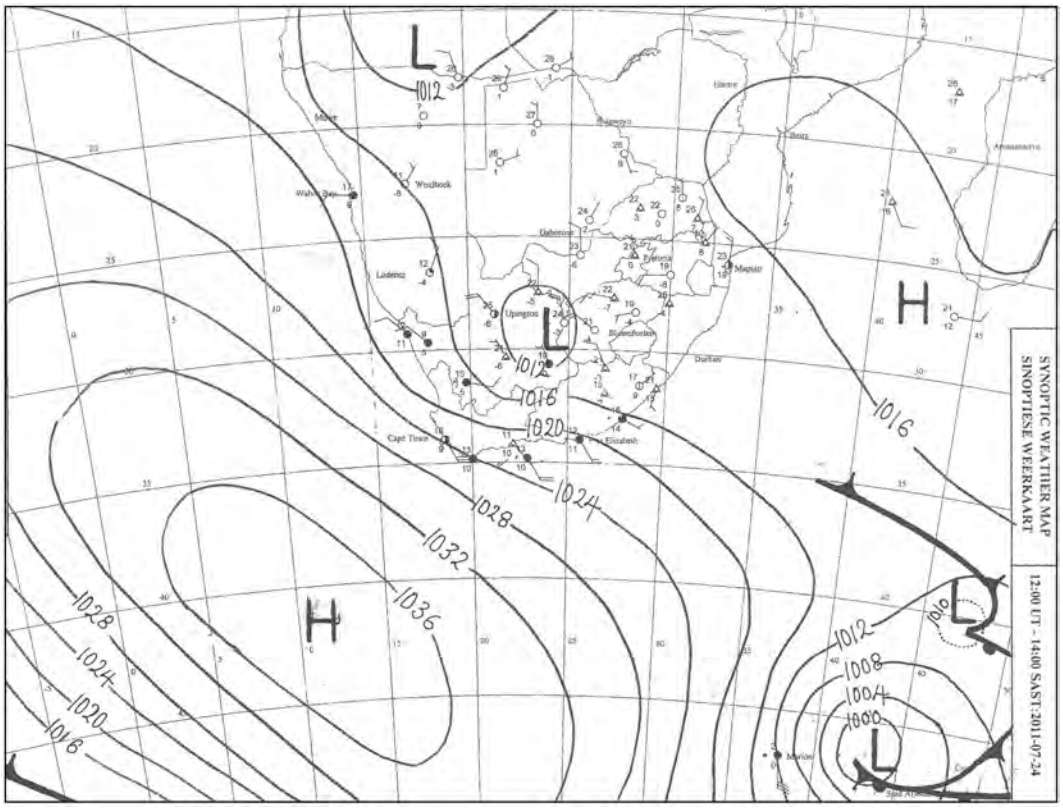

Figure 2.10: Synoptic chart from SAWS for 14h00 SAST on 24th July 2011 in which the South Atlantic High Pressure is moving south-eastwards after the passage of a cold front, seen dissipating to the south-east. Rainfall from this system was concentrated in the southern and eastern portions of the Western Cape, with up to 68 mm for the day, at George.

2.4.1.3 Ridging Anticyclone

A day or two after the passage of a cold front, the South Atlantic High Pressure cell can ridge south of the subcontinent. Moisture is picked up off the Indian Ocean and advected into an area of unstable conditions. The rainfall that results is usually confined to the eastern and central parts of the country with only orographically induced cloud evident in the far west, but when this system intensifies, the rain becomes more widespread in the eastern or central parts and the orographically induced cloud in the west increases to the point where it precipitates. This condition is known as a *black south easter*, named for the low, dark clouds that accompany this type of rain event. The normal white, fluffy or smooth *table cloth* on Table Mountain thickens and emits rain, often at a 45° angle or less, due to the intense wind, from the base of the darkened cloud. Ridging anticyclones typically cause rainfall in the eastern and southern portions of the Western Cape, as occurred in the example given in **Figure 2.10**.

The westerly wave, southern meridional flow and ridging anticyclone above are common weather scenarios, although a black south easter develops only infrequently, a few times per year. The cut-off low and west coast trough described below are not common.

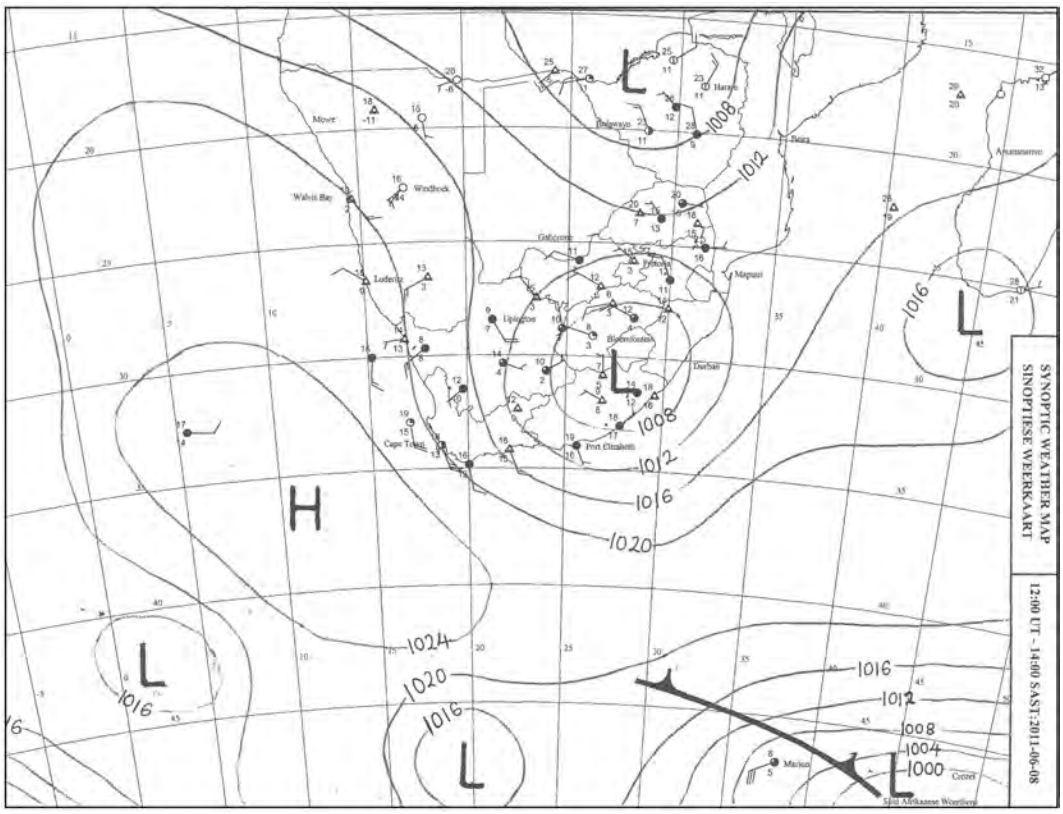

Figure 2.11: Synoptic chart from SAWS for 14h00 SAST on 8th June 2011 in which a cut-off low can be seen over the Eastern Cape. This system started south-west of the country on the 6th and intensified, exiting the country to the south-east on the 9th and dissipating thereafter. Rainfall from this system on this day (8th) reached 103 mm, in Ladismith.

2.4.1.4 Cut-Off Low

A cut-off low occurs when a cold front spawns a closed cyclonic cell that drifts northwards, out of the westerly wind belt. The cut-off low is a deep system with substantial uplift and generates heavy rain. As the low is out of the flow of the westerlies, it is often stationary or slow moving and the rain therefore falls on a relatively small area and can be for a period of days, usually causing floods. The example in **Figure 2.11** shows the most intense, third day of a four day cut-off low system, where rain occurred over the whole of the Western Cape, starting in the west and moving east. The floods of January 1981 that nearly obliterated the small town of Laingsburg were caused by a cut-off low. These systems can affect most of the country, but particularly the southern portions.

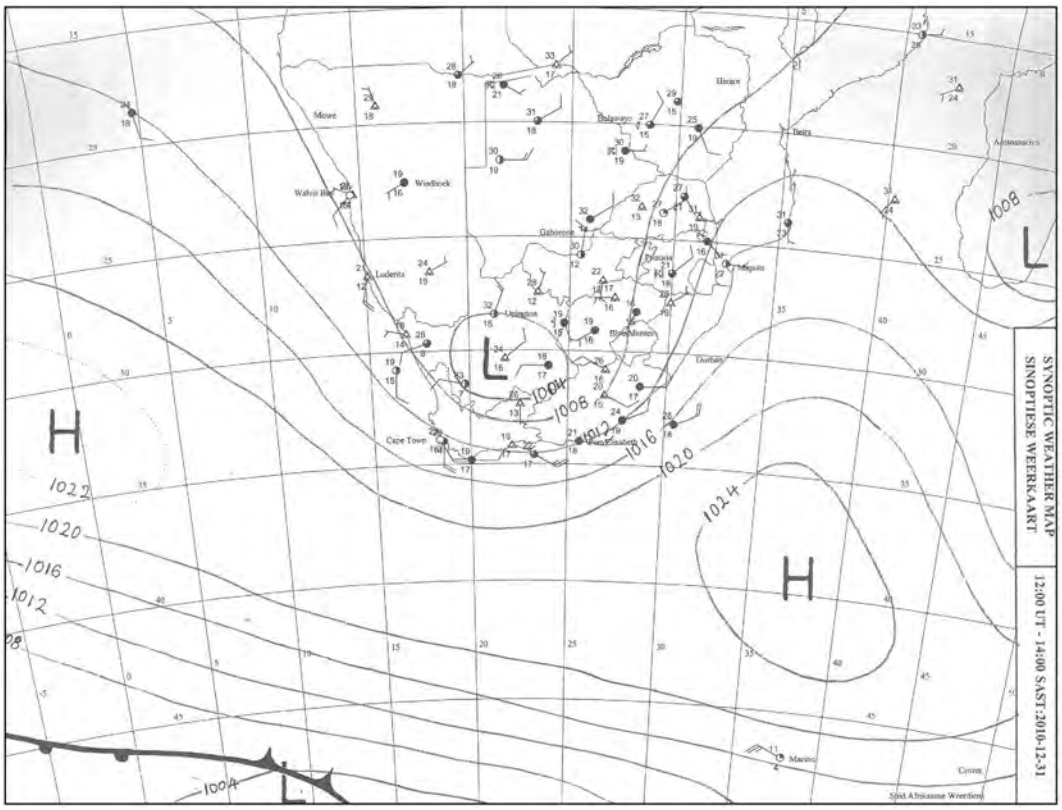

Figure 2.12: Synoptic chart from SAWS for 14h00 SAST on 31st December 2010 in which a trough near the west coast is causing significant rainfall in the Western Cape. Rainfall on this day reached 26 mm, at Beaufort West, and continued the next day, with up to 19 mm, at Excelsior Ceres.

2.4.1.5 West Coast Trough

This is the only weather pattern discussed here that may have no association with a frontal depression. Although the weather pattern may develop several times per year, rainfall from this system is less frequent. The rain that results usually falls in the central, southern and eastern parts of the country, but it is one of the few systems that can bring significant rain to the far west desert areas. The trough is a region of low pressure that develops west of the country, as the name suggests, and deepens and strengthens as it moves south-eastwards, as these systems generally do. The system shown in **Figure 2.12** was stationary for about two days, generating widespread rain over the Western Cape, with some heavy falls of rain and hail from thunderstorms. Rain typically occurs in the west if the system had its genesis far out in the Atlantic and had time to develop rain-bearing clouds by the time it makes landfall on the west coast.

2.4.2 Temperature

The study area experiences mostly moderate temperatures, although there are extremes of heat in the dry areas and cold on the mountain tops. Temperatures near the coast are more consistent (see Cape Town and Port Elizabeth), being moderated by the presence of the ocean and the more humid air. Inland temperatures are more extreme, with greater daily and seasonal ranges (see Oudtshoorn and Robertson). The effect of altitude reduces temperatures (see Calvinia). Interestingly, the annual average temperatures do not vary much, being from 16.5–19 °C for the selected stations.

2.5 Hydrogeology

2.5.1 Porosity and Permeability

The Table Mountain Group is largely composed of quartzose sandstones, a rock type that would generally exhibit a primary porosity of 5 to 30 % , depending on coarseness and sorting (Domenico and Schwartz, 1998, p.14). However, burial and diagenesis during the Cape Orogeny reached lowermost greenschist facies (not exceeding 300 °C), sufficient to result in conversion of most of the sandstones to quartzite (Frimmel et al., 2001). The changes in porosity that occur during diagenesis are complex and include mechanical rearrangement of the matrix, partial dissolution of sediment grains and precipitation of new minerals (the cement). In the case of the Table Mountain Group, silica was dissolved from the quartz sand grains and reprecipitated to the extent that the rock has been thoroughly recrystallized and virtually no primary porosity remains (Rosewarne, 2002b).

However, the Table Mountain Group contains abundant secondary porosity due to fractures (see **Figure 2.13**. The great thickness of quartzose sandstones has predisposed the rocks to brittle behaviour under stress and the thorough recrystallization of the Table Mountain Group formations has only made the units more competent and therefore subject to an even greater degree of brittle failure (Kotze, 2002). Fractures in the Table Mountain Group have developed in relation to folding, faulting and cleavage formation, but also include bedding planes, as can be seen in **Figure 2.14**. Up to a point, the more deformation, the greater the degree of fracturing and therefore secondary porosity. However, there is a limit to this and zones of extreme deformation, or cataclasis, often have experienced intense silicification that closes or partially blocks openings and thereby reduces permeability (de Beer, 2002).

In the absence of any porosity measurements for the TMG, general models of porosity can be instructive. For rocks with fracture porosity, three possible broad classes exist, as shown in **Figure 2.15**: one, single porosity from major fractures only; two, dual porosity of major fractures and intergranular, primary porosity; three, dual porosity of major and minor fractures. Kotze (2002) maintained the Table Mountain Group has a dual porosity of major and minor fractures, at least as was observed in the Peninsula aquifer in the Kammanassie Mountains. This dual fracture

Figure 2.13: Groundwater discharging as seeps from fractures in quartzite of the Skurweberg Formation on the Spout at Cederberg Tafelberg. The fractures are horizontal bedding planes and vertical joints.

porosity model may operate at numerous scales and in fact be a multiple level phenomenon with fractures or fracture systems being found at many scales, from regional or mega-fault structures, through local and outcrop scale, to hand specimen size. Mapping as done by Hartnady and Hay (2002c) using remote sensing techniques gives some indication of this at the regional to local scale in **Figure 2.16** and at the local to outcrop scale in **Figure 2.17**.

Groundwater discoveries support this multilevel fracture model because water strikes during drilling can give an order of magnitude difference in water yield. For example, borehole BK4 drilled in the Citrusdal Valley in 1997-8 yielded a 5 L/s blowyield until, at 220 m depth, a major water strike allowed blow yields of around 100 L/s to be realised (Hartnady and Hay, 2002a). The low yield was presumably from minor, more common fractures encountered through much of the borehole, and the very high yield corresponds to intersection of a major, regional scale fracture or fracture system.

Although the commonly held belief is that fracture density decreases with depth, it seems that this might only occur at a very low rate, or at great depths (more than 1 km) in the Table Mountain Group. Lin et al. (2007) recorded a very weak negative correlation between fracture density and depth over a vertical distance of 750 m in the Piekenierskloof Formation; in other words, there was only a marginal decrease in fracture density with depth.

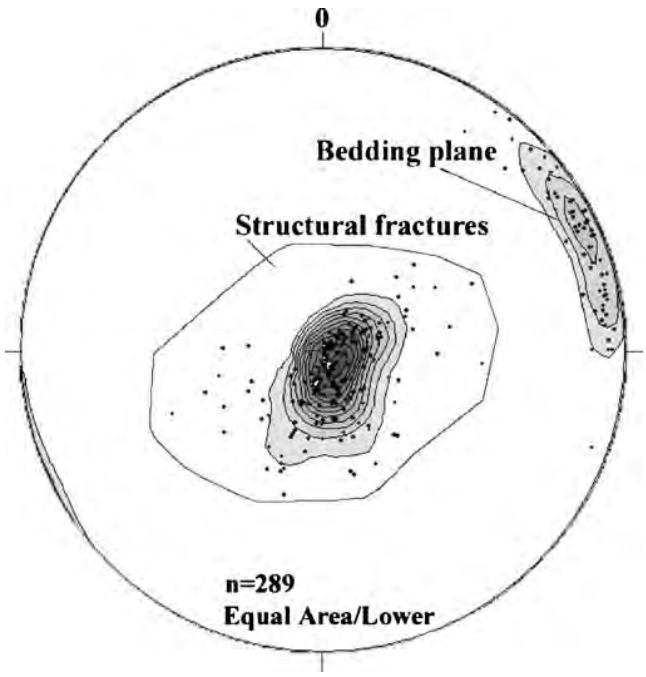

Figure 2.14: Fracture measurements (strike and dip) taken at surface in the Piekenierskloof Formation between Lamberts Bay and Graafwater, showing the separation between near horizontal bedding planes and near vertical structurally formed fractures. From Lin et al. (2007).

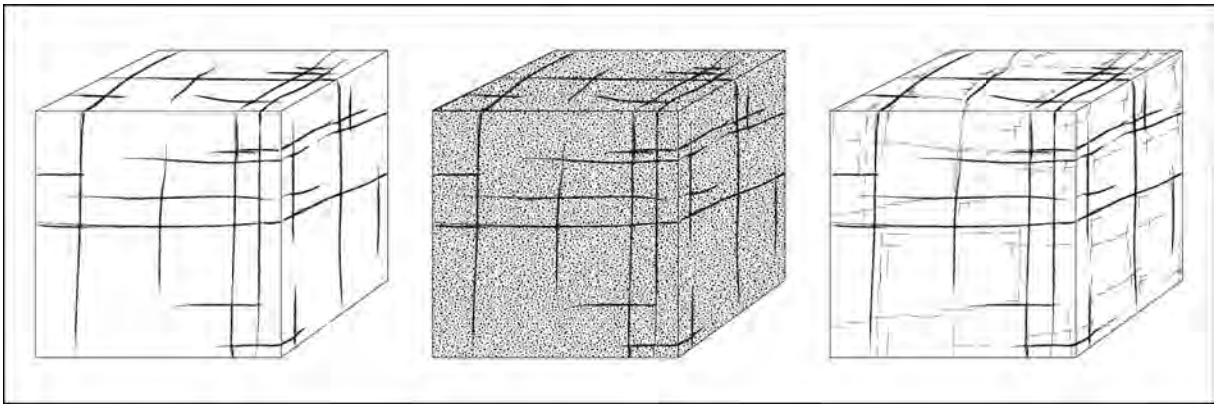

Figure 2.15: Theoretical models of possible fracture porosity: one, major fractures; two, major fractures and primary porosity; three, major and minor fractures. After Kruseman and De Ridder (1994) as cited in Woodford (2002).

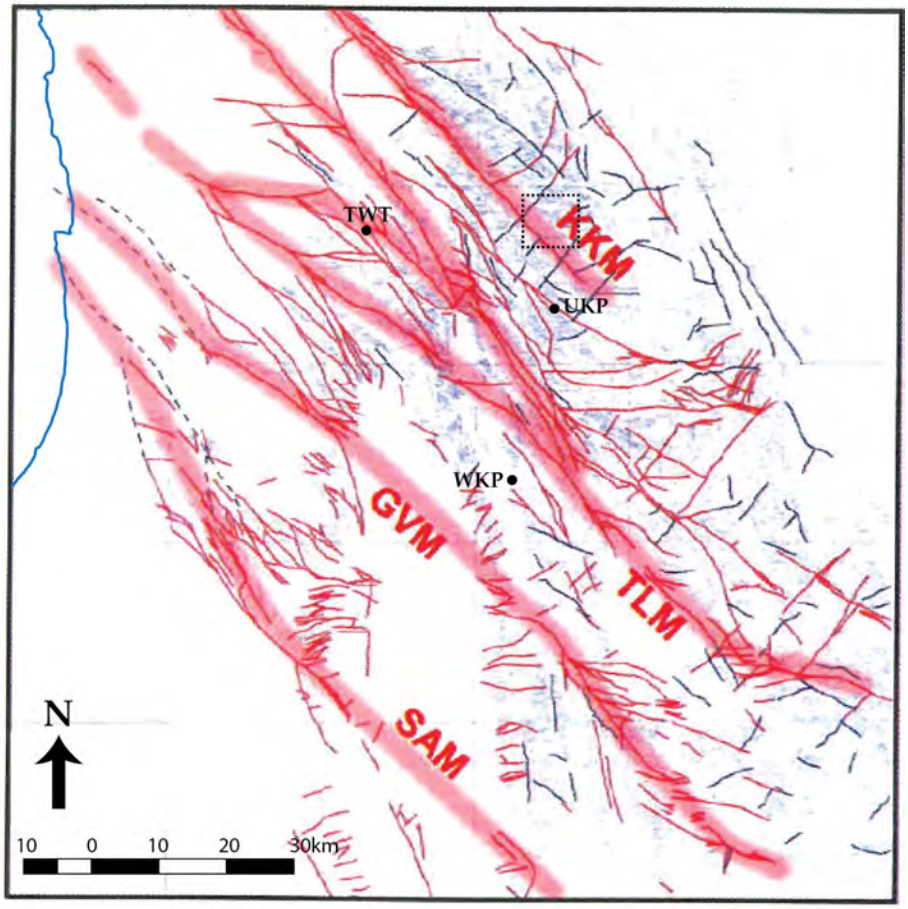

Figure 2.16: A fault and fracture trace map for the Cederberg–West Coast region showing mapped faults from the 1:250 000 geology maps as thin red lines, and additional mapped or remoted derived fracture traces, from Landsat, SPOT or aerial photographs, as thin black lines. The area includes outcrop of all formations within the Table Mountain Group. Large regions with few structures (in the south-west) are areas where the Malmesbury Group is exposed. SAM - Saron-Aurora megafault; GVM - Gydo-Verlorenvlei megafault; TLM - Twee Riviere-Leipoldtville megafault; KKM - Krakadouw-Klawer megafault. The dotted black square shows the location of **Figure 2.17**. From Hartnady and Hay (2002c).

2.5.2 Hydraulic Parameters

Aquifers can be defined in several ways, including geology, structure and spatial occurrence. The ability of an aquifer to conduct water is typically described by three hydraulic parameters: the hydraulic conductivity (K), the transmissivity (T) and the storativity (S). Hydraulic conductivity is a measure of permeability; transmissivity is a measure of the total flow possible along a vertical line through the aquifer and is calculated by multiplying the hydraulic conductivity by the aquifer thickness, and it gives some indication of the possible borehole yields or flow rates; storativity measures the amount of water released from a confined aquifer per unit drop in hydraulic head and gives an indication of how much water can be abstracted. All of these parameters are derived

location	aquifer	K m/d	T m^2/d	S	source
Lamberts Bay	Piekenierskloof	0.00069			Lin et al. (2007)
The Baths, Citrusdal	Peninsula	0.002 - 2	10 - 200	0.0001 - 0.001	Umvoto and SRK (2000)
Roode Elsberg, Hex	Peninsula	0.26			Brink (1981)
Villiersdorp	Peninsula	017			Brink (1981)
Kammanassie	Peninsula			0.01 - 0.05	Kotze (2002)
Lakenvalley, Hex	Skurweberg	0.26			Brink (1981)
Kouga Dam	Skurweberg	0.07			Brink (1981)
Villiersdorp	Skurweberg	0.3			Rosewarne (2002b)
Agter Witzenberg	Skurweberg	0.05			Weaver et al. (1999)
Kleinmond	Skurweberg		70 - 320	0.0001 - 0.0005	Parsons (2002)
St Francis on Sea	Skurweberg		100	0.0018 - 0.0033	Rosewarne (2002b)
Struisbaai	Pen/Skbg		15 - 200	0.0086	Weaver et al. (1999)
Uitenhage	Pen/Skbg		10 - 400	0.0002 - 0.05	Maclear (2002)
Cape Fold Belt	TMG			0.001	Vegter (1995)
Cape Fold Belt	TMG			0.0032 - 0.015	Weaver et al. (2002)

Table 2.1: Hydraulic parameters (K - hydraulic conductivity, T - transmissivity, S - storativity) for aquifers of the TMG, based on calculations from pumping tests, conceptual or numerical models and other estimates. Table is based on a compilation by Rosewarne (2002b).

from borehole pumping tests and are best suited to homogenous, isotropic, primary porosity aquifers. The Table Mountain Group may fit the characteristic of being homogenous, but it is anisotropic because of the preferential directions in which fractures have developed (see **Figure 2.14**) and it is of course a secondary porosity aquifer. In addition, the very size of the Table Mountain Group, even simply the depth at one locality, never mind the vast horizontal dimensions, makes the aquifer difficult to quantify, not only theoretically, but in a very practical sense; i.e. the cost and effort of drilling a fully penetrating borehole, even through just one formation (e.g. Peninsula), is in most cases immense. For these reasons there are few reliable estimates of the three hydraulic parameters for the Table Mountain Group.

Rosewarne (2002b) collated some hydraulic parameters for the TMG; these have been reproduced here in **Table 2.1** with some rearranging and additions.

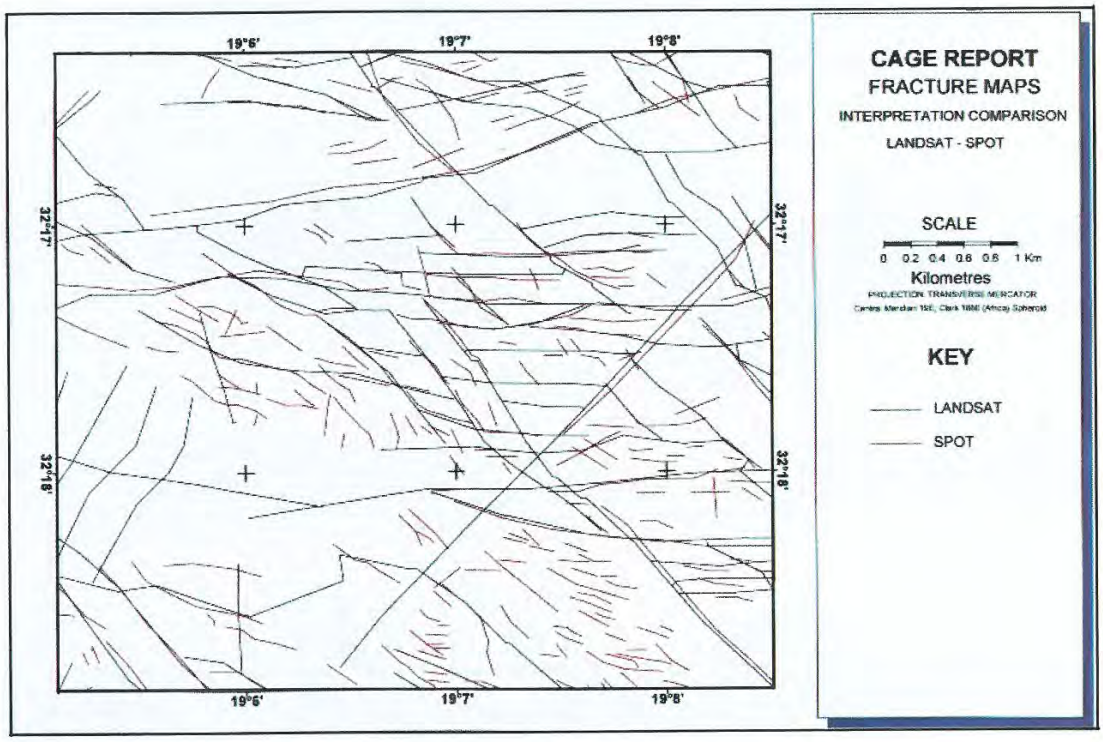

Figure 2.17: A detailed fracture trace map for a small area of Peninsula Formation outcrop, shown as the region in the dotted black square in **Figure 2.16**. Fracture traces derived from Landsat images (black lines) and SPOT satellite images (red lines). The diagrams shows how fractures occurs in parallel sets that often intersect and that many fractures are short and some, typically associated with local to regional faults, are much longer. From Hartnady and Hay (2002c).

2.5.3 Hydrostratigraphy

The Table Mountain Group is not a simple, single aquifer with a neat geometrical shape, but rather an interconnected aquifer system, semi-continuous in space, with an extremely complex three dimensional form and multiple aquifers. The highest parts of the aquifer are over 2000 m above sea level and form the crests and peaks of mountain ranges, mainly comprising the Peninsula Formation, but also the Nardouw Subgroup, especially the Skurweberg Formation. The lowest parts of the aquifer reach depths of 5–6 km below sea level along the Worcester and Kango Faults (see the cross-sections in Chapter 5), and in places the Table Mountain Group outcrops or subcrops beneath the sea bed, to a distance of at least tens of kilometres offshore. There is no location where all the Table Mountain Group formations occur, from Piekenierskloof or Sardinia Bay Formation to Rietvlei or Baviaanskloof Formation, however the succession from Peninsula to Rietvlei Formation is preserved in many areas and probably reaches 4000 m true thickness (perpendicular to the formation contacts), especially in the southern branch of the Cape Fold Belt where structural thickening has been substantial.

Hydrogeologists have traditionally only recognized the terms aquifer and aquitard for geolog-

ical units that do and do not conduct significant quantities of groundwater. These are relative terms and factors such as depth, thickness, economics and demand for water are almost as important as the actual hydraulic parameters of the unit in determining which term to apply. In addition, the term aquiclude is sometimes used as a synonym for aquitard, although Poehls and Smith (2009) maintain the term aquiclude should be reserved for extremely impermeable formations. It is important to realise that hydrostratigraphic units may or may not overlap with geological units; an aquifer may be only a part of a geological formation, or several geological formations may constitute one aquifer, and similarly for aquitards. Furthermore, there was no accepted heirarchy of hydrogeological units, such as the familiar geological *member*, *formation*, *group* and other categories.

Al-Aswad and Al-Bassam (1997) have created a hydrostratigraphical nomenclature, but even this is inadequate under many common geological situations where layers are lenticular, where folding has occurred and even more so in a faulted environment, where substantial flow along faults through aquitards connects different aquifers, or different aquifers are faulted into direct contact with each other. All of the above occurs in the Cape Fold Belt. For example, Rosewarne (2002a) found the Bokkeveld Group sandstone layers to deliver high yields, because leakage from the underlying Table Mountain Group into these sandstone layers occurred once they had been pumped. The high hydraulic head of the underlying Table Mountain Group was due to recharge in the adjacent Skurweberg mountain range and allowed this groundwater to leak upwards and recharge the Bokkeveld Group sandstones.

Using the Al-Aswad and Al-Bassam (1997) system yields a classification for the Cape Supergroup as shown in **Figure 2.18**. Each geological formation can be roughly evaluated as either an aquifer or aquitard. Aquitards may contain water bearing layers, such as the sandstone beds within the Graafwater Formation; equally, aquifers may only offer some portion of their thickness as an aquifer, the rest being an aquitard, such as the sandstone beds within the dominantly silty Floriskraal Formation, but the reason for calling the Floriskraal Formation an aquifer is that it bears water within a predominantly non-water bearing setting.

The proposed hydrostratigraphy attempts to simplify and highlight major aquifers and aquitards. Where aquifer-aquitard boundaries coincide with geological boundaries, no reclassification has been done. In the Witteberg and Bokkeveld Groups where the geology alternates regularly between arenaceous and argillaceous, the hydrostratigraphy mimics the geostratrigraphy, but in the TMG this is not the case. The Piekenierskloof and Graafwater Formations have limited areal extents.

The Piekenierskloof Formation is a significant aquifer in the Sandveld region (Lin et al., 2007). The Graafwater Formation may have fractured, water bearing sandstone layers, but their limited vertical and areal extent (Rust, 1977) will render them low yielding, unless they are connected via faults to the Piekenierskloof or Peninsula Formation.

The Peninsula Superaquifer may include some portion of the Pakhuis Formation, where this

is permeable, although Hartnady and Hay (2002b) consider the Pakhuis Formation to be an aquitard, based on the similarity in gamma and neutron-neutron downhole geophysical logging of the Pakhuis and Cederberg Formations. Superaquifer status is assigned on account of the extreme thickness (up to 2000 m) and areal extent over the Cape Fold Belt, as well as the high yielding nature of this unit (Hartnady and Hay, 2002a). The Cederberg Aquitard may include portions of the Pakhuis Formation where it is less permeable and portions of the Goudini Formation where the siltstone and shale layers are substantial enough to restrict groundwater flow. Although rather thin (100–200 m) the fact that this aquitard either separates the Peninsula Superaquifer from the Skurweberg aquifer or simply acts as a cap to the Peninsula Superaquifer, makes this unit of extreme importance in understanding groundwater flow in the Table Mountain Group. The Skurweberg Aquifer is centred on the highly fractured mature quartzites of the Skurweberg Formation, but includes portions of the underlying Goudini and overlying Rietvlei Formations where they are more permeable and have good connectivity with the Skurweberg Formation.

The Bokkeveld Group, although it contains sandstone aquifers that can yield substantial water at the local scale (Rosewarne, 2002a), acts as an aquitard on a regional scale, particularly as a confining layer to the Table Mountain Group. Good examples of this are seen in the Olifants River Valley (Geological Survey, 1973) and under the Little Karoo (Geological Survey, 1979) where the Bokkeveld Group confines the Table Mountain Group under the valley floors and allows deep groundwater to flow many kilometres from one side of the valley to the other and emerge in hot springs, under pressure gradients derived from mountain recharge areas (Diamond and Harris, 2000).

The Witteberg Group contains both substantial aquifers and aquitards. It probably acts as an aquitard on a regional scale, although the extensive structural deformation, particularly intense folding and thrusting, probably allow good connections between the various sandstone (aquifer) layers to the extent that in some areas these may act as a single aquifer. The great thickness and highly competent nature and therefore extensive fracturing of the Witpoort Formation mean this unit is potentially a significant aquifer, although low recharge because of low rainfall is probably a limiting factor for achieving high and sustainable borehole yields from this unit. The Witteberg Group tends to receive low rainfall because of its usual position inland and therefore in the rain shadow of mountains formed by the Table Mountain Group.

Overall, the Bokkeveld and Witteberg Groups possess similar hydrogeological characteristics, in that they both contain numerous minor aquifers that may be connected to each other, or to the larger aquifers in the Table Mountain Group, if structural features allow. These similarities suggest that the multiple aquifers and aquitards of these two groups can be collectively known as the Bokkeveld-Witteberg aquagroup (Al-Aswad and Al-Bassam, 1997). The Table Mountain aquagroup is essentially the Peninsula-Cederberg-Skurweberg configuration that persists over much of the Cape Fold Belt, with some localised variations at the base of the group, where other formations are present.

Below and above the Cape Supergroup lie thick aquitards that generally conduct little groundwater: the Saldanian basement of metasediments and granite beneath and the Dwyka Group above. The Cape Supergroup can therefore be termed the Cape aquasystem, bounded by these basement and cover mega-aquitards, and with a fixed configuration of the aquifer dominated Table Mountain aquagroup at the base, and the regular aquifer-aquitard alternations of the Bokkeveld-Witteberg aquagroup above.

In some instances, aquifers within the Cape aquasystem will be connected to more recent cover rocks of the West Coast, Sandveld, Bredasdorp or Algoa Groups, which contain calcarenites, unconsolidated sand and other lithologies that can form aquifers. These linkages occur mainly near the coast and are generally limited in area. The Sandveld region around Elands Bay is the largest area where the Table Mountain Group interacts with surficial rocks and sediments.

2.5.4 Significance of the Table Mountain Group

The Table Mountain Group is critical in sustaining surface water in the Western Cape (Roets et al., 2008; Colvin et al., 2009). Baseflow during the summer dry season is sustained through discharge of groundwater (le Maitre et al., 2002; Colvin et al., 2009) and it has been shown that peak or flood discharge surface water during rain events is mainly composed of groundwater that has discharge from the aquifer in response to increased hyrdaulic head caused by fast recharge of rainwater (Midgley and Scott, 1994). A substantial portion of the ecosystems of the Western Cape are directly dependant upon water, being wetlands, riparian zones and estuaries. Furthermore, these vegetation and plant communities are more important as habitat and for ecosystem services than the dryland areas. As such, the Table Mountain Group is the ultimate water source for most surface water and therefore controls both the natural and human environment through most of the Western Cape.

Various attempts have been made at calculating the groundwater yield potential of the Table Mountain Group. From the information presented above, it should be clear that this exercise is subject to two huge challenges, being the great size of the aquifer system and the sparse and often unreliable information. As a first step, Rosewarne (2002b) has collated pumping data from active wellfields, giving an indication of available water in particular locations, and Meyer (2002) gives the flow rates of the thermal springs in the Cape Fold Belt. These data are summarized in **Table 2.2**.

THERMAL SPRINGS		WELLFIELDS	
name	GL/a	name	GL/a
Baden	1.16	Albertinia	0.26
Brandvlei	4.00	Caledon	0.10
Caledon	0.28	Ceres	1.51
Calitzdorp	0.25	Hermanus	0.35
Citrusdal (The Baths)	0.91	Humansdorp	0.68
Goudini	0.35	Jeffreys Bay	0.80
Montagu	1.20	Lamberts Bay	0.13
Studtis	0.98	Plettenberg Bay	0.28
Toverwater	0.35	Steytlerville	0.07
Uitenhage	1.42	St Francis-on-Sea	0.73
Warmwaterberg	0.28	Uitenhage	1.58
TOTAL	11.2	TOTAL	6.5

Table 2.2: Point source (springs) or small area (wellfield) abstraction figures give an indication of possible yields for deep boreholes or small wellfields in the Table Mountain Group. Data from Meyer (2002) and Rosewarne (2002b).

Hartnady and Hay in Weaver et al. (2002) calculated groundwater yield for an area of less than 2000 km^2 in the Citrusdal region as 5–25 GL per 1 m decrease in hydraulic head, concluding that for a technically and probably environmentally acceptable decrease in head of 20 m, 100–500 GL could be withdrawn annually. Scaling up to the whole of the Table Mountain Group, they calculate an aquifer rock volume of 100 000 km^3, which, for a fracture porosity of 0.1-1 % gives a volume of 100 000 – 1 000 000 GL of groundwater, although much of this water is not available because of practical challenges, as well as potential environmental impacts. Similarly, Rosewarne (2002b) calculates an aquifer rock volume of 47 000 km^3 and using storatitivity values shown in **Table 2.1**, he concludes that 10 000 – 100 000 GL of groundwater is in storage, again, most of which is not available. However, even if only a small percentage of this groundwater is available, when compared to the total volume of all surface water reservoirs fed by Table Mountain Group catchments, 1500 GL, it should be clear that the aquifer system stores a very large amount of water.

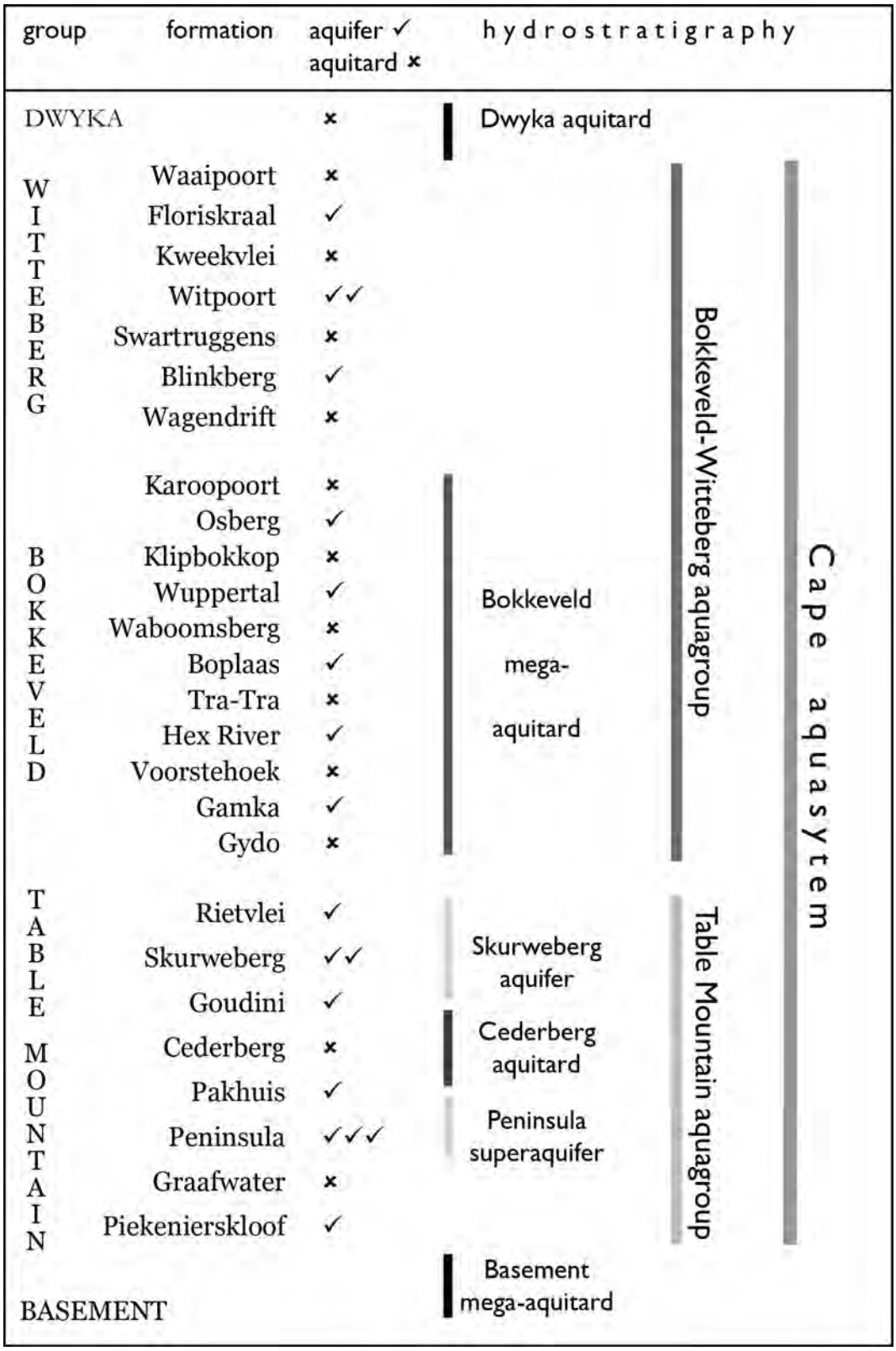

Figure 2.18: Proposed hydrostratigraphic classification for the Cape Supergroup in the western half of the Cape Fold Belt.

Chapter 3

Methods

3.1 Introduction

This chapter describes the methods used for collection of samples, laboratory preparation and instrumental analysis, including correction factors and equations. The locations of all the sample sites are shown on various maps and the major rainfall collection stations are all listed in a table with coordinates and elevations. Information on the calculation of regression lines is also included.

3.2 Sample Collection

3.2.1 Rain

Rainfall was collected at 15 sites across the Western Cape. Most of the collection stations operated for 2 years, from 2010 to 2012, with some having a continuous record and others an interrupted or shorter operational period. Factors that caused a station to cease operating were instrument problems from animal or weather damage, lack of access due to weather conditions and also human error. Maps of the sample locations are included below, approximately in a west to east direction, starting with Cape Town (**Figures 5.21 to 3.22**).

Rain collection depended on access to the rain gauge. Where gauges were easily accessible, rainfall was collected daily and emptied into a glass jar, from which a sample was taken at the end of each month. At remote sites, a cumulative collector (**Figure 3.2**) was erected and emptied at approximately the end of each month. In each case, the daily or monthly rainfall amounts were recorded. Bosman (1981) noted that plastic raingauges collect around 7 % less rainfall than standard metal raingauges, attributable to splash out from the receiving funnel and higher retention of raindrops on the plastic surface, which then evaporate. Given the extreme variation in rainfall in the field area due to orographic effects and that rainfall amount is used indirectly to weight isotope values, this discrepancy is considered acceptable. Furthermore, all rainfall for this study was collected using similar plastic raingauges and so the data is internally consistent.

station			location		
code	name	description	latitude	longitude	altitude
UCT	University of Cape Town	Department of Geological Sciences building	33° 57’ 31.9" S	18° 27’ 37.6" E	135 m
TMC	Table Mountain Cableway	upper cableway station	33° 57’ 26.6" S	18° 24’ 10.3" E	1074 m
TWT	Twaktuin	Twaktuin farm in Olifants River Mountains	32° 19’ 17.6" S	18° 49’ 31.9" E	412 m
UKP	Uitkyk Pass	crest of pass in Cederberg	32° 24’ 14.8" S	19° 06’ 05.4" E	1013 m
WKP	Wolfkop	house in Wolfkop Private Nature Reserve, south of Citrusdal	32° 38’ 19.2" S	19° 03’ 20.4" E	355 m
MTB	Matroosberg	nek between Matroosberg and Conical Peaks, Hex River Mountains	33° 22’ 27.2" S	19° 39’ 53.1" E	1910 m
DDN	De Doorns	Tweespruit farm near De Doorns in Hex River Valley	33° 26’ 34.3" S	19° 40’ 30.9" E	482 m
RVD	Riverndale	Riverndale farm, foot of the Langeberg, north-east of Heidelberg	33° 58’ 22.9" S	20° 59’ 56.2" E	251 m
RBP	Robinson Pass	crest of pass over Langeberg, north of Mossel Bay	33° 52’ 26.3" S	22° 01’ 54.7" E	885 m
BKK	Bakenskop	highest point of the Gamkaberg, Gamka Mountain Nature Reserve	33° 43’ 07.8" S	21° 55’ 28.4" E	1101 m
GST	Gamkaberg store	store shed at Gamka Mountain Nature Reserve	33° 40’ 20.0" S	21° 53’ 15.5" E	350 m
BBG	Blesberg	highest peak in the eastern Groot Swartberg	33° 25’ 03.8" S	22° 41’ 15.0" E	2080 m
KMN	Kammanassie	Vermaaks River Gorge in western Kammanassie Mountain	33° 36’ 11.4" S	22° 31’ 56.2" E	666 m
LTL	Lentelus	Lentelus farm in Bo-Kouga region	33° 40’ 42.2" S	23° 29’ 58.0" E	642 m
GKM	Goukamma	house near Goukamma railway station and Goukamma River	33° 02’ 21.1" S	22° 56’ 25.3" E	62 m

Table 3.1: Location information for the 15 rainfall collection stations of this study.

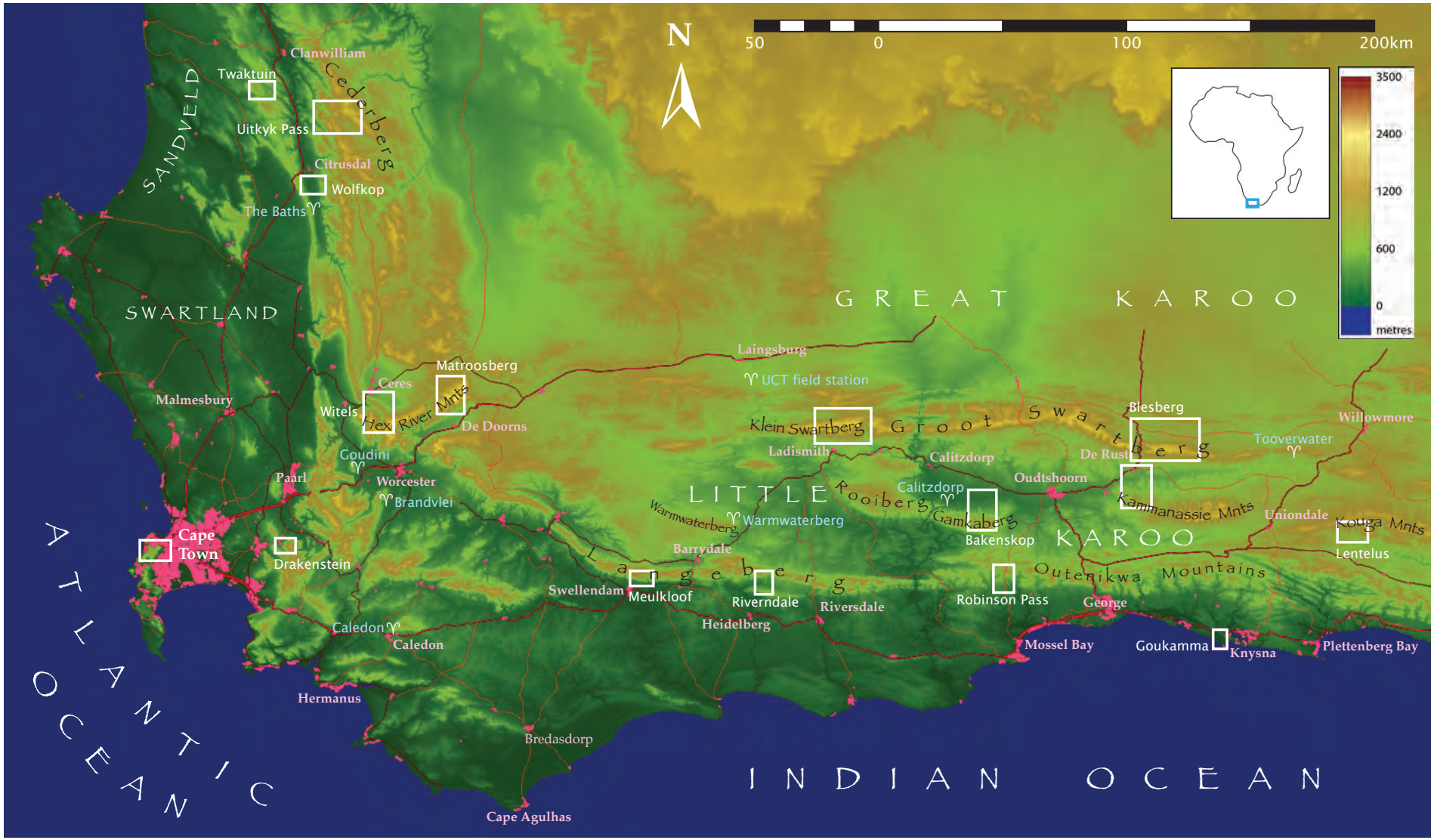

Figure 3.1: Map of the whole study area with white rectangles showing the areas for each of the detailed maps that follow. DEM from NASA (2013) and roads shapefile from NGI (2012).

For the monthly collectors, prevention of evaporation was achieved by use of a long thin plastic tube, as seen in the diagram, although oil was also added to some collectors, but it was found that this was unnecessary, as collectors without oil seemed to yield samples with acceptable isotope compositions. The oil contaminated some samples, but care was taken to avoid getting the oil into the laboratory preparation equipment and as a result, no effect on isotope values was observed. Spikes were placed on top to discourage birds from sitting on the rim and adding non-meteoric contributions to the funnel.

3.2.2 Surface Water

Surface water was collected from five rivers in the Western Cape. The water was collected directly from the surface of the flowing stream, except for one sample collected from the cold bottom water in a deep river pool. The sample locations are also shown in the maps in this chapter.

3.2.3 Groundwater

Groundwater was sampled from both natural sources, springs and seeps, and boreholes. If boreholes were not in frequent use, a short period of purging was done to flush water out from the borehole volume and associated piping and allow true aquifer water to be sampled. Springs and seeps were sampled at or as near as possible to the source, in cases where the spring was capped. The borehole locations are also shown in the maps in this chapter.

3.3 Sample Preparation

3.3.1 Mass Spectrometry

3.3.1.1 Hydrogen Isotopes

Sample preparation for hydrogen isotope analysis was done using established single sample preparation procedures (e.g. Tanweer et al., 1988; Schimmelman and DeNiro, 1993). The procedure starts by loading 100 mg ($\pm$3 mg) of Indiana zinc shavings into a glass tube of 3 mm internal diameter which was heated with a hot air gun under vacuum to degas the zinc, removed from vacuum and allowed to cool down before a 2 μL microcapillary pipette containing the sample water was dropped into the glass tube. The tube was then placed back on the vacuum line and evacuated after the sample had been frozen with liquid nitrogen, then sealed with an oxygen-propane flame; see **Figure 3.3**. The glass tube was then loaded into a furnace and baked at 450 °C for 30 minutes, allowing the following reaction to take place:

$$Zn + 2H_2O \rightarrow ZnO_2 + 2H_2 \quad .$$

This glass tube could then be loaded into the mass spectrometer to allow for analysis of the hydrogen gas.

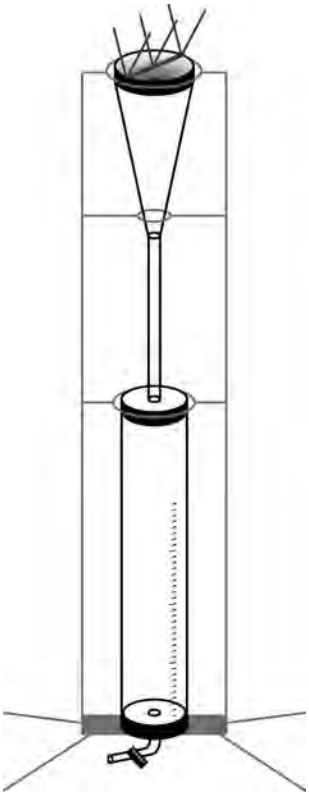

Figure 3.2: Cumulative rainfall collector, designed to collect rain for one month and prevent significant evaporation until collection.

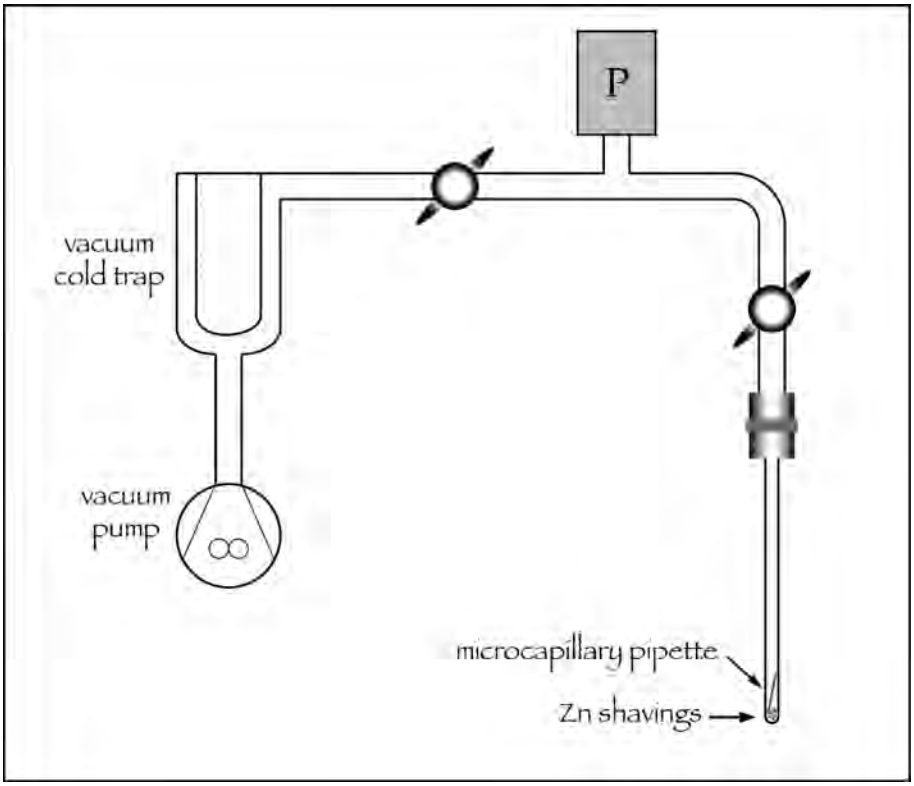

Figure 3.3: Vacuum line for preparing water samples for hydrogen isotope analysis.

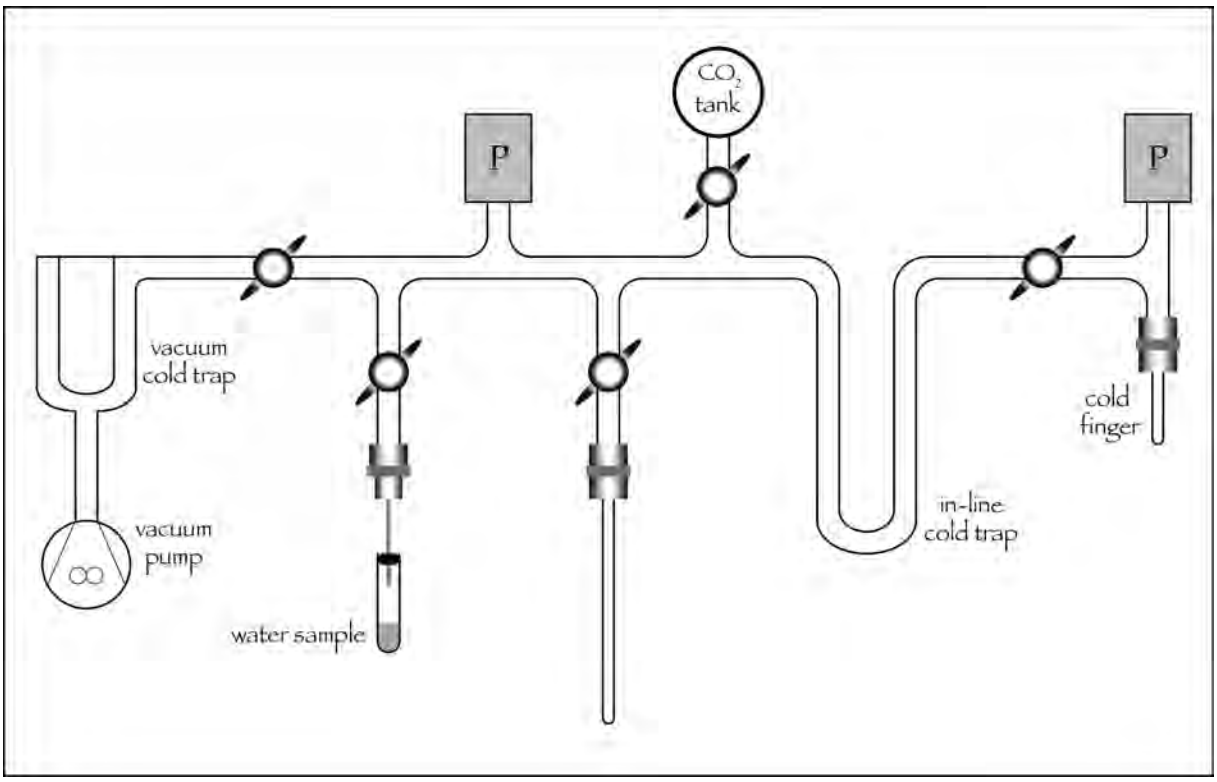

Figure 3.4: Vacuum line for preparing water samples for oxygen isotope analysis.

3.3.1.2 Oxygen Isotopes

Sample preparation for oxygen isotope analysis was done by the method of equilibrating sample water with CO_2 and analysing this, as described in Socki et al. (1992), based on that of previous workers, such as Epstein and Mayeda (1953). The method entailed injecting 2 mL of sample water into a 7 mL sealed plastic vial (vacutainer) that had been evacuated and then loaded with $\frac{1}{3}$ atm of CO_2. The vial was then submerged in a 25 °C water bath and agitated for 2 hours to allow oxygen exchange between the H_2O and CO_2 to reach equilibrium. Then the vial was placed onto the vacuum line and submerged in liquid nitrogen to freeze the H_2O and CO_2. Once frozen, the vial was opened to the vacuum to evacuate any gases. The liquid nitrogen was then moved to the in-line vacuum trap and nearly frozen 2-propanol (isopropyl alcohol) was placed around the vial to retain the ice but liberate the CO_2 as gas. Once all the CO_2 had frozen at the in-line cold trap, the vial was closed off from the vacuum line and the vacuum was opened again to remove any unwanted gases. After closing the valve to the vacuum pump, the liquid nitrogen was moved to the cold finger and the 2-propanol to the cold trap, to transfer the CO_2 where it could be measured with a pressure gauge. Unwanted gases can again be pumped away to vacuum in this step. Finally the CO_2 was frozen into a glass tube using liquid nitrogen, and flamed closed with an oxygen-propane torch.

For both hydrogen and oxygen isotope preparation, each batch of samples was accompanied by 2 laboratory standards, both duplicated. The two standards were initially CTMP2010, which

standard		$\delta D_{(SMOW)}$ (‰)	$\delta^{18}O_{(SMOW)}$ (‰)
CTMP2010	Cape Town Millipore Water 2010	-7.4	-2.69
ACTMP	Adam's CTMP2010	+1.6	-0.60
Evian	Evian bottled water	-70	-10.0
EvianA	Adam's Evian	-71.7	-10.20
RMW	Rocky Mountain Water	-129.5	-17.27

Table 3.2: Delta values for the various internal standards used in this study.

stands for Cape Town Millipore Water and is filtered 2010 University of Cape Town tap water and Evian bottled spring water, from the Alps. Later during the study, Evian was replaced with a more isotopically depleted water, RMW, which stands for Rocky Mountain Water, bottled spring water with a source in the American Rocky Mountains.

3.3.2 Laser Cavity Ringdown Spectroscopy

No sample preparation is generally needed for this method. One millilitre of sample water is injected into a vial which is capped with a septum and then put into an automated sample loading tray. Hydrogen and oxygen isotopes are analysed simultaneously. Only samples with traces of oil or other dirt were injected through a micropore filter to remove the contaminants.

Sample runs using this method made use of 3 standards: ACTMP (Adam's CTMP), EvianA (Evian Adam's) and RMW, reflecting the use of Adam West's laboratory in the Botany Department at the University of Cape Town.

3.4 Sample Analysis and Data Correction

3.4.1 Mass Spectrometry

A 2004 Thermo Corporation Delta Plus XP stable light isotope ratio mass spectrometer was used for conventional dual inlet analysis of hydrogen and oxygen isotope ratios at separate times. The machine was set to make 4 and 6 measurements of the δ value of the sample relative to the reference gas for H_2 and CO_2, respectively. Over years of experience it was found that the machine precision for hydrogen was better than the preparation procedure and so making more than 4 measurements would not improve overall accuracy. For CO_2 however, a slight memory effect seemed to occur as the first measurement was often slightly different from the other five, and the preparation procedure precision was slightly better, so 6 measurements resulted in the optimal balance between accuracy and time for analysis.

Each time the machine was switched over from hydrogen to carbon dioxide, a peak optimisation or focus procedure was performed, in which the ion source and other beam parameters were adjusted to reduce H_3 production and focus the beam squarely into the collector cups. This was

followed by an H_3-factor correction for the molecules of H_3 produced in the ion source, which interfere with the measurement of HD.

Data from the mass spectrometer were corrected using the following method. The first correction applied was for fractionation of oxygen between H_2O_l and CO_2, which at 25 °C has a fractionation factor of 1.0412. This equates to the CO_2 being 40.37 ‰ heavier than the water, once equilibrated. Then a correction was applied for the difference between the reference gas and SMOW. Finally, the sample values were adjusted by correcting the two laboratory standards (CTMP2010 and RMW) to their known values and applying the same correction to the samples. This was done by assuming the error between the measured and actual values varies linearly and therefore a straight line equation can be found that will transform the two standards from their measured values to their actual values, as shown in **Figure 3.5**.

The equation for a straight line is:

$$y = mx + c$$

where **y** is the unknown actual sample value, **m** is the gradient and **c** the intercept of the straight line, and **x** is the measured value of the sample. Both m and c can be calculated individually and the above equation used to calculate the actual sample value, or the equation below can be used to perform the calculation in one step:

$$SAMPLE_{actual} = \left(SAMPLE_{meas} \times \left(\frac{CTMP_{actual} - RMW_{actual}}{CTMP_{meas} - RMW_{meas}} \right) \right) + \left(RMW_{actual} - \left(RMW_{meas} \times \left(\frac{CTMP_{actual} - RMW_{actual}}{CTMP_{meas} - RMW_{meas}} \right) \right) \right)$$

As seen in **Figure 3.5**, a straight line is used to convert measured values (x-axis) to actual values, based on analysis of two standards (RMW and CTMP) of known value. For each analytical run of samples, the straight line will vary in both gradient and intercept. This method replaces the 'shift' and 'stretch' technique commonly used to correct measured values (e.g. Sharp, 2007, p.332).

3.4.2 Laser Cavity Ringdown Spectroscopy

A L2120-i Picarro wavelength scanning cavity ringdown spectrometer was used to analyse for oxygen and hydrogen isotope values simultaneously. Certain wavelengths of infrared light are scanned and the ringdown time is used to calculate the abundance of the various isotopes of oxygen and hydrogen (Lis et al., 2008). Six injections of microlitre amounts of sample were

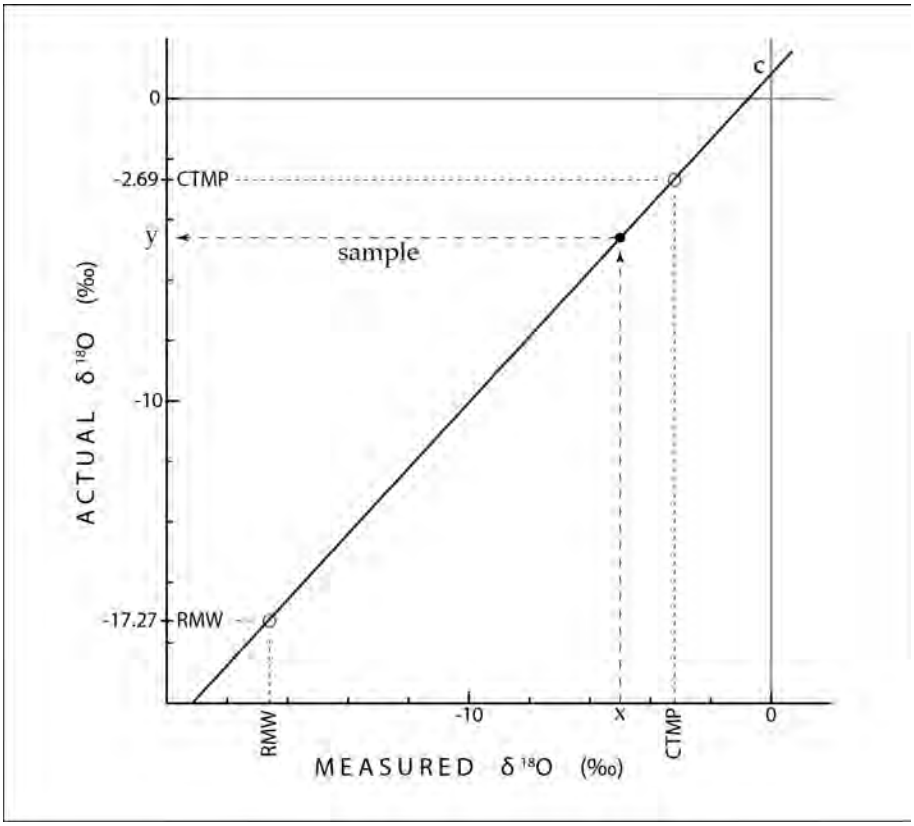

Figure 3.5: The final correction applied to isotope data to correct for instrument drift and laboratory preparation procedure variations. Two standards allow calculation of a straight line equation which is then applied to all the sample data for that run. The example is given for $\delta^{18}O$ but is equally applicable to δD.

made through a septum, vapourised and then transported by N_2 gas into the cavity for analysis. Standards were run at the beginning and end as well as after every ten to twelve samples during a given run. The first two injections show a clear memory effect and these values were discarded, the remaining four being averaged to give an instrument measurement. These instrument measurements were then corrected using the same final correction procedure as shown in **Figure 3.5**. Issues with contaminants, particularly organic compounds such as alcohols, have been noted (West et al., 2010), however, pure water samples tend to give good results. Quality assurance software was used to scan the raw data from the machine and highlight poor analytical indicators (West et al., 2011).

3.4.3 Standards

As shown in **Table 3.2**, several standards were used to correct for laboratory and instrument errors. An analysis of long term laboratory and mass-spectrometer precision can be made by looking at the raw data values for these working standards over time. These values are shown in **Tables 3.3 and 3.4** for δD and $\delta^{18}O$. The latter table shows rather stable values for the three standards, although a small possible drift in CTMP2010 from more to less negative values appears to occur over time. This is likely to be due to drift in the reference gas for the mass-spectrometer, although it could also be due to a change in the laboratory CO_2 tank or in the CTMP2010 standard. The mean difference in replicates (the two values against each date) is around 0.2 ‰ $\delta^{18}O$ for the three standards, which represents the overall precision of the laboratory preparation procedure and mass-spectrometer analysis.

Table 3.3 reveals substantial drift in the values for the three standards, although the period over which Evian was analysed is a bit short. Changes in hydrogen analysis results could be due to several factors. As with oxygen (carbon dioxide) analysis, there could be drift in the reference gas and in the working standards. The zinc used was changed around mid-2012, from batch S83B4 to S38r, and this in fact coincides with substantial changes in values. The 31-05-2012 sample run was the first with the new batch of zinc, the 08-08-2012 and 15-08-2012 again used the old batch, and from 20-08-2012 thereafter the new zinc was used. It can be seen that these changes coincide with the big changes in values. With this in mind, the drift in working standards appears reasonable. More importantly for precision, the mean difference in replicates can be seen to be a little over 1 ‰, which is assurance of the reliability of the preparation and analytical procedures.

The Picarro LASER instrument was only used twice, so no meaningful statements can be made about long term precision. Aside from the working standards, certain samples were run through the LASER and mass-spectrometer methods and the results were found to be similar, with approximately the same level of precision between instruments as within, as reported above.

The final correction procedure, making use of these measured values and adjusting them and the samples for each run to the known values, was able to produce data of acceptable accuracy.

δD ‰						
date	**CTMP2010**		**Evian**		**RMW**	
28-03-2011	-15.1	-12.8	-75.8	-76.0		
12-04-2011			-68.9	-70.2		
27-05-2011	-15.4	-13.3	-69.6	-67.2		
01-06-2011	-12.1	-9.8	-67.2	-59.7		
17-06-2011	-11.4	-11.3	-67.2	-70.3		
30-06-2011	-4.5	-0.6	-58.9	-59.2		
18-10-2011	-9.1	-12.2			-125.6	-125.7
13-12-2011	-4.1	-1.8			-119.6	-119.5
19-12-2011	-1.0	-1.1			-119.2	-119.1
03-02-2012	-2.0	-2.6			-115.8	-116.4
24-05-2012	-1.7	+0.4			-114.6	-115.2
31-05-2012	+9.0	+9.7			-104.6	-105.6
08-08-2012	-2.2	-3.0			-120.1	-121.6
15-08-2012	-0.7	-3.0			-122.9	-120.8
20-08-2012	+6.9	+6.3			-115.3	-116.0
04-10-2012	+12.9	+12.2			-98.0	-98.7
05-11-2012	+9.4	+7.9			-108.2	-108.0
21-02-2013	+8.7	+8.0			-105.0	104.2
03-04-2013	+11.5	+12.8			-100.0	-98.7
05-04-2013	+10.0	+9.9			-101.7	-102.2
02-05-2014	+7.8	-7.1			-107.6	-105.2
mean		-0.0075		-67.6		-111.8
maximum — minimum	+12.9 — -15.4		-58.9 — -76.0		-98.0 — -125.7	
standard deviation		8.9		5.7		8.7
mean difference		1.4		2.3		0.85
difference std. dev.		1.1		2.8		0.71

Table 3.3: Raw data for δD analyses of standards during this project. The values above are the mass-spectrometer values with the zinc correction applied.

$\delta^{18}O$ ‰						
date	**CTMP2010**		**Evian**		**RMW**	
15-03-2011	-4.46	-4.56	-10.5	-10.2		
12-04-2011			-10.44	-10.40		
26-05-2011	-5.75	-4.11	-9.76	-10.18		
02-06-2011	-4.10	-3.40	-9.65	-9.62		
07-06-2011	-3.27	-3.12				
20-06-2011	-3.48	-3.30	-9.61	-9.53		
07-07-2011	-3.63	-3.55	-9.61	-9.67		
01-08-2011		-2.54		-9.31		
03-08.2011		-4.25		-10.21		
04-08-2011		-3.86		-10.10		
12-08-2011		-3.63			-17.44	-17.59
24-10-2011		-3.61			-17.58	-17.77
21-12-2011	-3.53	-3.63			-17.50	-17.54
11-01-2012	-3.40	-3.09			-17.46	-17.61
01-02-2012	-4.58	-3.71			-17.56	-17.68
21-05-2012	-4.27	-4.16			-17.47	-18.09
28-05-2012		-3.63				-17.49
18-06-2012	-3.60	-3.80			-17.94	-18.45
18-07-2012	-3.62	-3.40			-17.82	-17.76
19-07-2012	-3.73	-3.68			-17.98	-17.86
23-07-2012	-4.04	-3.96			-17.57	-17.51
01-08-2012	-3.55	-3.67			-17.62	-17.51
10-10-2012	-4.57	-3.93				-17.27
11-10-2012	-3.42	-3.38			-17.61	-17.74
15-10-2012	-3.97	-3.82			-17.77	-17.83
06-11-2012	-3.67	-3.45			-17.44	-17.50
08-11-2012	-3.43	-3.49			-17.60	-18.47
19-02-2013	-3.18	-3.34			-17.56	-17.36
26-03-2013	-3.71	-3.35			-17.34	-17.42
27-03-2013	-3.41	-3.03			-17.13	-17.16
28-03-2013	-3.11	-3.05			-17.27	-17.36
04-04-2013	-2.92	-3.11				-17.01
02-05-2014	-3.42	-3.43			-17.19	-17.22
mean		-3.65		-9.92		-17.58
maximum — minimum	-2.54 — -5.75		-9.31 — -10.50		-17.01 — -18.47	
standard deviation		0.51		0.38		0.30
mean difference		0.28		0.15		0.18
difference std. dev.		0.35		0.16		0.22

Table 3.4: Raw data for $\delta^{18}O$ analyses of standards. The values above are the mass-spectrometer values with the reference gas and $CO_2 - H_2O$ equilibration corrections applied.

3.5 Data Analysis

A substantial portion of the analysis of stable isotope data consists of finding correlations and calculating regressions. The most common regression analysis is known as the *least squares method*. This assumes the x-variable is independent and accurately known, whereas the y-variable depends upon the x-value and has errors and random variations. An example of an independent x-variable would be time or distance, and a dependent y-variable could be temperature, rainfall or an isotope ratio. For analysis of one stable isotope ratio, say δD against one of these independent variables, the *least squares regression* is suitable. However, where both variables are dependent, such as δD and $\delta^{18}O$, no one should be treated as more certain than the other and so the *reduced major axis* form of a structural regression is suitable.

Least Squares Regression

To calculate a straight line of the form:

$$y = mx + c\,,$$

using the least squares regression:

$$\begin{aligned} m &= \frac{SP_{xy}}{SS_x} \\ \text{and} \quad c &= \bar{y} - m\bar{x}\,, \\ \text{where} \quad SS_x &= \sum_{i=1}^{n}(x_i - \bar{x})^2 \\ \text{and} \quad SP_{xy} &= \sum_{i=1}^{n}(x_i - \bar{x})(y_i - \bar{y})\,. \end{aligned}$$

Reduced Major Axis Regression

The RMA regression line is calculated in a similar way to above, with the single difference that the gradient, m, is calculated as follows:

$$\begin{aligned} m &= \sqrt{\frac{SS_y}{SS_x}} \\ \text{where} \quad SS_y &= \sum_{i=1}^{n}(y_i - \bar{y})^2\,. \end{aligned}$$

Weighted Regression Line Calculations

As noted by Hughes and Crawford (2012), weighting of isotopic values for monthly cumulative

rainfall by the rainfall amount produces regression lines (meteoric water lines) with higher gradients, as a result of minimising the influence of evaporated samples from low rainfall events. The difference in gradient between weighted and unweighted regression lines depends on the dataset. These meteoric water lines better characterise the average rainfall and especially heavier events that are more likely to play an important role in hydrological processes such as groundwater recharge. Calculation of such regressions uses methods similar to above, but by adding the rainfall term into the statistical quantities as follows:

$$SS_x = \sum_{i=1}^{n} (rain_i)(x_i - \bar{x})^2 \ ,$$
$$SS_y = \sum_{i=1}^{n} (rain_i)(y_i - \bar{y})^2 \ ,$$
$$SP_{xy} = \sum_{i=1}^{n} (rain_i)(x_i - \bar{x})(y_i - \bar{y}) \ .$$

3.6 Maps

The maps that follow were prepared using the QGIS programme with shapefiles of 1:50 000 tile data from the Chief Directorate for National Geo-Spatial Information of the South African Department of Rural Development & Land Reform. Dotted grey circles around some sampling sites are 5 km radius circles and will be mentioned in the Discussion chapter.

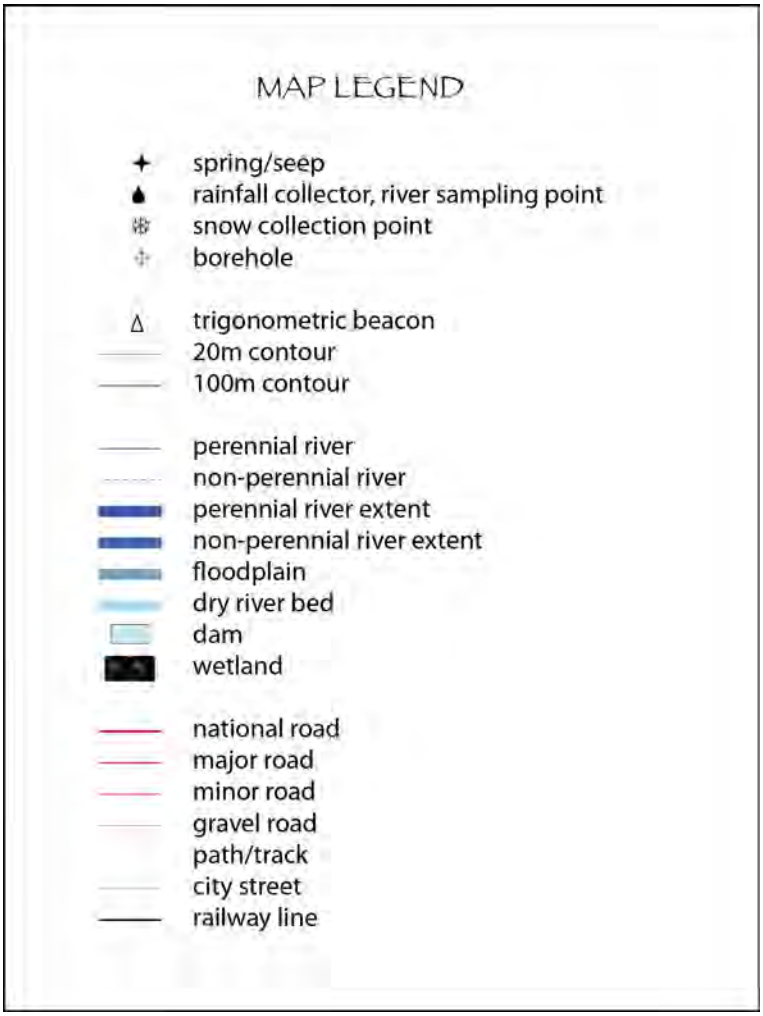

Figure 3.6: Legend for the location maps.

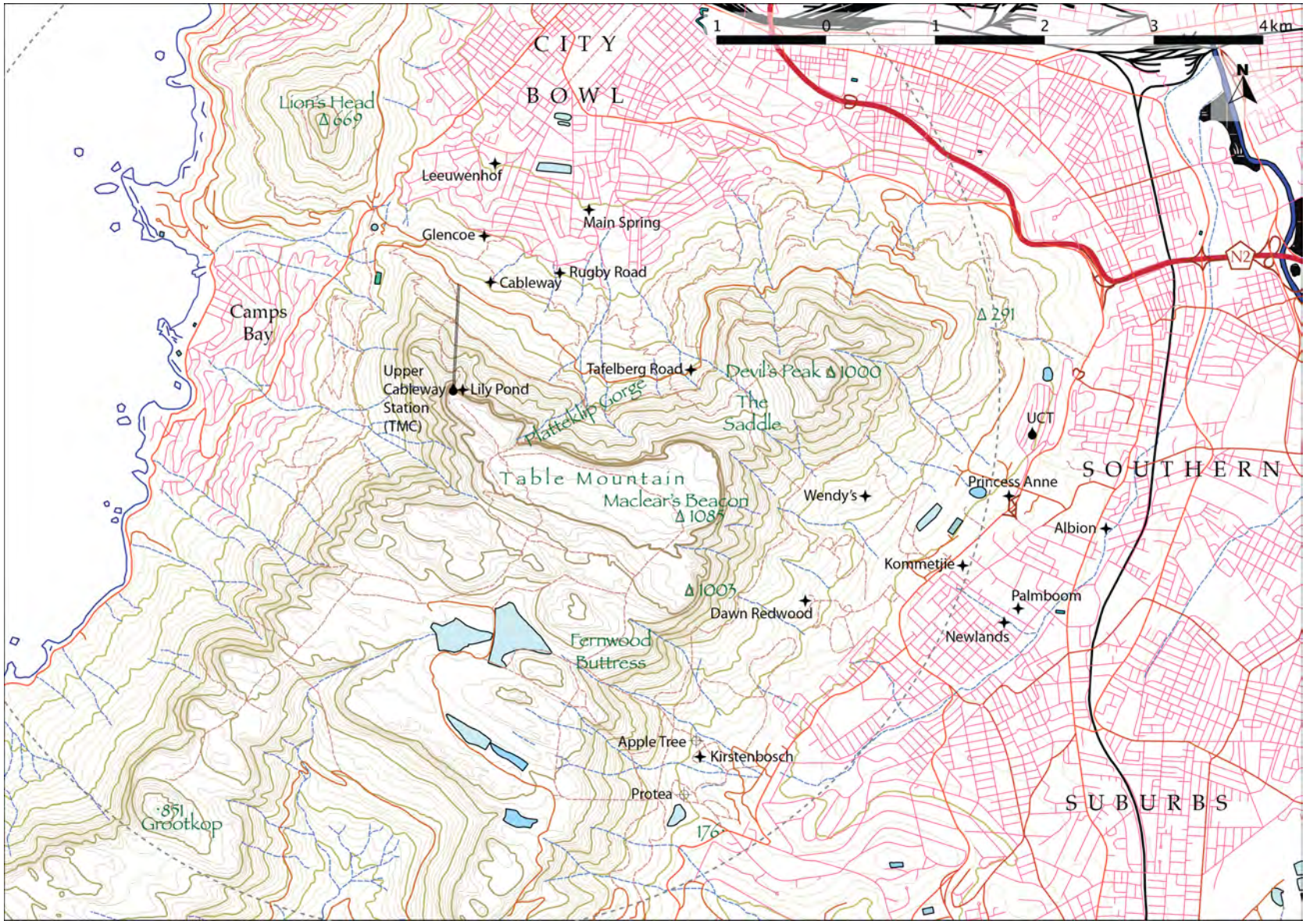

Figure 3.7: Locations of sampling points in the Cape Town area.

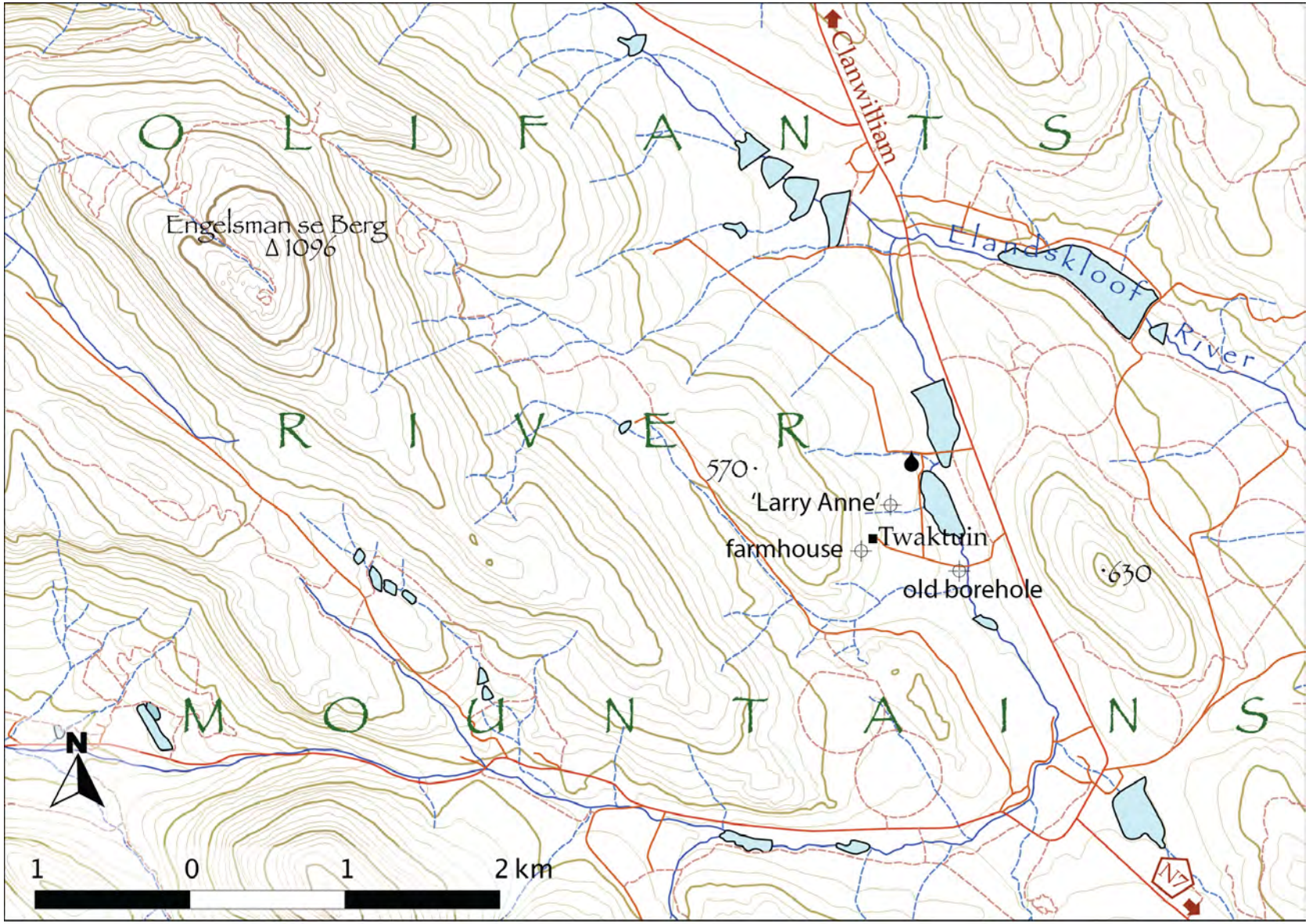

Figure 3.8: Locations of the rainfall collector and three boreholes sampled on Twaktuin Farm, south-west of Clanwilliam.

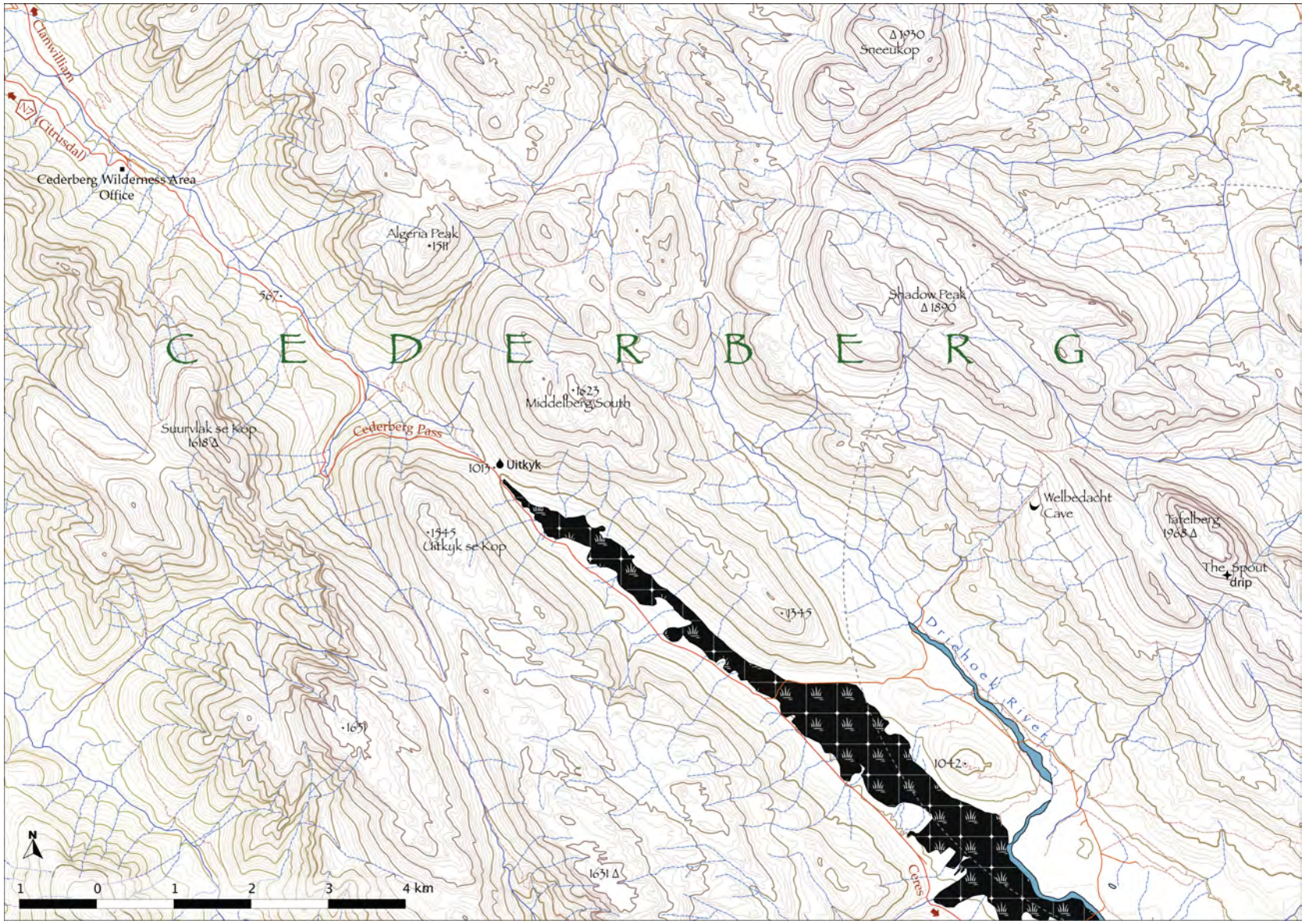

Figure 3.9: Locations of the rainfall collector and high altitude seep sampled in the Cederberg, south-east of Clanwilliam.

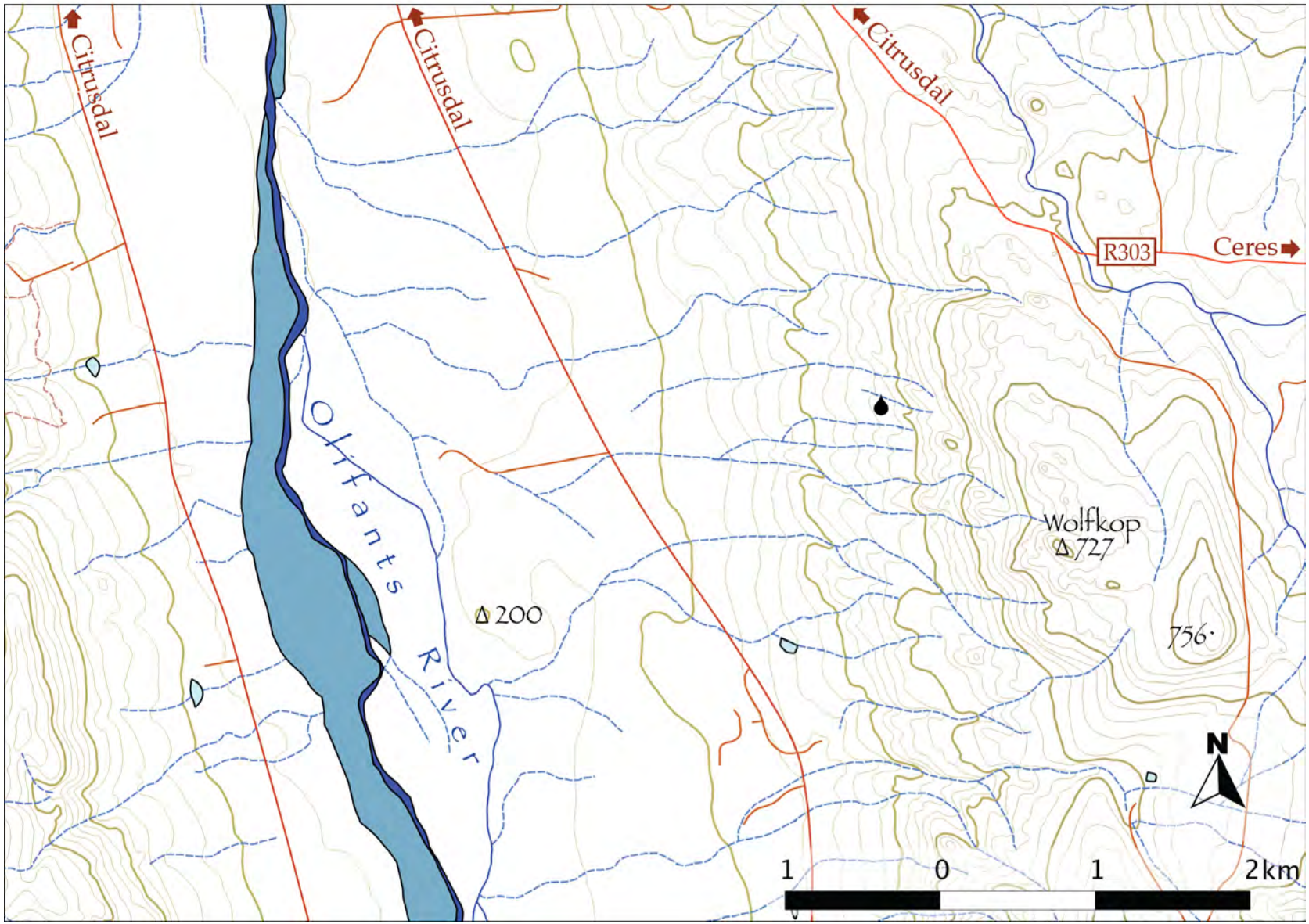

Figure 3.10: Location of the rainfall collector at Wolfkop Nature Reserve, south of Citrusdal.

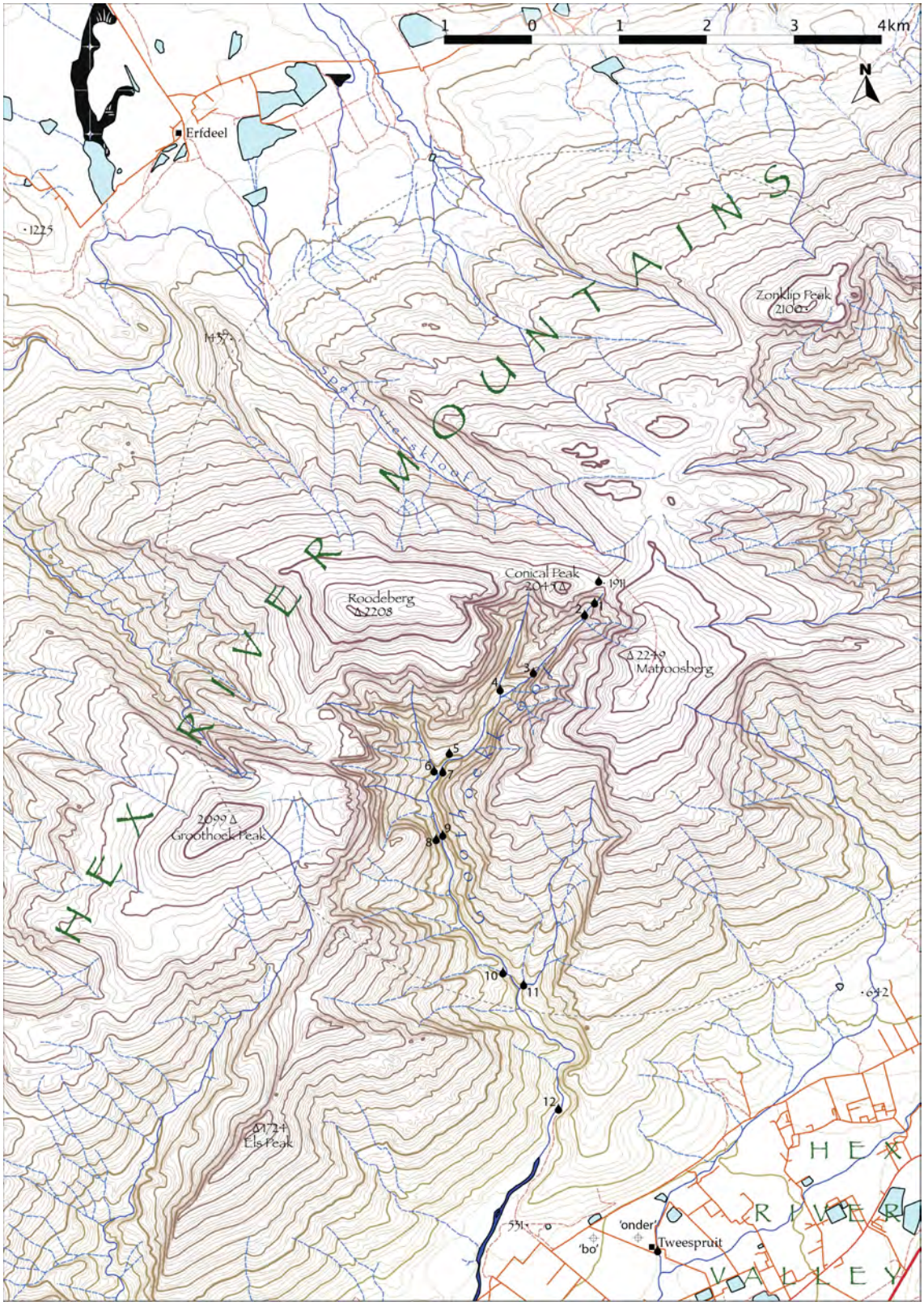

Figure 3.11: Locations of the Erfdeel and Tweespruit rainfall collectors and boreholes and the Groothoekkloof river samples in the vicinity of Matroosberg, the highest peak in the south-western Cape.

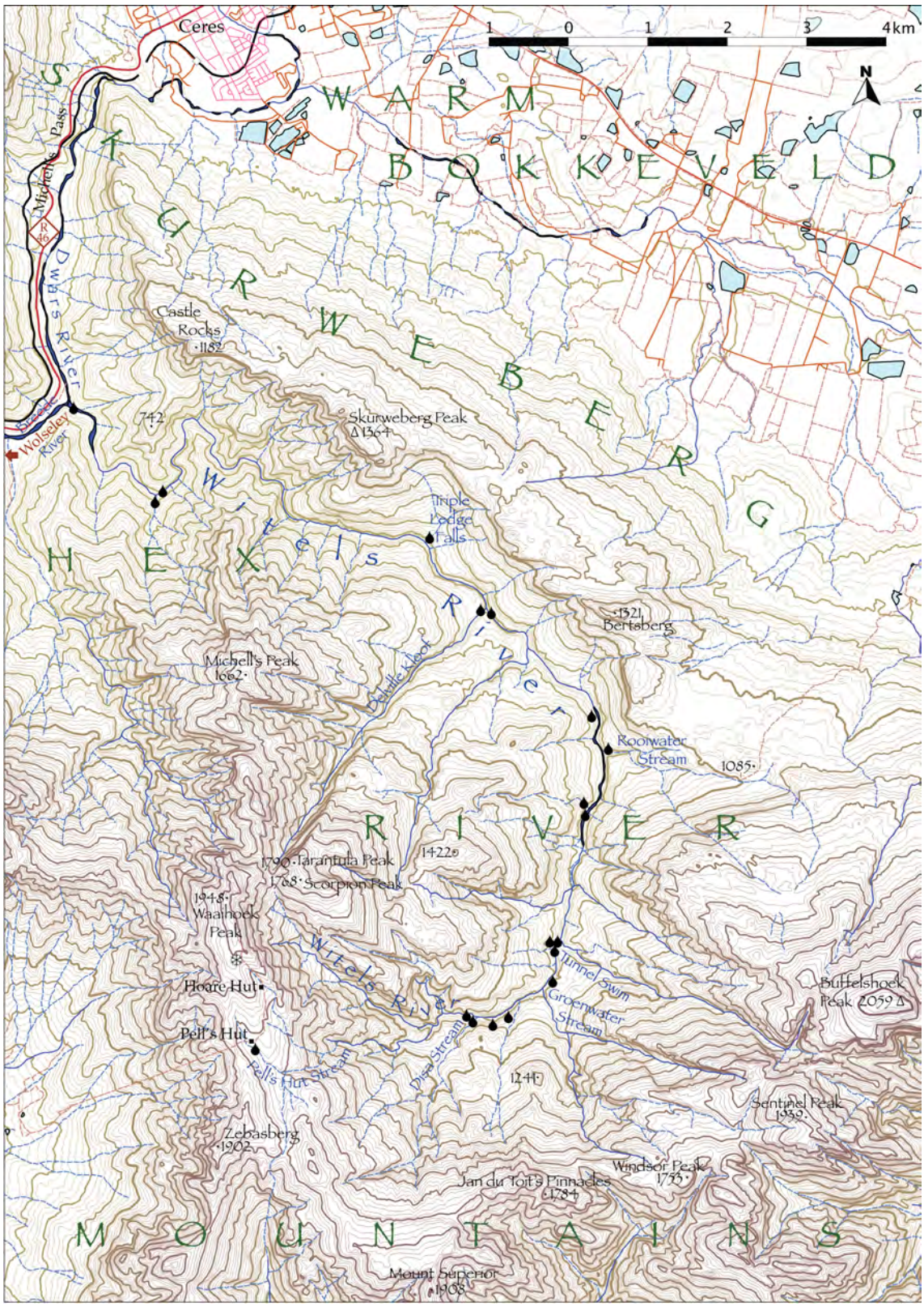

Figure 3.12: Locations of the Waaihoek Peak snow and Witels River samples taken in the Hex River Mountains, south of Ceres.

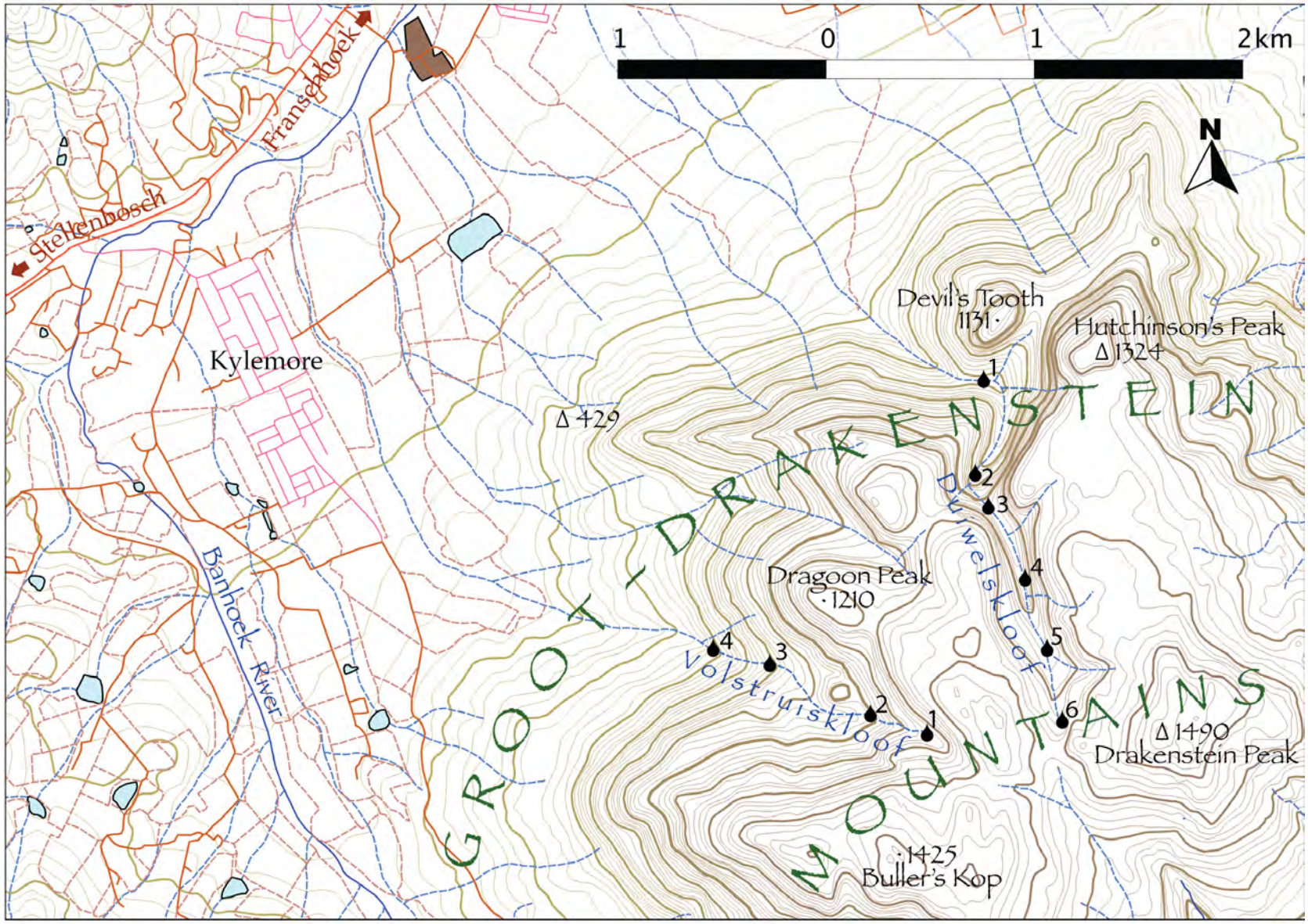

Figure 3.13: Locations of the Duiwelskloof and Volstruiskloof river samples taken in the Groot Drakenstein Mountains, east of Stellenbosch.

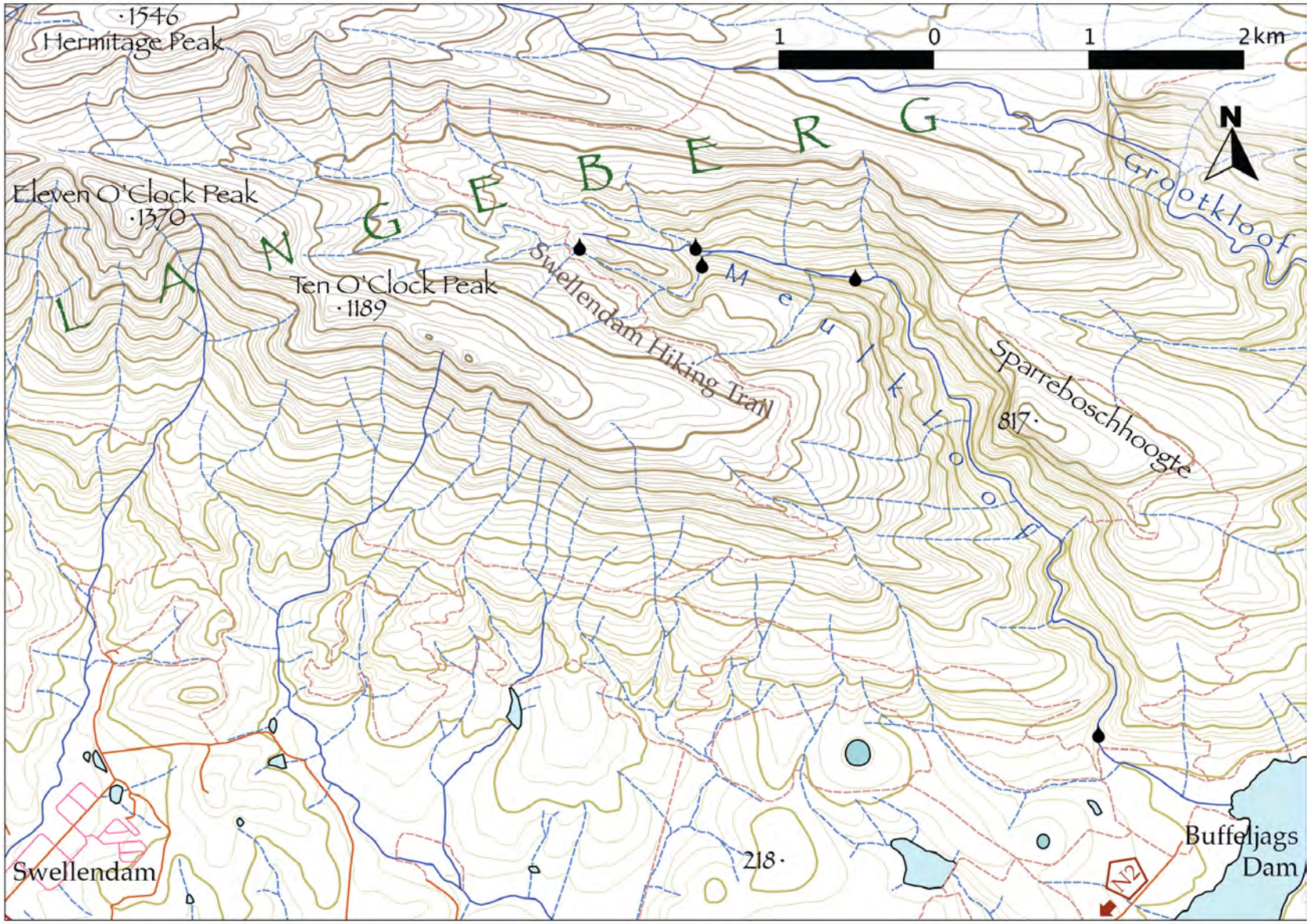

Figure 3.14: Locations of the Meulkloof river samples taken in the Langeberg, east of Swellendam.

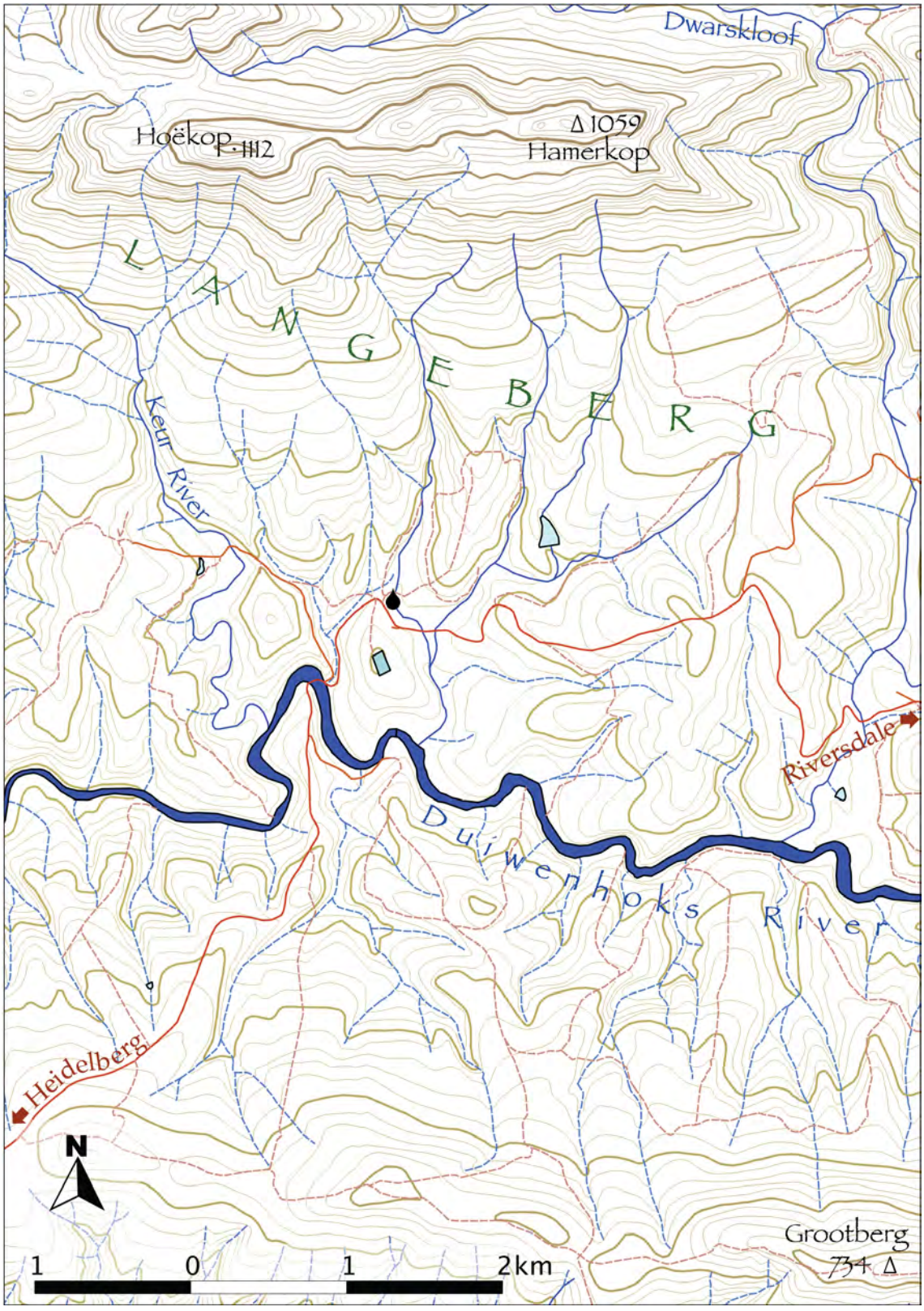

Figure 3.15: Location of the Riverndale rainfall collector, north of Heidelberg.

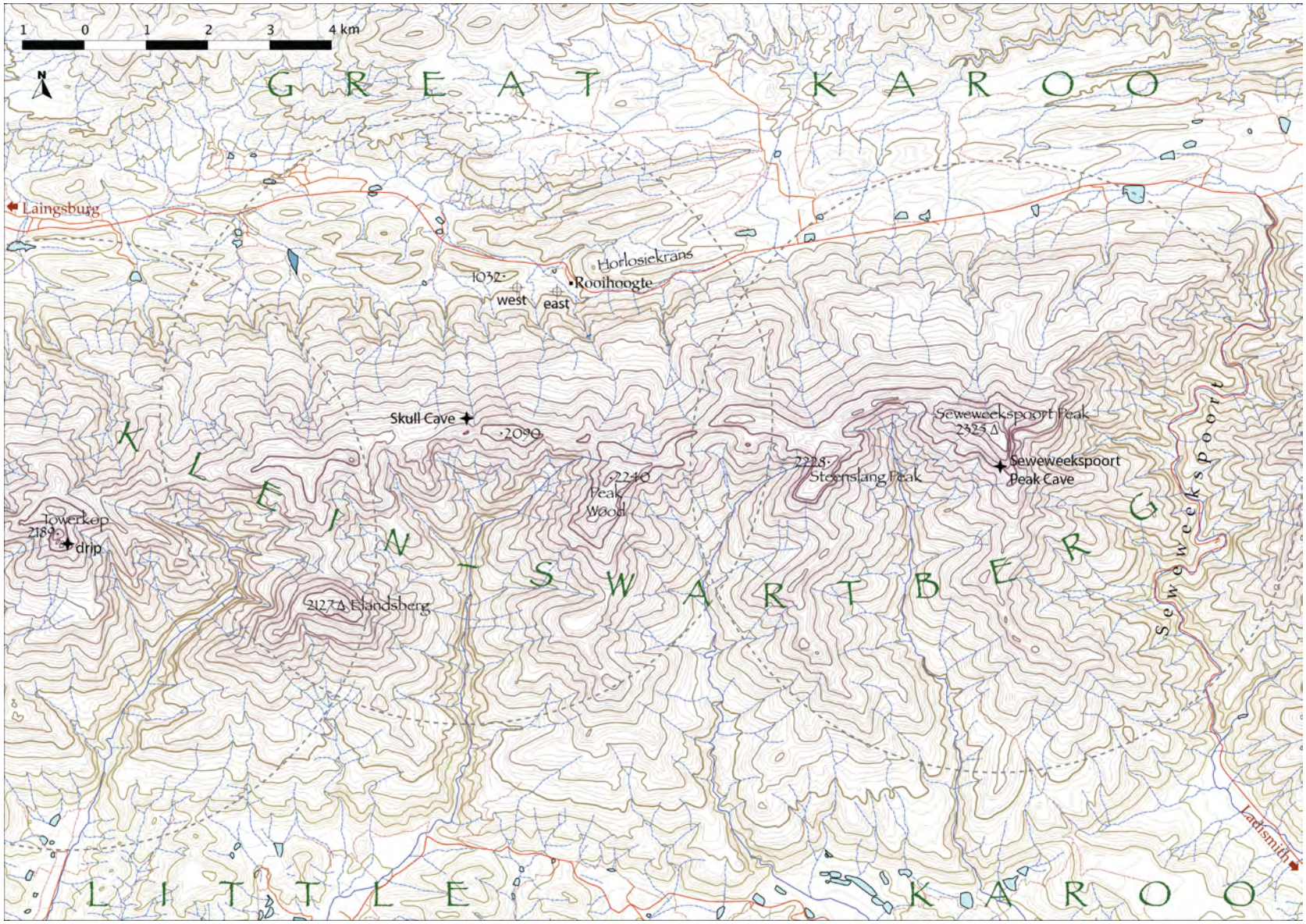

Figure 3.16: Locations of high altitude seeps in the Klein Swartberg and boreholes on Rooihoogte Farm.

Figure 3.17: Locations of the Bakenskop mountain and the store rainfall collectors as well as the boreholes at Gamkaberg, south-east of Calitzdorp.

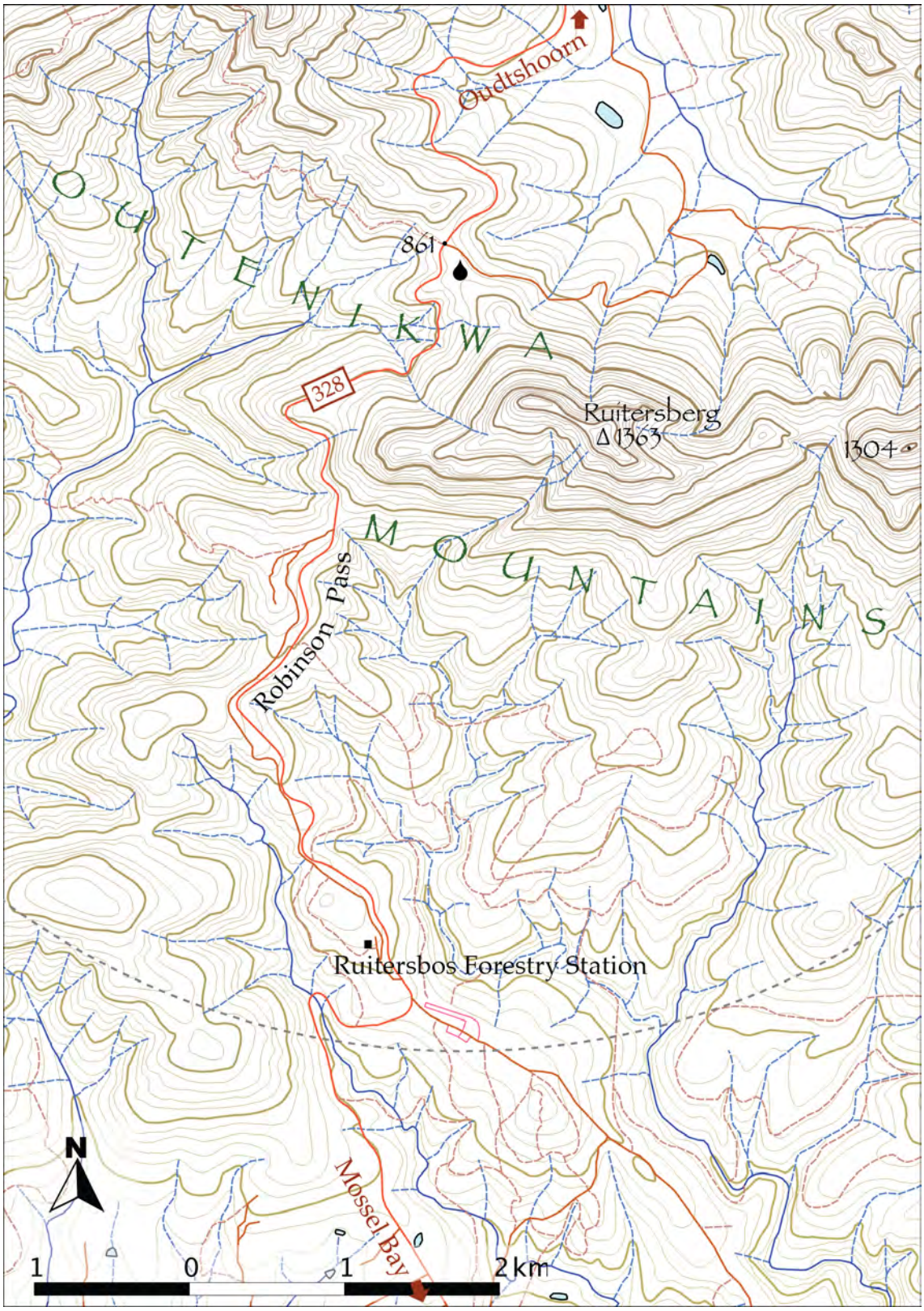

Figure 3.18: Location of the rainfall collector on Robinson Pass, north of Mossel Bay.

Figure 3.19: Location of the rainfall collector in the Kammanassie Mountains, south of De Rust.

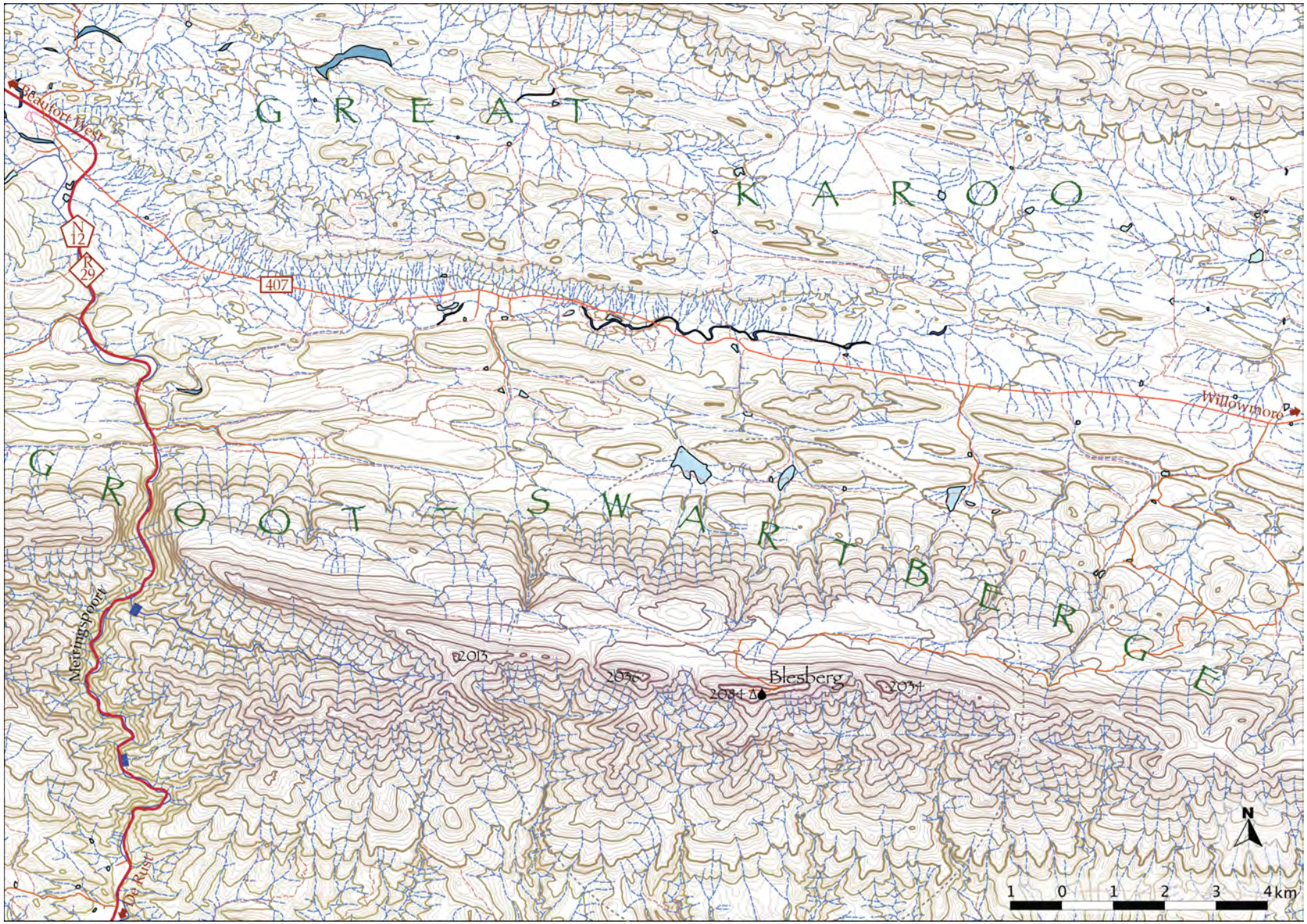

Figure 3.20: Location of the rainfall collector on top of Blesberg in the Groot Swartberg, north-east of De Rust.

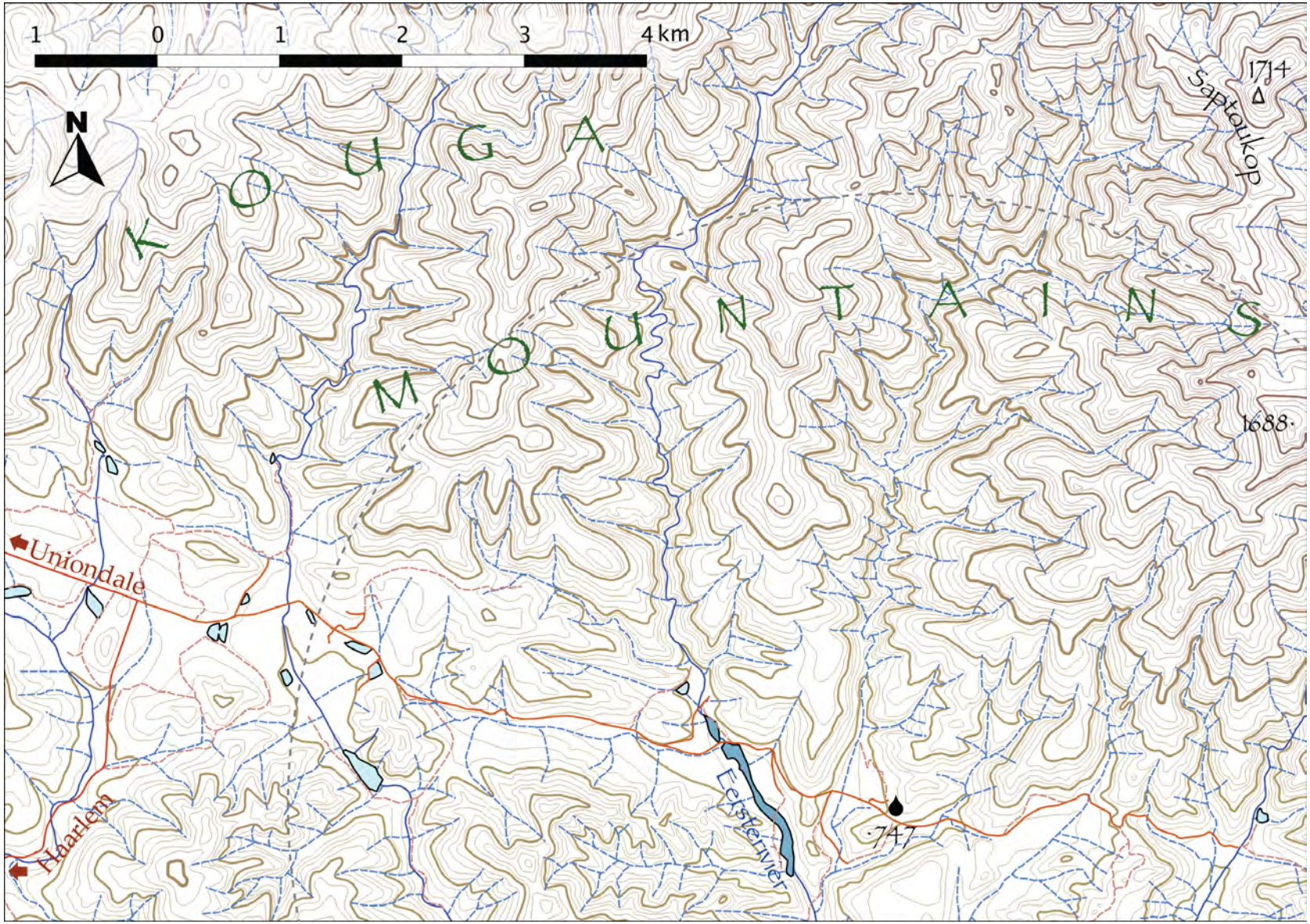

Figure 3.21: Location of the rainfall collector on Lentelus Farm in the Kouga Mountains, south-east of Uniondale.

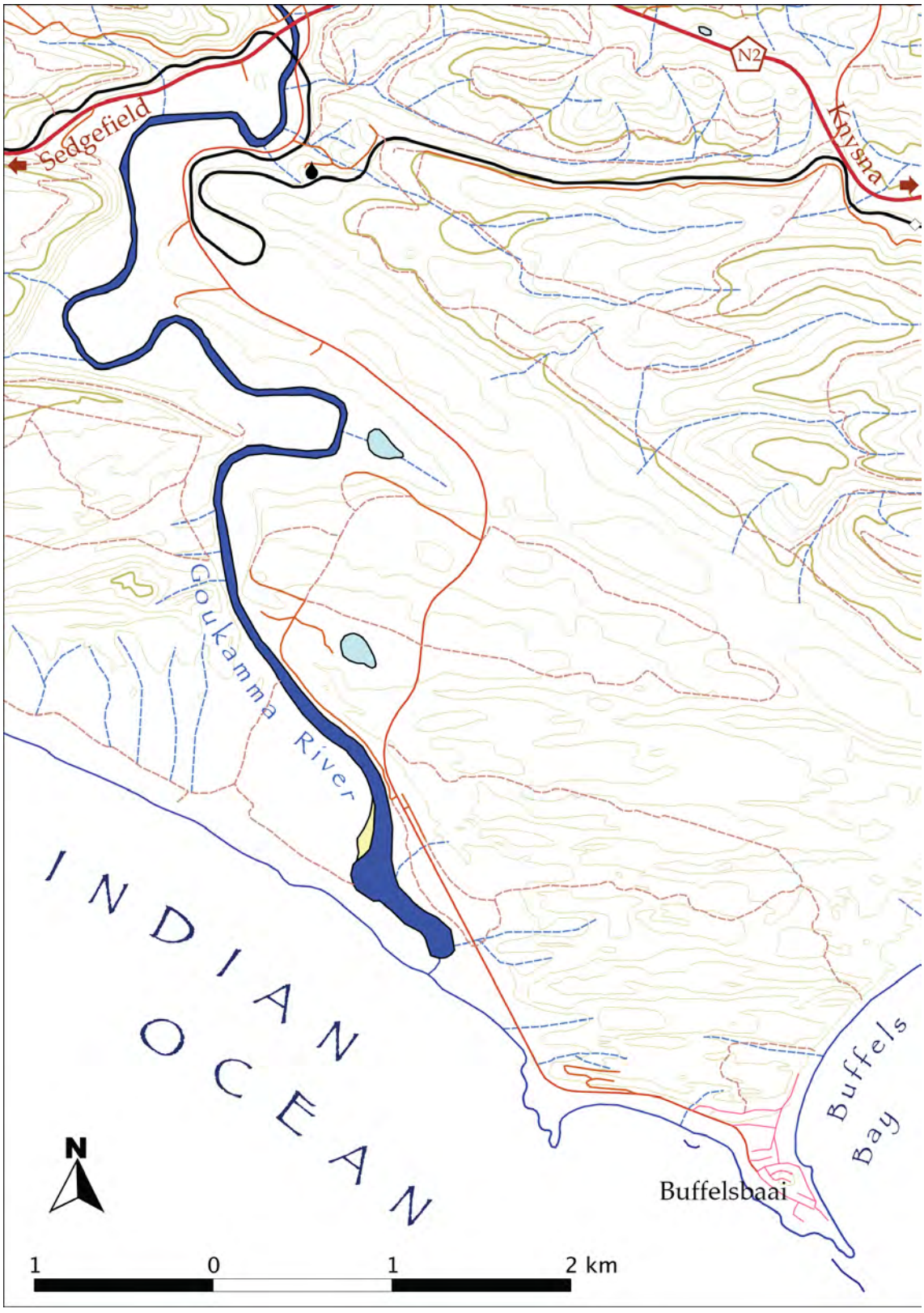

Figure 3.22: Location of the rainfall collector above the Goukamma River, west of Knysna.

Chapter 4

Results

4.1 Introduction

This chapter reports the data collected in this study, namely rainfall amounts and hydrogen and oxygen isotope values of various water samples, including rain, snow, river water and groundwater, the latter from both natural sources such as springs and seeps as well as from boreholes. The rainfall is presented as monthly amounts and some of the notable variations in space and time are described. Isotope data of rainfall is presented over time and compared with weather events to make sense of some of the outlier isotopic compositions. The rain isotope data is also analysed by generating means and weighted means for each rainfall station, d-excess values for these means, and meteoric water lines. Groundwater isotope data and the best-fit line through this data is compared to the rainfall isotope data and meteoric water lines. Mention is also made of other samples, such as surface water and snow. The isotope data for this study is reproduced in **Tables 4.5 to 4.10** at the end of this chapter.

4.2 Rain

In order to understand the hydrological impact of hydrogen and oxygen isotope ratios in monthly cumulative rainfall samples, the amount of rain for each month must be known. Isotope values from months with high rainfall have a greater effect on the isotope signatures in the hydrological cycle than months with low rainfall and therefore the isotope values need to be weighted accordingly when calculating means and meteoric water line equations. All the regular rainfall samples taken for this study are shown in **Table 4.1**.

	2010												2011												2012											
stn.	J	F	M	A	M	J	J	A	S	O	N	D	J	F	M	A	M	J	J	A	S	O	N	D	J	F	M	A	M	J	J	A	S	O	N	D
UCT	–	–	–	–	–	–	–	–	–	–	–	–	–	–	–	–	–	–	–	–	–	–	–	–	–	–	–	–	–	–	–	–	–	–	–	–
TMC					–	–	–	–	–	–	–	–	–			–	–	–	–	–	–	–	–	–	–	–	–									
TWT					–	–	–	–	–	–	–	–	–	–	–	–	–	–	–	–	–	–	–	–	–	–	–	–	–	–	–	–				
UKP								–	–	–	–	–	–	–	–	–	–	–	–	–		–	–	–	–	–	–	–	–		–	–				
WKP					–	–	–	–	–	–	–	–	–	–	–	–	–	–	–	–	–	–	–	–	–	–	–	–	–	–	–	–				
MTB					–								–	–	–	–	–	–	–	–	–	–	–	–	–										
DDN																		–	–	–	–	–	–	–	–					–					
RVD						–	–	–	–	–	–	–	–	–	–	–	–	–	–	–	–	–	–	–	–	–	–	–								
RBP						–	–	–	–	–	–								–																
BKK						–	–	–	–	–	–					–	–	–	–	–	–	–	–	–											
GST													–	–	–	–	–	–	–	–			–	–	–	–	–	–	–	–	–	–				
BBG						–	–	–	–	–	–	–	–	–	–	–				–	–	–	–			–	–	–	–	–	–					
KMN						–	–	–	–	–	–					–	–	–	–		–														
LTL						–	–	–		–	–		–	–	–	–	–	–	–	–	–	–	–	–	–	–	–								
GKM						–	–	–	–	–	–	–	–	–	–	–	–	–	–	–	–	–	–	–	–	–	–	–	–							

Table 4.1: Bars indicate the months for which total monthly rainfall was analysed for hydrogen and oxygen isotopic composition.

station code and name		elevation	continentality		MAP	SI	n	weighted mean & standard deviation				d-excess
			Atlantic	'sea'				δD	$\sigma_{\delta D}$	$\delta^{18}O$	$\sigma_{\delta^{18}O}$	
		(masl)	(km)	(km)	(mm/a)			‰	‰	‰	‰	‰
UCT	University of Cape Town	135	8	8	1210	0.63	36	-9.2	6.0	-2.89	1.19	14.0
TMC	Table Mountain	1074	3	2	1328	0.43	23	-13.9	5.7	-3.77	1.04	16.3
TWT	Twaktuin	412	48	45	510	0.76	17	-11.4	19.6	-2.96	3.41	12.3
UKP	Uitkyk Pass	1013	70	70	1177	0.81	20	-21.7	9.8	-4.67	2.23	15.6
WKP	Wolfkop	355	72	70	565	0.81	25	-15.9	11.4	-3.82	1.42	14.7
MTB	Matroosberg	1910	143	110	702	0.83	14	-43.1	9.6	-7.95	1.44	20.5
DDN	Tweespruit	482	133	105	213	0.91	6	-19.4	15.8	-3.14	2.09	5.8
RVD	Riverndale	251	242	42	671	0.40	23	-10.3	13.7	-3.44	2.38	17.2
RBP	Robinson Pass	885	330	30	1093	0.47	7	-23.3	11.3	-4.91	2.39	16.0
BKK	Bakenskop	1101	314	50	529	0.46	15	-29.2	12.2	-5.84	2.63	17.5
GST	Gamka Store	350	315	55	297	0.50	15	-15.6	13.5	-3.37	2.76	11.4
BBG	Blesberg	2080	410	65	735	0.50	18	-28.3	8.0	-6.16	1.04	21.0
KMN	Kammanassie	666	482	50	400	0.56	11	-36.3	23.1	-7.37	2.95	22.7
LTL	Lentelus	642	573	35	567	0.51	20	-26.9	20.4	-5.62	3.16	18.1
GKM	Goukamma	62	526	5	701	0.54	25	-14.3	15.3	-3.82	1.98	16.3
	all				713		275	-17.7	14.2	-4.22	2.33	16.0

Table 4.2: Continentality distance from Atlantic Ocean measured along a line of latitude; 'sea' distance is distance in any direction to the closest coast. Mean annual precipitation (MAP) and seasonality index (SI) based on 3 years of rainfall records; stable isotope weighted means and standard deviations using 'n' number of cumulative monthly rainfall samples. Deuterium excess for each station and the region, calculated from the weighted means.

These rainfall amounts should have been recorded when the rain was collected, however, due largely to human error, not all the figures were recorded or retained for each sample. In some cases people collecting rain forgot to record the amount, in other cases, the data was mislaid. However, it was possible to estimate these missing rainfall amounts by interpolation between South African Weather Service stations (SAWS, 2010-12), rainfall stations within this study and by using the SAWS monthly rainfall maps, examples of which are given in **Figure 4.1**. When estimating missing rainfall amounts, consideration was also given to factors known to affect rainfall, in particular the altitude, proximity and leeward or windward relationship to mountains, and distance from the sea.

The resultant rainfall figures, both measured and estimated, for each rainfall collection station are displayed in time series graphs in **Figure 4.14**. The most obvious pattern seen in these graphs is the seasonal signature caused by the higher rainfall occurring in winter from cold fronts (westerly waves) and the subsequent southerly meridional flow, as explained in Chapter 2. The second most noticeable pattern is the change from highly seasonal rain in the west to less seasonal in the east, as discussed below in **Section 4.2.2**.

4.2.1 Rainfall Amount

The average annual rainfall at the rain collection stations is shown in **Table 4.2**. Although this figure is only for three years and for most of the stations is based on many estimations, the averages do illustrate the range of rainfall amounts recorded and some general trends. Stations at higher latitude, altitude and nearer to the sea tend to receive more rain. Other factors, such as proximity to mountains, steepness of slopes and aspect (relative to rain-bearing winds) also influence the rainfall at a site. These were the factors used by Dent et al. (1987) and Beuster et al. (2009) to produce the MAP (mean annual precipitation) map for the south-western Cape, as discussed in Chapter 1.

Examination of the graphs in **Figure 4.14** shows how variable rainfall is across the Western Cape. Rainfall collection stations less than 50 km apart can receive vastly different quantities of rain in a month. For example, in August 2010, Twaktuin recorded 69 mm, Uitkyk Pass 215 mm and Wolfkop 84 mm. These sorts of variations are epitomized by the famous microclimates of Cape Town, as is revealed from the UCT and Table Mountain Cableway stations, less than 5 km apart, where in December 2010 those two stations recorded 17 mm and 60 mm respectively, and similarly for October 2012 with 44 mm and 123 mm. This variation is not always systematic; the generally wetter station may sometimes receive less rain. For example, in February 2011, Lentelus, which averages 80 % of the rainfall of Goukamma, recorded 65 mm in comparison to Goukamma's 39 mm; this is 160 %, or double the expected amount; or one could say that Goukamma was half as wet as would be expected from the Lentelus rainfall. Similarly, in November 2012 UCT recorded 6 0mm in comparison to the normally wetter Table Mountain Cableway's 44 mm.

4.2.2 Rainfall Seasonality

The seasonality index (SI), as described by Walsch and Lawler (1981), has been calculated for the rainfall collection stations in this study, according to the formula:

$$SI = \frac{1}{\bar{R}} \sum_{n=1}^{n=12} \left| \bar{x}_n - \frac{\bar{R}}{12} \right|$$

where $\bar{R}$ is the MAP and $\bar{x}_n$ is the mean monthly precipitation for month n.

The SI values may not be very meaningful after only 3 years of collection, however, they still provide a reasonable idea of seasonality. The SI values, as shown in **Table 4.2**, all fall within moderately seasonal categories: SI from 0.40 to 0.59 is "rather seasonal with a short drier season"; SI from 0.60 to 0.79 is "seasonal" and SI from 0.80 to 0.99 is "markedly seasonal with a long drier season" (Walsch and Lawler, 1981). There is a general decrease in SI eastwards, as would be expected given that summer rainfall gradually increases from Cape Town eastwards. To the east of the study area, seasonality will again increase eastwards as the winter rainfall decreases.

The two maps in **Figure 4.1** also show the strong seasonality of rainfall in South Africa. The June 2010 map shows a typical winter rainfall pattern with most rain occurring in the Western Cape, high amounts being on the Boland, Hex River and Tsitsikamma Mountains and some other substantial rainfalls along the coast of the Eastern Cape and KwaZulu-Natal as well as on the high ground around the Lesotho - Free State - Eastern Cape borders. The December 2012 map shows a typical summer rainfall pattern, although with above average rainfall amounts, especially those over the Karoo and Namaqualand, while the Western Cape experiences negligible rainfall, except for the futhest eastern portions.

4.3 Rain Isotopes

Four hundred and thirty-five water samples have been analysed for their hydrogen and oxygen isotope composition, excluding duplicates, repeats, laboratory standards or blanks. The graph in **Figure 4.2** shows the distribution of the water samples according to major water type and collection altitude of sample. Rain waters make up the bulk of the samples at 279, groundwaters are intermediate at 110 and surface waters the minority at 46 samples. The altitude distribution reflects the dominance of samples taken in settled areas, which are generally at lower elevations, either near the coast or in valleys, with two spikes at higher elevations due to the rain and groundwater samples taken on peaks or passes at 1000–1200 m, or on the high peaks of the Cape Fold Belt at 1800–2200 m.

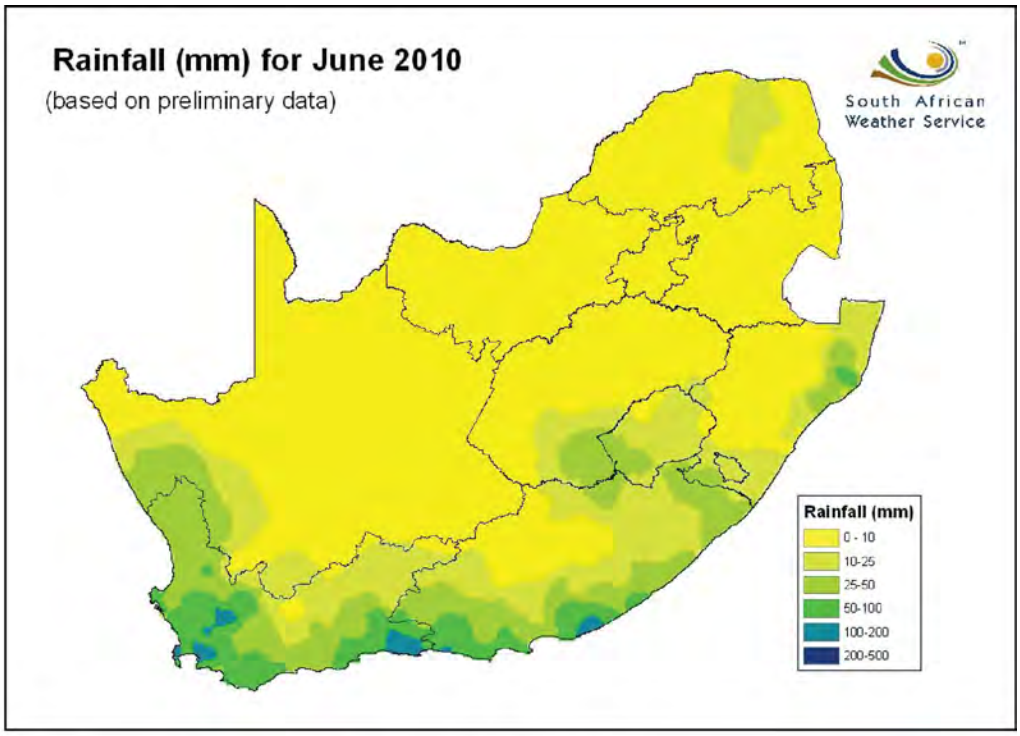

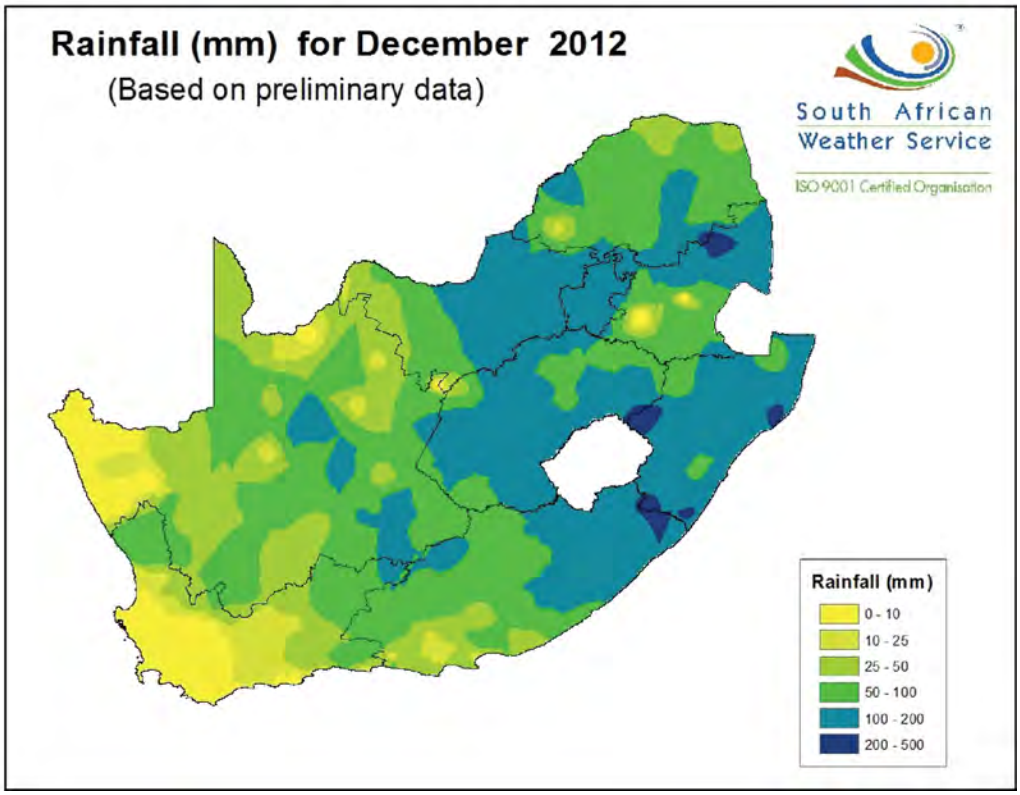

Figure 4.1: Two examples of the monthly rainfall maps produced by the South African Weather Service and available for download from their website (www.weathersa.co.za). The June 2011 map shows a typical winter rainfall pattern and the December 2012 map shows a typical summer rainfall pattern, although about 20 % wetter than normal.

4.3.1 Temporal Variations

Time series graphs have been plotted of all the isotope data from all the rainfall collection stations (**Figures 4.3 and 4.4**), separated into an eastern cluster (Riverndale, Robinson Pass, Bakenskop, Gamka Store, Blesberg, Kammanassie, Lentelus and Goukamma) and western cluster (UCT, Table Mountain, Twaktuin, Uitkyk, Wolfkop, Matroosberg and De Doorns) for ease of viewing. Several features stand out from these graphs. Firstly, although the isotope δ values correlate amongst stations some of the time, at other times they do not. In a few cases there may be field sampling errors, such as evaporation, causing a poor correlation. Most of the time, however, the samples are probably unaltered, based on discussions with the samplers, and the poor correlation indicates the spatial variation of isotope content of precipitation. This interpretation is reinforced by the observations made in **Section 4.2.1** showing how spatially variable rainfall amounts are. If the rainfall amounts are variable, the weather systems are heterogenous and it follows that the isotopic content of the rain may be varied.

Secondly, there is a general pattern of more negative δ values over winter and less negative δ values over summer, as would be expected for areas with a Mediterranean climate (e.g. Jaunat et al., 2013). This pattern is most noticeable in the eastern cluster, both for δD and $\delta^{18}O$. This pattern results from several of the meteoric water isotope effects, as mentioned in Chapter 1, such as the temperature effect and amount effect; in winter, temperatures are colder and rainfall amounts are greater, so rainout removes heavier isotopes faster and the lighter isotopes become more abundant in rain, resulting in more negative δ values. In summer the reverse is true; rainfall amounts are lesser and temperatures are warmer, resulting in less negative δ values. In particular, the effect of evaporation of raindrops during small amount rainfall events shifts the isotopic content to less negative or even positive δ values.

In the western cluster in particular, the data shows greater variation over summer and more similar values over winter. In winter, regional weather systems sweep over all the rainfall stations and produce rain of similar isotope content. In summer, weather systems may be more localised with the result that some stations receive almost no rain, others receive small, highly evaporated amounts with less negative or even positive δ values, and summer thunderstorms may deposit large amounts of rain with very negative δ values. As a result, summer isotopic ratios are less consistent between stations.

In addition to these general patterns, there are occasional spikes in δ values. July 2010 was a month with very negative δ values in the eastern cluster of rain collection stations. The weather systems that caused this month's rain have been compared to those in months without a negative spike in δ values, such as June 2010 or July 2011. For example, in July 2010 there were only two major rain producing systems, the first being a cold front followed by southerly meridional flow over 10–11th and the second being another cold front followed by south-westerly air flow on the 14–15th (SAWS, 2010-12). These rain producing weather systems are very similar to those for June 2010, in which a double cold front was followed by southerly meridional flow from 7–9th

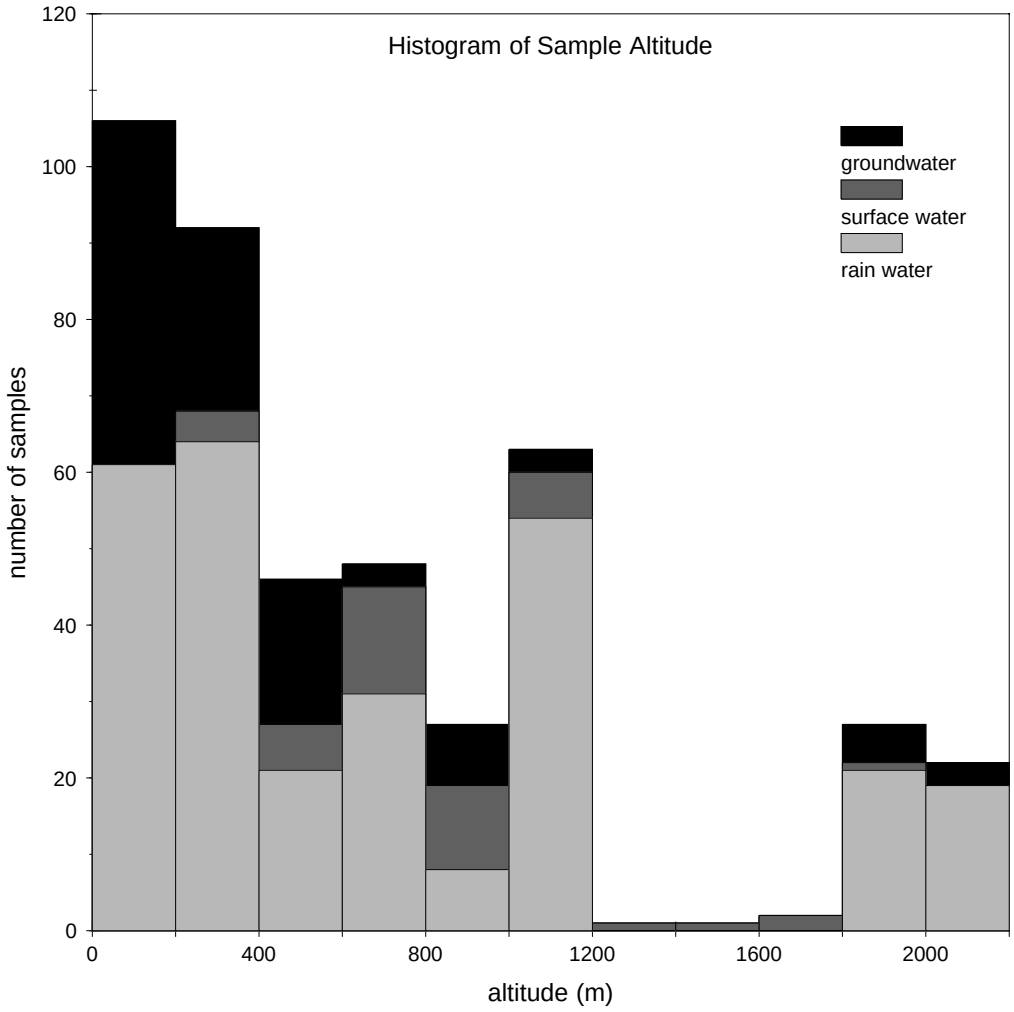

Figure 4.2: A plot of the distribution of the sampling altitude of all samples taken in this study.

and another double cold front was followed by southerly and then south-westerly flow over the 12–16th. For all these events, maximum daily rainfalls across the study area were typically in the 30–60 mm range, with averages being in the 10–20 mm range (SAWS, 2010-12). There is no unusual weather system or anomalously high rainfall for July 2010.

Temperatures at a weather station may undergo various changes as a weather system passes over. Maximum temperatures typically decrease as the cloudy, wet weather arrives and recover once clearing takes place, although may stay depressed if the southerly or south-westerly airflow is strong. Minimum temperatures however, may either decrease or increase, depending on the weather preceding the arrival of the cold front and the timing of the system (SAWB, 1996). Temperatures behaved variably in the June 2010 and July 2010 rainfall producing weather events, with no remarkable cold or change in July 2010. In the case of this distinctive spike in isotope values, it is therefore not easy to find something exceptional about the weather that could account for these results.

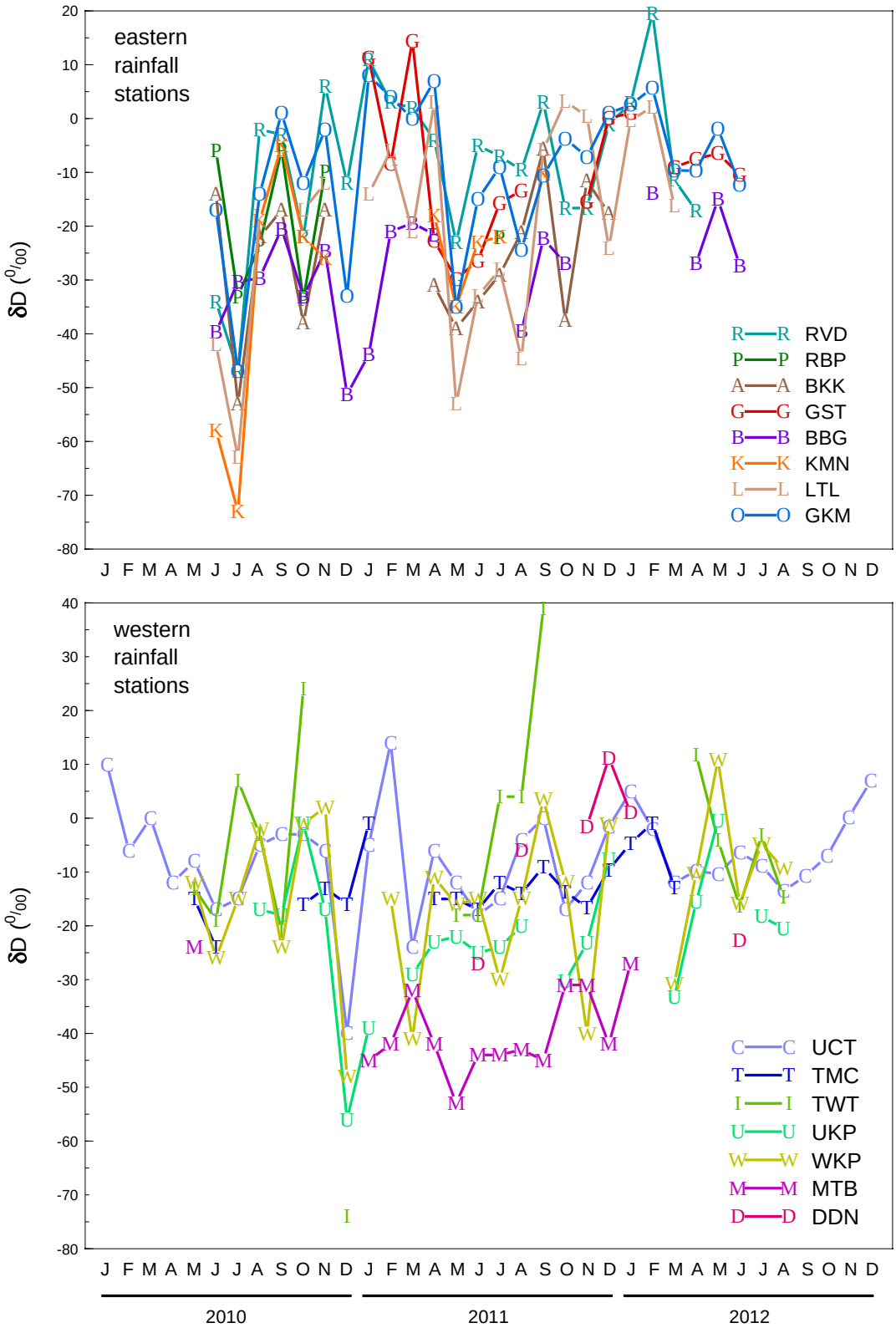

Figure 4.3: Time series graphs for δD for all rainfall stations, the eastern cluster on top and western cluster at the bottom. Stations with missing months have broken lines.

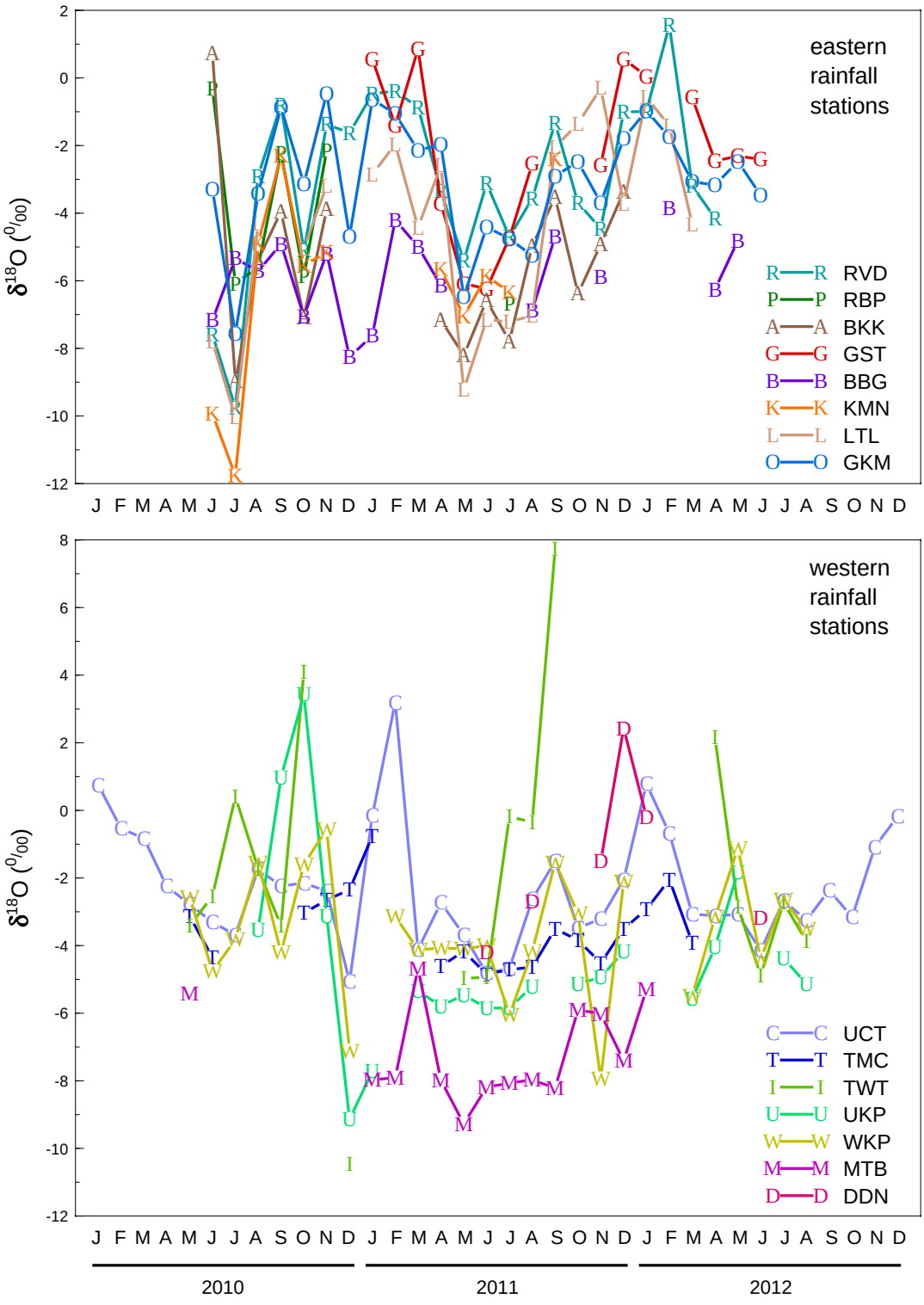

Figure 4.4: Time series graphs for $\delta^{18}O$ for all rainfall stations, the eastern cluster on top and western cluster at the bottom. Stations with missing months have broken lines.

December 2010 also features a negative spike in delta values, most noticeable for the Cederberg cluster of stations. In this case, it is easy to find the weather systems responsible for these results. During this month, several west coast troughs established and ridges of low pressure, connected to the summer rainfall producing *Kalahari Low*, penetrated far south into the Western Cape, but only twice did these result in appreciable rainfall in the Western Cape. The first occurred on 15–16th and delivered daily rainfall up to 60 mm at Vredendal, with lesser amounts of 30 mm at Lamberts Bay, 23 mm at Excelsior Ceres and other more minor amounts. The second event straddled the New Year, with up to 14 mm at Porterville on the 31st. Similar rainfalls occurred on 1st January 2011, such as 19 mm at Excelsior Ceres and 12 mm at Wellington, and it is quite possible that these were included in the December 2010 rainfall sample by the rainfall collectors. These low pressure systems produce convective style rain (thunderstorms) and hail was experienced by the author on top of Tafelberg at 1960 m in the Cederberg on 1st January 2011 (see **Figure 4.5**). The convective nature of these clouds can result in precipitation forming at high altitudes and hence low temperatures, which can result in relatively negative delta values, compared with the more stratified winter rainfall systems. Also, rainfall occurs in short, heavy showers in which minimal evaporation from raindrops occurs, reducing the extent to which the isotopic ratios will be driven to less negative delta values.

In November 2011 there was a very strong negative spike in the delta values for Wolfkop only. This can be traced to a low pressure trough extending southwards from the Kalahari on the 19th and causing convective rainfall. The rainfall amounts recorded were low, with daily totals of only 6 mm at Vredendal, 4 mm at Lamberts Bay and even lower elsewhere, but clearly the rain/hail that fell during this event must have been generated in systems with very low temperatures to account for the very negative delta values measured.

Some highly positive delta values, from +10 – +40 ‰ δD and +2 – +8 ‰ $\delta^{18}O$, were also measured, particularly at the Twaktuin station, but also at Uitkyk Pass, UCT and DeDoorns. These values have most probably been caused through extensive evaporation, both during the actual rainfall event of 19th November 2011 and possibly also from the rain gauge after the event. The latter is probably the reason for the extremely high spike at Twaktuin in September 2011, as there is no indication of similar behaviour at the other stations. However, the October 2010 spike is recorded at both Twaktuin and Uitkyk Pass and in that case probably reflects evaporation during rain drop descent. Similarly, the February 2011 measurements show more positive delta values at both UCT and Wolfkop, as well as for Wolfkop and DeDoorns in December 2011, and so these are likely to be real atmospheric isotopic enrichment during rain drop descent.

4.3.2 Means and Weighting

Mean delta values for each rain collection station have been calculated, both a simple arithmetic mean, and also a weighted mean, weighted according to the rainfall amount for each month (see **Table 4.2**). These results are shown in **Figure 4.6**, which demonstrates two significant patterns.

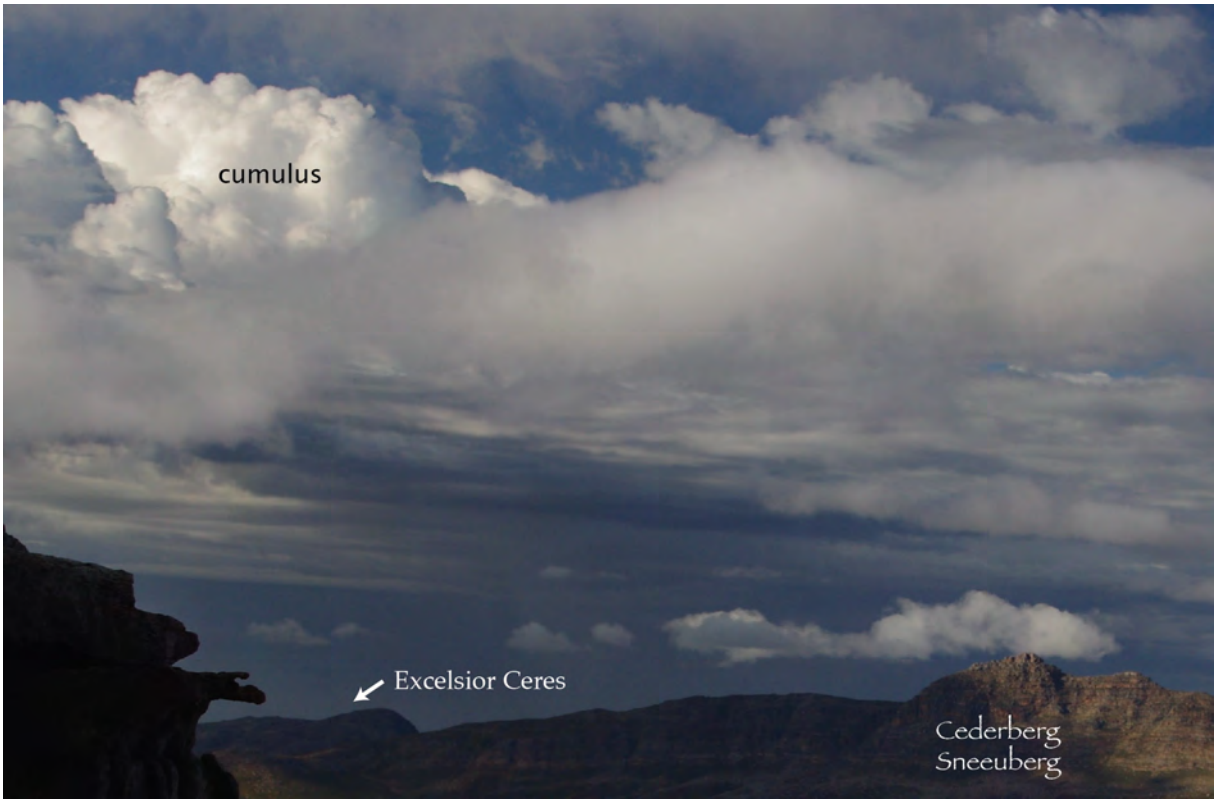

Figure 4.5: A view of the convective cumulus clouds and heavy rainfall (dark grey area in photo) that occurred in the West Coast and Cederberg region of the Western Cape over 31 December 2010 to 1st January 2011. Photograph taken from Cederberg Tafelberg, looking south over Sneeuberg and towards rain at Excelsior Ceres SAWS weather station.

Firstly, in all cases except one (δD at Uitkyk Pass), the weighted mean has a lower delta value for both δD and $\delta^{18}O$ than the unweighted mean, as is commonly observed in such studies (e.g. Iacumin et al., 2009). This is because the less negative delta values are associated with low rainfall events, mostly during summer where temperatures are higher and delta values of rain are less negative and where evaporation further increases the delta values. Put otherwise, the high rainfall, cold and isotopically more depleted winter rains bring the weighted means down towards more negative delta values.

Secondly, the degree of difference between the arithmetic mean and weighted mean is negatively correlated with the mean annual precipitation (see **Figure 4.7**). Sites with low total rainfall have more of the isotopically enriched very low rainfall months. These values drive the unweighted, or arithmetic, mean to unrealistically high delta values. When the weighted mean is calculated, the relatively few, but high rainfall months cause the weighted mean to have more negative delta values, so increasing the difference with the unweighted mean. It can be concluded that recording the rainfall amount when sampling rain is more important at drier locations, although still of value at all locations. According to Yurtsever and Gat (1981), when analysing the IAEA/WMO data: "The difference between the two means is not generally significant for stations

with a rather uniform monthly distribution of rainfall...". Our study, however, found that the correlation of difference between delta values with the seasonality index was very poor: δD and $\delta^{18}O$ vs SI gave Pearson's r correlations of 0.18 and 0.014 respectively, whereas the δD and $\delta^{18}O$ vs MAP correlations (as seen in **Figure 4.7**) are -0.71 and -0.65, respectively.

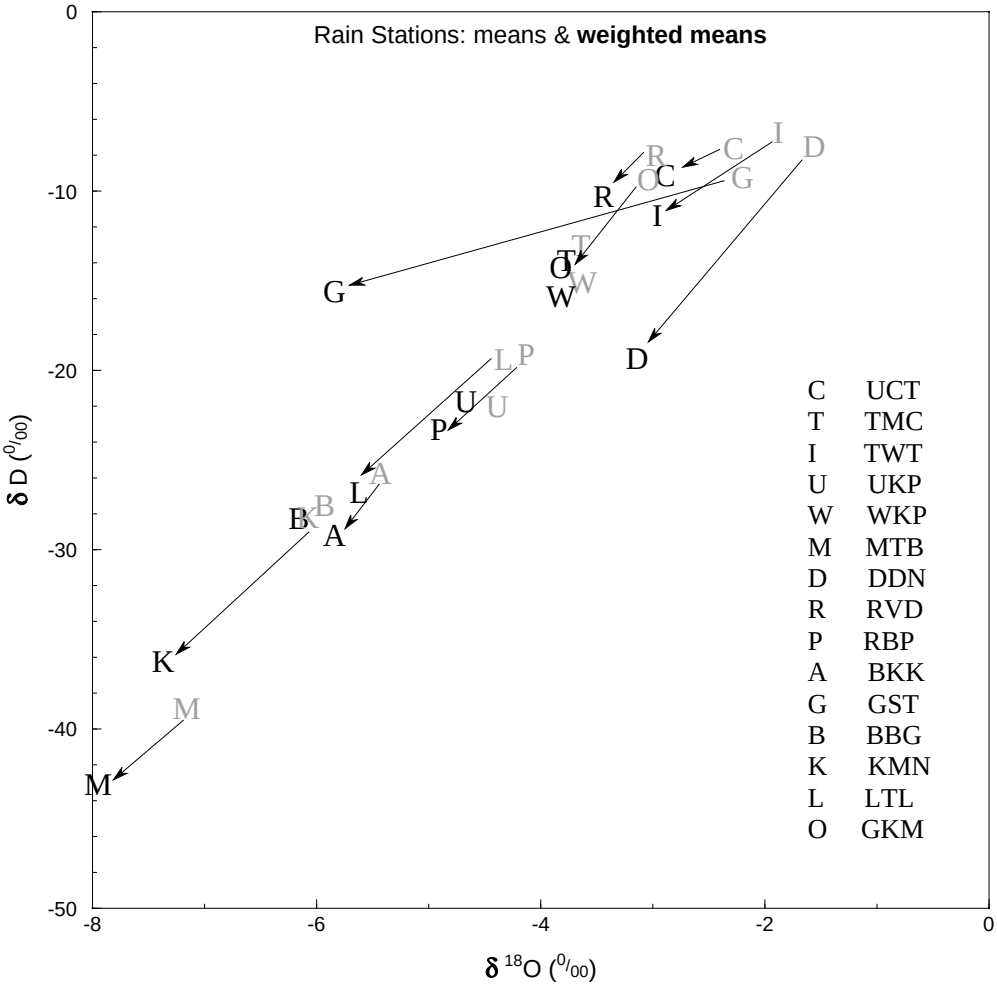

Figure 4.6: Arithmetic means and weighted means, by rainfall amount, for each rain collection station. Arrows show change from unweighted (arithmetic) means to weighted means.

The arithmetic and weighted mean δD and $\delta^{18}O$ values for UCT from this study compare favourably with previous studies in the Cape Town area, as shown in **Table 4.3**, although the results from this study are slightly less negative. There is a fair correlation between the amount of rainfall and the delta values, especially for δD, for the UCT data. The CTIA site is quite different, in terms of MAP and location, and most data is from 1960-80's and hence is not readily comparable, so it is displayed here more for interest.

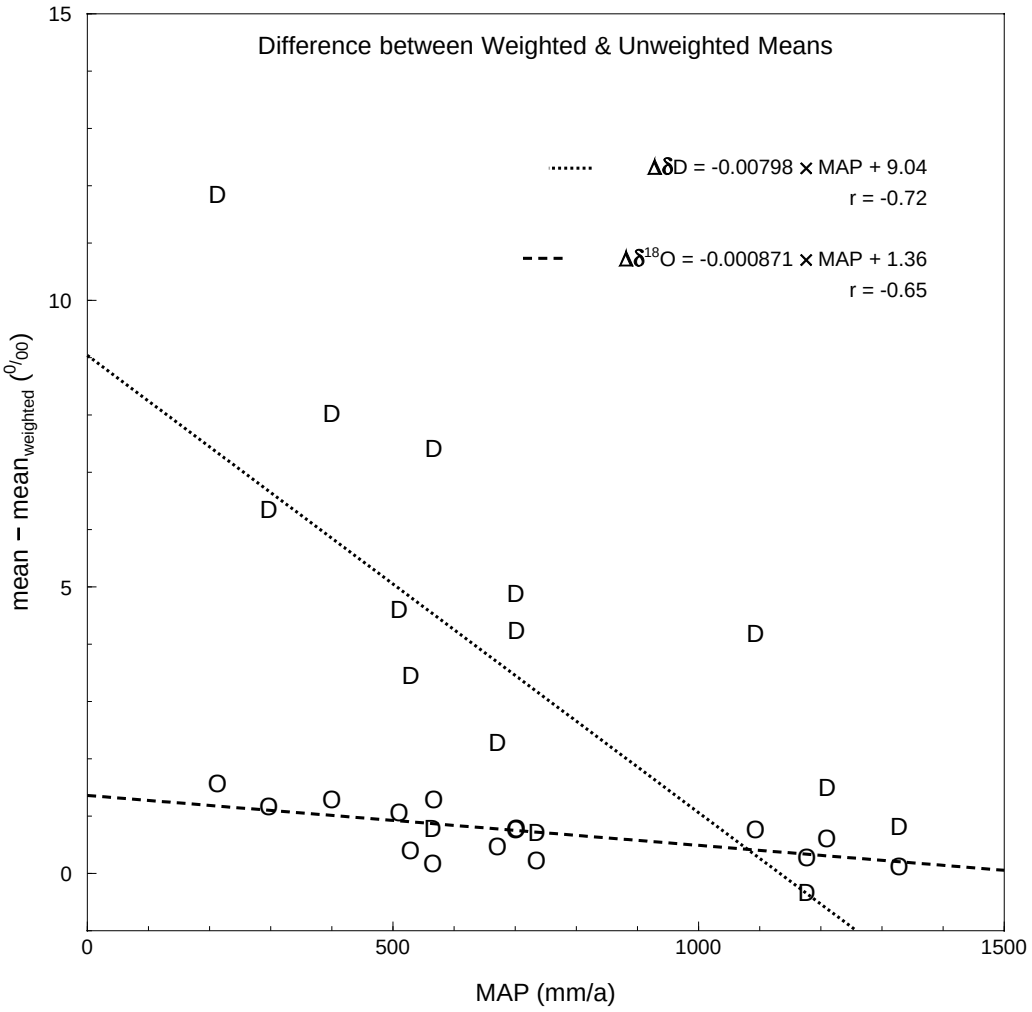

Figure 4.7: The difference between the mean and weighted mean for δD (D) and $\delta^{18}O$ (O) versus the MAP (mean annual precipitation), for each rain collection station.

			arithmetic		weighted		
study	altitude	MAP	δD	$\delta^{18}O$	δD	$\delta^{18}O$	source
	masl	mm	‰	‰	‰	‰	
UCT 2010–2012	130	1210	-7.6	-2.28	-9.2	-2.89	this study
UCT 1995–1997	130	1260	-13.0	-3.46	-11.7	-3.74	Diamond and Harris (1997)
UCT 1996–2008	130	1365	-8.5	-2.68	-12.5	-3.29	Harris et al. (2010)
'Malan'/CTIA	40	513	-8.2	-2.72	-12.8	-3.36	Rozanski et al. (1993)

Table 4.3: Arithmetic (unweighted) and weighted mean δD and $\delta^{18}O$ values of rainfall from various studies in Cape Town. CTIA refers to the Cape Town International Airport (DF Malan) where the IAEA/WMO GNIP station was located.

4.3.3 Deuterium Excess

The d-excess, often referred to simply as 'd' in the literature, is calculated for a sample of known δD and $\delta^{18}O$ values by the equation:

$$d - excess = \delta D - 8\delta^{18}O.$$

The d-excess values for the 15 rainfall collection stations range from 5.8 to 22.7 ‰ and average 16.0 ‰, which is similar to d-excess values from other studies in Mediterranean climates (Vreča et al., 2006; Argiriou and Lykoudis, 2006) (see **Table 4.2**). No correlations are apparent with MAP, seasonality or any other obvious geographic parameters, for example latitude and altitude, as can be seen in **Figure 4.8**. The best correlation is found against a continentality factor, which is the product of the distance between the rainfall station and the Atlantic Ocean (along a line of latitude due west) and the distance to the closest coast ('sea'). This factor is discussed further in Chapter 5, but even this correlation is rather poor, with a Pearson's r of only 0.42.

4.3.4 Local Meteoric Water Lines

All rain water isotope results have been plotted in the upper graph in **Figure 4.9**. The most noticeable feature of this graph is the well defined correlation between δD and $\delta^{18}O$, as is expected, according to isotopic fractionation, as described in the Introduction. This correlation defines the trend of the local meteoric water line. Using the data set to calculate lines of best fit (local meteoric water lines), the equations are as follows:

♢ unweighted rain water data: δD = 6.11$\delta^{18}O$ + 7.09

♢ rain water data, weighted by rainfall amount: δD = 6.15$\delta^{18}O$ + 8.21 .

Several points can be made about these equations. Firstly, there is only a small difference between the weighted and unweighted equations. This suggests that the statistical outliers, the rain water samples with unusual isotopic composition, are nearly symmetrical about the data. Additionally, the unweighted and weighted rain water means (n = 275) are, for δD and $\delta^{18}O$: -15.9 ‰ and -3.76 ‰ , -17.7 ‰ and -4.22 ‰. These also show only a small difference and if plotted together on a $\delta D - \delta^{18}O$ diagram, the two means lie along the same orientation as the two nearly parallel local meteroric water lines. The small shift between the two equations does however reveal that the unweighted line tends towards a lower gradient and lower intercept, both of which are a sign of evaporated waters. The bulk of the outliers are therefore the low rainfall, highly evaporated, summertime rainfall samples, as seen in the time series plots in **Figures 4.3 and 4.4**.

Local meteoric water lines have also been calculated for each of the rainfall stations and

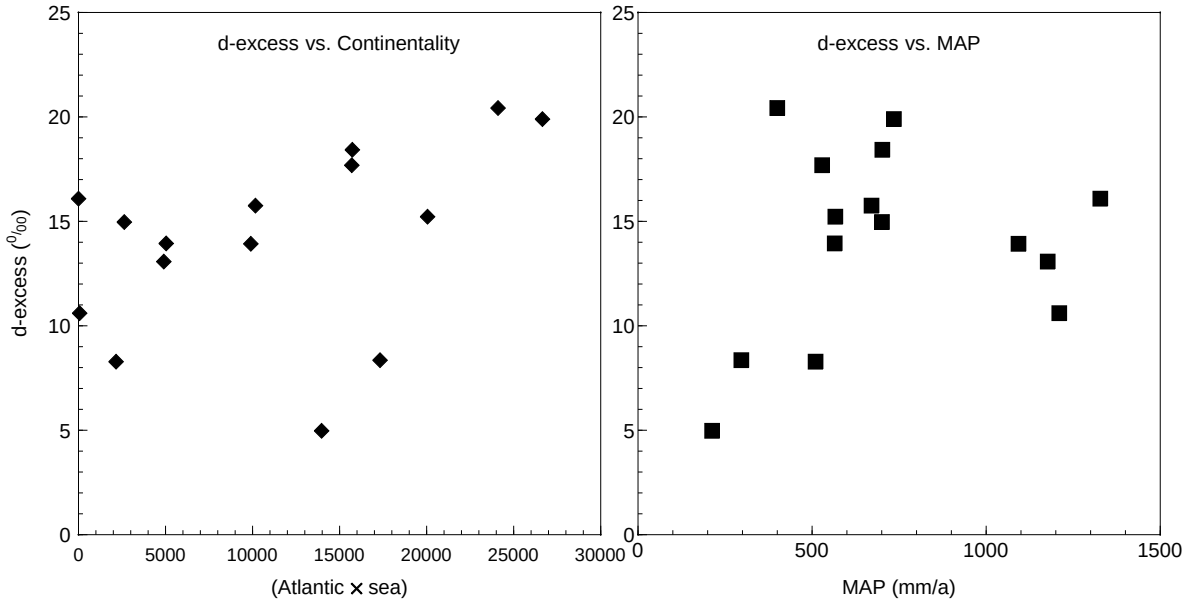

Figure 4.8: d-excess values for the weighted means for the 15 rainfall collection stations, plotted against a continentality factor and against MAP.

these are displayed in **Figure 4.10**. Ellipses have been drawn on the graph, using the standard deviations from **Table 4.2**, to show where most of the data actually lies; 67 % of points should lie within the 1σ ellipse and 98 % within the 2σ ellipse. The graph region was extended to show some separation in the meteoric water lines and allow labelling of each line.

The LMWL gradients range from 4.42 for Uitkyk Pass to 8.17 for Kammanassie, and intercepts from -3.0 for Bakenskop to 23.9 for Kammanassie. Although no single, clear correlation between these local meteoric water line equations and geographic factors such as mean annual precipitation, altitude or longitude is apparent, the equations do display geographic clustering (see **Figure 4.11**). The following groups can be distinguished by the similarity of their gradient and intercept values: a western cluster of UCT (University of Cape Town), TMC (Table Mountain Cableway) and TWT (Twaktuin) have gradients in the 5 to 6 range with intercepts from 6 to 7.5; the Hex River Mountain stations MTB (Matroosberg) and DDN (DeDoorns) have similar gradients, although different intercepts; the Langeberg-Gamkaberg group of RBP (Robinson Pass), BKK (Bakenskop) and GST (Gamka Store) all have gradients around 4.5 and intercepts close to zero; the eastern stations BBG (Blesberg), KMN (Kammanassie), LTL (Lentelus) and GKM (Goukamma) have high gradients, from 6.5 to 8.2, and high intercepts, from 10 to 24. Some stations do not fit into these groups, despite being geographical neighbours, these being Uitkyk Pass and Wolfkop, 30 km apart in the north-west, and Riverndale, less than 100 km from the Langeberg-Gamkaberg group in the south. The large range in gradients and intercepts for the 15 LMWLs is likely due to the short duration of sampling, whereby unusual weather (humidity, series of storms, drought) can affect the small dataset. Longer term monitoring should see some convergence in LWMLs.

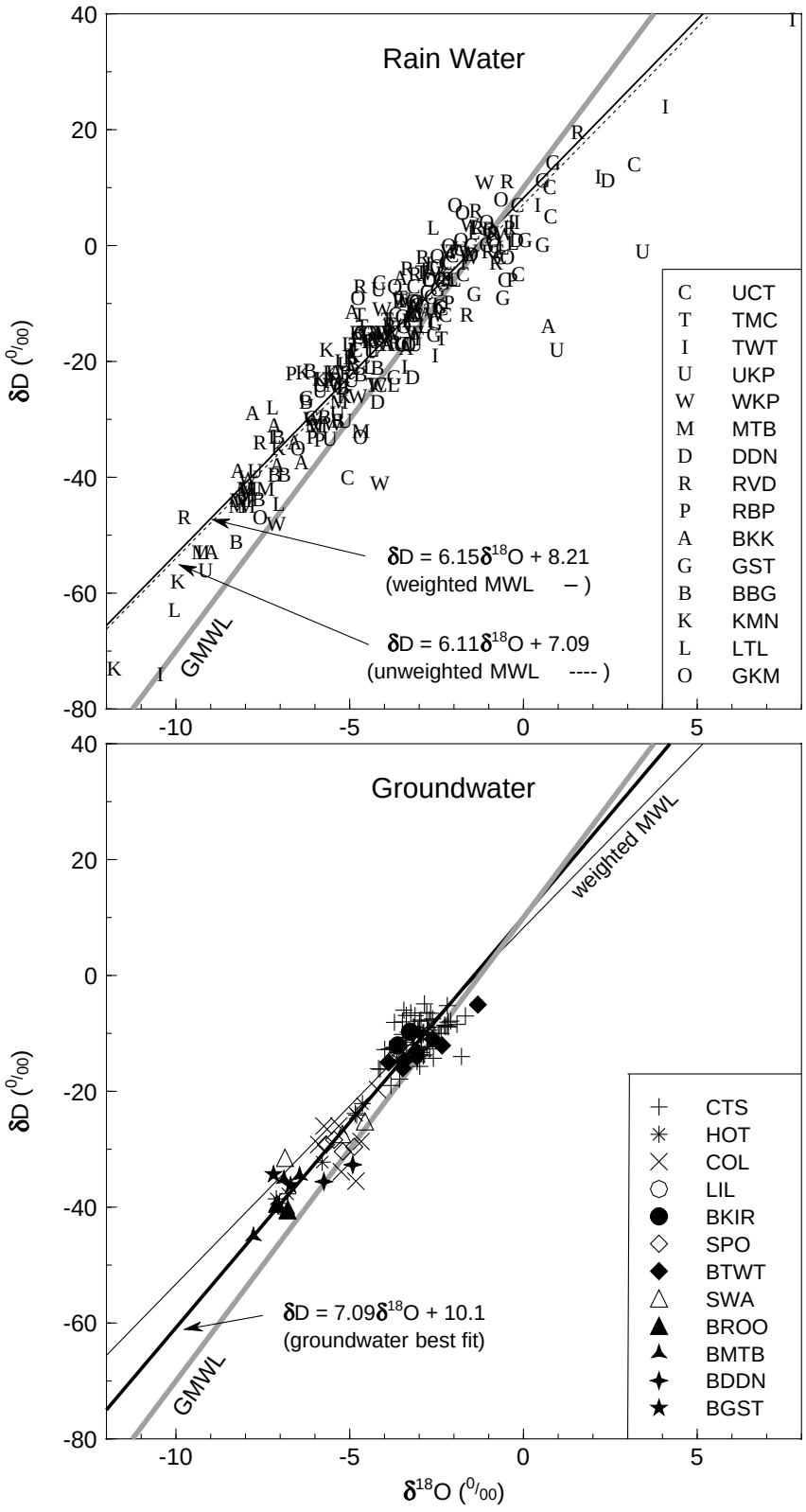

Figure 4.9: δD–$\delta^{18}O$ plots of all rain water and groundwater samples for this study. Key for the groundwater graph: CTS Cape Town springs; HOT hot springs; COL cold springs; LIL Table Mountain lily pond; BKIR Kirstenbosch boreholes; SPO Cederberg Tafelberg spout drip; BTWT Twaktuin boreholes; SWA Klein Swartberg seeps; BROO Rooihoogte boreholes; BMTB Matroosberg boreholes; BDDN DeDoorns boreholes; BGST Gamka Store boreholes.

The significance of the clustering of these local meteoric water lines is that they reveal affinities not seen when looking at the means and d-excess values. For instance, the two stations Matroosberg and DeDoorns, only 10 km apart, have very different means and d-excess values, and although the intercepts of their local meteoric water lines do show a large difference, the gradients are nearly identical, showing some parallels in meteoric processes between the two stations. A similar thing can be said for the 'sister' stations, Bakenskop and Gamka Store.

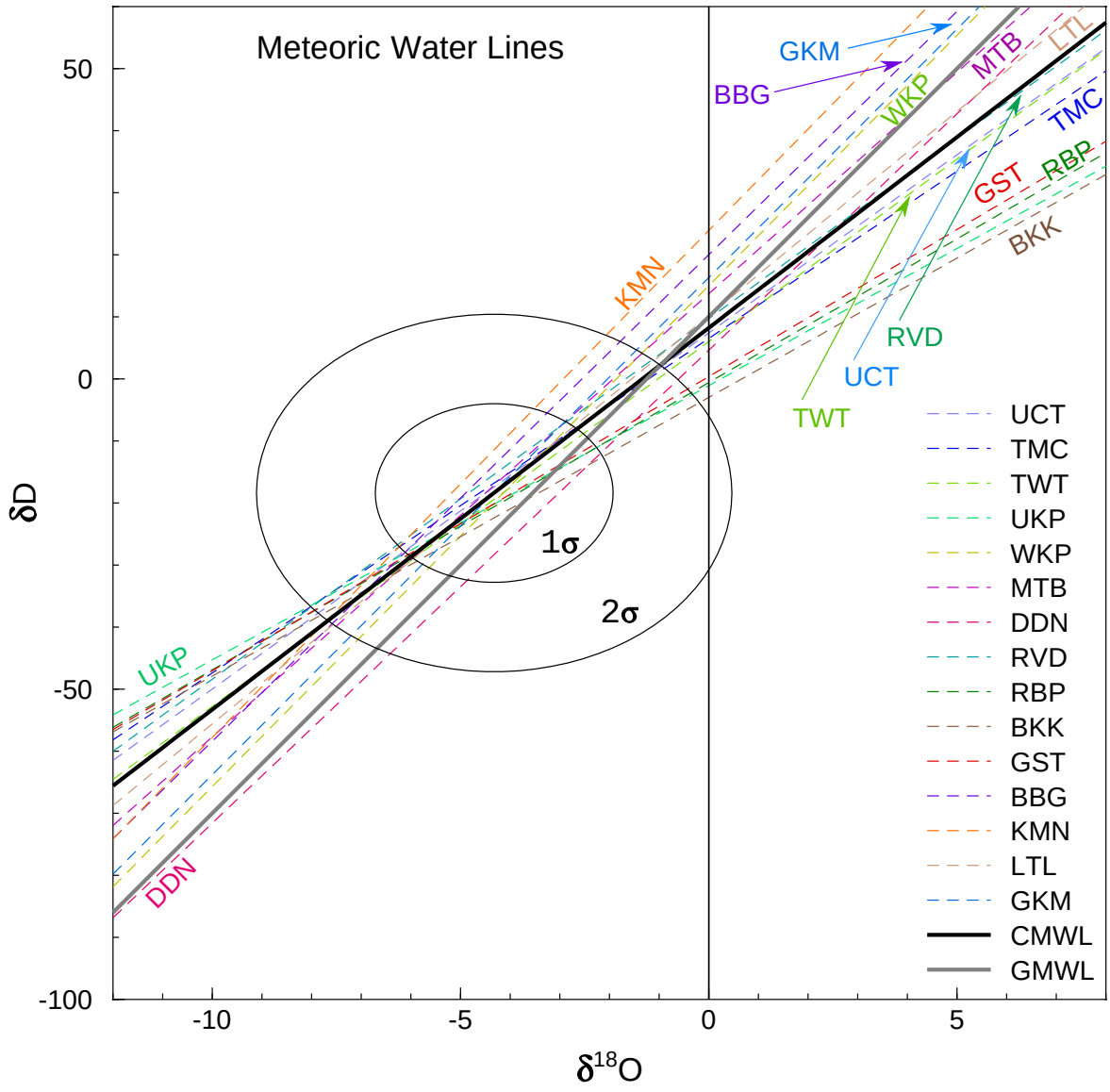

Figure 4.10: Local meteoric water lines for each of the 15 rainfall stations, calculated from monthly cumulative rainfall samples weighted by rainfall amount and using the RMA regression method. The LMWL for the all the stations (also weighted), called the Cape MWL (CMWL), and the GMWL of Craig (1961a) are also shown. The 1σ and 2σ distribution ellipses are for all rainfall data, showing how the graph has been extended well beyond the δ values found in this study, in order to show separation and allow labelling of the LMWLs.

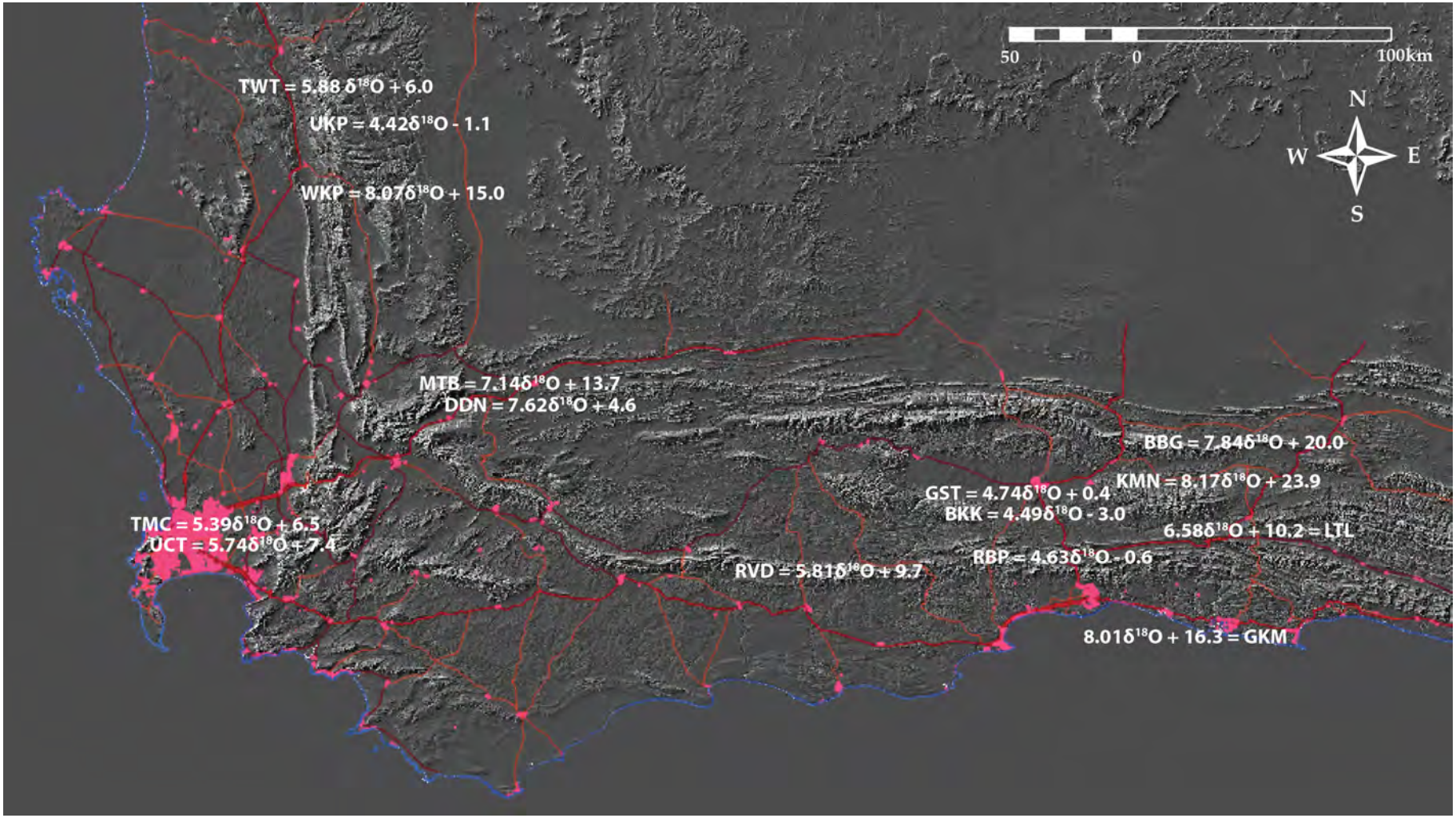

Figure 4.11: Local meteoric water line equations for each rainfall collection station, calculated with data weighted by monthly rainfall amount. The station code (e.g. BBG) lies approximately over the station location. Background image is a hillshade DEM (NASA, 2013) with roads and streets overlain (NGI, 2012).

4.4 Groundwater

Groundwater was sampled from a variety of sources: springs, seeps and boreholes. Except for the springs around Table Mountain, almost all of the groundwater was taken from sources discharging from the Table Mountain Group.

The Table Mountain springs lie below the unconformity between the overlying Table Mountain Group and the Cape Granite or Malmesbury Group, but they do not discharge from unaltered granitic or metamorphic rock. These springs discharge from areas with no bedrock outcrop and are likely to be discharging from an aquifer made of colluvial material such as scree and some weathered rock.

The springs and seeps around the Western Cape vary from widely known, high discharge rate hot springs such as Calitzdorp and Citrusdal, to virtually unknown drips that are used as high altitude water points by mountaineers, such as Cederberg Tafelberg Spout drip and the Klein-Swartberg Toverkop drip. The former, major springs, have often been capped and the ground is covered with recent material, both natural and anthropogenic, and so the exact geological formation at the discharge point is uncertain. Additionally, these larger springs mostly lie on faults and stratigraphic units can be juxtaposed, such as the Peninsula Formation of the Table Mountain Group and the Gamka Formation of the Bokkeveld Group at the Caledon hot spring (e.g. Council for Geoscience, 1997). In contrast, for the seeps, not only can the geological formation be identified, but the exact fracture from which the groundwater emerges is often visible.

The boreholes sampled are of moderate depths, around 30–100 m, and most (except for the Kirstenbosch boreholes) penetrate the Table Mountain Group, although the surface outcrop in some cases (e.g. DeDoorns) is Bokkeveld Group.

All groundwater data have been plotted in the lower graph in **Figure 4.9**. The contrast with the upper graph of all the rain water data is very noticeable, the lack of scatter being the result of the smoothing that occurs for the following reasons: small rain volume events with unusual isotopic signatures do not contribute to recharge; mixing of meteoric water takes place during recharge and subsequent underground flow, averaging out the composition of discharge. The former of these effects has been dubbed selection by Gat & Tzur (1967) (in Gat, 1981a). Using this data set to calculate a best fit line gives the following equation:

$\diamondsuit$ groundwater data, which cannot be weighted: $\delta D = 7.09\delta^{18}O + 10.08$.

This equation is substantially different from the rain water MWL equations and is much closer to the GMWL of Craig (1961a). The means for all the groundwater data are, for δD and $\delta^{18}O$: -16.9 ‰ and -3.8 ‰, respectively. These means are biased towards the Table Mountain springs, as about 60 % of the groundwater data is from these springs, which accounts for the relatively isotopically enriched values of these means.

Figure 4.12: The Seweweekspoort Peak Cave water point at 2020m in the Klein Swartberg. The fractured nature of the folded, duplexed and competent quartzite of the Peninsula Formation is apparent.

4.5 Surface Water

Water samples were collected from five rivers in the Cape Mountains. The extent of each river that was sampled falls wholly within the outcrop of the Table Mountain Group, although shortly downstream of the lowest sample the rivers exit onto other stratigraphic units, except for the Witels as described below.

Duiwelskloof and Volstruiskloof are both in the Drakenstein Mountains between Stellenbosch and Franschhoek where the Table Mountain Group is fairly flat lying on top of granite of the Stellenbosch Pluton of the Cape Granite Suite. The rivers are both very steep: Duiwelskloof has an average gradient of 30° over a distance of 2.4 km and Volstruiskloof drops 700 m in a distance of 1.5 km, giving an average gradient of around 45° (see **Table 5.7**). The rivers flow through Peninsula Formation and exit onto scree over granite at the foot of the mountains.

The Witels and Groothoekkloof Rivers both lie in the Hex River Mountains, but at opposite ends. The Witels lies in the western side of the Hex River Mountains, south of Ceres, and is the longest mountain river in the Western Cape, protected from the impact of agriculture and urbanisation by virtue of the mountainous terrain. This makes it potentially useful for understanding interaction between surface water and Table Mountain Group groundwater. The Witels has an

average gradient of 7.5° over the full 20 km length, starting at around 1900 masl and ending at 300 m in Michells Pass, but bar one high altitude sample, the main 16 km stretch of the river that was sampled drops only 600 m and so has an average gradient of only 3.5°. The Witels mainly flows through Peninsula Formation, but due to folded beds that dip north-east, it flows through Pakhuis, Cederberg and Goudini Formations for a portion of its course. The sampling of the Witels stops at its junction with the Dwars River in Michells Pass, an impacted river that drains the agricultural and urban land of the Ceres Valley. The Dwars (with the Witels) continue for a few kilometres in Table Mountain Group before exiting onto a substrate of Malmesbury Group in the Tulbagh–Wolseley Valley.

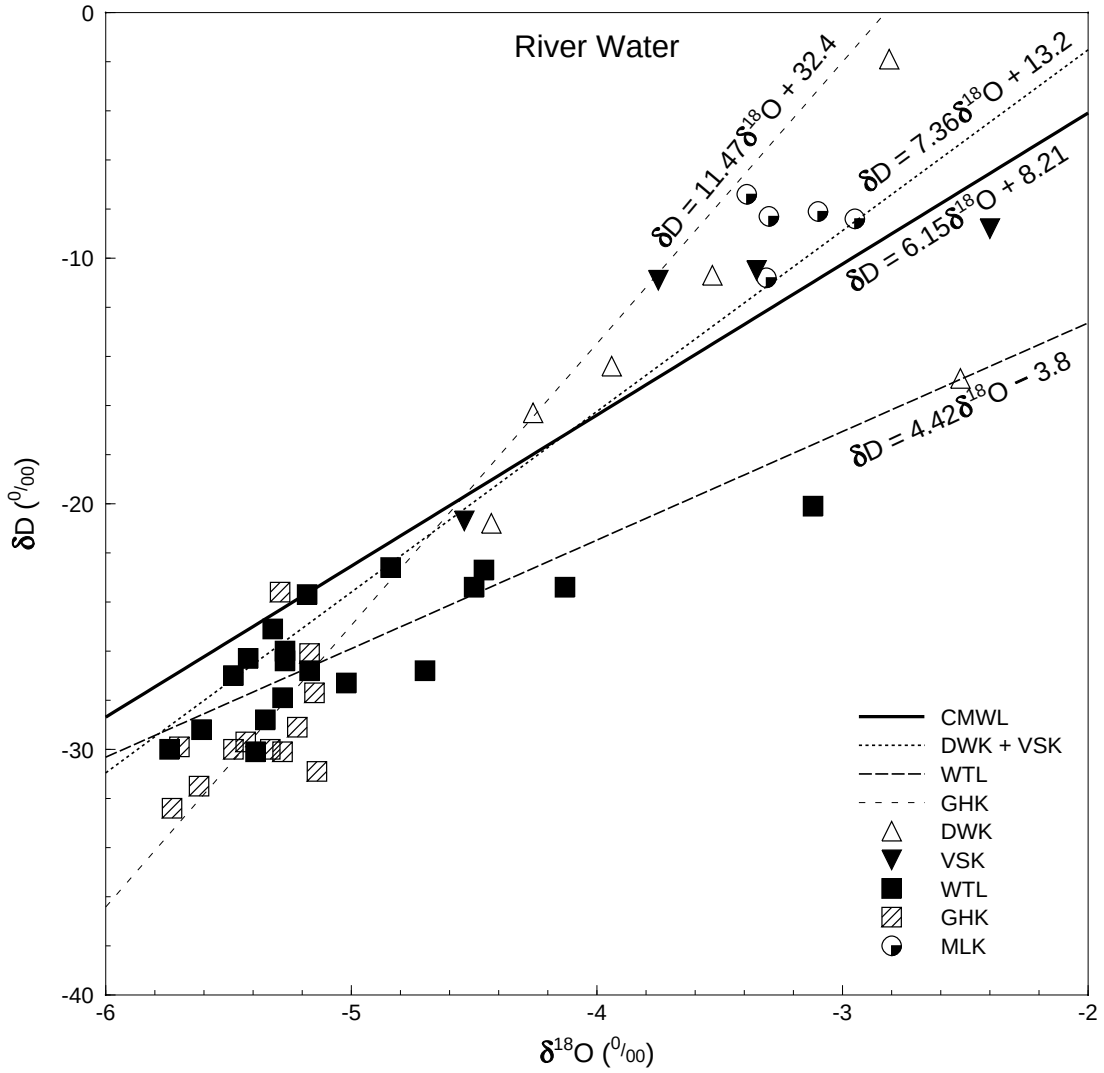

Figure 4.13: $\delta D - \delta^{18}O$ plot for all surface water samples. Best fit lines have been calculated for some data sets and the Cape Meteoric Water Line, as calculated from this study, has been added for reference.

The Groothoekkloof River arises in the highest mountains of the south-western Cape, namely

Matroosberg and Roodeberg in the far north-eastern Hex River Mountains, both over 2200 masl. It exits into Bokkeveld Group and covering gravels in the Hex River Valley Syncline at 500 masl, having flowed only through Peninsula Formation, although the high peaks above perennial water are capped with cliffs of the Skurweberg Formation and the catchment therefore includes outcrop of the Pakuis, Cederberg and Goudini Formations. This river's average gradient from perennial water at about 1800 m is around 13° (see **Table 5.7**).

Meulkloof River lies in the Swellendam region of the Langeberg Mountains. It's source is around Hermitage Peak, over 1500 masl, and it flows through Peninsula Formation only until it exits the mountains across a faulted contact with the Bokkeveld Group at 130 masl.

The $\delta D - \delta^{18}O$ plot of all surface water samples is shown in **Figure 4.13**. A clear separation exists between the two rivers from the higher mountains of the Hex River Mountains and the three other rivers located in lower mountain ranges. Best fit lines have been calculated for Groothoekkloof, Witels and a combined line for Volstruiskloof and Duiwelskloof. Meulkloof does not have enough of a linear spread of data to calculate a meaningful correlation. The correlation coefficient, Pearson's r, is only 0.53 for Groothoekkloof, but for Witels it is 0.81 and Volstruiskloof-Duiwelskloof it is 0.72, both of which are fair correlations. There is a large separation in the Witels and Groothoekkloof lines, and they straddle the MWL equations for De Doorns and Matroosberg, the two rainfall stations in the area.

The river water samples have a weak correlation with altitude, mainly between rivers. More detailed analysis of these results is necessary, as samples include those from not only the trunk stream, but also tributaries, and certain samples are highly evaporated after descent over exposed cliffs (trickling waterfalls). This will be done in the next chapter.

4.6 Other Samples

4.6.1 Snow

Six samples of snow and ice were taken from about 1900 masl on Waaihoek Peak on 29 July 2011. An unusual weather event occurred on 24–25th July 2011 when snow fell on some of the high peaks of the Cape Fold Belt from a *black south-easter*. This event can be summarised as follows. On the 2nd July a cold front and ensuing southerly meridional flow caused widespread light rain over the Western Cape with very cold ($0 - 10°C$) minimum daily temperatures. On the 4th July southerly meridional flow caused large amounts of rain (40–50 mm daily totals) on the south coast and light rain in the south-central mountain areas. Thereafter, a blocking high sat south of the country for nearly three weeks and prevented any cold fronts from causing rain until the 21st–22nd when a cold front brushed past, resulting in a few millimetres of rain along the south coast. This was followed by the South Atlantic High Pressure re-establishing itself south of the country, but this time with abundant moisture and resulting in rain falling from 23–25th mostly along the southern parts of the Province, with a maximum daily rainfall of 68 mm in George on the 24th.

On the 27th–28th a typical winter cold front caused widespread rain, and snow on the high peaks, across the Province.

Snow from both the black south-easter event and the following north-wester event was sampled near the top of Waaihoek Peak in the Hex River Mountains. It was possible to differentiate the two snowfalls from the granular snow (firn) which develops at the top of a snowpack due to freeze-thaw. The isotope results of these samples are shown in **Table 4.4**. Two different profiles were cored into the snow, WHK1-3 and WHK5-6 and a sample was also taken of rime ice (formed by sublimation directly from the atmosphere) that forms on these windy summits. The rime ice was formed during the recent north-wester, as it was on the western side of the rocks and would also not have survived the intervening sunny days between the south-east and north-west weather events.

sample ID	sample description	depth	δD	$\delta^{18}O$
		mm	‰	‰
WH1	recent powder snow from NW cold front	0-50	-60.6	-11.56
WH2	granular (melted and refrozen) top of SE snow	100-150	-38.3	-9.11
WH3	powder snow from SE at base of snowpack	300-400	-30.6	-9.16
WH4	rime ice stalactite on west facing rock	n/a	-20.5	-7.16
Wh5	granular snow at top of SE snowfall	100-200	-38.0	-8.69
WH6	podwer SE snow at base of snowpack	300-350	-33.6	-8.46

Table 4.4: Waaihoek Peak snow samples taken on 29 July 2011.

4.7 Summary

The stable isotope data from this study has a wide range of values because of seasonal variations, specific weather events, differing continentality and altitude of sample sites, and modification by evaporation. Some results can easily be attributed to such factors, whereas others have a less clear cause. Mean δD and $\delta^{18}O$ values for each rainfall station were calculated by weighting the monthly values by rainfall amount. Meteoric water lines for each station were also calculated using weighted data. The weighted results differ more from the unweighted results for less rainy areas, as weighting removes the effect of highly evaporated, low rainfall isotopically outlying data points.

Groundwater data is more tightly clustered than precipitation, as a result of selective recharge of more isotopically negative, higher rainfall events, and mixing of groundwater. Water from rivers tends to vary unsystematically isotopically down the length of the streams and each river's isotope data tends to form a cluster. Snow from a south-easter weather event has a markedly different isotope content to a subsequent north-wester weather system.

More detailed analysis of these and other results follows in the Discussion.

Figure 4.14: Monthly rainfall graphs for the 15 rain collection stations over January 2010 to December 2012. Estimates were made based on nearby rainfall stations from this study and SAWS, as well as monthly rainfall maps from the SAWS.

(a) Monthly rainfall as measured (solid bars) and estimated (striped bars) for the two Cape Town area stations.

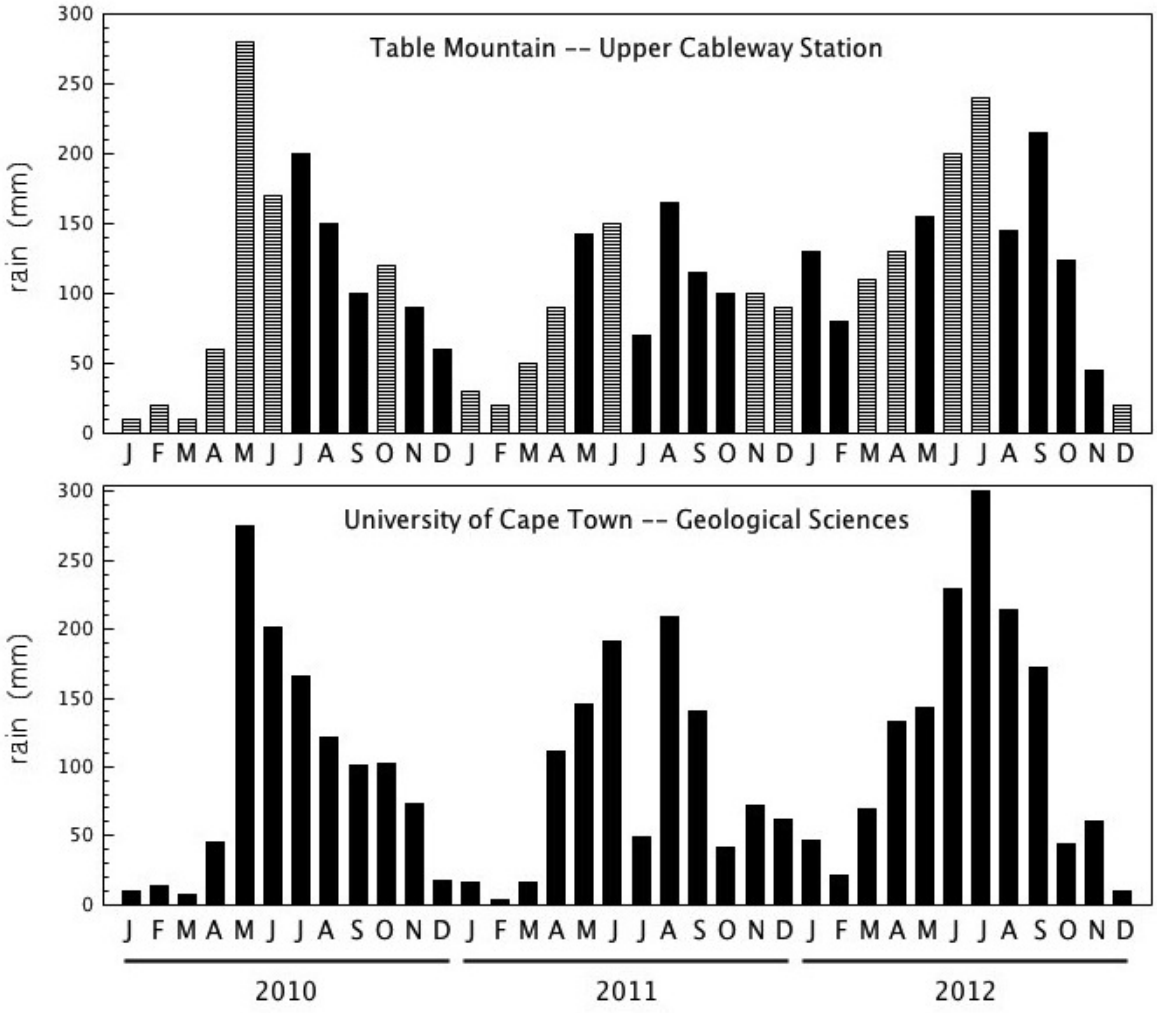

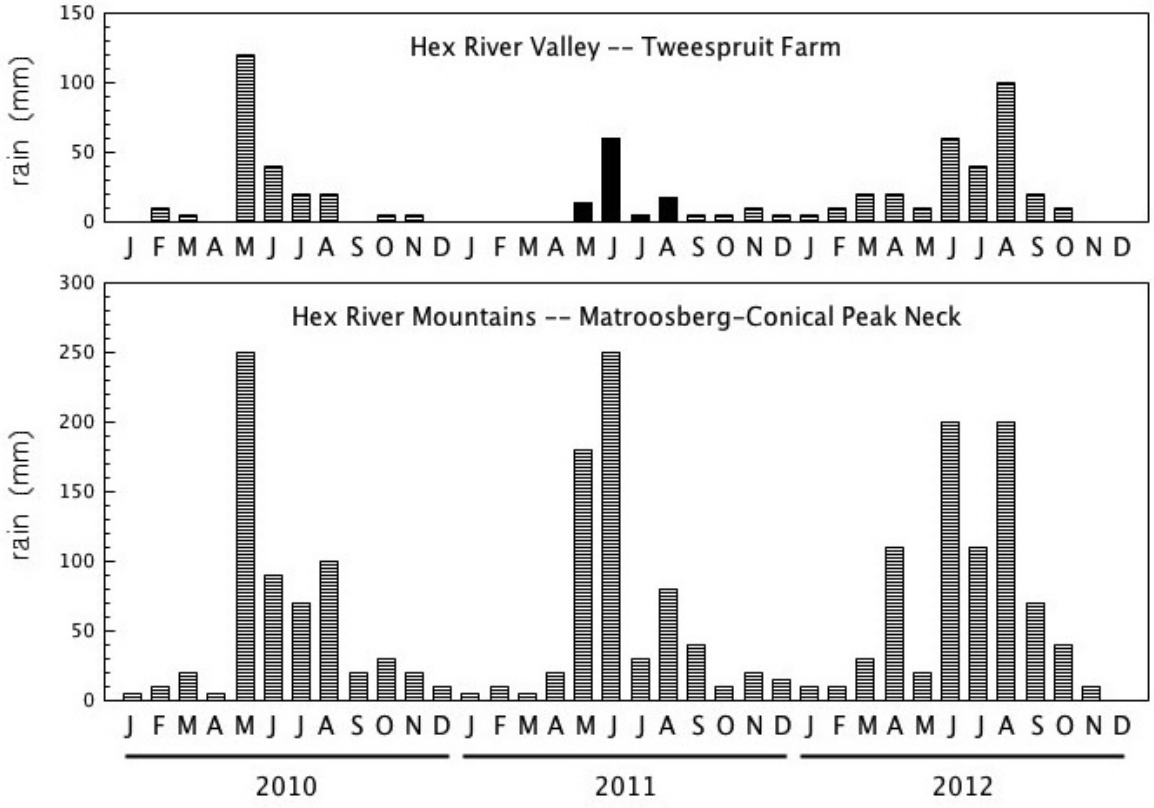

(b) Monthly rainfall as measured (solid bars) and estimated (striped bars) for the two Hex River region stations.

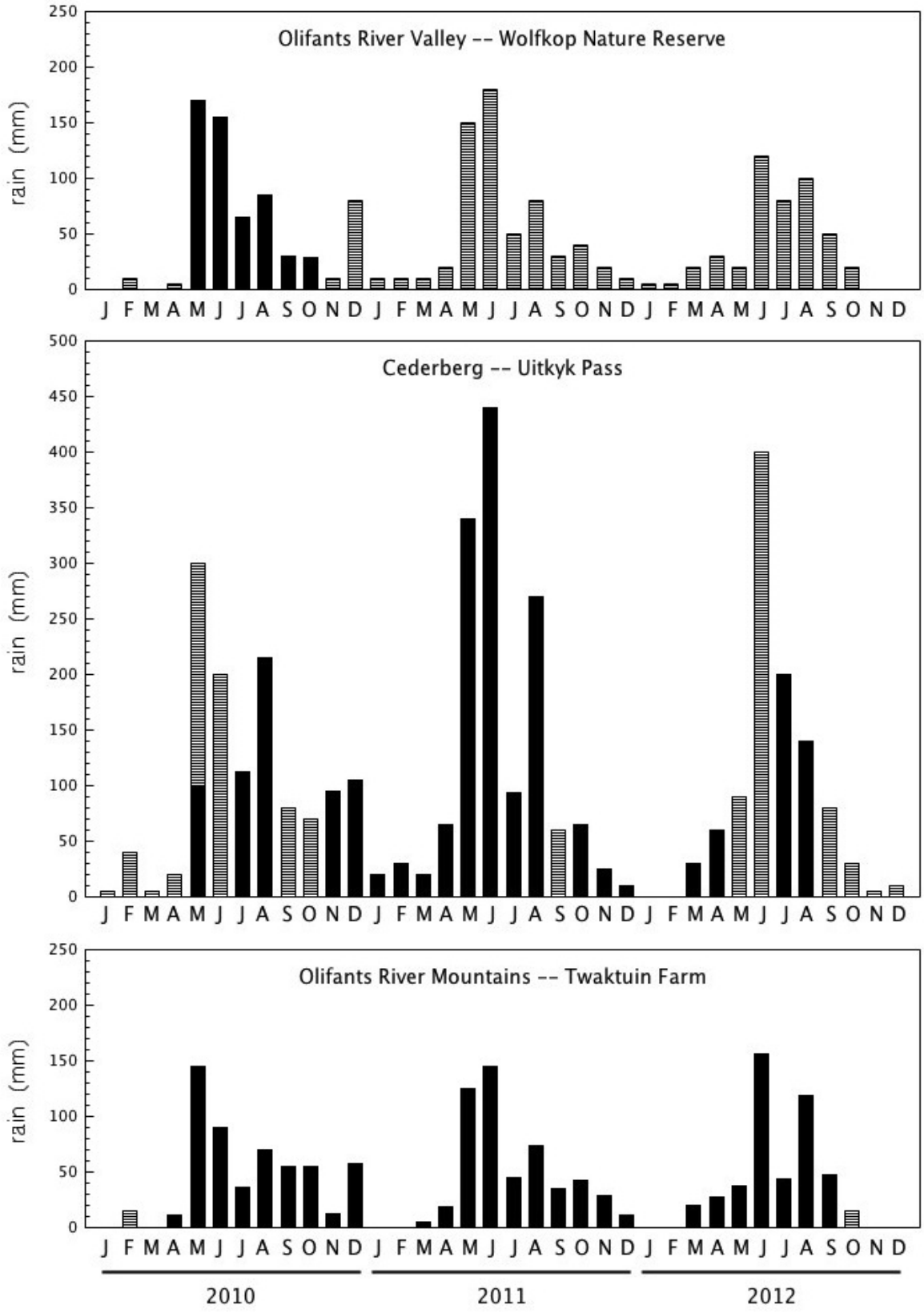

(c) Monthly rainfall as measured (solid bars) and estimated (striped bars) for the three Cederberg area stations.

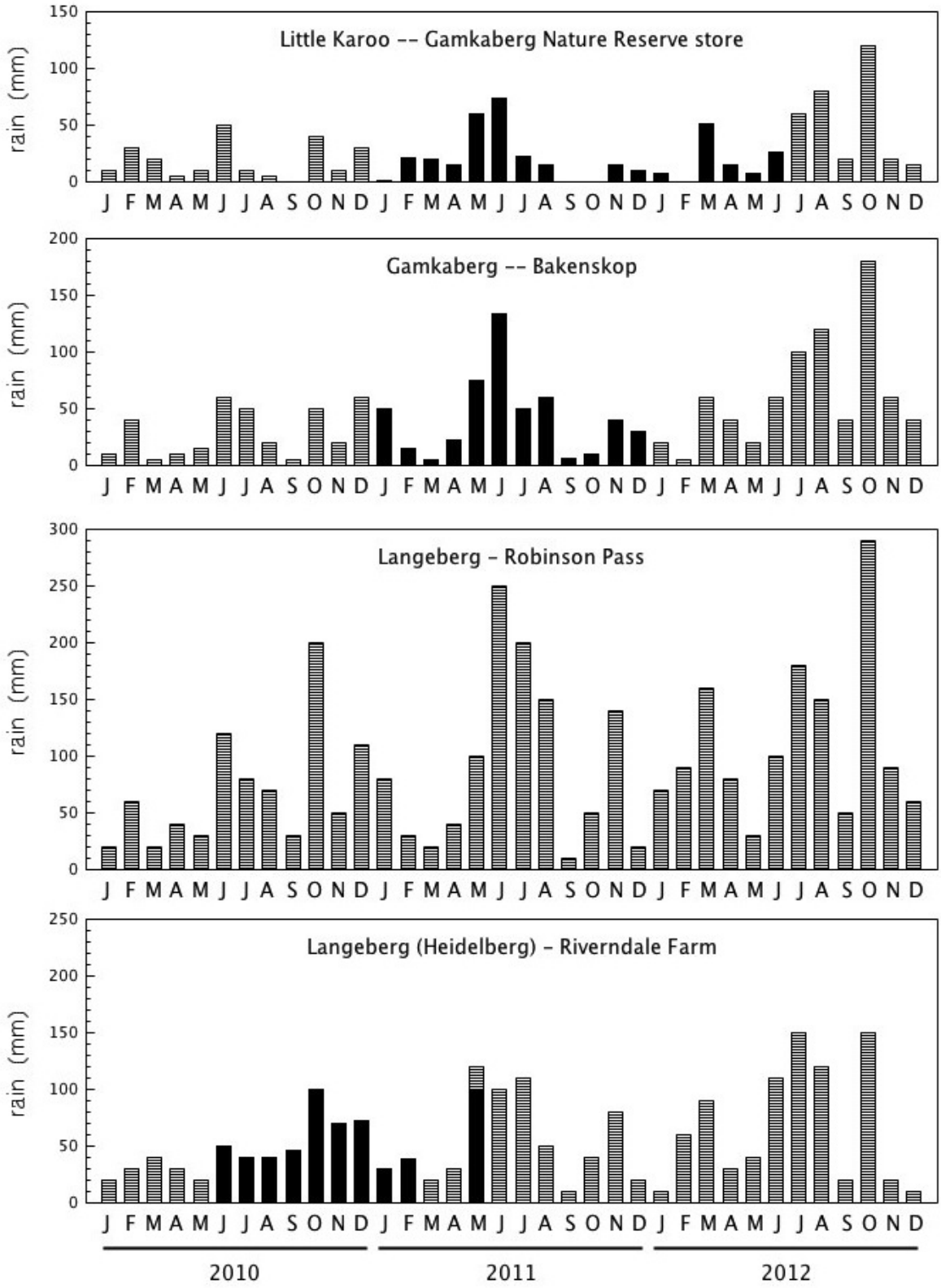

(d) Monthly rainfall as measured (solid bars) and estimated (striped bars) for the Langeberg and Gamkaberg region stations.

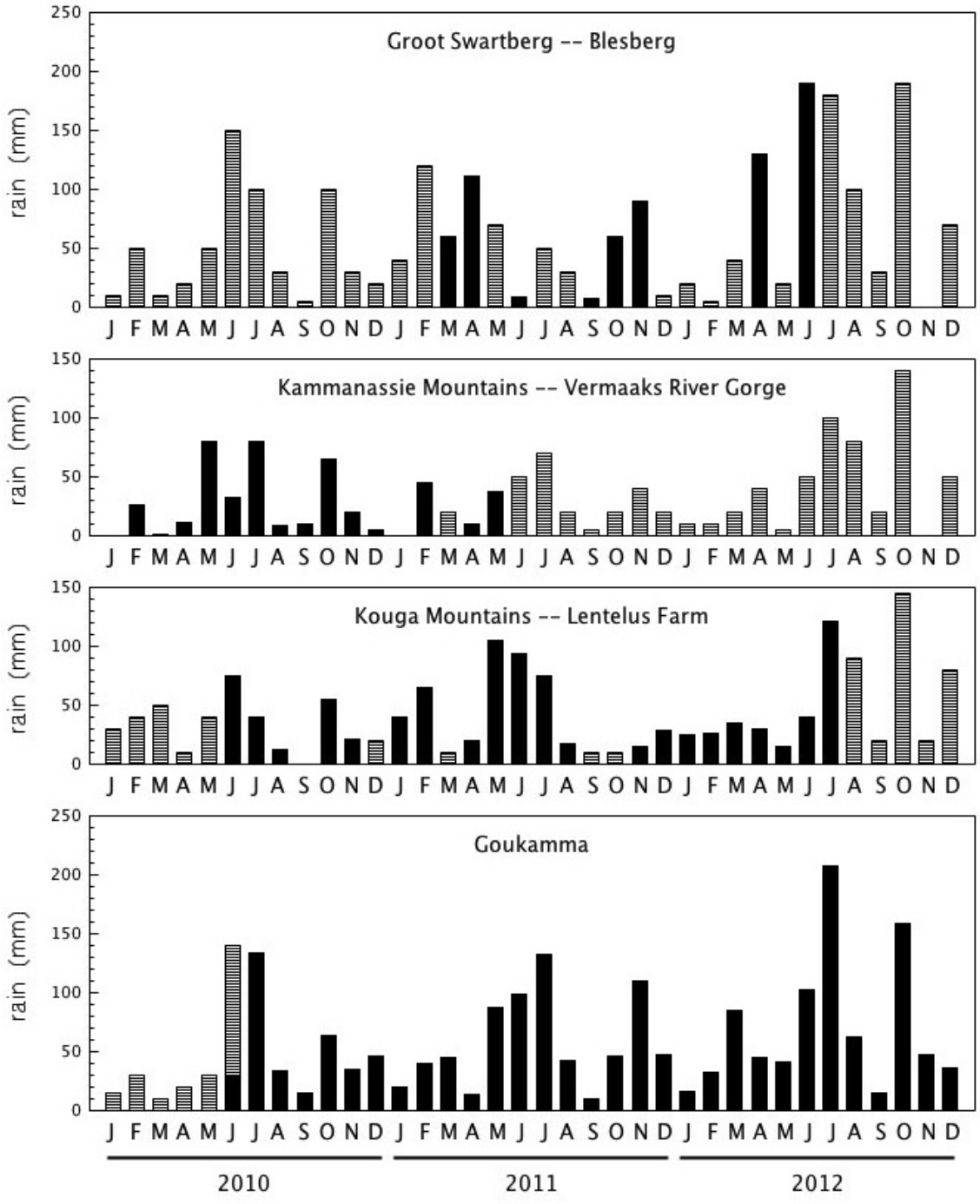

(e) Monthly rainfall as measured (solid bars) and estimated (striped bars) for the eastern region stations.

rain — 2010

	J		F		M		A		M		J		J		A		S		O		N		D	
	δD	$\delta^{18}O$	δD	$\delta^{18}O$	δD	$\delta^{18}O$	δD	$\delta^{18}O$	δD	$\delta^{18}O$	δD	$\delta^{18}O$	δD	$\delta^{18}O$	δD	$\delta^{18}O$	δD	$\delta^{18}O$	δD	$\delta^{18}O$	δD	$\delta^{18}O$	δD	$\delta^{18}O$
	‰	‰	‰	‰	‰	‰	‰	‰	‰	‰	‰	‰	‰	‰	‰	‰	‰	‰	‰	‰	‰	‰	‰	‰
UCT	9.7	0.75	-5.8	-0.54	0.4	-0.83	-12.1	-2.25	-8.4	-2.78	-17.0	-3.31	-15.0	-3.69	-4.9	-1.74	-3.3	-2.24	-3.3	-2.15	-6.2	-2.39	-39.9	-5.06
TMC									-15.0	-3.14	-24.4	-4.35							-16.3	-3.04	-13.1	-2.65	-16.0	-2.35
TWT									-13.5	-3.41	-18.8	-2.54	6.6	0.41	-2.7	-1.73	-21.4	-3.42	23.7	4.09			-74.4	-10.45
WKP									-11.7	-2.57	-25.8	-4.77	-14.7	-3.82	-1.5	-1.55	-24.1	-4.21	-0.9	-1.60	2.2	-0.56	-47.8	-7.12
UKP															-16.6	-3.53	-18.2	0.97	-1.0	3.43	-17.4	-3.12	-56.2	-9.14
MTB									-23.7	-5.43														
DDN																								
RVD											-33.8	-7.58	-47.5	-9.76	-2.4	-2.90	-3.0	-0.79	-21.5	-5.11	5.5	-1.37	-12.0	-1.63
RBP											-5.9	-0.32	-33.1	-6.08	-23.5	-5.6	-5.8	-2.22	-33.5	-5.86	-9.9	-2.14		
BKK											-13.6	0.72	-52.7	-8.97	-22.2	-5.39	-16.8	-3.95	-38.2	-7.08	-16.5	-3.88		
GST																								
BBG											-39.6	-7.17	-30.3	-5.34	-29.6	-5.72	-20.5	-4.91	-33.1	-7.06	-24.6	-5.19	-51.3	-8.26
KMN											-58.3	-9.94	-73.0	-11.77	-18.9	-4.90	-5.0	-2.30	-21.9	-5.55	-26.4	-5.15		
LTL											-42.3	-7.80	-62.9	-10.04	-17.8	-4.32			-16.5	-5.04	-12.1	-3.18		
GKM											-16.9	-3.30	-47.1	-7.60	-14.4	-3.43	0.9	-0.87	-12.1	-3.13	-1.9	-0.46	-32.5	-4.69

Table 4.5: Isotope data for rain for 2010. For locations of the rainfall stations, see the maps in Chapter 3.

rain — 2011

	J		F		M		A		M		J		J		A		S		O		N		D	
	δD	$\delta^{18}O$	δD	$\delta^{18}O$	δD	$\delta^{18}O$	δD	$\delta^{18}O$	δD	$\delta^{18}O$	δD	$\delta^{18}O$	δD	$\delta^{18}O$	δD	$\delta^{18}O$	δD	$\delta^{18}O$	δD	$\delta^{18}O$	δD	$\delta^{18}O$	δD	$\delta^{18}O$
	‰	‰	‰	‰	‰	‰	‰	‰	‰	‰	‰	‰	‰	‰	‰	‰	‰	‰	‰	‰	‰	‰	‰	‰
UCT	-5.2	-0.15	13.9	3.19	-23.6	-4.12	-5.8	-2.73	-12.3	-3.69	-18.3	-4.82	-14.6	-4.68	-3.8	-2.63	-0.1	-1.51	-17.0	-3.48	-12.0	-3.21	-1.6	-2.05
TMC	-1.2	-0.75					-14.8	-4.61	-14.7	-4.17	-16.9	-4.85	-11.6	-4.71	-14.4	-4.64	-9.2	-3.51	-13.6	-3.84	-17.4	-4.64	-9.6	-3.51
TWT									-17.7	-4.97	-17.7	-4.94	3.8	-0.19	4.2	-0.35	39.2	7.74						
UKP					-29.2	-5.35	-22.7	-5.79	-22.4	-5.46	-24.9	-5.85	-23.9	-5.85	-20.2	-5.21			-30.3	-5.13	-23.2	-4.94	-7.6	-4.17
WKP			-15.1	-3.13	-41.4	-4.13	-11.2	-4.07	-16.0	-4.10	-15.0	-4.00	-30.4	-6.06	-14.6	-4.17	3.5	-1.54	-11.8	-3.06	-40.0	-7.94	-1.1	-2.11
MTB	-44.7	-7.97	-41.9	-7.91	-31.9	-4.67	-42.4	-7.98	-52.9	-9.28	-44.4	-8.19	-44.0	-8.07	-42.9	-7.97	-44.6	-8.22	-30.9	-5.90	-31.3	-6.02	-41.8	-7.41
DDN											-27.0	-4.20			-6.0	-2.71					-1.5	-1.5	11.2	2.43
RVD	11.0	-0.47	3.2	-0.39	2.2	-0.87	-3.6	-3.35	-22.7	-5.41	-5.0	-3.12	-7.5	-4.70	-9.6	-3.57	3.0	-1.33	-16.7	-3.70	-16.6	-4.46	-1.1	-1.01
RBP													-22.1	-6.68										
BKK							-30.9	-7.16	-39.2	-8.21	-33.7	-6.58	-28.9	-7.79	-21.1	-4.97	-5.7	-3.53	-37.5	-6.38	-11.6	-4.92	-17.7	-3.37
GST	11.2	0.56	-8.4	-1.82	14.4	1.61	-22.7	-3.72	-29.8	-6.08	-26.4	-6.24	-15.7	-4.73	-13.4	-2.54					-15.4	-2.57	0.1	0.56
BBG	-43.9	-7.62	-21.1	-4.20	-19.4	-4.99	-21.6	-6.14							-39.5	-6.88	-22.3	-4.69	-26.9		-14.8	-6.55		
KMN							-17.5	-5.66	-34.5	-7.05	-23.0	-5.86	-21.7	-6.34			-10.2	-2.41						
LTL	-13.8	-2.86	-6.3	-1.96	-21.3	-4.43	2.9	-2.59	-52.7	-9.23	-32.5	-7.15	-27.7	-7.22	-44.7	-7.03	-5.8	-2.05	3.2	-1.35	0.4	-0.30	-24.1	-3.73
GKM	8.1	-0.64	4.4	-1.06	-0.1	-2.15	7.2	-1.96	-35.4	-6.48	-15.1	-4.41	-8.8	-4.76	-24.4	-5.26	-10.6	-2.90	-3.7	1.0	-1.79			

Table 4.6: Isotope data for rain for 2011. For locations of the rainfall stations, see the maps in Chapter 3.

rain — 2012

	J		F		M		A		M		J		J		A		S		O		N		D	
	δD	$\delta^{18}O$	δD	$\delta^{18}O$	δD	$\delta^{18}O$	δD	$\delta^{18}O$	δD	$\delta^{18}O$	δD	$\delta^{18}O$	δD	$\delta^{18}O$	δD	$\delta^{18}O$	δD	$\delta^{18}O$	δD	$\delta^{18}O$	δD	$\delta^{18}O$	δD	$\delta^{18}O$
	‰	‰	‰	‰	‰	‰	‰	‰	‰	‰	‰	‰	‰	‰	‰	‰	‰	‰	‰	‰	‰	‰	‰	‰
UCT	5.4	0.78	-2.5	-0.68	-11.9	-3.07	-9.8	-3.12	-10.4	-3.08	-6.4	-4.15	-8.8	-2.67	-13.5	-3.25	-10.8	-2.36	-7.1	-3.16	0.1	-1.08	6.9	-0.17
TMC	-4.7	-2.93	-1.0	-2.05	-12.9	-3.91	-13.7	-4.34			-8.7	-2.32	-7.6	-2.93	-20.8	-4.82	-22.4	-5.75						
TWT							11.8	2.15	-4.1	-2.86	-16.4	-4.88	-3.1	-2.73	-14.6	-3.88								
UKP					-33.3	-5.57	-15.6	-4.05	-0.5	-1.82			-18.3	-4.37	-20.5	-5.14								
WKP					-30.8	-5.49	-10.2	-3.16	10.9	-1.12	-15.9	-4.40	-4.8	-2.65	-9.4	-3.51								
MTB	-26.5	-5.30																						
DDN	1.0	-0.20									-22.72	-3.19												
RVD	2.9	-0.99	19.6	1.56	-11.4	-3.19	-17.1	-4.15																
RBP																								
BKK																								
GST	1.0	0.05			-9.1	-0.58	-7.6	-2.46	-6.5	-2.31	-10.5	-2.41												
BBG			-13.9	-3.86	-26.9	-6.26	-15.0	-4.81	-28.2	-7.02														
KMN																								
LTL	-0.3	-0.57	2.2	-1.42	-16.2	-4.33																		
GKM	2.5	-0.97	5.7	-1.75	-9.6	-3.07	-9.7	-3.17	-1.9	-2.47	-12.4	-3.47												

Table 4.7: Isotope data for rain for 2012. For locations of the rainfall stations, see the maps in Chapter 3.

Table Mountain springs

	2010-03		2010-11		2011-05		2011-10		2012-05		2012-09	
	δD	$\delta^{18}O$	δD	$\delta^{18}O$	δD	$\delta^{18}O$	δD	$\delta^{18}O$	δD	$\delta^{18}O$	δD	$\delta^{18}O$
	‰	‰	‰	‰	‰	‰	‰	‰	‰	‰	‰	‰
Redwood			-10.3	-2.96			-10.8	-3.36	-8.0	-3.48	-9.6	-3.03
Wendy's			-9.4	-2.74			-10.7	-3.38	-9.8	-3.32	-9.1	-2.77
Kirstenbosch	-13.7	-3.01	-9.4	-3.03	-12.4	-3.71	-12.9	-3.04	-10.2	-3.48	-10.1	-2.37
Kommetjie	-13.9	-2.88	-8.9	-2.16	-8.9	-3.16	-10.2	-2.89	-6.5	-3.24	-8.5	-1.91
Newlands	-13.3	-2.94	-7.5	-2.61	-6.9	-3.37	-10.2	-3.01	-6.5	-2.67	-7.9	-2.09
Palmboom	-13.7	-2.86	-10.0	-2.43	-4.9	-2.85	-9.9	-2.99	-7.7	-2.95	-8.9	-2.24
Princess Anne							-12.0	-3.21			-8.9	-2.57
Albion	-8.7	-2.18	-7.0	-1.67	-7.9	-2.99	-9.8	-2.87	-7.7	-2.71	-8.0	-2.17
CT Main	-15.7	-2.98	-12.7	-2.70	-12.8	-3.99	-13.3	-3.64	-10.7	-3.40	-12.3	-2.77
Cableway	-19.0	-3.81	-10.4	-3.17							-14.9	-3.06
Glencoe	-17.9	-3.56	-10.0	-3.19	-16.1	-4.17	-16.2	-4.12	-12.5	-3.74	-14.4	-3.04
Leeuwenhof	-14.0	-1.78	-5.2	-2.19	-8.1	-3.71	-11.5	-3.17	-6.4	-2.78	-14.3	-2.59
Tafelberg Rd			-8.6	-2.27	-6.0	-3.44	-12.7	-3.85	-7.0	-3.12	-12.3	-2.93

Table 4.8: Isotope data for the Table Mountain springs. For locations of the springs, see the Cape Town map in Chapter 3.

Western Cape rivers

	Duiwelskloof March 2011		Volstruiskloof March 2011		Witels February 2010		Groothoekkloof January 2012		Meulkloof March 2012	
	δD ‰	$\delta^{18}O$ ‰	δD ‰	$\delta^{18}O$ ‰	δD ‰	$\delta^{18}O$ ‰	δD ‰	$\delta^{18}O$ ‰	δD ‰	$\delta^{18}O$ ‰
1	-14.4	-3.94	-20.7	-4.54	-26.8	-4.70	-27.7	-5.15	-7.4	-3.39
2	-16.3	-4.25	-10.9	-3.75	-30.1	-5.39	-32.4	-5.73	-8.4	-2.95
3	-10.7	-3.53	-8.8	-2.40	-28.8	-5.35	-30.1	-5.28	-10.8	-3.31
4	-14.9	-2.52	-10.5	-3.35	-23.4	-4.13	-23.6	-5.29	-8.1	-3.10
5	-20.8	-4.43			-23.4	4.50	-29.9	5.70	-8.3	-3.30
6	-1.9	-2.81			-27.9	-5.28	-26.1	-5.17		
7					-30.0	-5.74	29.1	-5.22		
8					-20.1	-3.12	-31.5	5.62		
9					-27.3	-5.02	-30.0	-5.48		
10					-27.0	-5.48	-30.9	-5.14		
11					-29.2	-5.61	-30.0	-5.33		
12					-22.7	-4.46	-29.7	-5.43		
13					-26.0	-5.27				
14					-25.1	-5.32				
15					-26.8	-5.17				
16					-22.6	-4.84				
17					-26.4	-5.27				
18					-23.7	-5.18				
19					-26.3	-5.42				

Table 4.9: Isotope data for the five rivers sampled. For locations of the rivers and sample points 1→n, see the maps in Chapter 3.

groundwaters

sample type	location		date	δD ‰	$\delta^{18}O$ ‰
hot spring	The Baths	Citrusdal	May 2010	-22.1	-4.63
hot spring	Goudini Spa	Worcester	February 2011	-24.1	-4.80
hot spring	Brandvlei	Worcester	February 2011	-32.2	-5.79
hot spring	Caledon	Caledon	May 2011	-23.8	-4.84
hot spring	Warmwaterberg	Barrydale	September 2010	-37.7	-6.78
hot spring	Calitzdorp Spa	Calitzdorp	May 2011	-39.4	-7.02
hot spring	Tooverwater	Willowmore	May 2011	-38.6	-7.11
spring	Goudini cool	Worcester	February 2011	-19.7	-4.20
spring	UCT field station	Laingsburg	September 2010	-28.7	-4.67
spring	UCT field station	Laingsburg	September 2011	-33.9	-5.24
spring	UCT field station	Laingsburg	September 2012	-35.5	-4.82
seep	Lily Pond	Table Mountain	February 2011	-12.8	-3.60
seep	Lily Pond	Table Mountain	March 2012	-11.4	-2.95
seep	Tafelberg Spout	Cederberg	December 2010	-29.2	-5.68
seep	Tafelberg Spout	Cederberg	January 2011	-29.6	-4.87
seep	Tafelberg Spout	Cederberg	March 2011	-30.4	-5.20
seep	Tafelberg Spout	Cederberg	December 2011	-28.4	-5.45
seep	Toverkop water cave	Klein Swartberg	September 2010	-25.2	-4.56
seep	Toverkop water cave	Klein Swartberg	October 2011	-27.4	-5.21
seep	Skull Cave	Klein Swartberg	March 2011	-39.7	-6.83
seep	Seweweekspoort Peak Cave	Klein Swartberg	March 2011	-31.5	-6.86
borehole	'Protea'	Kirstenbosch	May 2012	-12.1	-3.62
borehole	'Apple'	Kirstenbosch	May 2012	-9.73	-3.26
borehole	house borehole	Twaktuin	February 2011	-15.5	-3.47
borehole	vlei borehole	Twaktuin	February 2011	-14.4	-3.07
borehole	C&D borehole	Twaktuin	February 2011	-11.3	-2.61
borehole	house borehole	Twaktuin	September 2011	-15.2	-3.88
spring	house spring	Twaktuin	September 2012	-14.9	-3.45
borehole	house borehole	Twaktuin	September 2012	-13.1	-3.09
borehole	vlei borehole	Twaktuin	September 2012	-12.1	-2.34
borehole	C&D borehole	Twaktuin	September 2012	-5.1	-1.31
borehole	Erfdeel 1	Erfdeel	February 2012	-34.6	-6.44
borehole	Grootvlak 1	Erfdeel	February 2012	-45.0	-7.77
borehole	Grootvlak 2	Erfdeel	February 2012	-35.2	-6.89
borehole	upper borehole	Tweespruit	July 2012	-32.7	-4.91
borehole	lower borehole	Tweespruit	July 2012	-35.6	-5.74
borehole	house borehole	Gamkaberg	June 2012	-36.3	-6.70
borehole	Tierkloof	Gamkaberg	June 2012	-34.4	-7.19
borehole	east	Rooihoogte	July 2012	-40.6	-6.79
borehole	west	Rooihoogte	July 2012	-39.4	-7.09

Table 4.10: Stable isotope data for various sample types. Hot springs have T > 37 °C. Locations are shown in the maps of Chapter 3.

Chapter 5

Discussion

5.1 Introduction

This chapter has two major parts. The first part contains findings on the isotope data for rainfall, surface water and groundwater separately, concentrating on the isotope effects, especially the altitude effect. The second part is made up of regional analyses of all data types within an area, such as the Cederberg or Hex River Mountains. The interpretations are proposed on the grounds of stable isotope evidence, but are checked against the geological and hydrogeological setting for feasibility. Attempts are made to draw conclusions that have relevance for groundwater flow in the Table Mountain Group.

5.2 Precipitation

Widespread collection of rainfall across the Western Cape has allowed a thorough consideration of hydrogen and oxygen stable isotope variations for the first time in this region. In particular, the rainfall stations vary greatly in their altitude, from 60–2080 m above sea level, their mean annual precipitation, from 200–1300 mm per year, and distance from the sea, from 2–110 km. Establishing the stable isotope variation with factors such as altitude, continentality and temperature allows for application to hydrological problems such as finding groundwater recharge areas (e.g. D'Alessandro et al., 2004).

5.2.1 Source Area and Pathway Effects

Precipitation in a given area may be derived from differing weather systems or the moisture causing the precipitation may have had different trajectories, hence the rainfall may display distinctive isotopic compositions (e.g. Peng et al., 2010; Breitenbach et al., 2010). South Africa receives precipitation from several types of weather systems, but these can broadly be divided into convective type summer rainfall over the eastern, central and northern parts of the country and frontal winter rain over the western and southern regions. The summer rain is brought over

land anticyclonically by the South Indian High Pressure cell, whereas the winter rain arrives with cyclonic frontal depressions from the southern Atlantic Ocean. Although the frontal depressions originate at approximately 60°S in the Atlantic Ocean and gather some of their moisture over the mid-latitude ocean before making landfall on the southern west coast of Africa, much of the water vapour in these weather systems has been derived from evaporation off the tropical sea surface (Rozanski et al., 1993). The summer rainfall systems develop over the land, but the air mass containing the moisture is derived from the mid-latitudes, 30-60°S, in the southern Indian Ocean. Moisture in the summer and winter rainfall in South Africa has therefore followed different trajectories since evaporation over the tropical ocean and has acquired additional moisture at different latitudes over different oceans at different temperatures of evaporation. It is therefore possible that the summer and winter rainfall may have different isotopic compositions.

Plotted in **Figure 5.1** is data from this study, for the winter rainfall region, and data from three other studies for other parts of South Africa, representing summer rainfall regions. No striking differences are apparent. This could be for two possible reasons: either there is no actual isotopic difference, or the amount of data is insufficient to show any differences.

For the latter, it is possible that the treatment of the data is deficient and a more detailed separation of the Western Cape rainfall is needed, based on weather patterns. This is because rainfall in the Western Cape, although dominated by winter frontal rain, does have elements of other rain-producing weather systems, especially further east, as with rainfall stations like Lentelus and Goukamma. A substantial quantity of the rainfall at these far eastern stations does in fact come from weather related to advection of moisture by the South Indian High Pressure cell. However, this explanation does not seem likely, as the rainfall stations in this study show no significant difference in average δD and δ^{18}O values, d-excess values (see **Table 4.2**) or meteoric water lines between the rainfall stations in the west, which are winter rain dominated, and those further east, with all-year round rain.

It is also possible the duration of sample collection is too short, being only 2 years and having some months not recorded. However, this also does not seem likely for the following reasons. The various Cape meteoric water lines calculated using different data sets do not vary much, in spite of these data sets being vastly different in size, as shown in **Table 5.1**. Also, a lot of groundwater data has been collected and groundwater isotopic values are known to reflect the longer term average precipitation isotope values (e.g Clark and Fritz, 1997). As the groundwater data overlap the precipitation data and the array of compositions is centred within the spread of precipitation data (see **Figure 5.1**), this can be seen as a validation that the precipitation samples are representative of longer term precipitation averages.

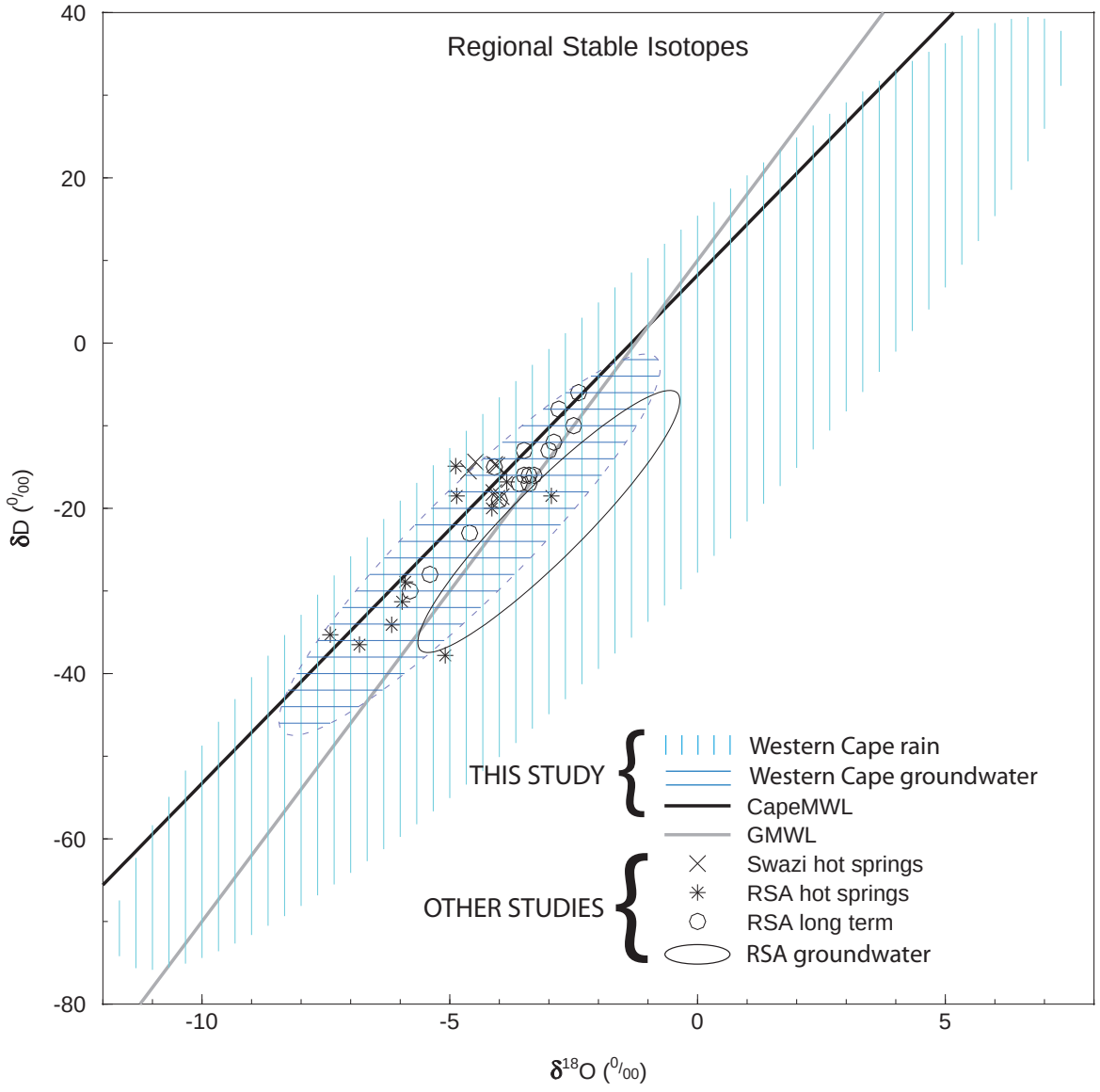

Figure 5.1: Comparison of isotope compositions of water from various South African studies with the results fields (shaded areas) for this study. Data for Swaziland hot springs from Mazor et al. (1974), RSA hot springs from Mazor and Verhagen (1983), RSA long term precipitation from Talma and van Wyk (2013) and RSA groundwater from West et al. (2014). The CMWL has the equation: $\delta D = 6.15\delta^{18}O + 8.21$.

meteoric water line equation	years		stations	reference
$\delta D = 6.1\delta^{18}O + 8.6$	1	1995-6	4	(Diamond and Harris, 1997)
$\delta D = 6.41\delta^{18}O + 8.66$	12	1996-2008	1	(Harris et al., 2010)
$\delta D = 6.15\delta^{18}O + 8.21$	2	2010-12	15	this study

Table 5.1: Meteoric water line equations calculated for rainfall in the Western Cape, illustrating the subtle differences in equations in spite of substantial differences in the date, duration and scale, as determined by the number of stations, for each study.

It does, however, remain possible that a more detailed analysis of South African isotope data will reveal a slight yet significant difference in isotopic composition for the summer and winter rainfall regions, but this is beyond the scope of this study. The alternative hypothesis may therefore be correct, which is that, in spite of different weather systems and moisture mass trajectories, there are no observable differences in isotope signatures between the summer and winter rainfall systems.

5.2.2 Isotope Effects

5.2.2.1 Temperature

Temperatures vary substantially across the Western Cape. This includes the daily maxima and minima, which are often over 40 °C in summer at low altitude, inland locations, and less than 0 °C in winter on mountains and at inland locations. Also, during precipitation events anticyclonic summer rain can occur with air temperatures over 20 °C whereas cyclonic winter precipitation frequently occurs as snow (SAWB, 1996). The isotopic content of precipitation is known to vary greatly temporally, and although correlations and patterns can at times be found with temperature, there is much noise in the data, associated with the complex dynamics of each and every weather system or rain event. Dansgaard (1964) states that, even if assuming no kinetic, exchange or evaporation effects, the isotopic composition of a sample of rain cannot be used to calculate the condensation temperature. This is because many other parameters, such as humidity, cloud height and rain event duration, also play a role in determining the eventual isotope composition of the rain.

The strong correlations of stable isotopes with average annual temperature reported in the literature (e.g Craig, 1961a; Dansgaard, 1964; Yurtsever and Gat, 1981) are summarized by Yurtsever and Gat (1981) as follows: "...it is evident that the spatial variations in the mean isotopic composition of precipitation of [GNIP] network stations are essentially correlated to the temperature variations." It is important to note that these correlations are based on long term averages of both the δD and $\delta^{18}O$ values of rainfall and of temperature (T) at each station and strong correlations are only formed with global or continental scale data sets and in particular at middle and high latitudes. This T-δ correlation is largely a product of the rainout process, where T reflects

species	gradient $\frac{\Delta‰}{1000km}$	location	reference
δD	13	Europe: Belgium to Poland - summer	Rozanski et al. (1982)
δD	33	Europe: Belgium to Poland - winter	Rozanski et al. (1982)
$\delta^{18}O$	1.6	Europe: Poland to Russia	Rozanski et al. (1993)
$\delta^{18}O$	3.8	Europe: Poland to Russia	Rozanski et al. (1993)
$\delta^{18}O$	3–4	North America: Atlantic to Rockies	Clark and Fritz (1997)
$\delta^{18}O$	10	Canada: Pacific to Prairies	Yonge et al. (1989)
$\delta^{18}O$	0.75	Amazon: Atlantic to Andes	Salati et al. (1979)

Table 5.2: Some examples of the continental effect from around the world.

distance from the tropical oceans and is therefore a proxy of the length of the air mass trajectory (Araguás-Araguás et al., 2000). At a single location where two (or more) weather system types produce precipitation, it has been shown that the rainout process has a greater effect in reducing the δ values of precipitation than seasonal changes in temperature of as much as 10 °C (Araguás-Araguás et al., 1998).

The situation in the Western Cape is that, in spite of the variety of climates in the study area, the mean annual temperatures at the 15 rainfall stations are between 16.5 and 19 °C. This small range in temperature makes it difficult to attempt a meaningful analysis of isotopic variations against average annual temperature. It may be possible to explore variations in stable isotopes against seasonal temperatures, but the precipitation during summer is erratic at many of the stations and more years of data would be needed. Isotopic trends will instead be explored against continentality and altitude, both also proxies for the rainout process.

5.2.2.2 Continentality

There is often a correlation between isotope composition of rainfall and distance from the coast (e.g. Liu et al., 2010). This has either been applied over large distances, 1000s of kilometres, and for this purpose the GNIP (IAEA/WMO) data has usually been used, such as Araguás-Araguás et al. (1998), or over a smaller scale, typically using non-GNIP data, such as Hunjak et al. (2013) who sampled around Croatia. The former studies often reveal a clear gradient in isotope values and result in a $\frac{\Delta\delta}{\Delta distance}$ ratio, whereas the latter studies may only find a difference between coastal and inland sites and not be able to calculate a meaningful gradient (e.g. Vreča et al., 2006). Some examples of calculated continental isotope gradients are given in **Table 5.2**.

Developing a continentality model for the Western Cape is challenging in several ways. Firstly, the area of study is only sub-continental and so isotopic depletion is limited, although this is offset by orographically induced rainout on the 2000 m high mountain ranges of the Cape. Secondly, the area is almost surrounded by ocean and so most locations are never further than 100 km

station	Atlantic distance	coast distance	Atlantic × coast
UCT	8	8	64
TMC	2	2	4
TWT	48	45	2160
UKP	70	70	4900
WKP	72	70	5040
MTB	143	110	15730
DDN	133	105	13965
RVD	242	42	10164
RBP	330	30	9900
BKK	314	50	15700
GST	315	55	17325
BBG	410	65	26650
KMN	482	50	24100
LTL	573	35	20055
GKM	526	5	2630
r for δD	-0.39	-0.44	-0.71
r for δ^{18}O	-0.44	-0.37	-0.68

Table 5.3: Calculation of a continentality factor, by multiplication of the distance to the Atlantic in a line due west and the distance to the closest coastline irrespective of direction. Correlation coefficients between weighted mean delta values at each station and the various distances are shown.

from the nearest stretch of coastline (see **Table 5.3**). Thirdly, several types of weather system are responsible for producing rain in the province and these may approach from any direction between north-west, through west, south-west and south, to south-east, a range of 180°. Ocean is located in all of these directions from the rainfall collection stations, but by very different amounts. For example, the Goukamma sampling station is very close to the Indian Ocean and rainfall approaching from the south will have travelled a mere 5km over land before reaching there, whereas a trough approaching from the Atlantic Ocean at the west coast will have travelled over 500km before arriving at this station. No simple single factor can therefore be expected to describe a continentality correlation and indeed, correlations between δD or $\delta^{18}O$ and 'distance-to-Atlantic' or 'distance-to-closest-coast' are poor, with Pearson's r values of -0.39 for δD – Atlantic, -0.44 for $\delta^{18}O$ – Atlantic, -0.53 for δD – coast and -0.37 for $\delta^{18}O$ – coast.

A factor that somehow combines the effects of multiple weather systems approaching from the Atlantic and Indian Oceans to represent the average length of rainout pathways to each rainfall station is needed. The two measurements of 'distance-to-Atlantic', which is a line from the rainfall station due west to the Atlantic Ocean, and 'distance-to-closest-coast', which is a line in any di-

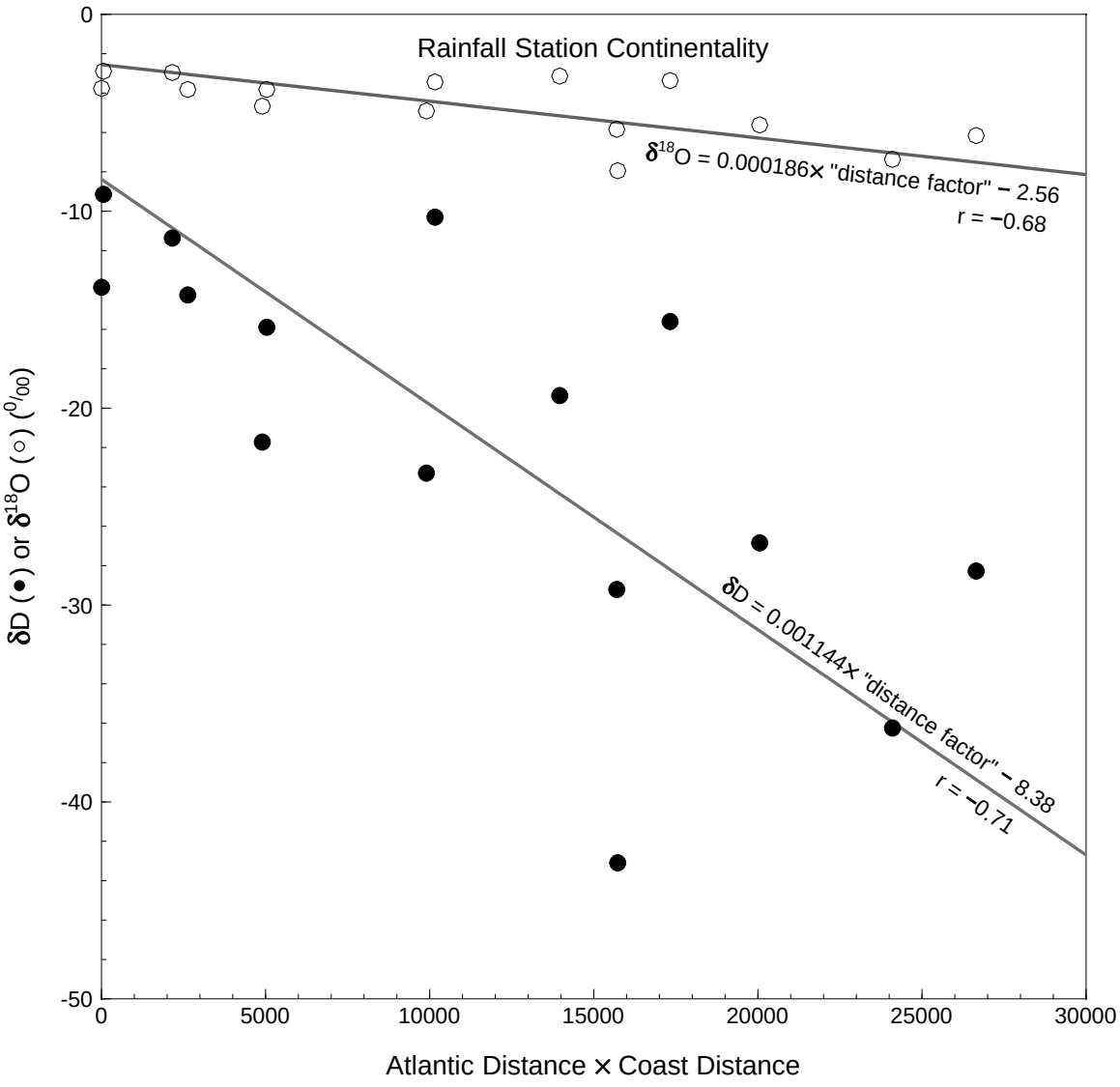

Figure 5.2: The continental effects calculated from this study.

location	**country**	$\delta^{18}O$ **gradient** $\frac{‰}{100m}$	**altitude** m asl	**reference**
Mt Cameroon	Cameroon	-0.16	0–4000	Gonfiantini et al. (2001)
Eastern Andes	Bolivia	-0.24	200–5200	Gonfiantini et al. (2001)
Hérault	France	-0.27	500–1800	Ladouche et al. (2009)
whole island	Taiwan	-0.20	0–2500	Peng et al. (2010)
Fuego volcano	Guatemala	-0.67	800–1200	Mulligan et al. (2011)

Table 5.4: Some examples of the altitude effect from around the world.

rection to measure the shortest distance to the coast from a rainfall station, have been multiplied to create a composite factor. Using this factor produces much better correlations; -0.71 for δD and -0.68 for $\delta^{18}O$ (**Figure 5.2**). The best fit lines to this data also have more realistic δD and $\delta^{18}O$ intercept values, close to those measured at UCT. These values are those expected for precipitation falling at the coast. Unfortunately this correlation does not allow easy comparison with isotope gradients that have been reported as $\frac{\Delta\delta}{\Delta distance}$, such as in Salati et al. (1979) or Rozanski et al. (1982).

5.2.2.3 Altitude

The altitude effect is the most easily measured and quantified meteoric isotope effect and many studies report values of $\frac{\Delta\delta}{\Delta altitude}$ for $\delta^{18}O$ and sometimes δD of precipitation at myriad locations around the world. **Table 5.4** shows a selection of these results from various recent studies; Clark and Fritz (1997, p.71) give results from similar studies in a slightly older selection of the literature.

The altitude effect is, as with the temperature and continental effects, also largely a consequence of progressive rainout as weather systems move up a mountain or escarpment and the heavier isotopes are depleted initially, leaving the subsequent precipitation to have lower and lower δ values. There is, however, an additional factor causing these lower δ values found at greater elevations and this is a reduction in the evaporative enrichment of raindrops as they descend below the cloud base, through unsaturated air. At higher elevations, the land surface is closer, or indeed above the cloud bottom, so reducing or eliminating the path length in which evaporative enrichment can occur.

Table 5.5 shows the altitude effect results calculated for this study. The range of $\frac{\Delta\delta^{18}O}{\Delta altitude}$ values can be seen to be similar to that reported in the literature, except that the Table Mountain and Cederberg region gradients seem on the low side. Unfortunately not many examples of $\frac{\Delta\delta D}{\Delta altitude}$ values have been reported in the literature. As would be expected from the physics governing isotopic fractionation of H and O in water, the δD gradients are around 6–8X that of $\delta^{18}O$.

locations	**distance***	**altitude change**		**gradient**	
				δ**D**	δ^{18}**O**
	km	m	masl	$\frac{‰}{100m}$	$\frac{‰}{100m}$
UCT - Lily Pond - TMC	6	940	135–1075	-0.48	-0.075
WKP - TWT - UKP - Cederberg Tafelberg	40	1550	350–1900	-1.1	-0.11
DDN - MTB	10	1430	480–1910	-1.6	-0.34
RVD - RBP	100	635	250–885	-2.0	-0.24
GST - BKK	6	750	350–1100	-1.8	-0.33
GKM - LTL	70	580	60–640	-2.2	-0.31
all stations: least squares regression	480	2020	60–2080	-1.2	-0.19
all stations: reduced major axis regression	480	2020	60–2080	-1.7	-0.27

Table 5.5: Altitude effect gradients calculated for this study. *Distance refers to the distance between the furthest of the listed locations.

The first point to note about the altitude effect calculations for this study is that many of the individually calculated gradients are similar, such as DeDoorns – Matroosberg and Gamka Store – Bakenskop, even though the altitudes are not the same and the pairs of stations are hundreds of kilometres apart. This is best seen graphically in **Figure 5.4**. Second to note, again most easily visible in the graphs, is the general agreement between the local gradients and the regional line calculated by using all the rainfall station data gathered in this study. Slight exceptions to this are the Table Mountain area (C – Lily Pond – T) and the Cederberg area (I – W – U – Spout).

Looking more closely at the data, there is a trend, especially noticeable in the δD gradients, of increasing gradient eastwards; the locations are arranged approximately in a west to east order in **Table 5.5**. This trend is not well displayed by the $\delta^{18}O$ gradients, however, the high gradients for DDN – MTB and to a lesser extent GST – BKK, the two locations which are disturbing the trend, are probably due to the evaporative enrichment of rain at DDN and GST, both of which are low altitude, low rainfall sites. The ratio of $\frac{\Delta\delta D}{\Delta\delta^{18}O}$ should be around 6–8X, and if less than this, is a sign of evaporative enrichment. Substantial evaporation of falling raindrops will increase $\delta^{18}O$ values more than δD values because of kinetic fractionation, and so increase the difference in $\delta^{18}O$ values between the high and low altitude sites, resulting in a steepening of the $\delta^{18}O$ gradient and therefore a reduction in the multiplication factor between the δD and $\delta^{18}O$ gradients.

The very low gradient in $\frac{\Delta\delta}{\Delta distance}$ reported for Table Mountain can be explained by the following argument. Normally weather systems move from low to high ground and so, as explained above, the altitude effect is a reflection of rainout of heavier isotopes at lower elevations. The dramatic topography of Table Mountain means that the high altitude station, TMC (1074 m), is only 2 km from the Atlantic Ocean coast, whereas the lower station, UCT (135 m), is 6 km further inland. This is a reversal of the usual situation in studies of the altitude effect, where the higher altitude station is also further inland (or in the direction of rain-bearing weather in the case of the

Andes and the Amazon in Gonfiantini et al. (2001)) than the lower altitude station. The altitude effects measured in these studies are the cumulative effect of altitude and distance on rainout. The Table Mountain sub-study is therefore an unusual and valuable example that demonstrates how the pure altitude component of rainout is less than is generally found in these other studies, where a composite distance and altitude induced rainout is being measured.

Two regression lines are plotted on each of the graphs in **Figure 5.4**; the altitude data is shown in **Table 5.6**. These lines have been regressed on all the rainfall station data (letters); they exclude the points for the high altitude seeps (symbols), such as the Lily Pond and Spout. The least squares method (thinner line) assumes no error on the x-variable as this is accurately known and does not change; this regression can be thought of as y on x. This method is appropriate for this type of analysis, where y (δ) is variable and imperfectly known and is dependent upon x (altitude), which is perfectly known and unchanging. However, these lines, for both δD – altitude and $\delta^{18}O$ – altitude are not good matches for the local gradient lines, as seen in the graphs and in the gradient values in **Table 5.5**, where the least squares gradients are at the low end of the spectrum.

The reduced major axis method of regression (thick lines) has been used throughout this study for the δD – $\delta^{18}O$ regressions and is ideally suited to data where both x and y have variance and neither are independent of the other. Interestingly, although this method is theoretically statistically sub-optimal for the δ – altitude regressions, the resulting regression lines and $\frac{\Delta\delta}{\Delta altitude}$ gradients seem to describe and fit the data better.

Figure 5.3: Map of the study area with sample locations and cross section lines indicated. Background DEM from NASA (2013) and roads shapefile from NGI (2012).

Island Mountains and Mountain Valleys

Island Mountains is a term coined here to describe sample collection points that are located at or near the top of a mountain peak and are therefore at a position much higher than the surrounding area.

The two rainfall collection stations, Blesberg and Kammanassie, which are only 25 km apart and have a 1400 m altitude difference, would seem to make a useful pair for a local estimate of the altitude effect. However, Blesberg, the highest station of the whole study, at 2080 m, has δD and $\delta^{18}O$ that would be expected for a station of half that height, based on the average altitude effect relationship for this study. In contrast, Kammanassie, with a moderate altitude of 666 m, has isotope ratios that would be expected for a station at triple the height. Only Matroosberg, at 1910 m, has more negative δ values than Kammanassie. The result of these departures from the average pattern is that the local altitude effect gradient is reversed between these stations, with δ values that increase with altitude.

The Blesberg mean δ values seem to fall on a line with Cederberg Tafelberg (Spout) and Cape Town's Table Mountain (and Lily Pond); see **Figure 5.4**. All four of these points lie to the right of the $\frac{\Delta\delta}{\Delta altitude}$ best fit regression line, meaning the δ values are less negative than expected, based on the average for this study. Robinson Pass, Bakenskop and Matroosberg are close to the average for all of the data. Kammanassie and Lentelus lie to the left of the average, meaning their δ values are more negative than would be expected for their altitude. These three sets of locations have morphological similarities that may account for their location on the δ–altitude plot. The first group can be thought of as "island peaks", sharply rising peaks that are much higher than the general surrounds. The last group can be thought of as "mountain valleys", where the elevation of the sample site is lower than that of the general surrounds. The intermediate group are at a position in the landscape where there are substantial amounts of higher and lower ground around, or, in the case of Bakenskop, on a plateau-like summit where the station is surrounded by lots of land at a very similar elevation (less than 100 m difference).

Rainout on the "island peaks" is not substantial, because of the sudden change in elevation, and so the isotopic signature is more typical of that for a site at lower elevation. The "mountain valleys" are the reverse, where the station elevation does not reflect the amount of rainout that occurs on the surrounding higher ground, and so the isotope composition tends towards those expected at these surrounding, higher elevations.

Table 5.6 summarizes the landscapes around some of the rainfall collection stations, as well as some high altitude seeps. The average altitudes were generated from the ASTER DEM (Advanced Spaceborne Thermal Emission and Reflection Radiometer Digital Elevation Model) by averaging the elevations of all pixels within a 5 km radius of the point of interest (ASTER, 2014). The seeps discharge high up in the mountains with minimal ground above the seep and so the discharge altitude cannot be much different to the recharge altitude, as there is very little more mountain available above the seep point for recharge to occur. These seeps can be thought of as proxies for

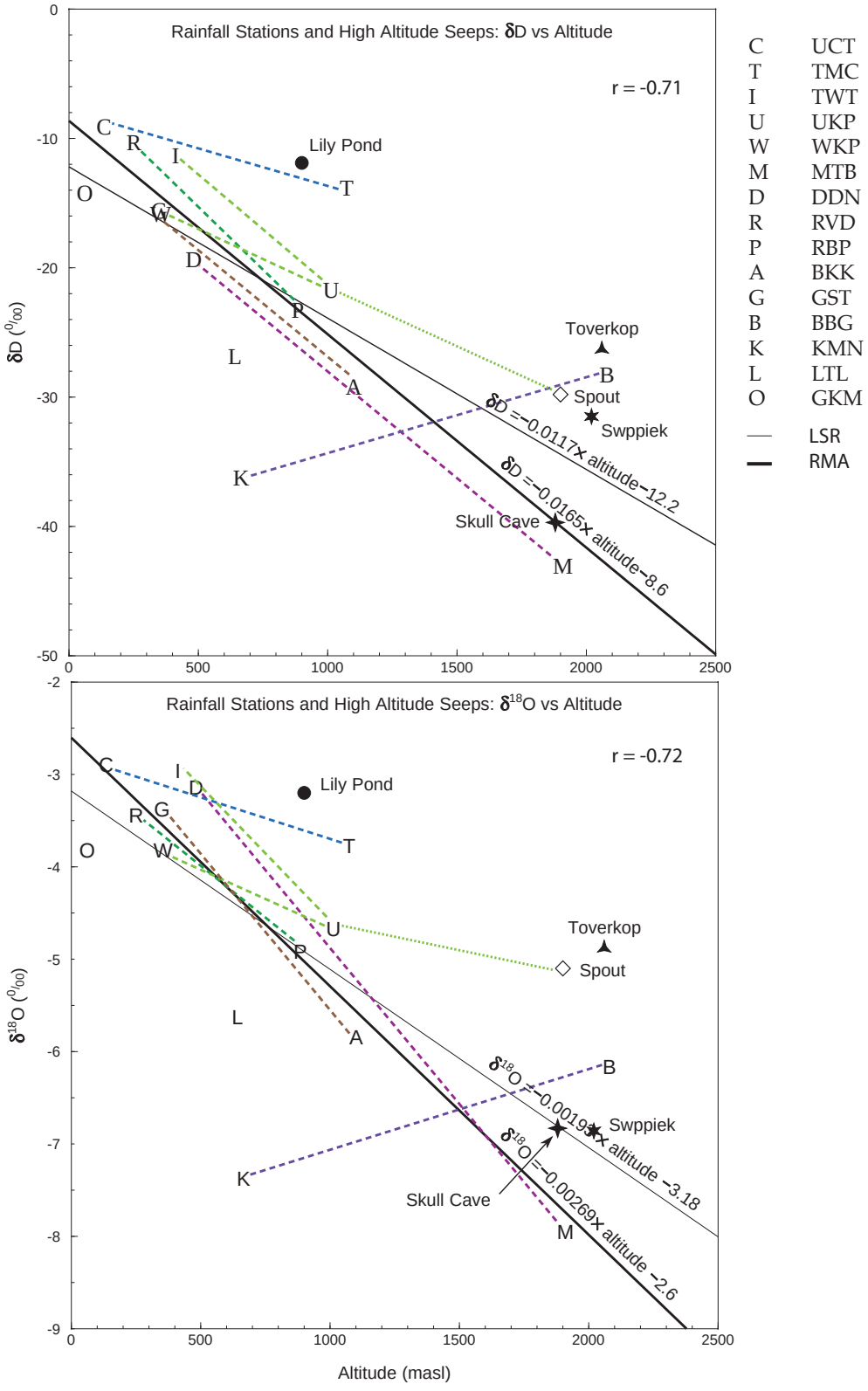

Figure 5.4: Relations between altitude and δ values. Letters indicate weighted averages of monthly precipitation at rainfall collection stations; symbols are high altitude seeps. Dashed lines connect rainfall nearby stations; dots to a nearby seep. Colours are from the theme colours for one of the stations in the pair. Both the RMA regression (thick line) and LSR (thin line) are shown, calculated from the rainfall station data, excluding the seeps.

station		elevations				stn - avg
		m asl in 5km radius from station				m
		station	**highest**	**average**	**lowest**	
Cederberg Spout		1900	1969	1266	940	+634
Table Mountain Cableway	TMC	1074	1086	289	0	+785
Table Mountain Lily Pond		900	1086	289	0	+611
Matroosberg	MTB	1910	2249	1561	550	+349
Robinson Pass	RBP	885	1363	723	350	+162
Bakenskop	BKK	1100	1106	772	350	+328
Toverkop	TVK	2060	2189	1281	550	+779
Skull Cave	SKC	1880	2240	1393	750	+487
Seweweekspoortpiek Cave	SWP	2020	2324	1368	650	+652
Blesberg	BBG	2080	2084	1329	600	+751
Kammanassie	KMN	666	1205	794	500	-128
Lentelus	LTL	710	1688	854	550	-144

Table 5.6: Relative position in the landscape of selected rainfall stations and high altitude seeps, which are proxies for rainfall. The last column summarizes the situation by showing the difference in height between the station or seep elevation and average elevation for an area of 5 km radius around the station.

rainfall at much the same elevation. It can be seen from **Table 5.6**, especially the final column, that some stations lie well elevated from the average surrounding landscape, Blesberg, Toverkop and Table Mountain being good examples – these are the "island peaks". Other stations are at similar altitudes to the average and only two, Lentelus and Kammanassie, are examples of the "mountain valleys". A good correlation exists between this difference from the average elevation, and the position on the δ–altitude graphs, as described above. A visual representation of the relative altitude of sampling points is shown in **Figure 5.5**.

The correlation is not exact, at least one reason of which is the seep data consists of between one and three samples only per seep. Much noise exists in isotope data, due to the specifics of the weather, and so single samples are not ideal, although being groundwater, these seep samples will be more stable and representative values than for rain. Another reason for the extreme position of Kammanassie is the large amount and isotopically negative rainfall in June and July 2010. The July value in particular, with 80 mm rainfall for the month, caused the average to be displaced towards low δ values.

In conclusion, due to the steep slopes and small area of the high peaks in the Cape Mountains, the altitude effect is supressed and the isotopic composition of rainfall on these summits is less negative than one might expect. The reverse is also true for valleys in mountainous areas, where the isotopic composition reflects a slightly higher altitude, closer to that of the average ground

elevation around the site, and not the specific, low, elevation of the valley floor. To get an accurate measure of the altitude effect, sites for rainfall collection should be chosen on broader peaks where substantial areas of high ground occur, such that the rainout process is significant enough to drive the isotope ratios to more negative δ values.

This altitude effect distortion is probably the reason the RMA regressions fit the data better than the least squares method, as the RMA regression assumes an error in 'x' as well as 'y'. As discussed above, the ground altitude at the rainfall stations is not always representative of the area around the location, which is what influences the isotope content of the rain, and so 'x', or altitude, can also be thought of as being subject to some error.

5.2.2.4 Amount

Correlations between δD or $\delta^{18}O$ and rainfall amount have been described by many authors since Dansgaard (1964) first reported it. As the amount of rainfall increases, the δ values decrease, both for single rainfall events (e.g. Dody and Ziv, 2013) and for monthly average rainfall amounts (e.g. Uemura et al., 2012). Reasons for the amount effect include, firstly, a drop in air temperature to cause condensation of progressively isotopically lighter vapour, as the heavier isotopes have already condensed and rained out of the air mass. Secondly, the more rain that has fallen, the more the air below the cloud becomes moist and so less evaporative enrichment of the raindrops occurs as they fall to the ground. And thirdly, similarly, in clouds with great vertical development where rain may form at high elevations, raindrops falling through the cloud may undergo isotope exchange with cloud droplets and vapour lower down, which will make slight rains tend towards heavier isotopic content, but will affect substantial rains less and so substantial rains will tend to retain their more negative isotopic signatures.

The data from this study is not ideally suited to quantification of an amount effect, primarily because the short period of sampling (two years) leads to averages for rainfall and isotope data possibly being far from the long term means. No correlations exists between the average annual rainfall and the weighted mean isotope values, as can be seen in **Figure 5.6**, both graphically and from the 'r' values that are near zero. For monthly data, a similar restriction on data quality results from the short duration of this study, as each month (e.g. July) may only be based on zero to three samples. At some stations there are months with no samples, although this is often due to a consistent lack of rain for that month(s) over two or three years, for example January at De Doorns. Nevertheless, for the stations with more complete records, comparison of mean monthly δD and $\delta^{18}O$ values with mean monthly rainfall has been done: see **Figure 5.7**.

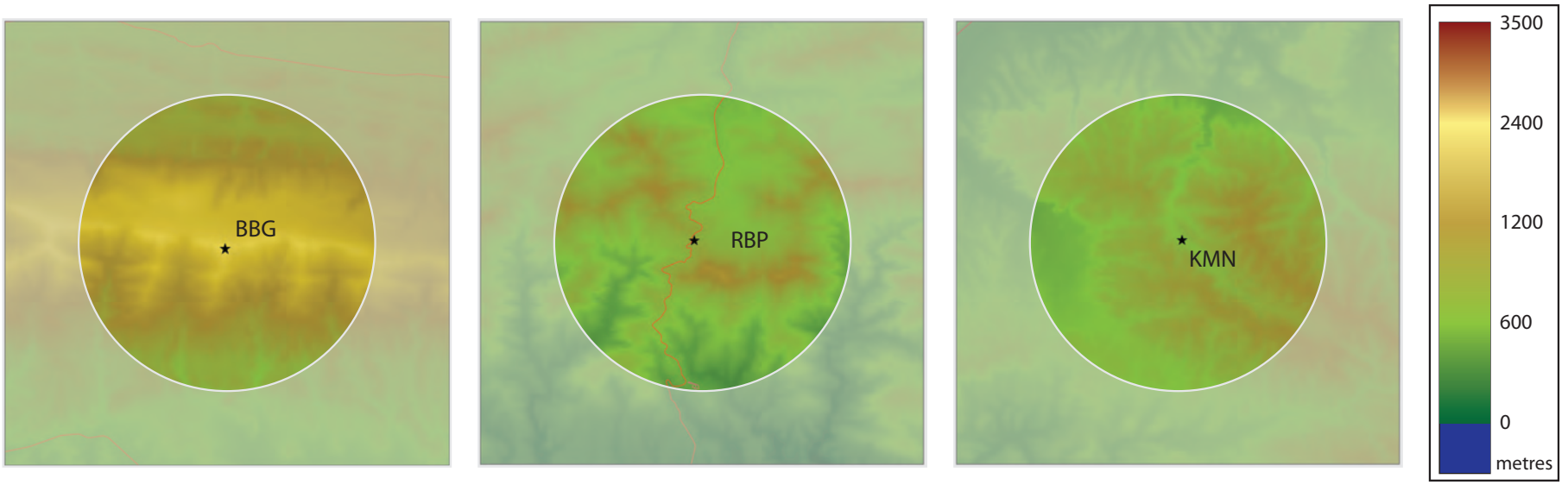

Figure 5.5: Digital elevation models for three of the rainfall collection stations with a highlighted circle of 5km radius around each station, illustrating the relative position in the landscape, in terms of altitude, of each station. Blesberg (BBG) is an example of an "island peak", Robinson Pass (RBP) of a station in a more or less representative position and Kammanassie (KMN) a "mountain valley". See **Table 5.6** for similar information in a numerical format for these and other sampling points.

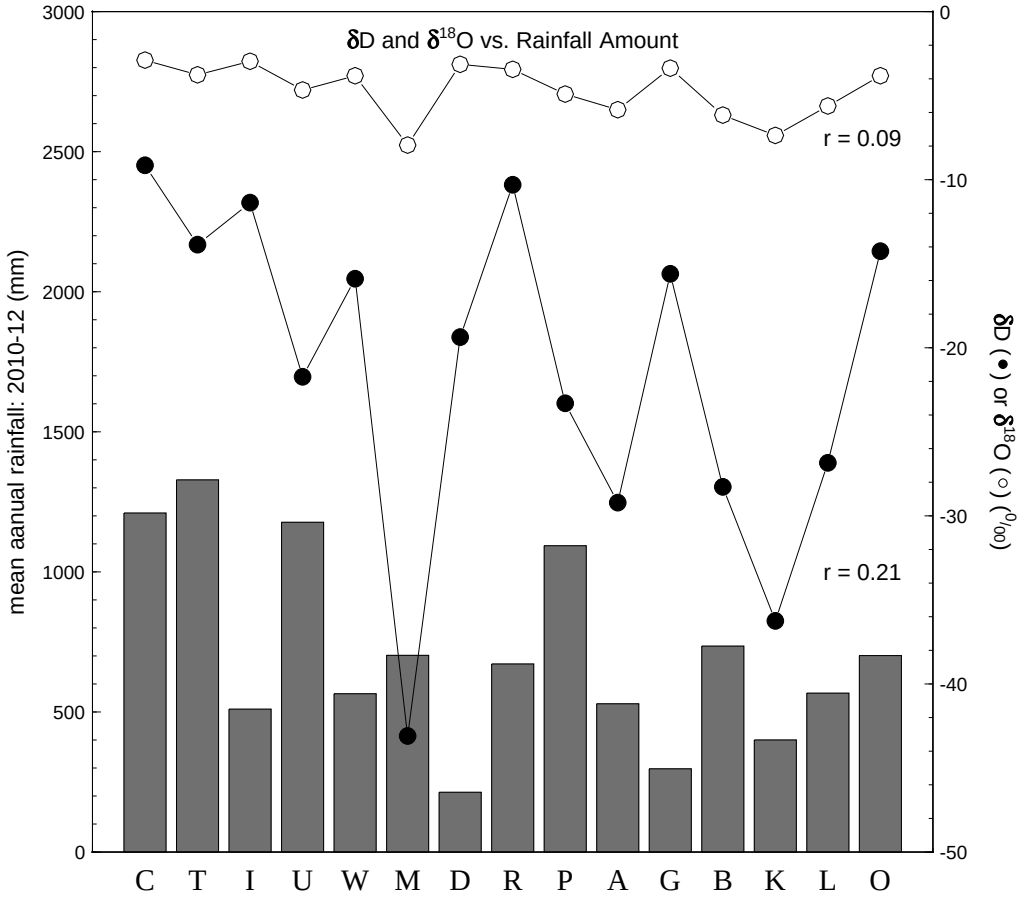

Figure 5.6: Comparison of weighted mean isotope composition and mean annual rainfall at each station: C = UCT, T = Table Mountain, I = Twaktuin, U = Uitkyk Pass, W = Wolfkop, M = Matroosberg, D = De Doorns, R = Riverndale, P = Robinson Pass, A = Bakenskop, G = Gamka Store, B = Blesberg, K = Kammanassie, L = Lentelus and O = Goukamma.

These stations were not selected on the grounds of displaying a "better" amount effect, but purely on the completeness of the record. The amount effect at these stations is generally noticeable in that there is a fair to good correlation between the δD or $\delta^{18}O$ values and rainfall amount. The Pearson's 'r' correlation coefficients shown on the graphs in **Figure 5.7** confirm the validity of the visual impressions given by the graphs. The Wolfkop station, however, shows no correlation between rainfall amount and δ values, due to some months with low rainfall having the isotopically lightest water, particularly March and December. The 30th March 2011 featured an unusual low pressure trough preceding a frontal depression over the Atlantic Coast area, causing widespread rain over the Western Cape and into the western parts of the Northern Cape, with falls of 8 mm at Clanwilliam and 10 mm at Excelsior Ceres. Rain from these systems is typically convective in nature (similar to thunderstorms) and generates rain of light isotopic composition. The rainfall of 31st December 2010 to 1st January 2011 has already been discussed in the previous chapter (Chapter 4), and was a significant event environmentally, causing floods and mass

wasting erosion in the Cederberg region, and resulted in rain and hail with highly negative delta values. A longer term record for a station like Wolfkop would be expected to see the influence of these unusual events decline and a better amount effect correlation develop.

The amount effects from the stations at UCT, Riverndale and Goukamma are all significantly better than that found by Harris et al. (2010) for UCT rainfall over 1996–2008, which gave 'r' values of -0.388 for δD–amount and -0.425 for $\delta^{18}O$–amount. Of the three stations shown in **Figure 5.7**, the UCT 2010–2012 record gave the poorest correlations with 'r' values of -0.51 and -0.68, similarly, but these are still substantially better correlations than the previous work. This suggests that some years have a particularly clear amount effect, exceeding the long term average. This finding emphasizes the value of long term monitoring in revealing average meteorological patterns and warns against overinterpretation of data based on short term precipitation records.

5.3 Surface Water

5.3.1 Altitude

The five rivers sampled reveal a wide range of isotopic compositions over an altitude range of approximately 130–1900 m (see **Figure 5.8**). The data for each river generally forms a cluster, with no significant correlations against altitude. The best correlation is at Volstruiskloof, which is the only river to have 'r' values more positive or more negative than +0.5 or -0.5, respectively (the threshhold for a reasonable correlation). However, removal of only one of the four Volstruiskloof data points reduces the remaining three points to a cluster. For the neighbouring river, Duiwelskloof, a better correlation can be created if the data point with the highest δ values is removed; this can be motivated as this sample is from the base of a very low flowing drip waterfall that flowed over exposed, sunny rock for many metres and has been substantially evaporated in the process. However, this still does not create a good correlation between isotope values and altitude. The outlier Volstruiskloof and Duiwelskloof points have been included in analyses and graphs.

5.3.2 Springs, Seeps and Tributaries

Samples of seeps and springs were taken along Groothoekkloof and in the Witels, often paired with a sample from the main stream just above mixing with the new source, but these showed surprisingly little variation. Similarly, tributaries were also sampled and paired with a sample in the main stream just upstream of mixing with the tributaries' waters, and again these often showed little difference. No systematic variation could be found between the isotope composition of a sample and the characteristics of its source, such as being a main stream or spring sample, or the size or average elevation of its sub-catchment, in the case of a tributary.

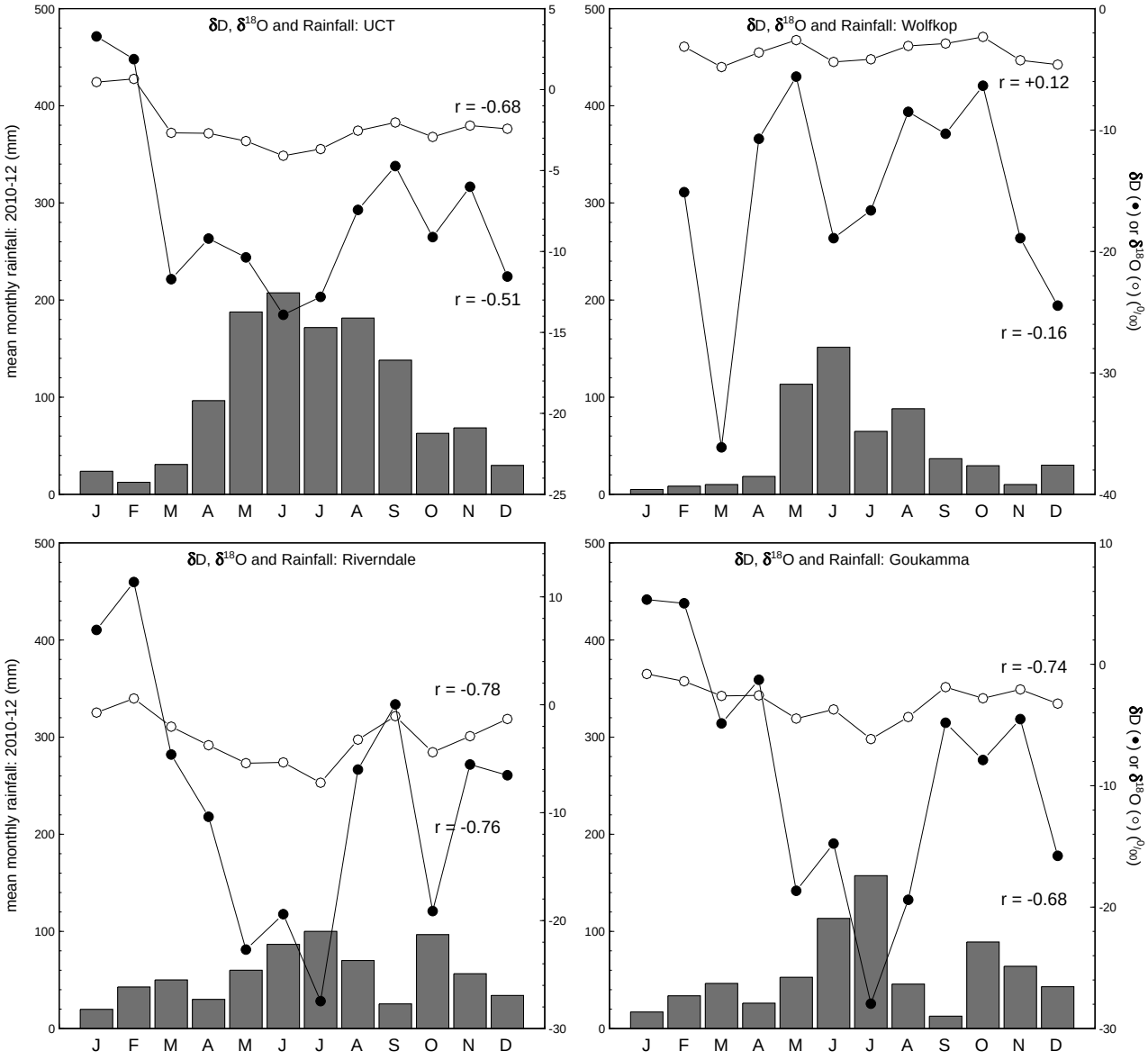

Figure 5.7: Mean monthly rainfall, δD and $\delta^{18}O$ values for the four rain stations with most complete record.

5.3.3 Baseflow

The rivers were all sampled in summer or early autumn when rainfall had been low for many months, with the exception of Meulkloof, near Swellendam in the southern Cape, which experiences all year round rainfall. The other rivers would all have been fed exclusively by groundwater (see **Section 2.5.4**), whether deeper groundwater discharging from fractured Table Mountain Group aquifers or shallow groundwater from soil and scree slopes. The surface water flows that remain steady over the dry season and are groundwater fed are known as baseflow.

Several factors could cause the baseflow to show little isotopic variation down the length of the river, as seen in **Figure 5.8**. The most obvious factor is that river samples are a mixture of the various groundwater sources that feed them, and so mixing of all the water sources would dilute any unusual isotope composition feeding into the river at any point. The rivers all have a steady increase in flow downstream, caused by addition of groundwater. However, the sampling of springs, seeps and tributaries directly showed that it is not mixing and dilution of surface water that is responsible for the lack of isotopic trends or changes, but rather the sources themselves that do not vary much.

Groundwater flow through the Table Mountain Group aquifers is directed by fracture networks that are aligned with structural features and bedding (Hartnady and Hay, 2002b). Groundwater does not simply flow from peaks to valley bottoms in the shortest distance as it would in a primary porosity aquifer. This complex flow dynamic means that water emerging as springs and seeps to feed surface water may come from a range of directions and be recharged at a variety of positions at different altitudes. This complexity is possibly the reason the rather limited surface water data set is unable to yield any patterns. Interestingly, the variations in δD and $\delta^{18}O$ values tend to decrease eastwards, as seen in the last two columns of **Table 5.7**. This could be caused by an increase in fracturing of the Table Mountain Group as one moves from the relatively undeformed strata of the Drakenstein Mountains in the west, through the syntaxial region of the Hex River Mountains to the southern Cape, known to have experienced the greatest tectonic deformation during the Cape Orogeny (Söhnge, 1983; de Beer, 2002). The greater the degree of fracturing, the more likely the groundwater becomes well mixed and variation in isotope composition is homogenised. The sample size of 5 rivers is perhaps a bit small to take this as a real trend, but it is interesting that greater river length, greater change in altitude or greater catchment size does not cause a greater range in isotope values.

Work by Negrel et al. (2011) on groundwater from shallow fractured rock aquifers showed substantial variation in isotope composition. This is in contrast to the more homogenous isotope compositions measured in this study and supports the model of complex and deep groundwater flow in the Peninsula aquifer.

code	river	mountain range	catchment						sampling		range	
			highest peak	height	highest sample	lowest sample	area	flow	length	gradient	δD	$\delta^{18}O$
				m asl	m asl	m asl	km^2	L/s	km	m/km	‰	‰
DWK	Duiwelskloof	Drakenstein Mountains	Drakenstein Peak	1490	1240	680	2	2	2.4	300	10.1	1.91
VSK	Volstruiskloof	Drakenstein Mountains	Buller's Kop	1425	1160	580	1.5	2	1.5	450	11.9	2.14
WTL	Witels	Hex River Mountains	Buffelshoek Peak	2060	1650	310	50	100	20	70	7.5	1.61
GHK	Groothoekkloof	Hex River Mountains	Matroosberg	2249	1800	580	15	10	8	150	8.8	0.59
MLK	Meulkloof	Langeberg	Hermitage Peak	1546	820	130	11	20	6	120	3.4	0.44

Table 5.7: Description of the five rivers sampled, with rough flow estimates and gradient for the sampled length.

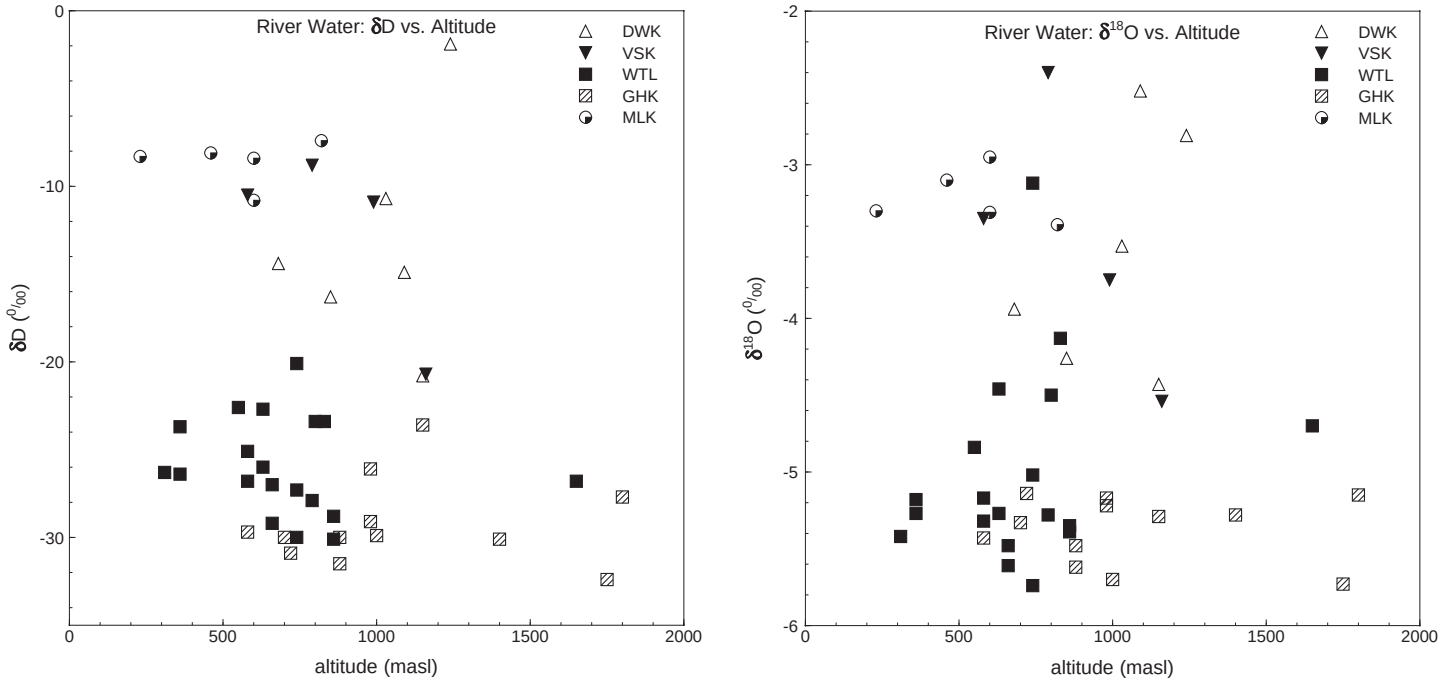

Figure 5.8: Plots of δD and $\delta^{18}O$ against altitude for surface water samples from five rivers in the Western Cape.

5.3.3.1 Sharp Relief

The lack of a distinct change in isotopic composition with altitude in the rivers and their sources (springs and seeps) suggests that the groundwater in each catchment does not vary significantly isotopically. The would occur if the rainfall is isotopically similar across the catchment, as might be expected because of the small size of these mountain catchments. This finding concurs with the rainfall analysis where it was found that the variation in isotopes is less than is expected given the range in altitude between sites. The average elevation around a site, in an area of 50–100 km^2, is as important as the actual altitude of the site in determining the isotopic composition of rainfall. This works for both sharp, high peaks that are much higher than the surrounding terrain, and for deep, steep valleys that are much lower than the surrounding terrain. So although the rivers traverse wide ranges of elevations, from peak to valley bottom, the range in isotopic composition for rainfall is more restricted than the elevation range would suggest.

The best fit lines shown for the five rivers in Chapter 4 also reveal something about the catchments. The line with the lowest gradient and intercept is for the Witels ($\delta D = 4.42\delta^{18}O - 3.8$), and is similar to typical evaporation lines (e.g. Gat, 1996). This river is the longest, the gradient is the lowest and the catchment is the largest, all of which are likely to contribute to evaporation in the area. If evaporation was occurring only in the main stream as it flows through the catchment, then the lowest samples would have the least negative isotope compositions. The samples with the least negative isotope composition are not concentrated towards the bottom of the river catchment and as seen in **Figure 5.8**, there is no systematic variation of isotope values against parameters such as altitude. This suggests that the evaporation is widespread and affects all waters in the catchment and is not simply the result of evaporation in the main stream.

5.3.3.2 Summary

Isotope compositions are clustered for each river sampled. Variation in each river is minimal and is generally poorly correlated with any obvious parameter, although it is known that rivers often display limited variation in isotope values (Fritz, 1981). The isotopic variation in rainfall has been shown to be smaller than would be expected, given the range of altitude. Furthermore, complex groundwater flow causing mixing, and also mixing and dilution along the length of the streams, will reduce the range in isotope compositions in the surface water. From the rivers sampled it seems that isotopes are unable to help pinpoint groundwater flow directions or recharge areas for the water that discharges into the streams via springs and seeps. Isotopes may still be of value for longer rivers or larger catchments, but appear to have little value in small, rugged mountain catchments. Decreasing range in isotope compositions within each river, as one moves eastwards, may reflect more complex groundwater flow and greater mixing, due to more intense fracturing related to position within the Cape Fold Belt, which has varying degrees of structural deformation from the Cape Orogeny.

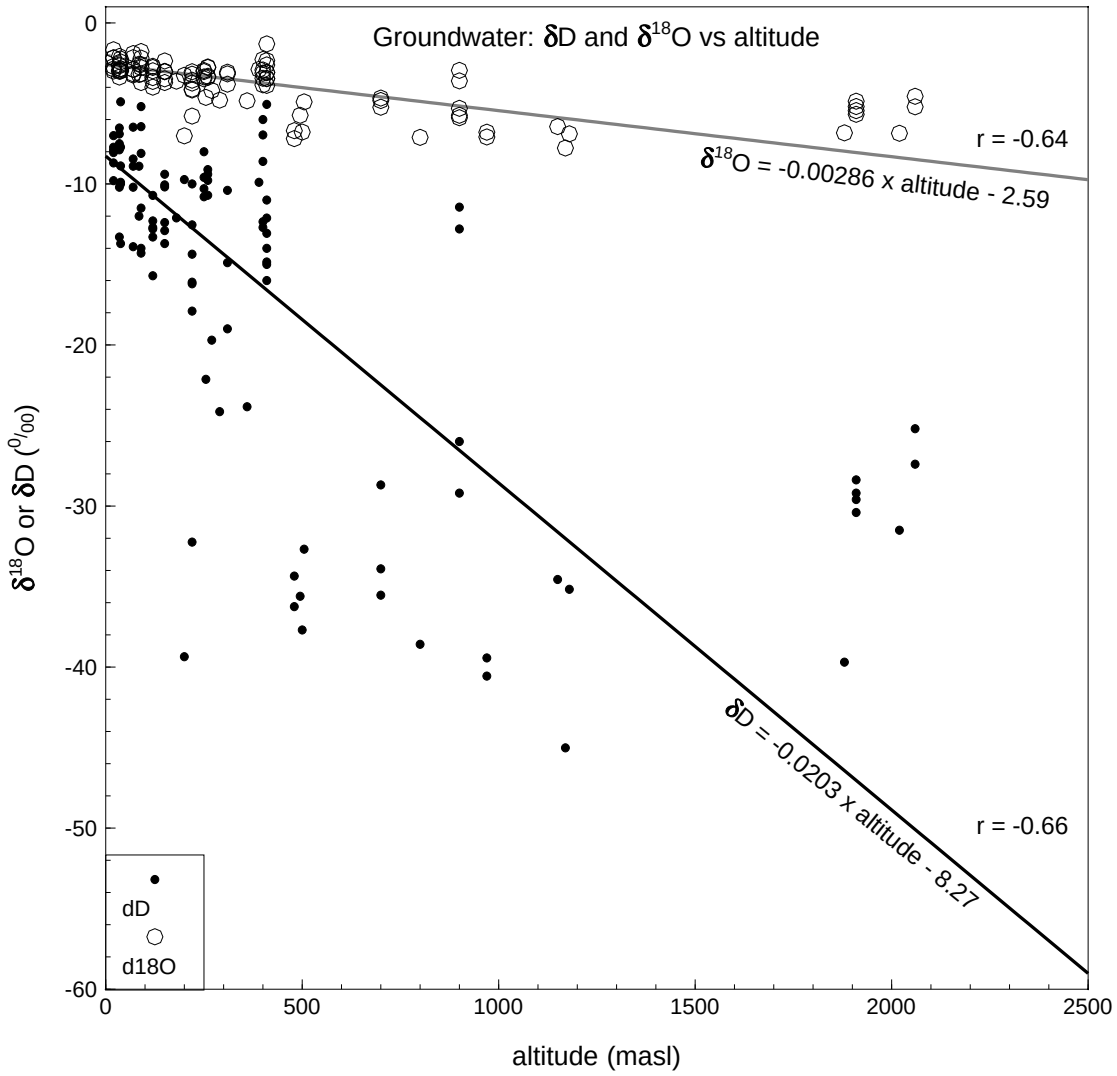

Figure 5.9: Groundwater isotope composition as a function of sampling (discharge) altitude.

5.4 Groundwater

5.4.1 Altitude

The isotope composition of recharge should be similar to that of the rainfall in the recharge area, although some changes will take place, primarily due to evaporation and selective recharge. Selective recharge takes place because not all rainfall events are the same in magnitude and intensity, and depending upon the recharge process, some of the rain may not recharge. This can occur when an event is too small and all the rainfall gets used up through interception, transpiration or evaporation. A larger event may generate recharge, but a portion of it will still be taken up in interception, transpiration and evaporation. More intense events may result in high runoff, none of which recharges locally, but may recharge in another area downslope. The isotope

composition of groundwaters can therefore vary from very similar to that of rain in the recharge area, to something quite different, and this variation may itself vary year to year, depending on changes in the weather and possibly also vegetation and soil.

Brandvlei hot spring, at 64 °C, is the hottest spring in the region (and in the country). No actively circulating groundwater in the Western Cape is therefore likely to reach temperatures over 70 °C and by far most of the groundwater circulates at temperatures between 0 °C and 20 °C. No isotope exchange between the water and host rock takes place at these temperatures (Clark and Fritz, 1997). Assuming a simple flow model from recharge area to discharge area with no mixing, the isotope composition of water at discharge must be the same as at the recharge area.

Groundwater flow through landscapes varies from highly local, over hundreds of metres or less, to regional, over distances of tens to hundreds, such as in the Perth Basin (Davidson, 1995) and sometimes even thousands of kilometres, such as in the Great Artesian Basin in Australia (White, 2000). In South Africa, the absence of large, unmetamorphosed sedimentary basins to form regional aquifers is the main reason groundwater flow is restricted in extent and quantity. The Karoo Basin contains mostly argillaceous rocks and the more arenaceous units are too well cemented to be highly transmissive primary porosity aquifers. Changes in rock type also tend to block flow as aquifers come up against impermeable units, for example the Table Mountain Group abutting the Malmesbury Group as on the Kango Fault (see **Figure 5.20**). Lastly, the highly dissected topography tends to make flow paths short, because of steep hydraulic gradients and short distances between wet, high altitude mountains, and dry, low altitude valleys where discharge feeds into rivers (Domenico and Schwartz, 1998, p.77).

A correlation exists between the isotopic composition of groundwater and altitude (**Figure 5.9**). The altitude plotted is that of the discharge point of springs and seeps, or that of the collar (ground level), if sampled from a borehole. The equations of the best fit lines describing the δD and $\delta^{18}O$ relationships with altitude have been plotted on the graph. These lines were calculated using the reduced major axis regression method, as the least squares regression method again generated lines of best fit with rather gentle gradients and unrealistically negative intercepts, as was noted for the regression of the rainfall station data against altitude, in **Figure 5.4**. These least squares regression equations are:

$$\delta D = 0.0134 \times altitude - 11.15 \quad (r = -0.66)$$

$$\delta^{18}O = 0.00184 \times altitude - 3.02 \quad (r = -0.64).$$

Where recharge areas are far from discharge points, the isotope composition of the groundwater might be different from the rainfall at the discharge area. In particular, because changes in altitude generate noticeable changes in rainfall (and hence recharge) isotope composition over relatively short distances, if groundwater flow paths were several kilometres and more, there

would be a poor correlation between groundwater delta values and altitude. The graph in **Figure 5.9** shows the opposite. The slopes and intercepts of the best fit lines similar to those for the rainfall station – altitude correlation (see **Figure 5.4**). This suggests that the flow paths, at least for the groundwater sampled in this project, are mostly short, and in particular, there are not large differences between the elevation of the recharge and discharge sites.

5.4.2 Hot Springs

Hot springs have always been a target for hydrological (e.g. Bond, 1953), hydrochemical (e.g. Kent, 1949) and isotopic (e.g. Mazor and Verhagen, 1976) studies. The hot springs of the Western Cape have been analysed for their stable isotope content previously, so an analysis of the changes over time is possible. From **Figure 5.10**, it is clear that there are no systematic changes between the three studies in 1971-2 (Mazor and Verhagen, 1983), 1995-6 (Diamond and Harris, 2000) and 2010-12 (this study). The 'random' variation in isotopic values of discharge at the springs, measured from month to month in the Diamond and Harris (2000) work is equal to the magnitude of variation seen over 40 years, between 1971 and 2011. It is possible that some of the larger shifts in isotope composition could reflect yearly or multi-year shifts in the average isotope composition of recharge. However, these large shifts (10 ‰ for δD and 2 ‰ for δ^{18}O) were recorded over months by Diamond and Harris (2000) over only 2 years at Laingsburg. It is possible that inter-annual shifts in isotope composition become compressed in the groundwater flow path and issue over monthly timescales, but this would require a piston-like flowpath with very little groundwater mixing, which is not likely given the depth and length of the flowpath.

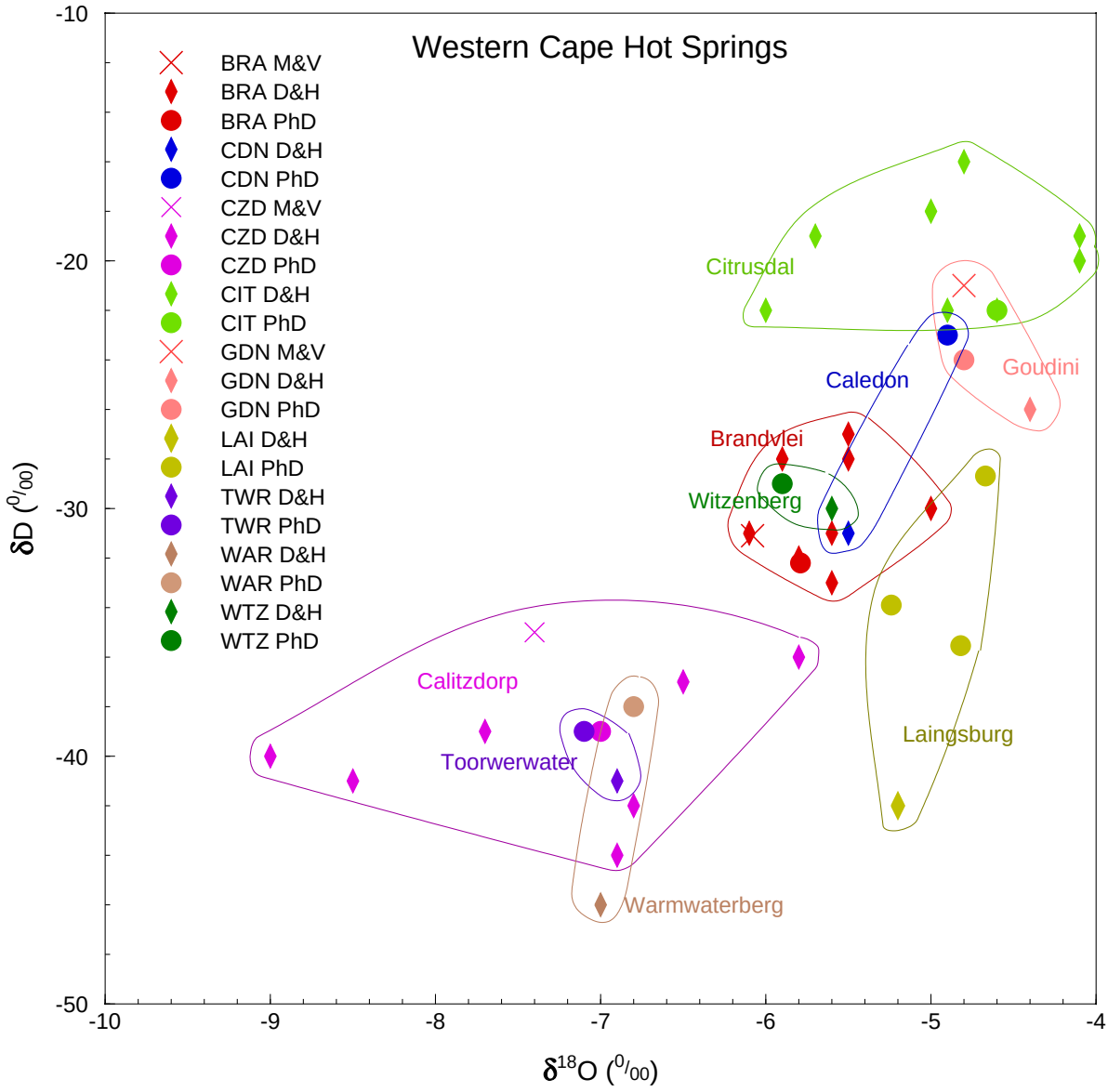

Figure 5.10: Stable isotope compositions for the Western Cape hot springs from three different studies, showing no obvious long term change. Data from Mazor and Verhagen (1983) (M&V), Diamond and Harris (2000) (D&H) and this study (PhD).

5.5 Regional Analyses

This study attempted an overview of stable isotopes of water in and around the Table Mountain Group, including rain, surface water and groundwater. In such a broad study, large areas naturally are neglected, but some areas have had sufficient analysis that a more detailed interpretation can be attempted in those areas. These interpretations should provide, firstly, an indication of the usefulness of stable isotope hydrology in unravelling the hydrogeology of the Table Mountain Group, and secondly, some actual insights into the flow of groundwater through the Table

Mountain Group. On the δD–δ^{18}O plots in this section, the symbol size is approximately that of the analytical error.

5.5.1 Cederberg

Substantial quantities (gigalitres per year) of groundwater are utilized by farmers in the Olifants River Mountains area (pers. comm. Robert Paterson of Twaktuin Farm). The possibility exists that this groundwater, or some of it, is recharged in the Cederberg and, by means of faults and fracture networks in the Peninsula Formation, passes beneath the Olifants River Valley before discharging to the west of the Olifants River Syncline in the Olifants River Mountains area. The cross section in **Figure 5.11** illustrates how the geology can allow this to occur, although the geometry of the Olifants River Syncline changes to the north and south of this line. In general, the syncline deepens and is dominated by a simple synclinal fold structure southwards, whereas northwards the syncline shallows and faults displace the Cederberg aquitard such that hydraulic connections are established between the Peninsula and Skurweberg aquifers. The fault shown in the Olifants River Syncline in the cross section does not quite achieve this linkage, but another fault, a few kilometres north of the cross section line, does.

The result of these changes in structure in the Olifants River Syncline is that futher south the Peninsula aquifer is more of a confined system under the Olifants River Valley, and does indeed transfer groundwater from the higher, eastern mountains, the Koue Bokkeveld range, to the lower, western range, the Warmbadberg, as shown in Diamond and Harris (2000). Evidence for this comes from the Citrusdal hot spring, The Baths, and is twofold: firstly, the temperature of discharge, at 43 °C, requires circulation to around 2 km depth, assuming a geothermal gradient of 20 °C/km and an input temperature for rain of 5–10 °C (Jones, 1992); secondly, as can be seen in **Figure 5.12**, the isotopic composition of the spring water is more negative than local rainfall at Citrusdal (Diamond and Harris, 1997) or Wolfkop, but matches rainfall at Uitkyk, 1000 m high in the Cederberg, which will be similar to rainfall in the Koue Bokkeveld ranges due east of the spring. Further north in the Olifants River Syncline movement of groundwater under a hydraulic gradient from the higher Cederberg range in the east to the lower Olifants River Mountains in the west may not be as easy due to the shallower syncline and the presence of the faults. These faults can lead to an upward leakage out of the Peninsula aquifer and directly into surface water, such as is postulated to occur at The Baths, or via the Skurweberg aquifer and then into surface water. The juxtaposition of the Peninsula and Skurweberg aquifers, because of the faulting, can also allow loss of groundwater from the Peninsula aquifer into the Skurweberg aquifer. The shallowness of the syncline also leaves a relatively thin layer of the Peninsula Formation remaining to conduct groundwater westwards, as seen in the areas just east and west of the Olifants River Valley in **Figure 5.11**.

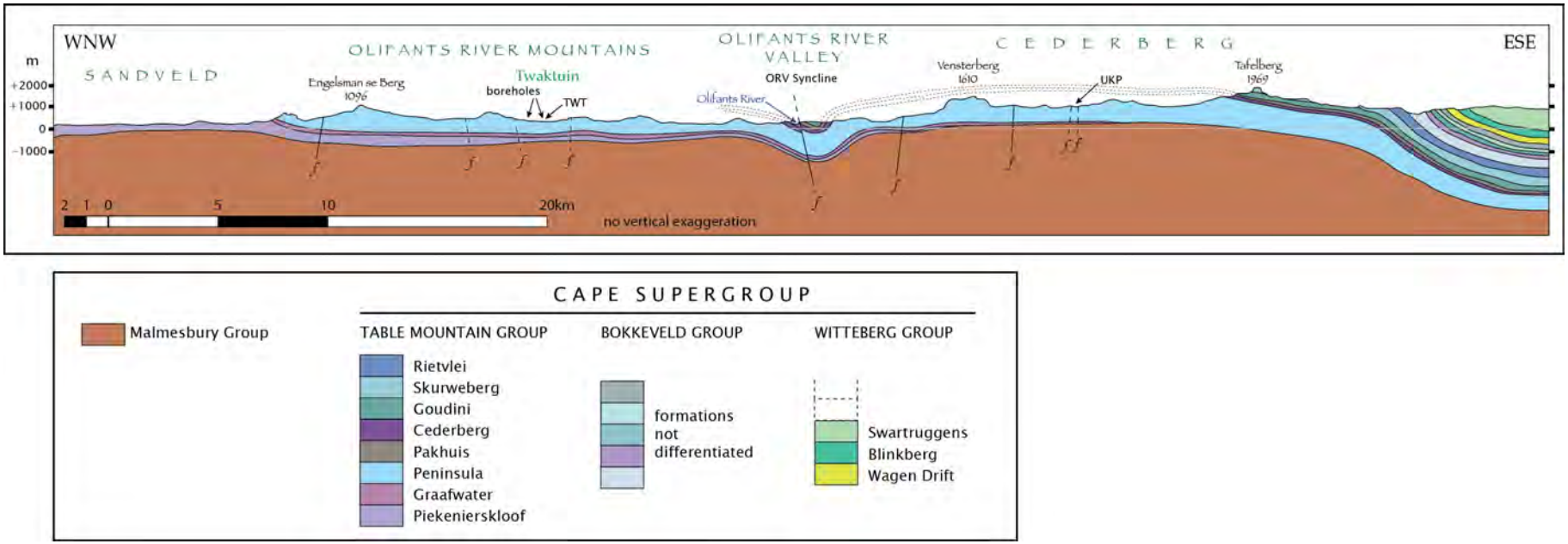

Figure 5.11: A geological cross section through the northern part of the western limb of the Cape Fold Belt, drawn from the Clanwilliam 1:250 000 geological map (Geological Survey, 1973). The section line is indicated on the map in **Figure 5.3**.

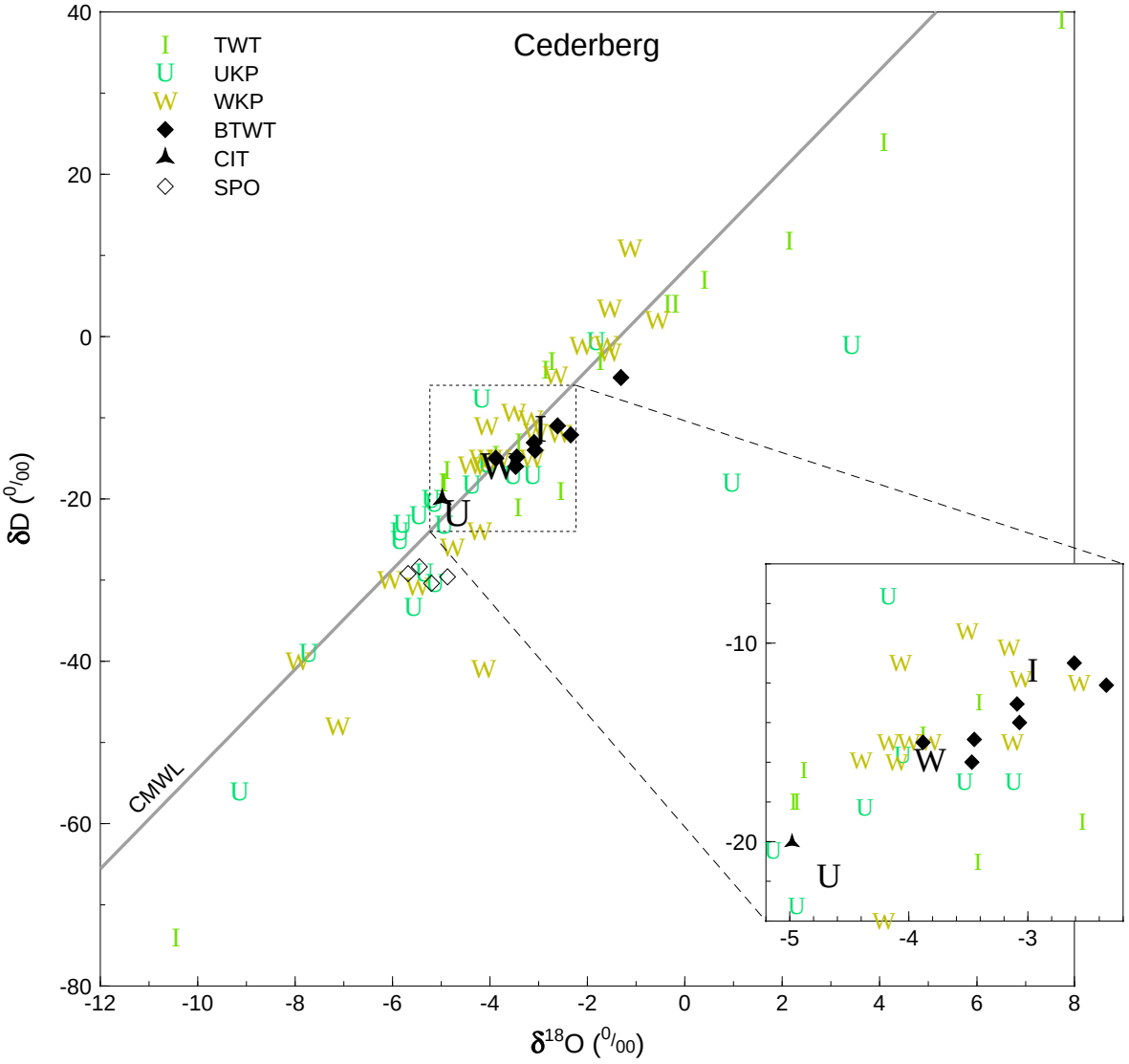

Figure 5.12: A δD – $\delta^{18}O$ plot for all data for the Cederberg region. Weighted means for Twaktuin (I), Uitkyk Pass (U) and Wolfkop (W) rainfall stations are shown as large black letters. Abbreviations: TWT = Twaktuin monthly rainfall, UKP = Uitkyk Pass monthly rainfall, WKP = Wolfkop monthly rainfall, BTWT = Twaktuin boreholes, CIT = The Baths hot spring, SPO = Tafelberg Spout seep.

Samples of groundwater from Twaktuin Farm in the Olifants River Mountains are compared **Figure 5.12** to possible sources of recharge: local rainfall at Twaktuin Farm; rainfall across the Olifants River Valley in the Cederberg at Uitkyk Pass; rainfall higher in the Cederberg, such as at the high altitude seep on Tafelberg at 1900 m. The groundwater discharging at this seep is from rainfall at around 1950 m on top of The Spout, a rock tower peak. The δ values of Twaktuin groundwater are more negative than the weighted mean for Twaktuin rainfall. The amount effect for Twaktuin has a similarly poor correlation to Wolfkop, primarily because of the 31 December 2010 thunderstorm event; Pearson's r values for Twaktuin are -0.12 for δD – rain-amount and

-0.30 for $\delta^{18}O$ – rain-amount. However, in general one can expect the heavier winter rains (more intense rainfall) are more likely to result in groundwater recharge and to have more negative δ values. The mean Twaktuin recharge δ values are probably more negative than the mean Twaktuin rainfall δ values. Also, the Farm is in a valley and the surrounding hills and peaks will contribute more negative isotopic value rainfall to recharge the groundwater of the area.

The δD and $\delta^{18}O$ values of Twaktuin groundwater are not as negative as Uitkyk Pass rainfall (**Figure 5.12**. They are however, similar to Wolfkop rainfall. The Wolfkop values represent all the lower elevation hills on the east of the Olifants River Valley, but these areas do not have the elevation necessary to produce a hydraulic head sufficient to drive groundwater to the Twaktuin region. If recharge is occurring east of the Olifants River Valley, it must be from the high peaks of the Cederberg proper, such as Vensterberg in the cross section. The isotopic evidence suggests that groundwater in the Olifants River Mountains area is locally recharged, as shown in the sketch in **Figure 5.13**. This fits with the geological structure of the region which shows numerous obstacles, as outlined above, to groundwater flow occurring in any significant quantities on such a regional scale.

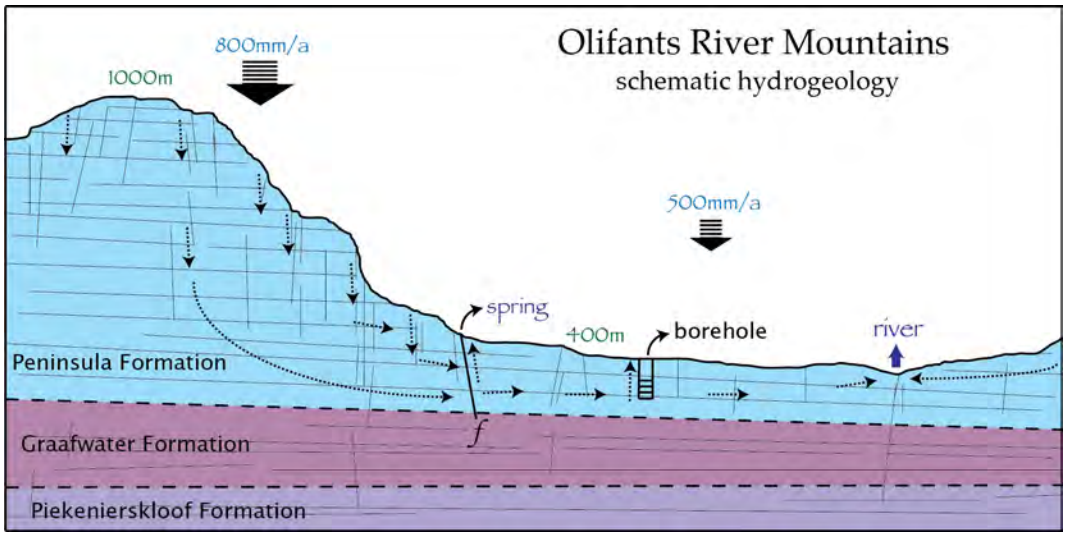

Figure 5.13: Sketch cross section showing the conceptual hydrogeological model suggested by isotopic compositions measured in this study.

The possibility does remain that there is a component of groundwater flow that is travelling east to west through the Olifants River Syncline, perhaps discharging closer to the Olifants River Valley, not as far west as Twaktuin, or contributing just a portion to groundwater in the Twaktuin area through limited flow in deep fractures near the base of the Peninsula Formation. More widespread monitoring of boreholes and springs in west of the Olifants River Valley could help shed light on the former possibility, whilst more detailed monitoring over time at Twaktuin and neighbouring farms' boreholes may reveal changes in isotopic composition as deeper groundwater is tapped later in the irrigation season, or after several low rainfall years.

Figure 5.14: Duplexes (piggyback thrusts) in the Hex River Mountains. Multiple thrust ramps can be seen, some of which have been labelled. The extensively fractured nature of the rock, both thrusts and near vertical jointing, are evident.

5.5.2 Hex River Mountains

The Hex River Mountains are formed by erosion into a large north-east trending anticline in the inland portion of the syntaxis (meeting zone of the western and southern limbs) of the Cape Fold Belt. East of the syntaxial region most folds trend east-west, while to the west and north of the syntaxis, folds trend north-south. The Hex River Mountains include several of the highest peaks in the Western Cape, including the second highest, Matroosberg, at 2249 m, just north-east of the cross-section in **Figure 5.17**. The Table Mountain Group, especially the Peninsula Formation, is structurally thickened in this region and duplexing is evident in the cliff forming outcrops of the Peninsula Formation, as seen in the annotated photograph in **Figure 5.14**.

The two surface water bodies sampled, the Witels and Groothoekkloof rivers, have been discussed in the Surface Water section above, but in summary they show a difference in the mean δD and $\delta^{18}O$ values. This probably reflects continental and altitude effects operating in concert to gause the Groothoekkloof isotope values to be more negative than the Witels.

Six snow and ice samples were taken at 1900 m elevation on Waaihoek Peak in the western Hex. They were taken by coring vertically into the thin snowpack, 0.2–0.4 m thick at two sites, and by removing a stalactite of rime ice hanging from a rock. The stalactite (*1) has the least negative δ values of the six samples. Four samples of snow (*2–*5) record the unusual weather

event described in Chapter 4, where a south-east wind caused widespread snow on mountains of the Western Cape. These samples show that the first snow to fall (the base of the snowpack, *2 and *3) had higher δ values than the later snow (*4 and *5). Snow from a more typical north-west wind from a frontal depression has the most isotopically negative signature (*6).

Previous snow samples (+) (Diamond and Harris, 1997; Harris et al., 2010) taken from Gydo Pass, Hex River Pass, Theronsberg Pass and Waaihoek Peak, all in the vicinity of the Hex River Mountains, overlap with the results from this study, as seen in **Figure 5.15**. The most negative cluster of points is from three different seasons, 1996, 2000 and 2011, and from three different locations, Theronsberg and Hex River Passes and Waaihoek Peak, suggest that this is a typical value for snow from a mid-winter north-west frontal storm in the south-western Cape: –55 > δD > –60, –10.5 > $\delta^{18}O$ > –11.5. The two less isotopically negative samples from the previous studies may have undergone melting, causing the lighter isotopes to be preferentially melted and removed (Arnason, 1981), or may have been rained upon and undergone exchange with heavier isotopes in rain, or may simply have been derived from a weather system that deposited snow of an isotopically heavier nature, such as was observed for the south-easter snowfall in this study.

The difference between the early and late south-easter snow is consistent in the two profiles sampled. It was possible to distinguish the top of the south-easter snowpack from the overlying north-west event snowfall, as the former was granular from freeze-thaw over a few sunny days prior to the north-west event, and the latter was still in powder form. The freeze-thaw process that turns powder snow to firn should have increased δ values at the top of the snowpack as the lighter isotopes are preferentially incorporated into snowmelt, so these points may have had lower δ values originally. A movement from less to more negative δ values during this precipitation event could occur if the temperature decreases or as a result of rainout. A decrease in temperature often accompanies the passage of a cold front, as the wind shifts from westerly to southerly, however, this snow was from a south-easter event. In this case the decrease in δ values during the event suggests that colder air from further south was being fed into the system as it developed and that perhaps increased rainout occurred for the later snow, as shown in **Figure 5.16**. The isotope composition of snow may be useful in understanding air mass trajectories during weather events. Clearly there are several processes at play, and complex relations occur between the three phases of water in this semi-alpine zone of the Cape Mountains. Unfortunately, there are probably insufficient data to draw major conclusions, except to note the large range in values that could be useful in meteorological and hydrological applications if such differences are consistent. A more comprehensive study with more widespread sampling of snow over a greater time frame would assist in identifying any trends.

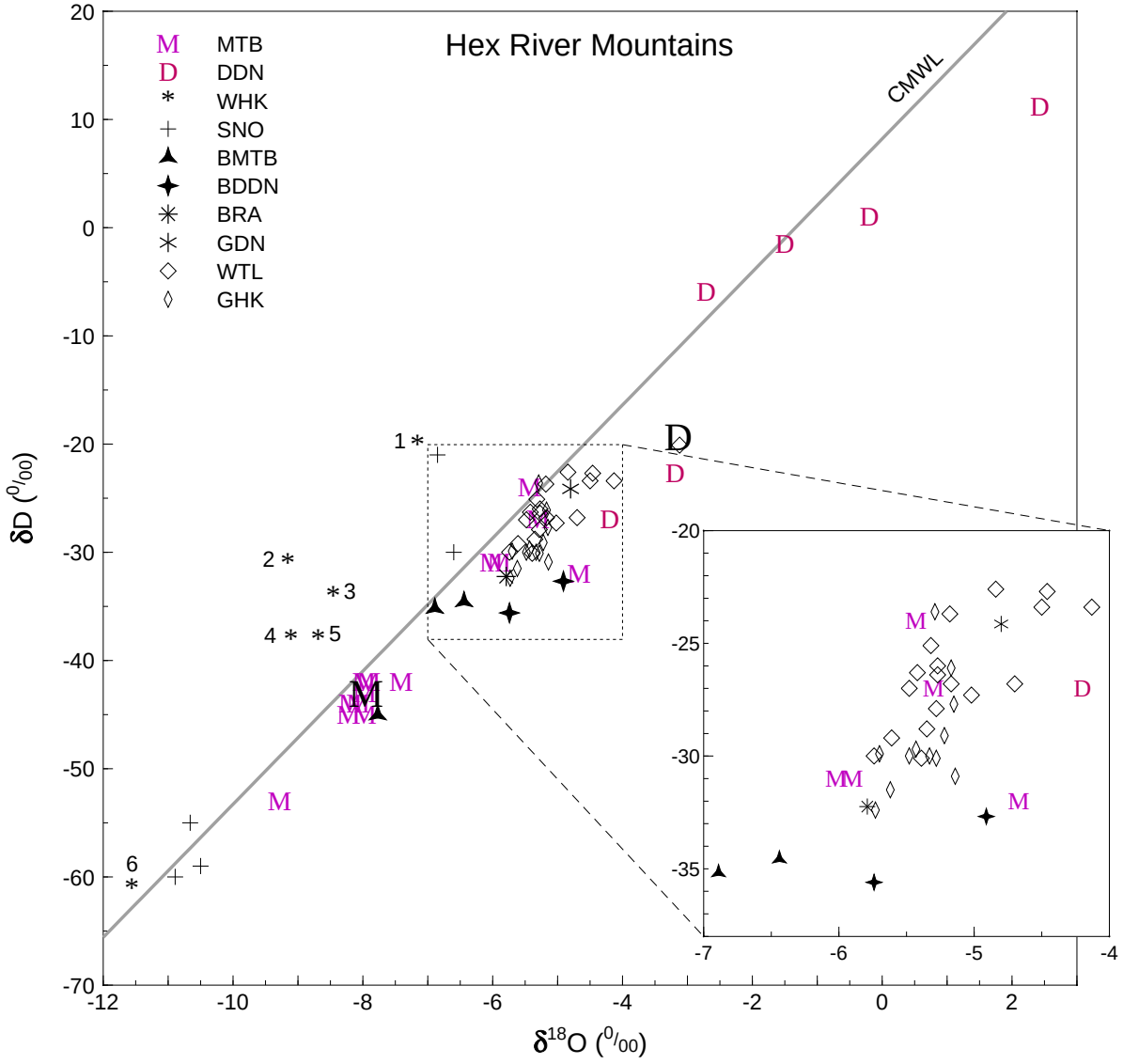

Figure 5.15: A δD – $\delta^{18}O$ plot for all data for the Hex River Mountains region. Weighted means for the Matroosberg (M) and DeDoorns (D) rainfall stations are shown as large black letters. Abbreviations: MTB = Matroosberg monthly rainfall, DDN = Tweespruit monthly rainfall, WHK = Waaihoek Peak snow, SNO = snow from previous studies, BMTB = Erfdeel boreholes, BDDN = Tweespruit boreholes, BRA = Brandvlei hot spring, GDN = Goudini hot spring, WTL = Witels River, GHK = Groothoekkloof River.

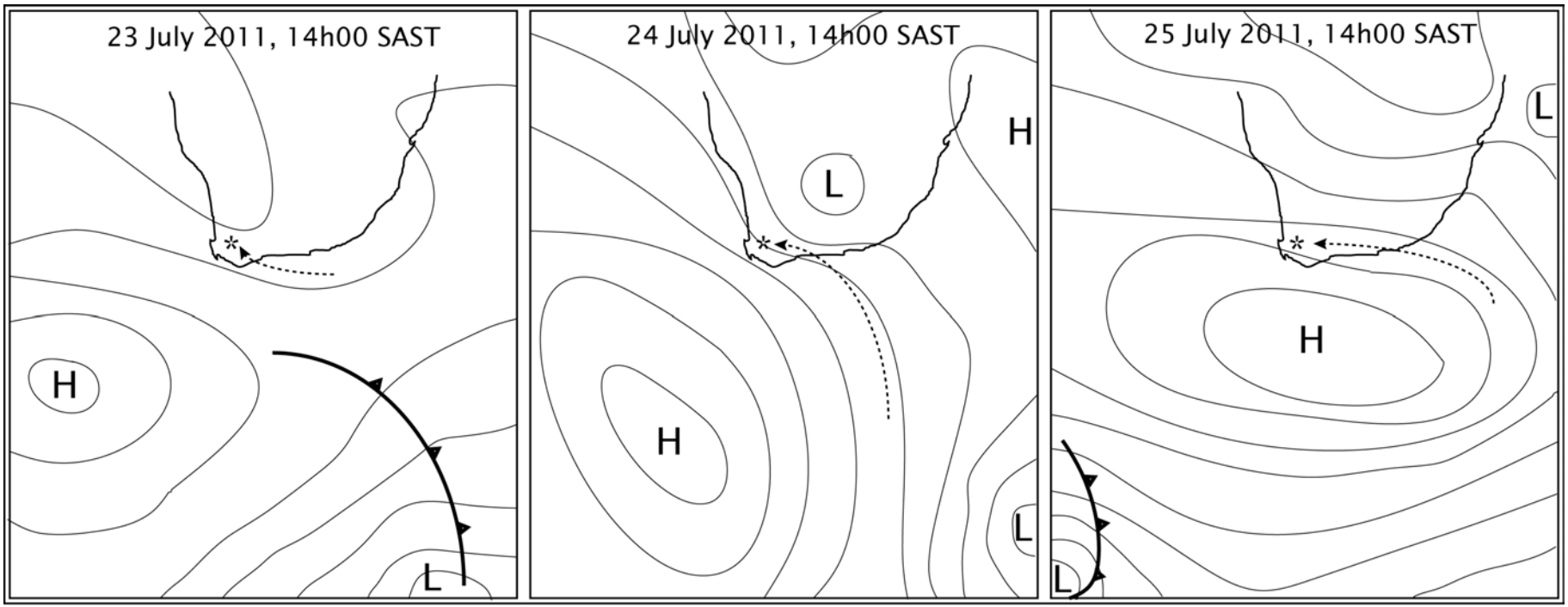

Figure 5.16: Simplified synoptic weather charts from SAWS (2010-12) with possible air trajectories for snowfall in the Hex River Mountains shown. The 23rd July shows a short air trajectory from warmer areas that caused rain. The 24th July shows a much longer air trajectory bringing very cold sub-antarctic air and resulting in snow. Later snow on the 25th July may have travelled even further and probably experienced more rainout over land, resulting in lighter isotope composition.

The most significant hydrogeological interpretations that can be made from the data for the Hex River Mountains region are from comparing the values for borehole water at Erfdeel, on the northern side of the Hex River Anticline (BMTB), and at Tweespruit, on the southern side (BDDN), with the rainfall data for the two stations in this area (see **Figure 5.17**). The mean δ values for rainfall at Tweespruit, the large 'D' in **Figure 5.15**, are less negative than the water from the two boreholes sampled on this farm. These boreholes are drilled into the Rietvlei Formation and although they may not penetrate deep enough to encounter the Skurweberg Formation (see **Figure 5.17**), the Rietvlei Formation is part of the Skurweberg aquifer. This large difference in δ values, 15 ‰ for δD and 2 ‰ for $\delta^{18}O$, can be accounted for by recharge at high altitude on the slopes of the Hex River Mountains. Based on a linear altitude effect between the DDN and MTB rainfall stations, using the gradients shown in **Table 5.5**, the δ values of the Tweespruit boreholes suggest an average recharge elevation for this groundwater of around 1200 masl. Weaver et al. (1999) showed a similar hydrogeological setting for groundwater flow in the Agter-Witzenberg Valley, north-west of Ceres, although with smaller differences in elevation.

Although the cross section shows the Skurweberg Formation only reaching around 1000 masl, the areas west and north of the section line contain outcrops up to 1500 m and 2000 masl, respectively. Additionally, the Goudini Formation, which is hydraulically part of the Skurweberg aquifer occurs at even higher elevations closer to the core of the Hex River Anticline. It is easy then for groundwater in the Skurweberg aquifer to have isotopic compositions similar to those found in the Tweespruit boreholes. However, it does suggest this groundwater originally was recharged in the Skurweberg or Goudini Formation outcrop areas and is flowing upwards through the stratigraphy in the Hex River Valley. This would probably have occurred naturally due to the hydraulic head in these lower formations being higher than that in the Rietvlei Formation, but it may also be enhanced by pumping, causing an upconing flow towards the boreholes. Should the isotope composition of the groundwater from the boreholes become lighter over time, this might suggest that deeper and deeper water from the Skurweberg aquifer is being abstracted. This is because the deeper parts of the aquifer (the Skurweberg and Goudini Formations) are recharged at higher elevation than the Rietvlei Formation and will therefore transmit groundwater with lower δ values. Long term monitoring of the isotope content of the boreholes may be useful to warn of depletion of the groundwater resource.

Groundwater from boreholes at Erfdeel displays a wider range of δ values than at Tweespruit, although in both cases the sample numbers are too low for this to be a firm observation. Two of the boreholes have similar and less negative δ values than the third, which has similar δ values to the weighted mean for the MTB rainfall station. The Erfdeel boreholes also tap the Rietvlei Formation, part of the Skurweberg aquifer, which reaches over 2000 m elevation south-east of the farm, two kilometres south of the section line. The range in isotope composition of the Erfdeep borehole water and the geological structure of the area suggest that groundwater recharge occurs from relatively low down on the mountain slopes, on the northern flank of the Hex River Anticline, to

high up, amongst the peaks on the hinge of the Anticline. The altitude range for groundwater recharge at Erfdeel can be estimated as 1300–2000 masl.

Groothoekkloof river samples display less negative δ values than the MTB rainfall station and the boreholes at Tweespruit and Erfdeel. This suggests that either the GHK samples, being from late summer, display an evaporated signature, or the Erfdeel groundwater was selectively recharged by the most isotopically negative rainfall, a phenomenon known as 'selection' (Gat, 1981a). If the latter is the case, it suggests that the groundwater responsible for creating summer baseflow in the Groothoekkloof river is mostly shallow circulating and recharged by rainfall of varied isotopic composition, whereas the groundwater being pumped out at Erfdeel taps deeper circulating water that has been selectively recharged in heavy winter rainfall events subject to colder temperatures and the amount effect to drive the isotope composition to more negative values.

The Erfdeel borehole δ values lie closer to the Cape Meteoric Water Line (**Figure 5.15**) than the Tweespruit borehole points that seem to lie on an evaporation line trend. As the recharge for the Tweespruit boreholes is on the eastern side of the Hex River Mountains, it is in the lee of the highest peaks. Rainfall here may take place through drier air that has lost some of its moisture when precipitating over the crest of the range. Evaporative enrichment during raindrop descent could account for these points being displaced from the CMWL.

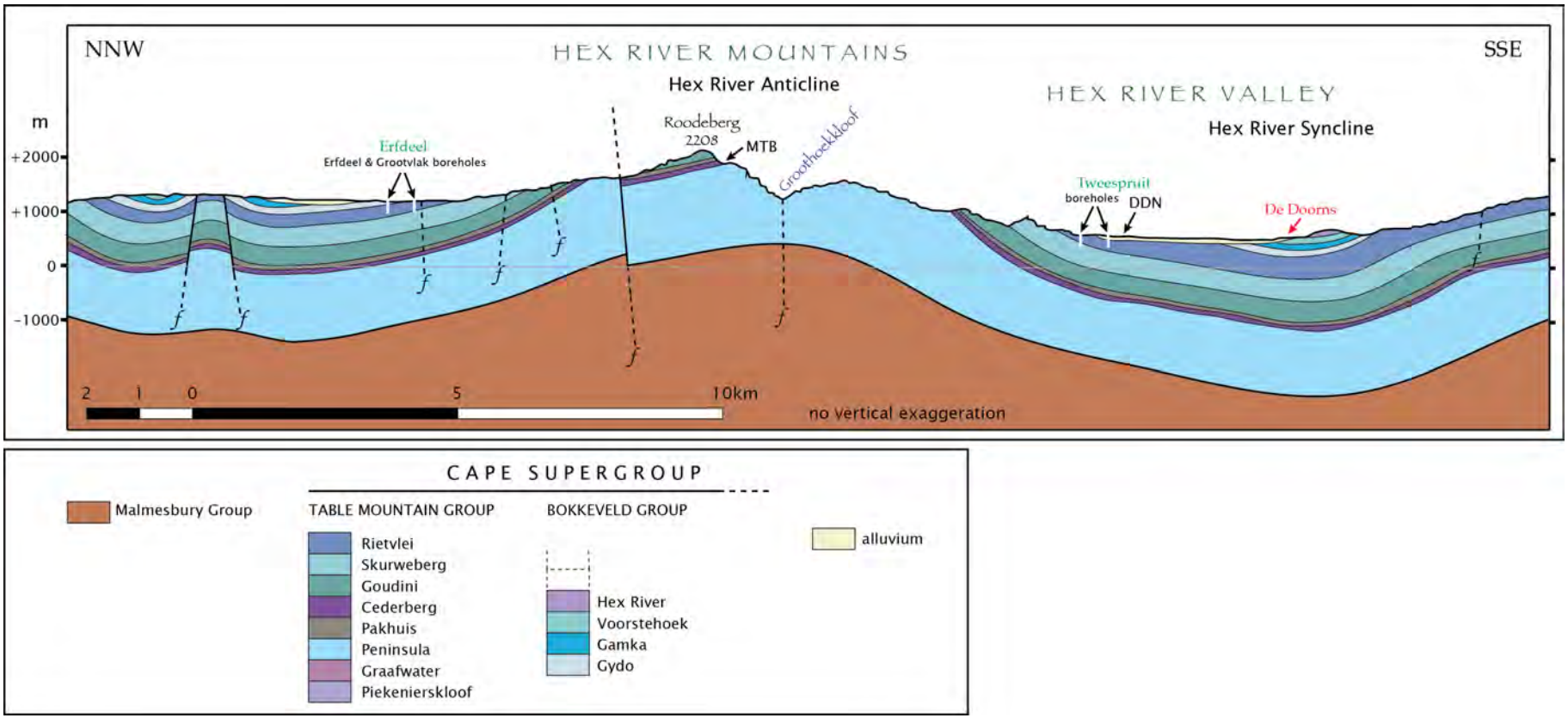

Figure 5.17: A geological cross section through the Hex River Mountains and Hex River Valley, drawn from the 1:250 000 geological map for Worcester (Council for Geoscience, 1997). Borehole positions and depths are illustrative only.

5.5.3 Langeberg – Gamkaberg – Swartberg

Gamkaberg Nature Reserve lies in the Little Karoo and the adjacent Gamka Mountain. The Little Karoo is a semi-arid area and the nature reserve gets its water from boreholes at the foot of the Gamkaberg. The Gamkaberg boreholes are drilled into Rietvlei Formation and perhaps some through unconformably overlying Enon Formation (**Figure 5.20**). They therefore abstract groundwater from the Skurweberg aquifer. The δ values for the groundwater from these boreholes are extremely low relative to rainfall collected at the same place, the Gamka Store location (GST). The groundwater has 20 ‰ lower δD and almost 4 ‰ lower $\delta^{18}O$ than the weighted mean for Gamka Store rain and almost 10 ‰ δD and almost 1.5 ‰ $\delta^{18}O$ less than the weighted mean for Bakenskop on the summit plateau of Gamkaberg. It is almost as negative as water from the hot springs at Warmwaterberg and Calitzdorp Spa. Three possible explanations could account for this result.

Firstly, as proposed by Diamond and Harris (2000) for the Calitzdorp Spa, the recharge area for this groundwater could be the Swartberg. That study did not collect high altitude rainfall and it was simply assumed that rainfall on the Swartberg around 2000 m would be isotopically negative enough to account for the very negative δ values at the Calitzdorp Spa (see **Figure 5.18 and 5.10**). Data from this study shows that this assumption was partly true: the high altitude seeps of the Klein Swartberg, to be discussed in the next regional analysis, do have δ values similar to Calitzdorp Spa discharge. On the other hand, the high altitude rainfall collected at 2080 m on Blesberg does not have such negative δ values and the weighted mean at Blesberg is similar to that of Bakenskop, at half the altitude.

The cross section in **Figure 5.20** shows that the Table Mountain Group has been eroded away over the inlier of Cango Group basement south of the Groot Swartberg and so no groundwater flow can occur from the Swartberg southwards along this line. However, to the north-west of Gamkaberg, the basement is much lower and the Table Mountain Group is continuous from the Swartberg, via the Huisrivier Mountains and the Rooiberg, to Gamkaberg and the Langeberg, as shown in Diamond and Harris (2000). Although this hydraulic connection exists, it is about 40 km, very folded and passes one major fault at the southern edge of the Swartberg. Groundwater would have to be recharged in the Peninsula aquifer in the Swartberg, move into the Skurweberg aquifer at the fault and then through the anticline of the Huisrivier Mountains and a syncline before discharging at the Gamkaberg boreholes. The water would have circulated to great depths and should be heated. For Calitzdorp Spa, the temperature of discharge is 52 °C, which is evidence for deep circulation and concurs with the isotopic evidence, but the Gamkaberg groundwater is not noticeably warm and therefore it is unlikely to have travelled this route. The Outeniqua Mountains (Langeberg) are very unlikely as sources of groundwater at the Gamkaberg boreholes because the discontinuity of the Skurweberg aquifer does not allow flow of groundwater to the northern side of the Gamkaberg. The Cederberg aquitard prevents groundwater flowing from the Peninsula aquifer into the Skurweberg aquifer without the presence of a major fault, of which

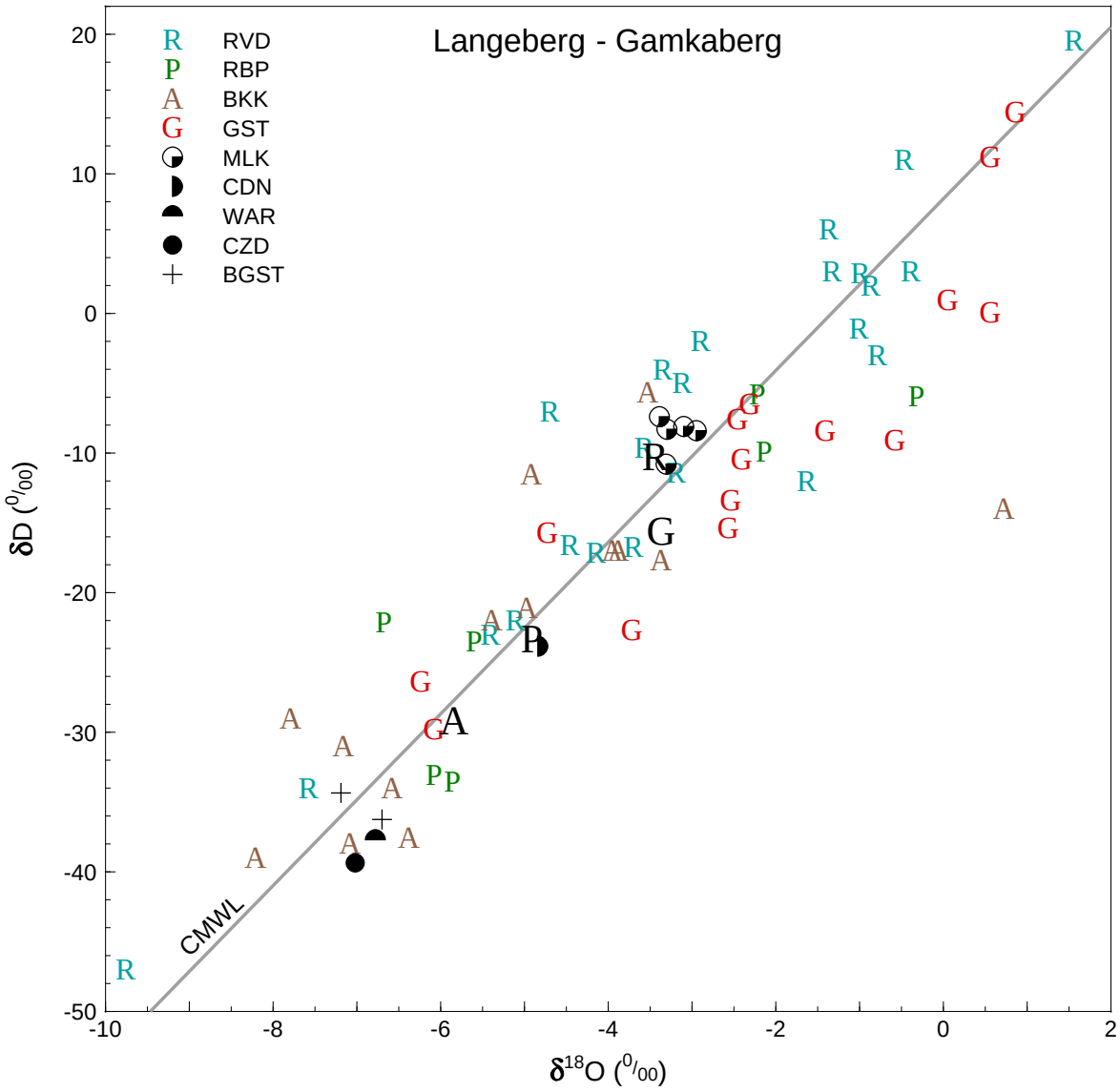

Figure 5.18: A δD – $\delta^{18}O$ plot for all samples taken in the Langeberg–Gamkaberg region, including rain, surface water and groundwater. Larger black letters indicate weighted means for rainfall at Riverndale (R), Robinson Pass (P), Bakenskop (A) and Gamka Store (G). RVD = Riverndale, RBP = Robinson Pass, BKK = Bakenskop, GST = Gamka Store, MLK = Meulkloof river, CDN = Caledon hot spring, WAR = Warmwaterberg hot spring, CZD = Calitzdorp hot spring, BGST = Gamkaberg boreholes.

none are mapped. The isotopic evidence also shows the Robinson Pass rainfall to have higher δD and $\delta^{18}O$ values than the Gamkaberg boreholes.

In the second and third possibilities, the recharge area is the crest of the Gamkaberg, around the Bakenskop rainfall collection station, but two possible factors may be causing the discrepancy between the weighted mean delta values at Bakenskop and the values found at the Gamkaberg boreholes. The first is *selection*, whereby heavy rainfall events, subject to the amount effect and hence with lighter isotope composition, are preferentially recharged over lighter rains with heavier isotope composition (e.g. Dogramaci et al., 2012). The second is that the 2010–12 rainfall at Bakenskop may have been less negative than normal. Although not generally reported in the literature, weighted mean annual isotope composition of rainfall has been shown to vary from year to year locally (Harris et al., 2010) and is discussed in **Section 5.21**. Specifically, observations at UCT show the 2010–12 weighted annual rainfall means lying at the less negative end of the spread of weighted annual means for 1996–2012, as seen in **Figure 5.24**, which supports the hypothesis that the sampled Bakenskop rainfall may not be typical. Lastly, a combination of *selection* and unusual rainfall isotope composition could be responsible for the discrepancy observed at Gamkaberg.

5.5.4 Swartberg to Goukamma

Figure 5.19 is a δD–$\delta^{18}O$ plot of all the samples analysed from the Klein Swartberg, north of Ladismith, to Goukamma, near Knysna. This graph provides some excellent examples of the amount effect at the moderate rainfall sites of Kammanassie and Lentelus, with MAP of 660 mm/a and 640 mm/a, respectively. The lowest δ values for these two sites are both from July 2010 where 80 mm and 40 mm, respectively, fell at these two locations. June 2010 also shows low values for Kammanassie and Lentelus where 30 mm and 75 mm, respectively, fell in that month.

Figure 5.19 shows the unexpected isotopic distribution of the Klein Swartberg high altitude seeps at Toverkop (2060 m), Skull Cave (1880 m) and Seweweekspoort Peak Cave (2020 m); these were discussed in **Section 5.2.2.3**. Two boreholes on the farm Rooihoogte on the northern side of the Klein Swartberg (due north of Skull Cave) were sampled are labelled BROO on **Figure 5.19**. The boreholes are drilled into the Rietvlei Formation and therefore abstract water from the Skurweberg aquifer. The Table Mountain Group here is tilted steeply to the north, dipping beneath the Bokkeveld and Witteberg Groups. The isotope composition of the Rooihoogte boreholes matches that of Skull Cave very closely, which suggests that recharge takes place at the crest of the range, which here is Goudini Formation and therefore also part of the Skurweberg aquifer, before travelling down-dip towards the Great Karoo. Another possibility is that recharge takes place at slightly lower altitudes, which would have less isotopically negative rainfall on average, but is subject to *selection*, whereby only the high volume rain events with the most negative isotope ratios recharge the aquifer.

As with the Tweespruit and Gamkaberg boreholes, it seems likely that the groundwater is

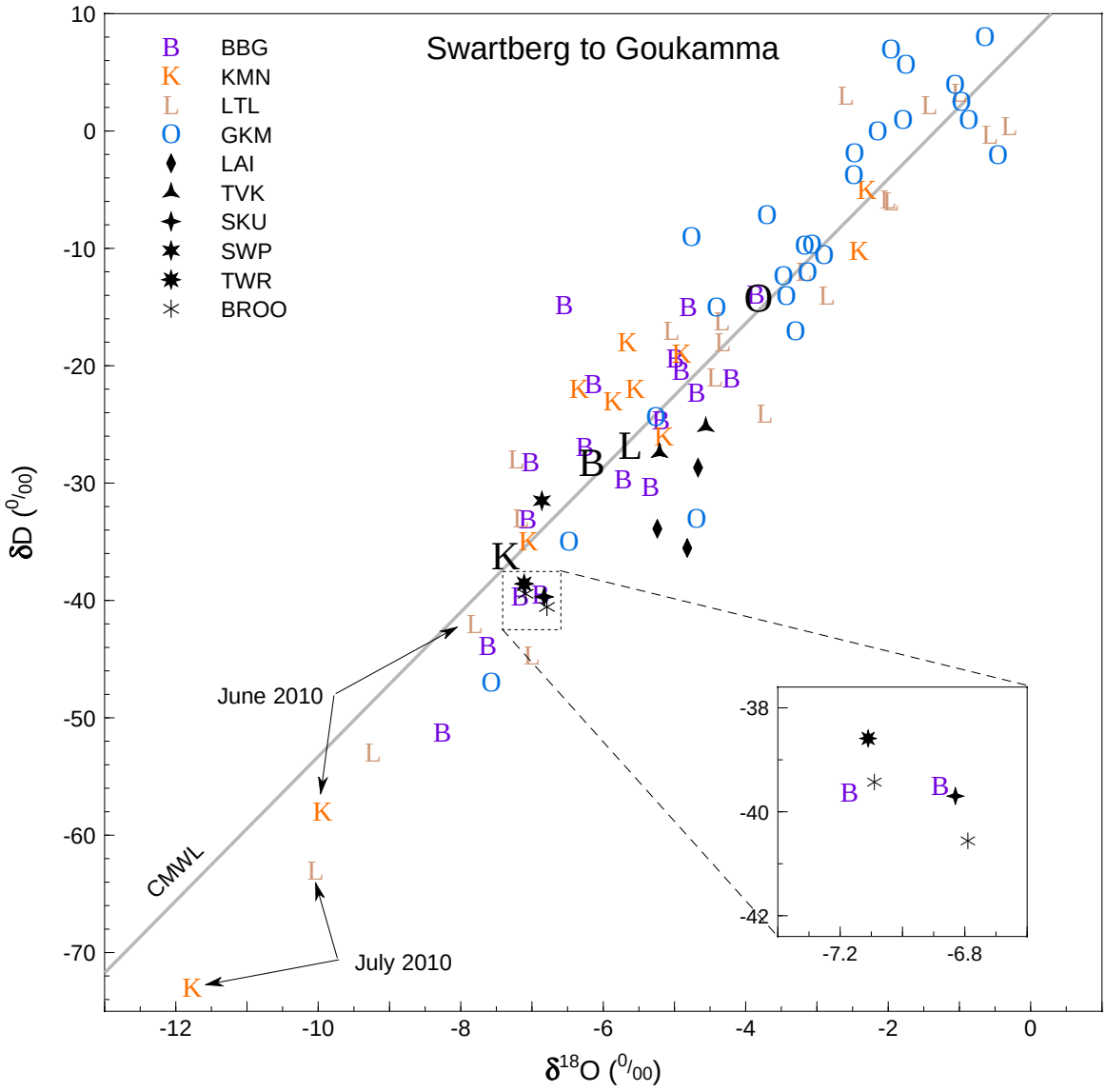

Figure 5.19: A δD – $\delta^{18}O$ plot for all samples taken in the Swartberg to Goukamma region. Larger black letters indicate weighted means for rainfall at Blesberg (B), Kammanassie (K), Lentelus (L) and Goukamma (O). BBG = Blesberg, KMN = Kammanassie, LTL = Lentelus, GKM = Goukamma, LAI = UCT field station spring, TVK = Toverkop seep, SKU = Skull Cave seep, SWP = Seweweek-spoort Peak Cave seep, TWR = Toowerwater hot spring, BROO = Rooihoogte boreholes.

recharged in the Goudini or Skurweberg Formations and discharged via the Rietvlei Formation, all part of the Skurweberg aquifer. To what extent this upgradient flow is natural or in induced by pumping remains open to speculation. From both the Gamkaberg and Swartberg (Rooihoogte) settings, the very negative nature of the borehole isotope values suggests the groundwater flow is already from the highest parts of the crest to the valley, whereas for Tweespruit there is space for the groundwater to be recharged at higher elevations, based on the calculated recharge elevation of 1200 m on the flanks of a 2000 m high mountain range.

Samples from a spring 10 km south of Laingsburg at the UCT Geological Sciences field station in the Great Karoo were taken in 2010, 2011 and 2012. This spring emerges from the Dwyka Group at about 700 m altitude and could be recharged in the south in low mountains of Witteberg Group rocks. The Witteberg Group contains quartzite formations that are extensively fractured, providing secondary porosity. The relatively negative δ values for the 'Laingsburg' spring suggest either a higher altitude of recharge than at the spring, or are the result of the local rainfall displaying a significant continental effect and amount effect. The continental effect is likely to be significant as this location is inland of 2000 m high mountain ranges in almost all directions, so rainout will have been substantial because of orographically driven rainfall. The amount effect is known from arid regions (Dody and Ziv, 2013) and has been seen in South African arid zone rainfall by Vogel and van Urk (1975).

The 'Laingsburg' spring samples plot quite far to the right of the Cape Meteoric Water Line, in the area on the δD – $\delta^{18}O$ plot associated with evaporated waters. This would be expected for precipitation, and hence all other meteoric waters, in an arid zone. It confirms that the recharge area is in the Karoo and not in the Table Mountain Group in the Cape Mountains, where less evaporated isotopic signatures are expected, as can be seen for most of the data in this study.

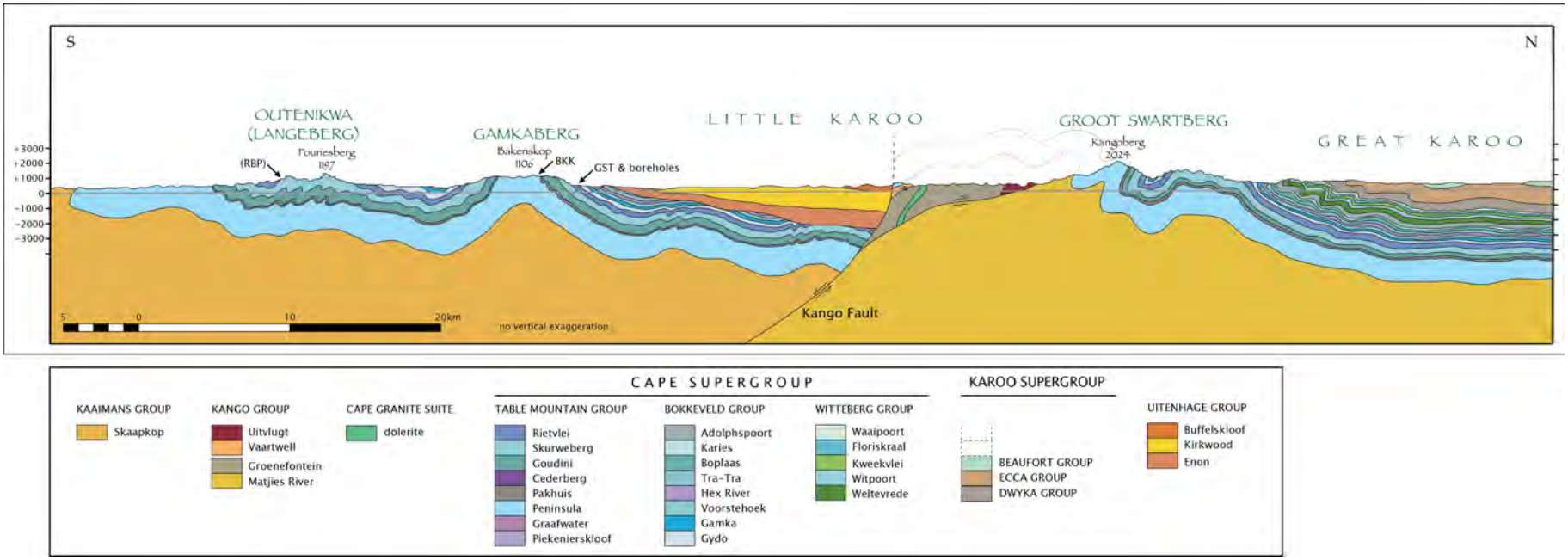

Figure 5.20: A geological cross section from the coastal plain to the Great Karoo, drawn from the 1:250 000 geological map for Ladismith (Geological Survey, 1991).

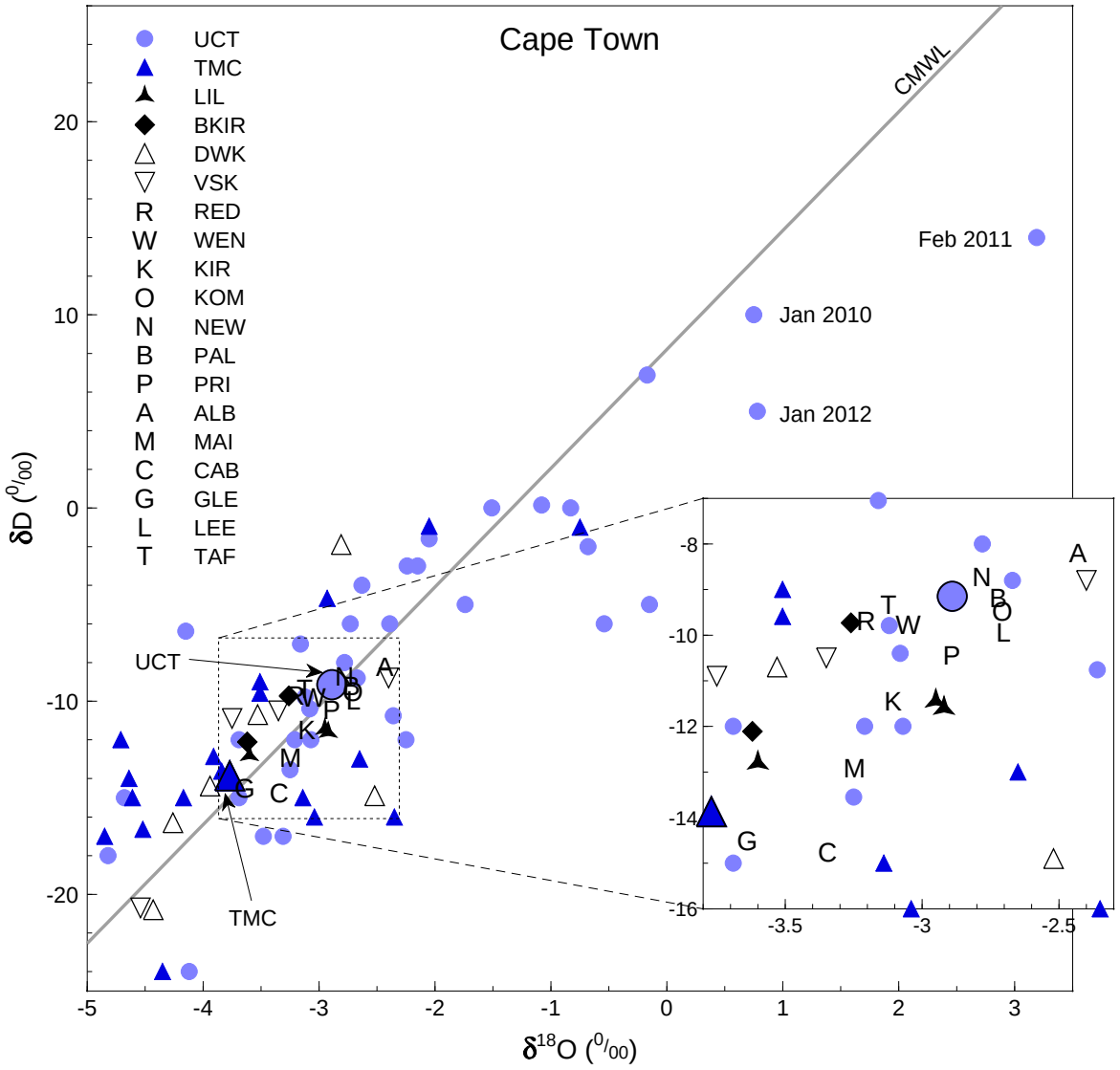

Figure 5.21: A δD versus $\delta^{18}O$ plot for all samples taken in the Cape Town region. The large circle and triangle indicate the weighted mean values for UCT and TMC rainfall. UCT = University of Cape Town, TMC = Table Mountain Cableway, LIL = Lily Pond seep, BKIR = Kirstenbosch boreholes, DWK = Duiwelskloof river, VSK = Volstruiskloof river, R = mean Redwood spring, W = mean Wendy's spring, K = mean Kirstenbosch spring, O = mean Kommetjie spring, N = mean Newlands spring, B = mean Palmboom spring, P = mean Princess Anne spring, A = mean Albion spring, M = mean Main CT spring, C = mean Cableway spring, G = mean Glencoe spring, L = mean Leeuwenhof spring, T = mean Tafelberg Rd spring.

5.5.5 Cape Town

Samples in the Cape Town area include regular samples over three years of the major springs that issue from the slopes of the mountain, both on the northern, city side and on the eastern, Kirstenbosch side. A detailed analysis of this data will be made, but first, a brief analysis of data from the two rainfall stations in the area, UCT and Table Mountain Cableway, will be made. As was mentioned in **Section 5.2.2.3**, the difference in isotope ratios between UCT and TMC is less than would be expected based on global averages for the altitude effect, because of both an "island peak" effect and because the higher location (TMC) is not in the direction of increasing rainout.

The UCT data shows some excellent examples of highly evaporated rainfall typical of summer months in a Mediterranean climate (e.g. Argiriou and Lykoudis, 2006). Table Mountain Cableway does not show the same degree of evaporative enrichment due to the shorter path of raindrops through the atmosphere in which evaporation can occur. The meteoric water lines of these two stations are similar in both gradient and δD-intercept values **Figure 4.10**.

The mean values for each of the sampled Cape Town springs have been plotted in **Figure 5.21**. The Kirstenbosch cluster of springs sit on the lower slopes below the east face of Table Mountain, Kirstenbosch being the most southerly and Albion one of the most northerly of those sampled. The Albion Spring (A) discharges water with the highest δ values of these springs and also happens to discharge at the lowest altitude. Its position places it furthest from the steep cliffs and the summit near the east face of Table Mountain, where the most isotopically light rainfall would be expected. The isotope values at Albion indicate the recharge area receives the least isotopically negative rainfall of all the Kirstenbosch springs, which corresponds with its geographic position and elevation. The opposite holds for Kirstenbosch (K), and to a lesser extent Redwood (R) and Wendy's (W), which have more isotopically negative discharge and are closer to the high cliffs of Table Mountain. The position of the spring waters on the δD – $\delta^{18}O$ graph roughly corresponds to the geographic position, resulting in a sequence from more to less negative δ values as the springs are located further from the site of highest rainfall on the southern end of the east face of Table Mountain, known as Fernwood Buttress. The sequence of springs, from most negative to most positive δ values is: Kirstenbosch (K) $\rightarrow$ Redwood (R) and Wendy's (W) $\rightarrow$ Princess Anne (P) $\rightarrow$ Kommetjie (O) and Palmboom (B) and Newlands (N) $\rightarrow$ Albion (A).

As this trend is based on the isotopic values of spring discharge, which is reliant upon isotopic changes inherited from precipitation in the recharge area, it suggests the position of a spring is closely related to the position of the recharge area. This in turn means long distance groundwater flow is probably not occurring. It also means if there is a distance between the spring and the recharge area, a similar distance exists for all the springs. The weighted average for UCT rainfall lies very close to many of these springs, especially Wendy's, Princess Anne and the Newlands, Palmboom and Kommetjie group, which are geographically also very close to UCT. All this evidence points to extremely local recharge on the lower slopes of the mountain. The most likely

aquifer for these springs is the scree and weathered material overlying the basement, comprising granite in the southern areas around Kirstenbosch and Redwood, and Malmesbury Group in the northern areas around UCT. The Table Mountain Group is not directly involved, except as a supply of boulders and sand that make up the scree material on the slopes of the mountain.

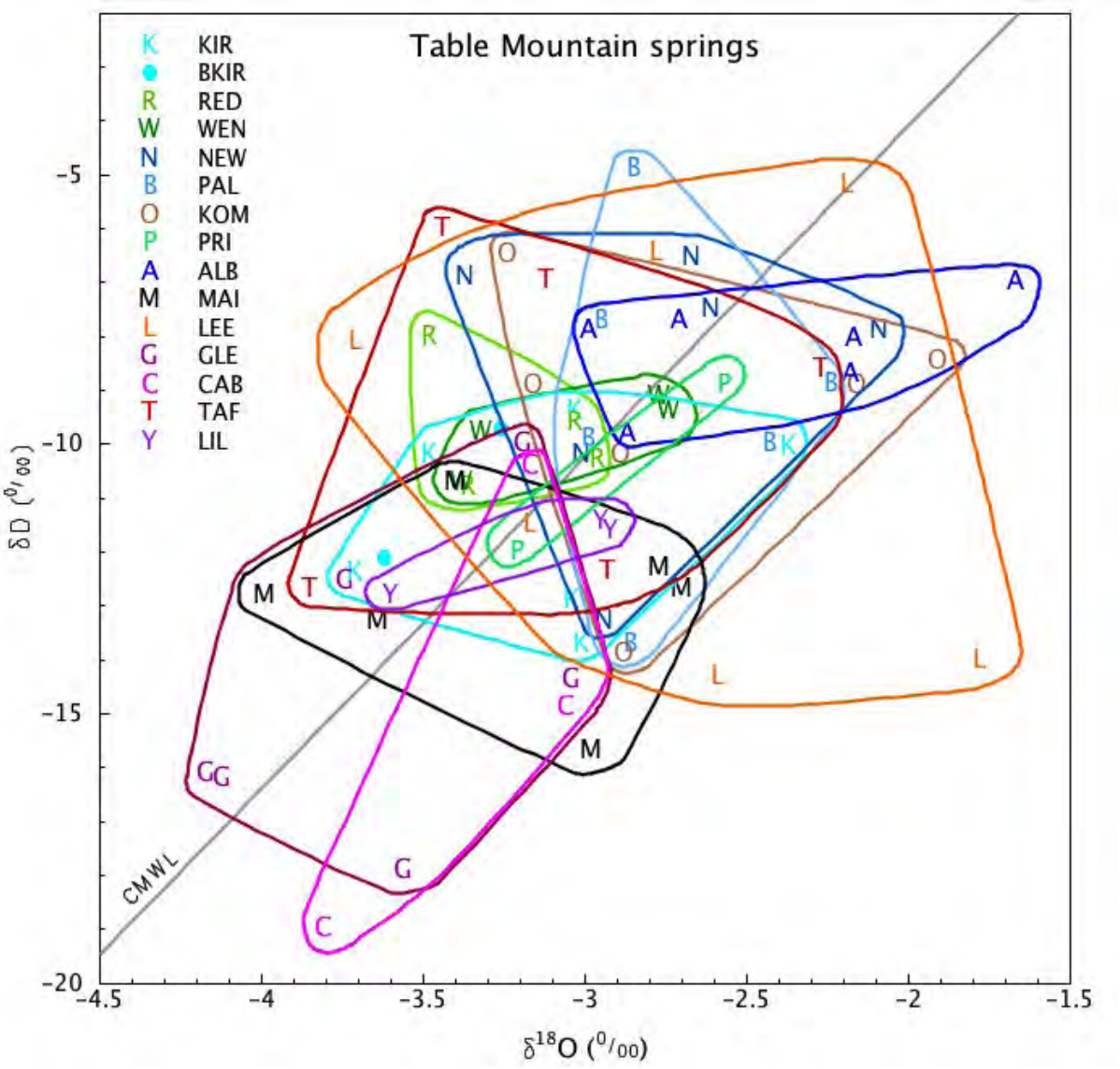

Figure 5.22: All the data for all the Table Mountain springs, with each springs' cluster of points circled. K = Kirstenbosch, BKIR = Kirstenbosch boreholes, R = Redwood, W = Wendy's, N = Newlands, B = Palmboom, O = Kommetjie, P = Princess Anne, A = Albion, M = main spring, L = Leeuwenhof, G = Glencoe, C = Cableway, T = Tafelberg Road, Y = Lily Pond.

Two boreholes at Kirstenbosch were sampled, "Protea" and "Apple Tree". Their isotope values are amongst the most negative of the Kirstenbosch springs and fall neatly within the distribution for the samples from the Kirstenbosch spring itself, as seen in **Figure 5.22**. They fit into the overall pattern noted above, where position on the δD – $\delta^{18}O$ diagram in **Figure 5.21** broadly

relates to geographic position relative to Table Mountain.

Several observations can be made from the isotope data for the springs analysed on the city side of Table Mountain. Cableway (C) and Glencoe (G) have the lowest δ values. These springs emerge from large scree fans that cover the north-west slopes of Table Mountain. Recharge into these screes is not only from rainfall directly onto their surfaces at 200–500 m elevation, but also from streams that drain the steep cliffs on the northern face of the western Table. These streams' catchments include areas up to the Upper Cableway Station at 1070 m. The similarity between the weighted mean for TMC and for Glencoe and Cableway springs confirm this as being part of the recharge area for these springs. An amount effect and selective recharge of heavier rainfall events will drive the Glencoe and Cableway recharge to lower δ values, compensated for by a shift to higher δ values from recharge occurring at lower elevation as well.

The Tafelberg Road spring (T) has less negative δ values, probably because its position below The Saddle, the area separating Devils Peak from Table Mountain, where recharge can only occur up to a maximum altitude of 700 m. The Leeuwenhof Spring (L) has the largest range of values of any of the springs by a factor of 2, as seen in **Figure 5.22**. This spring was sampled about 100 m from the source, an area of about half a hectare of seepage, because it is within the official residence of the Western Cape premier and access is restricted. The spring is undoubtedly the reason for the location of this historical homestead. The diffuse discharge area and the possibility for contamination from rain, Cape Town scheme water, stormwater or sewage leaks, as well as evaporation in the seepage area, explain the abnormally wide range in isotopic values at this spring. The position of the Leeuwenhof mean on the δD – $\delta^{18}O$ diagram, however, is consistent with its geographic position furthest from Table Mountain and at the lowest altitude of the city springs, and therefore subject to recharge at lower elevations with higher δ values. This suggests that dilution or alteration of isotope composition was minor.

The "main spring" (M) was sampled at the collection chamber in the "field of springs" east of Upper Orange Street in Oranjezicht. This collection chamber receives water from a few springs at the top of Oranjezicht, such as above Rugby Road cul-de-sac, and from the adjacent Stadsfontein at the field of springs, one of the original springs deciding the settlement of Cape Town by the Dutch East India Company in 1652. Assuming a similar relationship applies to the City Bowl springs as has been shown to apply to the Kirstenbosch springs, namely a positive correlation between distance from mountain and δ values, then the water from the "main spring" should be more isotopically negative than the position of the collection chamber on the map would suggest. The average position of these feeder springs would be in line with Glencoe's altitude and at the base of the large screen cones below Platteklip Gorge. Balancing these springs closer to the mountain is the position of Stadsfontein at the "field of springs." The expected isotope composition for the main spring should be intermediate to the Glencoe and Cableway values (closer to the mountain), and to Leeuwenhof (further from the mountain). This is indeed where the "main spring" plots in **Figure 5.21**.

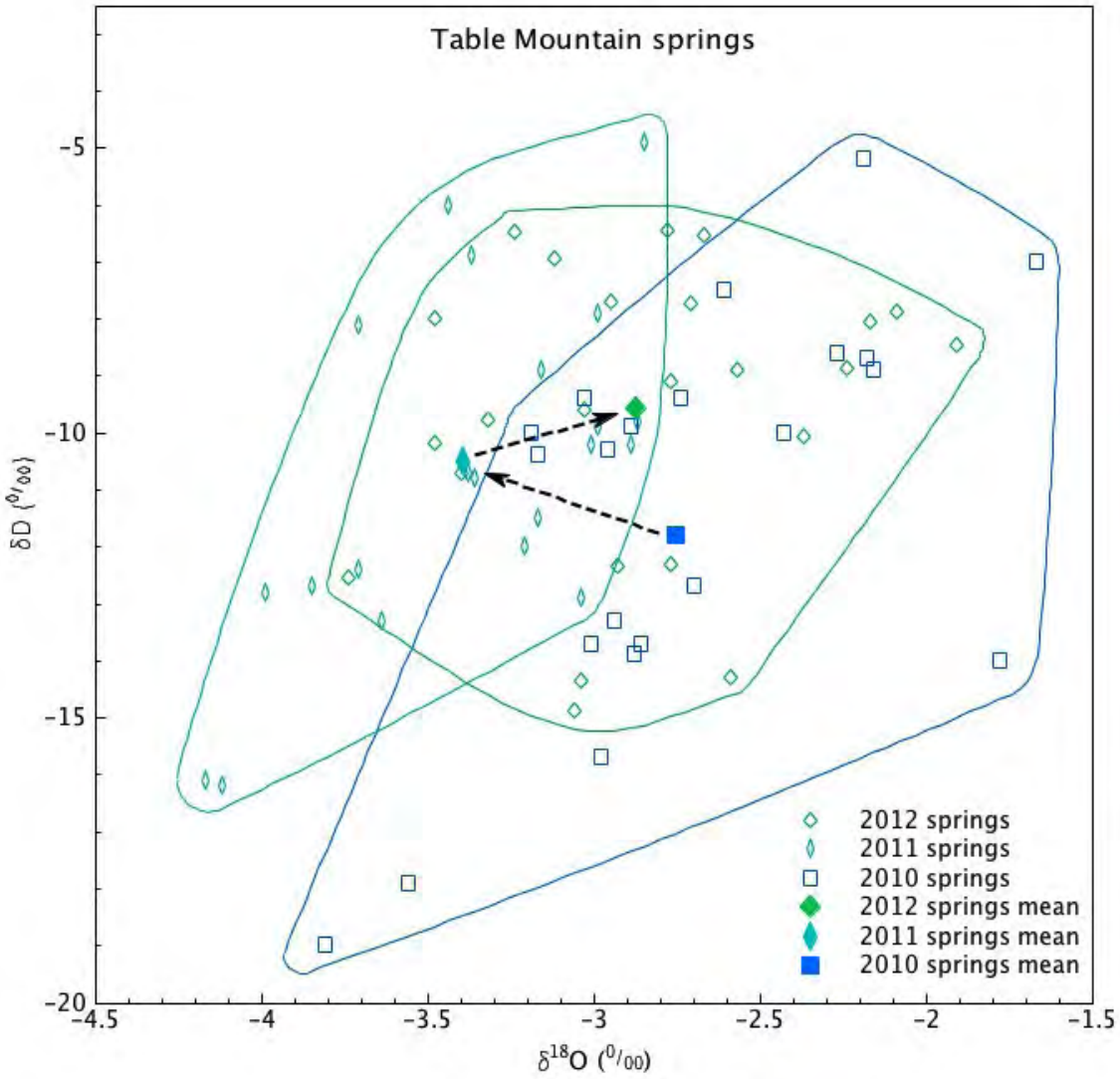

Figure 5.23: Data for all the Table Mountain springs plotted according to year, with the annual means also shown and arrows to indicate the yearly shift between annual means.

Groundwater Flow

Figure 5.23 shows the data for all the Cape Town springs plotted by year; most of the springs were sampled twice a year. A significant shift occurs in the isotope values, to the extent that less than 25 % of the 2010 samples fall within the range of the 2011 samples. This is clearly a significant shift and is quite unlike the random variability as noted for the hot springs in **Section 5.4.2**. The means for all the springs for the three years, 2010–2012, have also been plotted in **Figure 5.23** with arrows indicating the progression from year to year.

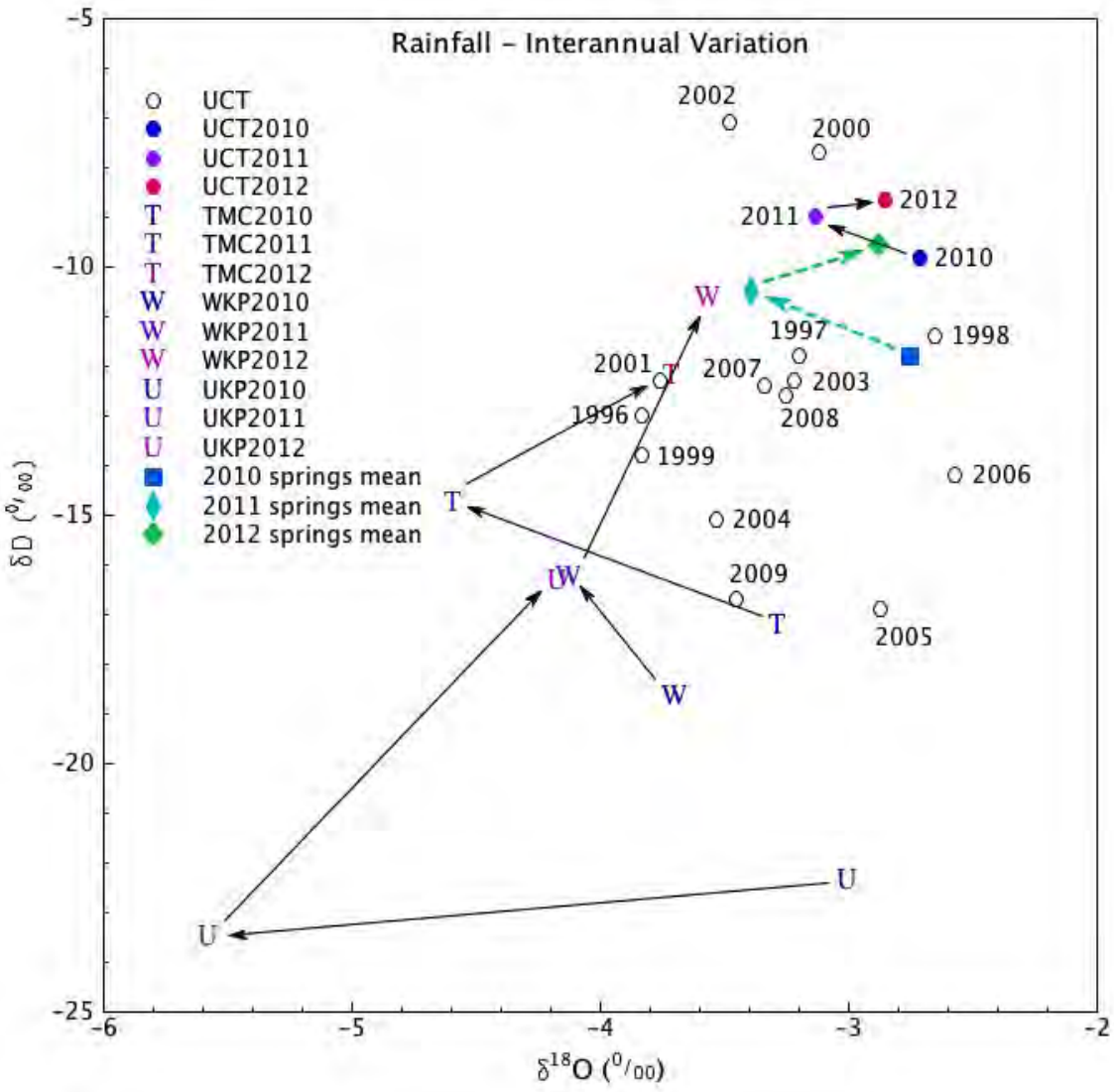

Figure 5.24: Weighted annual means for rainfall from several stations, including the long term records from UCT, as well as the average annual values for the Table Mountain springs, plotted in the δD – $\delta^{18}O$ space. UCT = University of Cape Town, T = Table Mountain Cableway, W = Wolfkop, U = Uitkyk Pass. Note the similarity in shift of annual means of UCT rain and Cape Town springs.

The weighted annual means for several of the rainfall stations have been plotted on **Figure 5.24**, including the long term records for UCT, from 1996 until this study. The shifts in the UCT annual means are interesting, if not somewhat puzzling, and some very large shifts can be seen, for example 1999 to 2000 and 2009 to 2010. The overall range in variation of these means is also noteworthy and suggests quite different weather conditions can dominate particular years.

Interestingly, the 2010–11–12 pattern in shifts of means at UCT mimics that of the Table Mountain springs, which have been added to the graph. Three of the other rainfall stations, Table Mountain Cableway (T), Uitkyk Pass (U) and to a lesser extent Wolfkop (W), also show similar

shifts in the weighted annual means. Seeing a similar pattern of shifts in annual mean values from more than one collection station is verification that these shifts are caused by widespread changes in weather conditions from year to year and not just site specific random variation. A small difference between the UCT averages and the spring averages probably reflects selection, altitude and amount effects, as the springs are recharged at higher elevations and during heavy rainfall events. Notwithstanding this small difference in actual isotope composition, the remarkable coincidence of the interannual shifts suggests that the Table Mountain springs discharge groundwater that has been recharged in that same year.

If recharge and discharge happens in the same year and the aquifer conforms to a piston flow model, then springs would only flow weeks to months after the first winter rain around April/May, in other words, around June/July, and cease flowing around November/December once the spring rains have passed. This is not seen, except in a few of the springs: Princess Anne and Rhodes Memorial (not sampled in this study) on the Kirstenbosch side, and Cableway and Tafelberg Road on the City Bowl side. The bulk of the springs flow perennially with little seasonal variation. Even after a drought, in which rainfall is well below average for a few years, all of the perennial springs continue to flow, although perhaps at lower rates (pers. comm. Caron von Zeil, Marius Bonthuis). Many of the springs are so reliable that they are used daily by the South African National Botanical Institute (Kirstenbosch), South African Breweries (Kommetjie), Provincial Government of the Western Cape (Leeuwenhof), City of Cape Town (Stadsfontein) and the public (Newlands) for industrial, irrigation and personal use. The aquifers are clearly able to sustain flow over a time period much greater than the half-year long rainy season.

The springs' aquifer must be able to accomodate longer term groundwater flow to sustain the steady, perennial flow, as well as shorter term groundwater flow to conduct the recently recharged groundwater with an isotope composition that is similar to the precipitation of that year. An attempt was made to isolate groups of springs to see if the higher flow rate springs showed less of a shift, or if those further from the mountain showed a greater delay in the isotope composition shift, but no trends could be found. A better data set, with monthly spring samples for all the springs would perhaps yield better resolution and show such trends. Nonetheless, it seems the aquifers are able to conduct recent recharge within months or less from the recharge area to the spring, as well as sustain groundwater flow over the summer months and through dry years.

A conceptual hydrogeological model is proposed whereby recently recharged groundwater is able to flow near the water table and at speed to discharge within weeks of heavy rain, usually at the start of winter. At the same time, slower movement of groundwater deeper in the aquifer is able to sustain discharge in the long term. This model is shown in a sketch cross section in **Figure 5.25**.

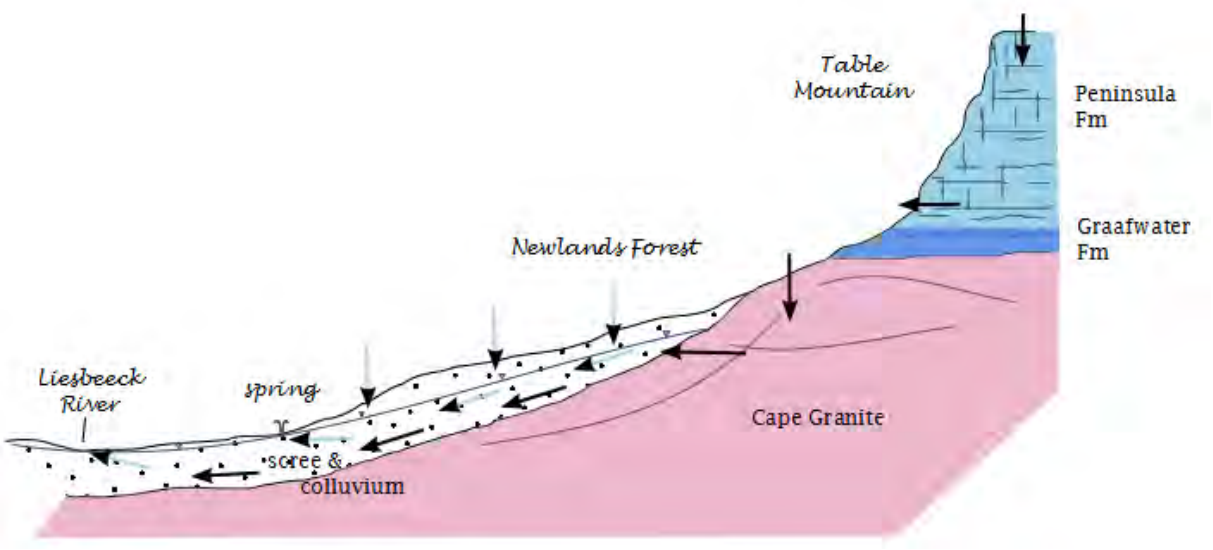

Figure 5.25: A sketch cross section looking south over Newlands Forest, showing a proposed conceptual hydrogeological model for the Kirstenbosch set of springs. Recently recharged groundwater is able to flow at shallow depths and discharge within weeks or months, whilst deeper groundwater is able to flow more slowly and sustain steady discharge over years. This model is equally applicable to the City Bowl springs.

Recharge Altitude

Figure 5.26 shows the weighted means for rainfall over 2010–12 at UCT and Table Mountain Cableway, and the mean for all the Cape Town spring samples, both those in the City Bowl and on the Kirstenbosch side of the mountain. As can be seen from the Figure, the springs plot in an intermediate position to UCT and TMC. Because the elevations of the rainfall stations are known, if a linear gradient for $\frac{\Delta\delta}{\Delta altitude}$ is assumed, the average recharge elevation for the springs can be interpolated. This works out to 304 masl.

The mean spring elevation is 156 masl, and so:

$$304masl - 156masl = 148m \ ,$$

which is the average altitude difference between spring recharge areas and discharge points. Given the typical topographic gradient of the lower slopes of Table Mountain is around 9°,

$$\Delta s = \frac{148m}{cosine9^\circ} = 946m \ ,$$

which is the average slope distance between recharge area and discharge point. Given that recharge occurs over a wide area, it would be reasonable to assume that recharge for each spring occurs in an area about 0.5–1.5 km upslope from the spring. Using the average distance of about 1 km, and an estimated duration of 2 months between rainfall and discharge for the shallow

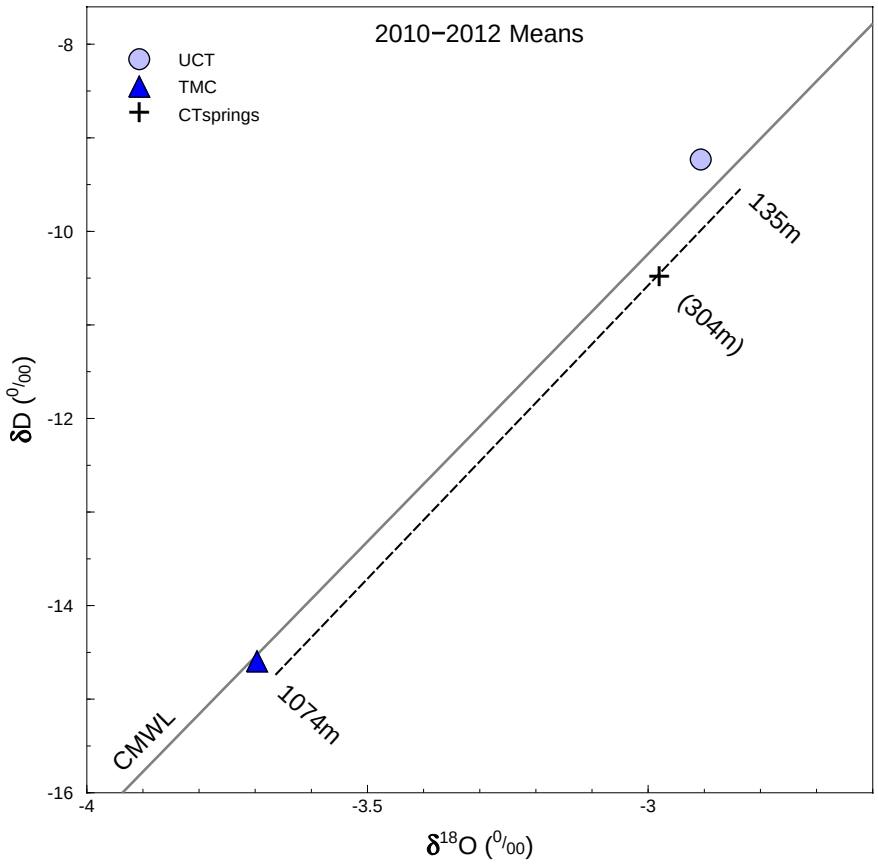

Figure 5.26: Calculation of average recharge altitude for Cape Town springs by interpolation between the altitudes of the UCT and Table Mountain Cableway (TMC) rainfall stations along a line of the same gradient as the Cape MWL.

groundwater component of the aquifer, a hydraulic conductivity of around 15–20 m/d is arrived at. This falls within the ranges of hydraulic conductivity of fine to coarse sand and gravel given in Domenico and Schwartz (1998, p.39).

These figures are rough values and will vary substantially between each spring, because of geological and topographic differences, and over different years, depending primarily upon rainfall amounts and intensities. Nonetheless, the calculation of recharge altitude and average flow path length based on isotope composition confirms the scree apron on Table Mountain as being the aquifer supporting the Cape Town springs, as presented in the conceptual model in **Figure 5.25**.

Chapter 6

Conclusions and Recommendations

This chapter summarizes the major findings of this study. The details of the data and reasoning behind these findings are to be found in both the Results and Discussion chapters above. Some key numerical results are repeated here.

1. **Weather affects isotopes** (p.100)
   The isotope composition of cumulative monthly samples of rain sometimes shows unusual values. With the help of records of past weather, individual weather systems can be found to be responsible for generation of unusual isotope composition (e.g. Dody and Ziv, 2013). In particular, convective rainfall events (thunderstorms) in summer can generate relatively negative δ values in precipitation in the Western Cape. Knowing the rarity of such weather systems can help determine whether the measured isotope composition is representative of that site.

   Recommendation: Weather records should be used when interpreting the isotope composition of rainfall.

2. **Weighted δ values of precipitation are more important in dry climates** (p.104)
   The difference between weighted and unweighted mean δ values for precipitation at a site is negatively correlated with mean annual precipitation. Weighting δ values of monthly precipitation samples by precipitation amount removes the effect of low volume rain events with extreme isotope composition, most particularly summer rains that are highly evaporated, with less negative or positive δ values. This has a greater effect on the mean in drier climates where highly evaporated and low volume rain events are more common than in wetter climates. This is in contrast to Yurtsever and Gat (1981), who found the difference in means is positively correlated with seasonality.

   Result: The weighted means for all rainfall for this study are: δD = -17.7 ‰ and $\delta^{18}O$ = -4.22 ‰, similar to those in drier parts of Jordan (Salameh, 2004).

Recommendation: Means should always be calculated by weighting δ values of monthly cumulative rain samples by the rainfall amount.

3. **The weighted LMWL is more relevant in hydrological studies** (p.108)
   The local meteoric water line equation is calculated using reduced-major-axis (RMA) regression between δD and $\delta^{18}O$. Weighting the monthly δ values by rainfall amount changes the best fit line and generally results in a steeper gradient and higher δD intercept. As low volume rains have less impact on hydrology, especially groundwater recharge, and weighting removes the effect of low volume rains, the weighted LMWL is more applicable to hydrological studies (Hughes and Crawford, 2012). Use of weighted data and the more applicable RMA regression method is either not done or not clearly stated in the global literature.

   Result: The weighted LMWL for this study, or Cape MWL is: δD = 6.15 $\delta^{18}O$ + 8.21, which is similar to those previously calculated for this area (Diamond and Harris, 1997; Harris et al., 2010).

   Recommendation: Local meteoric water lines should be calculated by weighted reduced-major-axis regression.

4. **Groundwater has a lesser spread of δ values than precipitation** (p.113)
   The range of δ values for groundwater at one site or across a region is less than for precipitation (e.g. Majumder et al., 2011). Groundwater averages out the short term variations in precipitation to reveal the long term mean δ values of precipitation. Where the recharge area is well defined, such as for high altitude mountain seeps in the Table Mountain Group, where there is very little aquifer above the discharge point, the isotope composition of the water from the seep is a good proxy for the local precipitation.

   Result: The ranges in values of δD and $\delta^{18}O$ are, for precipitation: -75 ‰ to +40 ‰ and -12 ‰ to +8 ‰; and for groundwater: -47 ‰ to 0 ‰ and -8 ‰ to -1 ‰ .

   Recommendation: High altitude mountain seeps in the Table Mountain Group can be collected instead of difficult and costly long term precipitation monitoring at high altitude.

5. **Western Cape stable isotope compositions are similar to South Africa** (p.129)
   In spite of having different climates, the isotope compositions for the Western Cape and for the rest of South Africa overlap. The current data sets have insufficient separation according to season, climatic region, weather events and other factors to be able to draw out trends, although there are most likely differences in means from different regions. Differences in mean isotope composition of precipitation at specific sites across Australia are also minor, in spite of vast distances and different climates (Liu et al., 2010).

Recommendation: More samples of meteoric water throughout South Africa are needed. In particular, thoughtful analysis of these samples, according to geographic and meteorological parameters, is needed to draw out regional patterns in stable isotope composition.

6. **The Western Cape displays a complex continentality effect** (p.133)
   Poor correlations are displayed between δ values and simple distance from sea parameters, such as have been used by Salati et al. (1979) and Yonge et al. (1989). A compound "distance to the Atlantic" and "distance to the closest coast" parameter shows much better correlations with δ values. This is likely because rain bearing weather systems can approach from any direction from NW, through W and S to SE, due to the Western Cape's position at the southern end of Africa. Continentality effects in regions where rain bearing weather systems can approach from more than one direction are likely to be complex.

   Recommendation: To calculate the best index of continentality for the Western Cape, generate average weather system tracks for different locations, or more simply measure the area of land between the rainfall station and the ocean within the semi-circle facing SW.

7. **Small and steep mountains display a reduced altitude effect due to reduced rainout** (p.136)
   Small, steep mountains do not generate sufficient rainout to drive isotope compositions towards the negative δ values that would be expected based on the site altitude. The isotope composition is a function of the average altitude over several square kilometres around a site. The reverse is also true: sites surrounded by higher elevation, such as valleys within mountains, record δ values that are more negative than would be expected based on the actual site altitude. The altitude effect gradients calculated for this study are on the low side compared to reported gradients from around the world (Clark and Fritz, 1997, p.71). This is because of the steep terrain gradients of the Cape Mountains and suggests that many of the altitude effects calculated worldwide are in fact combination effects of pure altitude change as well as rainout with distance.

   Result: Calculated altitude effect gradients varied from -0.48 to -2.2 $\frac{\Delta\delta D}{100m}$ and -0.075 to -0.34 $\frac{\Delta\delta^{18}O}{100m}$.

   Recommendation: Precipitation collection stations should be placed at an elevation that is representative of the general surrounds, rather than atop a high peak or in a deep valley. Where stations are in topographically unrepresentative positions, the average elevation around the site should be used when calculating altitude effect gradients.

8. **The amount effect varies between stations and over time at single stations** (p.143)
   The amount effect was not noticeable for average annual precipitation, but for mean monthly precipitation (e.g. Dansgaard, 1964; Rozanski et al., 1993). To calculate useful monthly means of precipitation and δ values, several years of monitoring are needed. The scale of the effect varied significantly between stations and even at a single station over different groups of years, emphasising the need for longer term monitoring to calculate reliable relationships.

   Recommendation: Long term monitoring is needed to calculate such isotope effects accurately. In the absence of longer term data, overinterpretation of trends should be avoided.

9. **Surface waters show little variation within catchments, suggesting complex groundwater flow paths with significant mixing in the Peninsula aquifer** (p.148)
   Samples from rivers showed great variation between rivers, but not within each catchment, despite substantial ranges in altitude and sometimes distance. The surface waters were sampled in late summer, so representing baseflow, made up of groundwater discharge. Direct samples of springs and seeps adjacent to rivers were also taken. The well averaged nature of surface water in each catchment suggests the groundwaters are well mixed between recharge and discharge points, which suggests complex flow paths through deep fracture networks in the Table Mountain Group, mostly the Peninsula Formation, in contrast to isotopically varied groundwater from shallow fracture networks (e.g. Negrel et al., 2011).

   Recommendation: Surface water samples should not be used to understand details of groundwater flow, but do offer averaged δ values for the catchment. The homogeneity of surface water baseflow can be used as a measure of groundwater mixing.

10. **Groundwater flow paths are often shallow and short** (p.151)
    A negative correlation exists between δ values of groundwater samples and the discharge elevation. If groundwater flow paths were long or variable in length, the recharge altitude, which is what determines the δ values, would not be correlated with the discharge altitude. The correlation suggests that much of the groundwater sampled circulates shallowly and has a short flow path of hundreds of metres to perhaps a kilometre or two. This means the aquifer is more easily impacted by surface activities and overabstraction.

    Recommendation: Determine the size and depth of the aquifer by comparing groundwater and precipitation isotope composition, to determine its vulnerability to surface impacts and overabstraction. Long term precipitation monitoring will be needed.

11. **Hot springs reveal long term, long distance, deep circulation in the Table Mountain Group** (p.153)

    Stable isotope composition of several hot springs did not change appreciably over 40 years, although significant variations occur in isotope composition of discharge, even on a monthly timescale. Interannual or interdecadal variations in recharge (precipitation) are not obvious and indicate that circulation is well mixed, deep and regional (e.g. Delalande et al., 2011). The Table Mountain Group is able to conduct deep (more than one or two kilometres), long distance (tens of kilometres) groundwater flow.

12. **Agricultural abstraction in the Olifants River Mountains taps locally recharged groundwater of the Peninsula aquifer** (p.155)

    Isotope composition of rainfall and groundwater in the Olifants River and Cederberg region revealed that groundwater being abstracted from the Peninsula Formation in the Olifants River Mountains was not coming from the Cederberg region and was being locally recharged. The aquifer is relatively limited in extent and more likely to become depleted.

    Recommendation: Local monitoring of hydrological parameters (water levels, rainfall) may be useful in warning of potential groundwater depletion, especially if climate change predictions of decreased rainfall come to pass. Stable isotopes can be employed to elucidate more details about the local groundwater circulation.

13. **Mountain recharge into the Skurweberg aquifer supplies agricultural boreholes on both sides of the Hex River anticline** (p.159)

    Comparison of the isotope composition of boreholes with precipitation has allowed the calculation of approximate recharge altitude. Groundwater abstracted from the Rietvlei Formation at 500 masl on the south side of the Hex River anticline is recharged in the Skurweberg or Goudini Formation at 1200 masl, and groundwater abstracted from the Rietvlei Formation at 1100 masl on the north side of the Hex River anticline is recharged in the Skurweberg or Goudini Formation at 1600 masl. The Skurweberg aquifer is an important, high yielding aquifer for agriculture in the Hex River Mountains region, as has been noted in the nearby Agter-Witzenberg Valley (Weaver et al., 1999). Increasing groundwater abstraction will draw water from deeper in the Skurweberg aquifer, which will have been recharged at higher elevation and therefore have more negative δ values.

    Recommendation: Where an aquifer is recharged over a range of altitudes, monitor stable isotope composition of borehole water to detect signs of overabstraction.

14. **Snow isotope composition varies greatly and preserves that of precipitation events**

    A profile through a snowpack revealed that the isotope composition changed both during a

precipitation event and between different events. Some of this change may have been due to post-depositional changes (Arnason, 1981).

Recommendation: Snow may be sampled to examine recent past precipitation events, but care must be taken to evaluate the degree of post-depositional change.

15. **Groundwater is recharged selectively during large amount rainfall events** (p.166)
    The isotope composition of groundwater discharge at Gamkaberg boreholes has more negative δ values than rainfall at the top of the Gamkaberg, so either selective recharge during isotopically more negative large amount rainfall events occurs (e.g. Dogramaci et al., 2012), or interannual variation in isotope composition of rainfall accounts for the relatively high δ values on top of Gamkaberg.

    Recommendation: Long term precipitation monitoring is needed to quantify the range of interannual variations in δ values.

16. **The Skurweberg aquifer conducts groundwater from the crest of the Klein Swartberg into the Great Karoo** (p.166)
    Boreholes on the northern side of the Klein Swartberg at 1000 masl discharge groundwater with δ values that match recharge at the crest of the range at 2000 m. The recharge occurs in the Goudini or Skurweberg Formation and is discharged through the Rietvlei Formation.

17. **Table Mountain springs are fed by groundwater from the scree aquifer** (p.173)
    Using the altitude effect calculated for Table Mountain it was shown that the typical groundwater flow path for each spring is 1 km long. The aquifer is the scree apron that lies on the middle to lower slopes of Table Mountain, contrary to popularly held belief that the Peninsula Formation is the aquifer (Bryant and Blake, 2014). The springs may be more susceptible to climate change and human activities on the lower slopes than would be the case if the Peninsula aquifer higher on the mountain was directly involved, being in a higher rainfall zone and further removed from human activities.

18. **Table Mountain scree aquifers allow layered groundwater flow to take place** (p.173)
    By tracking changes in annual mean δ values for precipitation and for the springs, the scree aquifer must allow shallow, fast groundwater flow to take place on top of slower, deeper groundwater flow. The former is needed to explain the identical pattern in shifts of annual mean δ values between rain and springs, and the latter is needed to explain the perennial flow of many of the springs. Changes in mean annual isotope composition are generally regarded as noise in data, caused by variations in the weather from year to year, and long

term averages are usually sought (Yurtsever and Gat, 1981). This study has shown the value of using shorter term data and in particular, the interannual changes in mean isotope composition to unravel hydrogeological relations.

Summary

In an international review on stable isotope hydrology, Gat (1996, p.253) stated: "In order to take full advantage of the possibilities of understanding groundwater formation, the detailed isotope effects of the recharge and runoff processes need to be established for different climate conditions and for each watershed. Such studies are still few and incomplete." And in the closing chapter of the Water Research Commission report on the Table Mountain Group, Pietersen and Parsons (2002, p.257) stated: "The WRC recognises the need to... Develop an understanding of the occurrence, attributes and dynamics of the TMG aquifer systems... ". This study has made a start on these recommendations and being regional in nature, has paved the way for more detailed work in and around the Cape Fold Belt.

Findings have been made regarding the continental and altitude effects. Both have been shown to contain more complexity than some other studies have shown, suggesting that either weather in the Cape is more complex, or that other studies have overlooked such details. Changes in mean annual isotope composition of precipitation have been shown to be useful tracers of groundwater flow, something which has not been done before.

Regarding the Table Mountain Group, this study has shown strong evidence for mountain recharge and flow of groundwater to adjacent valleys. Much of the groundwater in the Table Mountain Group has a short flow path of one or two kilometres or less, in keeping with the steep terrain of the Cape Mountains. Despite these short flow distances, groundwater appears to be well mixed, which indicates substantial fracture networks in multiple orientations. Recharge displays selection behaviour, where large amount rainfall events with lighter isotope compositions are favoured.

The range in isotope compositions, due largely to continental and altitude effects, allowed their use as hydrological tracers and helped develop conceptual models of groundwater flow in the Cape Fold Belt. With increasing pressure on water resources in the region, stable isotopes should be employed to help understand the hydrogeology and then better manage water resources to reduce environmental impacts and allow sustainable use of groundwater, at the same time as adding to the global picture on the behaviour of stable isotopes in the hydrological cycle.

Chapter 7

Abbreviations, Acronyms and Units

acronym	explanation
ASTER	Advanced Spaceborne Thermal Emission and Reflection Radiometer
CMWL	Cape meteoric water line
CTIA	Cape Town International Airport
CTMP	Cape Town millipore water
DEM	digital elevation model
GIS	geographic information system
GMWL	Global Meteoric Water Line
GNIP	global network for isotopes in precipitation
IAEA	International Atomic Energy Agency
LASER	light amplification by stimulated emission of radiation
LMWL	local meteoric water line
LSR	least squares regression
MAP	mean annual precipitation
masl	metres above sea level
MWL	meteoric water line
RMA	reduced major axis regression
RMW	Rocky Mountain Water
SAST	South African Standard Time
SAWS	South African Weather Service
SS	sum of the squares (statistical parameter)
SP	sum of the products (statistical parameter)
T	temperature
WMO	World Meteorological Organisation

symbol	explanation
mm	millimetre
m	metre
km	kilometre
μL	microlitre
mL	millilitre
L	litre
kL	kilolitre
ML	megalitre
GL	gigalitre
mg	milligram
s	second
h	hour
d	day
a	annum (year)
Ma	megannum (million years)

letter	abbreviation	explanation
		rainfall stations
C	UCT	University of Cape Town
T	TMC	Table Mountain Upper Cableway Station
I	TWT	Twaktuin
U	UKP	Uitkyk Pass
W	WKP	Wolfkop
M	MTB	Matroosberg
D	DDN	DeDoorns
R	RVD	Riverndale
P	RBP	Robinson Pass
A	BKK	Bakenskop
G	GST	Gamka Store
B	BBG	Blesberg
K	KMN	Kammanassie
L	LTL	Lentelus
O	GKM	Goukamma
		rivers
	DWK	Duiwelskloof
	VSK	Volstruiskloof
	WTL	Witels

	GHK	Groothoekkloof
		hot springs
	CIT	Citrusdal (The Baths)
	WTZ	Witzenberg (Tulbagh)
	GDN	Goudini
	BRA	Brandvlei
	CDN	Caledon
	WAR	Warmwaterberg
	LAI	Laingsburg (UCT field station)
	CZD	Calitzdorp
	TWR	Toowerwater
		Table Mountain (Cape Town) springs
K	KIR	Kirstenbosch
O	KOM	Kommetjie
P	PRI	Princess Anne Drive
N	NEW	Newlands
B	PAL	Palmboom
A	ALB	Albion
R	RED	Redwood
W	WEN	Wendy’s
M	MAI	Cape Town main spring (collection chamber)
C	CAB	Cableway
G	GLE	Glencoe Road
L	LEE	Leeuwenhof
T	TAF	Tafelberg Road
Y	LIL	Lily Pond

Table 7.1: Tables of Acronyms, Units and Abbreviations

Chapter 8

Acknowledgements

I would like to thank the following organisations and people:

Professor Chris Harris for supervision, funding, advice and climbing;

National Research Foundation and Water Research Commission for funding;

Dr John Lanham for analytical assistance on the mass spectrometer;

Dr Adam West for analytical assistance on the LASER spectrometer and advice;

for sampling rain:
Fayrooza Rawoot at University of Cape Town,
Sabine Lehmann, Marie Abraham and Kim van Reenen at the Table Mountain Aerial Cableway Company,
Robert and Anne Paterson at Twaktuin,
Patrick Lane at the Cederberg (Cape Nature),
Richard Humphris at Wolfkop,
Waldo and Didi Smith at Erfdeel,
Retief Jordaan at Tweespruit,
Jeremy Wakeford at Riverndale,
Jan Makampies at Ruitersbos (Cape Nature), Robinson Pass,
Tom Barry and team at Gamkaberg (Cape Nature),
Jan Coetzee, Theo Taute and team at the Groot Swartberg (Cape Nature),
Philip Esau and team at the Kammanassie (Cape Nature),
Dirk Versfeld and Rachel Moos at Lentelus,
Marina Botha at Goukamma;

for sampling boreholes:
Robert Paterson at Twaktuin,
Waldo Smith at Erfdeel,
Retief Jordaan at Tweespruit,
Tom Barry at Gamkaberg,
Geoff Grundlingh at Rooihoogte;

for sampling springs:
Caron von Zeil and Pixie Littlewort for assistance and passion for the Cape Town springs,
Marius Bonthuis at Cape Town Main (City of Cape Town),
Philip le Roux and Aida van Reenen at Kirstenbosch (South African National Biodiversity Institute),
Paul Teuchert at Kommetjie (South African Breweries),
the managers at the various hot springs;

and to all the friends and family who accompanied me on various missions to collect samples, service rainfall collectors and sample springs and seeps in the wild yet wonderful Cape Mountains:
Alexis Aronson,
Anyik Duku,
Phil Ginsberg,
John Glover,
Richard Halsey,
Martin Kleynhans,
Lucille Krige,
Mikhaela Levitas,
Elinor Milewski,
Sonia van Essen,
Luke Viljoen,
Xolani Zekani.

References

Adams, S., Titus, R., Pietersen, K., Tredoux, G., Harris, C., 2001. Hydrochemical characteristics of aquifers near Sutherland in the Western Karoo, South Africa. Journal of Hydrology 241, 91–103.

Al-Aswad, A.A., Al-Bassam, A.M., 1997. Proposed hydrostratigraphical classification and nomenclature: application to the Palaeozoic in Saudi Arabia. Journal of African Earth Sciences 24, 497–510.

Araguás-Araguás, L., Froehlich, K., Rozanski, K., 1998. Stable isotope composition of precipitation over southeast Asia. Journal of Geophysical Research 103, 28721–28742.

Araguás-Araguás, L., Froehlich, K., Rozanski, K., 2000. Deuterium and oxygen-18 isotope composition of precipitation and atmospheric moisture. Hydrological Processes 14, 1341–1355.

Argiriou, A.A., Lykoudis, S., 2006. Isotopic composition of precipitation in Greece. Journal of Hydrology 327, 486–495.

Arnason, B., 1981. Ice and Snow Hydrology, in: Gat, J.R., Gonfiantini, R. (Eds.), Stable Isotope Hydrology. International Atomic Energy Agency, Vienna. number 210 in Technical Reports Series. chapter 7, pp. 143–175.

ASTER, 2014. Advanced Spaceborne Thermal Emission and Reflection Radiometer. URL: http://www.jspacesystems.or.jp/ersdac/GDEM/E/index.html.

Barrow, D., Diamond, R.E., 2011. Stable isotopes of rain, surface water and groundwater in the Kogelberg, in: Groundwater: Our Source of Security in an Uncertain Future, Groundwater Division: Geological Society of South Africa, Pretoria.

Beaudoin, G., Therrien, P., 2014. AlphaDelta: Stable Isotope Fractionation Calculator. URL: http://www2.ggl.ulaval.ca/cgi-bin/alphadelta/alphadelta.cgi.

Belcher, R.W., Kisters, A.F., 2003. Lithostratigraphic correlations in the western branch of the Pan-African Saldania Belt, South Africa: the Malmesbury Group revisited. South African Journal of Geology 106, 327–342.

Bell, C.M., 1980. Deformation of the Table Mountain Group in the Cape Fold Belt south of Port Elizabeth. Transactions of the Geological Society of South Africa 83, 115–124.

Beuster, H., Thompson, I., Gögens, A.H., Jonker, V., Clarke, F.A., 2009. Application of geostatistical analyses to develop a new mean annual rainfall surface for the south-western Cape, in: South African National Committee for the International Association of Hydrological Sciences: Symposium 2009, p. 18p.

Bond, G., 1953. The origin of thermal and mineral waters in the middle Zambezi Valley and adjoining territory. Geological Society of South Africa 56, 131–148.

Bosman, H.H., 1981. Raingauges: Quality pays. Water SA 7, 190–191.

Breitenbach, S.F., Adkins, J.F., Meyer, H., Marwan, N., Kumar, K.K., Haug, G.H., 2010. Strong influence of water vapor source dynamics on stable isotopes in precipitation observed in southern Meghalaya, NE India. Earth & Planetary Science Letters 292, 212–220.

Brink, A.B., 1981. Engineering Geology of Southern Africa. volume 2: Case Study: Dams founded on rocks and The Table Mountain Group. Building Publications, Pretoria.

Broquet, C.A., 1992. The sedimentary record of the Cape Supergroup: A review, in: de Wit, M.J., Ransome, I.G. (Eds.), Inversion Tectonics of the Cape Fold Belt, Karoo and Cretaceous Basins of Southern Africa. A.A.Balkema, pp. 159–184.

Bryant, J., Blake, D., 2014. Investigating the springs and boreholes of Groote Schuur. Veld & Flora , 63.

Butler, M.J., Verhagen, B.T., Levin, M., 2000. Application of environmental isotope techniques to hydrological and pollution problems in the urban environment, in: Sililo, O. (Ed.), Groundwater: Past Achievements and Future Challenges. A.A.Balkema, Rotterdam, pp. 459–464.

Cavé, L.C., Weaver, J.M., Talma, A.S., 2002. The use of geochemistry and isotopes in resource evaluation: a case study from the Agter-Witzenberg Valley, in: Pietersen, K., Parsons, R. (Eds.), A Synthesis of the Hydrogeology of the Table Mountain Group - Formation of a Research Strategy. Water Research Commission, Pretoria. TT 158/01, pp. 143–149.

Clark, I.D., Fritz, P., 1997. Environmental Isotopes in Hydrogeology. CRC Press, Boca Raton.

Colvin, C., Riemann, K., Brown, C., Maitre, D.L., Mlisa, A., Blake, D., Aston, T., Maherry, A., Engelbrecht, J., Pemberton, C., Magoba, R., Soltau, L., Prinsloo, E., 2009. Ecological and environmental impacts of large-scale groundwater development in the Table Mountain Group) TMG aquifer system. Technical Report 1327/1/08. Water Research Commission. Pretoria.

Council for Geoscience, 1997. 3319 Worcester. 1:250 000 geological series. Council for Geoscience. Pretoria.

Craig, H., 1961a. Isotopic variations in meteoric waters. Science 133, 1702–1703.

Craig, H., 1961b. Standard for reporting concentrations of deuterium and oxygen-18 in natural waters. Science 133, 1833–1834.

CSAG, 2013. Climate Information Portal, Climate Systems Analysis Group, University of Cape Town. http://cip.csag.uct.ac.za/webclient2/app/.

da Silva, L.C., Gresse, P.G., Scheepers, R., McNaughton, N.J., Hartmann, L.A., Fletcher, I., 2000. U-Pb SHRIMP and Sm-Nd age constraints on the timing and sources of the Pan-African Cape Granite Suite, South Africa. Journal of African Earth Sciences 30, 795–815.

D'Alessandro, W., Federico, C., Longo, M., Parello, F., 2004. Oxygen isotope composition of natural waters in the Mt Etna area. Journal of Hydrology 296, 282–299.

Dansgaard, W., 1964. Stable Isotopes in Precipitation. Tellus 16, 436–468.

Davidson, W.A., 1995. Hydrogeology and groundwater resources of the Perth Basin. Technical Report Bulletin 142. Western Australia Geological Survey. Perth.

de Beer, C.H., 2002. The Stratigraphy, Lithology and Structure of the Table Mountain Group, in: Pietersen, K., Parsons, R. (Eds.), A Synthesis of the Hydrogeology of the Table Mountain Group - Formation of a Research Strategy. Water Research Commission, Pretoria. TT 158/01, pp. 9–18.

de Wit, M.J., Ransome, I.G., 1992. Regional inversion tectonics along the southern margin of Gondwana, in: de Wit, M.J., Ransome, I.G. (Eds.), Inversion Tectonics of the Cape Fold Belt, Karoo and Cretaceous Basins of Southern Africa. A.A.Balkema, Rotterdam, pp. 15–22.

Delalande, M., Bergonzini, L., Gherardi, F., Guidi, M., Andre, L., Abdallah, I., Williamson, D., 2011. Fluid geochemistry of natural manifestations from the Southern Poroto-Rungwe hydrothermal system (Tanzania): Preliminary conceptual model. Journal of Volcanology and Geothermal Research 199, 127–141.

Dent, M.C., Lynch, S.D., Schulze, R.E., 1987. Mapping mean annual and other rainfall statistics over Southern Africa. Technical Report 109/1/89. Water Research Commission. Pretoria.

Diamond, R.E., Harris, C., 1997. Oxygen and hydrogen isotope composition of Western Cape meteoric water. South African Journal of Science 93, 371–374.

Diamond, R.E., Harris, C., 2000. Oxygen and hydrogen isotope geochemistry of thermal springs of the Western Cape, South Africa: recharge at high altitude? Journal of African Earth Sciences 31, 467–481.

Dingle, R.V., Siesser, W.G., Newton, A.R., 1983. Mesozoic and Tertiary Geology of Southern Africa. A.A.Balkema.

Dody, A., Ziv, B., 2013. Factors affecting isotopic composition of the rainwater in the Negev Desert, Israel. Journal of Geophysical Research: Atmospheres 118, 8274–8284.

Dogramaci, S., Skrzypek, G., Dodson, W., Grierson, P.F., 2012. Stable isotope and hydrochemical evolution of groundwater in the semi-arid Hamersley Basin of subtropical northwest Australia. Journal of Hydrology 475, 281–293.

Domenico, P.A., Schwartz, F.W., 1998. Physical and Chemical Hydrogeology. John Wiley & Sons, Inc.

DTI, 2009. SA Risk and Vulnerability Atlas. URL: http://rava.qsens.net/themes/groundwater.

Emiliani, C., 1987. Dictionary of the Physical Sciences. Oxford University Press, Oxford.

Encyclopaedia Brittanica, 2013. Climate. URL: http://www.britannica.com/EBchecked/topic/121560/c

Epstein, S., Mayeda, T., 1953. Variation of 18O content of waters from natural sources. Geochimica et Cosmochimica Acta 4, 213–224.

February, E.C., Bond, W., Taylor, R., Newton, R., 2004. Will water abstraction from the Table Mountain aquifer threaten endemic species? A case study at Cape Point, Cape Town. South African Journal of Science 100, 253–255.

Friedman, I., 1953. Deuterium content of natural waters and other substances. Geochimica et Cosmochimica Acta 4, 89–103.

Frimmel, H.E., Fölling, P.G., Diamond, R.E., 2001. Metamorphism of the Permo-Triassic Cape Fold Belt and its basement, South Africa. Mineralogy and Petrology 73, 325–346.

Fritz, P., 1981. River Waters, in: Gat, J.R., Gonfiantini, R. (Eds.), Stable Isotope Hydrology. International Atomic Energy Agency, Vienna. number 210 in Technical Reports Series. chapter 8, pp. 177–202.

Fuller, A.O., Broquet, C.A., 1990. Aspects of the Peninsula Formation - Table Mountain Group, in: Geocongress ’90 - abstracts, Geological Society of South Africa. Geological Society of South Africa, Johannesburg. pp. 169–172.

Gabbott, S.E., Siveter, D.J., Aldridge, R.J., Theron, J.N., 2003. The earliest myodocopes: ostracodes from the late Ordovician Soom Shale Lagerstätte. Lethaia 36, 151–160.

Gat, J.R., 1981a. Groundwater, in: Gat, J.R., Gonfiantini, R. (Eds.), Stable Isotope Hydrology. International Atomic Energy Agency, Vienna. number 210 in Technical Reports Series. chapter 10, pp. 223–240.

Gat, J.R., 1981b. Historical Introduction, in: Gat, J.R., Gonfiantini, R. (Eds.), Stable Isotope Hydrology. International Atomic Energy Agency, Vienna. number 210 in Technical Reports Series. chapter 1, pp. 1–6.

Gat, J.R., 1996. Oxygen and hydrogen isotopes in the hydrological cycle. Annual Reviews in Earth and Planetary Sciences 24, 225–262.

Gaucher, C., Germs, G.J., 2006. Recent advances in South African Neoproterozoic-Early Palaeozoic biostratigraphy: correlation of the Cango Caves and Gamtoos Groups and acritarchs of the Sardinia Bay Formation, Saldania Belt. South African Journal of Geology 109, 193–214.

Geological Survey, 1973. 3218 Clanwilliam. 1:250 000 geological series. Department of Mines. Pretoria.

Geological Survey, 1979. 3322 Oudtshoorn. 1:250 000 geological series. Geological Survey. Pretoria.

Geological Survey, 1991. 3320 Ladismith. 1:250 000 geological series. Geological Survey. Pretoria.

Gonfiantini, R., 1981. The δ notation and the mass-spectrometric measurement techniques, in: Gat, J.R., Gonfiantini, R. (Eds.), Stable Isotope Hydrology. International Atomic Energy Agency, Vienna. number 210 in Technical Reports Series. chapter 4, pp. 35–84.

Gonfiantini, R., Roche, M.A., Olivry, J.C., Fontes, J.C., Zuppi, G.M., 2001. The altitude effect on the isotopic composition of tropical rains. Chemical Geology 181, 147–167.

Gresse, P.G., Theron, J.N., 1992. The Geology of the Worcester Area, explanation of sheet 3319. Technical Report. Geological Survey, Department of Mineral and Energy Affairs. Pretoria.

Gresse, P.G., von Veh, M.W., Frimmel, H.E., 2006. Namibian (Neoproterozoic) to Early Cambrian Successions, in: Johnson, M.R., Annhaeusser, C.R., Thomas, R.J. (Eds.), The Geology of South Africa. Geological Society of South Africa, Council for Geoscience, Pretoria. chapter 18, pp. 395–420.

Hälbich, I.W., 1992. The Cape Fold Belt Orogeny: State of the art 1970’s - 1980’s, in: de Wit, M.J., Ransome, I.G. (Eds.), Inversion Tectonics of the Cape Fold Belt, Karoo and Cretaceous Basins of Southern Africa. A.A.Balkema, Rotterdam, pp. 141–158.

Hammerbeck, E.C., Allcock, R.J., 1985. Geological Map of Southern Africa. Technical Report. Geological Society of South Africa. Pretoria.

Harris, C., Burgers, C., Miller, J., Rawoot, F., 2010. O- and H-isotope record of Cape Town rainfall from 1996 to 2008, and its application to recharge studies of Table Mountain groundwater, South Africa. South African Journal of Geology 113, 33–56.

Harris, C., Oom, B.M., Diamond, R.E., 1999. A preliminary investigation of the oxygen and hydrogen isotope hydrology of the greater Cape Town area and an assessment of the potential for using stable isotopes as tracers. Water SA 25, 15–24.

Hartnady, C.J., Hay, E.R., 2002a. Boschkloof groundwater discovery, in: Pietersen, K., Parsons, R. (Eds.), A Synthesis of the Hydrogeology of the Table Mountain Group - Formation of a Research Strategy. Water Research Commission, Pretoria. TT 158/01, pp. 168–177.

Hartnady, C.J., Hay, E.R., 2002b. Experimental deep drilling at Blikhuis, Olifants River Valley, Western Cape: Motivation, setting and current progress, in: Pietersen, K., Parsons, R. (Eds.), A Synthesis of the Hydrogeology of the Table Mountain Group - Formation of a Research Strategy. Water Research Commission, Pretoria. TT 158/01, pp. 192–197.

Hartnady, C.J., Hay, E.R., 2002c. Use of structural geology and remote sensing in hydrogeological exploration of the Olifants and Doring River catchments, in: Pietersen, K., Parsons, R. (Eds.), A Synthesis of the Hydrogeology of the Table Mountain Group - Formation of a Research Strategy. Water Research Commission, Pretoria. TT 158/01, pp. 19–30.

Hartnady, C.J., Newton, A.R., Theron, J.N., 1974. The stratigraphy and structure of the Malmesbury Group in the southwestern Cape. Bulletin of the Precambrian Research Unit, UCT 15, 195–213.

Harvey, F.E., Sibray, S.S., 2001. Delineating Groundwater recharge from leaking irrigation canals using water chemistry and isotopes. Groundwater 39, 408–421.

Hobday, D.K., Tankard, A.J., 1978. Transgressive-barrier and shallow-shelf interpretation of the lower Paleozoic Peninsula Formation, South Africa. Geological Society of America Bulletin 89, 1733–1744.

Horibe, Y., Kobayakawa, M., 1960. Deuterium abundance of natural waters. Geochimica et Cosmochimica Acta 20, 273.

Hughes, C.E., Crawford, J., 2012. A new precipitation weighted method for determining the meteoric water line for hydrological applications demonstrated using Australian and global GNIP data. Journal of Hydrology 464, 344–351.

Hunjak, T., Lutz, H.O., Roller-Lutz, Z., 2013. Stable isotope composition of the meteoric precipitation in Croatia. Isotopes in Environmental and Health Studies 49, 336–345.

Iacumin, P., Venturelli, G., Selmo, E., 2009. Isotopic features of rivers and groundwater of the Parma Province (Northern Italy) and their relationships with precipitation. Journal of Geochemical Exploration 102, 56–62.

IAEA, 2013. The Nubian Aquifer Project. URL: http://www-naweb.iaea.org/napc/ih/IHS projects nubian development.html.

Jasechko, S., Sharp, Z., Gibson, J., Birks, S., Yi, Y., Fawcett, P., 2013. Terrestrial water fluxes dominated by transpiration. Nature 496, 347–350.

Jaunat, J., Celle-Jeanton, H., Huneau, F., Dupuy, A., Le Coustumer, P., 2013. Characterisation of the input signal to aquifers in the French Basque Country: Emphasis on parameters influencing the chemical and isotopic composition of recharge waters. Journal of Hydrology 496, 57–70.

Johnson, M.R., van Vuuren, C.J., Visser, J.N., Cole, D.I., Wickens, H., Christie, A.D., Roberts, D.L., Brandl, G., 2006. Sedimentary rocks of the Karoo Supergroup, in: Johnson, M.R., Annhaeusser, C.R., Thomas, R.J. (Eds.), The Geology of South Africa. Geological Society of South Africa, Council for Geoscience, Pretoria. chapter 22, pp. 461–500.

Jolly, J.L., 2002. Sustainable use of Table Mountain Group aquifers and problems related to scheme failure, in: Pietersen, K., Parsons, R. (Eds.), A Synthesis of the Hydrogeology of the Table Mountain Group - Formation of a Research Strategy. Water Research Commission, Pretoria. TT 158/01, pp. 108–111.

Jolly, J.L., Kotze, J.C., 2002. The Klein Karoo Rural Water Supply Scheme, in: Pietersen, K., Parsons, R. (Eds.), A Synthesis of the Hydrogeology of the Table Mountain Group - Formation of a Research Strategy. Water Research Commission, Pretoria. TT 158/01, pp. 198–201.

Jones, M., 1992. Heat flow in South Africa. Handbook of the Geological Survey 14. Geological Survey. Pretoria.

Jordaan, L.J., Scheepers, R., Barton, E.S., 1995. The geochemistry and isotopic composition of the mafic and intermediate igneous components of the Cape Granite Suite, South Africa. Journal of African Earth Sciences 21, 59–70.

Kakiuchi, M., Matsuo, S., 1979. Direct measurements of D/D and 18O/16O fractionation factors between vapor and liquid water in the temperature range from 10 to 40C. Geochemical Journal 13, 307–311.

Kent, L.E., 1949. The thermal waters of the Union of South Africa and South West Africa. Transactions of the Geological Society of South Africa 52, 231–264.

Knox, A., 1911. The Climate of the Continent of Africa. Cambridge University Press, Cambridge.

Kotze, J.C., 2002. Towards a management tool for groundwater exploitation in the Table Mountain sandstone fractured aquifer. Technical Report 729/1/02. Water Research Commission. Pretoria.

Kotze, J.C., Verhagen, B.T., Butler, M.J., 2000. An aquifer model based on chemistry, isotopes and lineament mapping: Little Karoo, South Africa, in: Sililo, O. (Ed.), Groundwater: Past Achievements and Future Challenges. Balkema, Rotterdam, pp. 539–544.

Ladouche, B., Luc, A., Nathalie, D., 2009. Chemical and isotopic investigation of rainwater in southern France (1996-2002): Potential use as input signal for karst functioning investigation. Journal of Hydrology 367, 150–164.

Lawrence, J.R., White, J.W., 1991. The elusive climate signal if the isotopic composition of precipitation, in: Taylor, H.P., O'Neil, J.R., Kaplan, I.R. (Eds.), Stable Isotope Geochemistry: A Tribute to Samuel Epstein. The Geochemical Society, San Antonio. number 3 in Special Publication, pp. 169–185.

le Maitre, D.C., Colvin, C., Scott, D.F., 2002. Groundwater dependent ecosystems in the Fynbos Biome, and their vulnerability to groundwater abstraction, in: Pietersen, K., Parsons, R. (Eds.), A Synthesis of the Hydrogeology of the Table Mountain Group - Formation of a Research Strategy. Water Research Commission, Pretoria. TT 158/01, pp. 112–117.

Lin, L., Jia, H., Xu, Y., 2007. Fracture network characteristics of a deep borehole in the Table Mountain Group, South Africa. Hydrogeology Journal 15, 1419–1432.

Lis, G., Wassenaar, L.I., Hendry, M.J., 2008. High-Precision LASER spectroscopy D/H and 18O/16O measurements of microliter natural water samples. Analytical Chemistry 80, 287–293.

Liu, J., Fu, G., Song, X., Charles, S.P., Zhang, Y., Han, D., Wang, S., 2010. Stable isotopic compositions in Australian precipitation. Journal of Geophysical Research 115, 16.

Maclear, L.G., 2002. The hydrogeology of the Uitenhage Artesian Basin with reference to the Table Mountain Group aquifer, in: Pietersen, K., Parsons, R. (Eds.), A Synthesis of the Hydrogeology of the Table Mountain Group - Formation of a Research Strategy. Water Research Commission, Pretoria. TT 158/01, pp. 216 – 223.

Majumder, R.K., Halim, M.A., Saha, B.B., Ikawa, R., Nakamura, T., Kagabu, M., Shimada, J., 2011. Groundwater flow systems in Bengal Delta, Bangladesh revealed by environmental isotopes. Environmental Earth Science 64, 1343–1352.

Mazor, E., Verhagen, B.T., 1976. Hot springs of Rhodesia – their noble gases, isotopic and chemical composition. Journal of Hydrology 28, 29–43.

Mazor, E., Verhagen, B.T., 1983. Dissolved ions, stable and radioactive isotopes and noble gases in thermal waters of South Africa. Journal of Hydrology 63, 315–329.

Mazor, E., Verhagen, B.T., Negreanu, E., 1974. Hot springs of the igneous terrain of Swaziland – their noble gases, hydrogen, oxygen and carbon isotopes and dissolved ions, in: Isotope Techniques in Groundwater Hydrology. International Atomic Energy Agency, Vienna. volume 2, pp. 29–47.

Meyer, P.S., 2002. Springs in the Table Mountain Group, with special reference to fault controlled springs, in: Pietersen, K., Parsons, R. (Eds.), A Synthesis of the Hydrogeology of the Table Mountain Group - Formation of a Research Strategy. Water Research Commission, Pretoria. TT 158/01, pp. 224–229.

Midgley, J., Scott, D.F., 1994. The use of stable isotopes of water (D and ^{18}O) in hydrological studies in the Jonkershoek Valley. Water SA 20, 151–154.

Mulligan, B.M., Ryan, M.C., Cámbara, T.P., 2011. Delineating volcanic aquifer recharge areas using geochemical and isotopic tools. Hydrogeology Journal 19, 1335–1347.

NASA, 2013. Shuttle Radar Topography Mission. URL: http://www2.jpl.nasa.gov/srtm/.

Negrel, P., Pauwels, H., Dewandel, B., Gandolfi, J.M., Mascré, C., Ahmed, S., 2011. Understanding groundwater systems and their functioning through the study of stable isotopes in a hard-rock aquifer (Maheshwaram watershed, India). Journal of Hydrology 397, 55–70.

NGI, 2012. RSA National Geo-Spatial Information 1:50 000 shape files. URL: http://www.ngi.gov.za/.

Nkondo, M.N., van Zyl, F.C., Keuris, H., Schreiner, B., 2012. National Water Resource Strategy 2. Technical Report. Department of Water Affairs. Pretoria.

Parsons, R., 2002. Development of Groundwater Resources of the Arabella Country Estate, in: Pietersen, K., Parsons, R. (Eds.), A Synthesis of the Hydrogeology of the Table Mountain Group - Formation of a Research Strategy. Water Research Commission, Pretoria. TT 158/01, pp. 150–154.

Partridge, T.C., Botha, G.A., Haddon, I.G., 2006. Cenozoic Deposits of the Interior, in: Johnson, M.R., Annhaeusser, C.R., Thomas, R.J. (Eds.), The Geology of South Africa. Geological Society of South Africa, Council for Geoscience, Pretoria. chapter 29, pp. 585–604.

Partridge, T.C., Maud, R.R., 1987. Geomorphic evolution of southern Africa since the Mesozoic. South African Journal of Geology 90, 179–208.

Peng, T.R., Wang, C.H., Huang, C.C., Fei, L.Y., Chen, C.T., Hwong, J.L., 2010. Stable isotope characteristics of Taiwan's precipitation: A case study of western Pacific monsoon region. Earth & Planetary Science Letters 289, 357–366.

Pietersen, K., Parsons, R. (Eds.), 2002. A Synthesis of the Hydrogeology of the Table Mountain Group - Formation of a Research Strategy. TT 158/01, Water Research Commission, Pretoria.

Poehls, D.J., Smith, G.J., 2009. Encyclopedic Dictionary of Hydrogeology. Elsevier, Amsterdam.

Preston-Whyte, R.A., Tyson, P.D., 1988. The Atmosphere and Weather of Southern Africa. Oxford University Press, Cape Town.

Rangarajan, R., Ghosh, P., 2011. Tracing the source of bottled water using stable isotope techniques. Rapid Communications in Mass Spectrometry 25, 3323–3330.

Reeburgh, W.S., 1994. Global water reservoirs, fluxes and turnover times. URL: http://www.ess.uci.edu/ reeburgh/fig8.html.

Richey, D.G., McDonnell, J.J., Erbe, M.W., Hurd, T.M., 1998. Hydrograph separations based on chemical and isotopic concentrations: a critical appraisal of published studies from New Zealand, North America and Europe. Journal of Hydrology (NZ) 37, 95–111.

Roberts, D.L., Botha, G.A., Maud, R.R., Pether, J., 2006. Coastal Cenozoic Deposits, in: Johnson, M.R., Annhaeusser, C.R., Thomas, R.J. (Eds.), The Geology of South Africa. Geological Society of South Africa, Council for Geoscience, Pretoria. chapter 30, pp. 605–628.

Roets, W., Xu, Y., Raitt, L., El-Kahloun, M., Meire, P., Calitz, F., Batelaan, O., Anibas, C., Paridaens, K., Vandenbroucke, T., Verhoest, N., Brendonck, L., 2008. Determining discharges from the Table Mountain Group (TMG) aquifer to wetlands in the Southern Cape, South Africa. Hydrobiologia 607, 175–186.

Rosewarne, P., 2002a. Case Study: Ceres Municipality, in: Pietersen, K., Parsons, R. (Eds.), A Synthesis of the Hydrogeology of the Table Mountain Group - Formation of a Research Strategy. Water Research Commission, Pretoria. TT 158/01, pp. 160–163.

Rosewarne, P., 2002b. Hydrogeological Characteristics of the Table Mountain Group Aquifers, in: Pietersen, K., Parsons, R. (Eds.), A Synthesis of the Hydrogeology of the Table Mountain Group - Formation of a Research Strategy. Water Research Commission, Pretoria. TT 158/01, pp. 33–44.

Rozanski, K., Araguás-Araguás, L., Gonfiantini, R., 1993. Isotopic patterns in modern global precipitation, in: Swart, P.K., Lohmann, K.C., McKenzie, J., Savin, S. (Eds.), Climate Change in Continental Isotopic Records. American Geophysical Union. number 78 in Geophysical Monograph. chapter 1, pp. 1–36.

Rozanski, K., Sonntag, C., Munnich, K.O., 1982. Factors controlling stable isotope composition of European precipitation. Tellus 34, 142–150.

Rozendaal, A., Gresse, P.G., Scheepers, R., le Roux, J.P., 1999. Neoproterozoic to early Cambrian crustal evolution of the Pan-African Saldania Belt, South Africa. Precambrian Research 97, 303–323.

Rust, I.C., 1967. On the sedimentation of the Table Mountain Group in the Western Cape Province, D.Sc. thesis. Ph.D. thesis. Stellenbosch University.

Rust, I.C., 1973. The evolution of the Palaeozoic Cape basin, southern margin of Africa. Plenum, New York, New York. volume 1 of *The Ocean Basins and Margins*. chapter 6. pp. 247–276.

Rust, I.C., 1977. Evidence of shallow marine and tidal sedimentation in the Ordovician Graafwater Formation, Cape Province, South Africa. Sedimentary Geology 18, 123–133.

Saayman, I.C., Adams, S., Harris, C., 2000. Example of O- and H-isotope use to identify surface water pollution in groundwater, in: Sililo, O. (Ed.), Groundwater: Past Achievements and Future Challenges. A.A.Balkema, Rotterdam, pp. 599–603.

Saayman, I.C., Scott, D.F., Prinsloo, F.W., Moses, G., Weaver, J.M., Talma, S., 2003. Evaluation of the application of natural isotopes in the identification of the dominant streamflow generation mechanisms in TMG catchments. Technical Report 1234/1/03. Water Research Commission. Pretoria.

SACS, 1980. Stratigraphy of South Africa. volume Part 1: Lithostratigraphy of the Republic of South Africa, South West Africa/Namibia, and the Republics of Boputhatswana, Transkei and Venda. South African Committee for Stratigraphy, Geological Survey, Pretoria.

Salameh, E., 2004. Using environmental isotopes in the study of the recharge-discharge mechanisms of the Yarmouk catchment area in Jordan. Hydrogeology Journal 12, 451–463.

Salati, E., Dall'Olio, A., Matsui, E., Gat, J.R., 1979. Recycling of water in the Amazon Basin: an isotopic study. Water Resources Research 15, 1250–1258.

Sami, K., 1992. Recharge mechanisms and geochemical processes in a semi-arid sedimentary basin, Eastern Cape, South Africa. Journal of Hydrology 139, 27–48.

SAWB, 1996. The weather and climate of the extreme south-western Cape. South African Weather Bureau, Department of Environmental Affairs and Tourism. Pretoria.

SAWS, 2010-12. Daily Weather Bulletin, ISSN 0011-5517. Monthly. Pretoria.

Scheepers, R., Armstrong, R., 2002. New U-Pb SHRIMP zircon ages of the Cape Granite Suite: implications for the magmatic evolution of the Saldania Belt. South African Journal of Geology 105, 241–256.

Scheepers, R., Poujol, M., 2002. U-Pb zircon age of Cape Granite Suite ignimbrites: characteristics of the last phases of the Saldanian magmatism. South African Journal of Geology 105, 163–178.

Scheepers, R., Schoch, A.E., 2006. The Cape Granite Suite, in: Johnson, M.R., Annhaeusser, C.R., Thomas, R.J. (Eds.), The Geology of South Africa. Geological Society of South Africa, Council for Geoscience, Pretoria. chapter 19, pp. 421–432.

Schimmelman, A., DeNiro, M.J., 1993. Preparation of organic and water hydrogen for stable isotope analysis: Effects due to reaction vessels and zinc reagent. Analytical Chemistry 65, 789–792.

Schoch, A.E., Burger, A.J., 1976. U-Pb zircon age of the Saldanha Quartz Porphyry, Western Cape Province. Transactions of the Geological Society of South Africa 79, 239–241.

Schoch, A.E., Leterrier, J., de la Roche, H., 1977. Major element geochemical trends in the Cape Granites. Transactions of the Geological Society of South Africa 80, 197–209.

Schulze, R.E., Lynch, S.D., 2001. South African Atlas of Agrohydrology and Climatology. URL: http://planet.uwc.ac.za/NISL/Invasives/Assignments/GARP/atlas/atlas toc.htm.

Sharp, Z., 2007. Principles of Stable Isotope Geochemistry. Pearson Prentice Hall.

Shone, R.W., 2006. Onshore post-Karoo Mesozoic deposits, in: Johnson, M.R., Annhaeusser, C.R., Thomas, R.J. (Eds.), The Geology of South Africa. Geological Society of South Africa, Council for Geoscience, Pretoria. chapter 26, pp. 541–552.

Shone, R.W., Booth, P.W., 2005. The Cape basin, South Africa: A review. Journal of African Earth Sciences 43, 196–210.

Socki, R.A., Karlsson, H.R., Gibson, Jr., E.K., 1992. Extraction technique for the determination of oxygen-18 in water using preevacuated glass vials. Analytical Chemistry 64, 829–831.

Söhnge, A.P., 1983. The Cape Fold Belt - Perspective, in: Söhnge, A.P., Hälbich, I.W. (Eds.), Geodynamics of the Cape Fold Belt. Geological Society of South Africa, Johannesburg. number 12 in Special Publication. chapter 1, pp. 1–6.

Stats SA, 2006. Updated water accounts for South Africa: 2000. Technical Report. Statistics South Africa. Pretoria.

Sumner, G., 1988. Precipitation: Process and Analysis. John Wiley & Sons, Inc., Singapore.

Takai, K., Moser, D.P., DeFlaun, M., Onstott, T.C., Frederickson, J.K., 2001. Archaeal diversity in waters from deep South African gold mines. Applied and Environmental Microbiology 67, 5750–5760.

Talma, A.S., van Wyk, E., 2013. Rainfall and Groundwater Isotope Atlas, in: Abiye, T. (Ed.), The Use of Isotope Hydrology to Characterise and Assess Water Resources in Southern Africa. Water Research Commission, Pretoria. TT570/13. chapter 6, pp. 83–101.

Tankard, A.J., Hobday, D.K., 1977. Tide dominated back-barrier sedimentation, early Ordovician Cape Basin, Cape Peninsula, South Africa. Sedimentary Geology 18, 135–159.

Tankard, A.J., Jackson, M.P., Eriksson, K.A., Hobday, D.K., Hunter, D.R., Minter, W.E.L., 1982. Crustal Evolution of Southern Africa, 3.8 Billion Years of Earth History. Springer, New York.

Tanweer, A., Hut, G., Burgman, J.O., 1988. Optimal conditions for the reduction of water to hydrogen by zinc for mass spectrometric analysis of the deuterium content. Chemical Geology (Isotope Geoscience Section) 73, 199–203.

Thamm, A.G., Johnson, M.R., 2006. The Cape Supergroup, in: Johnson, M.R., Annhaeusser, C.R., Thomas, R.J. (Eds.), The Geology of South Africa. Geological Society of South Africa, Council for Geoscience, Pretoria. chapter 21, pp. 443–460.

Theron, J.N., Basson, W.A., 1989. Lithostratigraphy of the Rietvlei Formation (Table Mountain Group). Lithostratigraphic Series 7. Geological Survey. Pretoria.

Theron, J.N., Gresse, P.G., Siegfried, H.P., Rogers, J., 1992. The Geology of the Cape Town area, explanation of sheet 3318. Technical Report. Geological Survey, Department of Mineral and Energy Affairs. Pretoria.

Theron, J.N., Rickards, R.B., Aldridge, R.J., 1990. Bedding plane assemblages of *Promissum pulchrum*, a new giant ashgill conodont from the Table Mountain Group, South Africa. Palaeontology 33, 577–594.

Theron, J.N., Wickens, H., Gresse, P.G., 1991. The Geology of the Ladismith area, explanation of sheet 3320. Technical Report. Geological Survey, Department of Mineral and Energy Affairs.

Toerien, D.K., 1979. The Geology of the Oudtshoorn area, explanation of sheet 3222. Technical Report. Geological Survey, Department of Mines.

Toerien, D.K., Hill, R.S., 1989. The Geology of the Port Elizabeth Area, explanation of sheet 3324. Technical Report. Geological Survey, Department of Mineral and Energy Affairs. Pretoria.

Uemura, R., Yonezawa, N., Yoshimura, K., Asami, R., Kadena, H., Yamada, K., Yoshida, N., 2012. Factors controlling isotopic composition of precipitation on Okinawa Island, Japan: Implications for palaeoclimate reconstruction in the East Asian Monsoon region. Journal of Hydrology 475, 314–322.

Umvoto, SRK, 2000. Reconnaissance Investigation into the Development and Utilization of Table Mountain Group Artesian Groundwater using the E10 Catchment as a Pilot Study Area: CAGE project - interim report. Technical Report. Geohydrology and Project Planning Directorate, Department of Water Affairs & Forestry.

Urey, H.C., 1947. The thermodynamic properties of isotopic substances. Journal of the Chemical Society of London , 562–581.

Vegter, J.R., 1995. An explanation of a set of National Groundwater Maps. Technical Report TT 74/95. Water Research Commission, Department of Water Affairs & Forestry. Pretoria.

Vogel, J.C., van Urk, H., 1975. Isotopic composition of groundwater in semi-arid regions of southern Africa. Journal of Hydrology 25, 23–36.

Vos, R.G., Tankard, A.J., 1981. Braided fluvial sedimentation in the lower Palaeozoic Cape Basin, South Africa. Sedimentary Geology 29, 171–193.

Vreča, P., Bronić, I.K., Horvatiničić, N., Barešić, J., 2006. Isotopic characteristics of precipitation in Slovenia and Croatia: Comparison of continental and maritime stations. Journal of Hydrology 330, 457–469.

Walsch, R.P., Lawler, D.M., 1981. Rainfall seasonality: Description, spatial patterns and change through time. Weather 36, 201–208.

Weaver, J.M., Rosewarne, P., Hartnady, C.J., Hay, E.R., 2002. Potential of Table Mountain Group aquifers and integration into catchment water management, in: Pietersen, K., Parsons, R. (Eds.), A Synthesis of the Hydrogeology of the Table Mountain Group - Formation of a Research Strategy. Water Research Commission, Pretoria. TT 158/01, pp. 239–255.

Weaver, J.M., Talma, A.S., Cavé, C., 1999. Geochemistry and Isotopes for resource evaluation in the fractured rock aquifers of the Table Mountain Group. Technical Report 481/1/99. Water Research Commission. Pretoria.

West, A.G., February, E.C., Bowen, G.J., 2014. Spatial analysis of hydrogen and oxygen stable isotopes ("isoscapes") in ground water and tap water across South Africa. Journal of Geochemical Exploration 145, 213–222.

West, A.G., Goldsmith, G.R., Brooks, P.D., Dawson, T.E., 2010. Discrepancies between isotope ratio infrared spectroscopy and isotope ratio mass spectrometry for the stable isotope analysis of plant and soil waters. Rapid Communications in Mass Spectrometry 24, 1948–1954.

West, A.G., Goldsmith, G.R., Matimati, I., Dawson, T.E., 2011. Spectral analysis software improves confidence in plant and soil water stable isotope analyses performed by isotope ratio infrared spectroscopy (IRIS). Rapid Communications in Mass Spectrometry 25, 2268–2274.

White, M.E., 2000. Running Down. Kangaroo Press, Sydney.

Wikipedia, 2013a. Rain. URL: http://www.wikipedia.org/wiki/rain.

Wikipedia, 2013b. Ogallala aquifer. URL: http://www.wikipedia.org/wiki/Ogallala aquifer.

Woodford, A.C., 2002. Interpretation and applicability of pumping-tests in Table Mountain Group aquifers, in: Pietersen, K., Parsons, R. (Eds.), A Synthesis of the Hydrogeology of the Table Mountain Group - Formation of a Research Strategy. Water Research Commission, Pretoria. TT 158/01, pp. 71–84.

Yonge, C.J., Goldenberg, L., Krouse, H.R., 1989. An isotopic study of water bodies along a traverse of southwestern Canada. Journal of Hydrology 106, 245–255.

Young, G.M., Minter, W.E.L., Theron, J.N., 2004. Geochemistry and palaeogeography of upper Ordovician glaciogenic sedimentary rocks in the Table Mountain Group, South Africa. Palaeogeography, Palaeoclimatology, Palaeoecology 214, 323–345.

Yurtsever, Y., Gat, J.R., 1981. Atmospheric waters, in: Gat, J.R., Gonfiantini, R. (Eds.), Stable Isotope Hydrology. International Atomic Energy Agency, Vienna. number 20 in Technical Reports Series. chapter 6, pp. 103–142.